

# **European Congress of Chemical Engineering – 6**

Copenhagen, 16-20 September, 2007

## **ECCE-6 Book of Abstracts - Volume 2**

*Edited by*

**Rafiqul Gani & Kim Dam-Johansen**

*Technical University of Denmark,  
Department of Chemical Engineering,  
Søltofts Plads, Building 229,  
DK-2800 Kgs. Lyngby, Denmark*



**EFCE Event Number 669**

*September 2007*

*Technical University of Denmark  
Department of Chemical Engineering  
Søltofts Plads, Building 229,  
DK-2800 Kgs. Lyngby, Denmark*

*Tel: 45 45252800  
Fax: 45 45 882258  
E-mail: kt@kt.dtu.dk  
Internet: www.kt.dtu.dk*

*ISBN 978-87-91435-56-0*

*Printed at: ??*

*Cover Design by: ??*

*Photo of "Nyhavn" by Morten Jerichau has been used on the cover design*

## *Preface*

This two-volumes ECCE-6 book of abstracts contains the final camera ready abstracts of most of the papers presented at the conference. Each volume contains approximately 1150 pages with close to 500 abstracts per volume. In addition, a proceedings of the ECCE-6 in a CD-ROM (containing all submitted abstracts in their final version, the full manuscripts submitted by a large percentage of authors, the technical program, the author-program index and many more) has been prepared for distribution to all participants of ECCE-6.

ECCE-6 is the sixth in the series of congresses on chemical engineering launched by the EFCE in 1997 in Firenze, the venue for ECCE-1. Since 1997, ECCE has been organized in France (Montpellier, 1999), Germany (Nurnberg, 2001) and Spain (Granada, 2003). In 2005, the ECCE-5 was combined with the World Congress of Chemical Engineering in Glasgow. The objective of this biennial congress is to provide engineers, scientists, researchers, technologists, students and others a platform to present their latest results, to interchange ideas, to make new contacts, to establish new collaborations, and many more. The conference addresses the full spectrum of chemical engineering practice, including current trends and future needs.

Volume 1 includes the abstracts from themes 1, 3, 4, 6, special sessions 1-3, the EPIC-I symposium, the special workshop on education, and the symposiums on Chemical Product Design & Engineering (CPD&E) and Environmental Protection and Sustainability (EP&S). Volume 2 contains the abstracts from themes 2, 5 and the LMC Congress (ECCE-1 Symposium on Innovations in Food Technology). Out of a total of 1224 abstracts that were initially selected from more than 2000 submissions, about 500 will be presented in 12 parallel oral sessions while an equal number will be presented as posters in 4 plenary sessions, one on each day.

We would like to thank the members of the international scientific committee for their reviews, their advice during the selection process and the preparation of the technical program. We would like to thank all authors for submitting their abstracts. Also, we would like to thank the supporting group at the Department of Chemical Engineering for their help in getting these books ready for the printer. Special thanks in this respect goes to Mrs Eva Mikkelsen for the administrative/secretarial support, to Dr. Loic d'Anterrosches for the electronic transfer of necessary data, and the student helpers for various jobs related to getting the abstracts ready for the book. The following PhD-students (Kavitha, Merlin, Piotr, Bena-Marie, Leila, Elisa) and MSc-students (Christine, Reaz, Shafique) deserve special thanks. Also, we would like to acknowledge the help from Wonderful Copenhagen organization with respect to the selection of the background picture ("Nyhavn" by Morten Jerichau) on the front and back covers of the book volumes.

We hope that these books of abstracts will serve as a valuable record of reference of the contributions made at ECCE-6.

Rafiqul Gani & Kim Dam-Johansen

September 2007

Chemical Engineering Department,  
Technical University of Denmark



## ECCE-6 International Scientific Committee (ISC)

**Co-chairs:** Rafiqul Gani (DK), Kim-Dam-Johansen (DK), Ryszard Pohorecki (PL)

### Theme-Coordiators:

Theme	Theme Title	Coordinators
1	Sustainable process-product development through green chemistry	A. Kraslawski (SF)
2	Advancing the chemical engineering fundamentals	O Hassager (DK), J Drahos (CZ)
3	Multi-scale and/or multi-disciplinary approach to process-product innovation	J-C Charpentier (FR)
4	Systematic methods and tools for managing the complexity	E N Pistikopoulos (UK), B Braunschweig (F)
5	Integration of life sciences & engineering	J Villadsen (DK), F Muller (UK)
6	Educating chemical engineers for coming challenges	M Molzahn (DE)

### Chair-persons for Special Symposiums:

Symposium	Title	Coordinators
S1	Energy Issues	E H Stenby (DK)
S2	Multiscale Modelling	R Gani (DK)
S3	Biotechnology – Honouring Prof J Villadsen	K V Gernaey (DK)
S4	EPIC-1: 1 <sup>st</sup> European Process Intensification Conference	A. Stankiewicz (NL) A Gorak (DE)
S5	Innovations in Food Technology	A Friis (DK)
S6	The Future of European Chemical Engineering Education in a Globalized World	M Molzahn (DE)
S7	Environmental Protection & Sustainability	B Kawalec-Pietrenko (PL)
S8	Chemical Product Design and Engineering (CPD&E)	M E Vigild (DK), A A Broekhuis (NL)

### Topic Coordinators & Reviewers:

Abildskov, J.	DK
Achenie, L.E.K.	USA
Adjiman, C.	UK
Arlt, W.	DE
Azapagic, A.	UK
De Azevedo, S.F.	PT
Baldi, G.	IT
Bell, G.	UK
Brignole, E.	AR
Cameron, I.T.	AU
Diwekar, U.	USA
Drioni, E.	IT
Eden, M.R.	USA
Feise, H.	DE
Fischer, U.	CH
Galan, M.A.	ES
Gamse, T.	AT
Georgiadis, M.	GR
Gernaey, K	DK
Glarborg, P.	DK
Glavic, P.	SI
Gorak, A.	DE
Hampe, M.	DE
Hangos, K.	HU
Hao Wen	CN
Hvilsted, S.	DK

Jallut, C.	FR
Jensen, A.	DK
Jensen, N.	DK
Johannessen, T.	DK
Jonsson, G.	DK
Joulia, X.	FR
Kanamori, T.	JP
Keurentjes, J.	NL
Kiil, S.	DK
Kikkinides, S.	GR
Kontogeorgis, G.	DK
Kravanja, Z.	SI
Lapicque, F.	FR
Marechal, F.	CH
McKenna, T.	FR
Meyer, A.	DK
Meyer, T.	CH
Mollerup, J.	DK
Moon, I.	S. Korea
Narodoslawsky, M.	AT
Ng, K.M.	Hong Kong
Niklasson-Bjorn, I.	SE
Nordkvist, M.	DK
Nomen, R.	ES
O'Connell, J.P.	USA
Pilavachi, P.A.	GR

Pitt, M.	UK
Pérez-Cisneros, E.	MX
Pons, M.	FR
Povoa, A.	PT
Puigjaner, L.	ES
Rasmussen, M.S.	DK
Ribeiro, F.R.	PT
Roizard, C.	FR
Sadowski, G.	DE
Schembecker, G.	DE
Schenkel, B.	CH
Schouten, J.	NL
Schubert, H.	DE
Sorensen, E.	UK
Sovova, H.	CZ
Suter, G.	CH
Taylor, R.	USA
Thomsen, K.	DK
Tsotsas, E.	DE
Ulrich, J.	DE
Vigild, M.	DK
Von Rohr, P. R.	CH
Wiebe, L.	DK
Wild, G.	FR

## **Editorial Notes**

### **Inclusion of abstracts**

The conditions for inclusion of an abstract in the ECCE-6 books of abstracts have been the following:

- acceptance of the abstract in the technical program
- use of the supplied abstract template for the ECCE-6 book of abstracts
- not exceeding the 2-page limit as well as remaining within the specified page margins, etc.
- submission (uploading) of the final camera ready abstract document on time

Therefore, some authors may not find their abstracts included in these books. This does not effect their inclusion in the technical program and/or the form of presentation.

### **Guide to abstract-author search**

Because of the large number of abstracts, we have divided the book of abstracts into two volumes. Also, because of the very large number of authors involved (more than 3000 and not all of them registered in the database of authors), it has not been possible for us to link the author-index to the corresponding page numbers. Instead, we have linked the author-index to the session numbers and organized the abstracts according to the session numbers. In order to quickly and efficiently find the abstract of your interest, you may find the following guidelines useful:

#### **1. To find a paper on a specific topic**

Locate the theme and then the topic under the theme and then the session under the topic. The locations of these are indexed with page numbers (see the tables in the table of contents pages). Go to the corresponding page. On this page, a list of the abstracts corresponding to this session is given together with an indication of which abstracts have been included. The abstracts marked with “yes” can be found in the pages following the table, ordered as they appear on the table.

Alternatively, find the session number where the paper of your interest is to be presented. Go the corresponding page for the session and then find if the abstract of your interest is included. If yes, find the abstract within the pages corresponding to this session.

#### **2. To find an author and his/her papers**

In this case, the author-index linked to the session numbers (provided at the end of the book) can be useful. Note that this author index is in terms of session numbers and not page numbers. Also, only those authors who had signed-in to

the database are indexed. So , it is possible that authors listed in the technical program may not be found in this author-index.

Locate the surname of the author and the corresponding session number. Go to the contents page and find the page number where the session table is given. Find the abstract in the pages following the session table.



## Table of Contents – Volume 2

	Page
Preface	I
International Scientific Committee	III
Editorial notes	V
Table of contents	VII
Abstracts	1- 1128
Author Index	1129

### Abstracts-index according to themes

Theme/ Symposium	Title	Page
Theme-1	Sustainable process-product development & green chemistry	Vol-1
Theme-2	Advancing the chemical engineering fundamentals	1 – 792
Theme-3	Multi-scale and/or multi-disciplinary approach to process-product innovation	Vol-1
Theme-4	Systematic methods and tools for managing the complexity	Vol-1
Theme-5	Integration of life sciences and engineering	793 – 898
Theme-6	Educating chemical engineers for coming challenges	Vol-1
Invited-1	Multiscale modelling	Vol-1
Invited-2	Energy issues	Vol-1
Invited-3	Biotechnology: Honoring Prof John Villadsen	Vol-1
EPIC-1	European Process Intensification Conference – 1	Vol-1
LMC-Food	Innovations in food technology (LMC Congress)	899 – 1128
Education	Workshop on “The future of European chemical engineering education in a globalized world”	Vol-1
EP&S	Environmental Protection & Sustainability	Vol-1
CPD&E	Chemical Product Design & Engineering	Vol-1

## Abstracts-index according to session topics

<b>Session</b>	<b>Topic</b>	<b>Page</b>
Theme-2	Advancing the chemical engineering fundamentals	
T2-K	Keynote Lectures: Theme-2 .....	1
T2-1a	Thermodynamics: Hydrocarbons & Petrochemicals (T2-1a) .....	11
T2-1b	Thermodynamics: Applications of Equations of State (T2-1b) .....	21
T2-1c	Thermodynamics: Developments with SAFT EOS (T2-1c) .....	31
T2-1d	Thermodynamics: Molecular Simulation & Related Approaches (T2-1d) .....	39
T2-1e	Thermodynamics: General (T2-1e) .....	49
T2-1P	Thermodynamics (T2-1P) .....	61
T2-2a	Chemical Reaction Engineering: Kinetics & Modelling (T2-2a) .....	117
T2-2b	Chemical Reaction Engineering: Advanced Concepts (T2-2b) .....	127
T2-2c	Chemical Reaction Engineering: Practical Applications (T2-2c) .....	139
T2-2P	Chemical Reaction Engineering (T2-2P) .....	149
T2-3	Particulate Systems (T2-3) .....	197
T2-3P	Particulate Systems (T2-3P) .....	211
T2-4	Rheology (T2-4) .....	239
T2-4P	Rheology (T2-4P) .....	253
T2-5a	Multifase Flows - I (T2-5a) .....	259
T2-5b	Multifase Flows - II (T2-5b) .....	265
T2-5c	Multifase Flows - III (T2-5c) .....	279
T2-5P	Multifase Flows (T2-5P) .....	289
T2-6a	Interfacial & Colloidal Phenomena - I (T2-6a) .....	319
T2-6b	Interfacial & Colloidal Phenomena - II (T2-6b) .....	333
T2-6c	Interfacial & Colloidal Phenomena - III (T2-6c) .....	345
T2-6P	Interfacial & Colloidal Phenomena (T2-6P) .....	355
T2-7a	Transport Phenomena in Porous/Granular Media - I (T2-7a) .....	373
T2-7b	Transport Phenomena in Porous/Granular Media - II (T2-7b) .....	383
T2-7c	Transport Phenomena in Porous/Granular Media - III (T2-7c) .....	397
T2-7P	Transport Phenomena in Porous/Granular Media (T2-7P) .....	407
T2-8a	Membranes and Membrane Science - I (T2-8a) .....	437
T2-8b	Membranes and Membrane Science - II (T2-8b) .....	449
T2-8P	Membranes and Membrane Science (T2-8P) .....	461
T2-9	Crystallization (T2-9) .....	491
T2-9P	Crystallization (T2-9P) .....	505
T2-10a	Distillation, Absorption & Extraction - I (T2-10a) .....	537
T2-10b	Distillation, Absorption & Extraction - II (T2-10b) .....	547
T2-10c	Distillation, Absorption & Extraction - III (T2-10c) .....	561
T2-10P	Distillation, Absorption & Extraction (T2-10P) .....	571
T2-11a	Filtration - I (T2-11a) .....	599
T2-11b	Filtration - II (T2-11b) .....	609
T2-11P	Filtration (T2-11P) .....	621
T2-12a	Polymer Science & Engineering - I (T2-12a) .....	641
T2-12b	Polymer Science & Engineering - II (T2-12b) .....	651
T2-12P	Polymer Science & Engineering (T2-12P) .....	663
T2-13a	Catalysis - I (T2-13a) .....	671
T2-13b	Catalysis - II (T2-13b) .....	683
T2-13c	Catalysis - III (T2-13c) .....	693
T2-13P	Catalysis (T2-13P) .....	707
T2-14a	Electrochemical Engineering - I (T2-14a) .....	767
T2-14b	Electrochemical Engineering - II (T2-14b) .....	773
T2-14P	Electrochemical Engineering (T2-14P) .....	779

*Table of Contents*

<b>Session</b>	<b>Topic</b>	<b>Page</b>
Theme-5	Integration of life sciences & engineering	
T5-K	Keynote Lectures: Theme-5 .....	793
T5-1	Biochemical Engineering (T5-1) .....	799
T5-2	Design, Analysis & Control of Fermentation Processes (T5-2) .....	809
T5-3	Bio-transformation in the Laboratory and in Large Scale Production (T5-3) .....	821
T5-P	Integration of Life Sciences & Engineering - Poster (T5-P) .....	835

<b>Session</b>	<b>Topic</b>	<b>Page</b>
LMC/Food	Special Symposium - Innovations in Food Technology (LMC Congress)	
S-5D	Meals - Convenience, Gastronomy & Quality (Food-1a) .....	899
S-5Dd	Meals - Convenience, Gastronomy & Quality (Food-1b) .....	915
S-5E	White BioTech & Related Processes (Food-2a) .....	921
S-5Ee	White BioTech & Related Processes (Food-2b) .....	931
S-5F	Flexible Production, PAT & Modelling (Food-3a) .....	939
S-5Ff	Flexible Production, PAT & Modelling (Food-3b) .....	957
S-5G	Process & Product Innovation (Food-4a) .....	971
S-5Gg	Process & Product Innovation (Food-4b) .....	983
S-5H	Hygiene, Hygienic Design & Unit Operations (Food-5a) .....	993
S-5Hh	Hygiene, Hygienic Design & Unit Operations (Food-5b) .....	1009
S-5I	Modern Analysis: Chemical & Multivariate Analysis (Food-6a) .....	1019
S-5Ii	Modern Analysis: Chemical & Multivariate Analysis (Food-6b) .....	1033
S-5P-1	Innovations in Food Technology - Poster Session (LMC/Food - P1) .....	1039
S-5P-2	Innovations in Food Technology - Poster Session (Food - P2) .....	1087

*For the list of abstracts under each topic, go the corresponding page of the topic.*

*Table of Contents*

## Session T2-K: Theme-2 Keynote Lectures\*

<b>Abstract Number</b>	<b>Paper Title &amp; Authors</b>	<b>Included</b>
179	Prediction of properties of polymers through hierarchical simulations D N Theodorou	Yes
3203	Is Industrial Crystallization a Suitable Process for Protein Purification? – A Survey M J Jones, J Ulrich	Yes
4086	New solid foam reactor packings for multiphase applications J C Schouten, C P Stemmet, P W A M Wenmakers, J van der Schaaf, B F M Kuster	Yes
4091	Progresses on Seawater Desalination and Wastewater Treatment in the Logic of Process Intensification Strategy E Drioli, F. Macedonio	Yes

\* To be presented in different keynote sessions (see the technical program for details)

Session T2-K

## **Prediction of properties of polymers through hierarchical simulations**

D.N. Theodorou

*School of Chemical Engineering, National Technical University of Athens, 9 Heroon Polytechniou Street, Zografou Campus, 157 80 Athens, Greece*

### **1. Summary**

Predicting the physical properties of materials from their chemical constitution is highly desirable, but also very challenging, because of the extremely broad spectra of length and time scales governing their structure and molecular motion. This challenge can only be met through the development of hierarchical analysis and simulation strategies encompassing many interconnected levels, each level addressing phenomena over a specific window of time and length scales. We will discuss the fundamental underpinnings and example applications of new methods and algorithms for the hierarchical modelling of polymers. Questions to be addressed include: How can one equilibrate atomistic models of long-chain polymer melts at all length scales and thereby predict thermodynamic and conformational properties reliably? How can one quantify the structure of entanglement networks present in these melts through topological analysis and relate it to rheological properties? Can one address structural relaxation and plastic deformation phenomena in the configurationally arrested glassy state computationally? Are there ways to predict the microphase-separated morphology and stress-strain behaviour of multicomponent block copolymer-based materials, such as pressure sensitive adhesives? Is it possible to anticipate changes in the barrier properties of glassy polymers used in packaging applications as a consequence of modifications in the chemical constitution of chains?

Keywords: multiscale modelling, molecular simulation, polymers, rheology, diffusion

### **2. Extended Abstract**

Today's chemical engineers are called to contribute to the solution of important problems related to health, quality of life, energy, and the environment. A central, albeit perhaps not so visible, role in the solution of these problems is played by the design of materials with prescribed performance characteristics, products based on these materials, and processes for their manufacture and use.

Contemporary materials are very often engineered at the molecular level. Along with state-of-the-art synthesis, characterization, and testing techniques and high-throughput experimental approaches, computer modelling and simulation is gaining ground as a tool for quantifying structure-property-processing-performance relations in materials. A challenge faced by the modeller, especially in the case of polymers, is that structure in materials of engineering interest may exhibit characteristic length scales spreading over up to ten orders of magnitude, while the spectrum of characteristic times governing dynamics may cover more than twenty orders of magnitude. Clearly, hierarchical, or multiscale, modelling approaches are needed to connect atomic-level structure and interactions with the macroscopic properties of interest in applications in a predictive way (Kotelyanskii and Theodorou, 2004).

In this lecture we will present examples of hierarchical modelling strategies and algorithms for polymeric materials. Starting from polymer melts, we will show how connectivity-altering Monte Carlo simulations can ensure equilibration of high-molecular weight systems at all length scales, providing reliable estimates of thermodynamic and conformational properties (Theodorou, 2004); how systematic coarse-graining approaches can be used to reduce the number of degrees of freedom invoked in the molecular representation and thereby facilitate the simulation of polymers of complex chemical constitution; and how topological analysis of simulated configurations can provide valuable information about entanglements, which shape rheological properties (Tzoumanekas and Theodorou, 2006).

For self-organizing multicomponent polymeric materials (e.g. self-adhesive materials based on styrenic block copolymers) we will discuss how self-consistent field theoretical modelling can capture the microphase separated morphology starting from the system composition and the chemical constitution and architecture of its components. Morphology, in turn, can be used as a starting point for estimating the stress-strain behaviour of these materials using concepts of rubber elasticity theory.

In the design of gas separation membranes and packaging materials, controlling permeability properties is absolutely essential. We will discuss a hierarchical approach based on geometric analysis of accessible volume, multidimensional transition-state theory, and kinetic Monte Carlo simulation, for estimating the diffusivity of gases in glassy amorphous polymers (Theodorou, 2006).

## References

Kotelyanskii, M. and Theodorou, D. N. (Eds.), *Simulation Methods for Polymers*, Marcel Dekker, New York, 2004.

Theodorou, D.N., (2002) in: Nielaba, P., Mareschal, M. & Ciccotti, G. (Eds.), *Bridging time scales : Molecular simulations for the next decade*. Springer-Verlag, Berlin, pp. 69-128.

Tzoumanekas, C. and Theodorou, D.N., (2006) *Macromolecules*, 39, 4592-4603.

Theodorou, D.N., (2006) in: Yampolskii, Yu., Pinnau, I. & Freeman, B.D. (Eds.), *Materials Science of Membranes for Gas and Vapor Separation*, John Wiley, Hoboken, pp. 47-92.



## **Is Industrial Crystallization a Suitable Process for Protein Purification? – A Survey**

Matthew J. Jones and Joachim Ulrich

*Zentrum für Ingenieurwissenschaften, Verfahrenstechnik/TVT, Martin-Luther-Universität Halle-Wittenberg, 06099 Halle (Saale), Germany*

### **1. Summary**

Keywords: protein crystallization, industrial crystallization, downstream processing

### **2. Extended Abstract**

With the growing importance of protein products, demand for highly selective and cost effective separation methods with low environmental impact will increase. Industrial crystallization has the potential to satisfy all three requirements. However, for protein products, crystallization in the form of precipitation by salting-out is rarely used as anything other than an initial fractionating step prior to further purification, usually by chromatography. In contrast, protein crystal growth is well established for generating high-quality single crystals for structural studies. Despite being well established, the technique nonetheless relies upon empirical screening approaches when a new protein is to be crystallized. In part this is due to the absence of a general understanding of the factors influencing protein crystallization, which in turn is a consequence of the complexity of the problem: in addition to the "classic" crystallization parameters (temperature, pressure, concentration), account has to be taken of the effect of the precipitating agent required (its nature and concentration) as well as of the pH at which crystallization is carried out.

In the case of industrial crystallization, there is the added complication of the raw materials from which the protein product is to be isolated, either renewable resources or fermentation broths. Either of these represents complex systems containing

innumerable different compounds which may influence the processing requirements of the target protein.

This contribution will provide an overview of the state-of-the-art in protein crystallization with a view to developing large-scale processes for purification. Case studies based upon research carried out in our group will illuminate the difficulties that can be expected and which have to be addressed in the development of a process. Particular attention will be paid to mixing of the protein solution with the precipitant and to characteristics of enzymes, in particular their catalytic activity. The activity is an important characteristic and it is desirable to maintain the catalytic power of an enzyme during purification. In addition, the activity can be employed as a measure of the quality of a purification process. The enzyme urease, isolated from the jack bean, will be used as an example to highlight the effect of process conditions upon the activity. In addition, alternatives to standard batch crystallization by salting-out will be discussed.

## **New solid foam reactor packings for multiphase applications**

Jaap C. Schouten, Charl P. Stemmet, Patrick W.A.M. Wenmakers, John van der Schaaf, Ben F.M. Kuster

*Laboratory of Chemical Reactor Engineering, Department of Chemical Engineering and Chemistry, Eindhoven University of Technology, P.O. Box 513, 5600 MB Eindhoven, the Netherlands; Email: J.C.Schouten@tue.nl; Web: www.chem.tue.nl/scr*

### **1. Summary**

The chemical industry continually strives for more cost-efficient processes, and in doing so, considers the use of more advanced structured materials to optimize and intensify processes to the desired conditions. Solid foam materials are presented as highly efficient reactor packings for multiphase flow operation due to their improved hydrodynamic performance compared with more conventional packings, e.g. spherical particles, Raschig rings, and Sulzer packings. The advantages of these structured solid foam packings are a reduced pressure drop per packing height, improved hydrodynamic properties, and a greater window of stable operating conditions. The relatively high surface area ensures that adequate catalyst loadings may be applied. Improved gas-liquid contacting is advantageous to diminish mass transfer limitations under reaction conditions.

Keywords: gas-liquid-solid reactors, structured catalyst packings, solid foam materials, flow regimes, mass transfer, carbon nanofibres

### **2. Extended Abstract**

#### **2.1 Solid foam packings**

Solid foam packings represent a generation of commercially available materials combining relatively high specific surface area with low pressure drop per unit height. This is largely due to the open-celled structure with pore sizes ranging from 5 mm to 0.25 mm (5 to 40 pores per linear inch (ppi)), with relatively high voidages (up to 97%). Solid foams may be produced in a variety of materials (e.g., metal, carbon, ceramics, SiC, polymers). These materials enable high rates of gas-liquid mass transfer at relatively low levels of energy dissipation per unit volume of the reactor.

#### **2.2 Hydrodynamic characteristics**

This presentation outlines results obtained for gas-liquid flow through these solid foams in co-current and counter-current flow operation. The regimes of bubble flow, pulse flow, and trickle flow will be demonstrated with the associated flooding points (Figure 1). Hydrodynamic characteristics, such as frictional pressure drop and liquid holdup, will be presented for all three regimes. The overall gas-liquid mass transfer coefficient is correlated to the energy dissipation per unit of reactor volume. A comparison is presented between the foam packing characteristics and those of other packings, as Katapak-S and Sulzer packings, packed beds, monoliths, and micro-structured reactors.

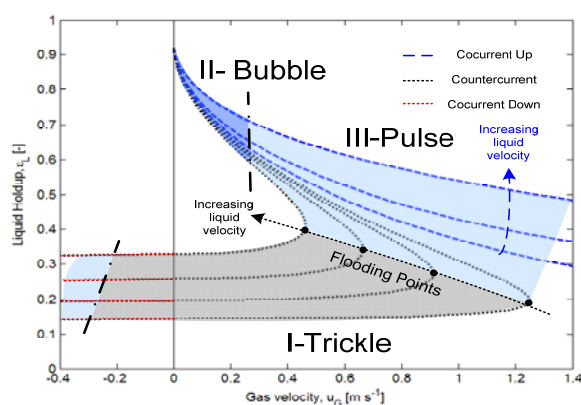


**Figure 1:** Flow regime map for co-current and counter-current gas-liquid flow.

### 2.3 Support for carbon nanofibers

It is also demonstrated that these solid foam materials are excellent carriers for immobilized active catalysts. For example, layers of entangled carbon nanofibers have been prepared on metallic as well as reticulated vitreous carbon foams (Figure 2). In this way the foam materials can be considered as the inverse of a packed bed, i.e. the void space and the packing have exchanged position, whereas entangled carbon nanofibers are the inverse of a porous catalyst particle.

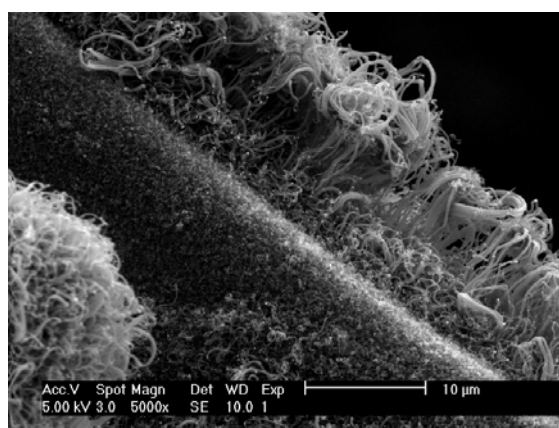


**Figure 2:** Carbon nanofibers grown on a nickel coated reticulated vitreous carbon foam by chemical decomposition of ethylene at 500 °C.

### 2.4 References

C.P. Stemmet, M. Meeuwse, J. van der Schaaf, B.F.M. Kuster and J.C. Schouten, *Chem. Eng. Sci.* (available online 1 March 2007).

C.P. Stemmet, J. van der Schaaf, B.F.M. Kuster and J.C. Schouten, *Chem. Eng. Res. Des.* **2006**, 84 (A12), 1134-1141.

C.P. Stemmet, J.N. Jongmans, J. van der Schaaf, B.F.M. Kuster and J.C. Schouten, *Chem. Eng. Sci.* **2005**, 60 (22), 6422-6429.

## **Progresses on Seawater Desalination and Wastewater Treatment in the Logic of Process Intensification Strategy**

E. Drioli,<sup>a, b</sup> F. Macedonio,<sup>a, b</sup>

<sup>a</sup>*Department of Chemical Engineering and Materials, University of Calabria, via P. Bucci cubo 45/A, 87030 Arcavacata di Rende, Italy*

<sup>b</sup>*Institute on Membrane Technology ITM-CNR c/o University of Calabria, via P. Bucci cubo 17/C, 87030 Arcavacata di Rende, Italy*

### **1. Summary**

*Water* is one of the simplest and most indispensable molecules in the world, whose growing scarcity and declining quality might negatively affect the overall quality of our life and the industrial and *sustainable* development of our society. Therefore, nowadays, the most advanced available scientific approach is devoted not only to the development of medicine, chemistry and computer sciences, but also to *Sustainability* and *Water Stress Problems* in the logic of *Process Intensification* [1, 2]. This is an innovative strategy which consists of the development of new apparatuses and avant-garde techniques that, compared to those commonly used today, are expected to bring drastic improvements in manufacturing and processing, substantially decreasing equipment size/production capacity ratio, energy consumption, or waste production and resulting in cheaper and more sustainable technical solutions.

In the present work, *Exergetic Analysis*, *Substitution Coefficient*, *Economic Evaluation* and *Metrics* (indicators consistent with Process Intensification Strategy) are presented and utilized for the analysis and comparison of different water treatment systems, in the attempt to show how they can drive to the choice of the most convenient and sustainable water treatment process.

Keywords: Water Stress, 3PE and Process Intensification Strategy, Integrated Membrane Operations.

### **2. Extended Abstract**

Membrane technologies are already dominant technologies in sea/brackish water desalination and wastewater treatment and reuse. Moreover, they respond efficiently to the requirement of Process Intensification because they have the potential to replace conventional energy-intensive techniques (such as distillation and evaporation); to realize the selective and efficient transport of specific components; to

reach advanced levels of automatization and remote control. These features offer the possibility of completely redesigned water treatment systems, based on the concept of *Integrated Membrane Operations*, which means coupling several membrane processes in order to overcome the limits of the single units, to use their synergic effects in terms of better performance of the overall system, decreasing water cost and brine disposal problem. In fact, an integrated seawater desalination system constituted by MF-NF-RO membrane operations in series and by Membrane Crystallizer units (MCr) on RO and NF retentate streams, allowed to increase plant recovery factor until about 93% [2], higher than that of a conventional RO process (about 40%) and much higher than that of a typical Multistage Flash operation (about 10%); an integrated water treatment system in which a fraction of the RO permeate was sent to a Membrane Distillation (MD) operation [3] allowed to reduce the concentration of contaminants in polluted waters under the maximum permissible concentration; an integrated MBR-RO process can be used for sewage/wastewater treatment and reuse. In all the cases, the treated obtained water is drinking water which meets both the most stringent water quality criteria and water cost.

The *Exergetic Analysis* and *Economic Evaluation* of the analyzed systems showed that energy consumption is the term which more influences water cost; it decreases significantly when a Pelton Turbine or a Pressure Exchanger System is used as Energy Recovery System or when thermal energy is available in the water treatment plant (Table 1).

Table 1: Water unit cost for the analysed water treatment systems.

Flow Sheet	MF-NF-RO	MF-NF-RO   MCr	MF-NF-RO   MCr	MF-NF-RO   MCr MCr	RO-RO	RO-MD
Unit cost* [\$/m <sup>3</sup> ]	0.46/0.39 <sup>a</sup>	0.68/0.63 <sup>a</sup>	0.59/0.54 <sup>a</sup>	0.73/0.69 <sup>a</sup>	0.74/0.50 <sup>a</sup>	0.97/0.73 <sup>a</sup>
Unit cost* <sup>b</sup> [\$/m <sup>3</sup> ]	0.46/0.39 <sup>a</sup>	0.55/0.51 <sup>a</sup>	0.47/0.43 <sup>a</sup>	0.54/0.51 <sup>a</sup>	0.74/0.50 <sup>a</sup>	0.80/0.56 <sup>a</sup>

\* Desalted water unit cost without consider the gain for the salts sale. (a) If Pelton turbine is used as energy recovery device. (b) If thermal energy is available in the plant or the stream is already at the operating temperature of the MD/MCr unit.

For the proposed systems some metrics have been calculated. It is important to underline that the results obtained with metrics agree with those obtained through exergetic and economic analysis of the proposed integrated membrane systems. Therefore, the use of the principles of Sustainable Development can help to the choice of the best alternative for two reasons: 1) they allow to avoid risks from unsustainable business practices; 2) a process that reduces costs by decreasing mass or energy metrics will be more economic profitable and will have less environmental impact.

## References

- [1] Charpentier, J. C, (2005) *Chemical Engineering Journal*, 107, 3–17.
- [2] Drioli, E., Curcio, E., Di Profio, G., Macedonio, F. and Criscuoli, A., (2006) *Chemical Engineering Research and Design*, 84 (A3), 209–220.
- [3] Macedonio, F., Drioli, E., *Desalination*, in press.

## **Session T2-1a: Thermodynamics: Hydrocarbons & Petrochemicals**

<b>Abstract Number</b>	<b>Paper Title &amp; Authors</b>	<b>Included</b>
866	Selection of Appropriate Thermodynamic Equations for Simulation of Separation Columns of Vinyl Chloride Unit of Iran Bandar Imam Petrochemical Company (BIPC) A Eliassi, M M Rabiei, A Kargari, H R Goodarzbod	Yes
1098	VLE Prediction via Equation of State Modeling of Compressed Liquid Densities S Sen	Yes
1440	Wax precipitation in crude oils: DSC and model analysis B Coto, C Martos, J J Espada, M D Robustillo, J L Peña	Yes
3881	VLE of normal and normal/iso paraffin mixtures covering a wide range of molecular weight S Bonomi, S Correra, V Calemma, J M Shaw	Yes

Session T2-1a



## **Selection of Appropriate Thermodynamic Equations for Simulation of Separation Columns of Vinyl Chloride Unit of Iran Bandar Imam Petrochemical Company (BIPC)**

**A. Eliassi<sup>a\*</sup>, M. M. Rabiei<sup>a</sup>, A. Kargari<sup>a</sup>, H. R. Goodarzbod<sup>b</sup>**

<sup>a</sup> *Chemical Industries Research Department, Iranian Research Organization for Science and Technology (IROST), No. 71, Forsat Street, Enghelab Ave., Tehran, Iran*

<sup>b</sup> *Research and Development Center, Bandar Imam Petrochemical Company, Mahshahr, Iran*

### **1. Summary**

In this paper, Peng-Robinson, Soave-Redlich-Kwong, Wilson, NRTL and UNIQUAC thermodynamic equations are considered for simulation of ten different separation columns of vinyl chloride unit of Iran Bandar Imam petrochemical company. The separation columns are related to different vinyl chloride unit sections namely: Ethylene Dichloride Recovery (EDC Recovery) & Oxychlorination Ethylene Dichloride Washing (OXY EDC Washing), O-EDC Purification, EDC Cracking & Vinyl Chloride Purification (VC Purification), Waste Water Treatment & VC Refining and HCl Recovery sections. Simulated quantities are: temperature, flow rate and average molecular weight of outlet flows of the mentioned separation columns. The results show that Wilson equation is the most appropriate equation for simulation of the separation columns of vinyl chloride unit.

**Key Words:** Equation of State, Activity Coefficient Equation, Phase Equilibria, Vinyl Chloride Unit, Simulation

### **2. Extended Abstract**

Selection of appropriate equation of state or activity coefficient equation for phase equilibrium calculations has a lot of effects on precision and accuracy of the calculated results. In this paper the ability of six different thermodynamic equations for simulation of separation columns of vinyl chloride (VC) unit of Iran Bandar Imam Petrochemical Company (BIPC) are considered. These equations are Peng- Robinson [1], Soave- Redlich- Kwong [2, 3], Wilson [4], NRTL [5] and UNIQUAC [6]. Three different quantities are calculated by five equation of states or activity coefficient equations. These quantities are composition error, temperature error and molecular weight error in compare to the experimental data. Finally, summation of all of these errors are calculated. Thermodynamic equation with the minimum error is selected as the appropriate equation for simulation of the considered separation column. The total calculated errors for each separation columns are reported in table 1 and a comparison between the errors which are obtained by different equations is shown in figure 1.

---

\* *Corresponding Author e-mail: [alieliassi@yahoo.com](mailto:alieliassi@yahoo.com)*

Table 3. Calculated errors for different separation columns by using five thermodynamic equation

	Peng-Robinson	SRK	Wilson	NRTL	UNIQUAC
<b>EDC Recovery &amp; EDC Washing</b>					
EDC Aborber	3.683	3.752	3.338	4.424	3.476
Stripper	13.018	13.363	11.400	12.663	12.787
<b>O-EDC Purification</b>					
Dehydration Column	7.316	7.607	6.170	9.718	6.523
Light Column	4.020	4.291	2.010	2.448	2.240
Heavy Columns	3.070	3.404	0.637	0.613	0.650
Recovery Column	6.532	7.422	4.320	4.507	4.381
<b>EDC Cracking &amp; VC Purification</b>					
HCl Column	1.993	1.686	0.492	0.601	20.566
VC Column	0.359	0.457	0.407	0.416	0.411
<b>Waste Water Treatment &amp; VC Refining</b>					
VC Refinary Column	1.869	1.783	1.357	1.358	1.361
<b>HCl Recovery</b>					
HCl Refinary Column	12.847	13.335	11.422	11.422	11.662

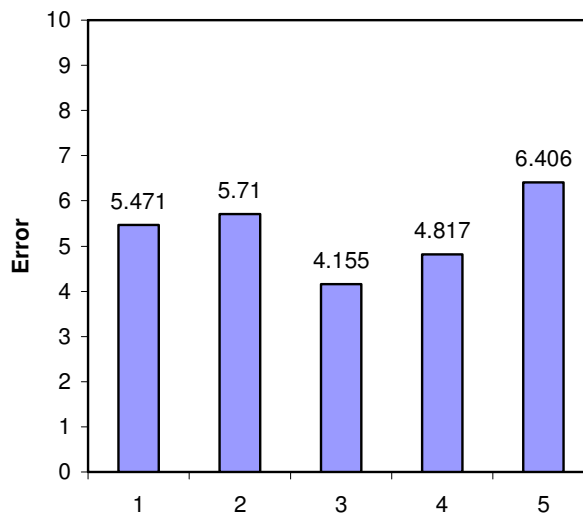


Figure 1. Error for different equations: 1. Peng-Robinson, 2. Soave-Redlich-Kwong, 3. Wilson, 4. NRTL, 5. UNIQUAC

### References

1. Peng, D.Y. and Robinson, D.B., (1976) *Ind. Eng. Chem. Fundam.*, 15, 59-64.
2. Redlich, O. and Kwong, J.N.S., (1949) *Chem. Rev.*, 44, 223-244.
3. Soave, G., (1972) *Chem Eng. Sci.*, 27, 1196-1203.
4. Wilson, G.M., (1964) *J. Am. Chem. Soc.*, 86, 127-130.
5. Renon, H. and Prausnitz, J.M., (1968) *AIChE Journal*, 14, 135-144.
6. Abrams, D.S. and Prausnitz, J.M., (1975) *AIChE Journal* 21, 116- 128.

## **VLE Prediction via Equation of State Modeling of Compressed Liquid Densities**

Sabyasachi Sen

*Thermodynamic Methods & Data Division, Invensys SimSci Esscor,  
26561 Rancho Parkway South, Suite 100, Lake Forest, California 92630, USA*

### **1. Summary**

The four-parameter PFV equation of state (EOS), along with virial-based (VB) mixing rules, is introduced. This EOS is shown to be a viable model for correlating compressed liquid densities. Interaction parameters obtained from correlating only compressed liquid densities of some targeted binary systems are used to successfully predict the corresponding vapor-liquid equilibria (VLE).

Keywords: PFV EOS, compressed liquid densities, VLE prediction, virial-based mixing rules

### **2. Extended Abstract**

The advent of high precision densitometers, especially since the mid 1980's, has resulted in an abundance of high quality liquid density measurements. The description of VLE also recognizes that, in a significant number of systems, non-ideality is concentrated in the liquid phase. Most commonly used P-V-T EOS's are continuous functions, purporting to describe some (or most) thermodynamic properties of the vapor and liquid phases, simultaneously.

This study combines the accuracy of modern density measurements, the notion of liquid phase non-ideality, and the dual phase design of P-V-T EOS's, to investigate the feasibility of predicting VLE from mixture liquid density data. This objective necessitates the EOS's employed in this investigation to predict pure and mixture liquid densities correctly, without sacrificing the accuracy of other properties (e.g., vapor pressures). This requirement precludes the use of most two-parameter cubic EOS's. An essential element of this investigation, therefore, is the introduction of the four-parameter PFV EOS amenable to simultaneously reproducing near-saturation compressed liquid densities, saturation vapor pressures and vapor densities (or, second virial coefficients), along with its corresponding set of virial-based mixing rules. This is a proof-of-concept study which does not focus on developing this EOS

or mixing rules, but simply employs these as vehicles to correlate compressed mixture liquid densities, and to predict VLE based on these liquid density data alone. The PFV EOS is fifth-order in molar volume ( $V$ ), has four parameters  $\{a, b, c, d\}$ , and is written as:

$$P = \frac{RT}{(V-b)} - \frac{a}{V(V+c)} - \frac{d}{V^3}$$

where  $T$  and  $P$  are pressure and temperature, respectively.

Compressed liquid densities of several binary and ternary systems are modeled. The PFV EOS is shown to be a viable model for correlating compressed liquid densities. VLE predictions based on the resulting interaction parameters are compared with VLE measurements. The results are quite encouraging, and, in some cases, very good. With some fine-tuning, this should be considered a viable approach to exploiting the large body of liquid density data available in the literature, as an alternate means to predicting VLE, especially in those instances where equilibrium vapor pressures and compositions are scarce and difficult, unsafe or expensive to measure.

An extension of the above idea is the simultaneous application of VLE and liquid densities. Several systems with only a few VLE data points are simultaneously correlated with mixture liquid densities to reliably extend VLE predictions over a wider concentration range.

## References

- Flebbe JL, Barclay DA, Manley DB. Vapor Pressures of Some C<sub>4</sub> Hydrocarbons and their Mixtures. *J Chem. Eng. Data*, 1982; 27(4):405-412.
- Arve DSC, Manley DB, Poling BE. Relative Volatilities from Mixture Liquid Densities for the n-Butane/1,3-Butadiene System. *Fluid Phase Equilib.* 1987; 35(1-3):117-126.
- Sen, S. Predicting VLE from Liquid Densities. *Eleventh International Conference of Properties and Phase Equilibria for Process and Product Design (PPEPPD)*, Hersonissos, Greece, 2007

## Wax precipitation in crude oils: DSC and model analysis

B. Coto<sup>a</sup>, C. Martos<sup>a</sup>, J.J. Espada<sup>a</sup>, M.D. Robustillo<sup>a</sup>, J.L. Peña<sup>b</sup>

<sup>a</sup>*Department of Chemical and Environmental Technology, Rey Juan Carlos University, E-28933 Móstoles (Madrid), Spain.*

<sup>b</sup>*Repsol-YPF, Alfonso Cortina Technology Centre, Móstoles (Madrid), E-28933, Spain.*

### 1. Summary

Wax deposition due to temperature decrease in crude oils is one of the flow assurance problems. Such deposition depends on crude oil nature, paraffin content and type, presence of additives, temperature conditions, etc. The problem prevention requires a detailed characterization of the crude oil. However, the direct experimental determination and quantification of the precipitation process is quite complex and time consuming and different experimental techniques have been used to carry out such study.

Application of the differential scanning calorimetry (DSC) technique has the advantage of its simplicity, fast response, and ability to be developed as routine essays. However, integration of the thermograms is not clearly defined for the complex petroleum mixtures and a procedure has to be developed.

In this work, a new method to study the wax precipitation from petroleum mixtures from DSC has been developed. Optimization of the method (temperature profile, DSC calibration) was carried out and an interpretation procedure (base line determination, peak assignment and integration) which yields the wax appearance temperature (WAT) and the wax precipitation curve was developed. Such method was applied to petroleum fractions with a narrower n-paraffin distribution than a crude oil. Experimental values of the cloud point temperature agree with the WAT values.

Keywords: wax precipitation, solid-liquid equilibrium, DSC.

### 2. Extended Abstract

DSC is calibrated in the low temperature range by using n-heptane, water and indium as reference substances. In the final optimized DSC conditions, about 10 mg of sample are used; temperature range from 80°C to -120°C; and the cooling/heating rate is 3°C/min. Several fractions of an aromatic crude oil from Middle East were analyzed.

Figure 1 shows the obtained heating thermogram of the fraction 370-427°C. Experimental thermograms above the WAT and at the low temperature are fitted to

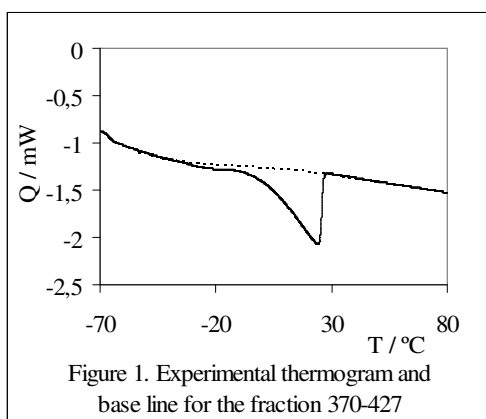


Figure 1. Experimental thermogram and base line for the fraction 370-427

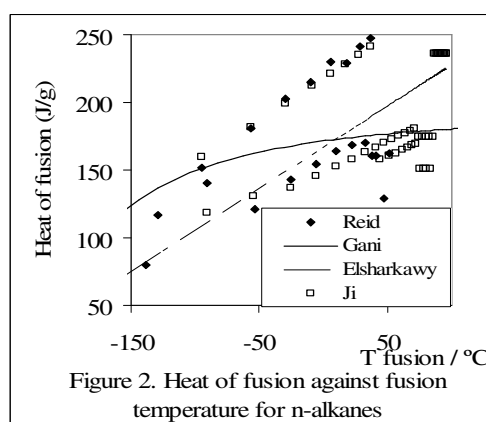


Figure 2. Heat of fusion against fusion temperature for n-alkanes

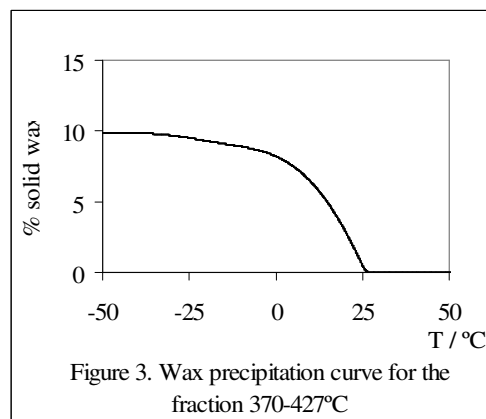


Figure 3. Wax precipitation curve for the fraction 370-427°C

polynomials representing the heat capacity of the liquid and the solid phases. Both functions are forced to be continuous and represent the base line.

In this work, a procedure to integrate the DSC thermograms has been developed based on values for pure n-paraffins. The correlation between heat of fusion and the fusion temperature was used to convert the DSC heat to precipitated mass. Such integration procedure yields both the wax appearance temperature (WAT) and the wax precipitation curve.

Figure 2 shows the heat of fusion against the fusion temperature for n-alkanes from 4 to 50 carbons. Experimental values and several correlation or prediction methods were included.

As there is not a unique and clear correlation between both magnitudes, the effect on the final results of the enthalpy-temperature correlation was checked.

Figure 3 shows results obtained from such procedure for the fraction 370-427°C when a linear fit between enthalpy-temperature of fusion is used. Value for WAT was about 25°C, which compares favorably with the experimental cloud point temperature (20°C).

Similar results are obtained for the rest of fractions considered and the procedure can be considered satisfactory.

However several additional tests have to be considered in the previous procedure. In mixtures, the n-paraffins precipitate at temperature lower than their fusion temperature and the heat of fusion is also changed. From the integration procedure the n-paraffin composition can be obtained and the solid liquid equilibrium conditions can be calculated by means of a model. The checking of this point is not easy to carry out. An iterative procedure was considered which depends both on the experimental curve integration procedure and the model calculations.

## **VLE of normal and normal/iso paraffin mixtures covering a wide range of molecular weight**

Susi Bonomi,<sup>a</sup> Sebastiano Corraera,<sup>b</sup> Vincenzo Calemma,<sup>a</sup> John M. Shaw<sup>c</sup>

<sup>a</sup>*Eni R&M Division, via Maritano, 26, 20097 San Donato Milanese, Italy*

<sup>b</sup>*Eni E&P Division, via dell'Unione Europea, 3, 20097 San Donato Milanese, Italy*

<sup>c</sup>*University of Alberta, NSERC, Chemical and Materials Engineering Building, Edmonton, Canada*

### **1. Summary**

In order to set-up a chemical reactor model, a thermodynamic description of the phase behaviour of reactants is a key requirement. Little experimental information is available to describe the thermophysical properties of mixtures of long chain linear or branched paraffins. Use of group contribution or other predictive EOS methods requires extrapolation well beyond the extant database and prediction uncertainty is a significant concern. For this reason, while building a complete model of a reactor for high molecular weight paraffinic mixtures, some thermodynamic data were measured in order to check the reliability of the thermodynamic part of the model. In particular, phase behavior and phase density measurements were performed on mixtures of a heavy paraffinic stream before and after hydrocracking. The first sample comprised only linear paraffins, while the second sample included branched isomers. These data were employed to assess the performance of a previously proposed thermodynamic model. In this paper, preliminary results of this assessment are described.

Keywords: Thermodynamics, EOS, Hydrocarbons, Phase Behavior

### **2. Extended Abstract**

The overall aim of this work is to develop and validate a mathematical model for the hydroconversion of normal and branched paraffinic alkanes coming from a Fischer-Tropsch reactor. A Gas-Chromatographic method was developed to characterize such mixtures and a correlation was developed to describe the properties of iso-paraffins (Corraera et al., 2006). Concurrently, an experimental campaign was performed where phase behavior and phase density data at elevated temperature and pressure were measured for a hydroconversion feed + hydrogen and hydroconversion product + hydrogen mixtures to assess the reliability of the thermodynamic model. The phase equilibrium experiments were conducted using an X-ray view cell described elsewhere in detail (Shaw et al., 1999). In this presentation only neat samples (i.e., without hydrogen) are discussed; Table 1 reports the overall composition of the samples, while the gas chromatogram of the second sample is shown in Figure 1. The measurement conditions were representative of the process conditions (temperature:

343-375°C, pressure: 35-60 bar), and were challenging to realize. The preliminary evaluation of the model performance shows that, without any tuning of the EOS, the model is able to predict values in the correct range and with the correct trend, but further tuning is necessary in order to achieve a satisfactory fit.

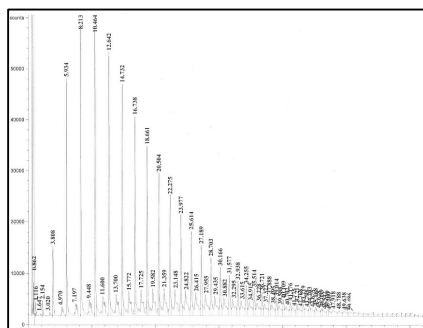


Figure 1: Gas-Chromatogram of the liquid hydrocracking product.

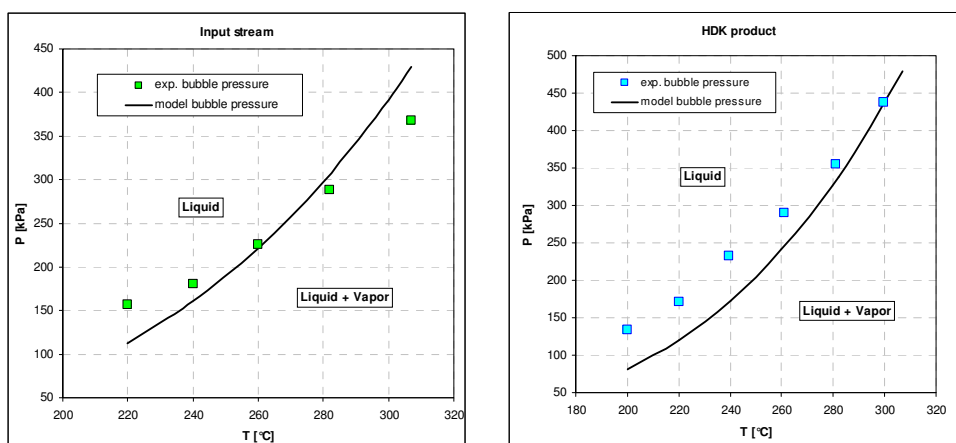


Figure 2: Model performance: input stream (2a) and HDK products (2b).

	C <sub>7</sub> -C <sub>9</sub>	C <sub>10</sub> -C <sub>14</sub>	C <sub>15</sub> -C <sub>22</sub>	C <sub>23+</sub>
Input stream	3.0	29.4	34.3	33.3
Products	4.0	34.8	40.4	20.8

Table 1: Stream compositions

## References

Correra, S., Molinari, D., Pellegrini, L., Calemma, V., (2006) *AICHE 2006 Spring National Meeting*, April 23 – 27, 2006, Orlando, FL.

Abedi, S. J.; Cai, H. Y.; Seyfaie, S.; Shaw, J. M., (1999) *Fluid Phase Equilibria*, 158-160, 775-781.



## Session T2-1b: Thermodynamics: Applications of Equations of State

<b>Abstract Number</b>	<b>Paper Title &amp; Authors</b>	<b>Included</b>
140	Modeling of Associating Mixtures for applications in the oil and gas and chemical industries G M Kontogeorgis, M L Michelsen, G Folas, N Solms, E H Stenby	Yes
1164	Mutual solubilities of hydrocarbons and water with the CPA EoS M B Oliveira, J A P Coutinho, A J Queimada	Yes
1170	Modelling Hydrogen-Bonding Fluid Mixtures using Insight Gained from Spectroscopy N Solms, J L Kofod, L Jensen, C P Passos, S O Derawi, S I Anderson, M L Michelsen, G M Kontogeorgis	Yes
2627	Surface tension of chain molecules - A combination of the gradient theory with the CPA EoS M B Oliveira, J A P Coutinho, A J Queimada	Yes
3209	Prediction and correlation of the phase behaviour of non-ideal binary systems by combining an equation of state with the COSMO-RS model O Spuhl, W Arlt	No

Session T2-1b

## **Modeling of Associating Mixtures for applications in the oil and gas and chemical industries**

Georgios M. Kontogeorgis, Michael L. Michelsen, Georgios Folas, Nicolas von Solms and Erling H. Stenby

*IVC-SEP Engineering Research Center, Department of Chemical Engineering, Technical University of Denmark, DK-2800, Lyngby, Denmark*

### **1. Summary**

The Cubic-Plus-Association (CPA) equation of state is applied in this work to phase equilibria of associating mixtures of importance to petroleum and chemical industries. Both binary and multicomponent systems are considered as well as various types of phase equilibria (VLE, LLE, VLLE, ...). Satisfactory results are obtained in many cases e.g. mixtures with gas-hydrate inhibitors like methanol and glycols but some limitations for mixtures with organic acids are also illustrated.

Keywords: equation of state, association, oil & gas, chemicals

### **2. Extended Abstract**

Thermodynamic properties and phase equilibria of many associating mixtures cannot often be modeled satisfactorily by conventional models e.g. cubic equations of state.

CPA (Cubic-Plus-Association) is an equation of state (EoS), which combines the SRK EoS with the association term of SAFT. For non-polar (non self-associating) compounds it reduces to SRK. The model was first published in 1996 and since then it has been developed and applied with success to binary systems containing water-alkanes and alcohol/glycol/acid-alkanes (both VLE and LLE) as well as ternary and multicomponent (V)LLE for water-alcohol (glycol)-alkanes and certain acid and amine-containing mixtures. The results for the multicomponent systems are predictions based on a single binary interaction parameter. Recent results include extension of the CPA model to glycol-aromatic hydrocarbons including multiphase multicomponent equilibria and gas hydrate calculations in combination with a van der Waals-Platteauw model.

CPA offers a substantial improvement over conventional models such as SRK in a number of cases, especially:

- liquid-liquid equilibria
- water-containing systems such as water-hydrocarbons (aliphatic, olefinic, aromatic)
- prediction of details of phase equilibria e.g. the azeotrope at low methanol concentrations of methanol-propane systems
- prediction of multicomponent multiphase equilibria from binary data (and parameters) without the need of multicomponent data.

This presentation will summarize some previous highlights but will mostly outline new applications of the model with special emphasis to those of relevance to the petroleum and chemical industries:

- mixtures with gas hydrate inhibitors
- systems containing acid gases ( $\text{CO}_2$ ,  $\text{H}_2\text{S}$ ), water, methanol and hydrocarbons over extensive temperature and pressure ranges
- reservoir fluids in presence of water and methanol, glycols
- mixtures with polar and hydrogen bonding chemicals including organic acids.

Some comparisons with conventional thermodynamic models especially those combining cubic EoS with local composition activity coefficient models will also be included.

One example of the performance of CPA for multicomponent systems is illustrated in figure 1.

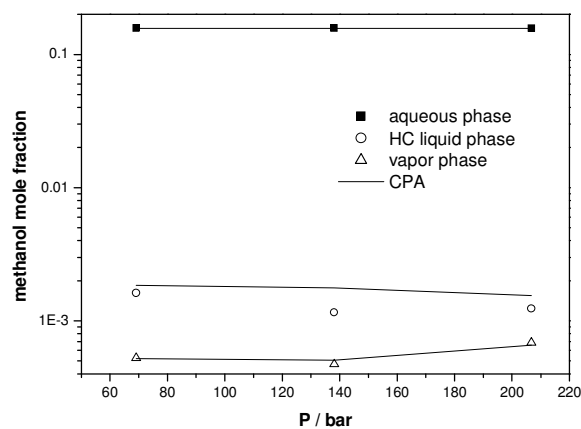


Figure 1: VLE for methanol – water – methane – propane – n-heptane with CPA at 284.14 K. The results (lines) are predictions using a single interaction parameter per binary (estimated solely from binary data).

## Mutual solubilities of hydrocarbons and water with the CPA EoS

Mariana B. Oliveira<sup>a</sup>, João A. P. Coutinho<sup>a</sup>, António J. Queimada<sup>b</sup>

<sup>a</sup> CICECO, Chemistry Department, Aveiro University, 3810 – 193 Aveiro, PORTUGAL

<sup>b</sup> LSRE – Laboratory of Separation and Reaction Engineering, Chemical Engineering Department, Faculty of Engineering, Porto University, Rua do Doutor Roberto Frias, 4200 - 465 Porto, PORTUGAL

### 1. Summary

In this work, it will be shown that an association equation of state known as CPA EoS is able to produce an excellent description of the mutual solubilities of water and several aliphatic and aromatic hydrocarbons in a wide range of pressures and temperatures, being the solubilities described with global average deviations below 30 %. The CPA EoS can be used as a predictive tool for the n-alkane family and for the aromatics is able to take in to account the solvation phenomena with water.

Keywords: CPA, Phase equilibria, Water, Hydrocarbons, High pressure

### 2. Extended Abstract

#### 2.1. Modeling

CPA is a thermodynamic model that combines the Soave-Redlich-Kwong EOS (SRK) for describing the physical interactions with the Wertheim's chemical association theory [1, 2, 3]:

$$Z = Z^{phys.} + Z^{assoc.} = \frac{1}{1 - b\rho} - \frac{a\rho}{RT(1 + b\rho)} - \frac{1}{2} \left( 1 + \rho \frac{\partial \ln g}{\partial \rho} \right) \sum_i x_i \sum_{A_i} (1 - X_{A_i}) \quad (1)$$

$$a(T) = a_0 \left[ 1 + c_1 (1 - \sqrt{T_r}) \right]^2 \quad (2)$$

$$X_{Ai} = \frac{1}{1 + \rho \sum_j x_j \sum_{B_j} X_{B_j} \Delta^{A_i B_j}} \quad \Delta^{A_i B_j} = g(\rho) \left[ \exp\left(\frac{\varepsilon^{A_i B_j}}{RT}\right) - 1 \right] b_{ij} \beta^{A_i B_j} \quad (3)$$

## 2.2. Results

Since the hydrocarbons studied in this work are all non self associating the CPA parameters are only the three ones required for the physical part ( $a_0$ ,  $c_1$  and  $b$ ). They have been estimated by a simultaneous regression of selected vapor pressure and saturated liquid density data. An excellent description of the experimental vapor pressure and liquid densities is achieved, with a global average deviation of 0.8 % for both properties. To provide a good description of the n-alkanes experimental data, a single temperature independent, binary interaction parameter was required. Using data from methane to decane it was possible to establish a generalized linear correlation for the binary interaction parameter with the carbon number. The global average deviations were of 30 and 26 % for the hydrocarbon solubility in the water-rich phase and for the water solubility in the hydrocarbon-rich phase, respectively.

Although the aromatic hydrocarbons are themselves non-self-associating, it is well known that aromatic compounds are able to cross-associate (solvate) with water. Using a solvation scheme approach both the binary interaction parameter  $k_{ij}$  and the cross-association volume  $\beta^{A_i B_j}$  are fitted to experimental equilibrium data. Results for the phase equilibria were obtained with global average deviations of 21 % for the aqueous phase and of 18 % for the hydrocarbon rich phase.

## 2.3. Conclusions

The ability of the CPA EoS for describing the phase equilibria of hydrocarbons + water systems can be successfully demonstrated for a large number of compounds in a broad range of pressures and temperatures.

## References

1. Voutsas, E. C., Boulougouris, G. C., Economou, I. G., Tassios, D. P., (2000) *Industrial & Engineering Chemistry Research*, 39,797 - 804.
2. Wu, J. Z., Prausnitz, J. M., (1998) *Industrial & Engineering Chemistry Research*, 37,1634 - 1643.
3. Michelsen, M. L., Hendriks, E. M., (2001) *Fluid Phase Equilibria*, 180,165 - 174.

## **Modelling Hydrogen-Bonding Fluid Mixtures using Insight Gained from Spectroscopy**

Nicolas von Solms, Jonas L. Kofod, Lars Jensen, Claudia Pereira Passos, Samer O. Derawi, Simon I. Anderson Michael L. Michelsen and Georgios M. Kontogeorgis

*Centre for Phase Equilibria and Separation Processes (IVC-SEP), Department of Chemical Engineering, Technical University of Denmark, DK-2800 Lyngby, Denmark*

### **1. Summary**

We have used two equations of state (CPA and PC-SAFT) for associating fluids to predict association in pure hydrogen-bonding fluids and fluid mixtures. We have used IR spectroscopy to measure hydrogen-bonding in fluid mixtures of alcohols and alkanes. Both models can predict association satisfactorily. Experimental measurement and modeling of hydrogen bonding can be used to obtain parameters and guidelines which improve model performance for more industrially relevant properties such as phase equilibrium.

Keywords: equation of state, PC-SAFT, CPA, hydrogen-bonding, spectroscopy

### **2. Extended Abstract**

The SAFT family of equations comprises some of the very few equations of state which explicitly account for the hydrogen-bonding interactions that exist in associating fluids such as water and alcohols. Two such equations are the Cubic-Plus-Association (CPA) and the recently developed Perturbed-Chain-SAFT (PC-SAFT) equations of state. Both these equations of state require 5 pure-component parameters to be specified for each associating fluid. Three of these are physical parameters (also required for non-associating fluids) whereas the remaining two parameters characterize the hydrogen bonding sites on the molecule. These five parameters are typically obtained by simultaneous fitting to experimental saturated liquid density and vapour pressure data. When so many parameters are required, the physical meaning of the parameters may be lost in the estimation procedure. It would thus be useful if further experimental data, specific to association fluids, could be used, when obtaining parameters for these fluids. Equations of state based on the Wertheim formalism (such as the SAFT variants) naturally calculate the degree of hydrogen bonding that exists in a pure fluid or mixture at given conditions. But IR and Raman spectroscopy can give us just such information experimentally.

In this work we investigate the ability of both CPA and PC-SAFT to predict the degree of hydrogen-bonding in a number of pure associating fluids (water and 1-

alkanols) over an extended temperature range. The effect of parameter estimation on these predictions was tested and found to be marked. It is thus clear that spectroscopic data can be used to obtain physically more meaningful parameters without comprising accuracy in predicting other, more useful, physical properties. CPA and simplified PC-SAFT (recently developed in our laboratory) were then used to predict the degree of hydrogen-bonding in binary mixtures consisting of an associating and a non-associating fluid. In general, both equations of state gave reasonable agreement with experimental spectroscopic data using parameters obtained only from density and vapour pressure data. The agreement could be improved by incorporating spectroscopic data into the parameter fit. Additional experimental data for binary systems have also been obtained using FTIR spectroscopy. Finally, in the literature there exist a number of inconsistencies arising from the confusion between non-bonded sites on a molecule and completely non-bonded molecules. These anomalies are pointed out and corrected.

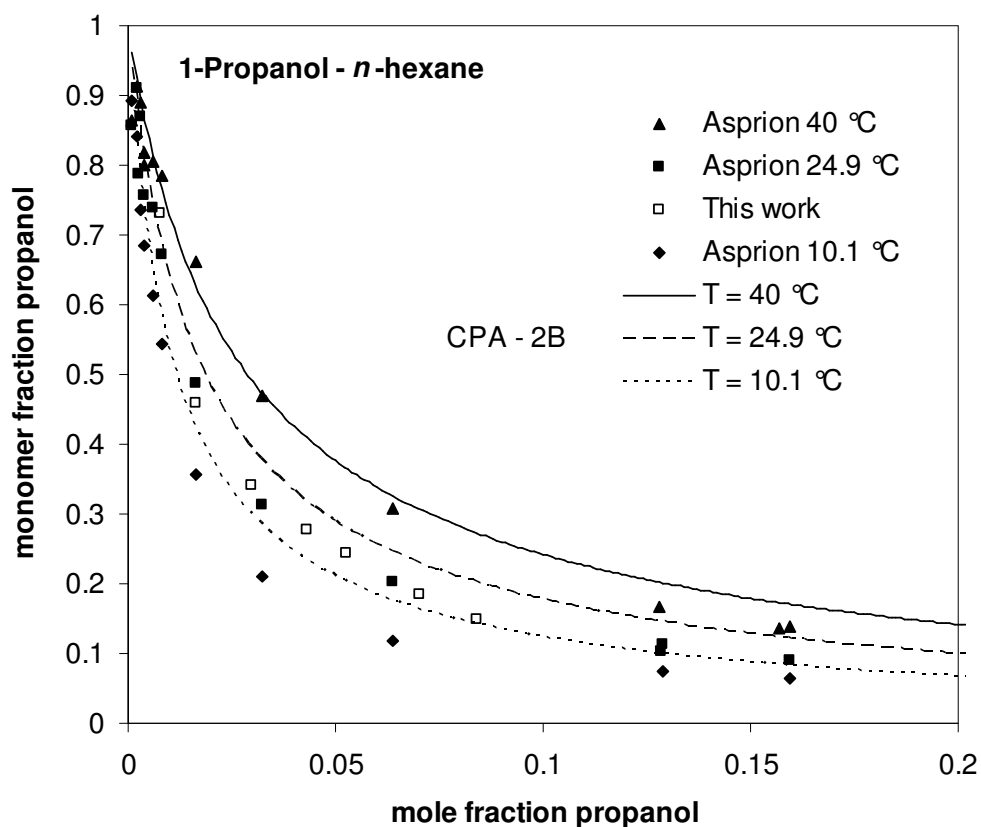


**Figure.** Monomer fraction 1-propanol as a function of overall mole fraction 1-propanol in the mixture 1-propanol-*n*-hexane. CPA predictions are shown at the three temperatures for which Asprion et al. obtained data (10.1 °C, 24.9 °C and 40 °C). For comparison data obtained in this work at 23.3 °C are also shown. The CPA predictions agree very well with the measured data, quantitatively predicting the effect of temperature. There is also good agreement between the data sets.



## Surface tension of chain molecules - A combination of the gradient theory with the CPA EoS

Mariana B. Oliveira<sup>a</sup>, João A. P. Coutinho<sup>a</sup>, António J. Queimada<sup>b</sup>

<sup>a</sup> CICECO, Chemistry Department, Aveiro University, 3810 – 193 Aveiro, PORTUGAL

<sup>b</sup> LSRE – Laboratory of Separation and Reaction Engineering, Chemical Engineering Department, Faculty of Engineering, Porto University, Rua do Doutor Roberto Frias, 4200 - 465 Porto, PORTUGAL

### 1. Summary

In this work the good modeling of phase equilibria provided by the CPA EOS is combined with the correct representation of interfacial tensions offered by the Gradient theory. Surface tensions for a series of n-alkanes, n-perfluoroalkanes and n-alcohols were accurately described in a broad temperature range. A discussion on the regression and selection of pure component parameters is also reported.

Keywords: CPA EoS, Gradient Theory, n-Alkanes, n-Alcohols, n-Fluoroalkanes

### 2. Extended Abstract

#### 2.1. Modeling

The CPA EoS, in terms of the compressibility factor, can be expressed as the sum of two contributions: one accounting for physical interactions, the SRK EoS, and another accounting for the association, the Wertheim association term [1]:

$$Z = Z^{phys.} + Z^{assoc.} = \frac{1}{1-b\rho} - \frac{a\rho}{RT(1+b\rho)} - \frac{1}{2} \left( 1 + \rho \frac{\partial \ln g}{\partial \rho} \right) \sum_i x_i \sum_{A_i} (1 - X_{A_i}) \quad (1)$$

$$a(T) = a_0 \left[ 1 + c_1 (1 - \sqrt{T_r}) \right]^2 \quad (2)$$

For n-alkanes and n-perfluoroalkanes the association term disappears while for alcohols the 2B association scheme applies.

The gradient theory is based on the phase equilibria of the fluid phases separated by an interface generalized for multicomponent mixtures by Miquieu *et al.* [2]:

$$\sigma = \int_{n_N^{vap}}^{n_N^{liq}} \sqrt{2\Delta\Omega(n) \sum_i \sum_j c_{ij} \frac{dn_i}{dn_N} \frac{dn_j}{dn_N}} dn_N, \quad \Delta\Omega(n) = \Omega(n) + p \quad (3)$$

where  $\Omega(n)$  is the grand thermodynamic potential and the influence parameter ( $c_{ij}$ ) is adjusted from surface tension data.

## 2.2. Results

The CPA pure component parameters are regressed simultaneously from vapour pressure and liquid density data. Average deviations of 2 % for vapour pressure and for liquid densities were obtained. For the calculation of interfacial tensions a quadratic correlation for the variation of the  $c_{ij}$  with reduced temperature is proposed. For heavier members calculations were also performed using the  $c_{ij}$  at the reduced temperature of 0.65. Accurate estimations of surface tensions were achieved (Figure 1), with global average errors of less than 1.2 % in the  $0.45 < Tr < 0.85$  range.

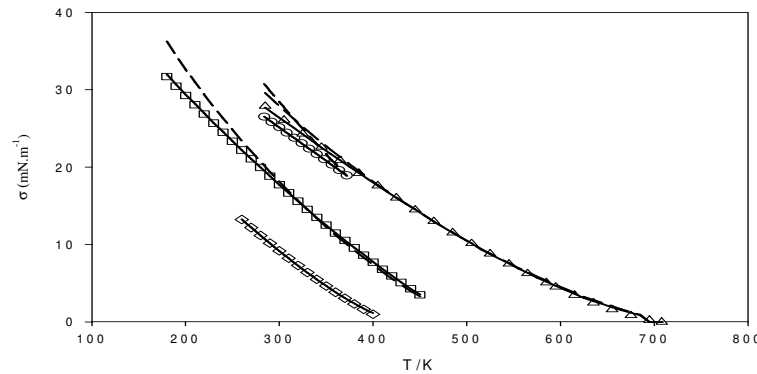


Figure 1: Surface tension. Experimental ( $\square$ ,  $C_6H_{14}$ ;  $O$ ,  $C_5H_{11}OH$ ;  $\diamond$ ,  $C_5F_{12}$ ;  $\Delta$ ,  $C_{15}H_{32}$ ) and gradient theory results (—) using a quadratic correlation; (---) using a constant value for  $c_{ij}$ .

## 2.3. Conclusions

The CPA pure compounds parameters showed to have a trend within the homologous series, and correlations were proposed allowing the CPA EoS to be used as a predictive tool.

The wide surface tension database that was evaluated in this work (57 fluids from 3 different families) ensures that the proposed model can be satisfactorily used for modelling surface tensions in a broad temperature range.

## References

1. Kontogeorgis, G. M., Voutsas, E. C., Yakoumis, I. V., Tassios, D. P., (1996) *Industrial & Engineering Chemistry Research*, 35,4310-4318.
2. Miqueu, C., Mendiboure, B., Graciaa, C., Lachaise, J., (2004) *Fluid Phase Equilibria*, 218,189 - 203.

## **Session T2-1c: Thermodynamics: Developments with SAFT EOS**

<b>Abstract Number</b>	<b>Paper Title &amp; Authors</b>	<b>Included</b>
205	Development of a Group Contribution Simplified PC-SAFT Equation of State A Tihic, G Kontogeorgis, M Michelsen, N Solms, L Constantinou	Yes
3198	Modeling of aqueous electrolyte solutions with an equation of state S Herzog, W Arlt, J Gross	Yes
3583	Thermodynamics And Phase Equilibria In Carbon Dioxide + Alkanol Systems From Statistical-thermodynamic Theory K Aim	No
4052	New molecular models for hydrogen fluoride, refrigerants and their mixtures M Pollock, C S Adjiman, A Galindo, G Jackson	Yes

Session T2-1c

## Development of a Group Contribution Simplified PC-SAFT Equation of State

Amra Tihic,<sup>a</sup> Georgios Kontogeorgis,<sup>a</sup> Michael Michelsen,<sup>a</sup> Nicolas von Solms<sup>a</sup>,  
Leonidas Constantinou<sup>b</sup>

<sup>a</sup>Center for Phase Equilibria and Separation Processes (IVC-SEP), Department of Chemical Engineering, Technical University of Denmark, Building 229, DK-2800 Kgs. Lyngby, Denmark

<sup>b</sup>Frederick Research Centre, Department of Chemical Engineering, P.O. Box 24729, Nicosia, Cyprus

### 1. Summary

The prediction of pure component thermodynamic properties and phase equilibria are required for the development of various processes in the chemical, pharmaceutical, food, gas processing, and petrochemical industry. Common characteristics of these applications are the complexity of molecules involved, the presence of various types of intermolecular forces (polarity, hydrogen bonding, etc.), and the frequent coexistence of many phases at equilibrium e.g. vapour-liquid-liquid or solid-liquid-liquid. Our work aims in developing a theoretically based engineering tool that can be used to predict thermodynamic properties of such complex mixtures when experimental data are insufficient.

The developed thermodynamic model is a group-contribution version of the simplified PC-SAFT equation of state (EoS) [2] where the parameters of the model are estimated via group contributions based on the so-called “conjugation principle” [3]. This type of model is designed to deal with systems containing polymers and associating fluids. In past years, similar SAFT- family models have been successfully applied to a number of complex systems over wide ranges of conditions. By our previously published work [1], this application has been extended.

The presentation covers the important steps in the development of the model and includes selected results for pure components and mixtures. Finally, potential industrial applications are presented.

Keywords: Equation of State, PC-SAFT, Pure parameters, VLE, LLE

### 2. Extended Abstract

#### The simplified PC-SAFT model

The general SAFT equation written as a sum of reduced Helmholtz free energy for mixtures of associating molecules is given as the following:

$$\tilde{a} = \frac{A}{kTN} = \tilde{a}^{id} + \tilde{a}^{hc} + \tilde{a}^{disp} + \tilde{a}^{assoc} \quad (1)$$

where the first term is the ideal gas contribution, the second term is the contribution of the hard-sphere chain reference systems, the third term is the dispersion contribution arising from the square-well attractive potential, and the last term is the contribution due to association. The exact expressions are available in the original paper [2]. In these expressions, three adjustable parameters are involved per non-associating species: the segment number ( $m$ ), the interaction energy ( $\epsilon/k$  in K), and the hard-core segment radius ( $\sigma$  in Å) that are typically estimated from vapour pressure and liquid density data over extended temperature ranges.

## Results

In order to ensure the validity of the group contribution scheme for parameters, an effort has been devoted to estimating PC-SAFT parameters for over 600 compounds from various chemical families, and methodically analysing parameters' behaviour when used by the model for mixture phase behaviour. The linear relationship of those newly estimated PC-SAFT parameters can be employed for various compounds as shown in Figure 1 where the group's segment number,  $m$ , is plotted as function of molecular weight [1]. A similar trend has been observed for other SAFT-family models. The success of this extrapolation further underlines the sound physical basis of the equation of state.

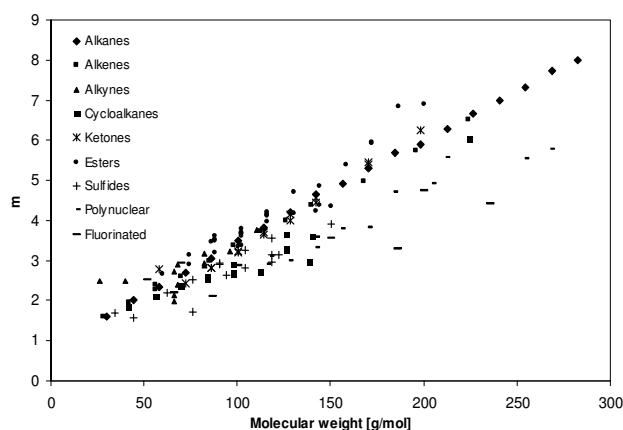


Figure 1: The segment number,  $m$ , versus molecular weight for different families of compounds.

## Conclusion

The analysis of the results showed that simplified GC PC-SAFT is quite successful in predicting and correlating VLE and LLE behavior in a variety of different types of binary system when using newly estimated PC-SAFT parameters.

## References

1. Tihic, A., Kontogeorgis, G.M., von Solms, N., Michelsen, M.L., (2006) *Fluid Phase Equilibria* 248, 29
2. von Solms, N., Michelsen, M.L., Kontogeorgis, G.M., (2003) *Ind. Eng. Chem. Res.*, 42, 1098
3. Constantinou, L., Gani, R., (1994) *AIChE J.*, 40, 1697

## **Modeling of aqueous electrolyte solutions with an equation of state**

S. Herzog,<sup>a</sup> W. Arlt,<sup>a</sup> J. Gross<sup>b</sup>

<sup>a</sup>*Chair of Separation Science and Technology, University Erlangen-Nuremberg, Egerlandstr. 3, D-91054 Erlangen, Germany*

<sup>b</sup>*Engineering Thermodynamics, Process & Energy Department, Delft University of Technology, Leeghwaterstraat 44, 2628 CA Delft, the Netherlands*

### **1. Summary**

In this contribution modeling results for aqueous electrolyte systems with an equation of state, namely the PC-SAFT equation of state in combination with the non-primitive mean spherical approximation are presented. The binary parameters for this model are adjusted to mean ionic activity coefficient data and to osmotic coefficient data at 298 K over the full solubility range of the salt. Using these adjusted parameters the liquid densities and vapor pressures in a temperature range from 273 to 373 K can be described without any further temperature dependent parameter.

Keywords: aqueous electrolyte systems, non-primitive mean spherical approximation (np MSA), PC-SAFT equation of state (EOS),

### **2. Extended Abstract**

Modeling of electrolyte systems is important for many industrial processes, e.g. for sour gas treatment, extractive distillation and suspension crystallization. If the electrostatic interactions for an electrolyte system in an equation of state (EOS) approach need to be considered, a theory from statistical mechanics, whether a perturbation theory or an integral equation theory, can be used. Such a theory needs to incorporate all relevant interactions, which are the ion-ion, the ion-dipolar and the dipole-dipole interaction and should compare well with molecular simulation data. One theory which individually accounts for all these interactions is the non-primitive mean spherical approximation (MSA) of Blum and Wei. Non-primitive indicates that the solvent is considered in its molecular structure, and not as a dielectricum. To calculate thermodynamic properties from the non-primitive MSA a set of three nonlinear equations has to be solved. Three parameters for each interaction are determined.

The MSA contributions are added to the non-electrostatic contributions of the PC-SAFT EOS in terms of the Helmholtz energy. The residual Helmholtz energy is calculated as

$$\frac{A^{res}}{NkT} = \frac{A^{hc}}{NkT} + \frac{A^{disp}}{NkT} + \frac{A^{assoc}}{NkT} + \frac{A^{MSA}}{NkT}$$

$$\frac{A^{MSA}}{NkT} = \frac{A^{CC}}{NkT} + \frac{A^{CD}}{NkT} + \frac{A^{DD}}{NkT}$$

In the equation ‘res’ denotes the residual term, ‘hc’ is for the hard chain contribution, ‘disp’ stands for the dispersive interactions, ‘assoc’ denotes the associating interactions. The MSA terms ‘CC’, ‘CD’ and ‘DD’ denote the ion-ion, the ion-dipole and the dipole-dipole interactions.

Using this theory mean ionic activity coefficient and osmotic coefficient data at 298 K, system pressures and liquid densities between 293 and 373 K of several aqueous electrolyte systems over the entire solubility range are described. However, because a simplification of the np MSA is used, namely the semirestricted np MSA only one ion diameter can be specified. This mean ionic diameter was adjusted for every aqueous electrolyte system to mean ionic activity coefficient and osmotic coefficient data at 298 K. Furthermore, the theory underestimates the solvation of the ions what can be seen by calculating the Gibbs enthalpy of solvation at infinite ion concentration. To compensate for this, a further solvation contribution is introduced. So in total two parameters, the mean ionic diameter and the additional solvation energy are adjusted for each aqueous electrolyte system. The liquid density and pressure plots over molality show that the model including the two temperature-independent parameters can be extrapolated up to 373 K.

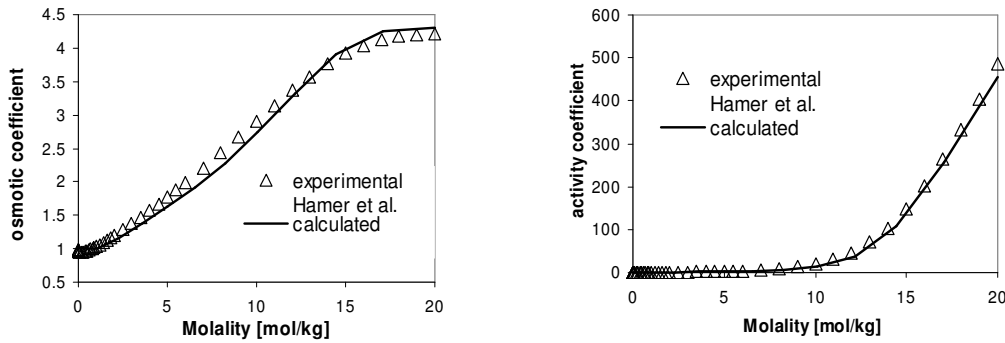


Figure 1: Osmotic coefficient and mean ionic activity coefficient at 298.15 K for the system water + LiBr over the full solubility range.

Our work on modeling of electrolyte systems using the np MSA indicates that the ion-dipole interaction is underestimated by the theory. To study the ion-dipole interaction more deeply we currently work on Monte Carlo simulations of a model ion-dipole system, consisting of Lennard-Jones molecules with point charges and point dipoles. Using these results we aim at evaluating the np MSA more deeply. In long term, it is planned to use our molecular simulation data to develop a better ion-dipole contribution and replace the one from the np MSA. Some results regarding the molecular simulations of the model system will be presented, too.



## **New molecular models for hydrogen fluoride, refrigerants and their mixtures**

M. Pollock, C. S. Adjiman, A. Galindo, G. Jackson

*Centre for Process Systems Engineering, Department of Chemical Engineering, Imperial College  
London, South Kensington Campus, London SW7 2AZ, UK*

### **1. Summary**

As a result of the depletion of the ozone layer and the subsequent banning of chlorofluorocarbons (CFCs) from use as refrigerants there has been great interest in accurately predicting phase equilibrium of replacement refrigerants and their mixtures with hydrogen fluoride (HF). HF is used in the production of replacement refrigerants by reaction with the original CFCs. Robust models for predicting accurately phase equilibrium are required by Industry for process design and simulation. There are many challenges in modeling these systems; hydrogen fluoride has a strong tendency to form hydrogen bonds, refrigerant molecules are non-spherical, mixtures of HF and refrigerants tend to contain azeotropes and exhibit liquid-liquid immiscibility, in addition there is limited experimental data available. In this work the Statistical Associating Fluid Theory for potentials of Variable Range (SAFT-VR) is used to overcome these challenges. Pure component models have been developed by optimizing to pure component vapour pressures and saturated liquid densities together with a quantum mechanical analysis to determine a physically meaningful and consistent value for the non-sphericity of refrigerant molecules. Mixture models have been developed by optimizing to mixture vapour liquid equilibrium data. In the case where the overall composition of the mixture is known, as opposed to the composition of the liquid phase in equilibrium, a model of experimental set-up has been developed so that mixture parameters can be obtained from raw data instead of correlated or mixture data.

Keywords: phase equilibrium, hydrogen fluoride, refrigerants, molecular models, SAFT-VR

### **2. Extended Abstract**

Since chlorofluorocarbons (CFCs) were banned from use as refrigerants, there has been great interest in accurately predicting phase equilibrium of replacement refrigerants and their mixtures with hydrogen fluoride (HF), which is used in the production of replacement refrigerants by reaction with the original CFCs. Accurate

prediction of phase equilibrium is required for process design and simulation. This is of industrial significance since a large proportion of capital and energy costs are related to separation processes, many of which are driven by phase equilibrium.

The Statistical Associating Fluid Theory with potentials of Variable Range (SAFT-VR) (Gil-Villegas et al., 1997; Galindo et al., 1998) is used to describe the phase behaviour of these highly polar systems. Pure component models for HF and a variety of refrigerants have been developed by optimising to pure component vapour pressures and liquid densities. Hydrogen fluoride is modelled as a 3 site molecule and the refrigerants are modelled as molecules with sites to represent their dipolar nature. Binary mixture data is used to further discriminate between different pure component models in order to determine the optimal association scheme. Quantum mechanical analysis (Sheldon et al., 2006) is used to determine a physically meaningful and consistent value for the non-sphericity of refrigerant molecules. The non-sphericity is determined by mapping the molecular dimensions, calculated using the Restricted Hartree-Fock formalism, onto a spherocylinder.

Asymmetric association models have been developed for the highly non-ideal and azeotropic mixtures HF + H<sub>2</sub>O and HF + R134a (1,1,1,2-tetrafluoroethane). In the classification of Van Konynenburg and Scott (1980), HF + H<sub>2</sub>O exhibits type 1A phase behaviour and HF + R134a, as most HF + refrigerant mixtures, exhibits Type 2A phase behaviour. Binary interaction parameters are obtained from parameter estimation to isothermal and isobaric vapour liquid equilibrium (VLE) data over a wide temperature and pressure range. In the case where the composition of the liquid phase in equilibrium is unknown a model of experimental set-up has been developed so that SAFT-VR mixture parameters can be obtained directly from raw experimental data as opposed to fitted data.

## References

- Galindo, A., Davies, L. A., Gil-Villegas, A. and Jackson, G., (1998) *Molecular Physics*, 93(2), 241-252.
- Gil-Villegas, A., Galindo, A., Whitehead, P. J., Mills, S. J., Jackson, G. and Burgess, A. N., (1997) *Journal of Chemical Physics*, 106(10), 4168-4186.
- Sheldon, T. J., Giner, B., Adjiman, C. S., Galindo, A., Jackson, G., Jacquemin, D., Wathelet, V. and Perpete, E. A., in *Multiscale Modelling of Polymer Properties*, Part I Chapter 7, editors Laso, M. and Perpete, E. A., Elsevier, The Netherlands (2006).
- Van Konynenburg, P. H. and Scott, R. L., (1980) *Philosophical Transactions of the Royal Society A*, 298(1442), 495-540.

## **Session T2-1d: Thermodynamics: Molecular Simulation & Related Approaches**

<b>Abstract Number</b>	<b>Paper Title &amp; Authors</b>	<b>Included</b>
554	Molecular simulation and macroscopic modeling of thermodynamic and transport properties of silicon-containing rubbery polymer – solvent mixtures I G Economou, Z A Makrodimitri, A Tihic, G M Kontogeorgis	Yes
1868	Thermodynamic Models from Fluctuation Solution Theory Analysis of Molecular Simulations Abildskov, S Christensen, GH Peters, FY Hansen, J P O'Connell	Yes
1874	Molecular Simulation Algorithms for Predicting Solid-Liquid Phase Equilibria R J Sadus	Yes
3623	Transferable Potentials for Nitrates and Phosphates J R Elliott	Yes

Session T2-1d

## **Molecular simulation and macroscopic modeling of thermodynamic and transport properties of silicon-containing rubbery polymer – solvent mixtures**

I.G. Economou<sup>a,b</sup>, Z.A. Makrodimitri<sup>a</sup>, A. Tihic<sup>b</sup>, G.M. Kontogeorgis<sup>b</sup>

<sup>a</sup>*Molecular Thermodynamics and Modeling of Materials Laboratory, Institute of Physical Chemistry, National Research Center for Physical Sciences “Demokritos”, GR-15310 Aghia Paraskevi Attikis, Greece*

<sup>b</sup>*IVC-SEP, Department of Chemical Engineering, Technical University of Denmark, DK-2800 Kgs. Lyngby, Denmark*

### **1. Summary**

Molecular Dynamics (MD) is used for the simulation of solubility and diffusivity of various gases and liquids in a number of silicon rubbery polymers. A united-atom force-field is used for the atomistic representation of polymer molecules. Long MD simulations on the order of several tens of ns are needed for the accurate estimate of physical properties. In addition, the simplified Perturbed Chain-Statistical Associating Fluid Theory (sPC-SAFT) is used for the calculation of small molecule solubility in polymers and for the calculation of the entire isotherms. In all cases, the agreement between experimental data and simulation or theory is very good.

Keywords: Molecular simulation, PC-SAFT, rubbery polymers, solubility, diffusivity.

### **2. Results and Discussion**

The accurate knowledge of thermodynamic and transport properties of polymer – solvent mixtures is highly important for novel material design, i.e. polymer membranes, and optimum process design, i.e. polymerization processes. Reliable experimental data over a wide range of conditions are often limited and expensive. Calculation of physical properties based on suitable theoretical models is, therefore, desirable. In this work, a family of relatively unexplored silicon-containing rubbery polymers, namely poly(sila-alkanes) are examined. These polymers are rooted to poly(dimethylsiloxane) (PDMS) by substituting carbon for oxygen. They have very low  $T_g$  and were shown to exhibit promising membrane material properties for hydrocarbon separation.

Molecular simulation using an atomistic force-field that accounts explicitly for bonded and non-bonded intra- and inter-molecular interactions developed based on *ab*

*initio* calculations for model oligomers is used for the elucidation of microscopic polymer melt structure [Makrodimitri *et al.*, 2006]. Accurate calculation of molecular mechanisms and microscopic structure permits reliable prediction of macroscopic physical properties. Solubility of various organic molecules (*n*-alkanes and *n*-perfluoroalkanes) and gases (noble gases, oxygen and nitrogen) is calculated using Widom's test particle method on well equilibrated polymer samples, as shown in Figure 1. Finally, long MD runs are used for the prediction of diffusion coefficients of small molecules in polymers. In all cases, simulation predictions agree well with limited experimental data available.

Despite its accuracy, molecular simulation substantial computational needs make it "too heavy" for engineering calculations and call for less detailed but equally accurate macroscopic models. In this respect, calculations using the simplified Perturbed Chain-Statistical Associating Fluid Theory (sPC-SAFT) [von Solms *et al.*, 2003] are presented for polymer – solvent isotherms. For some mixtures, sPC-SAFT predictions (no binary parameter used) are shown to be in excellent agreement with experiment (see Figure 1). In most cases, a single binary interaction parameter is used to tune the model to experimental data.

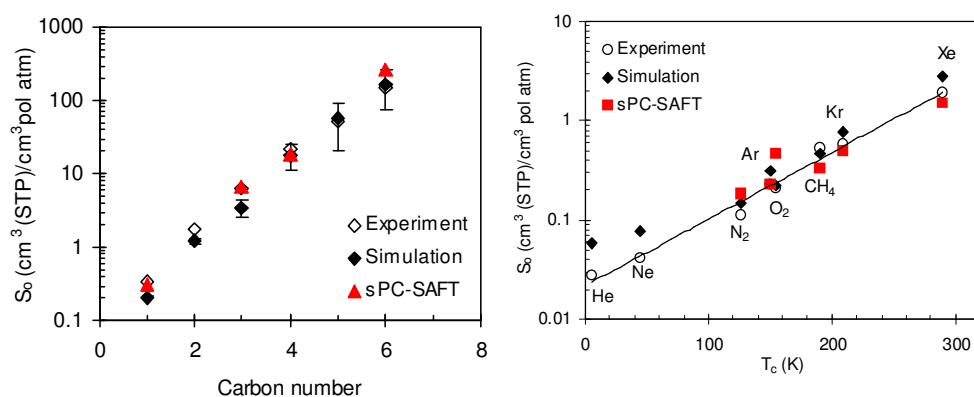


Figure 1: Experimental data, MD predictions and sPC-SAFT predictions for the infinite dilution solubility coefficient of (left) *n*-alkanes in poly(dimethyl silamethylene) (PDMSM) and (right) various gases in PDMS at 300 K and 0.1 MPa.

## References

- Economou, I.G., Makrodimitri, Z.A., Kontogeorgis, G.M. and Tihic, A. (2007) *Molec. Simul.*, in press.
- Makrodimitri, Z.A., Raptis, V.E. and Economou, I.G. (2006) *J. Phys. Chem. B.*, 110, 16047 – 16058.
- Makrodimitri, Z.A., Dohrn, R. and Economou, I.G. (2007) *Macromolecules*, 40, 1720 – 1729.
- von Solms, N., Michelsen, M.L. and Kontogeorgis, G.M., (2003) *Ind. Eng. Chem. Res.*, 42, 1098 – 1105.

## Thermodynamic Models from Fluctuation Solution Theory Analysis of Molecular Simulations

J. Abildskov,<sup>a</sup> S. Christensen,<sup>a</sup> G.H. Peters,<sup>b,c</sup> F.Y. Hansen,<sup>b</sup> J.P. O'Connell<sup>d</sup>

<sup>a</sup>CAPEC, Department of Chemical Engineering, Technical University of Denmark,,2800 Kgs. Lyngby, Denmark

<sup>b</sup>Department of Chemistry, Technical University of Denmark,,2800 Kgs. Lyngby, Denmark

<sup>c</sup>MEMPHYS - Center for Biomembrane Physics

<sup>d</sup>Department of Chemical Engineering, University of Virginia, 102 Engineers' Way, P.O. Box 400741, Charlottesville, VA 22904-4741, USA.

### 1. Summary

Most engineering approaches to property prediction (group contribution methods and equations of state) are driven and developed by parameterization revisions based on experimental data. Current global research trends indicate that atomic scale modeling R&D expenditures grow relatively faster than expenditures for experimental research. Also the price ratio for property determination by experiment versus atomic scale simulation clearly develops in favor of the latter. This suggests that 'experimental data'-driven approaches will be more and more difficult to develop and to maintain in future, unless we develop less data-demanding approaches or other less expensive means of providing equally reliable data.

Keywords: Fluctuations, Liquids, Simulation, Derivative, Properties

### 2. Extended Abstract

From isobaric-isothermal Molecular Dynamic (NPT-MD) simulations we calculate radial distribution functions (RDFs) for molecular pairs using for example the CHARMM force field. We integrate simulation results to obtain total correlation function integrals (TCFIs). Small errors in RDFs can lead to large errors in TCFIs. This problem was overcome by introducing a simple expression to reproduce the indirect interactions of the RDFs thereby ensuring finite TCFIs. The simple expression also allows extrapolation of RDFs, which allows integration to infinity. One output of this analysis is activity coefficient derivatives which can be used together with experimental data in the development of, for example, liquid phase Gibbs free energy models. Earlier works (Christensen et al., 2007) have included test systems of slightly and moderately non-ideal binary mixtures for which measured data exist, such as benzene/ethanol (at 298.15 K) and benzene/methyl acetate (at

303.15 K). When comparing the results of our computations with reliable data on both systems the results agreed to within experimental uncertainty.

The 'State Conditions Transferability' category of IFPSC 2006 tested prediction of binary vapor-liquid isotherms for mixtures of ethanol and the refrigerant HFF-227ea (1,1,1,2,3,3,3-heptafluoropropane). We also predicted this isotherm using Fluctuation Solution Theory (FST). The systems studied previously were nearly ideal and moderately non-ideal and at ambient temperatures. Both were at low pressures and remote from the pure component critical points. For the IFPSC system, we used the same method even though predictions are for conditions remote from those of the provided data, the pressures are elevated, and the temperatures are near the critical temperature of one of the components. The submitted results made assumptions appropriate for low pressures: Ideal vapors and no Poynting correction. We describe here the computational method and thermodynamic modeling for the entry submitted. Then we discuss results from using common modeling methods to estimate effects of elevated pressures. Finally, FST is best when the mixtures are very non-ideal, for example when the components are very different or have strong salvation, avoiding the 'small difference of large numbers' problem. To deal with cases near ideality we developed a strategy for choosing the number of parameters included in the macroscopic base model chosen for development. The selection is a trade off between precision in reproduction of the results from the FST analysis and standard deviation of parameters. Two different objective functions are investigated. One has been used previously (Christensen et al., 2007). The new one has advantages for systems with data at dilute conditions. Prediction of bubble point pressures using parameters from the two objective functions are compared with experimental data for the binary mixtures methyl acetate - n-pentane and methyl acetate - acetone.

## References

Christensen S., Peters G.H., Hansen F.Y., O'Connell J.P. and Abildskov J., (2007) *Molecular Simulation*, 33, 449-457.



## **Molecular Simulation Algorithms for Predicting Solid-Liquid Phase Equilibria**

Richard J. Sadus

*Centre for Molecular Simulation, Swinburne University of Technology, PO Box 218, Hawthorn  
Victoria 3122, Australia*

### **1. Summary**

Calculating solid-liquid phase equilibria via molecular simulation represents a considerable challenge because of the difficulty of interchanging molecules between two dense phases. This requirement means that techniques used for vapour-liquid-equilibria, such as the Gibbs ensemble are not viable. Other algorithms, such as histogram reweighting or Gibbs-Duhem integration are either computational expensive, or non self-starting. In this work, we examine an alternative algorithm for determining solid-equilibria, which combines elements of both equilibrium and non-equilibrium molecular dynamics. Results are presented which demonstrate the efficacy of the algorithm in predicting solid-liquid phase equilibria.

Keywords: molecular dynamics simulation, solid-liquid equilibria, phase behaviour, intermolecular potentials

### **2. Extended Abstract**

The phase behaviour of both pure systems and binary mixtures has been widely studied by molecular simulation, using techniques such as the Gibbs ensemble (Panagiotopoulos et al., 1988), Gibbs-Duhem (Metha and Kofke, 1994) or histogram reweighting algorithms (Sadus, 2002). The common aim of many of these investigations is to accurately predict the phase diagram using effective intermolecular potentials, most notable the Lennard-Jones potential. In contrast, other studies (Marcelli and Sadus, 1999; Nasrabad and Deiters, 2003; Wang and Sadus, 2006a&b) have used molecular simulation techniques, in conjunction with genuine two- and three-body intermolecular potentials, to determine the influence of various intermolecular interactions on phase behaviour. These studies have concluded that three-body interactions have a significant influence on phase behavior. Three-body interactions decrease the density of the liquid phase of pure fluids and they contribute significantly to the vapor-liquid critical point. In binary mixtures (Wang and Sadus, 2006a), three-body interactions are required to obtain good agreement between theory

and experiment for the pressure-composition behaviour. There is also some evidence (Sadus, 1998) that three-body interactions have a pivotal role in the transition between the different global phase behavior types of binary mixtures. □□ Previous investigations of three-body interactions on phase equilibria have been confined largely to pure fluids. Theoretical studies have been reported which indicate three-body interactions are important in solid phases. However, the direct molecular simulation of solid-liquid equilibria for both pure fluids and mixtures has mainly focused on predicting phase coexistence using an effective intermolecular potential. □□

The solid-liquid phase transition is difficult to determine accurately using traditional molecular simulation techniques. The high densities mean that it is not practical to use the Gibbs ensemble algorithm because of the difficulty of exchanging particles between the phases. Although this limitation is avoided by the Gibbs-Duhem technique, it is not self-starting which means it requires prior knowledge of one pair of coexistence data. Therefore, its ability to predict the phase boundary largely depends on the accuracy of the starting point data. In this work, we employed a novel approach (Ge et al., 2003) for locating the solid-liquid phase boundary which combines elements of both equilibrium and non-equilibrium molecular dynamics techniques. The approach yields reliable calculations and it avoids the problems encountered in both Gibbs ensemble and Gibbs-Duhem methods. Calculations are reported with both two-body and two-body + three-body intermolecular potentials. The analysis of the data and comparison with experiment allows us to draw conclusions regarding the relative importance of two – and three-body interactions on solid-liquid equilibria.

## References

- Ge, J., Wu, G.-W., Todd, B. D. and Sadus, R. J., *J. Chem. Phys.*, 119, 11017 (2003).
- Marcelli, G. and Sadus, R. J., *J. Chem. Phys.*, 111, 1533 (1999).
- Metha, M. and Kofke, D. A., *Chem. Eng. Sci.*, 49, 2633 (1994).
- Nasrabad, A. E. and Deiters, U. K., *J. Chem. Phys.*, 119, 947 (2003).
- Panagiotopoulos, A. Z., Quirke, N., Stapleton, M. and Tildesley, D. J., *Mol. Phys.*, 63, 527 (1988).
- Sadus, R. J., *Ind. & Eng. Chem. Res.*, 37, 2977 (1998).
- Sadus, R. J., *Molecular Simulation of Fluids: Theory, Algorithms and Object-Oriented*, Elsevier, Amsterdam (2002).
- Wang, L. and Sadus, R. J., *J. Phys. Chem.*, 125, 074503 (2006a).
- Wang, L. and Sadus, R. J., *Phys. Rev. E.*, 74, 031203 (2006b).

## Transferable Potentials for Nitrates and Phosphates

J. Richard Elliott<sup>a</sup>

<sup>a</sup>*Department of Chemical Engineering, University of Akron, Akron, OH 44325-3906 USA*

### 1. Summary

Nitrates and phosphates pose special problems when characterizing their molecular interactions. For nitrates, the nitro group is peculiar, exhibiting basic and weak acidic tendencies. Characterizing nitrate behavior requires careful analysis of a large database, including mixture data. For phosphates, only basic behavior is expected, but few data are available. Characterizing phosphates requires making the most of few data.

This presentation surveys the available data and characterizes the interactions for nitrates and phosphates. Correlations are developed for both vapor-liquid and liquid-liquid partition coefficients. These correlations form the basis for predictions that are relevant in environmental or biological applications.

Keywords: Nitrates, phosphates, environmental, vapor pressure, octanol-water partitioning

### 2. Extended Abstract

The Step Potential Equilibria And Discontinuous Molecular Dynamics (SPEADMD) model provides a basis for molecular modeling of thermodynamic and transport properties. It is based on Discontinuous Molecular Dynamics (DMD) and second order Thermodynamic Perturbation Theory (TPT). DMD simulation is applied to the repulsive part of the potential, complete with molecular details like interpenetration of the interaction sites, 110 degree bond angles, branching, and rings.[1,2] The thermodynamic effects of disperse attractions and hydrogen bonding are treated by TPT. This approach accelerates the molecular simulations in general and the parameterization of the transferable potentials in particular. Transferable potentials have been developed and tested for over 250 components comprising 25 families. These families include thiophene, fluorocarbon, alcohol, amine, aromatic, and ring compounds to name just a few examples.[3,4] Methods of predicting the thermodynamic properties are especially valuable when properties are difficult to

measure, as for chemicals that are explosive or toxic. This is the case for many nitrates and phosphates.

Nitrates are of special interest in defense and mining applications. New compounds are constantly being sought to enhance stability and reduce toxicity. Being able to leverage a few measurements for a few compounds and predict the properties of isomers and larger molecules is especially valuable. For environmental applications the octanol-water partition coefficient and vapor pressures are of particular interest. We have simulated all the nitrate compounds in the DIPPR database and characterized the interactions for a wide range of molecular structures. Vapor pressures are generally accurate to 15% error.

Phosphates have traditionally played roles as pesticides and nerve poisons. Very few data are available. Nevertheless, we have characterized the phosphate interactions and find accuracy to be near 15% for vapor pressure where data are available. Correlations for octanol-water partition coefficients and preliminary results for correlation of thermochemical properties based on quantum simulation are also presented.

## References

- 1 J. Cui and J. R. Elliott, *J. Chem. Phys.* 114 (2001) 7283.
- 2 O. Unlu, N. H. Gray, Z. N. Gerek, and J. R. Elliott, *Ind. Eng. Chem. Res.* 43 (2004) 1788-1793.
- 3 N. H. Gray, Z. N. Gerek, and J. R. Elliott, *Fluid Phase Eq.* Vol 228-229C (2005) 147-153.
- 4 F. S. Baskaya, N. H. Gray, Z. N. Gerek, and J. R. Elliott, *Fluid Phase Eq.* 236 (2005) 42-52.

## Session T2-1e: Thermodynamics: General

Abstract Number	Paper Title & Authors	Included
224	Heat capacity of liquids: database of recommended values and estimation by a group contribution method Z Kolská, M Záborský, V Růžička, J Kukul	Yes
280	Don't gamble with physical properties of polymers A A Kiss, A Belkou, A C Dimian, P Iedema	Yes
929	Determination of Critical Properties for Reactive Mixtures: Hydrodesulfurization of 4, 6-Dimethyldibenzothiophene M Alvarado-Morales, E S Pérez-Cisneros, T Viveros- García	No
3199	Solubility of CO <sub>2</sub> in Solutions of Hyperbranched Polymers. Search for Green Process Solvents M K Kozłowska, C S Schacht, B Jürgens, J Gross, T W Loos, P J Jansens	Yes
3647	Automatic generation of Global Phase Diagram from Equation of State A K S Patel, B A K Sunol	Yes
3699	Towards Fast Measurement of Multicomponent Diffusion Coefficients in Ionic Liquids E Kriesten, M Oertker, A Bardow, H J Koß, W Marquardt	Yes

Session T2-1e

## Heat capacity of liquids: database of recommended values and estimation by a group contribution method

Kolská Z.,<sup>a</sup> Zábranský M.,<sup>b</sup> Růžička V.,<sup>b</sup> Kukul J.<sup>c</sup>

<sup>a</sup>*Department of Chemistry, J. E. Purkinje University, České mládeže 8, 40096 Ústí nad Labem, Czech Republic*

<sup>b</sup>*Department of Physical Chemistry, Institute of Chemical Technology, Technická 5, 16628 Prague, Czech Republic*

<sup>c</sup>*Department of Computing and Control Engineering, Institute of Chemical Technology, Technická 5, 16628 Prague 6, Czech Republic*

### 1. Summary

A database of critically evaluated data on liquid heat capacities was updated and extended by including new data published in the literature from 2000 to 2006. Recommended data were used to develop a method for predicting heat capacity of liquids as a function of temperature by a three-level group contribution model by Marrero and Gani.

Keywords: liquid heat capacity, database, recommended data, estimation, group contribution method

### 2. Extended Abstract

Databases that contain recommended data on liquid heat capacities  $C_p^l$  for almost 2000 mostly organic compounds [1,2] were updated and extended. Experimental data on heat capacities of 411 pure liquid organic and some inorganic compounds that have melting temperature below 573 K, as well as of 50 ionic liquids, published in the primary literature between 2000 and 2006, were compiled and critically evaluated. Recommended values supplemented with an assessment of their uncertainty and presented in terms of parameters of correlating equations for temperature dependence of heat capacities will be provided by the end of 2007 as a report to the IUPAC project.

Current database of recommended values [1,2] was used to extend the group contribution method [3,4] to predict heat capacity of liquids as a function of temperature. The model development entailed a combination of the method by Marrero and Gani [3] and a relation for the temperature dependence of heat capacity:

$$\begin{aligned}
C_p^l = & c_p^\circ(T) + \left[ \sum_{i=1}^n N_i * [a_i + b_i * (T/100) + d_i * (T/100)^2] \right]_{\text{FIRST}} \\
& + \omega \cdot \left[ \sum_{j=1}^m M_j * [a_j + b_j * (T/100) + d_j * (T/100)^2] \right]_{\text{SECOND}}, \\
& + z \cdot \left[ \sum_{k=1}^o O_k * [a_k + b_k * (T/100) + d_k * (T/100)^2] \right]_{\text{THIRD}}
\end{aligned}$$

where indices  $i$ ,  $j$  and  $k$  mean the first, the second and the third level estimation, respectively,  $a_i$ ,  $a_j$ ,  $a_k$ ,  $b_i$ ,  $b_j$ ,  $b_k$ ,  $d_i$ ,  $d_j$ ,  $d_k$  are parameters for the temperature dependence of groups at individual levels,  $T$  is temperature (K),  $c_p^\circ(T)$  is the additional adjustable parameter,  $N_i$ ,  $M_j$ ,  $O_k$  are the numbers of occurrence of groups at individual estimation levels, parameters  $\omega$  and  $z$  are assigned unity and zero values, depending on the usage of the individual level group contributions.

We tested this model for 549 compounds from the current database for three cases: a) for the so-called hierarchic approach consisting in the parameter calculation in three subsequent steps for the first, second and third level parameters, resp. (and with calculation of the additional adjustable parameter in the first level only); b) for the similar approach similar as in the previous case with the additional adjustable parameter  $c_p^\circ$  being improved also at higher levels; c) and for the so-called non-hierarchic approach consisting in the parameter calculation in a single step.

Heat capacity predictions by the new model were compared with values obtained by two other group contribution methods [5,6].

This work was carried out within the IUPAC project number No. 2004-010-3-100 and within the Institutional Research Plans No. MSM 6046137307 and MSM 6046137306 and within the Grant No. IAA 400720710 of the Grant Agency of the Academy of Sciences of the Czech Republic.

## References

1. Záborský, M., Růžička, V., Majer, V.; Domalski, E. S., *Journal of Physical and Chemical Reference Data. Monograph No. 6*, American Chemical Society: Washington, D.C. (1996).
2. Záborský, M., Růžička, V., Domalski, E. S., (2001) *Journal of Physical and Chemical Reference Data*, 30, 1199-1689.
3. Marrero, J., Gani, R., (2001) *Fluid Phase Equilibria*, 183-184, 183-208.
4. Kolská, Z., Růžička, V., Gani, R., (2005) *Industrial & Engineering Chemistry Research*, 44, 8436-8454.
5. Záborský, M., Růžička, V. (2004) *Journal of Physical and Chemical Reference Data*, 33, 1071-1081.
6. Chickos, J. S., Hesse, D. G., Liebman, J. F., (1993) *Structural Chemistry*, 4, 261-269.



## **Don't gamble with physical properties of polymers**

Anton A. Kiss, Abdelghani Belkou, Alexandre C. Dimian, Piet Iedema

*University of Amsterdam, Nieuwe Achtergracht 166, 1018 WV Amsterdam, The Netherlands  
Email: ktony@science.uva.nl, alexd@science.uva.nl*

### **1. Summary**

This work explores some of the possible thermodynamic options (Sanchez-Lacombe, SAFT, Flory-Huggins, Soave-Redlich-Kwong) available in designing polymerization systems. Different results are predicted by these models with respect to monomer-polymer separation and polymer properties. The results show that it is essential to choose the right property model in order to get reliable results from simulation. High-pressure low-density polyethylene (HP-LDPE) process is used as a case study.

Keywords: polymerization systems, property model polymers, LDPE

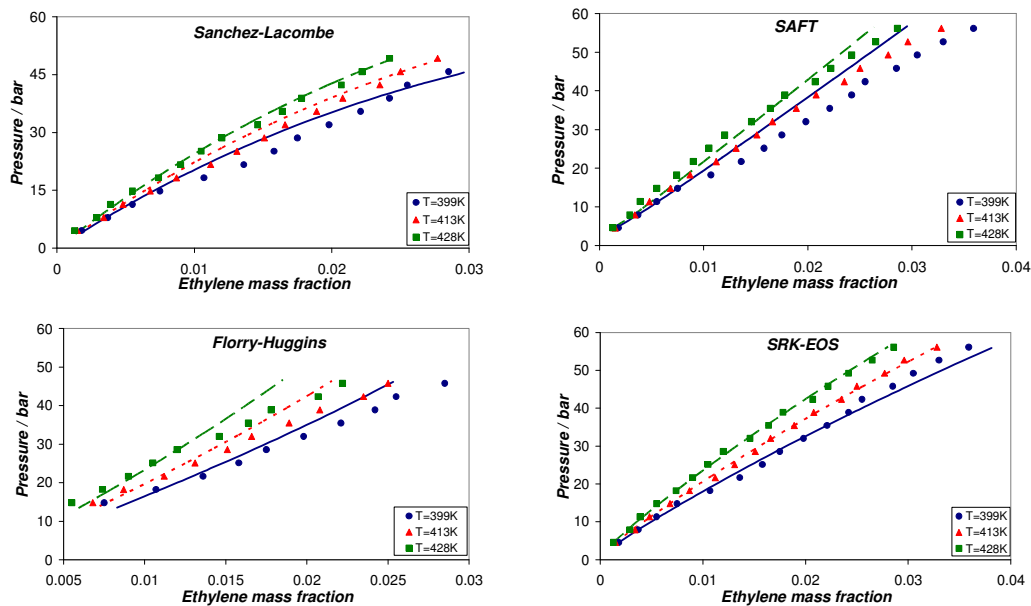
### **2. Extended Abstract**

The physical properties models are the base of any process modeling and simulation hence the appropriate selection of the property model influences all future steps of the simulation. In any polymerization system there is a separation of the polymer from monomer, which is recycled in case of incomplete conversion. Simulating such systems is not a trivial task because mixtures of small molecules and long-chain polymers are involved. Thus it is essential to choose a suitable property model to get reliable results from simulation. The problem is how to select the right property model for which reliable parameters can be calculated, when insufficient experimental data is available. To solve this problem we explore the most used property models available in polymerization systems (e.g. Sanchez-Lacombe, SAFT, Flory-Huggins, SRK), perform regression and parameters fitting, and show that different results are predicted with respect to monomer-polymer separation and polymer properties.

The property models used in this work describe with good accuracy the behavior of both conventional molecules and polymer chains. A major advantage of using equation-of-state (EOS) is that pure-component parameters of many conventional molecules encountered in polymer processes are already available in literature. Nevertheless there is a need to estimate somehow the binary interaction parameters for these models. When the binary parameters are not fitted to experimental data the models tested revealed unsatisfactory performance.

In this work the high-pressure low-density poly-ethylene (HP-LDPE) system was selected as case study.[1] Experimental data was used to calculate the model parameters.[2] The parameters should be segment-based or scalable to the size of the polymer. This condition is necessary because the size of the polymer changes in the process, and the model used must be able to accommodate this fact. [3]

Different results are predicted by the EOS models with respect to monomer-polymer separation and polymer properties. This has a major impact on the results of the simulation of a certain design. Since the analysis was limited to a single process we can not generalize the conclusions, but these results are an effective starting point in approaching other polymerization systems. Note that all calculations, including the industrial reactor simulations, were rigorously performed using the state-of-the-art software Aspen Polymers Plus that is a layered product built on top of Aspen Plus™.



Each EOS property model has exclusive characteristics that affect the results of modeling the pure monomer and polymer mixture behavior. Out of the four models used, Sanchez-Lacombe and Polymer-SRK EOS produced the best acceptable fit of the data. Both models are capable of predicting properties at both high and low-pressure, and give accurate results especially for high temperatures.

## References

Kiss, A. A., Bildea, C. S., Dimian, A. C. and Iedema, P. D. (2003) *Chemical Engineering Science*, 58, 2973-2984.

Hao, W., Elbro, H.S. and Alessi, P., *Chemistry Data Series*, XIV, DECHEMA (1992).

Stanley, H. H., and Radosz, M. (1990) *Industrial and Engineering Chemistry Research*, 29, 2284-2294.

## **Solubility of CO<sub>2</sub> in Solutions of Hyperbranched Polymers. Search for Green Process Solvents**

M.K. Kozłowska,<sup>a,b</sup> C.S. Schacht,<sup>a,b</sup> B. Jürgens,<sup>a</sup> J. Gross,<sup>a</sup> T.W. de Loos,<sup>a</sup> P.J. Jansens<sup>b</sup>

<sup>a</sup> Engineering Thermodynamics, Department of Process & Energy, Delft University of Technology, Leeghwaterstraat 44, 2628 CA Delft, The Netherlands

<sup>b</sup> Separation Technology, Department of Process & Energy, Delft University of Technology, Leeghwaterstraat 44, 2628 CA Delft, The Netherlands

### **1. Summary**

Hyperbranched Polymers (HBPs) are highly branched macromolecules, often existing as room-temperature liquids possessing no measurable vapor pressures. Their use as process solvents in the field of the separation technology was proposed in some recent publications [W. Arlt, M. Seiler, J. Rolker, DE 102002014707.0; J. Fang, H. Kita, K.-I. Okamoto, J. Membr. Sci. 182 (2001) 245-256.]. To determine the applicability of HBPs in adsorption/desorption cycles, vapor-liquid equilibrium data has been determined for the binary (Boltorn U3000 + CO<sub>2</sub>) system as well as for the ternary systems (Polyethylenimine + H<sub>2</sub>O + CO<sub>2</sub>) and (Polyglycerol + CH<sub>3</sub>OH + CO<sub>2</sub>). The solubility of CO<sub>2</sub> is the highest in hyperbranched polyester Boltorn U3000.

Keywords: hyperbranched polymers, green solvent, carbon dioxide, phase equilibria

### **2. Introduction**

Hyperbranched Polymers (HPBs) have recently attracted much interest due to their physical, thermal and chemical properties. In contrast to dendrimers, which build highly uniform and monodisperse structures [1-2], HBPs are randomly branched, polydisperse macromolecules [3]. They can easily be synthesized via economically favorable one-step reactions [4]. Seiler et al. [5-7] showed that HBPs can develop preferred interactions with one compound of a mixture, in other words, the fugacities of the compounds in mixtures are selectively altered by the addition of HBPs. This finding suggests that HBPs can be used as solvent or additive in separations based on adsorption to increase separation performance. The properties of HBPs can be tailored

by controlled functionalization of their end groups. Thus, they exhibit a high potential to being used in large scale industrial applications like removing carbon dioxide from waste gases.

### 3. Results and discussion

Using a Cailletet apparatus (Picture 1) the vapor-liquid equilibria of three different systems were determined including a Hyperbranched Polymer and CO<sub>2</sub>. Figure 1 shows the isopleths of the system Polyglycerol (PG-2) + CH<sub>3</sub>OH + CO<sub>2</sub> in a PT diagram. At a concentration of 15 wt % CO<sub>2</sub> and a temperature of 373 K a second liquid phase forms at around a pressure of 9.2 MPa to form a liquid-liquid-vapor phase split. A further increase of the pressure leads to the disappearance of the vapor phase at a pressure of ca. 9.8 MPa. Complete homogeneity will be reached at pressures above ca. 14.4 MPa. Pure Polyethylenimine (PEI-5) and Polyglycerol are too viscous to measure the phase behavior in PEI-5\CO<sub>2</sub> or PG-2\CO<sub>2</sub> systems in the Cailletet equipment. That is why these hyperbranched polymers are not appropriate for application as scrubbing agents in the pure state. However, the solutions of hyperbranched polymers in water or methanol can be used in gas separations based on absorption\desorption cycles.



Picture 1: Cailletet apparatus.

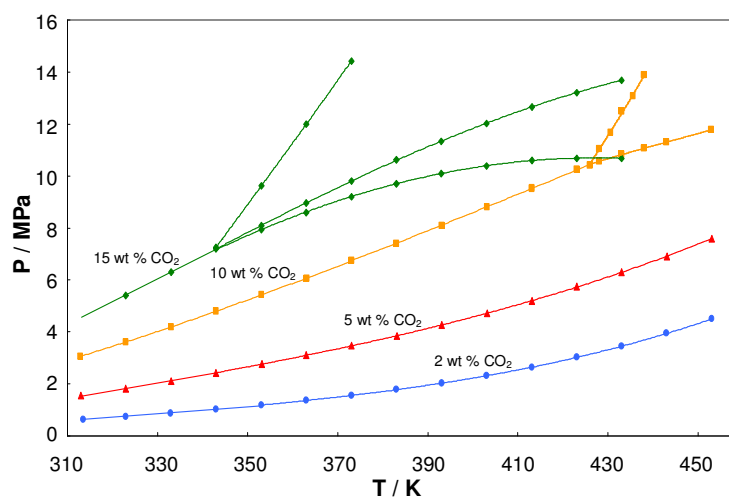


Figure 1: Bubble point curves for PG-2 (50 wt %) + CH<sub>3</sub>OH (50 wt %) + CO<sub>2</sub>.

### References

- [1] J.M.J. Fréchet, D.A. Tomalia, *Dendrimers and other Dendritic Polymers*, John Wiley & Sons, West Sussex, 2001.
- [2] F. Aulenta, W. Hayes, S. Rannard, *Eur. Polym. J.* 39 (2003) 1741-1771.
- [3] B. Voit, *J. Polym. Sci. A: Polym. Chem.* 38 (2000) 2505-2525.
- [4] C.R. Yates, W. Hayes, *Eur. Polym. J.* 40 (2004) 1257-1281.
- [5] M. Seiler, D. Köhler, W. Arlt, *Sep. Purif. Technol.* 30 (2003) 179-197.
- [6] M. Seiler, J. Rolker, W. Arlt, *Macromolecules* 36 (2003) 2085-2092.
- [7] M. Seiler, C. Jork, A. Kavarnou, R. Hirsch, W. Arlt, *AIChE J.* 50 (2004) 2439-2454.

## **Automatic generation of Global Phase Diagram from Equation of State**

A. Keyur S. Patel,<sup>a</sup> B. Aydin K. Sunol,<sup>a</sup>

<sup>a</sup>*Department of Chemical Engineering, University of South Florida, FL-33620 Tampa, USA*

### **1. Introduction**

For any separation processes, especially for the processes operating at high pressure, knowledge of global phase behavior (P-T-x-y projections) is very crucial for analysis of process under different operation region (P-T space) and eventually to determine the most suitable operating condition.

We propose a systematic strategy to calculate global phase diagram for binary system using equation of state model. As mentioned by Cismondi and Michelsen (2007), the strategy to compute the global phase diagram proposed by them doesn't take into account the possibility of appearance of solid phase. The authors also pointed out that the procedure can not detect type VI, or type VII phase behavior where closed liquid-liquid critical curve is present. Motivated by the need to improve reliability of global phase diagram calculations and importance to model the occurrence of solid phase for supercritical fluid technology, we developed a systematic strategy to calculate global phase diagram for binary system that can detect the presence of solid phase if any and can also check for existence of closed critical curves (type VI), if any.

Keywords: Global phase diagram, equation of state, homotopy continuation

### **2. Summary**

The method begins from the known thermodynamic point for pure component and traces the three phase line, two phase (for pure component) line and critical line in temperature-pressure-composition space. The phase equilibrium is tested for global phase stability while tracing the curve. If instability is detected or the occurrence of solid phase is encountered, the critical endpoint is located. Subsequently, new branches of phase equilibrium originating from endpoint are traced. To perform the phase stability test along a traced curve and to determine the existence of a closed critical curve, we use homotopy continuation based global method suggested by Sun and Seider (1995).

The procedure enables automatic generation of global phase diagram (GPD) which incorporates calculations of all important landmarks such as critical endpoints (CEP), quadruple point (Q point, if any), critical line, liquid-liquid-vapour line (LLV, if any), solid-liquid-liquid line (SLL if any) and solid-liquid-vapour lines (SLV). To demonstrate the ability we generated different type of phase diagrams using equation of state model.

The proposed strategy is completely general that can be applied to any equation of state model. Also, the algorithm doesn't assume any knowledge about the type of phase diagram. Homotopy continuation based global method is used to determine phase stability and to detect the existence of closed loop critical curve. Critical lines and three phase lines are traced using predictor-corrector type method. The predictive tool for global phase diagram can not only minimize experimental effort to determine phase behavior of unknown binary system, but also provides a valuable tool to determine the most suitable thermodynamic model which reproduces the experimental behavior with best accuracy. Such model, if used to simulate the chemical processes, can improve the accuracy of prediction significantly.

## References

Cismondi, M., Michelsen, M., (2007) *Journal of Supercritical Fluids*, 39(3),287-295.

Sun, A., Seider, W., (1995) *Fluid Phase Equilibria*, 103(2),213-49.

## **Towards Fast Measurement of Multicomponent Diffusion Coefficients in Ionic Liquids**

E. Kriesten,<sup>a</sup> M. Oertker,<sup>b</sup> A. Bardow,<sup>a</sup> H.-J. Koß,<sup>b</sup> W. Marquardt,<sup>a</sup>

<sup>a</sup>Process Systems Engineering, RWTH Aachen University, 52056 Aachen, Germany

<sup>b</sup>Chair of Technical Thermodynamics, RWTH Aachen University, 52056 Aachen, Germany

### **1. Summary**

The potential of model-based 1D Raman spectroscopy for the analysis of diffusion in electrolytes and ionic liquids is demonstrated. 1D Raman spectroscopy simultaneously determines concentrations of all components in a mixture with high temporal and spatial resolution. Through combination with model-based experimental analysis, multicomponent diffusion can be analyzed in a few fast experiments. This renders the study of slowly diffusing systems such as ionic liquids practicable.

Keywords: multicomponent diffusion, ionic liquids, Raman spectroscopy, parameter estimation, experimental design

### **2. Extended Abstract**

While transport properties play an important role in reaction and separations, data on multicomponent mixtures are rare today. For ionic liquids, studies have been limited to infinite dilution [1]. A complete set of mutual diffusion data is available only for one binary mixture [2]. Established diffusion measurement methods are laborious and time consuming. In multicomponent systems, several measurements have to be carried out since these methods are not capable of resolving all components.

To overcome these problems, the authors developed a novel method based on 1D Raman spectroscopy [3,4]. This measurement technique allows for the simultaneous detection of all concentrations at 400 positions in a vertical diffusion cell with high temporal resolution. The application of model-based methods for the design of optimal experiments and for efficient data analysis further reduces the experimental effort. It was shown that the method is capable of identifying multi-component diffusion coefficients from a single experiment. The method has already been applied to several systems of up to four components [5].

The novel method has a high potential for the analysis of electrolytes. Salt diffusion coefficients can readily be measured in the existing setup. As a first test system, diffusion of  $(\text{NH}_4)_2\text{SO}_4$  in aqueous solution has been investigated. From the measured

concentration profiles (Fig.1), a salt diffusion coefficient of  $D=1.06 \cdot 10^{-9} \text{ m}^2/\text{s}$  was estimated, which corresponds within 3 % to literature data. Even though water has a weak Raman signal these results show the potential of the novel diffusion experiments for aqueous electrolyte systems.

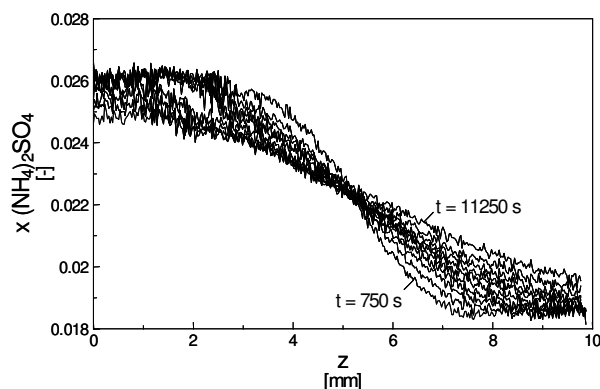


Figure 1: Concentration profiles of an ammonium sulfate diffusion experiment

Current investigations focus on ionic liquid (IL) systems due to the pressing need for diffusion data. In Fig. 2 the pure component spectrum of [EMIM] BTA recorded in our Raman setup is shown. The high signal-to-noise ratio is comparable to standard nonelectrolytic systems showing that Raman spectroscopy is well suited to study IL.

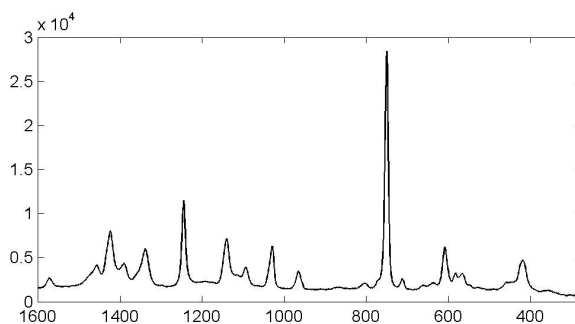


Figure 2: Pure spectrum of [EMIM] BTA

In this work, the Raman diffusion experiment is introduced and extensions to electrolyte systems are described. First results on ionic liquids are presented.

## References

- [1] Su., W.C., Chou, C.H., Wong, D.S.H., Li, M.H. (2007) *Fluid Phase Equilib.*, 252, 74–78.
- [2] Heintz, J. (2005) *Chem. Thermodynamics*, 37, 525–535
- [3] Bardow, A., Göke, V., Koß, H.-J., Marquardt, W. (2006) *AIChE J.*, 52(12), 4004-4015.
- [4] Bardow, A., Marquardt, W., Göke, V., Koß, H.-J., Lucas, K. (2003) *AIChE J.*, 49, 323.
- [5] Bardow, A., Göke, V., Koß, H.-J., Kriesten, E., Lucas, K., Marquardt, W. (2005), *Proc. of the 21st European Symposium on Applied Thermodynamics (ESAT)*, Jurata, Poland.



## Session T2-1P: Thermodynamics – Poster

Abstract Number	Paper Title & Authors	Included
1	The use of Cyclic coordinate search, BFGS and FRPR methods for estimation of parameters of GE models in Binary VLE A R Prasad, J S Babji, A A Kumar, C Sreedevi	Yes
9	Comparison of Local Composition Models for estimation of parameters in Binary Vapor Liquid Equilibria A R Prasad, J S Babji, A A Kumar	Yes
17	Correlation of Binary VLE by GE models: Comparison of Four Unconstrained Optimization Methods A R Prasad, J S Babji, A A Kumar, B U S N Babu	Yes
445	Determination of solubility parameters of polymers by using intrinsic viscosity method G Ovejero, P Pérez, M D Romero, E Díez, I Guzmán	Yes
472	Forecasting of Hydrate Formation Pressure for Natural Gas Using Artificial Neural Network A Heydari, K Shayesteh, H Shayeghi	Yes
552	Evaluation of statistical mechanics-based equations of state for complex fluid mixtures I G Economou, E K Karakatsani, A Grennerb, I Tsivintzelis, C Panayiotou, G M Kontogeorgis	Yes
783	Estimations on the selectivity of the nickel dithiolene in the olefins separation Q Han, H Wen, Y Zhao	Yes
795	Solubility of polyhydroxyalkanoates by Thermodynamic predictions N Jacquél, C Lo, H Wu, Y Wei, S Wang	Yes
806	Speeds of Sound, Isentropic Compressibilities and Excess Molar Volumes of Mixtures of 1-Alkanol + Dibutyl Ether at 293.15, 298.15 and 303.15 K I Mozo, I G de la Fuente, J A González, J C Cobos	Yes
827	Prediction of Speeds of Sound and Ultrasonic Studies of Hydroxyether + Organic Solvent Mixtures J A González, I Mozo, I García de la Fuente, J C Cobos, N Riesco	Yes
860	Determination of Cloud Points of Poly (propylene glycol) Aqueous Mixtures Using Particle Counting Method A Eliassi, A Parach	Yes
992	Application of the simplified PC-SAFT Equation of State to Complex Phase Equilibria of Ethylene Glycol Oligomers A Grenner, G M Kontogeorgis, N Solms, M L Michelsen	Yes
1004	Modeling of Vapor-Liquid Equilibrium in Gas-Aqueous	Yes

Session T2-1P

	Electrolyte System using Neural Network Models A Ghaemi, S Shahhoseini, M G Marageh	
1075	Modelling lubricating oil fractions by means of a pseudo-component model J J Espada, B Coto, R Grieken, J L Peña	Yes
1240	Develop a correlation of convective coefficient in a vertical evaporator with boiling processes inside pipes where the flow is stagnant J C García, J F León, J A Aguinaco	Yes
1473	Prediction of Binary Adsorption Equilibria M A Monsalvo, A A Shapiro	Yes
1745	Experimental data and correlation of surface tension of binary polymer solutions at different temperatures and atmospheric pressure M T Mazandarani, A Eliassi, M Fazlollahnejad	Yes
1636	Group-contribution based method for surface tension estimation A Martinho, H A Matos, R Gani	Yes
1766	Thermodynamic modelling of Butadiene Extractive Distillation Plant N Farhadian, M A Mosavian, S Maghsoudi	No
2312	Thermodynamics of pervaporation process in reacting systems A Toikka, A Penkova	Yes
2401	On the stability analysis of phase diagrams of multicomponent systems A Toikka, R Ralis	Yes
2429	Correlations for predicting solution gas-oil ratio, bubblepoint pressure and oil formation volume factor at bubblepoint of Iran crude oils M T Mazandarani, S M Asghari	Yes
2808	Development of Group Contribution Plus Property Models for Organic Systems H E González, J Abildskov, R Gani	Yes
2884	A new extended UNQUAC model for solid-liquid equilibria of organic solvents+iPBu-1 systems H Salimnezhad, F Feyzi	Yes
2913	Fatty acids systems under high pressure: caprylic + myristic acids and lauric + myristic acids M C Costa, M A Krähenbühl, A J A Meirelles, J L Daridon, J Pauly, J A P Coutinho	Yes
3106	Global Phase Equilibrium Calculation and Critical Phase Behavior from a Group Contribution Equation of State in Binary Mixtures N Reshadi, F Feyzi	Yes
3215	Predicting branching structure effects on the thermodynamic properties using COSMO-RS W Arlt, O Spuhl, L Wang	Yes
3573	Prediction of Wax Precipitation Using Solid Equation of State M V Sefti, H Mehdizadeh, A Mousavi	Yes

## **The use of Cyclic coordinate search, BFGS and FRPR methods for estimation of parameters of $G^E$ models in Binary VLE**

A. Ravi Prasad, J. Srinivasa Babji, A. Aravind Kumar and Ch. Sreedevi

*Department of Chemical Engineering, Andhra University, Visakhapatnam, 530 003, India*

### **1. Summary**

Isothermal binary VLE data of forty systems of varying non-ideality have been processed for estimating the parameters using three unconstrained optimization methods with six  $G^E$  models to bring out comparative evaluation of combination of methods and models for correlation of binary VLE data.

Keywords: parameter estimation,  $G^E$  models, Optimization methods

### **2. Extended Abstract**

The binary VLE data are needed in the design of distillation equipment and for testing of liquid mixture models. Most of the liquid mixtures encountered in commercial operations are non-ideal. The non-ideality in a liquid mixture can be concisely represented by the Excess Gibbs Energy ( $G^E/RT = g^E$ ). There are several empirical and semi theoretical models proposed in literature. The correlation of P-T-x-y data consists in determining the constants in the  $G^E$  models by minimizing the objective function  $\sum (g_{\text{exp}}^E - g_{\text{cal}}^E)^2$ . The constants can be obtained either by solution of sets of non-linear equations or using the methods based on optimization techniques. The  $g^E$  models proposed in literature can be classified as Single parameter, Two parameter and Multi parameter models. The  $g^E$  models can be broadly classified as classical models and models based of local composition concept. Often they are classified as Enthalpic models, entropic models and complete  $g^E$  models ( $g^E = h^E - TS^E$ ).

In this paper three unconstrained optimization methods of Cyclic coordinates search, Broyden-Fletcher-Goldfarb-Shanno (BFGS) and Fletcher-Reeves-Polak-Rebiere (FRPR) are used for estimation of parameters in six  $g^E$  models namely Margules, Van

e-mail : rpandra@rediffmail.com

Laar, Wilson, NRTL, UNIQUAC and CLC by minimizing the objective function in  $g^E$ . The results of processing the data of forty isothermal binary VLE data of systems of varying degrees of non-ideality are presented. For comparison of the method of optimization and  $G^E$  model combinations in correlating the data the results for the system Ethanol (1) Water (2) at 25°C are given in Table 1. The results are also compared with the results given DECHEMA data Series where the optimization method used was Nelder–Mead. The complete results of processing of the data of forty isothermal binary VLE systems are presented in the full paper.

**Table 1: Average Deviation in Vapor Composition for the system Ethanol (1) Water (2) at 25°C by six GE models and four Optimization methods**

Method	$G^E$ Model					
	Margules	Van Laar	Wilson	NRTL	UNIQUAC	CLC
DECHEMA	0.0027	–	0.0072	0.0047	0.0056	–
CCS	0.0020	0.0040	0.0060	0.0039	0.0053	0.0039
BFGS	0.0020	0.0038	0.0060	0.0037	0.0055	0.0040
FRPR	0.0031	0.0052	0.0077	0.0052	0.0071	0.0052

## Comparison of Local Composition Models for estimation of parameters in Binary Vapor Liquid Equilibria

A. Ravi Prasad, J. Srinivasa Babji and A. Aravind Kumar

*Department of Chemical Engineering, Andhra University, Visakhapatnam, 530 003, India*

### 1. Summary

Isothermal binary VLE data of forty systems of varying non-ideality have been processed for estimating the parameters using the unconstrained optimization method of Hooke Jeeves with Nineteen  $G^E$  models to bring out comparative evaluation of  $G^E$  models for correlation of binary VLE data.

Keywords: parameter estimation,  $G^E$  models, Optimization methods

### 2. Extended Abstract

The binary VLE data are needed in the design of distillation equipment and for testing of liquid mixture models. Most of the liquid mixtures encountered in commercial operations are non-ideal. The non-ideality in a liquid mixture can be concisely represented by the Excess Gibbs Energy ( $G^E/RT = g^E$ ). There are several empirical and semi theoretical models proposed in literature. The correlation of P-T-x-y data consists in determining the constants in the  $G^E$  models by minimizing the objective function  $\sum (g_{\text{exp}}^E - g_{\text{cal}}^E)^2$ . The constants can be obtained either by solution of sets of non-linear equations or using the methods based on optimization techniques. The  $g^E$  models proposed in literature can be classified as Single parameter, Two parameter and Multi parameter models. The  $g^E$  models can be broadly classified as classical models and models based of local composition concept. Often they are classified as Enthalpic models, entropic models and complete  $g^E$  models ( $g^E = h^E - TS^E$ ).

In this paper the unconstrained optimization method of Hooke Jeeves is used for estimation of parameters in Nineteen Local composition Models and the results of processing the data of forty isothermal binary VLE data of systems of varying degrees

of non-ideality are presented. The following Local composition Models are considered:

Wilson, T-K Wilson, Enthalpic Wilson, Effective Wilson, Modified Wilson, NRTL, Modified NRTL1, Modified NRTL2, UNIQUAC, Effective UNIQUAC, Modified UNIQUAC – I, Modified UNIQUAC – II, Modified UNIQUAC – III, CLC, Modified CLC, Nagata-Notoh, Nagata Notoh-I, Nagata Notoh-II and Nagata Notoh-III.

## Correlation of Binary VLE by $G^E$ models: Comparison of Four Unconstrained Optimization Methods

A. Ravi Prasad, J. Srinivasa Babji, A. Aravind Kumar and B. U. S. Naidu Babu

*Department of Chemical Engineering, Andhra University, Visakhapatnam, 530 003, India*

### 1. Summary

Isothermal binary VLE data of Hexafluoro benzene (1) / benzene (2) at 333.15 K is processed with 40  $G^E$  models using four unconstrained optimization methods to bring out the comparison of combination of  $G^E$  models and optimization methods.

Keywords: parameter estimation,  $G^E$  models, Optimization methods

### 2. Extended Abstract

The binary VLE data are needed in the design of distillation equipment and for testing of liquid mixture models. Most of the liquid mixtures encountered in commercial operations are non-ideal. The non-ideality in a liquid mixture can be concisely represented by the Excess Gibbs Energy ( $G^E/RT = g^E$ ). There are several empirical and semi theoretical models proposed in literature. The correlation of P-T-x-y data consists in determining the constants in the  $G^E$  models by minimizing the objective function  $\sum (g_{\text{exp}}^E - g_{\text{cal}}^E)^2$ . The constants can be obtained either by solution of sets of non-linear equations or using the methods based on optimization techniques. The  $g^E$  models proposed in literature can be classified as Single parameter, Two parameter and Multi parameter models.

In this paper four unconstrained optimization methods namely two variants of Pearsons method, Broyden and Fletcher-Reeves-Ploak-Rebiere are compared for estimation of parameters in isothermal binary VLE of the system Hexafluoro benzene (1) / benzene (2) at 333.15 K which shows double azeotropy using 40  $g^E$  models and results of processing the data are presented. The results of calculations in terms of Dy (absolute average deviation in y) are presented in Table 1. As can be observed from the results all the  $g^E$  models selected and optimization methods are correlating the data satisfactorily. The correlation by Scatchard Hamer model is the best with Pearson No. 2 method of optimization for this system.

e-mail : rpandra@rediffmail.com

**Table 1: Correlation of P-x-y data at 333.15 K of Hexafluorobenze (1) Benzene (2) by four methods of optimization using forty G<sup>E</sup> models**

Model	$\Delta Y$			
	Pearson No:2	Pearson No:3	Broyden	Ploak Rebiere
Andiappan and Mc Lean.	0.001303	0.001312	0.001312	0.001312
C.L.C.	0.000783	0.000788	0.000814	0.000783
Combinational Activity Coefficient.	0.001219	0.001223	0.001219	0.001219
Enthalpic Wilson.	0.008149	0.008135	0.008115	0.008115
Effective UNIQUAC.	0.003788	0.003780	0.003797	0.003797
Extended Van Laar.	0.003475	0.003382	0.003533	0.003534
Effective Wilson.	0.005061	0.005054	0.005054	0.005061
Heil Prausnitz.	0.002964	0.002966	0.002988	0.002964
Hiranuma.	0.003886	0.003840	0.003840	0.003839
Modified Wilson (Huang - Lee).	0.003830	0.003840	0.003842	0.003825
L.C.G.	0.003811	0.003832	0.003780	0.003768
L.E.M.F.	0.004232	0.004235	0.004224	0.004232
L.S.G	0.002094	0.002052	0.002209	0.002182
Margules	0.001826	0.001570	0.001566	0.001576
Malanowski	0.009815	0.009805	0.009812	0.009815
Modified C.L.C.	0.000526	0.000503	0.000479	0.000433
Modified N.R.T.L.	0.000691	0.000684	0.000670	0.000662
Nagata Notoh – I	0.003801	0.003773	0.003792	0.003766
Nagata Notoh – II	0.003888	0.003890	0.003882	0.003882
Nagata Notoh – III	0.003486	0.003488	0.003483	0.003481
Nagata Notoh	0.004610	0.004126	0.004171	0.004140
NRTL+ Enthalpic Wilson	0.003442	0.003440	0.003442	0.003439
Noda Ishida	0.001727	0.001863	0.001702	0.001701
N.R.T.L	0.001273	0.001291	0.001281	0.001281
Nagata Nagashima	0.001377	0.001359	0.001421	0.001432
Orye	0.003737	0.003737	0.003732	0.003726
Redlich Kister	0.001413	0.001387	0.001387	0.001386
Ruckensteien and Shulgin	0.000646	0.000625	0.000714	0.000705
Scatchered Hamer	0.000356	0.000358	0.000364	0.000364
Sigma	0.000758	0.000688	0.000691	0.000691
T. K. Wilson	0.004173	0.004215	0.004173	0.004162
Modified UNIQUAC –I	0.002264	0.003650	0.002275	0.002264
Modified UNIQUAC –II	0.002240	0.002287	0.002264	0.002252
Modified UNIQUAC –III	0.003464	0.003461	0.003428	0.003436
UNIQUAC	0.003753	0.003375	0.003356	0.003356
Van Laar	0.007908	0.007908	0.007907	0.007907
Wilson	0.003790	0.003789	0.003780	0.003785
Modified N.R.T.L. (Wu et al).	0.001251	0.001250	0.001260	0.001252
Zeta	0.005033	0.005079	0.005079	0.005079
Zeta Wilson	0.004858	0.004856	0.004861	0.004856



## Determination of solubility parameters of polymers by using intrinsic viscosity method

G. Ovejero<sup>a</sup>, P. Pérez,<sup>b</sup> M.D. Romero<sup>a</sup>, E. Díez<sup>a</sup>, I. Guzmán<sup>a</sup>

<sup>a</sup>Department of Chemical Engineering, Complutense University of Madrid, 28040 Madrid, Spain

<sup>b</sup>REPSOL-YPF, 28933 Móstoles, Madrid, Spain

### 1. Summary

The wide use of polymers in many fields emphasizes the need to analyze different polymer-solvent interactions; one of the most important properties of these systems is the Hildebrand solubility parameter ( $\delta$ ). For this reason, the objective of this work is to obtain the solubility parameter of a hydrogenated triblock styrene-butadiene-styrene copolymer (SBES), from intrinsic viscosity measurements.

Keywords: polymer, intrinsic viscosity, solubility parameter, SBES rubber

### 2. Extended Abstract

In polymer-solvent thermodynamics, the solubility parameter is a factor that indicates the capacity of a polymer to be dissolved into a solvent because to obtain a complete polymer dissolution, free energy of mixing has to be as negative as possible, what happens when enthalpic term of this state function, proportional to  $(\delta_s - \delta_p)^2$ , is the lowest. So the closer the solubility parameter of polymer ( $\delta_p$ ) and solvent ( $\delta_s$ ) are the better is the solubility and the compatibility between polymer and solvent.

To obtain intrinsic viscosity values from flow time measurement, Huggins and Kraemer equations were used [1]:

$$\frac{\eta_{sp}}{c} = [\eta] + K_H \cdot [\eta]^2 \cdot c \quad (1)$$

$$\frac{\ln(\eta_r)}{c} = [\eta] + K_K \cdot [\eta]^2 \cdot c \quad (2)$$

where  $c$  is the concentration of polymer solution,  $K_H$  is the Huggins coefficient, a constant for a series of polymers of different molecular weights in a given solvent and temperature and  $K_K$  is the Kramer coefficient.

Relative viscosity ( $\eta_r$ ) was obtained as the relation between the flow time of the polymer solution through a capillary tube of known diameter and length and the flow time of the pure solvent through the same capillary tube and specific viscosity ( $\eta_{sp}$ ) is defined as relative viscosity minus one and represents the increase in viscosity due to the polymer. So the intrinsic viscosity can be determined as usual as the common

intercept of the Kraemer and Huggins relationships, using  $\eta_r$  and  $\eta_{sp}$  experimentally obtained. As example, Fig 1 shows Huggins and Kraemer plots for cyclohexane in order to obtain the intrinsic viscosity. The results obtained are shown in table 1.

Table 1

Solvent	$\delta$ (MPa <sup>1/2</sup> )	$[\eta]$ (gdL <sup>-1</sup> )	Solvent	$\delta$ (MPa <sup>1/2</sup> )	$[\eta]$ (gdL <sup>-1</sup> )
<i>n</i> -hexane	14.92	0.29	cyclopentane	17.80	0.88
methyl-cyclohexane	16.42	0.84	toluene	18.24	0.80
cyclohexane	16.81	0.94	benzene	18.78	0.68

Related to intrinsic viscosity of a polymer solution, the higher its value is, the more compatible polymer and solvent are. As it can be seen in Fig 2, for non-polar solvents a plot of intrinsic viscosity vs. solubility parameters tends to follow a parabolic relationship.

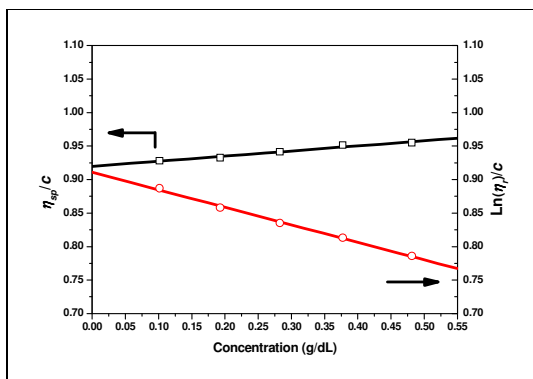


Figure 1

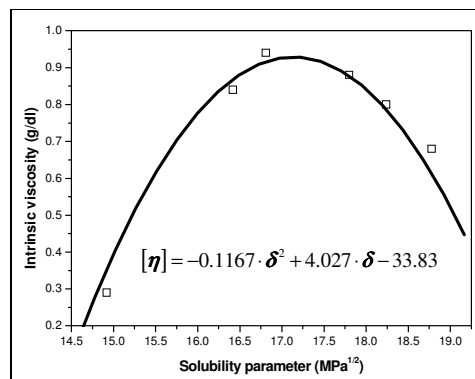


Figure 2

So, the solubility parameter of the polymer ( $\delta_p$ ) was determined [2] by getting the maximum of the plot intrinsic viscosity vs. solvent solubility parameter (eq. 3). The result obtained was 17.26 MPa<sup>1/2</sup> and is similar to other values found in literature for non-hydrogenated and non-vulcanized (SBS) rubbers [3], and to other found for random (SBR) rubbers [4]. The solubility parameter of polymer is closer to solubility parameter of cyclohexane and cyclopentane what indicates that these solvents are the most compatible with the polymer.

## References

- [1] Bustamante, P., Navarro-Lupi3n, J. and Escalera, E., (2005) *European Journal of Pharmaceutical Sciences*, 24, 229-237.
- [2] Brandrup, J. and Immergut, E.H., *Polymer Handbook*, John Wiley Interscience, New York (1989).
- [3] Sheehan, C. J., Bisio, A.L., (1966) *Rubbers Chemical&Technology*, 150-192.
- [4] Romdhane I.H., Plana, A., Hwang, S. and Danner, R.P., (1992) *Journal of Applied Polymer Science*, 45, 2049-2056.
- [5] Barton, A.F.M., (1975) *Chemical Reviews*, 75(6), 731-753.

## Forecasting of Hydrate Formation Pressure for Natural Gas Using Artificial Neural Network

Amir Heydari<sup>1</sup>, Keyvan Shayesteh<sup>1</sup>, Hossein Shayeghi<sup>2</sup>

<sup>1</sup> *Chemical Engineering Group, Technical Engineering Department, The University of Mohaghegh Ardabili, Ardebil, Iran, E-mail: Heydari.amir@gmail.com*

<sup>2</sup> *Technical Engineering Department, The University of Mohaghegh Ardabili, Ardabil, Iran*

### 1. Summary

Knowledge and prediction of natural gas hydrate formation conditions is one of the most important problems in oil and gas engineering. Although some mathematical models are available to predict temperature of hydrate formation, but there is no model for pressure. In this paper the Artificial Neural Network (ANN) technique have been applied for estimation of hydrate formation pressure. The neural network training and test data are 149 and 18 respectively and data are in the range of 32-74 F<sup>o</sup> for temperature, 50-4200 Pisa for pressure and 0.554-1 for specific gravity. The standard feed forward back propagation algorithm is used for training neural networks. The sub optimal neural network structure is 10-6-1 which is obtained using trail and error method. In comparison of performance analysis of ANN, the relative error (RE) was studied and maximum error is obtained 3.051 % and R-Square value is 0.9988. The ANN structure for pressure prediction is greater than temperature (7-5-1) and it's R-Square is better than temperature (0.9941). Thus it can be concluded that the proposed approach provides a good method for prediction of pressure and temperature of hydrates formation conditions.

Keywords: Pressure Forecasting, Artificial Neural Network, Hydrate, Natural gas

### 2. Extended Abstract

The use of Artificial Neural Network (ANN) in chemical and petrochemical areas has been increased recently. In this work, the ANN method is used for hydrates formation pressures. Simulation results based on ANN predictions show that the proposed is very effective and achieve goal performance. To check the reproducibility of the results, each of the networks studied was trained three times.

The ANN used here is a three-layer feed-forward network (see Fig. 1) with BP (stands for Back Propagation) learning as its teaching algorithm. Two hidden layers consist of 10, 6 neurons in each layer respectively, an input layer consists of two neurons (temperature and specific gravity) and an output layer consists of one neuron (pressure) was designed for prediction of hydrate formation in natural gas. Log-sigmoid is the transfer function that used here. By this function, output values have the range from 0 to 1 and therefore output data have been normalized in the range of [0, 1] by following equations:

$$P' = \text{Ln}(\text{Pressure}), P_{new} = \frac{P'_{old} - P'_{min}}{P'_{max} - P'_{min}}$$

Trainrp that is used in this study is a network training function that updates weight and bias values according to Resilient Back-Propagation (RPROP). All the ANNs calculations were carried out using Matlab mathematical software with artificial neural network toolbox.

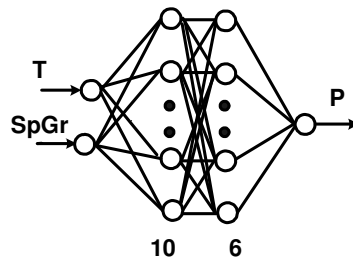


Fig. 1. Topology of the used neural network model

The R-square value for both the training and experimental data sets for the gas hydrate formation is 0.9988 that shows the model has captured the features accurately. These results prove that the proposed ANN can be used successfully for the prediction of hydrate formation in natural gas. The ANN structure for pressure prediction is greater than temperature (7-5-1) and its R-square is better than temperature (0.9941).

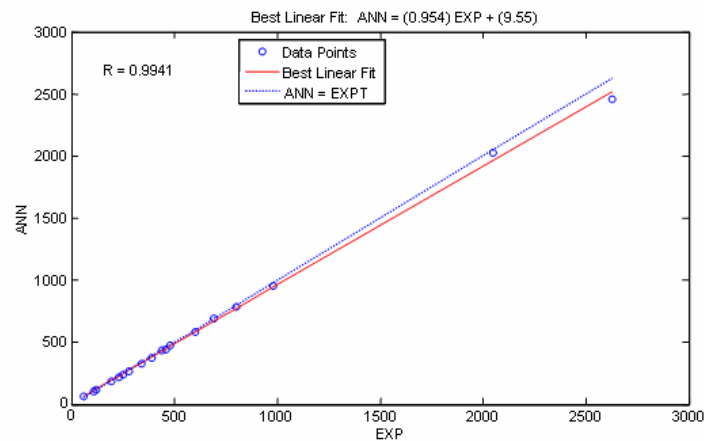


Fig. 2. Comparison of experimental data and estimated hydrate formation pressure by ANN

## References

- S.O. Yang, S.H. Cho, H. Leeb, C.S. Le, Measurement and prediction of phase equilibria for water + methane in hydrate forming conditions, *Fluid Phase Equilibria* 185 (2001) 53–63
- Kh.Fattah, Evaluation Of Empirical Correlations For Natural Gas Hydrate Predictions, *Oil and Gas Business Journal*, [www.ogbus.ru/eng/authors/Fatahh/Fatahh\\_1.pdf](http://www.ogbus.ru/eng/authors/Fatahh/Fatahh_1.pdf)
- A. Chouai, S. Laugier, D. Richon, Modeling of thermodynamic properties using neural networks Application to refrigerants, *Fluid Phase Equilibria* 199 (2002) 53–62
- D. L. Katz, R. L. Lee, *Natural Gas Engineering Producing and Storage*, McGraw Hill, New York, 1990
- A.Heydari, K.Shayesteh, L.Kamalzadeh, Prediction of hydrate formation temperature for natural gas using artificial neural network, *Oil and Gas Business Journal* [www.ogbus.ru/eng/authors/Heydari/Heydari\\_1.pdf](http://www.ogbus.ru/eng/authors/Heydari/Heydari_1.pdf)

## Evaluation of statistical mechanics-based equations of state for complex fluid mixtures

I.G. Economou<sup>a,b</sup>, E.K. Karakatsani<sup>a</sup>, A. Grenner<sup>b</sup>, I. Tsivintzelis<sup>b,c</sup>, C. Panayiotou<sup>c</sup>, G.M. Kontogeorgis<sup>b</sup>

<sup>a</sup>*Molecular Thermodynamics and Modeling of Materials Laboratory, Institute of Physical Chemistry, National Research Center for Physical Sciences "Demokritos", GR-15310 Aghia Paraskevi Attikis, Greece*

<sup>b</sup>*IVC-SEP, Department of Chemical Engineering, Technical University of Denmark, DK-2800 Kgs. Lyngby, Denmark*

<sup>c</sup>*Department of Chemical Engineering, Aristotle University of Thessaloniki, GR-54124 Thessaloniki, Greece*

### 1. Summary

Perturbed Chain-Statistical Associating Fluid Theory (PC-SAFT) and Non-Random Hydrogen Bonding theory (NRHB) are applied to predict and correlate the phase equilibria of multicomponent mixtures that exhibit highly non-ideal behavior, with emphasis to polar fluids of interest to chemical industry. Carefully selected mixtures over a wide range of conditions are used as benchmarks so that the accuracy of the models can be evaluated directly. In addition, the models are applied for the prediction of monomer fraction in pure self associating fluids and in their mixtures.

Keywords: statistical thermodynamics, equations of state, hydrogen bonding

### 2. Results and Discussion

Advances in applied statistical mechanics in recent years have resulted in a number of equations of state for real complex fluids with strong theoretical basis. Two of the most successful and widely used families of such models are based on perturbation theory and lattice fluid theory. By far, the most prominent perturbation theory today is the one based on Wertheim's first order thermodynamic perturbation theory, known as Statistical-Associating-Fluid Theory (SAFT). SAFT and its modifications / extensions have been applied to a wide range of complex fluids, including associating fluids, polymers and supercritical fluids. PC-SAFT is of one of the most successful models of this family. A simplified version of the model (sPC-SAFT) reduced computing time without compromising its performance [von Solms *et al.* 2003], while recently, the model was extended to strong polar fluids, both dipolar and quadrupolar (tPC-SAFT) [Karakatsani *et al.* 2006]. On the other hand, lattice fluid theory

originated from the work of Flory and Huggins and later of Sanchez and Lacombe has been used in industry and academia since 1970s. The most recent extension in this respect is the Non-Random Hydrogen Bonding Theory (NRHB), which accounts explicitly for hydrogen bonding as well as for the non random distribution of molecular segments and free volume [Panayiotou *et al.* 2007].

Hydrogen bonding is the most common reason for highly non ideal system behaviour. Often, the accurate description of thermodynamic properties in these systems is a demanding task. However, it is very useful in the process design and optimization. In this study the sPC-SAFT, tPC-SAFT and NRHB models were applied for the description of such systems in order to investigate their ability in the description of hydrogen bonding but also to underline similarities and differences between different approaches.

In Figure 1a the prediction of the liquid-liquid equilibrium of water – *n*-hexane system are presented. The incorporation of a polar term in the tPC-SAFT model significantly improves the correlation of phase equilibrium in this system. In Figure 1b predictions for the fraction of unbonded alcohol molecules in the binary 1-butanol – *n*-hexane mixture are shown. Both NRHB and sPC-SAFT predict very satisfactory and in close agreement with each other the monomer fraction of alkanol molecules.

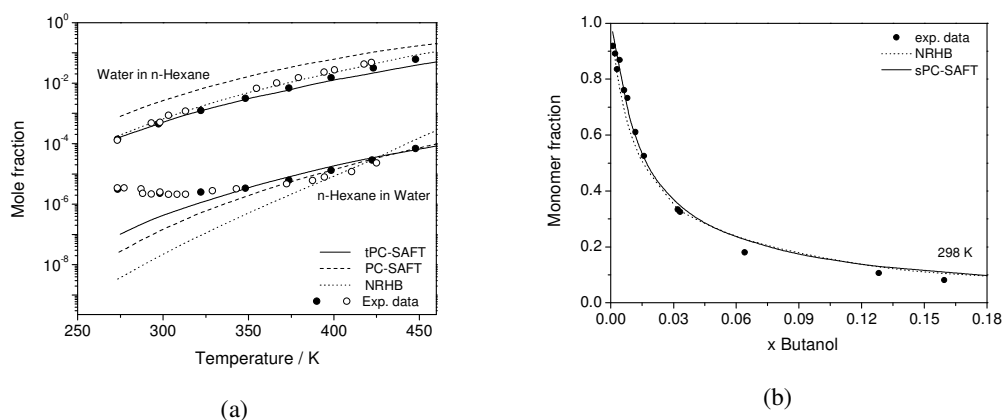


Figure 1: (a) Liquid-Liquid Equilibria of Water – *n*-Hexane mixture and (b) Monomer fraction of 1-Butanol in 1-Butanol – *n*-Hexane mixture.

In all cases, models were shown to correlate experimental data satisfactorily although significant differences can be found in specific cases, as for example in aqueous mixtures.

## References

- Karakatsani, E.K., Kontogeorgis, G.M. and Economou, I.G., (2006) *Ind. Eng. Chem. Res.*, 45, 6063 – 6074.  
 Panayiotou, C, Tsvintzelis, I. and Economou I.G., (2007) *Ind. Eng. Chem. Res.*, 46, 2628 – 2636.  
 von Solms, N., Michelsen, M.L. and Kontogeorgis, G.M., (2003) *Ind. Eng. Chem. Res.*, 42, 1098 – 1105.

## Estimations on the selectivity of the nickel dithiolene in the olefins separation

Qing-Zhen Han,<sup>a, b</sup> Hao Wen,<sup>a</sup> Yue-Hong Zhao,<sup>a</sup>

<sup>a</sup> Multi-Phase Reaction Laboratory, Institute of Process Engineering, Chinese Academy of Sciences, P.O. Box 353, 100080 Beijing, P. R. China

<sup>b</sup> Graduate University of Chinese Academy of Sciences, P.O. Box 4588, 100049 Beijing, P. R. China

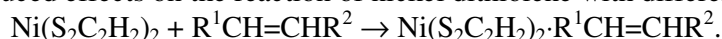
### 1. Summary

The reaction mechanism, as well as the chemical thermodynamics and dynamics, of complexing different olefins with Ni dithiolene is theoretically studied by using B3LYP method. Complete optimizations and frequency calculations of all the stagnation points existing in the reaction potential profiles are performed. It is shown that the reaction between the nickel dithiolene and the olefin is sensitive to both the structure of olefins and the carbon atom number in them. The increase of the carbon atom number in certain olefin will block the reaction and decrease the production rate. This enables one to separate the olefins with less carbon atoms and simple structure from the others with relatively more carbon atoms. Furthermore, we also find that, in some olefins with trans- or cis-structure, the reaction between nickel dithiolene and trans-structure olefins will be much easier and faster to occur than that of cis-structure olefins.

Keywords: olefins separation, nickel dithiolene, selectivity

### 2. Extended Abstract

The study on the transition metal dithiolene complex has been widely carried out since it can reversibly and selectively react with simple aliphatic olefins under mild conditions, without being poisoned by many impurities such as hydrogen, carbon monoxide, acetylene, hydrogen sulfide, and so forth. On account of that the specific structures of olefin complexes will make some influences on this reaction, we here, by means of density functional theory, perform a theoretical estimation of the olefin-structure-induced effects on the reaction of nickel dithiolene with different olefins:



In the present work eight kinds of olefins (ethylene, propylene, 1-butylene, 2-trans-butylene, 2-cis-butylene, 1-hexene, 3-trans-hexene, 3-cis-hexene) are considered. The complete optimizations of all the stagnation points and the corresponding frequency

calculations are performed for all reactions. The detailed calculation results of the activation energies, rate constants and equilibrium constants are presented in Table 1. It is shown that the reaction of complexing nickel dithiolene with each kind of olefins is a two-step process, and step-1 is the rate-determining step because the activation energy of step-1 is greater than that of step-2. Also, we find as the number of carbon atoms ( i.e. structure complex) in the olefins increases, most of the bond lengths in the transition states, intermediates, and products will become longer, while most of the bond angles will become smaller. Moreover, we show that the activation energy of step-1 (or step-2) will increase with the increase of the Carbon atom number of the olefins, while the reaction rate of step-1 (or step-2) will decrease, and the equilibrium constant will rapidly decrease from 12.12 to  $8.435 \times 10^{-6}$ . It is demonstrated that the reaction between the nickel dithiolene and olefins is sensitive to the number of carbon atoms (i.e. structure complex) of olefins. The increase of the carbon atom number in certain olefin will block the reaction, and decrease the production rate. This is beneficial to separate the olefins with less carbon atoms (e.g. ethylene and propylene) from the others with relatively more carbon atoms. Therefore, we may draw that the nickel dithiolene has a good selectivity for the separation of the olefins with less carbon atoms (e.g. ethylene and propylene). Notably, in some olefins with trans- or cis-structures, the reaction between nickel dithiolene and trans-structure olefin will be much easier and faster to occur than that of cis-structure olefin, while the product rate will become smaller. This work should be of some significance for estimating the reaction rate and product rate in olefin separation.

	$\Delta^\ddagger E_1$ kJ·mol <sup>-1</sup>	$\Delta^\ddagger E_2$ kJ·mol <sup>-1</sup>	$\Delta E$ kJ·mol <sup>-1</sup>	$k_1$ l·mol <sup>-1</sup> ·s <sup>-1</sup>	Keq
C <sub>2</sub> H <sub>4</sub>	122.9	89.90	-3.706	1.177E-11	12.12
C <sub>3</sub> H <sub>6</sub>	125.0	101.8	4.165	8.428E-14	0.5066
1-C <sub>4</sub> H <sub>8</sub>	128.2	99.48	4.354	1.827E-14	0.4694
1-C <sub>6</sub> H <sub>12</sub>	130.2	104.9	10.11	1.684E-15	0.0461
2-tr-C <sub>4</sub> H <sub>8</sub>	127.5	108.7	19.32	1.351E-14	0.0011
2-cis-C <sub>4</sub> H <sub>8</sub>	135.8	105.7	17.14	3.514E-16	0.0027
3-tr-C <sub>6</sub> H <sub>12</sub>	135.4	113.8	20.58	2.515E-15	0.0007
3-cis-C <sub>6</sub> H <sub>12</sub>	140.1	110.2	19.31	2.113E-17	8.435E-6

Table 1: Thermodynamic and dynamic Parameters of the Reaction adding olefins to Ni dithiolene.

## References

- Wang, K. and Stiefel, E. I., (2001) *Science*, 291, 106-109.
- Terry, P. A., Noble, R. D., Swanson, D. and Koval, C. A., (1997) *AICHE Journal*, 43, 1709-1716.
- Fan, Y. B. and Hall, M. B., (2002) *J. Am. Chem. Soc.*, 124, 12076-12077.
- Harrison, D. J., Nguyen, N., Lough, A. J., and Fekl, U., (2006) *J. Am. Chem. Soc.*, 128, 11026-11027



## **Solubility of polyhydroxyalkanoates by Thermodynamic predictions**

Nicolas Jacquel <sup>a</sup>, Chi-Wei Lo, <sup>b</sup> Ho-Shing Wu, <sup>b,c</sup> Yu-Hong Wei, <sup>c</sup> Shaw S. Wang <sup>b,c</sup>

<sup>a</sup> *Department of Chemistry and Process Engineering, Ecole Supérieure de Chimie, Physique et Electronique de Lyon, France*

<sup>b</sup> *Department of Chemical Engineering and Materials Science, Yuan Ze University, Taoyuan, 32003, Taiwan*

<sup>c</sup> *Graduate School of Biotechnology and Bioinformatics, Yuan Ze University, Taoyuan, 32003, Taiwan*

### **1. Summary**

This paper presents and develop a thermodynamic model to predict the solubility of polyhydroxyalkanoates in solvents. This model combines a new way to evaluate the polymer solubility parameters and regressions between experimental solubility and solubility parameters. Important parameters which influence solubility such as temperature and polymer molecular weight have been studied. Some experiments have also been carried out on PHB-*co*-Hx copolymers of different contents. Finally, a model which takes into account these parameters have been established and tested on 232 experimental points. Results show that this method could be very useful for the selection of a solvent with high efficiency, low price and low toxicity.

Keywords: solubility, polyhydroxyalkanoates, solubility parameter, PHAs, modeling

### **2. Extended Abstract**

Nowadays, the plastic materials are taking an important place in product design and engineering. Their varied physical properties make them very convenient in applications. However, these non degradable plastics are accumulating in the environment at the rate of 25 million tones per year. That is why the replacement solutions like the using of biopolymers (biodegradable polymers) have been envisaged. On that purpose, different kinds of polyesters –polyhydroxyalkanoates (PHAs), polylactides (PLAs), aliphatic polyesters and polysaccharides– have been studied for the last eighty years. PHAs have some very interesting physical properties and biodegradability. In fact, they could be used in packaging as well as in medical applications due to their biocompatibility and slow hydrolytic degradation.

The method described in this paper, demonstrated that using solubility parameters can lead to an evaluation of the solubility of polyhydroxybutyrate (PHB) in various solvent

systems. Firstly, the polymer solubility parameters are evaluated by a novel method, which place the polymer in the solubility map as the barycentre of all the solvents. Secondly, the regression established between experimental solubility and solubility parameters can lead to an easy method for predicting solubility. Important parameters which influence solubility have been studied, and from the data collected some correlations have been made to take into account the impact of these parameters. The final correlation, which links solubility to the solubility radius (evaluated with solubility parameters), temperature, the polymer molecular weight and the Hx content, have been tested on 232 experimental points. The solubility models of PHB polymer and poly(3-hydroxybutyrate-*co*-hydroxyhexanoate) (PHB-*co*-Hx) copolymer were given as

$$s = (141.7 + 0.454 \exp(0.063T) + 292.8 \exp(-0.210 \times 10^{-4} \times Mw)) \exp(-0.692 r)$$

and

$$s = (20.06 + 100.6 \exp(12.3 \cdot X_{Hx}) + 0.454 \exp(0.063 \cdot T) + 292.74 \exp(-0.211 \cdot Mw)) \exp((-0.272 - 0.422 \exp(-1351 \cdot X_{Hx}))r)$$

in which  $s$  denotes the solubility of PHAs,  $T$  is temperature,  $Mw$  is molecular weight,  $X_{Hx}$  is Hx molar fraction and  $r$  is solubility radius, respectively. Results show that although accuracy of this method is not high, but give interesting results to do a solvent selection before testing. Using this method coupling with their prices and low toxicity, solvents could be selected from their efficiency in solubilizing the polymer. This solvent screening method could also be very useful for the elimination of undesirable impurity, such as the elimination of residual endotoxin in PHAs that are intended for use in used for medical applications.

## References

- Ojumu T.V., Yu J. and Solomon B.O., (2004) *Afr J Biotechnol*, 3:18-24
- Terada M., and Marchessault R.H. (1999) *Int J Biol Macromol*. 25, 207-215
- Wei Y.H., Lo, C.W. Chien, C.C., Kung, S.S., Liao, C.S., Sun, Y.M. and Wu, H.S., (2005), *Trends in Chemical Engineering*, 9, 27-42

## Speeds of Sound, Isentropic Compressibilities and Excess Molar Volumes of Mixtures of 1-Alkanol + Dibutyl Ether at 293.15, 298.15 and 303.15 K

I. Mozo, I. García de la Fuente, J.A. González, J.C. Cobos

*G.E.T.E.F., Departamento de Termodinámica y Física Aplicada, Facultad de Ciencias, Universidad de Valladolid, E-47071, Tel +34 983423740., e-mail: isaias@termo.uva.es; Valladolid (Spain); fax: +34 983423136*

### 1. Summary

Studies on excess functions of binary liquid mixtures have been performed to understand the molecular interactions between the solution components, as well as for engineering applications. As continuation of our previous works on thermodynamic properties of binary systems containing 1-alkanols which present intermolecular self-association due to the presence of –OH groups in the molecules with organic solvents, we present here the density and speed of sound, measurements for 1-butanol, 1-pentanol and 1-hexanol + dibutyl ether systems. The measurements were carried out at 293.15, 298.15 and 303.15 K and atmospheric pressure using a vibrating tube densimeter and sound analyser Anton Paar model DSA-5000. The data were used to calculate excess molar volumes, isentropic compressibilities and the thermal expansion coefficients. The excess molar volumes are negative over the whole mole-fraction range, and slightly asymmetrical. The minimum is skewed towards the region of high mole fraction of dibutyl ether as the 1-alkanol chain is increased. For the same value of mole fraction, these hardly change with the temperature and decrease as the alkyl chain length of 1-alkanol increases. The isentropic compressibilities values are negative in all range of mole fraction, and decrease when the 1-alkanol increases. This behaviour is due to the formation of hydrogen bonds between the –OH group of the 1-alkanols and the etheric oxygen of the dibutyl ether. Solutions involving ethers are of high interest because of the possibility of studying a number of effects (e.g. steric or proximity effects, cyclization) on the interactions present in the mixture. Binary systems of ethers and 1-alkanols are particularly interesting due to their complexity, resulting from the partial destruction of the self-associating alcohols by the active molecules of ethers, and of the new OH-O bonds created.

Keywords: densities, thermal expansion coefficient, compressibility, interactions, structural effects.

### 2. Extended Abstract

In alkanols + n-alkanes mixtures there are several opposing effects: changes in self-association and physical interactions (dipole-dipole) between alkanol multimers and monomers lead to an increasing of volume; a decreasing in volume is obtained by

changes of free volume and interstitial accommodation. The magnitudes of these contributions are sensitive to the lengths of components molecules. So, as the length of the 1-alkanol is increased, the negative effect accompanying the fitting of the n-alkanes molecules into the alkanol multimer structure becomes progressively more important, and predominates for sufficient long alkanol molecules.

In linear ethers + n-alkanes mixtures the dipole-dipole interactions between ether molecules are weakened by the addition of the alkane. In the alkanol + ethers mixtures taken into account there are also interactions between unlike molecules, i.e. the new OH-O bonds created, which contribute negatively to excess molar volume. For all the mixtures studied, the  $V_m^E$  decreases as the chain length of the 1-alcohol increases (from 1-butanol to 1-hexanol). The results are in agreement with data available in the literature[1-2], where  $V_m^E$  for 1-alkanols with linear monoethers increases from methanol to 1-propanol and then decreases. It suggests that for longer 1-alkanols, the interactional contribution is practically the same, while the structural effects increases. For 1-butanol mixtures, we note that  $dV_m^E/dT$  is positive. In the case of system with 1-pentanol  $dV_m^E/dT \approx 0$  and for 1-hexanol  $dV_m^E/dT < 0$ . The observed behaviour may be attributed, in the case of 1-butanol system to the more self-associated character of this alcohol (large number of broken H-bonds with increasing temperature). It seems that the negative contribution to  $V_m^E$  from free volume effects increases with temperature and predominates in the case of systems with 1-hexanol. However, it might occur that the interactional contribution become sufficiently important in such a way that the sign of  $dV_m^E/dT$  is inverted.

### References

- [1] Serna, A., García de la Fuente, I., González, J.A., Cobos, J.C. and Casanova, C., (1995) *Fluid Phase Equilibria* 110, 361-367.
- [2] Villa, S., Riesco, N., Carmona, F.J., García de la Fuente, I., González, J.A. and Cobos, J.C., (2000) *Thermochimica Acta* 362, 169-177.

### Acknowledgment

The authors gratefully acknowledge the financial support received from the Consejería de Educación y Cultura of Junta de Castilla y León, under Project VA080A60.

## Prediction of Speeds of Sound and Ultrasonic Studies of Hydroxyether + Organic Solvent Mixtures

J.A. González<sup>a</sup>, I. Mozo<sup>a</sup>, I. García de la Fuente<sup>a</sup>, J.C. Cobos<sup>a</sup>, N. Riesco<sup>b</sup>

<sup>a</sup>*Dpto. Física Aplicada, Facultad de Ciencias, Universidad de Valladolid, Valladolid, 470071 Spain*

<sup>b</sup>*Department of Chemical Engineering, Loughborough University, Loughborough, LE11 3TU Leicestershire, U.K.*

### 1. Summary

As a part of a systematic study of mixtures containing hydroxyethers [1,2], we present a comparison between predictions on speeds of sound from different models for this type of systems. There is a number of theories, based in the intermolecular free length concept, which provide speeds of sound values on the basis of different expressions of the available volume. Here, we have considered the free length theory (FLT) and the collision factor theory (CFT). In addition, we have also used empirical equations such as Nomoto's equation, Junjie's equation and the Van Dael's equation, the two latter based on the ideal solution concept for the isoentropic compressibility. The better results are obtained from Nomoto's and Junjie's equations. On the other hand, the Rao's constant varies linearly on the concentration. This indicates that there is no association between unlike molecules [3] in the studied mixtures and that the interactions are of dipolar type [2].

Keywords: predictions, speeds of sound, compressibilities, Rao's constant, interactions

### 2. Extended Summary

Results from the different models applied are collected in Table 1. The more accurate predictions are obtained using the Nomoto's and Junjie's equations, which provide very similar results. Larger deviations are obtained from the Van Dael's equation for the systems with propylamine, which can be ascribed to the strong interactions between unlike molecules present in such solutions. Interactions in the investigated mixtures are of dipolar type, which is supported by the linear dependence on the molar fractions of the component liquids of the Rao's and Wada's constant (Fig. 1)

### References

- [1] González, J.A., Cobos, J.C., Carmona, F.J., García de la Fuente, I., Bhethanabotla, V.R., Campbell, S.W. (2001) *Phys. Chem. Chem. Phys.*, 3, 2856-2865.
- [2] Mozo, I., García de la Fuente, I., González, J.A., Cobos, J.C. (2006) *J. Mol. Liq.*, 129, 155-163.
- [3] Armes, P.S. Geetha, D. Rakkappan, C. (2006) *J.Mol. Liq.*, 126, 69-71

TABLE

Mean standard relative deviations<sup>a</sup> for  $u$  of hydroxyether + organic solvent mixtures at temperature  $T$  obtained in this work from the different models applied.

System	FLT	CFT	Nomoto	Junjie	Van Dael
2-alkoxyethanol + octane <sup>b</sup>	0.0072	0.0138	0.017	0.0048	0.020
2-alkoxyethanol + dibutylether <sup>b</sup>	0.0127	0.009	0.009	0.0022	0.010
2-(2-alkoxyethoxyethanol) + dibutylether <sup>b</sup>	0.0123	0.0127	0.0113	0.0083	0.0147
2-{2-(2-alkoxyethoxy)ethoxy}ethanol + dibutylether <sup>b</sup>	0.0583	0.015	0.0133	0.0133	0.020
2-alkoxyethanol + dibutylether <sup>c</sup>	0.0180	0.009	0.009	0.0023	0.0133
2-(2-alkoxyethoxyethanol) + dibutylether <sup>c</sup>	0.0093	0.0127	0.0103	0.009	0.0143
2-methoxyethanol + polyether <sup>b</sup>	0.0712	0.0025	0.0028	0.0045	0.0372
alkoxyethanol + propylamine <sup>b</sup>	0.0362	0.0048	0.0088	0.032	0.0902

<sup>a</sup>calculated as  $\frac{1}{N_s} \sum \sigma_r(u)$ ,  $N_s$ , number of systems; <sup>b</sup>system temperature 298.15 K;

<sup>c</sup>system temperature, 303.15 K

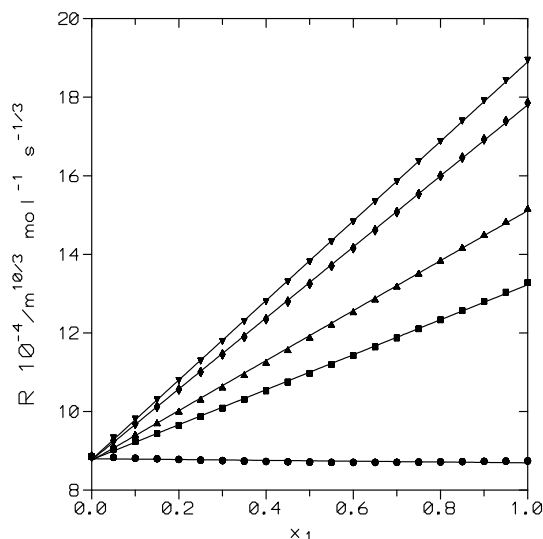


Fig. 1 Molar sound velocity,  $R$ , at 298.15 K for hydroxyether(1) + propylamine(2) mixtures. Points, experimental results using data from the literature: (●), 2-methoxyethanol; (■), 2-(2-methoxyethoxy)ethanol; (▲), 2-(2-ethoxyethoxy)ethanol; (▼), 2-(2-butoxyethoxy)ethanol; (◆), 2-{2-(2-methoxyethoxyethoxy)}ethanol. Solid lines, linear regressions.

### Acknowledgements

The authors gratefully acknowledge the financial support received from the Consejería de Educación y Cultura of Junta de Castilla y León, under Project VA080A06.

## **Determination of Cloud Points of Poly (propylene glycol) Aqueous Mixtures Using Particle Counting Method**

A. Eliassi\*, A. Parach

*Chemical Industries Research Department, Iranian Research Organization for Science and Technology (IROST), No. 71, Forsat Street, Enghelab Ave., Tehran, Iran*

### **1. Summary**

Cloud points of aqueous poly (propylene glycol) (PPG) mixtures at various concentration of PPG are determined using particle counting method. The number average molecular weight of the PPG is 2025 and its concentrations are changed from 1 up to 15 weight percents. In this method, initially an aqueous solution of PPG with a specified concentration at a specified temperature is made. At this condition, the number of particles in the solution is measured by a particle counter apparatus. Then by slowly increasing of the solution temperature, the number of particles is measured. The temperature at which a sudden increase in the number of particles is observed is noted as the cloud point. The increase of the particles is due to the formation of new liquid phase in the mixture. This procedure is repeated for various PPG concentration mixtures. We could determine the cloud point curve of the aqueous PPG mixture with an easy and rapid and precision method.

**Key Words:** Cloud Point, Particle Counter, Aqueous Polymer Solutions, Partial Miscibility

### **2. Extended Abstract**

Cloud point of a solution is temperature at which the solution becomes to formation of two phases. This phenomenon can be observed for some components which they have partial miscibility respect to each other. Determination of cloud point is very important from different point of view, such as designing of extraction apparatus and holding of a homogenous system at a stable condition respect to the composition of the system species. There are several methods for cloud point measuring. For example: visual observation [1], turbidimetry [2], light scattering [3], viscometry [4], thermo-optical methods [5] and so on. Particle counting method is a new method for cloud point measuring which has been introduced by Eliassi et al [6, 7]. The basis of this method for cloud point measuring is determining the number of particles in a mixture. Namely, when a new phase appears in a solution, this phase arise as a large number of small particles. At this time, the solution becomes cloudy due to the scattering of the light beam passing through the solution. So, if the number of particles in a solution is measured at various temperatures, it is expected that at the temperature where a new phase appear, a sudden change in number of particles would be observed and this temperature indicates the cloud point for the solution. A laser particle counter (Spectrex Corporation, Model PC-2000, United States), was used for particle counting. PPG2025 was prepared from Merk (Germany) and distilled water was used for preparing the solutions. All of solutions were prepared by mass, using an analytical balance with an accuracy of  $\pm 0.1$  mg. The samples compartment consists of a flow cell where PPG aqueous solution was

---

\* Corresponding Author e-mail: [alieliassi@yahoo.com](mailto:alieliassi@yahoo.com)

pumped by a pump to it from storage vessel kept at constant temperature water bath system. The temperature of the solution was recorded at the entrance of the cell by a thermocouple. The precision of the thermocouple was  $\pm 0.1^\circ\text{C}$ . The required time for determining the number of particles was 15 seconds. Therefore, the temperature of the water bath was changed and controlled by a thermostat with an appropriate rate to maintain the required temperature at the flow cell. At each temperature, the out put of the apparatus has been sent to a PC and finally the number of particles per cubic centimetre will be recorded by a printer.

Figure 1 shows the results of number of particles versus temperature for PPG2025+H<sub>2</sub>O mixture. Weight percent of PPG in this mixture is 10. According to this figure, on increasing the temperature of the solution from 7.1 to 8°C, the number of particles is nearly constant, but at 8.1°C, a sharp increase is observed which is due to appearance of first particles for formation of a new phase. Therefore, 8.1°C is recorded as the cloud point of this mixture. The similar experiments are done on 1%, 2%, 5% and 15% solution of PPG2025 in water. By using the obtained cloud point data we are able to draw the cloud point curve for the aqueous solution of PPG2025 from 0 up to 15 weight percent of PPG. This curve is shown in figure 2.

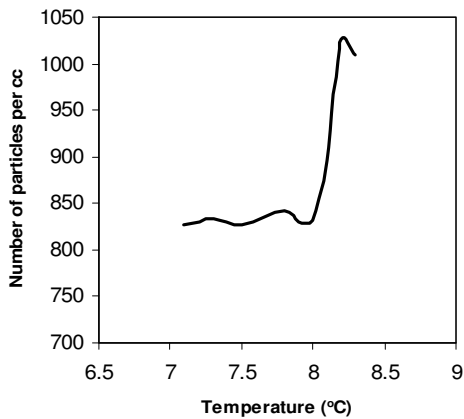


Figure 1- Number of particles versus temperature for a mixture of PPG2025+H<sub>2</sub>O (PPG%=10, H<sub>2</sub>O%=90).

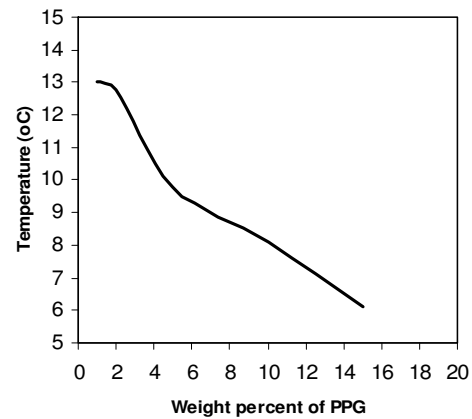


Figure 2- Cloud point curve of aqueous solution of PPG2025.

## Reference

1. Fischer, V., Borchard, W. and Karas, M., (1996) *J. Phys. Chem.*, 100, 15992.
2. Boutris, C., Chatzi, E. G. and Kiparissides, C., (1997) *Polymer*, 38, 2567.
3. Devanand, K. and Selser, J. C., (1991) *Macromolecules*, 24, 5943.
4. Nozary, S., Modarress, H. and Eliassi, A., (2003) *J. Appl. Poly. Sci.*, 89, 1983.
5. Bae, Y. C., Lambert, S. M., Soane, D. S. and Prausnitz, J. M., (1991) *Macromolecules*, 24, 4403.
6. Eliassi A., Modarress H. and Mansoori G. A., (2002) *Iranian J. Sci. Tech.*, 26, B2, 319.
7. Eliassi, A., Modarress, H. and Mansoori, G. A., *Study of Asphaltene Flocculation Using Particle Counting Method*, International Conference & Exhibition for Filtration and Separation Technology (FILTECH 2005), Germany (2005).



## **Application of the simplified PC-SAFT Equation of State to Complex Phase Equilibria of Ethylene Glycol Oligomers**

Andreas Grenner, Georgios M. Kontogeorgis, Nicolas von Solms, Michael L. Michelsen

*Center for Phase Equilibria and Separation Processes (IVC-SEP), Department of Chemical Engineering, Technical University of Denmark, DK-2800 Lyngby, Denmark*

### **1. Summary**

The final aim of this work is to obtain a model which can be used in the development of complex products such as pharmaceuticals, polymers, detergents and food ingredients. This type of modeling is challenging due to the complexity of the molecules involved. For equations of state of the SAFT type a major limitation is due to the procedure of obtaining pure compound parameters using vapor pressure and liquid density data. These data are, for complex compounds, often not available. One solution is to develop a group contribution scheme for PC-SAFT for estimating pure compound parameters from low molecular weight data and extrapolate to complex compounds. For associating compounds this is not trivial since the two parameters for association (association energy and volume) need to be fixed. In this work results will be presented for ethylene glycol oligomers with fixed association parameters. These compounds are widely used in petroleum and chemical industry e. g. ethylene glycol (MEG) is used to prevent gas hydrate formation and also as antifreeze, diethylene glycol (DEG) and triethylene glycol (TEG) are employed as dehydrating agent for natural gas, and tetraethylene glycol (TeEG) has been applied as extractant to produce high-purity aromatics. Also 1,2 propylenglycol (PG) was included in this study. New ethylene glycol oligomers parameters were estimated which yield good results for vapour-liquid equilibria (VLE) and liquid-liquid equilibria (LLE). All glycols are assumed to have four association sites. Complex VLE and LLE in binary systems with water, hydrocarbons, aromatics, methane and CO<sub>2</sub> were considered. Satisfying results were obtained in most cases. Various combining rules for the association parameters were applied in systems with solvation. The glycols + heptane LLE were studied; for MEG, DEG and PG very satisfying results were obtained while for TEG/TeEG + heptane larger deviations occur. In glycol + aromatics systems solvation was explicitly accounted for and very good results were obtained for glycol + aromatic LLE.



## **Modeling of Vapor-Liquid Equilibrium in Gas-Aqueous Electrolyte System using Neural Network Models**

Ahad Ghaemi,<sup>a</sup> Shahrokh Shahhoseini,<sup>b</sup> Mohammad Ghannadi Marageh<sup>c</sup>

<sup>a</sup>Department of Chemical Engineering, Iran University of Science and technology(IUST), Tehran, Iran

<sup>b</sup>Department of Chemical Engineering, Iran University of Science and technology(IUST), Tehran, Iran

<sup>c</sup>Jaber Ibn Hayan Research Laboratories, Atomic Energy Organization of Iran(AEOI), Tehran, Iran

### **1. Summary**

Solutions of weak electrolytes generally produce equilibrium systems with significant non-ideality and complexity due to the existence of ionic and molecular interactions. There are several equations reported in the literature to model equilibrium in electrolyte systems like Edward's model, three-parametric electrolyte-NRTL, UNIQUAC and UNIFAC. Several researchers have reported experimental data of NH<sub>3</sub>-CO<sub>2</sub>-H<sub>2</sub>O equilibrium system. These data are shown in Table 1 in different ranges of ammonia and carbon dioxide concentration liquid phase and temperature.

An artificial neural network (ANN), also called a simulated neural network or just neural network is an interconnected group of mathematical equation for information processing based on a connectionist approach to computation. . Figure 1 shows the architecture of the MLP with two hidden layers. Two neural network correlations for vapor-liquid equilibrium of electrolyte systems were developed based on an extensive database (Table 1). The model predictions were compared with the experimental data to calculate average relative deviation as a criterion to assess the model. The average relative deviations between the experimental data and calculated ammonia, carbon dioxide partial pressures and total pressure are less than 0.7%, 0.8%, 1.7% for both networks respectively, whereas average relative deviation of thermodynamic models is about 6% for the best reported cases

Keywords: VLE, Electrolyte, Neural network, Modelling, NH<sub>3</sub>-CO<sub>2</sub>-H<sub>2</sub>O system

### **2. Extended Abstract**

The literature contains several thermodynamic models that are presented to model NH<sub>3</sub> - CO<sub>2</sub> - H<sub>2</sub>O electrolyte system. Each of these models can reasonably predict the system only in a narrow rage of temperature, pressure or concentration. In this work, Multilayer Perceptron (MLP) and Radial Basis Function (RBF) artificial neural network (ANN) models were successfully used to model the system in a wide range of the conditions. The models were then validated employing an extensive vapor liquid equilibrium (VEL) database. The performance of these models to predict partial pressures of ammonia and carbon dioxide and the total pressure were evaluated by comparing their results with the experimental data, and the results of some

thermodynamic models. This comparison indicates that artificial neural networks are more accurate than other reported thermodynamic models.

### Vapor-liquid equilibrium (VLE) database of NH<sub>3</sub>-CO<sub>2</sub>-H<sub>2</sub>O system

Table 1: Equilibrium experimental data for NH<sub>3</sub>-CO<sub>2</sub>-H<sub>2</sub>O system

REFERENCES	Concentration, mole/ kg	
	H <sub>2</sub> O	
	NH <sub>3</sub>	CO <sub>2</sub>
Pexton and Bandger[9]	0-2	0.1-2
Badger and Wilson[10]	0.005-0.365	0.38-1.65
Van Krevelen et al.[7]	0.298-1.486	1.0-2.01
Otsuka et al.[11]	0.907-1.45	2.90-4.30
Takahashi [12]	1.4,8.5	6.5,21
Pawlikowski et al.[13]	0.3-1.5	0.5-2.3
Ellen M. et al.[14]	0.315-2.20	2.74-8.36
Ellen M. et al.[14]	0.851-5.44	3.12-9.57
Owens et al.[15]	0.268-0.864	1.14-2.354
Muller [16]	0.233-1.835	4.003-4.015
Muller[16]	0.644-3.07	7.65
Goppert et al.[17]	0-13	0-16
Muller et al.[18]	2-13	10-26
Kurz F. et al.[19]	0-9.69	6-12
Jadwiga Krop [20]	0.47-1.66	0.64-1.88
Jadwiga Krop [20]	0.39-0.97	0.6-1.8

Table 2: Performances and statistical tests of neural networks for NH<sub>3</sub>-CO<sub>2</sub>-H<sub>2</sub>O system

Networks	Neural regression stage	Mean relative deviation of parameter %		
		Total Pressure	NH <sub>3</sub> Pressure	CO <sub>2</sub> Pressure
MLP	Learning set	0.905	1.840	0.621
	Test set	0.549	1.705	0.654
	Whole data	0.681	1.617	0.589
RBF	Learning set	1.040	0.872	0.698
	Test set	0.779	1.646	0.824
	Whole data	0.469	0.903	0.595

### References

- G.R. Pazuki, H. Pahlevanzadeh, A. Mohseni Ahoeei, (2006) Fluid Phase Equilibria, 242,57–64,.
- Edwards, T.J., Newman, G., Newman, J. (1978) AIChE J.,24, 966-976,.
- Van Kervelen, D.W., Hoftijzer, P.J. and Huntjens, F. J. (1949),Rec. Trav. Chim. Pays-bas, 68, 91-216.
- Haykin S., *Neural networks A comprehensive Foundation*, Ontario, Canada, McMaster (1994).
- Thomsen K., Peter Rasmueesn(1999), Chem. Eng. Sci., vol. 54, pp. 1787-1802.

## Modelling lubricating oil fractions by means of a pseudo-component model

Juan J. Espada,<sup>a</sup> Baudilio Coto,<sup>a</sup> Rafael van Grieken,<sup>a</sup> José L. Peña<sup>b</sup>

<sup>a</sup>*Department of Chemical and Environmental Technology, Rey Juan Carlos University, E-28933 Móstoles (Madrid), Spain.*

<sup>b</sup>*Repsol-YPF, Alfonso Cortina Technology Centre, Móstoles (Madrid), E-28933, Spain.*

### 1. Summary

In the lubricating oil manufacturing process from vacuum distillates, the aromatic content is reduced by solvent extraction, frequently with furfural. These mixtures present very complex composition which makes difficult the description of the liquid-liquid equilibrium involved. In this work, a previously reported generalized model based on NRTL thermodynamic model and three pseudo-components was applied to model the aromatics extraction by furfural from SPD and HND lubricating oils. Extraction operation was simulated using AspenTech<sup>®</sup> and the generalized model. Physical properties (density and refractive index at 20°C) for the involved mixtures were calculated and compared to those values obtained by other methods reported showing similar accuracy.

Keywords: Aromatics extraction, furfural, liquid-liquid equilibrium, lubricating oil

### 2. Extended Abstract

The generalized model developed by Coto et al. was applied to SPD and HND lubricating oils with average boiling point ( $T_{50\%}$  ASTM D1160 standard test method) of 378°C and 528°C, respectively. The pseudo-component properties, the composition and the NRTL parameters were calculated for the selected lubricating oils from  $T_{50\%}$  and the relations proposed by Coto et al. Several experiments were carried out for SPD and HND lubricating oils by modifying the temperature and the furfural/feed ratio. To check the accuracy of the predictions obtained from the model, such experimental conditions were simulated with a commercial simulator, Aspen Plus<sup>®</sup>, and the generalized model.

Density ( $D_{20}$ ) and refractive index ( $RI_{20}$ ) both at 20°C, of each mixture (feed, raffinate and extract) for SPD and HND were calculated according to the mixing rule proposed by Coto et al. using the pseudo-component properties and the compositions in saturates, aromatics and polars obtained by simulation. Likewise, such properties were calculated through other methods reported in the literature. Figure 1 shows the comparison between experimental and calculated values for the selected properties using different methods. Density predictions by the methods proposed by Riazi-Daubert, Riazi-Roomi, and API are very similar, and all of them underestimate slightly such property. Values obtained with the method by Gomez and

the reported in this work based on the pseudo-component properties are the most accurate, showing no systematic deviations. Both methods consider the nature of the mixture and this results essential in the improvement of the prediction of density. Similar results were obtained for the predictions of  $RI_{20}$  as it is shown in Figure 1. The methods proposed by Riazi-Daubert and Riazi-Roomi underestimate the experimental values. However, no systematic deviations were found by using the generalized model based on pseudo-components.

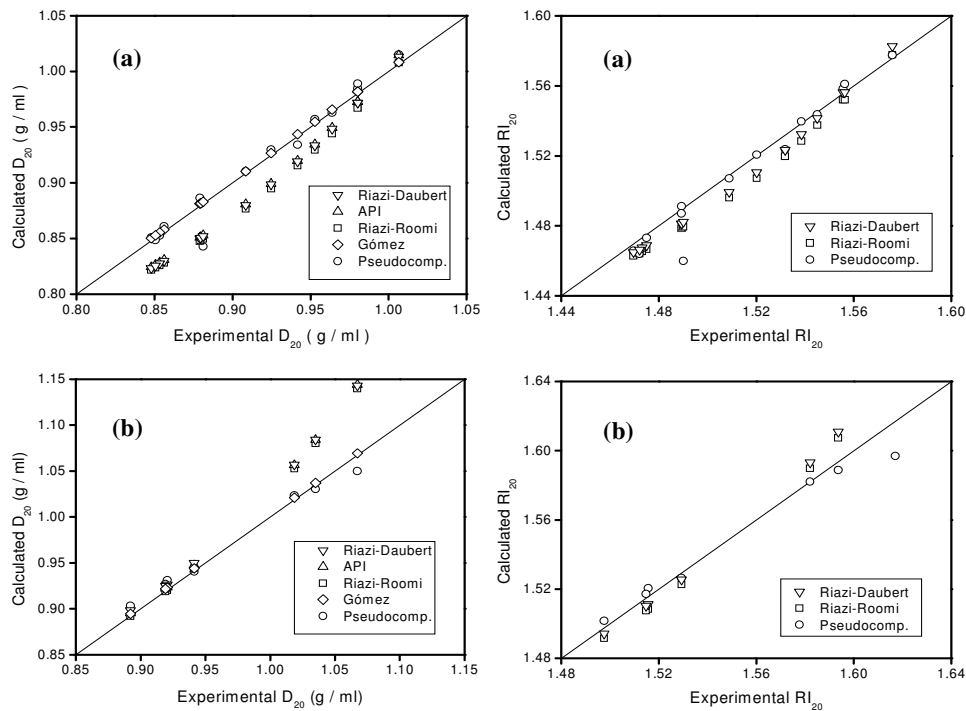


Figure 1. Comparison between experimental and calculated values for  $D_{20}$  and  $RI_{20}$  obtained by different methods. (a) SPD; (b) HND.

The generalized model predictions for the selected properties are of similar or better accuracy to other reported methods. This model can be applied to both light and heavy lubricating oils with similar accuracy. Furthermore, it is easier to apply than other methods, and it is fully predictive since only  $T_{50\%}$  and composition of the feed are required.

## References

Coto, B., van Grieken, R., Peña, J. L., Espada, J. J., (2006) *Chemical Engineering Science*, 61, 8028-8039.

Gomez, J. V., (1989). *Oil & Gas Journal*, 90, 49-52.

Riazi, M. R., *Characterization and Properties of Petroleum Fractions*, ASTM, USA (2005).

## **Develop a correlation of convective coefficient in a vertical evaporator with boiling processes inside pipes where the flow is stagnant**

**Juan C. García,<sup>a</sup> Juan F. León,<sup>a</sup> Jon A. Aguinaco,<sup>a</sup>**

<sup>a</sup>*Department of Chemical Engineering, School of Chemical Engineering, Faculty of Engineering University of Carabobo, 2001 Valencia, Venezuela*

### **1. Summary**

Actually there are many correlations to determinate the convective coefficient in boiling processes, condensation and processes without change phases. Nevertheless, a reliable correlation does not exist for vertical evaporators with boiling processes inside pipes where the flow is stagnant, reason which an average correlation of convective coefficient is require for processes inside pipes. This coefficient involve three processes: First, where there is a sensitive heat transference (Sub-cooling zone). Second there is latent heat transference (Stagnant boiling inside pipes) and third one there is sensitive heat transference (Overheating zone).

Keywords: *convective coefficient, heat transfer, boiling processes.*

### **2. Extended Abstract**

In order to determinate the number of experiment for the correlation was used a factorial design and them a statistical tool in order to reduce the number of experiment. On the other hand, the selection of the parameters involved in the correlation was relied in studies developed before where was determinated that the dimensionless parameters of a boiling processes and condensation are getting with utilization of Buckingham Theorem. For both processes the convection coefficient can depend for the difference between surface temperature and saturation,  $\Delta T = |T_w - T_{sat}|$ , the body force that arises from the difference between density liquid-steam,  $g(\rho_L - \rho_V)$ , latent heat  $h_{fg}$ , superficial tension  $\sigma$ , typical length  $L$  and the properties thermo physical from the liquid or steam:  $\rho, Cp, k, \mu$ . Additional for these particular case was added the mass flow ( $\dot{m}$ ), internal diameter of pipes ( $D_i$ ) and the level of liquid in the same ones ( $N_L$ ).

For the establishment of the define correlation was realize a lineal regression of the data, In which the exponents were modified for the diverse of dimensionless groups resting on existing correlations for reservoir boiling processes and forced convection for internal flow. Also, for every exponents supposition the quotient calculated between the experimental convective coefficient and the obtained one by the combination of  $\pi$  groups. (proportional constant) which must be a constant value for the diverse conditions, in such a way that having incorporated the above mentioned value in the correlation the equality was fulfilled to the diverse conditions. Nevertheless, for a relation of groups a particular behavior was observed. The

quotient between the experimental convective coefficient and the obtained for the combinations of  $\pi$  groups in the different conditions changes. However the above mentioned quotient keep constant value under conditions where the level of liquid inside pipes from the evaporator is equal, of such form an expression was realized where there is obtained a relation of this constant from the dimensionless group that involves water level in order to include this expression and obtain a definite correlation that represents the convective coefficient.

After incorporated this expression the definitive correlation is obtained.

$$h = 0,0083 \frac{k}{Di} \cdot \frac{L}{Di} \cdot \text{Re} \cdot \frac{h_{fg} \cdot \mu}{k \cdot \Delta T} \cdot \left( \frac{g \cdot (\rho_L - \rho_V) \cdot D^2}{\sigma} \right)^{1/4} \cdot \left( \frac{g \cdot \rho_V \cdot (\rho_L - \rho_V) \cdot Di^3}{\mu^2} \right)^{-1/2} \cdot \left( \frac{N_L}{Di} \right)^{-0,0008} \cdot \text{Pr}$$

Restrictions:

Vertical Cylinder

$$27 < \text{Re} < 240$$

All the properties involved in the previous expression are evaluated as liquid saturated to the saturation temperature, with the exception of the parameter, which is evaluated under the condition of saturated steam.

Due to the fact that the study for the determination of the correlation had certain limitations with the involved parameters it is suitable to introduce some restrictions that must be fulfilled in order to assure the reliability of the correlation showed previously. As it is observed, the correlation is used in vertical pipes where the water is stagnant and involves a process of boiling; in addition, the Reynolds number must be inside the notable range.

On the other hand, in order to assure the predictive power of the correlation there were realized a series of random experiments from which the convective coefficient was calculated, being the maximum deviation reported 1,70 %.

Finally, the following figure will show itself the behavior of the convective coefficient (obtained experimentally and across the new correlation) for the different conditions. In this figure there is verified that the correlation has been predicted close from the real values due to the results obtained by both methods are very similar.

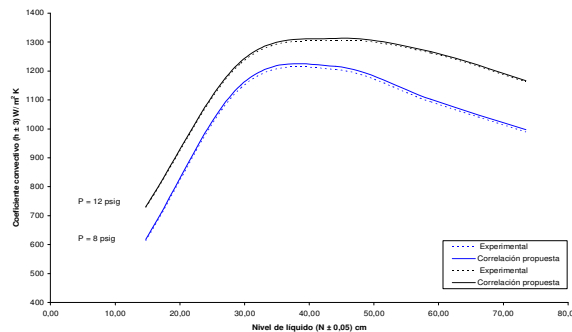


Figure 2 Behavior of the coefficient to different conditions

## References

- Incropera, F. P y DeWitt, D., *Fundamentos de transferencia de calor*, Editorial Prentice Hall, MX (1999).  
 Kern, D., *Procesos de transferencia de calor*, Editorial Continental, MX (1981).



## Prediction of Binary Adsorption Equilibria

M.A. Monsalvo,<sup>a</sup> A.A. Shapiro,<sup>a</sup>

<sup>a</sup>*Center for Phase Equilibria and Separation processes IVC-SEP, Department of Chemical Engineering, Technical University of Denmark, Building 229, DK-2800 Lyngby, Denmark*

### 1. Summary

The goal of this work is to extend the Multicomponent Potential Theory of Adsorption (MPTA) onto liquid mixtures. Comparison with experimental data shows good agreement and high degree of predictability.

Keywords: adsorption, potential theory, liquid mixtures, porous solids

### 2. Extended Abstract

In this work, we study the adsorption of liquid mixtures on porous solids on the basis of the MPTA (Shapiro and Stenby, 1998). The MPTA is based on the potential concept originally developed by Polanyi. In this theory the driving force for physical adsorption is measured by the adsorption potential that is a function of the distance from the solid surface. In this way, the adsorbate is considered as a heterogeneous substance segregated in the external field emitted by the adsorbent, with thermodynamic parameters that are function of the distance from the solid. The MPTA then uses a thermodynamic model to describe the equilibrium between bulk and adsorbed phases, and potential models for the fluid-solid interactions. With this approach few parameters are needed to predict adsorption equilibria. The MPTA has been so far used to successfully predict adsorption equilibria of multicomponent gas mixtures (Monsalvo and Shapiro, 2007). In spite of its industrial importance, adsorption from the liquid phase has been studied less extensively than adsorption from the gas phase, both experimentally and theoretically. The aim of this work is to extend the MPTA onto adsorption from liquid solutions.

#### 2.1 Description of the model and results

Adsorption is represented as a segregation of the mixture in the potential field emitted by the surface of the adsorbent. Each (*i*th) component of the mixture is affected by its own adsorption potential  $\varepsilon_i(z)$  depending on the distance *z* to the surface. An equilibrium state at a given temperature in the potential field is described by the equality of chemical potentials  $\mu_i$ :

$$\mu_i(P(z), x(z)) - \varepsilon_i(z) = \mu_{iB}(P_B, x_B) \quad (1)$$

Given pressure  $P_B$  and composition  $x_B$  in the bulk phase, the distributions of pressure and mole fractions along  $z$  are uniquely determined by system 1. In the case of adsorption in micropores, the variable  $z$  denotes the porous volume. Instead of the dependence  $\varepsilon_i(z)$ , the distribution of the porous volume by the value of potential  $z(\varepsilon_i)$  ( $\text{cm}^3/\text{g}_{\text{adsorbent}}$ ) is considered. This distribution can be obtained by the generalized Dubinin-Astakhov dependence (Stoeckli, 1998). The characteristic parameters of this dependence are the total pore volume  $z_0$  and the characteristics adsorption energy  $\varepsilon_{0i}$ :

$$z(\varepsilon_i) = z_0 \text{Exp}\left(-(\varepsilon_i / \varepsilon_{0i})^2\right) \quad (2)$$

Then the surface excess  $n_i^e$ , is calculated as (Shapiro and Stenby, 1998):

$$n_i^e = \int_0^\infty [\rho(z)x_i(z) - \rho(z)x_{Bi}] dz \quad (3)$$

Predictions of binary liquid adsorption equilibria are presented in Figure 1. The mixtures are thermodynamically described by the SRK equation of state. Fig. 1a shows adsorption isotherms at different temperatures on activated carbon. It can be seen that a good qualitative and quantitative agreement is obtained. An example of not-so-successful correlation is given by Fig. 1b. The MPTA can describe the mixture qualitatively well; however the match with experimental points is not very satisfactory. This may suggest that more advance thermodynamic models are required. Further testing of the theory and its combination with other thermodynamic models is necessary.

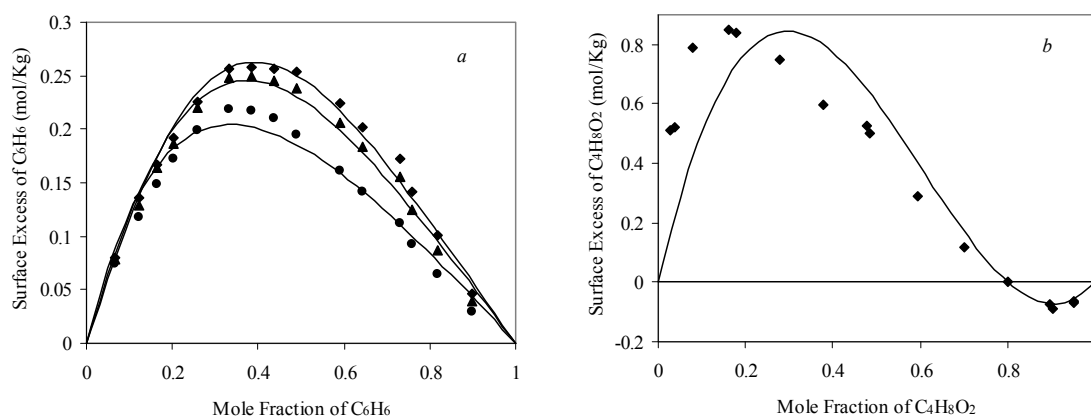


**Figure 1a** - Adsorption of  $\text{C}_6\text{H}_6$  on activated carbon from  $\text{C}_2\text{H}_5\text{OH}$  at:  $T = 283 \text{ K}$  ( $\blacklozenge$ ),  $T = 298 \text{ K}$  ( $\blacktriangle$ ), and  $T = 333 \text{ K}$  ( $\bullet$ ). **Figure 1b** - Binary adsorption isotherm of  $\text{C}_4\text{H}_8\text{O}_2 + \text{C}_6\text{H}_{12}$  at  $T = 303.15 \text{ K}$  on activated carbon. The full line (—) corresponds to the MPTA model + the SRK EoS.

## References

Monsalvo M., Shapiro A., (2007) *Fluid Phase Equilib.* 254, 91-100.

Shapiro A., Stenby E.H., (1998) *J. Colloid interface Sci.* 201, 146-157.

Stoeckli F., (1998) *Carbon* 36, 363-368.

## Group-contribution based method for surface tension estimation

Ana Martinho,<sup>a,b</sup> Henrique A. Matos,<sup>a</sup> Rafiqul Gani,<sup>b</sup>

<sup>a</sup> CPQ, Dept. of Chem. Eng. & Bio, Instituto Superior Tecnico, 1049-001 Lisboa, Portugal

<sup>b</sup> CAPEC, Dept. of Chem. Eng., Denmark Technical University, DK-2800 City, Lyngby, Denmark

### 1. Summary

A new method for surface tension estimation of pure organic compounds is presented. This property is estimated at 298 K through a group contribution (GC) based method working at three levels: the basic level that describe a wide variety of organic compounds, while second and third levels that provide additional structural information of the molecule, which the first order group is unable to provide. This GC-based method is therefore based on the molecular structure of the compound and is able to distinguish among some isomers through the higher than first order groups. Group contributions for surface tension (95, 42 and 8 for first, second and third order groups, respectively) have been regressed using a collected set of experimental data consisting of more than 420 compounds including C, H, N, O, F, Cl, Br and S atoms, some of which are complex polycyclic compounds. Compared to the currently used methods for surface tension estimation, this GC-based method provides a significant improvement both in accuracy and applicability.

Keywords: surface tension, group-contribution parameters, organic compounds

### 2. Extended Abstract

In this method, surface tension is based in Marrero & Gani estimation method by considering that each compound can be described by three types of group contribution sets: first-order groups, second-order group and third-order order groups.

The surface tension estimation model has the form of the following equation:

$$(\gamma - \gamma_0) = \sum_i N_i C_i + \sum_j M_j D_j + \sum_k O_k E_k \quad (1)$$

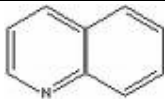
Where,  $\gamma$  is surface tension ( $\text{dyn.cm}^{-1}$ ) and  $\gamma_0$  is additional adjustable parameter or universal constant, equal to  $19.508 \text{ dyn.cm}^{-1}$ .  $C_i$ ,  $D_j$ ,  $E_k$  are the contributions of the first order group of type  $i$ , second order group of type  $j$  and third order group  $k$

( $\text{dyn.cm}^{-1}$ ), which are determined through a regression procedure, and  $N_i$ ,  $M_j$ ,  $O_k$  are the number of times that  $C_i$ ,  $D_j$  and  $E_k$  groups occurs, respectively.

Compared to other currently estimation methods for surface tension, the proposed one exhibit a great accuracy comparing with Sudgen method. Comparing with QSPR model the results are similar, however Marrero & Gani estimation present advantages in terms of accuracy for the most complex compounds and a faster, simpler and less resources need estimation response.

Table 1 shows an application example of the proposed estimation method. The compound in study is Quinone that belongs to nitrate hydrocarbons family, and has contributions of 1<sup>st</sup> and 3<sup>rd</sup> order

**Table 1-** Surface tension estimation for Quinone

<b>Quinone</b> Cas: 91-22-5 Molecular Formula: $C_9H_7N$				<b>Exp. Value</b> <b>(<math>\text{dyn.cm}^{-1}</math>)</b> <b>42.59</b>
First Order Group	Contribution <sup>(1)</sup>	Occurrences	Total	
ACH	1.453	7	22.396	
AC	1.683	2		
AN	8.858	1		
$\gamma = (22.396) + 19.505 = 41.902 \text{ dyn.cm}^{-1}$				
Relative Deviation				1.616%
Second-Order Group	Occurrences	Contribution	Total	
No group contributions of second order				
Third-Order Group	Contribution <sup>(1)</sup>	Occurrences	Total	
AROM.FUSED[2]	1.344	1	0.688	
PYRIDINE.FUSED[2]	-0.655	1		
$\gamma = (22.396 + 0.688) + 19,505 = 42.590 \text{ dyn.cm}^{-1}$				
Relative Deviation				0.000 %

(1) This surface tension group contribution were determined by Martinho *et al*, 2007

This model allows the prediction of surface tension of a wider variety of organic compounds by considering the strategy of group contribution. The comparison of the surface tension predicted value with experimental data is in very good agreement.

## References

- Delgado, E.J., Diaz, G.A., *SAR and QSAR in Enviromental Research*, 17 (2006) 483-496;
- Marrero, J., Gani, R., *Fluid Phase Equilibria*, 183-184 (2001) 183-208;
- Martinho, A , Matos, H.A., Gani,R., *Fluid Phase Equilibria*, (submitted for publication), 2007
- Poling, B. E., Prausnitz, J. M., O'Connell, J.P., *The properties of gases and liquids*, 5<sup>th</sup> ed., McGraw Hill, USA (2001);

## **Experimental data and correlation of surface tension of binary polymer solutions at different temperatures and atmospheric pressure**

M.Taghizadeh Mazandarani,<sup>a</sup> A.Eliassi,<sup>b</sup> M.Fazlollahnejad<sup>a</sup>

<sup>a</sup>*Chemical Engineering Department, Faculty of Engineering, Mazandaran University, P.O.Box:484, Babol, Iran, E-mail: [taghizadehfr@yahoo.com](mailto:taghizadehfr@yahoo.com), Tel: +98111-3234204, Fax: +98111-3234201*

<sup>b</sup>*Chemical Industries Research Department, Iranian Research Organization for Science and Technology (IROST), Tehran, Iran*

### **1. Summary**

Thermophysical properties are required both for engineering and product design. The surface tension of a liquid mixture is an important property which plays an important role in affecting the mass and heat transfer at the interface. In recent years, aqueous polymer solutions, especially poly(ethylene glycol) + water systems, have found widespread applications, mostly because of their use in two phase aqueous systems for separation of biomolecular mixtures. Despite the success of the aqueous two phase separation technique, data on the properties of phase systems that are necessary for the design of extraction processes and for the development of models that predict phase partitioning are few. Although reviewed surface tensions of pure liquid polymers are available, but experimental data for polymer solutions are extremely scarce. In this work, the surface tension ( $\sigma$ ) of aqueous solutions of various PEGs (poly ethylene glycol) with molecular weights of 200, 300 and 6000 in water and of poly(propylene glycol) (PPG) with a molecular weight of 2000 in ethanol were measured in the (293.2-338.2) K temperature range and atmospheric pressure. The results of measurements were fitted to linear equation relating surface tension of the solution to the mass fraction of polymer and the solution temperature. The coefficients of the equation are determined by linear multiple regression and the model results are compared with experimental data so that the absolute overall average mean relative deviation of the model is less than 0.55% for PEGs and 0.74% for PPG2000.

Keywords: Surface tension, polymer solution, correlation

## 2. Extended Abstract

**2.1. Materials.** Poly(ethylene glycol) with number-average molecular weights of 200 and 300, manufactured by Merk, and 6000, manufactured by Fluka, and Poly(propylene glycol) with a number-average molecular weight of 2000, manufactured by Riedel-deHaen, and ethanol absolute GR(>99.8%), manufactured by Merk, were used in this study. Double-distilled water was used in making the solutions.

**2.2. Apparatus and procedures.** The solutions were prepared by mass, using an analytical balance with +0.1 mg accuracy. The surface tension measurements were carried out using a tensiometer model K9 Kruss, Germany at temperatures of (298.2, 308.2, 313.2, 318.2, 328.2, and 338.2) K and atmospheric pressure. A constant temperature water bath was used to control the temperature of the solutions to an accuracy of +0.1 K. Each measurement was repeated five times and the surface tension data are fitted by the following relation:

$$\sigma(\text{mN/m}) = a + bw + cT(\text{K}) \quad (1)$$

where  $\sigma$  is the surface tension of the solution at the measured temperature, a, b and c are the coefficients of the equation, w is the mass fraction of polymer in the solution and T is the solution temperature. Values of the coefficients a, b and c were obtained by regression and reported in table 1.

**Table 1: coefficients of equation 1 for solutions of PEG (200, 300, and 6000) and PPG 2000**

a	b	c	r	RD%	ARD%
-0.1891	-20.8411	<b>PEG200</b> 68.0506	0.9959	-0.01422	<b>PEGs</b>
68.2448	-29.9762	<b>PEG300</b> -0.1944	0.9961	0.003634	0.545753
65.8374	-19.5177	<b>PEG6000</b> -0.2073	0.9968	0.029023	
23.35925	3.9983	<b>PPG2000</b> -0.0779	0.9881	0.0792164	<b>PPG</b> 0.742002

$$\text{RD}\% = \frac{100}{n} \sum \frac{\sigma_{\text{model}} - \sigma_{\text{exp.}}}{\sigma_{\text{exp.}}}, \quad \text{ARD}\% = \frac{100}{n} \sum \left| \frac{\sigma_{\text{exp.}} - \sigma_{\text{mod.}}}{\sigma_{\text{exp.}}} \right|$$

## References

- Baljon, A. R. C., Robbing. M. O., (2001) *J. Macromolecules*, 34, 4200.  
 Sauer, B. B., Dee. G. T., (2002) *J. Macromolecules*, 35, 7024.  
 Dan, N., (2000) *Langmuir*, 16, 4045.  
 Rahbari-Sisakht, M., Taghizadeh, M., Eliassi, A., (2003) *J. Chem. Eng. Data*, 48, 1221-1224.  
 Ho Sang Lee and won HO. JO, (1998) *J. Polymer*, 39, 2489.  
 Takuhei Nose and Naoe Kasemura, (1998) *J. Polymer*, 39, 6137.  
 Daniel Broseta, (1990) *J. Macromolecules*, 23, 132.

## **Thermodynamics of pervaporation process in reacting systems**

Alexander Toikka, Anastasia Penkova

*Department of Chemical Thermodynamics and Kinetics, Saint-Petersburg State University,  
Universitetskiy pr. 26, 198504, Saint-Petersburg, Russia*

### **Summary**

Pervaporation (evaporation through membrane) is a membrane process that has significant advantages for liquid separation in industry. The aim of this paper is to present some aspects of the thermodynamic approach of pervaporation. First of all the advantages of nonequilibrium thermodynamics are discussed. The thermodynamic–kinetic approach for the analysis of pervaporation in reacting systems is presented. The topological structure of diagrams of pervaporation of multicomponent systems, including reactive ones is considered. Experimental examples of pervaporation in reacting systems are presented and discussed.

**Keywords:** thermodynamics, membrane, pervaporation, reacting systems, nonequilibrium processes

Pervaporation is one of the main membrane separation processes with great advantages for the industrial application. The most widely utilized mode of operation is a vacuum pervaporation when the pressure gradient in membrane system exists. Because of it the pervaporation system should be considered as nonequilibrium system; accordingly the capacity of the use of classical thermodynamic methods (equilibrium approach) is rather limited. In the case of reacting systems the complexity of the analysis of pervaporation process increases. Nevertheless thermodynamic methods combined with kinetic approach and nonequilibrium theory give good opportunities for the analysis of such complex systems. In presented paper some aspects of thermodynamic theory of pervaporation and its application to reacting systems are considered.

Nonequilibrium approach for the thermodynamic analysis of membrane process including pervaporation is well-known. Kedem (1986, 1989) was one of the first who introduce some elements of nonequilibrium thermodynamics in the theory of pervaporation. First of all the theory was applied for the description of the coupling between fluxes. Unfortunately the further development of the thermodynamic theory of pervaporation was not so intensive and only few works of last decade were based on nonequilibrium thermodynamic approach.

Our consideration of pervaporation in reacting systems is based on the combined thermodynamic and kinetic method with the use of nonequilibrium theory. For the small fluxes (usual for the pervaporation) and the fast reaction the feed solution can be considered as a system in a chemically equilibrium state. Accordingly the residue curve map of reactive pervaporation process (similar to simple distillation of reactive mixtures) may be presented with the use of transformed concentration variables (Zharov, 1970, Barbosa and Doherty, 1987). For the fluxes we apply classical phenomenological equations (linear phenomenological laws). These equations are also used for the prediction of permeate compositions and the modeling of the process. In the case of low reaction rate additional parameters similar to Damköhler number can be taken into account.

The pervaporation process significantly depends on the nature of membranes and compounds of feed solutions. For example the sorption (the initial stage of pervaporation) can be considered as an equilibrium process if the rate of diffusion through membrane is low. In this case the data on equilibrium sorption were applied for the analysis of membrane mass transfer. Some example will be given on the base of our experimental data.

The brief review of the data on reactive pervaporation and the analysis of further opportunity of application and advantages of the thermodynamic approach for the study of pervaporation process in reacting systems will be presented.

**Acknowledgement.** This research was supported by Russian Foundation for Basic Research (grant 06-03-32493).

## References

- Kedem, O., (1986) in: R. Bakish (Ed.): *Proceedings of the First International Conference on Pervaporation Process in Chemical Industry*, P111.
- Kedem, O., (1989) *Journal of Membrane Science*, 47, 277-284.
- Zharov, V.T., (1970) *Zhurnal Fizicheskoi Khimii*, (*Journal of Physical Chemistry, USSR*), 44, 1967-1974.
- Barbosa, D., Doherty, M.F., (1987) *Proceedings of the Royal Society of London, Series A*, 413, 459-464.



## **On the stability analysis of phase diagrams of multicomponent systems**

Alexander Toikka, Richardas Ralis

*Department of Chemical Thermodynamics and Kinetics, Saint-Petersburg State University,  
Universitetskiy pr. 26, 198504, Saint-Petersburg, Russia*

### **Summary**

The calculation methods based on stability conditions are the strict thermodynamic approach that are significantly differ from more rife ones (i.e. methods based on fundamental equations such as Gibbs–Duhem relationships). One of the advantages of stability conditions is the opportunity to predict the properties of multicomponent mixtures on the base of binary data without model calculations. Stability conditions are thermodynamic inequalities; accordingly the results of their applications have the form of inequalities: e.g. the limitations on the values of thermodynamic properties (possible diapason of values) could be founded. In this lecture we consider some forms of thermodynamic inequalities and methods of the analysis of phase diagrams based on stability conditions; the new alternative approaches for calculation are discussed.

Keywords: thermodynamic stability, phase diagrams, multicomponent systems

The thermodynamic stability conditions can be directly used for the analysis and testing of equilibrium data. The significance of stability conditions is well known but the practical usage was limited by the capacities of computation methods. Due to the development of the computer technique the new possibilities of the use of stability conditions have been appeared; accordingly a number of papers on this topics were presented in scientific journals in recent years. The brief review and comparison of thermodynamic methods based on stability conditions and some new methods of the analysis of phase diagrams are considered in the present lecture.

Stability conditions give few ways for the analysis of phase equilibrium diagrams, mainly: 1. the problem of phase splitting; 2. the test of intrinsic agreement of thermodynamics data; 3. the limitation on the values of thermodynamics parameters. These applications of stability conditions are discussed in presented paper.

i. Michelsen, 1982, formulated one of the most known approaches to the first item (phase splitting or a number of equilibrium phases) as a solving of a flash problem. Michelsen's tests are based on Gibbs tangent plane criterion: e.g. condition

of convexity for the surface of internal energy. Some forms of equations of states are used for the calculations.

ii. For the test of the intrinsic agreement of experimental data the stability conditions can be used directly. The test consists of the substitution of the data for any pairs of states in stability condition equations (inequalities). In spite of the seeming simplicity of the test procedure some optimization procedure is needed (due to the great variety of the states to be compared). The examples of such calculation are presented in the lecture.

iii. For the estimation of the limitation on the values of thermodynamics parameters one should choose the states to be a base for calculation (reference states). For example, one can calculate the limitation on the parameters of multicomponent system using binary data. The variety of such kinds of computation is rather wide: e.g. a concentration limitation on the ternary azeotrope composition, etc. In a general case of  $n$ -component vapor–liquid or vapor–liquid–liquid systems the limitations on the composition or other properties could be determined on the base of the data on  $k$ -component sub-systems ( $k = n - 1, n - 2, \dots$ ) or another reference states. Limitations for other types of systems (including non-reactive and reactive) are determined in the similar way. For such calculations of the “limiting values of the equilibrium thermodynamic variables” we used the approach by Toikka and co-workers (e.g. see the review article by Toikka and Jenkins, 2002). In presented paper we propose the new calculation procedure that could be useful for practical applications.

One of significant advantages of stability analysis is the possibility to compare the properties of the system under different conditions. The most known relationship is the one for the heat capacity at constant pressure or volume. The general case is analogous to this one. The results could be presented as chains of inequalities for second derivatives of thermodynamic potentials under different conditions. Of practical interest is the following limiting case: the initial state is a single-phase state but the second phase can arise. It follows from stability conditions that the transition from a homogeneous region of the phase diagram to the heterogeneous one is accompanied by the jump in the value of these second derivatives. This conclusion can be compared with some known results for configuration effects and heat capacities. The analogous thermodynamic inequalities for the systems with chemical reactions also follow from the stability criteria.

In conclusion new examples of calculations of limiting values of thermodynamic variables based on the application of stability conditions are presented.

**Acknowledgement.** This research was supported by Russian Foundation for Basic Research (grant 06-03-32493).

## References

Michelsen, M.L., (1982) *Fluid Phase Equilibria*, 9, 1-19.

Toikka, A.M., Jenkins, J.D., (2002) *Chemical Engineering Journal*, 89, 1-27.

## **Correlations for predicting solution gas-oil ratio, bubblepoint pressure and oil formation volume factor at bubblepoint of Iran crude oils**

M.Taghizadeh Mazandarani , S. Mohammad Asghari

*Chemical Engineering Department, Faculty of Engineering, Mazandaran University, P.O.Box:484, Babol, Iran, E-mail: [taghizadehfr@yahoo.com](mailto:taghizadehfr@yahoo.com), Tel: +98111-3234204, Fax: +98111-3234201*

### **1. Summary**

Knowledge of the PVT parameters is a requirement for all types of petroleum calculations such as determination of hydrocarbon flowing properties, predicting future performance, designing production facilities and planning methods of enhanced oil recovery. The PVT properties can be obtained from a laboratory experiment using representative samples of the crude oils. However, the values of reservoir liquid and gas properties must be computed when detailed laboratory PVT data is not available. Over the last decade increased attention has been focused on models for predicting reservoir fluid properties from reservoir pressure, temperature, crude oil API gravity and gas gravity. Because of the availability of a wide range of correlations, it is beneficial to analyze them for a given set of PVT data belonging to a certain geological region. The present study develops empirical PVT correlations based on Al-Marhoun's correlations for estimating the solution gas-oil ratio, bubblepoint pressure and bubblepoint oil formation volume factor for Iran crude oils. Multiple regression analysis was used in developing those correlations. The evaluation is performed by using an unpublished data set of 55 bottomhole fluid samples collected from different locations in Iran. Based on statistical error analysis, the PVT correlations with their original coefficients and the modified coefficients were compared. The correlations developed in this study exhibit significantly lower average absolute error and deviation than the published ones.

Keywords: experimental data, PVT correlations, reservoir fluid, multiple regression

### **2. Extended Abstract**

PVT data of 55 reservoir oil samples collected from Iranian Central Oil Fields, Iranian Southern Oil Fields and Iranian Offshore Oil Fields, were used to develop the correlations presented in this study. A large number of PVT correlations for estimation of solution gas-oil ratio, bubblepoint pressure and bubblepoint oil FVF of

reservoir oils have been offered in the petroleum engineering literature over the last few years. The PVT properties depend on pressure, temperature and chemical composition or the geological condition. Therefore, to account for regional characteristics, PVT correlations need to be modified prior to their application. We developed our model based on Al-Marhoun's correlations for predicting the PVT properties for Iran crude oils. In this model, the bubblepoint pressure is predicted as a direct function of solution gas-oil ratio, specific oil and gas gravity and temperature as follows:

$$P_b = 1.09373 \times 10^{-4} R_s^{0.5502} \gamma_g^{-1.71956} \gamma_o^{2.5486} (T + 460)^{2.0967}$$

The correlation for the solution gas-oil ratio is usually derived from bubblepoint pressure correlation:

$$R_s = 994.3718 \gamma_g^{2.113367} P_b^{1.45558} \gamma_o^{-5.48944} (T + 460)^{-1.90488}$$

Oil FVF at bubblepoint pressure can be derived as a function of solution GOR, gas and oil relative density and temperature as follows:

$$B_{ob} = 0.99117 + 0.00021R_s - 2.32 \times 10^{-6} R_s \left(\frac{\gamma_g}{\gamma_o}\right) - 4.30 \times 10^{-7} R_s (T - 60)(1 - \gamma_o) + 0.00071(T - 60)$$

Where  $P_b$  is the bubblepoint pressure (psia);  $R_s$  is the solution gas-oil ratio (scf/STB);  $\gamma_g$  is dissolved gas relative density (air = 1);  $\gamma_o$  is oil relative density (water = 1); and  $T$  is the reservoir temperature (°F). As a typical example, the dependence of the bubblepoint pressure ( $P_b$ ) on temperature at different solution gas-oil ratio, oil gravity and gas gravity is shown in figure 1.

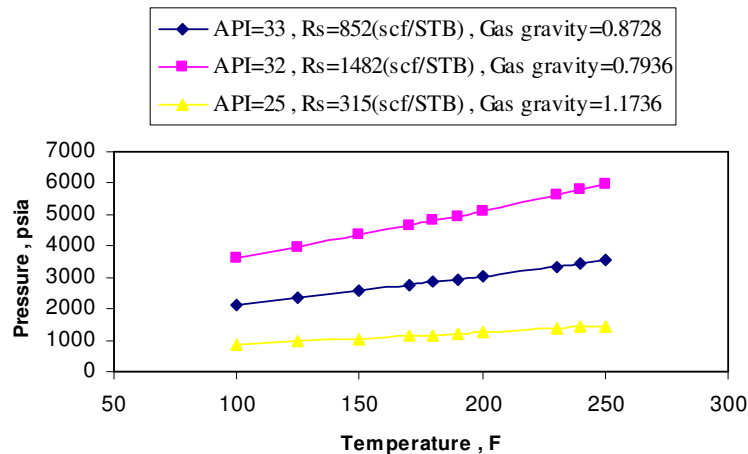


Figure 1: Effect of temperature on bubblepoint pressure at different  $R_s$ , gas and oil API gravity.

## References

- Al-Marhoun, M.A., (1988) *J. Pet. Technol.*, 40(5), 650-666.
- Mahmood, M. A., (1996) *J. Pet. Science and Engineering*, 16, 275-290.
- Alikhan, A. A., (1997) *J. Pet. Science and Engineering*, 17, 291-302.
- Al-Marhoun, M. A., (2004) *J. Pet. Science and engineering*, 1-13.

## **Development of Group Contribution Plus Property Models for Organic Systems**

Hugo E. González, Jens Abildskov, Rafiqul Gani\*

*CAPEC, Department of Chemical Engineering, Technical University of Denmark, DK-2800 Lyngby, Denmark*

### **1. Summary**

The description of different Group Contribution-Plus (GC-Plus) models for property prediction is highlighted on this work. A GC-Plus model for normal boiling point of cis-trans isomers has been developed, complementing a well established GC model with molecular mechanics tools. A model for predicting missing group interaction parameters using a set of atom connectivities and their regressed connectivity index interaction parameters is described in details. The performance of both models with experimental data is compared whenever is possible.

Keywords: UNIFAC, Group Contribution, Molecular descriptors, Connectivity Indices.

### **2. Extended Abstract**

Properties of chemicals play a very important role in the design of the chemical product and in the design of chemical processes that can manufacture them. In computer-aided model-based methods and tools for synthesis and design of the product-process, the applicability of the model and its reliability is governed by the property models used in the product-process model. In addition to reliability of the property models, another important need in product-process synthesis and design is that the models need to be predictive and fairly simple and easy to use. Group contribution (GC) based property models satisfy most of the above requirements and are therefore, routinely used in product-process synthesis and design. There are however some limitations, for example, they are not very reliable for complex chemicals or systems of complex chemicals; group parameters may not be available; not enough experimental data is available to develop a large set of group parameters; reliability is often dependent on how the chemical structure is represented by the groups. These limitations make the synthesis and design of high-value chemical products such as drugs, pesticides, structured polymers, etc., difficult with model-based methods since the necessary reliable property models are not available.

A complementary knowledge based on atomistic models, molecular descriptors and other techniques can be helpful to overcome the inherent limitations of the conventional group contribution methods. For example, features of the molecules like steric effects due to spatial conformation can be safely correlated using hybrid models that combine the simplicity and the predictive nature of GC-models with basic molecular/atomic knowledge for the property and model under study. This hybrid models (called GC-Plus models) should be simple enough to predict properties in an automatic fashion, and accurate in order to improve the performance of the conventional GC models.

This paper presents the current state of hybrid models for property prediction in organic systems: GC-Plus models have been developed for the automatic generation of missing group contributions (for pure compound property prediction) and for the generation of missing group interaction parameters for mixture property prediction models (UNIFAC-CI). Emphasis is given to the increase of the applicability range, specifically solid-liquid equilibria (SLE) calculations for mixtures (UNIFAC-CI) and accurate models for pure component property prediction of stereoisomers. The development of this hybrid models is based on molecular descriptors such as connectivity indices (CI) and molecular simulation methods (force fields).

Choosing properly the molecular/atomic based complement for the Group Contribution models -in terms of computational time- will derive in automated property models able to generate new and useful data for process simulation. Besides this, will be possible to fine-tune the parameters related with the models and to modify this models according the needs of the user. This property model development is the basis of a systematic computer aided framework that guides the user to create/select the appropriate property model, test its validity and then use it for the necessary calculations.

Case studies for problems from industry will be shown in order to exhibit the improvement gained in property prediction using GC-Plus models for organic systems involving either pure compounds and mixtures. A developed GC-Plus model for the prediction of normal boiling point combining molecular mechanics theory (MM2) and conventional GC methods will be highlighted and compared with experimental values.

The prediction of phase equilibria involving mixtures uncovered for the UNIFAC group contribution method and pure compound property prediction that are important in high-value chemical product design will be highlighted using the computer aided framework.

## References

Hugo Edson González , Jens Abildskov , Rafiqul Gani, Pascal Rousseaux, Brice Le Bert “A method for prediction of UNIFAC group interaction parameters”,*AIChE J.* 2007 vol. 53, No. 6, pp.1620-1632.

## **A new extended UNQUAC model for solid-liquid equilibria of organic solvents+iPBu-1 systems**

H. Salimnezhad, F. Feyzi\*

*Department of Chemical Engineering, Iran University of Science and Technology, Tehran 16846, Iran*

### **1. Summary**

The UNQUAC activity coefficient model is extended to predict solid-liquid equilibria of isotactic crystalline poly (1-butene), iPBu-1, in different organic solvents. The activity coefficient model used in this work is based on the concept of group-contribution and consists of combinatorial, residual and free volume terms. Free volume effects have been considered using the free volume term proposed by Danner et al. To account for branching of atom groups in the monomer structure of the polymer, a correction factor has been applied to the surface parameter of combinatorial and residual terms. The use of this correction factor has significantly improved the accuracy of the model and shows that the proposed activity coefficient model is a proper model for solid-liquid equilibria calculations in polymer solutions.

Keywords: UNIQUAC model, solid-liquid equilibria, iPBu-1, polymer solutions

### **2. Extended Abstract**

Understanding solid-liquid equilibria (SLE) is essential to developing and designing processes, such as crystallization and fractionation, and to preventing undesirable fouling of heat exchangers and polymerization reactors. Consequently, it is very important to use a suitable activity coefficient model in solid-liquid equilibria calculations.

Since the structures of polymers are very complicated, the description of SLE in polymer solutions is much more difficult than that for VLE in the same systems. Furthermore, due to their complex nature, experimental data of polymer solution systems are scarce. iPBu-1 that was discovered by Natta et al. about 50 years ago, nowadays has found several applications because of its excellent physical properties. In recent years Domanska et al. have produced sets of equilibrium data for SLE of iPBu-1 in different organic solvents, that some of these equilibrium data have been used in this work to evaluate the accuracy of the proposed model.

The UNIQUAC model is a fairly good predictive model for normal fluid mixtures in VLE and LLE calculations, but its applicability for SLE calculations of polymer solutions should be the aim of researches. In this work a free volume term has been added to UNIQUAC model in order to improve its accuracy of for iPBu-1 solutions. Free volume term, is the volume available to the center of mass of molecule and in

this work it is calculated by the equation proposed by Danner *et al.*, which is an expression based on hardcore volumes of molecules and gives the pure free volume effects. The molar hardcore volumes of different components have been calculated using Bondi's method.

In order to account for the branching of the atom groups in the monomer structure of a polymer, a correction factor has been applied to the surface parameter,  $q(n)$ , of the UNIQUAC model, and the value for this correction factor, has been set equal to 0.923 through mathematical optimization calculations. Finally, the applied activity coefficient model in SLE calculations is as below:

$$\ln \gamma_1 = \ln \frac{\Phi_1^*}{x_1} + \frac{z}{2} q_1 \ln \frac{\theta_1}{\Phi_1^*} + \Phi_2^* \left( l_1 - \frac{r_1}{r_2} l_2 \right) - q_1' \ln(\theta_1' + \theta_2' \tau_{21})$$

$$+ \theta_2' q_1' \left( \frac{\tau_{21}}{\theta_1' + \theta_2' \tau_{21}} - \frac{\tau_{12}}{\theta_2' + \theta_1' \tau_{12}} \right) + \ln \left( \frac{\varphi_1^{fv}}{\varphi_1^h} \right) + \left( \frac{\varphi_1^h - \varphi_1^{fv}}{x_1} \right)$$

$$q_i = 0.923 * \left( \sum_k v_k^{(i)} Q_k \right)$$

$$\varphi_i^{fv} = \frac{x_i (v_i - v_i^*)}{\sum_j x_j (v_j - v_j^*)}$$

$$\varphi_i^h = \frac{x_i v_i^*}{\sum_j x_j v_j^*}$$

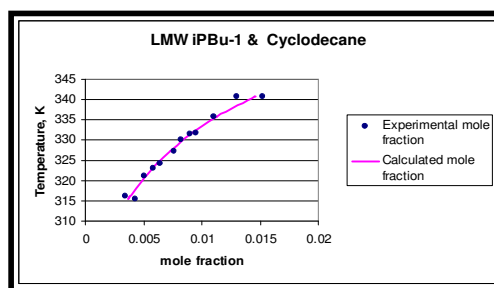


Figure 1: Calculated phase diagram for LMW iPBu-1 in cyclodecane

This modified activity coefficient model has been applied to 14 binary solvent+iPBu-1 systems including about 280 data points. Figure 1 illustrates an example of calculated phase diagrams using the proposed model for low molecular weight iPBu-1 in cyclodecane. The total average absolute deviation of the iPBu-1 mole fraction in the 14 polymer solutions was 20.54% for UNIQUAC model versus 17.00% for UNIQUAC-FV model, and 15.31% for the model finally proposed in this work. Concluding, using this activity coefficient model in SLE calculations, the experimental results obtained by Domanska *et al.* for the iPBu-1 solubility in different organic solvents, were predicted correctly.

## References

- Bondi, A., *Physical Properties of Molecular Crystal, Liquids and Glasses*, John Wiley Publications, New York, (1968)
- Danner, R. P., Kannan, D. C., Duda, J. L., (2005) *Fluid Phase Equilibria*, vol. 228-229, 321-328
- Domanska, U., Kozłowska, M. K., (2006) *J. of Molecular Liquids*, vol. 125, 76-85
- Domanska, U., Kozłowska, M. K., (2005) *Chem. Eou. J.*, vol. 11, 776-785
- Kozłowska, M. K., *et al.*, (2005) *J. of Chromatography A*, vol. 1068, 297-305
- Kozłowska, M. K., *et al.*, (2005) *Fluid Phase Equilibria*, vol. 236, 184-192
- Natta, G., *et al.*, (1955) *J. Am. Chem. Soc.*, vol. 77, 1708
- Prausnitz, J. M., Abrams, D. S., (1975) *AIChE*, vol. 21, 116-128



## Fatty acids systems under high pressure: caprylic + myristic acids and lauric + myristic acids

Mariana C. Costa<sup>a,d</sup>, M.A. Krähenbühl<sup>a</sup>, Antonio J.A. Meirelles<sup>b</sup>, J. L. Daridon<sup>c</sup>, J. Pauly<sup>c</sup>, J.A.P. Coutinho<sup>d</sup>

<sup>a</sup> LPT, Department of Chemical Processes (DPQ-FEQ), State University of Campinas (UNICAMP), P.O. Box: 6066, 13083-970, Campinas, São Paulo, Brazil.

<sup>b</sup> EXTRAE, Department of Food Engineering (DEA-FEA), State University of Campinas (UNICAMP), P.O. Box 6121, 13083-862, Campinas, São Paulo, Brazil.

<sup>c</sup> Laboratoire des Fluides Complexes, Groupe Haute Pression, Université de Pau et des Pays de l'Adour, Pau, France

<sup>d</sup> CICECO, Departamento de Química da Universidade de Aveiro, 3810.193 Aveiro, Portugal

### 1. Summary

The solid- liquid phase diagrams of two binary mixtures of saturated fatty acids, formed by caprylic acid (C8:0) + myristic acid (C14:0) and lauric acid (C12:0) + myristic acid (C14:0) were measured using high-pressure microscopy in the range of 0.1 to 90 MPa. Both systems were modeling using an approach previously developed by the authors for n-alkane mixtures.

Keywords: Solid-liquid equilibrium, high-pressure, phase diagrams, caprylic acid, lauric acid, myristic acid, modeling.

### 2. Extended Abstract

#### 2.1 Modeling

Equilibrium conditions are obtained from the equality of fugacities of each component in the liquid and solid phase.

The liquid phase fugacities can be written as:

$$f_i^L(T, P, x_i^L) = P x_i^L \phi_i^L \quad (1)$$

The solid phase fugacities at a pressure P are obtained by the equation:

$$\ln f_i^S(P) = \ln f_i^S(P_0) + (1/RT) \int_{P_0}^P \bar{V}_i^S dP \quad (2)$$

The fugacity of the component *i* in the solid phase at pressure  $P_0$  is calculated from its fugacity in subcooled liquid state at the same temperature *T*. The Poynting correction

term of Eq. (2) is simplified by the assumption that the partial molar volume of each component is proportional to the subcooled liquid molar volume. It is assumed that the liquid molar volume is pressure independent and that is the same for both compounds in the mixture, so that Eq. (2) can be written as [1, 2]:

$$f_i^s(T, P, x_i^s) = x_i^s \gamma_i^s [f_i^{0,L}(T, P_0)]^{1-\beta} [f_i^{0,L}(T, P_0)]^\beta \exp\left[-\frac{\Delta_{fus} H_i}{RT} \left(1 - \frac{T}{T_{fus,i}}\right)\right] \quad (3)$$

The activity coefficients  $\gamma_i^s$  of the rotator phase were described by means of the new Predictive UNIQUAC model [3, 4].

$$\frac{g^E}{RT} = \sum_{i=1}^n x_i \ln\left(\frac{\Phi_i}{x_i}\right) + \frac{Z}{2} \sum_{i=1}^n q_i x_i \ln \frac{\theta_i}{\Phi_i} - \sum_{i=1}^n x_i q_i \ln \left[ \sum_{j=1}^n \theta_j \exp\left(-\frac{\lambda_{ij} - \lambda_{ii}}{q_i RT}\right) \right] \quad (4)$$

with

$$\Phi_i = \frac{x_i r_i}{\sum_j x_j r_j} \quad \text{and} \quad \theta_i = \frac{x_i q_i}{\sum_j x_j q_j} \quad (5)$$

## 2.2 Results and Conclusions

The liquidus lines of the systems lauric acid + myristic acid and caprylic acid + myristic acid were determined with successfully for the first time under high pressure using a high pressure microscope. It was observed just a translation on liquidus line of both systems.

The changes in melting point due to the high pressure are reversible not affecting significantly the properties of foods with high percentage of saturated fatty acids in their composition.

The model, previously applied to alkanes, was used with success to describe the comportment of these systems under high pressure.

## References

1. Milhet, M., Pauly, J., Coutinho, J.A.P., Dirand, M., Daridon, J.L., (2005) Fluid Phase Equilib., **235**, 173-181.
2. Pauly, J., Daridon, J.L., Coutinho, J.A.P., Lindeloff, N., Andersen, S.I., (2000) Fluid Phase Equilib., **167**, 145-159.
3. Coutinho, J.A.P., Goncalves, C., Marrucho, I.M., Pauly, J., Daridon, J.L. (2005) Fluid Phase Equilib., **233**, 28-33.
4. Coutinho, J.A.P., Mirante, F., Pauly, J. (2006) Fluid Phase Equilib., **247**, 8-17.

## Global Phase Equilibrium Calculation and Critical Phase Behavior from a Group Contribution Equation of State in Binary Mixtures

N.Reshadi, F.Feyzi

*Department of Chemical Engineering, Iran University of Science & Technology, Tehran 16846, Iran*

### 1. Summary

A procedure is described to predict five different types of critical phase behavior of binary mixtures, using Elliott-Suresh-Donohue (ESD) equation of state. This procedure starts with two-phase flash to calculate solution critical points, and then stability of each calculated point is analyzed. Occurrence of an unstable point is used to determine the location of a critical endpoint. Then critical endpoint, in turn, is used as the starting point for constructing the three-phase line.

Keywords: Critical lines, LLE, LLVE, ESD EoS, Binary Mixtures

### 2. Extended Abstract

Five different types of critical phase diagrams have been constructed without adjusting any binary interaction coefficient using ESD EOS. Shape factor is calculated via two different methods: Correlated shape factor introduced by Elliott et al. (1990), and estimation using hydrocarbon group contributions (ESD-GC) by Elliott et al. (2002).

VLE, LLE and VLLE calculations are performed based on equality of fugacities. Then gibbs free energy minimization is performed to check for the stability of the phases in equilibrium. To predict the critical endpoints, phase stability analysis is applied.

The results are presented in Figures 1-2.

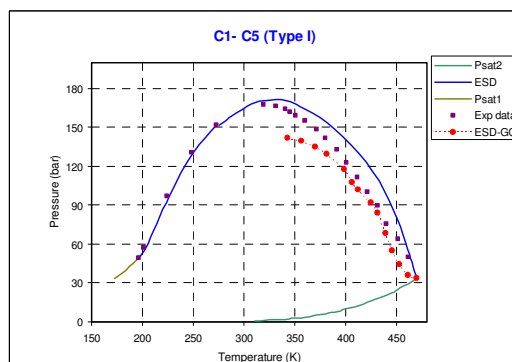


Fig.1. Phase behavior of Type I predicted for methane, n-pentane.  
Ref: Sage et. al. (1942)

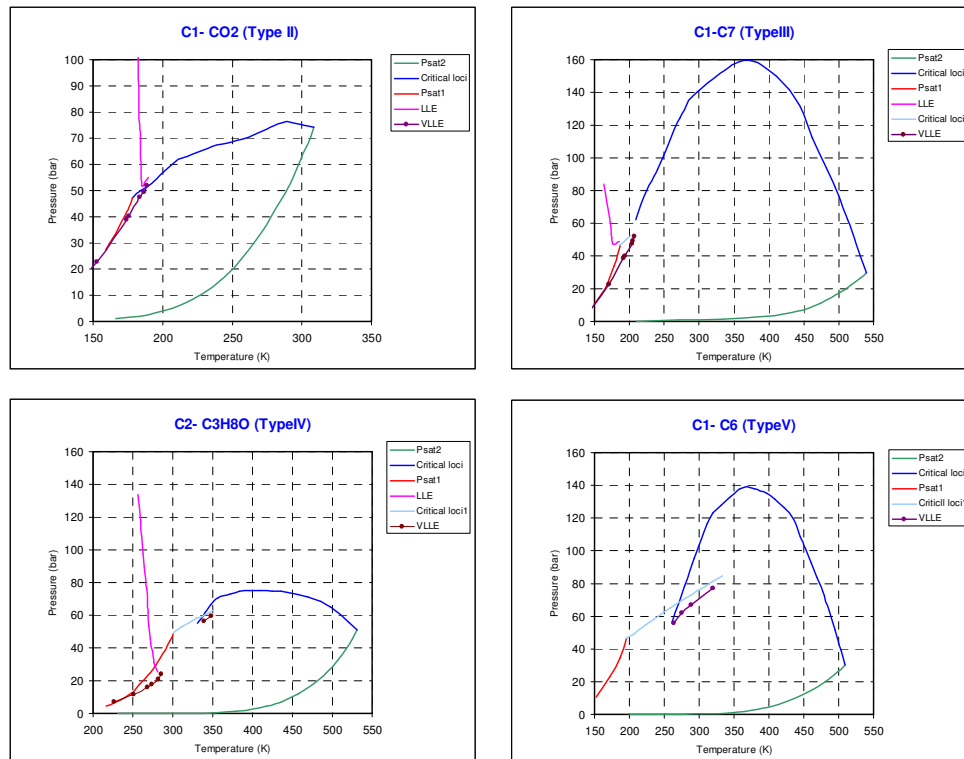


Fig.1. Phase behavior of Types II to V predicted for binary systems

While the method is completely predictive, very good results have been obtained in comparison with experimental data.

## References

- Elliott, J. R., Suresh, S. J., and Donohue, M. D., (1990) *Ind. Eng. Chem. Res.*, 29, 1476-1485.  
 Elliott, J. R., Natarajan, R. N., (2002) *Ind. Eng. Chem. Res.*, 41, 1043-1050.  
 Elliott, J. R., Critical Phase Behaviour, Private Communication.  
 Mickelsen, M., Cismondi, M., (2007) *J. of Supercritical Fluids*, 39, 287-295.  
 Eubank, P. T., (2006) *Fluid Phase Equilibria*, 241, 81-85.  
 Vega, L. F., and Llovell, F., (2007) *J. of Supercritical Fluids*, 41, 204-216.  
 Polishuk, I., Wisniak, J., Segura, H., Yelash, L. V., and Kraska, T., (2000) *Fluid Phase Equilibria*, 172, 1-26.  
 Prausnitz, J. M., Jiang, (2000) *Fluid Phase Equilibria*, 169, 127-147.  
 Mickelsen, M., *Fundamentals & Computational Aspects*, Tie-Line Publication, Denmark (2004)  
 Krenz, R., PhD Thesis, University of Calgary, Alberta, Canada (2005)  
 Sage, B. H., Reamer, H. H., Olds, R. H., and Lacey, W. N., (1942) *Ind. Eng. Chem.*, 34, 1108-1117.

## **Predicting branching structure effects on the thermodynamic properties using COSMO-RS**

Wolfgang Arlt, Oliver Spuhl, Liping Wang

*Chair of Separation Science and Technology, Friedrich-Alexander University Erlangen-Nuremberg, Egerlandstr. 3, 91058 Erlangen, Germany*

### **1. Summary**

Thermodynamic properties in COSMO-RS calculation show a high sensitivity to conformers of small molecules. In this work hyperbranched polyglycerine (PG) with 20 hydroxyl-groups has been chosen as a model of hyperbranched compounds to study the effects of branching on the thermodynamic properties, and also investigate if the thermodynamic properties of hyperbranched molecule system have a high sensitivity to conformers. The conformation search and analysis of the PG molecule has been made in vacuum, from which a best-guess starting structure has been found for the conformation search in solvent. Molecular dynamics simulations have been performed for the systems of PG/water, PG/ethanol and PG/ethanol/water mixtures, and the conformers of PG in the different solvents have been obtained. The effects of branching structure on the thermodynamic properties and the properties sensitivity to conformers have been investigated using COSMO-RS calculations.

Keywords: Hyperbranched compounds, Molecular simulation, COSMO-RS, Phase equilibria, Branching

### **2. Extended Abstract**

#### **2.1 Introduction**

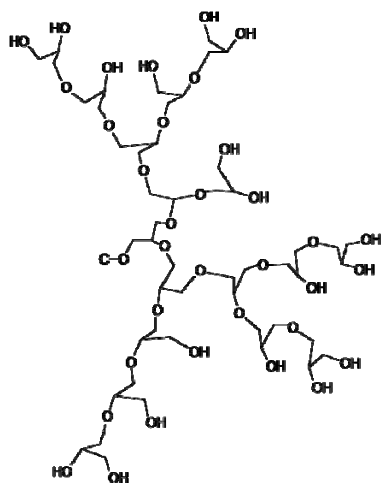
Hyperbranched compounds have been proposed to be used as separation agents, nanoscale catalysts, drug deliveries, and slow release agents for perfumes, herbicides and drugs. Most of these applications are based on their unique hyperbranched molecular structures. The backbone architecture of the hyperbranched molecules, especially the number and nature of the end functional groups will determine the properties for hyperbranched compounds.

## 2.2 Working procedure

The previous research work has shown that the a-priori prediction method COSMO-RS for thermodynamic properties requires many conformers to be included in the calculation of the chemical potential. The purpose of this work is to find a way to reduce this tedious work. The authors have much experience in phase equilibria with hyperbranched molecules, and PG is chosen as a model molecule to be studied. The following procedure is proposed to identify important conformers:

1. *Determination of three-dimensional (3D) molecular structure*  
From experimental data or synthesis knowledge, a two-dimensional topology of the hyperbranched molecule is determined, and then it is transferred using sketching programs like HyperChem into a three-dimensional structure.
2. *Optimization of initial structure, conformation search and analysis*  
The initial geometry is optimized by molecular mechanics with OPLS-AA force field to obtain a local energy minimum. From this point a conformation search and analysis is made in vacuum to obtain a best-guess starting structure for molecular dynamics simulation of the hyperbranched compound in solvent. The hyperbranched molecule conformers in solvent are extracted periodically when equilibrium is researched.
3. *Prediction of molecular structure effects on thermodynamic properties*  
The thermodynamic properties of the system are studied by the COSMO-RS model.

## 2.3 The model molecule PG



### Experimental data of PG:

Molecular weight: 1400 g/mol

No. of -OH group per molecule: 20

Degree of branching: 0.52

Figure 1: 2D topology of PG

## 2.4 Conclusions

Molecular dynamics simulation is an efficient tool to provide important conformers in solvent for COSMO-RS calculation. The structure of PG in the solvent water is very different from the lowest energy one in vacuum and PG expands in water. The COSMO-RS calculation indicates that the thermodynamic properties of PG hyperbranched compounds system do not show a high sensitivity to PG conformers.

## Prediction of Wax Precipitation Using Solid Equation of State

Mohsen Vafaie Sefti,<sup>a</sup> Hamid Mehdizadeh,<sup>a</sup> Ali Mousavi,<sup>b</sup>

<sup>a</sup>Department of Chemical Engineering, Tarbiat Modares University, Tehran, Iran

<sup>b</sup>Iran's Research Institute of Petroleum Industry, Pazhooheshgah, Blvd.Khairabad Junction, Old Qom Road, Tehran, Iran

### 1. Summary

In the traditional methods for wax precipitation prediction, the fugacity of solid is calculated using a hypothetical thermodynamic cycle. In this study, a new method based on TST solid equation of state is proposed to calculate the fugacities of solid phases. The multi-solid approach is used for description of solid phases. Obtained parameters for this equation of state is useful for future works.

Keywords: wax precipitation, solid equation of state, multi-solid

### 2. Extended Abstract

Wax Precipitation is a common problem in oil industries. It can increase the cost of process as a result of flow decrease or blocking the pipelines. So, different studies have been done to predict this phenomenon.

There are three different approaches to describe the solid state: solid solution, multi-solid and multi-solid solution. The last approach is used less than the others because of its difficulty. We use multi-solid approach because of its simplicity and limitation of used equation of state.

Based on the phase stability concept, each component or pseudo-component will appear in the solid phase in case of the following equation satisfaction:

$$f_i(P, T, z) - f_i^{0S}(P, T) \geq 0, \quad (i = 1, 2, \dots, N)$$

In which  $f_i^{0S}$  is the fugacity of pure component in the system condition. Calculation of solid(s) fugacity in different models is based on hypothetical thermodynamic cycle that was proposed by Prausnitz. Recently Twu et al. has proposed a method to calculate the fugacity of solid phase using an equation of state. In this approach a new  $\alpha$  function is defined for solid phase. The form of this  $\alpha$  function is as follows:

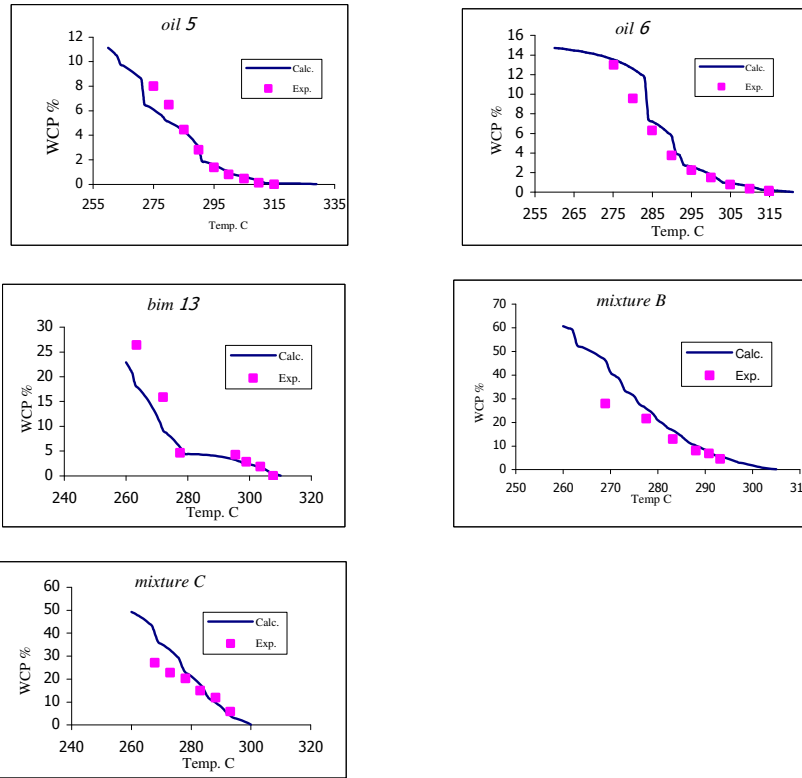
$$\alpha^S(T) = 1 + l_s(1 - T_r^{0.5}) + m_s(1 - T_r)^{n_s}(0.7 - T_r)$$

In which  $l_s$ ,  $m_s$  and  $n_s$  are the parameters that must be calculated for each component. This  $\alpha$  function is independent of pressure and so could be calculated in one pressure and used on the other pressures.

In order to obtain the parameters of the above correlation the concept of equality of different phases fugacities in equilibrium state at zero pressure is utilized. Therefore, an equation in the following form will be obtained:

$$-1 - \ln b^* - \ln(v^{*s} - 1) - \frac{1}{(w-u)} \frac{a^{*s}}{b^*} \ln\left(\frac{v^{*s} + w}{v^{*s} + u}\right) = \ln\left(\frac{f^L}{P}\right) - \frac{\Delta H^f}{RT} \left(1 - \frac{T}{T'}\right)$$

When the temperature and pressure are specified, the only unknown in the above equation is  $a^{*s}$ . Solving this equation, the value of  $a^{*s}$  and subsequently  $\alpha$  will be obtained. Regression of results in different temperatures on the proposed  $\alpha$  function results in  $l_s$ ,  $m_s$  and  $n_s$ . In order to solve the system of equations to calculate weight fraction of wax in each temperature, the dogleg method is used. Results of modeling for 5 different samples are shown in the following graphs.



## References

- Prausnitz, J., M., Lichtenthaler, R. N., and de Azevedo, E. G., *Molecular Thermodynamics of Fluid-Phase Equilibria*. Upper Saddle River, New Jersey: Printice Hall, 1999.
- Lira-Galeana, C., Firoozabadi, A., and Prausnitz, J. M., (1996) *AIChE*, 42, 239-248.
- Twu, C. H., Tassone, V., and Sim, W. D., (2003) *AIChEJ*, 49, 2957.
- Vafaie-Sefti, M., Mosavi-Dehghani, S. A. and Mohammad-Zadeh Bahar, M., (2000), *Fluid Phase Equilibria*, 173 ,65-80,
- Escobar-Remolina, J. C. M., (2006) *Fluid Phase Equilibria*, 240, 197-203.
- Feyzi, F., and Dalirsefat, R., (2007) *Fuel*, doi:10.1016/j.fuel.2006.11.034, Article in Press



## Session T2-2a: Chemical Reaction Engineering: Kinetics & Modelling

<b>Abstract Number</b>	<b>Paper Title &amp; Authors</b>	<b>Included</b>
543	Modelling of large reaction network through stochastic methods: application to oligomerization J R Shahrouzi, D Guillaume, P Galtier, P Rouchon, P Costa	Yes
725	The water-gas shift reaction in sub-critical water: Reaction kinetics and modeling G Akgül, A Kruse, M Olzman	Yes
752	Parameter estimation in a dynamic gas-liquid film model S C Cardona, J N Laboulais, M Bordera	Yes
1287	Towards the elucidation of a chemical reaction network for the palladium-catalysed phenylacetylene oxidative carbonylation reaction K Novakovic, M J Willis, A R Wright	Yes

Session T2-2a

## **Modelling of large reaction network through stochastic methods: application to oligomerization**

J. R. Shahrouzi<sup>a</sup>, D. Guillaume<sup>a</sup>, P. Galtier<sup>a</sup>, P. Rouchon<sup>b</sup>, P. Da Costa<sup>c</sup>

<sup>a</sup>*Institut Français du Pétrole, BP3 69390, Vernaison, France*

<sup>b</sup>*École des mines de Paris, 60 Bd Saint-Michel 75272 Paris cedex 06*

<sup>c</sup>*Université Pierre et Marie Curie, 4, place Jussieu, 75252, Paris cedex 05*

### **1. Summary**

Nowadays computer algorithms can be used to construct complex reaction networks, oligomerization for example, which involves thousands of species, intermediates and elementary steps whereas reduction of the rate parameters to tractable numbers can be achieved by application of single event concept. Classical deterministic simulation needs a complete construction of network for all possible reactions which is unrealistic due to the storage capacity and memory limitation of computers, specially when the number of carbon atoms rises. In this work, the stochastic simulation approach is applied for simulation and construction of oligomerization network instead of usual deterministic approach. The interest of this approach for our application is not to generate the complete network of all the possible reactions but to identify the population and evolution of the whole of the possible reactions at the present moment. This technique directs the model growth toward the most important and experimentally observed products at the expense of the unimportant part of the reaction network. In the case of limiting of network generation due to storage deficiency the stochastic simulation algorithm can be more satisfactory than deterministic network generation.

Keywords: stochastic simulation, network generation, oligomerization, single event

### **2. Extended Abstract**

Often a detailed kinetic network will grow to a prohibitively large size, because of the large number of isomers and species that can be built. Computer limitations such as storage size, the capability of the CPU memory and efficiency of the algorithm make us to fix some external limitations, such as the maximum carbon atom number and maximum number of species or reactions, for model termination [1].

For generating a detailed oligomerization network, seven types of elementary steps are proposed to represent the chemistry of the alkylcarbenium ions as follows: alkene protonation, ion deprotonation, hydride shift, methyl shift, protonated cyclo-propane (PCP) branching, oligomerization and  $\beta$ -scission. The number of single events involved in an

elementary chemical step is related to the symmetry changes associated with the formation of the activated complex out of the reactant. The elementary rate coefficient then follows from [2]:

$$k = n_e \tilde{k}$$

where  $\tilde{k}$  stands for the single event rate coefficient and  $n_e$  refers to number of single events.

In the present algorithm, we use the Monte Carlo Gillespie technique [3] to solve and generate the oligomerization network. The MC-Gillespie technique is an exact method for numerical integration of the time evolution of any spatially homogeneous mixture of molecular species that interact through a specified set of coupled chemical reaction channels. The technique is based on a fundamental equation giving  $a_j d\tau$  is the probability that a reaction  $r_j$  will occur in  $V$  in the next time interval  $d\tau$ . The deterministic rate constant  $k_j$  is related to  $a_j$  in different ways depending if the reaction is monomolecular or bimolecular.

In order to simplify the application of stochastic simulation algorithm we use three random numbers for selecting the next reaction time and the next reaction which should be fired. We define the propensity function for each component equal to summation of the propensity of all possible reaction which can be done in the moment  $t$ ,  $a_i = \sum_{j=1}^{M_i} a_j$  and  $a_0 = \sum_{i=1}^N \sum_{j=1}^{M_i} a_j$ .

According to Gillespie method the time of next reaction is,

$$\tau = \frac{1}{a_0} \ln \frac{1}{r_1},$$

the next component  $i$  which undergoes the next reaction can be determined by

$$\sum_{v=1}^{i-1} a_v < r_2 a_0 \leq \sum_{v=1}^i a_v$$

one reaction of the selected component is determined by third random number,

$$\sum_{v=1}^{j-1} a_v < r_3 a_i \leq \sum_{v=1}^j a_v$$

where  $r_1$ ,  $r_2$  and  $r_3$  are uniform random numbers between 0 and 1.

The results of this work show that the stochastic step by step simulation and generation with a limitation criteria on the number of species is more satisfactory than the stochastic simulation of the pre-generated deterministic network with the same limit. It seems that the application of stochastic simulation for step by step network generation method could be an advisable solution for simulating of very complex systems.

## References

- [1] Denis Guillaume, "Network Generation of Oligomerization Reactions: Principles," *Ind. Eng. Chem. Res.*, vol. 45, pp. 4554-4557, 2006.
- [2] E.Vynckier and G. F.Froment, "Modeling of the kinetics of complex processes upon elementary steps," in *Kinetic and thermodynamic lumping of multicomponent mixtures*. G.Astarita and S.I.Sandle, Eds. Amsterdam: Elsevier Science and Publishers B.V., 1991, pp. 131-161.
- [3] Daniel T.Gillespie, "A general method for numerically simulating the stochastic time evolution of coupled chemical reactions," *J. Comp. Phys.*, vol. 22, pp. 403-434, 1976.

## The water-gas shift reaction in sub-critical water: Reaction kinetics and modeling

G. Akgül<sup>a</sup>, A. Kruse<sup>a</sup>, M. Olzman<sup>b</sup>

<sup>a</sup>*Institut für Technische Chemie, Bereich Chemisch-Physikalische Verfahren (ITC-CPV), 3640 Karlsruhe, Germany*

<sup>b</sup>*Institut für Physikalische Chemie, Universität Karlsruhe, Germany*

The Water Gas Shift Reaction (WGSR) that is, the reaction of carbon monoxide and water to produce hydrogen and carbon dioxide, is an important fundamental reaction applied in industry. At accessible industrial temperatures and pressures, its rate is prohibitively low. However, it was shown that the WGSR could be accelerated if water as the reaction medium is used.<sup>1</sup> Water has generally attracted increasing attention as a chemical reaction medium, because its physical and chemical properties can be scaled over a considerable range by changing the temperature and the pressure. At near-critical ( $200\text{ °C} < T < 374\text{ °C}$ ,  $P > 22\text{ MPa}$ ) or supercritical conditions ( $T > 374\text{ °C}$ ,  $P > 22\text{ MPa}$ ),<sup>2</sup> it becomes, for instance, a good solvent for weakly polar molecules.

In this contribution, we report on kinetic investigations of the WGSR performed in an excess of water in a flow reactor at a pressure of 23 MPa and temperatures between 230 and 370 °C. The experimental results were analysed in terms of a complex reaction mechanism, and the assumption<sup>3</sup> that formic acid is an intermediate species in the WGSR could be experimentally confirmed. The occurrence of formic acid as an intermediate at hydrothermal conditions is the key to a better understanding of the kinetics and the mechanism of the WGSR.

Additionally, the effects of salts and oxygen were experimentally studied and compared with model calculations.

Keywords: water-gas shift reaction, sub-critical water

### References

Rice, S. F., Steeper, R. R., Aiken, J. D., (1998) *J. Phys. Chem. A*, 102,2673-2678.

Dinjus, E., Kruse, A.,(2004) *J. Phys. Condens. Matter*, 16, 1161 – 1169.

Melius, C. F., Bergan, N. E., Shepherd, J. E., (1990) *Proc. Combust. Inst.* 23, 217 – 223.

Book of Abstracts  
European Congress of Chemical Engineering (ECCE-6)  
Copenhagen, 16-20 September 2007

## Parameter estimation in a dynamic gas-liquid film model.

S. C. Cardona, J. Navarro-Laboulais, M. Bordera

*Department of Chemical and Nuclear Engineering, Universidad Politécnica de Valencia (UPV-EPVA),  
 Plaza Ferrándiz y Carbonell, 03801 Alcoy (Alicante), Spain.*

### 1. Summary

In this work, a general procedure for obtaining the maximum information from gas-liquid experiments through non-linear regression is proposed. The design of the experiments realized and the initial estimates of the parameters are important aspects studied in this work for obtaining  $\varepsilon$ ,  $k_L a$  and the kinetic rate constant  $k_2$ .

Keywords: structural identifiability, practical identifiability, parameter estimation, gas-liquid mass transfer.

### 2. Extended Abstract

The study of unsteady-state gas-liquid reactors needs of dynamic mathematical models for describing simultaneously the microscopic (interface level) and the macroscopic (reactor level) scales of the process. On the other hand, the knowledge of the different coefficients that characterize the model is fundamental. Although generalized correlations exist in the literature for those coefficients [1], in many cases it is necessary to estimate them from particular experimental data. The general procedure that we propose for getting information from experiments through non-linear regression is based, as the first step, on the structural identifiability analysis of the mathematical model [2] that let us to know their identifiable parameters  $p_i$ :

$$\begin{aligned} \frac{dx_1(t)}{dt} &= \frac{K_1 K_2 p_1}{K_2 - 1} U(t) - K_1 p_1 x_1(t) - N K_3 \frac{p_1 p_3}{p_2} (3x_1(t) - 4x_2(t) + x_3(t)) - \frac{K_1 p_1 x_1^2(t)}{K_2 - x_1(t)} & x_1(0) &= 0 \\ \frac{dx_i(t)}{dt} &= N^2 p_4 (x_{i+1}(t) - 2x_i(t) + x_{i-1}(t)) - p_5 x_i(t) + p_5 x_i(t) x_{N+i}(t) & x_i(0) &= 0 \quad i = 2, \dots, N \\ \frac{dx_{N+2}(t)}{dt} &= -\frac{2}{3} N^2 p_6 (x_{N+2}(t) - x_{N+3}(t)) + \frac{K_4 p_5}{K_2 p_2} x_2(t) - \frac{K_4 p_5}{K_2 p_2} x_2(t) x_{N+2}(t) & x_{N+2}(0) &= 0 \\ \frac{dx_{N+i}(t)}{dt} &= N^2 p_6 (x_{N+i-1}(t) - 2x_{N+i}(t) + x_{N+i+1}(t)) + \frac{K_4 p_5}{K_2 p_2} x_i(t) - \frac{K_4 p_5}{K_2 p_2} x_i(t) x_{N+i}(t) & x_{N+i}(0) &= 0 \quad i = 3, \dots, N \\ \frac{dx_{N+1}(t)}{dt} &= -\frac{N}{2} p_3 (3x_{N+1}(t) - 4x_N(t) + x_{N-1}(t)) - p_5 x_{N+1}(t) + p_5 x_{N+1}(t) x_{2N+1}(t) & x_{N+1}(0) &= 0 \\ \frac{dx_{2N+1}(t)}{dt} &= -\frac{N}{2} p_7 (3x_{2N+1}(t) - 4x_{2N}(t) + x_{2N-1}(t)) + \frac{K_4 p_5}{K_2 p_2} x_{N+1}(t) - \frac{K_4 p_5}{K_2 p_2} x_{N+1}(t) x_{2N+1}(t) & x_{2N+1}(0) &= 0 \end{aligned}$$

In this model a reactive gas A is bubbled through a liquid in which a non volatile solute B is present, reacting both substances together according to  $A+B \rightarrow \text{products}$ . We have assumed the unsteady state gas-liquid film model where a rigid liquid film of thickness  $\delta$  is next to the gas phase, and the original PDE system has been transformed to a ODE system using a finite-difference discretization scheme, dividing the liquid film in  $N$  slabs. The possible observable variables from the set of state variables present in our model are  $x_j$  (dimensionless molar fraction of A in the gas phase),  $x_{N+1}$  and  $x_{2N+1}$  (dimensionless A and B bulk molar concentrations, respectively). The seven parameters of the model are:

$$p_1 = \frac{1-\varepsilon}{\varepsilon} \quad p_2 = H \quad p_3 = \frac{D_A}{\delta} a \quad p_4 = \frac{D_A}{\delta^2} \quad p_5 = k_2 C_{B0}^b \quad p_6 = \frac{D_B}{\delta^2} \quad p_7 = \frac{D_B}{\delta} a$$

where the first four parameters are related with A, the last two are related with B, and  $p_5$  is related with the second order kinetic rate constant,  $k_2$ .

The next step considered in this work, is the estimation of these parameters from experimental data through non-linear regression [3]. We have used the Levenberg-Marquardt optimization algorithm implemented in Matlab. The elevated number of parameters of the model and their different sensitivity (as we have studied through practical identifiability analysis) does not let to estimate all the parameters from experiments with gas-liquid mass transfer plus chemical reaction. So, we propose another approximation that consists on a first stage without chemical reaction. This let us to obtain  $p_1$ ,  $p_2$  and  $p_3$  parameters but not  $p_4$ . The initial values of the parameters in the optimization algorithm is of paramount importance, and we establish how to set them for assuring the convergence of the algorithm to the correct solution.

On the second place, from experiments with gas-liquid mass transfer plus chemical reaction and considering the values of  $p_1$ ,  $p_2$  and  $p_3$  obtained previously, we can obtain only  $p_5$  but neither  $p_6$  nor  $p_7$ . Different metrics have been tested in this work for comparing the effect of the combination of observable variables and initial values of the parameters on the precision of the estimated parameters.

### Acknowledgments

The authors gratefully acknowledge the Conselleria d'Empresa, Universitat i Ciència de la Generalitat Valenciana for financial support of this work under project ref. GV06/083.

### References

- [1] Kantarci, N., Borak, F. and Ulgen, K.O., (2005) *Process Biochemistry* 40, 2263-2283.
- [2] Navarro-Laboulais, J., Cardona, S.C., Torregrosa, J.I., Abad, A. and López, F., (2006) *AIChE J*, 52, 2851-2863.
- [3] Englezos, P. and Kalogerakis, N., *Applied Parameter Estimation for Chemical Engineers*, Marcel Dekker, New York (2001).



## **Towards the elucidation of a chemical reaction network for the palladium-catalysed phenylacetylene oxidative carbonylation reaction**

K. Novakovic, M.J. Willis and A.R. Wright

*University of Newcastle, School of Chemical Engineering and Advanced Materials,  
Newcastle upon Tyne, NE1 7RU, UK*

### **1. Summary**

The palladium-catalysed phenylacetylene (*PhAc*) oxidative carbonylation reaction provides a novel *pH* and heat of reaction ( $Q_r$ ) oscillator operating in a stirred batch reactor. Furthermore, it provides the potential for the chemoselective synthesis of several commercially valuable products. The objective of this work is to determine reliable reaction network (rate determining reactions in a chemical mechanism) of the system. A reaction network is first requirement in the determination of the predictive kinetic model for use in reaction engineering studies, including process optimisation and scale-up.

Keywords: reaction networks, modelling, complex dynamics, experimental data

### **2. Extended Abstract**

Recently we have reported experimental study which achieves reproducible oscillations in both *pH* and heat output ( $Q_r$ ) during a palladium catalysed phenylacetylene oxidative carbonylation in an homogeneous catalytic system ( $PdI_2$ -*KI-Air-NaOAc* in methanol solution) (Novakovic et al. 2007). Experiments were performed in 11 HEL SIMULAR<sup>TM</sup> reaction calorimeter and the reaction exotherm,  $Q_r$ , was measured using power compensation reaction calorimetry (Barton and Rogers 1993). Recorded oscillations in  $Q_r$  were exothermic with no corresponding endotherm. Heat realised was in phase with *pH* fall, and decreased as *pH* increased. Magnitude of the heat realised during oscillations is significant. The total energy realised was calculated by integrating  $Q_r$  profile. This was performed automatically by the HEL iQ Evolution Software. An average of up to 586J/oscillation was calculated (Novakovic et al. 2007).

In this work, complex chemical dynamics associated with this reaction are studied using a three stage experimental programme. This divides the system into sub-systems in order to minimise the number of experiments needed for reaction network

elucidation. The experimental programme focuses on three aspects (1) the reaction pathway associated with catalyst activation (2) the pathway associated with catalyst regeneration (3) the overall reaction network. The first two steps are necessary for the understanding of how the catalyst affects the  $pH$  and the oscillations in  $pH$ . While the third stage is used to study the interaction between the catalytic system and the behaviour of both the reactant ( $PhAc$ ) and  $pH$ .

In the first set of experiments,  $PdI_2$  (the catalyst),  $KI$  (used primarily to facilitate  $PdI_2$  dissolution) and  $NaOAc$  (a buffer) in a methanol solution are purged with  $CO$ . Here, as no  $O_2$  is present the  $PdI_2$  is not regenerated hence the experimental data may be used to develop the reaction network and determine the rate constants associated with catalyst activation. A second subset of experiments is then performed with  $PdI_2$ ,  $KI$  and  $NaOAc$  in a methanol solution being purged with both  $CO$  and  $Air$ . The presence of  $O_2$  ( $Air$ ) allows for the regeneration of the catalyst to take place. Hence, using  $pH$  measurements (no  $Q_r$  is observed) the network obtained from the initial modelling studies is augmented with the new pathways and the corresponding rate constants are estimated. Finally, a third set of experiments is performed with  $PdI_2$ ,  $KI$ ,  $NaOAc$  in methanol solution purged with  $CO$  and  $Air$  with subsequent addition of the reactant,  $PhAc$ . Quantitative analysis is used to provide time-concentration profiles of the  $PhAc$  and the products formed. This data, together with on-line measurements of  $pH$  and  $Q_r$  are used to postulate and validate the final reaction network as well as estimate the associated rate constants.

Throughout the work the BatchCAD<sup>(TM)</sup> software package is used for kinetic fitting. The ordinary differential equation (ODE) structures of the reaction networks are postulated based on the observations and measurements made in experiments combined with the available literature. Subsequently, these ODEs are regressed to the recorded  $pH$ ,  $Q_r$  and species' time-concentration data. The structure of the reaction network is progressively modified until the simulation of the ODEs closely matches the recorded experimental data. The result is a reaction network and associated ODE model that may be used for subsequent chemical engineering design applications.

## References

- Novakovic, K., Grosjean, C., Scott, S.K., Whiting, A., Willis, M.J. and Wright, A.R., (2007) *Chemical Physics Letters*, 435, 142–147.
- Barton, J. and Rogers, R., *Chemical Reaction Hazards*, Institute of Chemical Engineering, UK (1993).

## Session T2-2b: Chemical Reaction Engineering: Advanced Concepts

Abstract Number	Paper Title & Authors	Included
600	An unusual application of chemical reaction engineering: the evolution of a crude oil reservoir. Of the use of intelligent lumping. R Bounaceur, G Scacchi, P M Marquaire, G Wild, F Dominé, R Michels	Yes
966	Rapid treatment of trace toluene in air with an air cleaner consisting of a continuous adsorption and desorption concentrator and photocatalytic reactor with a parallel array of nine light sources F Shiraishi, T Ishimatsu, K Tateishi, H Shima, H Yamamoto	Yes
2023	Internal diffusion coupled to hydrogenation kinetics in supported ionic liquid catalysts (Silicas) J-P Mikkola, L Myreen, P Virtanen, T Salmi, J Wärnå	No
2313	Hydrogenation of pyrolysis gasoline in pilot trickle-bed reactor with periodic modulated feed rate V Tukač, M Handlová, V Chyba, J Lederer, J Kolena, J Hanika, V Jiříčný, P Stavárek	Yes
3386	Experimental and model based analysis of single und multi stage membrane reactors for the oxidation of short-chain hydrocarbons in a pilot scale C Hamel, Á Tóta, F Klose, E Tsotsas, A S Morgenstern	Yes
3625	Super-Critical Fluids as Reaction Media for Fischer Tropsch Synthesis C B Roberts, E Durham	Yes

Session T2-2b

## **An unusual application of chemical reaction engineering: the evolution of a crude oil reservoir. Of the use of intelligent lumping.**

R. Bounaceur<sup>a</sup>, G. Scacchi<sup>a</sup>, P.M. Marquaire<sup>a</sup>, G. Wild<sup>a</sup>, F. Dominé<sup>b</sup>, R. Michels<sup>c</sup>

<sup>a</sup>*Département de Chimie Physique des Réactions (DCPR), Nancy-Université, CNRS, ENSIC, 1, rue Grandville, F - 54001 Nancy, France*

<sup>b</sup>*Carbochem, 12 chemin de Maupertuis, F - 38240 Meylan, France*

<sup>c</sup>*Géologie et gestion des ressources minérales et énergétiques (G2R), Nancy-Université, Faculté des Sciences, BP 239 F - 54506 Vandœuvre-lès-Nancy, France*

### **1. Summary**

This work is devoted to the prediction of the long time behaviour of the content of a crude oil reservoir. The petroleum is represented by a mixture of a finite number of typical components, the kinetics of which are described in a rigorous manner by complex radical reaction mechanisms. While the usually employed “pseudo-kinetic” laws cannot be extrapolated in temperature, the Arrhenius law holds true for real elementary reactions, so that predictions based on mechanisms built with elementary reaction rate equations can be extrapolated to temperatures usual in geochemistry. The resulting mechanism being however quite large, lumping is required to handle it. Two “informed lumping” techniques are proposed and their advantages and drawbacks are compared.

Keywords: kinetics, radical reactions, petroleum, pyrolysis, lumping

### **2. Extended Abstract**

Petroleum industry will still be with us for some time and the exploration of new reservoirs is still an important topic. Our knowledge about the origin of petroleum made tremendous progresses the last decades, however, it is still not possible to predict the actual form of a petroleum in a basin of a given age and approximately well known pressure and temperature history. The aim of the present paper is to use the tools of chemical reaction engineering to try to predict the approximate composition of an oil contained in a reservoir after secondary cracking.

The challenges are multiple: for a typical oil reservoir, the time scale is a few millions of years (a long time, even in academia), the pressure is high (some 20 MPa), the temperature relatively low (about 200 °C), the chemical composition of the mixture extremely complex; furthermore the reservoir may contain water and a lot of solids, some of which may react (sulfates can be reduced, other particles may have catalytic properties). It is however currently assumed that the main reactions happening are radical pyrolysis reactions. In the present paper, we will therefore neglect non radical reactions (catalytic or molecular).

Since the relevant pyrolysis reactions are very slow at the actual reservoir conditions, reaction rates have to be measured at higher temperatures, and the results extrapolated to the low temperatures of interest. Furthermore, it is of course impossible to handle separately all the numerous constituents of petroleum and their interactions during pyrolysis: different lumping strategies have been used to handle this complexity.

The classical approach of geochemistry consists in lumping the constituents of petroleum in a limited number of pseudo-compounds, as Kuo & Michael (1994): C1 (methane), C2 (ethane and ethene), C3-C5, C6-C14, stable aromatics (benzene, toluene, xylene, naphthalene), C<sub>15+</sub> saturates, C<sub>15+</sub> aromatics, resins, asphaltenes and coke. Arbitrary stoichiometry and rate laws are established using measurements at different temperatures usually between 300 °C and 500 °C.

Unfortunately the Arrhenius law used to extrapolate holds true for elementary reactions, but not for empirical rate laws obtained by fitting. For this reason, another approach was proposed (e.g. Dominé *et al.*, 2002), in which the oil is supposed to be a mixture of a limited number of model compounds the pyrolysis of which is described by a rigorously built set of radical reactions, whose rate equations are established. Since the resulting mechanism is still too complicated to be used directly, lumping has still to be done. Two ways of model reduction are proposed. The advantages and drawbacks of these are compared. Due to the principle used, they can be extrapolated to smaller temperatures, as long as no new reactions appear. The predictions of this technique are compared with the content of a real oil reservoir.

## References

- Dominé, F., Bounaceur, R., Scacchi, G., Marquaire, P.M. Dessort, D., Pradier, B., Brévert, O., (2002) *Organic Geochemistry*, 33, 1487-1499
- Kuo, L., Michael, G.E., (1994) ) *Organic Geochemistry*, 21, 911-925

## **Rapid treatment of trace toluene in air with an air cleaner consisting of a continuous adsorption and desorption concentrator and photocatalytic reactor with a parallel array of nine light sources**

F. Shiraishi,<sup>a</sup> T. Ishimatsu,<sup>a</sup> K. Tateishi,<sup>b</sup> H. Shima,<sup>b</sup> H. Yamamoto<sup>c</sup>

<sup>a</sup>Department of Systems Design, Bio-Architecture Center, Kyushu University, Fukuoka 812-8581, Japan

<sup>b</sup>I-Quark Corporation, 1-36-14, Matsushima, Higashi-ku, Fukuoka 812-0062, Japan

<sup>c</sup>Ars Research System Co., Ltd., 8-33-3, Momochihama, Sawara-Ku, Fukuoka 814-0001, Japan

### **1. Summary**

To rapidly treat a large amount of air containing trace volatile organic compounds, we have previously developed an air cleaner consisting of a continuous adsorption-and-desorption concentrator, with a honeycomb rotor loading zeolite particles, and photocatalytic reactor. In the present work, we miniaturized this air cleaner and investigated its performance. Toluene (1-3 ppm) in 1 m<sup>3</sup>-air was quickly reduced to almost zero concentration within 10 minutes and the toluene concentrated in a 0.0156 m<sup>3</sup> small box was decomposed in 30-60 min.

Keywords: air cleaner, trace toluene, photocatalytic reactor, continuous concentrator

### **2. Extended Abstract**

It is difficult to rapidly treat trace volatile organic compounds (VOCs) in air, because a film-diffusional resistance in the vicinity of the photocatalyst surface decreases remarkably the rate of decomposition because of low VOC concentrations. We previously developed an air cleaner consisting of a continuous adsorption-and-desorption concentrator and photocatalytic reactor and then treated the air containing formaldehyde (Shiraishi *et al.*, 2003). As a result, we found a high performance of this apparatus. The objectives of this work are to miniaturize this air cleaner and evaluate its applicability to the treatment of trace toluene in air.

A schematic of the air cleaner is shown in Fig.1. The fine zeolite particles-loading honeycomb rotor (12 cm in diameter and 5 cm in thickness) was slowly rotated at 1/12 r.p.m. The air containing trace toluene was continuously supplied to the 3/4 sectional area of the rotor at 0.27 m<sup>3</sup> min<sup>-1</sup> to adsorb toluene. On the other hand, the air in a loop, circulated at 0.09 m<sup>3</sup> min<sup>-1</sup>, was heated instantaneously and then supplied to the 1/4 sectional area of the

rotor to desorb toluene. When entering the small box ( $0.0156 \text{ m}^3$ ) in the loop, the desorbed toluene entered was decomposed in the photocatalytic reactor with a parallel array of nine 6W blacklight blue fluorescent lamps; the apparatus structure is detailed elsewhere (Shiraishi *et al.*, 2005a & b). The contaminated air was sucked from the reactor bottom by rotation of an electric fan at the reactor head and allowed to rise through the inside of each glass tube at a linear velocity of air ( $>11 \text{ m s}^{-1}$ ) that could neglect the film-diffusional resistance. The air cleaner was always set up in a closed room of  $1 \text{ m}^3$  and switched on to decompose toluene evaporated in a range of  $1\text{--}13 \text{ mg m}^{-3}$ .

A typical experimental result is shown in Fig.2. When only the concentrator was operated, the toluene concentration in the room decreased to the neighbourhood of a zero concentration in 10 min and then became constant, while that in the small box increased instantaneously and then became constant. When both the concentrator and reactor were operated, on the other hand, the toluene concentration in the room decreased more rapidly to a zero concentration, while that in the small box increased instantaneously, then decreasing and becoming zero. The experimental result clearly shows that the miniaturized air cleaner has a remarkably high performance. The photocatalytic activity and the ability of the rotor to adsorb toluene were very stable with repeated experiments.

## References

- Shiraishi, F., Yamaguchi, S., Ohbuchi, Y., (2003) *Chem. Eng. Sci.*, 58, 929-934.  
 Shiraishi, F., Ohkubo, D., Toyoda, K., Yamaguchi, S., (2005) *Chem. Eng. J.*, 114, 153-159.  
 Shiraishi, F., Toyoda, K., Miyakawa, H., (2005) *Chem. Eng. J.*, 114, 145-151.

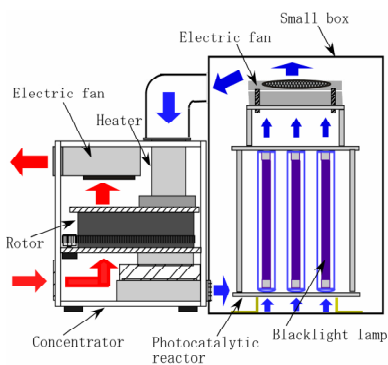


Fig.1 A schematic of air cleaner

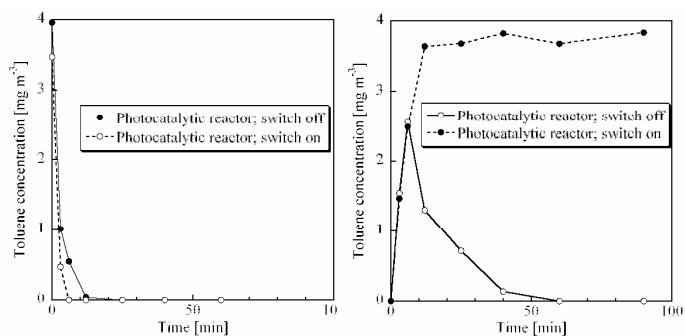


Fig.2 Time courses of toluene concentrations in a room (left) and small box (right) in photocatalytic decomposition of toluene by an air cleaner.



## Hydrogenation of pyrolysis gasoline in pilot trickle-bed reactor with periodic modulated feed rate

V. Tukač,<sup>a</sup> M. Handlová,<sup>a</sup> V. Chyba,<sup>a</sup> J. Lederer,<sup>b</sup> J. Kolena,<sup>b</sup> J. Hanika,<sup>c</sup> V. Jiříčný,<sup>c</sup>  
P. Stavárek<sup>c</sup>

<sup>a</sup>*Inst. Chem. Tech. Prague, Dept. Organic Technology, Technická 5, CZ-166 28 Prague 6, Czech Republic*

<sup>b</sup>*Unipetrol, a.s., div. VUANCH, CZ-436 70, Litvinov, Czech Republic*

<sup>c</sup>*Institute of Chemical Process Fundamentals, Czech Academy of Sciences, v.v.i., CZ-165 02 Prague 6, Czech Republic*

### 1. Summary

Comparison of both periodic and steady state hydrogenation of pyrolysis gasoline dissolved in toluene in pilot scale trickle bed reactor is given. Enhancement of reaction rate under periodic operation mode is followed by higher mean catalyst bed temperature and broader pressure drop fluctuation with respect to steady state ones.

Keywords: pyrolysis gasoline, trickle-bed reactor, hydrogenation, feed rate modulation

### 2. Extended Abstract

Hydrogenation of pyrolysis gasoline is widely applied in industry to prevent gum-formation and catalyst deactivation caused by dienes oligomerization. Advantages of trickle bed reactor, which is usually adopted for this hydrogenation, like continuous operation, simple construction, etc. are accompanied by drawbacks like bad external heat exchange, liquid maldistribution and mass transfer limitation, namely concerning transfer of hydrogen to catalyst. Promising solution of these disadvantages consists in periodic liquid feed rate modulation to create forced pulsing flow pattern in catalyst bed. Typical benefits are periodically renewal of wetted catalyst surface, more intensive interaction between gas and liquid phases in catalyst bed, higher mean reaction temperature and intensification of heat transport during liquid rich part of feeding period, which result in higher reactor throughput, increased productivity and also operation safety (Silveston and Hanika, 2004).

The goal of this work was to compare hydrogenation rate of pyrolysis gasoline under both steady-state continuous feed and periodic modulated liquid feed rate carried out in pilot scale trickle-bed reactor.

Trickle-bed reactor of 100 mm I.D. and 2000 mm height was equipped by automatic controlling and data acquisition system. Due to thick thermal insulation the reactor behavior was close to adiabatic one. Catalyst bed depth 1000 mm of pelleted 0.1 % palladium on alumina catalyst (Degussa Noblyst 1505, mean diameter 3 mm) was applied for selective diene/olefinic bonds hydrogenation. Adiabatic reaction temperature rise for pyrolysis gasoline was controlled by solvent dilution to 10 %wt. dienes solution in toluene. Temperature and pressure axial profiles in catalyst bed were scanned with distance of 100 mm by thermocouples and pressure transducers. An excess of hydrogen to stoichiometric demand at level 100 % was maintained in all experiments (Tukač et al., 2007).

During pilot plant tests a parametric sensitivity of the reactor both to inlet temperature and pressure, so as to parameters of periodic liquid feed rate modulation mode like period length, its split as well as ratio of peak to base liquid feed rate was found. Hydrogenation reactions in question exhibit important adiabatic temperature rise, which results in nonisothermal axial temperature profile. In case of periodic liquid feed rate modulation a higher mean temperature (Fig. 1) in the bed was found in comparison with steady state mode of operation with constant feed rate. It was stated, that mean reaction rate over whole catalyst bed (which represents reactor productivity) is higher at convenient modulation by 20 % (see Tab. I) in comparison to the value typical for steady state mode of constant feed rate.

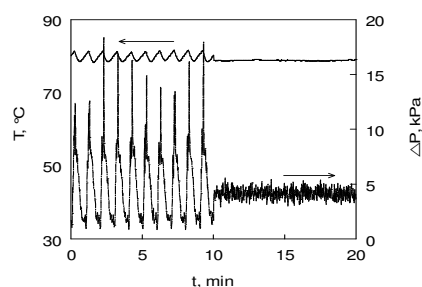


Fig. 1. Outlet temperature and pressure drop during transition from periodic to steady state operation, feed temperature 60 °C, mean feed rate 124,7 l/h, period 60 s, split 0.25

Tab. I: Enhancement factor of pyrolysis gasoline components (ratio of periodic to steady state reaction rate).

Compound	Enhancement factor
styrene	1.072
allylbenzene	1.130
3-methylstyrene	1.137
2- methylstyrene	1.155
4- methylstyrene	1.169
cyklopentadiene + isoprene	1.069
endo-dicyklopentadiene	1.090
indene	1.199
endo-dihydrodicyklopentadiene	1.084

Acknowledgement to the Ministry of Industry and Trade of the Czech Republic, grant no. FT-TA/039. and Ministry of Education, Youth and Sports of CR, grant no. MSM 604 6137301

## References

- Silveston, P. L., Hanika, J., (2004) *Canad. J. Chem. Eng.* 82, 1105-1142.  
 Tukač, V., et al., (2007), *Chem. Eng. Sci.*, doi: 10.1016/j.ces.2006.12.032

## **Experimental and model based analysis of single und multi stage membrane reactors for the oxidation of short-chain hydrocarbons in a pilot scale**

C. Hamel<sup>1</sup>, Á.Tóta<sup>2</sup>, F. Klose<sup>2</sup>, E. Tsotsas<sup>2</sup>, A. Seidel-Morgenstern<sup>1,2</sup>

<sup>1</sup>Max-Planck-Institut für Dynamik komplexer technischer Systeme, D-39106 Magdeburg, Germany

<sup>2</sup>Otto-von-Guericke-Universität, Institut für Verfahrenstechnik, D-39106 Magdeburg, Germany

### **1. Summary**

Based on an optimal distributed dosing of reactants and the resulting concentration and residence time effects the product spectrum can differ in a membrane reactor compared to a conventional fixed-bed reactor. In case of low oxygen concentrations the selectivity of the desired product ethylene can be increased significantly compared to the conventional fixed-bed reactor. The obtained results for the ODH of propane are similar even though the increase of the propylene selectivity is not so distinctive compared to ethylene. This reactor principle can be further enhanced using a multi stage reactant feeding with an increasing dosing profile (O<sub>2</sub> concentration and total volumetric flow rate). The developed detailed 2D models allow a good mathematical description of the exothermal reactions taking place in the membrane reactor.

Keywords: Membrane reactors, pilot plant, selectivity enhancement, propane, ethane

### **2. Extended Abstract**

In the field of chemical reaction engineering intensive research is devoted to develop new processes in order to improve selectivity and yields of intermediate products. Important example reactions are catalytic partial oxidations or selective hydrogenations [1]. For such reactions improved integral reactor performance can be achieved by optimised stage-wise dosing of one or several reactants [2]. Adjusted dosing profiles can be realised e.g. by feeding reactants separately through permeable reactor walls, e.g. through tubular membranes. Additionally, various types of stage-wise temperature profiles in combination with characteristic dosing and/or residence time profiles can be realised. The concept allows to improve significantly the selectivity and yield with respect to a desired intermediate product .

This contribution intends to provide insight into various aspects of multi-stage dosing concepts based on an experimental and model based analysis. For this aim the partial oxidations of ethane to ethylene and propane to propylene on a VO<sub>x</sub>/Al<sub>2</sub>O<sub>3</sub> catalyst were considered as model reactions. For the experimental study, a pilot scale set-up

has been constructed with a single stage packed bed membrane reactor and a three stage membrane reactor cascade. The inner/outer diameters were 21/35 mm, the effective membrane length 104mm, of the investigated asymmetric alumina and sinter metal membranes. A comparison with a conventional fixed-bed reactor operation was possible using the conventional co-feed-mode. Based on a preliminary theoretical analysis, a large set of experimental studies was carried out in a temperature range between 520/630 °C (ethane) and 350/500 °C (propane). The molar  $O_2/C_nH_m$  ratio was varied between 0.5 and 8. In the three-stage membrane reactor different dosing profiles could be realised, e.g. increasing (10-30-60), uniform (33-33-33) and decreasing (60-30-10) profiles.

Due to the separated and distributed feeding of the reactants, the resulting concentration and residence time profiles and the corresponding product spectra are distinctly different in membrane reactors compared to fixed-bed reactors. The analysis performed reveals for the investigated operation conditions a higher ethylene/propylene selectivity and simultaneously a higher conversion in membrane reactors (see figure 1 for different WHSV). In the presentation will be shown that improved performance could be achieved by combining optimised stage-wise temperatures profile with a stage-wise dosing of one or several of the reactants, respectively.

Reduced simple 1D and more detailed 2D models have been used to identify optimal operation parameters and to describe the concentration and temperature profiles, respectively.

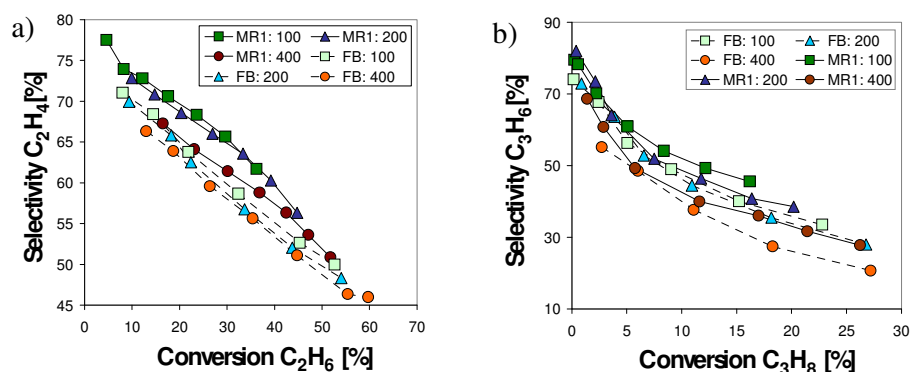


Figure 1: a) selectivity ethylene vs. conversion, b) selectivity propylene vs. conversion:  $C_2H_6^{in} = 1,5\%$ ,  $C_3H_8^{in} = 1\%$ ,  $O_2/C_nH_m = 1$ , WHSV = 100-400kg/m<sup>3</sup>, catalyst:  $VO_x/\gamma-Al_2O_3$ , (V: 1.4%), BET: 157m<sup>2</sup>/g, particle:  $d_p = 1.0$  mm

## References

- [1] Dixon, A.G., Int. J. Chem. React. Eng., Vol. 1, 2003, R6, 1-35
- [2] Hamel C., Thomas S., Schädlich K., Seidel-Morgenstern A., Chem. Eng. Sci., **58**, 2003, 4483-4492

## Super-Critical Fluids as Reaction Media for Fischer Tropsch Synthesis

C. B. Roberts,<sup>a</sup> E. Durham,<sup>a</sup>

<sup>a</sup>*Department of Chemical Engineering, Auburn University, Auburn, AL, USA*

### 1. Summary

Operating Fischer-Tropsch synthesis (FTS) in supercritical fluid (SCF) media offers certain advantages over conventional gas-phase FTS operation including in situ extraction of heavy hydrocarbons from the catalyst pores coupled with enhanced incorporation of 1-olefins in the chain growth process. In this study hydrocarbon product distributions in near-critical and supercritical hexane phase FTS (SCH-FTS) were studied over both alumina supported and silica supported cobalt catalysts in a high pressure fixed-bed-reactor system. All reactions were carried out in near-critical and supercritical regimes by tuning either the reaction temperature (230 °C-260 °C) or the reaction pressure (30 bar - 80 bar). Deviations from the standard Anderson-Schultz-Flory (ASF) chain growth model were observed under supercritical fluid conditions; however, the degree of deviation depends on the reaction conditions within the near-critical and supercritical regions and varies from gas-like density to liquid-like density within the supercritical region. Optimization of the SCF-FTS performance was achieved by operation within a specific region of temperature-pressure-density space. The supercritical fluid media was shown to offer comparable conversion to the gas phase, higher selectivity in the middle distillate fraction (gasoline and diesel), and lower methane and other light hydrocarbon selectivity.

Keywords: Fischer Tropsch Synthesis, Supercritical Fluids, Catalysis

### 2. Extended Abstract

Fischer Tropsch Synthesis (FTS) is a mature technology that utilizes gasified non-petroleum carbonaceous feedstocks (coal, natural gas) to meet the demand for liquid transportation fuels and chemicals. Fischer Tropsch Synthesis has received renewed interest in recent years for several reasons including both economic (the price and availability of crude oil) and environmental (the drive to utilize renewable energy resources such as biomass). FTS converts syngas (CO and H<sub>2</sub>) to a spectrum of hydrocarbon products (alkanes, alkenes, oxygenates, and branched compounds) with various chain lengths (C<sub>1</sub> to C<sub>30+</sub>) through surface catalyzed polymerization reactions. As the reactants are gasses and a large fraction of the product stream is liquid, the ideal reaction media would be able to readily transport gasses to the catalyst active sites and liquid products from the active site to the bulk reaction media. As the

reaction is strongly exothermic, the media would also be able to efficiently dissipate the produced heat to avoid catalyst deactivation and unwanted methane formation.

The process was originally carried out in the gas phase with a simple fixed bed reactor design. With a gaseous media, there is excellent transport of reactants to the catalyst active sites, resulting in high activity. However, the low density of the media results in poor extraction and transport of liquid products from the active site to the bulk media and poor heat dissipation from the catalyst active site. This results in poor activity maintenance and high methane selectivity. To counter this, liquid phase techniques were developed for FTS, utilizing slurry phase reactors where the reactant gases are bubbled through a heavy hydrocarbon liquid media. This media, being an excellent solvent for liquid hydrocarbons, alleviates buildup of liquid products on the active sites thereby allowing for improved activity maintenance. Moreover, the high media density also provides for more efficient heat dissipation, resulting in lower methane selectivity. While liquid phase FTS addresses the methane selectivity and activity maintenance issues in gas phase FTS, it does so at the expense of losing the simplicity of the gas phase, fixed bed reactor design coupled with lowering the catalyst activity due to decreased reactant transport rates.

Supercritical fluids (SCF) offer properties intermediate between gases and liquids and show promise for FTS, being miscible with gases, having intermediate diffusivities, being good solvents for liquids and solids, and providing for rapid heat dissipation. This paper presents the use of supercritical hexane as a reaction media for Fischer Tropsch Synthesis over conventional cobalt catalysts (e.g. 15% Co on alumina, 15% Co on silica). The influence of temperature (210 °C to 260 °C), pressure (20 bar to 80 bar), H<sub>2</sub>:CO ratio (0.5 to 2.1), syngas rate (50 SCCM/g to 150 SCCM/g), and supercritical fluid media (e.g. supercritical hexane) on conversion and product distribution was studied.

Supercritical phase Fischer Tropsch synthesis exhibits interesting behavior relative to gas phase operation, including comparable conversion with excellent activity maintenance, decreased methane selectivity, increased olefin selectivity, and higher product selectivity in the middle distillate fractions (gasoline and diesel). Deviations from the standard ASF product distribution have been observed in the near-critical region, with the degree of deviation being highly dependent upon the operating conditions (i.e. temperature, pressure, density, phase behavior). It was also observed that the use of supercritical hexane enhances the extraction of heavy products from the catalyst, restoring some catalytic activity lost during gas phase operation. Surface characterization studies indicate that the crystalline structure of the catalyst is less affected by the reaction when performed in the supercritical phase than the gas phase. Supercritical FTS shows a shift from gas phase FTS in terms of oxygen removal, favoring H<sub>2</sub>O over CO<sub>2</sub> far more than gas phase operation.

## References

Elbashir, N.O., Dutta, P., Manivannan, A., Seehra, M.S., Roberts, C.B., (2005) *Applied Catalysis A: General* 285, 169–180.

Elbashir, N. O., Roberts, C. B., (2005) *Ind. Eng. Chem. Res.* 44(3), 505-521.

## Session T2-2c: Chemical Reaction Engineering: Practical Applications

<b>Abstract Number</b>	<b>Paper Title &amp; Authors</b>	<b>Included</b>
1127	Catalytic Synthesis of Hydrogen Peroxide in a Capillary Microreactor S Maehara, M Taneda, K Kusakabe	No
2208	Using Online Calorimetry to Ensure Process Safety: Scaling Up Catalytic Epoxidation of Alkenes J Bu, C W Quah, K J Carpenter	Yes
2316	Direct Synthesis of Hydrogen Peroxide in a Catalytic Membrane Contactor A Pashkova , K Svajda , R Dittmeyer	No
2334	Mathematical Modeling of Two Separate Phases Enzymatic Membrane Reactor F Scura, G Barbieri, L Giorno, J Zhang, and E Drioli	Yes
2342	High purity hydrogen production in a Pd-Ag membrane reactor G Barbieri, G Tricoli, A Brunetti, E Drioli	Yes
3322	Role of the Precipitation Device on the Properties of Al <sub>2</sub> O <sub>3</sub> -TiO <sub>2</sub> Mixed Oxides G Mouret, K Mozet, H Muhr, E Plasari, M Martin	Yes

Session T2-2c



## Using Online Calorimetry to Ensure Process Safety: Scaling Up Catalytic Epoxidation of Alkenes

J. Bu, C.W. Quah, K. J. Carpenter

*Institute of Chemical and Engineering Sciences, Singapore  
No 1, Pesek Road Jurong Island, 627833, Singapore*

### 1. Summary

Manganese catalyzed epoxidation of styrene using  $\text{NaHCO}_3\text{-H}_2\text{O}_2$  buffer solution carried out in a semi-batch reactor exhibits characteristic features such as sudden exothermic heat release and spontaneous  $\text{O}_2$  gas generation due to  $\text{H}_2\text{O}_2$  decomposition. Hence, reaction calorimetry serves as an effective evaluation tool for process safety studies on this reaction system. In this paper, calorimetric data from reaction calorimeter (RC1e) shows that modification of the operating condition by using a low dosing rate effectively avoids the risks associated with potential thermal runaway and  $\text{O}_2$  pressurized explosion in any future large scale operations. Process optimization work based on various factors such as maximum production capacity, low material consumption, and minimal waste generation facilitates the formulation of a set of safe and efficient standard operating parameters, which are instrumental for scaling up epoxidation to the large-scale production. In addition, kinetic studies based on a second-order reaction carried out under optimized operating conditions, provides a preliminary design criterion for reactor sizing in large scale pilot plant production.

Keywords: catalyzed epoxidation, process safety, on-line calorimetry, kinetics studies, scale up

### 2. Extended Abstract

From the equation 1, the temperature of reactor,  $T_r$  could be related to the dosing rate ( $v$ ). Based on experimental data in Fig.1, the prime safety indicators,  $T_{r_{\max}}$  dramatically decreases as the dosing rate is reduced. The ratio of dosing rate ( $v$ ) to the initial volume of reactant ( $v/V_0$ ) serves as an indicative design factor for determining the safe dosing rate when scaling up to larger reactors. It was found that when the dosing rate ( $v/V_0$ ) is set to less than  $0.44 \text{ (hr}^{-1}\text{)}$ , the temperature rise will be less than 1%.

$$\sum (C_{pi} N_i) \frac{\partial T_r}{\partial t} = F(N_{styrene}, v\rho) - UA(T_r - T_j) \quad (1)$$

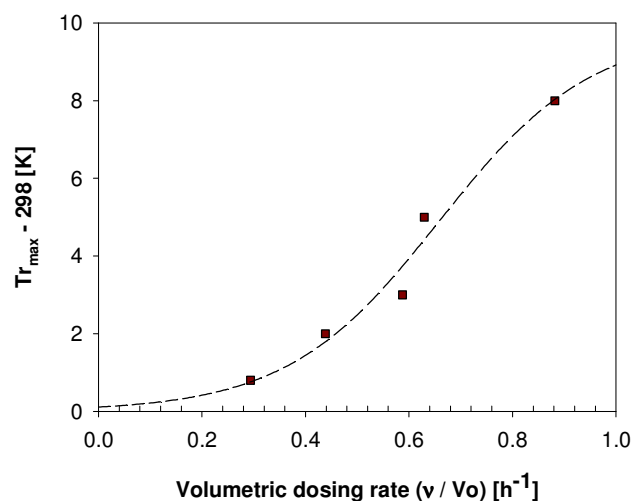


Figure 1: Temperature spike decreasing with dosing rate,

A graphical representation for the relationship of reaction time,  $t$  and the ratio of  $v/V_o$  against conversion,  $X$  can be plotted as shown in Fig. 2. Based on 100 ml of RC1e reactor, the optimized values of  $N_{A0}/V_o$ ,  $v/V_o$  and  $t$  are computed to be 0.766 [mol/Liter], 0.438 [ $h^{-1}$ ], and 1.5 h, respectively. For any scale-up, similarly, 100% conversion in any large scale reactors could be achieved after 1.5 h by using these scaling parameters.

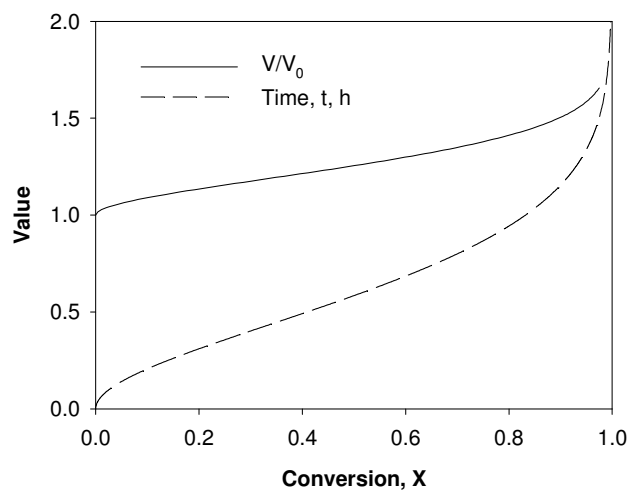


Figure 2: Scale up profile ( $V/V_o$ ; the ratio of total volume to the initial volume of reactant)

## References

Lane, B. S., Vogt, M., DeRose, V. J., and Burgess, K., (2002) *J. Am. Chem. Soc.* 124, 11946-11954.

## Mathematical Modeling of Two Separate Phases Enzymatic Membrane Reactor

F. Scura,<sup>a,b</sup> G. Barbieri,<sup>a</sup> L. Giorno,<sup>a</sup> J. Zhang,<sup>a</sup> and E. Drioli<sup>a,b</sup>

<sup>a</sup> National Research Council of Italy - Institute for Membrane Technology (ITM – CNR) Via Pietro BUCCI, c/o The University of Calabria, cubo 17/C, 87030 Rende CS, Italy

<sup>b</sup> The University of Calabria - Department of Chemical Engineering and Materials Via Pietro BUCCI, cubo 44/A, 87030 Rende CS, Italy

### 1. Summary

Lipases are useful biocatalysts in kinetic resolutions for they specific interaction with one of the two enantiomers present in a racemic mixture. The life time in terms of catalytic activity and stability is the major problems for their application at industrial level. The stability of lipase is increased by immobilization at the organic/aqueous interface within the porous structure of asymmetric membranes.

In this work, the modeling of a two separate phases enzymatic membrane reactor was developed considering the hydrolysis of S-naproxen methyl-ester.

Keywords: Enzyme membrane reactor, kinetic resolution, mathematical modelling

### 2. Extended Abstract

The modelled system consists in a catalytic membrane separating an organic phase containing the S-ester (reactant) and an inorganic phase for naproxen acid recovery (the reaction product); both the phases are continuously re-circulated. The S-naproxen ester diffuses from the organic bulk solution to the boundary layer and then into the enzyme layer inside the membrane, where it is catalytically converted into naproxen acid. The naproxen acid diffuses from the enzyme membrane layer towards the bulk inorganic solution in the other membrane side.

The slow reaction rate and the relative fast re-circulation allows the bulk phases to be considered as well mixed batch systems. Therefore, the dimensionless mathematical model consists of:

- the 1-D transient mass balance (partial differential equations) for S-enantiomer naproxen methyl-ester (reactant) and naproxen acid (product) inside the catalytic membrane;
- the ordinary differential equations for the evolution of reactant and product concentration in the organic and inorganic phases, respectively.

Same equations can be written for the R-enantiomer; however, due to the high selectivity of the catalyst for the S-ester the reaction rate of the R-ester is too low when compared to that of S-ester.

The naproxen methyl ester conversion and the naproxen acid production as a function of reaction time for different values of dimensionless parameters were calculated. Moreover, reactant and product profiles inside the catalytic membrane were obtained. The results shown that the performance depends on many factors such as: mass transport, reaction rate, membrane area to organic phase volume ratio and membrane thickness. In particular, a key role is played by the maximum velocity parameter of *Michaelis-Menten* kinetics to the effective diffusivity ratio ( $v_{MAX}/D_{effective}$ ). The model validated with some literature data shows interesting results for studying the catalytic membrane performance of such systems.

**Acknowledgement:** The “Ministero dell’Università e della Ricerca” Progetto “FIRB-CAMERE RBNE03JCR5 – Nuove membrane catalitiche e reattori catalitici a membrana per reazioni selettive come sistemi avanzati per uno sviluppo sostenibile” is grateful acknowledged for the financial support.

## High purity hydrogen production in a Pd-Ag membrane reactor

G. Barbieri<sup>a</sup>, G. Tricoli<sup>b</sup>, A. Brunetti<sup>a, b</sup>, E. Drioli<sup>a, b</sup>

<sup>a</sup>National Research Council of Italy - Institute for Membrane Technology (ITM – CNR) Via Pietro BUCCI, c/o The University of Calabria, cubo 17/C, 87030 Rende CS, Italy

<sup>b</sup>The University of Calabria - Department of Chemical Engineering and Materials Via Pietro BUCCI, cubo 44/A, 87030 Rende CS, Italy

### 1. Summary

The use of hydrogen as an energetic carrier is a fundamental goal to be achieved. However, a critical stage in its realization is the possibility of having a hydrogen-pure stream with a CO content lower than 10 ppm for use in PEMFC.



In this work WGS reaction was performed using a traditional reactor followed by a membrane reactor (TR+MR). A self-supported commercial Pd/Ag (23wt.%) membrane 60 microns thick was used. A commercial catalyst CuO/CeO<sub>2</sub>/Al<sub>2</sub>O<sub>3</sub> was used in a temperature range of 280-320°C up to 600 kPa.

Keywords: pure hydrogen, water gas shift, membrane reactor

### 2. Extended Abstract

Water gas shift reaction (WGS) is a necessary upgrading step in an integrated H<sub>2</sub> production plant using light hydrocarbon, and its development in a Pd-Ag membrane reactor, where reaction and separation take place in the same vessel, presents several advantages, such as

- Hydrogen permeate pure stream production that can be directly fed to a PEMFC
- High CO conversion: the selective removal of a product from reaction side allows the TR thermodynamic equilibrium limits to be exceeded, shifting the reaction toward the formation of further products.
- Positive effect of the feed pressure that facilitates the permeation by pushing the reaction towards further product formation.

In a simple MR the first part of the membrane is not exploited by the permeation, the H<sub>2</sub> production by reaction being necessary in order to create a driving force promoting the permeation. The configuration TR+MR in series allows a better membrane exploitation, because an already partially converted current reaches the MR, therefore the permeation also involves the first part of the membrane (*Barbieri*

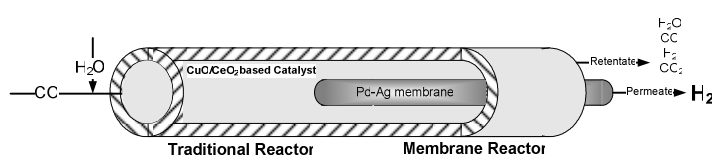


Figure 1 – Configuration of combined traditional and Membrane reactors

significant performance improvement in the MR.

and Bernardo, 2004). The space velocity and the reaction pressure effect on the CO conversion and H<sub>2</sub> recovery were analysed with special attention paid to a

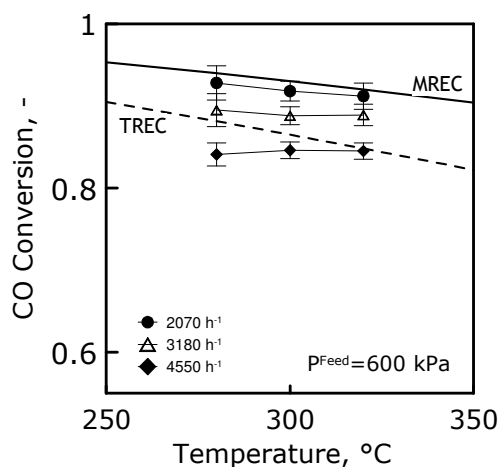


Figure 2 - CO Conversion as a function of Temperature at three different GHSV: 2,070 h<sup>-1</sup> (●), 3,180 h<sup>-1</sup> (Δ), 4,550 h<sup>-1</sup> (◆). Feed pressure=600 kPa.

CO conversion, always higher than that of a TR, also exceeds the TR equilibrium conversion (TREC) when a reaction pressure higher than 300 kPa is employed. In particular, 94.5% CO conversion was achieved at 320°C, 2070 h<sup>-1</sup> and 600 kPa with a gain of 10% with respect to the TREC and 20% to the TR, in the same operating conditions (Figure 2). In the meantime, 80% of the produced H<sub>2</sub> (equal to 70% of the H<sub>2</sub> extractable by the reaction) was recovered as pure stream. MR use also implies the possibility of working at high space velocity obtaining anyhow high CO conversion. In addition, the MR favours higher space velocity giving a very interesting performance. For instance, 91.7% and 88.5% CO conversion was measured at 3200 h<sup>-1</sup> and 4500 h<sup>-1</sup>, respectively, operating at 320°C, 600 kPa. Furthermore, no drops in the electrical performance were observed when the hydrogen permeated stream was directly fed to a commercial PEMFC.

### Acknowledgments

The Italian Ministry for Foreign affairs, Direzione generale per la promozione e la Cooperazione Culturale, Rome, Italy is gratefully acknowledged for co-funding this research. Johnson Matthey and Oleg M. Ilinitch (Engelhard, USA) are gratefully acknowledged for the membrane and catalysts supplied

### References

Barbieri, G.; Bernardo, P., Book of Carbon Dioxide Capture for Storage in Deep Geologic Formations – Results from the CO<sub>2</sub> Capture Project - Volume 1, Chapter 22, pp. 385-408. Elsevier, (2004).

## **Role of the Precipitation Device on the Properties of Al<sub>2</sub>O<sub>3</sub>-TiO<sub>2</sub> Mixed Oxides**

G. Mouret <sup>a</sup>, K. Mozet <sup>a</sup>, H. Muhr <sup>a</sup>, E. Plasari <sup>a</sup>, M. Martin <sup>b</sup>

<sup>a</sup> LSGC/CNRS UPR 6811 – Nancy Université/ENSIC - BP 20451 - 54001 NANCY Cedex, France

<sup>b</sup> IFP – Institut Français du Pétrole - BP 3 - 69390 Vernaison, France

### **1. Summary**

The quality of Al<sub>2</sub>O<sub>3</sub>-TiO<sub>2</sub> mixed oxides produced in continuous mode by using two original rapid mixers (the impinging jets and the sliding surface mixing device) as precipitation reactors are compared with ones obtained by a standard stirred tank. The properties of agglomerate particles strongly depend on the operating conditions and particularly on the type of precipitator used for their production.

Keywords: co-precipitation, mixed oxides, alumina, titanium dioxide, rapid mixers

### **2. Extended Abstract**

Recently, it is proved that Al<sub>2</sub>O<sub>3</sub>-TiO<sub>2</sub> mixed oxides could be excellent catalysts for many important industrial processes. To produce them, we have chosen a cost-effective route based on the precipitation by mixing of two reacting aqueous solutions, sodium aluminate and titanyl sulphate respectively, at 70°C and at pH = 9. The concentrations of both solutions are chosen in such a way that the final suspension at the outlet of the precipitator contains 60 g.L<sup>-1</sup> of solid phase. Two different Al<sub>2</sub>O<sub>3</sub>-TiO<sub>2</sub> catalysts are produced: the first one is composed of 10%, while the second one contains 30% of TiO<sub>2</sub>. The properties of the mixed oxides produced in continuous mode by two original rapid mixing systems are compared with ones obtained by a standard reactor (SR) equipped with a Rushton turbine. The first rapid mixer is composed of two opposite impinging jets (IJ) [Bénet et al. (2002)] immersed in the SR. The second one is a rotating disc reactor, also named sliding-surface mixing device (SSMD) [Rousseaux et al. (1999)].

In all cases, very porous agglomerates are obtained and their properties (particle size distribution, specific surface area and porosity) are measured. As illustration, Figure 1 shows the mean particle size as a function of principal operating parameters and the type of precipitator used. Here (and also in Figure 2), it is clearly proved that the reactor geometry is decisive for controlling the particle quality. In the case of the SSMD, the mean particle size is independent of the mean residence time, because in

this device, a very high shear rate value is produced. On the contrary, regarding SR, the mean particle size decreases as the mean residence time increases due probably to the combined effects of nucleation and agglomeration phenomena.

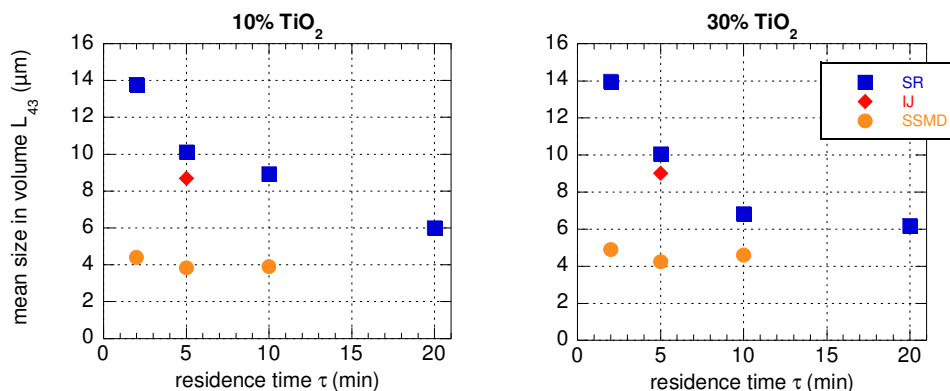


Figure 1 - Mean size of mixed oxide particles as a function of precipitation device and mean residence time.

In the case of Al<sub>2</sub>O<sub>3</sub>-TiO<sub>2</sub> mixed oxides used as catalysts, the mesoporosity is a matter of first importance. Under the same operating conditions, the mesoporosity attains the highest value when the impinging jets mixing device is used (see Fig. 2). In conclusion, the experiments reveal that the type of precipitator plays a major role on the properties of Al<sub>2</sub>O<sub>3</sub>-TiO<sub>2</sub> mixed oxides. Best results are given by the impinging jets device since it combines very high values of mesoporosity (more than 80%) and mean particle sizes similar to ones obtained by the standard reactor.

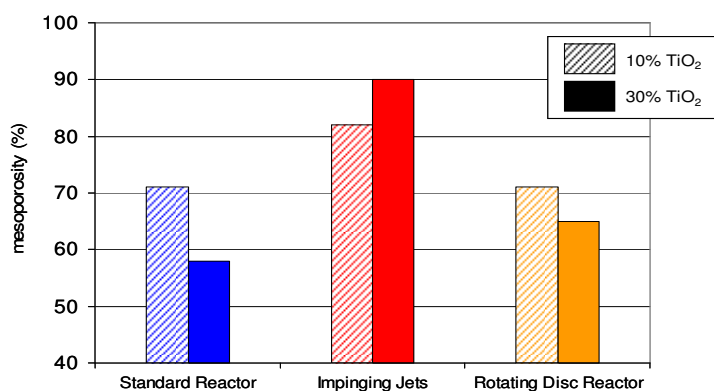


Figure 2 – Comparison of mesoporosities obtained with different reactor geometries at τ = 5 min.

## References

Bénet N., Muhr H., Plasari E. and Rousseaux J.M., (2002) *New technologies for the precipitation of solid particles with controlled properties*, Powder Technology, 128, 93-98.

Rousseaux J.M., Falk L., Muhr H., Plasari E., (1999) *Micromixing efficiency of a novel sliding-surface mixing device*, AIChE Journal, 45 (10), 2203-2213.



## Session T2-2P: Chemical Reaction Engineering – Poster

Abstract Number	Paper Title & Authors	Included
52	Estimating the Parameters of the Arrhenius Equation through Genetic Algorithm Technique using Maleic Anhydride Synthesis as Study Case E R Morais, G W C Oliveira, I R S Victorino, R M Filho	Yes
259	Efficient Synthesis, Structure Control and Homogeneous Catalytic Hydrogenation of Novel Arylidene Tetramic Acids. C Karaiskos, M Tzika, P Paraskevopoulou, J Markopoulos, O-I Markopoulou	Yes
271	Synthesis of some 3,4-bis-(bipyridilium chloride)-maleimides and their chromic behavior R Papadakis, ATsolomitis	Yes
406	Heterogeneous kinetics of the liquid phase synthesis and hydrolysis of isopropyl lactate P Delgado, M T Sanz, S Beltrán, B Saha	Yes
1012	Full factorial experimental design for heterogeneously catalysed esterification reactions A A I Citak, B D Deniz, C Izci	Yes
1138	Solid-state diffusion and crystal growth: two key steps for gas–solid reactions G Hu, K D Johansen, S Wedel	Yes
1262	Kinetic Modelling of a Polyphasic Reactor by Predetermination of Phases Equilibria Involved A J Bougrine, C Duriche, H Delalu	Yes
1279	Identifying Chemical Reaction Network Models S C Burnham, K Novakovic, M J Willis, A R Wright	Yes
1290	Reaction network determination using calibration free analytical data K Novakovic, M J Willis, AR Wright	Yes
1424	Establishment of a neural network model for ethylene production from naphtha feedstock M Ghadrđan, R Karimzadeh, R Bozorgmehri	Yes
1653	Modeling of Oxidative Dehydrogenation of Propane for Propylene Production in a Membrane Reactor M Fard Mostafavi, M R Omidkhah	Yes
1838	Modeling and simulation of industrial adiabatic fixed-bed reactor for the catalytic reforming of methane to syngas M T Mazandarani, H Ebrahim	Yes
2032	Modeling of rotating annular chromatographic reactor – application of statistical moments to indicate reasonable model simplifications E Molga, M Ciach	Yes

Session T2-2P

2090	Determination of the solubilities of mixed gases in mixed solvents using a novel HPNMR continuous flow system A Torres, J A Iggo, J Satherley, G Eastham, D Gobby	Yes
2616	Polymerization of Polypropylene Using Multi-Catalyst/Cocatalyst Systems and Investigation of Physical and Molecular Properties of Products A Ramazani, A Dashti, S Rezvantalab	Yes
2679	Simulation and sensitivity analysis of a multitubular fixed bed catalytic reactor to produce Phthalic anhydride O Gustavo, D Héctor	Yes
2731	Effect of pH and Hydrogen Peroxide on Ozonic Decomposition of NCW-1001 F Yamashita, N Shibata, T. Suzuki	Yes
2749	Photocatalytic oxidation of toluene F Jović, V Tomašić, S Zrnčević	Yes
2831	Cure reaction and heat transfer in the cylindrical mould V Kosar, Z Gomzi	Yes
3012	Mechanistic and reaction engineering aspects of nitrile hydrogenation P Schäringer, T E Müller, J A Lercher	Yes
3372	Modelling and simulation of a direct synthesis of dimethyl ether (DME) in a tubular reactor with a hybrid catalyst bed M Grzesik, A Ptaszek, J Skrzypek, P Ptaszek	No
3398	Inhibitory study and trickle bed reactor modeling for joint reactions of hydrodesulfurization, hydrodenitrogenation and hydrodearomatization during the hydrotreating of vacuum gas oils F Jimenez, V Kafarov, M Nunez, R M Filho	Yes
3405	A network of chemical reactions for modeling hydrocracking reactors R M C F da Silva, J L de Medeiros, O Q F Araújo	Yes
4069	The styrene photocatalytic degradation reaction S R Taffarel, M A Lansarin, C C C Moro	Yes

## Estimating the Parameters of the Arrhenius Equation through Genetic Algorithm Technique using Maleic Anhydride Synthesis as Study Case

E. R. Morais<sup>a</sup>, G. W. C. Oliveira, I. R. S. Victorino and R. Maciel Filho

*Laboratory of Optimization, Design and Advanced Control (LOPCA)  
Department of Chemical Processes, School of Chemical Engineering  
State University of Campinas (UNICAMP), Campinas, Brazil  
<sup>a</sup>erms@lopca.feq.unicamp.br*

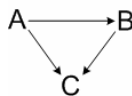
### 1. Summary

Maleic anhydride has numerous industrial uses and is of significant commercial interest worldwide. One of the synthesis routes for the production of maleic anhydride is based on the direct air oxidation of Benzene over vanadium pentoxide catalyst. An excess of air is applied, and a low Benzene concentration must be utilized in order not to exceed the flammability limit of the mixture, but the reactant Benzene cannot be recovered economically so the reactor must operate at high yields. The objective is to estimate the parameters set of the kinetic model, as the activation energy ( $E_i$ ) and the pre-exponential factor ( $A_i$ ), used in the calculation of the constant of Arrhenius ( $k_i$ ). This estimate is carried through Genetic Algorithms (GAs) with the purpose to minimize an objective function to be established, that considers the error between real values operation, values these that can be gotten from temperature or concentration reactor profiles for determined points throughout the reactor length supplied by literature, and the simulated theoretical values from the used model, so that a more adjusted kinetic model can be determined to be used in the reactor model. The results shown that, the method is a robust procedure which allows the reactor to be operated at high level of performance.

Keywords: kinetics, parameter estimation, optimization, genetic algorithms, fixed bed

### 2. Parameter Estimation

A high exothermic process of partial oxidation of benzene to maleic anhydride over  $V_2O_5$  catalyst has been assumed, it consists on a system of parallel and series equations with a classical triangular reaction scheme (Wohlfahrt and Emig, 1980; Westerink and Westerterp, 1988):



where  $A$  and  $B$  are benzene and maleic anhydride, respectively, while  $C$  denotes the combustion products ( $\text{CO}$ ,  $\text{CO}_2$ ,  $\text{H}_2\text{O}$ ).

The genetic code was coupled with the reactor model, and possesses the following characteristics: binary code; uses the elitism; search in niches and selection by tournament. The Arrhenius's Equation was linearized in accordance with Rodionova and Pomerantsev (2003). The kinetic parameters of reaction rate used from the literature together with the estimated values obtained with the optimization procedure are presented in the Table 1:

Parameters	Literature values		Estimated values	
	$A_i$	$Ea_i$ (Ea/R)	$A_i$	$Ea_i$ (Ea/R)
$k_1$ ( $\text{m}^3 \cdot \text{kg}_{\text{cat}}^{-1} \cdot \text{s}^{-1}$ )	$4,280 \times 10^3$	$-1,2660 \times 10^4$	$4,3198 \times 10^3$	$-1,2539 \times 10^4$
$k_2$ ( $\text{m}^3 \cdot \text{kg}_{\text{cat}}^{-1} \cdot \text{s}^{-1}$ )	$7,010 \times 10^4$	$-1,5000 \times 10^4$	$6,9543 \times 10^4$	$-1,5072 \times 10^4$
$k_3$ ( $\text{m}^3 \cdot \text{kg}_{\text{cat}}^{-1} \cdot \text{s}^{-1}$ )	$2,600 \times 10^1$	$-1,0800 \times 10^4$	$2,530 \times 10^1$	$-1,1545 \times 10^4$

Table 1: Kinetic parameters of reaction rate from the literature (Westerink, E. J., Westerterp, K. R., 1988) and estimated values.

The simulated temperature profile with the estimated kinetics parameters are compared to temperature profile obtained using the kinetics parameters from the literature as illustrated in Figure 1:

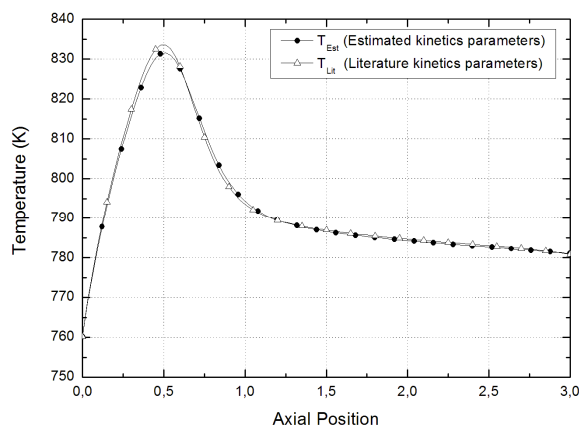


Figure 1: Axial temperature profile along the reactor length.

## References

- Rodionova, O.E., Pomerantsev, A. L., "Estimating the Parameters of the Arrhenius Equation", *Kinetics and Catalysis*, v 46, n 3, 2005, pp 305-308.
- Westerink, E. J., Westerterp, K. R., "Safe Design of Cooled Tubular Reactors for Exothermic Multiple Reactions: Multiple-Reaction Networks". *Chemical Engineering Science*, v 43, n 5, 1988, p 1051-1069.
- Wohlfahrt, K., Emig, G., "Compare Maleic Anhydride Routes". *Hydrocarbon Processing*, v 60, n 6, Jun, 1980, p 83-90.

## Efficient Synthesis, Structure Control and Homogeneous Catalytic Hydrogenation of Novel Arylidene Tetramic Acids.

Christos Karaiskos,<sup>a</sup> Maria Tzika,<sup>b</sup> Patrina Paraskevopoulou,<sup>c</sup> John Markopoulos,<sup>c</sup>  
Olga – Igglessi Markopoulou<sup>a</sup>

<sup>a</sup>Laboratory of Organic Chemistry, Department of Chemical Engineering, National Technical University of Athens, Zografos Campus, 15773 Athens, Greece

<sup>b</sup>Department of Chemistry and Biology, University of Siegen, Germany

<sup>c</sup>Department of Chemistry, University of Athens, Greece

### 1. Summary

Various products based on statines have been developed, over the last years, for the control of blood cholesterol and the prevention of heart diseases. Our research group has developed a series of arylidene tetramic acids, which can be submitted to a catalytic hydrogenation process, to afford novel statine analogues. Here, we present the efficient synthesis of novel arylidene tetramic acids and their catalytic hydrogenation.

Keywords: pharmaceutical synthesis, homogeneous catalysis, hydrogenation, statines, tetramic acids

### 2. Extended Abstract

#### 2.1. Synthesis of novel arylidene tetramic acids

Having investigated the physical and chemical properties, and also chemical transformations of arylidene tetramic acids (Figure 1), we can now present a complete range of these compounds. Our method allows for the efficient production (Table 1), and structure control of 5-arylidene tetramic acids. The activity of the tetramic ring depends on the functional groups of the structure. Therefore, the aromatic system can be stabilized or destabilized, depending on the nature of the groups, providing the means for accurate structure control.

The complexes of arylidene tetramic acids with transition metals demonstrate antibiotic activity, but another important possibility is the catalytic hydrogenation of arylidene tetramic acids at double bonds C(3)-C(4), and C(5)-C(6), which will afford statine analogues.

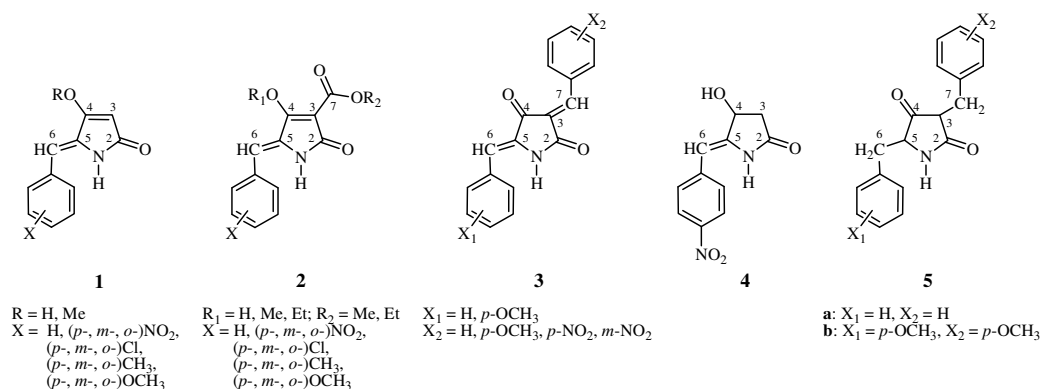


Figure 1. 5-Arylidene tetramic acids 1-3, and statine analogues 4-5.

Table 1. Conversion percentage for the synthesis of arylidene tetramic acids 1-3, and statine analogues 4-5.

Compounds	Conversion (%)	Compounds	Conversion (%)
1	80-90	4	60
2	55-70	5a	90
3	30-95	5b	70

## 2.2. Catalytic hydrogenation of arylidene tetramic acids

Statine analogues (Figure 1) can be produced with the catalytic hydrogenation of the respective 5-arylidene tetramic acids. This hydrogenation process must be enantioselective, and for that reason an homogeneous catalyst of Ru(II)-[(*S*)-BINAP] is employed. For the purposes of green chemistry, the reaction solvent is carefully chosen, and is preferably ethanol.

The hydrogenation process is very efficient, but only for substrates with certain functional groups (Table 1). A large number of experiments were performed, varying the temperature and pressure conditions, which illustrated the importance of process optimization.

The hydrogenation processes were performed using an Autoclaves Engineers' 300mL reactor controlled with a CT-1000 Control Tower. In conclusion we have achieved the synthesis of important novel arylidene tetramic acids, and their respective statine analogues.

## References

- Athanasellis G., Gavrielatos E., Igglessi-Markopoulou O., (2001) *J. Heterocyclic Chem.*, 38, 1203.
- Kitamura, M., Hsiao Yi, Ohta M., Tsukamoto M., Ohta T., Takaya H., Noyori R., (1994), *J. Org. Chem.*, 59.

## Synthesis of some 3,4-bis-(bipyridilium chloride)-maleimides and their chromic behavior

Raffaello Papadakis, Athanase Tsolomitis

*Laboratory of Organic Chemistry, School of Chemical Engineering, National Technical University of Athens, 15780 Athens, Greece*

### 1. Summary

A red shift in the absorption maxima is observed with increasing solvent polarity. A bathochromic shift which was also observed appears to be proportional to the electron withdrawing character of the imide N-substituent.

Keywords: viologens, pentacyanoferrate (II) complexes, solvatochromism

### 2. Extended Abstract

The viologens (1,1'-disubstituted 4,4'-bipyridilium dications) are a well known class of redox couples that undergo two reversible, one electron reduction to a radical cation and neutral form. Syntheses and photochromic properties of viologens have been discussed including such topics as matrix effects, molecular assembly, effects as counter-anion on photoreduction, and variety of color species of viologens have been reviewed<sup>1,2</sup>. On the other hand diarylmaleimide derivatives were also synthesized in an attempt to prepare photochromic compounds exhibiting photochromic reactivity even in polar solvents<sup>3</sup>, and in an attempt to shift the photosensitive wavelength longer than 450 nm<sup>4</sup>. A number of reports on dihetarylethenes with photochromic properties have been also reviewed<sup>5</sup>.

There have been also numerous studies on the thermal and photochemical reactions of unsaturated nitrogen heterocyclic ligands bound to pentacyanoferrate(II) and other metal centers.<sup>6,7,8</sup> The near UV-VIS spectra of these complexes are dominated by an intense metal-to-ligand charge transfer (MLCT) band assigned as  $P\pi^*(L) \leftarrow d\pi(M)$  in character. The energy of the MLCT band maximum is very sensitive to substituent changes of L (i.e., the energy of the  $\pi^*$  orbitals of the free L), with more electron withdrawing substituents causing red shifts in the MLCT maximum as well as greater ground state delocalization of the electron density into L ( $\pi$  back-bonding).

We report herein the synthesis of a number of new pentacyanoferrate(II) complexes of 3,4-bis-(bipyridilium)-N-substituted maleimides with the general chemical formula:  $Na_4[(CN)_5Fe-4,4'-bipy)_2-N\text{-substituted-maleimides}]^{-4}$  (**1**) where bipy is

bipyridine. These materials were prepared using conventional synthetic methods, following stepwise the series, starting from the commercial dichloromaleic anhydride, according to the reaction sequence: dichloromaleic anhydride→N-arymaleimide→3,4-bi-(bipyridilium)-N-substituted maleimide→**1**. For the latter reaction, which was done according to previously described procedures, Na<sub>3</sub>[Fe(CN)<sub>5</sub>(NH<sub>3</sub>)] and the bipyridilium maleimide were used. The final products were purified by recrystallization or by reprecipitation, the purity of these ligands was determined by elemental analyses<sup>9</sup>, <sup>1</sup>H and <sup>13</sup>C NMR spectroscopy. We are currently investigating the electronic and optical properties using cyclic voltammetry, HRS, single-crystal X-ray studies and Stark spectroscopy. Herein we present some solvatochromic properties of these ligands using the UV-VIS absorption spectra measured in both 1,4-dioxane and acetonitrile. These spectra feature intense UV absorptions due to  $\pi\rightarrow\pi^*$  intraligand transitions, together with intense, broad d(Fe<sup>II</sup>)→ $\pi^*(L)$  (L=bipyridil-maleimide ligand) visible MLCT bands, (table 1).

Compound 1	$\lambda_{\max}$ nm (log $\epsilon_{\max}$ )	
	in 1,4-dioxane	in acetonitrile
R (N-substituent)		
4-CH <sub>3</sub> OC <sub>6</sub> H <sub>4</sub>	543(3,57)	682(3,76)
	272(4,21)	275(4,24)
4-CH <sub>3</sub> C <sub>6</sub> H <sub>4</sub>	551(3,61)	723(3,80)
	274(4,21)	283(4,30)
C <sub>6</sub> H <sub>5</sub>	560(3,59)	742(3,82)
	278(4,27)	285(4,32)
3-ClC <sub>6</sub> H <sub>4</sub>	568(3,64)	748(3,81)
	282(4,29)	294(4,32)
4-ClC <sub>6</sub> H <sub>4</sub>	573(3,61)	764(3,81)
	287(4,30)	296(4,33)

Table 1: The results of the UV-Vis spectra of the compound 1

The observed positive solvatochromism pronounces interactions between the cyanide ligands and the solvent medium. These large red shifts are accompanied by significant increases in intensity. Using the previously reported techniques we will attempt to investigate the effect of the unavoidable nonplanar conformation of the adjacent 3,4-hetaryls, which partially block the interaction of aromatic substituents to the five-membered ring.

## References

1. M. Nanasawa, *Organic Photochromic and Thermochromic Compounds*, 341-346 (1999).
2. H. Kamogawa (1992) *Appl. Photochromic Polym. Syst.* 207-246.
3. T. Yamagushi, M. Irie. (2004) *Chem. Lett* 33, 1398-1399
4. T. Yamagushi, M. Matsuo, M. Irie (2005) *Bull. Chem. Soc. Jpn.*, 78, 1145-1148.
5. M. M. Krayuskin, N. D. Zelinsky (2001) *Chem. Heterocycl. Comp*, 37, 15-36.
6. J. E. Figard, J. D. Peterson (1978) *Inorg. Chem.*, 17, 1059-1063.
7. J. E. Figard, J. V. Paukstelis, E. F. Byrne, J. D. Peterson (1977) *JACS*, 99, 8417-25.
8. B. J. Coe et. al. (2006) *J. Amer. Chem. Soc.*, 128, 12192-12204.
9. Some differences in elemental analyses were observed due to hydration of the ligands.



## Heterogeneous kinetics of the liquid phase synthesis and hydrolysis of isopropyl lactate

P. Delgado,<sup>a</sup> M. T. Sanz,<sup>a</sup> S. Beltrán,<sup>a</sup> B. Saha<sup>b</sup>

<sup>a</sup>Department of Chemical Engineering, University of Burgos, 09001 Burgos. Spain

<sup>b</sup>Department of Chemical Engineering, Loughborough University, LE11 3TU, Loughborough, Leicestershire, United Kingdom

### 1. Summary

Separation and purification of lactic acid from fermentation broth is a daunting problem because of its non-volatile nature and also due to the presence of other organic impurities. Esterification of lactic acid with isopropanol followed by hydrolysis of isopropyl lactate to produce pure lactic acid is an effective technique for the recovery of lactic acid. Moreover, isopropyl lactate is used as a very important pharmaceutical intermediate. In the present work, esterification of lactic acid with isopropanol and the subsequent hydrolysis of the corresponding ester, i.e. isopropyl lactate, have been studied in a stirred batch reactor using macroporous and gelular cation-exchange resins. The influence of different operating parameters such as speed of agitation, catalyst particle size, reaction temperature, catalyst loading and initial reactants molar ratio has been studied for optimisation of the reaction condition. Additionally, the adsorption constants for water and isopropanol on Purolite<sup>®</sup> CT-124 (a gelular cation-exchange resin) have been determined by performing liquid phase adsorption experiments. Experimental kinetic data of esterification and hydrolysis reactions have been correlated simultaneously. The kinetic data have been correlated with both pseudo-homogeneous (PH) and adsorption based reaction rate models, e.g., Eley-Rideal (ER) and Langmuir-Hinshelwood-Hougen-Watson (LHHW). The non-ideality of each component in the liquid phase reacting mixture has been accounted for by using the activity coefficient *via* the use of UNIQUAC equation.

Keywords: Esterification, hydrolysis, lactic acid, isopropyl lactate, ion-exchange catalysis.

### 2. Extended Abstract

The objective of this research is to study the kinetic behaviour of the heterogeneously catalysed esterification of lactic acid with isopropanol and the subsequent hydrolysis of isopropyl lactate in a jacketed stirred batch reactor and to analyse the kinetic results by pseudo-homogeneous and heterogeneous rate models.

A comparison of the catalytic performance of six different commercial ion exchange resins (Purolite CT-124, CT-151, CT-175, CT-275, CT -145H, supplied by Purolite International Ltd.; Amberlyst 15 purchased from Aldrich) confirms the best catalytic activity of CT-124 and the lowest activity for Amberlyst 15 under otherwise identical conditions. It was found that the speed of agitation (varied between 250 and 400 rpm) and the catalyst particle size (between 300 and 710  $\mu\text{m}$ ) do not have any significant effect on the rate of esterification reaction delineating the absence of external and internal mass transfer resistances for the present system (Chakrabarti and Sharma, 1992).

Kinetic experiments were performed in the temperature range from 333.15 K to 363.65 K for the esterification and hydrolysis reactions. It was found that the reaction rate increases with an increase in reaction temperature. However, the equilibrium conversion was nearly equal in the range of temperatures considered for this work. In general, in most of the esterification reactions, the equilibrium constant is a weak function of the temperature because of the small value of the heat of reaction. The same behavior was observed in the reaction of lactic acid with methanol (Sanz *et al.*, 2002) and ethanol (Delgado *et al.*, 2007). A value for the activation energy of 59.47  $\text{kJ}\cdot\text{mol}^{-1}$  was found in the fitting procedure by applying the LHHW model for the esterification of lactic acid with isopropanol. The high value of the activation energy confirms the absence of mass transfer limitation. The catalyst loading was varied from 2.5 wt.% to 10 wt.% for the esterification and hydrolysis reactions. An increase in the catalyst loading leads to an increase of the reaction rate due to an increase in the total number of active catalytic sites. The initial molar ratio of isopropanol to lactic acid was varied from 2 to 10 for the esterification and hydrolysis reactions. The equilibrium conversion increases with an increase in the initial reactants molar ratio.

The adsorption constants were determined from independent sorption experiments that were performed for the binary non-reactive system (isopropanol + water). The adsorption constants were also calculated assuming Langmuir-type adsorption following the expression proposed by Pöpkén *et al.* (2000) using the Simplex-Nelder-Mead method and it was observed that water was more strongly adsorbed than isopropanol. For batch kinetic modelling, the activity coefficients of the components in the liquid phase were calculated by using the UNIQUAC equation. Amongst all the models used, best results were obtained for the LHHW model; nevertheless, due to the high polarity of the reacting medium, the PH model also provides a good agreement with the experimental batch kinetic data.

## References

- Chakrabarti, A., Sharma, M.M., (1993) *Reactive Polymers*, 20, 1-45.
- Sanz, M.T., Murga, R., Beltrán, S., Cabezas, J. L.(2002) *Ind. Eng. Chem. Res.*, 41, 512-517.
- Delgado, P., Sanz, M.T., Beltrán, S., (2007) *Chem. Eng. J.*, 126, 111-118.
- Pöpkén, T., Götze, L., Gmehling, J., (2000) *Ind. Eng. Chem. Res.*, 39, 2601-2611.

## Full factorial experimental design for heterogeneously catalysed esterification reactions

A. Alime Izci Citak,<sup>a</sup> B. Duygu Deniz,<sup>a</sup> C. Ertugrul Izci<sup>b</sup>

<sup>a</sup>Department of Chemical Engineering, Eskisehir Osmangazi University, 26480 Eskisehir, Turkey

<sup>b</sup>Physics Department, Anadolu University, 26470 Eskisehir, Turkey

### 1. Summary

The esterification kinetics of acetic acid with isobutanol in the presence of Amberlyst-36 as heterogeneous acid catalyst was investigated by applying experimental design. In order to examine the main factors and their interactions for the conversion of the acetic acid, 2<sup>3</sup> full factorial experimental design has been used. Effects of catalyst amount, speed of agitation and reaction temperature were selected as the factors with the high and low level. The statistical test showed that the reaction temperature, the catalyst amount and interaction of reaction temperature-catalyst amount are effective on the reaction rate but there is no influence of the speed of agitation. Regression equation formulated for reaction rate was represented as a function of response variables. Also, from the reaction rate data a pseudo-homogeneous model was developed and activation energy was determined as 83.3 kJ/mol.

Keywords: Esterification, experimental design, ion-exchange resin, isobutyl acetate, kinetics

### 2. Extended Abstract

#### 2.1. Introduction

Isobutyl acetate which is the product of this study is widely used in the industries of medicine, pesticide chemical, plastic, paint also used in the production of lacquer and similar coatings and in the food industry as flavouring agent. The method most widely used to synthesis an ester is reaction of the corresponding carboxylic acid with an alcohol. The reaction is catalysed by heterogeneous acid catalysts in the past years (Garcia et al., 2001; Saultani et al., 2001; Manahar and Divakar, 2004) These catalysts are non-corrosive and easy to separate from the reaction mixture. They can also be used repeatedly over a prolonged period without any difficulty in handling and storing them (Yadav and Rahuman, 2002; Sanz et al., 2002). Among solid catalysts, ion exchange resins have been used for relatively low temperature reactions and are available in a variety of forms and strengths (Harmer and Sun, 2001; Yadav and Rahuman, 2003; Ali and Merchant, 2006). In the present work, statistical design was applied to predict the behaviour of esterification reaction. Also, a pseudo homogeneous kinetic model was developed from the experimental data.

#### 2.2. Method

Experiments were performed according to the following procedure: 1,4-Dioxan and the ion exchange resin were charged into stirring batch reactor and in predetermined ratio isobutyl alcohol added into the reactor. After reaching desired temperature, acetic acid

was drained into the stirring batch reactor. This moment is considered as the beginning of the experiment. Samples were taken at regular intervals. The total reaction time was 8 hours and analysed by gas chromatography (Agilent 6890N GC) with a flame ionization detector.

### 2.3. Statistical Analysis

In order to examine the main factors and their interactions for the conversion of acetic acid in esterification reaction, a factorial of the type 2<sup>3</sup> has been used. In Table 1, x<sub>1</sub>, x<sub>2</sub> and x<sub>3</sub> represent the levels of speed of agitation, temperature and catalyst amount, respectively, and X<sub>1</sub>, X<sub>2</sub> and X<sub>3</sub> are the corresponding values in coded forms.

Table 1: The high and low levels of experimental factors

Levels of Variables	Speed of agitation (rpm)		Temperature ( °C)		Catalyst loading (g)	
	Actual (x <sub>1</sub> )	Coded(X <sub>1</sub> )	Actual (x <sub>2</sub> )	Coded(X <sub>2</sub> )	Actual (x <sub>3</sub> )	Coded(X <sub>3</sub> )
Low Level	300	-	45	-	0.2	-
High Level	500	+	75	+	0.5	+

Table 2: Design of trial runs (in coded form) for the conversion of the acetic acid in two replicate experiments

Trial No	X <sub>1</sub>	X <sub>2</sub>	X <sub>3</sub>	X <sub>1</sub> X <sub>2</sub>	X <sub>1</sub> X <sub>3</sub>	X <sub>2</sub> X <sub>3</sub>	X <sub>1</sub> X <sub>2</sub> X <sub>3</sub>	Y Conversion of the acetic acid	Y Conversion of the acetic acid	Y Total Conversion of the acetic acid	Y Average Conversion of the acetic acid
1	-	-	-	+	+	+	-	0.0497	0.0493	0.0990	0.0495
2	+	-	-	-	-	+	+	0.0490	0.0495	0.0985	0.0493
3	-	+	-	-	+	-	+	0.1315	0.1335	0.2650	0.1325
4	+	+	-	+	-	-	-	0.1316	0.1347	0.2663	0.1331
5	-	-	+	+	-	-	+	0.0521	0.0527	0.1047	0.0524
6	+	-	+	-	+	-	-	0.0513	0.0538	0.1050	0.0525
7	-	+	+	-	-	+	-	0.2531	0.2519	0.5050	0.2525
8	+	+	+	+	+	+	+	0.2573	0.2522	0.5096	0.2548

### 2.4. Results and Discussion

According to the results obtained from the experimental data in Table 2, It is found that largest factor effects are for temperature (0.1423), catalyst amount (0.0619) and the temperature-catalyst amount interaction (0.0588), although the interaction effect does not appear to have large an impact on the conversion of the acetic acid as the main effects. Also, it is determined that there is no effect of speed of agitation in the synthesis of isobutyl acetate. Since  $F_{0,05;1;8}=5.32$  the value of 95.0% confidence level, temperature(4132.65), catalyst amount(780.61) and the temperature-catalyst amount interaction(704.08) effects in giving F<sub>0</sub> greater than 5.32 have statically significance.

### References

- Harmer, M.A., Sun, Q., (2001) *Applied Catalysis A:General*, 221, 45-62.  
 Yadav, G.D. and Rahuman M.S.M., (2003) *Clean Tech Environ Policy*, 5, 128-135.  
 Garcia, R., Renedo, A., Martinez, M., Aracil, J., (2001) *Enzyme and Microbial Technology*, 30, 110-115.  
 Saultani, S., Engouser, J.M., Ghoul, M., (2001) *Journal of Molecular Catalysis B:Enzymatic*, 11, 725-731.  
 Manahar, B. and Divakar, S., (2004) *Process Biochemistry*, 39, 847-853.  
 Ali, S.H. and Merchant, S.Q., (2006) *International Journal of Kinetics*, 38, 593-612.  
 Sanz, M.T., Murga, R., Beltran, S., Cabezas, J.L., (2002) *Ind. Eng. Chem. Res.*, 41, 512-517.  
 Yadav, G.D. and Rahuman, M.S.M.M., (2002) *Organic Process Research&Development*, 6, 706-713.

## **Solid-state diffusion and crystal growth: two key steps for gas–solid reactions**

G. Hu, K. Dam-Johansen, S. Wedel

*Department of Chemical Engineering, Technical University of Denmark, 2800 Lyngby, Denmark*

### **1. Summary**

Gas-solid reactions with solid product formation usually involve nucleation and crystal grain growth of the solid product. Direct sulfation of limestone is an example of such reaction. Experimental results obtained with this reaction indicate that solid-state diffusion is most likely an intermediate step that is responsible for the transport of the product ions formed by chemical reaction to the nucleation/growth sites. For a gas-solid reaction with solid product formation, the whole reaction process may thus involve the following 5 steps: gas film diffusion, pore diffusion in product layer, chemical reaction, solid-state diffusion, and nucleation and crystal growth. The overall kinetics is usually significantly influenced by solid–state diffusion because of its slow nature. The significant influence of solid–state diffusion is an important reason for the special kinetic behaviour of such reactions. In addition, due to the involvement of nucleation and crystal growth, crystallographic properties of the solid reactant and product have a large influence on the overall kinetics as well since those properties determine whether nucleation and crystal growth can be oriented. The mechanism of gas–solid reactions with solid product formation is clearly more complicated than the widely used three–step modelling concept, i.e. gas film diffusion, product layer diffusion and chemical reaction.

Keywords: gas-solid reaction, nucleation, sulfation, limestone, solid-state diffusion.

Book of Abstracts  
European Congress of Chemical Engineering (ECCE-6)  
Copenhagen, 16-20 September 2007

## **Kinetic Modelling of a Polyphasic Reactor by Predetermination of Phases Equilibria Involved**

A.J. Bougrine, C. Duriche, H. Delalu

*Laboratoire Hydrazines et Procédés  
UMR 5179 Université Claude Bernard Lyon 1 – CNRS – Isochem/SNPE  
43, Bd du 11 Novembre 1918, 69622 Villeurbanne Cedex, France  
anne-julie.bougrine@univ-lyon1.fr*

### **1. Summary**

During the process of synthesis of a hydrazine, a transient miscibility gap appears. An experimental determination of the properties of the liquid-liquid equilibria involved permits to develop a predictive kinetic model for this polyphasic reactor. In fine, this study allows then to predict the behavior of the reaction mixtures in a plug-flow reactor according to the degree of conversion of the reaction whatever the operating conditions used.

Keywords : Hydrazine, kinetic modelling, polyphasic reactor, phases equilibria

### **2. Extended Abstract**

The know-how of our laboratory focuses on the development of integrated original processes, including the synthesis, extraction, purification and stability of solid or liquid hydrazines. The methods of preparation are selective and clean (chemistry in water with no use of organic solvent) and permit to produce and extract, by use of the particularisms involved in the phase diagrams, a hydrazine in conformity with the particularly restricting specifications (pharmaceutical or spatial applications as propellants).

Within the framework of the development of a process of synthesis of a hydrazine of pharmaceutical interest (hypoglycaemic drug), this work deals with the modelling of a plug-flow reactor which presents, in steady state conditions, a double diphasic and monophasic segment. This case arises in the second step of the elaboration of N-N bonding, by action of monochloramine with an excess of amine in strongly alkaline medium.

First step :  $\text{NH}_3 + \text{OCl}^- \rightarrow \text{NH}_2\text{Cl} + \text{OH}^-$  (monophasic medium)

Second step :  $\text{NH}_2\text{Cl} + \text{R}_1\text{R}_2\text{NH} \rightarrow \text{R}_1\text{R}_2\text{NNH}_2 + \text{HCl}$   
 $\text{HCl} + \text{NaOH} \rightarrow \text{NaCl} + \text{H}_2\text{O}$  (diphasic + monophasic medium)

In this configuration, amine and sodium hydroxide are responsible of a transient miscibility gap. The partial neutralization of excess NaOH by formed HCl leads, at the time  $t = t'$  and for the degree of conversion of the reaction  $\xi = \xi'$ , to a breaking of the polyphasic state and the continuation of the reaction in a homogenous medium.

The developed method consists in predicting the variation of the diphasic system according to  $\xi$ . The successive preparation of mixtures ( $\xi = 0$  ;  $\xi = 0.1$  ;  $\xi = 0.2$  ... ;  $\xi = \xi'$ ) allows to determine the variables  $C_i^\alpha, C_i^\beta, v^\alpha, v^\beta$  as a function of  $\xi$ , by physico-chemical analysis of the two phases in equilibrium. Then, it is possible to determine the value  $\xi'$  from which the medium becomes homogeneous.

Taking into account the distribution of the reagents between the phases in equilibrium, the evolution of the system is described by the following equation :

$$\frac{dC_i^\alpha}{dt} = -(k^\alpha \cdot C_i^\alpha \cdot C_j^\alpha) + \left( \frac{C_i^\alpha}{v^\alpha} \cdot \frac{dv^\alpha}{dt} \right) \quad \text{with} \quad C_{i,j}^\alpha = f(C_i^0, C_j^0, \xi, T) \quad \text{and}$$

$$v^\alpha = g(\xi, T)$$

The first term in brackets indicates the effect of the chemical transformation, whereas the second results from the variation of the volume  $v$ .

The presented work permits to establish the residence time of the diphasic and monophasic segments whatever the experimental conditions.



## Identifying Chemical Reaction Network Models

S. C. Burnham, K. Novakovic, M. J. Willis, A. R. Wright

*School of Chemical Engineering and Advanced Materials, Newcastle University, Newcastle-upon-Tyne, NE1 7RU, UK*

### 1. Summary

This presentation demonstrates the identification of underlying nonlinear ordinary differential equation (ODE) models that represent chemical reaction networks. The proposed method uses species' concentration and rate of heat evolution data which can be obtained from a reaction calorimeter. The identification procedure is demonstrated for a simulated Van de Vusse reaction system. It is shown that accurate estimates of the network rate constants and individual heats of reactions may also be generated.

Keywords: reactor modelling, differential equations, system identification

### 2. Extended Abstract

One of the key issues for fine chemical and pharmaceutical companies is to reach the market with many new products as quickly as possible. Within these industries multi-purpose plants which are suitable for a variety of customer specifications are often used. This leads to fast changing discontinuous processes incorporating batch or semi-batch reactors. A major problem facing these companies is the scale up of a process from laboratory to full-scale production in the shortest possible time, preferably avoiding pilot-plant testing.

Modelling and simulation studies are often used to assist scale-up. For conventional equation-based modelling software it is necessary to formulate mathematical equations in order to describe the process dynamics. In general, the behaviour of process design variables such as flow-rates, reactor volumes and inlet concentrations of species are well understood. However, obtaining knowledge of the chemistry, in particular the chemical reaction network remains a limiting step.

Traditional methods for determining reaction networks involve postulating a number of different structures which are then fit to experimental data. The reaction network whose ordinary differential equation (ODE) model provides the highest prediction accuracy with respect to the experimental data is taken to be the correct structure.

This is a time consuming procedure requiring both chemistry and modelling expertise.

From a system identification perspective, the task of identifying a useful network is one of determining the structure as well as the parameters of a set of non-linear ODEs. This is a non-trivial system identification task; however, recent work (Burnham *et al.*, 2007) has demonstrated that it is possible to elucidate the network by partitioning the problem into simpler subtasks. These subtasks are a) determine the number of reactions i.e. the number of rate expressions, b) define a set of all possible concentration terms, c) define the structure of the individual rate expressions, d) determine the structure of the individual species' ODEs, e) determine the kinetic rate constants and the individual heats of reactions.

The number of reactions is determined through assessment of the linear dependence of species derivatives. The method uses singular valued decomposition (SVD) to select the set of largest eigenvalues which represent a summed variance larger than a fixed threshold. The number of eigenvalues contained in this set represents the estimated rank of the matrix of species derivatives, which infers the number of independent reactions,  $\hat{l}$ . A concentration term is defined as the product of the reactant concentrations; the set is obtained by considering all theoretical reactions. To define the structure of the individual rate expressions it is assumed that the reaction has been performed in a reaction calorimeter and that reaction heat ( $Q_r$ ) data is available. Best subsets regression of the  $Q_r$ -time profile data against all combinations of  $\hat{l}$  possible concentration terms provides an estimate of the structure of the estimated  $\hat{l}$  rate expressions. The structure of the individual species' ODEs is determined by regression of the species' derivatives against the  $\hat{l}$  concentration terms in the estimated individual rate expressions. As each ODE expression must be physically consistent with the others in the sense of conservation of mass and adherence to the law of mass action kinetics, it is possible to extract the reaction network by finding matching concentration terms in the rate expressions. Finally, the kinetic rate constants and the individual heats of reactions are determined using standard kinetic fitting software.

The approach is demonstrated and critically assessed for a simulated four species, three reaction, Van de Vusse reaction scheme (Van de Vusse, 1964) operated in an isothermal constant volume batch process. The concentration measurements and the  $Q_r$  values were subjected estimated measurement error. The presentation demonstrates that the ODEs representing the underlying reaction network are obtained and furthermore accurate estimates of the network rate constants and individual heats of reactions are attained.

## References

- Burnham, S. C., Willis, M. J., and Wright, A. R. (2007). Identifying Chemical Reaction Network Models, *Submitted to The 8<sup>th</sup> Symposium on Dynamics and Control of Process Systems, Cancun, June.*
- Van, de Vusse J. G. (1964) Plug-flow Type Reactor Versus Tank Reactor. *Chem. Eng. Sci.*, 19, 994-997.

## **Reaction network determination using calibration free analytical data**

K. Novakovic, M.J. Willis and A.R. Wright

*University of Newcastle, School of Chemical Engineering and Advanced Materials,  
Newcastle upon Tyne, NE1 7RU, UK*

### **1. Summary**

A major bottleneck to the transition from chemical research to process development is that more quantitative information is needed for scale up, thermal safety and process optimisation studies. The quintessence of this information is the kinetic model of the reaction system that allows the chemical engineer to use modelling and simulation software to apply reaction-engineering principles and explore regions of parameter space not investigated experimentally. The first requirement in the determination of the predictive kinetic model is a reliable reaction network (rate determining reactions in a chemical mechanism). The experimental data required to determine a chemical reaction network are generally the species time-concentration data obtained from a series of experiments, using one of a number of analytical devices. The usual method used to obtain species' concentrations with these devices is to use an internal standard. This requires determination of a constant called the response factor which relates the area of the peak produced by a known concentration of the internal standard and the area of the peak produced by an unknown concentration of the species whose concentration is being measured. The aim of this work is to mathematically demonstrate that a network structure can be obtained without the need for response factor determination prior to sample analysis.

Keywords: Reaction network, analytical data, kinetic modelling

### **2. Extended Abstract**

The determination of a reliable reaction network that can be used in simulation studies is the initial requirement for reaction engineering applications such as scale up, moving from a batch process to a continuous one, thermal safety studies etc. The usual method used to determine a reaction network is to postulate a number of different structures which are then fitted to experimental data. The reaction network whose ordinary differential equation model provides the highest prediction accuracy with respect to the experimental data is taken to be the correct structure.

The experimental data used are generally the species time-concentration data obtained from a series of batch or fed-batch experiments, using one of a number of analytical devices, including GC (Gas Chromatograph), GC-MS (Gas Chromatograph-Mass Spectrometer), HPLC (High Performance Liquid Chromatograph) etc. The usual method used to obtain species' concentrations with these devices is to use an internal standard; a chemical that is inert to other components of the reaction system investigated and is present in each sample in known concentration. This requires determination of a constant called the response factor which relates the area of the peak produced by a known concentration of the internal standard and the area of the peak produced by an unknown concentration of the species whose concentration is being measured. The response factor differs with each species and needs to be determined prior to sample analysis therefore requiring a standard for each species, i.e. that each individual species has been synthesised.

A common problem is that some of the products and intermediates species standards are not available. This may be because the species cannot be isolated or synthesised or that obtaining a satisfactory purity for the standard is difficult and time consuming. Within process development, time to market is a critical process driver. The ability to differentiate between potential network structures while not being reliant on species standard characterisation would have the potential to remove a significant bottleneck in process development time. The aim of this work is to mathematically demonstrate that a network structure can be obtained without the need for response factor determination prior to sample analysis. As the ratio of the species area to the reference standard area observed through, for example GC-MS analysis, is directly proportional to the species concentration this data may be used directly to elucidate network structure.

The approach is demonstrated and critically assessed through simulated case studies addressing reaction systems where (1) there are differing numbers of species (2) some of the species are not detected by the analytical device (3) the reactant initial conditions relate to a known ratio of the species area to the reference standard area and (4) species of known initial concentration are not detected. Finally, the practicality of the method is demonstrated using experimental data obtained from the L-proline catalysed aldol reaction of p-nitrobenzaldehyde with acetone (Novakovic et al. 2006).

## References

Novakovic, K., Grosjean, C., Schütz, T., Willis, M.J., Wright, A.R. and Whiting, A., (2006) *17<sup>th</sup> International Congress of Chemical and Process Engineering, CHISA 2006*.

## **Establishment of a neural network model for ethylene production from naphtha feedstock**

M. Ghadrđan,<sup>a</sup> R. Karimzadeh,<sup>a</sup> R. Bozorgmehri,<sup>b</sup>

<sup>a</sup>*Department of Chemical Engineering, Tarbiat Modares University, Tehran, Iran*

<sup>b</sup>*Department of Chemical Engineering, Sharif University of Technology, Tehran, Iran*

### **1. Summary**

In this paper, the steam cracking process with naphtha feedstock is modeled by a multilayer, feed forward, fully connected neural network. Feed and steam residence times and coil outlet temperature were the input variables to the network. These input variables will help to generalize the model. The output variables of the network were hydrogen, methane, acetylene, ethylene and ethane yields. The cracked gas compositions were the output variables of the network. The optimum topology of network was a three layers network with fifteen neurons in hidden layer. The network outputs were in agreement with the experimental values.

Keywords: modelling, artificial neural network, thermal cracking, naphtha

### **2. Extended Abstract**

Thermal cracking of hydrocarbons could convert them into valuable raw materials, which can be used in the petrochemical industry for polymer production. Unfortunately, the absence of a simple predictive applied model of pyrolysis is an obstacle to the development of practical methods of conversion.

Neural networks have been used as a promising opportunity, when complex reaction systems can not be well identified, or in the case of lack of basic knowledge of reaction mechanisms. It has been claimed that Neural Networks are 120-5000 times faster than phenomenological models (Fontaine et al. 2001), and can therefore lead to significant reductions in computation times.

The topology of a neural network is determined by the number of layers in the ANN, the number of neurons in each layer and the transfer functions. A network with one hidden layer is able to approximate almost any type of nonlinear mapping (Cybenko 1989). The most suitable neural network topology turned out to be a network with fifteen nodes in the hidden layer (Figure 1). The input variables are chosen in a way to help generalize the neural network model, so that it can be used for a similar reactor of different geometry. The network was trained using 346 training data which was generated from a rigorous mathematical model of the thermal cracking reactor of

Tabriz petrochemical complex. The running program was written in VBA. The program is linked to HYSYS property package. Then, the generated data was transferred to the training program which was written in MATLAB. The comparison of experimental and calculated cracked gas composition for 70 test sets are shown in Figures 2-6. As it is obvious from the figures, the experimental and calculated values are in good accordance.

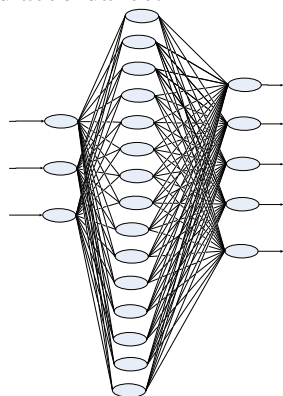


Figure 1: Optimum structure of ANN model for the reactor

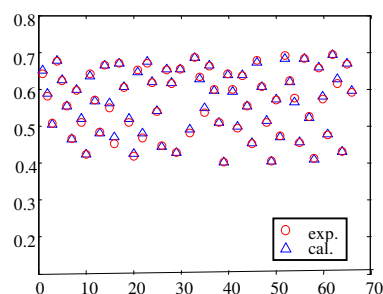


Figure 2: comparison of experimental and predicted values for H<sub>2</sub> yield

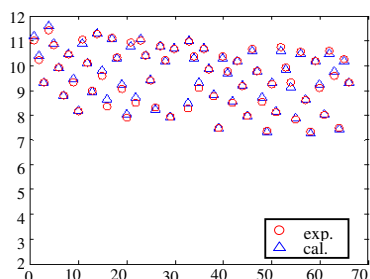


Figure 3: comparison of experimental and predicted values for CH<sub>4</sub> yield

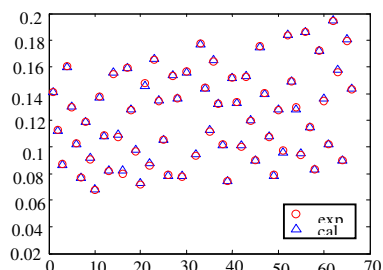


Figure 4: comparison of experimental and predicted values for C<sub>2</sub>H<sub>2</sub> yield

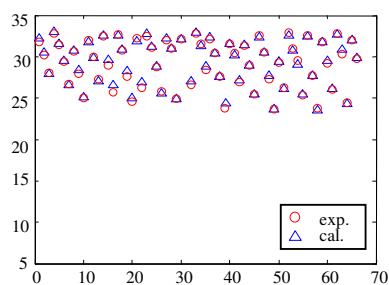


Figure 5: comparison of experimental and predicted values for C<sub>2</sub>H<sub>4</sub> yield

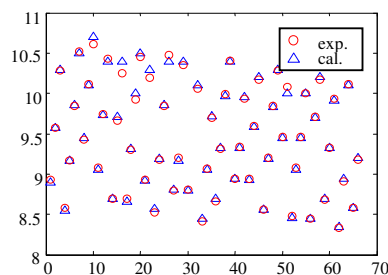


Figure 6: comparison of experimental and predicted values for C<sub>2</sub>H<sub>6</sub> yield

## References

- Cybenco, G.V., (1989) *Signals Syst.*, 2, 303–314.  
 Fontaine, J.L. and Germain, A., (2001) *Comp. Chem. Eng.*, 25, 7–8 1045–1054.

## Modeling of Oxidative Dehydrogenation of Propane for Propylene Production in a Membrane Reactor

M. Fard Mostafavi,<sup>a</sup> M.R. Omidkhah<sup>a</sup>

<sup>a</sup>Department of Chemical Engineering, Tarbiat Modares University, Tehran, Iran

### 1. Summary

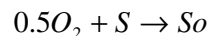
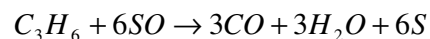
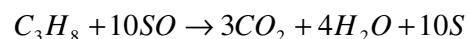
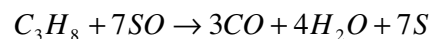
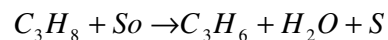
This study examines the oxidative dehydrogenation of propane in the membrane reactor and presents the oxygen diffusion model from the membrane into the reactor in order to complete dehydrogenation reaction. To calculate the diffusion coefficient of gas species in the reactor, Dusty Gas Model was employed. This model shows reasonable concurrence with empirical results compared to other diffusion models. Runge-Kutta method was applied to solve the equations. The findings of the aforementioned equations indicated a reasonable concurrence between the results accumulated from the experiments and modeling.

**Keywords:** modeling, oxidative dehydrogenation of propane, propylene, membrane reactor

### 2. Extended Abstract

#### Mechanism of oxidative dehydrogenation of propane over a V/MgO catalyst

A detailed discussion of the mechanism of oxidative dehydrogenation may be found in Romas et al (2000). The kinetic data were calculated in the temperature range between 450-550 °C. The reaction took place in the fixed-bed reactor that led to the produce propylene, water vapor and carbon oxides (Hou et al. 2001). The reactions are as below:



S: active site of catalyst

### Dusty Gas Model

The Dusty Gas Model (DGM) is being frequently used to model multi-component transfer through asymmetric composite membrane. The main model equation which is capable to predict molar flux densities ( $J_i$ ) for all components is shown below: (Burggraaf et al. 1996)

$$-\frac{p}{\mathcal{R}T} \nabla x_i - \frac{x_i}{\mathcal{R}T} \left( 1 + \frac{B_0^e}{D_{K,i}^e \eta} p \right) \nabla p = \sum_{j=1, j \neq i}^n \frac{x_j J_i - x_i J_j}{D_{ij}^e} + \frac{J_i}{D_{K,i}^e}, i = 1, n$$

$$\text{with } D_{K,i}^e = \frac{4}{3} k_0^e \sqrt{\frac{8\mathcal{R}T}{\pi M_i}} \text{ and } D_{ij}^e = \frac{\varepsilon}{\tau} D_{ij}$$

This model considers three gas phase transport mechanisms: Molecular diffusion; Knudsen diffusion; Viscous flux. The model was applied for two reactor configurations: R1 and R2 which are inert membrane reactor with permeation of  $O_2$  from the shell side and inert membrane reactor with permeation of  $O_2$  & He from the shell side respectively. The effect of dilution with inert gas in the configuration R1 is more beneficial than the configuration R2, so propane conversion in the configuration R1 is higher than the configuration R2.

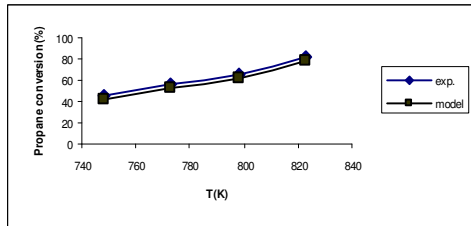


Figure 1. Variation of propane conversion with temperature (R1)

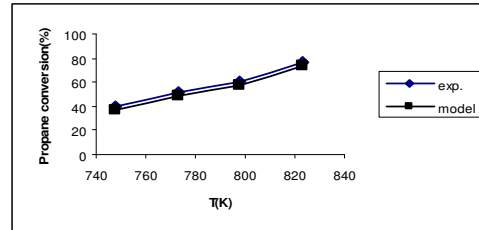


Figure 2. Variation of propane conversion with temperature (R2)

Experimental		Modelling		Absolutely error (%)		Approximately error (%)	
R1	R2	R1	R2	R1	R2	R1	R2
45	40	42	37	3	3	0.066	0.075
57	52	53	48	4	4	0.07	0.077
65	61	62	57	3	4	0.046	0.065
82	77	78	73	4	4	0.048	0.052

Table 1. Propane conversion for two reactor configurations

### References

- Burggraaf, A.J. and Cot, L., *Fundamentals of Inorganic Membrane Science and Technology*, Elsevier, (1996).
- Hou, K., Hughes, R., Ramos, R., Menendez, M. and Santamaria, J., (2001) *Using a Membrane Reactor for Oxidative Dehydrogenation of Propane*, *Chemical Engineering Science*, 53, 57-67.



## **Modeling and simulation of industrial adiabatic fixed-bed reactor for the catalytic reforming of methane to syngas**

M. Taghizadeh Mazandarani, H. Ebrahim

*Chemical Engineering Department, Faculty of Engineering, Mazandaran University, P.O.Box:484, Babol, Iran, E-mail: [taghizadehfr@yahoo.com](mailto:taghizadehfr@yahoo.com), Tel: +98111-3234204, Fax: +98111-3234201*

### **1. Summary**

Upgrading of natural gas (rich in methane) into more valuable chemicals, such as synthesis gas (syngas), has been investigated intensively in the past decade. Steam reforming of natural gas is widely used to produce syngas, a mixture of hydrogen and carbon monoxide in various proportions. Although the intensive research efforts have been performed on the kinetics and mechanism of the reaction, the preparation of catalyst and the evaluation of process and equipment, the detailed reactor modelling and simulation of SRM on an industrial scale is required. In this work an industrial adiabatic fixed-bed reactor for the catalytic reforming of methane to synthesis gas on a commercial supported Ni catalyst at high temperature and pressure ( $P_{tot} = 39$  bar,  $T_g = 894$  K), was simulated. Both external concentration and temperature gradients as well as intra-particle concentration gradients are taken into account. The intrinsic kinetics of the reforming and water-gas shift reactions were taken from Numaguchi and Kikuchi (1988). The gas-phase and solid-phase continuity and energy differential equations are solved simultaneously using MATLAB software. In this program the *finite volume* method is used for solving the corresponding continuity equations in solid phase (catalyst). The data taken from the *Khorasan petrochemical company* is applied to the proposed model to perform the simulation and the simulated results are then compared to the experimental data at the output of reactor.

Keywords: Simulation, steam reforming, finite volume, adiabatic fixed-bed reactor

### **2. Extended Abstract**

Adiabatic fixed-bed reactor for the catalytic reforming of methane to synthesis gas was simulated using a steady-state one-dimensional heterogeneous reactor model. The gas-phase and solid-phase continuity and energy equations are presented in Table 1 together with the corresponding initial and boundary conditions as well as Langmuir-Hinshelwood rate equations for steam reforming and the water-gas shift reaction. The calculated axial mole fraction profiles are shown in Figure 1.

**Table 1: Reactor model and reaction rate equations with corresponding boundary conditions**

<b>Gas phase</b>		$\frac{dy_i}{dZ} + \frac{k_g \times a_v \times \rho_f}{Q_m} (y_i - y_{i,s}^s) = 0$	(1)
		$\frac{dT_g}{dZ} + \frac{h_f \times a_v}{Q_m \times c_p} (T_g - T_s) = 0$	(2)
<b>Solid phase</b>		$T_g - T_s = -\frac{\rho_s \times (1 - \epsilon_B)}{h_f \times a_v} \sum_i R_{w,i} (-\Delta H_{f,i})$	(3)
		$\rho_f \frac{D_{e,i}}{r_p^2 \times X^2} \frac{d}{dX} \left( X^2 \frac{d}{dX} \left( \frac{y_{i,s}}{\rho_f} \right) \right) + R_{w,i} \times \rho_s = 0$	(4)
<b>Gas-phase boundary conditions</b>	$Z = 0$	$C_i = C_i^0, T_g = T_g^0$	(5)
<b>Solid-phase boundary conditions</b>	$X = 0$	$\frac{d}{dX} \left( \frac{C_{i,s}}{\rho_f} \right) = 0$	(6)
	$X = 1$	$\rho_f \frac{D_{e,i}}{r_p} \frac{d}{dX} \left( \frac{C_{i,s}}{\rho_f} \right)_{X=1} = k_g (C_i - C_{i,s}^s)$	(7)
	<b>Reaction</b>	<b>Rate equation</b>	
	$CH_4 + H_2O \leftrightarrow CO + 3H_2$	$r_1 = \frac{k_2^{NK} (p_{CH_4} - p_{H_2}^3 \times p_{CO} / K_{eq(2)})}{p_{H_2O}^{0.596}}$	(8)
	$CO + H_2O \leftrightarrow CO_2 + H_2$	$r_2 = k_3^{NK} (p_{CO} - p_{H_2} \times p_{CO_2} / K_{eq(3)})$	(9)

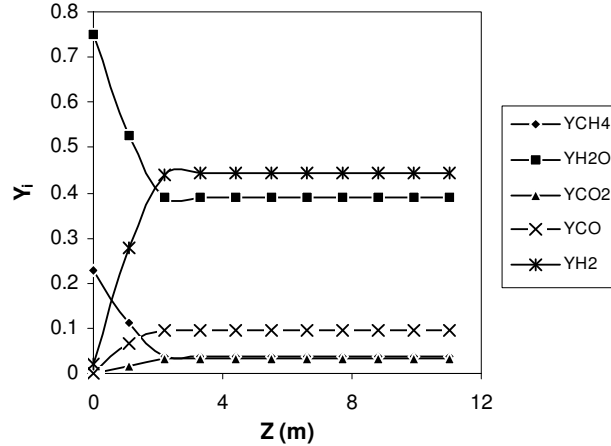


**Figure 1: Reactant and product mole fractions vs. axial reactor coordinate.**

### References

- De Smet, C. R. H. et al. (2001) *Chemical Engineering science*, 56, 4849-4861.  
 Xu, J., & Froment, G. F. (1989) *A.I.Ch.E. Journal*, 35, 88-96.  
 Numaguchi, T., & Kikuchi, K. (1988) *Chemical Engineering Science*, 43, 2295-2301.  
 De Groot, A. M., & Froment, G. F. (1996a) *Applied Catalysis A*, 138, 245-264.

## **Modeling of rotating annular chromatographic reactor – application of statistical moments to indicate reasonable model simplifications**

E. Molga,<sup>a</sup> M. Ciach<sup>a</sup>

<sup>a</sup>*Department of Chemical and Process Engineering, Warsaw University of Technology, ul. Warynskiego 1, 00-645 Warszawa, Poland*

### **1. Summary**

In a simple chromatographic separation process as well as in a reactive chromatography, statistical moments of concentration peaks can be expressed in terms of process parameters (Schneider and Smith, 1968; Suzuki and Smith, 1971). In this work the first absolute and the second central moments have been used to indicate a quantitative contribution of each stage process (axial dispersion, liquid-particle mass transfer, pore diffusion, adsorption rate) to the entire process of reactive chromatography. The results obtained, depending on the chosen operating conditions, can be used to indicate a significance of each stage process, so also to simplify a general model of the chromatographic reactor.

Keywords: process integration, rotating annular chromatographic reactor, reactor modelling, statistical moments

### **2. Extended Abstract**

In numerous papers on reactive chromatography the assumed simplifications of applied chromatographic reactors models usually are not quantitatively justified. A use of statistical moments gives a possibility to estimate a significance of each stage process, so also indicate possible model simplifications. In this paper, using the quite complex expressions derived by Suzuki and Smith (1971) for a reactive chromatography process, it has been found that the reaction kinetics (i.e. the reaction rate constant value) has not practical influence on the first and the second moments. So, analyzing a relative contribution of each stage process parameter to the moments calculated for a simple chromatographic separation, a significance of this process for a final efficiency of the reactive chromatography process can be also estimated.

The second central moment is a measure of the peak spreading, so the influence of each stage process parameter on this moment gives directly its contribution to the process efficiency. For each *i*-th reactant this moment can be expressed in terms of process parameters as follows:

$$\mu'_{2,i} = \frac{t_d^2}{12} + \frac{2L}{u} \left\{ \frac{D_L}{u^2} (1 + \delta_{o,i})^2 + \frac{(1-\varepsilon)}{\varepsilon} \left[ \frac{\varepsilon_p K_{A,i}^2}{k_{a,i}} + \frac{\varepsilon_p^2 d_p^2}{60} (1 + K_{A,i})^2 \frac{1}{D_{p,i}} + \frac{\varepsilon_p^2 d_p^2}{60} (1 + K_{A,i})^2 \frac{10}{k_{c,i} d_p} \right] \right\} \quad (1)$$

Then the contribution of each stage process  $\delta_{j,i}$  can be grouped as:

$$\mu'_{2,i} - \frac{t_d^2}{12} = \frac{2L}{u} (\delta_{d,i} + \delta_{a,i} + \delta_{p,i} + \delta_{e,i}) \quad (2)$$

where  $j$  means:  $d$  – dispersion,  $a$  – adsorption rate,  $p$  - pore diffusion and  $e$  - external mass transfer, respectively.

A series of calculations has been carried out for the hydrolysis of methyl formate with a simultaneous adsorption of the reaction products on the activated carbon. Such the reaction-adsorption system has been employed in the rotating annular chromatographic reactor (RACR) Cho et al. (1980). The results of calculations are shown in Fig. 1, where the contributions  $U_{j,A} = \frac{\delta_{j,A}}{\sum_j \delta_{j,A}}$  estimated for the reactant

A are plotted as a function of the liquid velocity  $u$ .

For the considered system, a significant contribution of the axial dispersion is observed at low liquid velocity, while at higher velocities the pore diffusion resistance dominates. At the indicated velocity  $u = 1.7 \cdot 10^{-4}$  m/s (applied in the cited above paper) a contribution of axial dispersion in a peak spreading is quite significant and equal to 64%, so the axial dispersion term can not be neglected in the process model.

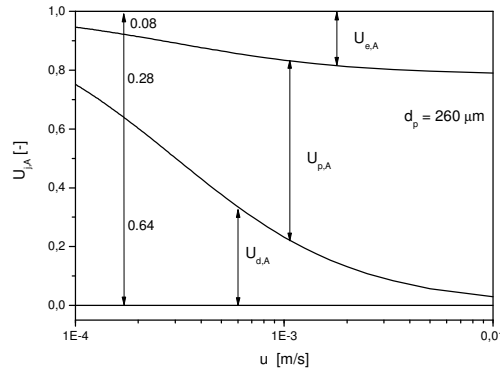


Figure 1: Dependence of the contributions  $U_{j,A}$  on the interstitial liquid velocity  $u$  calculated for the adsorbent particle size  $d_p = 260 \mu\text{m}$ .

## References

Cho, K.R., Carr, R.W., Aris, R., (1980), *Chemical Engineering Science*, 35, 74-81.

Schneider, P., Smith, J.M., (1968), *AIChE Journal*, 14, 762-771.

Suzuki, M., Smith, J.M., (1971), *Chemical Engineering Science*, 35, 74-81.

## Determination of the solubilities of mixed gases in mixed solvents using a novel HPNMR continuous flow system

Alexandre Torres,<sup>a</sup> Jonathan A. Iggo,<sup>a</sup> John Satherley,<sup>a</sup> Graham Eastham,<sup>b</sup> Darren Gobby<sup>b</sup>

<sup>a</sup>*Department of Chemistry, University of Liverpool, L69 7ZD Liverpool, United Kingdom*

<sup>b</sup>*Lucite International, Wilton Centre, TS10 4RF Redcar, United Kingdom*

### 1. Summary

Here is presented a new experimental system for determining VLE and gas solubilities using NMR spectroscopy technique, its advantages, and results that validate its reliability. It consists in a flow system in which the gas phase is continuously fed into the equilibrium cell (sapphire tube) by bubbling the gas into the liquid so that the equilibrium condition is rapidly obtained and maintained. The equilibrium cell is introduced in the NMR machine at all times, so the composition within it can be recorded at any time, and the equilibrium conditions (pressure and temperature) can be changed easy and fast with no need of modifying the system (manipulating the equilibrium cell).

Keywords: gas solubility, HPNMR (High Pressure Nuclear Magnetic Resonance), VLE (vapour-liquid equilibrium), homogeneous catalysis.

### 2. Extended Abstract

Homogeneous catalytic processes are widely used and important in industry. In gas-liquid homogeneous catalytic reactions the solubility of gases is a crucial parameter in the process. To obtain the desired performance of the reactions, the solubility of gases in liquids must be appropriate (high enough). Since the reaction occurs in the bulk of the liquid, the reactor design and the reaction kinetics are highly dependent on gas solubilities and *vice versa*. For kinetic modelling of the process it is essential to know/be able to predict reliably the concentrations of dissolved gases/gas solubility values in the working reactor. However, the modelling of gas solubilities in complex mixtures (mixed solvent-mixed feed gas), far from regions of "ideal" behaviour, is not trivial and relies on empirical correlations, thus the experimental determination of gas concentrations is necessary.

A new, high pressure NMR protocol has been developed for the quantitative measurement of gas solubilities in the pressure range 1 to 25 bar and a temperature

range from 295 K to 373 K. This new experimental method consists of a gas flow recycling system in which the equilibrium cell is in the magnet at all times. The liquid phase partially fills the equilibrium cell and a gas stream is bubbled through these solvents continuously as the gas is pumped by a reciprocating pump. The composition of the liquid phase in the equilibrium cell can be measured at all times. This system allows equilibrium to be established rapidly, and the temperature and pressure of the equilibrium cell can be readily varied. Thus, the composition of the liquid phase in equilibrium with the gas phase, as a function of temperature and pressure, can be rapidly and reliably determined.

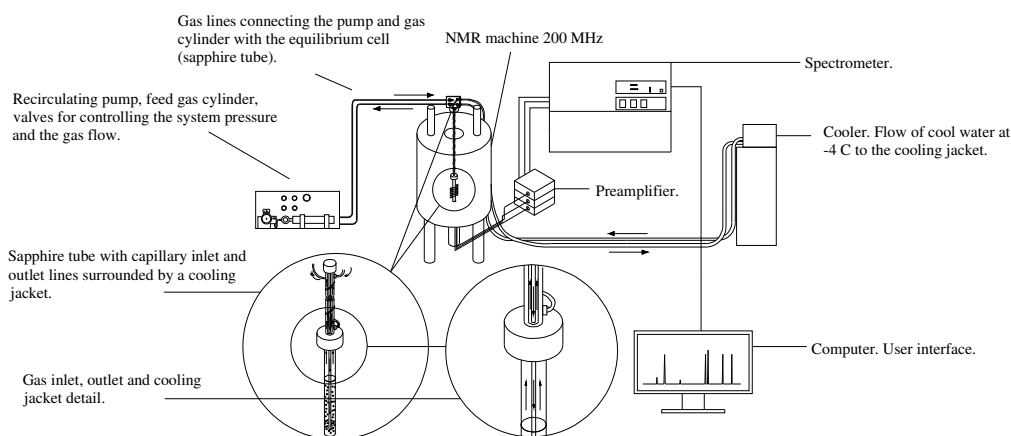


Figure 1: Experimental system. Sapphire tube connected to a recirculating pump, with an inlet and outlet of gas, introduced in the NMR machine connected to the spectrometer

In this work the solubilities, in liquid mixtures, of the gaseous reagents used have been determined experimentally and validated from previous experimental data reported in literature, as well as simulated using Aspen Plus.

## References

- Roe, D. C.; Kating, P. M.; Krusic, P. J.; Smart, B. E. *High resolution NMR techniques in catalysis*. Topics in catalysis. (1998), 5, 133-147.
- Horvath, I. T.; Millar, J. M. *NMR under high gas pressure*. Chem. Rev. (1991), 91, 1339-1351.

## **Polymerization of Polypropylene Using Multi-Catalyst/Cocatalyst Systems and Investigation of Physical and Molecular Properties of Products**

Ahmad Ramazani S.A.<sup>a</sup>, Ali Dashti<sup>a</sup>, Sima Rezvantab<sup>a</sup>

<sup>a</sup>*Chemical and Petroleum Engineering Department, Sharif University of Technology, Tehran, Iran*

To produce polypropylene with specific rheological and molecular weight distribution, polymerization of propylene has been done with different combinations of catalysts and cocatalyst types and their concentrations in slurry phase in semi-batch reactor. Two types of Titanium supported (Ziegler-Natta) catalysts with internal and external donors have been used with Triethylaluminum (TEA) and Triisobutylaluminum (TiBA) as cocatalysts in different concentrations. Also, effects of some main reaction parameters such as prepolymerization and polymerization conditions, hydrogen concentration, Al/Ti ratios on polymer yield and properties of product have been investigated. Obtained results from GPC tests showed that in appropriate combination of catalysts and cocatalysts, we are able produce broad molecular weight distribution and even bimodal polypropylene in one reactor with ZN catalysts.

Keywords: Polypropylene, Polymerization, Molecular Weight Distribution, Ziegler-Natta, Cocatalysts

### **Introduction**

Rheological, physical-mechanical and thermal properties of polypropylene is highly depends to molecular weight, molecular weight distribution (MWD) and tacticity of produced polymer. Although, high molecular weight polymer show better physical-mechanical properties than low molecular ones, in so many cases we should compensate between physical-mechanical and rheological properties due to process-ability and even clarity of final products. Polymers with same average molecular weight but with broader MWD present better rheological behavior and so better process-ability comparing with low MWD polymers. So it seems that by broadening MWD of polymers one can control both physical-mechanical and process-ability of polymers (Ahn et al. 1998, Cho et al. 2000, Kojoh et al, 1999). This work is devoted to study effects of catalyst/cocatalyst systems on molecular weight and MWD and some other physical properties of produced PP.

### **Materials and Experiments**

Two commercial magnesium supported titanium tetrachloride type Ziegler-Natta catalysts with internal donor (A, and B), Triethyl aluminum (TEA), and triisobutyl aluminium (TiBA) from Merck Inc. as cocatalyst have been used in this work. Also, Cyclohexyl dimethyl methoxy silane (C type donor) from Merck has been used as external donor. Polymerizations experiments have been done in a 1 liter high pressure commercial reactor from Buchi in slurry phase in pressure of 1-4 bars at 30 °C for prepolymerization and 65 °C for polymerization.

### **Results and Discussions**

Some experiments carried out to produce polypropylene with two different catalysts/cocatalyst and different Al/Ti ratios. Molecular weight distribution, thermal

behavior and tacticity of produced samples are studied, respectively, using High temperature GPC, DSC, and extraction with n-heptane method. Flow-ability of samples is also measured by MFI tester instrument at 190 °C.

In table (1) some properties of produced samples with TEA, TiBA and mixture of them are presented. Results show that polydispersity index (PDI) for sample that prepared with TEA cocatalyst is more than two times of the sample prepared by TiBA. Also the tacticity is less for sample prepared by TEA than the other one. But melting point is almost same for two samples where the prepared sample with a mixture of two cocatalysts show more tacticity index and considerably higher melting point where its MFI is almost same as MFI of the two other samples.

Table. 1. Comparison of some properties of PP samples (TEA/TiBA = 0.5).

Sample	Cocatalysts	PDI	Al/Ti	I.I	MFI	T <sub>m</sub> (°C)	Activity (Kg PP/gr Ti)
PP-1	TEA	6.576	231.9	88	0.8	161.925	-
PP-7	TiBA	3.153	338.179	92.5	0.9	161.658	26.784
PP-8	TEA + TiBA	3.537	250.3	94.5	0.8	166.697	38.964

In fig. 1 MWD of above mentioned samples are presented. This figure shows that average  $M_w$  for sample prepared by TiBA is considerably more than that of other samples. The most interesting point in this figure is obtaining a flat form for prepared samples with mixture of two cocatalysts. It seems that this broad pick could give better crystallinity and higher melting point for this sample. Although at high molecular weight, distribution behavior of MWD curve is almost combination of two other curves but at very low molecular weight the mentioned behavior is completely dominated by effects of TiBA and so we do not observe very low molecular weight chains (less than 10000). Other experimental results which are not presented here due to limit of space show that interring TEA cocatalyst with some delay after beginning polymerization with TiBA could broader molecular weight distribution and even produce somewhat bimodal distribution form.

### Conclusions

Presented results show that it is hard to give a two pick MWD (bimodal) curve by a system of Ziegler-Natta catalysts using two simultaneous cocatalyst but its possible to change molecular weight distribution considerably which could result in change of physical behavior of sample considerably.

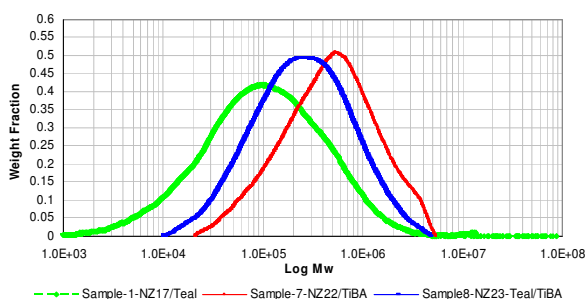


Fig. 1. MWD Curves of PP samples.

### References

- Ahn,T.O.; Hong, S.C.; Kim,J.H.; Lee,D.H; *Journal of Applied Polymer Science*, Vol.67, 2213-2222(1998).  
 Cho, H.S.; Choi, Y.H.; Lee, W.Y.; *Catalyst Today* 63 (2000) 523-530  
 Kojoh, Sh.; Kioka, M.; Kashiwa, N.; *European Polymer Journal*, 35 (1999) 751-755



## Simulation and sensitivity analysis of a multitubular fixed bed catalytic reactor to produce Phthalic anhydride

Orozco Gustavo A<sup>a</sup>, Durán Héctor A<sup>b</sup>

<sup>a</sup>Department of Chemical Engineering, Universidad Nacional de Colombia

<sup>b</sup>Department of Chemical Engineering, Universidad Nacional de Colombia

### 1. Summary

The objective of this paper is to find numerical solutions of one-dimensional and two-dimensional models under the reaction mechanism proposed by Calderbank [1] and using the kinetics parameters adjusted by Anastasov [2] for the anhydride phthalic reaction. The former with the purpose of carrying out comparisons among each one of the models, with the experimental temperature profiles (for axis tube  $r = 0$ ) of an industrial reactor; and in this way, determine the one with highest prediction grade. Finally it will be studied the effect of the temperature of the coolant and feed temperature by means of parametric sensitivity analysis using the two-dimensional models.

Keywords: o-xylene, hot-spot, parametric sensitivity, fixed bed reactors, phthalic anhydride.

### 2. One-dimensional and Two-dimensional models

The equations corresponding to each one of the models are well-known and can be found in reference [3]. Such group of equations forms a system of non linear ODE together with a system of algebraic equations for the one-dimensional heterogeneous case, and a system of PDE for the two-dimensional case. The solution of the one-dimensional system was solved by Runge-Kutta method together with iteration, for the solution of the algebraic system, supposing initially that the temperature of the bulk and pellet are the same. For the case of the two-dimensional model, the system was solved using a combination of the methods of Crank-Nicholson, relaxation and false transient [4]. The results obtained for the axis of the tube are shown next:

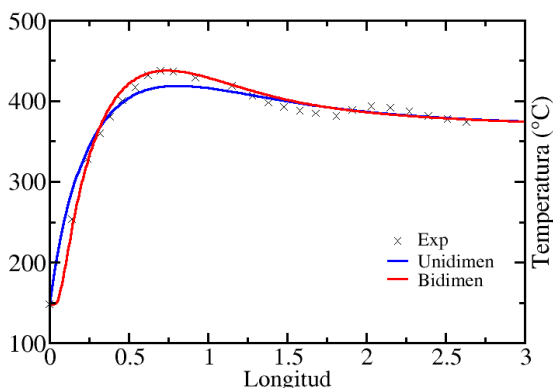


Figure 1. Comparison between one and two-dimensional models.  $P_{A0}=0.0121\text{atm}$ ,  $T_0=148^\circ\text{C}$ ,  $T_{\text{salts}}=366^\circ\text{C}$ ,  $Ker=0.92$ .

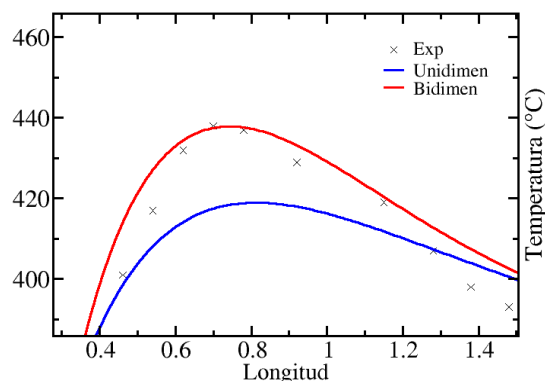


Figure 2. Amplification of figure 1, on hot-spot region. (x – Experimental profiles of an industrial reactor)

For the hot-spot region in Figures (1-2) it's seen that there are great deviations of the order of 20°C for the one-dimensional models and a slight deviation of the order of 5 cm for the prediction of hot-spot position, while the two-dimensional model shows a great prediction confronted with the profiles of industrial reactor.

### 3. Parametric sensitivity analysis

For the calculation of the sensitivities ( $\eta$ ) the definition used was the one given by Anastasov [5], with the purpose of studying the effect of the entrance temperature ( $T_o$ ) and the coolant temperature ( $T_c$ ). The results are shown next:

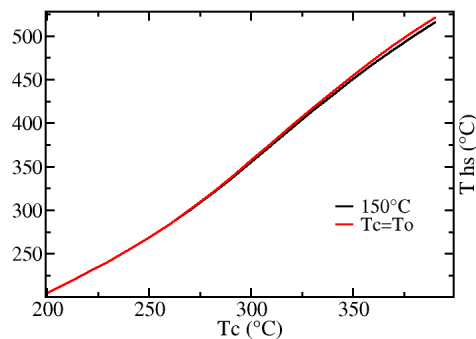


Figure 3. Influence of coolant temperature on hot-spot.  $P_{A0}=0.018$ ,  $T_o=150^\circ\text{C}$

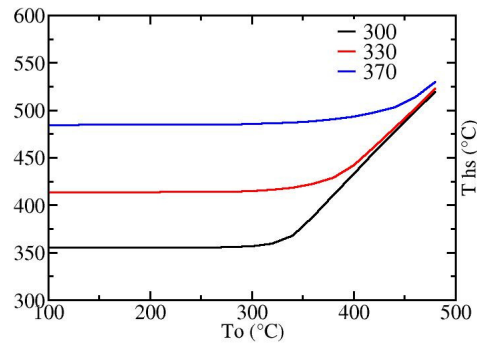


Figure 4. Influence of  $T_o$  on hot-spot  $P_{A0}=0.018$ ,  $T_c=300, 330, 370^\circ\text{C}$

The temperature of the coolant was varied between 200 and 400°C (the industrial value is between 350 and 390°C). There were also carried out two different simulations for  $T_o=T_c$  and  $T_o=150^\circ\text{C}$ . The sensitivities calculated for this case throw values that vary approximately between 1.1 and 2, obtaining the maxima values of  $\eta$  (1.8-2) in the area where the coolant temperature is between the 300 and 320 °C. For the entrance temperature, it was observed for the three coolant temperatures, that from a point, a remarkable change occurred in the sensitivities (Figure 4), since they pass of being approximately zero to be increased considerably; a thing showed in the slope change for the three curves, obtaining sensitivities between 1.5 and 2.1, for the three cases. Is important to mention that the apparent non-dependence, between the coolant temperature and the entrance temperature of the mixture, is broken approximately when the two values are the same i.e.  $T_o=T_c$ . But for lower mixture temperatures than the coolant, it was found that as the entrance temperature increases a shift of the hot point exists toward the entrance of the reactor.

### Bibliography

- [1] Chandrasekharan K. Calderbank P.H. (1976). *Chemical Engineering Science*, 32, 1435-1446.
- [2] Anastasov. A. (2003) *Chemical Engineering Science*, 58, 89-98.
- [3] Froment G., Bischoff K. *Chemical reactors analysis and design*. John Willey & Sons (1994).
- [4] Nikolov A., Anastasov A. (1992). *Chemical Engineering Science*, 47, 1291-1298.
- [5] Anastasov A. (2002) *Chemical Engineering Science*, 86, 286-297.

## Effect of pH and hydrogen peroxide on ozonic decomposition of NCW-1001

F. Yamashita,<sup>a</sup> N. Shibata,<sup>b</sup> T. Suzuki<sup>a</sup>

<sup>a</sup>*Department of Applied Chemistry, Kanagawa Institute of Technology, 243-0292 Atsugi, Japan*

<sup>b</sup>*Nomura Micro Science, 243 Atsugi, Japan*

### 1. Summary

The effect of pH and H<sub>2</sub>O<sub>2</sub> on ozonic decomposition of NCW-1001 (Polyoxyalkylene alkyl ether) was studied in a bubble column. In case of no hydrogen peroxide, Ro increased as pH increased, but Ra changed slightly in the range of pH=7-9. In the range of pH=10-11, Ro increased remarkably, however, Ra became smaller than that in the range of pH=7-9. This reason is that the ozone was used not for the decomposition of NCW-1001, but for the reaction with strong base. Where, Ra and Ro mean the alteration ratio for adsorbability on AER of NCW-1001 and the ozonic consumption rate, respectively. In case of addition of hydrogen peroxide, Ra and Ro were the same as those in case of no additions of hydrogen peroxide in the range of pH=7-9. But in the range of pH=10-11, as hydrogen peroxide dosage increased, Ro remarkably increased than that in case of no additions, though Ra did not increase.

Keywords: NCW-1001, ozone, pH, hydrogen peroxide, AOP

### 2. Extended Abstract

A bubble column was used as a reactor. Its diameter and height were 0.16 m and 1.0 m, respectively. A perforated plate was used as a gas sparger. Oxygen from a cylinder was used as a gas. Ozone was generated by an ozone generator (PO-10 by Fuji Electric Systems). Ultra pure water by MINIPURE TW-180R (Nomura Micro Science) was used as a liquid in a batch. NCW-1001 by Wako Chemicals was used as a non-ionic surfactant. The experimental conditions were in the range of QG=2L/min, C=20g/Nm<sup>3</sup>, pH=7-11 and H<sub>2</sub>O<sub>2</sub>=0-20mg/L. QG and C mean flow rate of O<sub>2</sub> and concentration of ozone in the gas. NCW-1001 solution was decomposed for 30 min in the bubble reactor.

The concentration of NCW-1001 was measured as Total Organic Carbon (TOC) by TOC analyzer (TOC-V, Shimadzu), and the alteration ratio of NCW-1001 was estimated by amounts adsorbed on Anion Exchange Resin (AER)

Figure shows the relationship between the consumption amounts of ozone and the residual ratios of TOC after AER treatment. In case of no hydrogen peroxide, as pH increased, Ro increased, but Ra changed slightly in the range of pH=7-9. In the range of pH=10-11, Ro increased remarkably, however, Ra became smaller than that in the range of pH=7-9. This reason is that the ozone was used not for the decomposition of

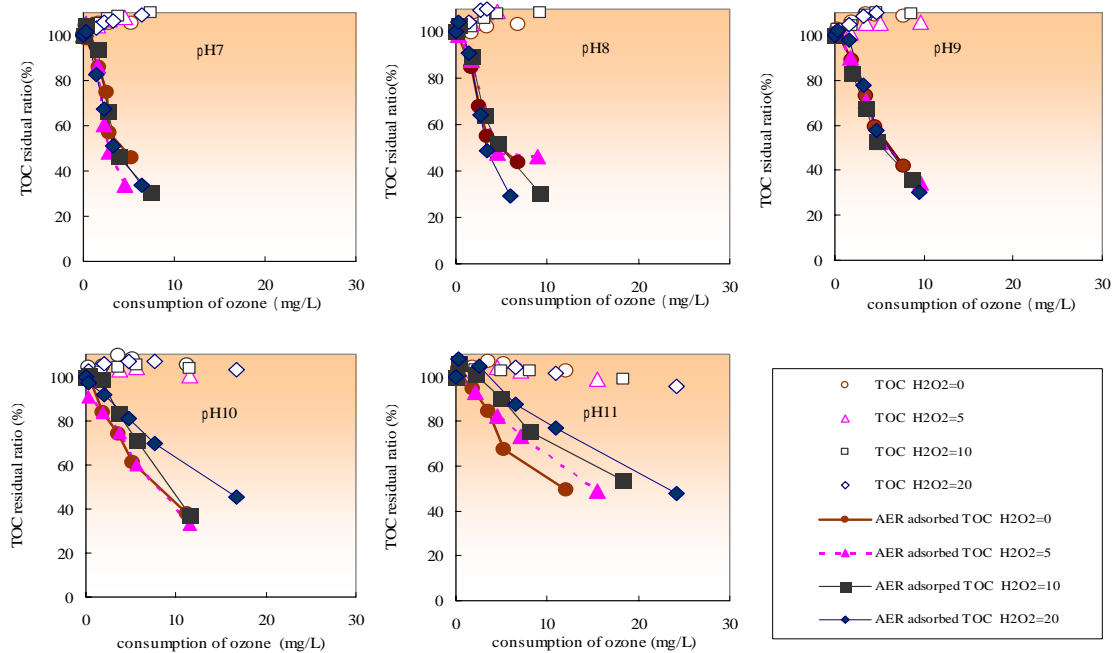
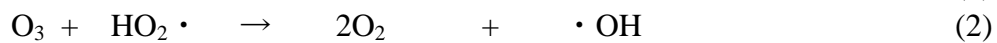


Figure. The relationship between the consumption amount of ozone and the residual ratio of TOC after adsorption treatment by AER.

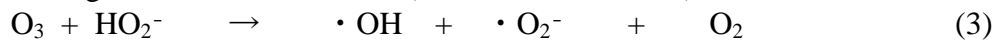
NCW-1001, but for the reaction with strong base. Where, Ra and Ro mean the alteration ratio for adsorbability on AER of NCW-1001 and the ozonic consumption rate, respectively.

In case of addition of hydrogen peroxide, Ra and Ro were the same as those in case of no additions of hydrogen peroxide in the range of pH=7-9. But in the range of pH=10-11, as hydrogen peroxide dosage increased, Ro remarkably increased than that in case of no additions, though Ra did not increase.

Ozone is decomposed at high pH according to Eqs. (1) and (2), and then hydroxyl radicals which are the most reactive species are formed.



Hydroperoxide ion reacts also with ozone and forms hydroxyl radical according to Eqs. (3) and (4). The formed hydroxyl radical increases more decomposition of ozone due to initiating radical chain reactions (Morioka et al., 1994).



Therefore, as hydrogen peroxide dosage increased, Ra decreased, although Ro increased at high pH. This indicates that the adsorbability of NCW-1001 on AER is remarkably increased by ozone molecules rather than hydroxyl radical.

## References

Morioka, T., Motoyama, N., Hoshikawa, H., Okada, M. and Moniwa, T., (1994) *Journal of Japan Water Works Association*, 63, 28-40.

## Photocatalytic oxidation of toluene

Franjo Jović, Vesna Tomašić, Stanka Zrnčević

*Department of Reaction Engineering and Catalysis, Faculty of Chemical Engineering and Technology, University of Zagreb, Savska cesta 16., HR-10000 Zagreb, Croatia*

### 1. Summary

Photocatalytic oxidation (PCO) is a promising way for the purification of contaminated air containing volatile organic compounds, VOC. In this study heterogeneous photocatalysis for the toluene degradation (used as model VOC) in the gas phase on commercial TiO<sub>2</sub> catalyst (*Degussa*, AEROXIDE TiO<sub>2</sub>, P25) was investigated. For this purpose laboratory annular fixed powder layer photocatalytic reactor (volume 0.5 dm<sup>3</sup>) was used. Illumination was provided by a 8 W black light tube located inside the inner tube of the reactor. The reaction products were analyzed on-line by a flame ionization detector on a gas chromatograph (GC *Varian* 3300), allowing detection of toluene on *Carbowax* 20M column. The influence of the water content, total gas flow rate and the toluene inlet concentration was studied. This work was aimed at describing basic features of the investigated photocatalytic reactor with particular focus on the reactor design and the development of the mathematical model. The proposed model was verified by comparing the experimental data with theoretical predictions. Generally, a good agreement was achieved, indicating that that proposed model could be used to describe photocatalytic degradation of toluene.

Keywords: photocatalytic oxidation, TiO<sub>2</sub>, toluene

### 2. Extended Abstract

The TiO<sub>2</sub>-mediated heterogeneous photocatalysis for the oxidation of VOC compounds at low concentrations has been extensively studied. Inlet concentrations of toluene were varied from (0.8 to 8.9)·10<sup>-6</sup> g dm<sup>-3</sup>, in a 0.04 – 0.410 dm<sup>3</sup> min<sup>-1</sup> air stream. The relative humidity was varied from 6 to 60 %. According to the possible reaction mechanism water has significant role in the photocatalytic reaction, but experimental results showed that the relative humidity has only negligible effect on toluene removal. At constant water vapor concentrations and considering that reaction intermediates and products are weakly or noncompetitively adsorbed, the Langmuir-Hinshelwood (LH) model can be used to describe toluene degradation kinetics (D'Hennezel et al., 1998):

$$r_A = \frac{kK_a C_A}{1 + K_a C_A}$$

where  $k$  is the reaction rate constant, and  $K_a$  - the adsorption equilibrium constant. Considering that at high concentration of toluene surface of the catalyst is saturated, Langmuir adsorption model can be applied.

The simple 1D model of the photochemical reactor was used. Following assumptions are considered: steady-state and isothermal conditions, negligible pressure drop ( $\Delta p = 0$ ), ideal flow ( $du/dr = 0$ ;  $dC_{A,g}/dr = 0$ ), reaction occurs on the catalytic surface in the reactor. Considering overall mass balances in the solid and gas phase, in a continuous tubular reactor at steady state are:

$$r_A = f(C_{A,s}) = k_g \cdot a \cdot (C_{A,g} - C_{A,s})$$

$$u \frac{dC_A}{dz} = k_g \cdot a \cdot (C_{A,g} - C_{A,s})$$

where:  $C_{A,s}$  and  $C_{A,g}$  are toluene concentrations at catalytic surface and in gas phase respectively, and  $k_g$  is mass transfer constant. It can be calculated using empirical correlation (Nicollella and Rovatti,1998). The initial conditions are at  $z = 0$ ,  $C_{A,g} = C_{A,0}$ .

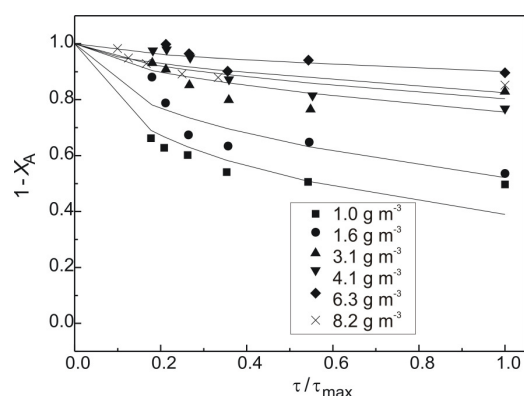


Figure 1: The model prediction results of the reaction rate of toluene degradation for various inlet concentrations

$C_A / \text{g m}^{-3}$	$k / \text{min}^{-1}$	$SD \times 10^2$	$K_a / \text{g}^{-1} \text{m}^3$	$SD \times 10^2$
1.0	27.90	3.156	0.2888	0.94
1.6	8.07	2.550		
3.1	1.98	2.647		
4.1	1.52	1.254		
6.3	0.61	1.217		
8.2	1.15	1.568		

Table 1: Estimated reaction rate constants,  $k$  and adsorption rate constant,  $K_a$ .

The reaction rate over a  $\text{TiO}_2$  catalyst at a low flow rate depends on the bulk gas to catalyst diffusion mass transport. The adsorption of the reactants onto the catalyst surface is also important, especially at higher inlet concentration where adsorption is probably rate limiting step. The proposed L–H kinetic model accurately describes reaction of the photocatalytic oxidation of toluene, although simpler model (pseudo-first reaction order) can be also used.

## References

- D'Hennezel, O., Pichat, P., Ollis, D. F., (1998) *J. Photochem. Photobio. A: Chem.*, **118**, 197-204.  
 Nicolella, C., Rovatti, M., (1998) *Chem. Eng. J.*, **69**, 119-126.

## Cure reaction and heat transfer in the cylindrical mould

Vanja Kosar, Zoran Gomzi

*Department of Reaction Engineering and Catalysis, Faculty of Chemical Engineering and Technology, University of Zagreb, Savska c. 16, HR-10000 Zagreb, Croatia, e-mail: vkosar@marie.fkit.hr*

### 1. Summary

The cure of unsaturated polyester was studied by using an experiment and a mathematical model of the process. The temperature-time profiles were recorded in the centre of the cylindrical mould filled with resin, also near the outer surface of the mould wall, and in the bulk of the air heated thermostat. A numerical model was developed by taking into account heat transferred by convection from the air to the mould surface and the heat transferred by conduction through the resin, as well as the heat generated by cure reaction. Introduction of the carbon base filler reduced the amount of heat generated in the composite. As a result, it lowered the temperature of the resin. The convection heat transfer coefficient was determined from independent experiments with glycerol inside the mould. Recording the temperature-time and conversion-time profiles developed within the sample, more extensive knowledge of the process can be obtained. The effects of the convection heat transfer to the mould, and the conduction heat transfer through the mould as well as the internal heat generated by the cure reaction is clearly shown, despite the complexity of the process.

Keywords: Curing, Polyester resin, Heat transfer coefficient, Mould, Mathematical model

### 2. Extended Abstract

In order to clarify the problem and to establish the mathematical model of the curing process in the mould, a few assumptions were made:

- 1.) Only radial heat transfer by conduction through the cylinder cross-section was considered.
- 2.) Heat was transferred by convection through the air-mould interface.
- 3.) Due to the large difference in heat conductivity between copper and resin, heat transfer through the mould wall was disregarded
- 4.) Within the given temperature interval thermal parameters  $c_p$ ,  $\lambda$ , and  $\rho$  are predicted as constants.

Based on above assumptions mathematical model of curing reaction in the cylindrical mould heated by air is given by:

$$\frac{\partial P}{\partial t} = r_A \quad (1)$$

$$r_A = A_r \exp\left(-\frac{E_a}{R_g T}\right) P^n (1-P)^m \quad (2)$$

$$\rho c_p \frac{\partial T}{\partial t} = \lambda \left[ \frac{\partial^2 T}{\partial r^2} + \frac{1}{r} \frac{\partial T}{\partial r} \right] + r_A \rho \Delta H_r \quad (3)$$

Equations (1)-(3) were numerically solved, subjected to the chosen boundary and initial conditions defined as:

*Initial condition:*

$$T(r,0) = T_0, T(R,0) = T_m = T_0, X_A(r,0) = 0$$

*Boundary condition:*

$$\lambda \frac{\partial T}{\partial r} = -h(T_m - T_{air}), \text{ for } r = R, \frac{\partial T}{\partial r} = 0, \text{ for } r = 0, \frac{\partial X_A}{\partial r} = 0, \text{ for } r = 0$$

The temperature-time history at the centre passes through the maximum, and normally decreases down to the mould wall temperature. Good agreements between experimental and estimated data were observed for temperature vs. time plots in the centre of the composite (Figure 1).

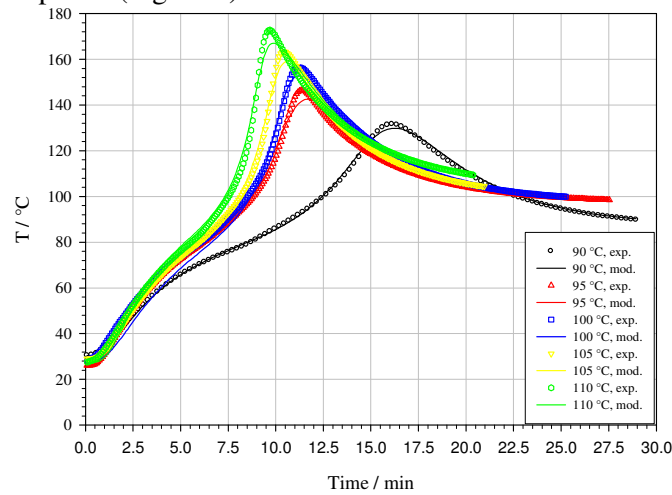


Figure 1: Comparison between simulation and experimental data

Evaluated parameters are presented in Table 1 as well as the *RMSD* as error criteria during the calculation,

$$RMSD = \sqrt{\frac{1}{N} \sum_{i=1}^N (\bar{y}_{i_{exp.}} - \bar{y}_{i_{teor.}})^2}$$

Table 1: Estimated model parameters

Air temperature, °C	$\Delta H_r, \text{ J g}^{-1}$	$A_r, \text{ s}^{-1}$	<b>RMSD</b>
90	139870.9	4430.67	0.1234
95	144911.6	5400.07	0.0895
100	165176.8	5143.03	0.1421
105	172012.4	5433.71	0.1145
110	177408.0	4618.86	0.2155

## References

- J. M. Vergnaud, J. Bouzon, *Cure of Thermosetting Resins: Modelling and Experiments*, Springer-Verlag, London, (1992).  
 A. Yousefi, P. G. Lafleur, R. Gauvin, *Polymer Composites* **18** (1997) 157-168.  
 V. Kosar, Z. Gomzi, *European Polymer Journal* **40** (2004) 2793-2802.  
 V. Kosar, Z. Gomzi, S. Antunović, *Thermochemica Acta* **433** (2005) 134-141.



## **Mechanistic and reaction engineering aspects of nitrile hydrogenation**

Peter Schäringer, Thomas E. Müller, Johannes A. Lercher

*Technische Universität München, Department Chemie, Lehrstuhl II für Technische Chemie, Lichtenbergstraße 4, 85747 Garching, Germany*

Liquid phase hydrogenation of nitriles is an important method for the production of primary amines, which find a variety of applications as intermediates in chemical and pharmaceutical industry. Raney-Co or supported Cobalt catalysts are frequently used due to the relatively high selectivity to primary amines. However, selectivities in excess of 95% can only be achieved, when ammonia is used as solvent. Thereby, thermodynamic control of the reaction is achieved as condensation reactions, where ammonia is released, are suppressed. However, liquid ammonia is difficult to handle and it is highly interesting to avoid, or at least to minimise, the addition of ammonia. This requires kinetic control of the reaction by optimizing catalyst properties and process conditions. In this study, nitrile hydrogenation in a stirred autoclave and a laboratory-scale trickle-bed reactor is compared. It is shown that changes in the distribution of ammonia between gas and liquid phase is the key parameter in terms of selectivity. Co-hydrogenation of acetonitrile and butyronitrile over Raney-Co provides detailed insight into the mechanism of alkyl group transfer, which leads to the formation of secondary and tertiary amines.

### Keywords

Multi-phase reaction, Trickle-bed reactor, Hydrogenation, Cobalt catalyst, Nitrile



## **Inhibitory study and trickle bed reactor modeling for joint reactions of hydrodesulfurization, hydrodenitrogenation and hydrodearomatization during the hydrotreating of vacuum gas oils**

F. Jimenez,<sup>a</sup> V. Kafarov,<sup>a</sup> M. Nunez,<sup>b</sup> R. M. Filho<sup>c</sup>

<sup>a</sup>*Department of Chemical Engineering, Industrial University of Santander, Kra 27 # 9. Tel. +57 76344746, Fax +57 76344684, Bucaramanga, Colombia*

<sup>b</sup>*Colombian Petroleum Institute -ICP, Piedecuesta, Colombia*

<sup>c</sup>*Campinas State University, Campinas, S.P., Brazil*

### **1. Summary**

Inhibition or promotion effects of water, likewise sulfur, basic nitrogen, non-basic nitrogen, mono-aromatics, di-aromatics, tri-aromatics, and poly-aromatics representative compounds, on the activity of NiMo/Al<sub>2</sub>O<sub>3</sub> hydrotreating (HDT) catalysts were investigated. Pure compounds selected for this work included: dibenzothiophene (DBT), carbazole (CBZ), acridine (ACR), tetralin (TET), naphthalene (NAF), anthracene (ANT), pyrene (PYR), and water, mixed with different real feed oils: vacuum gas oil, previously hydrotreated at high severity (VGO), light vacuum gas oil (LVGO), and parafinic base (PB). Experimental tests were carried out in a HDT pilot plant at 10 MPa, space velocity of 1.1 h<sup>-1</sup>, gas/oil ratio of 6.24, and temperatures between 330 and 370 °C. Obtained results showed that ACR presented inhibitory effects on hydrodesulfurization (HDS) and hydrodenitrogenation (HDN) of VGO and PB. CBZ showed inhibitory effects on HDS of PB but promoter effect on HDS and HDN of VGO. ANT presented promoter effects on HDS of medium VGO and PB, as well as reduction of basic nitrogen (BN), but no effects were found for the reduction of non-basic nitrogen (nBN). In another test using a heavy VGO and high concentrations of ANT were found an inhibitor effect for HDS and a promoter effect for HDN. Water had positive effects on the reduction of sulfur and nBN but it was an inhibitor for BN in VGO. No effects were detected in mixtures of water with PB, but water helped in the saturation of mono-aromatics and di-aromatics. Several possible explanations to these results are discussed.

Keywords: Inhibition, water effect, HDS, HDN, HDA

### **2. Extended Abstract**

A summary of the overall results for inhibitor and promoter effects with their strength, found in this investigation are presented in Tables 1 and 2.

Table 1. Summary of inhibitor and promoter effects on HDS, HDN and total HDA.

Light inhibition (-), moderated inhibition (--), strong inhibition (---), no effect (o), light promotion (+), moderated promotion (++), strong promotion (+++), very strong promotion (++++).

Compound	Feedstock	HDS	HDN				HDA		
			BN	nBN	total				
Acridine	VGOH + 2DBT	-	0,7%		--	12%			
Acridine	PB+1.5DBT	-	1,2%	o	0%	o	0%		
Carbazole	VGOH	o	0%	o	0%				
Carbazole	VGOH + 2DBT	+	1,5%	+++	15%	+++	40%		
Carbazole	VGOH +2DBT +0.5ACR	+	2,0%			++	15%		
Carbazole	PB+1.5DBT	-	0,5%	o	0%				
Anthracene	VGOH	++	3,0%	o	0%	++	15%		
Anthracene	VGOH +2DBT	+++	5,0%	o	0%	+++	45%		
Anthracene	VGOH +0.5CBZ	+++	6,0%	+	8%	++	22%		
Anthracene (10%)	MVGO	--	4,0%	+++	15%	+++	40%		
Tetralin (25%)	LVGO +3DBT	--	4,3%	++	12%	o	0%		
Tetralin (5%)	LVGO	o	0%	o	0%	o	0%		
Naphthalene (25%)	LVGO +3DBT	--	4,1%	o	0%	o	0%		
Naphthalene (5%)	LVGO	o	0%	o	0%	o	0%		
Pyrene (5%)	LVGO	o	0%	o	0%	o	0%		
Water (5%)	PB+1.5DBT	o	0%				o	0%	
Water (5%)	VGOH +2DBT	++	4,2%	---	20%	++++	50%	o	0%
Water +Acridine	LVGO			o	0,0%	++	8,0%		
Water +Tetraline	LVGO							++	8%
Water +NAF	LVGO							++	6%
Water +Pyrene	LVGO							--	12%

Table 2. Summary of inhibitor and promoter effects of water on aromatics families.

Light inhibition (-), moderated inhibition (--), strong inhibition (---), no effect (o), light promotion (+), moderated promotion (++), strong promotion (+++)

Compound	Feedstock	Aromatic family							
		mA	dA	tA	pA				
Water (5%)	PB+1.5DBT	o	0%	o	0%	o	0%	o	0%
Water (5%)	VGOH +2DBT	+	1,0%	o	0%	-	2,0%	--	5,0%
Water +Tetraline	LVGO	-	4,0%	+	2,0%	+	2,0%	+++	22%
Water +NAF	LVGO	-	4,0%	+	1,0%	+	5,0%	+++	20%
Water +Pyrene	LVGO	---	16%	-	7,0%	-	7,0%	---	15%

## **A network of chemical reactions for modeling hidrocracking reactors**

R.M.C. Ferreira da Silva<sup>a</sup>, J.L. de Medeiros<sup>b</sup>, O.Q.F. Araújo<sup>b</sup>

<sup>a</sup>*CENPES, PETROBRAS, Ilha do Fundão 21949-900, Rio de Janeiro, RJ, Brazil*

<sup>b</sup>*Escola de Quimica, Universidade Federal do Rio de Janeiro, 21949-900, Rio de Janeiro, RJ, Brazil*

### **1. Summary**

We studied some of the phases involved in the development of a HCC reactor model within a molecular-structure-based approach. Phase 1 considers a chemical description of HCC feeds. We use a discrete compositional model for a pre-hydrotreated heavy vacuum gasoil which constitutes a typical feed of a hydrocracking bed in the second stage of a HCC process. A set of hydrocarbon families is formulated to cover relevant functional molecular sub-structures quantifiable by analytical procedures of feedstocks and products. Each family has parameters defining its concentration and molecular weight distribution, and is complemented by a framework of rules for generation of molecular structures belonging to it. Feed parameters were estimated by reconciling property predictions with available characterizing data. Phase 2 is concerned with the HCC reactions network and the corresponding kinetic mechanisms. Empirical kinetic rules from the Literature were applied for proposing a HCC reaction network adopting molecule-based kinetics. Reactions rates were modeled according to several mechanisms involving gas-liquid equilibrium and adsorption equilibrium along an experimental isothermal reactor. In order to keep the model within tractable limits, kinetic and adsorption parameters were grouped into a primary and a secondary sets. The secondary set is calculated from the primary set via empirical proportionality factors. The primary set was estimated via non-linear regression of predicted properties over data of HCC products

Keywords: hydrocracking, HCC, compositional model, molecule-based kinetics

### **2. Extended Abstract**

The current petroleum market exhibits a trend of gradual increase in the participation of low quality crudes characterized by high contents of sulfur and/or nitrogen, besides high carbon/hydrogen ratios. In this scenario, the technology of Hydrocracking Processes (HCC) can guarantee stringent specified urban fuels by providing huge increases of hydrogen/carbon ratio of heavy fractions as well destroying contaminant heteroatoms and enhancing yields of naphtha and middle fractions by aromatic hydrogenation, paraffin cracking and ring opening of naphthenic molecules. This technology is, on the other hand, costly because it demands high usage of hydrogen

and extremely severe reactor conditions (temperature, pressure and spatial time). Thus it is not surprising that HCC plants are rare in the refinery context around the world. Inherently connected to this, modeling studies of HCC are also scarce. Plausible reasons derive from a large set of theoretical obstacles that characterize HCC like: (i) complex (true) chemical description of HCC feeds; (ii) complex chain of chemical transformations involved and associated chemical reaction network; (iii) complex behavior of reaction rates; and (iv) complex hydrodynamic, kinetic and thermal effects through the reactor. In this work we study some of the phases involved in the development of a HCC reactor model within a molecular-structure-based approach.

### **Compositional Model (CM) of HCC Feeds**

We formulate a discrete compositional model (CM) for representing a pre-hydrotreated heavy vacuum gasoil. A set of 47 hydrocarbon families was formulated to cover relevant functional molecular sub-structures quantifiable by analytical techniques over HCC feedstocks. Each family is represented by a typical individual having as adjustable parameters its concentration and the size of an alkyl lateral chain. The CM parameters were estimated for the gasoil by reconciling property predictions (like density, viscosities, NMR and mass spectrometry results etc) with available characterizing data. Results were statistically analysed.

### **HCC Reaction Network**

Empirical kinetic rules from the Literature were applied for proposing a HCC chemical reaction network adopting molecule-based kinetics. A total of 235 chemical reactions – involving 158 chemical species – were selected and organized into several classes like aromatics saturation, dealkylation of aromatics, dealkylation of naphthenics, cracking of naphthenic rings, cracking of paraffins, paraffin isomerization etc. The reactions rates were associated to a set of 75 feasible kinetic rules. Each kinetic rule presupposes a temperature dependent kinetic parameter. Reactions rates were modelled according to several mechanisms involving gas-liquid equilibrium and adsorption equilibrium along an isothermal reactor. In order to keep the model within tractable limits, kinetic and adsorption parameters were grouped into a primary and a secondary sets. The secondary set is calculated from the primary set via empirical proportionality factors suggested in the Literature. The primary set consists of 17 kinetic parameters and 2 Langmuir adsorption constants.

### **Reactor Model and Parameter Estimation of the Reaction Network**

The HCC isothermal reactor was modelled as a heterogeneous plug flow reactor with simultaneous flow of liquid and gas obeying one independent spatial (axial) coordinate. Gas and liquid were supposed permanently equilibrated along the reactor. As the set of conversion differential equations operates on the reactive mixture, the gas-liquid equilibrium has to be solved with conventional equations of state (e.g. Peng-Robinson) and separation algorithms (e.g. Flash[T,P]).

The primary set of HCC parameters has pretension to be universal (i.e. not feed dependent). It was estimated via non-linear regression by matching reactor predicted properties with characterizing data of HCC products. Statistical analysis was used to measure the quality of results.

## The styrene photocatalytic degradation reaction

S. R. Taffarel<sup>a</sup>, M. A. Lansarin<sup>a</sup>, C. Celso C. Moro<sup>b</sup>

<sup>a</sup> *Laboratory of Reactors, Kinetics and Catalysis (LARET) - Department of Chemical Engineering, Federal University of Rio Grande do Sul (UFRGS) - Eng. Luis Englert Street, s/n. CEP: 90040-040 – Porto Alegre – RS – BRASIL, e-mail: marla}@enq.ufrgs.br*

<sup>b</sup> *Institute of Chemistry (IQ), Federal University of Rio Grande do Sul (UFRGS) - Av. Bento Gonçalves, 9500, CEP 91501-970 – Porto Alegre – RS – BRASIL, e-mail: celso@iq.ufrgs.br*

### 1. Summary

In this study the aqueous styrene photocatalytic degradation reaction was evaluated using TiO<sub>2</sub> P-25 (Degussa) as catalyst. The experiments were accomplished in a batch reactor with temperature control, catalyst in suspension and a 28W UV lamp. Preliminary tests were made to determine the necessary contact time to reach the adsorption equilibrium and in order to separate the photolysis of the photocatalysis. Then the effects of the styrene initial concentration were evaluated, as well as, the catalyst concentration, the hydrogen peroxide addition and the initial pH of the solution. It was verified that the styrene degradation rate can be approached by a pseudo-first-order kinetics for styrene initial concentrations from 15.27 to 57.25 ppm, at 30°C. Besides, the addition of H<sub>2</sub>O<sub>2</sub> accelerates the degradation reaction until it reaches a certain optimum peroxide concentration in the reactor. Further H<sub>2</sub>O<sub>2</sub> additions resulted in reaction rate reduction.

Keywords: styrene, photocatalysis, batch reactor, kinetics, TiO<sub>2</sub>

### 2. Extended Abstract

In this study, the photocatalytic degradation of styrene has been investigated using TiO<sub>2</sub> as catalyst. The goals were: (i) to evaluate the kinetics of styrene disappearance, (ii) to examine the effect of several parameters such as catalyst mass, styrene initial concentration, the oxidants addition and pH change.

#### 2.1. Experimental

Titanium dioxide P-25 (Degussa) was used as catalyst. The reactant styrene was kindly given for the Innova Petroquímica Company. The experiments were carried out in a batch reactor with temperature control, catalyst in suspension and a 28W UV lamp which emits between 320 and 400 nm, with a maximum of 365 nm. The styrene and intermediates concentration was monitored using a gas chromatograph. Total organic carbon was analyzed by TOC analyzer. The radiant flux of the UV source was determined by a digital radiometer.

## 2.2. Results and Discussion

A non-appreciable styrene photodegradation occur in 90 min of irradiation without TiO<sub>2</sub> (photolysis). The same happens with TiO<sub>2</sub> but without irradiation (loss for the environmental). The styrene concentration variation due to the photocatalytic reaction reaches 95% degradation, in 90 min, for an initial concentration of 24.2 mg L<sup>-1</sup>. The photodegradation reaction can be approximated by a pseudo first-order kinetics, with apparent constant of 0.0445 min<sup>-1</sup>. It was also observed that increasing styrene initial concentration decreases the degradation rate. The Langmuir-Hinshelwood rate expression has been successfully used in this work for describe relationship between heterogeneous photocatalyst degradation rate and the initial pollutant concentration.

The effect of catalyst concentration was evaluated using the pseudo-first-order apparent kinetic constant for several initial catalyst concentrations. It was observed that the reaction constant kinetics increases with the catalyst concentration increment from 0.11 to 0.55g L<sup>-1</sup>; after that, decreases. Similar behavior was observed by several authors for different pollutants (Barakat et al, 2005; Gogate et al, 2002).

Regarding to the mixture initial pH effect, it was observed that the reaction presented a maximum degradation rate for pH 6.0. At this pH 6.0 value the TiO<sub>2</sub> surface is with low charge (near ZPC), a situation in which molecules probably reach its surface more easily, being the degradation rate in its maximum value (Evgenidou et al, 2005). When H<sub>2</sub>O<sub>2</sub> was added with several initial concentrations, at pH 6.0, the degradation rate pass by a maximum.

Chromatographic analysis of a sample collected during the styrene photocatalytic degradation revealed the benzaldehyde presence as intermediate. Experiments were carried out in order to analyze, simultaneously, styrene concentration, benzaldehyde concentration and total organic carbon (TOC). The results were used to do a mass balance, and CO<sub>2</sub> formed during reaction was calculated.

## 2.3. Conclusions

It can be concluded that in this work conditions the styrene degradation is a photocatalysed process and the adsorption equilibrium is reached in 40 min for three tested pH values (4.0, 6.25, 9.0). Besides, the amount of adsorbed styrene depends on the solution pH. In this case, the adsorption maximum happened in pH 6.25. Also, the styrene degradation kinetics can be approached by a pseudo-first order model, decreases with the increase of its initial concentration and it increases with the increment of catalyst concentration until reach a maximum of 0.55 g L<sup>-1</sup>. The degradation rate is maximum when pH is about 6.25 and H<sub>2</sub>O<sub>2</sub> concentration is 5.8 mmol L<sup>-1</sup>. There is benzaldehyde formation during the styrene photocatalytic degradation.

## References

- BARAKAT, M. A.; TSENG, J.M.; HUANG, C.P. (2005) *Applied Catalysis B: Environmental*, 59, 99–104.
- EVGENIDOU, E.; FYTIANOS, K.; POULIOS, I. (2005) *Journal of Photochemistry and Photobiology A: Chemistry*, 175, 29–38.
- GOGATE, P. R.; MUJUMDAR, S.; PANDIT, A. B. (2002) *Industrial and Engineering Chemical Research*, 41, 3370-3378.



## Session T2-3: Particulate Systems

<b>Abstract Number</b>	<b>Paper Title &amp; Authors</b>	<b>Included</b>
360	Enzyme Degradation during Spray Drying J Sloth, P Bach, S Kiil, A D Jensen	Yes
481	Effect of temperature on hydrodynamics of bubbling fluidized beds S Sanaei, N Mostoufi, R Radmanesh, R S Gharebagh, J Chaouki	Yes
556	Application of X-ray tomography to the characterization of single granules D B Medrano, G K Reynolds, A D Salman, M J Hounslow	Yes
2176	"Smart" polyesters for nanoparticles synthesis and stabilization A Voronov, A Kohut, W Peukert	Yes
2417	Electrostatic characterization of electrohydrodynamic atomization process for polymeric particle fabrication J Yao, J Xie, L K Lim, J Hua, C H Wang	Yes
2847	A three-dimensional population balance model of granulation employing mechanistic kernels R Ramachandran, J Poon, F Stepanek, F Doyle, J Litster, I Cameron, C Immanuel	Yes

Session T2-3

## Enzyme Degradation during Spray Drying

J. Sloth,<sup>a,b</sup> P. Bach,<sup>b</sup> S. Kiil,<sup>a</sup> A. D. Jensen<sup>a</sup>

<sup>a</sup>*Department of Chemical Engineering, Technical University of Denmark, Building 229, DK-2800 Kgs. Lyngby, Denmark*

<sup>b</sup>*Novozymes A/S, Krogshøjvej 36, DK-2880 Bagsværd, Denmark*

### 1. Summary

A method for evaluating the performance of enzyme containing formulations in terms of preserving the highest enzyme activity during drying is presented. The method is based on a combination of differential scanning calorimeter measurements and reaction kinetics modeling. The method is explained using a model enzyme and illustrated by a design study. Finally, the method is validated by comparing the results of the design study to the results of spray drying experiments.

Keywords: Spray Drying, Enzyme Inactivation, Formulation Design, Differential Scanning Calorimetry

### 2. Extended Abstract

Industrial enzymes are often subject to spray drying because product handling is easier and the enzyme storage stability is better in a powder product than in a liquid formulation. However, the enzymes may lose the native structure during the drying process due to the high temperatures prevailing in the spray dryer. This thermal inactivation may be reduced by mixing the enzyme containing feed with different compounds (e.g. carbohydrates and surfactants) prior to drying, i.e. design activity preserving formulations. In this work, a method for evaluating the performance of activity preserving formulations is presented, allowing fast formulation screening. Also, the method may help reduce the number of expensive pilot and full scale spray drying experiments when designing new or improving existing formulations.

The method for evaluating the performance of activity preserving formulations in terms of minimizing the enzyme degradation during spray drying is based on a combination of theory and experiments. In the following the principle of the method is illustrated using a concentrate of a model enzyme.

Firstly, a series of experiments using model enzyme samples with different water to enzyme ratios are conducted by differential scanning calorimetry to reveal the

relationship between the inactivation rate and the sample moisture content. Secondly, the experimental data is used to find reaction rate parameters in a first order reaction model, including an Arrhenius type expression for the rate constant. Also, the reaction order for the water concentration in the sample is identified. Finally, the rate of inactivation at different levels of moisture content and temperatures relevant for spray drying may be simulated.

Using the approach described above four different enzyme containing formulations are investigated in a design study. The formulation ingredients cannot be given in detail as this information is commercially sensitive but in general carrier materials, enzyme stabilizers and various amounts of a solute are mixed.

The reaction kinetics parameters are found for each formulation and the enzyme activity losses in the formulations as well as in the model enzyme concentrate are calculated at 80 °C and varying moisture contents (figure 1).

As seen in figure 1 the method described predicts that enzymes in Formulation 1 will suffer least inactivation during drying whereas Formulation 3 and 4 provides the poorest enzyme preservation. Thus, Formulation 1 is preferred.

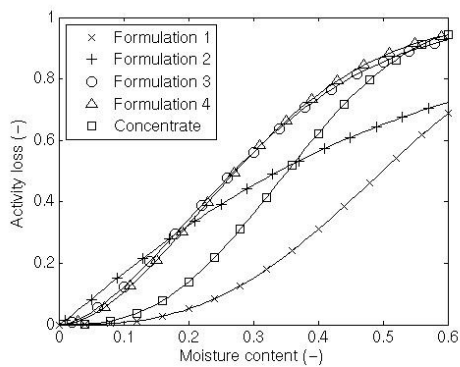


Figure 1: Prediction of enzyme inactivation during drying, using different formulations. T = 80 °C.

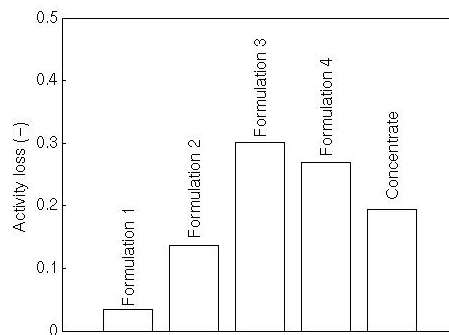


Figure 2: Inactivation of enzymes during actual spray drying. Formulations are identical to those of figure 1 and T = 80 °C.

The method for evaluation of enzyme containing formulations described above is validated by comparing the results of the design study to pilot scale spray drying experiments using a Niro Mobile Minor. For the concentrate and each of the four formulations used above a series of consecutive experiments are conducted and the activity loss is subsequently found by an assay. Qualitatively, the results are the same as those found above using the performance evaluation method described. Thus, the validity of the method is strongly supported by the results of the spray dryer experiments.

## **Effect of temperature on hydrodynamics of bubbling fluidized beds**

Sh. Sanaei,<sup>a</sup> N. Mostoufi,<sup>a</sup> R. Radmanesh,<sup>b</sup> R. Sotudeh-Gharebagh,<sup>a</sup> J. Chaouki<sup>c</sup>

<sup>a</sup> *Process Design and Simulation Research Center, Department of Chemical Engineering, University of Tehran, P.O. Box 11365/4563, Tehran, Iran*

<sup>b</sup> *Department of Chemical and Materials Engineering, University of Alberta, 536 CME Building, Edmonton, Alberta, Canada T6G 2G6*

<sup>c</sup> *Department of Chemical Engineering, École Polytechnique de Montréal, P.O. Box 6079 Station Centre-Ville, Montreal, Québec, Canada H3C 3A7*

### **1. Summary**

In order to explore the bubbling fluidized bed hydrodynamics at high temperatures, experiments were carried out at different temperatures in the range of 25-700 °C and different superficial gas velocities in the range of 0.17 - 0.87 m/s in a fluidized bed of sand particles. The fluidized bed used in the experiments was a 78 mm ID and 0.75 m height column. Time-position trajectory of particles was obtained by the radioactive particle tracking (RPT) technique. Hydrodynamic parameters such as velocity distribution of particles have been investigated by proper processing of the experimental time-position data. Plotting the velocity distribution shows two peaks corresponding to downward-moving particles (descending clusters) and upward-moving ones (bubble wake and ascending clusters). It can be concluded that mean velocities of upward and downward-moving particles increase by increasing the superficial gas velocity. In addition, mean velocity of downward-moving particles slightly increases by increasing temperature at each superficial gas velocity while mean velocity of upward-moving ones does not show a significant change.

Keywords: fluidized beds, high temperature, hydrodynamics, particle tracking

### **2. Extended Abstract**

A large number of research works on fluidization has been carried out over the past years at ambient temperature. However, industrial fluidized bed reactors operate at high temperatures. Obviously, there is a lack of study at high temperatures which is due to difficulties associated with measuring techniques under such a condition (Radmanesh et al., 2005). RPT technique, which was used in this study, provides the three-dimensional coordinates of a radioactive tracer moving inside the bed as a function of time. In a fluidized bed, particles can be categorized into two main groups (Stein et al., 2000; Mostoufi and Chaouki, 2004) which can be distinguished

by plotting the velocity distribution. As can be seen in Figure 1, velocity distribution, which has been obtained by proper processing [3] of the experimental time-position data, contains two peaks corresponding to downward and upward-moving particles.

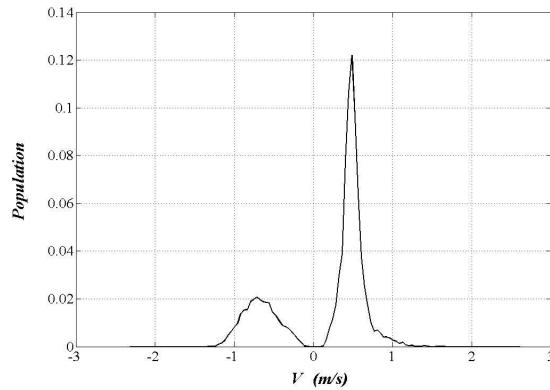


Figure 1: Velocity Distribution at Superficial Gas Velocity of 0.52 m/s and T=25 °C

Figure 2 shows mean velocities, which were obtained from the velocity distributions, against temperature. As can be seen in this figure, mean velocity of upward and downward moving particles increases by increasing the superficial gas velocity. Also, it can be concluded that mean velocity of descending particles slightly increases by increasing temperature at each superficial gas velocity while mean velocity of ascending particles does not show a significant change with temperature.

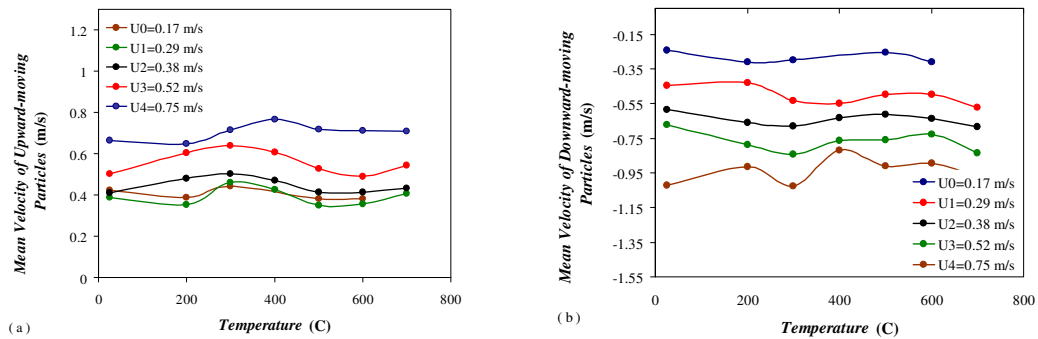


Figure 2: a) Mean Velocity of Upward-moving Particles as a Function of Temperature b) Mean Velocity of Downward-moving Particles as a Function of Temperature

## References

- Mostoufi, N., Chaouki, J., (2004) *Chemical Engineering Science*, 59, 4217-4227.
- Radmanesh, R., Mabrouk, R., Chaouki, J. and Guy, C., (2005) *International Journal of Chemical Reactor Engineering*, Vol. 3, Article A16.
- Stein, M., Ding, Y.L., Seville, J.P.K., Parker, D.J., (2000) *Chemical Engineering Science*, 55, 5291-5300.

## Application of X-ray tomography to the characterization of single granules

D. Barrera-Medrano<sup>a,b</sup>, G.K. Reynolds<sup>a</sup>, A.D. Salman<sup>a</sup>, M.J. Hounslow<sup>a</sup>

<sup>a</sup> Particle Products Group, Department of Chemical Engineering, University of Sheffield, Mappin Street, S1 3JD Sheffield, UK

<sup>b</sup> BASF Aktiengesellschaft, GCT/T – L540, D-67056 Ludwigshafen, Germany

### 1. Summary

X-ray tomography uses x-rays to evaluate, non-destructively, the internal structure of objects. It has widely been used in medical imagery since it was first discovered in the 1960s and 1970s. However its potential in the powder technology field has only started to be realized recently. A commercial desktop XRT system was used to evaluate the effect that different process/formulation parameters have on the internal structure of single granules made from comminuted limestone and polyethylene glycol; in a vertical-axis high shear mixer.

Keywords: granulation, x-ray tomography, granule structure

### 2. Extended Abstract

Fine particulate systems play a very important role both in day-to-day life and in human economy. Over 70% of industrial manufacturing processes (including pharmaceutical, chemical and food industries) involve small solid particles ranging from low-cost materials such as agricultural grains or sand, to the more specialized and expensive such as pharmaceutical products.

When dealing with particulate solids it is common in industry to aggregate them together in order to form larger entities by a granulation step, in order to improve the properties of the product (such as increased flowability or reducing of dustiness). This work focuses on wet granulation, which can be defined as the process of agglomerating fine powders in the presence of a liquid binder in order to obtain a smaller number of larger particles (granules).

The structure of granules is a key factor in determining the final properties of the product, whether as independent agglomerates or tablets. It would be therefore very important to understand how the structural characteristics of an agglomerate are going

to affect its properties, as well as how the way the agglomerates have been manufactured is going to affect the structure of the agglomerate. However, research has traditionally focused on trying to relate formulation/process parameters to the properties exhibited by the products, but usually the effect of these parameters on the structure is overlooked. In this research X-ray tomography (XRT) was used in order to study the structure of single agglomerates and how it is affected by the different parameters used in the granulation process.

XRT is a technique that uses x-rays to evaluate non-destructively the internal microstructure of objects. It has widely been used in medical imagery since it was first discovered in the 1960s and 1970s. However its potential in the powder technology area has only started to be realized recently. A commercial desktop XRT system was used to scan single granules and a method developed to analyze the raw data generated in terms of radial profiles of greyscale intensity within the granules in order to provide information of the internal structure of the granules.

Different granulation methods and materials were studied, with special emphasis on high-shear melt granulation of comminuted limestone with polyethylene glycol in a vertical-axis high-shear mixer, investigating the effect of process and formulation parameters in the structure exhibited by the resulting granules.

As an example, the presence of a core of melting binder was observed at early granulation times and lower impeller speeds. At low impeller speeds the cores were still present after granulation times of up to 15 minutes. The presence of a core of binder proves that immersion is the prevalent nucleation mechanism in the experiments performed. When the impeller speed is increased the core of binder is squeezed towards the surface of the granules and a spheronization process occurs. Impeller speed thus seems to be the variable that controls these processes for a given formulation.



## **"Smart" polyesters for nanoparticles synthesis and stabilization**

A.Voronov, A. Kohut, W.Peukert

*Institute of Particle Technology, Friedrich-Alexander University Erlangen-Nuremberg, Cauerstrasse, 4, 91058, Erlangen, Germany*

### **1. Summary**

Respond and conform to local changes in pH, temperature and solvent quality are well known for flexible polymer chains. Surface modification with polymers which provides possibilities for control and change of surface compositions thus allowing for demanded properties is significant for practical applications. Amphiphilic block copolymers recently gained a great interest, for example for biomedical applications. We synthesized a new class of amphiphilic polyesters forming stimuli responsive architectures. They offer adaptive properties, do not require a complex multistep synthesis and are accessible on larger scale. These polyesters are soluble in aqueous and organic media where they reveal inverse behaviour which could be correlated to their chemical structure. Polymers with such properties can find use in applications such as stimuli-responsive release, stabilization of colloidal nanoparticles and nanoreactors for the nanoparticles synthesis.

Keywords: amphiphilic invertible polyesters, smart polymeric nanoreactors, smart polymeric stabilizers.

### **2. Extended Abstract**

We developed and characterized the invertible polyesters based on poly(ethylene glycol) (PEG) of various molecular weights and aliphatic dicarboxylic acids. Obtained copolymers have been synthesized via polycondensation in solution. We believe that the possibility of conformational switching for polyester architectures can be reached with a controllable presence of oxygen atoms in a polymers main backbone. Our structural hypothesis suggests that the hydrophilic PEG and the hydrophobic aliphatic acid residues can change the polymeric micelle architecture in solvents of different polarities.

As it has been shown, the amphiphilic polyesters are able to form invertible architectures in media differing by polarity. These polymer architectures have been employed as nanoreactors for the synthesis of noble metal colloids (silver, gold, and palladium). The amphiphilic polyester architectures, which have hydrodynamic radii in toluene between  $14 \pm 1.4$  and  $18 \pm 1.2$  nm, possess a hydrophilic interior and a hydrophobic shell. Dispersed in organic solvents such as toluene or benzene, it has been achieved to transfer hydrophilic metal precursors through the solvent into the nanoreactors by liquid–liquid phase transfer. The precursors trapped into polymeric nanoreactors and are reduced by their hydrophilic poly(ethylene glycol) blocks. Nanoparticles stabilization occurs due to presence of hydrophobic (polymethylene) fragments outside of the micelle structure. Subsequently, reduction of the metal precursor led to the formation of 8 – 20 nm sized metal colloids stable both in a polar and nonpolar medium.

A new approach to building up self-adjustable invertible polyester coatings at solid surfaces was proposed recently. It was based on the functionalization of the solid surface with the reactive anchor copolymer poly(styrene-*alt*-maleic anhydride) due to the physical adsorption and on grafting the chains of developed amphiphilic polyester to the modified solid surface through a reaction between the functional groups of the anchor and the polyester. An essential increase in colloidal stability has been observed for the titania particles after their modification with the invertible polyester chains. Redispersion cycles show the ability of the modified titanium dioxide particles to be redispersed in media differing in polarity from the previous medium.

## Electrostatic characterization of electrohydrodynamic atomization process for polymeric particle fabrication

Jun Yao<sup>a</sup>, Jingwei Xie<sup>a</sup>, Liang Kuang Lim<sup>b</sup>, Jinsong Hua<sup>c</sup>, Chi-Hwa Wang<sup>a,b\*</sup>

<sup>a</sup> Department of Chemical and Biomolecular Engineering, National University of Singapore, 4 Engineering Drive 4, Singapore, 117576

<sup>b</sup> Singapore-MIT Alliance, E4-04-10, 4 Engineering Drive 3, Singapore 117576

<sup>c</sup> Institute of High Performance Computing, 1 Science Park Road, #01-01 The Capricorn, Singapore Science Park II, Singapore 117528

### 1. Summary

The electrostatics of electrohydrodynamic atomization (EHDA) process in a shuttle-chamber for polymeric particle fabrication was, for the first time, investigated. The electrical potential field between the spray nozzle and the ground plate inside the chamber was measured three-dimensionally and demonstrated that the electrical field strength increased with decreasing nozzle-plate distance and the variation became significant in the region closed to the nozzle where liquid spray occurred. It is deduced that the nozzle-plate distance may affect liquid spray significantly. Four liquids, two inorganic liquids (water, KCl) and two organic liquids (PLGA+DCM (w/v=7%), PLGA +Acetonitrile (w/v=8%)) were tested and the organic liquids were sprayed to fabricate micro-particles. For spraying inorganic liquids the currents scaling was  $I \sim Q^{1/2}$  but for spraying organic liquids the currents scaling was  $I \sim Q^{1/4}$ . The accuracy of current scaling depended on the values of  $\delta_{\mu}\delta^{1/3}$ , which was independent of the nozzle-plate distances (electric field strength). In addition, the spray current increased with decreasing nozzle-plate distance (or increasing liquid flow rate or liquid conductivity). As a result of spraying polymer solution with volatile organic solvent, particles with size of 0.61~36.10 $\mu\text{m}$  were fabricated. Particle size decreased with decreasing nozzle-plate distance as well as increasing conductivity of polymer solution or decreasing the liquid flow rate. For all cases of particle fabrication, Rayleigh limit was never reached and no coulomb fission was found to occur in the fabrication process.

Keywords: electrostatic, electrohydrodynamic atomization (EHDA), particle fabrication.

### 2. Extended Abstract

Electrohydrodynamic atomization (EHDA) process in a shuttle-chamber has been successfully applied in polymeric particle fabrication. Ding et al. (2005) reported an EHDA technique to fabricate uniform microparticles in the range of 1-15  $\mu\text{m}$ . Xie et al. (2006) employed EHDA to produce biodegradable polymeric micro-and nano-particles and systematically investigated

*J. Yao et al.*

the effects of processing parameters on the size and morphology of polymer particles. Present work aims to use electrostatic technology (Yao et al. 2006) to quantitatively investigate the electrostatic effect of working elements, i.e. nozzle-plate distance (electrical field strength), liquid conductivity, liquid flow rate on liquid spraying and particle formation, especially for the case of polymeric particle fabrication, where a low-conductivity organic solvent was used.

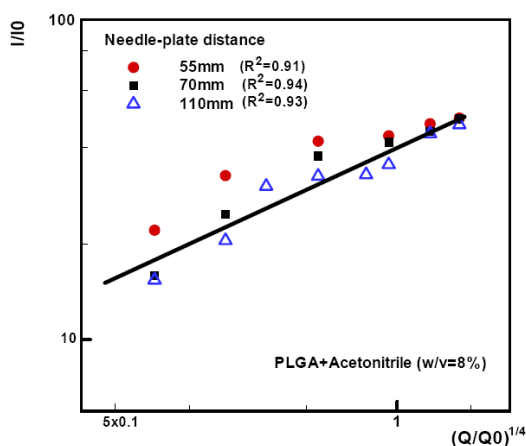


**Figure 1.** Spray current  $I$  versus flow rate  $Q$  in a dimensionless form for: (a) PLGA+DCM (w/v=7%); (b) PLGA+Acetonitrile (w/v=8%)

As indicated in Gañán-Calvo et al.(1997), for liquids with low viscosities and electrical conductivities ( $\delta_\mu \delta^{1/3} \gg 1$ ), the corresponding scaling law is given by  $I \sim Q^{1/4}$ , as shown by a straight line in Figure 1 for the solution of PLGA+Acetonitrile (w/v=8%).

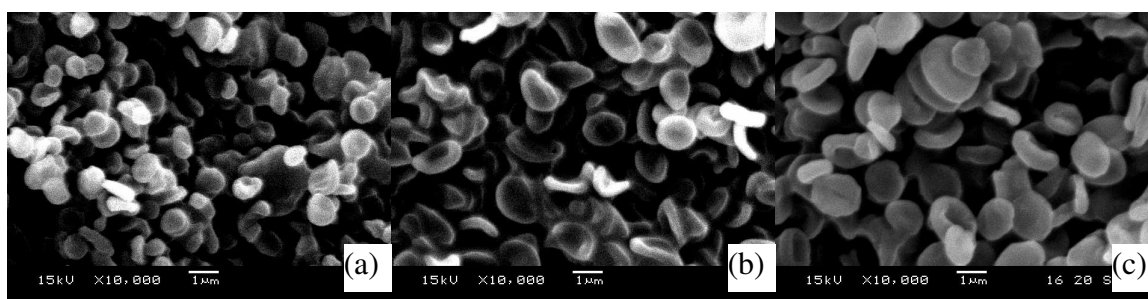


**Figure 2.** Effects of liquid flow rate on the particle morphology. Operating parameters:  $V_n$ (voltage applied on the nozzle) = 12kV,  $V_r$ (voltage applied on the ring) = 9kV. (a)-(c) acetonitrile, PLGA = 8% (w/v), nozzle-plate distance=110mm and flow rate: (a) 0.1ml/h (0.69~1.32 $\mu$ m); (b) 0.2ml/h (1.03~1.92 $\mu$ m); (c) 1.5ml/h (1.13~2.59 $\mu$ m).

During the fabrication process, the products formed on the plate were found to change with the liquid flow rate. In general, high liquid flow rate led to wet product without sufficient evaporation of organic solvent. In contrast, low flow rates resulted in fine dry powders on the ground plate.

## References

- Ding, L. N., Lee, T., Wang, C.H., (2005) *Journal of Controlled Release*, 102, 395-413.  
 Gañán-Calvo, A. M., Dávila, J., Barrero, A., (1997) *Journal of Aerosol Science* 28, 249-275.  
 Xie, J. W., Lim, L. K., Phua, Y. Y., Hua, J. S., Wang, C. H., (2006) *Journal of Colloid and Interface Science*, 302, 103-112.  
 Yao, J., Zhang, Y., Wang, C. H., Liang, Y. C., (2006) *AIChE Journal* 52, 3775-3793.

## **A three-dimensional population balance model of granulation employing mechanistic kernels**

R. Ramachandran,<sup>a</sup> J. Poon,<sup>a</sup> F. Stepanek,<sup>a</sup> F. Doyle III,<sup>b</sup> J. Litster,<sup>c</sup> I. Cameron,<sup>c</sup> C. Immanuel<sup>a</sup>

<sup>a</sup>*Department of Chemical Engineering, Centre for Process Systems Engineering, Imperial College, London, UK*

<sup>b</sup>*Department of Chemical Engineering, University of California at Santa Barbara, Santa Barbara, USA*

<sup>c</sup>*Particle & System Design Centre, School of Engineering, The University of Queensland, Brisbane, Australia*

### **1. Summary**

A dynamic model is presented for granulation processes, employing a three-dimensional population balance framework. As a first attempt to account for the multi-scale character of the process, the kernels used in the population balance model are derived using mechanistic representations of the underlying particle physics such as wetting kinetics and energy dissipation effects.

Keywords: pharmaceutical processes, population balances, nucleation, aggregation, multi-scale kernels

### **2. Extended Abstract**

Granulation is a particle production process of converting fine powdery solids into larger free-flowing agglomerates. It finds application in a wide range of industries (e.g. pharmaceuticals, fertilisers and minerals). Industrial granulation processes are operated in a highly inefficient manner with large recycle ratios within the process (3-4:1, recycle/product), and hence, an integrated systems model will be a crucial aid to alleviate this situation<sup>1</sup>. A modern view of granulation is a process that is governed by three predominant sub-processes: wetting and nucleation; consolidation and growth; and attrition and breakage<sup>2,3</sup>. An integrated model that accounts for these major sub-processes as well as the effects of the process inputs (binder addition, agitation rate, number of spray nozzles used for the binder spray, etc.) will enable an in-depth analysis, understanding, and efficient and effective control.

A suitable framework for the mathematical modelling of the granulation process is through population balances. A major challenge in developing these population

balances is the identification of appropriate kernels for the sub-processes (e.g., nucleation and aggregation). These issues have been addressed by several authors. The aim of this work is to develop a three-dimensional population balance model for granulation, accounting for the distribution of granules with respect to their size, binder content and porosity. The model incorporates the phenomena of wetting/nucleation, consolidation and aggregation. The nucleation and aggregation phenomena are represented by mechanistic kernels based on detailed particle-level information on these phenomena.

The kernel for the aggregation phenomenon is modelled using theory proposed for the case of porous and elastic granules with or without a binder layer<sup>4</sup>. The Smoluchowski formulation is employed to derive the dynamic kernel, drawing a parallel with the DVLO theory (a transition state theory that is well established in the emulsion polymerisation literature).

The nucleation stage is regarded as a crucial period during the initial stages of granulation because the nuclei size distribution obtained will impart a large influence on the resultant final granule size distribution. In the model presented here for the nucleation kernel, the initial focus is on the droplet controlled regime, where each droplet gives a single nucleus<sup>5</sup>. The proposed dynamic kernel is generic, and in addition to ideal situations, it also includes for situations wherein (1) the droplets do not wet the powder rapidly, and (2) once wetted, the penetration rate is not fast enough relative to the bed turnover rate, resulting in partial penetration of the droplet into the powder bed. The model adopts simplifying assumptions on certain other phenomena: (1) The droplets are well spread and do not overlap. (2) If primary particles (fines) are present, then the existent particles receive binder only if the droplets do not wet and penetrate the primary particles fast enough. Most of these assumptions are independent of the core wetting and nucleation phenomena, and could be more easily relaxed in a refined model in the future.

## References

1. Bardin, M., Knight, P.C. and Seville, J. P. K., (2004) *Powder Technology*, 140,169-175.
2. Iveson, S.M., Litster, J.D., Hapgood, K.P. and Ennis, B.J., (2001) *Powder Technology*, 117,3-39.
3. Biggs, C.A., Sanders, C., Scott, A.C., Willemse, A.W., Hoffman, A.C., Instone, T., Salman, A.D. and Hounslow, M.J., (2003) *Powder Technology*, 130,162-168.
4. Iveson, S.M., Litster, J.D., Hapgood, K.P. and Ennis, B.J., (2001) *Powder Technology*, 117,3-39.
5. Hapgood, K.P., Litster, J.D., Biggs, C.A. and Howes, P.B., (2002) *Journal of Colloids and Interface Science*, 253,353-366.

## Session T2-3P: Particulate Systems – Poster

Abstract Number	Paper Title & Authors	Included
147	Flow property measurement using the Jenike shear cell for 7 different bulk solids S Çagli, N Deveci, H Okutan, A A Sirkeci, Y Teoman	Yes
383	Drag on two co-axial rigid spheres moving normal to a plane: newtonian and Carreau fluids J P Hsu, S C Yang, J C Chen	No
438	Efficient Treatment and Control of Concentrated Particulate Waste Streams Q Omokanye, S Biggs	Yes
496	Solid-Solid Reactions in Fluidized Bed J S Murthy, T Sankarshana, S R Venna	Yes
722	Characteristics of Gas -Solid Fluidization in Tapered Beds J S Murthy, T Sankarshana	Yes
952	Characterization of metal powder suspension to improve the functionality of cemented carbides Y Komoda, D Takafuji, H Usui	Yes
999	Nonlinear Prediction of Fluidized Bed Pressure Fluctuation R Zarghami, N Mostoufi, R Sotudeh-Gharebagh	Yes
1222	A phenomenological Description of Mixing-Segregation Effects during Shear Deformation of Particulate Solids V Dolgunin, V Borshev, A Klimov, R Shubin	Yes
1298	On-line measurement of crystal complexity N Ferreira, N Faria, F Rocha	Yes
1346	Influence of hydrodynamic conditions on particle size distribution A A Öncül, D Thévenin	Yes
1830	Understanding the dissolution of a mineral material in formic acid H Grénman, J Gustafsson, T Salmi, D Y Murzin	No
2233	Prediction of product particle size distribution using batch grinding equation G Matijašić, K Žižek, M Hraste	Yes
2842	Gravity Separation Technology of Grain Materials Differ in Complex of Physical and Mechanical Properties of Particles V Dolgunin, O Ivanov, A Kudy, A Klimov	Yes
3514	Experimental Investigation of a Rotating Fluidized Bed in a Static Geometry J De Wilde, G B Marin, G J Heynderick, A de Broqueville	Yes
4033	Size Separation of Rubber Particles from Natural Rubber Latex by Hydrocyclone Technique K Pana-Suppamassadu, S Amnuaypanich	Yes

Session T2-3P



## **Flow property measurement using the Jenike shear cell for 7 different bulk solids**

Serkan ÇAĞLI<sup>a</sup>, Nuran DEVECİ<sup>a</sup>, Hasancan OKUTAN<sup>a</sup>, A. Ayhan SİRKECİ<sup>b</sup>, Yıldırım TEOMAN<sup>c</sup>

<sup>a</sup> *Department of Chemical Engineering, Istanbul Technical University, 34469, Maslak, Istanbul, Turkey*

<sup>b</sup> *Department of Mining Engineering, Istanbul Technical University, 34469, Maslak, Istanbul, Turkey*

<sup>c</sup> *Türkiye Sise ve Cam Fab. A. S., Vice Pres. Res. & Tech., 34330, 4. Levent, Istanbul, Turkey*

### **1. Summary**

In this study, instantaneous flow properties (cohesion, angle of internal friction) of 3 different sand samples (Yalıköy, Safaalanı and yellow), soda, limestone, dolomite and clay were measured at intrinsic moisture contents by using Jenike shear tester. Additional tests were also performed for low and high moisture contents of Yalıköy sand. Flowability of solids which is characterized by flow function (or flow index) was investigated for studied materials and a classification was made. It can be said that high moisture content and small particle size has an adverse effect on the flow.

Keywords: Shear testing, yield locus, Jenike shear tester, flow properties, flow function

### **2. Extended Abstract**

There are many industry branches which deal with solid materials in bulk form. The handling (storage, transportation and discharge) of these materials is an important operation in these industries. Some materials flow better than others and it is well known that wet and fine solid materials flow poorly and cause obstructions in the flow. Therefore, it is essential to understand the effect of material characteristics such as size, composition and moisture content on the static and dynamic behavior of solid materials in silos (bunker, bin). Determining the internal flow properties of bulk solids is the first mandatory step of silo design procedure and it is important for a proper and efficient bin design [1].

The standard method to characterize the flow properties of solid materials is the shear testing which provides the information for the yield locus of the solid in question. Shear testing is based on the information of shear stress values against normal stress values (graphically shown in  $\sigma$ - $\tau$  coordinates - namely Mohr diagrams) and these are obtained by sliding the material inside itself under defined load values. All of the

other flow properties (angle of internal friction, cohesion, flow function, kinematic angle of wall friction, etc.) of solids are also determined from the yield loci [2].

There are generally two types of bulk materials such as free flowing and cohesive in relation to their flow properties. A cohesive bulk material is named as Coulomb solid and expressed by a linear yield locus in soil mechanics:

$$\tau = \tan \phi \sigma + C \quad (1)$$

$\tau$  is the shear stress,  $\sigma$  is the normal stress,  $C$  is the cohesion and  $\phi$  is the angle of the internal friction of the material.  $\phi$  is an indication of the friction coefficient within the material [1, 2].

Shear tests were performed by the Jenike shear tester with standard size shear cell. The standard test method carried out in this study (standard test method for instantaneous flow using the Jenike shear cell) is defined in the publication of European Federation of Chemical Engineering [3, 4].

It has been found that cohesion values increase with increasing normal stress values and high moisture content and small particle size also increase the cohesion values. Beside, there is not significant difference between the angle of internal friction values at different stress levels. As these values don't give any idea about material flowability, it can be stated that these angle values are higher for the materials which have low moisture content and seem to have easy flow.

A classification has been made according to the flow functions (slope values of the defined equations) of the materials [5]. The material which has the hardest flow is clay and soda has the easiest flow among the studied materials. While clay and soda have been classified as cohesive and free flowing material, all other materials have been found in easy flowing material class. It can be said that high moisture content and small particle size has an adverse effect on the flow. While the flow of Yalıköy sand at low moisture content has been easier than its intrinsic moisture content, a more difficult flow hasn't been obtained at high moisture content as expected.

## References

- [1] P.C. Arnold, A.G. McLean, A.W. Roberts, *Bulk Solids: Storage, Flow and Handling* (Tunra Bulk Solids Handling Research Associates), 2nd Ed., The University of Newcastle Research Associates Ltd. Inc., NSW Australia, 1989.
- [2] A.W. Jenike, *Gravity Flow of Bulk Solids* (Bulletin No. 108), Utah Engineering Experiment Station, University of Utah, Salt Lake City-Utah, 1961.
- [3] D6128-00, *Standart Test Method for Shear Testing of Bulk Solids Using the Jenike Shear Cell*, ASTM International, West Conshohocken, USA, 2000.
- [4] *Standart Shear Testing Technique for Particulate Solids Using the Jenike Shear Cell*, Institution of Chemical Engineers (European Federation of Chemical Engineering), Rugby UK, 1989.
- [5] J.J. Fitzpatrick, S.A. Barringer, T. Iqbal, Flow property measurement of food powders and sensitivity of Jenike's hopper design methodology to the measured values, *Journal of Food Engineering*, 61 (2004) 399–405.

## **Efficient Treatment and Control of Concentrated Particulate Waste Streams**

Qanitalillahi Omokanye,<sup>a</sup> Simon Biggs<sup>a</sup>

<sup>a</sup>*Institute of Particle Science and Engineering, University of Leeds, Leeds, LS6 2JT, United Kingdom*

### **1. Summary**

Zeta ( $\zeta$ ) potential measurements are frequently used to predict the stability of colloidal systems under different solution conditions. Metal oxide particles are widely used in a range of products and processes as well as being a significant constituent of waste streams from many industrial activities such as minerals processing. In many cases, these oxide particle streams are highly concentrated and are within complex electrolyte solutions across a wide pH range (3 – 12). Here we investigate the effect of changing electrolyte conditions on particle-particle interactions for a model metal oxide dispersion by varying electrolyte type and concentration (1 mM – 1000 mM) across a range of pH. The shear yield stress was used as a primary characterization parameter for concentrated titania dispersions under different background solution conditions. Yield stress data can be used to infer particle-particle interactions for a bulk particle system and give a good measure of the stability of particles in a dispersion as well as the nature of individual particle-particle bonds. Of special interest here is the role that surface adsorbed ions can play in mitigating the particle-particle interactions within a settled bed network.

Keywords: zeta ( $\zeta$ ) potential, isoelectric point (iep), titania, shear yield stress, colloids

### **2. Extended Abstract**

A result of many industrial manufacturing, minerals extraction and water treatment processes is the production of particulate waste materials. Many of these waste streams consist of oxide particulates in aqueous dispersion; treatment and disposal of these wastes ultimately requires the application of a variety of unit operations such as filtration devices and thickeners. Typically, these processes must operate across a wide range of conditions, such as variable pH and electrolyte concentrations, and knowledge of how these dispersions behave over such a range of conditions is therefore essential for the efficient design and control of waste processing systems.

Basic theory for the stability of colloidal particles in aqueous dispersions requires summation of two independent components; the attractive van der Waals interaction and the repulsive electrical double layer component. An unstable dispersion can be created, if the repulsive electrical double layer interaction is suppressed in some way; the attractive component is largely insensitive to its surrounding medium in aqueous

conditions. A common route for instability to be induced or to occur naturally is through the addition of electrolyte in a process known as coagulation [1]. The net result of coagulation is the formation of aggregates which can settle to form a sediment bed; a key aspect of this sediment is that it will form a continuous network of particles bound to each other by the van der Waals interactions prevalent in that system. Adsorbed ions can have an influence on these short-range contact forces and it is this that we aim to investigate further here.

Classically, engineering design has concentrated on the hardware and its optimisation; here, we consider the detailed character of the dispersion and how this may be controlled and influenced to provide optimum operational conditions for existing unit operations. The electroacoustic zeta potentials and shear yield stresses for concentrated titania dispersions have been measured across a range of pH conditions and electrolyte concentrations (0.001 M – 1.0 M).

Some **key results** from these investigations are given below in Fig. 1 & 2. These data demonstrates how yield stress of concentrated aqueous titania dispersions can be controlled through the regulation of pH and addition of background electrolytes. The yield stress as a function of pH for titania in mixed electrolytes shows a clear correlation in the position of the iep with the  $\zeta$  potential data (Fig.2). The pH at which the maximum yield stress occurs corresponds to the iep in most low electrolyte concentration colloidal systems since this is the condition that produces the greatest attraction.

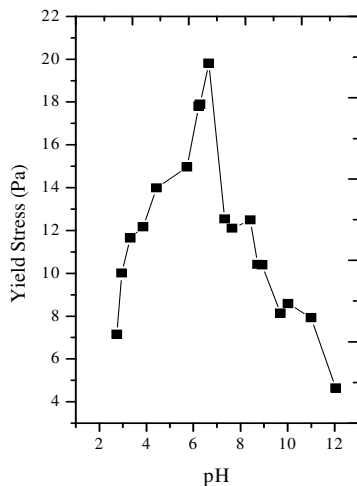


**Figure 1.** Yield stress of 41wt% titania in 0.01M mixed solution (NaCl and Na<sub>2</sub>SO<sub>4</sub>). The lines are drawn to guide the eye.

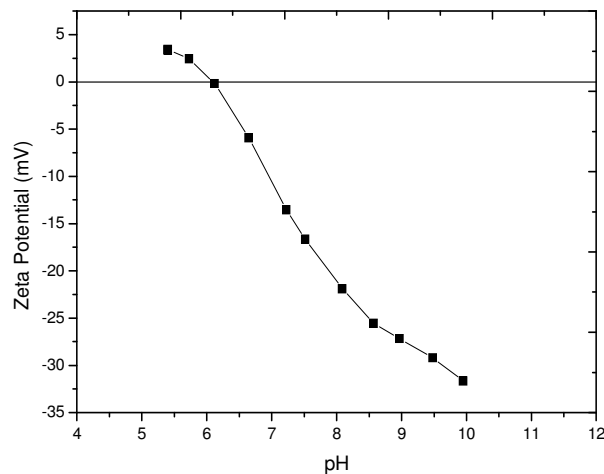


**Figure 2.**  $\zeta$  potential of titania calculated by the Colloidal dynamics Zeta probe for 4wt% titania in 0.01 M mixed solution (NaCl and Na<sub>2</sub>SO<sub>4</sub>).

## References

1. D.J. Shaw, Introduction to Colloid and Surface Chemistry. 1992. pp 210 – 243.

## **Solid-Solid Reactions in Fluidized Bed**

Josyula murthy<sup>a</sup>, Talapuru Sankarshana<sup>a</sup>, Surendar Reddy Venna<sup>a</sup>

<sup>a</sup>*University College of Technology, Osmania University, Hyderabad-500007, India.*

### **1. Summary**

The factors that affect the solid-solid reactions are rate of heat transfer, rate of diffusion and reaction kinetics methods. The rate of heat transfer and rate of diffusion are very slow since there is no mixing. In order to overcome these problems and to reduce the time of reaction and to obtain a desired conversion, an attempt is made to investigate these reactions employing fluidized bed technology. The addition reaction of Phthalic anhydride and p-Nitro aniline system forming phthaloyl derivative of p-Nitro aniline taking place between 80 - 120 °C is selected for investigations. The reactants are ground to fine powders and mixed with sand. The effect of variables viz. reaction temperature, stirrer speed and flow rate of fluidizing medium on maximum conversion, time for maximum conversion, rate constant and activation energy is studied. The experiments are performed based on statistically designed factorial experiments. It was observed that the time of reaction is reduced considerably and activation energy is reduced by about 14 times compared to that reported in literature. The results predicted by factorial design analysis are compared with results obtained from experiments under different conditions other than those used for the development of equations and found to agree within + 10%.

Keywords: Solid-Solid Reactions, Fluidization, Sintering, Factorial design

### **2. Extended Abstract**

Although solid- solid reactions are known to play an important role in industries, such as those associated with the manufacture of ferrites, semiconductors, ceramics, dry cells, cement production, catalyst preparation, fertilizers, drugs, metallurgy etc. have not received significant attention in chemical engineering literature. The usual manufacturing process involves mixing of the component solid reactants in fine powdered form and firing at high temperature to obtain the desired products.

The factors that affect the solid-solid reactions are rate of heat transfer, rate of diffusion and reaction kinetics. In conventional methods, the rate of heat transfer and rate of diffusion are very slow since there is no mixing. In order to overcome these problems and to reduce the time of reaction to obtain a desired conversion, an attempt is made to investigate these reactions employing fluidized bed technology.

The addition reaction of Phthalic anhydride and p-Nitro aniline system forming phthaloyl derivative of p-Nitro aniline taking place between 80-120oC is selected for investigations. To conduct the reaction, the reactants are ground to fine powders and mixed. To overcome the difficulty in fluidization of these cohesive types of powders, they are mixed with sand (an inert material) in 1:3 proportion and stirring is also provided for proper mixing and smooth fluidization and also to improve rate of heat transfer.

The hydrodynamic studies of fluidization of the mixed powder with stirring are first carried out in a glass column of 0.1m diameter and 1m height at atmospheric conditions. The reaction studies are conducted in a stainless steel column of the similar dimensions.

Heating of the reactants is carried by sending hot air at the required temperature.

The effect of variables viz. reaction temperature, stirrer speed and flow rate of fluidizing medium on maximum conversion, time for maximum conversion, rate constant and activation energy is studied.

The conventional single factor approach requires a large number of experiments to analyze the experimental data. Hence, the experiments are performed based on statistically designed factorial experiments to analyze the data and formulate the required mathematical equations for the desired response variables.

Development of model equations is done in two steps: 1. Modeling of the solid-solid reaction between phthalic anhydride and p-nitro aniline. 2. Development of relationship between kinetic parameters and the operating parameters.

Among the models proposed in the literature for solid-solid reactions for various mechanisms, Jander's model under diffusion controlled mechanism given by the equation:  $[1-(1-X)^{1/3}]^2 = k t$ , where X is the conversion, t is time and k is rate constant is found to be suitable.

It was observed that the time of reaction is reduced considerably and activation energy is reduced by about 14 times compared to that reported in literature. The equations are then formulated as per the factorial design analysis for the prediction of rate constant, activation energy, maximum conversion and time for maximum conversion in terms of operating variables.

The results predicted by factorial design analysis are compared with results obtained from experiments under different conditions other than those used for the development of equations and found to agree within + 10%. It is found that considerably less time for reaction and activation energy are required in a fluidized bed compared to that of conventional approach to obtain desired conversion for the reaction. These are attributed to good mixing and rate of heat transfer in addition to prevention of sintering in fluidization operation.

## Characteristics of Gas -Solid Fluidization in Tapered Beds

Josyula Surayanarayana Murthy<sup>a</sup>, Talapuru Sankarshana<sup>a</sup>

<sup>a</sup>University College of Technology, Osmania University, Hyderabad – 500 007, India.

### 1. Summary

The various problems associated with fluidization operation in cylindrical beds, could be overcome adopting tapered beds because of the decrease of superficial velocity with the height of the vessel. In the present work, various aspects of the fluidization phenomenon

have been experimentally studied in detail with respect to the effects of particle size, angle of the tapered bed employing a wide range of parameters like particle size (270-3600 $\mu$ m), and density (0.86 to 4.0 g/cc), apex angles of tapered vessels (5 to 30 degrees) and static bed height (0.08 to 0.55 m). The materials used include particles of sand of

different sizes, mustard, urea, magnetite and hematite. Correlations have been developed for all hydrodynamic characteristics. Correlations for some of the characteristics like minimum velocity for full fluidization, maximum velocity for defluidization and hysteresis are proposed for the first time in the literature to the best of the knowledge of the authors.

Keywords: tapered bed, fluidization, critical fluidization velocity, peak pressure drop

### 2. Extended Abstract

Gas solid fluidization has a wide range of industrial applications like catalytic reactions, combustion, gasification, granulation, drying etc. In a number of these applications, the feed is not of uniform size and also there could be reduction in size due to attrition and during operation. These lead to entrainment and also limitation of operating velocity. The various problems associated with fluidization operation in cylindrical beds, could be overcome adopting tapered beds because of the decrease of superficial velocity with the height of the vessel.

The fluidization characteristics are different from those of cylindrical beds and depend strongly on particle size and apex angle of the vessel. In the present work, various aspects of the fluidization phenomenon have been experimentally studied in detail with respect to the effects of particle size, angle of the tapered bed employing a wide range of parameters like particle size (270-3600 $\mu$ m), and density (0.86 to 4.0 g/cc), apex angles of tapered vessels (5 to 30 degrees) and static bed height (0.08 to

0.55 m).The materials used include particles of sand of different sizes, mustard, urea, magnetite and hematite.

In vessels with apex angle less than 10 degrees, there is no circulation of particles and also it is not possible to maintain stable partial fluidized bed region irrespective of particle size. However, in the case of particles greater than 450 $\mu$ m there is formation of slugs in the bed. For vessels with apex angle greater than 10 degrees, the circulation of particles and bubble formation along the walls are the main features of the fluidization phenomena. Accordingly, the variations in phenomena taking place as a function of apex angle and particle size are brought out clearly.

Correlations have been developed for all hydrodynamic characteristics. Correlations for some of the characteristics like minimum velocity for full fluidization, maximum velocity for defluidization and hysteresis are proposed for the first time in the literature to the best of the knowledge of the authors. Results predicted by the present correlations are also validated with additional experimental data. The correlations for fluctuation ratio, peak pressure drop and critical fluidization velocity are compared with the results predicted by the correlations available in literature. The trends of all hydrodynamic characteristics with particle characteristics, apex angle and static bed height are discussed.



## Characterization of metal powder suspension to improve the functionality of cemented carbides

Yoshiyuki Komoda <sup>a</sup>, Daisuke Takafuji <sup>b</sup>, Hiromoto Usui <sup>a</sup>

<sup>a</sup>Department of Chemical Science and Engineering, Kobe University, 657-8501, Kobe, Japan

<sup>b</sup>Department of Molecular Science and Material Engineering, Kobe University, 657-8501, Kobe, Japan

### 1. Summary

Cemented carbide is produced by sintering a mixture of metal carbide and binder. Both materials are formed into a granulated powder via suspension with the object of a uniform product and an easy material handling. In addition to excellent toughness and abrasion resistance, accurate and minute figuration is required as cemented carbide. Thus, how to produce the granulated powders is very important, because the interaction between materials in a suspension directly affect the property of final products. However, because of sedimentation of materials, the evaluation of particle agglomeration in a suspension had not been conducted, not to mention the control. In this study, the strength of particle interaction was evaluated by the measurement of viscosity; further the relationship between particle interaction and granulated powder characteristics was clarified. As the amount of surfactant addition into suspension was increased, the interaction was decreased gradually; however, up to a critical concentration the characteristics of granulated powder did not change. And too much addition of surfactant resulted in the decrease of strength of granulated powder.

Keywords: Cemented carbide, suspension rheology, surfactant, agglomeration

### 2. Extended Abstract

The raw material particles, which mainly consist of Tungsten carbide (WC), binder (Co) and other metal carbides, were suspended in an ethanol and its volume fraction was adjusted to 0.17. Diameters and specific densities of metal powders were ranging from 0.2 to 7 $\mu$ m and 7 to 15, respectively. Some suspensions contained non-ionic surfactant at the concentration of 0.1, 0.2, 0.5 and 1.0wt% to the metal materials.

The vertical tube viscometer (Fig.1) was assembled for the suspension viscosity measurement in order to minimize the effect of sedimentation. Suspensions flew out form a pressurized closed vessel via the vertical tube of 5mm in inner diameter and of 0.5, 0.75 and 1.0m in length. At that time, flow rate and pressure

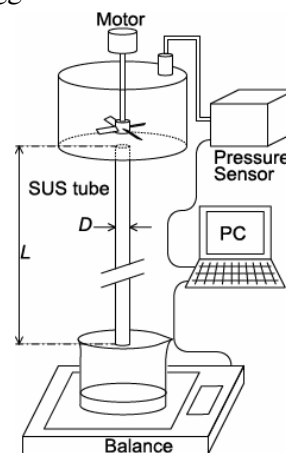


Fig.1 Apparatus Setup of Vertical Tube Viscometer

difference in tubes were measured by balance and pressure sensor, and simultaneously recorded. In this system, the inner pressure of the vessel and flow rate has decreased, as the suspension flew out from the vessel. By introducing Rabinowitsch - Mooney equation and Bagley collection, apparent viscosities in various shear rates were obtained.

It can be seen in Fig.2 that apparent suspension viscosities were correlated by Casson model and the effect of surfactant concentration,  $C_S$ , could not be distinguished up to  $C_S=0.2\%$ . However, suspension showed lower viscosity when  $C_S$  is higher than 0.5%. The inter-particle bonding energy was calculated by applying the experimental viscosity data to the thixotropy model proposed by Usui (Usui et al, 2001). Here, inter-particle bonding energy is defined as the energy required when an agglomeration is broken up into two pieces under a uniform shear rate.

Granulated powders were produced by spray drying from the suspensions used for a viscosity measurement. And the diameter measurement and the observation of the granulated powders were conducted. As shown in Fig.3, the effect of the addition of surfactant on both interaction and diameter could not clearly be seen up to  $C_S=0.2\%$ . When  $C_S$  was increased up to 0.5% or more, however, the size of granulated powder became small probably because of the small interaction between particles. From the SEM images, the granulated powder produced with the suspension with low concentration of the surfactant has rough surface and seems to be composed of agglomerations of raw material particles as shown in Fig.4 (a). On the other hand, the surface of the granulated powder from the suspension containing 0.5wt% of surfactant (Fig.4 (b)) was smooth but had some defects in some places. Since raw material particles were dispersed well and the agglomeration were packed loosely in a suspension, the granulated powder that the surface is smooth and breakable was produced. Although excessive addition of surfactant was proved to deteriorate toughness of granulated powder, it will be necessary to clarify the effect on the interaction between particles at a small amount of surfactant addition.

## References

Usui, H., Li, L., Kinoshita, S. and Suzuki, H., (2001) *Journal of Chemical Engineering of Japan*, 34(3), 360-368

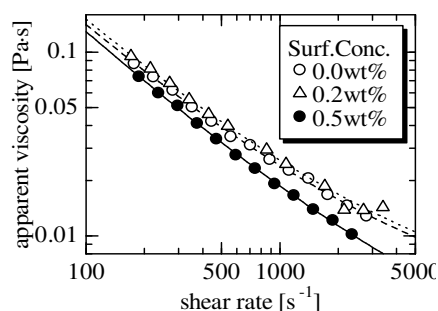


Fig.2 Effect of surfactant concentration on suspension viscosity

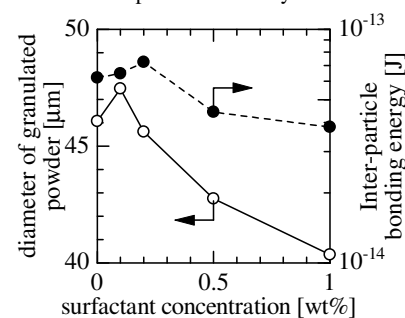
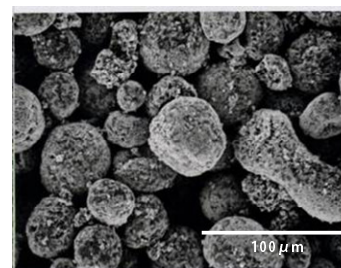
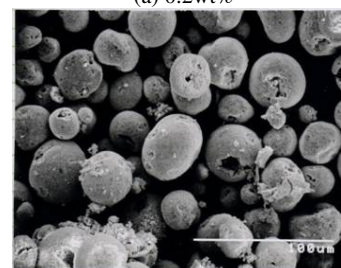


Fig.3 Effect of surfactant concentration on property of granulated powder



(a) 0.2wt%



(b) 0.5wt%

Fig.4 Appearance of granulated powders at  $C_S = 0.2$  and 0.5%

## **Nonlinear Prediction of Fluidized Bed Pressure Fluctuation**

R. Zarghami, N. Mostoufi, R. Sotudeh-Gharebagh

*Process Design and Simulation Research Center, Department of Chemical Engineering, University of Tehran, P.O. Box 11365/4563, Tehran, Iran*

### **1. Summary**

Nonlinear time series techniques have been applied to predict pressure fluctuation data in fluidized beds. The method of delays reconstructs the attractor dynamics by using time delay and embedding dimension to carry out analysis in the reconstructed state space. Several state space based prediction methods, i.e., nearest neighbors and local nonlinear prediction method, local linear method and Kernel regression method are used to predict of pressure fluctuation signals. The quality of a nonlinear prediction can be assessed by comparison of the predicted data for last segment of known sample time series of pressure signal with its original benchmark. Finally, chaotic invariants (dimension and entropy) of measured and predicted time series of pressure signals were compared.

Keywords: chaotic attractor, pressure fluctuation, prediction

### **2. Extended Abstract**

Several researchers (e.g., Daw and Halow, 1991; van den Bleek and Schouten, 1993; van der Stappen et al., 1993) have found characteristics of low-dimensional (typically less than five) nonlinear time series of pressure fluctuations in fluidized beds. The state of a fluidized bed (dissipative system) at a certain time could be determined by projecting all variables governing the system into a multidimensional space, i.e., the state space. The collection of the successive states of the system during its evolution in time is called the attractor. However, it is practically impossible to know all governing variables of a fluidized bed. Takens (1981) proved that the dynamic state of a system can be reconstructed from the time series of only one characteristic variable such as the local pressure in a fluidized bed. A time series of pressure measurements in a fluidized bed, extracted from Johnsson et al. (2000), for multiple bubble regime has been considered in this work. Determining the time delay and the embedding dimension is considered as one of the most important steps in nonlinear time series modelling and prediction. In the present study, the time delay value of 26 obtained from mutual information technique have been used. The embedding dimension of 20 considered using the Cao method (Cao, 1997). Prediction of future observations is an important problem in the analysis of time series and some existing nonlinear prediction methods, such as nearest neighbors (McNames, 1998), local nonlinear prediction method, linear method and Kernel regression method (Haerdle, et al., 1992), have been applied. First part of data, about 80 %, is considered as training section and last segment is used for prediction range. In general, the quality

of prediction was found to be good, see figure 1 for example. Correlation dimension and Kolmogorov entropy of measured and predicted time series of pressure signals were compared in the next step. The correlation dimension expresses the number of degrees of freedom of the system, whereas the entropy is measures of the predictability of the system and the sensitivity to initial conditions. The predictions errors corresponding to each method and values of dimension and entropy show that the Kernel method has a considerable advantage over other methods for the fluidized bed time series. This is mostly because the fluidized bed time series is a good example of a chaotic time series and the local nonlinear character of the Kernel method could best capture its local dynamics. The locally nonlinear predictor and the nearest neighbors showed comparable performance, while the locally linear method performed much worse. This confirms the suggestion that for chaotic time series nonlinear and locally linear prediction methods are preferred to traditional linear ones.

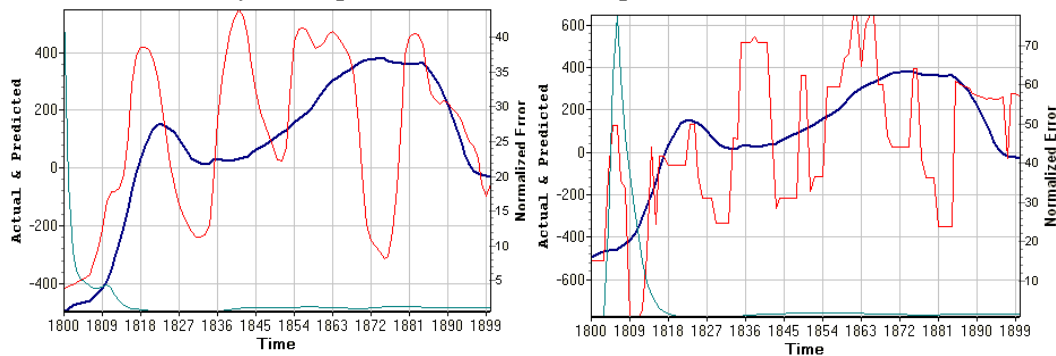


Figure 1: Actual values, predicted values and normalized error using: (left) Kernel regression method and (right) nearest neighbors method

## References

- van den Bleek, C.M., Schouten, J.C., (1993), *Chem. Eng. J.* 53, 75-87.
- Daw, C.S., Halow, J.S., (1991), In: Anthony, E.J. (Ed.), *Proc. Eleventh Int. Conf. Fluidized Bed Combustion. American Society of Mechanical Engineers*, New York, pp. 777-786.
- Cao, L., (1997), *Physica D* 110 45-50
- van der Stappen, M.L.M., Schouten, J.C., van den Bleek, C.M., (1993), *AIChE Symp. Series* 89 (296), 91-02
- Takens, F., (1981), In: Rand, D.A., Yong, L.S. (Eds.), *Proc. Dynamical Systems and Turbulence, in Lecture Notes in Mathematics* 898. Springer Verlag, Berlin, pp. 366-381.
- Johnssona F., Zijerveldb R.C., Schoutenb J.C., van den Bleekb C.M., Lecknera B., (2000), *International Journal of Multiphase Flow* 26 663-715
- J. McNames, (1998), *Proc. of the International Workshop on Advanced Black-box Techniques for Nonlinear Modeling*, 1998, pp. 112-128
- Haerdle, W., Vieu, P., (1992), *J. Time Ser. Anal.*, 13, No.3, 209-232.

## **A phenomenological Description of Mixing-Segregation Effects during Shear Deformation of Particulate Solids**

V. Dolgunin,<sup>a</sup> V. Borschev<sup>b</sup>, A. Klimov<sup>a</sup>, R. Shubin<sup>b</sup>

<sup>a</sup>*Department of Technological Equipment and Food Technology, State Technical University, 106 Sovetskaya str., 392000, Tambov, Russia*

<sup>b</sup>*Department of Mashine and Apparatus of Chemical Technology, State Technical University, 106 Sovetskaya str., 392000, Tambov, Russia*

### **1. Summary**

The mixing–segregation kinetics in the course of shear flow of particulate solids at low shear rates is studied analytically and experimentally. The experimental research was carried out by the use of the conveyor shear cell developed previously [1]. The phenomenological description of the segregation–mixing dynamics during shear flow of nonelastic cohesionless rough spherical particles is suggested. Only one experimental constant (segregation coefficient) is used to forecast the segregation–mixing dynamics. The method of the segregation coefficient determination is developed.

Keywords: particulate solids, shear deformation, mixing, segregation

### **2. Extended Abstract**

In our previous paper [1] we have suggested the experimental unit and method of segregation and mixing exploration during shear deformation of particulate solids.

In the present paper we are developing a phenomenological approach to the description of the segregation-mixing effects, observing by means of the conveyor shear cell [1]. As a result of investigation we are suggesting a mathematical simulation of the process of the nonuniform particles distribution in particulate solids undergoing shear deformation at low and moderate shear rates.

The mathematical description is based on the general mass transfer equation taking into account the fluxes of convection, segregation and mixing of particles, differing in size and density. Neglecting the mixing flux towards shear direction we formulated this equation adapted to the steady two-dimensional shear flow as follows

$$\partial c \rho_b / \partial \tau = -\partial (uc \rho_b) / \partial x + \partial (j_m - j_s) / \partial y \quad (1)$$

where  $c$  is the concentration of test particles;  $\rho_b$  is the bulk density;  $u$  is the mean particle velocity towards shear direction  $x$ ,  $(x, y)$  Cartesian coordinates,  $\tau$  is the time.

The mixing flux  $j_m$  is expressed on the basis of the analysis of chaotic transversal movements of particles (transversal mass transfer) in a restricted environment.

These chaotic movements are formally analogical to the quasidiffusional mixing of particles. That is why the mixing flux of particles is expressed as follows

$$j_m = -0,5s \cdot u_t (\partial c / \partial y) = -0,5s \cdot b \cdot d \cdot \sin(\pi/4 \cdot (d + s)/d) (\partial u / \partial y) (\partial c / \partial y) \quad (2)$$

where  $u_t$  is the mean transversal velocity of particles;  $s$  is the mean distance between particles;  $d$  is the average particle diameter,  $b = ((\pi/6)/(1-\varepsilon))^{0.33}$  is the geometrical parameter.

The segregation flux  $j_s$  is determined on the basis of the mechanism of hydromechanical segregation [2]. This mechanism presupposes that segregation takes place due to generation of the excess moment of forces acting on the nonuniform particles. This mechanism is adapted here for the conditions of the low shear rates, when the collision forces between particles are negligible. The adaptation allowed us to describe the segregation flux in the following way.

$$j_s = Kbd(du/dy)c\rho_b\Delta M_o \quad (3)$$

where  $\Delta M_o = (M - M_o)/M_o$  is the relative excess moment of gravity and frictional forces, acting on the test particle,  $M_o$  is the excess moment of forces acting on an average particle of the mixture;  $M$  is the analogous moment acting on a test particle of the mixture;  $K$  is the segregation coefficient.

In the present paper the method suggested for the segregation coefficient determination as the relative transversal velocity of the test particle in the conveyor shear cell is discussed. The coefficient is determined as follows

$$K = u_n / (\Delta M_o b d (du/dy)) \quad (4)$$

where  $u_n$  is the transversal test particle velocity.

It was found out that the segregation coefficient is the experimental constant, which doesn't depend on shear rate and size of large and small spherical cohesionless nonelastic test particles.

The adequacy of the developed mathematical simulation of the mixing-segregation dynamics is checked by comparison of experimental and calculated results. It is noteworthy, that the complex segregation-mixing process is forecasted by the method using only one experimental kinetic constant.

## References

1. Dolgunin V., Borschev V. and Klimov A. The conveyor shear cell for determination of particle tendency to segregation and mixing. 4<sup>th</sup> European congress of chemical engineering, full text of papers in CD-ROM; Granada, Spain, 2003.
2. Dolgunin V., Ukolov A. Segregation modeling of particle rapid gravity flow // Powder Technology. – 1995. – N 83. – P.95 – 103.

## On-line measurement of crystal complexity

A. Ferreira, N. Faria, F. Rocha

*Departamento de Engenharia Química, Faculdade de Engenharia, Universidade do Porto, Rua Dr. Roberto Frias, s/n 4200-465 Porto, Portugal*

### 1. Summary

This paper presents and describes an on-line method to determine the complexity level of a crystal or a population of crystals. Image analysis techniques are combined with discriminant factorial analysis leading to results that allow the computation of the complexity of crystals through a new parameter, the agglomeration degree of crystals. With this methodology it has been possible to distinguish, on-line and automatically, among three different classes of crystals, and within each class as per their complexity. It further describes the application of such methodology to the study of the influence of D-glucose on sucrose crystallization, namely on crystal size and morphology. The effect of supersaturation, growth rate and impurity concentration on the type, amount and complexity level of the agglomerates was also determined.

Keywords: crystal morphology, image analysis, agglomeration, sucrose, D-glucose

### 2. Extended Abstract

Developed by Pons *et al.* (1997, 1998) and adapted to the study of sucrose crystallization by Faria *et al.* (Faria *et al.* 2003; Fayo de Azevedo *et al.*, 2002), the image analysis technique has proved to be very effective in the quantification of crystal size distributions and morphology. In the present work this technique was applied, for the first time, as on-line method to determine the complexity level of a crystal or a population of crystals. Experiments were carried out in a laboratory-scale 4L batch crystallizer (Fig. 1-a). Information about the dissolved dry solids content was measured continuously by an on-line refractometer. Experiments were performed at constant temperature (35° C) starting at high supersaturations and leaving the system to evolve until near the saturation. For that, 16 g of crystals with mean size of 413 µm was used. Crystal images are acquired by a video camera located at the image analysis cell, where the solution flows at constant rate of 200 ml/min. These images (about 3 per second) are then treated, analysed and several numerical descriptors are extracted for each crystal using Visilog<sup>™</sup>5 (Noesis, les Ulis, France)(Faria *et al.* 2003). These data are then combined with discriminant factorial analysis leading to results that allow the computation of the complexity of crystals through the parameter

agglomeration degree of the crystals (Faria *et al.* 2003). With this methodology it was possible to distinguish automatically among three different classes of crystals (Fig. 1-b). The agreement between the automated and visual classification was about 90%. The experimental results are summarised in Fig. 2. The impurity decreases the growth rate and increases the crystals complexity. The formation of agglomerates increases with time.

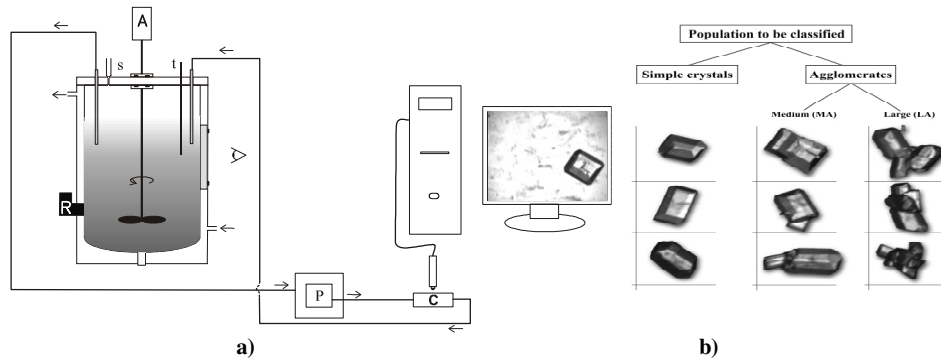


Fig. 1- a) Experimental apparatus: A, agitator; c, image analysis cell; P, peristaltic pump; R, refractometer ; s, seed vessel; t, thermocouple. b) Classification tree of sucrose crystals.

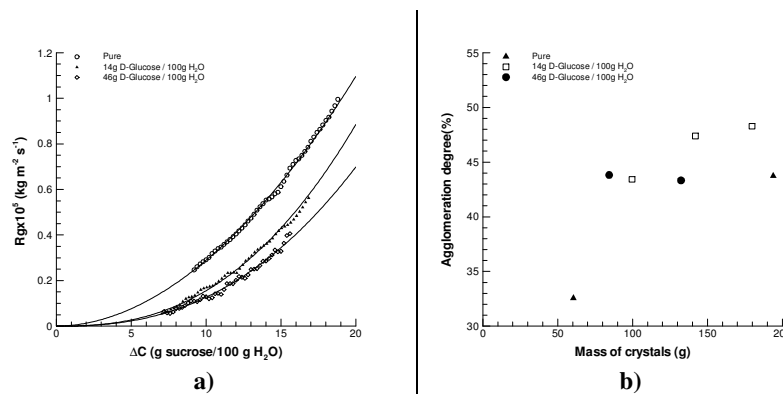


Fig. 2- Experimental results: a) Growth rate curves for pure and impure solutions; b) Impurity influence on the agglomeration degree.

## References

- Pons, M. N.; Vivier, H.; Dodds, J., (1997) *Part.Part. Syst. Charact.*, 14, 272-277.
- Pons, M. N.; Camarasa, E.; Vivier, H.; Faria, N.; Rocha, F.; Feyo de Azevedo, S., (1998) *Proceedings of World Congress of Powder Technology*, 33, Brighton.
- Feyo de Azevedo, S.; Rocha, F.; Faria, N.; Pons, M. N., (2002) *15<sup>th</sup> International Symposium on Indust. Crystallization, AIDIC, Sorrento, Italy*, III, 1377-1382.
- Faria, N.; Pons, M. N.; Feyo de Azevedo, S.; Rocha, F.; Vivier, H., (2003) *Powder Technology*, 133, 54-67.



## **Influence of hydrodynamic conditions on particle size distribution**

A. Alper Öncül, Dominique Thévenin

*Laboratory of Fluid Dynamics & Technical Flows (ISUT/LSS), University of Magdeburg "Otto von Guericke", Universitätsplatz 2, D-39106 Magdeburg, Germany*

### **1. Summary**

Publications describing how various particle properties are influenced by the hydrodynamic conditions are numerous, generally relying on experimental studies. As a complement, recent numerical investigations employing complex methods and models for population balance systems, micromixing, reactions rates... are developing at a rapid pace. Nevertheless, further improvements are still necessary in order to obtain a better, quantitative agreement between numerical results and experimental observations. Based on this idea, computations are performed in this work employing various recent numerical methods for several hydrodynamic conditions and possible improvements of the flow conditions are proposed.

Keywords: CFD, precipitation, mixing, particle size distribution, method of moments

### **2. Extended Abstract**

Investigation of crystallization processes under various hydrodynamic conditions is a wide and interesting subject embedded in the wider field of complex multiphase flows. This is due to the fact that the properties, quality and amount of the particulate product depend on the mixing conditions within the reactor. For instance, a good mixing increases the interaction between the ions of a solution during a reactive crystallization (precipitation) process, enhancing the reaction rate. As another example, a reactor providing high residence times may yield larger particles.

The particle size distribution (PSD) of a product can be considered as one of the essential criteria indicating the quality of the product. Therefore, the aim of the present work is to numerically determine the influence of the flow conditions on mean particle size and PSD in various reactors corresponding to different hydrodynamic and/or chemical conditions. The considered crystallization process takes place either within an aqueous solutions (similar to the conditions described in [1]) or within a micro-emulsion [2]. Zero-, two- and three-dimensional coupled

simulations of the turbulent flow and of the particle population have been performed using the industrial code FLUENT<sup>®</sup> 6.3 for the Computational Fluid Dynamics (CFD). Equations and source terms of the reaction kinetics, population balance model (PBM) and micromixing model have been defined via external user-defined scalars and functions. Various approaches for the population balance system (standard method of moments, MOM, as well as direct quadrature method of moments, DQMOM) and for micro-scale mixing (multi-environment, ME, as well as direct quadrature method of moments – interaction by exchange with the mean, DQMOM-IEM) have been compared.

The reconstruction of the obtained PSDs has been carried out according to several assumed mathematical function shapes using the first three moments of the PBM. Finally, the reconstructed PSDs and the mean particle size have been compared for the different conditions and compared as far as possible with corresponding experimental findings obtained from literature. As an example, the results obtained from the CFD simulations of BaSO<sub>4</sub> precipitation process in a tubular reactor are presented in Fig. 1 for various hydrodynamic conditions. In this particular case the computations have been performed based on MOM with a ME model employing three environments. Experimental data corresponding to the same parameters and conditions are obtained from literature [3]. Here, the effect of hydrodynamic conditions on the mean particle size at reactor outlet can be seen clearly. The predicted PSD at Re=30000 has been reconstructed using a Gaussian function. Considering these initial results, it can be concluded that such computations yield acceptable agreement with the experiments. A detailed discussion and possible improvements of the flow conditions will be proposed in the final contribution.

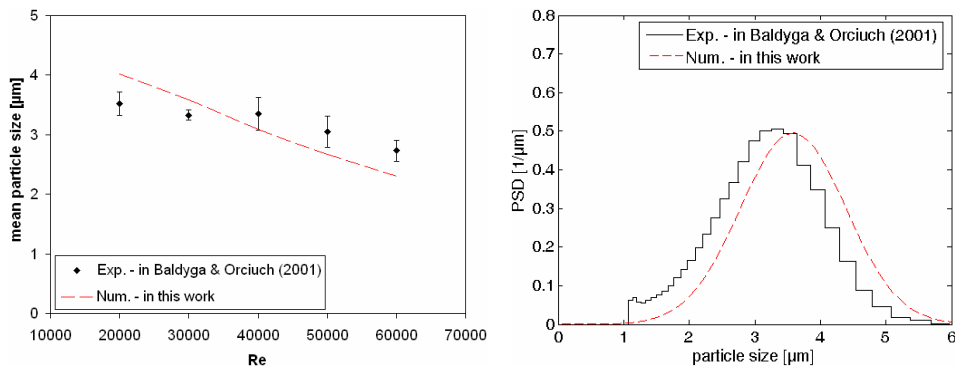


Figure 1: Numerical results in comparison to experimental findings. Left: mean particle size for various flow Reynolds numbers. Right: PSD at Re=30 000.

## References

- [1] Öncül, A. A., Sundmacher, K., Seidel-Morgenstern, A. and Thévenin, D., (2006). *Chemical Engineering Science*, 61, 652-664.
- [2] Öncül, A. A., Niemann, B., Thévenin, D. and Sundmacher, K., *Proc. of 16<sup>th</sup> European Symp. on Computer Aided Process Eng. & 9<sup>th</sup> Int. Symp. on Process Systems Eng.*, ISBN 978-0-444-52257-3, Paper No 1226, Garmisch-Partenkirchen/Germany, July 9-13, 2006.
- [3] Bałdyga, J. and Orciuch, W., (2001). *Chemical Engineering Science*, 56, 2435-2444.

## Prediction of product particle size distribution using batch grinding equation

G. Matijašić, K. Žižek, M. Hraste

*Department of Process Engineering, Faculty of Chemical Engineering and Technology, University of Zagreb, Marulićev trg 19, 10000 Zagreb, Croatia*

### 1. Summary

Mathematical description of comminution process implicates identification of a model which will enable an optimal design and process control. The conventional approach to the description of comminution process starts with an introduction of statistical functions: selection function and breakage function. By determining the mentioned functions it is possible to predict the particle size distribution of the comminution product using batch grinding equation.

Keywords: wet comminution, population balance, Laplace transform method, Runge-Kutta method

### 2. Extended Abstract

Wet grinding experiments were performed in planetary ball mill using mono- and polydispersed dolomite samples. Dolomite size domain was discretized in twelve geometric size intervals ( $\sqrt{2}$  basis). Selection function and breakage functions were derived experimentally, grinding each size interval independently. Obtained results were used in batch grinding equation:

$$\frac{dw_i(t)}{dt} = \sum_{j=1}^{n-1} b_{i,j} \cdot S_j \cdot w_j(t) - S_i \cdot w_i(t) \quad n \geq i \geq j+1 \quad (1)$$

Simple programme called GrindSIM was developed on the basis of well known analytical Reid's solution for batch grinding equation. Analytical solution was also found using Laplace transform method. Numerical solution was derived using Runge-Kutta method. Simulation was performed on five different polydispersed dolomite samples using all three methods.

Results according to all three methods reveal very good agreement with those obtained experimentally for all used polydispersed samples. Fig 1. shows comparison

of particle size distribution obtained according to solution of batch grinding equation and those derived experimentally for polydispersed sample P2 after 3 and 8 min of comminution. Maximal absolute deviation for model results was 1.24 % for all tested samples within 10 min time period.

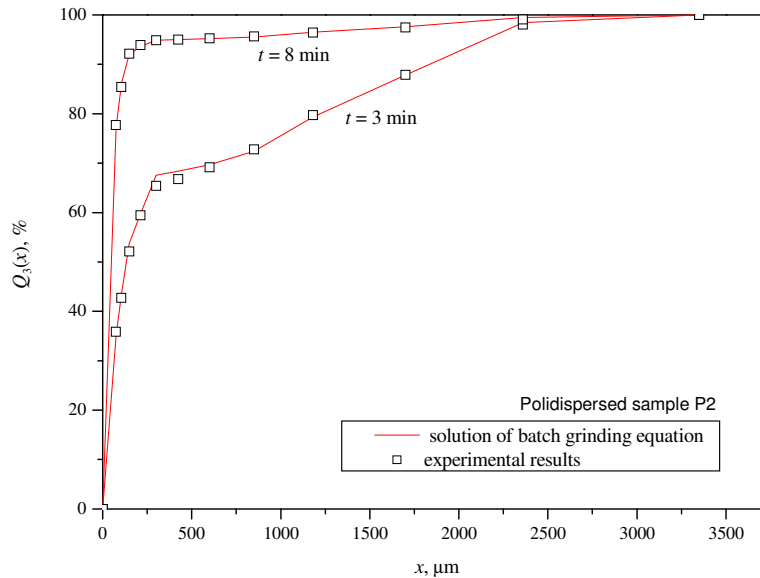


Figure 1: Comparison of particle size distribution according to results obtained through solution of batch grinding equation and experimentally for polydispersed sample P2 after 3 and 8 min of comminution.

Knowledge of selection and breakage functions for one-size intervals enables prediction of particle size distribution for polydispersed samples. Development of GrindSIM programme necessary requires analytical solution for batch grinding equation. Anyway, application of GrindSIM is limited to material properties and process conditions in which selection and breakage functions are obtained. The comprehensive use is possible if selection and breakage functions could be expressed in more general form involving process parameters and material properties dependence.

## References

- Reid, K. J., (1965), *A solution to the batch grinding equation*, Chemical Engineering Science, 20, 953-963
- Ramkrishna, D, Mahoney, A. W., (2002), *Population balance modeling. Promise for the future*, Chemical Engineering Science, 57, 595-606
- Rice, R. G., Duong, D. D., *Applied mathematics and modeling for chemical engineers*, Wiley, New York (1995).

## **Gravity Separation Technology of Grain Materials Differ in Complex of Physical and Mechanical Properties of Particles**

V. Dolgunin,<sup>a</sup> O. Ivanov<sup>a</sup>, A. Kudy<sup>a</sup>, A. Klimov<sup>a</sup>

*<sup>a</sup>Department of Technological Equipment and Food Technology, State Technical University, 106 Sovetskaya str., 392000, Tambov, Russia*

### **1. Summary**

Two-stage gravity separation technology of grain materials differ in particle size and their physical and mechanical properties (density, roughness, elasticity) is discussed. The separation process is organized by means of the use of segregation and migration effects in rapid shear gravity flows of particulate solids on rough chutes in the course of each separation stage. The cascade of chutes is used on the first stage to divide the grain mixture into some fractions and separate the fractions concentrating the products. The second stage consists in separation the fractions concentrating the products which organized by means of the principle of multi-stage separation with the countercurrent of nonuniform particles on the rough chute.

Keywords: particulate solids, gravity separation, segregation, migration

### **2. Extended Abstract**

There is an actual problem consisting in separation of grain materials differ in complex of physical and mechanical properties, e.g. in size and density simultaneously. The traditional solving this problem is characterized by low efficiency and reliability caused by multi-stage treatment of particulate mixtures. As a rule these technologies demand the application of a sieve classification and separation processes using gas and liquid flows such as flotation and sedimentation and lead to enlarged air and water consumption and use of the powerful source of vibration and pollute environment.

This problem is more complicated if the mixture contains abrasive particles of an angular shape. Due to the intensive abrasive wear in this case, there is a necessity to use rather thick sieves, which meshes are blocked very quickly.

These problems may be solved by means of the two-stage gravity separation technology with countercurrent flow of nonuniform particles on each separation stage. The separation process takes place due to segregation and migration effects of particles during their interaction in an aerated rapid shear gravity flow.

Thereby the segregation effects leads mainly to the particle separation on size whereas the migration effects results mainly in separation on physical and mechanical properties (density, roughness, elasticity) [1].

In the present paper the cascade gravity separation is suggested on the first separation stage. The gravity cascade separator consists of the cascade of rough perforated chutes (Fig. 1).

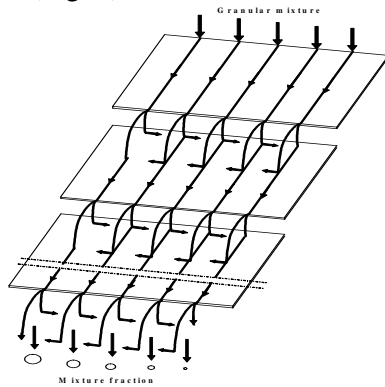


Fig. 1

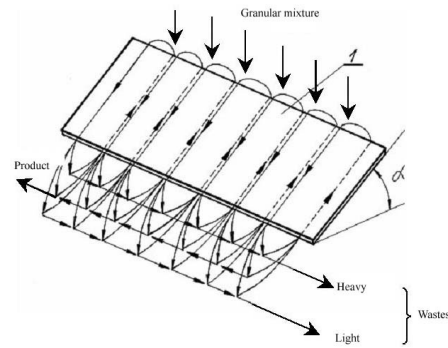


Fig. 2

The mixture flow discharging threshold of each chute is divided into parts. The parts differing in the test particle quantity are displaced towards each other. These multistage countercurrent displacements allow to distribute the mixture particles into some fractions according to the manifestation extent of the test particle properties. The cascade separation allows to provide conditions for selecting a lot of several fractions of particulate mixtures.

The fractions concentrating the products are separated finally on the second separation stage by means of using the principle of multi-stage separation "Multiseg" with the countercurrent of nonuniform particles on the rough chute (Fig. 2) [1].

This separator realizes the analogous separation mechanism combining the effects of segregation, migration and pneumatic classification in a transversally aerated gravity flow.

The gravity separation technology allows to separate particles differing not only in size but also in size and density, size and shape, size and roughness etc. simultaneously. This technology is characterized by high reliability because it has not sieves and does not need any reequipping at the change of the treated mixture properties due to the principle of self-separating particles. Besides it may be used to combine separation and heat-mass-transfer processes, for example drying, heating etc.

## References

1. Dolginin V. et al Gravity separation technology of particulate materials of high uniformity. *HUN-Pra-PARTEC International Conference on Practical Aspects of Particle Technology, Proceedings*, Budapest, Hungary, 2001, pp. 215-218
2. Dolgunin V.N. et al Model of segregation in a sheared flow of particulate solids and multifunctional modules for processes with separation / *Int. Congress of Chemical Engineering, Chemical Equipment Design and Automation. –CHISA–90.–Praha, 1990, P.36.*

## **Experimental Investigation of a Rotating Fluidized Bed in a Static Geometry**

J. De Wilde,<sup>a</sup> G.B. Marin,<sup>b</sup> G.J. Heynderickx,<sup>b</sup> A. de Broqueville

<sup>a</sup>*Department of Materials and Process Engineering (IMAP), Université catholique de Louvain, Réaumur, Place Sainte Barbe 2, B-1348 Louvain-la-Neuve, Belgium, dewilde@imap.ucl.ac.be*

<sup>b</sup>*Laboratorium voor Petrochemische Techniek, Ghent University, B-9000 Gent, Belgium*

### **1. Summary**

The new concept of a rotating fluidized bed in a static geometry is experimentally investigated. The rotating motion of the particle bed and the tangential fluidization of the solids are obtained by the tangential injection of the fluidization gas via multiple gas inlet slots in the outer cylindrical wall of the fluidization chamber. The solids experience a radially outwards centrifugal force. The gas, on the other hand, is forced to move radially inwards towards a chimney with one or more outlet slots, creating a radially inwards gas-solid drag force and fluidizing the solids radially.

For the experimental investigation of the new fluidization concept, one and the same non-optimized fluidization chamber design is used with either large diameter, low density polymer particles or small diameter, higher density Alumina particles. The fluidization chamber is operated in continuous mode, at different solids loadings and in the vertical and horizontal position.

Keywords: rotating fluidized bed, fluidization, centrifugal force, fluidized bed

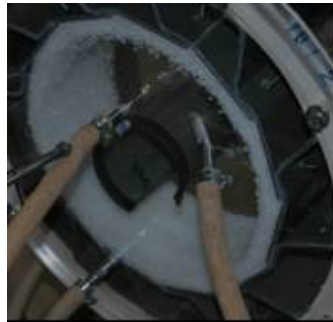
### **2. Extended Abstract**

In conventional rotating fluidized beds (Qian et al., 2001), a motor is used to rotate the fluidization chamber fast around its axis of symmetry. The fluidization gas is radially introduced in the fluidization chamber by means of gas distributors in the rotating outer cylindrical wall of the fluidization chamber. Obvious disadvantages of the conventional rotating fluidized bed technology are the use of a motor and the moving geometry, i.e. the rotating fluidization chamber. The latter may be at the origin of mechanical vibrations and makes sealing and particle feeding / removal to / from the fluidization chamber challenging. To overcome these difficulties, the new concept of a rotating fluidized bed in a static geometry is proposed and investigated with polymer and Alumina particles.

To induce a rotating motion in the static geometry, the fluidization gas is injected tangentially via multiple gas inlet slots at the outer cylindrical wall of the fluidization chamber (de Broqueville, 2004). As a result of the tangential gas-solid drag force, the solid particles in the fluidization chamber rotate as well and experience a radially outwards centrifugal force. By the action of the centrifugal force, the particles tend to form a rotating particle bed against the outer cylindrical wall of the fluidization

chamber. Except in the immediate vicinity of the gas inlets, the tangential gas-solid slip velocity is expected to be small, in contrast to the radial gas-solid slip velocity. The gas is moving radially inwards, forced to leave the fluidization chamber via an inner chimney with one or multiple outlet slots. As a result, the solids experience a radially inwards gas-solid drag force counteracting the radially outwards centrifugal force.

A rotating fluidized bed and a reasonable to good gas-solid separation can be obtained (Figure 1), provided that the solids loading and the particle bed rotational speed are sufficiently high. The behavior of the rotating fluidized bed is, however, very different with the polymer and the Alumina particles, in particular at higher solids loadings. Whereas the polymer particles tend to form a dense uniform bed, the Alumina particles tend to form a less dense and less uniform bed. With the current non-optimized fluidization chamber design, the radial fluidization is minimal with the polymer particles, but quite pronounced with the Alumina particles (Figure 1). Bubble formation is observed with the Alumina particles. Bubbles originating at the gas inlets are transported tangentially and radially or mainly tangentially, depending on the solids loading. Solids losses via the chimney are negligible with the polymer particles, but more pronounced with the Alumina particles as a result of the radial expansion, the bubble formation, and some recirculation near the chimney immediately downstream of the chimney outlet. An optimization of the fluidization chamber design and the operating conditions is necessary for each given type of particles.



1.3 kg polymer particles



1-1.5 kg Alumina particles

Figure 1.

## References

de Broqueville A., Catalytic polymerization process in a vertical rotating fluidized bed : Belgian Patent 2004/0186, Internat. Classif. : B01J C08F B01F; publication number : 1015976A3

Qian, G.-H., Bagyi, I., Burdick, I.W., Pfeffer, R., Shaw, H., Stevens, J.G., (2001) *AIChE J.*, 47(5), 1022-1034.



## Size Separation of Rubber Particles from Natural Rubber Latex by Hydrocyclone Technique

K. Pana-Suppamassadu,<sup>a</sup> S. Amnuaypanich,<sup>b</sup>

<sup>a</sup>Department of Chemical Engineering, King Mongkut's Institute of Technology North Bangkok, 10800 Bangkok, Thailand

<sup>b</sup>Department of Chemistry, Khon Kaen University, 40002 Khon Kaen, Thailand

### 1. Summary

In this research, the Reitema's optimum design hydrocyclone with a diameter of 8 mm was adopted to classify the size of rubber particles from NR latex. The feed pressure affected an efficiency of the separation, and the effective size separation occurred over the range of feed pressure approximately from 0.3 to 0.6 MPa. Increasing feed pressure further exhibited no significant enhancement of the size separation. From the simulation using a finite element method, flow topology illustrated a distinct variation within the same range of feed pressure used in the experiments. The flow patterns within series configurations i.e., the overflow-to-feed (OTF) and the underflow-to-feed (UTF) were also numerically studied for the first time. The flow field within the OTF was distinct from that of the UTF. A particle tracing showed the trend of very small particles reporting to the overflow, while relatively large particles reporting to the underflow.

Keywords: natural rubber, size separation, hydrocyclone, particle tracing

### 2. Extended Abstract

The Reitema's model hydrocyclone with a diameter of 8 mm illustrated the effective size separation of rubber particles over a range of feed pressure approximately 0.3–0.6 MPa. With a feed concentration of 0.05% w, the maximum effective separation interval was 200 nm occurred at the feed pressure of 0.5 MPa. The feed concentration of the rubber latex did not significantly affect the separation performance.

The underlying flow physics was also explored by the finite element method. The steady Navier-Stokes' and continuity equations are the governing equations:

$$\rho \frac{\partial \bar{u}}{\partial t} - \nabla \cdot \left[ -p\bar{I} + \eta(\nabla \bar{u} + (\nabla \bar{u})^T) \right] + \rho(\bar{u} \cdot \nabla)\bar{u} + \nabla p = \bar{F}$$

$$\nabla \cdot \bar{u} = 0$$

where  $\bar{T} = \sigma \hat{n} = \left[ -p\bar{I} + \eta(\nabla \bar{u} + (\nabla \bar{u})^T) \right] \hat{n}$ , and  $\bar{K} = \hat{\tau} \hat{n} = \eta(\nabla \bar{u} + (\nabla \bar{u})^T) \hat{n}$  are the total

boundary and the viscous boundary force per unit area, respectively. With the governing equations, the following boundary conditions were applied: (i) normal flow/pressure  $\hat{t}_1 \cdot \bar{u} = 0$ ,  $\hat{t}_2 \cdot \bar{u} = 0$ , and  $\hat{n} \cdot \bar{T} = -p_o$  at the inlet; (ii) outflow/pressure  $\bar{T} = -p_{atm} \hat{n}$  at the overflow and the underflow outlets; (iii) neutral  $\bar{T} = \bar{0}$  between the sub-domains; and (iv) slip/symmetry  $\hat{n} \cdot \bar{u} = 0$ ,  $\hat{t}_1 \cdot \bar{K} = 0$ , and  $\hat{t}_2 \cdot \bar{K} = 0$  at the walls.

From the simulation of a single hydrocyclone operating at the feed pressure of 0.7 MPa, the streamlines, and the Reynolds cell indicated a well-defined air core as illustrated in Fig. 1 and 2, respectively. To further investigate a possibility of the size separation enhancement, for the first time, the flow topology and the force field within the overflow-to-feed (OTF) and the underflow-to-feed (UTF) arrangements were investigated numerically as well. According to the simulation results, from flow topology and energy point of views, a balanced flow field occurred in the case of the UTF configuration and a less balanced occurred in the OTF configuration.

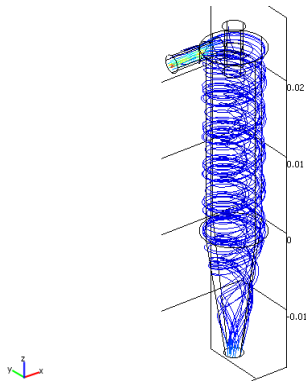


Fig. 1. Streamlines within the 8 mm hydrocyclone at the feed pressure of 0.7 MPa.

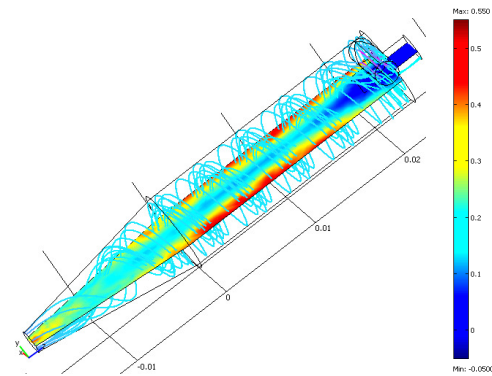


Fig. 2. Reynolds cell within the 8 mm hydrocyclone at the feed pressure of 0.7 MPa.

A particle tracing was conducted employing the Khan-Richardson force model i.e.,

$$F = \pi r_p^2 \rho (\bar{u} - \bar{u}_p)^2 (1.84 Re_p^{-0.31} + 0.293 Re_p^{0.06})^{3.45}$$

where  $Re_p = |\bar{u} - \bar{u}_p| 2r_p \rho / \eta$ . As the results, in the mean, a very small particle reported to the overflow, while a rather large particle reported to the underflow but the effective range of size separation was smaller compared to the experiments.

## References

Narasimha, M., Sripriya, R. and Banerjee, P.K., (2005) *International Journal of Mineral Processing*, 75, 53-68.

Coelho, M.A.Z. and Medronho, R.A., (2001) *Chemical Engineering Journal*, 84, 7-14.

Wolbert, D., Ma, B.-F., Aurelle, Y. and Seureau, J., (1995) *AIChE Journal*, 41, 1395-1402.

## Session T2-4: Rheology

<b>Abstract Number</b>	<b>Paper Title &amp; Authors</b>	<b>Included</b>
613	Effect of Reactor Conditions and Catalyst Design on Rheological Behavior of Polymers Produced in Catalytic Olefin Polymerization FBRs P Pladis, V Kanellopoulos, C Chatzidoukas, C Kiparissides	Yes
1191	Experimental analysis of thermal conductivity of carboxymethylcellulose sodium salt aqueous solutions in co-axial cylinder system L Broniarz-Press, K Pralat, K W Pyc	Yes
2473	Steady bubble rise and deformation in Newtonian and Bingham fluids and conditions for their entrapment J Tsamopoulos, Y Dimakopoulos, N Chatzidai, G Karapetsas, M Pavlidis	Yes
2775	Analytical Solution of Viscous Dissipation Effects of SPTT Viscoelastic Fluids for Purely Tangential Annuli non-Isothermal Flow S H Hashemabadi, S M Mirnajafizadeh	Yes
2778	The Prediction of Paint Properties from Rheological Data J Knoetz & P Moolman	Yes
3404	Linear viscoelastic retardation phenomena in selected polysaccharides system M Grzesik, P Ptaszek, A Ptaszek	Yes

Session T2-4

## **Effect of Reactor Conditions and Catalyst Design on Rheological Behavior of Polymers Produced in Catalytic Olefin Polymerization FBRs**

P. Pladis,<sup>a</sup> V. Kanellopoulos,<sup>a</sup> C. Chatzidoukas,<sup>a</sup> C. Kiparissides<sup>a</sup>

<sup>a</sup>*Department of Chemical Engineering, Aristotle University of Thessaloniki, and Chemical Process Engineering Research Institute, P.O. Box 472, Thessaloniki, Greece 54124*

### **1. Summary**

In the manufacturing of polyolefins it is of profound importance the control of molecular properties (e.g., MWD, CCD, etc.) to ensure the production of polymers with desired molecular characteristics that determine the molecular architecture of the polymer chains. In the present study, a fundamental rheological model is developed to investigate the effects of catalyst type, and reactor operating conditions on the polymer rheological properties produced in an industrial gas-phase olefin polymerization Fluidized Bed Reactor (FBR).

Keywords: catalytic, fluidized bed, rheological, olefin, polymerization

### **2. Extended Abstract**

Polyolefins are the most widely used plastics today due to their low production cost, reduced environmental impact, and wide range of applications. Polyolefins are commonly produced in low-pressure catalytic (e.g., Ziegler-Natta, metallocenes, etc.) bulk, slurry, and gas-phase reactors. The solid catalyzed gas-phase polyolefin production usually takes place in continuous fluidized bed reactors (FBR). In this process, prepolymerized catalyst (e.g., 20-80  $\mu\text{m}$ ) or polymer particles (e.g., 50-300  $\mu\text{m}$ , produced in an upstream reactor) are continuously fed into the FBR at a point above the gas distributor and react with the incoming fluidizing gas mixture of monomer(s) and nitrogen to form a broad distribution of polymer particles in the size range of 100-5000  $\mu\text{m}$  which are continuously withdrawn from the reactor at a point, preferably, close to the bottom of the bed.

In the present study, a multi-scale, integrated dynamic model is developed to assess the effect of polymer distributed properties on the rheological behavior of PE produced in a catalytic Ziegler-Natta gas-phase olefin copolymerization FBR (Dompazis et al, 2005). The proposed multi-scale reactor description comprises a

detailed kinetic model for the prediction of molecular weight distribution (MWD) and copolymer composition distribution (CCD), a random pore polymeric flow model (RPPFM) to follow the growth of individual polymer particles in the reactor and a population balance model to follow the dynamic evolution of PSD.

A detailed rheological model that includes reptation and Rouse relaxation terms (Ruymbeke et al, 2002; Doelder, 2006) has been employed in the present study. It is well-known that the proposed rheological model can provide quantitative predictions of polymer rheological properties in terms of the molecular properties (e.g., MWD, CCD, etc.). Numerical simulations were initially carried out, using the multi-scale model, to investigate the effect of reactor conditions, polymer crystallinity and catalyst design specifications on the distributed molecular properties as well as on the rheological behavior of PE. The model MWD were then used to calculate the rheological properties of the produced polymer.

In Figure 1 the dynamic evolution of the MWD of the polyethylene produced in a fluidized bed reactor is illustrated. As it can be seen, during the reactor start-up the molecular weight moves to higher values until it reaches its steady-state value. The corresponding rheological curves of the produced polymer is shown in Figure 2. It is clear that the Newtonian plateau viscosity value molecular weight is moving toward higher values. Using the present modeling methodology it is possible to obtain a quantitative relationship between the molecular properties (e.g., MWD, etc.) and a polymer end-use property (e.g., viscosity, MFI) and control of this property to ensure the production of polymers with desired molecular characteristics.

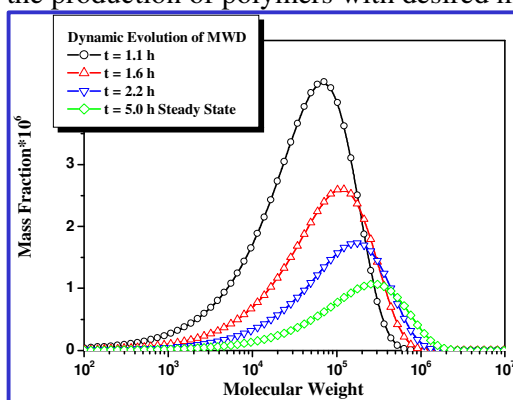


**Figure 1.** Dynamic evolution of the MWD of the produced PE during reactor start-up.

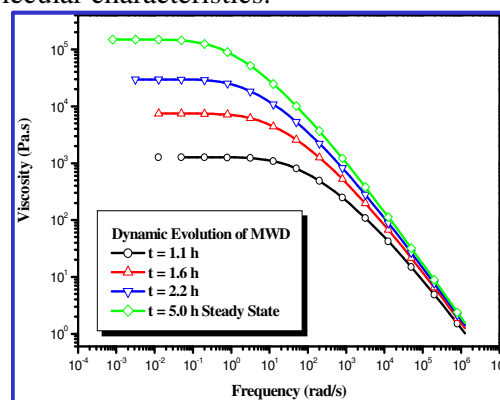


**Figure 2.** Dynamic evolution of the rheological curve during reactor start-up

## References

- Doelder, J. Den, (2006), *Rheologica Acta*, 46, 195.  
 Dompazis, G.; Kanellopoulos, V. Kiparissides, C. (2005) *Macromol. Mater. & Eng.* 290, 525.  
 Ruymbeke, E. Van, Keunings, R., Stephenne, V., Hagenaaars, A. and Bailly C. (2002) *Macromolecules*, 35, 2689-2699.

## **Experimental analysis of thermal conductivity of carboxymethylcellulose sodium salt aqueous solutions in co-axial cylinder system**

<sup>a</sup> L.Broniarz-Press, <sup>b</sup> K.Pralat, <sup>c</sup> K.W.Pyc

<sup>a</sup> *Department of Chemical Engineering and Equipment, Poznan University of Technology,  
pl. M. Skłodowskiej-Curie 2, PL 60-965 Poznan, Poland*

<sup>b</sup> *Polytechnic Institute, Higher Vocational State School of President Stanislaw Wojciechowski,  
Czestochowska 140, PL 62-800 Kalisz, Poland*

<sup>c</sup> *Department of Process Equipment, Lodz University of Technology,  
Wolczanska 175, PL 90-924 Lodz, Poland*

### **1. Summary**

In the paper the studies on the heat conductivity for aqueous solutions of carboxymethylcellulose sodium salt, have been presented. The new measuring installation which permitted to determine thermal conductivity of power-law fluids basing on the rheometric technique and very precise temperature measurement on outer cylinder, has been used. The evident effect of the shear rate on thermal conductivity of non-Newtonian fluids has been observed.

Keywords: non-Newtonian fluids, thermal conductivity, temperature- and shear-effects

### **2. Extended Abstract**

In papers of Lee and Irvine (1997), Kostic and Tong (1999), Shin and Lee (2000) as well of Lin *et al.* (2003) it was observed that thermal conductivity of non-Newtonian fluids depends not only on temperature, but also on shear rate.

In the present paper the results of experimental studies directed to the correlation of non-Newtonian fluids rheological behavior and thermal conductivity taking into account the shear rate effect, have been presented. The new measuring installation has been designed and taken into use to determine thermal conductivity of power-law fluids basing on the rheometric technique and very precise temperature measurement on outer cylinder. The liquids tested were water, glycerol (50%) and petrol, as Newtonian fluids, and carboxymethylcellulose sodium salt (of the molecular masses 250,000 and 700,000, Aldrich Comp.) aqueous solutions as non-Newtonian fluids (of

the polyelectrolyte concentrations in a solution ranged from 1000 to 5000 ppm). Experiments were performed in the range of temperature changed from 299K to 315K. The shear rate range studied was  $0 \leq \gamma \leq 750$  [s<sup>-1</sup>].

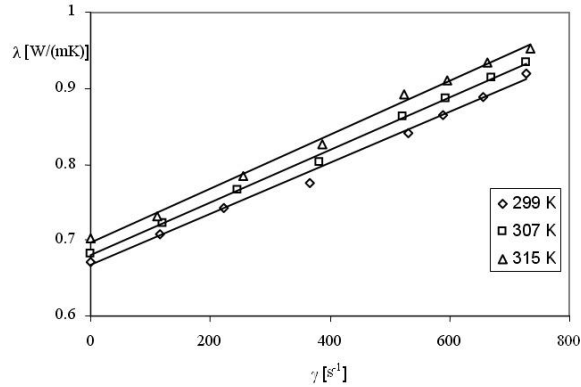


Figure 1: Thermal conductivity  $\lambda$  vs. shear rate  $\gamma$  for polymer ( $M = 700,000$  [kg/kmol]) solution of concentration of 1000 ppm

It was confirmed that the thermal conductivity  $\lambda$  of Newtonian liquids at  $T = \text{const}$  is independent of shear rate. For non-Newtonian aqueous solutions studied the relation of  $\lambda = f(T, \gamma)$  is evident and should be taken into account in all design practices. It has been found that for a given solution and at constant temperature the thermal conductivity increases linearly with shear rate increase. The increase of thermal conductivity with increase of molar mass of polymer solved in water was observed. The maximal effect was observed at temperature 315K for the carboxymethylcellulose sodium salt solution of the concentration of 1000 ppm (Figure 1).

## References

- Kostic, M., Tong, H., (1999) *American Society of Mechanical Engineering Proceedings, International Mechanical Engineering Congress and Exposition Papers*, 364-4, 15-21.
- Lee, D. L., Irvine, T. F., (1997) *Experimental Thermal Fluid Science*, 15, 16-24.
- Lin, S. X. Q., Chen, X. D., Chen, Z. D. and Bandopadhyay, P., (2003) *Journal of Food Engineering*, 57, 217-224.
- Shin, S., Lee, S.-H., (2000) *International Journal of Heat and Mass Transfer*, 43, 4275-4284.



## Steady bubble rise and deformation in Newtonian and Bingham fluids and conditions for their entrapment

J. Tsamopoulos, Y. Dimakopoulos, N. Chatzidai, G. Karapetsas, M. Pavlidis,

*Lab. of Comput. Fluid Dynamics, Dep. of Chem. Engineering, Univ. of Patras, 2600 Patras, Greece*

### 1. Summary

We examine the buoyancy-driven rise of a bubble in a Bingham fluid assuming axial symmetry and steady flow. Bubble pressure and rise velocity are determined, respectively, by requiring that its volume and center of mass remain constant. The continuous constitutive equation suggested by Papanastasiou (1992) is used to describe the viscoplastic behavior of the material. As the Bingham number increases, the yield surfaces at the equatorial plane and away from the bubble merge and the bubble gets entrapped. When the Bond number is small and the bubble cannot deform from spherical the critical Bingham number is 0.143, i.e. it coincides with the critical Bingham number for the entrapment of a solid sphere in a Bingham fluid.

Keywords: bubble dynamics, plastic materials

### 2. Extended Abstract

A viscoplastic fluid is a material that behaves either as a rigid solid or as a nonlinear viscous fluid and arises in the plastics, food and cosmetic industries, as well as in nature (e.g. lava). Bubble shapes in it affect many physical and chemical operations and the quality of the final products. The bubble rise in a Newtonian fluid has been extensively studied in the past (e.g. Ryskin & Leal, 1984), but not in a viscoplastic fluid (Dubash & Frigaard, 2004). We scale all lengths with the equivalent radius,  $R_b^*$ , of a spherical bubble with the same volume, velocities by balancing buoyancy to viscous forces, i.e. with  $\rho g R_b^{*2} / \eta_0$ , pressure and stresses with  $\rho g R_b^*$ . Consequently, the dimensionless groups that arise are the Archimedes number,  $Ar$ , the Bond number,  $Bo$ , and the Bingham number,  $Bn$ , the dimensionless yield stress. The flow is governed by the momentum and mass conservation equations. In order to describe the viscoplasticity of the fluid we employ the continuous Papanastasiou model and the von Mises criterion to determine the unyielded regions. The flow equations are solved numerically using the mixed finite-element/Galerkin method. The nodal points of the computational mesh are determined solving a set of elliptic differential equations to

follow the often large deformations of the bubble surface. The accuracy of solutions is ascertained by mesh refinement and by predicting very accurately previous experimental and theoretical results for Newtonian fluids. Fig. 1 shows that besides the unyielded material that always arises away from the bubble and surrounds it, it may also arise around its equatorial plane in contact with the bubble. In fig. 2a, we observe that the critical  $Bn$  at which the bubble will stop moving depends strongly on the shape of the bubble. Increasing  $Bo$ , the bubble deforms more easily, can squeeze through the material becoming more elongated and, hence, requires a larger  $Bn$  to entrap it. In fig. 2b, we show the evolution of the plastic boundary layer thickness (PBL), measured by the distance of the max in the  $u_\theta$  velocity to the unyielded material in contact with the bubble at the equatorial plane, with the  $Bn$  for creeping flow ( $Re=0.04$ ,  $Bo=0.01$ ). As  $Bn$  increases, the PBL decreases, in a manner identical to that in a rigid sphere, (Beris et al. 1985).

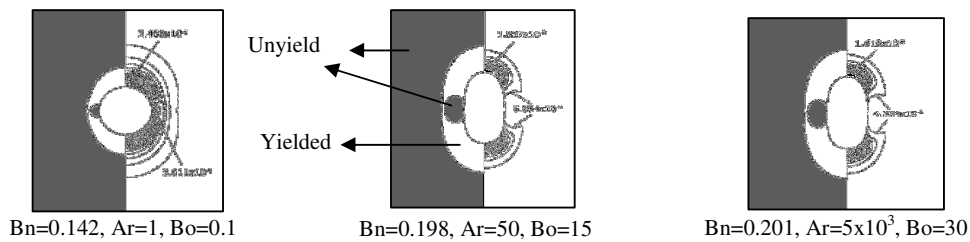


Figure 1: Yielded and unyielded domains (left half) and contour plots of the second invariant of the rate of strain tensor (right half) near the critical Bingham number.

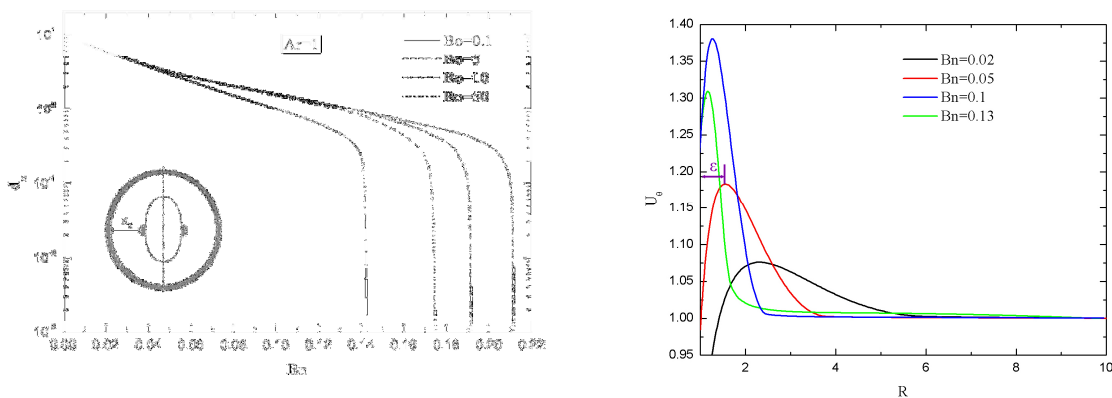


Figure 2: a) Variation of the distance between the two yield surfaces at the equatorial plane vs. the Bingham number, b) Dependence of the plastic boundary layer thickness on the Bingham number

## References

- Papanastasiou, T.C., (1992) *J. Rheol.*, 36, 389-407  
 Ryskin, G. and Leal, L.G., (1984) *J. Fluid Mech.*, 148, 19-35.  
 Dubash, N. and Frigaard, I.A., (2004) *Phys. Fluids*, 16, 4319-4330.  
 Beris, A., Tsamopoulos, J., Armstrong, R., Brown R. (1985) *J. Fluid Mech.*, 158, 219-244.

## **Analytical Solution of Viscous Dissipation Effects of SPTT Viscoelastic Fluids for Purely Tangential Annuli non-Isothermal Flow**

S.H. Hashemabadi, S.M. Mirnajafizadeh

*Computational Fluid Dynamics Research Laboratory, Department of Chemical Engineering, Iran University of Science and Technology, Tehran, 16846, Iran, Email: hashemabadi@iust.ac.ir*

### **1. Summary**

The flow in a very thin annulus where the gap between two cylinders is much smaller than the inner cylinder radius has been studied while outer cylinder rotates and inner cylinder is stationary. Effects of viscous dissipation of Simplified Phan-Thien Tanner (SPTT) viscoelastic fluid on velocity and temperature profiles have been investigated analytically. Exponential dependence of viscosity and relaxation time on temperature is modeled through Nahme Law. Inner cylinder is in constant temperature but the outer cylinder is subjected to two different thermal boundary conditions, constant temperature and insulated cylinder. Momentum and energy equations are solved by perturbation method and Nahme-Griffith number is considered as a perturbation parameter. The Results show while viscous dissipation increases for both boundary conditions, velocity profiles become nonlinear. For two constant temperature cylinders, increasing of viscous dissipation  $Na$ , causes a maximum temperature between two cylinders. While the outer cylinder is insulated, maximum temperature is placed near the insulated wall and increasing of viscous dissipation leads to increment of temperature. The results show, effects of viscous dissipation on temperature and velocity profiles are more considerable while physical properties of fluid depend on temperature.

Keywords: viscous dissipation, annulus, tangential flow, Phan-Thien Tanner model

### **2. Extended Abstract**

Consider the flow of SPTT viscoelastic fluid between coaxial cylinders in which the inner cylinder is stationary and the outer cylinder rotates with constant velocity. Since the slit width is small with respect to the radius  $R$  of the outer cylinder, curvature effects is ignored and the problem is solved for two parallel plates in cartesian coordinates. SPTT constitutive equation is given by the following equation:

$$Z(tr\tau)\tau + \lambda\tau_{(t)} = \eta\dot{\gamma} \quad (1)$$

Where  $\eta$ ,  $\lambda$ ,  $Z$  are the Newtonian viscosity coefficient, the relaxation time and the linear form of stress tensor coefficient respectively. The temperature dependency of relaxation time and viscosity are considered by a Nahme type law (Becker and McKinley, 2000) as follows:

$$\lambda = \lambda_0 e^{-\theta}, \quad \eta = \eta_0 e^{-\theta} \quad (2)$$

The dimensionless momentum and energy equations are:

$$\frac{d\phi}{d\xi} = C^* e^{\theta} (1 + 2\varepsilon De^2 C^{*2}) \quad (3)$$

$$\frac{d^2\theta}{d\xi^2} = -Na C^{*2} e^{\theta} (1 + 2\varepsilon De^2 C^{*2}) \quad (4)$$

The dimensionless groups are defined as

$$\phi = \frac{v_x}{V}, \theta = \frac{T - T_0}{T_0}, \xi = \frac{y}{B}, De = \frac{\lambda_0 V}{B}, C^* = \frac{CB}{\eta_0 V}, Na = \frac{\eta_0 V^2}{KT_0} \quad (5)$$

Two types of boundary conditions are used: Firstly two walls are considered with constant temperature and secondly one wall with constant temperature and the other is insulated. The momentum and energy equations are solved for constant physical properties first and then by using the perturbation technique and Nahme-Griffith number as perturbation parameter, the dimensionless velocity and temperature profiles for constant temperature plates are obtained:

$$\phi = (1 + 2\varepsilon De^2 C^{*2}) C^* \xi - Na \left[ \frac{1}{12} C^{*3} + \frac{1}{3} C^{*5} \varepsilon De^2 + \frac{1}{3} C^{*7} (\varepsilon De^2)^2 \right] (\xi - 3\xi^2 + 2\xi^3) + \dots \quad (6)$$

$$\theta = \frac{1}{2} Na C^{*2} (1 + 2\varepsilon De^2 C^{*2}) (\xi - \xi^2) + Na^2 \left( \frac{1}{24} C^{*4} + \frac{1}{6} C^{*6} \varepsilon De^2 + \frac{1}{6} C^{*8} (\varepsilon De^2)^2 \right) \times \left[ 2 \left( \frac{1 + 4\varepsilon De^2 C^{*2}}{1 + 6\varepsilon De^2 C^{*2}} \right) (\xi^2 - \xi) - (2\xi^3 - \xi^4 - \xi) \right] + \dots \quad (7)$$

When the lower plate is at constant temperature and the upper one is insulated:

$$\phi = (1 + 2\varepsilon De^2 C^{*2}) C^* \xi + Na \left( \frac{1}{6} C^{*3} + \frac{2}{3} C^{*5} \varepsilon De^2 + \frac{2}{3} C^{*7} (\varepsilon De^2)^2 \right) (3\xi^2 - \xi^3 - 2\xi) + \dots \quad (8)$$

$$\theta = Na C^{*2} (1 + 2\varepsilon De^2 C^{*2}) \left( \xi - \frac{\xi^2}{2} \right) + \frac{1}{3} Na^2 \left\{ \left( \frac{1}{8} C^{*4} + \frac{1}{2} C^{*6} \varepsilon De^2 + \frac{1}{2} C^{*8} (\varepsilon De^2)^2 \right) \times \left[ 8 \left( \frac{1 + 4\varepsilon De^2 C^{*2}}{1 + 6\varepsilon De^2 C^{*2}} \right) (\xi^2 - 2\xi) + (\xi^4 - 4\xi^3) + 8\xi \right] \right\} + \dots \quad (9)$$

As  $\varepsilon De^2$  approaches to zero, above equations are converted to Newtonian fluid solutions that were presented by Turian and Bird. The results illustrate while Nahme number increases, the velocity profile strengthens and flow is completely different with isothermal situation. Also, the maximum of temperature profile increases, and for small Nahme-Griffith number, there is no temperature changes across the channel.

## References

Becker, L. E. and McKinley, G. H., (2000) The stability of viscoelastic creeping plane shear flows with viscous heating, *J. Non-Newt. Fluid Mech.*, 92, 109-133.

Turian, R. M. and Bird, R. B., (1963) Viscous heating in the cone-and-plate viscometer-II, Newtonian fluids with temperature-dependent viscosity, *Chem. Eng. Sc.*, 18, 689-696.

## The Prediction of Paint Properties from Rheological Data

*JH Knoetze\* & PL Moolman*

*Department of Process Engineering, University of Stellenbosch, Private Bag XI, MATIELAND 7602, South Africa*

\*Email: [jhk@sun.ac.za](mailto:jhk@sun.ac.za)

### 1. Summary

Paint can be regarded as a complex mixture of mutually interacting components, usually formulated for specific application conditions. Though all other properties can be acceptable, a coating will usually not meet with success if the rheology is not acceptable. Rheological measurements were performed using a MCR 300 (Paar-Physica, Stuttgart, Germany). Rotational (ROT) and oscillatory (OSC) measurements were performed on a series of paint mixtures at constant temperature. A total of 43 paint properties were measured. Models were developed using both Multiple Linear Regression as well as Artificial Neural Networks to predict the paint properties from the rheological data as well as from the composition data, resulting in 3 different model types. Accurate predictions for the critical paint properties that are used for quality control (*Krebs Viscosity, Opacity, Gloss and Dry Film Thickness*) are possible as long as raw materials are varied within plus/minus 20% of the standard formulation.

Keywords: paint properties, paint rheology, modelling paint properties, rheological modelling

### 2. Extended Abstract

Paint can be regarded as a complex mixture of mutually interacting components, usually formulated for specific application conditions. Rheology is the science of deformation and flow. All forms of shear behaviour can be viewed as lying between two extremes: the flow of ideal viscous liquids on the one hand and the deformation of ideal elastic solids on the other. The behaviour of all real materials, such as paint, is based on the combination of both the viscous and the elastic portion and therefore, it is called visco-elastic materials.

Rheometry is the measuring technology used to determine rheological data and this includes technology such as the measuring systems, instruments and test and analysis methods. Visco-elastic materials can be investigated using rotational and oscillatory rheometers. Rotational tests characterise flow behaviour which can be expressed in terms of the viscosity.

To a degree matched by few other areas, rheology determines the success for coatings. Though all other properties can be acceptable, a coating will usually not

meet with success if the rheology is not acceptable. Experienced formulators say that more than half the cost of new product development is consumed in “getting the rheology right”. Moreover, apparently “minor” changes in a raw material or process can cause significant and unexpected variability in product rheology. For all these reasons, rheological analysis is a vital and cost-effective tool for the coatings industry. The development of relationships between paint properties and the relevant rheological test methods has been identified as a major gap in the coatings industry.

Rheological measurements were performed using a MCR 300 (Paar-Physica, Stuttgart, Germany). Rotational (ROT) and oscillatory (OSC) measurements were performed on all the paint mixtures. Rotational measurements were: Constant high shear (HS), constant low shear (LS), flow curve (FC) and three-interval-thixotropy-test (3-ITT). Rotational measurements were performed with the cone and plate measuring system CP50 (diameter = 50mm, angle = 1°, cone-plate distance = 50 µm). The measurements were performed in a controlled shear rate (CSR) mode and the resulting shear stress ( $\tau$ ) was measured and used for modelling purposes. Oscillatory measurements were:

Amplitude sweep (AS), frequency sweep (FS), time sweep (TS), three-interval-thixotropy-test (3-ITT), and extra low frequency test (XLF). Oscillatory measurements were performed with the plate and plate measuring system PP50 (diameter = 50 mm, plate-plate distance = 0.25 mm). The measurements were performed in a controlled shear deformation (CSD) mode and the resulting shear stress ( $\tau$ ) and phase angle ( $\delta$ ) was measured and used for modelling purposes. All measurements were performed at a constant temperature ( $23 \pm 0.2^\circ\text{C}$ ).

A total of 43 paint properties were measured. This includes properties where the relationship between rheology and the specific paint property is well established, e.g. sagging, spatter, etc. Other paint properties were also measured where the relationship between rheology and the specific paint property is not that well established, e.g. gloss, burnish, water permeability, etc. All properties were measured according to international standards such as American Standard Test Methods (ASTM) and Coatings Research Group International (CRGI).

Models were developed using both Multiple Linear Regression as well as Artificial Neural Networks to predict the following paint properties from the rheological data as well as composition data: Dry Burnish 20, Dry Burnish 60, Dry Burnish 85, Wet Burnish 20, Wet Burnish 60, Wet Burnish 85, Water Permeability, Krebs viscosity, Sag, Open time, Gloss 20, Gloss 60, Gloss 85, Dirt Pick-Up, Opacity, Hiding Power and Dry Film Thickness. Accurate predictions for the critical paint properties that are used for quality control (*Krebs Viscosity*, *Opacity*, *Gloss* and *Dry Film Thickness*) are possible as long as raw materials are varied within plus/minus 20% of the standard formulation.

## **Linear viscoelastic retardation phenomena in selected polysaccharides systems**

M. Grzesik,<sup>a</sup> P. Ptaszek,<sup>b</sup> A. Ptaszek<sup>b</sup>

<sup>a</sup>*Institute of Chemical Engineering, Polish Academy of Science, Baltycka 5, 44-100 Gliwice, Poland*

<sup>b</sup>*Faculty of Food Technology, Agricultural University of Cracow, Balicka 122, 30-149 Cracow, Poland*

### **1. Summary**

The aim of present study was to determine the viscoelastic properties of the model mixtures of the selected pasted polysaccharides. The initial material was maize starch (SK), mixed with guar gum (GG). Rheological tests were performed in time domain. Theoretical analysis covered adaptation of some achievements of phenomenological theory of viscoelasticity, which were applied during interpretation of results obtained for mentioned above mixtures of biopolymers. The emphasis was placed on description of retardation behaviours with the aim of continuous rheological Burger's model.

Keywords: viscoelasticity, polysaccharides, regularization, continues Burger's model

### **2. Extended Abstract**

Polysaccharides are main constituent of human's food. They are used also as food texturing agents and to grant food with proper resistance. Polysaccharides, due to their biodegradability and renewability found wide applications in pharmaceutical, ceramic, and textile industries, and also in biotechnology. Discussed compounds are characterized by very complicated structure, and exhibit many interesting, from practical point of view, rheological phenomena. Complex hydrodynamic behavior of polysaccharides and their solutions allows to apply them as pilot testing materials in emerging technologies. It seems to be reasonable to undertake researches dealing with viscoelastic phenomena of water based solutions of polysaccharides. It gives unequivocal opportunity to characterize investigated material in linear area, and also it is start point to model phenomena connected with non-linear viscoelasticity and thixotropy.

The aim of present study was to determine the viscoelastic properties of the model mixtures of the selected pasted polysaccharides. The initial material was corn starch (SK), mixed with guar gum (GG).

Starch is plant storage material, which is composed of two alpha glucans: essentially linear amylose, and branched amylopectin. The linear amylose (chain length 500 to 6000 glucose units) has a small degree of branching but it is predominantly regarded as a single chain. The chain of amylopectin contains only up to 30 glucose units. Regular corn starch (SK) produced by National Starch was used in this research. The

production of guar gum bases on its extraction from the leguminous shrub *Cyamopsis tetragonoloba*. By means of chemical compound guar is a galactomannan with (1-4)-linked  $\beta$ -D-mannopyranose backbone with branch points from their 6-positions linked to  $\alpha$ -D-galactose. Guar gum (GG) was supplied by Regis (Poland).

Rheological measurements were performed using rotary rheometer RS-150 (Haake, Germany) equipped with coaxial cylinder system. Temperature was controlled by ultrathermostat F9 (Haake, Germany) with 0.1°C accuracy. The principle of rheological measurements was to search for linear viscoelastic area by step function, and finally to create creeping curves. This investigation relied on conducting few deformation measurements in time function for different stress  $\tau_0$  values. Next, the function of susceptibility for creeping was calculated according to following formula:

$$J(t) = \frac{\gamma(t)}{\tau_0}$$

and if obtained curves matched each other that indicated on linear viscoelasticity of the system. Obtained in such way curves, also known as creeping susceptibility curves, were used for further analysis. The measurements were executed in the following manner: starch paste or hydrocolloid solution (95°C), prepared in water bath (95°C±1°C) and mixed for 30 min., was placed in measuring cylinder previously heated to 95°C. Next sensor was cooled down to desired temperature during one hour, and was kept at this temperature for the next 30 minutes. Next measurement was performed.

One of the relationships describing retardation phenomenon is continuous Burger model, which can be described as:

$$J(t) = \underbrace{J_g + \frac{1}{\eta} \cdot t}_{\text{Maxwell's element}} + \underbrace{\int_0^{\infty} L(\lambda) \left[ 1 - \exp\left(-\frac{t}{\lambda}\right) \right] d\lambda}_{\text{Kelvin-Voigt's element}}$$

To estimate function  $L(\lambda)$  and other parameters, regularization method of Tikhonov was used.

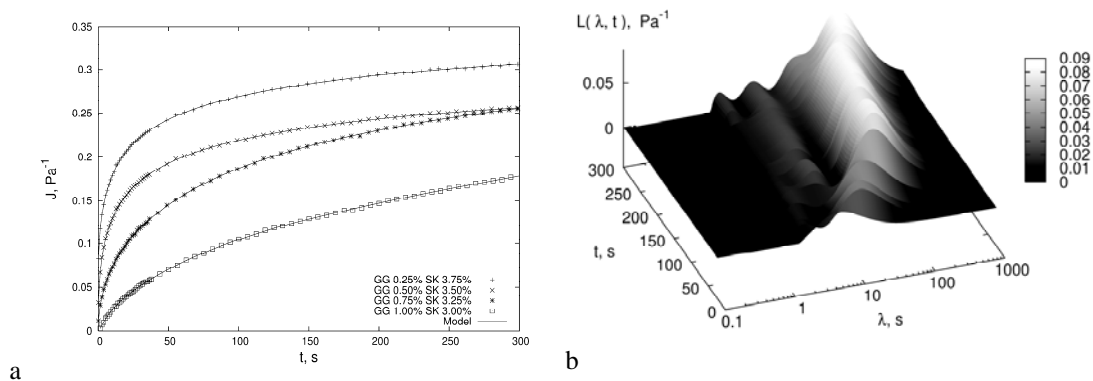


Figure 1: a. Creeping curves for mixtures maize starch with guar gum (GG) addition. b. Evolution of retardation spectra for mixtures maize starch with guar gum addition.

## References

Tikhonov A.N., Goncharsky A.V., Stepanov V.V., Yagola A.G., *Numerical Methods for the Solution of Ill-Posed Problems*. Kluwer, Dordrecht, 1995



## Session T2-4P: Rheology – Poster

<b>Abstract Number</b>	<b>Paper Title &amp; Authors</b>	<b>Included</b>
915	Characterization of time dependent behaviour of non fat and full fat stirred yoghurt A. Cancela, R. Maceiras, E. Álvarez	No
3066	Rheological Study of Phenolic Resol Resins Cure After Gelation J C Domínguez, M V Alonso, M Oliet, F Rodríguez	Yes
3394	Process rheo-kinetics of the bitumen modification by isocyanate-based reactive prepolymer M J Martín-Alfonso, P Partal, F J Navarro, M García-Morales, C Gallegos	Yes

Session T2-4P

## **Rheological Study of Phenolic Resol Resins Cure After Gelation**

J.C. Domínguez, M.V. Alonso, M. Oliet, F. Rodríguez

*Departamento Ingeniería Química, Facultad de Química, Universidad Complutense,  
Avda Complutense S/N. 28040 Madrid. Spain. Tlf.: +34 913 944 246, Fax: + 34 913 944 243,  
e-mail: [jucdomin@quim.ucm.es](mailto:jucdomin@quim.ucm.es)*

### **1. Summary**

Rheological kinetic curing studies of a phenolic resol resin were performance. Shear deformation was applied in order to obtain rheological properties during curing reactions. Samples precuring treatment was applied; gelation point was overcome. Arrhenius and Kiuna kinetic models were used in modelling. Kinetic parameter for both model were found to predict the behaviour of complex viscosity of phenolic resin during curing process.

Keywords: curing, rheology, resin, resol, phenolic

### **2. Extended Abstract**

Chemorheological curing behavior of 5 different samples of phenolic resol resins after gelation was studied in order to determine their kinetic curing parameters. The curing of thermosetting resins is a complex phenomenon, which occurs with relevant changes in their rheological properties (1, 2). Phenol-formaldehyde commercial resol resins tested were supplied by Hexion Chemical Iberica S.A. Rheological runs were performed by using an ARES Rheometer with 25 mm upper parallel plate and 42 mm lower parallel plate. Lower plate was fixed for sample immersion in a silicon surrounding fluid - Dow Corning 200® Fluid 100cst -just to get sample stability. 2 mm initial gap was fixed. Autotension option was used in order to keep axial force constant, 100 g, and avoid contact loss between sample and geometry. Isothermal curing runs (80, 85, 90, 95 and 100°C) were carried out for 30 minutes. Frequency was previously fixed at 1 Hz; therefore, constant frequency test were performance. Initial temperature was 25°C and temperature ramp to set temperature was 20°C/min for all samples and curing temperatures. Linear viscoelastic region (LVR) was determined through strain sweep after isothermal curing to delimit it for each temperature. Strain sweeps were carried out at 60°C, 1 Hz and strain from 0.01 % to 1 % strain. Applied strain was always inside LVR.

Kiuna model is frequently applied to study the cure stage of epoxy/amine resins (3). In this work a particular case of this method is used to study the cure of the samples after gelation. In Arrhenius model, Andrade equation is proposed to set viscosity dependence on temperature,  $\eta_0(T)$ . Viscosity increase along curing process is described using a function  $\alpha$  defined as  $\ln(\eta/\eta_0)$ . Function  $\tau$  represents the elapsed cure time and the rate of

advance of curing process at temperature described by function  $K(T)$ . Arrhenius model assumes  $\alpha(\tau)$  as a first order polynomial  $\alpha=\tau$ . An exponential form equation is used for  $K(T)$  model equation. In order to get best fitting model  $\alpha(\tau)$  was proposed as a second and third order polynomial. Figure 1 shows  $K(T)$  fits for all models.

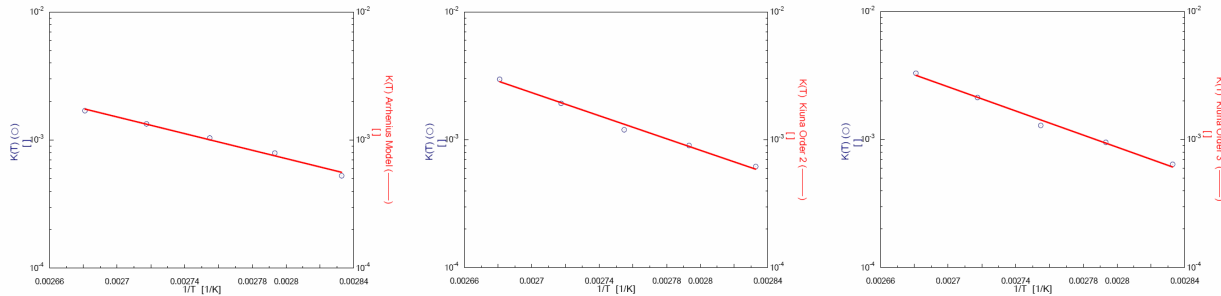


Figure 1: Sample 2:  $K(T)$  fitting for Arrhenius, Kiuna order 2, 3 models.

Table 1 shows kinetic parameters for each model. Andrade equation parameters were not possible to fit because slight heterogeneous precuring with small differences in  $\eta_0$  values.

Table 1: Average kinetic model parameters for all samples

	<b>Arrhenius</b>	<b>Kiuna Order 2</b>	<b>Kiuna Order 3</b>
<b><math>E_k</math> (kJ/mol)</b>	70.50 ± 11.83	90.58 ± 14.83	95.05 ± 12.20
<b><math>A_1</math> (s<sup>-1</sup>)</b>	16.26 ± 3.28	23.11 ± 4.91	24.37 ± 5.22
<b><math>a_1</math></b>		-0.080	-0.14
<b><math>a_2</math></b>			0.01

Kiuna model fits experimental values getting excellent SQR values. For example, SQR values for order 3 are about half in relation order 2. Arrhenius model exhibited an acceptable  $K(T)$  fitting; however, the results showed that this model was not appropriate for highest temperatures because a non-linear behavior for  $\ln(\eta)$  was found. Kiuna model is proposed as good fitting model simulate resol curing behavior. Kiuna order would be fixed depending on the accuracy needed in simulation. When high accuracy is needed then an order 3 is recommended, while low accuracy involves order 2 for simplify the calculus.

Predicted kinetic parameters values are in accordance with those obtained in previous works by DSC and mt-DSC. In addition, Arrhenius model kinetic parameter becomes closer than Kiuna to these parameters.

**References**

1. Pascault, J. P., Sauterreaux, H.; Verdu, J., Williams, R. J. J., *Thermosetting Polymers*, Marcel Dekker, USA (2002).
2. Sperling, L. H., *Introduction to physical polymer science*, John Wiley & Sons, USA (1992).
3. Kiuna, N., Lawrence, C. J., Fontana, Q. P. V., Lee, P. D.; Selerland, T., Spelt, P. D. M., (2002) *Composites: Part A*, 33,1497-1503.

## **Process rheo-kinetics of the bitumen modification by isocyanate-based reactive prepolymers**

M.J. Martín-Alfonso, P. Partal, F.J. Navarro, M. García-Morales and C. Gallegos.

*Department of Chemical Engineering, University of Huelva , Facultad de Ciencias Experimentales, Campus 'El carmen', 21071 Huelva, Spain*

### **1. Summary**

The aim of the present work was to study the mixing process of bitumen and reactive isocyanate-based prepolymers. An increase in viscosity is observed during the modified binder processing, which depends on mixing temperature. However, bitumen modification is observed on a time-scale of days. The results showed that the reactive polymer addition improved bitumen properties at high in-service temperatures, leading to an increase in the binder viscosity at 60°C. It was also found by AFM observations at 50°C that the reactive polymer MDI-PEG leads to a new microstructure displaying a higher level of stiffness.

*Keywords:* Processing, rheology, modified bitumen, isocyanate prepolymer

### **2. Extended Abstract**

Knowledge on the process kinetics of polymer-bitumen blends is of great interest since it provides information on the behavior of the binder in different stages of the mixing operation. In addition, the mixing process gives rise to significant changes in the microstructure of the blend, which can be detected by following the variation of the rheological parameters along time. The mixing process can be followed by measuring the viscosity of the blend as a function of time. Once the values of viscosity become constant, the mixing process is considered to be finished (García-Morales et. al. , 2006)

This work studies the mixing process of bitumen (penetration grade of 150/200) and reactive isocyanate-based prepolymers (polyethyleneglycol functionalized with polymeric MDI, MDI-PEG). Measurements of the evolution of viscosity with time, at different temperatures, were carried out with the experimental device known as "rheomixer" (Figure 1A). The increase of viscosity, found during processing, seems to be the result of chemical reactions, between -NCO groups of the reactive polymer and hydroxyl (-OH) and amine (-NH) groups of polar compounds present in bitumen (Singh et al , 2003).

The flow behavior of the blends during curing at 60°C is shown in Figure 1B. As can be observed, a remarkable increase in viscosity of the modified bitumen appears after the first week of curing. This tendency continues (although at a smaller extent), after 15 and 30 days of curing. As result, MDI-PEG bitumen modification seems to be the result of a short-term modification (during processing) and a long term bitumen modification due to curing effects, providing the most relevant increase in viscosity.

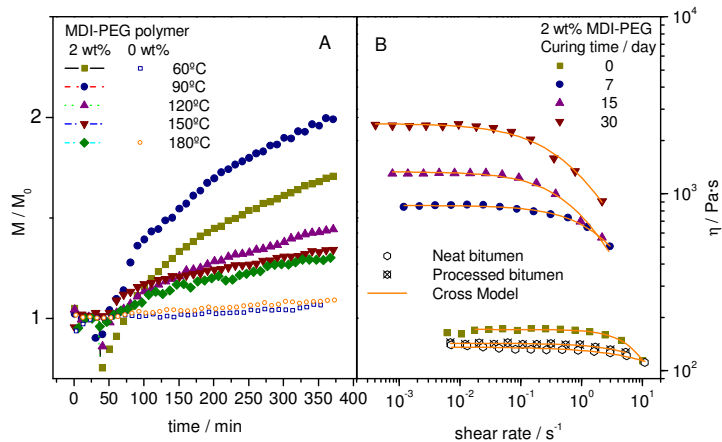


Figure 1. Evolution of torque during processing for blends of bitumen and MDI-PEG (2 wt%), manufactured with the rheomixer at different temperatures (A) Viscous flow curves at 60°C for a selected 2 wt% MDI-PEG modified bitumen, as a function of curing time (B)

The microstructure of the blends obtained after processing and curing was studied by Atomic Force Microscopy (AFM). Figure 2 shows images corresponding to the neat bitumen and MDI-PEG modified bitumen (mixed at 90°C), containing 2 wt% of polymer and cured for a period of 11 months, analyzed by AFM at 50°C. Polymer addition contributes to the development of a new microstructure which has been proved to present a more satisfactory performance at high temperatures, due to the above reported formation of chemical bonds between polymer and polar compounds within bitumen.

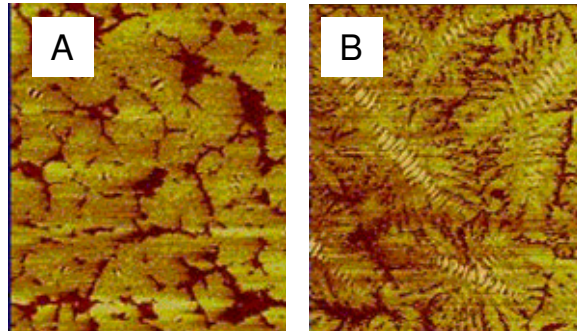


Figure 2. AFM micrographs at 50°C for the neat bitumen (A), as well as for modified bitumen sample containing 2 wt% (B) of MDI-PEG after a period of curing of 11 months (micrograph dimensions: 50x50  $\mu\text{m}$ )

### Acknowledgments

This work is part of a research project sponsored by MCYT-FEDER program, (Research Project MAT2004-06299-C02-02). The authors gratefully acknowledge its financial support.

### References

- Garcia-Morales M, Partal P, Navarro FJ, Martinez-Boza FJ, Gallegos C. *Rheol. Acta* 45: 513-524 (2006)  
 Singh B. H, Tarannum, M. Gupta. *J. Applied Polymer Sci.* 90:1365–1377 (2003)

## Session T2-5a: Multifase Flows – I

<b>Abstract Number</b>	<b>Paper Title &amp; Authors</b>	<b>Included</b>
1031	On the Interrelation of Flooding- and Complete Dispersion Characteristics in Agitated Gas-Liquid Contactors E Babalona, J Markopoulos	No
1133	The Effect of Particle-Particle Interaction Forces on the Sedimentation and Re-Suspension Properties of Silica Slurries D Harbottle, D Rhodes, M Fairweather, S Biggs	Yes
1727	Effect of the impeller type on the break up of the bubbles in a stirred tank M Martín, F J Montes, M A Galán	Yes
2954	On interactions of stationary particles and rising bubbles P Basařová, V Machoň, M Hubička, D Horn, M Fugasová	No

Session T2-5a



## **The Effect of Particle-Particle Interaction Forces on the Sedimentation and Re-Suspension Properties of Silica Slurries**

A. David Harbottle,<sup>a</sup> B. Dominic Rhodes,<sup>b</sup> C. Mike Fairweather,<sup>a</sup> D. Simon Biggs<sup>a</sup>

<sup>a</sup>*Institute of Particle Science and Engineering, University of Leeds, Leeds, LS2 9JT, England*

<sup>b</sup>*Nexia Solutions, Cumbria, England*

### **1. Summary**

The presentation summarises experimental data which looks at the effects of suspension chemistry on the transportation and flow properties of colloidal silica in pipes. Mono-dispersed colloidal silica was chosen to produce ideal experimental slurries with an aim of generating data sets for computational model validation. A variety of laboratory based analytical equipment has been utilised to characterise the slurries, such as, LUMiFuge® Stability Analyser, Malvern Mastersizer 2000 and Nanosizer ZS, Brookfield HB DV-II+ Pro viscometer and Veeco Bioscope™ II Atomic Force Microscope. Sediment bed erosion rates and particle flow characteristics were investigated in a 25mm horizontal flow loop, applying techniques such as Particle Imaging Velocimetry (Dantec Dynamics) and Ultrasonic Velocity Profiler (Met Flow).

Keywords: Colloid, Flow properties, Particle Imaging Velocimetry

### **2. Extended Abstract**

Experimental observations on the sedimentation and re-suspension characteristics of colloidal silica as a function of the strength of the particle-particle interaction forces are reported. Silica slurries are encountered mainly in mining operations, with efficient transportation leading to substantial environmental and cost savings. In this study mono-dispersed silica is used to produce model slurries where the physical and chemical properties are easily controlled and understood. Stability of the silica slurries have been studied using a variety of analytical techniques, investigating the effect of particle surface charge on the settling rate and sediment packing structure. The transition from a stable to a flocculated state is induced by a pH change and/or a change in the strength of an appropriate electrolyte. Through controlling the strength of the particle interactions, the packing structure of the sediment can be manipulated. When there is strong attraction between the particles, the resulting sediment bed consists of a random arrangement of particles with a low bed density and high bed

porosity. For a weakly attractive system, a denser sediment is observed due to the individual particles packing more efficiently. The sediment bed yield stress then becomes a function of the packing structure of the particles, ultimately influencing the re-suspension and transport properties of the particles in the pipe.

A 25mm horizontal pipe loop applying techniques such as Particle Image Velocimetry (PIV) and Ultrasonic Velocity Profiling (UVP) was used to look at the erosion and re-suspension properties of consolidated sediment beds (figure 1.). In order to enable movement of particles settled on the pipe invert, the driving forces which are acting to set the bed in motion and lift the particles (pressure gradient, shear stress) have to exceed the resistive forces (mechanical and fluid friction) which are acting to hold the bed in place. The reaction forces are assessed in this study through analysis of the re-suspension characteristics in the laminar and turbulent flow regimes, along with consideration for re-suspension in transitional flow, where a sharp peak is observed in the axial velocity fluctuations.

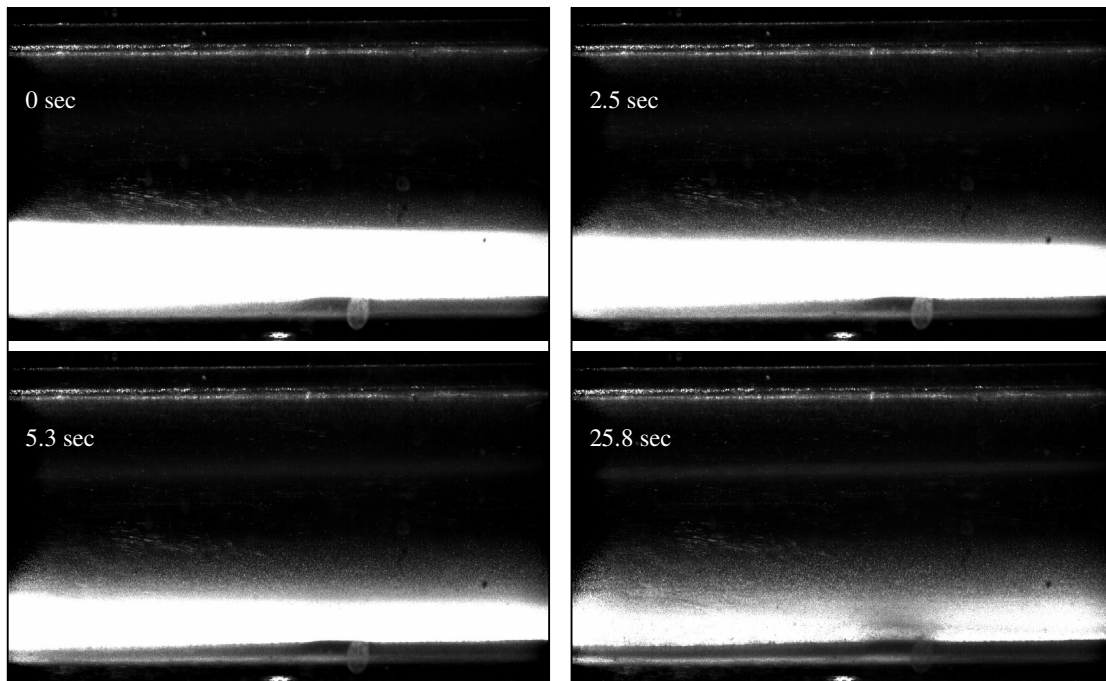


Figure 1: Typical image sequence of a sediment bed eroding in the laminar/turbulent transition ( $Re \approx 2000$ ) using 50Hz Particle Image Velocimetry.

## **Effect of the impeller type on the break up of the bubbles in a stirred tank**

Mariano Martín, Francisco J. Montes, Miguel A. Galán.

*Universidad de Salamanca, Departamento Ingeniería Química y Textil, Plaza de los Caídos, 1-5, 37008, Salamanca, Spain, Telf: 00 34 923 294479; Fax: 00 34 923 294574  
mariano.m3@usal.es; javimon@usal.es; magalan@usal.es*

### **1. Summary**

The effect of different impellers on the bubble break up has been experimentally studied and modelled using population balances. The different behaviour of the impellers, based on its physical effect on the bubbles as well as on the effect of the flow pattern developed in the tank, determines the main break up mechanism and can be quantified using the Weber number and studying the energy applied in a region surrounding the impeller.

Keywords: Impellers, Bubbles, Population balances, Break - up

### **2. Extended Abstract.**

So far, one of the most important problems in modelling gas – liquid dispersions generated inside stirred tanks using population balances has been the multiple parameters involved in the equations. These parameters refer to the coalescence and break up phenomena of the bubbles. Although in an industrial case standard impellers, such as the Rushton turbine or the A series turbines, are widely used and so the particular parameters can be obtained, a more systematic study can provide some insight about the break up phenomenon, basic to improve the mass transfer efficiency in stirred tanks.

In the first place, CFD commercial code, CFX 5.7<sup>®</sup>, discoloration and high speed video techniques, were used in order to study the hydrodynamics generated inside the tank and the development of dispersions monitoring the bubble break up processes and evaluating the break up mechanisms responsible for the bubble mean size. Five different impellers, standard ones, like the propeller or the Rushton turbine and non standard ones, several turbines and blades were tested.

Secondly, bubble stability in the flow is the basis for the theoretical study of the break up process, which leads to the development of a dispersion. Bubbles break as a result of the deformation caused by the stress fields developed by the impellers. The deformation of the bubbles depends on the relationship between the forces that try to maintain bubble shape, those related to the surface tension, and the inertial forces resulting from the flow inside the tank. The dimensionless number considering that relationship is the Weber number, (Kolmogorov, 1949, Hinze, 1955, Bhavaraju et al., 1978; Walter and Blanch, 1986; Parthasarathy and Ahmed, 1994; Barabash and Belevitskaya, 1995).

A model using the results from these studies and population balances (Prince and Blanch, 1990, Pohorecki, et al 2001) has been used to evaluate the contribution of different break up mechanisms and their effect on the bubble mean diameter in a dispersion, monitoring the Weber critical number and the energy required for the break up processes.

It was verified that each impeller shows a particular behaviour on the bubbles according to its geometry and the flow pattern developed inside the tank. The critical Weber number for each impeller depends on the break up mechanisms responsible for the bubble mean size of the dispersions generated by each one, lower values are found for direct break up of the bubbles, meanwhile the effective energy applied to the bubbles in the neighbourhood of each impeller, although within the range of the dissipated energy given by the literature, depends on the physical effect of the impeller on the bubbles.

For the air - water system, the optimal values for the critical Weber number and the energy needed for the break up meet the values previously reported by Shimizu, (Shimizu et al. 2000) and the one given by Wu, (Wu and Patterson, 1989),  $We_c = 1$  and  $\epsilon_{max} = 20 \cdot \epsilon$  respectively. Good results for all the five impellers can be found using these mean values.

**Acknowledgment:** The support of the Ministerio de Educación y Ciencia of Spain providing a F.P.U. fellowship to M. Martín is greatly welcomed. The funds from the project reference CTQ 2005 – 01395/PPQ are also appreciated.

## References.

- Barabash, V. M., Belevitskaya, M. A., (1995) *Theoretical Foundations of Chemical Engineering*, 29, 4, 333-342
- Bhavaraju, S. M., Russell, T. W. F; Blanch, H. W., (1978) *A.I.Ch.E. J.*, 24, 3, 454-466
- Hinze, J. O., (1955) *A.I.Ch.E. J.*, 1, 289-295.
- Kolmogorov, A. N., (1949) *Dokl. Akad. Nauk. SSSR* 66, 825-828
- Parthasarathy R., Ahmed, N., (1994) *Transactions of the Institution of Chemical Engineers, Part A*, 72, 565-572.
- Pohorecki, R.; Moniuk, W.; Bielski, P.; Zdrójkowski, A., (2001). *Chemical Engineering Science*, 56, 6157-6164
- Prince, M. J., Blanch, H. W., (1990) *A.I.Ch.E. J.*, 36, 10, 1485-1497
- Shimizu, K., Takada, S., Minekawa, K., Kawase, Y., (2000) *Chemical Engineering Journal*, 78, 21-28
- Walter, F. J., Blanch, H. W., (1986) *Chemical Engineering Journal*, 32, 1, B-7 - B-17
- Wu, H., Patterson, G. K., (1989) *Chemical Engineering Science*, 44, 10, 2207-2221

## Session T2-5b: Multifase Flows – II

Abstract Number	Paper Title & Authors	Included
1121	Innovative $\mu$ -PIV measurement technique for film flow investigations S Paschke, I Ausner, J U Repke, G Wozny	Yes
1198	Mixing time of surface active agent solutions L B Press, S Rozanska, I Szrajbrowska	Yes
1437	Bubble Size Distribution and Two-Phase Pressure Drop in Thin-Gap Microchannel J Kristal, J Havlica, V Jiricny	Yes
2194	Hydrodynamics of one-dimensional gas-solid flow F J Collado	Yes
2254	Influence of the Liquid Phase Physical Properties on Unsteady-State Hydrodynamics in Periodically Operated Trickle-Bed Reactors B Brkljac, T Bludowsky, W Dietrich, M Grünwald, D W Agar	Yes
3146	Transition from the perfect core-annular flow in a constricted tube to unsteady – stratified, bubbling, pulsing and spray – flow regimes M Zacharioudaki, Y Dimakopoulos, J Tsamopoulos	Yes

Session T2-5b

## **Innovative $\mu$ -PIV measurement technique for film flow investigations**

S. Paschke,<sup>a</sup> I. Ausner,<sup>a</sup> J.-U. Repke,<sup>a</sup> G. Wozny<sup>a</sup>

<sup>a</sup> *Institute of Process Engineering, Technical University Berlin, Strasse des 17. Juni 135 – KWT 9, 10623 Berlin, German*

### **1. Summary**

By using Computational Fluid Dynamics (CFD) simulations it is possible to investigate the film flow behavior in packed columns. To validate these, accurate experimental measurements are required.

With a new developed micro Particle Image Velocimetry ( $\mu$ -PIV) method it is possible to measure the three dimensional velocity field on industrial used wall materials. The first results show that with this special technique the influence of reflections and refractions on account of the wavy surface are minimized. A comparison between the velocity profiles for a water-glycerol mixture with the Nusselt solution show a good agreement especially for low Reynolds numbers.

Keywords: Micro-PIV measurements, film flow, CFD simulation, validation, 3D velocity profile

### **2. Extended Abstract**

In a multitude of process engineering applications film flows can be found, e.g. in packed columns for distillation and absorption or falling-film evaporators. It was found that e.g. the separation efficiency of such processes strongly depends on the hydrodynamics of the liquid flow behavior. For prediction of the flow behavior and the design of film flow apparatus, a detailed knowledge of the fluid dynamic on the surface in dependence on the process and system parameters is urgently required. With the aid of CFD simulations it is possible to investigate the flow behavior inside complex geometries. However, it is necessary to validate the CFD simulations with accurate measurements.

The liquid phase inside film flow apparatus mainly flows as closed film flow or after break-up as rivulet and droplet flow. Normally, in industrial applications the wetted surface is often strong corrugated. With the additional formation of waves on the liquid surface, the flow behavior becomes very complex. Therefore, researchers of previous studies have investigated the liquid flow from the backside through a

transparent wall in order to avoid reflection and refraction effects due to the wavy vapor-liquid interface. The transparent wall material is different to materials, which are used in industrial applications, and due to that the flow properties like liquid spreading can be changed.

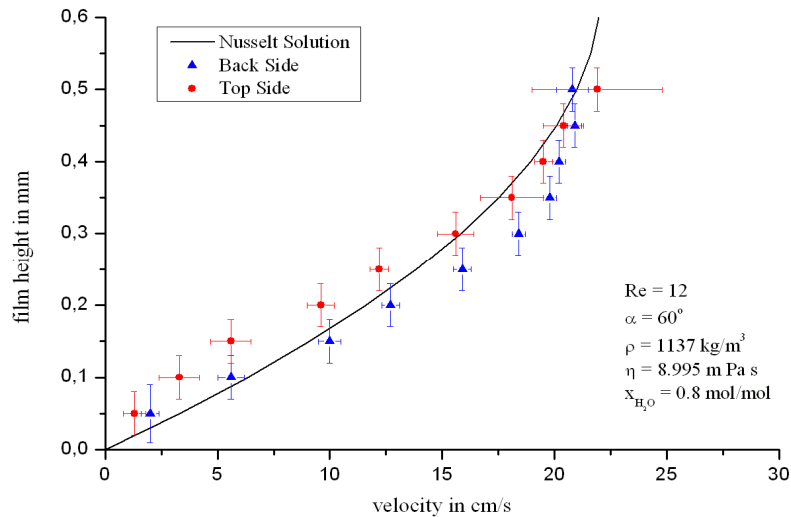


Figure 1: Velocity Profile for a water-glycerol mixture, measured from the backside (triangle) and through the liquid surface (circle) for  $Re=12$ . The line present the analytical Nusselt solution.

To analyze the flow behavior on non-transparent materials, a new micro Particle Image Velocimetry ( $\mu$ -PIV) method is developed and will be presented in this contribution. This method enables the measurement of a three dimensional velocity field from the top side of the flow through the wavy interface. First measurements are carried out from the top side and from behind through a transparent glass wall with water-glycerol mixtures at different Reynolds numbers. A comparison of the velocity profiles for the different cases show the feasibility of this new measurement technique (see figure 1). Consequently, flow investigations on industrially used wall materials like stainless steel are carried out.

Further measurements are conducted with water-glycerol on a flat inclined stainless steel plate under different Reynolds numbers. The results are compared with own CFD simulations as well as other correlations published in the literature. The comparison of the three-dimensional velocity field shows good agreements and leads to further investigations in more complex technical geometries. This enables the analysis of multiphase flow processes, e.g. three-phase flows in packed columns (Repke et al.).

*The authors would like thank the German Research Foundation (Deutsche Forschungsgemeinschaft) for the financial support.*

## References

- Repke, J.-U., Ausner, I., Paschke, S., Hoffmann, A. and Wozny, G, (2007) *Trans IChemE Chemical Engineering Research and Design*, 85, 50-58



## Mixing time of surface active agent solutions

L. Broniarz-Press, S. Rozanska, I. Szrajbrowska

*Department of Chemical Engineering and Equipment, Poznan University of Technology,  
pl. M. Skłodowskiej-Curie 2, PL 60-965 Poznan, Poland*

### 1. Summary

One of the basic properties of the surfactant solutions is their ability to reduce the interfacial tension and form the micelle associates. The phenomenon depends on the surfactant concentration in a solution and surfactant structure as well as on the kind and the concentration of salt present. The paper deals with the experimental studies directed to mixing time in drag reducing micellar solutions. It has been shown that in TTAB/NaSal aqueous solutions agitated the dumping of turbulent vortex in microscale exists. The effects of the decrease of mass transport in the tank volume and increase of the mixing time, have been observed too.

Keywords: mixing time, energy dissipated, surfactant solution, conductometric method, optical method

### 2. Extended Abstract

In cationic surfactant solutions, for example ammonium quaternary salts, the spherical micelles, rod-like micelles and their unusual form called the worm-like micelles, have been formed. The worm-like micelles are formed mainly in the systems accompanied with sodium salicylate (NaSal). In literature the characteristic feature of the rod-like structures is usually connected with the fact that in a lot of cases they can substitute the high-molecular polymer additives. The last ones found the application in drag reduction of tube flow, at the crude oil (Chen *et al.*, 2005) output and as thickeners of the cosmetics.

In the paper the experimental studies directed to determination of mixing time  $t_m$  for tetradecyltrimethylammonium bromide (TTAB) aqueous solutions in the agitated vessel equipped with turbine impeller of six straight blades, have been presented. Sodium bromide (NaBr) and sodium salicylate (NaSal) were used as additives promoting the micelle association process. In order to estimate the mixing time the optical method accompanied with the numerical analysis of a film, has been chosen. In optical method the pigment ultramarine (loftsmann) has been applied. To check the

correctness of the results obtained the conductometric technique has been used, additionally. In the study the model Newtonian fluids were distilled water and glycerin aqueous solution of concentration of 47%. It was found that mixing time in a tank equipped with Rushton turbine for Newtonian fluids agitated at  $Re > 6400$   $Ne^{-1/3}$  can be determined by the Ruszkowski (1994) relationship:

$$t_{95} = 5.9D^{2/3}\epsilon^{-1/3}\left(\frac{D}{d}\right)^{1/3} \quad (1)$$

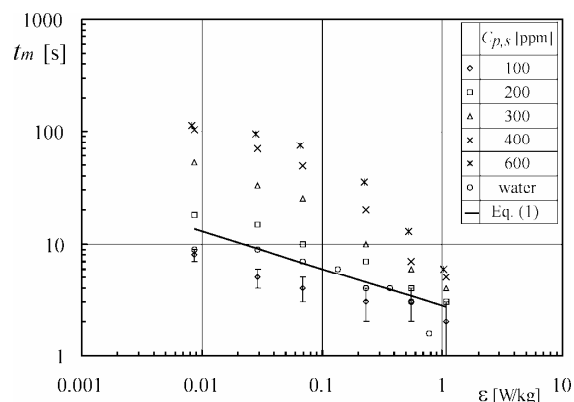


Figure 1: Comparison of the mixing times for TTAB/NaSal with data for distilled water and Ruszkowski proposal

In Figure 1 the exemplary relationships of  $t_m = f(\epsilon)$  for TTAB/NaSal solutions are presented. For surfactant solution concentration equal to 100 ppm the experimental points run below Ruszkowski proposal (1). Its results from fact, that in TTAB/NaSal solution at the surfactant concentration 100 ppm only spherical micelles or relatively short cylindrical micelles can be present. At higher TTAB/NaSal concentrations the considerable increase of mixing time with surfactant concentration increase is evident. The literature data showed, that in quaternary ammonium salt with sodium salicylate, the unusually long wormlike micelles, have been formed (Qi and Zakin, 2002). The growth of mixing time was connected with micelle association. It is additionally seen that with the increase of energy dissipation coefficient  $\epsilon$ , the decrease in differences between mixing times is observed.

## References

Chen, H., Han, L., Luo, P. and Ye, Z., (2005) *Journal of Colloid and Interface Science*, 285, 872-874.

Ruszkowski, S., A rational method for measuring blending performance and comparison of different impeller types, *Proceedings of 8<sup>th</sup> European Mixing Conference*, Institute of Chemical Engineering, Rugby, UK, 283-291 (1994).

Qi, Y. and Zakin, J. L., (2002) *Industrial and Engineering Chemistry Research*, 41, 6326-6336.

## **Bubble Size Distribution and Two-Phase Pressure Drop in Thin-Gap Microchannel**

J. Kristal, J. Havlica and V. Jiricny

*Institute of Chemical Process Fundamentals, The Academy of Sciences of the Czech Republic,  
Rozyjova 135, 165 02, Praha 6 – Suchbøl, Czech Republic*

### **1. Summary**

Present study experimentally investigates the two-phase flow in a rectangular microchannel. Reaction mixture for organic electrochemical oxidation (Rode 2004) is used as a liquid phase. Hydrogen generated on cathode inside the microchannel forms the gas phase. Flow in the thin-gap microchannel is visualized using digital camera for a range of operating conditions. Image processing is then used for the evaluation of bubble size distribution. The applicability of previously proposed correlations for two-phase frictional pressure drop to thin-gap channel is investigated.

Keywords: rectangular microchannel, bubble size distribution, pressure drop

### **2. Extended Abstract**

Process intensification in production of fine chemicals can be achieved using various types of microreactors. One of suitable arrangements for electrochemical reactions is a thin-gap microreactor. Thin-gap microreactor can be used as a single-pass flow-through reactor, with electrodes built in front and rear walls. In case of electroorganic oxidation, the desired reaction takes place on anode, whereas on cathode hydrogen is generated from the solvent as a counter reaction. Evolution of gas leads to formation of a two-phase system inside the microreactor.

Bubble presence near the electrode has negative effect on reactor efficiency due to the hindrance of electrode active surface. If the bubble covers large part of electrode (bubble diameter is much larger than reactor thickness), it blocks electrode surface from the bulk liquid. Only a thin liquid film exists between the bubble and electrode. Mass transfer from the bulk liquid to this film is slow and the electrode area is not fully utilized for the reaction. Therefore, for the efficient reactor design, the understanding of the bubble size distribution and flow patterns is essential.

Another parameter considered in reactor design is the pressure drop. For individual microreactor the pressure drop is not so important because of its low value. However, in the case of reactor stack, pressure drop can play significant role when

determining optimal operating condition. Two-phase pressure drop has been intensively studied during last years and several correlations are already available in literature.

Present study experimentally investigates the two-phase flow in a rectangular microchannel. Cross section of the microchannel is 10×0.1 mm, and orientation is vertical. Flow in the thin-gap microchannel is visualized using digital camera for a range of operating conditions. Image processing is than used for the evaluation of bubble size distribution. The applicability of previously proposed correlations for two-phase frictional pressure drop to thin-gap channel is investigated. Finally, two-phase pressure drop is identified with flow patterns existing in microreactor.

### **References**

Rode, S., Altmeyer, S. and Matlosz M., (2004) *J. Applied Electrochemistry*, 34, 674-680

## Hydrodynamics of one-dimensional gas-solid flow

Francisco J. Collado

*Department of Mechanical Engineering, Maria de Luna 3, Univ. Zaragoza , E-50018 Zaragoza, Spain*

### 1. Summary

The usual way to model vertical, one-dimensional, gas-solid flows states two continuity equations for each of the phases, plus the mixture momentum equation by the simple addition of the gas and solid momentum ones. So, we have three nonlinear first-order differential equations, and we want to determine four continuous functions: the gas and solids velocities, the gas (or solids) void fraction, and the gas pressure. Therefore, we need one more differential equation. Recently, a new approach for modelling one-dimensional, gas-solid flow has been suggested by the author: if the two phases have different velocities then they cannot travel along the same distance (the length of control volume) in the same time. Thus, the new model would suggest that the fourth equation would be the gas-solid velocity ratio constancy throughout the duct. So, new mass, momentum and energy equations for one-dimensional, gas-solid flow have been recently proposed by the author, which allow to derive a new pressure drop correlation successfully tested against data. In this work, the ability (and thus the correctness) of the new proposal to predict the one-dimensional axial profile of the solid void fraction is checked against recent and careful particle distribution measurements.

Keywords: gas-solid flow, hydrodynamics, slip ratio, pressure drop

### 2. Extended Abstract

The classic gas and solid continuity equations (Arastoopour and Gidaspow, 1979) for a one-dimensional, gas–solid flow are  $W_G = v_G \rho_G \phi A_c$  and  $W_S = v_S \rho_S (1 - \phi) A_c$ , respectively. Where subscript G is for gas, subscript S for solid and  $\phi$  is for gas void fraction. Then, we can easily derive the gas-solid velocity ratio, or slip ratio

$$v_G/v_S = (W_G/W_S)(\rho_S/\rho_G)((1-\phi)/\phi). \quad (1)$$

In other works (Collado and Muñoz, 1997; Collado et al., 2002), the author has already suggested to consider this slip ratio constant along the line at steady state.

Quite recently, Tortora et al. (2006) have carefully measured particle distributions in the riser of a pilot-scale circulating fluidized bed (CFB) (14-cm inner diameter, 5.77-m height) using electrical impedance tomography (EIT) and gamma densitometry tomography (GDT). FCC catalyst particles, generally spherical in shape and with a density of  $1275 \text{ kg/m}^3$ , were used in all experiments. All the terms in Equation (1) have been carefully measured, and so, allowing check the former assumption of slip ratio constancy.

Fig. 1 shows the axial profile of the measured slip ratio along the CFB riser. Four combinations of motive airflow (low: “LG” and high: “HG”) and solid flux (low: “LS” and high: “HS”) were tested. For high solid flux, it would seem that the slip ratio constancy is verified from the beginning, whereas for low solid flux, this constancy would clearly fail at the bottom of the riser, although after about 0.9 metres, the slip ratio profile would tend to stabilize.

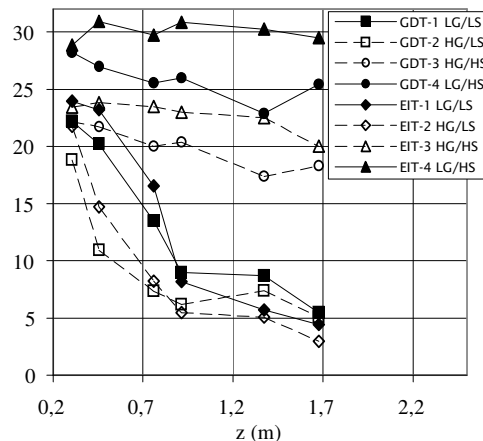


Figure 1: Measured axial profile of slip ratio

The author thanks to Dr. Paul Tortora and Dr. Steven Trujillo the data kindly supplied.

## References

- H. Arastoopour, D. Gidaspow, Analysis of IGT pneumatic conveying data and fast fluidization using a thermohydrodynamic model, *Powder Technology* 22 (1979), pp. 77-87.
- F.J. Collado and M. Muñoz, New considerations on the mass and energy balances in one-dimensional two-phase flow at steady state, *Powder Technology* 92 (1997), pp. 195-204.
- F. J. Collado, E. Sevilla, C. Valcarcel, Thermodynamics of gas-solid flow, *AIChE Journal*, 48 (2002), pp. 1100-1108.
- P. R. Tortora, S. L. Ceccio, T. J. O’Hern, S. M. Trujillo, J. R. Torczynski, Quantitative measurement of solids distribution in gas-solid riser flows using electrical impedance tomography and gamma densitometry tomography, *International Journal of Multiphase Flow*, 32 (2006), pp. 972-995.

## **Influence of the Liquid Phase Physical Properties on Unsteady-State Hydrodynamics in Periodically Operated Trickle-Bed Reactors**

B. Brkljac<sup>a</sup>, T. Bludowsky<sup>a</sup>, W. Dietrich<sup>a</sup>, M. Grünewald<sup>a</sup>, D. W. Agar<sup>a</sup>

<sup>a</sup>*Department of Biochemical and Chemical Engineering, Universität Dortmund  
Emil-Figge-Str. 66, 44227 Dortmund, Germany*

### **1. Summary**

The effect of the liquid phase viscosity and surface tension on the trickle bed reactor hydrodynamics was systematically investigated. Surface tension and viscosity were independently varied in order to modify liquid wetting properties. Two-phase pressure drop and dynamic liquid hold-up were determined at different gas and liquid flow rates and different liquid operating modes. The results reveal the importance of the pressure drop and liquid hold-up determination in both increasing and decreasing liquid flow rate operation modes and of the independent investigation of liquid properties on the complex trickle-bed reactor hydrodynamics.

Keywords: Trickle-bed reactors, Multiphase Flow, Hydrodynamics, Pressure drop, Liquid hold-up

### **2. Extended Abstract**

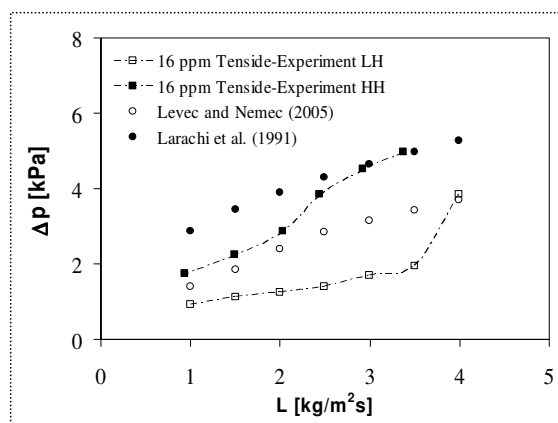
Trickle-bed reactors (TBRs) are extensively used for heterogeneously catalysed multiphase reactions in various industrial sectors, ranging from petrochemical and chemical plants to wastewater treatment and biochemical manufacturing processes [1]. The forced periodic operation of TBRs is one approach which has attracted extensive attention in chemical engineering research over the past few decades and this work has clearly demonstrated the substantial enhancement of performance that is feasible in laboratory-scale reactors. The deliberate manipulation of the liquid flow rate results in a dynamically fluctuating wetting of the catalyst surface, which allows the circumvention of the major shortcomings in steady-state operation: strong mass transfer resistance for the gaseous reactant and hot-spot formation [2, 3].

Despite considerable research in this field, periodic operation is still long way from being a viable alternative to conventional steady-state TBR operation in industrial applications. Even though a variety of modelling approaches and abundant experimental data are available, theoretical predictions of the trickle-bed reactor performance under periodic conditions still remain unsatisfactory.

The relative permeability hydrodynamic model proposed by Saez and Carbonell [4] represents a promising starting point for modelling TBR hydrodynamics as it has

already been successfully employed for the modelling of unsteady-state multiphase flow through porous media [5]. In order to examine its validity, an investigation of the quantitative influence of the liquid phase physical properties is necessary. The liquid phase surface tension and viscosity were systematically varied in order to modify liquid wetting properties. Water was selected as the reference liquid, with the surface tension being manipulated by addition of a tenside and viscosity by addition of glycerine. This strategy permitted surface tension and viscosity to be varied independently. Besides physical properties, both decreasing and increasing liquid flow operation modes were examined as the underlying structural elements of periodic operation.

The two phase pressure drop and dynamic liquid hold-up were measured under steady-state conditions for aqueous-solution/N<sub>2</sub> systems in a laboratory trickle-bed reactor packed with  $\gamma$ -Al<sub>2</sub>O<sub>3</sub> spheres. Furthermore, static liquid hold-up was determined for all solutions employed. The pressure drop for a tenside solution is presented in Figure 1. One of the important results obtained shows that the relative permeability model is superior to purely empirical correlations and provides a good



starting point for modelling of hydrodynamics under unsteady-state operation. Literature permeability coefficients do not adequately predict hydrodynamic behaviour when liquid phase physical properties are modified and do not differentiate between upper and lower hysteresis branches. Therefore for an improved description of unsteady-state hydrodynamics experimental determination of permeability parameter is necessary.

Figure 1. Pressure drop for tenside solution

The dynamic model thus derived has been successfully validated by periodic experimentation. Experimental and simulated results will be compared and discussed in detail with respect to the specific influence of the liquid physical properties. A reliable dynamic model represents an important first step in the prediction of mass transfer and reaction processes in periodically operated TBR. Furthermore, the modification of the wetting properties is seen as a promising technique for 'levelling the playing field' between gas and liquid in both steady-state and periodic TBR operation.

## References

- [1] Al-Dahhan, M.H. et al., (1997) *Industrial & Engineering Chemistry Research*, 36, 3292-3314.
- [2] Haure, P. M., Hudgins, R. R. and Silveston, P. L., (1989) *AIChE Journal*, 35, 1437-1444.
- [3] Lange, R., et al., (1994) *Chemical Engineering Science*, 49, 5615-5621.
- [4] Saez, A. E. and Carbonell, R. G., (1985) *AIChE Journal*, 31, 52-62.
- [5] Crone, S., Bergins, C. and Strauss, K., (2002) *Transport in Porous Media*, 49, 291-312.



## **Transition from the perfect core-annular flow in a constricted tube to unsteady – stratified, bubbling, pulsing and spray – flow regimes**

M. Zacharioudaki, Y. Dimakopoulos, J. Tsamopoulos

*Lab. of Comput. Fluid Dynamics, Dep. of Chem. Engineering, Univ. of Patras, 2600 Patras, Greece*

### **1. Summary**

A Volume Tracking algorithm is implemented for locating the interface between two immiscible, incompressible, Newtonian fluids in a tube with a periodically varying, circular cross-section. Initially, the fluids are stationary and stratified in an axisymmetric arrangement so that one is around the axis of the tube (core fluid) and the other one surrounds it (annular fluid). A constant pressure gradient sets them in motion. The main parameters of the problem are: The Reynolds and Weber numbers, the fluids viscosity ratio, the volume fraction occupied by the core fluid and various geometric characteristics of the tube, while the fluids are of equal density. We present a parametric study of the conditions under which the stratified (trickling) flow is stable or turns into pulsing, bubbling or spray flow. In the first two cases, the flow of the core fluid becomes discontinuous forming one large (slug flow) or several smaller (bubbling flow) drops along the axis of the tube. The latter flow pattern is promoted, when capillarity increases. On the contrary, when the Weber and Reynolds numbers increase, the more viscous fluid penetrates the less viscous one forming a finger which eventually breaks forming many smaller and off-centered drops.

Keywords: two-phase flow, trickling flow, slug flow, volume tracking

### **2. Extended Abstract**

Our motivation for studying the two-phase flow in a circular tube with sinusoidal variation in its cross-section is that this is the simplest of the primarily shearing flows of two fluids, which can approximate the flow that takes place in a packed-bed reactor. Previously, we simulated two-phase flow either in this geometry (Kouris & Tsamopoulos, 2001a, 2002a) or in a straight tube (Kouris & Tsamopoulos, 2001b, 2002b), albeit under conditions that the flow remained stratified, steady or unsteady. Here we present transitions of stratified flow to pulsing, bubbling or spray flow. To this end, we used the Volume Tracking algorithm for locating the interface between the two fluids. The surface tension force is approximated using the continuous surface

force method. A boundary-fitted coordinate transformation is applied and all terms appearing in the continuity and momentum equations are approximated using centered finite differences in space and forward finite differences in time. The well-known failure of centered finite differences arises as the Reynolds number increases and leads to non-physical oscillations and failure of convergence with mesh refinement. These problems are resolved and computations with Reynolds as large as 500 converged by approximating the convective terms in the momentum equations by third-order upwind differences using Lagrangian Polynomials. In each time step, the incompressibility condition is enforced by a transformed Poisson equation, which is linear in pressure, but with variable coefficients and is solved by LU decomposition. As the Reynolds number increases from values leading to stratified flow, a wave develops on the interface which is convected downstream and the time averaged value of the total flow rate and the temporal frequency of the time periodic solution increase also. Decreasing the volume fraction of the core fluid or increasing the interfacial tension results in the transition from stratified flow to the pulsing (in which one large drop of the core fluid arises) and to bubbling flow (in which several drops are formed). The transition to the spray regime occurs as the Weber increases. Initially, the interface develops a wave, fig1b which then grows forming a finger of the annular more viscous fluid pointing towards the less viscous one, fig.1b,c. Due to inertia this finger extends and is torn off the main body of the annular fluid and creates drops of the annular fluid inside the continuous stream of the core fluid, fig. 1e,f. The spray regime arises also when the core fluid is the more viscous one, but in this case the fingers are pointing towards the annular fluid.

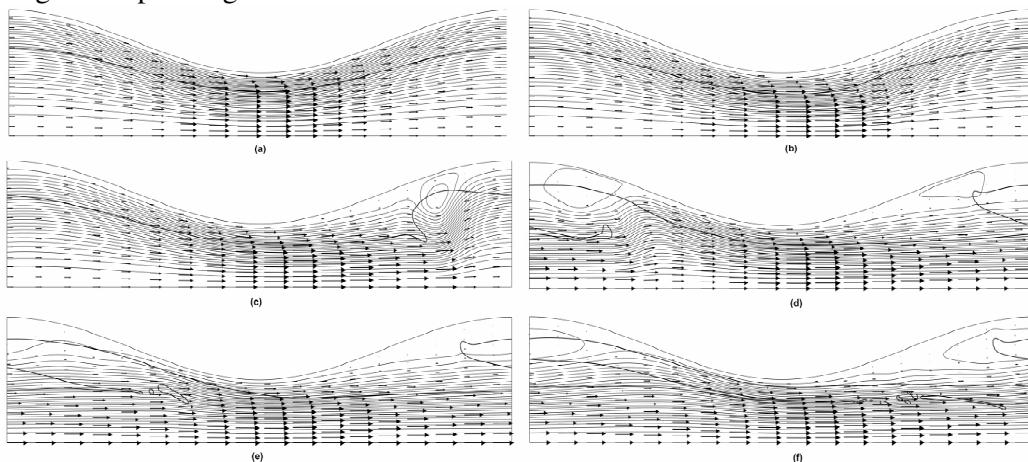


Figure 1 Time evolution of the flow field and the liquid-liquid interface at (a)  $\tau=0.4$ , (b)  $\tau=1.6$ , (c)  $\tau=2.8$ , (d)  $\tau=4.4$ , (e)  $\tau=5.2$  and (f)  $\tau=6.4$ . The results are for  $Re=500$ ,  $We^{-1}=0.01$ , the volume fraction of the core fluid is 0.49 and the core fluid is 5 times less viscous than the annular one.

## References

- Kouris, Ch. and Tsamopoulos, J., (2001a) *J. Fluid Mech.*, 432, 31-68.
- Kouris, Ch. and Tsamopoulos, J., (2001b) *Phys. Fluids*, 13, 841-858.
- Kouris, Ch. and Tsamopoulos, J., (2002a) *J. Fluid Mech.*, 470, 181-222.
- Kouris, Ch. and Tsamopoulos, J., (2002b) *Phys. Fluids*, 14, 1011-1029.

## Session T2-5c: Multifase Flows – III

<b>Abstract Number</b>	<b>Paper Title &amp; Authors</b>	<b>Included</b>
755	Solids Flow Pattern in Gas – Flowing Solids – Fixed Bed Contactors N Nikačević, M Petkovska	Yes
771	Simulation and measurement of gas holdup in bubble columns F Yamashita, T Suzuki	Yes
822	Structural and Practical Identifiability of a dynamic gas-liquid film model. J N Laboulais, S C Cardona	Yes
2857	Axial Dispersion Model for Simulation of an Airlift Bioreactor I Sikula, J Markoš	Yes

Session T2-5c

## **Solids Flow Pattern in Gas – Flowing Solids – Fixed Bed Contactors**

Nikola Nikačević,<sup>a</sup> Menka Petkovska<sup>a</sup>

<sup>a</sup>*Department of Chemical Engineering, Faculty of Technology and Metallurgy, University of Belgrade, Karnegijeva 4, 11000 Belgrade, Serbia*

### **1. Summary**

Solids Flow Pattern in Gas – Flowing Solids – Fixed Bed Contactors was investigated experimentally and theoretically. Tracer experiments were performed in a bench scale system in order to determine: residence time distribution (RTD) curves and dynamic responses of static holdup. A differential mathematical model with following assumptions: (a) axial dispersion in the dynamic zone for fast moving particles, (b) exchange of particles in two active stagnant zones, (c) dead zone for flowing solids that are inactive, was developed. Variation in operational conditions showed that the solids flux has more influence on the flow pattern than the velocity of gas. When solids flux was decreased, deviation from plug flow becomes more significant.

Keywords: multiphase systems, gas – flowing solids – fixed bed contactors, residence time distribution, solids flow model, axial dispersion

### **2. Extended Abstract**

Gas – flowing solids – fixed bed contactors are multiphase systems with counter-current flow of gas and fine particles through a packed bed of larger particles. These contactors show a good potential for a broad range of processes: adsorption, gas purification, heat recuperation, and catalytic reactors with separation *in situ*.

In a bench scale system, two types of experiments were performed. In the first case, RTDs of flowing solids were determined. Fine alumina particles were a flowing phase, and alumina particles of a different colour (all other properties being the same) represented a tracer for the step change. The step response curves (F) were obtained by the colour analysis of the particles at the outlet. The colour intensity profile was related to the fractions of tracer via the calibration curve.

In the second type of experiments, the dynamic behaviour of the static particles was investigated in step change measurements. The response curves, which represent the mean fraction of the tracer in the static holdup ( $x_{st}$ ) as a function of time, were obtained also by colour analysis of digital photographs. Additionally, the dynamic

holdup was measured as the mass of fast moving particles and static holdup was determined by weighting the particles entrapped in the packed bed.

Experiments were carried out in seven different series, varying the operational conditions in order to investigate their influence on the solids flow pattern. Four different solids fluxes, in a wide range of values ( $S=0.313\text{--}2.29\text{ kg/m}^2\text{s}$ ) were used. Gas velocities were varied broadly ( $U_g=0.041\text{--}0.123\text{ m/s}$ ) in four different series.

The RTD measurements confirmed that the flow of particles in gas – flowing solids – fixed beds is close to plug flow. The deviation from desirable (plug) flow pattern originate from two sources: back-mixing and the presence of stagnant solids which are not completely inactive. A differential, material balance model was developed to describe these phenomena. The model assumes existence of several flowing solids zones: dynamic for fast moving particles and stagnant zones for particles temporarily settled on the packing. Model presumes plug flow with axial dispersion for dynamic zone and exchange of particles between dynamic and stagnant zones. Particles that are inactive correspond to a “dead” zone, and they were treated as a part of a packing.

Complex hydrodynamic behaviour of the stagnant particles was described by an approximate exchange model. Its optimized parameters (exchange rates and fractions of two stagnant zones) were obtained on the base of both experimental sets. In the balance equation for the dynamic zone, the optimized parameter was Peclet number which is a measure of the axial mixing. Figure 1 shows results for both types of experiments, presented by: a) percentage of tracer as a function of dimensionless time ( $\theta=t/t_m$ ) – F curve and b) percentage of tracer in static holdup as a function of time –  $x_{st}$  curve. The model results, which are presented by the lines in Figure 1, are in very good agreement with the selected experimental series.

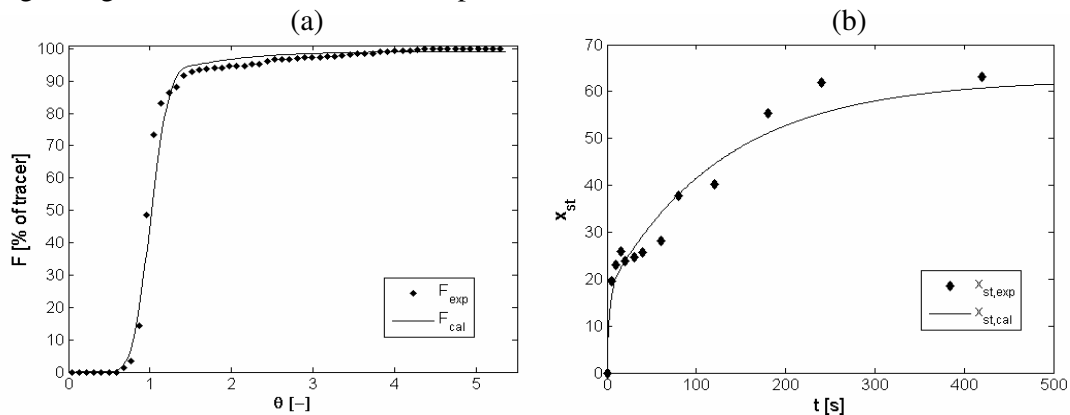


Figure 1. Comparison between model and experimental results for one series ( $S=1.22\text{ kg/m}^2\text{s}$   $U_g=0.123\text{ m/s}$ ). (a) RTD results (b) Response curve for static particles

The model calculations, as well as experimental results, showed a minor influence of the gas velocity and a considerable influence of the solids flux on the solids flow pattern. The results confirmed that for high solids fluxes, the particles would approach a plug flow pattern. When solids flux was decreased, deviation from plug flow becomes more significant. For the static holdup, regardless of operational conditions, it can be concluded that the exchange between the static and the dynamic particles is relatively intensive, but not complete (a “dead” zone exists). These conclusions were quantified through the values of the model parameters.

## Simulation and measurement of gas holdup in bubble columns

F. Yamashita, T. Suzuki

*Department of Applied Chemistry, Kanagawa Institute of Technology, 243-0292  
Atsugi, Japan*

### 1. Summary

The effects of gas inlet height  $H$ , arrangement of gas spargers, gas density  $De$  and viscosity  $Vis$  and inclination of a bubble column on gas holdup  $E_G$  were simulated by FLUENT software.  $E_G$  decreased with increasing gas inlet height, because the region under the gas inlet became bubble-free. Liquid circulates in the bubble column, however, bubbles don't fall into the region under the gas inlet.  $E_G$  for the gas sparger set in the center of the bottom of the bubble column was much larger than  $E_G$  for the gas sparger set near the wall, because the gas sparger set near the wall caused maldistribution of bubbles.  $E_G$  decreased with increasing inclination angle, because bubbles rise along the upper wall of the bubble column. Though Hikita et al. (1980) has reported that  $E_G$  is proportional to  $De^{0.062}Vis^{0.107}$ , the simulation results have showed that  $E_G$  does not depend on density  $De$  and viscosity  $Vis$  of gas for a constant bubble diameter. If bubble diameters depend on  $De$  and  $Vis$  of gas, it is possible that  $E_G$  by the simulation will change.

Keywords: simulation, gas holdup, gas inlet height, bubble column, gas density

### 2. Extended Abstract

#### 1) Conditions of simulation

Fluent software was used to simulate  $E_G$ . The conditions of simulation were as follows: 2D, 5 mm Mesh, Euler-Euler method, k- model, constant bubble diameter of 5 mm.

#### 2) Effect of gas inlet height $h$ on $E_G$

Fig.1 shows the effect of gas inlet height  $H$  on gas holdup  $E_G$  in a 16 cm wide and 2 m high bubble column. The width of gas inlet is 5cm.  $E_G$  decreased with increasing  $H$ , because the region under the gas inlet became bubble-free. Liquid circulates in the bubble column, however, bubbles don't fall into the region under the gas inlet. The simulation results showed a good accordance with experimental results.

#### 3) Effect of arrangement of gas spargers on $E_G$

Fig.2 shows the effect of geometrical arrangement of gas sparger on the bottom of the bubble column on  $E_G$ .  $E_G$  for the gas sparger set in the center of the bottom of the

bubble column was much larger than  $E_G$  for the gas sparger set near the wall, because the gas sparger set near the wall caused mal- distribution of bubbles. The effect of arrangement of gas spargers on  $E_G$  is now experimentally under investigation.

**4) Effect of inclination of bubble column on gas holdup  $E_G$**

Fig.3 shows the effect of inclination of the bubble column on  $E_G$ .  $E_G$  decreased with increasing inclination angle, because bubbles rise along the upper wall of the bubble column. The simulation results showed the same tendency as the experimental results.

**5) Effect of density  $D_E$  and viscosity  $V_{is}$  of gas on  $E_G$**

Though Hikita et al. (1980) has reported that  $E_G$  is proportional to  $De^{0.062}Vis^{0.107}$ , the simulation results have showed that  $E_G$  does not depend on  $De$  and  $Vis$  of gas for a constant bubble diameter of 5 mm. If bubble diameters depend on  $De$  and  $Vis$  of gas, it is possible that  $E_G$  by the simulation will change. Fig.4 shows the effect of kinds of gas on  $E_G$ .  $E_G$  depended on the measuring methods of  $E_G$ .  $E_{G,mano-Air}$  was much larger than  $E_{G,mano-H_2}$ .  $E_{G,eye-Air}$  was nearly equal to  $E_{G,eye-H_2}$ . It is not clear from these results if  $E_G$  depends on kinds of gas.

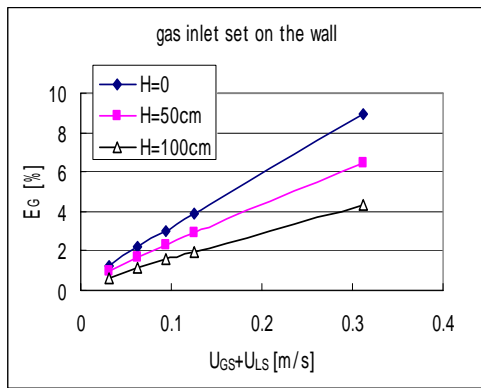


Fig.1 Effect of gas inlet height on  $E_G$ .

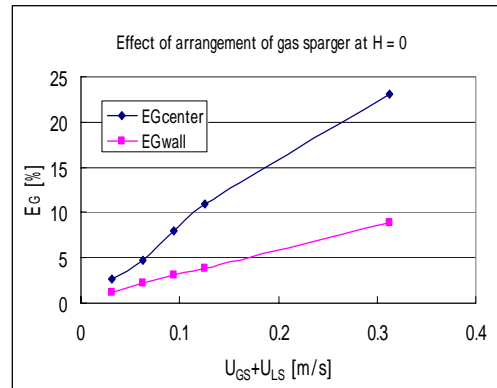


Fig.2 Effect of arrangement of gas spargers on  $E_G$ .

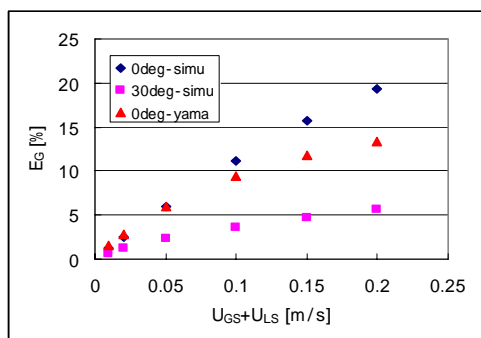


Fig.3 Effect of inclination of bubble column on  $E_G$ .

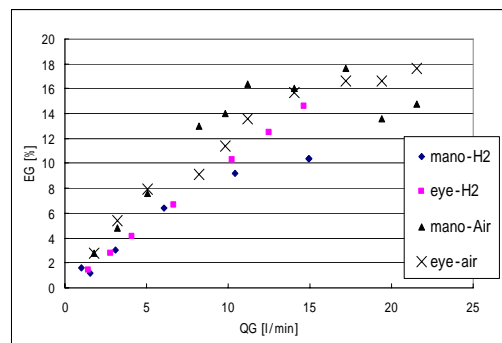


Fig.4 Effect of kinds of gas on  $E_G$ .

**References**

Hikita, H., Asai, S., Tanigawa, K., Segawa, K., Kitao, M., (1980) *The Chemical Engineering Journal*, 20, 59-67.



## **Structural and Practical Identifiability of a dynamic gas-liquid film model.**

J. Navarro-Laboulais, S.C. Cardona

*Universidad Politécnica de Valencia (UPV-EPVA). Department of Chemical and Nuclear Engineering.  
Plaza Ferrandiz y Carbonell, 03801 Alcoy (Alicante) SPAIN*

### **1. Summary**

The structural and practical identifiability analysis of a dynamic gas-liquid model combining both the macroscopic and the microscopic scales, confirms that the gas-liquid mass transfer process could only be well characterized determining the volumetric mass transfer coefficient,  $k_L a$ , together with the reciprocal of the diffusion time,  $D/\delta^2$ . A systematic error in the determination of  $k_L a$  is done when  $D/\delta^2$  is disregarded in the calculation of the mass transfer coefficient. The simultaneous measurement of the chemicals in the gas and in the liquid phase reduces significantly this error.

When a chemical reaction is considered, the fast and slow chemical regimes should be considered separately. A global second order kinetics model has also been analysed and shows that physical magnitudes like the gas hold-up,  $\epsilon$ , could be theoretically measured from purely chemical magnitudes, but inaccurately. The chemical rate constant could only be determined under certain circumstances from measurements just in the solution. The system is well characterized when additional measurements in the gas phase are done.

Keywords: gas-liquid mass transfer coefficient, structural identifiability, practical identifiability, Fisher information matrix, optimization.

### **2. Extended Abstract**

The mathematical models used to describe the gas-liquid mass-transfer processes usually have two spatial-temporal scales which refer to the physical mass-transfer itself at the gas-liquid interface level, and the modeling of the reactor configuration which considers the mixing processes and the chemicals distribution in the whole volume of the reactor. The *double-film*, *surface-renewal* and *film-renewal* models are developed assuming a steady state at the macroscopic scale which in some cases could not be attained or checked.

A dynamical gas-liquid model has been developed in this work based on unsteady state double film model including the macroscopic description of the reactor to analyse theoretically which parameters of the model and how accurately could be estimated from macroscopic measurements.

The problem of structural identifiability is related to the uniqueness of the solution of an input-output system, while the practical identifiability problem is related with how accurate those parameters could be determined. The structural

identifiability analysis has been carried out using the similarity transformation approach [1,2] while the practical identifiability analysis was done based on the determination of the Fisher Information Matrix of the model [3].

The gas-liquid model analysed considers a an unstationary semi-batch bubble column, given by the following set of differential equations:

$$\frac{dy_A(t)}{dt} = \frac{RT}{PV} \frac{1-\varepsilon}{\varepsilon} F_i \left( \frac{y_{A0}}{1-y_{A0}} U(t) - \frac{y_A(t)}{1-y_A(t)} \right) + \frac{RT}{P} \frac{1-\varepsilon}{\varepsilon} D_A a \left( \frac{\partial C_A(z,t)}{\partial z} \right)_{z=0} \quad (1)$$

$$\frac{\partial C_A(z,t)}{\partial t} = D_A \frac{\partial^2 C_A(z,t)}{\partial z^2} - k_2 C_A(z,t) C_B(z,t) \quad \forall z \in [0, \delta] \quad (2)$$

$$\frac{\partial C_B(z,t)}{\partial t} = D_B \frac{\partial^2 C_B(z,t)}{\partial z^2} - k_2 C_A(z,t) C_B(z,t) \quad \forall z \in [0, \delta] \quad (3)$$

$$\frac{dC_A^b(t)}{dt} = -D_A a \left( \frac{\partial C_A(z,t)}{\partial z} \right)_{z=\delta} - k_2 C_A^b(t) C_B^b(t) \quad (4)$$

where  $y_A$  and  $y_{A0}$  are the molar fraction of component A in gas phase at reactor outlet and inlet, respectively,  $F_i$  is the inert gas molar flow rate,  $\varepsilon$  the gas hold-up fraction,  $R$  the ideal gas constant,  $T$  the reactor temperature,  $P$  the total pressure,  $V$  the volume of the liquid phase,  $U(t)$  the unit step function,  $a$  the interfacial specific area,  $D_A$  and  $D_B$  the diffusion coefficient for A and B respectively in the liquid phase,  $k_2$  is the second order kinetic rate constant,  $C_A$  and  $C_B$  the molar concentrations for A and B in the liquid film and  $C_A^b$  and  $C_B^b$  the molar concentration for A and B in the liquid bulk.

The structural identifiability analysis of this model demonstrates the impossibility of uncouple  $k_L a$  in its constituents even when experiments with or without chemical reactions are combined. This result disagrees with the classical procedures, i.e. Danckwerts-plot method, based on fast chemical reactions to determine simultaneously the mass-transfer coefficient and the interfacial area of gas-liquid equipment.

The practical identifiability analysis shows that the measurement of chemical substances only in the liquid phase leads to systematic errors on parameter determination. The simultaneous measurement of the concentration in the gas phase avoids these errors.

The authors wish to acknowledge the Ministerio de Educación y Ciencia for the financial support for this work under contract CTQ2006-10783/PPQ (Project DATO3)

## References

1. Vajda, S.; Godfrey, K. R.; Rabitz, H. *Mathematical Biosciences* 1989; 93: 217-248.
2. Chapman, M. J.; Godfrey, K. R.; Chappell, M. J.; Evans, N. D. *Mathematical Biosciences* 2003; 183: 1-14.
3. Lin, Z. P.; Zou, Q. Y.; Ward, E. S.; Ober, R. J. *IEEE Signal Processing Letters* 2005; 12: 855-858.

## **Axial Dispersion Model for Simulation of an Airlift Bioreactor**

Sikula, I., and Markoš, J.\*

*Institute of Chemical and Environmental Engineering, Faculty of Chemical and Food Technology,  
Slovak University of Technology, Radlinského 9, 812 37 Bratislava, Slovak Republic*

### **1. Summary**

The airlift reactors have potential application in biotechnology industries due to their simple construction and less shear stress imposed on shear sensitive cells compared with the mechanically stirred tanks.

This work was focused on mathematical modeling of the fermentation process in an internal loop airlift reactor (IALR). Simulation results were verified on the batch fermentation of the gluconic acid by the strain *Aspergillus niger* which has been chosen as a model system. The fermentation was carried out in three laboratory IALRs (each one with different scale: 12, 40 and 200 liters, respectively) and performed in growth or non-growth conditions. Model of the ILALR is based on the material balance of each compound taking a part of reaction. From the various hydrodynamic and mixing point of view the reactor was divided into four main parts: bottom, riser, separator and downcomer. Each zones of that reactor were modeled separately according to mixing properties within (ideal mixing or plug flow with axial dispersion).

Parameters of the model, such as axial dispersion coefficient, mass transfer coefficient of oxygen, gas hold-ups, and circulation velocities, were predicted using experimentally determined correlations.

The results of the simulations and experiments are in sufficient agreement.

**Acknowledgement:** This work was supported by the Slovak Scientific Grant Agency in the framework of the Grant VEGA 1/3573/06.

**Keywords:** airlift bioreactor, gluconic acid fermentation, mathematical modeling, scale-up

---

\*corresponding author, E-mail: [jozef.markos@stuba.sk](mailto:jozef.markos@stuba.sk)

Book of Abstracts  
European Congress of Chemical Engineering (ECCE-6)  
Copenhagen, 16-20 September 2007

## Session T2-5P: Multifase Flows – Poster

Abstract Number	Paper Title & Authors	Included
46	The residence time distribution of the gas phase in circulating fluidised beds M Van de Velden, J Baeyens, J Degève, J P K Saville	No
166	Instability study of an annular liquid sheet of polymer produced by atomization. E P Herrero, E M M Valle, M A Galán	Yes
598	Experimental investigation of air-water two-phase flow in a 1mm x 1mm cross section channel R Negera, B Wittgens, L Sætran, P Skjetne	Yes
718	Parameters characterising the pulsing flow for cocurrent flow of gas and foaming liquid in a pressurised trickle-bed reactor D Janecki, G Bartelmus, A Szczotka	Yes
823	Solid – liquid mass transfer in a fixed – bed reactor operating in induced pulsing flow regime G Bartelmus, A Gancarczyk, T Krótki, T Mokrosz	Yes
842	Hydrodynamic behaviour and gas-liquid mass transfer in a three-phase inverse turbulent bed reactor D Hadjiev	Yes
855*	Simulation of entrained air separation from paper machine circulation water using CFD A Laari, A Haapala, T Stoor, I Turunen	Yes
862*	Prediction of bubble size and interfacial area in bubble column CFD simulations through solution of population balance equations M R Kamali, A Laari, Z Sha, I Turunen	Yes
1186	Vibration Field Effect Upon Gas-Liquid Mass Transfer V Kholmer, L Grinis	Yes
1216	Power consumption for non-aerated Na-CMC solutions in multiple bioreactors agitated L B Press, S Woziwodzki, M Ochowiak	Yes
1881	Hydrodynamics and Gas-Liquid Mass Transfer in a Rectangular Bubble Column A E M Cachaza, B E D Martín, C F J Montes, D M A Galán	Yes
2116	The effect of liquid viscosity on the void friction in a two-phase gas-liquid flow in narrow mini-channels J Sowiński, M Dziubiński	Yes
2356	Hydrodynamic Correlations for the Design of Conical Spouted Beds with Open-Sided Draft-Tube	Yes

Session T2-5P

	H Altzibar, G Lopez, J Bilbao, S Alvarez, M J San José, M Olazar	
3266	Mass transfer coefficient and gas hold-up in rectangular air-lift columns	No
	M Dziubiński, P Budzyński, M Orczykowska	
3300	Gas hold-up and bubble diameters in a gassed pulsation reactor	No
	P Budzyński, M Dziubiński, P M Domagalski	
3627	A visualisation technique for quantifying mixing time in stirred tank	Yes
	E Brunazzi, S Pintus	
3750	Hydrodynamics of "jet" type outflow from process installations	Yes
	H Fidos, M. Dziubiński, R. Krokos	

\* These two posters will be presented in session T3-P (theme-3, topic-5)

## **Instability study of an annular liquid sheet of polymer produced by atomization.**

E. P. Herrero; E.M.M. Del Valle<sup>a</sup> and M.A. Galán.

*Dep. Chem. Eng. Univ. of Salamanca, P/Los Caídos, 37008, Salamanca, Spain; <sup>a</sup>[emvalle@usal.es](mailto:emvalle@usal.es)*

### **1. Summary**

A temporal stability analysis was carried out to model the atomization of a swirling viscous annular liquid sheet emanating from an air-blast atomizer subject to inner and outer inviscid swirling air streams. The dimensionless dispersion equation that governs the instability of a viscous annular liquid sheet under swirling air streams was obtained. Numerical solutions to the dispersion equation under a wide range of flow conditions were obtained to investigate the effect of the liquid and gas flow on the maximum growth rate and its corresponding unstable wave number. The theoretical behaviour predicted by the dispersion diagrams was compared with the experimental results obtained by the same authors in previous works from the atomization of alginate solution using an air-blast atomizer. It was found that the instability model proposed justify the experimental effects found for the atomization of the fluid and under the work range for alginate flow rate and viscosity and air flow rate.

Keywords: atomization; air-blast atomizer; instability; growth rate

### **2. Extended Abstract**

During the last decade atomization techniques as air-blast or twin-fluid atomization has been widely used [1-4]. Unfortunately, the process of air-blast atomization is very complex and its physical mechanisms are not fully understood [1].

Theoretical and experimental studies on the mechanism of atomization have been carried out by Rayleigh, Tyler, Weber, Haenlein, Ohnesorge and Castleman [1]. Detailed reviews of earlier work have been published by Giffen and Muraszew [5], and more recently by Chigier [6], and Lefebvre [1] from these studies it can be concluded that the wave mechanism has been found the widest acceptance among the mechanisms of atomization. According to this theory the disintegration of liquid sheets or liquid jets is caused by the growth of unstable waves at the liquid-gas interface due to the aerodynamic interactions between the liquid and the gas.

There exists a dominant or most unstable wave number corresponding to the maximum growth rate and when the amplitude of the disturbance reaches a critical

value, the wave detaches from the sheet to form ligaments, which rapidly collapse, forming drops.

The main aim of this work is to develop a temporal stability analysis to model the atomization of a swirling viscous annular liquid sheet emanating from an air-blast atomizer subject to inner and outer inviscid swirling air streams. The dimensionless dispersion equation that governs the instability of a viscous annular liquid sheet under swirling air streams was derived. Numerical solutions to the dispersion equation under a wide range of liquid viscosity values, and flow conditions were carried out to investigate the effects of the liquid and gas on the maximum growth rate and its corresponding unstable wave number.

It has been observed that when the liquid flow decrease, the growth rate increase, which indicates smaller drops. When the liquid viscosity decrease, the growth rate increases, this indicates shorter breakup length and smaller drops.

The theoretical behaviour predicted by the dispersion diagrams were compared with the experimental results obtained from the atomization of alginate solution using an air-blast atomizer. It was found that the instability model proposed justify the experimental effects found for the atomization of a fluid and under the work range for alginate flow rate and viscosity and air flow rate.

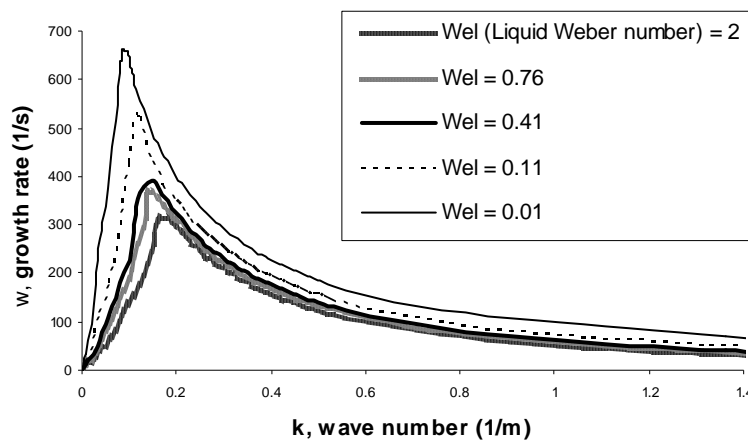


Figure 1: Example of dispersion diagram ( $We_{air} = 35128$ ;  $Z$  (Ohnesorge number) = 0.2;  $We_{liquid} = 0.01 - 2$ )

## References

- (1) Lefebvre, A. H., *Atomization and sprays*, Hemisphere, New York (1989).
- (2) Robitaille, R., et. al., (1999) *J. Biomed. Mater. Res.* 44, 116-120.
- (3) Orive, G, et. al., (2003) *Int. J. Pharm.* 259, 57-68.
- (4) Sugiura, S., et. al., (2005) *Biomaterials.* 26, 3327-3331.
- (5) Giffen, E., Muraszew, A., *The atomization of liquid fuel*, John Wiley, New York (1953).
- (6) Chigier, N., *Energy combustion and the environment*, McGraw-Hill, New York (1981).



## **Experimental investigation of air-water two-phase flow in a 1mm x 1mm cross section channel**

R. Negera<sup>a</sup>, B. Wittgens<sup>b</sup>, L. Sætran<sup>a</sup>, P. Skjetne<sup>b</sup>

<sup>a</sup>*Department of Energy and Process Engineering, Norwegian University of Science and Technology, Trondheim, Norway*

<sup>b</sup>*SINTEF Materials and Chemistry, Trondheim, Norway*

### **1. Summary**

In this paper an investigation of air-water flow pattern in a horizontal 1mm x 1mm PMMA (Polymethyl Methacrylate) square channel is presented. The effect of entrance condition on the flow patterns is shown. The flow patterns observed are also compared with flow patterns in channels of sizes in the ranges of several centimeters down to micrometers to evaluate the effect of channel size reduction. In addition, the flow at two 90° bends at 1 mm distance from each other is investigated.

Keywords: gas-liquid flow, two-phase flow, flow in small channel

### **2. Extended Abstract**

The main mechanical feature of miniaturized equipment are small rectangular channels in a limited volume, thus lots of turnings are necessary to accommodate the total length of the channel required for a specific process. Therefore, this study focuses on the investigation of gas-liquid two-phase flow in square channels with 90 degree bends. From a chemical engineering point of view, miniaturized system utilizes alternative measures for a given operation, e.g. mixing by means of diffusion in thin fluid layers instead of turbulent flow.

An air–water two-phase flow in a 1mm x 1mm cross sectional channel made of PMMA is investigated for two entrance conditions. The first system consists of a T-mixer, where air and water streams enter directly to the channel section, the second system consists of a mixing area prior to the channel configuration. The flow patterns obtained are also compared with the data presented by Mandhane et. al (1974), Tripplett et al. (1999) and Serizawa et al.(2002) to analyze the flow pattern change as the channel size decreases from the order of several centimetre, down to millimetre and micrometer, respectively. The flow parameters for the different studies considered are summarized in Table 1. In addition, the effect of 90 degree bends on the flow pattern is investigated.

The flow pattern maps for the two entrance conditions considered are shown in Figure 1. Comparing the two flow maps, the transitions from slug flow to stratified wavy and wavy is similar for both conditions. However, transitions from annular to stratified wavy and then to wavy occurs at lower liquid flow rate in the case where there is a

mixing area at the entrance. Furthermore, a churn flow is observed in this case which was not observed when there was a T-shaped entrance to the channel. The other difference observed between the cases is that the annular pattern without liquid film on the right side wall occurs at high gas flow rate when there is no mixing area before the entrance.

Experiments	Channel size	Superficial velocity[m/s] ranges		Re ranges	
		Liquid	gas	liquid	gas
Serizawa et al. (2002)	20, 25 and 100 $\mu\text{m}$	0.0032 - 17.5	0.0022 - 295.3	0.064 - 1750	0.003 - 1980
This study	1 mm	0.0003 - 0.0167	0.067 - 4.33	0.3 - 16.7	4.5 - 279.4
Triplett et al. (1999)	1.09 mm	0.02 - 8.0	0.02 - 80	21.8 - 8720	1.46 - 5846
Mandhane et. al (1974)	1.27 cm – 16.5 cm	0.003 - 6.1	0.03 -152.4	38.1 - 1.01x 10 <sup>6</sup>	25.5 - 1.69x 10 <sup>6</sup>

Table 1: Flow parameters of the different experiments compared in the study.

The flow patterns are in good agreement with the maps done for similar size channels by Triplett et al. (1999) and for micro size channel by Serizawa et al. (2002). However, the map did not agree well with the work of Mandhane et al. (1974) for conventional size channels, since the effect of gravity has created more stratified flow in the conventional channels in much of the flow rate we considered. At the 90 degree bends, for a given liquid flow rate, the flow passes through the bends with out changing its pattern at low gas flow rate. As the gas flow rate increases, the flow gets more deformed at the bend. This causes the formation of a new liquid plug at the second bend and/or breaking off of a passing air slug to create one or more bubbles. Thus a bubbly pattern is created here which was not been observed in the channel section up stream the bend.

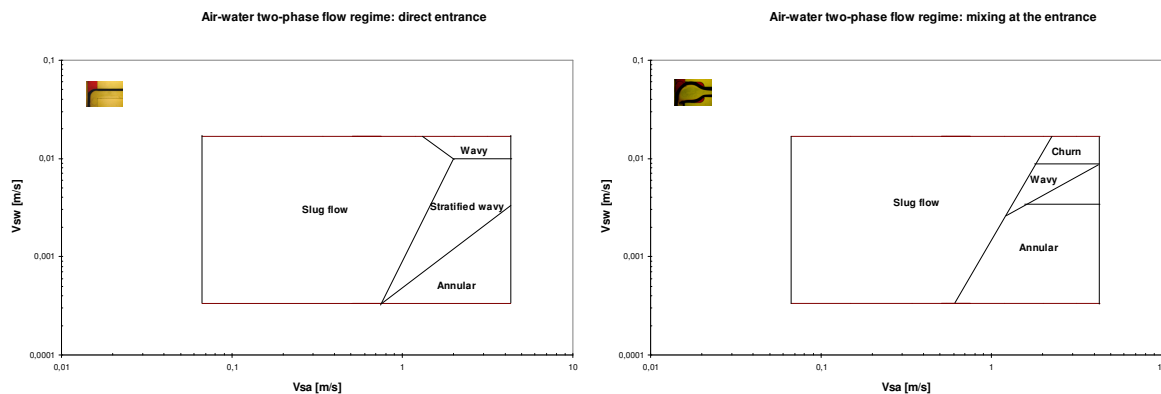


Figure 1: Flow maps for the two entrance conditions (a) direct entrance (b) mixing area at the entrance

**References**

Mandhane, J. M., Gregory, G. A., and Aziz, K., (1974) *Int. J. Multiphase Flow*, 1, 537 – 553.  
 Serizawa, A., Feng, Z. and Kawara, Z., (2002) *Exp. Thermal Fluid Science*, 26, 703 – 714.  
 Triplett, K. A., Ghiaasiaan, S. M., Abdei-Khalik, S. I. and Sadowski, D. L., (1999) *Int. J. Multiphase Flow*, 25, 377 – 394.

## **Parameters characterising the pulsing flow for cocurrent flow of gas and foaming liquid in a pressurised trickle-bed reactor**

D. Janecki<sup>a</sup>, G. Bartelmus<sup>b</sup>, A. Szczotka<sup>b</sup>

<sup>a</sup>*Department of Process Engineering, University of Opole, Dmowskiego 7/9, 45-365 Opole, Poland*

<sup>b</sup>*Polish Academy of Sciences, Institute of Chemical Engineering, Baltycka 5, 44-100 Gliwice, Poland*

### **1. Summary**

The aim of the present work was to experimentally determine the parameters characterizing the pulse flow of liquids through bed i.e. the frequency of pulsation and the velocity of pulses travelling along the bed and next to work out the correlation equations enabling their assessment. The research was carried out in a pressure reactor (pressures up to 2 MPa) having 0.05 m in diameter and being 1.5 m long. Physicochemical properties of the gas and liquid phases were changed in the research and the concentrations of water solutions of aliphatic alcohols were chosen in such a way so that the systems would form foams of various lifetime as a result of their contact with the gas in packing. The experimental data which were obtained as a result of the research were correlated depending on the operational parameters of the reactor and physicochemical properties of gas and liquid phases. The knowledge of the examined in the present work parameters is extremely important to model the operation of a three-phase system in the pulsing flow regime.

Keywords: trickle bed reactors, foaming systems, pulsing flow

### **2. Extended Abstract**

Trickle-bed reactors are commonly used in the branches of industry where great streams of substrates are processed (among others in petrochemical and kerosene industries) (Al-Dahhan et al. (1997), Dudukovic M.P. et al. (2002)). Foaming is a very common phenomenon occurring in many industrial processes. So far very little has been learned about the hydrodynamics of cocurrent flow of gas and foaming liquid through a fine packing bed and scant literature data often provide only qualitative observations concerning the behaviour of systems in case foaming occurs. The aim of the present work was to experimentally determine the parameters characterizing the pulse flow of liquids through bed i.e. the frequency of pulsation

and the velocity of pulses travelling along the bed and next to work out the correlation equations enabling their assessment.

The research was carried out in a pressure reactor (pressures up to 2 MPa) having 0.05 m in diameter and being 1.5 m long. Physicochemical properties of the gas and liquid phases were changed in the research and the concentrations of water solutions of aliphatic alcohols were chosen in such a way so that the systems would form foams of various lifetime as a result of their contact with the gas in packing. The method of measuring the changes in conductivity of the two-phase gas-liquid mixture flowing through bed was used to determine the parameters characterizing the pulsing flow of fluids.

The experimental data which were obtained as a result of the research were correlated depending on the operational parameters of the reactor and physicochemical properties of gas and liquid phases. It was state, that the velocity of pulses ( $V_p$ ) in case of every tested system was lower than the real gas velocity ( $v_g$ ). It means that gas always penetrates pulse in systems with low value of surface tension. No influence of foaming on the velocity of pulses was observed while comparing weak and strong foaming systems. Therefore, a common dependence for all experimental data was derived (mean relative error –  $e_Y=10.5\%$ , correlation coefficient –  $R=0.957$ ):

$$\frac{V_p}{v_g} = \left[ 1.6818 Re_{gr}^{-0.2857} - 0.213 \left( \frac{\rho_{aN}}{\rho_g} \right)^{0.406} \right] Re_{Lr}^{0.358} \quad (1)$$

where:  $Re_{\alpha} = v_{\alpha} r_{\alpha} d_p / \mu_{\alpha}$  – modified Reynolds number,  $\rho$  – density,  $\mu$  – viscosity,  $d_p$  – particle diameter,  $\alpha=g,L$  – refers to the gas and liquid phases,  $N$  – refers to normal conditions.

It is very difficult to determine the influence of real velocities of both phases on the frequency of pulsations ( $f_p$ ) because this dependence is different for systems forming strong and weak foams. The only parameter, which formulates the distinctiveness of the properties of the liquids tested, is the flow parameter  $\psi$ . Thus, that parameter was introduced into the correlation equations. For systems forming strong foams the following relationship was obtained ( $e_Y=33.4\%$ ,  $R=0.936$ ):

$$f_p = 0.2354 + 0.63\psi^{1.2916} Re_{gr}^{0.2697} We_{Lr} \quad (2)$$

where:  $We_{Lr} = d_p v_L^2 \rho_L / \sigma_L$  – Weber's number,  $\sigma_L$  – liquid surface tension.

The relation which, with  $e_Y=28.3\%$  and  $R=0.824$ , approximates experimental data for the systems forming weak foams has the form:

$$f_p = 0.343 Re_{gr}^{0.1655} + 0.0062\psi^{1.22} Re_{gr}^{0.447} We_{Lr} \quad (3)$$

The knowledge of the examined in the present work parameters is extremely important to model the operation of a three-phase system in the pulsing flow regime.

## References

- Al-Dahhan M.H., Larachi F., Duduković M.P., Laurent A., (1997) *Industrial Engineering Chemistry Research*, 36, 3292-3314.  
 Dudukovic M.P., Larachi F., Mills P.L., (2002) *Catalysis Review*, 44, 123-246.

## **Solid – liquid mass transfer in a fixed – bed reactor operating in induced pulsing flow regime**

G. Bartelmuś<sup>a</sup>, A. Gancarczyk<sup>b</sup>, T. Krótki<sup>a</sup>, T. Mokrosz<sup>b</sup>

<sup>a</sup>*Department of Process Engineering, University of Opole, Dmowskiego 7/9, 45-365 Opole, Poland*

<sup>b</sup>*Polish Academy of Sciences, Institute of Chemical Engineering, Bałtycka 5, 44-100 Gliwice, Poland*

### **1. Summary**

The aim of the present study was to evaluate both the liquid holdup and the liquid/solid mass transfer coefficients in a packed column operating with periodic liquid feeding of the BASE-IMPULSE type. The experiments were carried out for SLOW MODE of pulsing, applying electrochemical method of measuring the liquid holdup values and the limiting current method of measuring the local (in axial direction) mass transfer coefficients. The effect of changes of the physicochemical properties of the liquid phase and operating conditions on the local and averaged value of measured parameters were analyzed thoroughly. The equation correlating the measured values of liquid holdup was worked out. The experimentally determined values of mass transfer coefficient were shown by means of the enhancement coefficient defined as the ratio of the values of mass transfer coefficients determined in the induced pulsing flow and trickling flow regimes (for  $w_L = \text{idem}$ ).

Keywords: trickle-bed, induced pulsing flow, liquid holdup, liquid/solid mass transfer

### **2. Extended Abstract**

The aim of the present study was to determine experimentally the values of liquid/solid mass transfer coefficients ( $k_{LS}$ ) in a trickle-bed reactor (TBR) operating in a pulsing flow regime induced by means of cyclic changes in the flow rate of the liquid phase (LIPF-liquid induced pulsing flow) between the high and low value (BASE-IMPULSE method). The experiments were performed in a PCV column of 0.057 m in diameter and filled with a 1.37 m high layer of glass spheres of 3 mm in diameter.

The research presented in this paper was carried out for water and water solutions of glycerol (30 wt.% and 45wt.% respectively); nitrogen was used as the gas phase.

The knowledge of liquid holdup is necessary to determine the real values of liquid velocities in packing. That is why, the measurements began with determining the values of this parameter. The dynamic liquid holdup was determined by

electrochemical method. In order to state the axial changes of the averaged in the cross section of the column dynamic holdup values 5 conductometric cells (every spaced at the distance of 0.225 m) were placed along the bed. The results of experiments show that for water and glycerol solutions the values of averaged in time dynamic liquid holdup are changing insignificantly along the bed (~5%), regardless of duration of base and impulse as well as method of pulse induction. The data of  $\varepsilon_{Ld}$  obtained experimentally for SLOW mode of LIPF regime were correlated.

The following formula was obtained:

$$\varepsilon_{Ld} = 2.287 Re_L^{0.412} Ga_L'^{-0.306} \quad (1)$$

where:  $Ga_L' = d_p^3 \rho_L (\rho_{Lg} + \Delta P/H) \mu_L^{-2}$ ,  $Re_L = d_p \rho_L w_L / \mu_L$

Eq.(1) correlates 390 experimental points with the mean relative error  $e_y = 2.64\%$  and standard deviation  $\sigma_{st} = 1.93\%$ .

The liquid-to-solid mass transfer rate was determined electrochemically, based upon the measurement of the density of the current of electrochemical reaction whose rate is controlled by diffusion of ions to the surface of an electrode (cathode). The electrolyte used in the research contained 0.01 mol/l of potassium ferricyanide, 0.05 mol/l of potassium ferrocyanide and the so-called current carrier-potassium chloride. The role of the cathode was played by the platinum spheres of diameters equal to that of inert packing and positioned at 0.22m intervals along the axis of the bed.

The effect of changes of the physicochemical properties of the liquid phase and operating parameters (such as: the base and impulse liquid feed rate, duration of base and pulse, gas flow rate) on local and averaged values of measured coefficients were analysed thoroughly. The obtained experimental data base made it possible to determine the values of the so-called enhancement coefficient ( $\varphi$ ) pointing out how much higher values of mass transfer coefficient are obtained in LIPF regime in relation to the values of this coefficient obtained in GCF regime at the same average real velocity of the liquid phase in bed. It allows us to estimate the benefits resulting from the operation of reactor in the induced pulsing flow.

The result of the measurements indicate that if the operating parameters of the reactor are properly selected, then the dynamic work of the column makes it possible to obtain the increase in mass transfer coefficient ( $k_{LS}$ ) by even 30% (Fig.1). The analysis of the influence of the changes in the velocities of both phases on the value of the enhancement coefficient seems to indicate that the high value of  $\varphi$  is, first of all, the result of a better covering of the packing surface with liquid.

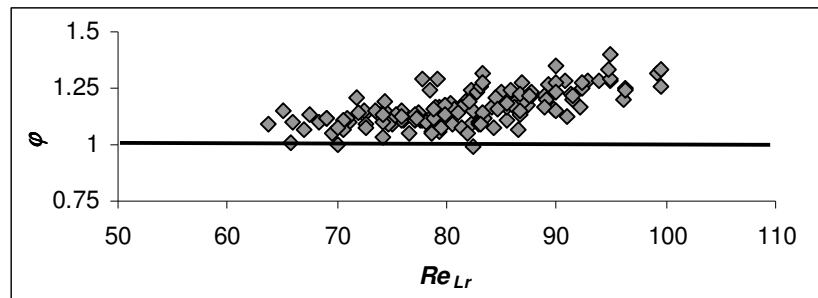


Fig.1. Enhancement coefficient ( $\varphi$ ) vs. real Reynolds number. System nitrogen-water solution of salts,  $w_g = 0.15 \text{ m/s}$

# Hydrodynamic behaviour and gas-liquid mass transfer in a three-phase inverse turbulent bed reactor

D. Hadjiev

Laboratoire de Biotechnologie et Chimie Marine, Université de Bretagne Sud, Research Centre, rue Saint Maudé, 56100Lorient, France

## 1. Summary

In this work, hydrodynamic characteristics and gas-liquid mass transfer in a laboratory scale inverse turbulent bed reactor were studied. In order to characterize internal flow in the reactor, the residence time distribution (RTD) was obtained by the stimulus-response technique using sodium chloride as tracer. The bed expansion -  $\varepsilon_{bed}$ , the gas hold-up -  $\varepsilon_g$ , and the volumetric gas-liquid mass transfer coefficient -  $k_{l}a$  were evaluated for a range of fluid dynamic conditions including different solid hold-up (0-0.2), air superficial velocities (0-0.014 m/s), liquid superficial velocities (0-0.05), and surface tensions (32 – 72 mNm as well as surface roughness. The volumetric gas-liquid mass transfer coefficient was found independent on the solid hold-up but it was influenced by the solid phase roughness and the surface tension. Increasing the former, up to 30% increase in the  $k_{l}a$  was observed, while up to 50% decrease in the same parameter was detected with the decrease in surface tension. The results enhance a previously suggested hypothesis which considers that the solid and liquid form a pseudo-fluid in the inverse turbulent bed reactor.

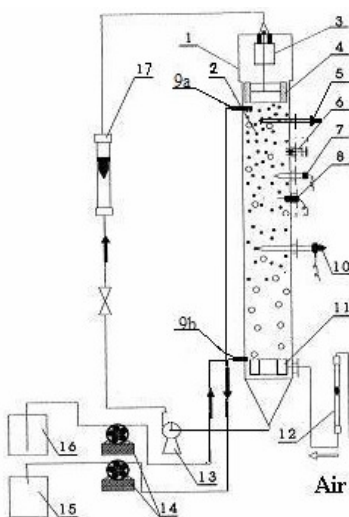
Keywords: fluidized bed, hydrodynamics, bed expansion, mass transfer coefficient

## Extended Abstract

Biofilm reactors with microorganisms immobilized on small suspended particles e.g. fluidized bed, airlift, inverse fluidized bed and circulating bed reactors have been used for organic matter and ammonia removal from industrial wastewaters. They allow higher biomass concentrations to be obtained, and higher volumetric loading rate of pollutants can be treated at the required removal efficiency.

### Experimental set-up

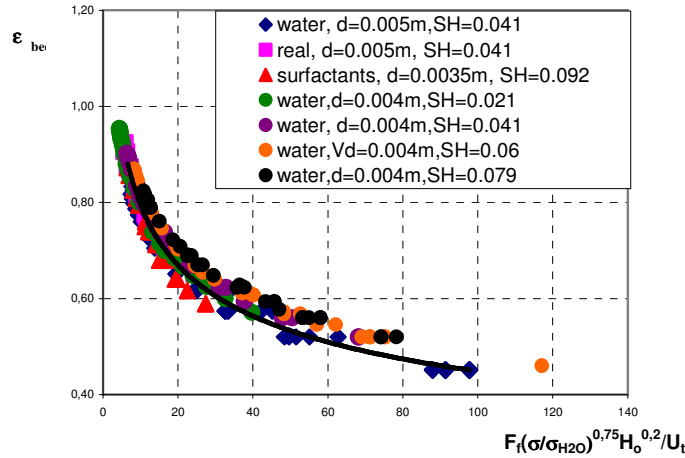
Experiments were carried out in an inverse fluidized bed reactor given in the Figure. The solid carriers were obtained by coating expanded PS beads with a PAC. The reactor consisted of a glass column of 0.1 m internal diameter. The height of the fluidization section between the air injection point and the liquid level was 1 m. The gas distributor with diameter of 0.09m was mounted in the bottom lid. It was designed to assure bubble size up to 1mm and uniform spreading in the column. An AALBORG, USA gas flow controller (12) and a liquid controller (17) made by Burkert (France) were used to measure both flowrates. The reactor was continuously fed using a Masterflex L/S pump (Cole-Parmer Instruments) (14) which assures flow rates from 0.006 to 10.2 l/h. The superficial liquid velocity was varied in the range from 0.01 to 0.03 m/s using a centrifugal pump (13). The superficial gas velocity was between 0.003 m/s and 0.014 m/s.



Experimental set up: 1. column, 2. support, 3. liquid phase distributor, 4. gas outlet, 5,10. O<sub>2</sub> electrodes, 6. sampling, 7. pH electrode, 8. temperature probe, 9a,b conductivity cells, 11. gas distributor, 12,17. flow meters, 13. recycling pump, 14. feed pump, 15,16. tanks

### Bed expansion

The study concerning the bed expansion in an inversed fluidized bed reactor with a medium recycle was carried out with coated and non-coated carriers in water and in a real suspension of *Pseudomonas putida*, cultivated in saccharose medium. Various solid holdups, solid phase density and liquid and gas velocities were used. Part of the results is presented below to illustrate the influence of the various parameters on the bed expansion in the case of a turbulent inverse bed. Applying the dimensional analysis approach, an expression can be proposed to evaluate the



bed porosity for various liquid and gas flow rates and different physicochemical properties. It takes into account the influence of the surface tension which is very important in the case of bioparticle fluidization. This expression:

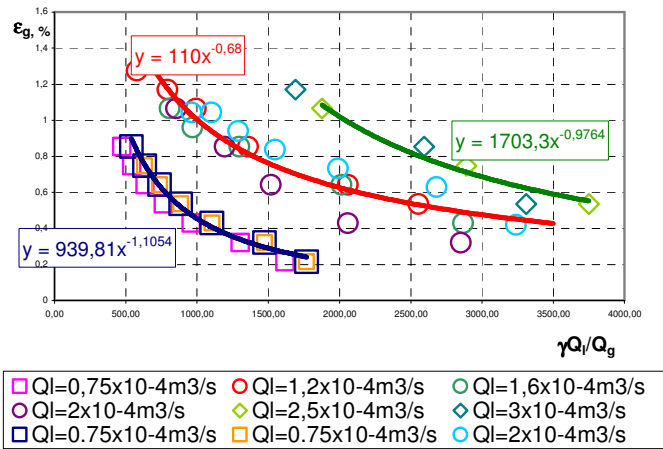
$$\epsilon_{bed} = 1.4125 \left[ \frac{F_f H_o^{0.2}}{U_t} \left( \frac{\sigma}{\sigma} \right)^{0.75} \right]^{-0.2492}$$

can describe satisfactorily all experimental data obtained with model and real systems.

### Gas hold-up

The study concerning the gas hold-up in the inversed fluidized bed reactor with a medium recycle was carried out with coated and non-coated carriers in water and in real solutions of *Pseudomonas putida* in saccharose mediums. Various solid hold-ups, solid phase densities and gas and liquid flowrates were used.

As it can be seen, three different regimes can be clearly outlined. They can be described by correlation expressions:



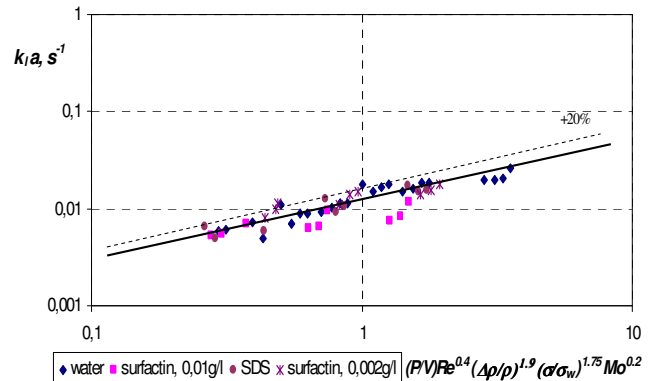
where respectively:  $A = 9.3981$ ,  $k = -1.1054$  - for “fixed” expanded bed;  $A = 1.1$ ,  $k = -0.68$  - for dispersed bubble regime and  $A = 17.033$ ,  $k = -0.9764$  -for coalesced bubble regime.

### Mass transfer coefficient

Following evaluation of the coefficients by trial and error the final form of the equation has been determined:

$$k_1 a = 0.0039 + 0.076 \times \lg \left[ \left( \frac{P}{V_{\text{reac}}} \right) \text{Re}^{0.4} \left( \frac{\Delta \rho}{\rho} \right)^{1.9} \left( \frac{\sigma}{\sigma_w} \right)^{1.75} \text{Mo}^{0.2} \right]$$

The figure compares experimental and calculated volumetric coefficients for 45 data sets.





## **Simulation of entrained air separation from paper machine circulation water using CFD**

A. Laari,<sup>a</sup> A. Haapala,<sup>b</sup> T. Stoor,<sup>b</sup> I. Turunen<sup>a</sup>

*<sup>a</sup>Department of Chemical Engineering, Lappeenranta University of Technology, Laboratory of Process and Product Development, PO Box 20, FIN-53851, Lappeenranta, Finland*

*<sup>b</sup>Department of Process and Environmental Engineering, University of Oulu, Fibre and Particle Engineering Laboratory, PO. Box 4300, FIN-90014, Oulu, Finland*

### **1. Summary**

Separation of entrained air bubbles from paper machine circulation water is studied both experimentally and by CFD simulations. A multiphase CFD model is developed taking into account the development of bubble size distribution due to bubble coalescence through the solution of population balances. The interaction of the moving bubbles and fibers is also considered by using a homogeneous model with characteristic rheological properties describing the additional viscous forces in fiber containing solutions. It is demonstrated that in the flow cases like this CFD is a valuable tool which allows structural optimization of the channel geometry to maximize air removal efficiency.

Keywords: entrained air, paper machine, degassing, CFD

### **2. Extended Abstract**

Entrained air is a common problem in paper and pulp industry. It can cause detrimental effects, for instance, on product quality, machine runnability, and pumping and washing efficiency. Different methods are used in paper mills to remove entrained air including active methods, such as vacuum deaeration tanks and deaeration pumps. Passive deaeration methods are used in wire pits and flumes. Also, chemical deaeration is frequently used by addition of degassing chemicals.

In this work gas removal efficiency is studied both experimentally and by CFD simulations. An experimental device to study air separation was constructed from transparent polyacrylate plates. The length of the rectangular air separation channel is 2.06 m, height is 0.22 m and depth 0.05 m. The studied solution is circulated by pump from the circulation tank back to the air separation channel through a 50 mm pipe connection. Before the entrance, a controlled volumetric flow of gas is fed and

dispersed into the pumped solution using a sintered porous plug. The size of the dispersed bubbles is measured by photometrical method. Flow fields of the liquid and gas bubbles are studied by Particle Image Velocimetry (PIV).

CFD simulations were carried out by using ANSYS CFX 10.0. A 2D model was used to decrease the computational load. The upper boundary of the gas removal domain is defined as a degassing boundary. This boundary definition allows gas bubbles to escape from the liquid phase. Runs were simulated using different feed rates, bubble sizes and volume fractions. The results were compared to experimental results for flow fields and gas removal efficiency. A reasonable agreement between the measured and calculated values was found to exist.

Some results from the simulations are shown in Fig. 1. Liquid and gas feed enters the channel from the downright corner. Feed rate is 1.0 m/s, gas volume fraction 0.2 and bubble size 200  $\mu\text{m}$ . The liquid feed generates a vortex near the entrance with liquid and gas flowing backwards at the channel surface. Most of the gas bubbles are separated at this vortex. Further downwards in the channel the flow is laminar which allows the rest of the bubbles to escape from the system. At the end of the channel some bubbles are sucked into the exit pipe.

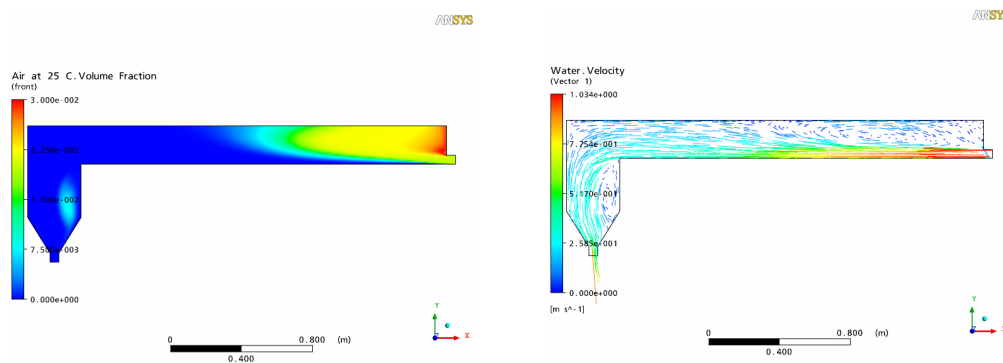


**Figure 1.** Simulated air volume fraction and liquid velocity field in a gas separation channel. Feed rate is 1.0 m/s, gas volume fraction 0.2 and bubble size 200  $\mu\text{m}$ .

The developed CFD model will be further enhanced to include physical properties of pulp suspensions, like viscosity, interfacial surface tension and bubble drag force. Also, the solution of population balances will be implemented. This makes it possible to study the effect of bubble coalescence and presence of degassing chemicals on the air removal efficiency.

## Prediction of bubble size and interfacial area in bubble column CFD simulations through solution of population balance equations

M.R., Kamali, <sup>a</sup> A. Laari, <sup>a</sup>, Z. Sha, <sup>b</sup> I. Turunen <sup>a</sup>

<sup>a</sup> *Lappeenranta University of Technology, Department of Chemical Technology, Laboratory of Process and Product Development, PO. Box 20, FIN-53851, Lappeenranta, Finland, kamali@lut.fi, arto.laari@lut.fi, ilkka.turunen@lut.fi.*

<sup>b</sup> *Tianjin University of Science and Technology, College of Marine Science and Technology, TEDA Street 13, No. 29, Tianjin, 300457, P. R. China, zsha@tust.edu.cn.*

### 1. Summary

In bubble column reactors the bubble size and the interfacial area available for gas-liquid mass transfer is determined by continuous coalescence and breakage of bubbles. These variables can be predicted by solution of discretized population balance equations for dispersed phases. In the current work a CFD-PBE coupled model is coded and tested for bubbly flow. The method is based on inhomogeneous flow field for different bubble size groups in Eulerian multi-dispersed phase systems. It is an improved method compared to available commercial packages for prediction of bubble size distribution and interfacial area in multiphase systems.

Keywords: bubble column, CFD-PBM coupled, population balances, bubble coalescence, antifoaming agent.

### 2. Extended Abstract

In the current model, in order to find local bubble size distribution, dispersed phase is divided into several phases. Theoretically, the higher the number of phases the more accurate the calculated variables should be. Each phase consists of several size groups. This classification is done by discretization of bubble sizes in different categories. Each size group is considered as a scalar variable. The local size fraction, number, volume and mass for each scalar variable are found based on solution of population balance equations.

Following equation shows scalar transport equation for different bubble size classes in each dispersed phase.

$$\frac{\partial}{\partial t}(n_i \rho_j) + \nabla \cdot (n_i \rho_j U_j) = \rho_j (B_{Bi} - D_{Bi} + B_{Ci} - D_{Ci}) = S_i \quad i = 1, \dots, N_c \quad j = \text{Disp. phase}$$

In this equation  $n$  is the population density and  $S$  is the source which is calculated by considering bubble breakage (B) and coalescence (C) for each bubble class. In the solution of these discretized equations it is necessary to ensure that at least two moments of the size distributions are conserved. In practice, these moments are chosen to conserve the total number and volume (or mass) of the distribution. This ensures that the numerical solution does not cause any error in the total number or mass of the bubbles. Some special techniques or correction factors has to be implemented to ensure the moment conservation.

Current CFD-PBE coupled approach is based on the Multi Phase Multi Size Group model presented by Sha et. al (2006) and can be used for different G/L/S multiphase systems. Solution of Navier-Stokes equations and turbulence models in Eulerian-Eulerian approach can give required variables in each control volume of calculation domain. These values are used to often or simultaneously calculate coalescence and breakage rates and finally size distribution at that control volume in other PBE related codes. Bubble coalescence model include some solution composition dependent experimental parameters, which has to be estimated based on experimental data. In order to save the computation time, PBE solution codes are called only in the beginning of each time step in transient calculations. This model was implemented in ANSYS CFX 10 and tested to calculate flow hydrodynamics and bubble size distributions in a cylindrical column with a diameter of 0.19 m and height of 1.7 m. To minimize the computational load a 2D model was used in the calculation.

Experimental data was collected from similar column using industrial wastewater with different concentrations of antifoaming agent. The experimental data included bubble size distribution, average gas hold up and flow hydrodynamics for liquid and gas phase. Bubble size distribution was measured using photometrical method. Flow fields of gas and liquid were measured by using Particle Image Velocimetry (PIV). The experimental results were compared to the results from CFD calculations to verify the developed CFD model.

## References

- Sha Z., Laari A., Turunen I., *Chem. Eng. Technol.*, 29, 550-559, 2006  
Wang et al., *AIChE Journal*, 52, No.1, 125-139, 2006

## **Vibration Field Effect Upon Gas-Liquid Mass Transfer**

V. Kholmer,<sup>a</sup> L. Grinis,<sup>a</sup>

<sup>a</sup>*Civil Engineering Department, Sami Shamoon College of Engineering 84100 Beer Sheva, Israel*

### **1. Summary**

The behaviour of two-phase liquid-gaseous mixtures plays an important role for many technological processes. In this research we investigated experimentally the effect of vibration parameters on the mass transfer efficiency. Bubble residence time in the liquid as well as its mean diameter and gas hold-up were chosen as the main parameters characterizing gas-liquid mass transfer efficiency. Obviously, bubbles with longer residence time having more uniform distribution result in mass transfer efficiency improvement. The goals of the present research are to study the effect of such vibration parameters as amplitude and frequency on the mass transfer efficiency and to develop the device for gas bubbles entrainment from the liquid surface. The effect of the device design parameters on the gas hold-up was also studied experimentally. It was shown that the proposed vibration-assisted device improves considerably the parameters characterizing the gas-liquid mass transfer and makes it possible to dissolve all the gas feed to the absorber. This fact allows to use this device for liquid saturation by relatively expensive gases. The simplicity of the design and the possibility of controlling the parameters, which insure proper mass transfer process, make the proposed method suitable for various applications in chemical and process industries.

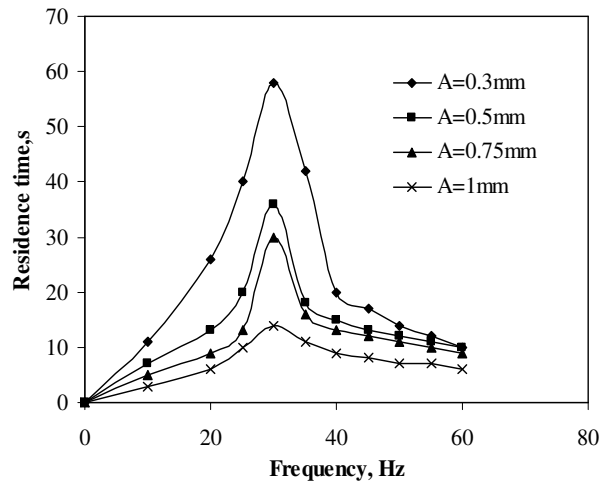
Keywords: vibration, mass transfer, liquid, bubble.

### **2. Extended Abstract**

The uniform distribution of gas in liquid bulk is required in many fields of chemical technology that widely employ two-phase liquid-gaseous mixtures. At the same time, the increase in gas bubbles residence time accompanied by decrease of their size and coalescence is also strongly desirable. A number of studies [ ] have been performed on the effect of vibrations on the gas bubble behaviour in the liquid. The common conclusion of these studies is a plausible effect of vibration field employment on the reduction of the bubble size and decrease of the bubble rise velocity. The improving effect is due to generation of submerged turbulent jets as well as to intensive breakage of the bubbles. The main benefits of the phenomenon are decrease of the bubble rise velocity and increase of the interfacial area which result in gas-liquid mass transfer enhancement.

In the present study we performed three sets of experiments. In the first set of experiments we used the plate vibrating in the rectangular vessel. In the second and the third sets we used the plate vibrating in the cylindrical bubble column. The first set of experiments dealt mainly with the effect of vibration parameters upon the gas bubbles mean diameter and residence time in the liquid. We tried also to determine the effect of the distance between the vibrating plate and the outlet gas orifice on the abovementioned bubble parameters. In the second and the third sets of experiments we tested the effect of the vibrating plate design and its location upon the bubble residence time in the liquid and the gas holdup. In the second set of experiments the gas was injected into the column (similar to the technique which was used in the first set) while in the third set the gas was entrained into the liquid bulk from its surface. It should be noticed that the experimental apparatus for all sets was almost the same with some slight differences.

Results of investigation of the amplitude of pulsations effect on the bubble residence time are presented on figure. The best results (the longest residence time) were obtained for the smaller values of the pulsation amplitude. It seems that for bigger amplitude values (more than 0.5 mm) occurring liquid downward streams enforce the bubble movement out of the region of effective vibration field action thus weakening its effect. As a result of this phenomenon the bubble residence time in the liquid bulk decreases with the vibration amplitude increase. For the investigated amplitude range the vibration frequency increase results in the bubble residence time increase up to its maximum value for the frequency of about 30 Hz. The further increase of the vibration frequency results in the bubble residence time decrease.



The effect of the plate fractional closed area  $\varphi$  value on the gas holdup was also investigated. Three series of experiments were performed for  $\varphi$  values of 0.3, 0.75 and 0.85. The vibration amplitude value varied from 0.5 mm to 4 mm for constant frequency value of 30 Hz. In all experiments the optimal (according to the results of the previous experiments) depth of the plate submergence (3 cm) was used. The obtained experimental results show the strong positive effect of the  $\varphi$  value decrease for the investigated amplitude range. In other words, the increase of the holes areas results in the gas holdup growth.

## **Power consumption for non-aerated Na-CMC solutions in multiple bioreactors agitated**

L. Broniarz-Press, S. Woziwodzki, M. Ochowiak

*Department of Chemical Engineering and Equipment, Poznan University of Technology,  
pl. M. Skłodowskiej-Curie 2, PL-60965 Poznan, Poland*

### **1. Summary**

Multiple impeller vessels are generally used in many industries, because of the advantages of the longer residence time, lower decrease of heat exchange area in scale-up treatment, lower power consumption per impeller as compared to single-impeller systems. The obtained data showed that in double impellers systems power consumption depends on distance between impellers. The optimal distance between impellers with the smallest power consumption has been proposed. For three and more impellers it has been shown that mixing power consumption depends on number of impellers.

Keywords: mixing, double impellers, power consumption, biochemical processes

### **2. Extended Abstract**

The experiments were carried out in a flat bottomed cylindrical vessel with internal diameter  $T = 0.19$  m and liquid level  $H/L = 2.3T$ . Three type of impellers ( $D = 0.065$  m) were used: Rushton turbine (RT), six pitched blade turbine (PBT) and six flat blade turbine (FBT). The influence of distance between impellers on power consumption has been investigated for double impeller systems whereas the influence of impellers number on mixing power requirements has been studied for vessels equipped with three, four and five impellers. The experiments were carried out with various Na-CMC solutions (non-elastic shear thinning fluids) of concentrations of 0.1% to 1.7%. The Reynolds number changed from 100 to 10,000.

It has been found that the power characteristics for non-Newtonian fluids agitated were of similar form as the power characteristics in turbulent Newtonian flow regime. The reduction of mixing power was observed in transitional region of fluid flow at  $Re_m \in (100, 1000)$ . At greater values of Reynolds number the mixing power consumption in non-Newtonian fluids studied is similar in a level to that observed in Newtonian fluids. The literature data by Metzner and Otto (1957), Calderbank and Moo-Young (1961), Broniarz-Press *et al.* (1997), as well as Paul *et al.* (2003)

suggested that in standard tank equipped with single impeller, the reduction of mixing power exists only in the range of  $Re_m \in (100,200)$ .

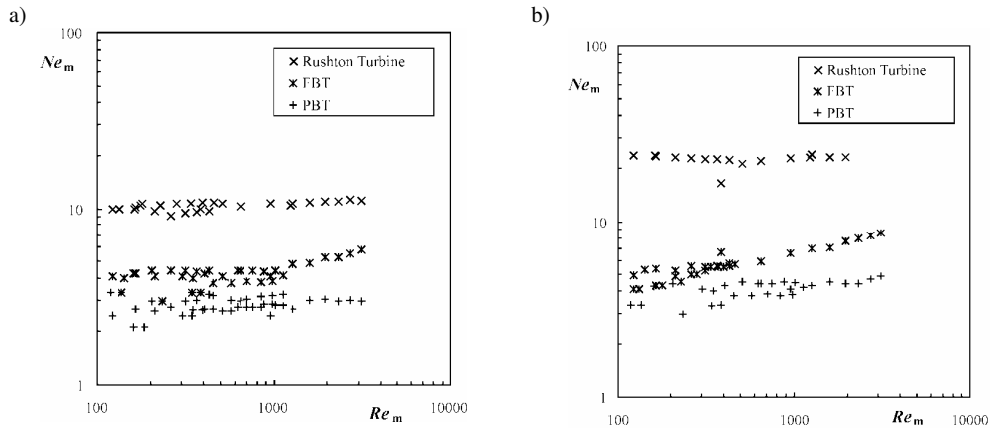


Figure 1: The exemplary relations of  $Ne_m = f(Re_m)$  for: a) three impeller systems, b) five impeller systems

It has been shown that for double Rushton turbine system the relation of power number  $Ne_m$  vs. Reynolds number can be described by  $Ne_m \propto Re_m^{-0.1}$  whereas for FBT's and PBT's it is related by  $Ne_m \propto Re_m^{-0.25}$ . For vessels equipped with three, four and five impellers it has been found that the mixing power reduction is smaller in comparison with double impeller systems. The effect is connected with the distance between impellers. The enlargement of number of impellers causes the reduction of distance between them and the change in the hydrodynamic conditions. It has been shown that mixing power for three and more impellers is not proportional to the number of impellers. The hydrodynamic interactions between particular impellers lead to the reduction of total power requirements. The increasing of molecular weight of Na-CMC caused the increase in mixing power reduction. The phenomena can be interpreted by the fact that the Na-CMC<sub>700,000</sub> molecule is like a spaghetti, and during mixing process this molecule is developing.

## References

- Broniarz-Press, L., Borowski, J. and Agacinski, P., (1997) *Chemical Engineering and Apparatus*, 36,12-17.
- Calderbank, P. H., Moo-Young, M. B., (1961) *Transactions of the Institution of Chemical Engineers*, 39,337-347.
- Metzner, A. B., Otto, R. E., (1957) *American Institute of Chemical Engineering Journal*, 3,3-10.
- Paul, E. L., Atiemo-Obeng, V. A., Kresta, S. M., *Handbook of Industrial Mixing. Science and Practice*, Willey-Interscience, US (2003).



## Hydrodynamics and Gas-Liquid Mass Transfer in a Rectangular Bubble Column

A. Elena M. Cachaza<sup>a</sup>, B. Elena Díaz Martín<sup>a</sup>, C. Francisco J. Montes<sup>a</sup> and D. Miguel A. Galán<sup>a</sup>

<sup>a</sup> *Department of Chemical Engineering, University of Salamanca, Plaza de los Caídos s/n., 37008 Salamanca, Spain*

### 1. Summary

This work presents the estimation of the efficiency of oxygen mass transfer in a two dimensional bubble column using an air- water system related to the hydrodynamics developed inside the reactor at different aspect ratios and superficial gas velocities. It's also presented a study of the interfacial area between the phases (bubble size), its relationship with the superficial gas velocity and its influence in the volumetric mass transfer coefficients ( $k_L a$ ) measured.

Keywords: hydrodynamic, gas-liquid mass transfer, volumetric mass transfer coefficient, interfacial area, bubble column

### 2. Extended Abstract

Bubble columns (BC) are multiphase reactors widely employed in chemical, biochemical and petrochemical industrial processes due to their advantages such as simple construction and excellent heat and mass transfer. The main objective of the design and operation of this multiphase equipment is the maximization of its performance, that is, the calculation of the optimum conditions for mass and heat transfer. Transfer phenomena taking place across the gas-liquid interface of the bubbles, depend strongly on the mixing capacity of the system and, therefore, on the existing flow regimes inside the bubble column.

For volumetric mass transfer coefficient ( $k_L a$ ) measurements in BCs, the dynamic gas absorption method has been popularly used in BCs for its simplicity and reliability. In the dynamic method, the measured transient concentration profiles of the introduced gas represent not only the extent of gas-liquid mass transfer rate but also the phase mixing. Hence, a reactor model is needed to estimate  $k_L a$  values by fitting the experimental data. Based on its advantages, the dynamic method has been chosen in this work and  $k_L a$  values have been estimated using two reactor models: (1) the continuous stirred tank reactor (CSTR) model, which assumes perfect mixing for both phases and constant gas concentration in the gas phase; and (2) the axial dispersion model (ADM). Both of them are completed with another model provided by the gas sensor used for the measurement of the dissolved gas concentration.

Despite the extended use of the dynamic method, there are still some unsolved problems when calculating accurate values of  $k_L a$ . Among them, the position of the oxygen sensor in the bubble column has been pointed out as a variable determining the resulting  $k_L a$  value. This variable is also studied in this research in order to determine its influence on the calculated mass transfer coefficients.

Another important parameter in the design of mass exchangers and chemical reactors using gas bubbling is the interfacial area, i.e., the bubble diameter. Its importance comes

from the fact that the mass transfer phenomenon takes place across this gas-liquid interface and it is influenced by the superficial gas velocity that modifies the number, the size and the shape of the bubbles. [1]

In this way, the work presented has the following main parts:

- (1) The study of the influence of the hydrodynamics in the determination of the volumetric mass transfer coefficients.
- (2) The fitting of the experimental results to the CSTR and AD mass transfer models considering the existence of a sensor delay in the measurements and the comparison of the  $k_L a$  estimated by both of them in the 2D bubble column reactor at the tested operating conditions. The models are as follows:

a. CSTR [2]

i. Assumptions:

1. Well- mixed liquid phase. Actually, the model assumes perfect mixing for both phases.
2. Oxygen depletion from the gas bubble negligible. The gas concentration in the gas phase is constant.
3. Mass balance for oxygen based on a statistic liquid volume

ii. In the bulk liquid phase:

$$\frac{dC_L}{dt} = k_L a \cdot (C_L^* - C_L)$$

iii. In the proximity of the sensor:

$$\frac{dC_S}{dt} = k_S \cdot (C_L - C_S)$$

b. One dimensional AD model [3]

i. Assumptions:

1. The local gas hold up is equal to the overall gas hold up  $\epsilon_G$
2. Liquid velocity negligible.

ii. Liquid phase:

$$\frac{\partial C_L}{\partial t} = D_L \frac{\partial^2 C_L}{\partial z^2} + \frac{k_L a}{\epsilon_G} \cdot (HC_G - C_L)$$

iii. Gas phase:

$$\frac{\partial C_G}{\partial t} = D_G \frac{\partial^2 C_G}{\partial z^2} - u_G \frac{\partial C_G}{\partial z} - \frac{k_L a}{\epsilon_G} \cdot (HC_G - C_L)$$

(3) The relationship between mass transfer and the position of the gas sensor in the BC.

(4) The influence of the interfacial area of bubbles on the mass transfer coefficient ( $k_L$ )

## References

- [1] Pohorecki, R., Moniuk, W., Zdrójkowski, A. and Bielski, P. Hydrodynamics of a pilot plant bubble column under elevated temperature and pressure (2001) *Chemical Engineering Science* 56, 1167-1174
- [2] Gourich, B., EL Azher, N., Soulami Bellhaj, M., Delmas, H. Bouzidi, A. and Ziyad, M. Contribution to the study of hydrodynamics and gas-liquid mass transfer in a two- and three-phase split- rectangular airlift reactor (2005) *Chemical Engineering and Processing*, 44, 1047-1053.
- [3] Han, L. and Al- Dahhan, M.H. Gas- Liquid mass transfer in a high pressure bubble column reactor with different sparger designs (2006) *Chemical Engineering Science* 62, 131-139

## **The effect of liquid viscosity on the void friction in a two-phase gas-liquid flow in narrow mini-channels**

J. Sowiński, M. Dziubiński

*Technical University of Łódź, Faculty of Process and Environmental Engineering.*

*Wolczanska 213 90-924 Lodz, Poland*

### **1. Summary**

Investigations of phase fractions in the two-phase liquid–gas flow with liquids of viscosities differing from water viscosity are presented in the paper. In experiments two channels 15 mm wide and with different slit sizes 1.23 mm and 2.31 mm were used. Liquid phase was water and aqueous saccharose solutions. The fraction of gas phase was determined on the basis of an image of two-phase mixture flowing in the channel, recorded by a quick DDC camera. From the experiments it followed that liquid viscosity had a significant effect on phase fractions in the flowing two-phase mixture. The experimental data were correlated using a drift flux model.

Keywords: void fraction, two-phase flow, mini channel, narrow channel, viscosity.

### **2. Extended Abstract**

In narrow mini-channels important differences can be observed in two-phase flow hydrodynamics as compared to bigger ducts. This refers first of all to flow structures, phase fractions and flow resistance. Studies published so far have referred mainly to the description of flow hydrodynamics of two-phase water-air mixture [1-4]. There are no works dedicated to the flow of two-phase mixtures with liquids of higher viscosities [2].

The aim of experiments was to investigate the effect of liquid viscosity on phase fractions in the two-phase liquid-gas flow in narrow mini-channels and to compare the obtained results with relations available in the literature.

In the experiments two channels 15 mm wide with slit size 1.23 mm and 2.31 mm were used. The two-phase mixture flowing in the channel was filmed with a quick MV-D752 – 160 Photonfocus camera and the image was recorded on a hard disc. Next, basing on the recorded image phase fractions in the flowing two-phase mixture were determined.

Liquid phase in the experiments was water and two aqueous solutions of saccharose (saccharose 1 and saccharose 2). Viscosities and densities of the tested liquids were:

$\mu_w=0.001$  Pa·s,  $\rho_w =1000$  kg/m<sup>3</sup>,  $\mu_{s1}=0.004$  Pa·s,  $\rho_{s1} =1160$  kg/m<sup>3</sup>,  $\mu_{s2}=0.0097$  Pa·s and  $\rho_{s2} =1185$  kg/m<sup>3</sup>, respectively. The gas phase was air. Apparent liquid and gas flow velocities ranged from 0.011 to 2.30 m/s and from 0.011 to 5.65 m/s, respectively.

As a result of the investigations a very distinct effect of liquid viscosity on the gas fraction in the flowing two-phase mixture was observed. It was found that with an increase of liquid viscosity the gas phase fraction decreased. An attempt was made to correlate the experimental values of gas phase fraction by means of the following relation based on the drift model [2,3] – cf. Fig. 1 for examples of experimental data.

$$v_G = \frac{u_{SG}}{\epsilon_G} = C_0 v_m \quad (1)$$

where:  $u_{SG}$ - superficial gas velocity,  $v_G$  – mean gas phase velocity,  $v_m$  – mixture flow velocity,  $\epsilon_G$  – gas void fraction,  $C_0$  – distribution parameter

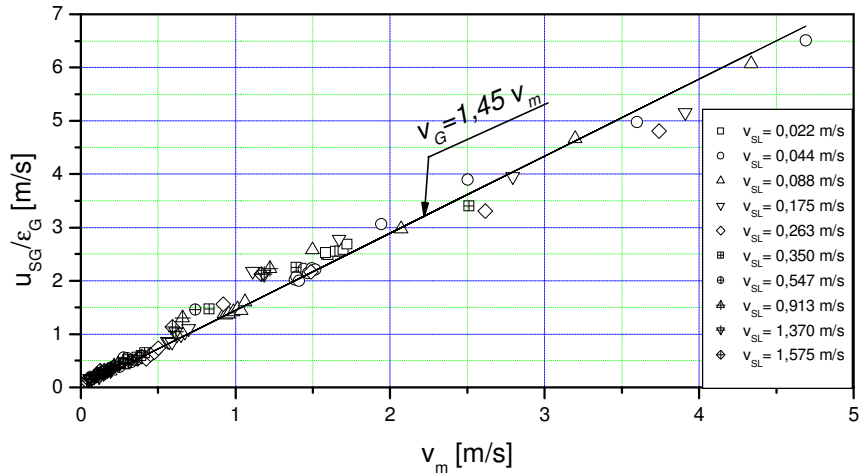


Fig 1. Drift-flux correlation for sccharose 1,  $\delta=2.31$  mm

A very distinct influence of liquid viscosity on distribution parameter  $C_0$  was observed. It assumed the lowest values for the flow with water ( $C_0= 1.23$ ), while the highest for the solution of saccharose 2 ( $C_0=1.76$ ).

### References

- [1] English N.J., Kandlikar S.G.: *An experimental investigation into the effect of surfacants on air-water two-phase flow in minichannels*, 3<sup>rd</sup> International Conference on Microchannels and Minichannels, June 2005, 13.
- [2] Dziubiński M.: *Hydrodynamika przepływów mieszanin dwufazowych ciecz-gaz*, Politechnika Łódzka, Łódź, 2005.
- [3] Mishima K., Hibiki T.: *Some characteristic of air-water two-phase flow in small diameter vertical tubes*, Int. J. Multiphase Flow 1996, 22, 703.
- [4] Ide H., Fukano T.: *Experimental research on the correlations of holdup and frictional pressure drop in air-water two-phase flow in capillary rectangular channel*, Experimental Thermal Science 2005, 29, 833.

## Hydrodynamic Correlations for the Design of Conical Spouted Beds with Open-Sided Draft-Tube

H. Altzibar, G. Lopez, J. Bilbao, S. Alvarez, M.J. San José, M. Olazar

*Department of Chemical Engineering, University of the Basque Country, P.O. Box 644, 48080 Bilbao, Spain. [martin.olazar@ehu.es](mailto:martin.olazar@ehu.es). Phone: 946012527. Fax: 946013500*

### 1. Summary

The hydrodynamics and performance of conical spouted beds provided with open-sided draft tube have been studied for the treatment of fine particles. The results have been compared with those obtained with non-porous draft tubes in a previous paper under the same experimental conditions. Correlations for calculation of the minimum spouting velocity and operation pressure drop have been developed.

Keywords: hydrodynamic correlations, conical spouted bed, open-sided draft tube, minimum spouting velocity, pressure drop.

### 2. Extended Abstract

Spouted beds with fully conical geometry combine the features of the cylindrical spouted beds (such as the capacity for handling coarse particles, small pressure drop, cyclic movement of the particles and so on) with those inherent to their geometry, such as stable operation in a wide range of gas flow-rates. This versatility in the gas flow-rate allows for handling particles of irregular texture, fine particles and those with a wide size distribution and sticky solids, whose treatment is difficult using other gas-solid contact regimes. Moreover, operation can be carried out with short gas residence times (as low as milliseconds) in the dilute spouted bed [1].

In the past, such spouted beds have been widely used for drying, granulating, and mixing, but attempts have recently been made to make better use of their flexibility by using them for gasification, pyrolysis, combustion and three phase reactions [2].

A crucial parameter that limits the scaling up of spouted beds is the ratio between the inlet diameter and particle diameter. In fact, the inlet diameter should be smaller than 20-30 times the average particle diameter in order to achieve spouting status. The usual solution in conventional spouted beds is the use of a draft-tube. Nevertheless, the hydrodynamics with this tube is different to that of plain beds.

A hydrodynamic study of conical spouted beds with draft-tube, Figure 1, has been carried in a previous paper [3]. In this one, conical spouted beds with open-sided draft-tubes have been studied in order to check its potential application in the

handling of fine particles, Figure 2. Different types of tubes have been used. Thus, draft-tubes of different diameter (lower or higher than the inlet diameter), different opening wide, length above the bed, ring(s) at different levels and closed and open upper outlet have been used. Moreover, stable operation regimes have been delimited.

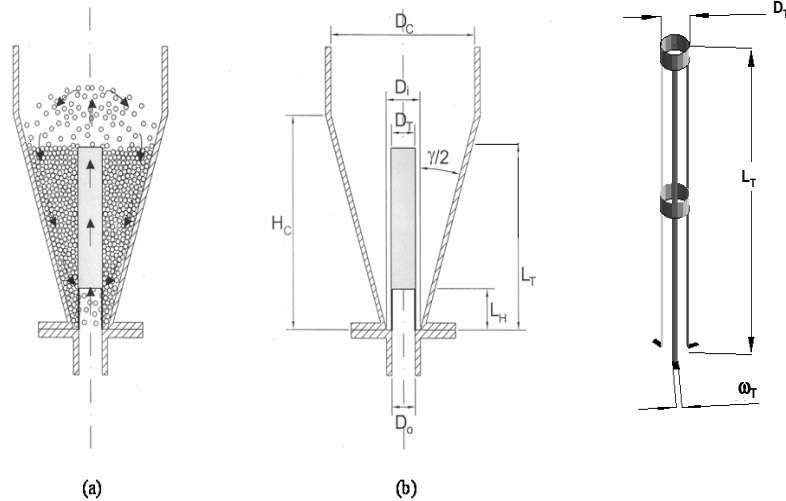


Figure 1. Conical contactors with (non-porous) draft tube. (a) Zones in the bed. (b) Geometric factors

Figure 2. Scheme of the open-sided draft tube

Beds provided with open-sided draft-tube require a higher velocity to open the spout than beds with a solid draft-tube. Likewise, operation pressure drop is also higher. The values of these parameters are intermediate between those for plain beds and non-porous draft-tube spouted beds. Nevertheless, the solid circulation rate (turbulence) is much higher with open-sided draft-tube, which is due to the solid cross-flow from the annulus into the spout. Aeration of the annulus is also improved with this type of device.

Based on dimensional and statistical analysis, correlations have been determined for the minimum spouting velocity (1) and operation pressure drop (2).

$$(\text{Re}_0)_{ms} = 0,632 * Ar^{0,474} * \left(\frac{H_0}{D_0}\right)^{1,30} * \left(\frac{A_0}{At}\right)^{0,284} * \left(\tan\left(\frac{\gamma}{2}\right)\right)^{0,429} \quad (1)$$

$$\frac{\Delta P_s}{H_0 \rho_b g} = 0.0029 * \left(\tan\left(\frac{\gamma}{2}\right)\right)^{-0.195} * \left(\frac{H_0}{D_0}\right)^{-0.770} * \left(1 + \left(\frac{|\Delta D|}{D_0}\right)\right)^{-0.122} * \left(\frac{A_0}{A_r}\right)^{1.28} * ((\text{Re}_0)_{ms})^{1.07} \quad (2)$$

## References

1. Olazar, M.; San José, M. J.; Zabala, G.; Bilbao, J. Chem. Eng. Sci., 49, 4579(1994)
2. Lu, W.J., Chang, C.M., Chem. Eng. Sci., 49, 1465(1994).
3. H. Altzibar, S. Alvarez, M.J. San José, R. Aguado, J. Bilbao, M. Olazar, in Fluidization XII, (in press), (2007)

## **A visualisation technique for quantifying mixing time in stirred tank**

E. Brunazzi, S. Pintus

*Department of Chemical Engineering, University of Pisa, Via Diotisalvi 2, I-56126 Pisa, Italy*

### **1. Summary**

A non intrusive optical technique has been developed allowing to quantifying the mixing evolution and mixing time in stirred tank reactor. This paper describes the novel technique which has been applied to study a non standard geometrical configuration.

Keywords: mixing time, light absorption, image analysis, visualisation

### **2. Extended Abstract**

A technique for quantifying the mixing evolution in a transparent stirred tank is proposed. It consists of capturing on video a colorisation-decolorisation process in a stirred vessel and apply the fundamentals of light absorption imaging technique in combination with image analysis. The advantages of the method developed are that

- 1) there is no disturbance of the fluid flow,
- 2) no preliminary calibration is necessary,
- 3) it allows to quantify the mixing evolution in the whole vessel.

This paper describes protocols for carrying this method out. In addition examples of experimental results obtained for both a standard and a non standard geometrical mixing system are given and discussed.

The results indicate that the technique has significant potential to provide insight to study and compare mixing efficiency of different impellers or mixing systems.

### **Acknowledgement**

This work was financially supported by the “Ministero dell’Istruzione, dell’Università e della Ricerca Scientifica” (PRIN 2005). The authors are also grateful to Ing. Francesco Adorisio for his help in the experimentation.

Book of Abstracts  
European Congress of Chemical Engineering (ECCE-6)  
Copenhagen, 16-20 September 2007



## Hydrodynamics of „jet” type outflow from process installations

H. Fidos,<sup>a</sup> M. Dziubiński,<sup>a</sup> R. Krokos,<sup>a</sup>

<sup>a</sup>*Department of Chemical Engineering, Technical University of Lodz, Wolczanska str. 213, 90 – 924 Łódź, Poland*

### 1. Summary

Emergency outflows of liquids through disrupted pipeline walls operating under pressure were studied. Attention was focussed on outflows from horizontal fissures of different lengths and on the analysis of volume rate and range of the outflowing liquids. The experimental liquid was water. Experimentally measured parameters were compared with theoretically calculated values.

Keywords: outflow, pipeline, discharge.

### 2. Extended Abstract

A schematic diagram of an experimental set-up is shown in Fig. 1. The exchangeable section of the installation was equipped with a flange which enabled mounting of flat covers with orifices of different shapes and cross-sections. The orientation of this section could be changed. Fissures 1 mm wide and 24.4, 64.4 and 90 mm long were applied in the study. The covers were built from two spliced layers of organic glass.

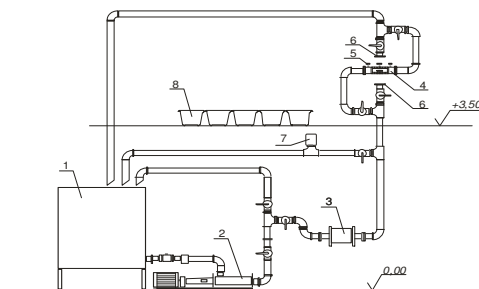


Fig. 1. Schematic diagram of the experimental set-up: 1 – storage tank, 2 – screw pump, 3 – electromagnetic flowmeter, 4 – measuring section, 5 – pressure transducer, 6 – flanges for vertical mounting of the measuring section, 7 – pneumatic valve, 8 – measuring vessels.

The outflowing liquid jet was directed to measuring vessels with inlets of rectangular cross-section arranged on a big plane. Such method of reception of the outflowing liquid jet enabled the estimation of its propagation on a plane. The time of outflow of the jet received in the measuring vessels was determined, the mass of liquid in

particular vessels was specified, the jet range was specified and the size of liquid jet was measured by the volumetric method.

The jet range was determined for the jet axis in its final position (in the plane of inlet to the measuring vessels) and confirmed with theoretical ranges calculated on the basis of the equation for oblique projection.

$$z_i = 2 \cdot \beta \cdot \sqrt{\frac{p_o \cdot y}{\rho \cdot g}} \quad (1)$$

The velocity coefficient is defined by the equation

$$\beta = \frac{Q_v}{S_o} \sqrt{\frac{\rho}{2p_o}} \quad (2)$$

Figure 2 shows a comparison of experimental and theoretical values of the range of liquid jet flowing out from the fissure in the pipe wall.

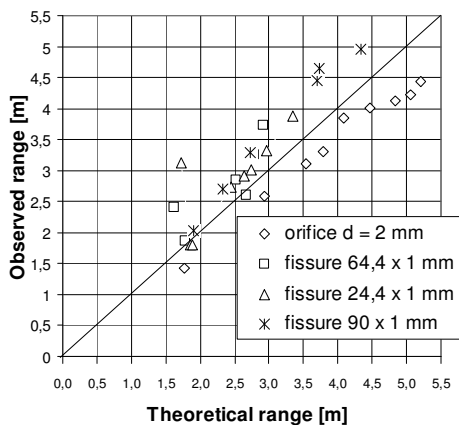


Fig. 2. Comparison of theoretical and experimental values of the jet range

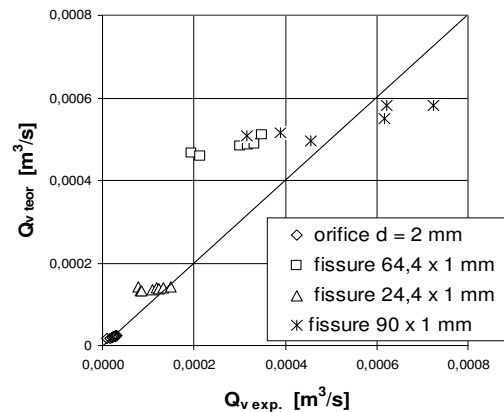


Fig. 3. Comparison of theoretical and experimental values of jet volume.

A subsequent value which theoretical determination is very suitable for the analysis of emergency outflow from pipelines, is the liquid volume rate. For the scope of the performed measurements this value was calculated basing on the equation:

$$Q_{v_o} = \varphi \cdot S_o \sqrt{2gH} \quad (3)$$

The value of outflow coefficient  $\varphi$  was determined based on literature data. The assumed outflow coefficient was equal to 0.65. Figure 3 shows a comparison of theoretical and experimental volume rates of the liquid.

As follows from the diagram Fig. 2, the range of jet from the fissures of determined shapes can be estimated basing on equation (1) with an error not exceeding 35%. As can be seen in the Fig. 3, the theoretical values of the liquid volume are overestimated.

## References

Troskoleński A.T, *Hydromechanika techniczna*, PWT, Warszawa, 1954.

Mitosek M, *Mechanika płynów w inżynierii i ochronie środowiska*, PWN, Warszawa, 2001.

## Session T2-6a: Interfacial & Colloidal Phenomena – I

<b>Abstract Number</b>	<b>Paper Title &amp; Authors</b>	<b>Included</b>
143	Interfacial Tension Behavior in Oil-Water Systems Related to Crude Oil Recovery V Hornof, G H Neale	Yes
626	The Experimental Study on Mean Drop Size in a Horizontal Mixer-Settler Extractor A Khakpay, H Abolghasemi, M G Maragheh, A S Khorshidi	Yes
1095	A study of how surface wetting may affect the coating layer when coating paper C G Berg, N C Berg	Yes
2197	Interfacial instability on bubble surface during chemisorption S P Karlov, D A Kazenin, A V Vyazmin, D A Polyanin	Yes
2760	Three-phase behavior of surfactant-polymer mixture S B Chen, G Q Zhao	Yes
3602	Effect of surfactant on stagnant slow aggregation kinetics of polymer colloids M Lattuada, H Wu, M Morbidelli	Yes

Session T2-6a

## **Interfacial Tension Behavior in Oil-Water Systems Related to Crude Oil Recovery**

Vladimir Hornof and Graham H. Neale

*Department of Chemical Engineering, University of Ottawa, P.O. Box 450, Stn.A, Ottawa, ON, Canada  
K1N 6N5*

### **1. Summary**

Liquid-liquid interfaces are present in many systems of industrial importance. The behavior of the interface between two immiscible or partially-miscible liquids is governed by its interfacial tension. Many systems of interest involve mass transfer or chemical reaction at the interface and as a consequence, interfacial tension may become time dependent (transient) and often both time and location dependent (dynamic). Of particular interest in the present work is the situation when an acidic crude oil is being displaced by an injected alkaline solution inside the porous rock of an oil reservoir. The resulting interfacial phenomena and their effect on oil displacement patterns and ultimate recovery will be discussed in reference to experimental results obtained in the authors' laboratory.

Keywords: interfacial tension, dynamic interfacial tension, interfacial reaction, flow in porous media, crude oil displacement

### **2. Extended Abstract**

Interfacial tension is an important property of systems consisting of two phases. Liquid-liquid interfaces are often encountered in both nature and industry. In immiscible liquid-liquid systems, such as that composed of pure octane and pure water, the interfacial tension between the two components is essentially constant. However, most real-life oil-water systems do not fall into that simple category. Often, surface-active substances are present. These may be a part of the original system, or they may have been added to the system for a specific purpose. Surface-active substances may also enter the system through interaction of resident fluids with their surroundings. For example, in the process of enhanced oil recovery by an injection of aqueous fluids, surface-active substances may be extracted from the surrounding rock or soil, or, alternatively, they may be produced through oxidation of reactive oil components by oxygen dissolved in water. Of particular interest in the present investigation is the case in which a surfactant is produced *in-situ* via a chemical reaction occurring at the interface. Such a situation is encountered when an alkaline solution is injected into an oil reservoir with a crude oil containing dissolved acidic components. Interfacial chemical reaction between the alkali and the oil-borne

acids produces surface-active substances that become adsorbed at the interface. Such systems rarely attain a true equilibrium, and consequently the oil-water tension at the interface is dependent on time (i.e., transient in nature). When the reacting oil-water interfaces are continuously moving and changing, as in the case of two-phase flow during which the crude oil is being continuously displaced by injecting an alkaline solution inside a porous rock, the interfacial tension becomes also location-dependent and it thus acquires a truly dynamic character. Resulting interfacial tension gradients give rise to Marangoni flows. The exact behavior of a chemically reacting, flowing two-phase system (for example, in terms of displacement instabilities and oil recovery) then becomes very difficult to predict and simulate. Often, unexpected flow patterns are observed. This is also due to the fact that both added and *in-situ* generated surface-active substances may undergo adsorption on solid surfaces, thus altering the wettability of the rock, usually from strictly water-wet to at least partially oil-wet. This may also produce a strong effect on the flow patterns observed and, ultimately, on the recovery of oil from the reservoir. The above mentioned phenomena will be discussed with reference to experimental results obtained in the authors' laboratory.

## The Experimental Study on Mean Drop Size in a Horizontal Mixer-Settler Extractor

A. Khakpay<sup>a</sup>, H. Abolghasemi<sup>a</sup>, M. Ghannadi-Maragheh<sup>b</sup>, A. Salimi-Khorshidi<sup>a</sup>

<sup>a</sup>Department of Chemical Engineering, University of Tehran, Tehran, Iran

<sup>b</sup>Department of Chemical Engineering, Amir Kabir University of Technology, Tehran, Iran

### 1. Summary

In this work, the effects of impeller speed and holdup on mean drop size,  $D_{32}$ , was investigated in a mixer settler. Two series of experiments, with and without surfactant, were performed to analyze the presence effect of surfactants on  $D_{32}$ . In first series, without surfactant, a correlation was derived, so that  $D_{32}$  found to be dependant on impeller speed with a power law function having an exponent of -1.208. Moreover,  $D_{32}$  depends on holdup with an increasing linear function. In second series, using two surfactants (Sodium Dodecyl Sulfate and Aniline),  $D_{32}$  at low surfactant concentration decreased significantly with an increase in surfactant concentration, whereas  $D_{32}$  didn't depend on surfactant concentration at high surfactant concentration. For both surfactants, in surfactant concentration between 0.003 and 0.005 %wt, a critical zone was observed. Also, the results showed that the decreasing rate of  $D_{32}$  decreased with an increase in impeller speed, likewise the increasing rate of  $D_{32}$  decreased when the holdup increased for both surfactants. A correlation was obtained for each surfactant and compared with experimental results. The exponent of power law function, in comparison with first series of experiments, was decreased about 9.9% and 16.7% for system containing Aniline and SDS, respectively.

Keywords: mean drop size, surfactant, impeller speed, holdup, mixer-settler

### 2. Extended Abstract

#### 2-1. Effect of impeller speed on mean drops size

Hinze and Kolmogorov were predicted that  $D_{32}$  proportioned with a power function of impeller speed that is well verified with our system. The same results were presented by Masbernat et al. [1]. When surfactants were added to the liquid-liquid emulsion, the decreasing rate of  $D_{32}$  decreased with an increase in impeller speed and the exponent of the power function increased to -0.766 and -0.641 for SDS and Aniline, respectively.

#### 2-2. Effect of holdup on mean drops size

In system without surfactant,  $D_{32}$  was increased with an increase in holdup with linear fashion. The same results were presented by Masbernat et al. [1]. When surfactants were

added to the system, the increasing rate of  $D_{32}$  decreased with an increase in holdup and the slope of linear function, in comparison with the system without surfactant, decreased about 77.3% and 60.5% for SDS and Aniline, respectively.

### 2-3. Effect of surfactant concentration on mean drop size

Results show that for both surfactants, the curves ( $D_{32}$  versus surfactant concentration) consist of two distinct regions: a significant decrease of  $D_{32}$  in the range of surfactant concentration between 0 and 0.003 wt %, and a plateau region at surfactant concentrations above 0.005 wt %. The same results have been presented by Denkov et al. [2]. In the surfactant concentrations between 0.003 and 0.005 wt %, a critical zone is observed. In this zone,  $D_{32}$  has a minimum value.

### 2-4. Correlation of mean drop size

The correlation for predicting of  $D_{32}$  for system without surfactant is:

$$\frac{D_{32}}{D_i} = 0.872(1 + 1.937\phi)We_i^{-0.604} \quad (1)$$

Average Absolute Relative Deviation, %AARD, for this correlation was about 3% which shows that equation (1) has a good agreement with experimental data. For investigation of accuracy of the correlation, we compared this correlation with Godfrey's correlation and %AARD was calculated [3]. %AARD for Godfrey's correlation is about 7.8%. Consequently, we decreased the %AARD about 61.5%.

In addition, the correlation for predicting of  $D_{32}$  for SDS is:

$$\frac{D_{32}}{D_i} = 0.562(1 + 1.65\phi)We_i^{-0.523} \quad (2)$$

And for aniline is:

$$\frac{D_{32}}{D_i} = 0.766(1 + 1.807\phi)We_i^{-0.581} \quad (3)$$

The amount of %AARD for SDS was measured about 16.7% and for aniline was about 9.9%. In these correlations, the exponents of Weber number were -0.523 and -0.581 for SDS and aniline, respectively. These exponents had some deviation from Hinze and Kolmogorov theory. The SDS system had more deviation than the aniline system. It can be due to the fact that the effect of SDS on interfacial tension is more pronounced than aniline. If we compare equations (2) and (3) with equation (1), we can conclude that all constants of equations (2) and (3) were decreased when surfactant was added to the system. This decrease for SDS system is more than aniline system.

## References

- Desnoyer, C., Masbernat, O. and Gourdon, C., (2003) *Chemical Engineering Science*, 58, 1353 – 1363.  
Tcholakova, S., Denkov, N. D. and Danner, T., (2004) *Langmuir*, 20, 7444-7458.  
Godfrey, J. C. and Slater, M. J., *Liquid-liquid extraction equipment*, Wiley, USA (1994).



## **A study of how surface wetting may affect the coating layer when coating paper**

C.-G. Berg<sup>a</sup>, N.-C. Berg<sup>b</sup>

<sup>a</sup>*Process Design Laboratory, Department of Chemical Engineering, Åbo Akademi University, Biskopsgatan 8, FIN-20500 Åbo, Finland, E-mail: cberg@abo.fi*

<sup>b</sup>*Equitor LTD, P.O.Box 20, FIN-02701 Grankulla, Finland*

### **1. Summary**

Light Weight Coated (LWC) paper and many other paper grades are made in coating units producing 100 000 ton paper/year or far more. The paper prize for LWC has during the last years been around 600 euros/ton paper, and for extraordinary coated paper grades much more. Single industrial coating units are considered to be the step that controls final quality and hence one of the most essential components when controlling annual turnovers greater than 60 000 000 euro/year. We may now say that the scale of economics calls for advanced and reliable multi-disciplinary models, to assist high-tech product innovation in the field of paper coating. Advanced drying studies have further shown that chemical additives in the base paper or coating color may reduce or increase energy efficiency, productivity and quality considerably, (e.g. paper ink interaction, print mottle etc.). Our work will therefore aim to illuminate the knowledge of dynamic drainage, which is needed to enhance conventional or novel surface treatment techniques (sym-sizing, plasma, curtain coating, etc.), that are dependent of fine tuning of the in-plane and out-of-plane drainage mechanisms such as surface wetting.

Keywords: drying, porous media, colloidal system, wetting, sorption

### **2. Extended Abstract**

#### **The paper coating process**

The formulation of a high-performance paper coating necessarily requires a strong understanding of the underlying interfacial and colloidal interaction mechanisms dominating first in the wet state and then during dewatering and consolidation. There are simultaneous interactions between pigments, polymers (stabilizers, binders and thickeners) and other coating components. The distribution of components within the dry coating layer and especially at its surface determines the optical and mechanical properties and printability of the final product. The extremely fast and harsh drying process of coated paper is impossible to measure. The objective of this work will therefore be to explore and illuminate basic liquid state and movement already in the

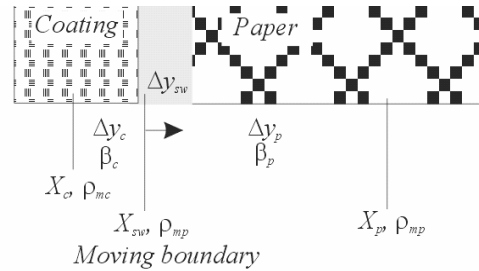
initial phase (less than 100-300 milliseconds) when coating color is brought to the surface of the hygroscopic paper (i.e. coating solid contents from 55 % to 65 %) [1,2].

### Defining surface wetting

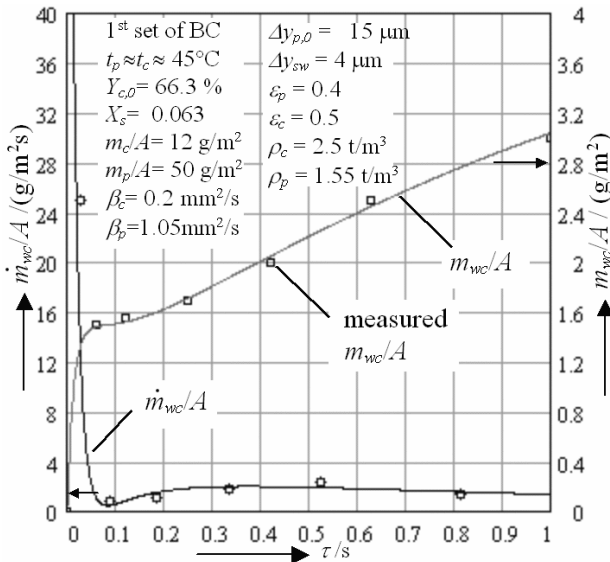
We start by defining that a homogenous flux of water (or water vapor when changing indexing) through any surface may be written in the following form [1],

$$\frac{\dot{m}_w}{A} = \frac{\beta_w}{\Delta y} (\rho_{mbd0} X_0 - \rho_{mbd1} X_1) \quad (1)$$

A set of differential equations including sinks and sources are solved using equation (1) and property variables and problem formulation shown in the figure to the right.  $\Delta y_{sw}$  is the surface-wetting layer, and could also be called a boundary storage zone.



### Calculated surface wetting



The figure to the right shows calculated and measured drainage values of LWC-paper as a function of contact time,  $\tau$ . Boundary conditions are included in the figure, these are: paper temperature,  $t_p$ , coating temperature,  $t_c$ , measured and calculated drainage  $m_{wc}/A$ , measured and calculated mass flux  $\dot{m}_{wc}/A$ , the moving boundary  $\Delta y_c$ , the calculated moisture content of the surface wetting zone  $X_{sw}$ , the calculated moisture content of the coating color  $X_c$ , the dryness of the coating color  $Y_c$ , the mass transfer coefficients,  $\beta_c$ ,  $\beta_p$ , and geometrical boundary conditions.

Novell curtain coating and spray coating methods highlight now the role of surface wetting and surface chemistry, mainly due to small application pressures. There is therefore an increasing need to understand the development of both coating systems and measurement methods when we are trying to fulfil the need of the end consumer.

### References

Berg C-G., Berg N-C. and Karlsson M, 2005, *A Study of Surface Wetting when Coating Paper*. *Drying Technology journal*. 23, (11) pp 2105-224. ISSN 0737-3937  
 Yamazaki, K.; Nishioka, T.; Hattori, Y.; Fujita, K., 1993, *Print mottle effect of binder migration and latex film formation during coating consolidation*, *Tappi Journal*, May 1993, Vol. 76(5), page 79-84.

## **Interfacial instability on bubble surface during chemisorption**

S.P. Karlov, D.A. Kazenin, A.V. Vyazmin, D.A. Polyaniin

*Department of Chemical Engineering, Moscow State University of Environmental Engineering, Staraya Basmannaya str. 21/4, 105066, Moscow, Russia*

### **1. Summary**

Interference laser spectroscopy was used to study the macrokinetics of absorption of carbon dioxide by aqueous solutions of chemisorbents. Chemisorption was shown to be a complex and multistage process. Its evolution included the occurrence of a diffusion-controlled chemical reaction close to the interphase boundary, the appearance of instability, and the development of convection in the liquid phase. The main rules governing stability loss during chemisorption were considered.

Keywords: interference spectroscopy, chemisorption, instability, convection

### **2. Extended Summary**

The problem of generation and time evolution of convective structures arisen due to chemical reactions became a subject of numerous studies in connection with the search for intensive mass transfer mechanisms than molecular diffusion. The phenomena of chemo-gravitational and capillary instability manifest itself in the appearance of convective flows on the interface due to gravitation and surface forces.

With the use of interference microscope we could visualized at a real time the evolution of interfacial phenomena on a spherical bubble of carbon dioxide formed on the end of microsyringe needle and mounted in the water solution of a base. This gave the possibility to describe in detail the principle stages of instability, to estimate its duration and to suggest a physical interpretation of the experimental pattern. Polarizing interference microscope is schematically represented in Figure 1.

The chemisorption cell (7) is made from transparent optic glass which gives the possibility to inspect the gas-liquid interface and the volumes of phases near the interface. The experimental patterns shown in Figure 2 attest the complex time and spatial character of the evolution of chemisorption.

The appearance of the reaction product at the bubble surface is observed after some period which may last several seconds after the inert gas is substituted by carbon dioxide (Fig 2a). One can see the flows of the liquid heated due to of reaction. At this stage the reaction seems to proceed via the diffusion-kinetic mechanism. At the same time the movement of the liquid along the interface is detected. Such behavior is inherent in chemo-capillary instability which intensifies mass transfer at the interface.

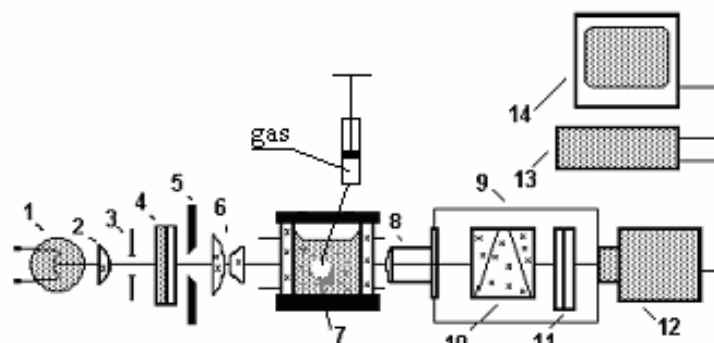


Figure 1: Polarizing interference microscope: (1) filament lamp; (2) lens; (3) aperture; (4) polarizer; (5) slit-shaped aperture; (6) condenser; (7) cell; (8) microlens; (9) polarizing interference unit; (10) prism; (11) analyzer; (12) TV camera; (13) video type recorder, and (14) TV monitor

Later on, the film of reaction product becomes more and more thick and starts to precipitate along the bubble surface to its bottom as if it is a separate quasi phase, possessing its own surface tension. This corresponds to the chemo-gravitational mechanism of instability.

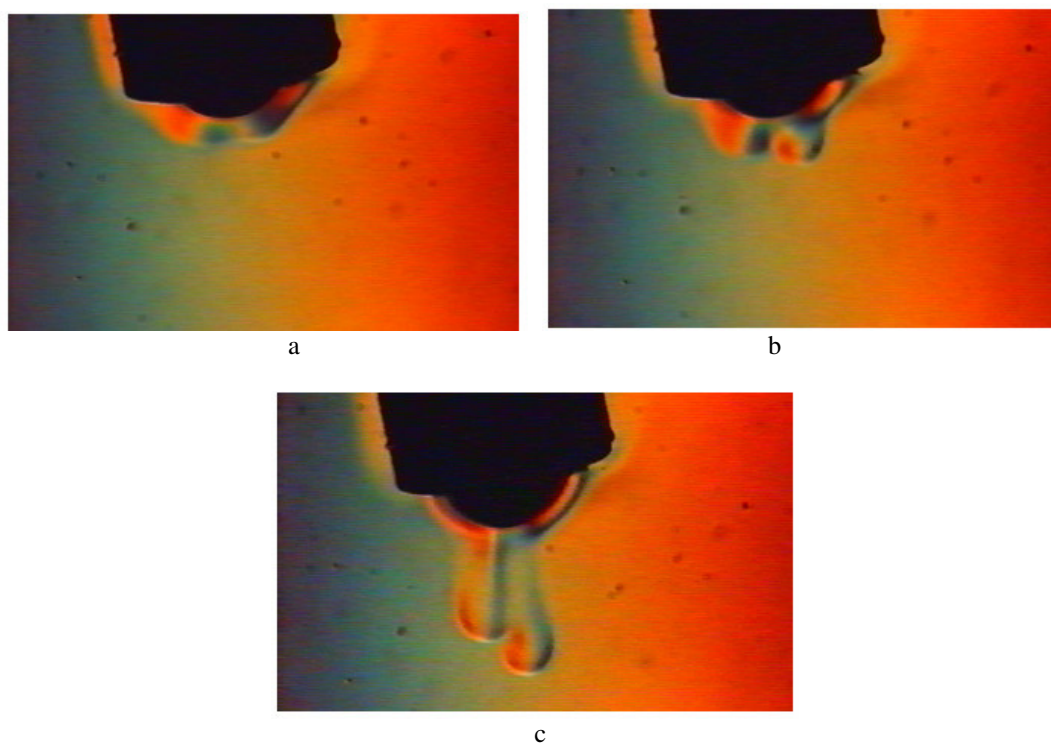


Figure 2: Interference patterns corresponding: (a) at the moment of instability generation on the interface; (b) to the appearance of droplets; (c) to the movement of product droplets from the interface

At the last stage, droplets of reaction product are formed at the bottom part of the bubble. The size of droplets is defined by the chemical composition of the water solution. Periodically droplets leave the surface and precipitate into the surrounding liquid without intermixing.

## Three-phase behavior of surfactant-polymer mixture

S. B. Chen, G. Q. Zhao

*Department of Chemical and Biomolecular Engineering, National University of Singapore, Singapore 117576, Republic of Singapore*

### 1. Summary

Phase separation of nonionic surfactant in the presence of associative polymer was studied experimentally. Slightly above the cloud point, the solution could separate into three macroscopic phases if the surfactant concentration falls within a certain range: a cloudy phase in between two transparent phases. The formation of three phases could be observed a few hours after the solution turned cloudy, depending on the solution composition. It is interesting to find that the volume of the middle cloudy phase shows a linear relation with the global polymer concentration, implying that most of polymer stays in this phase. This finding is verified by composition analysis using UV to measure both the surfactant and polymer concentrations in each of the three phases. We also found that the bottom phase is a surfactant rich micellar solution, while the top phase is both surfactant and polymer lean.

Keywords: surfactant, cloud point, micellar solution, associative polymer, phase separation

### 2. Extended Abstract

Hydrophobically modified polymers (HMP) are a class of water-soluble polymers onto which hydrophobes are chemically attached either to both ends or along the hydrophilic polymer backbone. An HMP/surfactant mixture can undergo an *associative phase separation* into a phase enriched in both polymer and surfactant and a dilute phase. For hydrophobically modified hydroxyethyl cellulose (HMHEC) with nonionic surfactant, our prior work<sup>1</sup> reported for the first time that at sufficiently high surfactant concentrations, HMHEC solutions can separate into three macroscopic phases if the temperature is above the cloud point temperature (CPT). To seek a better understanding, we continue our investigation on the three-phase separation behavior of HMHEC aqueous solutions in the presence of TX114 or TX100, focusing on the time evolution of phase volume fractions and the composition in each of the phases.

Phase separation kinetics at different HMHEC concentrations with fixed surfactant concentration showed that the bottom phase emerges some time after the formation of the top and middle phases, and the time lag is substantial at high HMHEC concentrations. The clouding and phase separation have been attributed to substantial aggregation of free and mixed micelles, leading to the formation and growth of droplets, which are rich in surfactant and polymer and big enough to scatter light strongly. The slow phase

separation observed is thought to arise from the high viscosity of HMHEC solutions because the droplets must diffuse to encounter each other and get coalesced so as to gradually become a continuous phase.<sup>2</sup>

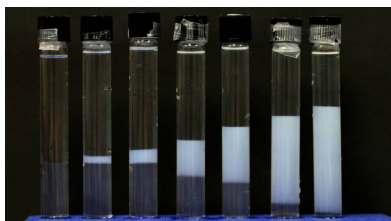


Figure 1: Photo of the three-phase separation for 6wt% TX114 and HMHEC at various concentrations: 0, 0.05, 0.1, 0.2, 0.3, 0.4, and 0.5 wt% (from left to right). The picture was taken after 7 days at 35 °C, when the individual phase heights no longer changed (except for the first two samples from the right).

It is interesting to observe a certain relation from Figure 1 between the phase heights and the global HMHEC concentration. Indeed, the volume fraction of the middle phase changes linearly with the global polymer concentration, implying a strong likelihood that a majority of polymer stays in the middle phase, while most of surfactant exists in the bottom phase. To verify the above speculation, we determined the composition in each phase for some typical three-phase separation samples, shown in Table 1.

		Height [cm]	HMHEC [wt%]	TX100 [wt%]
0.2%hmHEC +4%TX100	Top phase	7.3	0.10±0.01	0.20
	Middle phase	1.3	1.03±0.07	5.9
	Bottom phase	1.4	< 0.1 <sup>a</sup>	23.4
0.3%hmHEC +6%TX100	Top phase	6	0.13±0.01	0.31
	Middle phase	1.9	1.23±0.11	5.1
	Bottom phase	2	< 0.1	23.9
0.4%hmHEC +4%TX100	Top phase	6.2	0.16±0.02	0.33
	Middle phase	2.6	1.12±0.12	5.1
	Bottom phase	1.2	< 0.1	23.5

Table 1: Composition analysis for HMHEC/TX100 at 70 °C. <sup>a</sup>Estimated upper limit.

It is found that the surfactant and polymer concentrations are the highest in the bottom and the middle phase, respectively. We note that the low HMHEC concentration in the bottom phase cannot be determined precisely due to the high surfactant concentration. The considerable surfactant concentration in the middle phase can be explained by the association between HMHEC and surfactant. When CPT is reached, the solution undergoes an associative phase separation. Since a majority of HMHEC stays in the cloudy phase, it must take up a considerable amount of surfactant to form mixed micelles. When the global surfactant concentration is high enough, a portion of surfactant originally staying in the cloudy phase in the form of free micelles will aggregate and diffuse away slowly, and hence the new phase (bottom phase) emerges some time later. It could be explained by segregative phase separation.

## References

- Zhao, G. and Chen, S. B., (2006) *Langmuir*, 22, 9129-9134.  
 Zhao, G., Khin, C. C., Chen, S. B., Chen, B.-H. (2005) *J. Phys. Chem. B*, 109, 14198-14204.

## **Effect of surfactant on stagnant slow aggregation kinetics of polymer colloids**

Marco Lattuada, Hua Wu, Massimo Morbidelli

*ETH Zurich, DCAB, Institute for Chemical and Bioengineering, Hoenggerberg, CH 8093 Zurich, Switzerland*

### **1. Summary**

In this work, we have investigated the effect of surfactant addition on the slow reaction-limited aggregation kinetics of model polymer colloids (polystyrene latexes). Our experimental results, obtained by following in time the change of few average moments of the cluster mass distribution through light scattering, indicate that surfactant redistribution greatly affects aggregation kinetics by narrowing the cluster mass distributions compared to the aggregation of surfactant free latexes. The greater is the amount of surfactant added, the stronger are the deviations from the aggregation kinetics of surfactant free latexes.

Keywords: aggregation, polymer colloids, surfactants, population balance equations, light scattering

### **2. Extended Abstract**

The aggregation under stagnant conditions of colloids has been investigated for many years. A universal behaviour has been proposed almost twenty years ago by Weitz's group. Two different aggregation regimes have been identified: a fast or diffusion-limited aggregation regime and a slow or reaction-limited aggregation regime. While the diffusion-limited regime is rather well established and verified, many real-life systems show strong deviation from the expected reaction-limited universal behaviour. These deviations are particularly common in the case of polymer colloids. Despite the large number of experimental and modelling work published in the literature, no entirely satisfactory quantitative description has been provided of this effect.

In this work, we demonstrate that many of the observed discrepancies are caused by the anomalous behaviour of surfactants adsorbed on particles surface. We have carried out aggregation kinetics experiments on polymer colloids, with different amount of surfactant coverage, starting from particles stabilized only by fixed charges. The aggregation kinetics has been monitored by means of light scattering, which allows a few independent moments of the cluster mass distribution to be measured as a function of time.

Our experimental results indicate that polymer colloidal systems do follow the universal behaviour when no surfactant molecules are adsorbed on the particle surface, and

stabilization is only due to fixed charges. On the other hand, even small amounts of surfactant generate an anomalous kinetic behaviour, which can be quantitatively accounted for when redistribution of surfactant molecules on the particle surface during aggregation is considered. This redistribution of surfactant molecules generate a progressive slow down of the aggregation process, which leads to changes in the cluster mass distribution. In particular, progressively larger amounts of surfactants generate progressively narrower cluster mass distributions. In addition, a model based on population balance equations has been developed to quantitatively reproduce the time evolution of the experimentally measured cluster mass distribution moments.

## **References**

- Lin, M.Y., Lindsay, H.M., Weitz, D.A., Klein, R., Ball, R.C., and Meakin, P., (1990) *Journal of Physics: Condensed Matter*, 2, 3093-3113.
- Lattuada, M., Wu, H., Sandkühler, P., Sefcik, J., Morbidelli, M., (2004) *Chemical Engineering Science*, 59, 1713-1798.
- Sandkühler, P., Sefcik, J., Morbidelli, M. (2004) *Journal of Physical Chemistry B*, 108, 20105-20121.



## Session T2-6b: Interfacial & Colloidal Phenomena – II

<b>Abstract Number</b>	<b>Paper Title &amp; Authors</b>	<b>Included</b>
441	COSMO-RS and COSMOmic: Thermodynamic Properties of Interfaces and Micelles from Ab Initio Quantum Chemistry F Eckert	Yes
465	Mesoscopic simulation of surfactant oligomers behavior in aqueous solution and interface H Wu, J B Xu, H Wen	Yes
784	Dissipative Particle Dynamics Simulation of Polymers Adsorption under Shear B W Hao, J B Xu	Yes
1061	Model Studies during the Preparation Steps of Supported Hydroteating Catalysts Examined by Raman Spectroscopy P Beato, K Johannsen, A Nielsena, X Faber	Yes
3264	Prediction of partitioning coefficients: potential for drug formulations and bioseparation technologies W Arlt, I Smirnova, L Mokrushina, M Buggert	Yes

Session T2-6b

## **COSMO-RS and COSMOmic: Thermodynamic Properties of Interfaces and Micelles from *Ab Initio* Quantum Chemistry**

Frank Eckert

*COSMOlogic GmbH & Co KG, Burscheider Str. 515, D-51381 Leverkusen, Germany*

### **1. Summary**

COSMO-RS is a novel predictive method for the thermodynamic properties of pure and mixed fluids. COSMO-RS calculates the thermodynamic data from molecular surface polarity distributions, which result from quantum chemical calculations of the individual compounds in the mixture. The different interactions of molecules in a liquid, i.e. electrostatic interactions, hydrogen bonding and dispersion, are represented as functions of surface polarities of the partners. Using a novel, very rigorous and efficient thermodynamic solution for such pair-wise surface interactions, which goes beyond the limitations of the quasi-chemical approximation, COSMO-RS finally converts the molecular polarity information into standard thermodynamic data of fluids, i.e. vapor pressures, activity coefficients, excess properties, etc. Due to the almost general applicability of modern quantum chemical methods, COSMO-RS can be applied in many situations, where group contributions fail. This presentation reports some novel extensions and applications of the COSMO-RS methodology towards the prediction of solvent interfaces, surfaces and micellar properties: COSMOmic.

Keywords: COSMO-RS, micelle, surface properties, thermodynamic property prediction, quantum chemistry

### **2. Extended Summary**

COSMO-RS [1,2] is a novel predictive method for the thermodynamic properties of pure and mixed fluids. In contrast to group contribution methods, which depend on an extremely large number of experimental data, COSMO-RS calculates the thermodynamic data from molecular surface polarity distributions, which result from quantum chemical calculations of the individual compounds in the mixture. The different interactions of molecules in a liquid, i.e. electrostatic interactions, hydrogen bonding and dispersion, are represented as functions of surface polarities of the partners. Using a novel, very rigorous and efficient thermodynamic solution for such pair-wise surface interactions, which goes beyond the limitations of the quasi-chemical approximation, COSMO-RS finally converts the molecular polarity information into standard thermodynamic data of fluids, i.e. vapor pressures and heat of vaporization, activity coefficients, excess enthalpy and Gibbs free energy, phase diagrams, solubility, Henry constant etc. The quantum chemical basis of COSMO-RS is COSMO [3] the "Conductor-like Screening Model",

which belongs to the class of QM continuum solvation models (CSMs). CSMs are an extension of the basic QM methods towards the description of liquid phases and describe a molecule in solution through a quantum chemical calculation of the solute molecule with an approximate representation of the surrounding solvent as a continuum. Due to the almost general applicability of modern quantum chemical methods, COSMO-RS can be applied in many situations. New or complicated multifunctional chemical compounds, reactive intermediates, and even ions and zwitterions can be handled. Electronic and hydrogen bonding intramolecular interactions are well described and isomer differences in thermodynamic data can be resolved. Although some problems still exist for electrolytes, COSMO-RS appears to be a rather general predictive method for the thermodynamics of simple and complex fluid systems.

This presentation reports some novel extensions and applications of the COSMO-RS methodology towards the prediction of solvent interfaces, surfaces and micellar properties: COSMOmic. Describing micelles or biomembranes as liquid layers based on COSMO-RS, partition coefficients of solutes are determined very efficiently and without the need of additional fitting of parameters. Results of MD simulations of micelles or membranes are taken as an input to describe the statistics of the atomic distribution of the micelle. Together with COSMO/DFT calculations of the molecules that build up the micelle, as well as for the solutes of interest, this is all that is needed for a COSMOmic calculation. Figure 1 shows an example of a planar micelle, here a phospholipid biomembrane. Each layer is taken as a liquid, composed from each atom of the molecules in the given slice. Free energy of solutes in the membrane is calculated for a large number of positions and orientations. This gives a probability distribution and hence a free energy profile for the solutes in the membrane, as shown in Figure 2 for octanol and octane in a DMPC phospholipid bilayer in water. From this probability distribution, the lipid-water partition coefficient can be derived, as well as the free energy difference between the water phase (outermost layer) and all other layers.

Figure 1: Membrane described by liquid layers, various solute orientations and positions [4]

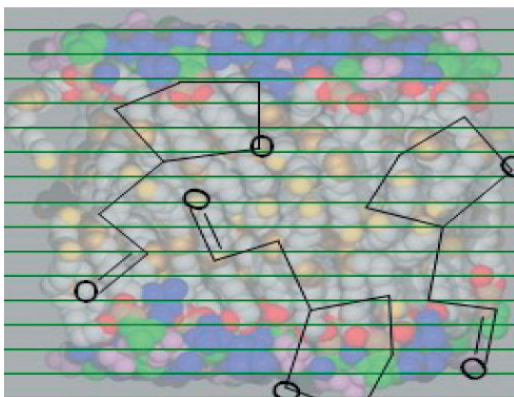
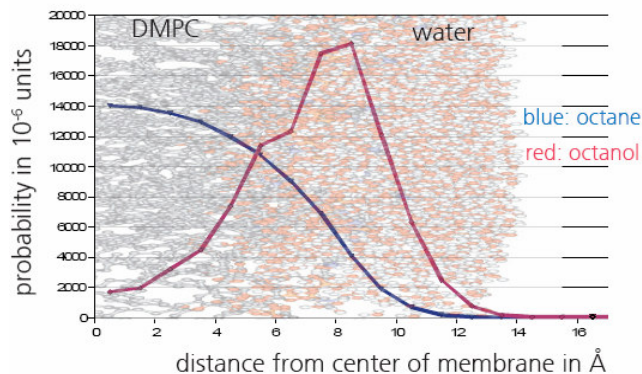


Figure 2: Probability distribution of octanol and octane in DMPC bilayer membrane



## References

- Eckert, F. and A. Klamt, (2002). *AIChE Journal*, **48**, 369.  
 Klamt, A. and F. Eckert, (2000). *Fluid Phase Equilibria*, **172**, 43.  
 Klamt, A. and G. Schüürmann, (1993). *J. Chem. Soc. Perkin Trans. II*, 799.  
 Courtesy of P. Tieleman, University of Calgary.

## Mesoscopic simulation of surfactant oligomers behavior in aqueous solution and interface

Hao Wu<sup>a,b</sup>, Jun-Bo Xu<sup>a,b</sup>, Hao Wen<sup>a</sup>

<sup>a</sup> Multi-phase Reaction Laboratory, Institute of Process Engineering, Chinese Academy of Sciences, No. 1  
2<sup>nd</sup> North Lane, ZhongGuanCun, HaiDian District, Beijing 100080, China

<sup>b</sup> Graduate School of the Chinese Academy of Sciences, 100049 Beijing

### 1. Summary

In recent years, new classes of surfactants have been synthesized and have attracted such attention from academics and industries. One of them is the surfactant oligomers<sup>[1]</sup>, consisting of two or more conventional single-chain surfactants with hydrophilic head connected by spacer groups. Both experimental studies and computer simulations indicate that the surfactant oligomers exhibit better performance compared to the conventional single-chain counterpart. The efficiency of surfactants is related to its structure. However, its effect is not fully understood. Dissipative particle dynamics (DPD)<sup>[2]</sup>, a coarse-grained method introduced by Hoogerbrugge and Groot, is performed in this paper to better understand the behavior of surfactant oligomers in aqueous solution and oil/water interfaces. The interfacial tension was calculated by Irving-Kirkwood method.

Keywords: surfactant oligomer, dissipative particle dynamics, mesoscale simulation

### 2. Extended Summary

The critical micellar concentration (CMC) of dimeric or trimeric surfactant is much lower than that of their single-chain counterpart. All surfactants show self-assembling properties due to their amphiphilicity in an aqueous medium. They all form spherical micelles at the concentration not far above their CMC. The transition from spherical to cylindrical micelles appears with increasing surfactant concentration. Lamellar micelles will appear with further increasing the surfactant concentration. For dimeric and trimeric surfactants, cylindrical micelles transform into extremely long “wormlike” or “threadlike” micelles before the transition to lamellar micelles. These results are in qualitative agreement with experimental observations. The average aggregation numbers ( $AN$ ) of micelles increase with a power law of  $AN \propto c^\alpha$  when the surfactant concentration  $c \gg \text{CMC}$ . The self-diffusion coefficients will drop with a power law of  $D \propto c^{-\alpha}$  when wormlike micelles are formed.

The surface area  $A$  occupied by one surfactant at the interface is an important characteristic of a surfactant, which decreases slightly when the carbon number  $m$  of alkyl chain increases. In the case of surfactant oligomers, our simulation indicates that  $A$  also decreases slightly when  $m$  is small. Due to the pre-micellar aggregation, the relationship between  $A$  and  $m$  become unclear as the value of  $m$  larger than 16. The

variation of  $A$  with the spacer length is complex. For the diametric  $m-s-m$  surfactants with a hydrophobic spacer  $s$ ,  $A$  has a maximum when  $m$  is approximate 9 ~ 15. For the relative trimeric surfactants,  $A$  increase slightly while  $m$  increase.

The efficiency of surfactants is measured by the reduced surface tension at a given surfactants amount. In short, mostly the efficiency increases while the carbon number  $m$  of alkyl chain increases. For some of the diametric and trimeric surfactants with long spacer groups, the efficiency meets a maximum value when  $m$  is approximate 9 ~ 15. With the increase of spacer length  $s$ , the efficiency has a minimum when  $s$  is approximate 3 ~ 6.

## References

- Zana, R.; Levy, H., Papoutsi, D., Beinert, G., (1995) *Langmuir* 11, 3694  
Groot, R. D., Warren, P. B., (1997) *J. Chem. Phys.* 107, 4423

## **Dissipative Particle Dynamics Simulation of Polymers Adsorption under Shear**

B. Wen Hao<sup>a</sup> and Jun-Bo Xu<sup>a,b</sup>

<sup>a</sup>*Multi-Phase Reaction Laboratory, Institute of Process Engineering, Chinese Academy of Sciences, P.O.Box 353, 100080 Beijing, China*

<sup>b</sup>*Graduate University of Chinese Academy of Sciences, P.O. Box 4588, 100049 Beijing, China*

### **1. Summary**

In the present work, a new method to create solid walls in dissipative particle dynamics (DPD) was put forward according to the comparison between existing solid boundary methods and Lee-Edwards boundary method. Then it was used to simulate the adsorption of block copolymers on solid-liquid interface. The simulation shows that the block copolymer adsorbed on the solid surface will performed as an adsorbent deactivator. An effective barrier will form by the adsorbed block copolymer molecules to prevent the adsorption of other molecules or tiny particles represented by beads R in the simulation system.

Keywords: dissipative particle dynamics, boundary method, polymer adsorption, meso-scale simulation

### **2. Extended Abstract**

Polymers adsorbed onto surfaces have application in many important technical problems, such as wetting, adhesion, colloid stabilization and lubrication. Here dissipative particle dynamics was used to simulate the adsorption of block copolymers on solid-liquid interface. In order to investigate the protective effect of block copolymers, some beads R which were needed to repel away from the solid surface were added to the simulation systems. This study was motivated by the problem of controlling the agglomerative effect of soot in lubricating oil.

First the reason of density and velocity distortion near the solid boundary was analyzed through the comparison between existing solid boundary methods and Lee-Edwards boundary method. Then a new method to create solid walls in dissipative particle dynamics that suitable for many complex boundary shapes was put forward: the density of solid beads was adjusted to decrease the density distortion near the boundary; reflection method was used to guarantee the wall's impenetrability, specular reflection was found to be the best reflection method that can produce minimum velocity distortion near boundary; the dissipative parameter between solid beads and liquid beads was magnified to depict the velocity profile near boundary accurately.

Then this boundary method was used to simulate the adsorption of block copolymers on solid-liquid interface and its protective effect to the solid surfaces. The simulation shows that the block copolymer adsorbed on the solid surface will performed as an adsorbent deactivator. An effective barrier will form by the adsorbed block copolymer molecules to prevent the adsorption of other molecules or tiny particles represented by beads R in the simulation system. The adsorption amount of beads R at a certain R concentration can be calculated to evaluate the protect effect of block copolymers. The effects of molecular structure, concentration, interactions with solid wall and solvents of block copolymer were inspected. The adsorption amount of beads R will decrease rapidly with increasing the concentration of block copolymer, or with decreasing the repulsion parameter between the preferential block and the solid surface. Moreover, the barrier formed by block copolymers appears to be greater as the polymeric chain length increases or as the block copolymer is more soluble. A better protect effect can be obtained by using diblock copolymer, rather than using tri-block copolymer. The shear to the simulation system will weaken the effective barrier formed by the block copolymer, the beads R will be more likely to adsorb onto the solid surface with the increase of the shear rate.

## References

- Irfachsyad, D., Tildesley, D.J., and Malfreyt, P., (2002) *Phys. Chem. Chem. Phys.*, 4, 3008-3015.  
Goujon, F., Malfreyt, P., and Tildesley, D.J., (2004) *Chem. Phys. Chem.*, 5, 457-464.  
Visser, D.C., Hoefsloot, H.C.J., and Iedema, P.D., (2005) *J. Comput. Phys.*, 25, 626-639.



## Model Studies during the Preparation Steps of Supported Hydrotreating Catalysts Examined by Raman Spectroscopy

P. Beato<sup>a</sup>, K. Johannsen<sup>a</sup>, A. Nielsen<sup>a</sup>, X. Faber<sup>a</sup>

<sup>a</sup> Haldor Topsoe, Nymøllevej 55, DK-2800 Lyngby, Denmark

### 1. Summary

NiMo and CoMo catalysts supported on alumina are used for hydrotreating of different oil fractions for production of green fuels such as ultra low sulphur diesel. Preparation of the catalyst is usually done by dissolving different metal precursors in basic or acidic aqueous media. Molybdenum, as the principal component in the solution, is known to form small oxidic clusters in solution, the so called polyoxometalates (POM's). Depending on pH, concentration, temperature and elemental composition of the solution, different types of POM's are formed and different chemical compositions can be obtained. It is now generally accepted, that the structure and composition of the POM in solution has a significant effect on the properties of the final impregnated catalyst. During impregnation and calcination of the catalyst complex chemical and physical interactions between the dissolved species and the alumina surface take place, which further influence the properties of the active catalyst.

In order to understand the formation of an active catalyst and be able to further improve its performance, it is therefore necessary to monitor each individual preparation step.

In this work we present our studies using *in situ* Raman spectroscopy on model systems of Ni/Co, Mo/W and P impregnated on alumina to evaluate the structural development of the POM from solution to the final catalyst.

Keywords: Raman, *in-situ*, hydrotreating, NiMo, green chemistry

### 2. Extended Abstract

Molybdenum precursors typically used for the preparation of the impregnation liquids include MoO<sub>3</sub>, ammonium heptamolybdate (AHM), ammonium dimolybdate (ADM) or phosphomolybdic acid (PMA), while Ni and Co are typically introduced as carbonates or nitrates. Depending on the conditions in solution, Ni or Co can be incorporated into the POM structure and are thereby generate a mixture of the NiMo or CoMo on a molecular level. The idea is that this intimate mixture will enhance the dispersion of the elements in the final catalyst and thereby prevent segregation.

Alternatively to the *in situ* generation of mixed elemental POM's in solution, it is also possible to selectively synthesize POM's with the desired stoichiometric composition.

P. Beato et al.

Typically, the second approach is more time and cost intensive and has therefore more model character. However, these model compounds are very useful as they can be used as references for the observed Raman spectra in more realistic systems. Especially in the case of Molybdenum, mixtures of POM's are usually observed in solution which makes it difficult to assign the spectra to the separate species.

We have performed a systematic study of the interaction of the Ni/Co, P and Mo in aqueous solution under various conditions. As an example *Figure 1* shows the structural evolution of  $H_3PMo_{12}O_{40}$  in aqueous solution with increasing pH (a) and the subsequent structural effects during the addition of Ni (b).

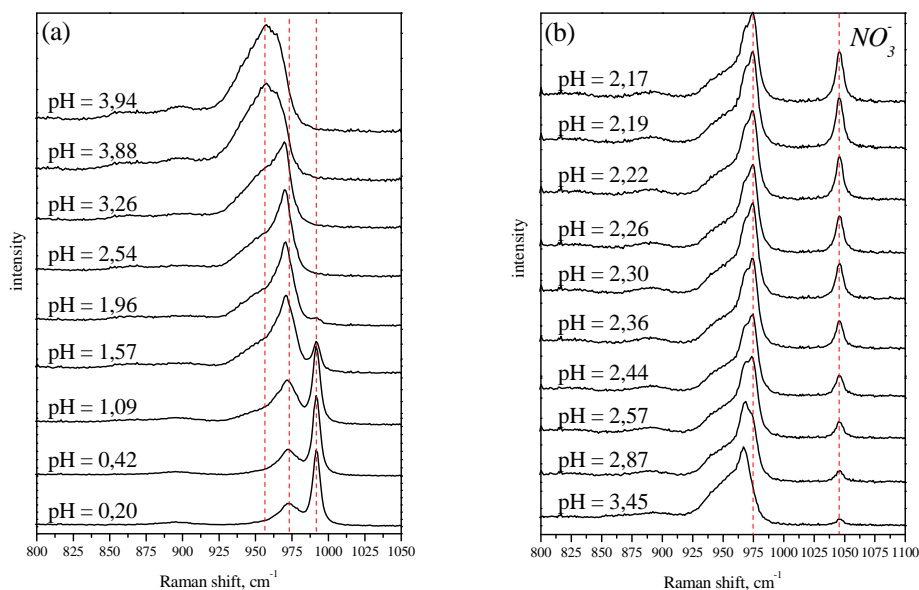


Figure 1. Structural evolution of  $H_3PMo_{12}O_{40}$  in aqueous solution with increasing pH (a).  $NaHCO_3$  was used to increase the pH. Subsequent structural evolution during the addition of Ni (b). Ni was introduced as  $Ni(NO_3)_2$ .

## References

- Topsøe, H., Clausen, B.S. and Massoth, F.E., *Hydrotreating Catalysis – Science and Technology*, Springer Berlin (1996).
- Bergwerff, J.A., Van de Water, L.G.A., Visser, T., De Peinder, P., Leliveld, B.R.G., De Jong, K.P. and Weckhuysen B.M., (2005) *Chemistry - A European Journal* 11, 4591-4601.
- A. Griboval, P. Blanchard, E. Payen, M. Fournier, J.I. Dubois, (1998) *Catal.Today* 45, 277-283.

## Prediction of partitioning coefficients: potential for drug formulations and bioseparation technologies

W. Arlt, I. Smirnova, L. Mokrushina, M. Buggert

*Chair of Separation Science & Technology, Friedrich – Alexander University Erlangen – Nuremberg  
Egerlandstr. 3, 91058 Erlangen, Germany*

### 1. Summary

In the present paper, the group-contribution UNIFAC and the *a priori* COSMO-RS models are applied to predict micelle/water partition coefficients. The models allow predictions based on the molecular structure only. The practical implementation of the models is examined by studying a number of homologous series of organic solutes in aqueous solutions of nonionic (polyethoxy alcohols) and ionic surfactants (SDS, DTAB). Good quantitative agreement with experimental data from literature has been achieved. Factors which seem to be important in the calculation and to influence the prediction results are discussed. Among these are interfacial contribution and conformation analysis. Compared to UNIFAC, the COSMO-RS method opens up new perspectives, since ionic components, steric isomers, and inorganics can be modelled.

Keywords: partitioning, micellar solution, COSMO-RS, UNIFAC, bioseparation

### 2. Extended Abstract

#### Introduction

Solubilisation of solutes in micellar solutions is a process having a wide range of applications. Some examples are: detergency, enhancing the aqueous solubility of hydrophobic drugs, separation of products of biosynthesis. In such applications, the possibility to predict the solute partitioning is of special value. Presently, only few models exist allowing the prediction of micelle/water partition coefficients,  $K_{mw}$ . All of them belong to the class of linear correlations between some molecular properties and  $\log(K_{mw})$  values. The aim of this work is to show that models based on estimation of chemical potentials or equivalently of activity coefficients can be effectively utilised to predict the drug partitioning between polar (water) and nonpolar (octanol/micelle) phases, and the prediction can be achieved quantitatively based solely on the chemical structure of the substances.

#### Modelling

UNIFAC model is a group-contribution tool, which allows calculations based on functional group parameters giving additive contributions to the system properties [1]. In order to consider micellar systems in the frame of this model, we have introduced the

interfacial contribution to the activity coefficient in terms of the Gibbs-Thompson theory (UNIFAC-IF) [2].

*COSMO-RS model* is based on quantum mechanics and allows an *a priori* prediction of thermodynamic properties such as activity coefficients. In the COSMO model [3], the solute molecule is considered to be embedded in a cavity surrounded by a virtual conductor. The transfer from this state to the real solvent is done by applying the COSMO-RS concept [4] by means of statistical thermodynamics (here different conformers of all components of the mixture are taken into account).

## Results

We illustrate the practical implementation of the theoretical framework by examining a variety of homologous series of organic substances (including drugs) in aqueous solutions of nonionic and ionic surfactants.

Figure 1 shows the predicted micelle/water partition coefficients (COSMO-RS) versus the experimental values taken from literature in the aqueous solutions of the *nonionic surfactant*, Triton X100. Both models demonstrate a quantitative agreement with the experimental data. The average errors are below 11% and 17% for the COSMO-RS and UNIFAC-IF models, correspondingly.

Figure 2 illustrates the potential of the COSMO-RS model to predict  $K_{mw}$  in the aqueous solutions of *ionic surfactants*. The predicted  $K_{mw}$  of a series of organics in aqueous solution of sodium dodecyl sulphate (SDS) are plotted versus the experimental values. The results are in reasonable agreement with the experimental data [7]. The average error is lower than 16%.

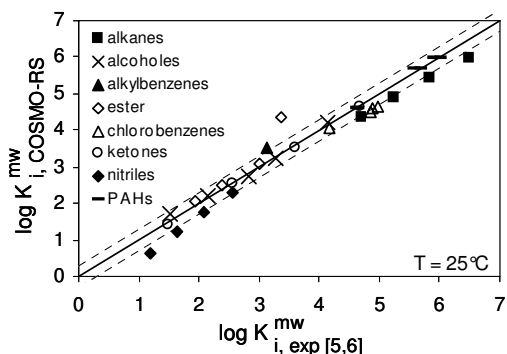


Figure 1: Comparison of experimental and predicted partition coefficients of solutes in aqueous Triton X100 solutions at 25°C using COSMO-RS

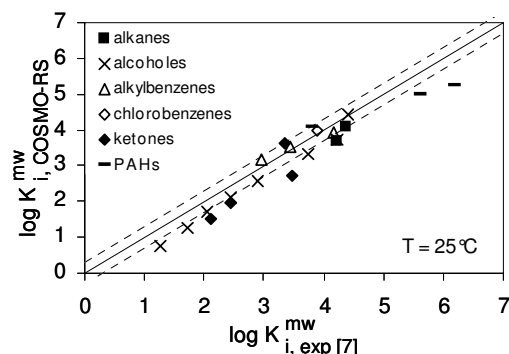


Figure 2: Comparison of experimental and predicted partition coefficients of solutes in aqueous SDS solutions at 25°C by COSMO-RS

## References

- Fredenslund, A., Gmehling, J., and Rasmussen, P., *Vapor-Liquid Equilibria using UNIFAC – a group-contribution method*, Elsevier, Amsterdam (1977)
- Buggert, M., Mokrushina, L., Smirnova, I., Schomäcker, R., and Arlt, W., (2006) *Chem. Eng. Technol.*, 29, 567-573
- Klamt, A., (1995) *J. Phys. Chem.*, 99, 2224-2235.
- Klamt, A. and Schüürmann, G., (1993) *J. Chem. Soc. Perkin Trans.*, 2, 799-805
- Edwards, D.A., Luthy, R.G., and Lui, Z., (1991) *Environ. Sci. Technol.*, 25, 127-133
- Suslov, D.A. and Solomonov, B.N., (1995) *Zhurnal Fizicheskoi Khimii*, 69, 1264-1267
- M.H. Abraham, H.S. Chadha, J.P. Dixon, C. Rafols, C. Treiner. (1995) *J. Chem. Soc. Perkin Trans.*, 2, 887-894

## Session T2-6c: Interfacial & Colloidal Phenomena – III

<b>Abstract Number</b>	<b>Paper Title &amp; Authors</b>	<b>Included</b>
222	Surfactant-based separation technique in the removal of dissolved organics from water I V Rao, P V Reddy	Yes
1849	Industrial Case-study: Re-emulsification of expired highly viscous emulsion product L T Yee, N W Kiong, C W Jae, M Venugopa	Yes
1979	Crystallization of proteins on polymeric membranes: how porosity, thickness and roughness affect the heterogeneous nucleation kinetics E Curcio, G Profio, E Fontananova, S Simone, E Drioli	Yes
3630	Synthesis of Mesoporous Silica using Mixed Surfactant Templates: Predictions from Ternary Liquid Crystal Phase Diagrams S E Rankin, R Xing, M S Rahman, S M Vyas, H-J Lehmler, B L Knutson	Yes

Session T2-6c

## Surfactant-based separation technique in the removal of dissolved organics from water

I.V. Rao<sup>a</sup> and P. Venkat Reddy<sup>b</sup>

<sup>a</sup> *University College of Technology, Osmania University, Hyderabad – 500 007, India*

<sup>b</sup> *Department of Chemical Engineering, IIT Bombay, Mumbai-400076, India*

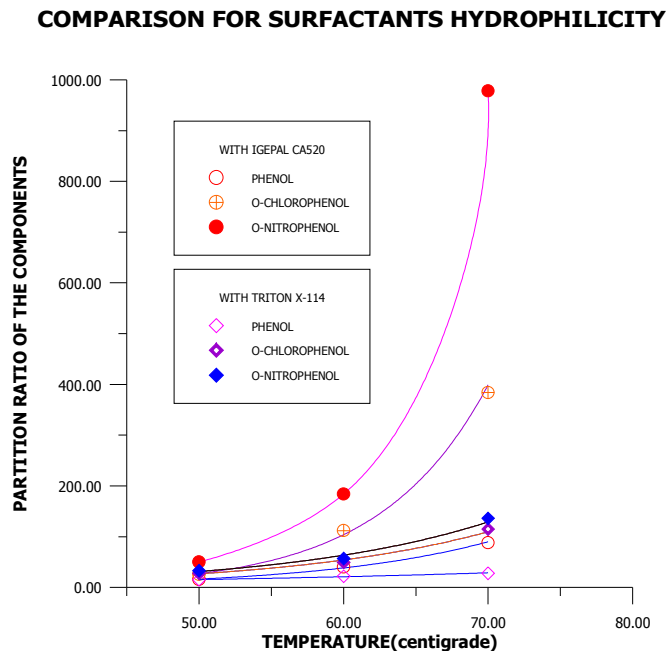
### 1. Summary

Separation techniques based on the use of surfactants have several important advantages over traditional separation methods. Aqueous solutions of certain surfactant micelles exhibit phase separation behaviour upon temperature alteration. This phenomenon can be exploited in separation science for the development of extraction, purification and pre-concentration schemes for different solutes. Since the addition of just a small amount of an appropriate nonionic surfactant to the aqueous sample solution is required, this approach is convenient and fairly benign, eliminating the need for the use of organic solvents as in conventional liquid-liquid or solid-liquid extraction. The technique of extracting dissolved species such as phenol, o-chlorophenol and o-nitrophenol from water via nonionic surfactant micelle-mediated phase separation was studied. The effect on extraction efficiency, solute distribution coefficient and phase volume ratio of pertinent experimental parameters such as surfactant hydrophilicity, temperature and additives was systematically evaluated. Surfactant hydrophilicity was examined by monitoring the extraction parameters for two members of the homologous series of octylphenoxypolyethoxyethanols with varying ethylene oxide units.

Keywords: cloud point, nonionic surfactant, hydrophilicity, salting-out, partition coefficient

### 2. Extended Abstract

The cloud point technique was used to recover phenol, o-chlorophenol and o-nitrophenol from aqueous solutions using octylphenoxypolyethoxyethanol as the nonionic surfactant. The concentrations of solutes and surfactants were analysed with the help of Shimadzu UV-160 spectrophotometer. The experiments indicate that increase in temperature resulted in increased recovery of the solutes. It was also observed that surfactant hydrophilicity affects the extraction with Igepal CA-520 (5 ethylene oxide moles) showing higher extraction than Triton X-114 (7.5 ethylene oxide moles), as shown in Fig.1. Recovery of phenols follows the order of o-nitrophenol > o-chlorophenol > phenol and is increased in the presence of sodium chloride; a salting-out electrolyte.



The presence of salting-out electrolytes is preferred both to decrease the cloud point and to increase the efficiency of extraction. It was also observed that as the surfactant hydrophilicity increases, the solute distribution coefficient decreased for all the solutes studied.

Figure 1. Effect of temperature, surfactant hydrophilicity and solute structure



## **Industrial Case-study: Re-emulsification of expired highly viscous emulsion product**

Lim Tau Yee<sup>a</sup>, Ng Wai Kiong<sup>a</sup>, Choi Won Jae<sup>a</sup>, Murugapillai Venugopa<sup>b</sup>

<sup>a</sup>*Institute of Chemical and Engineering Sciences, Agency for Science, Technology and Research (A\*STAR)*

<sup>b</sup>*Pesek Road, Jurong Island, Singapore 627833*

### **1. Summary**

The aim of this work is to conduct a technical feasibility study to minimize the loss of emulsion product by developing a small-scale process to re-emulsify expired emulsion (phase separated). Our results revealed that it was technically feasible to recover phase separated emulsion product using a small batch dynamic mixing process. It is hoped that this work could serve as a reference industrial case-study in exploring the recovery of expired highly viscous emulsion product during prolonged storage using a small-scale batch process.

Keywords: re-emulsification, viscous emulsion, mixing, centrifugation, stability

### **2. Extended Abstract**

A continuous industrial-scale static mixing process is used to emulsify a highly viscous feed into oil-in-water emulsion product. Unfortunately, during prolonged storage, some product could not be utilized before the shelf-life expired and separated into two immiscible phases (expired emulsion) leading to economic losses. In open literature, there were few technical reports on re-emulsification of expired highly viscous emulsion, which was normally treated as know-how in industries. The aim of this work is to conduct a technical feasibility study to minimize the loss of emulsion product by developing a small-scale process to re-emulsify this leftover product. An attempt is made to apply a batch dynamic mixing process at laboratory-scale to achieve similar product specifications as that of the original product produced by large-scale static mixing. Surfactant and bio analysis were carried out to evaluate the need to replace the separated aqueous phase containing surfactants and stabilizers. It was found that arising from the growth of micro-organisms in the expired emulsion, only negligible quantities of surfactants and stabilizers remained in the aqueous phase. Therefore, all re-emulsification work was carried out using additional surfactants, de-ionized water and the recovered oil phase. The original and re-emulsified products were characterized using optical microscopy (droplet shape and size), laser diffraction (droplet size distribution)<sup>1</sup>, viscometer (dynamic viscosity), Karl Fisher titration (water content) and centrifuge (relative stability against centrifugation)<sup>2,3</sup>. In order to mimic large-scale continuous static

mixing, special considerations in terms of the number of the mixing stages and residence time distribution need to be accounted for in the batch process.

Our results revealed that it was technically feasible to recover phase separated emulsion product using a small batch dynamic mixing process. While the droplet size distribution of recovered product was slightly smaller as compared with the original product, there was a small improvement in viscosity of the recovered product. Measurements also showed that the original and the re-emulsified emulsions contained approximately same water contents. After centrifugation at 6,000 rpm for 15 minutes, it appeared that the recovered product and the original had similar relative stability against centrifugation force and could imply roughly similar shelf life. It is hoped that this work could serve as a reference industrial case-study in exploring the recovery of expired highly viscous emulsion product during prolonged storage using a small-scale batch process.

### **References**

- Roland, I., Peil, G., Delattre, L., and Evrard, B., (2003) *Int. J. Pharm.*, 263, 85-94.  
Sobisch, T., and Lerche, D., (2004) *Chemistry Preprint Archive*, 5, 7-18.  
Sobisch, T., Lerche, D., and K uchler, S., (2002) *Chemistry Preprint Archive*, 6, 5-11.

## **Crystallization of proteins on polymeric membranes: how porosity, thickness and roughness affect the heterogeneous nucleation kinetics**

E. Curcio<sup>a,b</sup>, G. Di Profio<sup>a,b</sup>, E. Fontananova<sup>a,b</sup>, S. Simone<sup>b</sup>, E. Drioli<sup>a,b</sup>

<sup>a</sup>*Department of Chemical Engineering and Materials, University of Calabria, via P. Bucci CUBO 44/A – 87030 Rende (CS) Italy*

<sup>b</sup>*Institute on Membrane Technology (ITM-CNR), via P. Bucci CUBO 17/C – 37030 Rende (CS) Italy*

### **1. Summary**

The innovative use of polymeric membranes as solid substrates promoting heterogeneous nucleation of proteins has been recently proposed. Experimental evidences for shorter induction times, accelerated nucleation rates and excellent diffractometric quality – obtained for various proteins (lysozyme, trypsin, catalase etc.) – make this technique attractive and simultaneously increase the need for a better understanding of the role of the membrane in the early stage of nuclei formation. This work investigates, both theoretically and experimentally, the effect of the morphological parameters of the membrane structure (porosity, thickness, roughness) on the crystallization kinetics of proteins, so creating the premise for a micro-scale design and a better engineering of the crystallization process.

Keywords: membrane crystallization, heterogeneous nucleation, protein crystallization, microporous hydrophobic membranes

### **1. Extended Abstract**

The rate of solvent extraction, related to physico-chemical properties of the membrane by Dusty Gas Model under the regime of Knudsen-limited diffusion, determines the supersaturation level of the solution and induces – in some cases – important modification in the crystalline habit.

The Gibbs energy barrier to the formation of critical nuclei on a polymeric membrane, calculated as difference between the energy gained upon formation of a bulk phase and the energy required to form new surface area, was evaluated by solving the appropriate energy balance including the positive contributions of interfacial free energies of the nucleus-liquid ( $\gamma_L$ ) and nucleus-substrate ( $\gamma_i$ ) interfaces, and the negative contribution for the liquid-substrate ( $\gamma_S$ ) interface displaced.

Based on geometrical analysis, the Young equation - strictly valid for smooth, planar and homogeneous surfaces - has been modified in order to take into account the effect of porosity  $\varepsilon$  (eq.1) and roughness coefficient  $r$  (eq.2) on the observed contact angle  $\theta$ :

$$(\gamma_s - \gamma_i) = \gamma_L \left( \cos \theta + \frac{4\varepsilon(1 + \cos \theta)}{(1 - \varepsilon)(1 - \cos \theta)} \right) \quad [1]$$

$$(\gamma_s - \gamma_i) = \frac{1}{r} \gamma_L \cos \theta \quad [2]$$

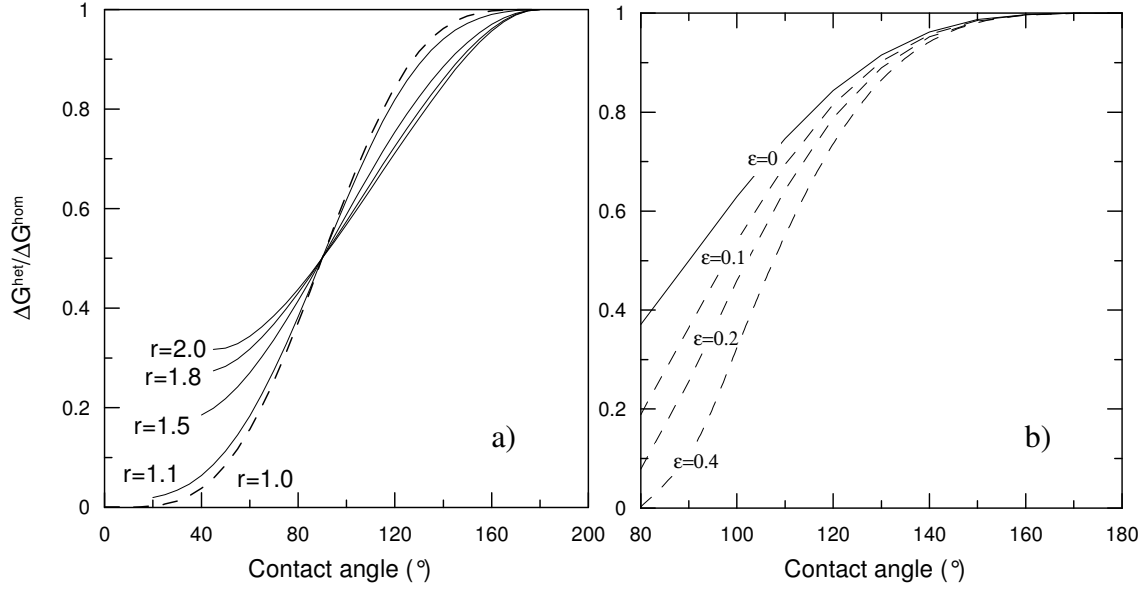


Figure 1: Heterogeneous/Homogeneous nucleation Gibbs energy ratio as a function of contact angle and: a) membrane roughness; b) membrane porosity.

Model predictions (figure 1), based on the contact angle data of protein solutions, porosity data from SEM and gas permeability tests, and AFM measurement of surface roughness, significantly diverge from results of Volmer theory (valid under the same hypothesis of Young equation) already at porosity  $> 0.1$  and for surfaces moderately hydrophobic (contact angle:  $90-110^\circ$ ).

A substantial agreement with the nucleation rates measured for lysozyme and catalase on different polymeric supports (LiCl or poly-vinylpyrrolidone modified poly-vinylidene fluoride membranes, Teflon, modified poly-etheretherketone membranes) has been verified.

Modifications of the shape and size of crystals grown on different membranes, in most cases resulting in the elongation of the longitudinal axis, have been also observed.

## References

- Curcio, E., Di Profio, G. and Drioli, E., (2003) *Journal of Crystal Growth*, 247,166-176.  
 Di Profio, G., Curcio, E. and Drioli, E., (2005) *Journal of Structural Biology*, 150, 41-49.

## **Synthesis of Mesoporous Silica using Mixed Surfactant Templates: Predictions from Ternary Liquid Crystal Phase Diagrams**

Stephen E. Rankin,<sup>a</sup> Rong Xing,<sup>a</sup> Mohammed S. Rahman,<sup>a</sup> Sandyha M. Vyas,<sup>b</sup> Hans-Joachim Lehmler,<sup>b</sup> and Barbara L. Knutson<sup>a</sup>

<sup>a</sup>*Department of Chemical and Materials Engineering, University of Kentucky, 177 Anderson Hall, Lexington, KY 40506-0046, USA. E-mail: srankin@engr.uky.edu*

<sup>b</sup>*Department of Occupational and Environmental Health, University of Iowa, 222 IREH, Iowa City, IA 52242, USA. E-mail: hans-joachim-lehmler@uiowa.edu*

### **1. Summary**

We discuss the use of ternary liquid crystal phase diagrams of mixed surfactants in water for predictive synthesis of mesoporous silica. Specifically, we examine the hypothesis that the phase of a mesoporous material can be predicted by substituting the volume of water needed at a particular point in the phase diagram with the equivalent volume of condensed silica. This hypothesis has some merit because both water and silica are protic, polar media and because both substances form tetrahedrally coordinated clusters. In practice, the hypothesis works quite well at predicting the structure of silica-surfactant mesophases formed from a mixture of a cationic surfactant and a surfactant with a single glucopyranoside headgroup. The phase diagram measured using polarized optical microscopy matches the mesostructures measured by XRD, and TEM of silica-surfactant composites formed by acid-catalyzed polycondensation in concentrated solutions. However, the mesophase of the material is not always well predicted for the same cationic surfactant mixed with a maltoside-terminated surfactant. Differences may be due to the specific hydrogen bonding environment near the sugar headgroup. The success of this hypothesis in mixtures of cationic hydrogenated and cationic fluorinated surfactants will also be examined using a combination of polarized optical microscopy, TEM, XRD, and gas adsorption.

Keywords: materials, templating, nanotechnology, lyotropic, liquid crystal

### **2. Extended Abstract**

Surfactant micelle templating is a well-established technique for the preparation of metal oxides with pores of uniform size, shape, and connectivity.[Ying 1999] The structure of these materials mimics that of lyotropic liquid crystals, where a metal oxide serves as the polar microphase, and the surfactant tails form the apolar microphase. This mimicry is particularly clear when materials form by hydrolysis of

metal alkoxides in a concentrated surfactant solution. Attard et al. [1995] first demonstrated that the structure of a lyotropic surfactant phase could be directly captured as a mesoporous metal oxide by adding tetramethoxysilane (TMOS) to a hexagonal liquid crystal, and then removing the methanol generated by hydrolysis.

Here, we explore the extension of this concept to binary surfactant templates. Reasons to use pairs of surfactants as templates include tuning of the pore characteristics and incorporation of organic and inorganic functionality in the walls of the final material. We seek conditions under which the structure of the final material can be predicted by simply replacing the water at a particular point in the ternary phase diagram of the surfactant/water system with an equivalent volume of metal oxide – an approach similar to that of Albertius et al. [2002].

Figure 1 shows an example of the ternary phase diagram of n-octyl- $\beta$ -D-glucopyranoside, cetyltrimethylammonium bromide (CTAB), and water determined by polarized optical microscopy (POM). Representative POM textures are shown in the upper left part of the diagram. For this surfactant system, the phase of templated silica is well predicted from this ternary diagram, [Xing 2007a] and the x-ray diffraction (XRD) patterns of a few as-synthesized materials on the right hand side are shown, which are consistent with the expected phase. Synthesizing materials with a given phase fails for this system only because of instability of samples with high surfactant content, or surfactant decomposition during ammonia treatment [Xing 2007b].

This approach is not as successful for all systems. Instructive cases will be discussed in which the material does not match the liquid crystal phase, either because of differences in hydrogen bonding between water and silica (for maltoside surfactants) or nonideal tail mixing (fluorinated / hydrocarbon surfactant mixtures).

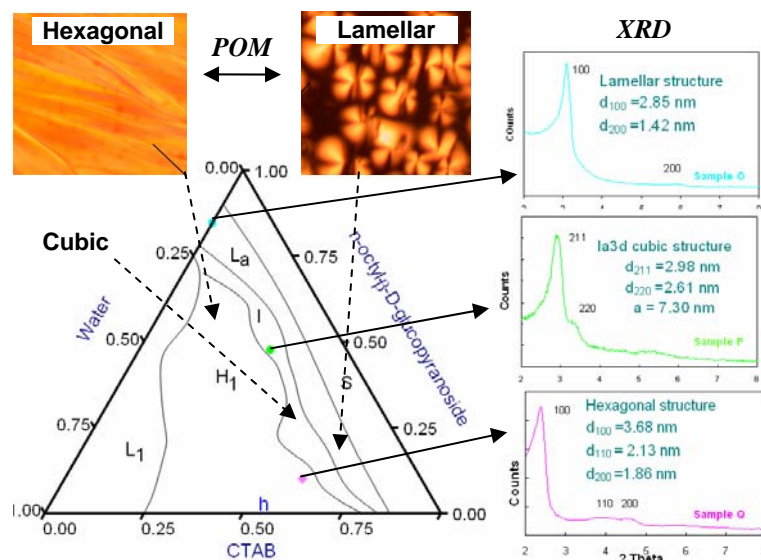


**Figure 1.** Ternary phase diagram of CTAB,  $C_8G_1$  and water (lower left) determined by polarized optical microscopy (POM), and x-ray diffraction (XRD) patterns of calcined materials prepared based on the indicated compositions.

## References

- Albertius, P.C.A., Frindell, K.L., Hayward, R.C., Kramer, E.J., Stucky, G.D., Chmelka, B.F. (2002) *Chem. Mater.*, 14, 3284-3294.
- Attard, G.S., Glyde, J.C., Göltner, C.G. (1995) *Nature*, 378, 366-368.
- Xing, R., Rankin, S.E. (2007a) *J. Colloid Interface Sci.*, in press.
- Xing, R., Rankin, S.E. (2007b) *Micropor. Mesopor. Mater.*, in press.
- Ying, J.Y., Mehnert, C.P., Wong, M.S. (1999) *Angew. Chem. Int. Ed.*, 38, 56-77.

## Session T2-6P: Interfacial & Colloidal Phenomena – Poster

Abstract Number	Paper Title & Authors	Included
219	Using of hydrogen peroxide for increasing of biologically active carbon filter work efficiency I Kozyatnyk, N Klymenko	Yes
385	Electrical interaction between two long, parallel particles covered by an ion-penetrable charged membrane in oil-water interface S Tseng, L F Cheng, J P Hsu	Yes
488	The effect of polyacrylamides on the flocculation and settling behaviour of kaolinite dispersions M S Nasser and A E James	Yes
1188	Thin film flow of a liquid down smooth and rough surfaces L B Press, D Dulcka, S Woziwodzki	Yes
1204	Sedimentation in Micellar Solutions of Tetradecyltrimethylammonium Bromide J Rozanski, L B Press	Yes
2555	Phase Inversion in Liquid – liquid Batch Stirred system M Amouei, P K Parsi, M A Moosavian, A A Davoodi	Yes
2596	Study on effective parameters on adhesion in segmented polyurethanes M Amrollahi, G M M Sadeghi, M Haghshenas	Yes
4053	A Dynamics Behavior of Two-Dimensional Colloidal Aggregates using Discrete Element Method (DEM) T Kangsadan, S Promkotra	Yes

Session T2-6P



## Using of hydrogen peroxide for increasing of biologically active carbon filter work efficiency

Ivan Kozyatnyk and Natalia Klymenko

*Institute of Colloid Chemistry and Chemistry of Water, Ukrainian National Academy of Sciences, 42 Vernadsky Avenue, Kyiv 03680, Ukraine, e-mail: koziatnik@ukr.net, klimenko@carrier.kiev.ua*

### 1. Summary

The study addresses the influence of hydrogen peroxide on the efficiency of fulvic acids filtration through biologically active carbon. The paper authors defined optimal conditions for the application of hydrogen peroxide in the processes of BAC filtration. The authors also determined that the hydrogen peroxide concentration of 5 mg/L is the most effective as this concentration level allows increasing the oxygen content in the solution of natural organic compounds. The study showed that in the process of the filter loading the microorganisms consume oxygen released after the  $H_2O_2$  decomposition.

Keywords: activated carbon, bioregeneration, hydrogen peroxide

### 2. Extended Abstract

Using of activated carbon (AC) with inoculated microorganisms (BAC) is the most effective method for the advanced removing of the organic compounds from natural and waste water. Inoculation of AC by microorganisms and supporting of the optimal condition of their life is one of the most fundamental circumstances of the BAC successful using.

Hydrogen peroxide, except enrichment of liquid by oxygen, can be oxidizing agent for the dissolved organic matters in presence such catalyst as AC. Ability of AC to be catalyst in oxidation-reduction reaction is well known. Granulated activated carbon (GAC) is successfully used as adsorbent and catalyst in heterogenic catalysis owing to well developed surface, porous structure and flexible regulated characteristics.

The main goal of this work was to estimate hydrogen peroxide influence on fulvic acids filtration efficiency through BAC. Another aim was to determine rational condition of  $H_2O_2$  using in BAC filtration processes

As sorbent was used activated carbon KAU with such structural and sorption characteristics: effective mesoporous surface  $S_{me} = 630 \text{ m}^2/\text{g}$ ; volume of adsorption space  $V_a = 0,39 \text{ cm}^3/\text{g}$ ; volume of micropores  $V_{mi} = 0,12 \text{ cm}^3/\text{g}$ . As adsorbate were used fulvic acids (FA). They were receive by Forsit method from high-moor peat. Plant work was controlled by analysis of the water samples, which were taken from different height of the column. They were analyzed on content of fulvic acids (COD, TOC) and dissolved oxygen.

Decomposition degree of  $H_2O_2$  under initial concentration 1 mg/l is 94-96%. Therefore concentration of the released oxygen is not more than  $\sim 0.95 \text{ mg/l}$ . Under  $H_2O_2$  initial concentration  $H_2O_2$  10 mg/l the decomposition degree is 86-88% at the first moments. It is apparently conditioned by the spending of some part of hydrogen peroxide on the reaction with AC surface. At  $H_2O_2$  initial concentration 5 mg/l the quantity of  $H_2O_2$

released after oxidation at AC surface is ~4.8 mg/l. If dissolved in water oxygen is taken into account this value of oxygen will prevent of anaerobic process in AC loading. Value of limit specific adsorption of fulvic acids without H<sub>2</sub>O<sub>2</sub> is 102.5 mg/g and in presence of H<sub>2</sub>O<sub>2</sub> (10 mg/l) – 135 mg/g. As we can see from this data presence of H<sub>2</sub>O<sub>2</sub> in the system leads to some increasing of  $a_{\infty}$  value. It is probably stipulated for catalytic oxidation of some part of dissolved fulvic acids (up to 20-21%). Changing in the surface oxygen content groups on the AC KAU after contact with H<sub>2</sub>O<sub>2</sub> can confirm trustful of this assumption.

Thus, using of hydrogen peroxide solution with concentration 5 mg/l is the most expedient because it allows enrichment fulvic acids solution by oxygen without using it for AC surface oxidation and partly use of catalytic reaction of fulvic acids oxidation.

Experimental dates were compared in the both columns on the height of 15 cm where experimental was going for 14 months. Native biofilms was formed on AC for this time.

Earlier we showed that efficiency of organic matters solution filtration through the BAC is expediently estimated by comparing of equal and dynamic adsorption capacity of AC. It is known when biodegradation processes in the layer of AC is absence, equal capacity is always bigger or in ideal case at the absence of mass transfer resistance is equal to dynamic capacity. Increasing of the dynamic capacity above equal is evidence that the bioregeneration of AC is going on as a result of adsorbed compound biodegradation. Presence of hydrogen peroxide in fulvic acids solution which is entered to the BAC filter lead to the increasing of adyn value for 81 %. At the same time  $a_{eq}$  in presence of H<sub>2</sub>O<sub>2</sub> is bigger  $a_{eq}$  at it absence for 27 %. That is why we can suppose that in biofiltration process influence of hydrogen peroxide is stipulate for both catalytic oxidation of part of organic substrate and intensification of the biological processes in BAC layer. The last is probably conditioned by amount of oxygen solution which is passed through BAC filter.

Amount of oxygen in solution decreased from 3.8 mg/l at height 15 sm to 1.8 mg/l at height 90 sm after setting of stationery regime of filtration. According to the dates from such amount of oxygen is not enough for normal life of aerobic biocenose.

Under filtration of the fulvic acids solution with H<sub>2</sub>O<sub>2</sub> though AC layer oxygen concentration was not lower than 3 mg/l both at the top and the bottom of the AC layer. The initial concentration of the oxygen was 4-4.5 mg/l. It is confirmation that the oxygen released at the catalytic decomposition of H<sub>2</sub>O<sub>2</sub> is consumed by microorganisms.

## Conclusion

Using of H<sub>2</sub>O<sub>2</sub> at concentration 5 mg/l is the most expediently because it allows to enrichment NOM solution such as fulvic acids by oxygen without using it for AC surface oxidation. Oxygen can be partly used for catalytic oxidation of the fulvic acids. This approach may be recommended for the enrichment of the waste and natural water by oxygen during advanced treatment by biologically active carbon.

## **Electrical interaction between two long, parallel particles covered by an ion-penetrable charged membrane in oil-water interface**

S. Tseng,<sup>a</sup> L. F. Cheng,<sup>b</sup> J. P. Hsu<sup>b</sup>

<sup>a</sup>*Department of Mathematics, Tamkang University, Tamsui, Taipei 25137, Taiwan*

<sup>b</sup>*Department of Chemical Engineering, National Taiwan University, Taipei10617, Taiwan*

### **1. Summary**

The electrical interaction between two parallel, infinite, particles of elliptical cross section, each is covered by an ion-penetrable charged membrane layer, immersed in a water/oil interface is calculated. The effects of the key parameters of the system under consideration on the electrical interaction are discussed. The membrane layer may contain acidic dissociable functional groups. We conclude the followings: (1) The rate of decrease in the electrical potential as the separation distance between two particles varies in oil phase is slower than that in water phase. (2) For constant total amount of fixed charge in membrane layer, the thinner the membrane the greater the electrical interaction force. (3) The higher the pH or the larger the equilibrium dissociation constant, the greater the interaction force. (4) The closer the shape of a particle to a cylinder the smaller the interaction force. (5) The interaction force when the major axis of a particle is parallel to oil-water interface is smaller to that when it is perpendicular to oil-water interface.

Keywords: electrical interaction, rod-like particles, ion-penetrable membrane, oil-water interface

### **2. Introduction**

The stability of a colloidal dispersion depends largely on two competitive forces between colloidal particles, the van der Waals attractive force and the electrostatic repulsive force. The former is related to the physical properties of colloidal particles and the dispersion medium, and the latter, for rigid entities, is a function of the charged conditions on particle surface. A colloidal dispersion remains stable if the magnitude of the electrostatic repulsive force exceeds that of the van der Waals attractive force. Although previous studies on these forces are ample in the literature, most of them focused on the case where only one

dispersion medium is present. Also, relevant analyses are often limited to the interactions between two identical particles of simple geometries.

Surfactants or stabilizers are often introduced into an emulsion system to improve its stability. Relevant problems are of practical significance in medical, pharmaceutical, cosmetic, and food areas. Many attempts have been made to investigate systems involving oil/water interface. In this study, our previous analysis (Hsu et al., 2003) on the electrical interaction between two rod-like particles covered by an ion-penetrable membrane in a water-oil interface is extended to the case in which the radii of two particles can be different and level of electrical potential is arbitrary. Also, the membrane layer contains dissociable functional groups, the degree of dissociation of which is a function of the electrical potential. This condition is of practical significance because it provides a more realistic description for biocolloids and particles covered by an artificial membrane layer such as polymer layer

### 3. Theory

We consider the interaction between two parallel, infinitely long particles each of them comprises a rigid core and an ion-penetrable membrane, which contains uniformly distributed dissociable functional groups. Three types of particles are examined, including that the cross section of a particle is a circle, a prolate, or an oblate. The linear sizes of the cross section of two particles can be different, and both are immersed in the oil-water interface. The portion of a particle in the oil phase and that in the water phase depend on the contact angle. For simplicity, we assume that the oil-water interface is flat throughout the system. Both the water phase and the oil phase contain  $a:b$  electrolytes, but the concentration in the former is much higher than that in the latter. The resolution of the present problem involves solving the governing equations for the electric field, a modified Poisson-Boltzmann equation subject to appropriately assign boundary conditions. The solution obtained is then used to evaluate the electrical force between two particles based on Maxwell stress tensor. Numerical simulations are conducted to examine the influences of the key parameters of the system under consideration on the general behaviours of the electrical force between two particles. These include the linear size of a particle, the thickness of the membrane layer surrounding a particle, the relative sizes of two particles, the shape of a particle, the amount of electrolytes in the oil phase, the contact angle, the pH value in the aqueous phase, the dissociation constant of the functional groups in the membrane layer, and the valence of electrolytes.

### Acknowledgment

This work is supported by the National Science Council of the Republic of China.

### Reference

Hsu, J. P., Jiang J. M. and Tseng, Jiang (2003) *Colloids and Surfaces B*, 27,49-58.

## The effect of polyacrylamides on the flocculation and settling behaviour of kaolinite dispersions

M.S.Nasser and A.E. James

*Department of Chemical Engineering, University of Manchester, M60 1QD Manchester, UK*

### 1. Summary

The effects of the surface charge and molecular weight of cationic and anionic polyacrylamide (PAM) on the floc size, effective floc density and settling rate of kaolinite suspensions has been investigated at pH 7. At optimum polymer concentrations, the kaolinite floc sizes were larger and the settling rates were greater in the presence of anionic PAM than cationic PAM. The difference in the floc sizes of the flocculated slurries may be attributed to floc structure-related adsorption. Cationic polymer chains adsorb via hydrogen bonding interactions between OH groups at the particle surface and polymer's amide groups, these electrostatic attractions between the positively charged polymer and the negatively charged kaolinite produce dense and close floc structures. For anionic PAM, however, although the adsorption still occurs through hydrogen bonding between the OH groups at the particle surface and polymer's amide groups, the interactions appear to be weakened as a consequence of electrostatic repulsion between the negatively charged polymer and negatively charged kaolinite surface. These repulsive forces allow the polymer molecules to be extended and produce loops and tails, which lead to the formation of large open-structure flocs having low density.

*Key words:* kaolinite; polyacrylamide; floc size; settling rate; effective floc density.

### 2. Extended Abstract

The equipment used here to measure the flocs size was modified by the authors from the original design of Tambo and Watanabe [1] (see Fig. 1a). The basic function of the flocculation unit in the setup is to enable flocs to be produced in different conditions. The function of the sliding trap is to allow individual flocs pass through then to settle in the settling column. As flocs can change size through interactions with other particles and flocs, the measurements of the flocs should be performed in a dilute suspension in order to avoid additional flocculation during analysis. In this study, a 0.005 volume fraction was found sufficient to provide the required dilution. A parallax correction unit is fitted at the bottom of the settling column in order to reduce refraction arising from the effects of curvature. A measuring tape was attached to the column and digital camera was used to capture the flocs. An image analysis tool (UTHSCA, Texas,) was used to analyse the data (see Fig. 1b). According to results of Tambo and Watanabe [1], the effective floc density, can be estimated using a modified Stokes' Equation:  $\rho_e = \frac{135\mu_w V_s}{4.g.d_f^2}$ , where  $\mu_w$  is the dynamic viscosity of water,  $d_f$  is the floc diameter,  $V_s$  is settling rate and  $g$  is the gravitational force.

The characteristic of the six different PAM used as flocculants and the experimental results are summarized in Table 1. In a previous paper [2] we have determined the optimum flocculant dosage for kaolinite suspensions flocculated using these PAM.

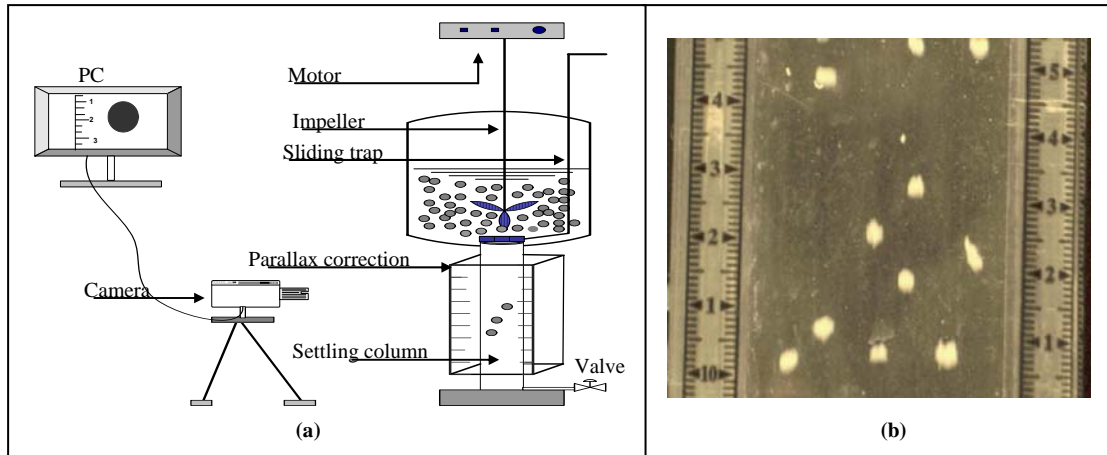


Figure 1: (a) Flocculation unit used for floc size measurements and (b) Typical photographs of kaolinite-PAM flocs of 0.005 volume fraction flocculated using C492 at optimum concentration and pH 7

The results show that using similar molecular weight and surface charge density the floc sizes of the kaolinite produced by anionic polyacrylamides are larger but less dense than those produced by cationic polyacrylamides. The difference in the floc sizes and floc densities may be attributed to floc structure-related adsorption. The adsorption of the anionic and cationic polyacrylamides occurs through hydrogen bonding between the silanol and aluminol OH groups at the particle surface and polymer's primary amide functional groups. But the repulsion between the negatively charged anionic polymer and negatively charged kaolinite surface allow the polymer molecules to be extended and produce loops and tails, which lead to the formation of larger and open-structured flocs of less dense than those in the cationic polymers.

Table 1: Floc sizes, settling rates and effective floc densities for kaolinite suspensions using optimum PAM concentrations at pH 7

Polymer type	Charge type	M. weight $\times 10^{-6} /$ $(\text{g mol}^{-1})$	Charge density (%)	Optimum concentration $/(\text{mg kg}^{-1})$	Floc size $/(\text{cm})$	Settling rate $/(\text{cm s}^{-1})$	Floc density $/(\text{g cm}^{-3})$
C 446	3-4	Cationic	35	240	0.199	1.152	0.0101
C 496	5-7	Cationic	35	240	0.232	1.652	0.0106
C 492	5-7	Cationic	10	240	0.260	1.811	0.0093
A130LMW	3-4	Anionic	35	120	0.220	1.280	0.0092
A 130	10-12	Anionic	35	60	0.311	1.890	0.0068
A100	10-12	Anionic	10	60	0.341	2.143	0.0064

Further investigation is undertaken to study the rheological behaviour and the particle-particle interaction forces for the kaolinite-PAM suspension and correlate that to the flocs structure (i.e. floc size and strength).

## References

- [1] Tambo, N., and Watanabe, Y., (1979) *Water Research*, 13,409-419.  
 [2] Nasser, M. S, and James, A. E., (2006) *Separation and Purification Technology*, 52, 241-251.

## Thin film flow of a liquid down smooth and rough surfaces

L. Broniarz-Press, D. Dulaska, S. Woziwodzki

*Department of Chemical Engineering and Equipment, Poznan University of Technology,  
pl. M. Skłodowskiej-Curie 2, PL 60-965 Poznan, Poland*

### 1. Summary

The flow of viscous liquids in thin films down a vertical or inclined to horizontal plates under the influence of gravity and surface tension is of both fundamental and practical importance in a wide variety of separation and heat/mass transfer processes. The paper deals with the results of the studies on the effect of plate roughness on a mean film thickness of Newtonian liquids. It has been shown that in the laminar region of the falling liquid flow the small artificial roughness ( $d_r \leq 710 \mu\text{m}$ ) does not effect on the mean thickness of the thin layer. The effect of the wall roughness was found as the evident one in turbulent film flow down the surfaces studied. The film thickness values increased with increase of the grain size values.

Keywords: falling film, film thickness, rough plate

### 2. Extended Abstract

The flow of liquids in thin films down a vertical or inclined to horizontal plates under the influence of gravity and surface tension is of both fundamental and practical importance in a wide variety of separation and heat/mass transfer processes. The occurrence of waves on the film surface as well as the solid wall roughness are known to enhance greatly the rates of mass and heat transfer (Broniarz-Press, 1991). The small thickness of a film compared to the characteristic sizes is usually encountered in nature and patterns of liquid flows (Broniarz-Press, 2004). In the present work the results of the studies on the effect of plate roughness on a mean film thickness of Newtonian liquids, have been presented.

The experiments were performed using two types of plates of 241 mm width and 1165 mm length: smooth constructed from organic glass and rough (coated with grains of abrasive material of various size distributions). The plates were inclined to horizontal at an angle  $\theta$  equal to  $24^\circ$ . The grain-size distributions of the modified plates used ranged as follows:  $d_r \in (125,300) \mu\text{m}$  for plate P100,  $d_r \in (300,710) \mu\text{m}$  for coated plate P40 and  $d_r \in (1.00,2.36) \text{ mm}$  for P16 one. The experimental data were elaborated using the dimensionless relationship of the reduced mean thickness  $s_r$  of a film on equivalent Reynolds number  $Re_e$ .

$$s_r = \frac{s}{\delta_{e,\theta}} = C Re_e^A \quad (1)$$

where:

$$Re_e = \frac{4\Gamma}{\eta} = \frac{4ws\rho}{\eta}, \quad \delta_{e,\theta} = \left( \frac{\eta^2}{g\rho^2 \sin \theta} \right)^{1/3} \quad (2)$$

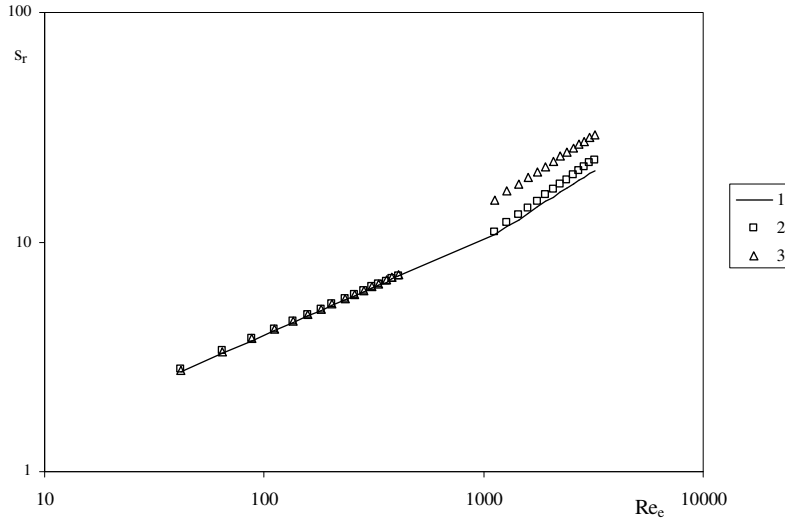


Figure 1: Reduced liquid film thickness vs. modified Reynolds number: 1 – smooth plate, 2 – plate P100, 3 – plate P40

It has been shown (Figure 1) that in the laminar region of the falling liquid flow the artificial roughness used had no effect on the mean thickness of the thin layer. The effect of the wall roughness was found as the evident one in turbulent film flow down the surfaces studied. The increase in thickness values in a film flowing turbulently down the plate P40 (in comparison with the data for smooth plate obtained) was practically independent of Reynolds number. The increase in values of  $s_r$  was about 50.6%. For a plate P100 the increase of reduced mean thickness with the increase of Reynolds number was observed. For example, at  $Re_e = 1100$  the degree of an increase was 13.8%, and at  $Re_e = 4000$  24.6%, respectively.

## References

- Broniarz-Press, L., *Transfer Processes Enhancement Using Passive Turbulization of a Stream*, Poznan University of Technology Publishers, Poland (1991).  
 Broniarz-Press, L., *Liquid Falling Film Hydrodynamics and Transfer Processes in Film-Apparatus*, Poznan University of Technology Publishers, Poland (2004).



## **Sedimentation in Micellar Solutions of Tetradecyltrimethylammonium Bromide**

J. Rozanski, L. Broniarz-Press

*Department of Chemical Engineering and Equipment, Poznan University of Technology,  
pl. M. Skłodowskiej-Curie 2, PL 60-965 Poznan, Poland*

### **1. Summary**

In this paper the results of experimental studies on the sedimentation process of barium carbonate in aqueous solutions of tetradecyltrimethylammonium bromide (TTAB), have been presented. As the additives assisting in micellar association the sodium bromide and sodium salicylate (NaSal), have been used. It has been shown that in TTAB solutions of concentrations about 1CMC and 2CMC, the sedimentation process proceeds faster than in clear water. The reason of that observation can be a fact that the cationic surfactants are adsorbed on the barium carbonate molecule surface. As the result it causes the both, reduced surface charge and decreased repulsion between particles. Aggregation is induced by the hydrophobic interactions between particles. For the sake of bigger mass, the molecules fall faster. Growth of the TTAB concentration to 10CMC level and addition of sodium bromide into a solution causes slowing down the sedimentation process. It is the result of the growth in fluid density and viscosity.

Keywords: sedimentation, surfactant solution, tetradecyltrimethylammonium bromide

### **2. Extended Abstract**

In dilute solution the molecules of surfactant cover the interface with the hydrophilic part uniaxially oriented to water. Above the value of CMC the surfactant builds up the spherical micellar structures. The increase of concentration of surface-active agent in a solution causes the transformation of micelles from spherical form to rodlike structure. The transformation takes place when the solution concentration is equal to so-called second critical micellization concentration (CMC<sub>2</sub>). The sphere-rod transition of the alkyltrimethylammonium halides micelles can be caused by addition of salt too (Imae and Ikeda, 1986). The longest micellar associates (called wormlike micelles) in alkyltrimethylammonium halides solutions with added sodium salicylate, have been formed (Qi and Zakin, 2002).

The idea of using cationic surfactant to alter the suspension stability is not new (Gupta and Basu, 2005). In this paper the results of experimental studies on the sedimentation process of barium carbonate (of mean particles diameter of 25 µm) in aqueous solutions of tetradecyltrimethylammonium bromide (TTAB), have been presented. As the additives

assisting in micellar association the sodium bromide and sodium salicylate (NaSal), have been used. The critical micelle concentration (CMC) of the TTAB is  $1.3 \text{ g/dm}^3$ . The sedimentation tests were carried out in the transparent cylinder of  $1 \text{ dm}^3$  volume and height of 34 cm. The experimental results were presented in form of relationships the height of suspension column  $h$  vs. sedimentation time  $t$ .

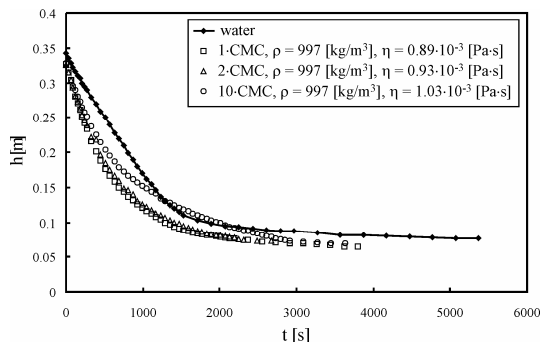


Figure 1: Sedimentation curves of barium carbonate in water and aqueous solutions of TTAB ( $T = 298\text{K}$ )

It has been shown that in TTAB solutions of concentrations about 1CMC and 2CMC, the sedimentation process proceeds faster than in clear water (Figure 1). The reason of that observation can be a fact that the cationic surfactants are adsorbed on the barium carbonate molecule surface. As the result it causes the both, reduced surface charge and decreased repulsion between particles. Aggregation is induced by the hydrophobic interactions between particles. It will facilitate the approach of molecules to each other and the greater agglomerates are formed. For the sake of bigger mass, the molecules fall faster. Growth of the TTAB concentration to 10CMC level and addition of sodium bromide into a solution causes slowing down the sedimentation process. It is the result of the growth in fluid density and viscosity. The sedimentation velocity for barium carbonate falling in TTAB/NaSal system was lower than this one in the clear solvent observed. The growth of the viscosity of this solution has been observed. It can be the result of the decrease of sedimentation velocity.

## References

- Imae, T. and Ikeda, S., (1986) *Journal of Physical Chemistry*, 90, 5216-5223.  
 Qi, Y. and Zakin J. L., (2002) *Industrial and Engineering Chemistry Research*, 41, 6326-6336.  
 Gupta, J. K. and Basu S., (2005) *Colloids and Surfaces, A: Physicochemical and Engineering Aspects*, 255, 139-143.

## Phase Inversion in Liquid – liquid Batch Stirred system

M. Amouei, P. Khadiv-Parsi\*, M.A. Moosavian, A.A. Davoodi

*Department of Chemical Engineering, University of Tehran, Tehran, Iran.*

*\*Email: kpars@ut.ac.ir*

### 1. Abstract

The aim of this research is the study of speed of rotation or energy input in the range of 400 to 800 rpm in a batch liquid-liquid system of toluene and water. It was also studied the presence of sodium chloride and magnesium sulphate in the system.

It was shown that the increase of energy input had more obvious effect on O/W dispersion at lower values of holdup. Also, shown that the ambivalence region of phase inversion curve was shifted down ward and became wider as a result of decrease in interfacial tension.

It was observed that inorganic salt used in both single and dual (mixed) shapes enhanced phase inversion for O/W dispersion. Therefore, the more the ionic strength, the more the tendency to inversion is.

Keywords: phase inversion, holdup, ambivalence region, delay time, dispersed phase, drop.

### 2. Extended Abstract

#### Introduction

Due to the different natures of molecular forces existed in aqueous and organic phases, there is a noticeable difference between O/W and W/O dispersion when separation of two phases occurs. Therefore, it is very important to select exactly the dispersed or drop phase [1].

Most of works have been done in stirred vessels and columns with mechanical parts. The main purpose of these works was the determination of ambivalence region related to the curve of critical hold up versus speed of rotation in a batch system [2-5].

#### Apparatus

The experiments were conducted in a batch mixed vessel or contactor. The vessel was made of pyrex glass which contained an stainless steel impeller and its shaft in the shape of hollowed cylinder, comprising two parallel disks attached by vertical rods. In order to detect phase inversion points, a conductivity meter has been used.

#### Results and discussion

Figure1. shows the behavior of the ambivalence region for systems of W/n-C<sub>7</sub> and w/toluene.

The upper curve represents inversion of O/W to W/O dispersion and the lower one represents vice versa.

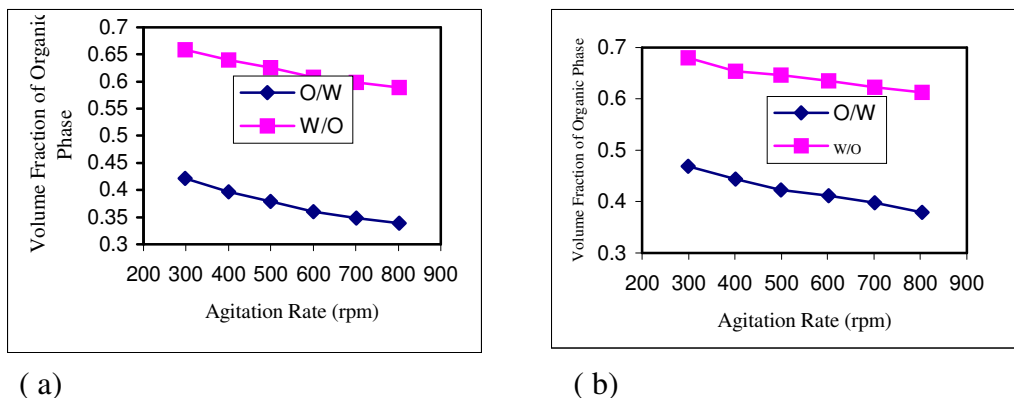


Figure 1. a) Ambivalence region for the system of W/n-C7. b) Ambivalence region for the system of W/Toluene.

As seen from these figures, for drop holdups less than 0.5, phase inversion does not take place, neither for the organic drops (upper curve) nor for the aqueous phase drops (lower curve).

### Conclusion

Experiments showed a difference between phase inversion behavior of two initial dispersions of O/W and W/O. The O/W dispersions inverted to W/O dispersion at lower holdup when rotation or energy input increased, while this was vice versa for W/O dispersion. It was strongly related to secondary dispersions formed in W/O.

It was found that the interfacial tension widened the ambivalence region accompanied with a downward shift.

Adding salt to an O/W dispersion enhanced the phase inversion which was more obvious for salt with higher charge. Also, mixture of two salts of NaCl and MgSO<sub>4</sub> was examined and revealed that mixed salts behaved well with respect to a separate salt ( data not shown).

### References

- Yeo, L. Y., Matar, O. K., Perez de Ortiz, E. S., Hewitt, G.F., *Multiphase Sci. Technol.*, 12, p. 51 (2000).
- Khdiv-Parsi, P. and M.-A. Moosavian, *Can. J. Chem. Eng.*, 82, 256-264 (2004).
- Yeo, L. Y.; Matar, O. K.; Perez de Ortiz, E. S.; Hewitt, G. F., *Chem. Eng. Sci.*, 57, 1069-1072 (2002).
- Khdiv-Parsi, P. and M.-A. Moosavian, *Iran. J. Chem. & Chem. Eng.*, 23,79-88 (2004).
- Khdiv-Parsi, P. and M.-A. Moosavian, *Iran. J. Chem. & Chem. Eng.*,23,89-96 (2004).

## Study on effective parameters on adhesion in segmented polyurethanes

M. Amrollahi<sup>a</sup>, G. Mir Mohamad Sadeghi<sup>a\*</sup>, M. Haghshenas<sup>b</sup>

<sup>a</sup> Department of Polymer Engineering, Amirkabir University of Technology, 15875/4413 Tehran, Iran

<sup>b</sup> Jihad Research Institute, Ministry of Agriculture, 16<sup>th</sup> Km. Karaj Road, Tehran, Iran

### 1. Summary

Phase separation in segmented polyurethanes is an important phenomenon which affects on characteristic properties of polyurethanes. Morphology, formation and distribution of microdomains (hard segments and soft segments) are effective parameters on adhesion and interfacial interaction of polyurethane system. In this work segmented polyurethanes based on 4,4'-diphenylmethane diisocyanate (MDI) and 1,4-butanediol (BDO) were synthesized and the effect of hard segment content as well as type of polyol on adhesion properties of synthesized polyurethanes has been studied and also correlation between microstructural factors on final behavior (peel strength and tack resistance) of polymer well defined.

Keywords: polyurethane, adhesion, phase separation, peel strength, tack resistance

### 2. Extended Summary

#### 2.1. Introduction

Segmented polyurethanes that consist of alternating soft and hard segments offer unique possibilities of tailor-made polymers by varying block length and composition [1]. Thermodynamic immiscibility between hard and soft segments induces phase separation and generates a two-phase morphology in these segmented block copolymers. There are some reports on evaluation of structure-properties in these segmented polyurethanes [2-4].

In the present study the effect of hard segment content, type of polyol on the thermo-mechanical properties as well as swelling behaviour and adhesion properties such as tack and peel strength of synthesized Polyurethanes has been studied.

#### 2.2. Experimental

The polybutadiene-ol were prepared locally [5] with low vinyl microstructures and Mn being about 2500 gr/mol. PTMG and polycaprolactone with Mn about 2500 obtained from Merck and used as received. Polybutadiene-ol and other polyols were degassed at 50 °C for 24 hr before use. MDI (4,4'-diphenylmethane diisocyanate), BDO(1,4-butane diol) from Merck were used after drying at 50 °C and 800 mm-Hg vacuum for 8 hr. Toluene and Dimethyl-formamide were used to measure swelling ration of polyurethanes.

Aluminium and glass were chosen as substrate to evaluate adhesion properties of polyurethanes.

#### Synthesize method

All the polyurethanes synthesized using one-shot method. The procedure was as follows: Polyol, MDI and BD were mixed vigorously for a few minutes. The above mixture was poured in a rectangular mould. The mould was preheated and coated with silicon before use. The mould was in a 85°C oven for 3 days. All of tests were carried out on the specimens that maintained in a desiccator for 7 days. Final cross linked products (networks) were insoluble in common solvents. Polyurethanes were synthesized in various molar ratios and hard segment contents of 25 %, 40% and 55%.

#### 5. Analytical techniques

A VPO Knauer apparatus was used to determine Mn of polyols. Toluene as solvent at 90° C and benzyl was used for calibration. A Polymer-Lab DSC was used. The DSC runs were performed under nitrogen using a heating rate of 10 °C/min with sample weight of 10 mg .The static mechanical properties were carried out by MTS tensile machine with a separation speed of 500 mm/min. Peel strength and tack of adhesives were measured according to ASTM D-3221 and ASTM D-1002 respectively.

#### Conclusion

Experiments showed that as the hard segment content of polyurethanes as well as type of polyol affect on mechanical and adhesion properties of polyurethanes. As hard segment content increases, storage modulus of polyurethane increases but damping decreases. Moreover in polybutadien-ol, low temperature damping of network increases. Peel strength of ester-type polyurethane is higher than two others. Hard segment content affects broadness of damping peak of network in DMTA analysis.

#### References

- Speckhard,T.A;Cooper,S , (1986) *Rubb.Chem.Tec.*, 59 ,405-413  
Cuve,L;Pascault,J.P.;Boiteux,G.;Boiteux,G. (1993) *Polymer*, 33,18  
Ono,K;Shimada,H,Nishimura,T, (1977) *J.Appl.Polym.Sci.*, 21,3223, 1977  
Huang, G. *J. Appl. Polym. Sci.* (1997) ,63,1309  
Mir Mohamad . Sadeghi G., Morshedian,J., Barikani M.(2003) *Polym.International* ,52 ,1083.

## **A Dynamics Behavior of Two-Dimensional Colloidal Aggregates using Discrete Element Method (DEM)**

T. Kangsadan<sup>a</sup>, S. Promkotra<sup>b</sup>

<sup>a</sup>*Chemical and Process Engineering Program, The Sirindhorn International Thai-German Graduate School of Engineering, King Mongkut's Institute of Technology North Bangkok 10800, Thailand*

<sup>b</sup>*Geotechnology Department, Faculty of Technology, Khon Kaen University 40002, Thailand*

### **1. Summary**

Two-dimensional (2D) colloidal aggregates of polystyrene microspheres were formed on the air-liquid interface and characterized by digital video microscopy. Since, these 2D colloidal aggregates can be treated as the granular material or discontinuum materials, the dynamics behavior can be easily monitored and investigated with the used of the Discrete Element Method (DEM) computer simulation. The aggregates occurred due to the force interactions between particles that also depend on their chemical conditions and environments. The force interactions that influence the behavior of colloidal particles were the spring-and-dashpot and the van der Waals forces. These can be implemented along with appropriate conditions in the conventional DEM and the dynamics behavior of 2D colloidal aggregates could be obtained. The results from the simulation could be further studied in a statistical mechanical analysis of contact forces and stress and the compressive behaviors of clusters and rearrangement mechanisms of the aggregates. Unfortunately, the main focus of this paper is to introduce another computer simulation method, DEM that can be easily applied and mimic the behavior of colloidal aggregates. The simulation results have been verified with the experiments.

Keywords: discrete element method, dynamics behavior, colloidal aggregates

### **2. Extended Abstract**

The compressive deformations of 2D colloidal aggregates formed on the air-liquid interface were examined to characterize the mechanical properties of particles by digital video microscopy and orientations of particles as coordination number (Kangsadan, 2006). In order to have a better understanding of this system, the dynamics behavior and force interaction must be studied from the initial dispersed condition to the equilibrium state. Due to the complexity of the interaction force to be experimentally studied, the computer simulation was developed.

## Methodology

The dynamics behavior of 2D colloidal aggregates can be investigated using a computer simulation DEM since these particles can be treated as discontinuum materials. In DEM simulations, the dynamics and mechanical interactions of each particle are explicitly modeled with the soft-particle methodology which allowing the interparticle penetration to be considered explicitly. A detailed description of the motion on each particle at discrete points in time is monitored by applying Newton's Law directly. The elastic restitution and friction influence the particles' collision, which have a finite duration, and the magnitude of the interaction depends on the penetration path. The equations of colliding motion of particles can then be solved in regular incremental steps. The difficulties in this computer modeling are the models of collisions and friction between particles--contact force model to varying degrees of realism and accuracy. In the conventional DEM simulations, the contact force model is the spring and dashpot which is the combination of the elastic and viscous damping forces (representing the long-ranged interaction force). It has been known that the colloidal aggregates behave as elastic and plastic and has the van der Waals interaction force which is representing the short-ranged interaction force (Tatemoto et al., 2005). Therefore, the contact force model for the colloidal particles is the spring and dashpot and van der Waals forces.

## Result and Discussion

The computer simulation results indicated that the DEM could mimic the behavior of 2D colloidal particles, polystyrene microspheres of 4  $\mu\text{m}$  (also 40  $\mu\text{m}$ ) in diameter. Recall that the effect of van der Waals force is insignificant comparing to the other forces acting on the particle (such as the gravity force and the drag force) at the molecular level. In addition, it had been found that the ratio of gravity force to van der Waals force of larger particle was similar to that of smaller particle (Tatemoto et al., 2005). Therefore, the effect of the van der Waals force was not depended on the particle size and became significant in morphology.

From the experiment of 2D colloidal particles, polystyrene microspheres of 25  $\mu\text{m}$  in diameter by suspended in ethanol of 0.1 vol% solid fractions to eliminate the charges and dropped on the viscous liquid, glycerol-water solution to minimize the vibrations, the particles had been aggregated and formed the monolayer in a small chamber. The results from the experiment and the computer simulation were in good agreement. The colloidal particles were dropped into the chamber and became dispersed was similar to the initial condition set by the computer simulation. Then, particles started to move toward the side-walls and bounced back. The small colloidal aggregates were formed and became the large clusters, nearly the hexagonal crystal. All of these phenomena could be seen in the computer simulation.

## References

- Kangsadan, T. and Promkotra, S., (2006) *International Conference on Modeling in Chemical and Biological Engineering Science (CBES2006)*.
- Tatemoto, Y., Mawatari, Y., and Noda, K., (2005) *J. Chemical Engineering Science*, 60, 5010-5021.



## **Session T2-7a: Transport Phenomena in Porous/Granular Media – I**

<b>Abstract Number</b>	<b>Paper Title &amp; Authors</b>	<b>Included</b>
2425	Brownian dynamics simulations of tracer diffusion and dynamics in polyelectrolyte gels H Zhou, S B Chen	Yes
3164	Modeling of two-stage heat pump fluidized bed drying of protein S V G Alves, O Y Guzev, O A Filho	Yes
3236	Steady-State and Dynamic Systems for Diffusion Parameters Determination: Advantages and Disadvantages K Soukup, P Schneider, O Šolcová	Yes
3345	Modelling of diffusion of molecules in biporous structure supports R Mesnier, L Sorbier, M Quintard	Yes

Session T2-7a

## Brownian dynamics simulations of tracer diffusion and dynamics in polyelectrolyte gels

Huai Zhou and Shing Bor Chen

*Department of Chemical & Biomolecular Engineering, National University of Singapore, Singapore, 119260*

### 1. Summary

Brownian dynamics simulation was used to study tracer diffusion in polyelectrolyte gels. In this paper, a coarse-grained bead-spring lattice model was used along with a truncated Lennard-Jones potential representing the excluded volume effect and a screened electrostatic interaction accounting for charge effect. The electrostatic effect gives rise to different diffusion behaviors between the case in which the tracer particle and gel beads were oppositely charged and the case in which they are likely charged. The explanation of the behavior of tracer particle self-diffusion in polyelectrolyte gels was also discussed.

Keywords: Brownian dynamics simulation, polyelectrolyte gel, tracer diffusion, mesoscopic scale.

### 2. Extended Abstract

Theoretical investigations on tracer diffusion in polyelectrolyte gels are scarce as compared to those for static properties. In this paper, Brownian dynamics (BD) simulation was employed to study the diffusion behaviour of charged tracer particle in a polyelectrolyte gel network, which can be either rigid or flexible, and is represented by a coarse-grained bead-spring lattice. In BD simulation, the solvent is treated as a continuum, and its effect on the tracer is random force and drag force. The Langevin equation (1) describes the motion and dynamics of the tracer and the network beads:

$$\zeta \frac{dr}{dt} = -\frac{\partial U(r)}{\partial r} + R(t) \quad (1)$$

where  $\zeta$  is the friction coefficient,  $R(t)$  is the forces due to the incessant collision of the solvent molecules with the Brownian particle, and  $U(r)$  is the interaction potential consisting of a truncated Lennard-Jones potential representing the excluded volume effect, a screened electrostatic interaction accounting for charge effect, and a Harmonic spring force (for network beads) simulating the connectivity and flexibility. Periodic boundary conditions were used as usual. The tracer and gel beads are of equal size. The screened electrostatic interaction derived by Wiese and Healy (1970) was adopted.

In this work, the tendency of mean square displacement and diffusion coefficient with varying bead size, spring constant and charge condition was primarily investigated. The short time diffusion coefficient is obviously different from the long-time diffusion coefficient either in a polyelectrolyte gel network or in a neutral gel network. The self-diffusion coefficient of tracer particle decreases with increasing volume fraction of gel beads, spring constant and charge density of the cubic lattice, respectively. Fig.1(a) shows the results for the case where each bead carries 3 elementary charges, the normalized Debye length is 0.5, the normalized spring constant is 80. The diffusivity of tracer particles at various volume fractions of gel beads are compared, indicating a ‘confined effect’, which is caused by reduction of free space for tracer particle with the increase of the volume fraction.

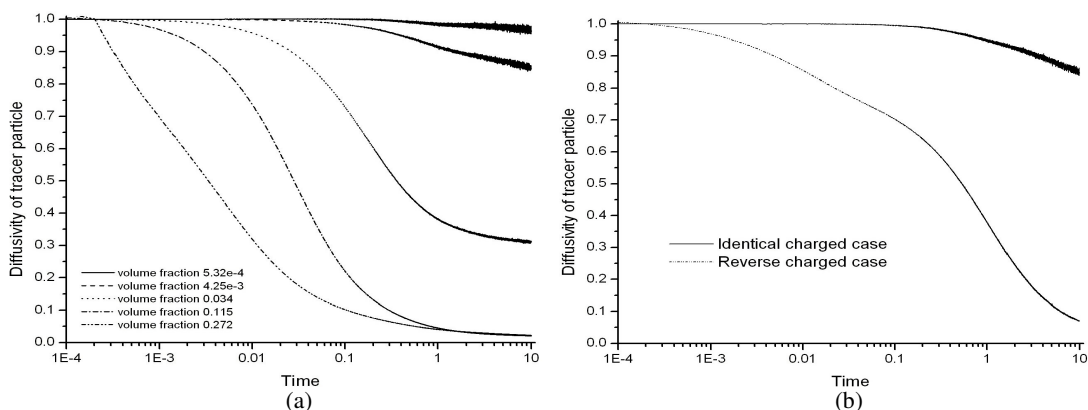


Fig.1 Diffusivity of charged tracer particle in polyelectrolyte gel network

In addition, the diffusion behaviours of tracer particle show a significant difference between the case in which the tracer particle and gel beads are reversely charged and the case in which they carry charges of the same sign, as shown in Fig.1(b), in which the diffusivity are calculated under conditions similar to those in Fig.1(a) with the volume fraction being fixed at about 5.32e-4. The obvious disparity in the diffusivity for the two cases may arise from the different behaviour of local electrostatic interaction between the tracer and a network bead, which appears to depend on the sign of charge.

## References

Wiese, G. R. and T. M. Healy, (1970) *Tran. Faraday Soc.*, 66,490-499.

## **Modeling of two-stage heat pump fluidized bed drying of protein**

S.V. Goncharova-Alves<sup>a</sup>, O.Yu.Guzev<sup>a</sup>, O. Alves-Filho<sup>b</sup>

<sup>a</sup>*Mendeleev University of Chemical Technology of Russia, Miusskaya sq., 9, 125047, Moscow, Russia*

<sup>b</sup>*New and Improved Drying Technologies, Elvevegen, 25, 7031, Trondheim, Norway*

### **1. Summary**

The experimental investigations of atmospheric two-stage heat pump fluidized bed drying of protein were carried out. The influence of drying stages number and drying time on the final product quality characteristics (residual moisture content, color, bulk density, shrinkage) was investigated. The mathematical modeling of drying kinetics was made using the experimental data. The modeling results showed that the proposed mathematical model is adequate to experimental data.

Keywords: heat pump drying, protein, modeling.

### **2. Extended Abstract**

There is an increase effort to adopt the international GMP standards in the pharmaceutical industry and other fields in Russia. Among the requirements of these standards is the manufacture of the highest quality products. Without conformity to such standards the Russian producers in the field of pharmaceutical industry will not have the needed edge to succeed in this highly competitive international market.

Drying is an essential unit operation in processing and production of pharmaceutical powders. This process has a great impact on the final product quality and energy utilization. The traditional technologies for drying of pharmaceutical are the vacuum freeze-drying, spray drying and fluidized bed drying. These technologies have limitations concerned to powder final quality, product residence time and production cost.

An innovative technology is atmospheric two-stage fluidized bed heat pump drying [Alves-Filho O., 2004; Alves-Filho O., 2006]. This technology allows to obtain the highest quality and predefined structure of the final product and to significantly reduce energy consumptions.

This process includes two stages, the first is fluidized bed freeze drying and the second is fluidized bed drying at medium temperature. The gentle conditions of atmospheric freeze drying allow improvement of product quality as well as preservation of the material structure. It promotes intensive mass and heat transfer during medium temperature drying and reduction in material residence time or production cost.

The main advantages of heat pump drying technology are:

recovering of the latent heat of the air exhaust in the drying chamber and consequent energy reduction in the order of 35 to 50%;

the closed drying cycle reduces product contamination and inlet gas filtering is much simpler compared to open cycles;

there is no environmental pollution by fine dried particles usually transported and discharged into surroundings in open cycles.

The experimental investigations of atmospheric two-stage heat pump fluidized bed drying of protein were carried out. The scheme of the laboratory atmospheric heat pump fluidized bed drier is presented on the Figure 1.

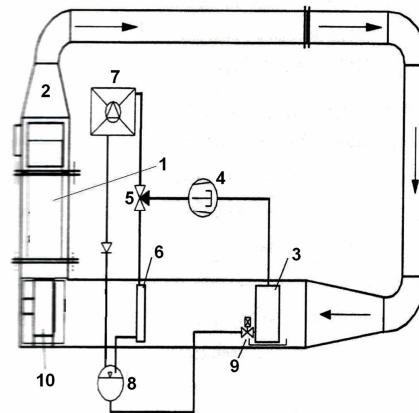


Fig. 1. Laboratory atmospheric heat pump fluidized bed drier: 1 – drying chamber; 2 – cyclone; 3 – refrigerant evaporator; 4 – compressor; 5 – three-way valve; 6 – internal refrigerant condenser; 7 – external refrigerant condenser; 8 – receiver; 9 – throttle valve; 10 – fan

The influence of drying stages number and drying time on the final product quality characteristics (residual moisture content, color, bulk density, shrinkage) was investigated.

The mathematical modeling of drying kinetics was made. The modeling objective was the determination of the optimal drying stages time to get the required residual moisture content and to preserve the quality characteristics of the final product. The modeling results show that the proposed mathematical model is adequate to experimental data and can be used to optimize the process.

## References

- Alves-Filho O. *Atmospheric freeze and medium temperature drying technologies for fish and marine products / Dehydration of products of biological origin*, Norway (2004).
- Alves-Filho O., Goncharova-Alves S.V., Guzev O.Yu. *Multistage drying of pharmaceutical powders and modeling of mass transfer*, (2006) *15th International Drying Symposium (IDS 2006): proceedings of symposium*, V. B, 1110-1117.

## **Steady-State and Dynamic Systems for Diffusion Parameters Determination: Advantages and Disadvantages**

K. Soukup, P. Schneider, O. Šolcová

*Institute of Chemical Process Fundamentals, Academy of Sciences of the Czech Republic, CZ-16502  
Prague, Czech Republic*

### **1. Summary**

The chromatographic method in the single pellet string column (SPSC) together with counter-current gas diffusion measurements are discussed and compared. From both methods transport characteristics of porous solids can be determined. Diffusion measurement methods are suitable for cylindrical shaped porous materials while SPSC allows to measure peculiarly shaped porous materials, too. On the other hand, diffusion methods are appropriate also for powder materials. The obtained transport characteristics from chromatographic and diffusion measurements are compared.

Keywords: transport parameters, mass transport, Single-Pellet String Column, Wicke-Kallenbach diffusion cell, Graham's diffusion cell

### **2. Extended Abstract**

Two groups of methods (dynamic/steady-state) commonly used for pore-structure characterization (effective diffusion coefficients and transport parameters,  $\langle r \rangle \psi$  and  $\psi$ ) are discussed. Transport parameters are constants of the porous medium and play an irreplaceable role in modelling and design of chemical and biochemical processes (Petrisans et al.). The chromatographic technique in the single-pellet string column configuration (SPSC) which represents the dynamic methods and steady-state counter-current gas diffusion measurements in Wicke-Kallenbach and Graham's diffusion cells were used and the results compared.

In SPSC (Scott et al.), particles are packed one by one into a column with diameter that exceeds only slightly (10–20 %) the particle dimension. A pulse of tracer gas is injected into the carrier-gas stream, which flows at constant flow rate through the column. Diffusion cell (Šolcová & Schneider) consists of two flow-through compartments separated by an impermeable disk with fixed samples. For the classic Wicke-Kallenbach cell outlet gas streams from both compartments are chromatographically analysed whereas experiments in the Graham's cell is based on the direct measurement of the net volumetric diffusion flux.

The main advantage of the SPSC chromatographic method is that it enables determination of transport parameters for variously shaped porous materials (asterisks, asterisks with hole, leness, extrudates, washcoats, etc.), while the diffusion cell methods requires cylindrically shaped pellets only. Another advantage of SPSC is the averaging of obtained transport parameters over many pellets (usually hundreds of pellets as compared with several pellets forced into the diffusion cell). On the other hand, in steady-state diffusion cell measurements with nonadsorbable gases only diffusion transport process takes place, while in the chromatographic column other processes, such as convection and axial dispersion and transport of the tracer through a laminar film around solid particles must be taken into account.

Sample	Diffusion			SPSC		
	$\langle r \rangle \psi$ [nm]	$\psi$ [-]	$\langle r \rangle^{*}$ [nm]	$\langle r \rangle \psi$ [nm]	$\psi$ [-]	$\langle r \rangle^{*}$ [nm]
ICI	2.7	0.037	73	2.27	0.027	84
G43-a	7.8	0.031	252	1.95	0.013	302
G4	60	0.09	663	18	0.034	526
G1	153	0.19	803	47	0.055	861

$$^{*}) \langle r \rangle = (\langle r \rangle \psi) / \psi$$

Table 1: Transport parameters from diffusion measurements and SPSC method

The obtained transport parameters from diffusion methods and SPSC are compared in Table 1. It can be seen that for all samples the mean transport pore radii are in a good agreement. Differences between parameters  $\psi$  (which is defined as the ratio of transport pore porosity to transport pore tortuosity) could be explained by the different diffusion path-length (tortuosity) under steady-state and dynamic conditions.

#### Acknowledgement

The financial support of the Grant Agency of the Czech Republic (203/03/H140) and Grant Agency of Academy of Sciences of the Czech Republic (A4072404) is gratefully acknowledged.

#### References

- Petrissans, A., Petrissans, M., Zoulalian, A., (2006) *Chemical engineering journal*, 117, 31–38.  
 Scott, D. S., Lee, W., Papa, J., (1974) *Chemical Engineering Science*, 29, 2155–2167.  
 Šolcová, O., Schneider, P., (2003) *Applied Catalysis A*, 244, 1–9.



## Modelling of diffusion of molecules in biporous structure supports

Raphaël Mesnier<sup>a</sup>, Loïc Sorbier<sup>a</sup>, Michel Quintard<sup>b</sup>

<sup>a</sup> IFP LYON, BP3, 69390 Vernaison, FRANCE

<sup>b</sup> IMF Toulouse, Allée du Professeur Camille Soula, 31400 Toulouse, FRANCE

### 1. Summary

Residual oils treatments are a big issue for refiners. They are usually hydrotreated by biporous (meso and macroporous) catalysts. In this study, we try to understand the link between transport properties of large probe molecules representative of residual oils and the texture of this kind of catalyst. Diffusion coefficients in porous media are measured by pulsed field gradient NMR (PFG-NMR). This technique allows us to determine two diffusion coefficients: one in macroporosity and an other in mesoporosity. A model was built where mesoporous domains are homogenized by using upscaling theories. The non linear adsorption of probe molecule is described by a Langmuir isotherme. Simulations are compared to experimental data which are obtained in measuring decrease of concentration of probe molecule in a solution in contact with biporous support. The biporous behaviour of this kind of system is discussed.

Keywords : biporous structure, diffusion, up-scaling, size effect, PFG-NMR

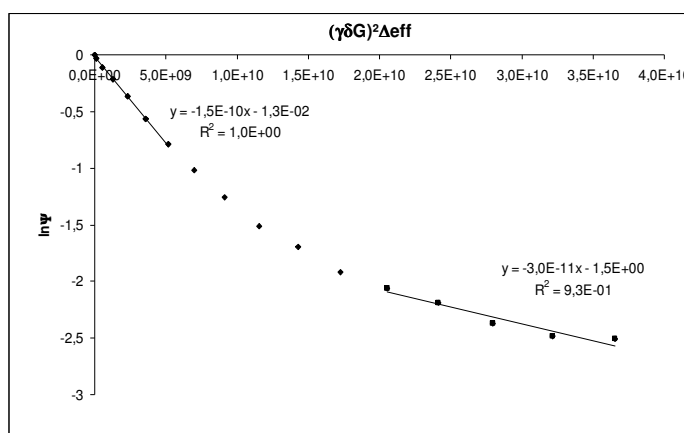
### 2. Extended Abstract

The quality of crude oils, the environmental norms and the needs of transport sector involve the development of residual oil treatment. The control of hydrotreating processes requires an overall understanding of the various stages of the catalytic reactions taking place, especially the ones concerning the transport of the molecules of the load to the active sites. Vacuum residues mainly contain asphaltenes which lead to problems associated to diffusion in the porosity of hydrotreating catalysts supports, because of their size. In the industry, the used hydrodemetalation catalysts are porous support having two scales of porosity : a macroporosity, in order to have a great porous volume and accessibility, and a mesoporosity to have a great active area.

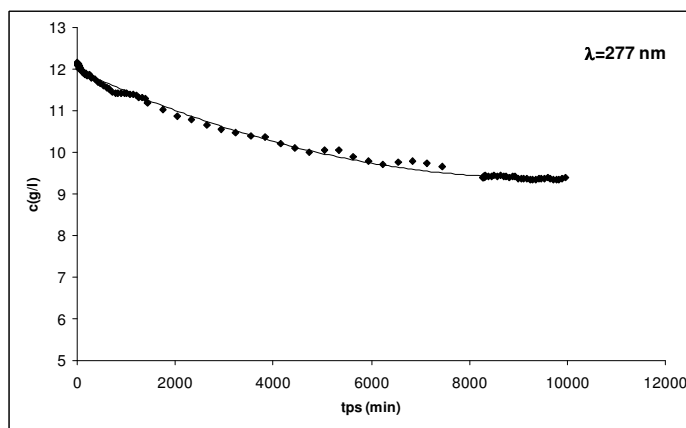
In our study, we measured the diffusion coefficients of three molecules of different sizes in this kind of support. These molecules are supposed to be representative of asphaltenes. Diffusion coefficients have been measured at a microscopic level by pulsed field gradient NMR (PFG-NMR). Based on these results, we built a model describing the kinetics of the diffusion of molecules at a macroscopic level, i.e., for a catalysts pellet. Using upscaling theories, the mesoporous domain can be homogenized and this leads to an effective diffusion coefficient. The macro-scale model will follow by a subsequent upscaling using this mesopore effective diffusion coefficient and the molecular diffusion coefficient in the macropores. The resulting macro-scale model takes into account the non linear adsorption of the molecules (Langmuir type) in mesoporosity. In fact, the accurate description of

mesoporosity is not easy with the actual experimental techniques. Therefore, the idea is to determine experimentally the diffusion properties in the mesoporous domain, and the macropore structure as a starting point for the upscaling theory. This is the objective of this paper.

Indeed, PFG-NMR measurements show there are two diffusion coefficients in biporous structures. It was verified that the value of the diffusion coefficient measured in the macropores is the same as the value in a free liquid. For the mesoporosity, it was found that the diffusion coefficient depends on the mesopore size and diffusing molecules. In addition, we can see an evolution of the effective diffusion coefficient with the mesoporous pore structure. Biporous structures are good candidates for a double-porosity behaviour, i.e., rapid diffusion in the macropores followed by a relaxation of the concentration in the mesoporous domain. Based on our experimental data, a numerical solution over a structure close to the real structure shows that relaxation time in the mesoporous domain is fast with regard to transport in macroporous network, at least for molecules of intermediate sizes. Therefore, this suggests that a single macro-scale effective diffusion coefficient may be used for the description at the pellet-scale.



Diffusion decays of PS  $M_w=3\ 000\ \text{g}\cdot\text{mol}^{-1}$  in Biporous support



modelisation of concentration of PS  $M_w=3\ 000\ \text{g}\cdot\text{mol}^{-1}$  in bath containing biporous support

## References

- Kortunov, P.V., Skirda, V.D., (2005) *Colloid Journal*, 67 (5), 573-580.  
 Whitaker, S., *The Method of Volume Averaging*, Kluwer Academic Publishers, The Netherlands (1999).

## Session T2-7b: Transport Phenomena in Porous/Granular Media – II

Abstract Number	Paper Title & Authors	Included
848	Transient natural convection in stored granular media J G A Acevedo, E Tsotsas	Yes
1627	Effect of liquid flow rate and bed void fraction on the hydrodynamics and performance of a trickle-bed bioreactor M C Díaz, S Revah, R L Oehmichen	Yes
2179	Effective diffusivities of gases in a reconstructed porous body P Čapek, V Hejtmánek, L Brabec, A Zikánová, M Kočířík	Yes
2199	Influence of the interfacial reaction rate on macroscopic systems F J Valdes-Parada, M Sales-Cruz, J Alvarez-Ramirez, J A Ochoa-Tapia	Yes
2293	Prediction Of Shelf-life Of Beverages Stored In Pet Bottles With Passive And Active Walls R. Di Felice, D. Cazzola, S. Cobror, L. Oriani	Yes
3159	Production of cylindrical carbon xerogel monoliths: effect of sample diameter on drying-induced cracks A Léonard, M Crine, W Jomaa	Yes

Session T2-7b

## Transient natural convection in stored granular media

J.G. Avila-Acevedo and E. Tsotsas

*Thermal Process Engineering, Otto-von-Guericke-University Magdeburg, Universitaetplatz 2,  
D-39016 Magdeburg, Germany*

### 1. Summary

In the present work the transient natural convection taking place in a cylinder filled with a saturated porous medium is studied. A mathematical model is developed, and the parameters influencing heat transfer are identified. Results from simulations are compared with experiments allowing for model validation. A criterion for neglecting the effect of natural convection is established.

Keywords: Transient heat transfer, natural convection, porous media, homogeneous model

### 2. Extended Abstract

With the aim of analyzing and understanding the heat transfer phenomenon associated with moisture migration during the storage of granular materials [1], the transient heat transfer in a cylinder filled with a saturated porous medium is studied in the present communication. The saturated medium has a uniform initial temperature. The side wall of the cylinder undergoes a sudden change to a lower temperature at  $t = 0$ , while the ends of the packed cylinder are considered to be insulated. A homogeneous model is derived, where the porous medium is considered to be isotropic with local thermal equilibrium between the phases, following [2]. The Darcy law is assumed for the flow and the Boussinesq approximation is used for accounting density variations. The problem is transformed into a dimensionless form where the most relevant parameters appearing are the aspect ratio of the cylinder ( $R/H$ ) and the modified porous media Rayleigh number

$$Ra_b = \frac{Kg\rho_0\beta H}{\mu\alpha^*} (T_0 - T_w).$$

The latter depends on temperature difference, fluid properties (density  $\rho$ , viscosity  $\mu$ , coefficient of thermal expansion  $\beta$ ), bed properties (bed permeability  $K$ , fluid based bed thermal diffusivity  $\alpha^*$ ), and silo height  $H$ .

A finite differences method with central differencing scheme is used for the numerical solution of the problem and can predict well the results of the analytical solution existing for the case without free convection ( $Ra_b = 0$ ). Cases with free convection ( $Ra_b > 0$ ) have been analyzed systematically by variation of the Rayleigh number (changes of interstitial fluid, air or water, particle sizes and of the magnitude of the temperature jump) and the aspect ratio. Comparison with experimental results (transient cooling of small

cylinders packed with glass beads and filled with water) reveals a good agreement, as it is shown in Fig. 1. The model describes properly the real cooling process, following the trend for faster cooling at higher convection intensities. Minor deviations may be attributed to the influence of the wall on bed structure.

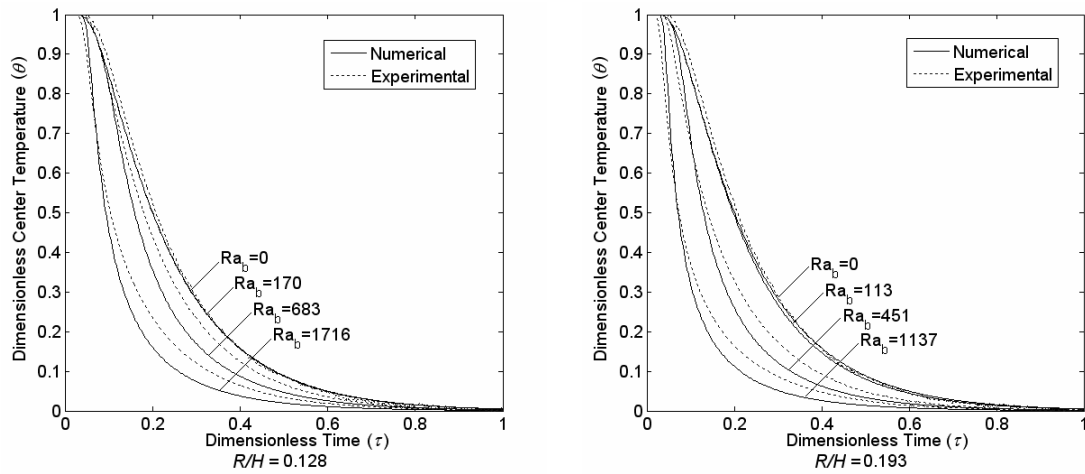


Fig. 1. Comparison between numerical and experimental results for different  $R/H$

Furthermore, the effect of Rayleigh number and aspect ratio on natural convection has been analyzed systematically by identifying time constants for attainment of thermal equilibrium. A criterion for neglecting the effect of natural convection on heat transfer is established by observing the change of these time constants as functions of the parameters mentioned above.

In summary, free convection has been found to have a very small influence on heat transfer in small cylinders filled with particles and air, as frequently used in the lab for the determination of packed bed thermal conductivity. However, it may have a strong influence in large, industrial silos. A similar influence is obtained at the lab scale by exchanging the air with water, providing us with a system for comfortably imitating free convection in industrial equipment and validating the model. With the help of this model it is possible to simulate and study different cases of storage conditions, establishing criteria for identifying situations with a strong influence of natural convection in practice.

## References

- Schneider, M.; Tsotsas, E.; *On the predictability of silo rain: Modelling moisture migration in beds of particulates after drying*. Proceedings of the 1<sup>st</sup> Nordic Drying Conference, Trondheim/Norway, 2001, Paper No. 15
- Nield, D.A., Bejan, A., *Convection in Porous Media*, 2<sup>nd</sup> edition. Springer Verlag, New York (1999).

## Effect of liquid flow rate and bed void fraction on the hydrodynamics and performance of a trickle-bed bioreactor

Martín Cruz-Díaz<sup>a,b</sup>, Sergio Revah<sup>a</sup>, Ricardo Lobo-Oehmichen<sup>a\*</sup>

<sup>a</sup>*Departamento de Ingeniería de Procesos e Hidráulica, Universidad Autónoma Metropolitana-Iztapalapa. San Rafael Atlixco 186, C.P. 09340, México, D.F., MEXICO*

<sup>b</sup>*División de Química y Bioquímica, Tecnológico de Estudios Superiores de Ecatepec, Av. Tecnológico S/N Esq. Av. Hank González, Valle de Anahuac, C.P. 55120, Ecatepec, Edo. de Mex, MEXICO*

### 1. Summary

Hydrodynamics has a strong influence on substrate elimination capacity in trickle-bed bioreactors (TBB). The present study reports the influence of liquid mass flow rate and bed void fraction ( $\epsilon$ ) on the TBB liquid residence time distribution (RTD), gas-liquid pressure drop, liquid hold-up, and biofilm wetting efficiency ( $J_w$ ). Most RTD are well represented by an axial dispersion model. It is also shown that the hydrodynamic parameters increase as superficial liquid mass flow rate increases and as bed void fraction diminishes. The TBB isopropyl alcohol (IPA) mineralization capacity follows the same trend, except at the lowest bed void fraction (0.44), when the TBB turns anaerobic due to excessive biomass growth. TBB IPA elimination capacity was not affected by liquid flow.

Keywords: trickle-bed bioreactor, hydrodynamics, residence time distribution

### 2. Extended Abstract

Elimination capacity in TBB is determined by the micro-organisms kinetic properties and the hydrodynamic characteristics of the flowing phases. Although hydrodynamics is known to influence TBB behaviour [1], it has been scarcely studied. The TBB catalyst is a biofilm supported on an inert packing. This biofilm grows with operating time and alters considerably the characteristics of the bed and the hydrodynamics of the flowing phases. The aim of this paper is to report the effects of superficial liquid mass flow rate and bed void fraction on the hydrodynamic parameters gas-liquid pressure drop, total and dynamic liquid hold-up, biofilm wetting efficiency, and residence time distribution, in an IPA-removing TBB.

**Materials and methods.** Experiments were carried out in an acrylic TBB (0.143 m id by 1.6 m of total packed length of 316 SS 1.0 in Pall rings with  $\epsilon=0.95$ ). An acclimatized microbial consortium was used to remove IPA. The superficial liquid mass flow rates used were 6.8, 9.8, 11.8, y 13.8 kg/m<sup>2</sup>s, while gas mass flow rate was kept at 0.063 kg/m<sup>2</sup>s, with an IPA average inlet load of 180 g/m<sup>3</sup>h. Sets of experiments were performed at bed void fractions of 0.94, 0.86, 0.7, 0.6, and 0.44, corresponding to different stages of biofilm growth.

**Results and discussion.** DTR (Fig. 1) show channelling, recirculation, and stagnant zones, thus deviating from plug flow. Axial dispersion model seems to be adequate to describe flow.

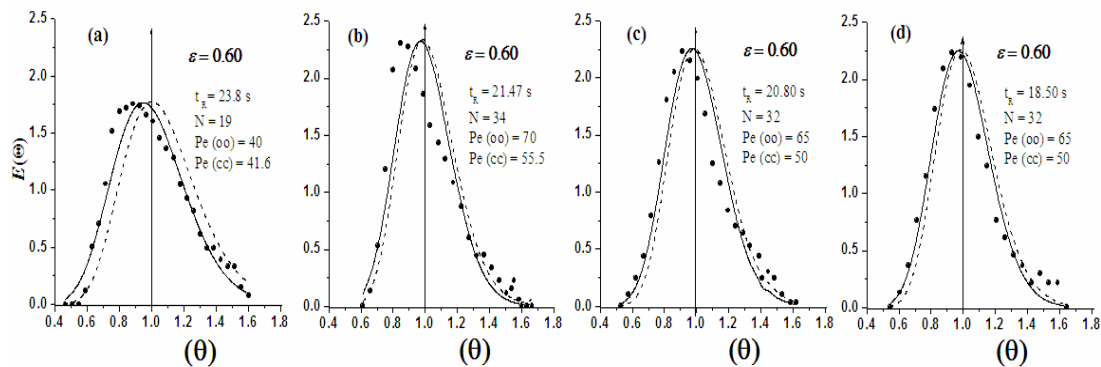


Figure 1. RTD at  $\varepsilon=0.6$  for liquid mass flow rates. a)  $6.8 \text{ kg/m}^2\text{s}$ ; b)  $9.8 \text{ kg/m}^2\text{s}$ ; c)  $11.8 \text{ kg/m}^2\text{s}$ , and d)  $13.8 \text{ kg/m}^2\text{s}$ . (—) Axial dispersion model; (----) n-CSTR model.

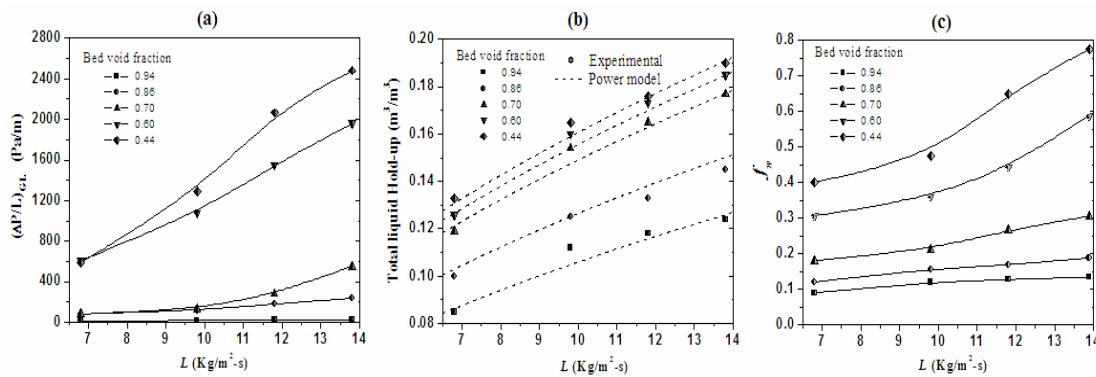


Figure 2. a) Gas-liquid pressure drop; b) Total liquid hold-up, and c) Biofilm wetting efficiency, as a function of superficial liquid mass flow rate and bed void fraction..

Gas-liquid pressure drop, total and dynamic liquid hold-up, and biofilm wetting efficiency (Fig. 2) increased with increasing liquid flow rates and with diminishing bed void fraction. At constant  $\varepsilon$ , increased liquid flow rate had a small effect on the IPA degradation rate, although it increased its conversion to  $\text{CO}_2$ . The best TBB performance was obtained at  $\varepsilon=0.6$ , with an 88 % of IPA removal and 67.3 % mineralization. At  $\varepsilon=0.44$ , the TBB turned anaerobic and there was a large reduction in IPA removal rate and mineralization (not shown). Results may be explained in terms of the amount of biomass present, wetting efficiency and the available area for liquid-biofilm contact.

## References

Trejo-Aguilar, G., Revah, S. Lobo-Oehmichen, R. (2005). *Chem. Eng. J.* 113, 145-152.



## Effective diffusivities of gases in a reconstructed porous body

Pavel Čapek<sup>a</sup>, Vladimír Hejtmánek<sup>b</sup>, Libor Brabec<sup>c</sup>, Arlette Zikánová<sup>c</sup>, Milan Kočířík<sup>c</sup>

<sup>a</sup>*Institute of Chemical Technology, Prague, Technická 5, 16628 Prague, Czech Republic*

<sup>b</sup>*Institute of Chemical Process Fundamentals ASCR, v.v.i., Rozvojová 135, 16502 Prague, Czech Republic*

<sup>c</sup>*J. Heyrovský Institute of Physical Chemistry ASCR, v.v.i., Dolejškova 3, 18223 Prague, Czech Republic*

### 1. Summary

Two models of a porous body, a 3D replica obtained by the stochastic reconstruction and a random pore network, are evaluated with reference to the effective diffusivity of gases. The stochastic reconstruction technique employs limited morphological information that has been extracted from images of 2D cuts through the porous medium. The pore network is derived in such a way that the total porosity, pore-size function, and mercury intrusion curve agree well with experiment. A simulator of steady diffusion flow in the pore network overestimates the effective diffusivity while the direct calculation of the effective diffusivity by exploiting random-walk simulation in the 3D replica delivers a value which is less than its experimental counterpart. However, both the deviations are acceptable.

Keywords: stochastic reconstruction, pore network, random walk, diffusivity

### 2. Extended Abstract

A method of the 3D stochastic reconstruction based on statistical information extracted from images of 2D cuts through a porous body is applied to reproduce a sample of  $\alpha$ -alumina with the total porosity  $\phi = 0.404$ . 3D replicas of  $\alpha$ -alumina conforming to the reference and simulated microstructural descriptors are generated by the simulated annealing technique. The main idea behind this technique of combinatorial minimisation is to gradually transform a chaotic (“high-energy”) configuration of void and solid voxels into a structured, “minimum-energy” configuration, where “energy” is given by the sum of squared deviations between reference (experimentally determined) and simulated functions carrying morphological information. A set of these functions, i.e. microstructural descriptors, considered here includes the two-point probability function and the lineal-path function for the void phase. The analysis of the 2D images showed that the microstructure is statistically homogeneous (invariant under translation of the spatial coordinates) and isotropic (invariant under rotation) and, hence, the descriptors are only the functions of the lag distance.

The reconstructed pore space is analysed and transformed onto an equivalent 3D pore network of irregular topology. Since visual inspection of the 3D replicas reveals that the

pore space is well represented by pores of convergent-divergent shapes, a chamber-and-throat network with nodes arranged on the simple cubic lattice is chosen for the transformation. If the network is to be of irregular topology, the mean coordination number of the network has to be reduced by removing bonds selected at random. The mean coordination number of 4.0, which is a typical value for many porous solids, is taken into consideration in this work. Each network throat is formed by two obelisks, mutually connected. Their larger, square bases take size of adjacent cubic chambers; the smaller, rectangular bases of the same size represent the narrowest cross-section area of a throat. The rectangular shape of throats is chosen in order to raise randomness in the pore morphology. The throat aspect ratio is drawn from the uniform distribution. The chamber volume distribution (CVD) and the throat size distribution (TSD) are deduced from the pore size function of the reconstructed porous body. Parameters of CVD and TSD are systematically changed in such a way that the pore size function of the pore network fits well the reference one. Note that no throat is allowed to be larger than the adjacent chambers and no chambers can overlap. Since this procedure is not particularly sensitive to throat sizes, the exact course of TSD is determined by comparison of simulated and experimental mercury intrusion curves. Systematic changes of TSD parameters result in good agreement between the simulated and experimental curves.

A simulator of steady diffusion flow in the pore network is used for prediction of effective diffusivities of inert gases (isobaric counter-current diffusion in binary mixtures involving H<sub>2</sub>, He, N<sub>2</sub>, and Ar). For each network bond comprising a throat and halves of two adjacent chambers, a general expression for the diffusion flow rate as the function of nodal mole fractions, pore geometry, and transport properties of gases (e.g. bulk binary diffusivity,  $D_{AB}$ ) is derived. These flow rates have to fulfil the mass conservation law in all network nodes, which are located in the centres of gravity of chambers. By imposing a macroscopic gradient of mole fractions across the pore network, unknown values of the nodal mole fractions are determined by solving the corresponding system of non-linear equations. Finally, the total flow rate through the network boundary is computed and the effective diffusivity is evaluated from Fick's first law. In addition to these network calculations, the ratio of the bulk binary diffusivity to the effective diffusivity,  $F = D_{AB} / D_{AB}^{eff}$ , in the 3D replica is directly estimated by performing random-walk simulation, which is based on calculation of the mean-squared displacement versus time for a number of Brownian particles taking discrete steps in the pore space. Both predicted values of the ratio  $F$  (7.41 and 9.81 predicted by the network calculation and by random-walk simulation, respectively) are quite consistent with the experimental value of 8.1. Note, that the ratio  $F$ , which is identical, in form, to the formation factor, slightly deviates from Archie's law  $F = \phi^{-2} = 6.13$  in our particular case.

## **Influence of the interfacial reaction rate on macroscopic systems.**

Francisco J. Valdes-Parada<sup>a</sup>, Mauricio Sales-Cruz<sup>b</sup>, Jose Alvarez-Ramirez<sup>a</sup>, J. Alberto Ochoa-Tapia<sup>a</sup>

<sup>a</sup> *Departamento de Ingeniería de Procesos e Hidráulica, Universidad Autónoma Metropolitana - Iztapalapa, México D.F., 09340, México*

<sup>b</sup> *Departamento de Procesos y Tecnología, Universidad Autónoma Metropolitana - Cuajimalpa, México, D.F., 1850, México*

### **1. Summary**

In this work, the effects of including a reaction term in the porous catalytic pellet-fluid boundary are analyzed. The analysis is carried out in two typical reaction systems, namely a stirred tank reactor and a plug flow reactor, both are assumed to operate in isothermal conditions and steady state, although the analysis can be extended to systems and conditions more complicated. The results strongly depend of macroscopic parameters like the Thiele modulus, the Biot and Péclet numbers, as well as the ratio between the internal and external areas of the porous catalytic pellet. The conditions under which the highest deviations are presented respect to the assumption of flux continuity at the dividing surface are more probably to be exhibited by materials with fractured structure.

Keywords: jump condition, interfacial reaction, porous media, continuous stirred tank reactor, plug flow reactor

### **2. Extended Abstract**

The development of models for macroscopic transport processes in multiphase systems has been the subject of intense research activity in the last decades. Most of the efforts have been devoted to the derivation of macroscopic conservation equations which are usually valid in the homogeneous regions (i.e., constant porosity) of a system. This gives rise to the problem of describing transport phenomena in the transition zone (the inter-region) between two (or more) homogeneous regions. This difficulty can be tackled by posing the corresponding jump boundary conditions that match the transport equations of the homogeneous regions at the dividing surface (Ochoa-Tapia and Whitaker, 1995). Moreover, the use of new materials in the reaction-transport processes enhances the idea that the conditions under which the imposition of the condition of mass flux continuity may fail. Recently, Valdés-Parada et al. (2006), using the method of volume averaging (Whitaker, 1999), proposed a jump boundary condition for the mass flux at the micropore-macropore boundary which involves a reaction term.

In this work, we carry out an analysis to determine the effect of including the reaction term proposed by Valdés-Parada et al. (2006) in the modelling of the steady-state diffusive mass transport with first-order kinetics taking place in a porous catalytic pellet within a CSTR and a plug-flow tubular reactor.

The results given in Figure 1 show a strong dependence with the Thiele modulus ( $\Phi$ ), the Biot number ( $Bi$ ). More explicitly, for  $\Phi > 5$  and  $Bi \in [1, 10]$  the results from the model that takes in account the surface reaction term exhibit the highest deviations from those assuming continuity in the mass flux. Of all the output variables computed, the interfacial mass flux exhibited the biggest deviations.

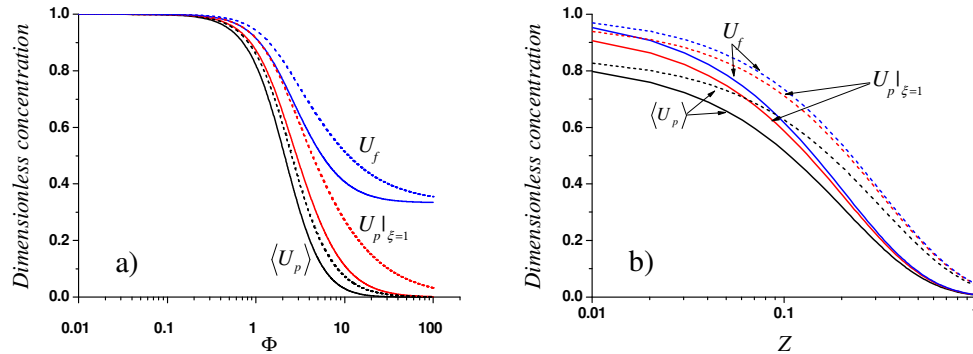


Figure 1: Fluid, interfacial and average concentration vs. a) the Thiele modulus ( $Bi = 10$ ,  $\psi_p = 0.1$  and  $\tau_R = 20$ ), b) dimensionless position ( $Pe = 1$ ,  $\psi_p = 100$ ).  $\epsilon_{\gamma\omega} = 0.84$  and  $A_{\omega}^{T\omega} = 10000$ . (—) Results from considering a reaction and (---) imposing continuity conditions at the dividing surface.

As above mentioned, these conditions are more likely to be exhibited, for example, by materials with highly fractured porous surface (Coppens, 1999). The results from this analysis can also be extended to more complicated systems and transport mechanisms.

## References

- Coppens M.O. (1999) *Catalysis Today*, Vol. 53, 225-243.  
 Ochoa-Tapia J.A., Whitaker S. (1995) *International Journal of Heat and Mass Transfer*. 38, 14, 2635-2646.  
 Valdés-Parada F.J., Goyeau B., Ochoa-Tapia J.A. (2006) *Chemical Engineering Science*, 61, 1692-1704.  
 Whitaker S., *The method of volume averaging*, Kluwer academic publishers, USA, (1999).

## Prediction of shelf-life of beverage stored in PET bottles with passive and active walls

R. Di Felice<sup>a</sup>, D. Cazzola<sup>a</sup>, S. Cobror<sup>b</sup>, L. Oriani<sup>b</sup>

<sup>a</sup>Department of Chemical and Process Engineering, University of Genova, I-16145 Genova, Italy

<sup>b</sup>Cobarr Gruppo Mossi & Ghisolfi, Strada Savonese 9, I-15040 Rivalta Scrivia, Italy

### 1. Summary

The aim of this paper is to provide a framework whereby gas permeation rates through plastic packaging walls, and hence food shelf life, may be estimated from the computed change of gas concentration in the container as a function of time. Although the approach is quite general, specific attention is given to the case of liquid filled PET bottles (with both passive and active gas scavenging walls), with either oxygen or carbon dioxide as the permeating gas. The work demonstrates how basic chemical engineering principles can be applied to the problem in hand: the net flux of the permeating component across the container boundaries is inserted in the overall material balances, which take into account mass transfer and chemical reaction within the boundary material.

Keywords: Food packaging, PET bottles, shelf-life, passive wall, active wall

### 2. Extended Abstract

Two situations are considered: when the walls simply provide a passive resistance to the flux (as is the case for standard PET or PET aided by some other low permeability material) and when an active gas scavenger is incorporated within the boundary material. For the first case (passive barrier) a theoretical analysis has been carried out to establish whether effectively steady conditions would prevail within the bottle wall. Having demonstrated that this is the case for the vast majority of practical cases, permeability data relative to oxygen and carbon dioxide have been collected from many source in the scientific literature and have been further verified with specific oxygen transmission rate (OTR) experiments carried out in the our laboratory. A general dependency of permeability on the material structural condition has been found for PET layers. The validity of the Nielsen relationship for the reduction of permeability for PET blends

$$\frac{P}{P_0} = \frac{1 - \varepsilon_p}{1 + \frac{\alpha \varepsilon_p}{2}}, \quad (1)$$

(where  $\varepsilon_p$  is the volumetric fraction of the passive material in the final blend and  $\alpha$  is its aspect ratio) has also been verified.

All this information has been utilised to provide a numerical routine for the prediction of oxygen (or carbon dioxide) concentration in a container as a function of time; these predictions have been verified by comparison with data on gas concentration in water filled bottles (and carbonated-water filled bottles, for the CO<sub>2</sub> measurements) maintained under controlled conditions for periods of up to 6 months.

Analysis for the case of an active scavenger wall differs from the above approach due to the reaction of the scavenging material with the oxygen, which results in a gas flux changing continuously with time until all of the scavenger has been consumed. This situation has been modelled by Cussler and co-workers who formulated the unsteady state material balance equations for oxygen and the scavenger component in the barrier wall; the gas flux follows from the calculated concentration profiles. Clearly, such numerical predictions require knowledge of the kinetic constant for the oxygen-scavenger reaction. For the specific oxygen scavenger investigated in this work, the kinetic constant was first estimated from data obtained using test bottles prepared with varying scavenger concentration, then utilised to carry out predictions for other bottles of differing shape and volume. Overall the results were very good, with predictions always close to measured gas concentration, thereby supporting the general procedure proposed in this work.

## References

- Nielsen L.E., 1967, Models for the permeability of filled polymer systems *J. Macromol. Sci.* A1(5) 929-942.
- Nuxoll E.E., Siegel R.A. and Cussler E.L., 2005, Layered reactive barrier films. *J. of Membrane Science* 252 29-36.
- Yang C., Nuxoll E.E. and Cussler E.L., 2001, Reactive barrier films. *AIChE J.* 47 295-302.

## **Production of cylindrical carbon xerogel monoliths: effect of sample diameter on drying-induced cracks**

A. Léonard<sup>a</sup>, M. Crine<sup>a</sup>, W. Jomaa<sup>b</sup>

<sup>a</sup>Laboratory of Chemical Engineering, University of Liège, Sart Tilman – B6c, 4000 Liège, Belgium

<sup>b</sup>TREFLE, University Bordeaux 1 - ENSAM, Esplanade des Arts et Métiers, 33405 Talence, France

### **1. Summary**

Upstream from pyrolysis, drying is a critical step for the production of crack-free carbon xerogel monoliths. The effect of the diameter size on the cracking tendency was investigated for cylindrical samples, both experimentally and numerically using a thermo-hygro-mechanical model. Results showed that the drying conditions have to be drastically softened to avoid crack formation when drying large size materials.

Keywords: resorcinol-formaldehyde xerogel, carbon xerogel, convective drying, crack, modelling

### **2. Extended Abstract**

#### *1.1. Introduction*

Carbon xerogels can be obtained by convective drying of resorcinol(R)-formaldehyde(F) hydrogels, followed by pyrolysis (Léonard et al., 2005). Adapting the synthesis conditions allows tailoring the carbon xerogel pore texture so that a wide range of applications can be considered for these materials (adsorbents, catalysts supports, electrode material, energy storage device, column packing materials, ...). Drying constitutes a particularly critical step when carbon monoliths are required, *e.g.* for electrodes or supercapacitors. Indeed, when the drying conditions are too severe, the mechanical stresses caused by differential shrinkage may lead to sample cracking. In this work, we focus on the effect of the gel size on the mechanical stresses induced during drying, both from an experimental and modelling point of view.

#### *1.2. Materials and methods*

Hydrogels were prepared by sol-gel polycondensation of resorcinol, solubilised in deionised water with formaldehyde, in the presence of Na<sub>2</sub>CO<sub>3</sub>, a basification agent usually called catalyst (C). Since the Na<sub>2</sub>CO<sub>3</sub> concentration controls the gel texture and its shrinkage behaviour, the R/C molar ratio was fixed at 300 in order to get a volume reduction after drying close to 65%. The molar ratio R/F and the dilution ratio were fixed

at 0.5 and 5.7, respectively. Cylindrical samples with diameters of 23 and 46 mm were obtained by casting 5 ml or 50 ml solution into glass moulds, respectively. After gelation under saturated atmosphere at 70°C during 24h, the gels were dried in a convective rig controlled in air relative humidity, temperature and velocity. A camera was used to follow the development of cracks during the drying process. The velocity was kept constant at 2 m/s for all the experiments while the temperature and relative humidity were adjusted in order to produce crack-free monoliths. As the cracks are induced by drying stresses, a coupled thermo-hygro-mechanical model was used to simulate the stress state of the samples during the drying process (Léonard et al., 2006).

### 1.3. Results and discussion

A series of experiments showed that the drying conditions have to be softened to avoid cracking when the sample size increases. For the large samples, the temperature has to be set to 40°C, together with 60% RH, to obtain crack-free monoliths. Small samples withstand more severe drying conditions, *i.e.* 70°C and 15% RH. Images obtained from the camera revealed that cracks initiation occurs quite early in the drying process, indicating a mechanical response to hydrous strains. Simulations results confirmed the experimental ones. The drying conditions, as well as the sample size, were proved to have a large influence on the stress state within the sample during drying. This latter was evaluated through the determination of the maximal Von Mises stress.

### 1.4. Conclusions

The diameter of cylindrical resorcinol-formaldehyde samples was shown to have an impact on their cracking behaviour. The production of carbon monoliths by pyrolysis of dried RF xerogels requires optimising the drying step according to the material size. Simulation of the drying-induced stresses using a thermo-hygro-mechanical model confirmed the effect of both the sample size and the drying conditions on the maximal Von Mises stress developing within the sample. In order to validate these results and to develop a relevant cracking criterion, Brazilian tests will be carried out to determine the failure strength at various water contents. Other synthesis conditions, *i.e.* R/C ratios, as well as other samples shapes will also be considered.

### Acknowledgements

A. Léonard is grateful to the FRS-FNRS (Fund for Scientific Research, Belgium) for a Postdoctoral Researcher position. A. Léonard also thanks the FRS-FNRS for supporting her scientific stay at the TREFLE Laboratory.

### References

- Léonard A., Job N., Blacher S., Pirard J.P., Crine M., Jomaa W., (2005) *Carbon*, 43, 1808-1811.  
Léonard A., Crine M., Jomaa W., *Modelling of the convective drying of resorcinol-formaldehyde resins: influence of the drying conditions on the induced stress tensor*. In: Farkas I (Ed.), *Drying 2006*, 273-278 (2006).



## **Session T2-7c: Transport Phenomena in Porous/Granular Media – III**

<b>Abstract Number</b>	<b>Paper Title &amp; Authors</b>	<b>Included</b>
1374	Determination of equilibrium, kinetic and thermodynamic parameters for the adsorption of cadmium (II) onto Castanea sativa shell G Vázquez, R F Bea, M S Freire, J G Álvarez, G Antorrena	Yes
1925	Viscous stabilization of drying front: three-dimensional pore network simulations T Metzger, E Tsotsas	Yes
2015	Immiscible and Miscible Displacement in Heterogeneous Porous Media: From Soil Column Experiments to a Dynamic Large-Scale Network Simulator C A Aggelopoulos, C D Tsakiroglou	Yes
2972	Time and bed height dependent concentration vs. particle radius profiles in packed-bed adsorption columns: Non-equilibrium model simulation studies A R Özdural	Yes

Session T2-7c

## **Determination of equilibrium, kinetic and thermodynamic parameters for the adsorption of cadmium (II) onto *Castanea sativa* shell**

G. Vázquez, R. Fernández-Bea, M. S. Freire, J. González-Álvarez, G. Antorrena

*Department of Chemical Engineering, University of Santiago de Compostela, School of Engineering, Rúa Lope Gómez de Marzoa, 15782 Santiago de Compostela, Spain*

### **1. Summary**

A study on the removal of Cd(II) ions from aqueous solutions by *Castanea sativa* shell was conducted in batch conditions. The influence of different variables, such as adsorption time, temperature and initial concentration, on cadmium uptake was evaluated. Results indicated that cadmium adsorption equilibrium could be described by the Freundlich adsorption model, predicting the heterogeneity of the shell. The adsorption process followed a pseudo-second order adsorption model with adsorption capacity decreasing with increasing temperature, which indicated that the sorption of cadmium onto shell could be exothermic. The activation energy of the adsorption was calculated as equal to 19.2 kJ/mol, which is inside the range (8-22 kJ/mol) of diffusion-controlled processes. Equilibrium sorption capacity increased when the initial cadmium concentration was increased.

Keywords: cadmium adsorption, chestnut shell, equilibrium, kinetics, thermodynamic parameters

### **2. Extended Abstract**

*Castanea sativa* shell is generated as a residue of a food factory during the peeling process in the “marrón glace” production. Apart from its use as fuel, the shell has little application, and although other similar lignocellulosic materials have received considerable attention as adsorbents of cations from wastewaters, there is no much information in the literature on the utilization of chestnut shell as adsorbent. Therefore, in this work, we proposed the study of the adsorption of cadmium ions from aqueous solutions onto the chestnut shell.

There are several parameters which determine sorption rate, like structural properties of the adsorbent, metal ion properties, initial concentration of metal ions, pH and temperature. In general, the characteristics of the adsorption behaviour are inferred in terms of both adsorption kinetics and equilibrium isotherms. They are also important tools to understand the adsorption mechanism for the theoretical evaluation and interpretation of thermodynamic parameters.

Two adsorption models have been applied to evaluate the experimental data: the Lagergren pseudo-first order kinetic model and the Ho's second-order rate equation. The dynamic behaviour of the adsorption was investigated analysing the effect of concentration (15.3, 50.5 and 87.3 mg/L) at 25°C and temperature (15, 25 and 35°C) at an initial cadmium concentration of 20 mg/L. In addition, Langmuir and Freundlich isotherms were used to describe the adsorption equilibrium at the three temperatures essayed.

Chestnut shell was air-dried, ground and sieved to a particle size less than 2 mm, and then it was treated with formaldehyde in acid-medium. Adsorption experiments were conducted in a series of Erlenmeyer flasks covered with a Teflon sheet to prevent contamination. 100 mL of cadmium ion solution were transferred in the flasks together with 1g of pre-treated chestnut shell, and placed in a water bath shaker maintained at the desired temperature. When the adsorption process was completed, the solutions were filtered and analyzed for residual cadmium (II) ion concentrations.

For all cases essayed, the amount of cadmium adsorbed increased rapidly with time at the beginning and became slow towards the end of the process. The adsorption equilibrium was attained within four days. The efficiency of adsorption was increased with increasing contact time and initial cadmium concentration, and with decreasing temperature.

Experimental results have indicated that the pseudo-second order reaction model provided the best description of the data with correlation coefficients higher than 0.99 for all initial cadmium concentrations and temperatures. It was found that the values of the rate constant and the equilibrium sorption capacity obtained from model equations were affected by the two variables analysed. Thus, the rate constant decreased slightly from  $5.32 \cdot 10^{-3}$  to  $4.53 \cdot 10^{-3}$   $\text{g} \cdot \text{min}^{-1} \cdot \text{mg}^{-1}$  and the capacity increased from 1.3 to 4.4 mg/g with an increase in initial cadmium concentration from 15.3 to 87.3 mg/L. The data also showed that, when the temperature increased from 15 to 35°C, the rate constant also increased (from  $4.2 \cdot 10^{-3}$  to  $7.1 \cdot 10^{-3}$   $\text{g} \cdot \text{mg}^{-1} \cdot \text{min}^{-1}$ ), whereas the equilibrium sorption capacity was little affected (from 1.4 to 1.2 mg/g). A linear relationship between the rate constant and the reciprocal absolute temperature was found and therefore, the variation of the pseudo-second order rate constants with temperature could be represented in an Arrhenius form. The rate constant of sorption,  $k_0$ , took the value of  $12.72 \text{ g} \cdot \text{mg}^{-1} \cdot \text{min}^{-1}$  and the activation energy for sorption,  $E$  of 19.2 kJ/mol, which is inside the range (8-22 kJ/mol) of diffusion-controlled processes. These results suggested that the rate-controlling step for the adsorption of cadmium on chestnut shell is likely not chemical in nature.

Freundlich equation represented a better fit to the experimental data than the Langmuir equation. This result predicts the heterogeneity of the adsorption sites on chestnut shell. The values of  $n$ , greater than unity, indicated that cadmium (II) ions are favourably adsorbed by *Castanea sativa* shell at all the temperatures studied.

## **Viscous stabilization of drying front: three-dimensional pore network simulations**

T. Metzger and E. Tsotsas

*Thermal Process Engineering, Otto-von-Guericke-University, P.O. 4120, D-39016 Magdeburg, Germany*

### **1. Summary**

In this study, a recently developed pore network drying model (see reference), which accounts for liquid viscosity, is applied to three dimensions for the first time. Isothermal convective drying is simulated for a cubic network (25x25x50) with pore throats of mono-modal radius distribution. The role of liquid viscosity is assessed by comparison with non-viscous drying of the same network. Simulation results are presented as 3D phase distributions, moisture profiles and drying rate curves.

Keywords: capillary porous media, phase distributions, drying rate curves, viscosity

### **2. Extended Abstract**

If viscous effects are negligible, liquid is always pumped out of the largest meniscus throats by capillary forces and drying can be modelled as an invasion percolation process. Due to random distribution of throat size, the liquid phase gradually splits up into clusters (see Figure 1a). As long as the liquid is connected over the whole network, capillary pumping experiences no constraint. During this period, no drying front occurs, but saturation level drops more or less uniformly throughout the network (see Figure 2a). In the presence of a diffusive gas-side boundary layer, lateral vapour transfer ensures that liquid is evaporated at a constant rate. Gas penetrates into the depth of the network until a saturation is reached at which the liquid phase consists of small disconnected clusters and a receding evaporation front is observed (see Figure 2a). Drying rate drops due to the additional vapour transfer resistance in the network.

For important viscous effects, differences in capillary pressure are not enough to pump liquid from the largest meniscus throats to other evaporating meniscus throats. Concerning drying behaviour, several periods must be distinguished. At the very beginning, when only some of the near surface throats are emptied, distances for capillary flow are so short that capillary forces still dominate over viscosity. Later on, as gas penetrates deeper into the drying body, distances for capillary flow get longer; additionally, surface saturation drops so that local evaporation rates at the remaining surface menisci increase (due to increased lateral diffusion in boundary layer). Both effects contribute to the viscous stabilization of the drying front (see Figure 1b) that has a strong reduction effect on drying rates. As drying proceeds, this front recedes into the porous medium and can widen up because of reduced overall evaporation rates (see Figure 2b). In this limit, drying behaviour approaches the non-viscous one.

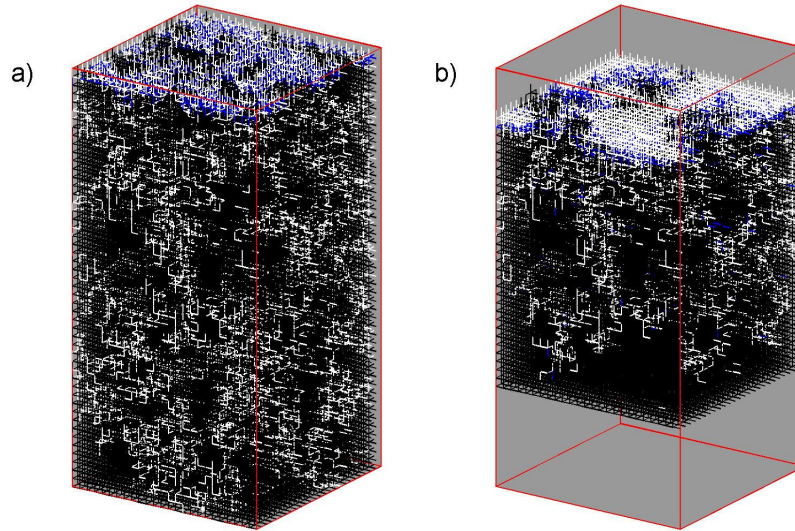


Figure 1: Phase distributions for (a) non-viscous and (b) viscous case at network saturation 0.8; white lines represent gas-filled throats, black is for liquid throats and blue for partially filled throats. The networks are open for evaporation at the top, periodic boundary conditions are assumed in the two horizontal directions. (For better readability of the viscous case, dry layers at the top and completely saturated layers at the bottom are not shown.)

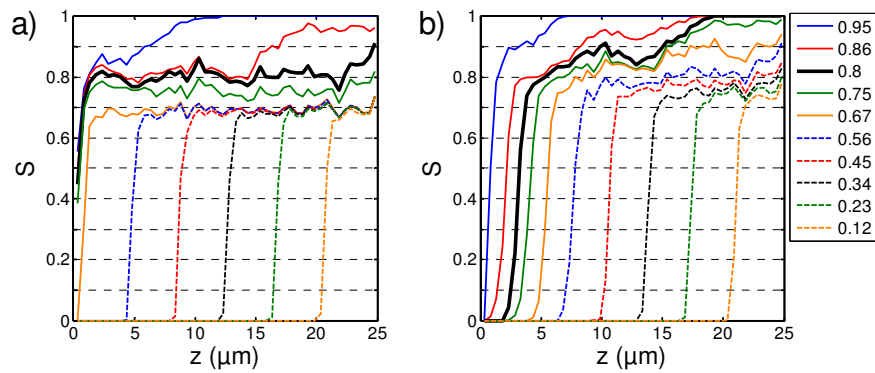


Figure 2: Saturation profiles at different network saturation (see legend) for (a) non-viscous and (b) viscous case.

In conclusion, the relative size of viscous effects (quantified by a Capillary number) are decisive for phase distributions and drying rates in intermediate stages of the drying process – and especially the duration of the constant drying rate period.

## Reference

Metzger, T., Irawan, A. and Tsotsas, E. (2007) *Drying Technology* 25, 49-57.

## Immiscible and Miscible Displacement in Heterogeneous Porous Media: From Soil Column Experiments to a Dynamic Large-Scale Network Simulator

C.A. Aggelopoulos<sup>a,b</sup>, and C.D. Tsakiroglou<sup>a</sup>

<sup>a</sup>*Foundation for Research and Technology Hellas – Institute of Chemical Engineering and High Temperature Chemical Processes, Stadiou str., Platani, 26504 Patras, Greece*

<sup>b</sup>*Department of Physics, University of Patras, 26500 Patras, Greece*

### 1. Summary

The capillary pressure and relative permeability curves of porous media can be estimated from transient immiscible displacement tests with history matching. The hydrodynamic dispersion coefficients of porous media are usually estimated from miscible displacement experiments by fitting the advection-dispersion equation to the transient evolution of the solute concentration at the outlet of the porous medium.

Keywords: porous media, multiphase flow, dispersion, heterogeneity, simulation

### 2. Extended Abstract

Immiscible and miscible displacement tests are performed on undisturbed and heterogeneous soil columns (length=30 cm, diameter=5 cm). Multipoint measurements of the electrical resistance are employed to determine the axial distribution of the fluid saturation and the solute concentration breakthrough curves. The porous medium is regarded as a system of parallel flow paths quantified by a permeability distribution function. The miscible and immiscible displacement in such a multiregion model are described by a mixed system of algebraic and differential equations, the parameters of which are estimated by inverting (1) the transient response of the solute concentration averaged over three cross-sections, and (2) the transient responses of the total pressure drop and fluid saturation averaged over five successive segments, respectively. In this manner, (1) the dispersivity  $\alpha_L$  & degree of micro-heterogeneity (expressed by the variance of permeability at micro-scale,  $\sigma_{k^*}^2$ ) (Table 1), and (2) the capillary pressure curve, relative permeability curves and macro-heterogeneity (expressed by the variance of permeability at macro-scale,  $\Sigma_{k^*}^2$ ) (Fig.1a,b) are estimated. The micro-heterogeneity is significant (Table 1), as mixing of sand, clay and silt creates pore structures dominated by multiple pore length scales.

$u_{p0}$ (m/s)	$\alpha_L$ (cm)	$\sigma_{k^*}$	$u_{p0}$ (m/s)	$\alpha_L$ (cm)	$\sigma_{k^*}$
1.50e-6	2.96	1.40	3.76e-6	1.20	1.34
2.63e-6	4.0	2.36	5.26e-6	1.74	1.24

Table 1: Estimated parameter values of the multi-region model

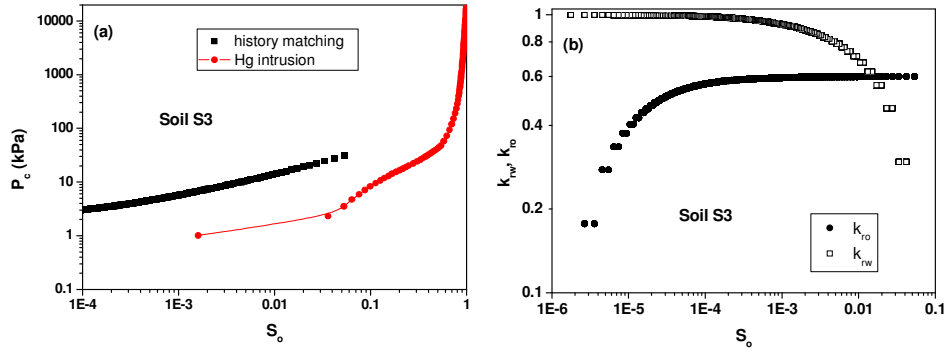


Figure 1: (a) Oil/water capillary pressure curve estimated by the multiregion model as compared to the equivalent capillary pressure curve resulting from Hg intrusion data. (b) Water,  $k_{rw}$ , and oil,  $k_{ro}$ , relative permeability curves estimated by the multiregion model (permeability of soil column S3:  $k=50$  mD; estimated  $\Sigma_{k^*} = 0.16$ )

Permeabilities are chosen randomly from a distribution function and are assigned to the nodes of a cubic network (macro-heterogeneity). In order to simulate rate-controlled drainage in such a network, the pressure field is calculated by solving the system of equations resulting from mass balances in the nodes. Based on the calculated flow rates, a time interval is so selected that the displacement is completed in no more than one unit cells. Then, the fluid saturation in each node is updated, and the procedure is repeated until no change of saturation and total pressure drop occur. The simulated axial fluid saturation profile, and total pressure drop are sensitive to macro-heterogeneity (Fig.2), and network simulator could be employed for the inverse modeling of the two-phase flow tests performed on heterogeneous soil columns.

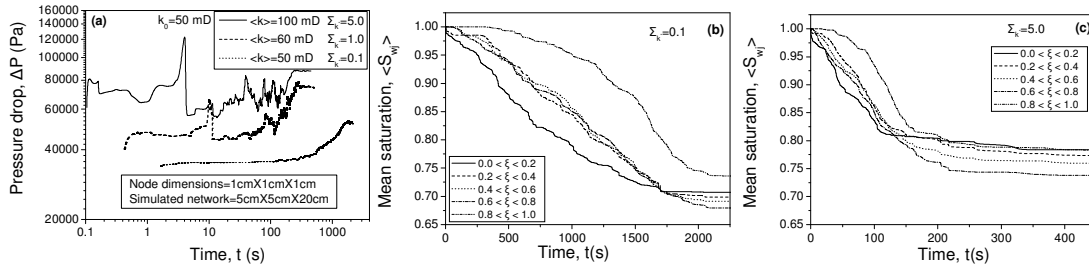


Figure 2: Sensitivity analysis of the large scale network simulator with respect to macro-heterogeneity. (a) Transient response of the pressure drop across the network. (b) (c) Water saturations averaged over five successive segments of the network (dodecane displaces water downwards,  $u_0=1.88e-6$  m/s).

### Acknowledgements

This work was supported by European Commission, in the course of 6th Framework Program, Subprogram: “Global Change and Ecosystems”, contract number: SSPI-CT-2003-004017-STRESOIL.



## **Time and bed height dependent concentration vs. particle radius profiles in packed-bed adsorption columns: Non-equilibrium model simulation studies**

Ahmet R. Özdural

*Department of Chemical Engineering, Hacettepe University, TR-06532 Ankara, Turkey*

### **1. Summary**

A new mathematical model and a simulation program have been developed for the prediction of the intra-particle uptake profiles at packed bed adsorption processes. It is shown that the methodology presented in this work allows quantitative investigations of solute adsorption dynamics within a single adsorbent particle of the packed-bed column, which adds a new tool to the available methods for characterizing and optimizing adsorption processes.

Keywords: intra-particle uptake, packed-bed adsorption, non-equilibrium model

### **2. Extended Abstract**

Usually the understanding of packed-bed adsorption and mathematical modeling approaches to describe intraparticle adsorption and transport of solutes are limited to data obtained from finite bath and packed bed breakthrough studies, with the change of solute concentration in the fluid phase as the only source of information. This approach corresponds to the end result of the actual amount of adsorbed solutes overlaid within the adsorbent and has limited use for the development and verification of models describing intraparticle transport. The validity of the assumption of local equilibrium (LE) conditions is uncertain in the dynamic state in a packed-bed adsorption column [1]. Here the non-equilibrium model proposed by Özdural et al. [2] is employed, where external mass transfer and intraparticle transport are included as separate identities. The mechanism of intraparticle diffusion is based on homogeneous (solid) diffusion. Fluid-solid interphase concentrations are related with Langmuir isotherm. Eq. (1) gives the intra-particle parabollic profile expression where  $q(r,x,t)$  is the  $x$  (bed height),  $r$  (radial position within the particle), and  $t$  (time) dependent solid concentration. Eqs. (2) and (3) give  $a_0(x,t)$  and  $a_2(x,t)$  values where  $r_p$  is the particle radius,  $k_f$  is film mass transfer coefficient,  $D_s$  is homogeneous diffusivity,  $c(x,t)$  is the bulk liquid concentration,  $c_s^*(x,t)$  is the liquid concentration at the interphase,  $q_s^*(x,t)$  is the solid concentration at the interphase and  $Bi = k_f \cdot r_p / D_s$ .

$$q(r, x, t) = a_0(x, t) + a_2(x, t)r^2 \quad (1)$$

$$a_0(x,t) = q_s^*(x,t) - a_2(x,t)r_p^2 \quad (2) \quad a_2(x,t) = (Bi/2)[c(x,t) - c_s^*(x,t)] \quad (3)$$

The non-equilibrium adsorption column modeling of Özdural et al [2] makes it possible to evaluate  $c(x,t)$ ,  $c_s^*(x,t)$  and  $q_s^*(x,t)$  values. Thus the time and bed height dependent  $a_0$  and  $a_2$  values can be determined through Eqs. (2) and (3). Once  $a_0$  and  $a_2$  are determined for a certain bed height and time, their values are substituted into Eq. (1) so as to resolve particle concentration profile for the above mentioned specified time and bed height. Fig. 1 and Fig. 2 illustrates time change of “intra-particle concentration vs. particle radius” profiles at different bed locations.

Figure 1.

Time change of, intra-particle concentration vs. particle radius, profiles at packed-bed adsorption column. Distance = 1/5 of bed height

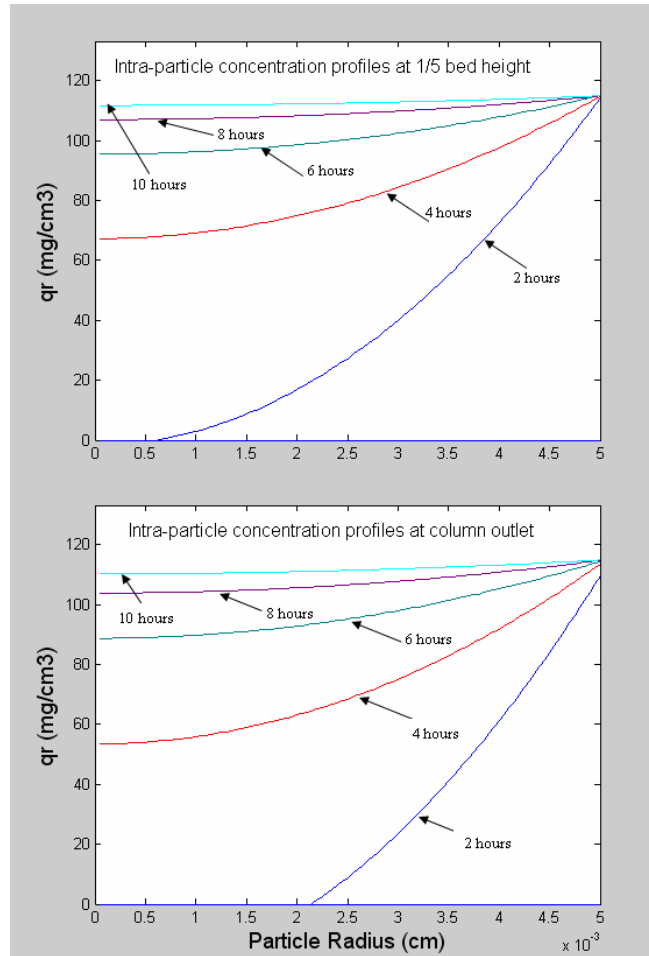


Figure 2.

Time change of, intra-particle concentration vs. particle radius, profiles at packed-bed adsorption column. Distance = bed outlet

**Parameters for Fig. 1 and Fig. 2:**  $k_f = 1.467 \times 10^{-3}$  cm/s,  $D_s = 2.1 \times 10^{-8}$  cm<sup>2</sup>/s,  $D_a = 6.79 \times 10^{-3}$  cm<sup>2</sup>/s,  $c_0 = 1.0$  mg/cm<sup>3</sup>,  $L = 20$  cm,  $r_p = 50$  μm,  $R_{\text{column}} = 0.66$  cm,  $\epsilon = 0.43$ , superficial velocity = 500 cm/h Langmuir parameters:  $q_m = 121$  mg/cm<sup>3</sup> solid,  $K = 0.0529$  mg/cm<sup>3</sup>

## References

- Skoog, D.A., West, D.M., Holler, F.J. and Crouch, S.R., *Fundamentals of Analytical Chemistry (8th Ed)*, p. 930, Brooks Cole, Belmont (2003).  
 Özdural, A.R., Alkan, A. and Kerkhof, P.A.J.M., (2004) *Journal of Chromatography A*, 1041, 77-85.

## Session T2-7P: Transport Phenomena in Porous/Granular Media – Poster

Abstract Number	Paper Title & Authors	Included
352	Influence of the adsorbent particle size distribution on the adsorption parameters from stirred tank dynamic experiments J A Hernández, J O Marroquin, B Castro, G C Laredo, J A Ochoa	Yes
729	Mathematical modeling of hydrodynamic processes in high-porous open cell ceramic foams A S Shaimardanov, A I Kozlov, A V Jensa, V A Kostikov, E M Koltsova	Yes
1208	The break-up of jet in non-Newtonian systems M Ochowiak, L B Press, S Woziwodzki	Yes
1450	Hydrodynamics in a Packed Bed Reactor with Low Tube-to-Particle Diameter Ratio C C Araiza, F L Isunza	Yes
1707	Dynamics of flow pattern in baffled mixing vessel with axial impeller O Brůha, T Brůha, I Fort, M Jahoda	Yes
1937	Drying kinetics of granular Nylon-6 S Suherman, M Peglow, E Tsotsas	Yes
2120	Heat transfer on a sphere at different inflow turbulence L Bogusławski	Yes
2131	A non-isothermal pore network drying model: influence of gravity V K Surasani, T Metzger, E Tsotsas	Yes
2140	Expansion of starch during thermal pressure forming S Jan, Ž Rudolf	Yes
2911	Mathematical modelling of the Drying Curves of hemispherical solids S Simal, M C Garau, J Cañellas, J Bon	Yes
3045	Mathematical modeling of transport and separation properties of permselective membranes L Seda, J Kosek	Yes
3383	Numerical Investigations of Fluid Flow and Lateral Fluid dispersion in Bounded Granular Beds in a Cylindrical Coordinates System A Soleymani, I Turunen	Yes
3589	Heat exchange between a fluidised bed and an immersed cylinder: estimation of local heat transfer coefficient F D Natale, A Lancia, R Nigro	Yes
4037	The effect of biofilm growth on hydrodynamic properties of	No

Session T2-7P

	bioreactors	
	M Karrabi, P Séchet, C Morra, C Geindreau, J Martins, ACartellier	
4054	A Study of Force Response in Pellets of Herbal Spa Salts using Discrete Element Method (DEM) Computer Simulation. T Kangsadan, S Promkotra	Yes

## **Influence of the adsorbent particle size distribution on the adsorption parameters from stirred tank dynamic experiments**

J.A. Hernández<sup>a</sup>, J.O. Marroquin<sup>b</sup>, B. Castro<sup>b</sup>, G.C. Laredo<sup>b</sup>, J.A. Ochoa<sup>c</sup>

<sup>a</sup> *Centro de Investigaciones en Ingeniería y Ciencias Aplicadas (CIICAp), Universidad Autónoma del Estado de Morelos (UAEM); Av. Universidad No. 1001 Col. Chamilpa, C.P. 62210, Cuernavaca, Mor., México.*

<sup>b</sup> *Instituto Mexicano del Petróleo, Programa de tratamiento de crudo maya. Eje Central Lázaro Cárdenas 152, México D. F. C. P. 07730 México.*

<sup>c</sup> *Área de Ingeniería Química, Universidad Autónoma Metropolitana, Unidad Iztapalapa, Av. San Rafael Atlixco 186, Col. Vicentina, México, D. F. CP 09340 México.*

### **1. Summary**

The parameters that affect the separation of n-heptane from a binary mixture conformed of n-heptane and iso-octane, by adsorption in a microporous material called IMP-C12 are presented. The procedure involves a mass transfer model that considers a mean particle size calculated from the particle diameter distribution. Experimental adsorption curves of n-heptane were determined in a stirred tank by previously probed that iso-octane is not adsorbed by the IMP-C12. The system of nonlinear differential equations was solved by the finite differences method. The model reproduced with good accuracy ( $R^2=0.99$ ) the experimental adsorption kinetics with a determined mean particle size obtaining a Biot number and an intra-particle diffusivity coefficient. In order to predict the n-heptane adsorption kinetics and validate the model, solute transfer simulations were performed. The results (simulations and experimental kinetics test) were in good agreement provided that the process uses the same particle diameters distribution. The influence of the mean particle size in the adsorption kinetics was studied considering different particle diameters distribution. The results showed that particle size is essential to predict with good accuracy the adsorption curves, therefore it is extremely important to have a homogeneous (size and shape) particle distribution to determine adsorption kinetics.

Keywords: adsorption kinetics, mass transfer, particle size distribution

### **2. Extended Abstract**

In order to predict or evaluate the performance of an industrial separation procedure involving adsorption, the mathematical description of the dynamic process is required. The packed column with porous particles as adsorbent is a conventional operation in the industries for mixture separation. Normally, in the common operation, for modeling adsorption kinetics it is necessary to know the model parameters (i.e. adsorption equilibrium parameters and effective intra-particle diffusivity). Experimental data from

tank systems are used to obtain equilibrium parameters and transport parameters for adsorbents. Although, while performing batch adsorption experiments, the estimation of the intra-particle diffusivity becomes more difficult when the stirring speed is slow, in which the liquid-solid interface mass transfer resistance is not negligible. The objective of the present work is evaluate the importance of the particles size distribution on the adsorption parameters (equilibrium parameters and effective intra-particle diffusivity) of n-heptane from binary mixtures (n-heptane/isooctane) into IMP-C12 in a stirred tank. Additionally, an analysis was made to test the efficiency of the mathematic model to predict the adsorption process in a batch system. The validation of the model was made with experimental data obtained by the stirred tank.

In order to theoretical part, someone assumptions are considered. The molecules it is assumed that the suspension is well mixed. The porous particles of different size are considered spherical and suspended in the fluid; therefore, only radial transport takes place through the porous particles. We assumed that the transport and adsorption in all different size particles is represented by the mean diameter. According to different authors, the mass transport equations that govern the adsorption kinetics in a well mixed batch system that contains spherical porous particles where the inter-particle diffusion is considered, the solute concentration variation in the adsorbent porous particle is described by the following equation:

$$\varepsilon_{\gamma} \frac{\partial C_{\gamma}}{\partial t} + (1 - \varepsilon_{\gamma}) \frac{\partial C_{\kappa}}{\partial t} = \varepsilon_{\gamma} \frac{1}{r^2} \frac{\partial}{\partial r} \left( D_{\gamma} r^2 \frac{\partial C_{\gamma}}{\partial r} \right) \quad 0 \leq r \leq r_p \quad (1)$$

and to describe the solute concentration change in the bulk fluid when there is change of volume:

$$\varepsilon_{\beta} \frac{dC_{\beta}}{dt} + C_{\beta} \frac{d\varepsilon_{\beta}}{dt} = \frac{A_{fp}}{V} k_f \left( C_{\beta} \Big|_{r=r_p} - C_{\beta} \right) \quad (2)$$

In order to experimental part, adsorption kinetics were carried out. Two particle size distribution of IMP-C12 were considered. The effective intra-particle diffusivity of n-heptane on IMP-C12 and Biot number were estimated for a stirred micro-reactor at two different speeds of agitation (300 and 450 rpm). This model was solved using the well known method of explicit finite differences. This study shows that the particle size distribution is strongly important to predict the adsorption kinetics when the mass transfer type-model is used. Therefore if the particle size diameter is homogeneous and with a same particle size, it is possible to estimate the effective intra-particle diffusivity of the n-heptane into IMP-C12 in batch system and predict with good accuracy the adsorption kinetics. Particle size diameter, intra-particle diffusivity and Biot number (at low stirring rates) are significant factors for the simulation of the adsorption process. Volume variation predictions were well represented by the proposed model.

## **Mathematical modeling of hydrodynamic processes in high-porous open cell ceramic foams**

A.S. Shaimardanov, A.I. Kozlov, A.V. Jensa, V.A. Kostikov, E.M. Koltsova

*Department of Cybernetics of Chemical Engineering, D. Mendeleev University of Chemical Technology of Russian, Miusskaya pl., 9, 125047 Moscow, Russia*

### **1. Summary**

On the basis of equations of Navier-Stokes using the method of final elements, the hydrodynamic stream structure in a cell and in a layer of open-cell foam is considered. Hydrodynamic resistance of highly porous cellular material is determined during the transfer of liquid and gaseous media. Experimental data are compared.

Keywords: porous media, ceramic foam, pressure drop, mathematical modeling.

### **2. Extended Abstract**

Support and development of up-to-date level of industrial catalytic processes requires radical solutions in the field of producing new-generation catalysts possessing unique physicochemical and mechanical properties along with high operation characteristics. As such promising modern catalysts the block catalysts based on high-porous open cell metal foams can be considered, which are prepared by the polymer matrix replication and are characterized by high permeability, reliable work in the external diffusion zone, etc. Cellular metals were developed for filtration of gases, liquids, metal melts and are virtually unknown as catalyst supports.

Structure of high-permeable high-porous foam metals represents a 3D-skeleton formed by crosspieces conjoined in the nodes in four and having in cross-section the form of a curvilinear triangle. Spatial dislocation of the nodes is not random but possesses certain regularity. Due to such organization open cell structure can be considered as a group of elementary cells in form rather close to regular dodecahedron whose vertices correspond to the nodes while the edges are formed by strips connecting the nodes. However, the angles between faces in a regular dodecahedron are such that can't allow full volume filling with regularly aligned dodecahedra.

In terms of the work on thesis the foam metal elementary cell geometry was developed that provide the volume filling with the regular packing. Such foam cell is characterized by diameter of its generating sphere and interception degree (overlapping degree) – the distance from the center of the cell generating sphere to the plane intercepting a spherical segment referred to the cell diameter. The overlapping degree affects the window diameter – diameter of a circle resulting from spherical surface intersection with the

secant plane, as well as on the obtained foamed material porosity. To exclude overlapping of the neighbor windows, overlapping degree is limited by some minimum value.

For comparing the modeled foam structure with the real structure, the correlation of one of the model geometry parameters (overlapping degree) with the real structure parameters (porosity, specific surface) was found. Both the stationary and the turbulent (k-e model) flow driven by the applied constant pressure drop was considered. Mathematical modeling of the flow was based on Navier-Stokes equations and was realized using the numerical simulation packages (ANSYS and Fluent).

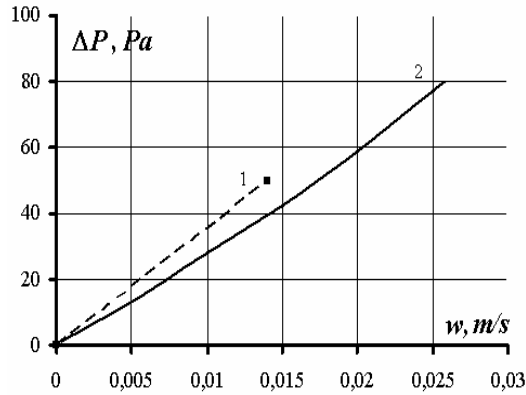


Fig. 1. Dependence of pressure drop on velocity of a water for open cell metal foam with  $d_c=0.9$  mm, with porosity  $\Pi=0.9$ , height of layer  $L=15$  mm.

1 – experimental data; 2 – laminar model.

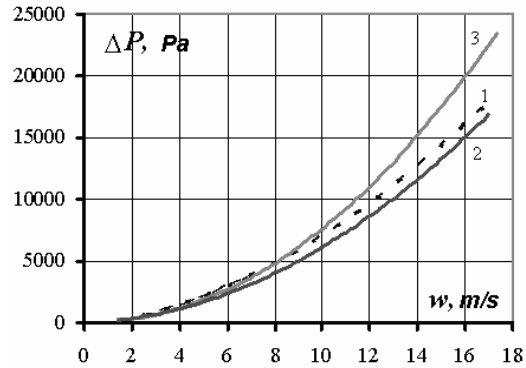


Fig. 2. Dependence of pressure drop on velocity of air for open cell metal foam with  $d_c=2.1$  mm, with porosity  $\Pi=0.9$ , height of layer  $L=70$  mm.

1 – experimental data; 2 – turbulent model; 3 – laminar model.

## References

- Bespalov, A.V., Grunskii, V.N., Kozlov, A.I., Tatarinova, I.N., and Vanchurin, V.I., (2005) Khim. Prom-st. Segodnya,, no. 3, pp. 9-13.  
 Tishchenko, S.V., Kozlov, A.I., Grunskii, V.N., and Bespalov, A.V., (2005) Khim. Prom-st. Segodnya, no. 2, pp. 42-51.



## The break-up of jet in non-Newtonian systems

M. Ochowiak, L. Broniarz-Press, S. Woziwodzki

*Department of Chemical Engineering and Equipment, Poznan University of Technology, pl. M. Skłodowskiej-Curie 2, PL 60-965 Poznan, Poland*

### 1. Summary

The phenomenon of break-up of jet into drops has been applied mainly to separation technologies in chemical, pharmaceutical, and metallurgical industries. The paper deals with the experimental analysis directed on the breakup of flexible, semi-rigid and rigid polymers solutions flowing through a ring-shaped orifice nozzle. Non-Newtonian effects on the break-up of a liquid jet into drops was studied using microphotography method. Analysis of the photos of jet break-up showed that the break-up length of non-Newtonians aqueous polymers solutions depends on liquid flow rate, rigidity and concentration of polymer in a solution.

Keywords: break-up, jet, nozzle, polymer solution, non-Newtonian system

### 2. Extended Abstract

The addition of polymers to a solvent can affect the breakup of jets. The break-up length is defined as the length of the continuous portion of the jet, measured from the nozzle to the break-up point where drop formation occurs. The length of jet is very important parameter for description of dispersion effect (Harrison et al., 1998, Mun et al., 1998-1999, Akimoto et al., 2004, Broniarz-Press et al., 2004). Knowledge of the jet length has practical significance in fire fighting and cleaning of boiler pipes, where the large length of jet is desirable, as well as in combustion engine, where the short length of jet is recommended.

In the paper the experimental analysis directed to the breakup of polymers solutions flowing through a ring-shaped orifice nozzle, has been presented. The main elements of the test installation were ring-shaped orifice nozzle, reservoir, pump, measurement units of liquid flow and digital camera. Three types of polymer molecule were considered in this work. Xantan gum (XG) was a rigid polymer, a semi-rigid was carboxymethylcellulose sodium salt (Na-CMC), and a flexible chain was characteristic for polyacrylamide (PAA). The various aqueous solutions studied were power-law fluids and presented different rheological characteristics as a result of polymer rigidity. The observations were carried out for Reynolds number (Metzner and Reed, 1955) values

$$Re_L = \frac{w^{2-n} d^n \rho}{8^{n-1} K} \left( \frac{4n}{3n+1} \right)^n \in (25,5900) \quad (1)$$

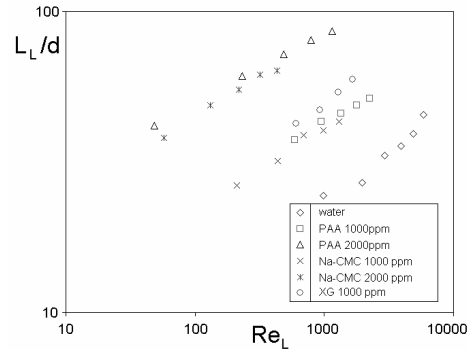


Figure 1: Effect of liquid flow rate and type of polymer solution on break-up length

An analysis of the photos of the jets break-up showed that the length of jets depends on both, liquid flow rate and type of polymer solutions used (Figure 1). High molecular polymers added to a solvent involve the changes in the rheological properties of liquid and the length of break-up  $L_L$  of jets. For all polymer solutions used the length of jets was determined from the correlation relationship:

$$\frac{L_L}{d} = C Re_L^A \quad (2)$$

where the values of  $C$  and  $A$  were dependent on the type of polymer solution and its rheological behavior.

## References

- Akimoto, K., Homma, S., Koga, J., Matsumoto, S. and Tryggvason, G., (2004) *Proceedings of the International Conference on Multiphase Flow*, 410, Yokohama, Japan.
- Broniarz-Press, L., Ochowiak, M., Poltorak, I. and Jackowska, A., (2004) *Chemical and Process Engineering*, 25, 727-732.
- Harrison, G. M., Mun, R., Cooper, G. and Boger, D. V., (1999) *Journal of Non-Newtonian Fluid Mechanics*, 85, 93-104.
- Metzner, A. B. and Reed, J. C., (1955) *American Institute of Chemical Engineering Journal*, 1, 434-440.
- Mun, R. P., Byars, J. A. and Boger, D. V., (1998) *Journal of Non-Newtonian Fluid Mechanics*, 74,285-297.

## Hydrodynamics in a Packed Bed Reactor with Low Tube-to-Particle Diameter Ratio

C. Castillo-Araiza and F. López-Isunza

*Departamento de Ingeniería de Procesos e Hidráulica, Universidad Autónoma Metropolitana –Iztapalapa.  
Av. San Rafael Atlixco 186, Col. Vicentina, C.P. 09340, México, D.F., MEXICO*

### 1. Summary

There is a major interest to incorporate the hydrodynamics into models of packed bed catalytic reactors for a class of highly exothermic reactions, performed in low tube/particle diameter ratios ( $d_t/d_p$ ); one of the aims is the simulation and design by the prediction of the spatial and temporal profiles of concentration and temperature, and the velocity field. The partial oxidation of o-xylene with air to produce phthalic anhydride belongs to this class and it is performed in catalytic reactors with  $d_t/d_p \sim 3$ . This work compares model predictions following the classical approach that model the heat transport in a packed bed with no hydrodynamics, versus those that include the hydrodynamics and a radial void fraction profile. Thus the heat transport parameters (wall heat transfer coefficient  $h_w$ , and thermal conductivity  $k_{er}$ ) are estimated in the same reaction system without reaction. These parameters are different when the hydrodynamic is incorporated into the heat transfer model; however the temperature predictions are similar making it difficult to discriminate between them. Model simulations when the reaction takes place showed that temperature profiles were sensitive to the values of the heat transfer parameters.

Keywords: Packed bed, hydrodynamics, low tube/particle diameter ratio, velocity field, model prediction

### 2. Extended Abstract

Some studies (Lerou and Froment, 1977; McGreavy et al., 1986) have found that for packed beds with low  $d_t/d_p$ , the bed voidage has a strong impact on the radial and axial velocity profiles, that will be reflected upon the calculations in catalytic fixed bed reactors, showing large reactor model sensitivity (Froment, 1967). It was observed that changes in the effective Peclet number for mass transfer has a negligible effect on the temperature profiles and conversion, whereas a 10% increase in effective thermal conductivity or in wall heat transfer coefficient have a large effect on temperature profiles and conversion. Smith (1973) has analyzed the relative importance of heat and mass transfer effects in packed bed reactors and concluded that the radial temperature gradient is the most important heat transfer limitation. On the other hand, the partial oxidation of o-xylene to phthalic anhydride has been the subject of a large number of studies in the last 50 years, and the prediction of temperature measurements from both industrial and pilot reactors for this reaction, has been carried out using pseudo-homogeneous or pseudo-heterogeneous reactor models. Normally, these models have omitted two

important aspects: the presence of porosity and velocity profiles; a sensitivity analysis to the heat transport parameter; both aspects affect the prediction of temperature measurements.

In this work a Navier Stokes-Darcy-Forchheimer equation was employed to predict the velocity profiles in this type of reactor, where the viscous and inertial terms in the Ergun (1952) expression were determined by fitting the experimental data on pressure drop in the packed bed at several air mass flow rates. To describe the radial void fraction profile in the packed bed the empirical expression developed by de Klerk (2003) was used.

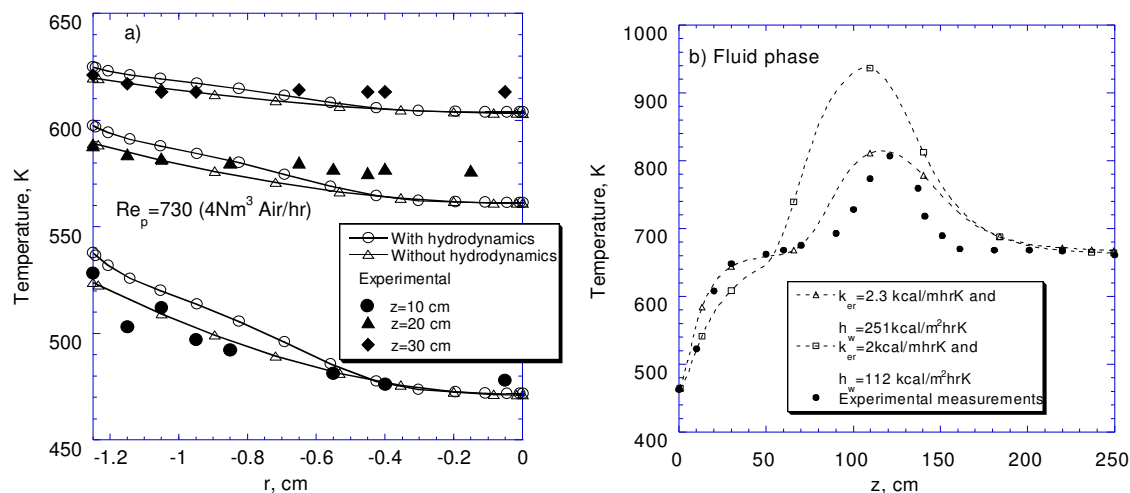


Figure 1. a) Comparison of measured versus predicted radial temperature profiles without reaction to estimate  $h_w$  and  $k_{er}$ ; b) temperature predicted at  $4\text{Nm}^3$  air/hr,  $176\text{ gr o-xylene/hr}$ ,  $T_w=661\text{ K}$ ,  $T_o=463\text{ K}$ .

Heat transfer experiments in the absence of chemical reaction were performed to estimate the  $h_w$  and  $k_{er}$ . A pseudo-homogeneous 2D model was employed. Firstly, the classical approach was used to estimate these parameters assuming plug-flow and constant void fraction ( $k_{er}=2\text{ kcal/m hr K}$  and  $h_w=112\text{ kcal/m}^2\text{ hr K}$ ); secondly, the hydrodynamics and void fraction distribution were incorporated into the heat transfer model to estimate these parameters ( $k_{er}=2.3\text{ kcal/m hr K}$  and  $h_w=251\text{ kcal/m}^2\text{ hr K}$ ). Model simulations of the heat transport in the packed bed showed that very similar predictions of radial and axial temperature profiles were obtained in all cases, making difficult to discriminate between them (Figure 1a; only radial). Then, the reactor simulation, incorporating the estimated heat transport parameters was carried out using a pseudo-heterogeneous model 2D, with Calderbank's (1977) kinetics, and an (empirical) irreversible deactivation profile (López-Isunza & Kershenbaum, 1992). Figure 1b shows the comparison between the model predictions using the estimated heat transfer parameters (with & without hydrodynamics), versus experimental results from an industrial single-tube reactor (López-Isunza, 1983). The results show the effect of the parameter values on the temperature profile. Those parameters estimated using the bed hydrodynamics give the best prediction.

## References

- Chandrasekharan K.; Calderbank P.H. (1980). *Chemical Engineering Science*, 35, 341.  
 de Klerk A. (2003). *American Institute of Chemical Engineers Journal*, 49, 2022.  
 Ergun S.(1952). *Chemical Engineering Progress* 1952, 48, 89.  
 Froment G. F. (1967), *Industrial Engineering Chemical*, 59, 18.  
 López-Isunza F. (1983). *Ph.D. Thesis*, Imperial College, University of London, UK.  
 López-Isunza & Kershenbaum (1992), *Chemical Engineering Science*,  
 Lerou J.J.; Froment G.F. (1977). *Chemical Engineering Science*, 32, 853.  
 McGreavy C.; Foumeny E.A.; Javed K (1986). *Chemical Engineering Science*, 41, 787.  
 Smith J.M. (1973). *The Chemical Engineering Journal*, 5(2), 109.

## **Dynamics of flow pattern in baffled mixing vessel with axial impeller**

O. Brůha,<sup>a</sup> T. Brůha,<sup>b</sup> I. Fort,<sup>c</sup> M. Jahoda<sup>b</sup>

<sup>a</sup>*Department of Physics, Faculty of Mechanical Engineering, Czech Technical University, Technická 4, CZ-166 07 Praha 6, Czech Republic*

<sup>b</sup>*Department of Chemical Engineering, Institute of Chemical Technology, Prague, Technická 5, CZ-166 28 Praha 6, Czech Republic*

<sup>c</sup>*Department of Process Engineering, Faculty of Mechanical Engineering Czech Technical University, Technická 4, CZ-166 07 Praha 6, Czech Republic*

### **1. Summary**

The mechanically agitated system under turbulent regime of flow with or without internals radial baffles, draft tubes coils etc. consists of wide spectrum eddies with size varying from main circulation loop of agitated batch down to the dissipative vortices corresponding to the micro-scale eddies. This study deals with theoretical and experimental analysis of oscillations of the primary circulation loop in axial flow impeller system with radial baffles. Investigated oscillations are sources of the flow macro-instability phenomenon characterized by additional macro vortices appearing in agitated batch.

Keywords: mixing, axial impeller, primary circulation loop, oscillation, macro-instability

### **2. Extended Abstract**

The paper deals with experimental and theoretical study of oscillations of the primary circulation of agitated liquid in flat-bottomed cylindrical stirred tank of inner diameter  $T=0.29$  m filled with water to the tank diameter height  $H=T$ . The vessel was equipped with four radial baffles (width of baffles  $b=0.1T$ ) and stirred with six pitched blade impeller (pitch angle  $45^\circ$ , diameter  $D=T/3$ , width of blade  $w=D/5$ ), pumping downwards. The experiments were concentrated on the lower part of the vessel, namely on the time and space pulsations of the primary loop, initiated by the impeller pumping action. The attention was focused on this space as this area is supposed to be a "birth place" of the flow macro-instabilities in an investigated system. The occurrence of this phenomenon has been studied and described by several authors, see References. The flow was observed in a vertical plane coming through the vessel axis. Flow patterns of agitated liquid were visualised by means of aluminium micro

particles spread in water and illuminated by a vertical light knife 5 mm wide and located in the half of the sector between adjacent baffles. The impeller speed was adjusted at 400 rpm and the off bottom clearance was  $T/3$ . The visualized flow was scanned by a digital camera, records and shots obtained were of satisfactory quality. The defined exposure time allowed to obtain information on approximate local flow speed. Experimental conditions were set up so that the regime of agitated liquid flow was turbulent. The analysis of the record and shots as well as theoretical findings resulted in following conclusions:

The primary circulation loop oscillates within the limits 0.2 – 0.7 of surface level height and the mean oscillations frequency is  $f_{osc} = 0.63$  Hz. This value is significantly lower than the impeller frequency  $N = 6.67$  Hz. The flow field corresponding to the primary loop has an elliptical shape with a core. The flow in the elliptical annular area is intensive and streamlined (it can be considered as a stream tube), while the core is steady and chaotic. The flow in the remaining upper part is markedly steadier. The main diameter of the primary loop is not constant, it increases in time and after reaching a certain value the loop disintegrates and collapses. This development is characterized by a certain periodicity, see value above, and the period proved to be correlated to the flow macro-instability occurrence. According to the balance of mechanical energy dissipated in the primary circulation loop it is possible to explain the instability of this loop observed. Impeller power output is dissipated both in the bulk flow (just below the impeller and in the whole space above the rotor), in the primary circulation loop (growing of its kinetic energy) and in the turn of primary flow at the bottom (change of direction from downwards to upwards) and by friction along the vessel wall. But a part of the impeller power output is consumed by increasing the kinetic energy of the primary loop. When the primary loop reaches the level of disintegration, the whole impeller power output is dissipated. In this moment, any flow alteration requiring additional energy, for instance even a very small vortex separation from the primary loop, leads to the loop collapse.

## References

- Brůha, O., Fořt, I., Smolka, P. and Jahoda, M. (1996) *Collection of Czechoslovak Chemical Communications*, 61, 856-867.
- Hasal, .P., Montes, J.-L., Boisson, H.-C. and Fořt, I. (2000) *Chemical Engineering Science*, 55, 391-401.
- Hasal, .P., Fort, I. and Kratena, J. (2004) *Chemical Engineering Research and Design*, 82 (A9), 1268-1281.
- Roussinova, V.T., Kresta, S.M. and Weetman, R. (2004) *AIChE Journal*, 50, 2986-3005 .
- Paglianti , A., Montante, G. and Magelli, F. (2006) *AIChE Journal*, 52, 426-437.
- Ducci, A. and Yianneskis, M. (2007) *AIChE Journal*, 53, 305-315.

## Drying kinetics of granular Nylon-6

S. Suherman\*, M. Peglow, E. Tsotsas

*Thermal Process Engineering, Otto-von-Guericke-University, 39106 Magdeburg, Germany.*

*\*Present Address: Dpt. of Chemical Engineering, Diponegoro University, Semarang, Indonesia.*

### 1. Summary

In this study, the drying kinetics of granular nylon-6 has been investigated. Single particle drying experiments were carried out in a magnetic suspension balance (MSB) using dry air as drying agent. The comparison of measured and simulated data using Vrentas-Duda diffusion model shows a satisfactory prediction of mean particle moisture content and drying rates.

Keywords: drying, nylon, polymer, diffusion, free volume theory.

### 2. Extended Abstract

In the production of polymers, drying is one of the major recovery operations employed to obtain a final saleable product from a reaction process. Since it consumes large amounts of energy, the drying process deserves attention towards both energy savings and improvement of the quality of dried polymer. Beside that, the drying rate of many polymers decreases rapidly to low values and then tends very slowly to zero at the end of drying. This phenomenon is sometimes called tail of the drying curve or plateau diffusion. It is characterized by very slow diffusion phenomena when moisture contents close to zero are achieved. Therefore, the determination and prediction of drying kinetics is a demanding task, and could be helpful in the selection of adequate drying systems (Suherman, et al, 2006).

Popular example of granular polymer is nylon-6. The big problems in drying of nylon are low temperature limits (70-80°C) and the oxidative deterioration and discoloration at low moisture content. Usually nylon is dried in vacuum condition or in recirculating dehumidified air (dew point lower than -18 °C). For these conditions the drying time ranges from 10 to 24 h (Melvin, 1995).

In this work, the prediction of residual moisture content is based on the assumption that the drying process is mainly controlled by diffusion of moisture within the particle and mass transfer kinetics at the phase boundary. The free volume parameters in Vrentas and Duda diffusion model are determined from thermodynamics (Vrentas, 1977; Hong, 1995), except  $D_0$  (constant pre exponential factor) and  $\xi$  (ratio of solvent and polymer jumping unit), which are estimated from experimental data by fitting. The fitting procedure is conducted by minimizing the sum square of error (SSE) between mean particle moisture obtained from measurement and simulation.

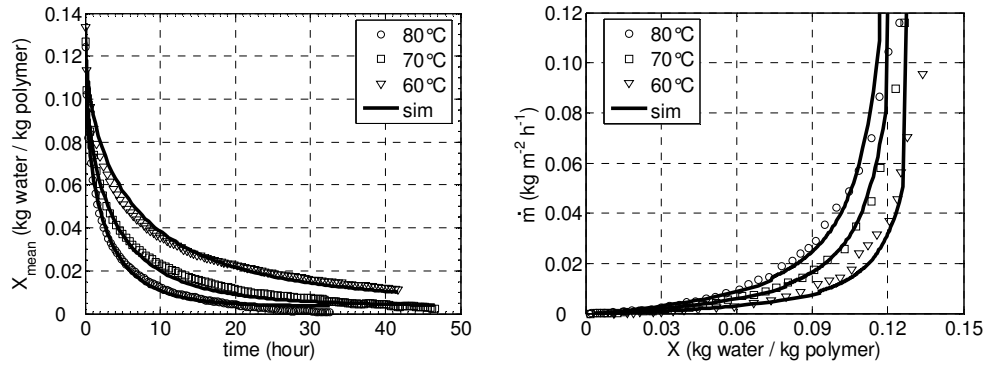


Fig. 1. Comparison between measurement and simulation; (i) mean particle moisture content, and (ii) drying rates.

Figure 1 shows the comparison between experimental and simulation data for different gas temperatures. Both the temporal change of moisture content (left diagram in Fig.1) and the drying rates (right diagram in Fig. 1) are predicted well by the diffusion model. It should be pointed out that the initial drying rates were an order of magnitude smaller than the theoretical first period drying rate for the given process conditions ( $Sh=2$ ,  $Y=0.5$  g/kg). Consequently, the entire drying process of nylon 6 is controlled by the internal diffusion of moisture. For small moisture contents ( $X < 0.01$ ) the diffusion coefficient decreases tremendously (see Fig. 2) since the water vapour in nylon 6 is comparatively immobile at the lower water content, and considerably mobile at higher water contents. This phenomenon has also been reported by Kowasaki, 1964.

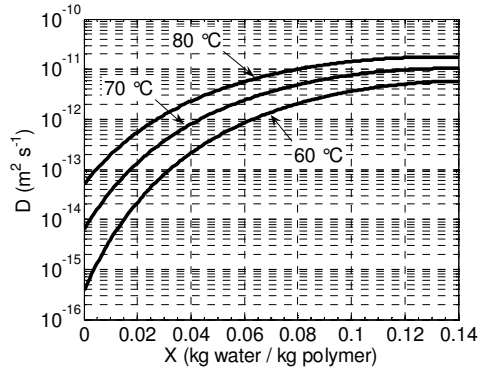


Fig 2. Dependency of diffusion coefficient on particle moisture content and temperature ( $\xi = 0.49$ ;  $D_0 = 4.02 \times 10^{-8}$  m<sup>2</sup>/s).

## References

- Hong SU, (1995), *Ind. Eng. Chem. Res.*, Vol. 34, 2536-2544.
- Kowasaki K., and Sekita, Y., (1964), *J. Poly. Sci., Part A*, Vol.2, 2437-2443.
- Melvin I, and Kohan, (1995), *Nylon Plastics Handbook*, Hanser Gardner Publications, Munich.
- Suherman, Peglow, M., and Tsotsas, E., (2006), *Drying Kinetics of Granular and Powdery Polymers*, Proc. of 15th Int. Drying Symp. (IDS 2006), 1867-1874
- Vrentas, J.S., and Duda, J.L., (1977), *J. Polym. Sci., Polym. Phys. E* Vol. 15, No. 3, 403-416.



## Heat transfer on a sphere at different inflow turbulence

L. Bogusławski

*Chair of Thermal Engineering, Poznań University of Technology, Pl-60 965 Poznań, Poland*

### 1. Summary

In the paper results of experimental investigations of influence of the flow turbulence level on average heat transfer on spheres of different diameters will be presented.

Keywords: heat transfer coefficient, sphere, flow turbulence

### 2. Extended Abstract

Heat transfer process from solid surface to external flow is a function of many parameters. For forced convection of heat from surface the main parameter which stimulated this process is the average flow velocity. Nevertheless many literature data indicated that increase of turbulence level of external flow cause increase of heat transfer coefficient even when average velocity doesn't change. This cause that in many application accuracy of estimation of heat transfer intensity can be not sufficient, because it is very difficult to determine the level of turbulence in external flow generated by different flow sources. In this case average velocity can be the same but level of turbulence, as the simplest parameter of turbulent flow structure, can be different because turbulent flow generated by different flow sources can be characterised by different flow structures.. Very often the average flow velocity is not good enough to describe turbulent flow structures when they influence on heat transfer processes on surfaces.

To estimate influence of turbulence level of external flow on average heat transfer coefficient on a simple surface geometry, sphere, the experimental tests were performed. The flow was generated by nozzle diameter of  $D$ . For different distances from nozzle outlet it was possible to get turbulence level in free jet from about 0,5% till about 20% with no change of the average flow velocity. The constant temperature anemometer was used to measure level of flow turbulence. The average heat transfer coefficient on spheres diameters of  $d$  was measured in steady-state thermal conditions by means of an electrical heating system. Heat transfer convection from spheres diameter of 0.01m, 0.02m, 0.03m and 0.05m was measured at different turbulence level of inflow. The constant temperature anemometer (CTA) TSI 1050 with hot wire probe was used to measure level of flow turbulence. For measurements of distribution of local heat transfer coefficient the surface probe connected to CTA bridge was used. All data were recorded by digital acquisition system.

Investigations indicated that increase of turbulence level of flow cause increase of average heat transfer from isothermal surface of sphere to ambient air even when the average inflow velocity doesn't change i.e. Reynolds number of average flow remain

constant (Figure 1). For sphere diameter of  $d = 0.03\text{m}$  increasing of flow turbulence to 22% cause increase of average heat transfer coefficient about 30%. Heat transfer process on spheres of larger diameter is more sensitive on increasing of external flow turbulence. There is no evidence that diameter of nozzles generated flow influence on heat transfer process in tested range of sphere to nozzle diameters rate

Analysis of local heat transfer distributions around sphere surfaces indicated that increasing of heat transfer process is not uniform and depend on external flow turbulence intensity.

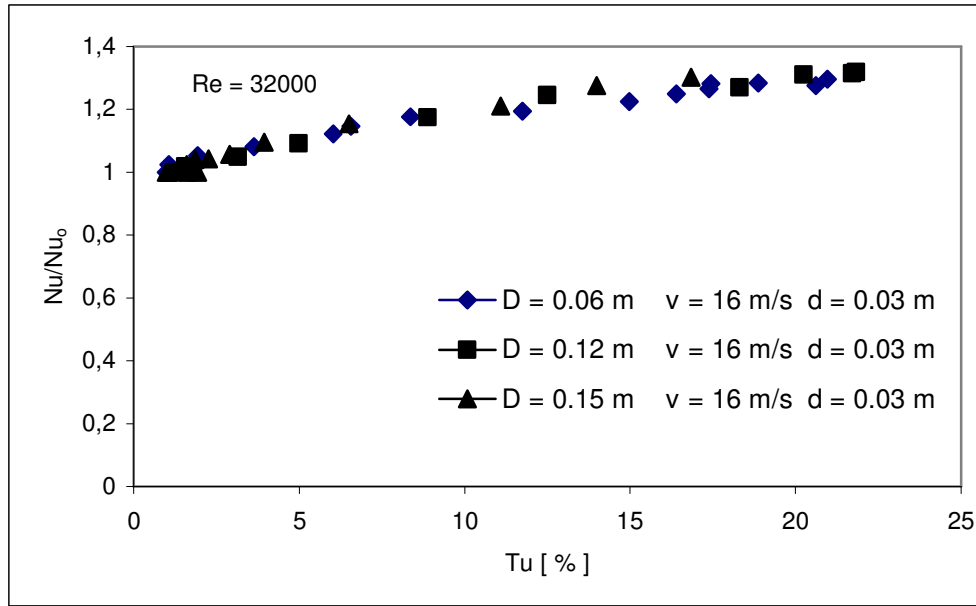


Figure 1. Distribution of the average heat transfer coefficient on the sphere surface diameter of 0.03m at different inflow turbulence level.

Performed measurements show that level of turbulence intensity of external flow can influence in essential manner on heat transfer process on solid surfaces of different kinds thermal equipments.

## References

- L. Bogusławski. *Losses of heat from sphere surface at different inflow conditions* (in polish), XVI Thermodynamics Conference, Kołobrzeg, vol. 1, 135-140, (1996).
- F.P.Incropera and D.P. De Witt. *Fundamentals of Heat and Mass Transfer*, John Wiley and Sons, New York 2001
- S.Whitaker. *J. of AICHE*, vol. 18, 361-371, (1972).

# A non-isothermal pore network drying model: influence of gravity

V. K. Surasani, T. Metzger, E. Tsotsas

*Thermal Process Engineering, Otto-von-Guericke-University, P.O. 4120, D-39016 Magdeburg, Germany*

## 1. Summary

The concept of immiscible displacement as an invasion percolation (IP) process driven by heat and mass transfer is used in a pore network model for convective drying of capillary porous media. The coupling between heat and mass transfer occurs at the liquid-gas interface through temperature dependent equilibrium vapor pressure, surface tension and phase change enthalpy (in evaporation and condensation). The interfacial effects due to capillary forces and gravity are combined in an invasion potential  $\Phi$ ; viscous forces are neglected. Simulation results show stabilized invasion patterns and finite drying front width by the influence of gravity.

Keywords: capillary porous media, mono-modal pore size distribution, invasion percolation, phase distributions, temperature field

## 2. Extended Summary

### Modeling

Void space in the porous medium is envisaged as a network of throats and pores in the manner of 2D square lattice. The definitions of pore and throat conditions during drying and the discretized boundary layer formed due to convective air flow [1] are shown in Figure 1. The sum of vapor flow rates over the control volume CV equals zero for every gas pore i:

$$\sum_{j=1}^4 \dot{M}_{v,ij} = \sum_{j=1}^4 A_{ij} \frac{\delta}{L} \frac{P\tilde{M}}{RT} \ln\left(\frac{P - P_{v,i}}{P - P_{v,j}}\right) = 0 \quad (1)$$

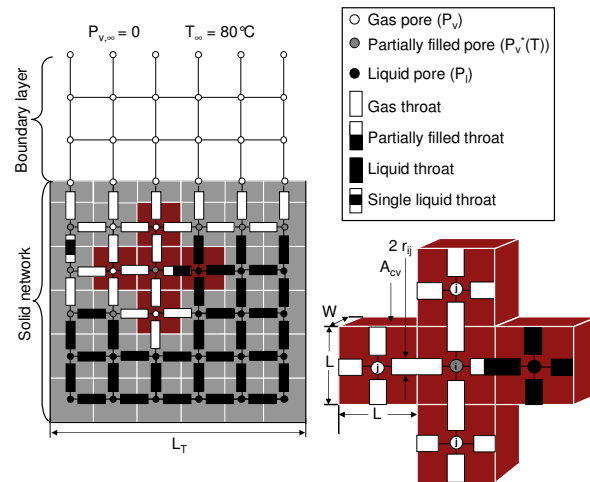


Figure 1: Pore network with boundary layer, pore and throat conditions and control volume.

$$\frac{dH_i}{dt} = - \sum_{j=1}^4 A_{ij} \lambda_{ij} \frac{T_i - T_j}{L} - \Delta h_{v,i} \sum_{j=1}^{lm} \dot{M}_{ev,ij} \quad (2)$$

$$\Phi = \frac{-2\sigma(T_{ij})}{r_{ij}} + (\rho_l - \rho_g) g h_{ij} \quad (3)$$

The enthalpy balance, Eq. (2), incorporates Fourier's law of heat conduction and heat sinks/sources due to evaporation/condensation at menisci within the CV. The linear system of vapor transport, Eq. (1), has to be solved for unknown vapor pressures, from which cluster evaporation rates are computed. For every liquid cluster, the meniscus with the highest invasion potential  $\Phi$ , Eq. (3), is chosen to empty. An appropriate time step is used to update phase distributions and temperatures, by Eq. (2), and this procedure is repeated until required saturation is achieved.

*Simulation results*

Simulations are carried out on 51x51 pore network with mono-modal pore size distribution ( $40 \pm 2 \mu\text{m}$ ), throat length 500  $\mu\text{m}$  and solid properties as for glass. Drying air at 80°C is flowing parallel to the top edge of the network; the remaining faces are impermeable to heat and mass fluxes. Phase distributions, and temperature fields are presented without and with gravity in Figure 2.

In absence of gravity, i.e. with Bond number  $B = 0$ , capillary forces alone will determine the order of throat invasion; they are given by random throat radius distribution and current local temperatures. If temperature gradients are low, then the gas phase will rapidly invade the depth of the pore network creating many liquid clusters in the whole network. In convective drying, the porous medium heats up from the surface; this leads to favorable invasion of near surface throats (influence of temperature dependent surface tension in  $\Phi$ ). This thermal stabilization becomes important for weakly disordered networks.

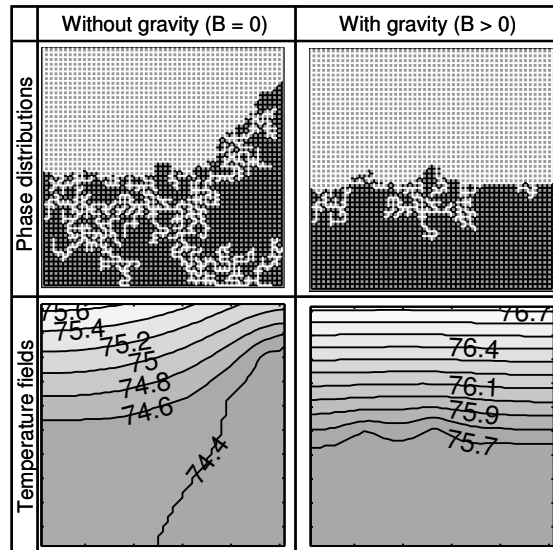


Figure 2: Results for network saturation 40 %.

For the given geometry, gravity counteracts capillary forces. Throat invasion order is then determined by invasion potential  $\Phi$ , which combines both effects. Capillary pumping is limited to a finite drying front in which small clusters will form (see Figure 2 with gravity). This front recedes into the network without major changes of its width. The observed drying rates are low because of the increased resistance to vapor diffusion for a stabilized front. The above-mentioned thermal stabilization of the drying front is now superimposed by a gravitational stabilization [2]. This is also studied by a comparison with isothermal drying simulations.

**References**

V. K. Surasani, T. Metzger and E. Tsotsas, Consideration of heat transfer in pore network modelling of convective drying, submitted to Int. J. Heat and Mass Transfer.  
 J. B. Laurindo and M. Prat, Drying Technology 16(9&10), 1769-1787, 1998.

## **Expansion of starch during thermal pressure forming**

Skočilas Jan and Žitný Rudolf

*Czech Technical University in Prague, Faculty of Mechanical Engineering, 166 07, Prague 6, Technická 4.*

### **1. Summary**

The contribution is aimed to the processes of thermal treatment of starch-based materials for biologically degradable packaging products. The combined heating of starch-based suspension (direct ohmic heating and thermal processing of starch based suspensions) was performed in a closed mould. The sample expands significantly (approximately 3 times) during heating and this expansion is accompanied by gradual formation of crust and a porous layer in the core. The time course of the sample expansion was detected by a grid of thermocouples and compared with the recorded pressure inside the mold. The mathematical models of the combined ohmic heating of starch suspension was formulated. The finite element model is based upon the concept of two overlapping 2D meshes: the fixed mesh represents the heating plates and the crust, while the moving (expanding) mesh describes the expanding core (foam). The foam behavior is modeled according to the idea of expanding spherical bubble, filled by a saturated steam and with viscoelastic walls. Besides the finite element model also a simplified model of a homogeneous sample (expanding homogeneous foam) will be presented. Parameters of models are identified by comparing the theoretical predictions with the experimental data.

Keywords: starch, thermal forming, finite element method, mould filling, expansion

### **2. Extended Abstract**

The technology of pressure thermal forming in a mould is aimed to the replacement of plastics by starch-based biodegradable materials. Pressure thermal process design, scale up, modeling and operational parameters optimization are still difficult, because basic mechanisms controlling the starch-based material expansion and the formation of crust, are not clearly identified. Fig.1 shows the experimental stand designed for monitoring the process parameters (temperatures and pressure) when baking thin potato-starch samples between two planar heating plates (in a closed mould).

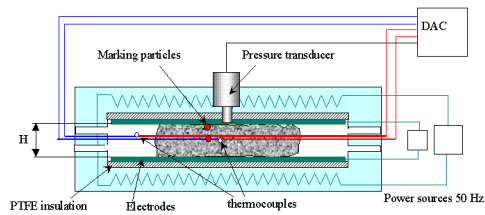


Figure 1. Schematic sketch of the apparatus

2D finite element model was developed based upon enthalpy balances at an element level (Lagrangian approach). The model operates with two overlapping meshes of finite elements (fixed mesh represents crust and heating plate, expanding mesh describes the flowing core).

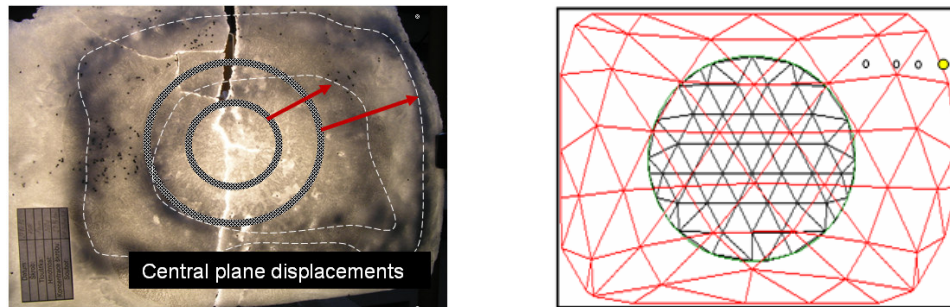


Figure 2. Expansion of sample obtained by marking particles and predicted by model

This model assumes that a driving force for the liquid core expansion is a radial pressure profile, corresponding to the radial flow of evaporated steam (the model assumes in fact a radial squeezing flow of liquid displaced by a growing crust). Our new experiments, based upon measured radial temperature profiles, indicate that the actual mechanism of the sample expansion might be different – the time course of volumetric expansion advances the pressure increase recorded at a centre of the heating plate. Possible explanation of the delayed pressure peak is a blockade of venting gaps located around the mould perimeter by the expanded sample.

These observations motivated development of a new model, based upon the concept of an expanding bubble, Fan (1999). This approach enables to formulate either a simple integral model represented by a single bubble (assuming uniform temperature, pressure, water content and the expansion rate) or a 2D FEM model considering the two overlapping layers: the expanding core formed by a manifold of elastic bubbles (foam) and a permeable crust sticking at wall.

## References

Fan J., Mitchell J.R., Blanshard J.M.V. (1994): *Journal of Food Engineering*, 23, 337-356, 1999.

## Mathematical modelling of the Drying Curves of hemispherical solids

Susana Simal<sup>a</sup>, M. Carme Garau<sup>a</sup>, Jaume Cañellas<sup>a</sup>, José Bon<sup>b</sup>

<sup>a</sup>Department of Chemistry, Univ. of Illes Balears, Ctra. Valldemossa km. 7.5. 07122. Palma de Mallorca, Spain. e-mail: susana.simal@uib.es

<sup>b</sup>Food Technology Department, Univ. Politècnica de Valencia, Cno. Vera s/n. 46071. Valencia, Spain.

### 1. Summary

Conventional air-drying is the most frequently used drying operation in food and chemical industry. The drying kinetics are greatly affected by air temperature and material characteristic dimension. The drying curves of halved and deseeded apricots at different temperatures (from 50 to 90°C) have been evaluated and a diffusional model, solved by a finite elements method, has been proposed to simulate the drying kinetics. The effect of the external resistance on the mass transfer curves was taken into account when modelling. Due to the geometry of the system considered, a hemisphere losing water only through the flat section, both the effective water diffusion and the mass transfer coefficient ( $k_c$ ) were identified from the experimental results. The mean relative error estimated for the simulation of the experimental drying curves was of  $2.9 \pm 1.0\%$ .

Keywords: diffusional model, mass transfer, hemisphere, external and internal resistances, apricot

### 2. Extended Abstract

The governing equation for a hemispherical shape is as follows (eq. 1) (Bon et al, 1997), where  $W_1$  is the local moisture content dependent on the position and on the time ( $t$ ), and  $D_{\text{eff}}$  is the effective moisture diffusion coefficient ( $\text{m}^2/\text{s}$ ).

$$\frac{\partial W_1(r, \alpha, t)}{\partial t} = \frac{1}{r^2} \frac{\partial}{\partial r} \left( D_{\text{eff}} r^2 \frac{\partial W_1(r, \alpha, t)}{\partial r} \right) + \frac{1}{r^2 \sin \alpha} \frac{\partial}{\partial \alpha} \left( D_{\text{eff}} \sin \alpha \frac{\partial W_1(r, \alpha, t)}{\partial \alpha} \right) \quad [1]$$

The boundary conditions considered were those related to the thermodynamic equilibrium and solid symmetry. The initial condition is the initial moisture content of the solid. To take into account the effect of the external resistance to mass transfer, the second boundary condition can be expressed:

$$t > 0 \rightarrow D_{\text{eff}} \rho_{\text{dm}} \frac{\partial W_1(0, \alpha, t)}{\partial r} = k_c (\varphi_s - \varphi_\infty) \quad [2]$$

$$t > 0 \rightarrow \frac{D_{\text{eff}} \rho_{\text{dm}}}{r} \frac{\partial W_1(r, \pi/2, t)}{\partial \alpha} = k_c (\varphi_s - \varphi_\infty) \quad [3]$$

The effect of temperature on the diffusivity is generally described by the Arrhenius equation. The parameters in the Arrhenius equation ( $D_o$  and  $E_a$ ) were identified to minimise the mean relative error calculated (MRE) through the comparison of experimental and estimated average moisture contents.

The function “fminsearch” of the Optimization Toolbox of MATLAB 7.1 (The MathWorks Inc.) was used to find this minimum. To solve the partial differential equation for the drying process through a Finite Element Method (FEM), the function “parabolic” of MATLAB was used.

### Results

Figure 1 shows the drying curves of apricots at different drying air temperatures, from 50 to 90°C. As it was expected, increasing air temperature affected the drying curves and decreased the final drying time.

The identified  $D_o$  and  $E_a$  figures are shown in equation 4 together with the results obtained for the mass transfer coefficient adjusted to an empirical relationship (eq. 5).

$$D_{\text{eff}} = 5.25 \times 10^{-2} \exp\left(\frac{-46278.0}{RT}\right) \quad [4] \quad k_c = \left[\frac{939.9}{T}\right]^{-6.72} \quad [5]$$

Figure 1 also shows and the calculated moisture content vs. drying time for the experiments carried out at different air drying temperatures. As can be seen, the model provided a very accurate simulation of the drying curves being the mean relative error of  $2.9 \pm 1.0\%$ .

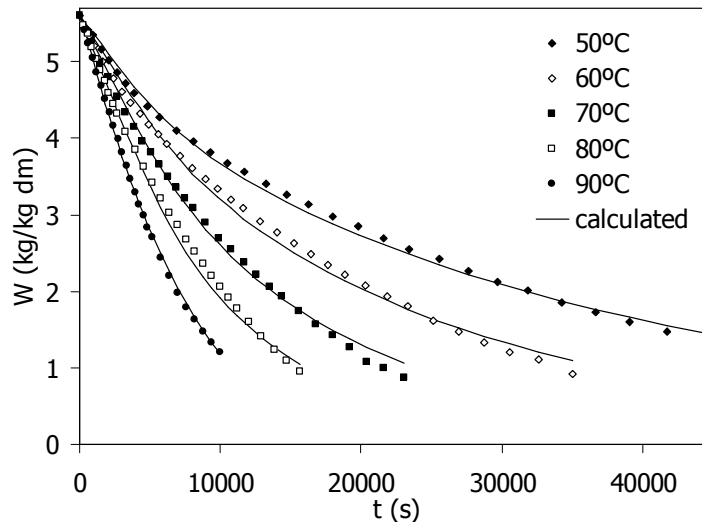


Figure 1: Experimental and calculated drying curves of apricots.

### References

- Pinto, L.A.A.; Tobinaga, S. (2006). *Drying Technology* 24, 509-516.  
 Bon, J.; Simal, S.; Rosselló, C.; Mulet A. (1997). *Journal of Food Engineering* 34, 109-122.



## **Mathematical modeling of transport and separation properties of permselective membranes**

L. Seda and J. Kosek

*Department of Chemical Engineering, Institute of Chemical Technology in Prague, 166 28 Prague 6, Czech republic*

### **1. Summary**

The relations between type and concentration of ionic species, structure and fixed surface charge density of reconstructed porous media and the ionic permselectivity of these media are presented. We demonstrate the solution of Poisson, Navier-Stokes, continuity and mass balance equations with finite element method to obtain electric potential, pressure, velocity and concentration fields to address the above mentioned problem. The ionic permselectivity of reconstructed porous domains with various setup of charged surfaces was carried out and the obtained simulation results are compared with experimental observations.

Keywords: concentration polarization, electroosmotic flow, reconstructed porous media, ionic permselectivity

### **2. Extended Abstract**

Porous media with fixed surface charge are involved in many practical applications which utilize externally applied electric field or where the induced electric field is important, e.g., capillary electrochromatography, electrodialysis, nanofiltration and other membrane separation processes. In electric field driven applications the electroosmotic flow is an important mechanism of convective transport of the electrolyte solution. Although one of the practical problems is to find the relation between concentrations of charged species in electrolyte or the electroosmotic flow of the electrolyte and the porous structure of the medium, most current case studies assume the so called pseudohomogeneous (space-averaged) porous medium represented by space-averaged parameters, for example by effective diffusivity of species or averaged fixed charge on the surfaces of permselective membranes. We have developed the software which allows us to predict the transport and separation properties of porous medium (e.g., perfusion flow and ionic permselectivity) in dependence on: (i) the porous micro-structure, (ii) type and distribution of the fixed charge, and (iii) type and concentration of the electrolyte.

The ionic system is described by the set of partial differential equations. The distribution of electrostatic potential  $\varphi$  is governed by the Poisson equation, velocity and pressure

distributions are obtained from the solution of Navier-Stokes equations and from the continuity equation of an incompressible liquid. The steady-state local molar balances of species in the ionic system without chemical reaction are described by the Nernst-Planck equations.

We employed the finite element method for processing of mentioned equations. The resulting set of nonlinear equations was solved by Newton's method and the set of linear equations was processed by LU factorization.

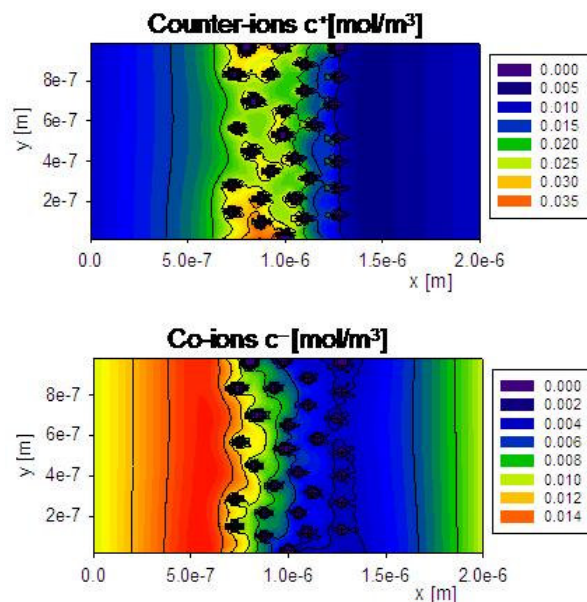


Fig. 1. Concentration profiles in spatially 2D micro channel packed by particles with fixed surface charge.

Concentration profiles of ionic species in spatially 2D micro-channel packed with particles with fixed negative charge groups on their surface are visualized in Fig. 1. The negatively charged co-ions (bottom profile) are excluded from the packed zone because of electrostatic interactions and on the other hand the positively charged counter-ions are enriched there. Because of applied outer electric potential gradient the ions are forced to motion. Due to the exclusion of co-ions from the middle part of the channel the concentration polarization of co-ions is developed and the system embodies the ionic permselectivity. The obtained results with various setups of porous media are further compared with experimental studies.

## References

- Seda, L., Kosek, J.: Predictive modeling of ionic permselectivity of porous media *Computers and Chemical Engineering*, in print (2007).
- Kosek, J., Stepanek, F., Marek, M.: *Modeling of transport and transformation processes in porous and multiphase bodies*, in *Advances in Chemical Engineering*, Vol. 30 „Multiscale Analysis“, edited by Marin G.B., Elsevier (2005).

# **Numerical Investigations of Fluid Flow and Lateral Fluid dispersion in Bounded Granular Beds in a Cylindrical Coordinates System**

Azita Soleymani and Ilkka Turunen

*Department of Chemical Engineering, Laboratory of Process and Product Development, University of Lappeenranta, PO Box 20, FIN-53851, Lappeenranta, Finland*

## **1. Summary**

Results are presented from a numerical study examining the flow of a viscous, incompressible fluid through random packing of non-overlapping spheres at moderate Reynolds numbers. By using a laminar model including inertial terms and assuming rough walls, numerical solutions of the Navier-Stokes equations in three-dimensional porous packed beds resulted in dimensionless pressure drops in excellent agreement with those reported in a previous study. This observation suggests that no transition to turbulence could occur in the range of the Reynolds number studied. For flows in the Forchheimer regime, numerical results are presented of the lateral dispersivity of solute continuously injected into a three-dimensional bounded granular bed at moderate Peclet numbers. In addition to numerical calculations, to describe the concentration profile of solute an approximate solution for the mass transport equation in a bounded granular bed in a cylindrical coordinates system is proposed. Lateral fluid dispersion coefficients are then calculated by fitting the concentration profiles obtained from numerical and analytical methods. Comparing the present numerical results with data available in the literature, no evidence has been found to support the speculations by others for a transition from laminar to turbulent regimes in porous media at a critical Reynolds number.

Keywords: porous media, direct numerical simulation, laminar regime, dispersion coefficient, turbulence

## **2. Extended Abstract**

Transport phenomena in disordered systems are a subject of considerable scientific and engineering importance. In particular, fluid flow through granular beds has attracted attention due to its importance in many important industrial processes, such as chromatographic separation technology, packed bed reactor and contacting device design, catalytic exhausters, modeling of contaminant transport in hydrogeological and environmental systems and studies of perfusion in biological media.



Figure 1: Particle configuration for the simulations of the present study. The side wall of the duct is roughened to avoid exiting the higher velocity region near the tube wall

In the present study, a cylindrical bed of 3000 nonoverlapping spherical particles is employed as the porous matrix (Figure 1). Simulations were performed using a model based on the Navier-Stokes equations, including inertial terms but without a turbulence model, to examine the fluid flow in a granular bed. Assuming rough walls, the simulation results for pressure drop across the bed agreed well with the correlation of [Fand et al., 1987] for the range of conditions studied in the second post-Darcy (“turbulent”) flow regime, despite the absence of a turbulent model in the formulation. To investigate the fluid dispersivity, the spread of the solute continuously injected into the three dimensional bounded granular bed composed of randomly packed monodisperse spheres is recorded. For these simulations, the solvent is flowing in the laminar Forchheimer regime. The calculated results for the dispersion coefficients, which were isotropic, were found to be in excellent agreement with those of [Han et al., 1985] and [Harleman and Rumer, 1963]. The simulation results highlight the need for an improved experimental database for flow in porous media. The lateral dispersion coefficients are predicted by applying a method similar to the so-called concentration-based methods that utilize solutions of the advection-diffusion equation to calculate the dispersivity from the measured concentration and mean velocity data. To this end an analytical solution for the advection-diffusion equation in the cylindrical coordinates is presented.

## References

- R. M. Fand, B.Y. Kim, A. C. C. Lam and R.T. Phan, (1987) *J. Fluids Engineering*, 109, 268 .  
N. Han, J. Bhakta, and R.G. Carbonell, (1985) *AIChE J.* 31, 277.  
D. R. F. Harleman, R. R. Rumer, (1963) *Journal of Fluid Mechanics*, 16, 385.

## Heat exchange between a fluidised bed and an immersed cylinder: estimation of local heat transfer coefficient

Francesco Di Natale<sup>a</sup>, Amedeo Lancia<sup>a</sup>, and Roberto Nigro<sup>a</sup>

<sup>a</sup>*Dipartimento di Ingegneria Chimica, Università di Napoli "Federico II",  
P.le Tecchio, 80, 80125 Napoli, Italy*

### 1. Summary

This work reports experimental results on the local heat transfer coefficient on the surface of a horizontal cylinder immersed in a fluidised bed. Experimental runs are carried out at ambient pressure and temperature on several bed materials. The heat transfer coefficient is mainly related to particle convective mechanisms and it is the highest on the lateral surface of the cylinder and the lowest on its upper face. The maximum heat transfer coefficient results from an optimal compromise between the local values of the particle concentration and velocity on the exchange surface.

Keywords: Fluidisation, local heat transfer coefficient, bed material properties

### 2. Introduction

The bed structure near an immersed surface mainly consists of a region characterized by gas velocity and void fraction higher than the bulk of the bed, leading, in some cases, to the formation of indigenous bubbles and whose characteristics strongly depend on the shape of the submerged object. This structure characterizes the interactions between the fluidized bed and the immersed surface, playing a crucial role in several industrial processes.

Experimental evidences point out that heat transfer coefficient is strongly related to the bed structure. In particular, it depends on the overall fluidization regime, the size and the shape of the exchange surface as well as on its orientation respect to the main gas stream.

In particular, this work is a first attempt to test the reliability of heat transfer measurements in describing the local bed structure near an immersed surface. In particular, this work reports the evaluation of local heat transfer coefficients on the surface of a horizontal cylinder immersed in a bubbling fluidized bed. The effect of bed material properties and gas velocity are considered.

### 3. Experimental analysis

The experimental rig consists in a 1500 mm height, 120 mm ID fluidization column with a porous plate distributor. Dried air is used as fluidizing gas. The immersed surface consists in a thermal insulating horizontal cylinder (L=100mm, OD=30 mm) placed 300 mm above the distributor. The heat transfer probe is a brass parallelepiped centrally inserted in the cylinder. It contains a 60 W heater cartridge and presents an

effective rectangular exchange surface of 30mm length and 6 mm width. A first k-type thermocouple is placed on the center of the exchange surface while a second one is located on the thermal insulating surface. The time averaged heat transfer coefficient,  $h$ , is determined by measuring the probe power input and the average temperature differences between the two thermocouples. Heat transfer losses by conduction in the thermal insulating cylinder are negligible. The horizontal cylinder can rotate on its longitudinal axis to allow the estimation of heat transfer coefficient at different angular positions. Four types of bed materials are considered: ballotini (avg. Sauter diameter  $d_p = 210 \mu\text{m}$  and  $500 \mu\text{m}$ ), silica sand ( $d_p = 210 \mu\text{m}$ ) and carborundum ( $d_p = 300 \mu\text{m}$ ).

Experimental results show that the value of the heat transfer coefficient depends on exchange surface position. For all the investigated materials  $h$  is the highest on the lateral surface of the cylinder ( $0^\circ$ ) and the lowest on its upper face ( $+90^\circ$ ). Particle convection is known to be the leading heat transfer mechanism. It directly increases with local surface renewal frequency and solid concentration. According to previous studies, the former is the highest on the lower face of the surface (Kim et al., 2003) and the latter is maximum on the upper one (Buyevich et al., 1986). Hence, the angular position for the maximum heat transfer can be considered as an optimal compromise between these variables.

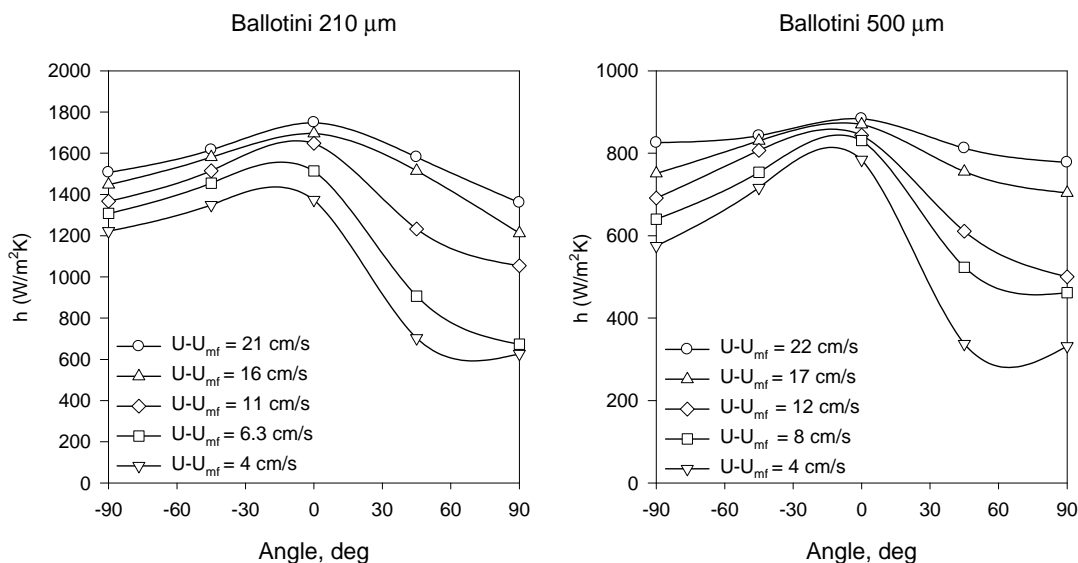


Figure 1: Heat transfer coefficient in function of excess gas velocity and angular position for 210 and 500  $\mu\text{m}$  ballotini

## References

- Buyevich Y.A., Korolyov V.N., Syromyatnikov N.I., in "Heat and Mass transfer in fixed and fluidized bed", Van Swaaj W.P.M., Afgan N.H. eds., (1986), Springer & Verlag
- Kim, S. W.; Ahn, J. Y.; Kim, S. D.; Hyun Lee, D., Heat transfer and bubble characteristics in a fluidized bed with immersed horizontal tube bundle; *Int. J. Heat Mass Transf.*, 2003, 46(3), 399-409

## **A Study of Force Response in Pellets of Herbal Spa Salts using Discrete Element Method (DEM) Computer Simulation.**

T. Kangsadan,<sup>a</sup> S. Promkotra<sup>b</sup>

<sup>a</sup> *Chemical and Process Engineering Program, The Sirindhorn International Thai-German Graduate School of Engineering, King Mongkut's Institute of Technology North Bangkok 10800, Thailand*

<sup>b</sup> *Geotechnology Department, Faculty of Technology, Khon Kaen University 40002, Thailand*

### **1. Summary**

Even though the spa popularity in Thailand has been increased, but the spa business is still small and has to import the spa salts from foreign countries. However, there are large sources of rock salts in the north-eastern region of Thailand that can be modified and produced as spa salts. This can be farther developed into the herbal spa salt which can be sold as a higher value product. The spa salts are normally sold in a viscous-creamy liquid or a pellet form, which is the main focus of this study. Since, the herbal spa salts comprising of herbs and spa salts were considered to be an inhomogeneous material, the force interaction would influence the force distribution and affect the mechanical properties, especially in the fracture of material during the compression (making pellets). The Discrete Element Method (DEM) computer simulation was used as a study tool to observe and investigate the dynamic and static behaviors of such materials. The force distribution under compression was studied to predict the location of the fracture in the pellet and how the fracture was propagated.

Keywords: Discrete Element Method, Force Response, Herbal Spa Salts

### **2. Extended Abstract**

The preliminary study and experiment on the herbal spa salt had been performed by Dr. Sarunya Promkotra at the Geotechnology Department, Faculty of Technology, Khon Kaen University. This research solely focuses on the chemistry and properties of spa salts, the production of herbal spa salts based on the mixture of the ingredients at the laboratory scale, and economic analysis.

Since, the force interaction between herbs and salts particles will affect the mechanical properties of the system, the appropriate condition of process during the production must be well designed. The interaction forces between particles under compression depend on the rearrangement mechanisms and compressive behaviors of particles. Therefore, the study of the two-dimensional (2D) particles of herbs and salts

will essentially provide the information on the force interaction prior and during the compression. In addition, the results can predict the fracture of these materials during the compression, especially for the pellet form.

## 2.1 Methodology

Since, these 2D particles can be treated as discontinuum materials, the dynamics behavior can be monitored and investigated with the used of the DEM computer simulation. In DEM simulations, the dynamics and mechanical interactions of each particle are explicitly modeled with the soft-particle methodology which allowing the interparticle penetration to be considered explicitly. A detailed description of the motion on each particle at discrete points in time is monitored by applying Newton's Law directly. The elastic restitution and friction influence the particles' collision, which have a finite duration, and the magnitude of the interaction depends on the penetration path. The equations of colliding motion of particles can then be solved in regular incremental steps. The difficulties in this computer modeling are the models of collisions and friction between particles--contact force model to varying degrees of realism and accuracy. The spring force and viscous damping, called the spring and dashpot force, can be implemented to mimic the collision behavior of these particles.

The dynamics of 2D of herbs and salts particles were influenced by the gravitational force. Once stable assemblies of particles (reaching the static equilibrium) were formed (Kangsadan, 2000), then the compressive deformation into the pellet experiment could be performed to study the force distribution, the particle orientations and rearrangement mechanisms.

## 2.2 Result and Discussion

The distribution of forces in static granular media relates to the particle spatial distributions, interactions, and polydispersity. The simulation results of particles without friction were presented, in an effort to analyze the connection between particle packing disorder and force distributions. In the limit of strong stiffness, the stress response function (to a small perturbing force in the pile) was shown to reflect a hierarchy of force dependencies (chains), and to depend on the boundary conditions (Wu et al., 2000). The inhomogeneities of the force distribution in real granular piles suggest that the behavior of such materials may not exhibit elastic properties. In particular, when an external force is applied to such a structure, a force is induced on particles elsewhere in the system, as transmitted along an irregular path where particles make contact.

## References

Wu, D. T. and Kangsadan, T., (2000). **Theory and Simulation of Stress Correlations and Response Functions in Granular Piles.** *MRS. SYMPOSIUM BB. The Granular State. April 24 - 28, 2000. San Francisco, California U.S.A.*

Kangsadan, T., (2000). **Statistical Mechanical Studies of Granular Materials using Discrete Element Simulation.** *Master Thesis. Colorado School of Mines*



## Session T2-8a: Membranes and Membrane Science – I

<b>Abstract Number</b>	<b>Paper Title &amp; Authors</b>	<b>Included</b>
177	A membrane based process for the upgrading of biogas to substituted natural gas (SNG) and recovery of carbondioxide for industrial use B Norddahl , J du Preez	No
1591	A CAPE tool to simulate the pervaporation process for recovering an aroma contributor of orange juice W A Araujo, M E T Alvarez, M R W Maciel	Yes
1882	Determining the dehydration performance of a hydrophobic DDR zeolite membrane J Kuhn, K Yajima, T Tomita, J Gross, F Kapteijn, P J Jansens	Yes
2001	Natural gas sweetening by the use of a facilitated blend membrane M B Hägg, L Deng, T J Kim	Yes
2380	Mass transport with varying diffusion- and solubility coefficient through a catalytic membrane layer E Nagy	Yes
3539	Mathematical modelling of multicomponent transport in silicalite-1- $\alpha$ -alumina membrane V Fíla, B Bernauer, M Kočířík, P Hrabánek, V Navara, A Zikánová	Yes

Session T2-8a

## **A CAPE tool to simulate the pervaporation process for recovering an aroma contributor of orange juice**

W.A. Araujo, M.E.T. Alvarez, M.R. Wolf-Maciel<sup>a</sup>

*Separation Process Development Laboratory (LDPS), School of Chemical Engineering, State University of Campinas (UNICAMP), CP 6066, ZIP CODE 13081-970, Campinas-SP, Brazil.*  
<sup>a</sup>wolf@feq.unicamp.br

### **1. Summary**

Flavor and odor components of food are often lost during processing, which leads to a final product with poorer quality when compared to fresh made ingredients. This scenario is not different in orange juice and other fruit processing industries. Comparative studies of quantitative data of volatiles to odor threshold data and multivariate relationship studies between chemical composition and sensory characteristics describe ethyl butyrate (EB) as one of the key contributors to fresh orange aroma. Pervaporation constitutes one membrane process for separating dilute species in liquid solutions that has been extensively studied for aroma recovery. This process is based on a selective transport through a membrane associated with permeate evaporation on the downstream side of the membrane. In this work, pervaporation process simulation using a poly (dimethylsiloxane) membrane was investigated for separation and EB recovery from a binary mixture (EB-water). A simulator named PERVAP was, for the first time, applied to study separation of aroma compounds from a low concentration solution. Simulated process data was compared to experimental data available in open literature. PERVAP is, essentially, predictive and it was originally developed and evaluated for ethanol/water separation.

Keywords: pervaporation, juice, aroma, membrane, simulator

### **2. Extended Abstract**

PERVAP simulator is supported by a mathematical predictive approach used for modelling pervaporation process. The group contribution method UNIFAC was applied for predicting activity coefficients in the feed,  $\gamma_{i,F}$ , and diffusion coefficients of components in membrane,  $D_i^m$ , were determined using the free-volume theory. Pure components and polymer properties were used to obtain the parameters required by free-volume theory. Binary interaction parameter between solvent and polymer,  $\chi$ , was

predicted by a group-contribution lattice-fluid equation of state (GCLF-EOS). The free volume parameters are presented in Table 1. The fluxes were calculated using equation 1:

$$J_i = \frac{D_i^m}{\ell \bar{\gamma}_i^m} \left( x_{i,F} \gamma_{i,F} - \frac{x_{i,F} \alpha p}{1 + (\alpha - 1)x_{i,F}} \right) \quad i=\text{ethyl butyrate}; F=\text{Feed}; m=\text{membrane} \quad (1)$$

where  $J$  = permeate flux ( $\text{mol}/\text{m}^2\cdot\text{h}$ ),  $D$  = diffusivity in the membrane ( $\text{cm}^2/\text{s}$ ),  $C$  = concentration ( $\text{mol}/\text{m}^3$ ),  $x$  = molar fraction,  $\ell$  = membrane thickness (m),  $\alpha$  = selectivity, and  $p$  = permeate relative pressure. Fluxes are illustrated in Figure 1. The simulated data was compared to experimental data of EB/water obtained using a PDMS membrane.

Components	$\hat{V}_1^*$	$K_{11}/\gamma$	$K_{21}-Tg_1$	$Do$	$\chi$	$\xi$	$E$
EB	0.919	$1.090 \times 10^{-3}$	-35.00	$11.60 \times 10^{-4}$	0.007	2.096	0
water	1.071	$2.180 \times 10^{-3}$	-152.29	$8.55 \times 10^{-4}$	0.003	0.236	0

Table 1- Free-volume parameters estimated and predicted used in the diffusion coefficient prediction.

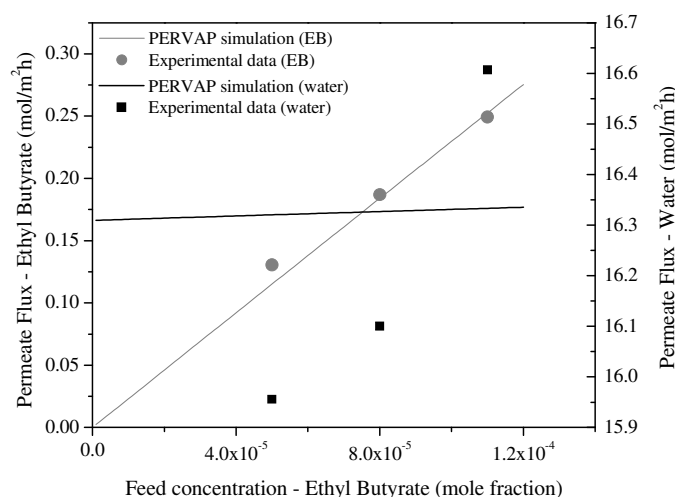


Figure 1 – Experimental fluxes compared to calculated flux using PERVAP.

### 3. References

- Alvarez, M.E.T., Moraes, E.B., Wolf-Maciel, M.R., (2006) *16th European Symposium on Computer Aided Process Engineering and 9th International Symposium on Process Systems Engineering*, Amsterdam, 21A, 619-624.
- Baudot, M., Marin, M., (1997) *Trans IChemE*, 75, 117-142.
- Burgard, D.R., In: Rouseff, R.L., Leahy, M.M., *Fruit Flavors*, American Chemical Society, USA (1995), 21-32.
- Pereira, C.C., Ribeiro-Jr, C.P., Nobrega, R., Borges, C.P., (2006) *Journal of Membrane Science*, 274, 1-23.
- Sampranpiboon, P., Jiratananon, R., Uttapap, D., Feng, X., Huang, R.Y.M., (2000) *Journal of Membrane Science*, 174, 55-65.

## Determining the dehydration performance of a hydrophobic DDR zeolite membrane

J. Kuhn<sup>a/c</sup>, K. Yajima<sup>b</sup>, T. Tomita<sup>b</sup>, J. Gross<sup>c</sup>, F. Kapteijn<sup>a</sup>, P.J. Jansens<sup>c</sup>

<sup>a</sup>Delft University of Technology, Ceramic Membrane Centre, The Pore, Julianalaan 136, 2628BL Delft, The Netherlands

<sup>b</sup>NGK Insulators, LTD. NCM Project, New Products Development Center, 2-56 Suda-cho, Mizuho, Postal Code 467-8530, Nagoya, Japan

<sup>c</sup>Delft University of Technology, Process & Energy Laboratory, Leeghwaterstraat 44, 2628CA, Delft, The Netherlands

### 1. Summary

Permeation of water, ethanol and methanol through an all-siliceous DDR zeolite membrane has been measured under pervaporation conditions. Although the membrane is hydrophobic it shows excellent performance in dewatering ethanol. Selectivities up to 10,000 and pure water fluxes up to  $4.6 \text{ kg}\cdot\text{m}^{-2}\cdot\text{hr}^{-1}$  have been measured. The permeation data are modeled using the Maxwell-Stefan equations.

Keywords: membrane, DDR, pervaporation, dehydration

### 2. Extended Abstract

The polarity of a zeolite is an important parameter determining the transport and separation properties in zeolite packed beds and membranes. Conventionally hydrophilic membranes are used for dehydration of solvents. For zeolite membranes this usually implies a low silica to aluminum ratio. The high aluminum content, however, results in decreased chemical stability [1] and reduced membrane quality causing inter-crystalline transport [2]. Since the DDR

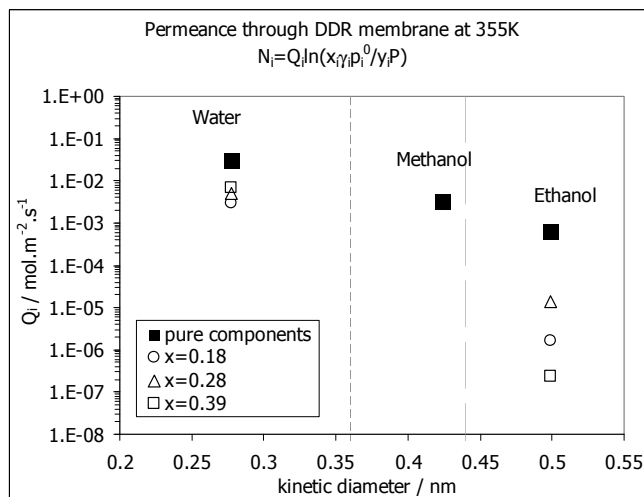


Figure 1: Flux/dimensionless driving force ( $Q_i$ ) of pure water, ethanol and methanol and for water-ethanol mixtures at 355K and water molar fractions of 0.18 to 0.39. The dashed lines indicate the DDR pore size.

membrane does not contain aluminum, there is no measurable contribution of inter-crystalline transport. Moreover, its potential application in acidic environments is promising.

All-silica DDR is a hydrophobic zeolite, with a pore size of 3.6 x 4.4 Å, able to separate water from many solvents based on size exclusion [3]. An all-silica DDR membrane (NGK, Japan) has been used to study the permeation of pure water, methanol and ethanol, as well as water/ethanol mixtures in pervaporation mode. The membrane showed to be insensitive to increased feed side pressure (up to 12 bar), indicating the absence cracks leading to viscous flow. The presence of water decreases the ethanol permeance and vice versa, although the presence of ethanol has less influence on the water permeance, as can be seen in figure 1. Adsorption isotherms of water, methanol and ethanol on all-silica DDR will be measured and the permeation results are modeled using Maxwell-Stefan based equations [4]:

$$-\rho \frac{\theta_i}{RT} \frac{\partial \mu_i}{\partial z} = \sum_{\substack{j=1 \\ j \neq i}}^n \frac{q_j N_i - q_i N_j}{q_{i,sat} q_{j,sat} \mathcal{D}_{ij}} + \frac{N_i}{q_{i,sat} \mathcal{D}_{i,M}}$$

$$i = 1, 2 \dots n$$

where the driving force is expressed as

$$\frac{\Delta \mu_i}{RT} = \ln \left( \frac{x_i \gamma_i P_i^0}{P^p y_i} \right)$$

The support layers were found to contribute significantly to the resistance to mass transfer, which was described with the Dusty Gas Model, assuming a combination of viscous flow and Knudsen diffusion [5].

In spite of its hydro-phobic character, the all-silica DDR membrane has shown to exhibit good dewatering properties for water/ethanol mixtures. High fluxes of pure water (up to 4.6 kg.m<sup>-2</sup>.hr<sup>-1</sup>) and excellent selectivities (up to 10.000) and fluxes (up to 1 kg.m<sup>-2</sup>.hr<sup>-1</sup>) for water/ethanol mixtures have been measured.

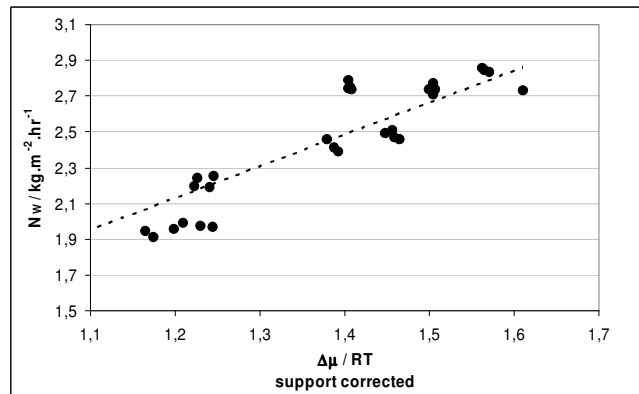


Figure 2: Pure water flux through all-silica DDR layer, plotted against the dimensionless driving force, corrected for the support resistance.

## References

- 1 Y. Cui, H. Kita, and K. I. Okamoto, *Journal of Membrane Science*, vol.236, 17 (2004)
- 2 M. Noack, P. Kolsch, V. Seefeld, P. Toussaint, G. Georgi, and J. Caro, *Microporous and Mesoporous Materials*, vol.79, 329 (2005)
- 3 Yajima, K., Nakayama, K., Niino, M., Tomita, T., and Yoshida, S., *Proceedings of the 9th ICIM9*, 401, (2006)
- 4 R. Krishna, J. A. Wesselingh, *Chemical Engineering Science*, vol.52, 861 (1997)
- 5 F. T. de Bruijn, L. Sun, Z. Olujic, P. J. Jansens, and F. Kapteijn, *Journal of Membrane Science*, vol.223, 141 (2003)

## Natural gas sweetening by the use of a facilitated blend membrane

May-Britt Hägg, Liyuan Deng, Taek-Joong Kim

*Department of Chemical Engineering, Norwegian University of Science and Technology (NTNU),  
NO-7491 Trondheim, Norway*

### 1. Summary

The sweetening of natural gas (NG) is today basically done by the use of amine solutions, requiring large columns for both absorption of the CO<sub>2</sub> and regeneration (desorption) of the amine. A very attractive solution is the use of polymeric membranes which will selectively permeate the CO<sub>2</sub> while the NG is being withheld on the feed side. Such membrane solutions have existed for more than 20 years, and there are several installations around in the world especially for onshore treatment. These membranes are, however, not optimised with respect to flux and selectivity, and may require a fairly large permeation area (large foot print) as well as having a fairly high methane loss. The objective of the current study is to develop a stable CO<sub>2</sub>-selective membrane which is optimised with respect to flux and selectivity, hence reducing both permeation area and costs.

Keywords: Natural gas, CO<sub>2</sub>, membranes, separation

### 2. Extended Abstract

Materials like cellulose acetate (CA) and polyimides (PI) are typical materials used for natural gas sweetening today. They are produced either as spiral wound membranes or hollow fibres respectively. The PI usually exhibit higher selectivity between CO<sub>2</sub>-CH<sub>4</sub> than that of CA, however, the CA may have higher flux. The most favourable configuration is the hollow fibre modules due to high packing densities (m<sup>2</sup> permeation area per m<sup>3</sup> module volume), see figure 1. Up until now, natural gas sweetening by membrane separation has however not been the first choice; mainly because the performance of these commercial membranes do not exhibit optimum performance with respect to flux and selectivity. Also the CH<sub>4</sub> loss may be too high. A membrane process will, however, require pre-treatment of the gas, and this may be rather costly. A commercial CA membrane today may have a flux for CO<sub>2</sub> around 0.15 m<sup>3</sup>(STP)/(m<sup>2</sup> h bar) and a selectivity of CO<sub>2</sub>/CH<sub>4</sub> ~12. The goal should be at least both a doubled flux and selectivity for a membrane in order to be commercially

attractive for separation (Baker 2002). This is hence the primary goal for selectivity and flux of the membrane development at NTNU for NG application in order to design a simpler system with reduced permeation area (resulting in smaller footprint, light weight) and also reduce the loss of valuable gas.

In the current work to be reported here, experimental results which meet these goals will be presented. The membrane is a blend of polymers developed within the membrane research group, Memfo, at NTNU. The membrane contains a facilitated transport polymer (PVAm) which selectively transport the  $\text{CO}_2$  (Kim et al. 2004), while the other polymer component in the blend (PVA) adds mechanical strength to the membrane (Deng et al. 2006). The transport of  $\text{CO}_2$  through the membrane is facilitated by a fixed carrier (equation 1 and figure 2), hence flux and selectivity in favour of  $\text{CO}_2$  compared to  $\text{CH}_4$  is increased. The membrane is currently being tested at varying process conditions (temperature, pressures) and for relevant gas mixtures.

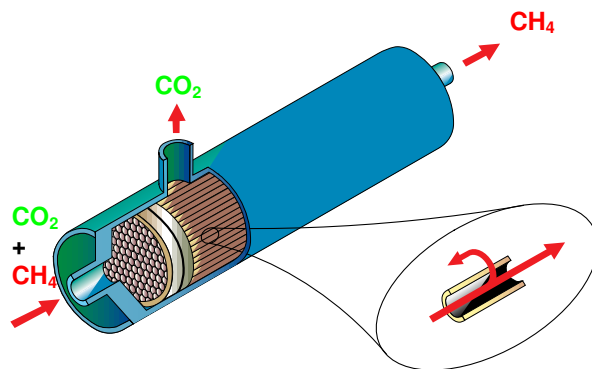


Figure 1: Typical hollow fibre membrane module (Hägg & Quinn 2006)

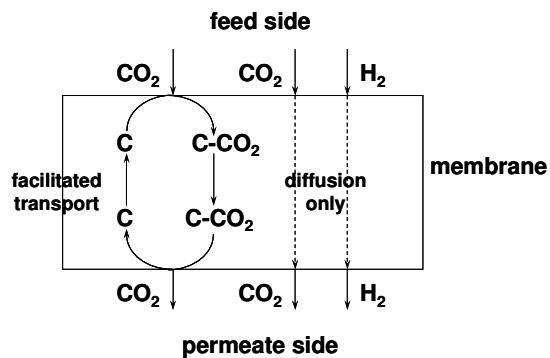


Figure 2: Gas permeation through a membrane with facilitated transport in addition to solution-diffusion (Hägg & Quinn 2006)

## References

- Baker R., (2002) *Ind. Eng. Chem. Res.*, 41, 1393-1411
- Deng L. et al. (2006) *Desalination*, (Proceedings Euromembrane 2006)
- Hägg MB and Quinn R (2006) *MRS Bulletin*, 31, 750-755
- Kim T-J et al.,(2004) *J.Polym.Sci. Part B: Polym.Phys.*, 42, 4326-4336



## **Mass transport with varying diffusion- and solubility coefficient through a catalytic membrane layer**

E. Nagy,<sup>a</sup>

<sup>a</sup>*Research Institute of Chemical and Process Engineering, University of Pannonia , H-8200 Veszprém, Hungary*

### **1. Summary**

The catalytic membrane reactor is widely recommended to apply for heterogeneous reactions. This reactor with segregated feed of reactant(s), and/or with separation of products improves safety, selectivity and efficiency of the catalytic processes. Thus, the hydrogenation, dehydrogenation, oxidation reactions, etc., with different membranes, are the most common examples of the conversion enhancement (Marcano and Tsotsis, 2002; Saracco et al., 1999). To accomplish these, one could use a membrane that has been made catalytic through, e.g., catalytically active particles, as metallic complexes, activated carbon or metallic clusters, dispersed throughout the membrane phase. Recently Nagy (2007) developed mathematical models which define the concentration distribution and the mass transfer rate in membrane layer with dispersed catalyst particles. Depending on the particle size both the pseudo-homogeneous as well as heterogeneous models were recommended. These models assume constant diffusion in both membrane layer and catalyst particles and constant solubility coefficient of the reactant in the catalyst particles. In the reality, both parameters might depend on the concentration and/or on the inhomogeneity of the membrane layer. General mathematical models were developed to describe the mass transport in such nonlinear system taking into account the external mass transfer resistances as well.

Keywords: catalytic membrane layer, dispersed catalyst particles, variable diffusion coefficient, variable solubility coefficient, nonlinear mass transfer;

### **2. Extended Abstract**

The mass transport through catalytic membrane layer, with dispersed catalyst particles, can be given by means of homogeneous and/or heterogeneous models. When the catalyst particles are enough small,  $d_p \ll \delta$  ( $d_p < 1-3 \mu\text{m}$ ,  $d_p$ - particle size,  $\delta$ - thickness of the membrane layer) then the pseudo-homogeneous model is recommended. In this paper this model is applied to predict the mass transfer rate in the case of variable diffusion

coefficient and solubility as well as accompanied by first-order, irreversible chemical reaction.

### 2.1. Variable solubility coefficient

Both the solubility curves (e.g. Flory-Huggins theory) and the adsorption isotherms (e.g. Langmuir, Freundlich) can be strongly concentration dependent. These curves can be approached by two- or three linear isotherms (Nagy, 1999). Thus, the concentration boundary layer is divided into two or three segments with various solubilities. Considering e.g. a Langmuir isotherm [ $a_d = a_{sat}Ka/(1+Ka)$ , where  $a$ - concentration in the membrane;  $a_d$ - concentration in the catalyst particle;  $K$ -Langmuir constant] and approaching it by two or three linear isotherms [ $a_d = H_i a + C_i$  ( $C_i$ - constant,  $i=2$  or  $3$ ;  $i^{\text{th}}$  sub-layer)], the mass balance equation system to be solved is as follows (for details see Nagy, 2007, 1999):

$$D_i \frac{d^2 a}{dx^2} - \frac{6\beta_p \varepsilon}{(1-\varepsilon)d_p} (H_i a + C_i) = 0$$

Depending on the curvature of the isotherm or of the solubility curve, the mass transfer rate can be strongly differed from that obtained by linear isotherm.

### 2.2. Variable diffusion coefficient

The diffusion coefficient might vary as a function of the concentration [ $D=D(a)$ ] and/or space coordinate [ $D=D(x)$ ]. The solutions of these systems are different in the two cases. The membrane layer is divided into  $N$  sub-layers ( $N$  value must be high enough due to the assumption of constant diffusivity in these sub-layers) with their constant diffusivity and then the differential equation system obtained can be solved analytically. For the case of the concentration dependent diffusivity the concentration distribution in the membrane layer must be known in order to determine the correct values of  $D(a)$ . When the diffusion coefficient depends on the space coordinate, the mass transfer rate at the membrane interface can be expressed without knowing the concentration distribution in the catalytic membrane layer. The concentration distribution and the mass transfer rates will be expressed by closed, explicit mathematical equations for pseudo first-order, irreversible chemical reaction.

The mass transfer rate should be replaced into the differential mass balance equation given for the tube (or shell) side of the membrane layer and the effect of the concentration dependency on the outlet concentration will be shown. As case study the oxidation of alkenes by means of peroxide (t-BuOOH) will be studied.

## References

- Markano, J.G.S., Tsotsis, T.T., *Catalytic Membranes and Membrane Reactors*, Wiley-VCH, (2002).  
 Saracco, G. Neomagus, H.W.J.P., Versteeg, G.F., van Swaaij, W.P.M., (1999), *Chemical Engineering Science*, 54 1997-2017  
 Nagy E., (2007), *Industrial & Engineering Chemistry Research*, 46, 2295-2306.  
 Nagy E., (1999), *Chemical Engineering Journal*, 72, 43-51

## Mathematical modelling of multicomponent transport in silicalite-1- $\alpha$ -alumina membrane

V. Fíla<sup>a</sup>, B. Bernauer<sup>a</sup>, M. Kočířík<sup>b</sup>, P. Hrabánek<sup>b</sup>, V. Navara<sup>a</sup>, A. Zikánová<sup>b</sup>

<sup>a</sup>*Department of Inorganic Technology, Institute of Chemical Technology, Technická 5, 166 28 Prague 6, Czech Republic*

<sup>b</sup>*J. Heyrovský Institute of Physical Chemistry, Academy of Sciences of the Czech Republic, Dolejšková 3, 18223 Prague 8, Czech Republic*

### 1. Summary

The present study is mainly focused on mass transport modelling through composite silicalite-1 membranes and support contribution to the overall mass transport and separation properties of prepared membranes. Overall transport properties of a membrane are determined, i.a. by number and nature of defects as well as textural properties of a support. Pore size distribution of support and interaction of pore surface with permeating species determine transport, which effects species composition on zeolite layer/support interface and consequently separation efficiency of a composite membrane.

The dynamic mass transfer of nitrogen and methane through a silicalite-1/ $\alpha$ -alumina membrane is examined as a model system. The dynamic permeations of binary mixtures and single components in a semi-open Wicke-Kallenbach cell [1] were used to measure total pressure difference and gas mixture composition in a closed compartment. These data were treated by a mathematical model based on dusty-gas and Maxwell-Stefan theory where the effects of support layer were taken into account during calculations. Resulting system of PDEs, ODEs and AEs is solved by a home-made general simulation FORTRAN program that is based on a method of lines with orthogonal collocation discretization in spatial coordinate. The textural and transport parameters were estimated by a multi-response regression method.

Keywords: composite membrane, silicalite-1 membrane, separation, simulation, dynamics

### 2. Extended Abstract

The new software for modelling of multicomponent dynamic mass transfer in composite membranes was developed. The modular structure approach allowing building up a multilayer membrane model accounting for different mass transfer mechanisms was used. To describe the contributions of different mass transfer mechanisms to the overall mass transfer in the individual layers, the typical approach dividing a composite membrane into different regions with corresponding transport mechanism is applied and has been already described elsewhere [2]. To be able to simulate heterogeneous structures, e.g. microporous layer with defects, the models,

like dusty gas model, activated Knudsen diffusion and surface diffusion are employed as transport paths. The surface diffusion of adsorbed molecules is calculated according the generalized Maxwell-Stefan model [3] in combination with the Ideal Adsorbed Solution theory. The different level of interactions between the molecules transported by different transport paths are considered, i) no interaction along the layer between molecules transported by different transport paths, ii) full interaction along the layer assuming the adsorption equilibrium between the adsorbed and gas phase, iii) combination of both above mentioned cases. Each layer is divided into sub-layers of given thickness and inside of these sub-layers the transport mechanisms described in i) is applied. At the interfaces of sub-layers the adsorption equilibrium or continuity of gas composition is assumed.

The samples of comparison of experimental and calculated results are shown on following figure.

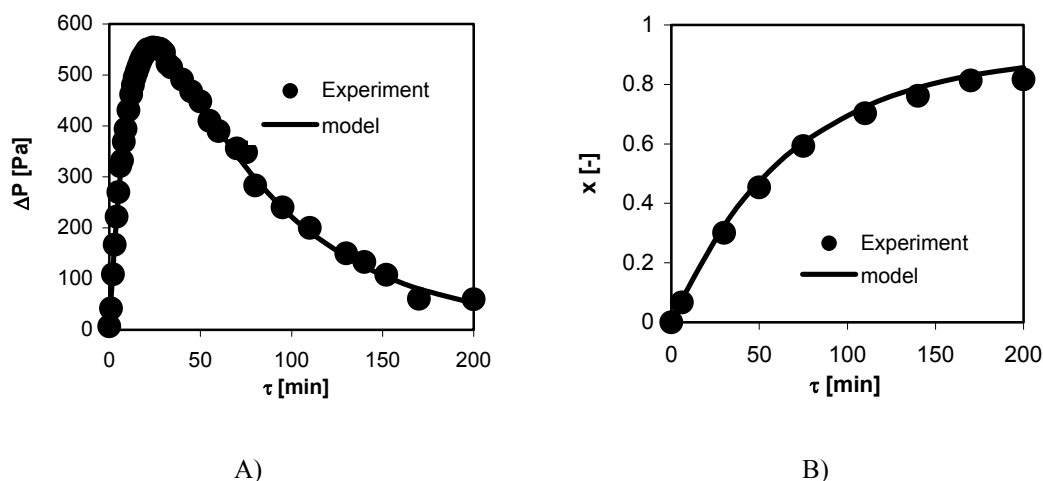


Figure 1: Pressure uptake (A) and CH<sub>4</sub> relative pressure (B) in close compartment of semi-open W-K cell as the function of time, after step change of concentrations in open compartment from pure N<sub>2</sub> to mixture containing 20 mol. % CH<sub>4</sub> and 80 mol. % N<sub>2</sub>, initial total pressure 99.5 kPa.

#### Acknowledgment

The financial support of this research by the Grant Agency of the ASCR under project number 1QS401250509, by the Ministry of Education, Youth and Sports under project number MSM 604 613 73 01 and by the EC under project NanoMemPro is gratefully acknowledged.

#### References

- [1] Zikánová A., Bernauer B., Fíla V., Hrabánek P., Hradil J., Krystl V. and Kočířík M., *Studies in Science and Catalysis 142*, p. 1513-1520, R. Aiello, G. Giordano and F. Testa (Eds.), Elsevier Science B. V., Amsterdam (2002).
- [2] Hanebuth, M., Dittmeyer, R., Mabande G.T.P., Schwieger W., (2005) *Catalysis Today*, 104, 352-359
- [3] Kapteijn, F., Moulijn, J.A., Krishna R., (2000) *Chemical Engineering Science*, 55, 2923-2930

## Session T2-8b: Membranes and Membrane Science – II

<b>Abstract Number</b>	<b>Paper Title &amp; Authors</b>	<b>Included</b>
763	Hydrodynamics and concentration polarization in NF/RO spiral wound modules with ladder-type spacers: experimental and numerical work M N de Pinho, V Semiao, V Geraldes	No
1717	In-Situ Preparation of Immobilized Liquid Membranes Using Inorganic Supports and Non-Volatile Liquids F F Krull, P Wasserscheid, T Melin	Yes
1861	Metal affinity chromatography with a chitosan/ceramic membrane C J Muvdinova, D P Jeanjean, M Barboiu, M P Belleville, M Rivallin, G Rios	Yes
2341	Measurement of adsorption equilibrium and kinetics of water and alcohols on pervaporation membrane top layer pellets by gravimetric vapor adsorption B Bettens, J Degrève, B V Bruggen, H M V Veen, C Vandecasteele	Yes
2345	Catalytic zeolite membrane reactors for CO-free hydrogen production P Bernardo, C Algieri, G Barbieri, E Drioli	Yes
2353	Experimental characterization and modelling of affinity membrane J Labanda, J Llorens	Yes

Session T2-8b

## **In-Situ Preparation of Immobilized Liquid Membranes Using Inorganic Supports and Non-Volatile Liquids**

Florian F. Krull<sup>a</sup>, Peter Wasserscheid<sup>b</sup>, Thomas Melin<sup>a</sup>

<sup>a</sup> *Institut für Verfahrenstechnik of RWTH Aachen University, Turmstr. 46, 52056 Aachen, Germany*

<sup>b</sup> *Chair of Chemical Reaction Engineering of University Erlangen-Nürnberg, Egerlandstr. 3, 91058 Erlangen, Germany*

### **1. Summary**

Commonly, preparation of Immobilized Liquid Membranes (ILM) is done manually and in a discontinuous manner employing organic supports and low-volatile liquids. On the one hand the loss of membrane function due to evaporation of the membrane phase in gas separation applications prohibits the long term and industrial use of ILM. On the other hand, the complicated and tedious manual batch preparation of ILM represents another application barrier that has to be overcome.

By employing non-volatile ionic liquids as membrane phase in a chemically and thermally inert inorganic support, a membrane configuration showing long term stability is obtained. In contrast to organic supports, inorganic supports generally display a wall thickness of more than 200  $\mu\text{m}$ . Thus, the adjustment of the effective membrane thickness, i.e. the liquid layer thickness inside the porous support, deserves closer attention.

In this work an innovative in-situ preparation of ILM using inorganic supports and non-volatile liquids is presented. To adjust the liquid layer thickness, the wetting kinetics of (a)symmetric porous supports is modeled and evaluated experimentally.

Keywords: Immobilized Liquid Membrane, In-Situ Preparation, Inorganic Support, Non-Volatile, Liquid Layer Optimization

### **2. Extended Abstract**

Immobilized Liquid Membranes (SLM) consist of a mesoporous support and a liquid, which is immobilized in the support due to capillary and interfacial forces. Although liquid membranes have been of interest in research for more than thirty years, only few industrial applications have been put into practice. This can clearly be related to the lacking mechanical and long term stability of the membrane configurations. In literature mainly combinations of an organic support and a volatile organic liquid are found. These systems suffer from evaporation of the liquid phase and the chemically

or thermally provoked change of the support's properties like pore size and wettability. Novel materials like chemically and thermally inert inorganic supports and non-volatile ionic liquids or liquid molten salts can overcome these stability problems.

Since the permeability of membranes is reversely proportional to the thickness of a membrane, a minimum thickness would be required to reach maximum permeability. This changes if the SLM concept is combined with a facilitated transport concept using carrier species. These species reversibly react with a permeating component of a mixture and enhance the selectivity of the membrane. The time for reversible reaction with a desired component competes with the time for diffusion of undesired components. Hence an optimum membrane thickness with respect to the carrier is required.

In contrast to organic supports of defined small thickness inorganic supports are mostly available with thickness greater than 200  $\mu\text{m}$ , being unfavourable for non-carrier mediated transport membranes. On the other hand a method for adjustment of the membrane thickness allows for preparation of SLM with optimized thickness for carrier mediated transport.

In our current work we have developed a method for in-situ-preparation of SLM inside a module already installed in a gas separation process allowing for adjustment of the membrane thickness within an asymmetric capillary inorganic support. This in-situ preparation leads one step further to industrial application, since the membrane preparation takes place after mounting the support to the module. Even water and oxygen sensitive liquids can be employed as membrane phase in an easy way in contrast to complex manual preparation in glove-boxes. The method is based on a model accounting for the wetting kinetics of the support. Since this model is formulated in a dimensionless way, results can be transferred to different membrane-liquid configurations.



## **METAL AFFINITY CHROMATOGRAPHY WITH A CHITOSAN/CERAMIC MEMBRANE**

C. J. Muvdinova, D. Paolucci-Jeanjean, M. Barboiu, M.-P. Belleville, M. Rivallin, G.Rios

European Membrane Institute, IEM/UMII – Place Eugène Bataillon – Casse Courrier 047, 37095 Montpellier Cedex 5, France.  
Corresponding author: [carlos.muvdi@iemm.univ-montp2.fr](mailto:carlos.muvdi@iemm.univ-montp2.fr)

### **1. Summary**

In this study a hybrid chitosan/ceramic membrane is proposed with the aim of performing protein purification. This investigation proposes a two-step method for the fabrication of this hybrid membrane: the first one is the coating of chitosan (CTS) onto the surface of the ceramic support by filtration. The second one involves the chemical modification of the chitosan layer. The chitosan is firstly cross-linked with epichlorohydrin then it reacts with iminodiacetic acid (IDA), on which the metal-ion is fixed by metal-chelation.

Keywords: chitosan, affinity, protein, metal, chromatography

### **2. Extended Abstract**

Affinity chromatography, mostly based on column configurations, is nowadays widely employed in protein purification. Unfortunately, due to high pressure drop, these systems are not appropriate for industrial applications where big volumes of non-clarified biological solutions have to be treated. In recent years, great interest has been paid to membranes as chromatographic media. This relatively new method combines the high-resolution separation of chromatography with the low pressure drop induced by the short-wide-bed of macroporous membrane systems, which generally involve organic supports [1, 2].

In this study, a hybrid chitosan/ceramic membrane is proposed for the purification of proteins by metal-affinity chromatography (histidine-tagged proteins mainly). Thanks to the attractive properties of chitosan, such as biocompatibility and non-toxicity, it was chosen to activate the ceramic support before the immobilization of the affinity ligand. Concerning the ceramic support, it will be in charge of conferring membranes the mechanical and chemical strength required for industrial applications [3, 4].

In the first stage of the study, a four step protocol was developed for membrane preparation: Chitosan is firstly coated onto a tubular alumina support (length 13cm;

inner diameter 0.7cm; pore diameter 1.8 $\mu$ m) by cross-flow filtration of a chitosan solution. Then, the chitosan layer is cross-linked with epichlorohydrin. Iminodiacetic acid (IDA) is grafted on cross-linked chitosan. Finally the copper-ion is fixed by dead-end filtration with a 100ppm Cu<sub>2</sub>SO<sub>4</sub> solution at a flow rate of 1ml/min. Tests show these membranes have a copper adsorption capacity of 1.5 g of Cu<sup>2+</sup>/m<sup>2</sup> of membrane.

Protein retention is tested with Bovine Serum Albumin (BSA) as a model protein. Experiments are carried out in dead-end filtration, with a 40ppm BSA solution at a flow rate of 0.25ml/min. Analyses show a BSA retention capacity of 0.33 g BSA/m<sup>2</sup> of membrane; total capacity achieved in 230min. Protein retention is then followed by rinsing and elution steps.

This work is interesting in two aspects: in one hand, it proposes a new method to elaborate membrane media for protein purification and, in the other hand, it contributes in the study of this promising new membrane application process, nowadays not well known.

## References

- [1] Charcosset, C., (1998) *Journal of Chemical Technology and Biotechnology*, 71, 95-110.
- [2] Gaberc-Porekar, V., Menart, V., (2001) *Biochemical and biophysical methods*, 49, 335-360.
- [3] Klein, E., (2000) *Journal of Membrane Science*, 179, 1-27.
- [4] Wu, C., Suen, S.-Y., (2003) *Journal of Chromatography A*, 996, 53-70.

## **Measurement of adsorption equilibrium and kinetics of water and alcohols on pervaporation membrane top layer pellets by gravimetric vapor adsorption**

B. Bettens<sup>a</sup>, J. Degève<sup>a</sup>, B. Van der Bruggen<sup>a</sup>, H. M. Van Veen<sup>b</sup>, C. Vandecasteele<sup>a</sup>

<sup>a</sup> Department of Chemical Engineering, K.U.Leuven, W. de Croylaan 46, B-3001 Leuven, Belgium  
Tel.: +32 16 32 23 44, Fax: +32 16 32 29 91, [ben.bettens@cit.kuleuven.be](mailto:ben.bettens@cit.kuleuven.be)

<sup>b</sup> Department of Energy Efficiency in Industry, Energy Research Centre of the Netherlands, ECN, Westerduinweg 3, 1755 ZG Petten, The Netherlands

### **1. Summary**

In this study, vapor sorption experiments were carried out with water, methanol and ethanol (single components and mixtures) on a Cahn D-100 microbalance to measure the weight change of calcinated silica membrane top layer pellets exposed to different activities of the components. Adsorption isotherms as well as adsorption kinetics are used to derive diffusion and sorption coefficients for both single components and components in a mixture. Focus is on selective sorption and the concentration dependence of the diffusion coefficient. Comparison to previous pervaporation measurements indicates that the vapor adsorption results can be used to predict the pervaporative transport through microporous ceramic membranes.

Keywords: pervaporation, vapor adsorption, silica membrane pellets,

### **2. Extended Abstract**

The pervaporative transport through microporous ceramic membranes is governed by adsorption and diffusion processes. The selectivity of both processes towards components in a mixture determines the partial fluxes through the membrane and the selectivity of the total process. Hence, knowledge of both processes allows predicting the membrane's performance.

From previous pervaporation experiments on aqueous alcohol (methanol, ethanol, isopropanol, butanol) mixtures, it was concluded that strong interaction effects (flux coupling) between the components in the mixture have a large impact on the membrane's performance [1].

In this study, vapor sorption experiments were carried out with water, methanol and ethanol (single components and mixtures) on a Cahn D-100 microbalance to measure the weight change of calcinated silica membrane top layer pellets exposed to different activities of the components. The composition of the adsorbed vapor is obtained by means of a Turbomass Mass Spectrometer (gas chromatography/mass spectrometry, GC/MS) and a Turbomatrix Headspace Sampler (PerkinElmer). When placing a sample in the Turbomatrix Headspace Sampler and connecting it to the GC/MS, it becomes possible (via an accurate temperature and pressure control) to desorb vapors from the sample and to determine its composition. Adsorption isotherms are correlated to Langmuir adsorption models. Increasing the temperature decreases the sorption capacity of the pellets. Adsorption kinetics are used to derive diffusion and sorption coefficients for both single components and components in a mixture. Focus is on selective sorption and the concentration dependence of the diffusion coefficient. Comparison to the previous pervaporation measurements indicates that the vapor adsorption results can be used to predict the interaction effects in the pervaporative transport through microporous ceramic membranes.

## **References**

1. B. Bettens, J. Degrève, B. Van der Bruggen, C. Vandecasteele, Transport of binary mixtures in pervaporation through a microporous silica membrane: Shortcomings of Fickian models, *Separation Science and Technology*, 42:1-23, 2007

## Catalytic zeolite membrane reactors for CO-free hydrogen production

P. Bernardo,<sup>a</sup> C. Algieri,<sup>a</sup> G. Barbieri,<sup>a</sup> E. Drioli<sup>a, b</sup>

<sup>a</sup> National Research Council - Institute for Membrane Technology (ITM - CNR)  
Via Pietro BUCCI, c/o The University of Calabria, cubo 17C, I-87030 Rende CS, Italy

<sup>b</sup> The University of Calabria - Department of Chemical Engineering and Materials  
Via Pietro BUCCI, cubo 44A, I-87030 Rende CS, Italy

### 1. Summary

In the hydrogen production from hydrocarbons, a final purification is required to reduce the carbon monoxide amount to the desired level (e.g., less than a few tens ppm for PEM fuel cells). Among several approaches, CO selective oxidation (Selox) is the most simple and cost-effective purification method, without excessive hydrogen consumption [1]. A highly selective catalyst is necessary because of the high ratio of H<sub>2</sub> to CO in the reformat stream. Typically, Pt-supported catalysts as fixed bed or monoliths [1–3] are used; catalytic membrane reactors (MRs) has been recently investigated in a few papers [4,5].

The focus of the present work is on the use of catalytic zeolite (Pt-Y) membranes for CO selective oxidation in continuous flow MRs.

Keywords: CO Selox, membrane reactors, zeolite membranes, Pt-Y.

### 2. Extended Abstract

The use of a catalytic membrane, with the zeolite layer containing catalytic Pt clusters, has numerous advantages over conventional fixed bed reactors: the catalytic surface directly available, reduced by-pass and pressure drop.

In this work, tubular zeolite Y membranes were Pt-loaded by ion-exchange, and their catalytic performance for the CO Selox was tested in a continuous MR.

The reactor was operated in a *flow-through* mode, with the reactant mixture forced to pass through the catalytic membrane. The feed mixtures (CO, O<sub>2</sub>, H<sub>2</sub>, N<sub>2</sub> and CO<sub>2</sub>) simulated a dry reformat gas stream (H<sub>2</sub> c. 50-60 % molar).

Experimental results were collected at 200°C, varying the reaction pressure up to 500 kPa. In particular, the permeate stream composition was analyzed on-line by a microgaschromatograph (Micro GC 3000A, Agilent) equipped with TCD detectors

and Molsieve 5A PLOT and PLOT Q columns and with a CO detection limit of 5 ppm.

A negligible effect of the *reverse water gas shift* reaction was observed for these catalytic systems by cutting off the CO inlet.

The catalytic MRs succeeded in bringing the outlet CO concentration in the range 50–10 ppm in one stage, starting from 1% (10,000 ppm) CO and using a low O<sub>2</sub> amount (O<sub>2</sub>/CO feed ratio =1). Moreover, the good selectivity measured (ca. 50% at O<sub>2</sub>/CO = 1) is important for the reduced hydrogen consumption (< 1%).

The catalytic membranes characterized by lower permeance resulted in a lower CO concentration at the reactor exit, reaching the steady state in a few minutes. Moreover, their behaviour was stable in reaction tests of several hours.

The reaction pressure improved the MR performance. However, for the less permeable catalytic membranes a reduced pressure effect was observed: good MR performance were also reached at low reaction pressure values.

The obtained results indicate the potential of practical application of the catalytic Pt-Y MR for the CO Selox stage into a fuel processor producing CO-free hydrogen to be used also for PEM fuel cells.

### Acknowledgements

The Ministry of University and Research of Italy, Progetto “FIRB-CAMERE RBNE03JCR5”, is gratefully acknowledged for co-funding this research.

### References

- [1] Oh, S. H. and Sinkevitch, R. M., (1993) *Journal of Catalysis*, 142, 254-262.
- [2] Kahlich, M. J., Gasteiger, H. A., Behm, R. J., (1997) *Journal of Catalysis*, 171, 93-105.
- [3] Ahluwalia, R. K., Zhang, Q., Chmielewski, D. J. Lauzze, K. C. and Inbody, M. A., (2005) *Catalysis Today*, 99 (3-4), 271-273.
- [4] Hasegawa, Y., Ueda, A., Kusakabe, K., Morooka, S., (2002) *Applied Catalysis A*, 225, 109-115.
- [5] Bernardo, P., Algieri, C., Barbieri, G., Drioli, E., (2006) *Catalysis Today*, 118, 90-97.

## EXPERIMENTAL CHARACTERIZATION AND MODELLING OF AFFINITY MEMBRANE

J. Labanda, J. Llorens

*Department of Chemical Engineering, University of Barcelona, Martí i Franquès 1, 08028 -Barcelona, Spain*

### 1. Summary

The present study proposes a model to explain the adsorption process through ion-exchange membrane adsorbers. The model is defined by the continuity equation, expressed as a differential mass balance of the solute over a section of the membrane, and the Langmuir isotherm. The proposed model uses dimensionless variables that were defined by characteristic times of the global process. To examine the validity of the model, the adsorption of an anionic dye (Orange G) through the ion-exchange membrane adsorbers was investigated as a function of dye and KCl concentration, obtaining strong correlation between fitted and experimental breakthrough curves.

Keywords: membrane chromatography, ion-exchange membrane adsorbers, dynamic adsorption, breakthrough curve, anionic dye

### 2. Extended Abstract

Membrane chromatography has been studied as an alternative to conventional resin-based column chromatography for the isolation and purification of macromolecules. Membrane chromatography operates in convective mode, which can significantly reduce diffusion and pressure drop limitations commonly encountered in column chromatography (Ghosh, 2002).

A mathematical model has been developed to predict the performance breakthrough curves of affinity membranes. This model can be used to describe the affinity-membrane processes in which the adsorption mechanism between solute and adsorbent is Langmuir adsorption. The total solute mass transfer from the liquid-phase to the solid-phase is controlled by four time dependent processes:

$$Pe = \frac{t_{disp}}{t_{process}} = \frac{v \cdot L}{D} ; K_{ads} = \frac{t_{process}}{t_{ads}} = \frac{k_a \cdot c_o \cdot L}{v} ; r = \frac{t_{des}}{t_{ads}} = \frac{k_a}{k_d} \cdot c_o$$

where  $Pe$  is the axial Peclet number,  $K_{ads}$  is the dimensionless adsorption constant and  $r$  is ratio between adsorption and desorption constants.

Then, the continuity equation, expressed as a differential mass balance of the solute over a section of the membrane, is written by dimensionless variables as follows:

$$\frac{\partial C}{\partial \tau} + \frac{\partial C}{\partial \zeta} = \frac{1}{Pe} \cdot \frac{\partial^2 C}{\partial \zeta^2} - m \cdot \frac{\partial C_s}{\partial \tau} \quad (1)$$

where  $C$  is the ratio between the current and feed solute concentration in the liquid-phase,  $C = c/c_o$ ,  $C_s$  is the ratio between the current and equilibrium feed solute concentration in the solid-phase,  $C_s = c_s/c_{s\_eq\_o}$ ,  $\zeta$  is the dimensionless coordinate along the membrane,  $\zeta = z/L$ , and  $\tau$  is the dimensionless time defined as the ratio of current time and the characteristic time of the process,  $\tau = t/t_{process}$ . The mass transfer of solute from liquid-phase to the solid-phase is described by a second order kinetic reversible equation and the Langmuir isotherm:

$$\frac{\partial C_s}{\partial \tau} = K_{ads} \cdot \left( C + \frac{I}{r} \right) \cdot (C_{s\_eq} - C_s) \quad ; \quad C_{s\_eq} = \frac{(r/p) \cdot C_{eq}}{1 + r \cdot C_{eq}} \quad (2)$$

Experimental work has been done in order to valid the model using Sartobind Membrane Adsorber and solutions of Orange G (C.I.=16230) at different dye concentrations and KCl concentrations. Figure 1 shows that the experimental and modelling results are in good agreement, although some model predictions differ a little of the experimental data. This fact could be due to the membrane may have some dead volume which cannot be reached by convective flow and diffusion of the solute become more significant.

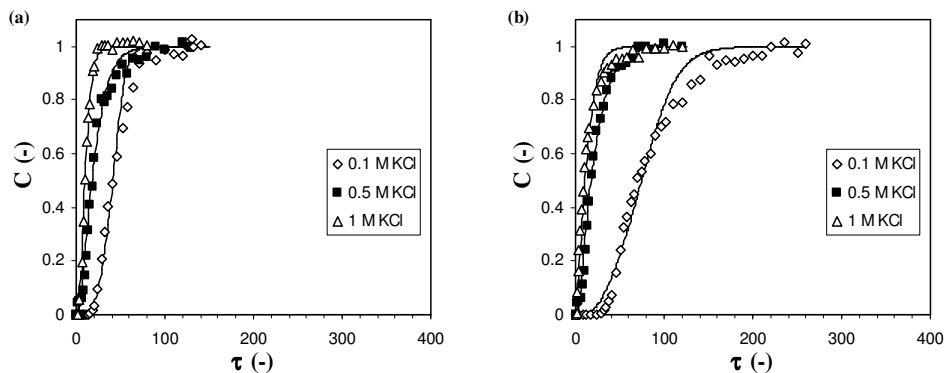


Figure 1. Experimental and calculated breakthrough curves as a function of KCl concentrations and Orange G concentrations: (a)  $10^{-3}$  M, and (b)  $5 \cdot 10^{-4}$  M.

The adsorption process was significantly affected by the dye and KCl concentrations, since the electrostatic repulsion between chloride and dye anions intensified the desorption rate constant and, at the same time, it reduced the adsorption rate constant. Whereas the axial diffusion coefficient was independent of KCl concentration.

## References

Ghosh, R, (2002) *Journal of Chromatography A*, 952, 13-27.



## Session T4-8P: Membranes and Membrane Science – Poster

Abstract Number	Paper Title & Authors	Included
814	Pervaporation of mixtures involved in the esterification of lactic acid with ethanol P Delgado, M T Sanz, S Beltrán	Yes
912	Treatment of Pharmaceutical Waste Water by Hybrid Separation Processes E Csefalvay, K Koczka, P Mizsey	Yes
1418	Mathematical modeling of transfer processes and chemical reactions in catalytic membrane reactors E M Koltsova, S V Tsaplin, A A Mochalova, V V Vasilenko	Yes
1580	Self-cleaning properties of RO membrane coated with TiO <sub>2</sub> particles S S Madaeni, N Ghaemi	Yes
1852	Trade-off between hydrogen production and temperature hot spots in the design of a membrane reactor G Chiappetta, G Clarizia, E Drioli	Yes
1884	Estimating the adsorption characteristics of a methylated amorphous silica membrane from permeation data J Kuhn, P J Jansens, F Kapteijn, J Gross	Yes
2095	Polyvinylamine/polysulfone composite membrane with excellent performance by facilitated transport for CO <sub>2</sub> capture from exhaust gas of power plant T J Kim, M B Hägg	Yes
2283	Unsteady and steady-state gas permeation through active porous walls R D Felice, D Cazzola, M Garbero, P Ottonello	Yes
2351	Permeation of organic molecules in water and ethanol-water solution by reverse osmosis J Labanda, J Llorens	Yes
2357	Membrane processes in the purification of electronic grade chemicals A Garea, P Portilla, A Irabien	Yes
2921	PEUF process with electrochemical regeneration for the recovery of copper P Cañizares, A Pérez, J Llanos, M González-Mohino	Yes
2942	Influence of the nature of the ionic liquid on the selective transport of the substrates and products of transesterification reactions through supported liquid membranes based on ionic liquids F J Hernández-Fernández, A P de los Ríos, F Tomás-Alonso,	Yes

Session T2-8P

2946	D Gómez, M Rubio, G Villora MFI-type zeolite dispersed in rubbery polymers: influence on surface and transport properties	Yes
2976	G Clarizia, C Algieri, E Drioli Stability studies of supported liquid membranes based on ionic liquids using SEM/EDX techniques	Yes
3323	A P de los Ríos, F J Hernández-Fernández, F Tomás-Alonso, J M Palacio, D Gómez, M Rubio, G Villora Gas separation simulation in hollow fiber membrane modules for multi component mixtures: Calculation of the performance and required area	No
	T Mohammadi, M Pir, M Mahdyarfar	

## **Pervaporation of mixtures involved in the esterification of lactic acid with ethanol**

P. Delgado, M.T. Sanz, S. Beltrán

*Department of Chemical Engineering, University of Burgos , 09001 Burgos, Spain*

### **1. Summary**

In this work, pervaporation experiments were performed for some binary feed mixtures involved in the esterification of lactic acid with ethanol: water/ethanol, water/ethyl lactate and water/lactic acid. The commercial (Sulzer Chemtech) hydrophilic membranes PERVAP<sup>®</sup> 2216 and PERVAP<sup>®</sup> 2201 were used for studying these systems. The effect of feed composition and operating temperature on the membrane performance was studied. Both membranes showed to be water selective as indicated by its higher flux when compared with other components. It was found that the permeation rate increased with the feed water content and the operating temperature.

Keywords: pervaporation, esterification, lactic acid, ethanol

### **2. Extended Abstract**

Lactate esters are biodegradable, non-toxic and can be used in the food industry for preservation and flavouring purposes, as well as in the pharmaceutical and cosmetic industries. Methyl, ethyl, isopropyl and n-butyl lactates are usually produced by conventional esterification of lactic acid with the corresponding alcohol, being equilibrium-limited reactions [1]. Higher ester yields can be obtained by shifting chemical equilibrium towards products formation by hybrid processes such as reactive distillation and pervaporation-aided reactors. Pervaporation-esterification coupling has attracted most attention in recent years due to the selective removal of water from the reaction medium by hydrophilic membranes.

In the case of quaternary systems, the transport through the membrane is a very complex phenomenon with interactions between the components of the mixture and the components and the membrane. Previous to the pervaporation study of the quaternary mixture involved in our reacting system, pervaporation performance of different binary feed mixtures was considered: water/ethanol, water/ethyl lactate and water/lactic acid.

The experiments were carried out with a laboratory pervaporation set-up with a test cell unit (170 cm<sup>2</sup> effective membrane area, Sulzer Chemtech) following the procedure described elsewhere [2].

For ethanol/water feed mixtures, experiments were performed with PERVAP<sup>®</sup> 2216 and PERVAP<sup>®</sup> 2201 membranes (Sulzer Chemtech). As can be observed in Figure 1 higher permeate fluxes were obtained with PERVAP<sup>®</sup> 2201 membrane. The increase of ethanol flux is almost linear as the feed water concentration increases. This behaviour shows that ethanol flux is not primarily influenced by its own chemical potential gradient, but by the water permeation. The separation factor values obtained were also better with this membrane. PERVAP<sup>®</sup> 2201 was chosen for further experiments as it showed better results for ethanol/water mixtures.

In Figure 2 the total permeate flux and the permeate composition are plotted as function of water concentration in the feed. As the feed concentration of water increases, the water concentration in the permeate remains relatively constant averaging 95% for all the systems. Ethanol/water and ethyl lactate/water systems have similar permeation behaviour whereas lactic acid/water shows a different behaviour; the lactic acid-water mixtures have much higher total permeate flux. Lactic acid contains a carbonyl group, which has a high capacity of hydrogen bonding with the alcohol groups of the polyvinyl alcohol top layer of the membrane [3].

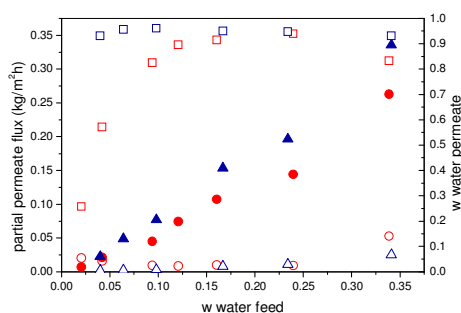


Figure 1. Influence of water feed concentration for PERVAP<sup>®</sup> 2216 (red) and PERVAP<sup>®</sup> 2201 (blue), on partial permeate flux: water  $\blacktriangle$ ,  $\bullet$ , ethanol  $\triangle$ ,  $\circ$ , and permeate concentration  $\blacksquare$ ,  $\square$  ( $T_{\text{pervaporation}} = 327.15$  K).

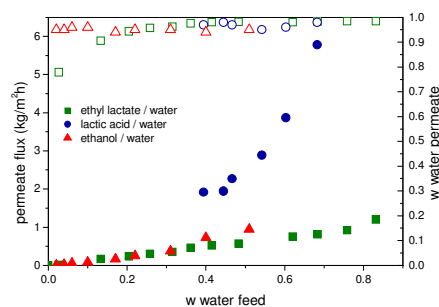


Figure 2. Influence of water feed concentration for PERVAP<sup>®</sup> 2201 on permeate flux (solid symbols) and permeate concentration (open symbols) for the binary mixtures studied.  $T_{\text{pervaporation}} = 327.15$  K

For all the binary feed mixtures, the effect of temperature was also studied in the range from 327.15-348.15 K. Permeate flux was promoted with increasing temperature. A positive temperature dependence of permeation flux is not necessarily an indication of a diffusion dominating process because the driving force for pervaporation is also increased due to the increasing vapour pressure. It was found that temperature dependence of the permeation rate can be expressed by an Arrhenius-type relation.

## References

- [1] Delgado P., Sanz M.T., Beltrán S., (2007) *Chem. Eng. J.*, 126,111-118.
- [2] Sanz M.T., Gmehling J., (2006) *Chem. Eng. Technol.*, 29, 473-480.
- [3] Van Baelen D., Van der Bruggen B., Van den Dungen K., Degreve J., Vandecatelee C., (2005) *Chem. Eng. Sci.*, 60, 1583-1590.

# Treatment of Pharmaceutical Waste Water by Hybrid Separation Processes

E. Cséfalvay<sup>a</sup>, K. Koczka<sup>a</sup>, P. Mizsey<sup>a</sup>

<sup>a</sup>*Department of Chemical Engineering, Budapest University of Technology and Economics, H-1111 Budapest, Hungary*

## 1. Summary

Waste water from a pharmaceutical industry is treated by a hybrid separation process. The steps of the hybrid process are the following: i) conventional filtration to remove solid particles; ii) distillation to clean the waste water from volatile organic content; iii) nanofiltration and reverse osmosis to concentrate the not biodegradable components. The recovered solvents can be reused or recycled into the technology. Since the pharmaceutical waste water contains salts and high molecular weight organic compounds, which can not be decomposed by biodegradation, the membrane filtration technique helps to concentrate them. The concentrated effluent can be further treated in an incinerator plant. Permeate of the membrane filtration can either be lead to an optional biological treatment or into waste water pipe, if it meets the emission limits.

Keywords: pharmaceutical waste water, distillation, hybrid separation process, membrane filtration

## 2. Extended Abstract

Latest environmental regulations urge industrial companies to apply preventive environmental politics. In the pharmaceutical industry, however, the production of an active ingredient can not enable the technology to be changed basically. In this case, instead of preventive environmental politics, attention is focused on the treatment of the wastes. Usually, there are many engineering options for achieving the treatments. According to the EU Directives, biological treatment is aided. [1] Nevertheless in certain cases the biological treatment can not be achieved but physical-chemical processes can offer a solution for this problem and they come increasingly to the front. Hybrid processes including distillation combined with membrane techniques are promising alternatives for industrial waste water treatment, therefore more and more experiments are performed to support their industrial application.

The aim of the work is to give an optional process for the treatment of a pharmaceutical wastewater regarding the EU Directives.

The waste water is actually a process water of the production of an active ingredient. The ingredient is produced by fermentation therefore the waste water contains carbohydrates, a part of the feed of the fermentation, the product of fermentation and a slight concentration of solid particles. It contains among other compounds of high molecular weight, which are hardly biodegradable and it may contains traces of the ingredient. Since the ingredient production technology applies also solvent extraction, the waste water has a little solvent content, too.

The waste water has a chemical oxygen demand of 42,000 mg/L. Out of this initial value 19,000 mg/L share is due to the solvent content and 6,000 mg/L to the solid particles. In order

to accomplish the removal of solvents, the solid particles need to be eliminated, since they can damage and/or disturb the subsequent part of the hybrid separation process. Figure 1 shows a schematic drawing of the applied treatment technology. After the conventional filtration of the solid particles, the initial chemical oxygen demand is reduced to 36 000 mg/L. The pre-treated waste water is then fed into the distillation column. A reflux ratio of 10 is applied. Related to the total amount of waste water (100%), about 5% of the waste water is removed as solvents.

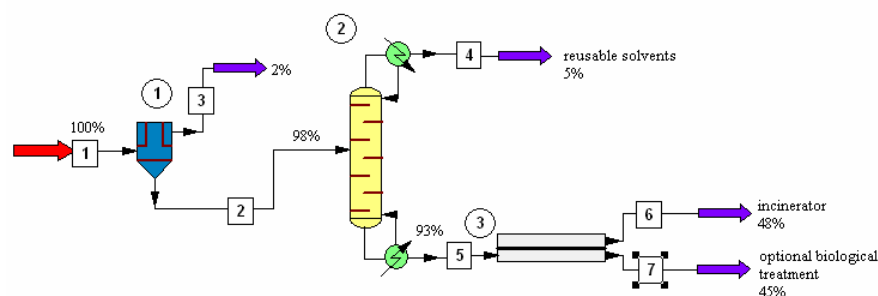


Figure 1: A schematic drawing of the applied treatment technology

The distillate contains methanol, ethanol, isobutyl-acetate, and toluene traces. The high molecular compounds remain in the bottom of the column. In the next step of the treatment the bottom product is filtered by membrane. In our experiments, two different types of membranes are tested in order to determine whether the nanofiltration or the reverse osmosis membrane show better rejection and flux. First, nanofiltration of bottom product is investigated. The experiment is carried out at room temperature and a pressure of 10 bar is used. Only one-tenth of the optimal flux is observed. After a yield of 7%, the permeate has a chemical oxygen demand of 5 800 mg/L. In this case nanofiltration is proven to be not effective adequately. Then a reverse osmosis membrane is tested at room temperature and at an operating pressure of 30 bar. One-sixth of the optimal flux is observed. Both the nanofiltration and reverse osmosis membrane show much smaller flux than it is expected. The great decrease in flux can be explained by the high salt content of the waste water. Regarding the rejection estimated by conductivity, a rejection of 95% can be achieved in reverse osmosis. The chemical oxygen demand of the permeate of the reverse osmosis increases during the experiment. Table 1 shows the chemical oxygen demand values of permeate of reverse osmosis membrane in the yield of permeate.

Yield of permeate (%)	COD of RO permeate(mg/L)
20	973
40	2900
45	3070

Table 1: Chemical oxygen demand of the permeate of reverse osmosis membrane in the function of the yield of permeate

The permeate of the reverse osmosis membrane contains the not biodegradable compound in negligible amounts therefore it can be further treated with biological tools. The Hungarian emission limit for the COD is 1000 mg/L so the first 20% can be lead into the waste water pipe. The energy content of the not biodegradable organic compound enriched in the concentrate of reverse osmosis can be used in an incinerator plant.

## References

- [1] Mizsey, P., (1994) Journal of Hazardous Materials, 37, 1-13.

## **Mathematical modeling of transfer processes and chemical reactions in catalytic membrane reactors**

E.M. Koltsova, S.V. Tsaplin, A.A. Mochalova, V.V. Vasilenko

*Department of Cybernetics of Chemical Technological Processes, Mendeleev University of Chemical Technology of Russia, 125047, The Russian Federation, Moscow, Miusskaya sq., 9*

### **1. Summary**

The aim of this work was investigation of mass transfer processes and chemical reactions proceeding in catalytic membrane reactors (CMR). These reactors are of great interest for chemical engineering since they enable to remove the equilibrium point to the side of forming the target products and enable to intensify the chemical processes. One of the perspective ways of using these reactors is getting hydrogen (for example by means of sulfur-iodine cycle).

Keywords: mathematical modeling; catalytic; membrane reactor; hydrogen; sulfur-iodine.

### **2. Extended Abstract**

As a method of investigation of mass transfer processes and chemical reactions proceeding in catalytic membrane reactors the method of mathematical modeling was chosen. As the result of this modeling the time-dependent model with distributed parameters describing the processes proceeding inside the CMR was developed. For the forming of this mathematical model the block principle was used concerning the following: model structure of mathematical model, model of mass transfer processes, kinetic model of chemical reactions and the structure of threads. For describing the processes inside the membrane of CMR the assumption that porous medium of the membrane is a nature fractal was used.

Novation of this work consists in the fact that mathematical description of mass transfer processes is based on the usage of differential equations with time-derivative of fractional order. The worked out mathematical model enables to determine (in the assumption of all starting value assignment) concentrations of all the components of the reactions in any place of the reactor at any moment of time.

The above mentioned mathematical model of mass transfer processes and chemical reactions proceeding in catalytic membrane reactors was materialized by means of the worked out program product in order to simplify the processes of working with it and

estimation of the results. Solving the equations of the model was carried out by means of the numerical methods of solving the equations of mathematical physics and chemistry based on the use of the diversity schemes. The adequacy of exit data was estimated for the process of propane dehydration.

The worked out program product gives the possibility of exporting the results into the sheets of Microsoft Office Excel by means of using the DDE-technology of the application interaction. The integration of this program product into larger products by means of including the functions, procedures and the whole modules of the program product is also possible.

The exit data of the worked out program product will be useful during the analysis of work of the CMR for the aim of determining for it optimal (concerning the chosen criterion) technological (temperature and pressure inside the CMR) and constructional (length of the apparatus, width of the catalyst layer, width of the mount) values.

The work was carried out under support of grants RFBR № 05-08-18001-a and № 07-08-00654-a.



## **Self-cleaning properties of RO membrane coated with TiO<sub>2</sub> particles**

S. S. Madaeni, N. Ghaemi

*Department of Chemical Engineering, Razi University, Kermanshah, Iran*

### **1. Summary**

Fouling is one of the most important problems in membrane processes. The deposition of particles and their sticking on the surface, results in the formation of layers on the surface of membrane. These layers, together with particles left inside the membrane lead to a fluid-passing resistance and as a result the output flux in the lapse of time is reduced. In this research, TiO<sub>2</sub> particles on the surface of composite RO membrane were self-assembled and radiated by UV light. The coating of membrane surface with TiO<sub>2</sub> particles and radiation with UV light, results in a creation of photocatalytic property with an increased hydrophilicity on the surface of membrane. The flux, through a coated and UV light irradiated membrane, has increased to a large extent in comparison with a neat membrane. In this research, the performance of photocatalytic decomposition and ultrahydrophilicity under UV irradiation, which create the self-cleaning speciality in a TiO<sub>2</sub> coated membrane and an increase in the flux, have been studied.

Keywords: self-cleaning membrane, photocatalysis, ultrahydrophilicity, TiO<sub>2</sub>.

### **2. Extended Abstract**

Nowadays membrane processes are of great importance in many fields of industries. However, one of the main barriers to greater use of membrane technology is membrane fouling [1]. Various approaches have been performed to reduce fouling. A recently established approach is use UV-catalysts such as TiO<sub>2</sub> for this purpose. The TiO<sub>2</sub> photocatalyst can effectively degrade the pollutants, especially organic materials effectively with UV light. The photocatalytic, related to the properties of oxidative decomposition and the photoinduced ultrahydrophilicity of titanium dioxide, has attracted much interest from the view points of basic and applied sciences [2]. Among different applications of photoactive TiO<sub>2</sub> thin films, one concerns self-cleaning surfaces, which rely both on photocatalysis and photohydrophilicity mechanisms [3].

TFC-SR reverse osmosis composite membranes were used. This is a hydrophilic membrane with the top layer of poly vinyl alcohol. In order to coat the membrane surface with TiO<sub>2</sub> particles, it was immersed in a transparent colloidal solution containing 0.003 wt. % of TiO<sub>2</sub> particles for 1 hour. After that, the membrane was washed with an excess amount of water and then illuminated by UV lamp for 10 minutes. The treated membrane was kept in distilled water for 15 minutes before usage in the experiment rig. All experiments were carried out in a reverse osmosis rig with a cross flow cell at 23 ± 1 °C temperature and a transmembrane pressure of 20 bars. For radiation, a 400W UV lamp was used. Whey from feta cheese manufacturing process was used as feed.

The SEM micrographs are shown in Fig. 1.  $\text{TiO}_2$  particles were uniformly distributed on the membrane surface. However some particles form larger clusters. The whey proteins are more important factors in creating fouling. Fig. 2 shows that the flux of whey using  $\text{TiO}_2$  coated membrane is much higher compared to flux of the neat membrane. This is due to the hydrophilicity and photocatalytic properties of  $\text{TiO}_2$  particles radiated on the membrane surface by UV light. The photocatalysis produces oxidant reagents such as: hydroxyl radicals and superoxide radical anions which are strong oxidant reagents. These groups decompose the contaminations, especially organic compounds. On the other hand, the ultrahydrophilicity created by the  $\text{TiO}_2$  particles results in an increment in the membrane flux and spread of water layer all over the surface. The movements of these layers decontaminate the deposited specimen on the surface. In this way,  $\text{TiO}_2$  particles by their photocatalytic and ultrahydrophilicity properties prevent the deposition of proteins and organic compounds. So the membrane will clean its surface and it can be claimed that the membrane has the self-cleaning property.

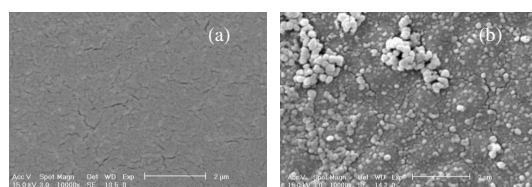


Figure 1. SEM images of (a) neat and (b) coated membrane with  $\text{TiO}_2$  particles

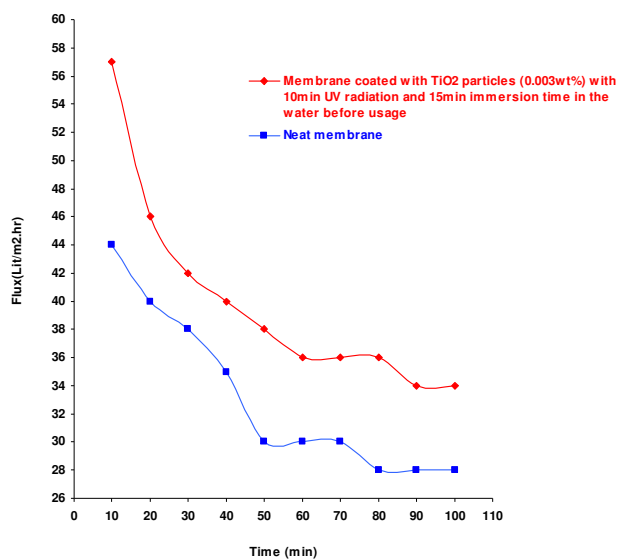


Figure 2. Flux of whey versus time for neat and coated membrane with  $\text{TiO}_2$  particles

## References

- [1] Chen, D., Weavers, L. K. and Walker, H. W., (2006) *Water Research*, 40, 840-850.
- [2] Yamamoto, S., Nagata, S., Takayama, A. and Yoshikawa, M., (2006) *Nuclear Instruments and Methods in Physics Research B*, 249, 374-376.
- [3] Langlet, M., Permpoona, S., Riassetto, D., Berthome, G., Pernot, E. and Joud, J. C., (2006) *Journal of Photochemistry and Photobiology A: Chemistry*, 181, 203-214.

## **Trade-off between hydrogen production and temperature hot spots in the design of a membrane reactor**

G. Chiappetta, G. Clarizia, E. Drioli

*Research Institute on Membrane Technology, ITM-CNR, c/o UniCal via P. Bucci, cubo 17/C, 87030 Arcavacata di Rende (CS), Italy*

### **1. Summary**

Computer simulations showed as a proper choice of sweep gas temperature and flow rate makes the membrane reactors inherently safer than conventional systems in carrying out exothermic reactions since they allow to control temperature hot spots without modifying the global yield and the H<sub>2</sub> recovery in water gas shift reaction. In order to minimize the hot spot intensity, an effective heat exchange is suggested. This result can be achieved operating on the effective radial thermal conductivity or, in alternative, on the catalyst distribution, without reducing the hydrogen recovery.

Keywords: non-isothermal conditions, modelling, water gas shift reaction, catalyst mass distribution

### **2. Extended Abstract**

Hydrogen worldwide demand is increasing rapidly for its potential as energy carrier and clean fuel, meeting the environmental restrictions for a sustainable development. At present, hydrogen is mainly produced from a variety of fossil fuels by either steam-hydrocarbon reforming or autothermal reforming for light feedstocks or partial oxidation using pure oxygen for heavy feedstocks, coal and coke [1]. The water gas shift reaction (WGSR) represents a fundamental step in the main industrial routes to produce hydrogen [2], specially where the CO content must be minimized as for fuel cell applications or for adjusting the CO/H<sub>2</sub> ratio of the syngas produced.

The opportunity to carry out this exothermic reaction, limited by thermodynamic equilibrium, in a membrane reactor (MR) offers some important advantages with respect to a conventional packed bed reactor if an appropriate design of the unit is performed. Pd-based membranes, that present the highest selectivity values to hydrogen, are adequate to withstand the high operation temperature and pressure values.

Mass and heat transport phenomena in MR have been investigated by means of a two-dimensional pseudo-homogeneous model that considers both axial convective and

radial diffusive contributions. The effect of some important parameters (e.g. sweep gas temperature and flow rate, reaction temperature and pressure) on CO conversion and temperature hot spot managing has been analysed in order to improve the MR performance.

At high feed pressures, the influence of the sweep gas temperature and flow rate on the performance of the membrane reactor is less remarkable than at low feed pressure. At 20 bar is more convenient to operate with a sweep gas at lower temperature (e.g. 500 K) than lumen temperature in terms of hydrogen recovery and CO conversion. On the other hand, at 1.1 bar it is strongly suggested to use a large sweep gas flow rate at the same temperature of the feed stream in order to achieve high CO conversion and H<sub>2</sub> recovery. For what concerns the effect of membrane surface and reactor volume ( $S_m/V_r$ ) ratio on the reactor performance, it is more important at low feed pressures (see figure 1).

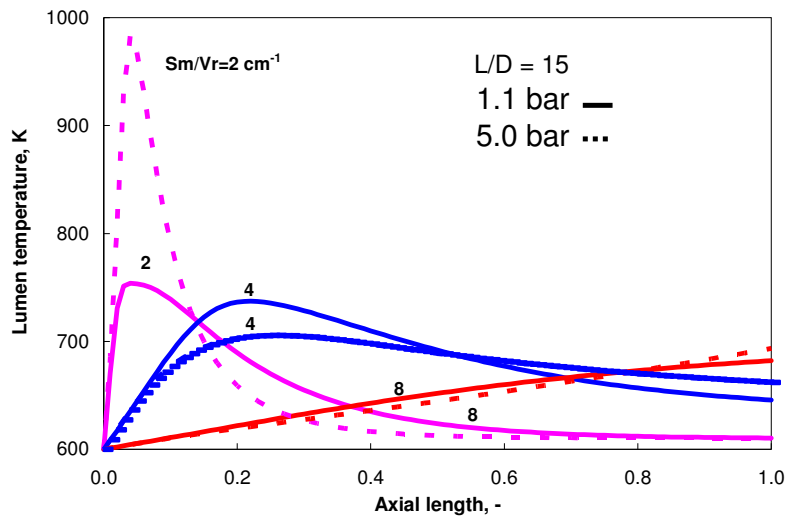


Figure 1. Lumen temperature vs. axial length at different  $S_m/V_r$  values.

A catalyst mass that increases linearly along the membrane reactor is more efficient than an exponential distribution to control the temperature hot spots. However, if at high pressures (20 bar) the advantage of a linear catalyst distribution is moderated, it becomes progressively more significant at 5 bar and 1.1 bar with respect to an exponential distribution.

## References

- [1] Conte M., Iacobazzi A., Ronchetti M., Vellone R., (2001) *J. Power Sources*, 100, 171-187.
- [2] Newsome D.S., Kellog P., (1980) *Catal. Rev. Sci. Eng.*, 21(2), 275-318.

## Estimating the adsorption characteristics of a methylated amorphous silica membrane from permeation data

J. Kuhn<sup>a/b</sup>, P.J. Jansens<sup>b</sup>, F. Kapteijn<sup>a</sup>, J. Gross<sup>b</sup>

<sup>a</sup>Delft University of Technology, Ceramic Membrane Centre, The Pore, Julianalaan 136, 2628BL Delft, The Netherlands

<sup>b</sup>Delft University of Technology, Process & Energy Laboratory, Leeghwaterstraat 44, 2628CA, Delft, The Netherlands

### 1. Summary

This research is aimed at a simple method of estimating the adsorption characteristics of membranes from permeation data. Permeation of methanol and ethanol through methylated amorphous silica membranes (ECN, The Netherlands) have been performed, and assuming the transport can be described by the Maxwell-Stefan equation, the Langmuir adsorption parameter is estimated.

Keywords: adsorption, membrane, amorphous silica, methanol

### 2. Extended Abstract

Knowing the adsorption behavior of permeating components on microporous membranes is crucial when determining the membrane performance. To describe the mass transport through a membrane using the Maxwell-Stefan equations, data on the adsorption on the membrane material is required. Although in most cases the adsorption data can be measured from bulk material, the adsorption behavior at a membrane can deviate significantly [1].

Using the Maxwell-Stefan equations [2], the method proposed here provides a simple way to estimate the adsorption characteristics of the membrane. By assuming a uniform zeolite membrane thickness,  $\delta$  (m), and introducing the Langmuir isotherm, the Maxwell-Stefan equation for single component transport through a microporous membrane reduces to

$$N_i = -q_{i,sat} \rho \mathcal{D}_{i,M} \frac{\ln \left( \frac{1 + b_i p_{i,o}}{1 + b_i p_{i,\delta}} \right)}{\delta}$$

The diffusion coefficient can be assumed to be independent of loading (weak confinement) or the loading dependency of the diffusion coefficient can be taken into account (strong confinement). The most simple loading dependency is the so-called

vacancy diffusion, where the diffusion coefficient is assumed to decrease linearly with increasing loading.

$$D_i = D_i(0) \theta_v$$

with  $\theta_v = 1 - \sum_i^n \theta_i$

From the ratio of pure component fluxes measured under pervaporation conditions at different permeate pressures the Langmuir adsorption parameter can be calculated. Assuming isothermal transport and, the ratio of the fluxes at different permeate pressures are for weak and strong confinement respectively:

$$\frac{N_i^A}{N_i^B} = \frac{\ln \frac{(1+b_i p_{i,0})}{(1+b_i p_{i,\delta}^A)}}{\ln \frac{(1+b_i p_{i,0})}{(1+b_i p_{i,\delta}^B)}} \quad , \text{and} \quad \frac{N_i^A}{N_i^B} = \frac{(b_i p_{i,0} - b_i p_{i,\delta}^A)(1+b_i p_{i,\delta}^B)}{(b_i p_{i,0} - b_i p_{i,\delta}^B)(1+b_i p_{i,\delta}^A)}$$

By calculating the adsorption parameter at different temperatures, the heat of adsorption can be estimated using an Arrhenius type of temperature dependence of the Langmuir adsorption parameter [3].

The pure component single site Langmuir adsorption parameter and the heat of adsorption of methanol and ethanol on a methylated amorphous silica membrane (provided by ECN, The Netherlands) were estimated using this method. Pervaporation experiments were conducted at 338, 347, and 360K and the permeate pressure was varied between 10 and 200 mbar.

The obtained adsorption isotherm for methanol is compared with literature data [4] on bulk silica (Figure 1). A lower uptake compared to literature data can be expected, since on bulk silica adsorption in all pores is measured, while in this method only the adsorption in pores which are relevant to permeation is taken into account. The proposed method allows for a fast and easy estimate of the adsorption behavior on microporous membranes relevant for the permeation process.

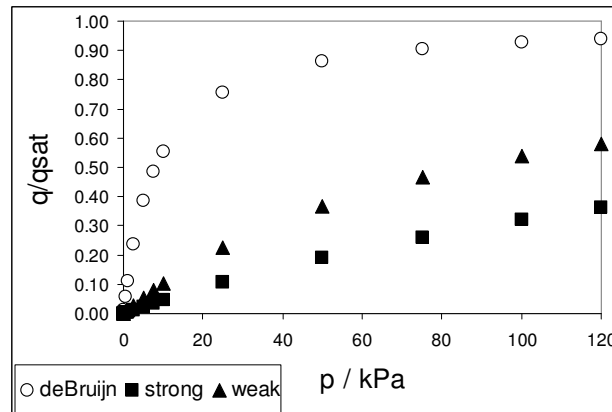


Figure 1: adsorption isotherm measured from silica flakes (open symbols), and estimated assuming strong confinement (cubes) and weak confinement (triangles)

**References**

- 1 T. E. Clark, H. W. Deckman, D. A. Cox, and R. R. Chance, Journal of Membrane Science, vol.230, 91 (2004)
- 2 R. Krishna, R. Baur, Chemical Engineering Journal, vol.97, 37 (2004)
- 3 Bakker, W. J. W., Structured Systems in Gas Separation thesis, Delft University of Technology (1998)
- 4 de Bruijn, F. T., J.Gross, Z.Olujic, P.J.Jansens, F.Kapteijn, Industrial and Chemistry Research (2007) in press

## **Polyvinylamine/polysulfone composite membrane with excellent performance by facilitated transport for CO<sub>2</sub> capture from exhaust gas of power plant**

Taek-Joong Kim, May-Britt Hägg

*Department of Chemical Engineering, Norwegian University of Science and Technology (NTNU), NO-7491 Trondheim, Norway*

### **1. Summary**

The removal of CO<sub>2</sub> by absorption into aqueous alkanolamine solutions is widely used in the chemical industry. However the membrane application for CO<sub>2</sub> capture is getting more attention because of its simplicity, lower energy cost compared to the conventional alkanolamine absorption method.

Especially facilitated transport membrane is attractive with high permeance and selectivity at the same time overcoming the drawbacks of the previous liquid membrane or ion exchange membrane.

CO<sub>2</sub> is transported through this membrane by both the solution-diffusion and the fast “hops” between reactive fixed-site-carriers while N<sub>2</sub> is transported only by the solution-diffusion.

Unlike the normal membranes which may lose separation ability when swollen by the water vapor in the system, this polyvinylamine membrane shows enhanced CO<sub>2</sub> transport in the presence of water molecules by reversible formation of bicarbonates. The performance of this membrane was tested under different pressure, temperature and humidity conditions.

Keywords: CO<sub>2</sub>, membranes, facilitated transport, separation

### **2. Extended Abstract**

Polyvinylamine solution of carefully adjusted concentration to obtain a required thickness was cast onto polysulfone support. The dried polyvinylamine/polysulfone composite membrane was then cross-linked with ammonium fluoride solution.

Permeance and selectivity of the membrane were measured with an experimental setup equipped with humidifiers to study the effect of water vapour in the system as well. This humidified gas system study is important because combustion gas may always contain water vapour which can affect the performance of normal membranes seriously.

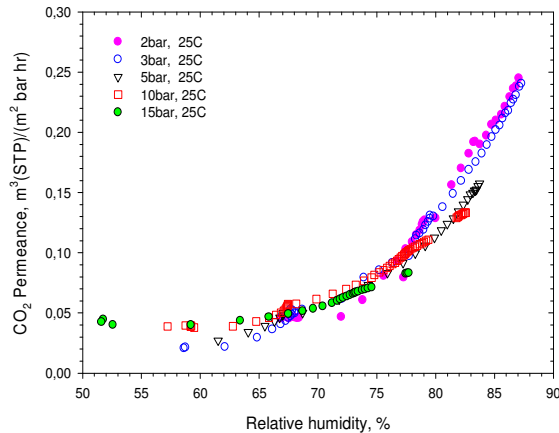


Fig. 2: Effect of temperature on permeance (PVAm/PSf, feed gas: 10%CO<sub>2</sub> + 90%N<sub>2</sub>).

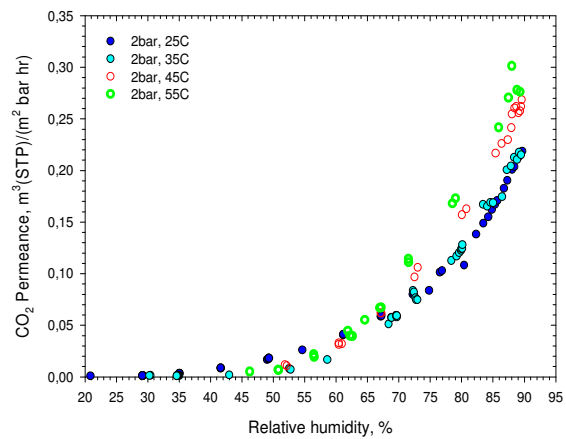


Fig. 1: Effect of feed pressure on permeance (PVAm/PSf, feed gas: 10%CO<sub>2</sub> + 90%N<sub>2</sub>).

The membrane performance was tested at various conditions (pressure of 2-15bar and temperature of 25-55°C and relative humidity of 20-95%).

It was found out that both CO<sub>2</sub> permeance and CO<sub>2</sub> selectivity over N<sub>2</sub> were dependent on humidity change in the system. The permeance increased continuously with humidity and temperature increase, while the selectivity (CO<sub>2</sub>/N<sub>2</sub>) showed more complex behaviour depending on temperature and pressure. Permeance decreased with increasing pressure while selectivity increased, which needs complicated explanation by the typical facilitated transportation characteristics and membrane compaction caused by pressure.

This polyvinylamine fixed-site-carrier membrane showed good CO<sub>2</sub> capture performance (permeance, selectivity and durability) under the presence of water vapour in the system, which implies a potential of replacing the conventional CO<sub>2</sub> capture process even without water removal unit.

## References

Kim, T-J., Li, B. and Hägg, M-B, (2004) *Journal of Polymer Science: Part B*: 42, 4326-4336.



## **Unsteady and steady-state gas permeation through active porous walls**

R. Di Felice,<sup>a</sup> D. Cazzola,<sup>a</sup> M. Garbero,<sup>b</sup> P. Ottonello<sup>b</sup>

<sup>a</sup>*Department of Chemical and Process Engineering, University of Genova, I-16145 Genova, Italy*

<sup>b</sup>*Cobarr Gruppo Mossi & Ghisolfi, Strada Savonese 9, I-15040 Rivalta Scrivia, Italy*

### **1. Summary**

Steady and unsteady-state gas permeation rates through packaging walls containing active (scavenger) materials are determined as functions of the system's physical parameters and the scavenger load. With the simplifying assumptions of constant scavenger concentration and first order reaction kinetics, steady-state analysis shows that there is a minimum quantity of scavenger that must be added to the packaging wall if any reduction of gas permeation is to be achieved. Unsteady-state studies have established the dependence of the time needed to reach stationary behaviour on the system's physical parameters.

**Keywords:** Food packaging, Oxygen scavenger, Permeation Rate, Steady-state, Unsteady-state

### **2. Extended Abstract**

There are various ways to improve the barrier properties of plastic packaging walls, which can generally be classified as providing either passive or active protection. Passive protection consists in simply supplementing the original plastic material with a further component with superior barrier properties, so that the overall performance is improved. Examples are the addition of polyamide or ethylene vinyl alcohol compounds to the polymer.

Active protection, on the other hand, implies the addition of a scavenging compound to the plastic matrix; this reacts with, and thus consumes, the permeating gas, thereby greatly reducing, for example, contact of a sensitive food product with oxygen. Examples of oxygen scavengers in current employment are iron, ascorbic acid, photosensitive dyes, enzymes, unsaturated fatty acids and immobilised yeasts.

In cases where the use of an active scavenger is contemplated, it is clearly important to be able to quantify its effectiveness with regard to the amount of oxygen, or other contaminant, which permeates the packaging wall to reach the packaged contents.

Steady and unsteady-state gas permeation rates through packaging walls containing active (scavenger) materials are determined as functions of the system's physical parameters and the scavenger load. With the simplifying assumptions of constant scavenger concentration and first order reaction kinetics, steady-state analysis shows that there is a minimum quantity of scavenger that must be added to the packaging wall if any reduction of gas permeation is to be achieved. Unsteady-state studies have established the dependence of the time needed to reach stationary behaviour on the system's physical parameters.

We have been able to quantify (analytically for the steady-state case and numerically for the unsteady-state case) gas transmission rates in active packaging walls, enabling a desired performance criterion to be realized function of the dimensionless parameter  $\Phi = L(k/D)^{0.5}$  where  $L$  is the wall thickness,  $k$  the kinetic constant and  $D$  the diffusion coefficient.

The parameter  $\Phi$  is exactly analogous to the Thiele modulus, which characterises diffusion and reaction in a porous solid.

Computed steady-state dimensionless gas fluxes are shown in Figure 1 as a function of  $\Phi$ .

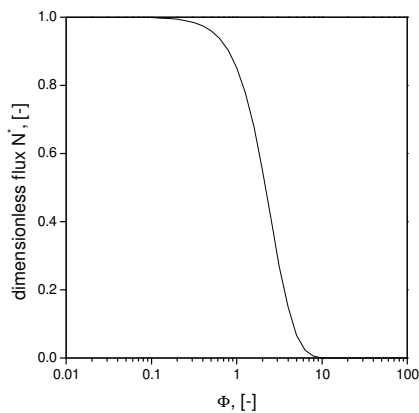


Figure 1 – Gas fluxes at  $x=L$  as a function of  $\Phi$ .

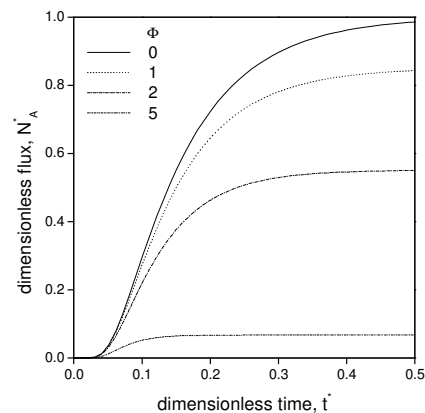


Figure 2 – Dimensionless flux at  $x=L$  as a function of time for various  $\Phi$ .

Some interesting conclusions may be drawn from Figure 1. It is clear that once the system has been fixed (i.e. the wall thickness and diffusion coefficient have been specified and the scavenger type defined), then an estimate may be obtained of the appropriate amount of scavenger to include within the polymer structure. Thus, in order to have a tangible effect on the gas transport,  $\Phi$  must be greater than 0.1; on the other hand,  $\Phi$  values larger than around 10 indicate that an unnecessary excess of the active compound has been used.

Unsteady-state gas fluxes are represented in Figure 2. It is evident that the time required to reach steady-state conditions depends on the parameter  $\Phi$ : the higher the value of  $\Phi$ , the smaller will be the duration of the unsteady-state transition. For a typical PET bottle ( $L = 0.3$  mm,  $D_A = 2.7 \cdot 10^{-13}$  m<sup>2</sup>/s); for  $\Phi=0$ , 40 hours are required to reach steady state conditions; for  $\Phi=5$ , this time reduces to 10 hours.

## PERMEATION OF ORGANIC MOLECULES IN WATER AND ETHANOL-WATER SOLUTIONS BY REVERSE OSMOSIS

J. Labanda, J. Llorens

*Department of Chemical Engineering, University of Barcelona, Martí i Franquès 1, 08028 – Barcelona, Spain*

### 1. Summary

The permeation of different organic molecules in water solvent and in 12% ethanol in ethanol-water mixture by hydrophilic reverse osmosis membrane was studied. Initially, the membrane was characterized by solutions of NaCl in water and in ethanol-water. The permeate flux of the ethanol-water mixture was lower than that of the pure water for the hydrophilic membrane and the result was theoretically analyzed. The solute rejections increased with permeate flux and they were than 90% in water solvent, and they were decreased significantly in presence of ethanol.

Keywords: reverse osmosis, ethanol-water mixtures, solute rejection, organic molecules, Spiegler-Kendem model.

### 2. Extended Abstract

There is usually a difference in solute rejection and flux in organic solvents when compared with performance in aqueous solutions (Machado *et al.*, 1999). In most cases, rejection of the same molecule in an organic solvent is significantly lower than in aqueous solution for the same membrane and operating conditions (Su *et al.*, 2005). Swelling and deformation of the membranes when exposed to organic solvents is common and is dealt with by conditioning the membranes through gradual solvent change (Shukla *et al.*, 2002).

In this study, the influence of feed pressure and feed solute concentrations on the permeate flux and rejection of organic molecules have been analyzed in water solvent and in 12% (v/v) ethanol in ethanol-water mixture at 20°C through low pressure reverse osmosis membrane, UTC-70, which was supplied by Toray.

The membrane was conditioned to the solution, since the membrane's performance may have to be described for each individual solute-solvent-membrane system. The solution-diffusion model of Spiegler-Kendem has been used to predict the permeate flux.

Initially, the membrane was characterized by different NaCl concentrations in water solvent. The experimental data was adjusted with good agreement to the model. Permeate fluxes increased linearly with increasing pressure when the osmotic pressure of the solution was counteracted by the applied pressure between both sides of membrane. Linear relationships with transmembrane pressure were also obtained for ethanol-water mixtures. The ethanol-water fluxes were much lower than those of the water.

As water had the highest affinity for hydrophilic membranes, the addition of ethanol had a stronger effect on the solvent permeability. Therefore, ethanol-water mixture showed lower permeabilities than water ones. This fact could be due to the polarity differences and surface phenomena (i.e., swelling), since the presence of a relative low alcohol concentrations decreases the mixture polarity, leading to higher resistance at the membrane-solvent interphase. As a result, ethanol has lower affinity for hydrophilic membranes.

Figure 1 shows the solute rejections as a function of permeate flux for both solvents. The solute rejections increased with permeate flux tending to the reflection coefficient of the solute,  $\sigma$ . The Spiegler-Kedem model was well correlated with the experimental data for the best values of solute permeability,  $w$ , and reflection coefficient,  $\sigma$ . The solute rejections were higher than 90% in water solvent, and they were decreased significantly in presence of ethanol. The higher rejection in water solvent than in ethanol-water mixture could suggest that the complexation of water molecules with the solute molecules makes their effective size larger in water solvent than in ethanol-water mixture. This sharply decline of solute rejections with ethanol-water mixture can be attributed to the reduction of solvent flux although solvent permeability increased.

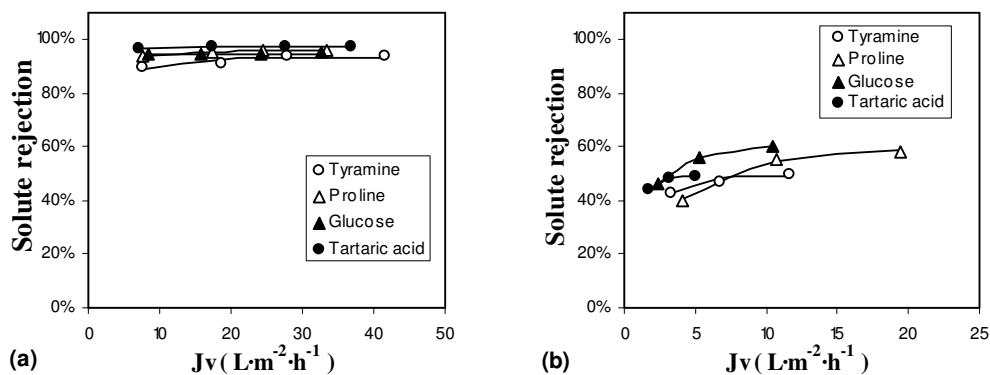


Figure 1: Solute rejections as a function of solvent fluxes: (a) water solvent and (b) 12% ethanol in ethanol-water mixture.

## References

- Machado, D.R., Hasson, D. and Semita, R., (1999) *Journal of Membrane Science*, 163, 93-102.  
 Su, B., Wang Z., Wang, J. and Wang, S., (2005) *Journal of Membrane Science*, 251, 189-200.  
 Shukla, R. and Cheryan, M., (2002) *Journal of Membrane Science*, 198, 75-85.

## **Membrane processes in the purification of electronic grade chemicals**

A. Garea, P. Portilla, A. Irabien

*Departamento de Ingeniería Química y Química Inorgánica, Universidad de Cantabria ,  
Avda. Los Castros, s/n, 39005 Santander, Cantabria, Spain*

### **1. Summary**

The manufacturing of high purity wet chemicals for the Semiconductor Industry requires the purification of these chemicals to the specifications of the determined grades by the introduction of some advanced separation technologies based on distillation, ion-exchange, and membranes. The aim of this work is the use of membranes to the purification of hydrofluoric acid, which is considered the key chemical of semiconductor technology for structuring the silicon or silicon oxide surfaces.

Keywords: membranes, semiconductor, electronic grade, high purity chemicals

### **2. Extended Abstract**

The quality requirements for wet processing chemicals have been increasing during the last 30 years in line with the increasing complexity of the semiconductor devices. In addition, the overall product portfolio of wet processing chemicals expands due to the introduction of new technologies, which also leads to a change in volume consumption of chemicals.

Specifically, the big volume products of the past, sulphuric acid and hydrogen peroxide are hit by new cleaning technologies. Among the main products still used for cleaning purposes during the manufacturing process are sulphuric acid, hydrogen peroxide, 2-propanol, and ammonium hydroxide, whereas the group of chemicals used for structuring the silicon or silicon oxide surfaces includes hydrofluoric acid as the key chemical of semiconductor technology [1].

According to the complexity of the manufacturing process and the sensitivity of highly integrated devices, specific quality requirements have been developed and established by the industry, with the SEMI® base standards for wet chemicals. It is important to notice that the development of more and more stringent specifications

was related to the introduction of the multielement atomic absorption (AAS), inductive coupled plasma-optical emission spectroscopy (ICP-OES), inductive coupled plasma-mass spectroscopy (ICP-MS), and the high resolution-inductive coupled plasma-mass spectroscopy (HR-ICP-MS).

The manufacturing of high purity wet chemicals (with different specifications of metallic impurities such as EG/MOS, 10-500 ppb ; VLSI, 10-100 ppb; ULSI, < 10 ppb; SLSI, < 1 ppb ; XLSI, < 100 ppt) requires (i) the selection of materials, (ii) the filtration to remove the particles, and (iii) the purification to the specifications of the determined grades by the introduction of some advanced separation technologies based on distillation, ion-exchange, and membranes [1].

Taking into account that the aqueous hydrofluoric acid (HF) is the only cleaning and etching material that exposes the base silicon surface in the production process of the integrated circuits, the ultrapurity of the HF is an important concern both in the virgin and the processed product. The etching rate of silicon dioxide generally increases with the increase of the concentration of HF but delamination problems may arise, so wafer oxide removal operations generally tend toward the use of lower concentrations of HF, around 0.1 to 5 % [2].

Under these considerations, this work is focused to the use of membranes to the purification of hydrofluoric acid, being analysed the behaviour of reverse osmosis and nanofiltration membranes in order to advance the chemical process fundamentals.

### **Acknowledgements**

This research is financially supported by the Spanish Ministry of Science and Technology (Project CTM2006-00317/TECNO).

### **References**

- [1] Sievert, W.J., (2003) *Semiconductor Fabtech*, 13<sup>th</sup> ed. 175-179.
- [2] Mukherjee, D., Kulkarni, A. and Gill W.N., (1996) *Journal of Membrane Science*, 109, 205-217.

## PEUF process with electrochemical regeneration for the recovery of copper

P. Cañizares, A. Pérez, J. Llanos, M. González-Mohino

Department of Chemical Engineering, Faculty of Chemistry, University of Castilla-la Mancha. Av. Camilo José Cela, 10. 13005 Ciudad Real, Spain.

### 1. Summary

Copper is a valuable and toxic metal present in effluents such as metal surface treatment or electronic industries. The removal of this heavy metal ion has been widely studied using the polymer enhanced ultrafiltration (PEUF) technique. In the vast majority of the works previously published, polymer regeneration step has been carried out by a chemical technique that involves a decrease in pH followed by an ultrafiltration step in which permeate contains the target ion [1]. In electrochemical regeneration, metal is electrodeposited in the cathode of an electrochemical cell meanwhile polymer remains in solution and can be recycled [2]. This regeneration technique offers the clear advantage of lacking of a discharge effluent with metallic content.

Keywords: Copper, Ethoxylated Polyethylenimine, PEUF, Electrochemical Regeneration.

### 2. Extended Abstract

In this investigation, the removal of  $\text{Cu}^{2+}$  from a synthetic effluent has been confronted using partially ethoxylated polyethylenimine (PEPEI) as water-soluble polymer. Firstly, the values of temperature (T), transmembrane pressure ( $\Delta P$ ) and pH have been studied and optimised with polymer solutions (0.06 % w/w) in total recirculation mode, in order to maximize the value of the design parameters (permeate flux and rejection coefficients) [3]. Secondly, the loading capacity of PEPEI at pH 6 in respect of  $\text{Cu}^{2+}$  ions was determined. This study resulted in a loading capacity of PEPEI of 208 mg  $\text{Cu}^{2+}$ /g PEPEI, which represent a value in the same order than that obtained for the non-ethoxylated polyethylenimine [4].

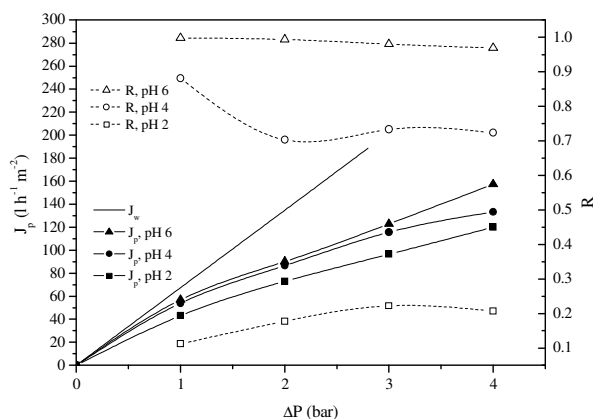


Figure 1: Influence of transmembrane pressure on permeate fluxes and metal rejection coefficients.  $T = 50\text{ }^\circ\text{C}$ ,  $C_{\text{PEPEI}} = 0.06\text{ \% w/w}$ ,  $C_{\text{Cu}} = 125\text{ ppm}$ ;  $v_t = 3.2\text{ m s}^{-1}$ .

This means that the partial substitution of primary amines by hydroxyl groups does not clearly affect polymer capacity to bind copper ions.

Next, the influence of pH on copper retention has been studied, what allows the determination of the optimal working pH for retention and regeneration steps, if the latter were carried out chemically. Fig. 1 represents the influence of pH on permeate fluxes and metal rejection coefficients. From this figure, one can establish that, if the regeneration step were carried out chemically, it would be necessary a pH lower than 2 to assure low metal rejection coefficients. To finish with ultrafiltration experiments, both concentration polarization and fouling phenomena were studied and modelled for PEPEI and PEPEI-Cu solutions in discontinuous mode. The main conclusion of this last study is that fouling is the main phenomenon that causes flux decline at the conditions tested in the present work.

In respect of the polymer electrochemical regeneration study, it comprised two stages. Firstly, voltamperometric analyses of increasing complexity solutions were carried out. From these experiments, one can determine the optimal operation voltage in order to avoid competitive reactions (-0.7 V in respect of Ag/AgCl) and verify that the polymer does not suffer any oxidation or reduction process. Secondly, the influence of pH on the electrodeposition process for solutions with  $\text{Cu}^{2+}$ , PEPEI and  $\text{Na}_2\text{SO}_4$  as electrolyte was studied at constant voltage (Fig. 2). An optimal pH value less extreme (pH = 3.3) was obtained for electrochemical regeneration than that necessary if the regeneration were carried out chemically (pH = 2).

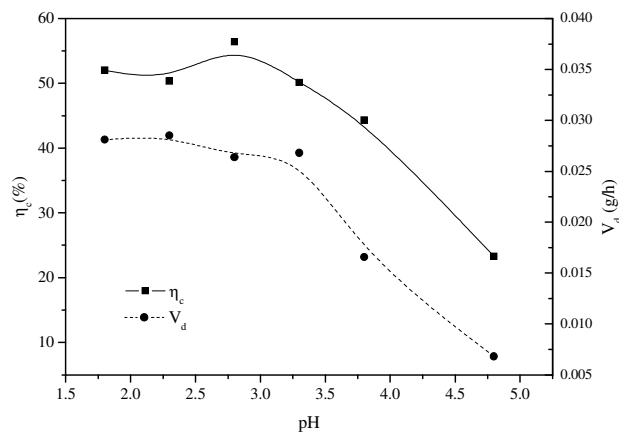


Figure 2: Influence of pH on current efficiency ( $\eta_c$ ) and deposition velocity ( $V_d$ ) for experiments at constant voltage.  $C_{\text{PEPEI}} = 0.1$  % w/w,  $C_{\text{Cu}} = 200$  ppm;  $V = -0.7$  V vs. Ag/AgCl., pH = 2.

## References

- [1] Cañizares, P., Pérez, Á., Camarillo, R., Llanos, J., López, M. L., (2007) *Desalination*, 206 602-613.
- [2] Barron-Zambrano, J., Laborie, S., Viers, Ph., Rakib, M. and Durand, G. (2004) *Journal of Membrane Science*, 229, 179-186.
- [3] Cañizares, P., De Lucas, A., Pérez, Á. and Camarillo, R. (2005) *Journal of Membrane Science*, 253, 149-163.
- [4] Kislenco, V. N. and Oliynyk, L.P. (2002) *J. Polym. Sci. Pol. Chem.*, 40, 914-922.



## **Influence of the nature of the ionic liquid on the selective transport of the substrates and products of transesterification reactions through supported liquid membranes based on ionic liquids**

F. J. Hernández-Fernández\*, A. P. de los Ríos, F. Tomás-Alonso, D. Gómez, M. Rubio and G. Vállora

*Department of Chemical Engineering, Faculty of Chemistry, University of Murcia, P.O. Box 4021, Campus de Espinardo, E-30100, Murcia, Spain.*

*\*E-mail: fjhernan@um.es*

### **1. Summary**

The present work seeks to broaden the field of application of supported ionic liquid membranes to the selective separation of the substrates and products of a transesterification reaction, for possible use in future integrated reaction/separation processes. This work analysed the transport of vinyl butyrate, 1-butanol, butyl butyrate and butyric acid, substrates and products of a transesterification reaction, through ILs based on the 1-n-alkyl-3-methylimidazolium cation (n-butyl, n-octyl) and the hexafluorophosphate, tetrafluoroborate or bis{(trifluoromethyl)sulfonyl}imide anions immobilized in Nylon membranes, evaluating the influence of the hydrophobic/hydrophilic character of the ionic liquids on the behaviour of the resulting supported liquid membranes.

Keywords: supported liquid membranes, ionic liquids, selective transport, transesterification reaction

### **2. Extended Abstract**

Supported liquid membranes (SLMs) is recognized as one of the most promising membrane-based techniques [1]. Although SLMs have been widely studied for the separation and concentration of a variety of compounds and present many potential advantages over other separation methods, there have been very few large scale applications of SLM due to insufficient membrane stability, which can be due to the loss of the solvent from the membrane. One potential solution of this problem is employing ionic liquids (ILs) as a liquid membrane phase. Ionic liquids are organic salts that are liquid close to room temperature. They normally consist of an organic cation, being the most commonly used dialkylimidazolium and tetraalkylammomium salts, and a polyatomic inorganic anion (e.g.  $\text{BF}_4^-$ ,  $\text{PF}_6^-$ ) [2]. The use of ILs as liquid membrane phase results in the stabilization of the SLM because ionic liquid have

negligible vapour pressure and their solubility in the surrounding phases can be minimized by adequate selection of the cation and the anion [3].

This work analysed the transport of vinyl butyrate, 1-butanol, butyl butyrate and butyric acid, substrates and products of a transesterification reaction, through ILs based on the 1-n-alkyl-3-methylimidazolium cation (n-butyl, n-octyl) and the hexafluorophosphate, tetrafluoroborate or bis{(trifluoromethyl)sulfonyl}imide anions immobilized in Nylon membranes, evaluating the influence of the hydrophobic/hydrophilic character of the ionic liquids on the behaviour of the resulting supported liquid membranes.

The experimental device consisted in a diffusion cell made of two independent compartments of equal volumes separated by the SLM. Control experiments were performed without ionic liquids, showing no selectivity for the transport. However, significant permeability difference between the organic compounds was observed when ionic liquids were supported in the Nylon membranes.

In order to analyze the influence of the hydrophobic/hydrophilic character of the ionic liquids on the efficiency of separation, this parameter has been measured as the partition coefficients of each ionic liquid between octanol and water ( $K_{ow}$ ). It has been observed that an increase in the hydrophilic character of the ionic liquid is in agreement with an increase in the efficiency of separation. The best results were obtained when [bmim<sup>+</sup>] [BF<sub>4</sub><sup>-</sup>] was supported in the Nylon membrane. The evolution of different organic compounds concentration in the receiving phase using this SLM can be observed in the Figure 1.

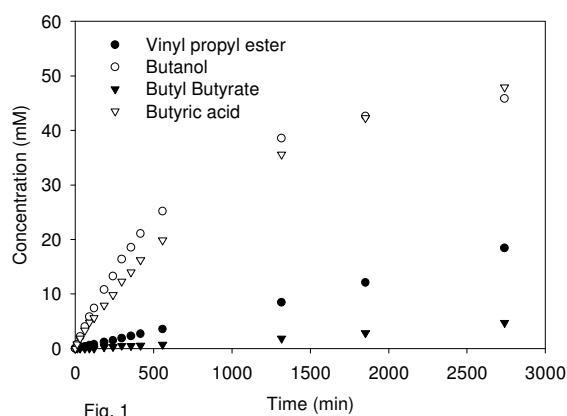


Fig. 1

### Acknowledgment

This work was partially supported by the CICYT CTQ2005-09238/PPQ grant.

### References

- [1] J. T. F. Keurentjes, L. J. W. M. Nabuurs, E. A. Vegter., (1996) *Journal of Membrane Science*, 113, 351–360.
- [2] J. F. Brennecke, E. J. Maginn., (2001), *AIChE Journal*, 47, 2384-2389.
- [3] F. J. Hernández, A. P. de los Ríos, M. Rubio, F. Tomás-Alonso, D. Gómez, G. Vllora., (2007), *Journal of Membrane Science*, 293, 73-80.

## **MFI-type zeolite dispersed in rubbery polymers: influence on surface and transport properties**

G. Clarizia, C. Algieri, E. Drioli

*Research Institute on Membrane Technology, ITM-CNR, c/o University of Calabria via P. Bucci, cubo 17/C, 87030 Arcavacata di Rende (CS), Italy.*

### **1. Summary.**

The effect of MFI zeolite in different rubbery polymers (PDMS and SBS) has been investigated. Mixed matrix membranes, prepared by dry-inversion phase method, have been characterised morphologically by scanning electron microscopy (SEM) and contact angle measurements. Transport properties have been measured at different temperatures using pure gases. The experimental results showed that MFI filler acts as a molecular sieve in the hybrid membranes by facilitating the permeation of smaller molecules and hindering that of larger molecules.

Keywords: gas separation, mixed matrix membrane, rubbery polymers, zeolite

### **2. Extended Abstract**

The combination of organic and inorganic phases by means of the dispersion of a filler in a polymer matrix is an interesting route to modify the physical and transport properties of various materials [1, 2]. Adhesion problems can represent a significant limit in the development of mixed matrix membranes based on glassy polymers, which are widely used for separations on industrial scale. On the contrary the performance of the rubbers, in principle less appropriate to achieve remarkable separation factors, can be favourably improved via adequate inorganic fillers without defects at the interfaces polymer-crystal [3]. In this framework the effect of MFI-type zeolite, dispersed into different rubbery polymers, has been investigated.

Microscopic investigations showed as the membrane morphology and the zeolite distribution within the polymer matrix are strongly affected by the filler concentration. In fact at low zeolite contents, a stratification close to the bottom side was observed, while at high zeolite concentrations the crystal distribution seems homogeneous along the membrane cross section (see figure 1).

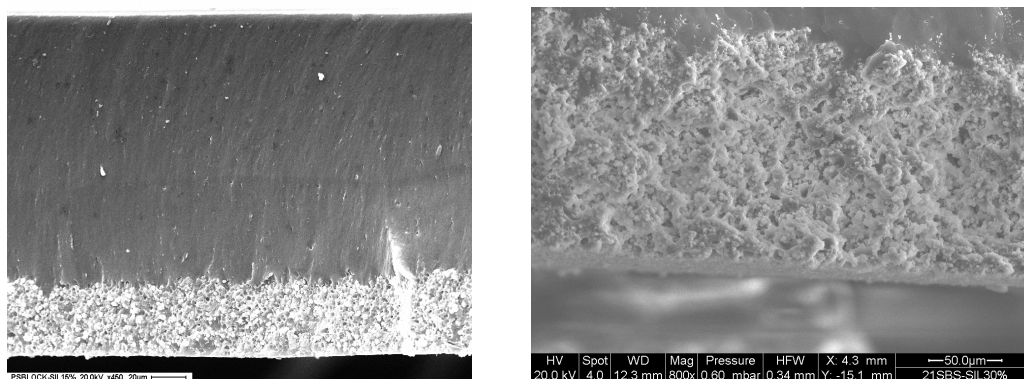


Figure 1. Cross section of different hybrid samples (a: MFI-SBS, 15 wt.%; b: MFI-SBS, 30 wt.%)

Water contact angle measurements showed an increase of the hydrophobic character of the hybrid samples as a function of the zeolite content for all polymer matrices. However, significant differences between bottom and upper (exposed to air) membrane sides have been observed due to the filler distribution, as above discussed. For what concerns the transport properties, the presence of the zeolite filler determines, according to a different behaviour of permanent gases at temperature changes, the inversion of the permeation rate order of some species with respect to the original polymer. In fact, the permeability of the more condensable gases, characterised by a big kinetic diameter and also by a significant solubility value, results more affected by the zeolite presence due to molecular sieving prevailing on the surface adsorption mechanism. Although the gas species investigated have kinetic diameter smaller than zeolitic channels, the partial pore blockage of the zeolite pores by the polymer chains justifies this behaviour. Nevertheless, this trend becomes less important as operating temperature rises.

## References

- [1] Moore T.T., Koros W.J., (2005) *J. Molecular Structure*, 739, 87-98.
- [2] Li Y., Guen, H.-M., Chung T.-S., Kulprathipanja S., (2006) *J. Membrane Sci.*, 275, 17-28.
- [3] Clarizia G., Algieri C., Drioli E., (2004) *Polymer*, 45, 5671-5681.

## Stability studies of supported liquid membranes based on ionic liquids using SEM/EDX techniques

A.P. de los Ríos <sup>a\*</sup>, F.J. Hernández-Fernández <sup>a</sup>, F. Tomás-Alonso <sup>a</sup>, J.M. Palacio <sup>b</sup>, D. Gómez <sup>a</sup>, M. Rubio <sup>a</sup> and G. Vllora <sup>a</sup>

<sup>a</sup>Department of Chemical Engineering, Faculty of Chemistry, University of Murcia, P.O. Box 4021, Campus de Espinardo, E-30100, Murcia, Spain

<sup>b</sup>Institute of Catalysis and Petrochemistry, Spanish Council for Scientific Research (CSIC), Campus de la UAM, Cantoblanco, 28049, Madrid, Spain.

\*E-mail: aprios@um.es

### 1. Summary

This work evaluates the operational stability of six different supported liquid membranes (SLMs) based on ionic liquids (ILs). [bmim<sup>+</sup>][PF<sub>6</sub><sup>-</sup>], [bmim<sup>+</sup>][BF<sub>4</sub><sup>-</sup>] and [bmim<sup>+</sup>][NTf<sub>2</sub><sup>-</sup>] were used as supporting phase in Nylon<sup>®</sup> membranes. Scanning electron-microscopy (SEM) combined with Energy Dispersive X-ray (EDX) analysis was used to characterize the membrane surface morphologically and examine the global chemical composition of the membranes and the distribution of the ILs within them.

Keywords: supported liquid membranes; ionic liquids; SEM-EDX spectroscopy; operational stability.

### 2. Extended Abstract

Among membrane-based separation processes, the use of supported liquid membranes (SLMs) has received growing attention during recent years [1]. SLMs are porous supports whose pores are filled with a liquid; among their numerous advantages is the fact that the amount of solvent needed in the SLM process is minimal and that the processes of extraction and stripping are combined into one single stage. Nevertheless, their industrial application is still limited, mainly due to concerns about SLM stability and long-term performance [2]. Supported liquid membranes with conventional liquids eventually deteriorate due to liquid vaporization, dissolution into a contacting phase, and displacement from the porous structure under low-pressure gradient (<10 kPa). A recently revealed clean alternative to the classical organic solvents are ionic liquids [3]. They are organic salts that are liquid close to room temperature and they normally consist of an organic cation and a polyatomic inorganic anion.

In a previous work [4], SLMs based on ionic liquid were successfully applied for the selective separation of the substrates and products of a transesterification reaction. All the assayed SLMs showed excellent operational stability when tested over eight continuous cycles of 48 hours each. On the basis of these results, our aim in this work was to microscopically characterize by SEM-EDX the operational stability of six different SLMs based on ILs. Nylon<sup>®</sup> membranes were used as supporting membranes, in which three ILs ([bmim<sup>+</sup>][BF<sub>4</sub><sup>-</sup>], [bmim<sup>+</sup>][PF<sub>6</sub><sup>-</sup>] and [bmim<sup>+</sup>][Tf<sub>2</sub>N<sup>-</sup>]) were immobilized.

In the first step, the resulting supported liquid membranes were analyzed by SEM and EDX. The EDX spectra referenced to the F K $\alpha$  peaks found that Nylon membranes impregnated with [bmim<sup>+</sup>][PF<sub>6</sub><sup>-</sup>], [bmim<sup>+</sup>][BF<sub>4</sub><sup>-</sup>] and [bmim<sup>+</sup>][NTf<sub>2</sub><sup>-</sup>] showed the expected concentration of ILs in the bulk of membranes, in complete agreement with the morphological appearance of samples evidenced by SEM micrographs. In the cases of [bmim<sup>+</sup>][PF<sub>6</sub><sup>-</sup>] and [bmim<sup>+</sup>][BF<sub>4</sub><sup>-</sup>], a thin layer of ionic liquid were present on the membrane surface as was evidenced by SEM micrographs.

In the second step, stability experiments were performed keeping the membranes with supported ILs immersed for a week in a diffusion cell with hexane/hexane in both – feed and receiving- compartments. The EDX analyses showed that in all cases the ionic liquid was not displaced from the membrane pores. Furthermore, SEM micrographs of Nylon membranes impregnated with [bmim<sup>+</sup>][BF<sub>4</sub><sup>-</sup>] and [bmim<sup>+</sup>][NTf<sub>2</sub><sup>-</sup>] showed the same morphological appearance than before the immersion in hexane. However, SEM micrographs of Nylon membrane impregnated with [bmim<sup>+</sup>][PF<sub>6</sub><sup>-</sup>] evidenced that part of the ionic liquid layer present on the membrane surface before the immersion in hexane was rinsed during contact with the hexane solution, which could be due to a little solubilization of the ionic liquid in hexane.

### Acknowledgment

This work was partially supported by the CICYT CTQ2005-09238/PPQ grant. A. P. de los Ríos and F.J. Hernández-Fernández have fellowships from the Spanish Ministry of Education and Science and the University of Murcia, respectively.

### References

- [1] G. Muthuramam and K. Palanivelu, (2006), *Dyes Pigments*, 70, 99-104.
- [2] M. Teramoto, Sakaida, S.S. Fu, N. Ohnishi, H. Matsuyama, T. Fukui and K. Arai, (2000), *Separation and Purification Technology*, 21, 137-142.
- [3] M.J. Earle and K.R. Seddon, (2000), *Pure and Applied Chemistry*, 72, 1391 –1398.
- [4] F. J. Hernández, A. P. de los Ríos, M. Rubio, F. Tomás-Alonso, D. Gómez, G. Vllora., (2007), *Journal of Membrane Science*, 293, 73-80.

## Session T2-9: Crystallization

<b>Abstract Number</b>	<b>Paper Title &amp; Authors</b>	<b>Included</b>
680	Crystallizing the Right Polymorphic Form: An Integrative Approach C Wibowo, S W Lin, K M Ng	Yes
886	Investigation, mathematical modelling and simulation of the crystallisation process in a circulation crystalliser M I Dorofeeva, E M Koltsova, A Lieb, M Kind	Yes
1504	Tailoring Morphology and Particle Size Distributions via Crystallization J Heinrich, J Ulrich	Yes
2854	The application of different seeding techniques for solution crystallization of ammonium sulphate R Lakerveld, A N Kalbasenka, H J M Kramer, P J Jansens, J Grievink	Yes
3158	Contribution of crystal-impeller and crystal-crystal collisions to the secondary nucleation A Imran, E Wolf, H J M Kramer, P J Jansens	Yes
3894	Towards Predictive Simulation of Single Feed Semibatch Reaction Crystallization Å C Rasmuson, M Ståhl	Yes

Session T2-9



## Crystallizing the Right Polymorphic Form: An Integrative Approach

C. Wibowo,<sup>a</sup> S. W. Lin,<sup>b</sup> K. M. Ng<sup>c</sup>

<sup>a</sup>*ClearWaterBay Technology, Inc., 4000 W. Valley Blvd., Suite 100, Pomona, CA 91789, USA*

<sup>b</sup>*Mitsubishi Chemical Group Science and Technology Research Center Inc., 1000 Kamoshida-cho, Aoba-ku, Yokohama 227-8502, Japan*

<sup>c</sup>*Department of Chemical Engineering, Hong Kong University of Science and Technology, Clear Water Bay, Kowloon, Hong Kong*

### 1. Summary

An integrative approach is presented for synthesizing a process to crystallize a specific polymorphic form. By considering crystallization compartments, metastable zones and crystallization kinetics of different polymorphs, strategies for obtaining the desirable form can be developed. The progress of crystallization is followed by visualizing how the process paths move around different regions of a solid-liquid equilibrium phase diagram.

Keywords: crystallization, polymorph, active pharmaceutical ingredient, process development

### 2. Extended Abstract

One of the most important issues in the development of crystallization processes for active pharmaceutical ingredients (APIs) is to obtain the desired polymorphic form of the product. While identical in chemical composition, polymorphs of the same API may exhibit markedly different physical and chemical properties. For example, different crystal shapes can have a considerable influence on downstream processing steps such as filtration, washing, and bulk solids handling, while a difference in solubility can affect the bioavailability and efficacy of the drug. Thus, selecting the right polymorph for formulation and being able to produce it in a consistent manner are exceedingly important in pharmaceutical processing. As an additional challenge, interconversion among polymorphs may occur during and after the manufacturing process.

Polymorphic crystallization is controlled by both thermodynamics and kinetics. An integrative approach which combines fragmented and incomplete data, experimental observations, physical insights and modeling related to these factors, has been

developed for the development of a process to produce a desired polymorphic form (Lin et al., 2007). The approach begins with a representation of the equilibrium phase behavior of the system in the form of a phase diagram. The crystallization compartments and the metastable zones are identified. Crystallization kinetics is determined either qualitatively or quantitatively. The necessary experimental work, calculations and polymorph recovery strategy development are expected to take place side-by-side in an iterative manner. This iterative scheme would converge to a handful of process alternatives that satisfy the overall objective, as summarized in Figure 1. The rationale behind the process alternatives is made clear by visualizing how the process paths venture into different regions in composition space. Experiential heuristics are also identified to guide the user in making decisions during each step. By implementing the proposed approach, the manufacturing process can be strictly monitored and ensuring the correct polymorphic form is consistently obtained.

## References

Lin, S. W., Ng, K. M. and Wibowo, C., (2007) *Ind. Eng. Chem. Res.*, 46, 518-529.

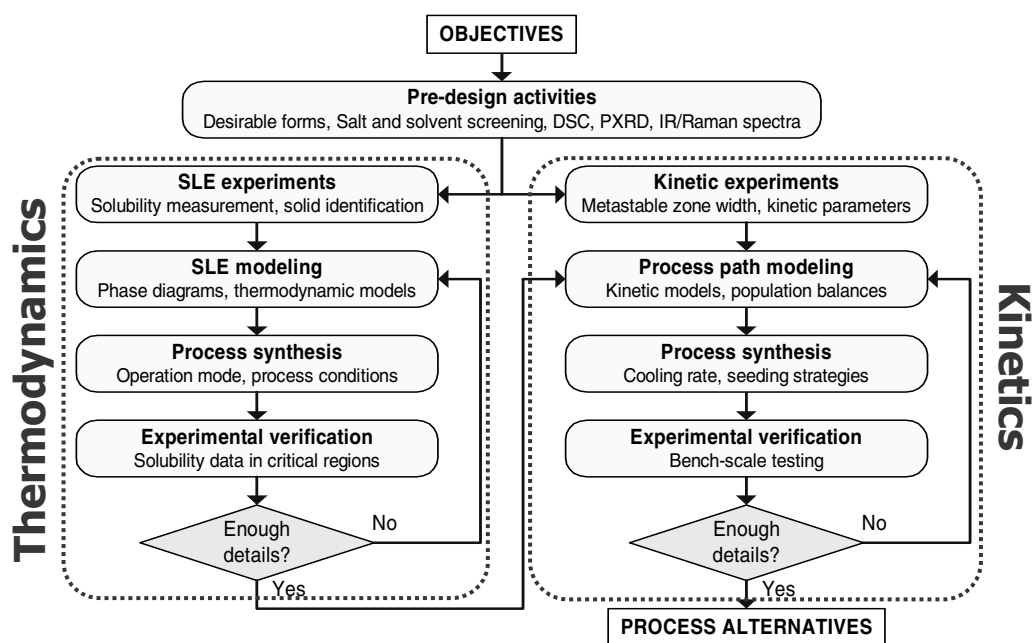


Figure 1. Integrative approach for developing polymorphic crystallization processes.

## **Investigation, mathematical modelling and simulation of the crystallisation process in a circulation crystalliser**

M. I. Dorofeeva,<sup>a</sup> E. M. Koltsova,<sup>a</sup> A. Lieb,<sup>b</sup> M. Kind<sup>b</sup>

<sup>a</sup>*Department of Cybernetics of Chemical Engineering, D. Mendeleev University of Chemical Technology of Russian, Miusskaya pl., 9, 125047 Moscow, Russia*

<sup>b</sup>*Institute of Thermal Process Engineering (TVT), University of Karlsruhe (TH), Kaiserstr. 12, Geb. 10.91, 76131 Karlsruhe, Germany*

### **1. Summary**

The industrial crystallisation of well soluble substances is often dominated by secondary nucleation, in particular contact nucleation, and crystal growth. In different crystallisers types the attrition is mainly caused by the crystals impact onto stirrer blades, pumps, etc. The ultimate objective is to quantitatively describe a crystallization process, which is governed by the formation and growth of attrition fragments.

Keywords: secondary nucleation, attrition, crystallization, mathematical modelling, ammonium sulphate

### **2. Extended Abstract**

For the investigation of attrition and growth mechanisms a number of experiments have been carried out with the crystallizing system ammonium sulphate in the lab-scale. They have been carried out attrition experiments for different seed crystals in size under variation of the volumetric flow and, as a result, under variation of the impingement velocity of the crystals, and crystallization experiments under variation of volumetric flow, nozzle diameter and feed rate. All experiments have been lead in a continuously operated 5.85-liter-forced circulation crystalliser (FC-crystalliser), which uses a particularly gentle pump to circulate the suspension at minimal attrition of crystals. The attrition behavior of crystals has been investigated by imposing to them additional mechanical stress with the help of an impingement device implemented in the slurry loop. This device consists of a nozzle and an orthogonal positioned cylinder. The formation of attrition fragments was preceded by crystals collides with this cylinder. During all experiments the particle size distribution and the mean particle size were measured with the help of a laser diffraction spectrometer.

During crystallization experiments the supersaturation of the solution was obtained via density measurement.

The attrition process and the crystallization process were quantitatively described. The mathematical model of the attrition process is based on the theoretical considerations of Gahn and Mersman. While mathematical modeling each of the processes was subdivided in separate zones. The process only with crystals attrition was subdivided in only one zone – the attrition. The crystallization process with crystals attrition and their subsequent growth was subdivided in mixing, cooling, attrition, growth and sampling zones. Mass, energy and population balances have been presented for each zone. Necessary model parameters have been determined in the process of experimenting. Equation of particle number conservation for the attrition zone, growth rate equation and growth parameters of the ammonium sulphates crystals have been selected in the process of calculations. Median crystals size, supersaturation and particle sizes distribution have been calculated for all experiments conditions and compared with the experimental findings. During calculations the influence of volumetric flow, nozzle diameter, target size and feed rate on a product characteristics have been determinate.

The mathematical model of the industrial crystallization process in a FC-crystalliser has been designed, because the purpose of the modeling is an opportunity to predict the median crystals size and the particle size distribution. The mathematical model includes mixing, attrition (axial-pump), growth (crystalliser) and sampling zones. During calculations it has been revealed, that change of a product characteristics has oscillatory character. The influence of pumps propeller frequency, propeller blades number, feed rate and feed concentration on a product characteristics and on parameters of their fluctuations have been determinate. With the help of calculations process optimization for the reception a product of certain size at a minimal power input has been done. The operating mode of the triple-blades axial-pump has been chosen, the pump has been picked up and its operating mode has been chosen.

For the calculation of all considered processes a Delphi 7.0 program has been developed. The program allows executing calculations for different crystal's system and operation conditions.

This work was supported by grant of PRO3 e. V. (Pro3 process engineering expertise network) and grant RFBR № 07-08-00357-a.

## **References**

Gahn, C., Mersman, A., (1999) Brittle fracture in crystallization processes, *Chemical Engineering Science*, 54,1273-1292.

## **Tailoring Morphology and Particle Size Distributions via Crystallization**

J. Heinrich,<sup>a</sup> J. Ulrich,<sup>a</sup>

*<sup>a</sup>Department of Thermal Separation Processes, Martin-Luther-University Halle-Wittenberg, D-06099 Halle (Saale), Germany*

### **1. Summary**

The design of crystallization equipment depends on a sound knowledge of the underlying kinetics that are determined by a number of simultaneously occurring processes such as nucleation, growth, attrition and agglomeration and where applicable polymorphic transformation. Consequently, the determination of rate constants still requires high resource expenditure in form of number of experiments and amounts of starting material to retrieve the necessary information. The objective of this study is to speed the determination of kinetics by combining “in-situ” measurement techniques, time dependent batch trials and a model based experimental design and analysis strategy to derive kinetic constants. Additionally, experimental data will highlight how the crystal properties of the model system can successfully be tailored to satisfy specified needs.

Keywords: crystallization, kinetics, population balance, in-situ measurement probes, model based experimental analysis

### **2. Extended Abstract**

Crystallization from solution is not only a standard separation technique, but it is also a powerful method to design and tailor particle properties that satisfy consumer needs. Beside morphology, purity and form, the mean particle size and particle size distribution are important properties of a crystalline product [Ulr04]. However, this high potential in tailoring specific particle properties still requires high resource expenditure. Combining “in-situ” measurement techniques, time dependent batch trials and a model based experimental design and analysis strategy the required number of experiments can significantly be reduced by maximizing the information content of the experimental data at the same time. Although each technique for its own has been widely validated and proven to be beneficial, the combination is seldom employed [Hei07].

The crystallization of ammonium chloride that has rarely been studied in literature will serve as a model system. Experimental data are recorded using a batch laboratory crystallizer equipped with an “in-situ” MTS 3D-ORM and a SensoTech LiquidSonic probe measuring chord length distribution and supersaturation, respectively. The chord length distribution is converted to a corresponding particle size distribution using the method described by Worlitschek et al. [Wor05].

Experimental results will focus on the crystallization behaviour of ammonium chloride from a kinetic as well as particle properties point of view. It will be presented how the morphology can successfully be changed from an dendritic to an elliptical shape using an additive, leading to a reduced rate of crystal breakage (see figure 1).

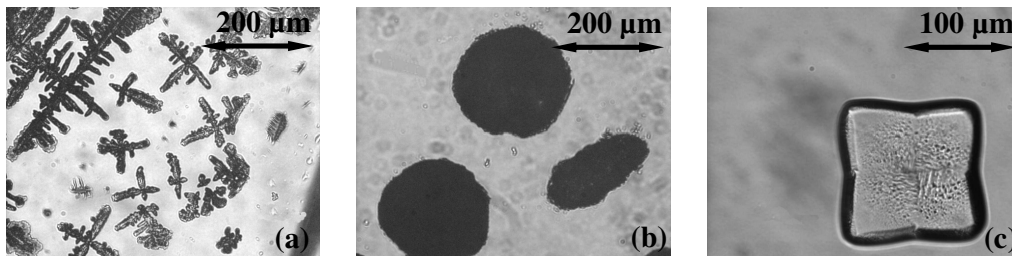


Figure 1: (a)  $\text{NH}_4\text{Cl}$ -Water (stirred solution), (b)  $\text{NH}_4\text{Cl}$ -Water-Additive (stirred solution), (c)  $\text{NH}_4\text{Cl}$ -Water-Additive (stagnant solution)

Furthermore, it will be illustrated how different process conditions alter agglomeration kinetics and how it can be avoided. The experimental work and optimization of crystal properties is supported by using a model based experimental analysis strategy. The model is given by a two-dimensional population balance model, incorporating growth, nucleation and attrition as described according to Baumann et al. [Bau83]. Estimated kinetic parameters will be presented.

Based on new experimental data, the study will show how the crystal properties of ammonium chloride can be tailored successfully. Moreover, it will be highlighted that the combination of “in-situ” measurement techniques, time dependent batch trials and model based experimental design and analysis strategy is a powerful tool. It allows to base decisions on all knowledge that is available in form of experimental data and differential equations. This leads to a significantly reduced time in the development and optimization of new crystallization processes.

## References

- Baumann, K.-H., (1983) *Crystal Research and Technology*, 18(12), 1547-1553.
- Heinrich, J., Ulrich, J., (2007) in *PARTEC 2007 – Proceedings, International Congress on Particle Technology*, Nürnberg, Germany, CD-ROM
- Ulrich, J., Jones, M. J., (2004) *Chemical Engineering Research & Design*, 82, 1567-1570.
- Worlitschek, J., Hocker, T., Mazzotti, M., (2005) *Particle & Particle Systems Characterization*, 22(2), 81-98.

## The application of different seeding techniques for solution crystallization of ammonium sulphate

R.Lakerveld<sup>a</sup>, A.N. Kalbasenka<sup>b</sup>, H.J.M. Kramer<sup>a</sup>, P.J. Jansens<sup>a</sup>, J. Grievink,<sup>c</sup>

<sup>a</sup>Process & Energy Department, Delft University of Technology, 2628 CA Delft, The Netherlands

<sup>b</sup>Delft Center for Systems and Control, Delft University of Technology, 2628 CD Delft, The Netherlands

<sup>c</sup>Product & Process Engineering, Delft University of Technology, 2628 BL Delft, The Netherlands

### 1. Summary

Seeding was applied to a 75L draft tube crystallizer operated in evaporative fed-batch mode for an ammonium sulphate water system. Seeding can be applied to improve product quality and reproducibility compared to unseeded operation. The use of ground seeds is complicated by breeding fragments adhering to the surface and lack of stability due to the presence of lattice strain. It demands a careful preparation procedure and causes partial dissolution upon introduction in the crystallizer. Seeds that are prepared from product slurry do not suffer from this drawback. However, the large median size and broad crystal size distribution (CSD) of this seeding material result in excessive nucleation and a broad final product CSD. Seeds that are produced with primary nucleation in the seeding vessel can combine the favorable properties of previous seeding methods. An anti-solvent was used to produce a large amount of nuclei and therefore a large specific area. The weak point of this procedure is the occurrence of agglomerates which reduces the specific surface area. Ultrasound is an interesting process actuator to circumvent this drawback.

Keywords: Batch crystallization, Seeding, Ultrasound, Nucleation, Crystal growth

### 2. Extended Abstract

The design and operation of solution crystallization processes still pose many challenges despite its wide application in chemical industry. In case of batch-wise operation, the reproducibility between the batches is one of these challenges. Fed-batch experiments show a strong dependency of the final product on the initial conditions of a batch. Primary nucleation results in ill-defined initial conditions and therefore seeding is often applied as an additional process actuator. This contribution will analyze in more detail the influence of seed quality on the reproducibility between batches and the final product quality for an ammonium sulphate water system. The aim is to find the critical seed mass for ideal growth, which means that the number of crystals do not change. A high seed load is needed for ideal growth if a system is very sensitive for nucleation. A high seed load is often not practical and results in a small product size. Therefore, also an experimental critical seed load is

defined as the seed load that improves reproducibility and product quality in terms of median size and distribution width compared to unseeded operation.

Seeding with ground seeds was applied to a 75L draft tube (DT) crystallizer operated in evaporative fed-batch mode. It was found experimentally that the surface of the seeds in the seeding vessel heals and breeding fragments dissolve. The median size of the seeds increased and reached a steady state after approximately 60 minutes ( $L_{50} = 220 \mu\text{m}$ ). The seed mass was the only degree of freedom for the experiments.

Figure 1 shows the results of the seeding experiments with ground seeds in a seeding chart. It shows the ratio of seed to product mass ( $C_s$ ) as function of product size ( $L_p$ ). The graph also contains the results obtained by Hojjati et al. (2005) for cooling crystallization of ammonium sulphate on lab-scale. It is interesting to note that the results are well comparable despite the significant differences in crystallization method, scale and yield. It can be concluded that ideal growth is only reached with seed masses that are in the same order of magnitude as the final yield.

Seeding can improve the reproducibility and product quality compared to unseeded operation. In our specific case the minimum seed load was 2.8% of the final yield. For lower seed masses partly dissolution of the seeds and nucleation events were detected, which resulted in poor reproducibility and product quality. Excessive nucleation was observed for experiments in which the product slurry of a previous batch was used as seeding material. These seeds did not have the tendency to dissolve as was the case for the ground seeds.

Seeding experiments are also done in a bubble column crystallizer to investigate the source of nucleation. The bubble column does not have any moving parts or a circulation pump. The mixing is provided by the upward velocity of the bubbles and supersaturation is generated by simultaneously cooling and evaporation. Ideal growth is already approached for a low seed mass (see figure 1). It demonstrates that attrition is the main source of nucleation in the DT crystallizer.

Current research focuses on the combination of the favorable properties of the ground seeds and the product slurry seeds. The aim is to produce small seed crystals with primary nucleation in the seeding vessel for which different approaches are investigated. An anti-solvent was used to produce a large amount of nuclei. The main obstacle is to prevent agglomeration of the particles. Experiments in the 75L crystallizer showed a very rapid outgrowth of the seed material indicating a reduced surface area due to agglomeration. Ultrasound is an alternative method to produce seed crystals with a high specific surface area (Virone et al., 2005). Current research progresses in this direction.

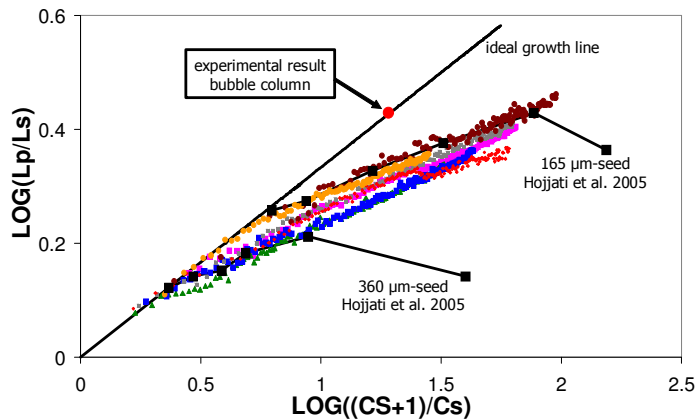


Figure 1: Seed chart. dotted lines are results from 75L DT

## References

- Virone, C., Ter Horst, J.H., Kramer, H.J.M., Jansens, P.J. (2005) *Journal of Crystal Growth*, 275, e1397 - e1401  
 Hojjati, H., Rohani, S. (2005) *Chemical Engineering and Processing*, 44, 949-957



## **Contribution of crystal-impeller and crystal-crystal collisions to the secondary nucleation**

A. Imran, E. Wolf, H.J.M. Kramer, P.J. Jansens

*Process & Energy Department, Delft University of Technology, Leeghwaterstraat 44, 2628 CA Delft, The Netherlands*

### **1. Summary**

A secondary nucleation model mainly based on the findings of Ottens (1973) and Evans (1974) considering both crystal-impeller collisions and crystal-crystal collisions was investigated using experimental data obtained from two crystallizers of different scale and configuration which are operated continuously in an evaporative mode for the crystallization of ammonium sulfate. The crystal size distribution (CSD) prediction is consistent with the measured data for all investigated experiments.

Keywords: crystal-impeller collisions, crystal-crystal collisions, secondary nucleation, industrial crystallization.

### **2. Extended Abstract**

It is now well-established that secondary nucleation plays an important role in determining the product crystal size distribution in most forms of industrial suspension crystallizer. Possible mechanisms of secondary nucleation are numerous though one which is widely reported concerns contact or collision breeding which occurs as a result of impacts of crystals with each other and/or with other solid objects, e.g. vessel walls or a rotating impeller. Ottens et al. (1972) was the first to develop a mechanistic description of the mechanical interaction of the crystals with the crystallizer hardware in which the nucleation rate of the crystals is assumed to be proportional to the product of collision energy and frequency of collision. Moreover a lower bound of integration was introduced into the distribution in order to account for the phenomenon that larger crystals are more prone to attrition. Another approach towards the simulation of the dynamics of the crystallization process was introduced by Ó Meadhra (1995), who determined an attrition function for the parent crystals under growing conditions. Gahn and Mersmann (1999) developed a more fundamental approach of the generation of secondary nuclei based on material properties and physical concepts. Although these models can be used to describe the steady-state CSD, they fail to describe the dynamics in a crystallization process and to

predict the nucleation behavior for different process conditions. In present contribution, a secondary nucleation model is developed based on the work of Ottens (1973) and Evans (1974), which considers both crystal-impeller and crystal-crystal collisions. The aim of the research is develop a model, which is capable to describe the dynamic behavior of the crystallization process and can predict the nucleation behavior, not only for different impeller frequencies, but also for different scales and configuration.

Two crystallizer types, a 22-liter Draft Tube (DT) crystallizer and an 1100-liter Draft Tube Baffled (DTB) crystallizer are used which differ both in scale and configuration, to investigate the effect of the impeller frequency and the effect of scale on the CSD. The CSD description obtained using gPROMS simulations is consistent with the measured data for all investigated experiments. Not only the changes in the CSD due to different impeller frequencies, but also the changes due to scale and configuration are well described and model is able to capture the sustained cyclic behavior in DTB crystallizer. The developed model contains seven parameters out of which four parameters are considered to be system dependent. Three of the model parameters, the

number of nuclei per unit energy ( $\Omega$ ), the lower bound of integration for crystal-impeller and for crystal-crystal collisions are found to be the function of impeller frequency. A correlation was found between the impeller speed and the model parameter that describes the  $\Omega$ . An almost parallel linear fit on log-normal scale is found for  $\Omega$  in the 22L DT crystallizer (Figure 1) and in the 1100L DTB crystallizer. The relation is attributed to the time available for healing of the crystal corners between two subsequent collisions with the impeller. It was found that in the 22-liter DT-crystallizer crystal-impeller collisions are dominating while crystal-crystal collisions are of less importance. Nevertheless, crystal-crystal collisions cannot be neglected and are especially pronounced at low impeller frequencies. In the 1100-liter DTB-crystallizer the term of the secondary nucleation rate equation describing crystal-crystal collisions seems to be more important. This effect cannot be attributed only to crystal-crystal collisions, but suggest the existence of a different secondary nucleation mechanism. Since the supersaturation in the DTB-crystallizer is higher and the circulation time is larger compared to the DT-crystallizer, it is expected that also the surface breeding could occur in this crystallizer. Dedicated experiments are discussed to validate this hypothesis.

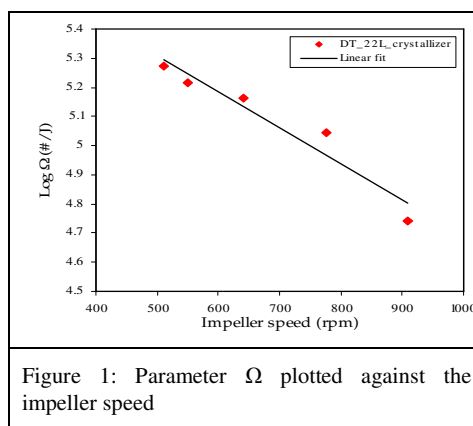


Figure 1: Parameter  $\Omega$  plotted against the impeller speed

## References

Evans, T. W., Sarofim, A. F., and Margolis, G., *AIChE J.*, 20, 950–959, 1974.

Ottens, E. P. K., Janse, A., and de Jong, *Journal of Crystal Growth*, 13/14, 500–505, 1972.

## **Towards Predictive Simulation of Single Feed Semibatch Reaction Crystallization**

Åke C. Rasmuson; Marie Ståhl

*Department of Chemical Engineering and Technology, Royal Institute of Technology, KTH, SE 100 44 Stockholm, Sweden*

### **1. Summary**

In the present work a population balance model is developed of single feed semi-batch reaction crystallization of benzoic acid. The model accounts for chemical reaction, meso- and micromixing, nucleation, crystal growth and growth rate dispersion and is evaluated against experimental data. When mixing is described as engulfment with inertial-convective mesomixing, and growth rate dispersion is accounted for, the model quite well captures the influence of process conditions (reactant concentrations, agitation rate, feed point location, feed pipe diameter, total feeding time and crystallizer volume) on the product weight mean size. It is also found that the kinetics of nucleation and crystal growth have a strong influence on the results of the simulations, influencing the product weight mean size as well as the response to changes in the processing conditions.

Keywords: reaction crystallization, precipitation, kinetics, mixing, population balance modelling

### **2. Extended Abstract**

Reaction crystallization or precipitation is used in the production of both inorganic and organic compounds, e.g. photographic materials, organic fine chemicals and pharmaceuticals. A common procedure is to feed one reactant into an agitated solution of the other reactant in a semi-batch (fed-batch) process. In reaction crystallization processes, the solubility of the formed compound is normally low or very low, and a region with high supersaturation and subsequent rapid nucleation and growth will form around the feed point. Nucleation starts before the solution has been completely homogenized, and the crystallization proceeds under conditions of partial segregation. Hence, the mixing conditions in the crystallizer will have a significant influence on the final product characteristics.

In the present work, a model is developed of single feed semi-batch reaction crystallization. A population balance model is combined with a mechanistic model of

meso- and micromixing to account for chemical reaction, mixing, nucleation, crystal growth and growth rate dispersion. The aim is to correctly describe the influence of process conditions on the product weight mean size. Two mechanistic mixing models are evaluated, and the simulation results are compared with experimental data on single feed semi-batch reaction crystallization of benzoic acid. Results for 1-litre scale experiments were published by Åslund and Rasmuson (1992), and results for 10-litre and 200-litre experiments were published by Torbacke and Rasmuson (2004). The experiments show that the product crystal weight mean size increases with decreasing reactant concentrations, and with decreasing feed rate. At low feed point mixing intensity, the mean size increases with increased mixing but at high levels this trend vanish or even becomes reversed. At low feed rates, the mean size increases with decreasing feed pipe diameter. At high feed rates the influence of the feed pipe diameter is more complex. It is found experimentally that micromixing is of some importance in most experiments, but especially the rate of mesomixing governs the process.

In the modelling and simulation of the process, it is found that when the engulfment model with inertial-convective mesomixing is adopted and growth rate dispersion is accounted for, the model quite well captures the influence of the agitation rate, the feed point location, the feed pipe diameter, the reactant concentrations, and the total feeding time on the product weight mean size. However, the results are sensitive to the kinetics of nucleation and growth. When incorrect crystallization kinetics are used, not only the magnitude of the weight mean size becomes incorrect but also the influence of the processing conditions can essentially vanish. It is found that the optimum kinetic representation is not independent of scale, i.e. a better description of experimental data is obtained when different kinetic parameter values are used for the different scales. This is likely due to that the mixing description do not fully capture the varying conditions in the different scales of experiment.

Previously determined kinetics of nucleation and growth estimated from T-mixer experiments (Ståhl et al., 2001, Ståhl et al., 2004) do not give satisfactory simulation results. A re-evaluation of the T-mixer experiments has been performed. Even though the new parameters do not give the best representation of the semi-batch experiments, the results are encouraging and suggest that further work on determination of reaction crystallization kinetics as well as on describing the mixing in agitated tank crystallizers, will allow for successful model-based predictions of the product size distribution of full scale crystallizers.

## References

- Åslund, B., Rasmuson, Å. C., (1992) *AIChE J*, 38, 328-342.  
Ståhl, M., Åslund, B. L., Rasmuson, Å. C., (2001) *AIChE J*, 47, 1544-1560.  
Ståhl, M., Åslund, B. L., Rasmuson, Å. C., (2004) *Ind Eng Chem Res*, 43, 6694-6702.  
Torbacke, M., Rasmuson, Å. C., (2001) *Chem Eng Sci*, 56, 2459-2473.  
Torbacke, M., Rasmuson, Å. C., (2004) *AIChE J*, 50, 3107-3119.

## Session T4-9P: Crystallization – Poster

Abstract Number	Paper Title & Authors	Included
685	An insight into interparticle forces and filterability of potassium sulphate crystals precipitated with ethanol and acetone M Louhi-Kultanen, A L Arnalot, L Nyström, J Kallas	Yes
1432	Cellular automata for simulation of crystallization in different mediums E R Abasheva, E M Koltsova	Yes
1734	Crystallization of Ammonium-Perchlorate from Solution of Electrolytically Produced Sodium-Perchlorate in a Pilot-Scale Plant Ž Andrić	Yes
1915	Synthesis of Small Crystals of LTA Zeolites without used Organic Compounds S Alfaro , M A Valenzuela, P Bosch	Yes
1928	Correlation of Fluid Atomization and Particle Formation in the SAS Process by Optical Laser Analysis R Schatz, A Braeuer, A Leipertz, E Schlücker	Yes
2192	Material effects on the ammonothermal crystallization of bulk GaN N Alt, E Meissner, D Kilian, E Schlücker	Yes
2226	Experimental study of different configurations to perform preferential crystallization for enantioseparation G Ziomek, M P Elsner, A S Morgenstern	Yes
2264	Influence of selected process parameters on attrition intensity in DTM type crystallizers with a jet-pump – a general neural network's approach K Piotrowski, K Pentos, M Malasinska, A Matynia	Yes
2736	Controlling of Chaos in the Process of Crystallization of Dibasic Lead Phosphite M V Cherenkov, E M Koltsova	Yes
2763	Crystallization of a polymorphic drug in a stirred tank C Herman, V Gelbgras, V Halloin, B Haut	Yes
2871	Process conditions and granulometric properties of crystals A Sander, J P Kardum	Yes
2899	CSD and the kinetic parameters of crystallization of K <sub>2</sub> SO <sub>4</sub> J P Kardum, A Sander, M Kirinčić, M Kalšan	Yes
2910	Supersaturation profiles of L-sorbose water solutions in the cooling batch crystallization process B Wierzbowska, J Koralewska, K Piotrowski, A Matynia, K	Yes

Session T2-9P

3023	Wawrzyniecki Synthesis and Characterization of Hydrotalcite-like Compounds Produced via Hydrothermal Treatment W N Budhysutanto, Y P Diego, H J M Kramer, M Reedijk, A G Talma, P J Jansens	Yes
3757	Solvent Influence on Organic Crystal Agglomeration E M Ålander, Å C Rasmuson	Yes

## **An insight into interparticle forces and filterability of potassium sulphate crystals precipitated with ethanol and acetone**

M. Louhi-Kultanen,<sup>a</sup> A. Llansana Arnalot,<sup>b</sup> L. Nyström,<sup>a</sup> J. Kallas<sup>a</sup>

<sup>a</sup>*Department of Chemical Technology, Lappeenranta University of Technology,  
P.O. Box 20, FI-53851 Lappeenranta, Finland*

<sup>b</sup>*Acciona Water, Mas Blau II Business estate, Garrigues Avenue, 22 – 2nd Floor,  
08820 El Prat de Llobregat, Barcelona, Spain*

### **1. Summary**

Solvent effects on formation of secondary crystals, in semibatch operating precipitation, were studied with potassium sulphate using acetone and ethanol as an anti-solvent. Zeta potential measurements were carried out to investigate the attractive or repulsive interaction of primary crystals forming firstly via primary nucleation and crystal growth by varying the pH of the solution. Particle size characterization was conducted using optical microscopy and image analysis. In addition to crystal size investigation to characterize the end product, the filterability of obtained crystals was determined using a Nutsche pressure filter. The obtained results showed that acetone yielded smaller crystal sizes and lower filterability than ethanol with the used precipitant feed rates. The isoelectric point for the acetone solution was obtained at a pH range of 5.5 to 6.5, whereas for the ethanol solution the isoelectric point was expected to be around a pH lower than 3.5 based on extrapolation. The zeta potential values varied less as a function of pH in acetone solutions than in ethanol solutions.

Keywords: precipitation, filterability, potassium sulphate, zeta potential, image analysis

### **2. Extended Abstract**

The present work focuses to study the influence of chemical composition on a semibatch salting-out process and downstream processing, on the filterability of the precipitate. The solvent effects on the formation of secondary crystals in precipitation and the filterability of the obtained crystals were studied with salting-out precipitation of potassium sulphate using ethanol and acetone as anti-solvents. In many applications the filterability of the crystals is a criterion used to define how good the crystals obtained by crystallization are, i.e. how trouble-free the solid-liquid

separation is and what is the required filtration time. This comes from the entire integrated crystallization process where crystallization as a unit operation is followed by solid-liquid separation in downstream processing. The main subject of the present work was to investigate salting out precipitation using two precipitants and characteristics of obtained crystals based on image analysis and filterability study, and zeta potential study of a solid-liquid suspension. The chosen compound was potassium sulphate which was precipitated from aqueous solutions with ethanol and acetone as studied anti-solvents. Based on the experimental results obtained, it seems that the feed rate has a greater influence on the primary particle size than the pH. As the size of the primary particles change with the feed rate, so does the zeta potential.

According to the obtained zeta potential results, it can be expected that in acetone solutions the primary crystals tend to form secondary crystals more easily. The external appearance of aggregates salted-out with acetone did not increase the permeability of the crystal cake to such an extent that the filterability with acetone exceeded the cake permeability of the crystal cake obtained using ethanol as the precipitant. Also greater equivalent circle diameter values when using ethanol prove that the crystal size ranges were different. The primary crystals obtained with acetone remained small causing a higher specific crystal surface in the filter cake in spite of varying precipitation conditions. The main conclusion drawn was that out-salting with ethanol yielded crystals more easy to filter than acetone.

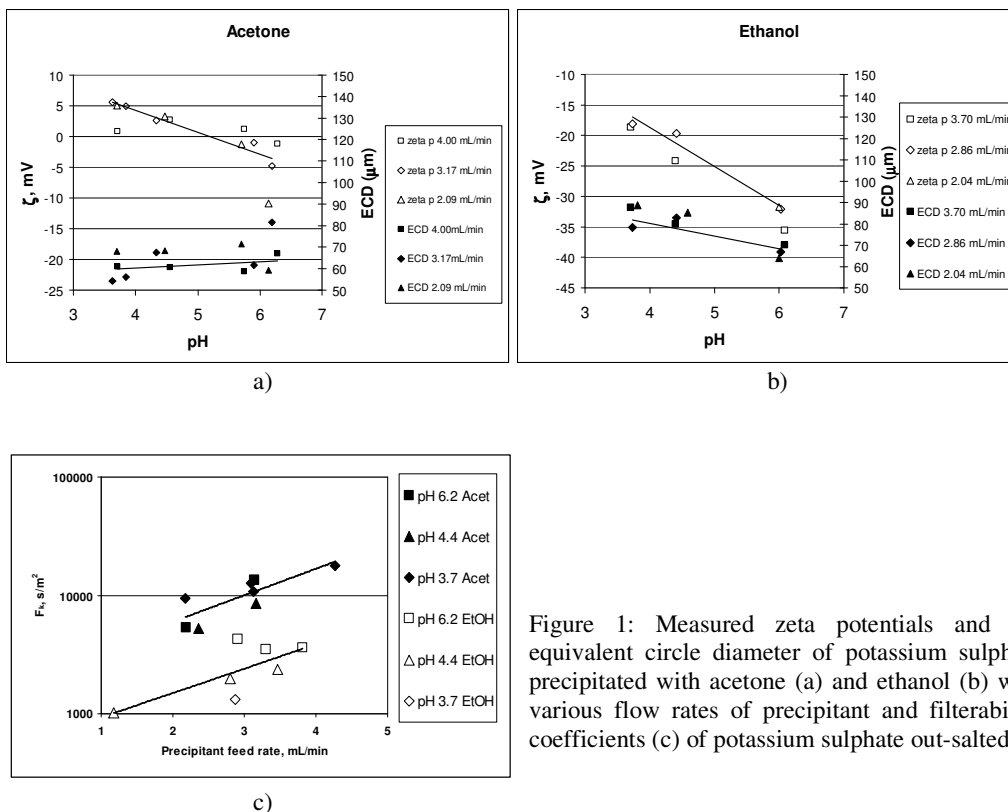


Figure 1: Measured zeta potentials and the equivalent circle diameter of potassium sulphate precipitated with acetone (a) and ethanol (b) with various flow rates of precipitant and filterability coefficients (c) of potassium sulphate out-salted.



## Cellular automata for simulation of crystallization in different mediums

E.R. Abasheva, E.M. Koltsova

*Mendeleev's University of Chemical Technology of Russia, Department of Cybernetics of Chemical Technological Processes, 125047, Russia, Moscow, Miusskaya pl., 9.  
Tel. 007 (499) 978 65 89, Fax: +007 (495) 200 42 04, E-mail: [kolts@muctr.edu.ru](mailto:kolts@muctr.edu.ru)*

### 1. Summary

This work is devoted to the researching and simulating of crystallization processes in different mediums by cellular automata. The cellular automaton is an instrument for the simulation of processes and phenomenon, existent in open systems, where processes have liminal character. Cellular automation theory for describing of micro-, macro- and nanostate crystallization processes was developed. Growth of ammonium chloride crystal in conditions of rest and turbulent mixing, glass crystallization processes, Fe- nanothread crystallization and melting in silicon dioxide nanoporous were researched and simulated.

Keywords: cellular automation, crystallization, simulation

### 2. Extended Abstract

The crystallization processes need high level of technology and the strict observance of all demands for process parameters. Carrying out of sufficient investigations in this field is important for making and perfection of modern effective techniques of crystal growth. Theoretical research takes place in present work by mathematical models.

The mathematical models of crystallization process in different mediums are developed by way of cellular automation. Theory of cellular automation lies in the base of simulation. Cellular automations are mathematical models of system, which describe its evolution. The cellular automation is net, that consist of elements (cells) that change their state in the discrete points of time, conform to the law in the dependence of past element state and its closest neighbors by net [1]. For example, in general case mass transfer at every step (by time) are presented by following law:

$$C_{ij}^{(n+1)} \rightarrow C_{ij}^{(n)} + \frac{1}{m} \left( \langle DC_{kl}^{(n)} \rangle - DC_{ij}^{(n)} \right),$$

where  $(k,l) \in O(i,j)$  – cells of near neighborhood;  $\langle DC_{kl}^{(n)} \rangle$  – the middle value of multiplying of diffusion coefficient to the concentration in the near neighborhood cells;

$$\langle DC_{kl}^{(n)} \rangle = \frac{1}{6} \sum_{k,l} DC_{kl}^{(n)},$$

where  $D$  – diffusion coefficient;  $m$  – parameter characterized by discretization of time and space.

The mathematical model of ammonium chloride crystal growth from solution in conditions of rest and turbulent mixing was developed by cellular automation theory. Optimal process parameters were defined. The simulation of turbulent mixing was based on algorithm developed in works [2,3]. The influence of turbulization on crystal growth was investigated by developed cellular automation model.

The mathematical model of glass producing was developed in this work, which gives representation about phenomena, taking place in the glass production processes. The model allows to calculate an optimum composition, processing and cooling regimes for obtaining of optically homogeneous or nonhomogeneous glass. This model also ensures clearing out of dependency of liquation ability from prescribed process parameters.

The mathematical model of iron crystallization process in mesoporous silicon dioxide matrix was developed by means of cellular automation. Simulation was based on experimental investigation from work [4]. In view of incompleteness of process information we set up hypotheses about nanomaterial production processes. They are the hypotheses about initial and boundary conditions, hypotheses of iron crystallization, hypotheses about particle diffusion in porous. The cellular automata model allows to monitor the evolution of iron nanothread formation and melting in pores.

The work was carried out under support of grant RFBR № 05-08-18001.

## References

1. Koltsova E.M., Tretyakov Y.D., Gordeev L.V., Vertegel A.A. *Nonlinear dynamics and thermodynamics of irreversible processes in chemistry and chemical technology*. M: Chemistry, 2001. – 408 p.
2. Vanag V.K., Virchenko A.Y., Vanag K.V. *Simulation of mixing effect in self-catalyzed reaction by probabilistic cellular automaton*. // Applied nonlinear dynamics, 1996, №3, T. 4, P. 87–96.
3. Ayt A.O., Vanag V.K. *Simulation of kinetic nonequilibrium phase change in condition of turbulent mixing by cellular automata*. // J. Phys. Chem., 1996, T. 70, №8, P. 1385-1390.
4. Eliseev A.A. *Synthesis and properties of nanostructures in mesoporous oxide matrices*. Ph. D. diss. M.: MSU, 2004 – 154 p.

## **Crystallization of Ammonium-Perchlorate from Solution of Electrolytically Produced Sodium-Perchlorate in a Pilot-Scale Plant**

A. Mr Živko Andrić<sup>a</sup>

<sup>a</sup>19. December AD, Chemical process and product R&D department, Podgorica, Montenegro

### **1. Summary**

Production of ammonium-perchlorate, a key oxidative compound in the composite rocket fuels, is initiated on a semi-industrial scale, with original solutions in the crystallization step. As a result, a satisfactory product is obtained, from the point of granulation, crystal shape, moisture content and crystal packing density.

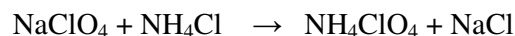
Keywords: rocket fuels, ammonium-perchlorate, electrolysis, crystallization, granulation

### **2. Extended Abstract**

Large scale application of ammonium-perchlorate in the composite rocket fuels defines this compound as an important strategic material. The high content of oxygen in ammonium-perchlorate (54.5% w/w) and the fact that during the thermal decomposition does not yield solid residue, determines its application as an exceptional and irreplaceable oxidative compound in the composite rocket fuels. The fraction of ammonium-perchlorate in the composite rocket fuels is usually around 70-75% w/w, while the energetic performances of the fuel are increased even for 50% compared to the conventional fuels.

Based on these facts, and especially due to the specificity and needs of its own production process, in company "19. December" AD, Podgorica, Montenegro, is initiated production of ammonium-perchlorate on a semi-industrial scale, with original solutions for the crystallization of ammonium-perchlorate, which is a key step in production of this compound.

The core reaction in the process of crystallization is the reaction of double exchange:



First, the technological parameters of sodium-perchlorate production from sodium-chlorate by electrolytic reaction are investigated, followed by definition of key crystallization parameters in the system:  $\text{NH}_4\text{ClO}_4 - \text{NaCl} - \text{H}_2\text{O}$ . As a result of the

crystallization, the product is obtained, which satisfies known and valid standards, especially from the point of granulation, crystal shape, moisture content and crystal packing density.

## Synthesis of Small Crystals of LTA Zeolites without used Organic Compounds

S. Alfaro <sup>a\*</sup>, M. A. Valenzuela <sup>a</sup>, P. Bosch <sup>b</sup>

<sup>a</sup>Laboratorio de Catálisis y Materiales, ESIQIE-Instituto Politécnico Nacional, Zacatenco, 07738, México D.F., México, \*salfaroh@ipn.mx

<sup>b</sup>Instituto de Investigaciones en Materiales, Universidad Nacional Autónoma de México, 04510, México D.F., México

### 1. Summary

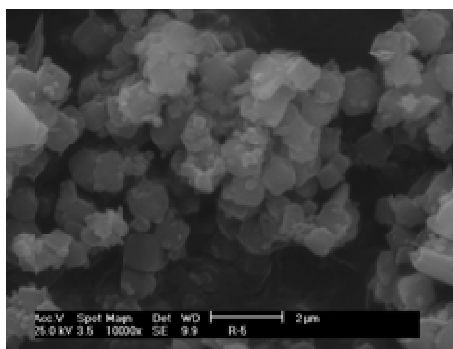
Small crystals of zeolites LTA were obtained in absence of organic templates using a crystallization temperature of 373 K. The as-synthesized samples were characterized by X-ray diffraction (XRD), scanning electron microscopy (SEM), Nitrogen adsorption (BET) and CO<sub>2</sub> adsorption-desorption. During the zeolites synthesis, the aging time was found to be a crucial factor for the control of the crystal size. Samples aged between 72 to 144 h presented an average crystal size of ca. 200 to 500 nm.

Keywords: Crystal growth, Small crystals, Hydrothermal synthesis, Zeolite LTA, Aging time

### 2. Extended Abstract

Zeolites are crystalline alumino-silicate or silicate materials, which have a highly regular and open microporous structure formed by a three-dimensional network of SiO<sub>4</sub> and AlO<sub>4</sub> tetrahedra. The tetrahedra are linked together to give cages connected by pore openings of defined size; depending on the structural type, the pore sizes range from 0.3 to 1 nm approximately. The synthesis of small or nanocrystal like zeolites is crucial to prepare new materials as ultra-thin zeolite films in membranes among other examples. In addition, the reduction of the crystal size to the nanometer scale is the basis for unique applications in microelectronics devices. The crystallization of zeolite nanoparticles has been usually performed at the lowest possible temperature for a particular zeolite, which results in a relatively long synthesis. Therefore, a reduction of the crystallization time and optimization of the conditions yielding zeolite nanoparticles is highly desirable. Several authors have already reported on the synthesis of nanocrystalline zeolite A. However, the drawback of these synthesis procedures is generally that large amounts of the comparatively expensive organic template tetramethylammonium hydroxide (TMAOH) have to be employed in order to promote nucleation and, thus, the formation of nanocrystals.

Small crystals of zeolites LTA, were obtained from gels with the follow composition:  $\text{Al}_2\text{O}_3 : 1.2\text{SiO}_2 : 2.5\text{NaOH} : 145\text{H}_2\text{O}$ . The gels were aged from 24 to 144 h, then the mixture was transferred to a Teflon-lined stainless steel autoclave and the hydrothermal reaction was carried out for 24 h under static conditions in a convection oven preheated at 373 K. X-ray diffractograms of the 623 K treated samples and aged at different times were compared and samples aged for 72 and 144 h, clearly show sharp and intense peaks which can be attributed to LTA zeolite (JCPDS = 89-5422 card). In addition, SEM image of the sample with 144 h of aging time has morphology like a cube shape, that is characteristic of the LTA zeolites and no aggregates are present, the surface area and pore volume were determined by  $\text{N}_2$  adsorption. Finally the small crystals of LTA zeolites were characterised by TPD (temperature-programmed) experiments using  $\text{CO}_2$  and  $\text{H}_2$  as probe-molecule to know the adsorption capacity and their possible applications as an adsorbent for  $\text{CO}_2$  removal from flue gases and as  $\text{H}_2$  storage.



SEM image showing small crystals of LTA zeolites obtained by hydrothermal method

The authors are grateful to the financial support of Project SIP 2007-0134, and COFAA, IPN.

## References

- Szostak, R. *Molecular Sieves - Principles of Synthesis and Identification*, 1st ed.; Van Nostrand Reinhold: New York, 1989; 2nd ed.; Blackie: London, (1998).
- E.E. McLeary, J.C. Jansen, F. Kapteijn, (2006) *Microporous Mesoporous Mater.* 90 198-220.
- S.S. Hayrapetyan, H.G. Khachatryan, (2005) *Microporous Mesoporous Mater.* 78 151-157.
- L. Tosheva, V.P. Valtchev, (2005) *Chem. Mater.* 17 2494-2513.
- B.A. Holmberg, H. Wang, J.M. Norbeck, Y. Yan, (2003) *Microporous Mesoporous Mater.* 59 13-28.

## **Correlation of Fluid Atomization and Particle Formation in the SAS Process by Optical Laser Analysis**

R. Schatz,<sup>a</sup> A. Braeuer,<sup>b</sup> A. Leipertz,<sup>b</sup> E. Schlücker<sup>a</sup>

<sup>a</sup>*Department for Process Technology and Machinery, University of Erlangen-Nuremberg, Cauerstrasse 4, 91058 Erlangen, Germany*

<sup>b</sup>*Department of Engineering Thermodynamics, University of Erlangen-Nuremberg, Am Weichselgarten 8, 91058 Erlangen, Germany*

### **1. Summary**

The supercritical antisolvent (SAS) method was examined using optical laser analysis detecting propagation, concentration and the corresponding state of phase within the injected solution atomized inside the precipitation chamber. Evaluating these results with respect to the properties of particles produced allows an insight on the particle formation process.

Keywords: SAS, supercritical antisolvent, elastical light scattering, linear Raman scattering

### **2. Extended Abstract**

A variety of supercritical fluid atomization processes are used for the production of fine powders particularly in the pharmaceutical industry. Important properties such as particle size, morphology and particle size distribution can be influenced by varying parameters such as concentration, pressure and temperature.

However, the requirement of high pressure equipment and the expeditious process complicate the analysis of the particle formation mechanism. The supercritical antisolvent (SAS) method was examined using optical laser analysis detecting propagation, concentration and the corresponding state of phase within the injected solution atomized inside the precipitation chamber. A pulsed, piezoelectric actuated injector was used to atomize an ethanol solution of acetaminophen into supercritical carbon dioxide. Elastical light scattering and linear Raman scattering were applied as optical measuring techniques to analyze the process of mixture formation.

Evaluating these results with respect to the properties of particles produced allows an insight on the particle formation process.

**References**

Braeuer, A., Schatz, R., Schlücker, E., Leipertz, A., (2006) *ICLASS 2006*, Paper ID ICLASS06-274.



## **Material effects on the ammonothermal crystallization of bulk GaN**

N. Alt,<sup>a</sup> E. Meissner,<sup>b</sup> D. Kilian,<sup>a</sup> E. Schlücker<sup>a</sup>

<sup>a</sup> *Department for Process Technology and Machinery, University of Erlangen-Nuremberg, Cauerstrasse 4, 91058 Erlangen, Germany*

<sup>b</sup> *Crystal Growth Laboratory, Fraunhofer Institute Integrated Systems and Device Technology, Schottkystrasse 10, 91058 Erlangen, Germany*

### **1. Summary**

Different metals and ceramics were investigated for applicability in the ammonothermal GaN crystallization. The effects of these materials on the crystal growth process are presented.

Keywords: GaN, gallium nitride, ammonothermal, bulk crystal growth, supercritical ammonia

### **2. Extended Abstract**

Gallium nitride is an essential material for the semiconductor industry, e.g. for laser diodes. Up to now single crystals can not be grown in an adequate size and quality for industrial scale production. A promising method for growing such bulk crystals is the ammonothermal process. Due to the extreme reaction conditions at high pressure and temperature in a supercritical ammonia atmosphere, the requirements of the materials are extensive. Especially chemical resistance behaviour of the materials used is important to prevent contaminations in the grown crystals. For this reason different metals and ceramics were investigated for applicability in the ammonothermal process. Catalytic effects on crystal growth, contamination of the crystals, and chemical behaviour of these materials were examined by microscopy, SEM, and EDS measurements. Evaluation of these results allows the improvement of crystallizers and consequently the quality of the produced crystals.



## **Experimental study of different configurations to perform preferential crystallization for enantioseparation.**

Grzegorz Ziomek,<sup>a</sup> Martin P. Elsner,<sup>a</sup> Andreas Seidel-Morgenstern,<sup>a,b</sup>

<sup>a</sup>Max Planck Institute for Dynamics of Complex Technical Systems, Sandtorstr. 1, 39106 Magdeburg, Germany

<sup>b</sup>Otto von Guericke University, Universitätsplatz 2, 39106 Magdeburg, Germany

### **1. Summary**

In this presentation influence of the important crystallization process variables like initial seed size distribution and temperature for different crystallizer configurations has been analyzed experimentally using threonine-H<sub>2</sub>O as a model system. The influence of initial seed size distribution on the productivity and product quality will be shown. By varying size of particles used as a seeds, nucleation as well as growth kinetics are influenced. It will be demonstrated that by appropriate changing of free operating parameters the process performance can be controlled and improved. Parallel to the experimental analysis, a modeling approach will be also presented.

Keywords: Enantioseparation, Process intensification, Crystallization, Optimization

### **2. Extended Abstract**

The separation of chiral compounds is of large interest since most of the (bio-)organic molecules are chiral. Usually only one of the enantiomers shows the wanted properties with regard to therapeutic activities or metabolism, whereas the other enantiomer may be inactive or may even cause some undesired effects (Jacques et al., 1994). In recent years, besides the most commonly used classical resolution via formation of diastereomers, direct crystallization methods have become increasingly important. An attractive process is enantioselective preferential crystallization (Elsner et al., 2005) In a batch crystallizer racemic mixture of conglomerate forming systems tend to reach an equilibrium state in solution in which the liquid phase has racemic composition and the solid phase is 1:1 mixture of crystals of both enantiomers. However, before approaching this state, it is possible to preferentially produce just one of the enantiomers after seeding with homochiral crystals.

Among all available crystallizer configurations the batch mode is obviously the easiest one. The principle of batch process is quite simple: the vessel is filled with a supersaturated solution of the racemate (enantiomers E<sub>p</sub> and E<sub>c</sub>). After addition of homochiral seeds e.g., merely E<sub>p</sub> is crystallizing within a limited time period. In order

to gain the target enantiomer as a product of high purity, the process must be stopped before the nucleation of the undesired counter-enantiomer occurs (Lorenz et al., 2006). During this batch crystallization, the concentration of the desired enantiomer in the solution is decreasing, whereas the concentration of the counter-enantiomer remains constant. Based on analysis of these concentration profiles a more attractive and effective operation mode using two batch crystallizers coupled via liquid phase (see Fig. 1) has been studied (Ziomek et al., 2007). In each vessel one of both enantiomers is seeded and grows subsequently. An exchange of the crystal free liquid phases between the crystallizers leads to an increase of driving forces and consequently process productivity.

The influence of important process variables like initial seed size distribution, exchange flow rates between crystallizers, and temperature has been analyzed experimentally using threonine-H<sub>2</sub>O as a model system. The influence of initial seed size distribution on the productivity and product quality will be shown. By varying size of particles used as a seeds, nucleation as well as growth kinetics are influenced. It will be demonstrated that by appropriate changing of free operating parameters the process performance can be controlled and improved. Parallel to the experimental analysis, a modeling approach will be also presented.

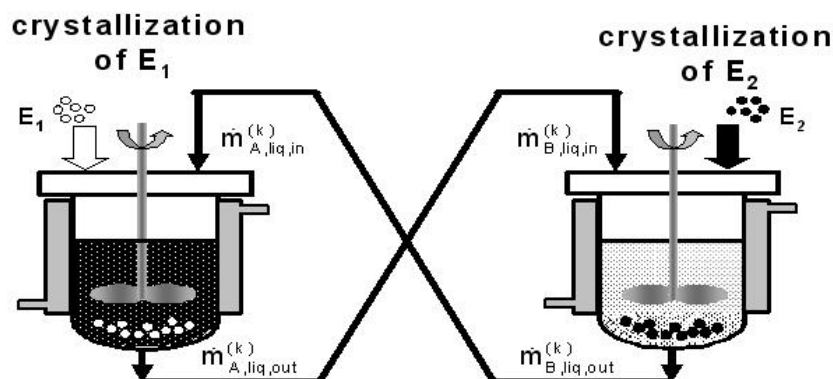


**Fig. 1:** Basic concept of arrangement for two crystallizers with simultaneous exchange of crystal-free liquid phase

## References

- Jacques, J., Collet, A., Wilen, S.H., (1994): *Enantiomers, racemates and resolutions*, Krieger, Malabar
- Elsner, M.P., Fernández Menéndez, D., Alonso Muslera, E., Seidel-Morgenstern, A. (2005): 17 (S1), S183-S195
- Lorenz, H., Perlberg, A., Sapoundjiev, D., Elsner, M.P., Seidel-Morgenstern, A., (2006) Chem. Eng. and Proc., doi, 10.1016/j.cep.2005.11.013
- Ziomek, G., Elsner, M.P. Seidel-Morgenstern, A., (2007) Submitted to Chemical Engineering Science

## **Influence of selected process parameters on attrition intensity in DTM type crystallizers with a jet-pump – a general neural network's approach**

Krzysztof Piotrowski,<sup>a</sup> Katarzyna Pentos,<sup>b</sup> Monika Malasinska,<sup>b</sup> Andrzej Matynia<sup>b</sup>

<sup>a</sup>*Department of Chemical & Process Engineering, Silesian University of Technology, 44-101 Gliwice, Poland*

<sup>b</sup>*Faculty of Chemistry, Wrocław University of Technology, 50-370 Wrocław, Poland*

### **1. Summary**

Secondary contact nucleation is a main source of nuclei in industrial mass crystallization processes. Overcoming this phenomenon provides one with a method for precise process control. Respecting complex interactions between constructional (DTM MSMPR / MSCPR crystallizer with a liquid jet-pump) and hydrodynamic factors a feedforward multilayer artificial neural network was used for creating a numerical model of this process. It enables one to predict with significant accuracy attrition intensity in NaCl crystals suspension for various technological conditions.

Keywords: DTM crystallizer, attrition degree, liquid jet-pump, neural network model

### **2. Extended Abstract**

For properly designed industrial-scale mass crystallization process main source of nuclei is a complex secondary nucleation, based mainly on attrition, breakage and abrasion phenomena. In the most common crystallizer constructions with internal circulation of suspension this desirable (if strictly controlled) effect results from the mechanical collisions between: crystal-crystal, crystal-agitator (or pump rotor) and crystal-apparatus wall (or/and other interior equipment). However, in case of too intensive attrition action an excessive number of nuclei arise, causing difficulties in process control and making creation of the product of desirable crystal size distribution impossible. Facing the complex interrelations between hydrodynamic and constructional factors the exact prediction of attrition action in the assumed process environment is an important engineering challenge. Application of original constructions of crystallizer with a liquid jet-pump creates new possibilities of providing stable and intensive enough internal circulation of suspension inside the vessel simultaneously reducing the undesirable excessive attrition effects. Experimental tests of the attrition resistances in NaCl crystal populations (hardness

via Vickers method  $16 - 24 \text{ MN/m}^2$ ) of initial mean size within the range of  $L_m = 0.441 - 1.52 \text{ mm}$  were performed. Crystal volumetric concentration in the suspension was adjusted in the  $\varphi = 2 - 10 \%$  range, while the suspension residence time in the crystallizer was changed within the  $\tau = 900 - 7200 \text{ s}$  range. Two different constructions of laboratory-scale crystallizer with a jet-pump were taken under consideration: DTM MSMPR (Draft Tube Magma Mixed Suspension Mixed Product Removal crystallizer) and a more complex design with internal hydraulic classification system – DTM MSCPR (DTM Mixed Suspension Classified Product Removal crystallizer). Both laboratory crystallizers, loaded with the crystal suspension of possibly narrow, closely restricted crystal size distribution (saturated solution,  $\rho = 1198 \text{ kg m}^{-3}$ ,  $T = 298 \text{ K}$ ) were working under steady state hydraulic mode through the selected residence time. A resulting, final crystal size distribution was determined with Laser Particle Size Analyzer COULTER LS-230. Each measurement was repeated twice (repeatability test). Taking under consideration complex entirety of analyzed phenomenon (e.g. influence of hydrodynamics in macro- and microscale, etc.) a feedforward multilayer artificial neural network was used for creation a numerical model of this process based on the experimental data set (60 input-output vectors). The net was composed of three inputs (representing: mean residence time of suspension, crystals volumetric concentration in the suspension and initial mean size of crystals) and six output neurons, representing: mean size of crystal population after the process, attrition degree (defined as a ratio of the difference of mean sizes – before and after the test – to the initial mean size) and final value of coefficient of variation (CV) – a set for DTM MSMPR and a set for DTM MSCPR crystallizer, respectively. The 30 neural network configurations with 4 – 24 hidden neurons arranged into 1 – 2 hidden layers were a subject of statistical tests (RMSD – Root Mean Square Deviation). An optimal configuration proved to be a 3–6–6 structure, trained for 8600 iterations with learning rate set as 0.1. Its statistical accuracy was as follows: for DTM MSMPR apparatus RMSD for attrition degree was 0.8810 %, for  $L_m - 0.0145 \text{ mm}$  and for CV – 0.9847 %. For DTM MSCPR apparatus RMSD for attrition degree was 0.5724 %, for  $L_m - 0.0157 \text{ mm}$  and for CV – 0.9164 %. The resulting, numerical neural model enables one to predict (and then eventually control) with the significant accuracy attrition intensity of NaCl crystals in various technological conditions, including: mean size of the process magma, its volumetric concentration and mean residence time in the apparatus. Based on experimental data, thus devoid of any simplifying assumptions, the model can correctly render all possible hidden, strongly nonlinear intrinsic interrelations and feedbacks between these three process factors, imposing simultaneously the hydraulic regime resulting from the selected geometrical arrangement of the vessel interior of two different constructional solutions (mixed and classified product removal). The experimental and simulated data, however connected strictly quantitatively only with the laboratory-scale crystallizers used, can provide one with at least qualitative information about attrition behavior of NaCl crystal suspensions in a large-scale liquid jet-pump crystallizer of diversified internal hydraulic regimes, making the comparative study as well as selection of the optimal process conditions possible.

This work was supported by the Ministry of Science and Higher Education of Poland under grant No. N205 071 31.

## **Controlling of Chaos in the Process of Crystallization of Dibasic Lead Phosphite**

M. V. Cherenkov, E. M. Koltsova

*Department of Cybernetics of Chemical Technological Processes, Mendeleev University of Chemical Technology of Russia, 125047, Miusskaya pl. 9, Moscow, Russia*

### **1. Summary**

In this paper three algorithms of control of chaos (destochastization, control with proportional feedback and control with time-delayed feedback) in the process of continuous mass crystallization of dibasic lead phosphite are offered.

Keywords: chaos, crystallization, control, dibasic lead phosphite

### **2. Extended Abstract**

In this paper three algorithms of control of chaos (destochastization, control with proportional feedback and control with time-delayed feedback) in the process of continuous mass crystallization of dibasic lead phosphite are offered.

The first method involves a corrective action in compliance with the required values of the dynamic variables and, therefore, involves a feedback as a necessary component of the system. An algorithm based on the Poincare cross section was developed by Ott, Grebogi, and Yorke, which is referred to as the acronym of their names (the OGY algorithm). For today the OGY-method has quite a number of modifications. The second attractive for scientists method is the time-delayed feedback one. It was offered in 1992 by the Lithuanian physicist K. Pyragas. The main advantage of his idea is the continuity of the method. In other words, when one uses the OGY-method and its modifications the algorithm starts working when a system gets, for example, to the given area of an unstable fixed point, that takes some time, but when using the Pyragas' method the algorithm is supposed to be switched on any time when it is necessary due to a feedback principle. The efficiency of Pyragas' method and its modifications for the physical, chemical and a number of other systems was demonstrated.

Another approach to the stabilization of the stochastic behavior of dynamic systems involves external disturbances without feedback. This method of suppression of chaos is referred to as the destochastization method. We show the possibility of using of each method for controlling chaos in the process of continuous mass crystallization of dibasic lead phosphate.

Book of Abstracts  
European Congress of Chemical Engineering (ECCE-6)  
Copenhagen, 16-20 September 2007



## **Crystallization of a polymorphic drug in a stirred tank**

C. Herman, V. Gelbgras, V. Halloin, B. Haut

*Université Libre de Bruxelles, Belgium*

### **1. Summary**

The crystallization behaviour of a drug presenting several polymorphic forms is investigated. The study is focused on a reference pharmaceutical crude product. The objective of this paper is, on the one hand, to identify the mechanism of the polymorphic transition, and, on the other hand, to model the influence of the operating parameters on the kinetics of this transition. This involves to characterize the polymorphic forms, and to obtain some experimental crystallization data.

Keywords: crystallization, polymorphism, modelling, Computational Fluid Dynamics, mixing

### **2. Extended Abstract**

Crystallization by cooling followed by separation of the crystals from the resulting suspension is the most frequent method of choice to achieve the required purity of active pharmaceutical ingredients. However, this method may generate several types of polymorphs if uncontrolled.

Hereafter, the crystallization behaviour of a drug presenting several polymorphic forms is investigated.

In this process, the crude product is initially dissolved in an alcohol at high temperature and stirred. The cooling of this solution in a controlled manner induces the crystallization of the drug, but in a non-desired crystallographic form (morph II). In order to obtain the desired crystallographic form (morph I), the temperature is further reduced under 0°C and the system is kept at this constant maturation temperature. After a latency period, the polymorphic transition from morph II to morph I is observed.

The objective of this work is, on the one hand, to identify the mechanism of the polymorphic transition, and, on the other hand, to model the influence of the operating parameters on the latent period, in order to reduce it.

**In a first step**, the two morphs are characterized by different techniques: optical and electronic microscope, Infra – Red and Raman spectroscopy, XR diffraction, and Differential Scanning Calorimetry. Solubility curves of the two morphs are experimentally measured.

**In a second step**, the nature of the polymorphic transition is investigated. For this purpose, the industrial installation has been reproduced in the lab, on a small-scale pilot installation. Using it, and some other measurement apparatus, as a FBRM Lasentec probe, it is shown that the polymorphic transition follows a mechanism of dissolution-recrystallization mediated by the solvent.

**In a third step**, the influence of two operating parameters on the latent period is modelled.

Firstly, a model of the influence of the temperature on the latent period is developed. For this purpose, thermodynamic calculations, fed by the data obtained in the first step, and latent period measurements on the small-scale installation, using different maturation temperatures, are performed.

Secondly, a model of the influence of mixing on the latent period is developed. For this purpose, Computational Fluid Dynamics simulations of the flow in the tank and latent period measurements on the small-scale installation, using several impellers and different rotation speeds, are performed. It appears that the latent period can be well correlated to local hydrodynamic characteristics such as the Kolmogorov micro-scale.

Based on the developed models, optimal operating conditions are derived, and validated against experimental data, for different reactor scales.

## References

Escudié R., Bouyer D., Liné A., (2004) *Characterization of trailing vortices generated by a rushon turbine*, AIChE Journal, 50, 75-86

Garcia E., Hoff C., Veesler S., (2002) *Dissolution and phase transition of pharmaceutical compounds*, Journal of Crystal Growth, 237-239, 2233-2239

Kundu P.K, (2002) Cohen I.M., *Fluid Mechanics*, USA

Mersmann A., (1995) *Crystallization Technology Handbook*, New York

Mullin, (2001) *Crystallization*, London

Pohorecki R., Baldyga J., (1983) *The use of a new model of micromixing for determination of crystal size in precipitation*, Chemical Engineering Science, 38, 79-83

Sarkar D., Rohani S., Jutan A., (2006) *Multi-objective optimization of seeded batch crystallization processes*, Chemical Engineering Sciences, 61, 5282-5295

## Process conditions and granulometric properties of crystals

Aleksandra Sander, Jasna Prlić Kardum

*Faculty of Chemical Engineering and Technology, University of Zagreb, 10000 Zagreb, Croatia*

### 1. Summary

Granulometric properties of crystals (mean crystal size, crystal size distribution and crystal shape) are very sensible to process conditions (mixing rate, cooling rate, cooling profile, seeding, type of impeller, batch time, etc). Selection of the appropriate process condition, in order to obtain the required product quality, is of a great importance. To achieve that, the influence of various process conditions on the granulometric properties of crystals, have been investigated on a laboratory scale batch cooling crystallizer. Three different salts were used for crystallization from water solution: two inorganic (potassium chloride, potassium sulphate) and one organic (pentaerythritol).

Keywords: batch crystallization, cooling rate, granulometric properties, mixing rate, seeding

### 2. Extended Abstract

The intensity of cooling and mixing strongly influence the shape, the mean crystal size and the CSD of the KCl crystals. To produce crystals of better quality (regular shape, bigger size and narrow CSD) the process must be conducted at slow cooling and high mixing rate.

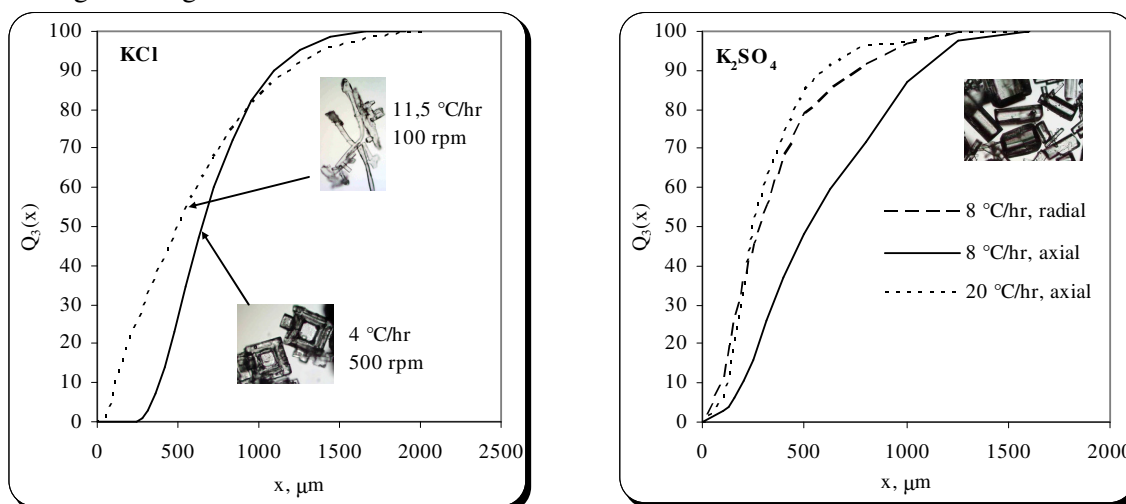


Figure 1: Cumulative crystal size distributions at different process conditions

Cooling rate does not influence the shape of the  $K_2SO_4$  crystals, but it affects the crystal size and CSD in the same manner as on the KCl. The usage of the impeller that produces the axial flow is recommended, because the improvement in the final CSD (it shifts to the larger size ranges) was observed, when compared with the impeller with radial flow.

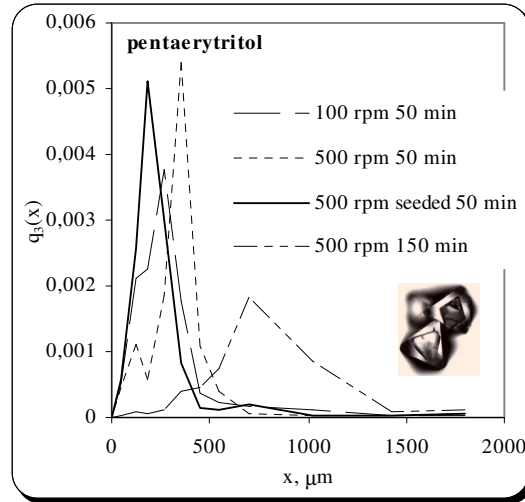


Figure 2: Crystal size distributions of pentaerythritol at different process conditions

The pentaerythritol crystal shape does not depend on the applied operating conditions. Well mixed conditions (higher mixing rate) result with production of bigger crystals. The final CSDs are bimodal for all cooling modes (convex, natural and linear), higher batch time and low mixing rate. Crystals obtained from seeded crystallization experiments results with unimodal CSD. The mean crystal size remains the same for all seed sizes and loadings.

## References

- Hu, Q., Rohani, S., Wang, D.X. and Jutan, A., (2005) *Powder Technology*, 156, 170-176.
- Choong, K.L., Rohani, S., (2004) *Chemical Engineering Science*, 59, 313-327.
- Prlić Kardum, J., Sander, A., Glasnović, A., (2005) *Chem.Biochem.Eng.Q.*, 19 (1), 39-47.

## CSD and the kinetic parameters of crystallization of $K_2SO_4$

J. Prlić Kardum, A. Sander, M. Kirinčić, M. Kalšan

*Faculty of Chemical Engineering and Technology, University of Zagreb, Zagreb, Croatia*

### 1. Summary

A study of a cooling crystallization of a potassium sulphate water solution in a batch reactor is described in this paper. The effect of hydrodynamics conditions on the crystallization process were investigated by using different type of impellers. Two types of impellers were investigated; the four-pitched blade impeller which generates axial flow and the six blades Rushton turbine which generates radial flow. The experiments were performed at four different linear cooling rates in the range from 8-20 °C/h at same mixing rate of 700 rpm for both types of impeller.

Keywords: batch crystallization, CSD, crystallization kinetic, potassium sulphate

### 2. Extended Abstract

Influence of the cooling rates to the metastable zone width was investigated. The experimental data shows that higher cooling rate expands the metastable zone for all types of impeller and influences the crystal size distribution.

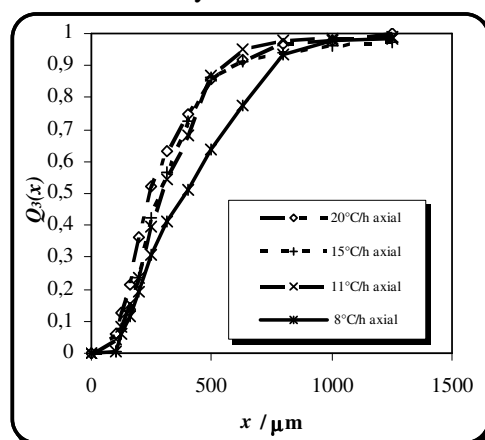


Figure 1: Cumulative crystal size distributions for different cooling rates and propeller that produces axial flow

At low cooling rates, supersaturation was kept at constant value for a long period. It results with improved conditions for mass transfer and crystals would grow. Bigger crystals were obtained at lower cooling rates.

It is stated that radial flow (Rusthon turbine) is particularly inappropriate for nucleation process, and for crystallization. Nucleation started at lower temperature and higher supersaturation. This conditions result with high nucleation's rate and large number of nucleation centre. Also, the obtained crystals were settling on the wall of the reactor, baffles and stirrer. The great part of obtained crystals was agglomerated.

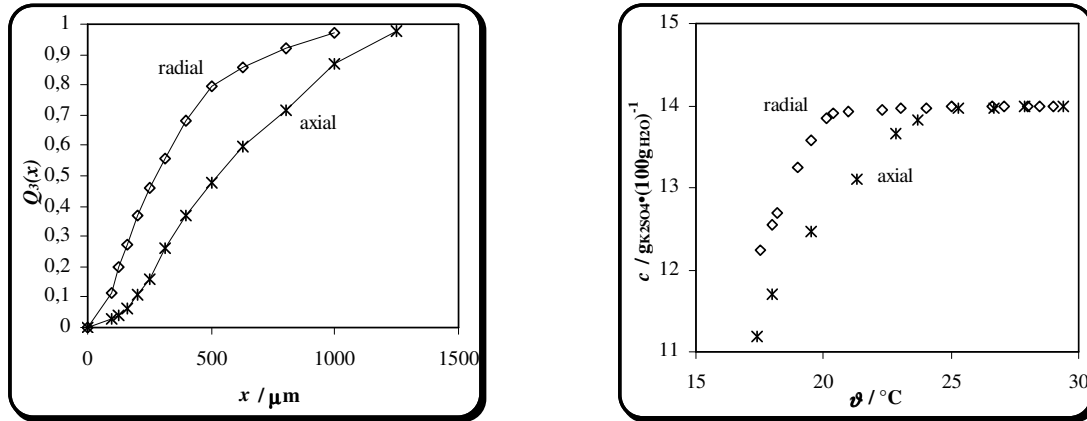


Figure 2: Cumulative crystal size distributions and concentrations vs temperature for different type of impellers

Nucleation order,  $n$  and constant of nucleation,  $k_n$  were determined for different cooling rates. Nucleation order is bigger at radial flow (nucleation started at higher supersaturation).

	$k_n / (\text{kg}_{\text{K}_2\text{SO}_4} / \text{kg}_{\text{H}_2\text{O}})^{1-n} \text{s}^{-1}$	$n$	$r / ^\circ\text{C} \cdot \text{h}^{-1}$	$g$	$k_g / (\text{kg}_{\text{K}_2\text{SO}_4} / \text{kg}_{\text{H}_2\text{O}})^{1-n} \text{s}^{-1}$
<b>Axial flow</b>	$1.96 \cdot 10^{-4}$	6.47	8	1.44	0.0640
			11	1.43	0.1284
			15	1.38	0.2345
			20	1.13	0.1720
<b>Radial flow</b>	$1.43 \cdot 10^{-4}$	7.10	8	1.22	0.0479
			11	1.18	0.2130
			15	1.10	0.2041
			20	0.76	0.1606

Table 1: Crystallization kinetics parameters

Relation between the rate of concentration drop in a solution and supersaturation has been approximated with a power law equation. For used impellers, reaction orders do not change much for different cooling rates, except at the biggest cooling rates that results with the smallest crystals.

## References

- Lyczko, N., Espitalier, F., Louisnard, O. and Schwartztruber, J., (2001) *Chemical Engineering Journal*, 86, 233-241.  
 Mohamed, H. A., Abu-Jdayil, B. and Al Khateeb, M., (2002) *Chemical Engineering and Processing*, 41, 297-302.

## Supersaturation profiles of L-sorbose water solutions in the cooling batch crystallization process

Bogusława Wierzbowska,<sup>a</sup> Joanna Koralewska,<sup>a</sup> Krzysztof Piotrowski,<sup>b</sup> Andrzej Matynia<sup>a</sup>, Krzysztof Wawrzyniecki<sup>a</sup>

<sup>a</sup>*Faculty of Chemistry, Wrocław University of Technology, 50 – 370 Wrocław, Poland*

<sup>b</sup>*Department of Chemical & Process Engineering, Silesian University of Technology, 44 – 101, Gliwice, Poland*

### 1. Summary

L-sorbose, an intermediate product in L(+)-ascorbic acid synthesis, is effectively separated from postprocessing mixture (purification process) by multistage batch crystallization operations. Water solutions of L-sorbose tend to form stable supersaturated systems, characterized by high values of maximum supercooling depending on saturation temperature of initial solution (concentration) and its cooling rate. This effect of undesirable accumulation of undischarged supersaturation makes some disturbances both in mass crystallization process yield and in crystal product quality (excess nucleation effects). The experimental results concerning time–distribution of supersaturation in the seeded water solutions of L-sorbose (55–75 mass % range) in a batch DT MSMR crystallizer (linear cooling rate  $(1.39 – 8.33) \cdot 10^{-3} \text{ K s}^{-1}$ ) are presented and discussed.

Keywords: L-sorbose, batch crystallization, supersaturation, DT MSMR crystallizer, cooling rate

### 2. Extended Abstract

L-sorbose is a second, intermediate product in L(+)-ascorbic acid synthesis according to Reichstein procedure. An industrial scale crystal product should be composed of, according to the assumed technology yield, 97.0 – 98.8 mass % of L-sorbose. The required chemical purity results the most often from the subsequent batch mass crystallization from its postprocessing water solutions.

An characteristic property of this purification step is that water solutions of L-sorbose tend to form stable supersaturated systems, characterized by high values of maximum supercooling: from ca.  $\Delta T = 10$  up till 50 K, depending on saturation temperature of initial solution in a batch crystallizer (its concentration), as well as on a cooling rate applied. It reveals a direct influence both on mass crystallization

process yield and crystal product quality (crystal size distribution, their uniformity, shape and chemical purity).

The experimental results concerning time–distribution of supersaturation in the seeded water solutions of L-sorbose during batch mass crystallization process with adjusted cooling rate value providing linear decrease of temperature with the process time are presented. The tests were performed in a laboratory DT (Draft Tube) MSMPR (Mixed Suspension Mixed Product Removal) crystallizer of internal circulation of suspension equipped with a propeller agitator. Laboratory test stand performance (temperature reduction regime) was controlled by means of PC computer system.

Crystallizer was fed with water solutions of L-sorbose of initial concentration adjusted to fit within the 55 – 75 mass % range (corresponded to saturation temperature range of  $T_{\text{eq}} = 324.5 - 368.5$  K), cooled with a linear cooling rate selected individually from the  $R_T = (1.39 - 8.33) \cdot 10^{-3}$  K s<sup>-1</sup> range.

On the basis of laboratory test results it can be concluded, that with the decrease of saturation temperature of the batch solution introduced into the crystallizer (lower initial concentration values) supersaturation in the solution reaches during crystallization process only slightly higher values in a whole time range tested. In a final process temperature ( $T_f$ ) for two extreme cases under study ( $T_{\text{eq}} = 324.5$  and 368.5 K) a difference between final supersaturation values in these two solutions was 1.9 mass % only. The discharge of supersaturation, continuously generated while the process, runs smoothly in all water solutions of L-sorbose under investigation.

Supersaturation value in a final process temperature ( $T_f$ ) is also crystallization time,  $\tau_{\text{cr}}$ , dependent (where crystallization time is defined as  $\tau_{\text{cr}} = (T_{\text{cr}} - T_f)/R_T$  and  $T_{\text{cr}}$  is a temperature value corresponding to a spontaneous crystallization event observed in the solution), thus – indirectly – cooling rate dependent. For the solution characterized by  $T_{\text{eq}} = 324.5$  K (corresponding to L-sorbose concentration of 55 mass %) relatively short batch crystallization time ( $\tau_{\text{cr}} = 1920$  s resulting from the highest value of  $R_T = 8.33 \cdot 10^{-3}$  K s<sup>-1</sup>) is responsible for the fact, that the residual supersaturation in the solution in a final process temperature is as high as 5.0 mass %. Contrary, lower values of linear cooling rate applied correspond to higher crystallization process yields. For example, in case of  $R_T = 1.39 \cdot 10^{-3}$  K s<sup>-1</sup>, thus  $\tau_{\text{cr}} = \text{ca. } 2 \cdot 10^4$  s, the undischarged residual supersaturation in a postprocessing mother solution reaches only 0.3 mass %, what is profitable from the mass balance (thus economic) point of view.

This work was supported by the Ministry of Science and Higher Education of Poland under grant No. 3T09B 122 27.



## Synthesis and Characterization of Hydrotalcite-like Compounds Produced via Hydrothermal Treatment

W.N. Budhysutanto,<sup>a</sup> Y. Perez de Diego,<sup>a</sup> H.J.M. Kramer,<sup>a</sup> M. Reedijk,<sup>b</sup> A.G. Talma,<sup>b</sup> P.J. Jansens<sup>a</sup>

<sup>a</sup>*Process and Energy Laboratory, Delft University of Technology, 2628CA Delft, The Netherlands*

<sup>b</sup>*Akzo Nobel Chemicals Research bv, Velperweg 76,6800 SB Arnhem, The Netherlands*

### 1. Summary

A novel method of producing hydrotalcites-like compounds by hydrothermal process is introduced. In contrast with precipitation method, this novel method produces fewer impurities thus eliminating the requirement of product purification. Different magnesium oxide sources, reactant pre-treatment and operating temperatures were investigated. Magnesium oxide provided by Martin Marrietta reacted faster compared to the one provided by Nedmag due to its high surface area. Pre-treatment by milling increased the reactivity of the aluminium source by making it amorphous and the magnesium oxide by increasing its surface area. Two different polytypes were observed at different temperatures. Polytype 3R1 was produced at temperature below 90°C and the other polytype, 3R2, was produced at higher temperature.

Keywords: hydrotalcite, anionic clay, hydrothermal process, polytype

### 2. Extended Abstract

Hydrotalcites-like compounds (HTlc) are stacks of metal hydroxides layers with anions in between, compensating the charges, and also water. Despite of many possible application of HTlc, currently they are used commercially in pharmaceutical, PVC and catalyst industry. Wide spread use of the material is still limited due to their complex production process. HTlc is generally produced by precipitation of acid/basic solution in batch reactor. This process includes the removal of acid/base material from the starting solution via a washing process, which is of course time consuming, expensive and waste productive. A novel hydrothermal method to produce HTlc has been proposed. This method does not use acid/basic starting materials, thus eliminating the requirement of product washing. It has been found that this synthesis method produced different polytypes, namely 3R1 and 3R2, along with other impurities, such as brucite and boehmite [1]. The aim of this study is to optimize the process condition with respect to the impurities and reaction rate.

### 2.1. Magnesium Source

Two magnesium oxide sources were used in this research: Martin Marietta MgO and Nedmag MgO. The reaction with Martin Marietta MgO seems to perform faster, indicated by less amount of MgO found in the end product. Moreover, using Nedmag MgO as a magnesium source boehmite impurities were produced. The use of Martin Marietta MgO, on the other hand, resulted in higher brucite levels compared to Nedmag MgO. As Martin Marietta MgO has almost five times higher BET surface area than Nedmag MgO, this indicates that surface area is one of the key variables for the reaction rate. At high temperatures, the dissolution of MgO is determined by the diffusion of hydroxyl ions, which increases with the surface area [2]. The formation of boehmite impurities could be explained by the slow dissolution of Nedmag MgO, which causes the gibbsite to be transformed into boehmite in the absence of dissolved MgO.

### 2.2. Reactant Pre-Treatment

It has been found that the reactivity of the reactants was increased when it is pre-treated by milling [3]. Several milling techniques were investigated: dry milling, wet milling, and ultrasound milling. Mechanical activations by dry and wet milling amorphized the gibbsite, increasing its solubility and reactivity, while ultrasound milling did not give this effect to the material. Activation of MgO occurred by all the milling techniques. In this case, amorphization was not observed, but particle size decreased considerably, consequently increasing the specific surface area and thus the reactivity. Activation of both gibbsite and MgO resulted in a drastic reduction of batch time from 24 hours to 1 hour at 170 °C.

### 2.3. Reaction Temperature

Varying the reaction temperature, not only increase the reaction rate, but also produced different polytypes. At temperatures up to 90 °C, a polytype 3R1 is formed. Beyond this temperature, a different polytype namely 3R2 polytype is formed. The optimum temperature for the 3R2 polytype formation is observed at 170 °C.

The hydrothermal synthesis process of hydrotalcites-like compounds appears to be highly efficient conversion process generating a high product yield, short reaction times and minimal waste streams. The key factors determining the performance of the process appeared to be the nature of the solid reactants, especially of the magnesium source and the temperature. In addition it was shown that both crystalline reactants could be activated by wet milling leading to a significant reduction of the batch time of the process. Different polytypes could be obtained depending on the reaction temperature.

## References

1. Newman, S., Jones, W., O'Connor, P., Stamires, D.N., (2002) *Journal of Material Chemistry*, 12, 153-155.
2. Fruhwirth, O., Herzog, G.W., Hollere, I. and Rachetti, A., (1985) *Surface Technology*, 24, 301-317.
3. Stamires, D., Jones, W., Daamen, S., (2002) *United States Patent* US 6,593,265 B2.

## **Solvent Influence on Organic Crystal Agglomeration**

Eva M. Ålander and Åke C. Rasmuson

*Department of Chemical Engineering and Technology, Royal Institute of Technology, 100 44  
Stockholm, Sweden*

### **1. Summary**

The agglomeration of ibuprofen and paracetamol during crystallization in different pure solvents has been investigated. Narrowly sieved crystals were suspended as seeds and were allowed to grow and agglomerate in supersaturated solutions at constant temperature. To quantify the degree of agglomeration, particles from each experiment were examined by image analysis. Surfaces of large and well-grown crystals have been characterized by contact angle measurements. The surface free energy components of the crystal faces have been estimated using three probe liquids and the Lifshitz-van der Waals acid-base theory. The data were used for estimation of the solid-liquid interfacial free energy and the crystal-crystal adhesion free energy of pairs of faces in different solvents. It is found that there is a dependence of the degree of agglomeration on solvent selection that can be correlated to the independently estimated free energy of adhesion.

Keywords: crystallization, agglomeration, contact angle measurements, adhesion free energy

### **2. Extended abstract**

The crystallization process is a critical step in the manufacture of pharmaceutical compounds. In this step properties such as the polymorphic form, particle size, crystal habit, surface properties and mechanical strength can be controlled to achieve a required product quality. Among important parameters like supersaturation generation, feed and mixing conditions the selection of solvent is crucial. The solvent very much determines the productivity and yield of the process, but also the crystal size, shape and agglomeration. Agglomeration is in principal a three steps process: crystals collide, adhere and grow together. After collision, physico-chemical and fluid mechanical forces compete and determine the time available for crystalline bridging between crystal faces. All three steps are influenced by the properties of the solvent.

In previous work the influence of solvent composition on crystal agglomeration of paracetamol was studied [1-3]. The agglomeration behaviour in the crystallization experiments correlated to large extent to the solvent polarity and to the free energy of adhesion between crystal faces in various solvents. The paracetamol product is less agglomerated and the agglomerates are weaker when the crystallization is carried out in polar solvents where the crystal-solvent interactions are stronger, e.g. in water.

In recent work the agglomeration behaviour of (RS)-ibuprofen crystals has been investigated. In comparison with the paracetamol crystal, the important faces of the ibuprofen crystal expose a more pronounced difference in hydrogen bonding ability. Also the morphologically dominant face of the ibuprofen and paracetamol crystal displays very different hydrophilicity, as is indicated by the water contact angle of 71° and 21°, respectively. The fully seeded isothermal crystallization experiments were carried out in four organic solvents (toluene, ethyl acetate, ethanol, and methanol) within the solvent polarity range 0.099-0.762. Particles from each experiment were examined under a microscope by image analysis. Each particle is characterized for the number of crystals per agglomerate (C/A-number) using a set of calibration particles. The ibuprofen product of all experiments is only to minor extent agglomerated. Hence, differently from the results of paracetamol, the agglomeration behaviour of ibuprofen is independent of solvent and polarity (See Figure 1a). Surfaces of large and well-grown ibuprofen crystals have been characterized by contact angle measurements. The surface free energy components of a crystal face are estimated using three probe liquids (water, formamide, and diiodomethane) and the Lifshitz-van der Waals acid-base theory [4]. The free energy of adhesion between pairs of the characterized crystal face in different solvents, including the solvents of the crystallization experiments, can then be calculated. It turns out that the observed degree of agglomeration of paracetamol and ibuprofen in the crystallization experiments of different solvents agree with the trend of the estimated free energies of adhesion (See Figure 1). When the attractive adhesion forces are too weak the hydrodynamic forces can easily keep the crystals apart thus reducing agglomeration. Hence, the results gives support to that the agglomeration behavior is linked to the crystal surface chemistry and to the crystal-solvent interactions.

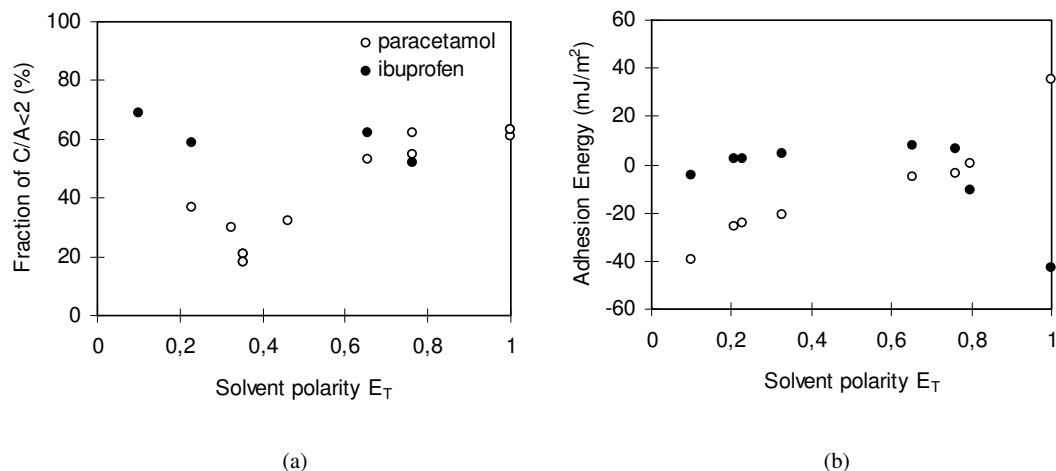


Figure 1: Change in a) degree of agglomeration (represented by the number fraction of particles in a sample having a C/A number less than 2) and b) free energy of adhesion (between two morphologically dominant faces) with solvent polarity.

## References

1. Ålander, E., Uusi-Penttilä, M. and Rasmuson, Å., (2004) *Ind. Eng. Chem. Res.*, 43, 629-637.
2. Ålander, E. and Rasmuson, Å., (2005) *Ind. Eng. Chem. Res.*, 44, 5788-5794.
3. Ålander, E. and Rasmuson, Å., (2006) *AIChE J.*, in press.
4. van Oss, C. J., Good, R. J. and Chaudhury, M. K., (1988) *Langmuir*, 4, 884-891.

## Session T2-10a: Distillation, Absorption & Extraction – I

<b>Abstract Number</b>	<b>Paper Title &amp; Authors</b>	<b>Included</b>
731	Revamping gas absorption solvents with functionalized ionic liquids L M G Sánchez, G W Meindersma, A B de Haan	Yes
801	Benefits of Entrainer-based Reactive Distillation over Reactive Distillation for the Synthesis of Fatty Acid Esters M C Jong, A C Dimian, N J M Kuipers, A B de Haan	Yes
1177	Structure and Activity Relationships for CO <sub>2</sub> Regeneration from Aqueous Amine Based Absorbents P Singh, G F Versteeg	Yes
2328	Adsorptive isomer distillation of gasoline related molecules S I Andersen, A Leerskov, P J Mune	Yes

Session T2-10a

## Revamping gas absorption solvents with functionalized ionic liquids

L.M. Galán Sánchez<sup>a</sup>, G.W. Meindersma<sup>b</sup>, A.B. de Haan<sup>b</sup>

<sup>a</sup>Separation Technology, University of Twente, P. O. Box 217, 7500 AE Enschede, The Netherlands

<sup>b</sup>Process System Engineering Group, Eindhoven University of Technology, P.O. Box 513, 5600 MB Eindhoven, The Netherlands

### 1. Summary

A study of the Room Temperature Ionic Liquids (RTILs) as promising absorption solvents for recovery of CO<sub>2</sub> and separation of olefins from paraffins is presented. The solubility of C<sub>2</sub>H<sub>4</sub>, C<sub>2</sub>H<sub>6</sub> and CO<sub>2</sub> into standard and designed RTILs is measured at temperatures and pressures up to 343 K and 1 MPa. In the structures of the designed RTILs functional groups are included to improve the solvent performance in targeted gas absorption. The higher gas loads are attained with the designed RTILs solvents. Gas solubility increases when temperature decreases and pressure rises. The functionalized RTILs enhanced the absorption ( $\chi$ ) of CO<sub>2</sub> and C<sub>2</sub>H<sub>4</sub> around 5 and 3 times respectively, compared to that on the standard ionic liquids. The designed RTILs are able to merge in one solvent the behaviour exhibited by chemical and physical solvents used in absorption processes. The gas loads achieved and the possibility for regeneration strongly positioned RTILs as an alternative to the traditional solvents.

Keywords: Absorption solvents, Ionic liquids, CO<sub>2</sub> absorption, olefin/paraffin separation

### 2. Extended Abstract

Ionic liquids are potential solvents for gas absorption operations due to its properties, such as a very low vapour pressure and the possibility to design its constitutive ions for task specific purposes. Characterization of ionic liquids as solvents for gas absorption systems is essential for its industrial application. An approach of the factors which influence gas absorption, diffusion and mass transfer in ionic liquids is presented here. The study of solvent bulk properties and absorption behaviour was performed for common and functionalized ionic liquids.

The performance of ionic liquid solvents in two absorption applications was determined. The absorption of CO<sub>2</sub> and the separation of olefins from paraffins were chosen as examples. The solubility of C<sub>2</sub>H<sub>4</sub>, C<sub>2</sub>H<sub>6</sub> and CO<sub>2</sub> into different Room Temperature Ionic Liquids (RTILs) was measured at temperatures between 303 K and 343 K and pressures

up to about 1 MPa. The RTILs used were alkyl imidazolium-based cations paired with several anions:  $[\text{BF}_4]^-$ ,  $[\text{DCA}]^-$ ,  $[\text{NTf}_2]^-$ ,  $[\text{OTf}]^-$ ,  $[\text{NO}_3]^-$ . To improve the performance of the solvent for gas absorption, some of the RTILs used were designed for carrying out the specific separation. For the  $\text{CO}_2$  absorption, the ionic liquids were functionalized with an amine group, while in the case of the  $\text{C}_2\text{H}_4/\text{C}_2\text{H}_6$  separation, the liquids were functionalized with metallic salts.

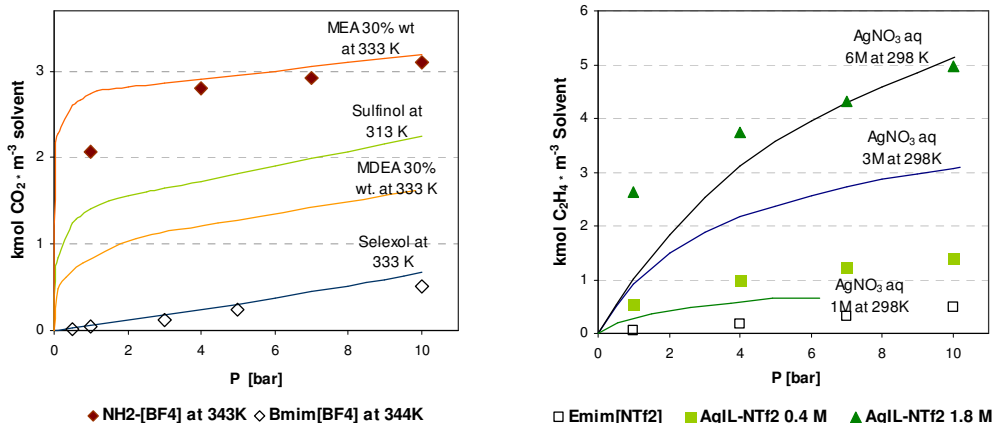


Figure 1: CO<sub>2</sub> Solvent capacity of RTILs at 343 K. Figure 2: C<sub>2</sub>H<sub>4</sub> Solvent capacity of RTILs at 303 K.

The results indicated that, in general, the gas solubility into RTILs decreased with a raise in temperature and increased at higher pressures. A chemical enhancement of the gas absorption was observed when functionalized RTILs were used as absorption solvents, see Figs. 1 and 2. The influence of the specific bulk and surface properties of the ionic liquid, such as density, viscosity and surface tension, on the ion mobility was more evident with functionalized RTILs. The effect of the bulk properties is reflected in the absorption kinetics and mass transfer resistances. The rise of ion mobility and species accessibility caused by an increase in temperature almost cancelled out the expected effect of a temperature rise on the C<sub>2</sub>H<sub>4</sub> absorption when a functionalized RTIL for the olefin/paraffin separation was used. The chemical enhancement of the CO<sub>2</sub> absorption into amine-functionalized RTILs was almost threefold the gas volumetric load in comparison with non-functionalized RTILs. The selectivity of the C<sub>2</sub>H<sub>4</sub>/C<sub>2</sub>H<sub>6</sub> separation was improved up to 10 times when ions of metallic salts were included in the RTIL structure. Regeneration of the RTILs was possible and the conditions varied with the RTIL properties. The factors that influence the diffusion, mass transfer, kinetics depend on the anion and cation of the RTIL and the accessibility to the active species in the RTILs.

It was possible to change the ionic liquid structure in order to improve its performance as a gas solvent. The CO<sub>2</sub> load of ionic liquids increased almost threefold with primary amine groups incorporated to the ionic liquids structure. The non-functionalized ionic liquids exhibited lower CO<sub>2</sub> loads and the absorption behaviour was similar to physical solvents for CO<sub>2</sub> absorption. Ionic liquids can merge in one solvent the behaviour exhibited by chemical and physical solvents used in absorption.



## **Benefits of Entrainer-based Reactive Distillation over Reactive Distillation for the Synthesis of Fatty Acid Esters**

M.C. de Jong<sup>a</sup>, A.C. Dimian<sup>b</sup>, N.J.M. Kuipers<sup>c</sup>, A.B. de Haan<sup>a</sup>

<sup>a</sup>*Process Systems Engineering, Eindhoven University of Technology, P.O. Box 513, 5600 MB Eindhoven, The Netherlands*

<sup>b</sup>*HIMS, Faculty of Science, University of Amsterdam, Nieuwe Achtergracht 166, 1018 VW Amsterdam, The Netherlands*

<sup>c</sup>*Separation Technology, University of Twente, P.O. Box 217, 7500 AE Enschede, The Netherlands*

### **1. Summary**

For the synthesis of fatty acid ester a conventional Reactive Distillation (RD) process and the Entrainer-based Reactive Distillation (ERD) process were compared with the aid of process models. In ERD an entrainer improves the conversion by continuously removing water. This results in a significantly smaller reactive section compared to conventional RD. Secondly, only one column is necessary, instead of two. Therefore ERD could become an economically interesting alternative process for the production of fatty acid esters.

Keywords: Reactive Distillation, Entrainer, Modelling, Fatty Acids

### **2. Extended Abstract**

Where in conventional Reactive Distillation (RD) a reaction column and a recovery column are necessary to reach high conversions, Entrainer-based Reactive Distillation (ERD) may take place in only one column. ERD not only uses separation to improve reaction, but also the introduction of an entrainer feed to make the separation feasible by increasing the relative volatility of one of the products. ERD appears to be advantageous for the synthesis of fatty acid esters. The entrainer increases the relative volatility of water (by-product) compared to the alcohol (reactant), such that during the reaction the water can be continuously removed by distillation by breaking the azeotrope. In this way the chemical equilibrium is shifted such that higher conversions can be obtained.

The ERD column consists of a reactive section with a distillation section placed on top, in where the entrainer is responsible for removing the water out of the reactive section. The top vapour is condensed and two phases are obtained through decantation: an aqueous phase and an entrainer rich phase which is refluxed back into the column. Of course adding an entrainer also has disadvantages: the most important one is that pollution of the

product has to be prevented, therefore the entrainer should not enter the reactive section. The more entrainer is added the more critical this is.

### Objective and Approach

The conceptual feasibility of ERD for the synthesis of fatty acid esters is already shown by Dimian et al.. This work will concentrate on the gains that can be obtained using ERD with regarding to conventional RD.

The objective of this work was to compare the ERD process with a conventional RD process for the synthesis of fatty acid esters. An operating window was constructed which contains the necessary conditions to be able to produce fatty acid esters by ERD. Within this operation window both processes were compared and the advantage of ERD, which can be expressed in decreasing number of stages and the omission of a recovery column, was weighted against the constraints that are introduced together with the entrainer. The comparison was done by process models made in Aspen Plus<sup>®</sup> for the esterification of lauric acid with isopropanol using a heterogeneous catalyst.

### Results

From the Aspen Plus<sup>®</sup> simulations can be seen that the entrainer in the distillation section indeed enhances the water removal from the reactive section without entering the reactive section itself and thus the equilibrium is favourably shifted. It also causes a higher alcohol concentration and therefore a higher reaction rate in the reactive section. The operating window in which this occurs is determined by the entrainer to feed ratio. A minimal value has to be reached to make the process work. When a certain value is exceeded (maximum) the entrainer completely ends up in the bottom of the distillation section, which results in a decreasing product purity. Within this operating window the number of stages in the reactive section necessary to achieve a certain conversion is significantly smaller for the reaction section for ERD than for the conventional RD column. The entrainer to feed ratio shows an optimum with respect to the capacity of removing water, however product purity is not influenced. It is desirable that the entrainer does not reach the reactive section. This can be prevented by introducing heat at the top stage of the reactive section. The more entrainer is added the more entrainer ends up in the bottom of the distillation section, such that more energy is needed to prevent the entrainer from entering the reactive section. Thus, the optimal entrainer to feed ratio is a compromise between water removal capacity/number of reactive stages and the amount of entrainer in the bottom of the distillation section which has to be prevented from entering the reactive section.

### Conclusion

Within the operation window where ERD can be used, its use results in a significantly smaller reactive section compared to conventional RD. Therefore ERD could become an economically interesting alternative process for the production of fatty acid esters.

### References

Dimian, A.C., Omota, F. and Blik, A., (2004) *Chemical Engineering and Processing*, 43, 411-420.

## Structure and Activity Relationships for CO<sub>2</sub> Regeneration from Aqueous Amine Based Absorbents

Prachi Singh<sup>a</sup> and Geert F. Versteeg<sup>b</sup>

<sup>a</sup>*Department of Chemical and Biochemical Engineering, Clarkson University, P.O.Box 5705, Potsdam, NY 13699-5705, USA.*

<sup>b</sup>*Faculty of Science and Technology, Twente University, P.O. Box 217, 7500 AE, Enschede, The Netherlands*

### 1. Summary

A study to determine the structure and activity relationships of various amine based CO<sub>2</sub> absorbents was performed in which, the desorption of CO<sub>2</sub> from saturated absorbent at 80 °C and atmospheric pressure was measured to assess the initial desorption rate and desorption capacities at pseudo equilibrium. Evaluation of desorption capacity at 80 °C will give a better understanding for more energy efficient and lower circulation rate absorbent for CO<sub>2</sub> absorption process.

Keywords: Absorption, Desorption, CO<sub>2</sub>, Amine, Acid gas, Kinetics.

### 2. Extended Abstract

Although the absorption of acid gases such as CO<sub>2</sub> in aqueous amine solutions like e.g. MEA (monoethanolamine) from natural gas concerns proven technology, the removal of CO<sub>2</sub> from flue gases is not as straightforward as it could be expected. In these currently used systems a major part of the operational costs is caused by the solvent regeneration (up to 40%). In industrial processes, very high temperatures (>100 °C) are used to regenerate MEA solutions. Usually high pressure steam is applied, which provides the heat of reaction and enables the transport of CO<sub>2</sub> out of the reactor. The regeneration process is usually done at the temperature in excess of the boiling temperature, as the chemical kinetics of regeneration increases with temperature. Although desorption processes often act as regenerative processes for absorption systems, studies devoted to desorption are not as numerous as those concerning absorption. More specifically, the relationship of structure and regeneration characteristics of various amines based absorbent for CO<sub>2</sub> is hardly studied.

Therefore, a screening method has been developed for the desorption of CO<sub>2</sub> from various loaded amine based aqueous absorbents. It is aimed that in this investigation screening of various compounds on their regeneration at low temperature, atmospheric pressure with rapid regeneration rate and low evaporation solution loss especially. Desorption of CO<sub>2</sub>

from various amine based absorbents was measured to assess the amount of CO<sub>2</sub> desorbed and the overall rate of desorption at 80 °C. In this study the effects which were investigated are the chain length, number of functional groups, different functional groups at the  $\alpha$ -carbon, cyclic amine and substituted cyclic amines. From this study the solvents which showed the lower desorption capacities at pseudo-equilibrium were found to be more suitable, as they will decrease the solvent circulation rate in the CO<sub>2</sub> capture process. Hence, that will be economically beneficial for the whole CO<sub>2</sub> capture process. Also the evaluation of the desorption rate at 80 °C will give the indication of more energy efficient absorbent, that might result in a decrease in energy cost for the CO<sub>2</sub> absorption process. Based on the results a better understanding of the structural effect on CO<sub>2</sub> desorption will be developed. Hence, these results could be an advantage in the development of an improved amine based CO<sub>2</sub> absorbent, which will lead to a better approach for development of new technologies in the CO<sub>2</sub> capture area.

## References

Blauwhoff P.M.M., Versteeg G.F. Van Swaaij W.P.M., A study on the reaction between CO<sub>2</sub> and alkanolamines in aqueous solutions. *Chemical Engineering Science* 1984, pp 207-225.

Hook Robert J., 1997: An Investigation of Sterically Hindered Amines as Potential Carbon Dioxide Scrubbing Compounds, *Industrial Engineering & Chemistry Research* Vol. 36, pp 1779-1790.

Caplow M. 1968: Kinetics of Carbamate formation and Breakdown, *Journal of American Chemical Society* Vol 90, pp 276.

Chakraborty A.K., Astarita G., Bischoff K.B. 1986: CO<sub>2</sub> Absorption in Aqueous Solutions of Hindered Amines. *Chemical Engineering Science* Vol 41, pp 997-1000.

Chakraborty A.K., Astarita G., Bischoff K.B. Damewood J.R. Jr. 1988: Molecular orbital Approach to Substituent Effects in Amine-CO<sub>2</sub> Interactions. *Journal of American Chemical Society* Vol 110, pp 6947.

Sartori G., Savage D.W. 1983: Sterically hindered amines for CO<sub>2</sub> Removal from gases. *Industrial Engineering Chemistry Fundamentals* Vol 22, pp-239-249.

## **Adsorptive isomer distillation of gasoline related molecules**

S.I. Andersen, A. Leerskov, P.J. Mune

*Haldor Topsøe A/S, R&D Refinery, Nymøllevej 55, DK-2800 Kgs. Lyngby, Denmark*

### **1. Summary**

The importance of highly branched isomers as octane improvers in gasoline is well known. Where isomerization processes are well described and used, the further separation of the effluent streams of these reactors into high RON (research octane number) compounds and low RON compounds is complex and energy demanding. Simple distillation of isomers requires large and very effective columns and high reflux ratios.

Various technology solutions have been proposed and are used in the refining industry. Apparently, the most common ones are adsorption processes either as simulated moving bed, chromatographic separation or pressure swing adsorption. Most of these processes are technologically complicated and require extensive posttreatment of product streams.

In an attempt to enhance the separation, we have developed the novel concept of adsorptive distillation. The process consists of a hybrid between extractive distillation and adsorption. The process uses a packed column, which is operated at isothermal conditions, and the packing is made up from beads or extrudates of an adsorbent with specificity for a given molecular structure or type. The paper describes the development of the process with the aim to separate n-heptane and methylcyclohexane boiling at 98°C and 101°C, respectively.

Keywords: C7 isomers, adsorption, extraction, distillation



## Session T2-10b: Distillation, Absorption & Extraction – II

<b>Abstract Number</b>	<b>Paper Title &amp; Authors</b>	<b>Included</b>
341	New Approach to Energy Efficient Chemical Process Design A Lucia, A Amale, R Taylor	Yes
368	Methods for Extractive Distillation Flow Sheets Synthesis L Ivanova, A Timoshenko, E Anokhina	Yes
399	Multicomponent rectification: Representation of number of stages as function of reflux ratio J Bonet, M I Galan, J Costa, X M Meyer, M Meyer	Yes
431	Conceptual Process Design for Aromatic/Aliphatic Separation with Ionic Liquids G W Meindersma, A B de Haan	Yes
1576	A Systematic Synthesis Framework for Extractive Distillation Processes S Kossack, K Kraemer, R Gani, W Marquardt	Yes
3286	Energetic Analysis of a Crude Distillation Plant: a Case Study M Mascia, M Errico, G Tola	Yes

Session T2-10b



## **New Approach to Energy Efficient Chemical Process Design**

Angelo Lucia<sup>a</sup>, Amit Amale<sup>a</sup>, Ross Taylor<sup>b</sup>

<sup>a</sup>*Department of Chemical Engineering, University of Rhode Island, Kingston, RI 02881 USA*

<sup>b</sup>*Department of Chemical & Biomolecular Engineering, Clarkson University, Potsdam, NY 1369 USA*

### **1. Summary**

The shortest stripping line approach, originally described in Lucia et al. (2006), is used to address two open issues in process synthesis and design – the sensitivity of energy efficient designs to trace components in product streams and finding non-pinch, energy efficient solutions. Trace component sensitivities are handled by a two-level design procedure that uses a process target in an outer loop and the shortest stripping line approach in an inner loop to generate portfolios of minimum energy designs and to show that Underwood's method corresponds to the global minimum in the stripping line distance. Mixed Integer Nonlinear Programming (MINLP) and process targets are used to find non-pinch solutions to multi-unit processes.

Keywords: energy efficient process design, shortest stripping lines, Underwood equivalence, non-pinch solutions

### **2. Extended Abstract**

Distillation remains the most versatile means of separation and will continue to be used in some capacity to address a wide variety of separation needs. Therefore, new synthesis and design methodologies for overall energy efficiency must extend the current knowledge base for finding minimum energy requirements in distillation and also address processes involving multiple units. The particular design and optimization approach presented in this talk is based on the novel concept of shortest stripping lines. Through new global optimization formulations, the proposed methodology

- 1) Is a unification of existing methods for finding minimum energy needs in the presence of feed, saddle, or tangent pinch points and applies to all distillations.
- 2) Finds minimum energy solutions that do not correspond to pinch points.
- 3) Is unaffected by the number of components.
- 4) Can be combined with other synthesis methods like attainable regions.
- 5) Uses a back-to-front philosophy to identify correct processing targets for processes with multiple units (e.g., reaction/separation/recycle, hybrid separation schemes) such that overall energy consumption is minimized.
- 6) Can be used to provide portfolios of minimum energy designs.

- 7) Can provide starting values for more detailed rating optimization calculations.
- 8) Can be used to establish that longest and shortest paths are unifying geometric principles for the design of energy efficient chemical processes.
- 9) Solves problems other synthesis methodologies cannot.
- 10) Enhances the teaching and practice of energy efficiency in process design through a simple and straightforward theory that is easily understood.

This talk focuses on two important open issues in process synthesis and design.

- 1) The sensitivity of design methodologies and energy demands to trace component compositions in product streams.
- 2) The synthesis and design of non-pinch energy efficient multi-unit processes.

General optimization formulations are given and numerical results are presented that show that these issues can be resolved using the shortest stripping line methodology. A two-level design procedure is proposed to address the sensitivity of energy demands to trace compositions in product streams. This two-level approach uses key component recoveries instead of product compositions to fix the desired separation. Non-key recovery fractions (or equivalently bottoms product compositions) are adjusted in an outer loop while the corresponding shortest stripping line distance is computed in an inner loop. As a result, our two-level design procedure generates a portfolio of minimum energy designs for a variety of feasible product compositions. The two-level design procedure also provides a framework within which we can establish that Underwood's method can be shown to correspond to the minimum of all shortest stripping line distances for the desired separation. Thus Underwood's method is a global minimum in the stripping line distance under the conditions that separation requirements are specified in terms of recovery fractions.

A second important and equally important attribute of the shortest stripping line approach is its ability to easily find non-pinch energy efficient solutions. The concept of processing target for a reacting mixture is used to study the trade-offs between reactive distillation and reaction-separation-recycle (RSR) processes. Equilibrium and kinetically controlled reaction systems are studied and clearly show that the most energy efficient design configurations often involve non-pinch separators.

Finally, we close by noting that the shortest stripping line approach is a unifying geometric design procedure that encompasses many methods for energy efficient synthesis and design including the McCabe-Thiele method, Underwood's method (as presented in this talk), boundary value methods, and others. Moreover, it can find solutions other methods cannot – either by itself or when combined with other design methodologies such as the two-level design procedure for energy portfolios and attainable regions. Thus in our opinion, the shortest stripping line approach lays the foundation for the next generation of energy efficient process synthesis and design tools.

## References

Lucia, A., Amale, A. and Taylor, R., (2006) *Industrial & Engineering Chemistry Research*, 45, 8319-8328.

## Methods for Extractive Distillation Flow Sheets Synthesis

Ludmila Ivanova, Andrey Timoshenko, Elena Anokhina

*Lomonosov's Moscow State Academy of Fine Chemical Technology Chemistry and Technology of Basic Organic Synthesis Dpt., 86, Vernadskogo ave., 119571, Moscow, Russian Federation*

### 1. Summary

The graph-theoretical approach was used for the extractive distillation flow sheets construction. We propose to synthesize the extractive n-component distillation flow sheet manifold by transformation of graphs explicated the separation of (n+1)-component mixture in the sequence of simple columns. The initial flow sheet was presented as oriented graph in which nodes characterize columns and fractions, and edges describe flow relationships between them. The transformation leads to the manifold of extractive distillation flow sheets which workability must be verified. Thus, we have developed a universal algorithm for synthesizing workable flowsheets for extractive distillation of multicomponent azeotropic mixtures.

Keywords: extractive distillation, flow sheets synthesis

### 2. Extended Abstract

Distillation is one of the most widely used industrial methods in the separation of multicomponent mixtures. Those processes often accounts for up to 70% of the total productive power consumption in chemical industry. This raises the problem of flowsheet optimization with energy consumption decreasing. Thermodynamically reversible distillation is the least energy-consuming. However, it is unfeasible because of its specific features [1]. One can only approach thermodynamic reversibility by optimizing flowsheet structure and/or using diabatic distillation. The well known examples are Petlyuk [1] and dividing-wall wall [2] columns. In this case only one feature of the reversible distillation was used – the components with the intermediate volatilities full distribution between the products. From this standpoint, of great interest are flow sheets with the partially thermally coupled columns which thermodynamic efficiency lies between the simple and Petlyuk columns. The investigation of partially thermally coupled complexes is difficult because of their quantity for the multicomponent mixtures distillation. More than that, the methods were proposed for their creation only some years ago [3]. These ones are based on the initial graph transformation of the simple distillation columns sequences. Also one can use for this operation the residue curve graphs [4]. Now this graph-theoretical approach may be used not only for the zeotropic but also for the extractive distillation

flow sheets construction. We propose to synthesize the extractive n-component distillation flow sheet manifold by transformation of graphs explicated the separation of (n+1)-component mixture in the sequence of simple columns. It is possible because in the extractive distillation there are no thermodynamical restrictions on the products composition [5]. The initial flow sheet have to be presented as oriented graphs in which nodes characterize columns and fractions, and edges describe flow relationships between them. This graph describes the separation sequence. The next step of the synthesis is to split the feed flow into two individual flows: the n-component mixture and the extractant. This structure already almost fully represents the extractive distillation flowsheet. It is only necessary to create a cycle for the extractant by merging two nodes which are explicated extractant flow. Thus we obtain the extractive distillation flow sheet graph. Note that, depending on the vapor-liquid equilibrium pattern, more than one edge may leave the "extractant" node (the extractant may also be necessary for separating the mixture in the second column of the system).

Since the extractive distillation system has a closed (without taking into account losses) cycle for the extractant, one of the conditions of operability of flow sheets synthesized using the proposed algorithm is the presence of a cycle in the orgraph. A cycle must include at least two nodes representing columns. A second condition of operability of the proposed flow sheets is the introduction of the extractant into the column in which an azeotropic pair of components is separated. Thus, we have developed a universal algorithm for synthesizing workable flowsheets for extractive distillation of multicomponent azeotropic mixtures. More than that now we can construct the extractive distillation flow sheets with partially coupled columns for separation of multicomponent mixtures using simultaneously two proposed methods of synthesis [3,5].

The part of this work was supported by the Russian Foundation for Basic Research.

## References

- [1] Petlyuk F.B., V.M. Platonov and Slavinskij D.M. (1965) *Int. Chem. Eng.*, 5, 555–561.
- [2] Kaibel G., Schoenmarkers H., *Process Synthesis and Design in Industrial Practice*. Proc. ESCAPE-12 (Computer Aided Process Engineering,10), Eds. J. Grievink and J.V. Schijndel, Elsevier, Amsterdam (2002).
- [3] Timoshenko, A.V. and Serafimov L.A., (2001) *Theor. Found. Chem. Eng.*, 35, 567–572
- [4] Timoshenko A. V., Anokhina E. A. and Buev D. L., (2004) *Theor. Found. Chem. Eng.*, 38, 160–164
- [5] Ivanova L.V., Timoshenko A.V., Timofeev V.S. (2005) *Theor. Found. Chem. Eng.*, 39, pp. 16–23.

## Multicomponent rectification: Representation of number of stages as function of reflux ratio

J. Bonet<sup>a,b</sup>, M.-I. Galan<sup>a</sup>, J. Costa<sup>a</sup>, X.-M. Meyer<sup>b</sup>, M. Meyer<sup>b</sup>

<sup>a</sup>*Department of Chemical Engineering, University of Barcelona, Martí i Franquès 1, E-08028Barcelona, Spain*

<sup>b</sup>*Laboratoire de Génie Chimique, UMR-CNRS 5503, INPT-ENSACET, 5 rue Paulin Talabot, 31106 Toulouse Cedex 01, France*

### 1. Summary

The aim of this work is to provide a guideline for distillation column designers to correlate the number of stages and the reflux and to propose an initial value which could be near the optimum. The Gilliland graphical representation of the number of stage in front of the reflux is recalculated and extended to more points and systems by rigorous simulation. The optimal feed plate is assured and systems disregarded by Gilliland are taken into account. All this data are used to plot a graphic of the quotient, with its minimal values, of the number of stages and the reflux. An equation is proposed to fit these data. The rule of thumb that asserts the optimal reflux is from 1.2 to 1.5 times its minimal value is verified.

Keywords: distillation, Gilliland correlation, rule of thumb, optimal reflux

### 2. Extended Abstract

Gilliland (1940) found a graphical representation where several systems followed the same representation with small deviations. Until then, usually, the number of stages ( $N$ ) is represented directly as function of the reflux ratio ( $r$ ); the system is fed at its optimal plate (figure 1). The minimal reflux ratio ( $r_{\min}$ ) and the minimal number of stages ( $N_{\min}$ ) are the horizontal and vertical asymptotes. It has been demonstrated that the elbow of this curve corresponds to a flat minimum where is the optimal operation zone (Bonet et al, 2005). It is quite intuitive to imagine that, the investment costs are too high at the left side and the operating costs are too high at the right side.

When the Gilliland's cases are recalculated by rigorous simulation, the coincidence of curves is observed when the asymptotic limiting conditions of the minimal reflux and minimal number of stages are transformed to definite points (figure 2a). Gilliland (1940) postulated that his correlation has to be used with caution for mixtures of abnormal volatilities such as ethanol and water. Gilliland correlation can be applied independently to each column section (Youssef et al, 1989). Gilliland correlation is still used nowadays at the first steps of column design and it is used as a base for new shortcut models (Gadalla et al, 2003).

The representation of all the evaluated points including abnormal volatility systems on the Gilliland graphic does not show a so nice curve as for his studied cases (figure 2b). However, all the points give us an idea of a general tendency. The first calculated points where the reflux costs are predominant are symbolized by squares and the points where the investment costs are predominant are symbolized by rounds. Another feasible representation of the data would be observed on figure 2c. Whereas the optimal zone at the Gilliland representation is rather disperse, it is more delimited for this other representation. Figure 2d shows a zoom of the optimal zone with a starting point for a column design and the representation of a proposed equation to correlate the points.

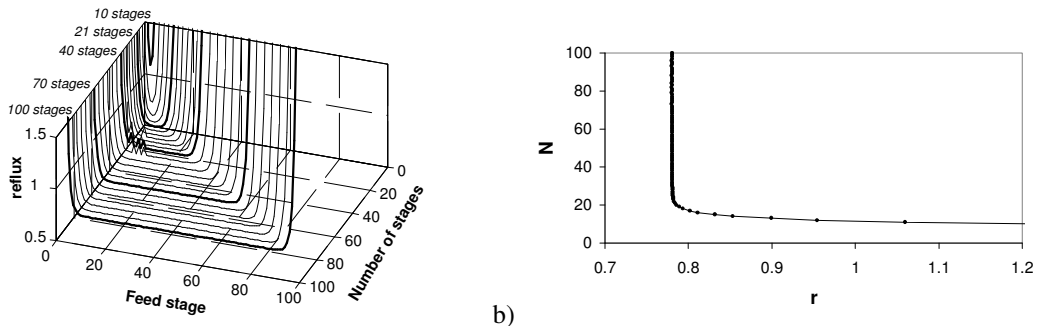


Figure 1- Analysis of a methanol (0.1) – acetone (0.1) – water (0.8) feed mixture, feed at boiling point,  $P=101325$  Pa,  $D/F= 0.2063$  and  $x_B(\text{acetone})=0.995$ . (a) Reflux, number of stages and feed stage; (b) reflux and number of stages at optimal feed stage.

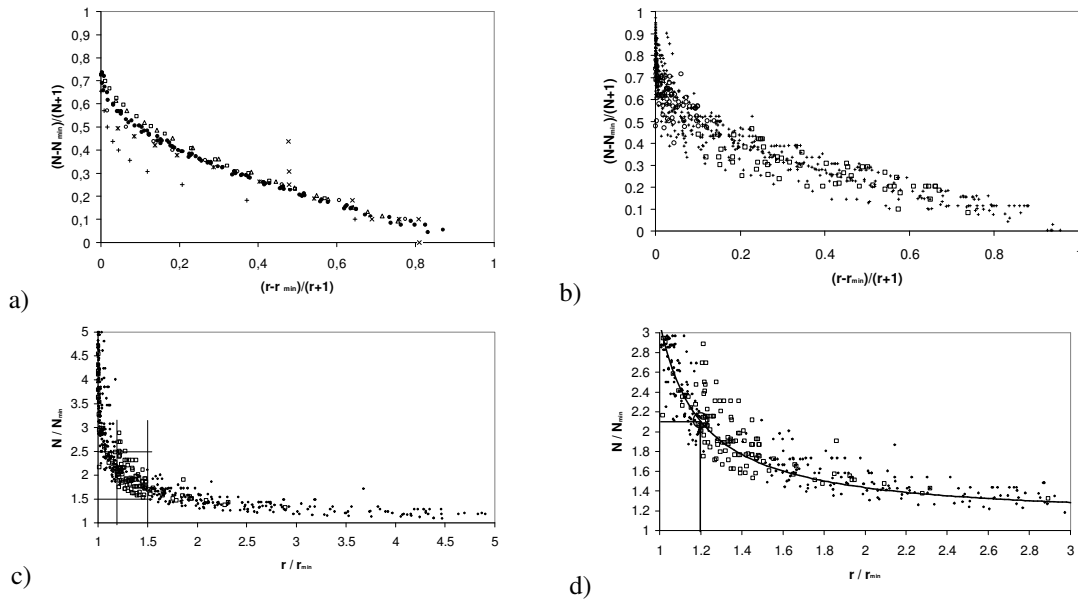


Figure 2- Graphical correlations of the number of stages in front of the reflux. (a) Gilliland graphic and cases; (b) Gilliland graphic for all cases; (c) proposed graphic for all cases; (d) detail of the proposed correlation and design values.

## References

- Bonet, J., Galan, M-I., Costa, J., They, R., Meyer, X-M., Meyer, M., Reneaume J-M., (2005) *Institution of Chemical Engineers Symposium Series*, 152, 344-352.  
 Gilliland, E.R., (1940) *Industrial and Engineering Chemistry*, 32(9), 1220-1223.  
 Youssef, S., Domenech, S., Pibouleau, L., (1989) *Chemical Engineering Journal*, 42(3), 153-165.  
 Gadalla, M., Jobson, M., Smith, R., (2003) *Chemical Engineering Research and Design*, 81(A8), 971-986.

## Conceptual Process Design for Aromatic/Aliphatic Separation with Ionic Liquids

G.W. Meindersma and A.B. de Haan

*Department of Chemical Engineering and Chemistry/SPS, Eindhoven University of Technology, P.O. Box 513, 5600 MB Eindhoven, The Netherlands*

### 1. Summary

The investment and annual costs for a separation of aromatic hydrocarbons from a naphtha feed (~10 % aromatics) can be 35 to 70 % lower for an extraction with ionic liquids compared to an extraction with sulfolane. Aromatic hydrocarbons (benzene, toluene, ethyl benzene and xylenes) and C<sub>4</sub> - C<sub>10</sub> aliphatic hydrocarbons are normally separated by liquid extraction, extractive distillation or azeotropic distillation. The application of ionic liquids for separation processes is promising because of their non-volatile nature [1]. This facilitates solvent recovery using techniques as simple as flash distillation or stripping.

Keywords: ionic liquids, extraction, Rotating Disc Contactor, naphtha cracker, cost evaluation

### 2. Extended Abstract

Ionic liquids are organic salts that are liquid at low temperature (<100°C) and they consist of cations based on methylimidazolium [Rmim], 1-butylpyridinium [R-N-bupy] and others, and organic or inorganic anions.

Most ethylene cracker feeds contain 10 to 25% of aromatic components, depending on the source of the feed (naphtha or gas condensate). The aromatic compounds are not converted to olefins and even small amounts are formed during the cracking process in the cracker furnaces [2]. Therefore, they occupy a part of the capacity of the furnaces and they put an extra load on the separation section of the C<sub>5</sub><sup>+</sup>-aliphatic compounds. If a major part of the aromatic compounds present in the feed to the crackers could be separated upstream of the furnaces, it would offer several advantages: higher capacity, higher thermal efficiency and less fouling. The energy requirement of a thermal cracker is about 8.5 GJ/ton feed. The improved margin will be around € 20/ton of feed or € 48 million per year for a naphtha cracker with a feed capacity of 300 ton/hr, due to the lower operational costs. The application of ionic liquids for extraction processes is promising because of their non-volatile nature. This facilitates solvent recovery using techniques as simple as flash distillation or stripping.

The extraction of toluene from a mixed toluene/heptane stream was used as a model system. The extraction with the ionic liquid 4-methyl-N-butyl-pyridinium tetrafluoroborate ([mebupy]BF<sub>4</sub>) was evaluated in a pilot plant Rotating Disc Contactor (RDC). With the NRTL interaction parameters determined for this separation, a process model could be developed using ASPEN Plus 12.1 [3]. The data measured in the pilot plant and the data calculated with the model are in reasonable agreement with each other. With the results of process simulations for the separation of toluene from a mixed toluene/heptane stream, an economic evaluation of the process was made and compared to the extraction process with sulfolane.

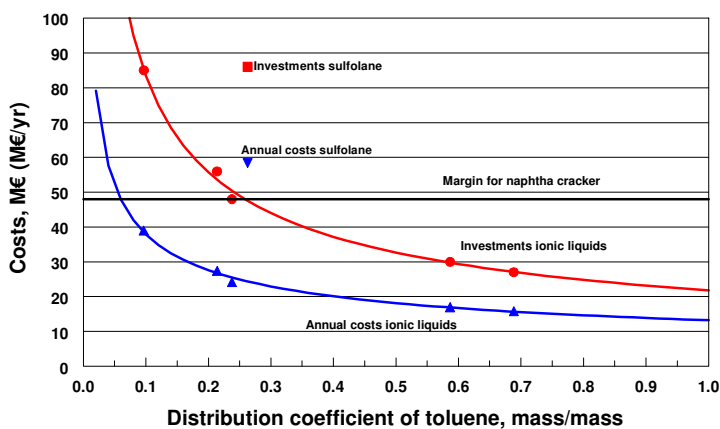


Figure 1. Investment and variable costs for extraction with ionic liquids and sulfolane.

due to the fact that the regeneration of the ionic liquid is much simpler than that of sulfolane. Since also the energy costs are lower, the total annual costs with the ionic liquid process are estimated to be M€ 27.4, compared to M€ 58.4 for sulfolane. In Figure 1, the investment and annual costs for the extraction of aromatics with sulfolane and several ionic liquids is depicted.

The main conclusion of the process evaluation is that ionic liquids which show a high aromatic distribution coefficient,  $D_{\text{arom}} = 0.6$  mass fraction, with a reasonable aromatic/aliphatic selectivity,  $S = 40$ , could reduce the investment costs of the aromatic/aliphatic separation to about M€ 25 to 30 and the annual costs to M€ 16 to 17.

## References

- Meindersma, G.W., Podt, J.G. and De Haan, A.B., (2005), Selection of ionic liquids for the extraction of aromatic hydrocarbons from aromatic/aliphatic mixtures, *Fuel Process. Technol.* 87 (1) 59–70.
- Zimmermann, H; Walzl, R, *Ullmann's Encyclopedia of Industrial Chemistry* (electronic version 2000), Ethylene, 5. Production, 5.1.1 Cracking Conditions.
- Meindersma, G.W., Podt, J.G., De Haan, A.B., (2006), Ternary liquid-liquid equilibria for mixtures of toluene+n-heptane+an ionic liquid, *Fluid Phase Equilib.* 247 (1-2) 158-168.

The total investment costs in the sulfolane extraction were estimated by UOP, the supplier of this process, to be about M€ 86 for a naphtha feed of 300 t/hr containing about 10% aromatic hydrocarbons. The investment costs for an extraction process with the ionic liquid [mebupy]BF<sub>4</sub> was estimated to be M€ 56, including an ionic liquid inventory of M€ 20. The lower investment in the ionic liquid process is mainly



## **A Systematic Synthesis Framework for Extractive Distillation Processes**

S. Kossack<sup>a</sup>, K. Kraemer<sup>a</sup>, R. Gani<sup>b</sup>, W. Marquardt<sup>a</sup>

<sup>a</sup>*Process Systems Engineering, RWTH Aachen University, D-52064 Aachen, Germany*

<sup>b</sup>*Department of Chemical Engineering, Technical University of Denmark, DK-2800 Lyngby, Denmark*

### **1. Summary**

The effectiveness of an extractive distillation process relies on the choice of the extractive agent. In this contribution heuristic rules for entrainer selection and the design of entrainers through computer-aided molecular design are reviewed. The potential of the generated alternatives is then evaluated by their selectivity at infinite dilution and the rectification body method (RBM). It is shown that a screening based on selectivity alone is not sufficient and can possibly lead to an unfavorable entrainer choice. The minimum entrainer flowrate and the minimum energy demand as calculated from the modified RBM allow a more comprehensive evaluation of different entrainer alternatives. In a third step a rigorous MINLP optimization of the entire extractive flowsheet for the remaining entrainer candidates is executed to determine the best entrainer. Since a number of alternative entrainers have already been eliminated, only a few optimization runs are necessary. The whole framework allows the systematic generation and evaluation of entrainer alternatives and is illustrated with the case study of the separation of acetone and methanol.

Keywords: extractive distillation, entrainer design, CAMD, RBM, MINLP

### **2. Extended Abstract**

In extractive distillation an additional entrainer is used to alter the relative volatility of close-boiling or azeotrope forming components to facilitate an economic separation in a distillation process. Compared to a conventional distillation setup, the choice of the entrainer is an important degree of freedom. In this contribution a systematic synthesis framework for extractive distillation is proposed, in which this and other degrees of freedom are fixed successively.

As shown in fig. 1, the synthesis framework proposed is essentially a three step process. The framework starts with the generation of entrainer candidates in the first step. While several heuristics have been developed to find suitable entrainers for a given azeotropic mixture, additional entrainer candidates are designed here through Computer-Aided Molecular Design (CAMD) [Harper and Gani 2000]. This allows the generation of feasible entrainer candidates systematically based on thermodynamic group contribution methods.

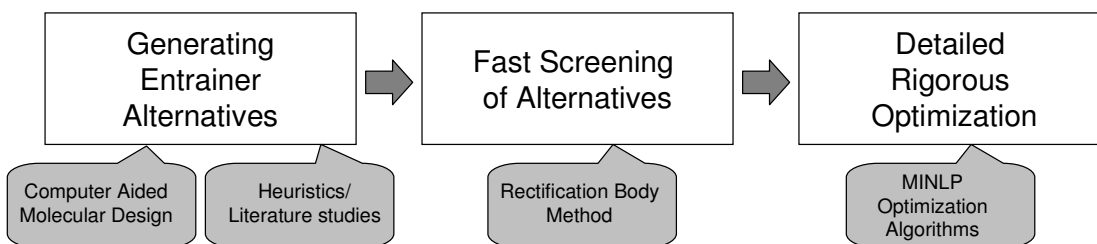


Fig. 1: Outline of the proposed synthesis framework

For the evaluation of these entrainer candidates a number of methods, such as the selectivity at infinite dilution have been proposed. Here, the Rectification Body Method (RBM) for extractive distillation is used to further screen the selected set of entrainers in terms of minimum energy demand and minimum entrainer flowrates. The minimum entrainer flowrate is determined from the analysis of the nonlinear pinch equations, the minimum energy demand from the tailored shortcut models [Brüggemann & Marquardt, 2004].

Once the entrainer choices have been narrowed down to two or three candidates through these intermediate screening methods, a rigorous MINLP optimization is started. Here the entire process is optimized with respect to an economic merit function. In this last step the optimal number of stages, the optimal feed stage, reflux policies and the optimal entrainer flowrate are determined. Information from the shortcut step can be used for the initialization of the MINLP optimization model [Kossack et al. 2006], which greatly increases stability and convergence.

The separation of the azeotropic mixture of acetone/methanol is used as an illustrative case study for the proposed synthesis framework. In case of pure acetone as the product of the extractive distillation column, DMSO and water are the best entrainer choices, since the minimum energy demand rises steeply for other entrainer choices. In the case of methanol as the distillate product of the extractive column, this rise is not as steep. Here, chlorobenzene, mesitylene and p-Xylene are selected as possible entrainer choices. For these remaining choices of entrainer candidates, the entire extractive process consisting of two columns is rigorously optimized using MINLP optimization techniques. Not surprisingly, the detailed economic evaluation supports the results obtained with the shortcut method.

The proposed framework thus allows the systematic generation and evaluation of extractive flowsheets. The candidate space of possible entrainers is successively reduced until only a small number of candidates remain. The best alternative is then found through a rigorous optimization.

This work was funded by the Deutsche Forschungsgemeinschaft (DFG) under grant MA 1188/26-1.

## References

- Harper, P.M., and Gani, R., (2000) *Computers and Chemical Engineering*, 24, 677-683.  
 Brüggemann, S., and Marquardt, W., (2004) *AIChE Journal*, 50, 1129-1149.  
 Kossack, S., Kraemer, K., and Marquardt, W., (2006) *Industrial & Engineering Chemistry Research*, 45, 8492 - 8502.

## **Energetic Analysis of a Crude Distillation Plant: a Case Study**

M. Mascia, M. Errico, G. Tola

*Dipartimento di Ingegneria Chimica e Materiali, Università degli Studi di Cagliari, piazza d'Armi, 09123 Cagliari, Italy*

### **1. Summary**

This work presents the results of the energetic analysis of an existing Crude Distillation Unit. The analysis started from the simulation of the existing plant and field data of compositions, flow rates and temperatures. The sequence of thermally coupled columns thermodynamically equivalent to the unit was identified. All the sequences of thermally coupled columns suitable for the considered separation were designed. The simulation of all the sequences was performed and the energy demand of all the units were obtained. On the basis of the energy demands, the sequences were compared and the best sequences identified. The results allowed to identify scopes for energy savings which can be obtained by revamping the existing plant, mainly relocation of the feed and re-piping of the side units.

Keywords: Crude Distillation Unit, Energy Saving, Thermal Coupling, Column Sequences

### **2. Extended Abstract**

In the refining industry, Crude Distillation Unit is the most energy and power intensive process and contribute significantly to the energy demand of the whole plant<sup>1</sup>. This work presents an industrial case study which deals with a energetic analysis of an existing crude oil distillation systems to study energy efficiency. The aim of the work was to identify scopes for energy efficiency improvements. The first step of the work was the simulation of the existing plant. Based on field data, a rigorous simulation of the main column along with side strippers and pump-arounds, was performed by the commercial software Aspen Plus: the PETROFRAC model was utilized to simulate the unit. The model allows the stage by stage calculation of flow rates, compositions and temperatures in each column section. The results obtained from the simulation were compared with the plant data in terms of flow rates and product quality utilising laboratory ASTM D-86 curves. The difference between the values of temperatures, flow rates and compositions obtained by the model and those measured in the plant never exceeded 5%.

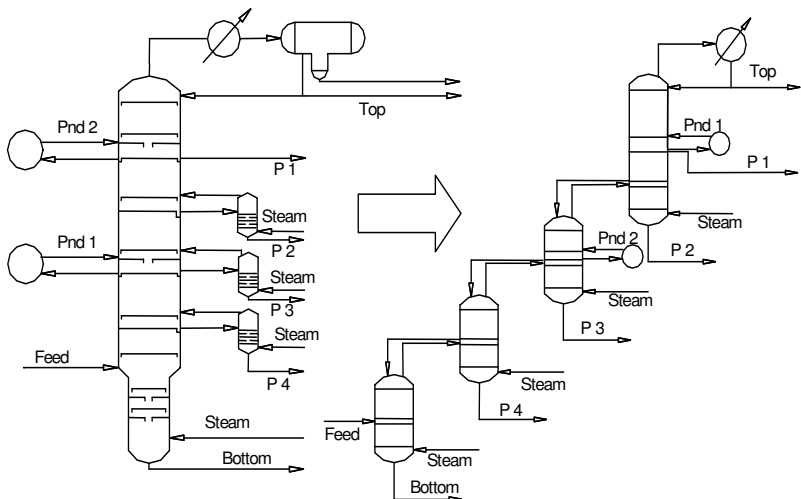


Figure 1: Flow sheet of the Crude Distillation Unit considered in this work and the thermodynamically equivalent sequence of thermally coupled columns

The model was then used to analyse the process conditions of the plant, in order to reduce its energy demand. The topping column, along with sidestrippers, was first considered as a sequence of thermally coupled columns<sup>2</sup>, as sketched in Figure 1. The other 13 thermally coupled schemes which can be utilised for the considered separation were then identified<sup>3</sup>. All the column in the

different sequences were designed<sup>4</sup>, using grouped pseudo components as key components, and rigorous simulations of all the units in the sequences were implemented.

The simulations were optimised in order to obtain the requested characteristics of the product streams. Then the energy demand of each configuration was obtained, and the values were compared.

The results are shown in Figure 2 normalising the energy demand of each configuration with respect to the actual configuration (bar number 1). The inset shows the plant configuration thermodynamically equivalent to the best sequence (bar 4): as can be seen from the figure, it is possible to achieve a good energy saving (10%), through the revamping of the existing plant.

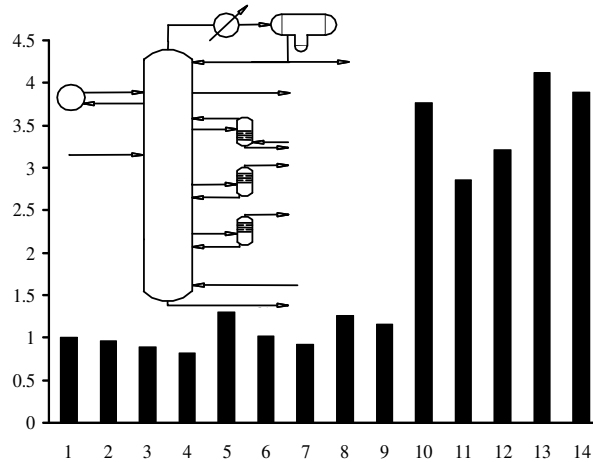


Figure 2: Total energy demand of the different sequences normalised with respect to the value of the existing plant; inset shows the configuration thermodynamically equivalent to the best sequence

## References

1. Gadalla, M., Olujic, Z., Jobson, M., Smith, R., (2006) *Energy* 31, 2398–2408
2. Liebmann, K., Dhole V. R., Jobson, M., (1998), *Chem.Eng. Res. Des.*, 76(A3), 345-347.
3. Rong, B., Kraslawski, A., Nystroem, L., (2001) *Comp. Chem. Eng.* 25, 807-820.
4. Carlberg, N. A., Westerberg, A.W., (1989) *Ind. Eng.Chem. Res.*, 28, 1379-1386.

## Session T2-10c: Distillation, Absorption & Extraction – III

<b>Abstract Number</b>	<b>Paper Title &amp; Authors</b>	<b>Included</b>
607	Mass Transfer Characteristics of Modular Catalytic Structured Packing M Behrens, Ž Olujićb, P J Jansens	Yes
644	Non-linear dynamics of packing layers in watered scrubbers M A Serimbetov, A M Brener	Yes
1357	Study and Design of a Heat Integrated Hybrid Pervaporation-Distillation Process M T P Gómez, A Klein, J U Repke, G Wozny	Yes
1611	Genetic Algorithm Approach in Prediction of Mass Transfer and Axial Dispersion Coefficients of Rotating Disc Liquid-Liquid Extraction Contactors D Bastani, M Shahalami	Yes

Session T2-10c

## Mass Transfer Characteristics of Modular Catalytic Structured Packing

M. Behrens<sup>a</sup>, Ž. Olujić<sup>b</sup>, P. J. Jansens<sup>b</sup>

<sup>a</sup>*Air Products and Chemicals, Walton-on-Thames, KT12 4RZ, Surrey, UK*

<sup>b</sup>*Process & Energy Department, Delft University of Technology, Leghwaterstraat 44, 2628 CA Delft, The Netherlands*

### 1. Summary

A parallel channel model has been developed to describe the hydraulics and mass transfer performance of a modular catalytic structured packing. This model that accounts for various combinations of reaction and separation elements, does not require any adjustable parameter, and was validated using results of devoted total reflux distillation experiments.

Keywords: mass transfer, catalytic packing, reactive distillation, structured packing

### 2. Extended Abstract

Combining heterogeneously catalysed chemical reaction with thermal separation in one unit appears to be an effective way to intensify industrial processes, where applicable. Further significant improvements in this direction are expected from a new generation of structured packing based modular contactors which allow certain flexibility with respect to the variation in the reaction to separation requirements in a single unit. However, little is known about hydraulic and mass transfer performance characteristics of such complex contactor-separator configurations. In other words, information essential for scale-up, design and operation of industrial scale units is still missing. To fill this gap, the mass transfer performances of Sulzer KatapakSP 11 and 12 (see Fig. 1) packings with respectively one and two corrugated sheets between catalyst pockets, have been evaluated experimentally using total reflux distillation column with internal diameter of 0.45 m.

Experiments have been performed at atmospheric pressure with an aqueous system and an organic mixture, including the reference structured packing MellapakPlus 752.Y. In general, better efficiencies were obtained with aqueous system. The “11” packing with one corrugated sheet separating catalyst pockets, containing closed flow channels only, proved to be prone to liquid maldistribution in preloading region. In all cases the best mass transfer efficiency was observed around the loading point.

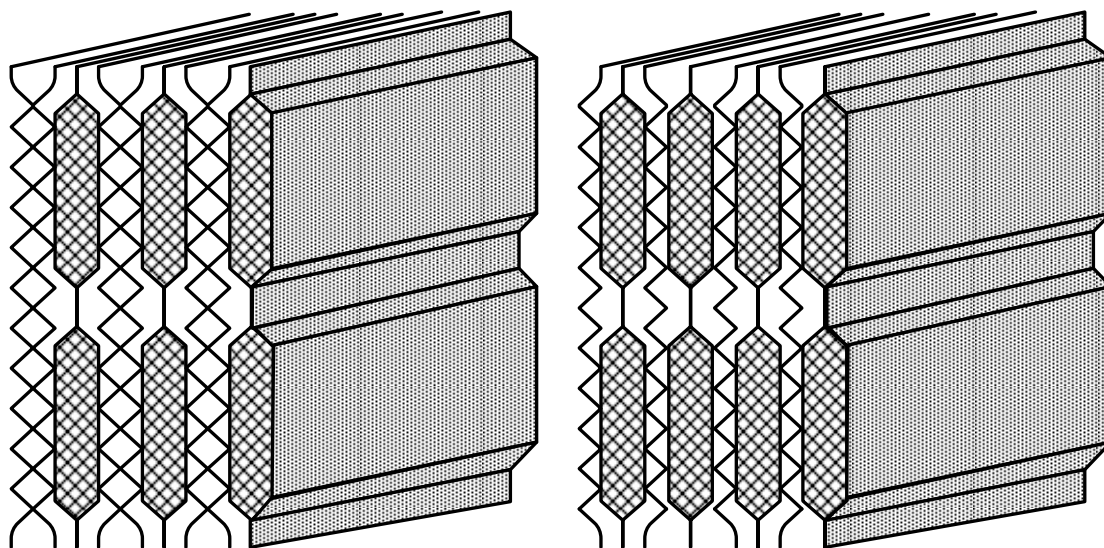


Figure 1 - Schematics of Katapak SP12 (left hand side) and Katapak SP11 structures

Taking a predictive model developed originally for common corrugated sheet structured packings, which was later extended to so-called high capacity packings, as a building block, a new, parallel channel model was developed that makes a distinction between catalyst filled pockets in the reaction section and the open and/or closed channels in separation section. With this simple approach it appeared possible to account properly for specific geometric features of modular catalytic structured packing, without using any empirical, packing type specific constant. The new model proved to be capable of predicting properly the mass transfer efficiency around the loading (design) point.

Further reading: Marcel Behrens, *Hydrodynamic and Mass Transfer Performance of Modular Catalytic Structured Packing*, D. Sc. Thesis, Delft University of Technology, Delft, 2006.



## Non-linear dynamics of packing layers in watered scrubbers

M.A. Serimbetov and A.M. Brener

*State University of South Kazakhstan, Tauke Khan av. 5, Shimkent, 162012, Kazakhstan*

### 1. Summary

A regularity of phases distribution in packed towers determines the efficiency of transport phenomena. In its turn the distribution of interacting phases in an apparatus is dependent on the packing structure. The aim of this work is to carry out methods for modelling the dynamics of tower packings composed from heavy elements of complex shape. Peculiarities of packing layers dynamics in this case are explained by possibility of elements space re-orientation under the influence of gas and liquid flow. This re-orientation leads to changing the drift coefficient within the bounds from initial value to certain minimum. In our paper we submit the model differential equation describing the non-linear dependence of the drift coefficient on average velocity of gas flowing past the packing layer. The hydrodynamic regimes from the rest layer to the fluidization have been described by numerical experiments and qualitative analyzes. The estimations for scaling effect based on the submitted model approach have been obtained and compared with experimental data.

Keywords: hydrodynamics, packed towers, drift coefficient, scaling.

### 2. Extended Abstract

The correct mathematical model describing hydrodynamics of packing layer composed from heavy elements of complex shape has to take into account that elements drift coefficient  $\xi$  can change because of the influence of gas flow to elements space orientation [1, 2]. This coefficient changes from certain initial value  $\xi_0$  for the rest packing under the low gas velocity to such minimum  $\xi_{\min}$  as possible for the element shape under the high gas velocity. The other factor influencing the drift coefficient is widening of packing layer with gas velocity growth.

The velocity of elements re-orientation with gas velocity increasing depends both on the force of gas-element interaction and on the current deviation of drift coefficient from its minimum. On the base of the mentioned heuristic assumptions we submit the model equation for searching the dependence of drift coefficient on gas velocity  $W$  :

$$\frac{d\xi}{dW} = -k\xi W^2 (\xi - \xi_{\min}). \quad (1)$$

The boundary condition is determined by the rest packing structure:

$$\xi|_{W \rightarrow 0} = \xi_{st} \quad (2)$$

From (1), (2) it follows:

$$\xi = \frac{\xi_{\min} (S + \xi_{\min})}{(S + \xi_{\min}) - S \exp(-k \xi_{\min} W^3/3)}, \quad (3)$$

where  $\xi_{st} - \xi_{\min} = S$ .

Figures 1 and 2 depict some characteristic results of numerical tests for drift coefficients both of single element of the ellipsoid form and of the packing layer as a whole.

Here:  $\xi_{\min} = 20$ ;  $\xi_{st} = 110$ ; 1-  $k = 0.00005$ , 2-  $k = 0.0001$ , 3-  $k = 0.0005$ , 4-  $k = 0.001$ , 5-  $k = 0.005$ , 6-  $k = 0.01$ .

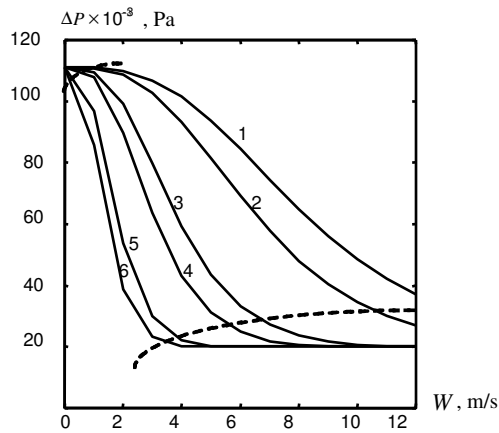


Figure 1: Drift coefficient of single element.

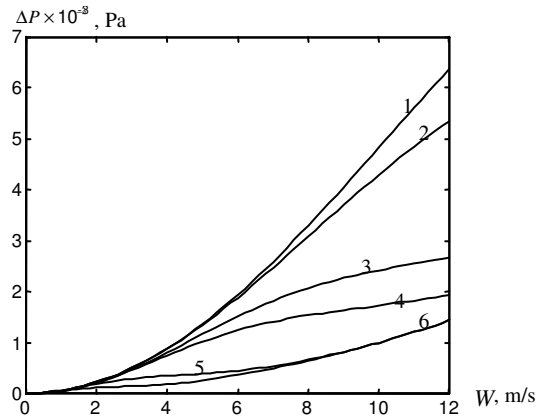


Figure 2: Drift coefficient of layer.

In our report we present results of our investigations for packing elements of different shapes, which are used in the industrial packed towers.

By analyzing the empiric data the model expression has been generalized for packing layer consisting from annular or dumb-bell elements with allowing for the layer widening. The modified model with allowing for peculiarities of the packing structure nearby the tower walls has been submitted too. The mentioned factor plays a great role as main scaling effect.

## References

1. Akhberdiev, A.S., Brenner, A.M. Hydrodynamic characteristics of fluidized packing with elements of complex shape, (2002) *Theor. Found. of Chemical Technology*, V.35, 6,1-6. (In Russian)
2. Serimbetov, M.A, Akhberdiev, A.S., Hydrodynamics and drops motion in scrubbers packed by elements of complex shape, (2001) *Science and Education of South Kazakhstan*, 23, 138-140. (In Russian)

## Study and Design of a Heat Integrated Hybrid Pervaporation-Distillation Process

M.T. Del Pozo Gómez, A. Klein, J.U. Repke, G. Wozny

*Institute for Process Engineering, Berlin Technical University, Strasse des 17. Juni 135, 10623 Berlin, Germany*

### 1. Summary

The separation of homogenous azeotropic mixtures is a common problem in the chemical industry. High energy consuming techniques are the primarily used in practice. Hybrid-Pervaporation-Distillation processes have been intensely studied in the last decade. The saving in energy costs and the need of no additional substance in the procedure are the major benefits of it. In the present paper, a novel membrane configuration is presented, a mathematical model is described and finally the advantages of the new heat-integrated flow-sheet are demonstrated. In the study, the heat integrated process yields to a reduction in the energy consumption and to an increase in the permeate flux, what means a smaller necessary membrane area. As a result, the new process presents lower operation and investment costs.

Keywords: hybrid process, pervaporation, heat integration, azeotropic mixtures

### 2. Extended Abstract

The core of the novel heat-integration concept, is to utilize the distillate vapor stream of a distillation column as heating medium in the pervaporation membrane (fig.1). The vapor condenses partially and energy is released into the module. The homogeneous azeotropic binary mixture of isopropanol (IPA) –water is taken as an example. Without internal heat support, the temperature along the module decreases significantly, and a heat exchanger is needed before the next pervaporation membrane. In the new pervaporation proposal there is no need of external energy support. Another

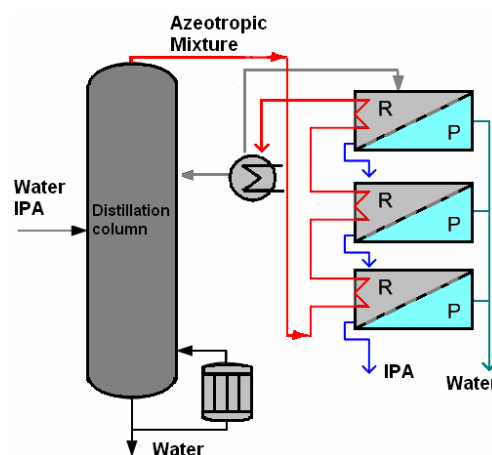


Fig 1: Hybrid process flow sheet principle (new heat-integrated approach)

benefit is that the heat transfer is realized directly inside of the module (fig.2) therefore, the temperature decrease along the membrane is minimized and the permeate flux can be increased (fig.3). In consequence the membrane area and energy supply in the process can be reduced.

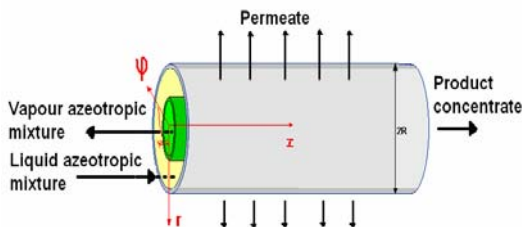


Fig 2: Heat integration inside the membrane-module

For the investigation of the new concept a model for the novel process with internal and with external heat exchangers was developed in gPROMS®. The dynamic column model described in Repke et al. (2006) was used, the membrane parameters were taken from Sommer S. (2003) and its characterization is done experimentally in a built laboratory plant (Klein 2006). In fig.3

the heat integrated process with internal heat exchangers is compared with the process with external heat exchangers in the case of a three membrane module pervaporation system.

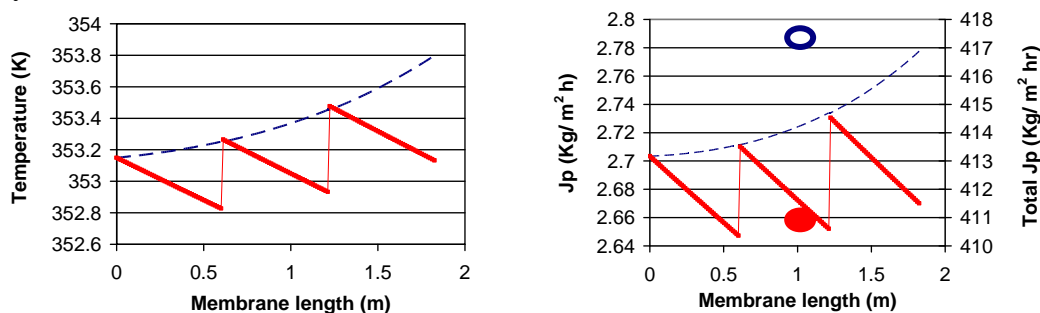


Fig3: Left temperature drop, right permeate flux along a three pervaporation membrane system. Dashed line is for the heat integrated system and filled line is for the system with external heat exchangers. The dot is the aggregate of the permeate going out along the membranes (Total Jp), empty dot for the case with internal heat exchangers and filled dot for the case with external heat exchangers.

As a result, the heat integrated system presents lower temperature drop and a higher permeate flux ( $J_p$ ) (fig.3) in each membrane module; what reduces the required membrane area (for a constant exit product purity). Moreover, no external heat support is required because the energy for the pervaporation can be obtained from the condensation energy of the distillation product. Therefore an important energy save in the whole hybrid distillation/pervaporation process can be done. In the presentation, this new concept will be described and its feasibility demonstrated and discussed.

## References

- Repke, J.-U., Forner, F. and Klein, A., (2006) *Chem. Eng. Techn.*, 28
- Klein, A., Repke, J.-U., del Pozo Gómez, M. T., Wozny, G., (2006) *AJChE Annual Meeting, San Francisco, California*, 409 Separation Design.
- Sommer, S., (2003) *PhD Thesis*, RWTH Aachen, Germany.
- Wijmans, J.G., and Baker, R.W., (1993), *Journal of Membrane Science*, 79, 101-113

This research project is funded by EFRE (request number 10134788)

## Genetic Algorithm Approach in Prediction of Mass Transfer and Axial Dispersion Coefficients of Rotating Disc Liquid-Liquid Extraction Contactors

Dariush Bastani and M. Shahalami

*Chemical and petroleum Engineering Department, Sharif University, Tehran, Iran*

### 1. Summary

This paper presents a new application of Genetic Algorithm to predict the parameters of the model of a rotating disc liquid-liquid extraction contactor. Mass transfer mechanism inside the drops of the dispersed phase was modeled by Handlos&Baron circulating drop model with considering the effect of forward mixing. In order to achieve RDC model parameters, a least-square function of differences between the simulated and experimental concentration profiles was considered. The criterion to distinguish that this approach is more applicable is the calculation of the 95% confidence limit in plug flow number of transfer units. The calculated Results using this method were compared with the result obtained using the NAG software (Numerical Analysis Group). The comparisons justify the use of Genetic Algorithm as a successful method for optimization of mass transfer and axial dispersion coefficients of Liquid-liquid extraction columns.

**Keywords:** Liquid-Liquid Extraction, Rotating Disc Contactor, Genetic Algorithm

### 2. Extended Abstract

The overall objective of the design of a liquid-liquid extraction column is to combine a model of the mass transfer with a model of the phase flow behavior in order to predict the accurate mass transfer and axial dispersion coefficients to calculate the column dimensions required [1]. Genetic Algorithm is a computational method that emulates biological evolutionary theories to solve optimization problems. . A GA operates typically through a simple cycle of four stages [2]:

1. Creation of a population of string;
2. Evaluation of each string;
3. Selection of best string;
4. Genetic manipulation to create the new population of string.

A brief list of results obtained using NAG software and GA are summarized in Table 1.

In figures 1 and 2 the predicted and experimental plug flow number of transfer units using GA approach and NAG library are compared. As these figures show, more agreements between  $PN_{ODP}$  and  $E_{N_{ODP}}$  values are attained when GA was applied.

The criterion to distinguish that this approach is more applicable is the calculation of the 95% confidence limit in plug flow number of transfer units. The less 95% confidence limit means the more accurate prediction. This parameter is calculated using the following relation:

$$95\% \text{Confidence Limit} = 2 * \sqrt{\frac{\sum \left( \frac{EN_{ODP} - PN_{ODP}}{EN_{ODP}} \right)^2}{n-1}} \quad (1)$$

n is the number of experiments. The values of predicted 95% confidence limits in plug flow number of transfer units when Genetic Algorithm and NAG library were applied, were 6.02% and 13.21% respectively.

Table .1. Experimental operating conditions and predicted values of parameters

Run No.	$E_{N_{ODP}}$	$K_c \times 1000$	$E_c$	$SSD \times 10^6$	$P_{N_{ODP}}$	$K^*_c \times 1000$	$E^*_c$	$SSD^* \times 10^6$	$P^*_{N_{ODP}}$
1	2.237	1.016	1.38	3.04	2.349	0.922	1.3	1.31	2.259
2	2.402	1.470	2.64	0.07	2.581	1.33	2.56	0.0345	2.409
3	2.895	2.018	2.75	1.64	2.676	2.2	2.88	1.09	2.847
19	3.394	3.996	1.99	0.84	3.664	4.5	2.097	0.789	3.350
20	2.753	2.556	1.54	0.01	2.717	2.22	1.354	0.00959	2.738
21	3.458	3.733	2.09	0.14	3.490	3.8	2.222	0.196	3.537
22	3.259	2.425	2.73	0.03	3.547	2.5	3.009	0.0192	3.292
23	3.618	4.089	2.27	0.05	3.646	4.2	2.402	0.0636	3.654
24	1.682	2.294	0.49	0.34	1.622	2.29	0.555	0.23	1.669
25	1.788	2.661	0.64	0.53	1.770	2.522	0.674	0.578	1.768
26	2.023	2.701	0.64	0.59	2.291	2.97	0.719	0.576	2.271
27	1.922	2.461	0.79	0.31	1.882	2.4	0.813	0.256	1.938
28	2.011	2.854	0.80	0.17	1.956	2.4	0.655	0.189	2.087
29	2.540	3.485	0.80	0.69	2.522	3.802	0.915	0.854	2.645
30	2.713	5.374	1.69	7.60	3.100	5.48	1.762	4.32	2.764
31	2.516	2.513	0.91	0.94	2.347	2.3	0.947	0.821	2.437
32	2.653	3.286	0.94	0.98	2.428	3.33	1.039	0.708	2.677
33	3.186	3.507	1.23	0.38	3.317	3.331	1.257	0.369	3.252
34	1.744	2.507	0.60	0.17	1.753	2.355	0.580	0.149	1.75
35	2.924	3.316	0.78	0.26	2.889	3.8	0.915	0.364	3.03
36	1.242	1.380	0.52	0.82	1.219	1.461	0.609	0.89	1.291
37	1.499	1.258	0.44	2.11	1.371	1.3	0.531	1.93	1.439
38	1.512	1.441	0.66	0.65	1.272	1.33	0.575	0.613	1.400
39	1.915	2.226	1.39	0.15	1.910	2.3	1.539	0.24	1.946
40	2.230	2.348	1.45	0.001	2.121	2.36	1.546	0.00098	2.225
41	2.840	2.445	2.94	0.03	2.932	2.11	2.688	0.0216	2.815
42	2.014	2.032	1.46	0.02	2.101	1.9	1.486	0.0123	2.0198

\* : predicted by GA method.

$PN_{ODP}$  by this model

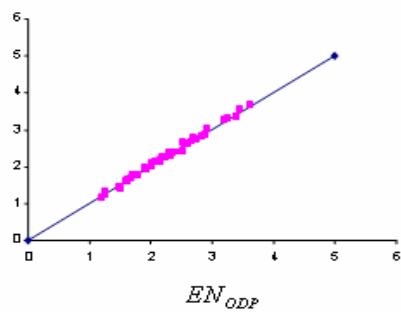


Fig.1. Comparison between experimental and predicted values of  $N_{ODP}$ , using GA.

$PN_{ODP}$  by NAG

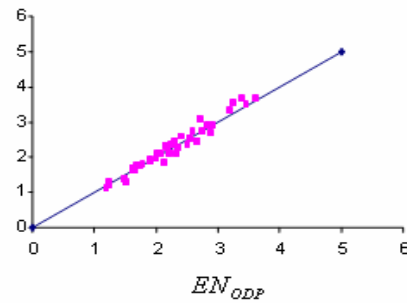


Fig.2. Comparison between experimental and predicted values of  $N_{ODP}$ , using NAG

**References**

[1] Bastani, D., "Liquid-Liquid extraction column performance evaluations for two column diameters and two chemical systems.", Ph.D. Thesis, Victoria University of Manchester, 1990.  
 [2] D. E. Goldberg, "Genetic Algorithms in search, Optimization, and Machine learning", Addison-Wesley, 1989.

## Session T2-10P: Distillation, Absorption & Extraction – Poster

Abstract Number	Paper Title & Authors	Included
123	Impact of texturation by DIC on solvent extraction of anthocyanins from Hibiscus sabdariffa B B Amor, K Allaf	Yes
250	Measurements of Ternary Diffusion Coefficients of Aqueous Blended Alkanolamine systems: Diethanolamine + N-methyldiethanolamine + Water P H Lin, C C Ko, M H Li	Yes
377	Investigation of application of extractive distillation method in chloroform manufacture L S Gordeev, M B Glebov, E M Koltsova, N V Hitrov	Yes
565	Mass transfer study using an electrochemical method M A Cancela, R Maceiras, E Álvarez, X R Nóvoa	No
570	Heat effect on mass transfer in N-Methyldiethanolamine aqueous solutions M A Cancela, R Maceiras, E Álvarez	No
1248	Hydrometallurgical Treatment of a Zinc Concentrate by Atmospheric Direct Leach Process S M C Santos, M R C Ismael, M J N Correiaa, M T A Reis, A Deep, J M R Carvalho	Yes
1303	Copper recovery from ammoniacal media using hollow fibre contactors M L F Gameiro, M R C Ismael, M T A Reis, J M R Carvalho	Yes
1458	Thermodynamic topological analysis at infinite and finite conditions for reactive mixtures of acetates C A Cardona, F A Perdomo, F E Lopez	Yes
1912	Regimes of extractive distillation in ethanol production N Vyazmina, D Baranov, A Vyazmin	Yes
2011	Design and Construction of a Novel Oldershaw-type Distillation Column for Measurement and Scale-up of Tray Efficiencies M Rahmati, M M Shafaghieh, H Amouei	Yes
2118	Supercritical fluid extraction of bioactive compounds from sunflower leaves: comparison of analytical and pilot-scale extraction L Casas, C Mantell, M Rodríguez, A Torres, F A Macías, E J M Ossa	Yes
2213	Sorption Dynamics of Rare Metals into a Matrix-Type Microcapsule Containing an Organophosphorus Extractant K Kondo, M Matsumoto, E Kamio	Yes
3629	Characterizing a Brazilian Petroleum Residue by Molecular	Yes

Session T2-10P

	Distillation Process	
	A Winter, B C Batistella, M R W Maciel, R Filho, L C Medina	
3680	Carbon dioxide absorption from flue gases using Sodium Hydroxide as liquid solvent	Yes
	F Yazdanbakhsh, A Soltani, H Hashemipour	
4025	Numerical simulation to determine the mass transfer Coefficient in gas - liquid phase in an absorbed column	Yes
	B Sohbi	



## **Impact of texturation by DIC on solvent extraction of anthocyanins from *Hibiscus sabdariffa***

Bouthaina BEN AMOR,<sup>a</sup> Karim ALLAF,<sup>a</sup>

<sup>a</sup>*University of La Rochelle -Pole science and Technology, «Laboratory Mastering agro-industrial technologies LMTAI EA 3166», avenue Michel Crépeau, 17042 La Rochelle, FRANCE*

### **1. Summary**

The aim of this study is to investigate the effect of the “Instantaneous Controlled Pressure Drop” DIC (Détente Instantanée Contrôlée) on the yield of extraction of Total Monomeric Anthocyanins from *Hibiscus sabdariffa* calyces. It was concluded that the DIC has a positive effect on the yield of extraction of anthocyanins from *Hibiscus sabdariffa*. Between the different combinations of the parameters of DIC, the experiment 2 (1.8 bars; 18s) have proved to be the best treatment giving an improvement of 130, 119 and 127% for TMA, Dp-3-sam and Cyn-3-sam respectively.

Keywords: Anthocyanins, Extraction, DIC, *Hibiscus sabdariffa*

### **2. Extended Abstract**

Anthocyanins exist widely in fruits, flowers, and vegetables and are responsible for their bright colors such as orange, red, and blue. Anthocyanins are beneficial for skin and vascular health and are also known to coat the surface of cell membranes and protect them from enzymatic and free radical damage. Roselle (*Hibiscus sabdariffa*), which produces enlarged fleshy, dark red, edible calyces with a unique taste, is also known to contain a large amount of anthocyanins. Delphinidin-3-sambubioside and cyanidin-3-sambubioside are the major anthocyanins of Roselle.

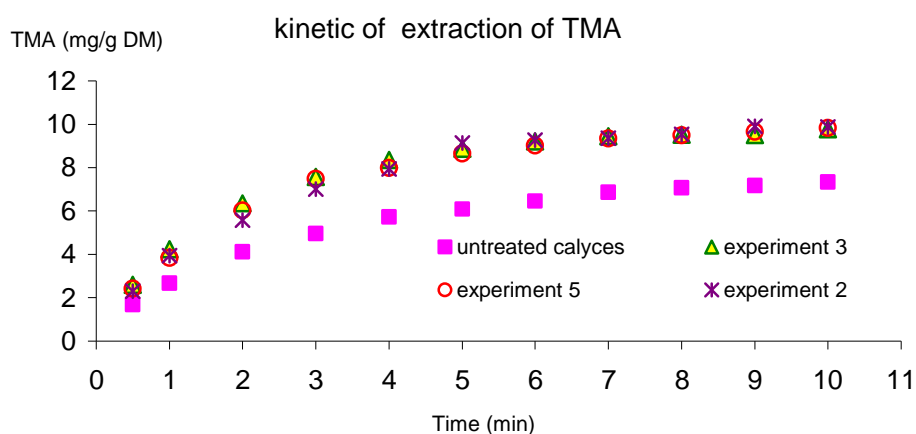
The extraction kinetics implies multiple steps. However, the main part of the operation is limited by diffusion, because of the natural structure of the plant which opposes a resistance to any liquid penetration; then the process is very slow and solvent is, sometimes, choose in order to improve the diffusion. Similar considerations would intervene even with supercritical fluid as solvent. Some other recent alternative extraction methods (ultrasonification, microwaves...) are proposed in order to intensify transfer processes but they remain too costly techniques for scaling up.

For improving technological aptitude of raw material in terms of extraction, one may modify the initial structure by cutting, grinding, etc. In our laboratory, we proposed to carry out studies concerning the effect of structure expansion. In several cases, we proved that the higher the expansion rate, the better the diffusivity constant. So we applied a swelling operation using the well-known process of “Instantaneous

Controlled Pressure Drop” DIC (Détente Instantanée Contrôlée) witch was developed in our laboratory since some years (Allaf *et al.*, 1989, Allaf *et al.*, 1994). Firstly, this process was used for swell-drying various fruit and vegetable; it assures a high quality by improving the hydration kinetics and capacity. DIC treatment is based on fundamental studies concerning the thermodynamics of instantaneity (Allaf, 2002). It consists on a thermo-mechanical processing induced by subjecting the product to an abrupt transition from high steam pressure towards vacuum. This process is also used for the extraction of essential oils and other volatile molecules by instant autovaporization (Allaf *et al.*, 1998); it allows the plant (seeds, fruit, flower, etc.) to get higher global diffusivity and improves the availability of some of its compounds.

The present work aims to improve the capability to extract anthocyanins from dried calyces of Roselle by modifying the “raw material” structure.

After DIC treatment, we have investigated the kinetics of the aqueous extraction of anthocyanins from treated and non treated Roselle calyces. Total anthocyanins content in the aqueous extract was evaluated by differential pH method absorbance at 520 nm (Giusti M. and Wrolstad R. E. 2001)). Individual anthocyanins were quantified by HPLC. Response surface methodology (RSM) was used for quantifying the effect of the processing parameters on the extraction yield of anthocyanins.



The comparison between the kinetics of extraction of Total Monomeric Anthocyanins (TMA) from the untreated and the different DIC experiments shows that there was an improvement in the kinetic of extraction for all the DIC experiments and that the maximum of Total Monomeric Anthocyanins extracted from dried calyces of roselle is obtained within a short time (between 3 and 6 min) compared to untreated calyces (about 10 min).

Concerning the yield of axtraction, the optimum processing conditions selected for the global extraction yield obtained from response surface analysis were as follows: pressure level: 180 KPa; processing time: 9 s. The DIC treated calyces of Roselle according to optimum processing conditions gave the highest amount of TMA, Dp-3-sam and cyn-3sam with an improvement reaching respectively 130%, 119 and 127% compared to untreated Roselle.

## References

1. Giusti M. and Wrolstad R. E. (2001). Characterization and Measurement of Anthocyanins by UV-Visible Spectroscopy. *Current Protocols in Food Analytical Chemistry*. NY, John Wiley & Sons.

## Measurements of Ternary Diffusion Coefficients of Aqueous Blended Alkanolamine systems: Diethanolamine + N-methyldiethanolamine + Water

Po-Hsun Lin<sup>a</sup>, Chih-Chiang Ko<sup>a</sup>, Meng-Hui Li<sup>a,b</sup>

<sup>a</sup>*R&D Center for Membrane Technology and Department of Chemical Engineering, Chung Yuan Christian University, Chung Li, Taiwan 32023, Republic of China*

<sup>b</sup>*Corresponding author*

### 1. Summary

Ternary diffusion coefficients of aqueous blended alkanolamine systems diethanolamine (DEA) + *N*-methyldiethanolamine (MDEA) + water using the Taylor dispersion technique have been measured for temperatures 30, 40 and 50 °C. The systems studied were aqueous solutions containing the total amine concentrations of 2, 3, and 4 kmol·m<sup>-3</sup> with three (or four) molar amine ratios. The corresponding mutual diffusion coefficients of aqueous DEA and aqueous MDEA solutions were also measured. Working equations for the ternary diffusion coefficients presented by Leaist et al. (1998) was adopted to obtain the ternary diffusion coefficients. The main diffusion coefficients ( $D_{11}$  and  $D_{22}$ ) and the cross coefficients ( $D_{12}$  and  $D_{21}$ ) are reported as function of temperature and concentration of alkanolamines. The predicted values from the Onsager phenomenological coefficients, the activity, and partial molar volume of component are also performed and compared with the measured values.

Keywords: ternary diffusion coefficient, aqueous blended amines solutions, diethanolamine, *N*-methyldiethanolamine, Taylor dispersion technique

### 2. Extended Abstract

#### 2.1. Experimental

The ternary mutual diffusion coefficients of DEA + MDEA + H<sub>2</sub>O were measured in a Taylor dispersion apparatus which has been described in Chang et al. (2005).

#### 2.2. Working equations

The working equation to calculate ternary diffusion coefficients is as follows,

$$v(t) = v_{\max} \left( \frac{t_R}{t} \right)^{1/2} \left[ W_1 \exp \left( -\frac{12D_1(t-t_R)^2}{r^2t} \right) + (1-W_1) \exp \left( -\frac{12D_2(t-t_R)^2}{r^2t} \right) \right] + B_0 + B_1t \quad (1)$$

where  $v_{\max}$  is the height of the eluted solute peak relative to the baseline,  $t_R$  the mean retention time,  $r$  the inner radius,  $B_0$  the baseline detector voltage,  $B_1t$  is representing a small linear drifts in the baseline signal.  $D_1$  and  $D_2$  denote two overlapping Gaussians, centered on time  $t_R$  with variances  $r^2L/24D_1U$  and  $r^2L/24D_2U$  where  $L$  is the length of the tube,  $U$  the mean speed of stream. After the values of  $a$ ,  $b$ ,  $D_1$ , and  $D_2$  determined from the refractive index profile for solution stream with solutes concentration ( $\bar{c}_1$ ,  $\bar{c}_2$ ), the ternary mutual diffusion coefficients,  $D_{11}$ , can be calculated as (similar equations for  $D_{12}$ ,  $D_{21}$ ,  $D_{22}$ ) (Deng and Leaist, 1991):

$$D_{11} = D_1 + \frac{a(1-a-b)}{b}(D_1 - D_2) \quad (2)$$

### 2.3. Results

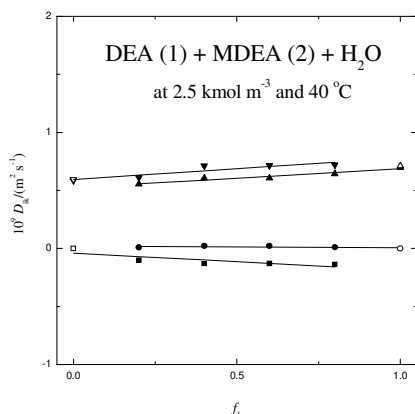


Figure 1 Ternary diffusion coefficients:

▲,  $D_{11}$ ; ■,  $D_{12}$ ; ●,  $D_{21}$ ; ▼,  $D_{22}$ .

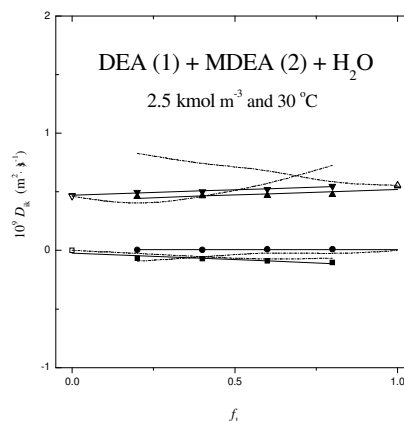


Figure 2. Comparison between predicted (Onsager equation) and experimental values.

Figure 1 shows the ternary diffusion coefficients and Figure 2 the comparison between the predicted results from Onsager phenomenological coefficient equation. Except for  $D_{11}$ , the predicted values for  $D_{22}$ ,  $D_{21}$ ,  $D_{12}$  are generally follows the trend of the experimental values.

### References

- Chang, L.-C., Lin, T.-I., and Li, M.-H., (2005). *J. Chem. Eng. Data*, 50, 77-84.  
 Deng, Z. and Leaist, D. G., (1991). *Can. J. Chem. Eng.*, 69, 1548-1553.  
 Leaist, D. G., Li, Y., and Poissant, R., (1998). *J. Chem. Eng. Data*, 43, 1048-1055.  
 Snijder, E. D., Riele, M. J. M. T., Versteeg, G. F., and van Swaaij, W. P. M., (1993). *J. Chem. Eng. Data*, 38, 475-480.

## **Investigation of application of extractive distillation method in chloroform manufacture**

L.S. Gordeev, M.B. Glebov, E.M. Koltsova, N.V. Hitrov

*D. Mendeleev University of Chemical Technology of Russia, Dep. Cybernetics of Chemical technol. Processes, Miusskaya sq., 9, Moscow, Russia; tel. 007-495-8499-9786589, e-mail glebov@muctr.ru , fax: 007-495-8499-2004204*

### **1. Summary**

The research of a purification process of chloroform from impurities by a method of an extractive distillation is submitted. Comparison the schemes of chloroform purification is executed on the basis of two separation agents: ethylen glycol and monophenyl glycol. On the basis of economical criterion the expediency of usage of the separation agent monophenyl glycol is showed.

Keywords: Extractive distillation, chloroform, mathematical model

### **2. Extended Abstract**

Chloroform finds wide application in a number of industries: in manufacture of chladones, pesticides, in a medical industry, agriculture etc. The available data on consumption of chloroform for last years in Russia show about growing demand for it. Chloroform, manufactured on a basis of methane chloration, contains impurities of ethane – ethylene type and requires a special purification stage. The basic difficulty of chloroform purification is separation of closely boiling cis-dichloroethylene - chloroform and 1,1-dichloroethane - chloroform mixtures.

In research an extractive distillation method for the decision of the specified task of chloroform purification is offered. For this purpose the selection of the separating agent by authors have been carried out and for the chosen separating agents on the basis of the carried out experimental researches the thermodynamic model of vapour – liquid equilibrium in multicomponent system 1,1 - dichloroethane - cis-dichloroethylene - chloroform - carbon tetrachloride - separating agent have been constructed. With use of the basic equation of extractive distillation the efficiency of application of chosen separating agents have been proved. The best separating agents have appeared the substances of a glycol class.

The calculation of change of a relative volatility of closely boiling components at the introducing of the separating agent was conducted on an equation

$$\lg \frac{(\alpha_s)_m}{\alpha_m} = \frac{F_{1s} - F_{2s}}{1 - x_s} \quad (1)$$

where  $(\alpha_s)_m$ ,  $\alpha_m$  express average value of a factor of a relative volatility of the first and second components in all range of their concentrations accordingly in presence and in absence of the separating agent. A function F for a ternary system consisting from components 1 and 2 given mixture and separating agent ("s") is determined by expression

$$F = x_1 \lg \gamma_1 + x_2 \lg \gamma_2 + x_s \lg \gamma_s \quad (2)$$

Here  $x_s$  - concentration of the separating agent in a mixture.

The value of selectivity S

$$S = \frac{(\alpha_s)_m}{\alpha_m} \quad (3)$$

expresses mean increase of relative volatility coefficient of components of considered binary mixture conditioned by presence of the separating agent.

On laboratory experimental installation of extractive distillation the research of separation of 1,1- dichloroethane and cis-dichloroethylene from chloroform have been executed. With use of obtained experimental data the adequacy to mathematical model of extractive distillation in the plate column have been established. The mathematical model was based on the equilibrium approach to the description of process taking into account the efficiency of a plate. The carried out numerical experiment the basic regime and constructive data of extractive distillation process, including distribution of the extractive agent on height of a column has allowed to determine. It have been obtained, that for achievement of the required total contents of 1,1- dichloroethane and cis-dichloroethylene in bottom product of extractive distillation column (less than 0,02 % of weights) it is required to support the concentration of the separating agent in a column from 70 up to 85 % mol. The research polystationarity of extractive distillation process have been carried out.

Modeling of stationary modes of operations of the flow chart of chloroform purification from impurities including a column of methylene chloride separation, column of carbon tetrachloride separation, extractive distillation column of 1,1- dichloroethane and cis-dichloroethylene separation, evaporator for separating agent separation and column for manufacturing of grocery chloroform have been executed. By results of modeling the conclusion about expediency of industrial realization of the offered flow chart of chloroform purification by extractive distillation, have been made.

This work was supported by the grant RFBR N<sup>0</sup> 07-08-00498-a

## **Hydrometallurgical Treatment of a Zinc Concentrate by Atmospheric Direct Leach Process**

S.M.C. Santos, M.R.C. Ismael, M.J.N. Correia<sup>a</sup>, M.T.A. Reis, A. Deep, J.M.R. Carvalho

*CPQUTL – Centre of Chemical Processes of UTL, DEQ-Department of Chemical Engineering, Instituto Superior Técnico, Av. Rovisco Pais, 1049-001 Lisboa, Portugal*  
*Phone: +351-21-8417311, Fax: +351-21-8499242, Email: jcarv@ist.utl.pt*

### **1. Summary**

A hydrometallurgical method is proposed to recover zinc and other valuable metals from a zinc sulphide concentrate. The effect of several variables on the leaching efficiency was investigated. The results showed that using 5% of solids, it was possible to leach 95% of zinc after 2h, with a solution of 0.5 mol/L H<sub>2</sub>SO<sub>4</sub> and Fe<sub>2</sub>(SO<sub>4</sub>)<sub>3</sub> at 80°C. Copper extraction was 60% after 2h of leaching at 80°C, with 10% of solids and a solution of 1.0 mol/L FeCl<sub>3</sub>, 0.5 mol/L HCl and 1.0 mol/L NaCl. The addition of O<sub>2</sub> to the leaching system showed a clear improvement on zinc extraction.

Keywords: Sulphide ores; Atmospheric leaching; Iron (II) oxidation

### **2. Extended Abstract**

The conventional method to recover zinc from sulphide minerals involves the roast-leach-electrowinning process. As the policy on discharge of SO<sub>2</sub> becomes stricter, hydrometallurgical routes are becoming more attractive. In atmospheric leaching, ferric ion, in either sulphate or chloride media, can be used to leach zinc sulphide, according to the equation: [1,2]



In this study, the zinc concentrate, which contains Zn-40%; Fe-12%; Cu-4%; Pb-0.84%; As-7000 mg/kg; Hg-400-1000 mg/kg; Sb-500 mg/kg; In- 60-250 mg/kg; Tl-200 mg/kg; and Bi-50 mg/kg was supplied by Somincor, Portugal. Leaching tests were carried out in a five-necked round bottom reactor (1 L, 13 cm diameter) heated on an oil bath. The agitation was achieved with a single round peddle impeller (6.5 cm diameter). Samples were collected at regular time intervals, and analysed by Atomic Absorption Spectroscopy. The concentration of the Fe(II) was assessed by a standard volumetric method [3].

The results indicate that the percentage of metals extraction increased with time. After 1 h of reaction, approximately 90% of the final metals extraction was obtained. As seen in Table 1, the best results for the recovery of zinc (95%) were obtained under conditions of 0.5 mol/L H<sub>2</sub>SO<sub>4</sub> and 0.5 mol/L Fe<sub>2</sub>(SO<sub>4</sub>)<sub>3</sub>, solid/liquid ratio of 5% (w/v) and 80°C reaction temperature.

Table 1: Variables influence on metals extraction.

Variables investigated	Solid/liquid ratio (%)	T (°C)	speed (rpm)	[H <sub>2</sub> SO <sub>4</sub> ] (mol/L)	[Fe <sub>2</sub> (SO <sub>4</sub> ) <sub>3</sub> ] (mol/L)	[HCl] (mol/L)	[FeCl <sub>3</sub> ] (mol/L)	[NaCl] (mol/L)	Zn (%)	Cu (%)	In (%)	Ag (%)
Solid/liquid ratio	5	80	320	0.5	0.5	-	-	-	95	18	96	-
	7	80	320	0.5	0.5	-	-	-	81	17	-	-
	10	80	320	0.5	0.5	-	-	-	61	10	63	-
Temperature	5	40	320	0.5	0.5	-	-	-	52	7	-	-
	5	80	320	0.5	0.5	-	-	-	95	18	96	-
[Fe <sub>2</sub> (SO <sub>4</sub> ) <sub>3</sub> ]	5	80	320	0.5	0.25	-	-	-	57	13	-	-
	5	80	320	0.5	0.5	-	-	-	95	18	96	-
[H <sub>2</sub> SO <sub>4</sub> ]	5	80	320	0.25	0.5	-	-	-	82	16	-	-
	5	80	320	0.5	0.5	-	-	-	95	18	96	-
	5	80	320	2	0.5	-	-	-	95	26	-	-
Chloride medium	10	80	350	-	-	0.5	1	0	70	44	-	53
	10	80	350	-	-	0.5	1	1	69	56	-	60
	10	80	350	-	-	0.5	1	2	71	56	-	60

Metals extraction can be improved if the re-oxidation of Fe(II) to Fe(III) is performed. Figure 1 shows the improvement on zinc extraction when air, O<sub>2</sub> and H<sub>2</sub>O<sub>2</sub> were used to re-oxidize Fe(II).

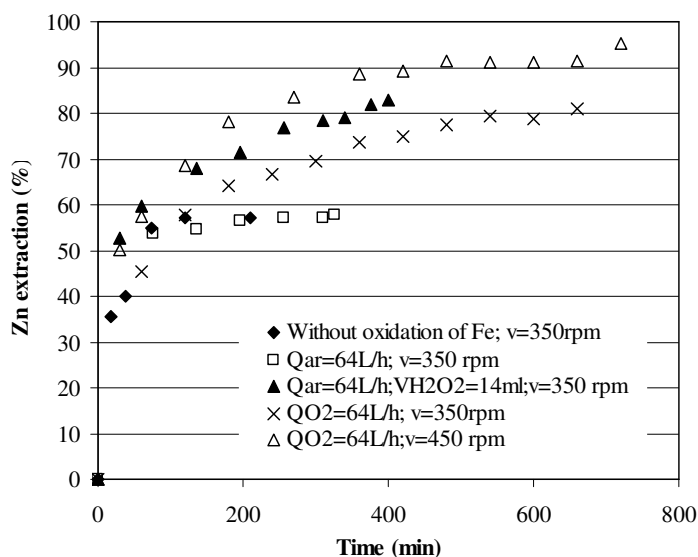


Figure 1: Comparison of effect on zinc leaching with and without oxidation of Fe(II). Experimental conditions: [H<sub>2</sub>SO<sub>4</sub>]=0.5M; [Fe<sub>2</sub>(SO<sub>4</sub>)<sub>3</sub>]=0.25M; s/l=5%; T=80°C

Without the addition of any oxidant, after 60 minutes of reaction almost all the iron is in the form of Fe(II). However, when O<sub>2</sub> was used to oxidize Fe(II) to Fe(III), after 10h of reaction 45% of the iron is Fe(III). The oxidation of iron decreases the amount of initial oxidant needed and improves the recovery of the metals.

## References

- [1] Dutrizac, J. E., Pratt, A.R., Chen, T.T., (2003) *The Mechanism of Sphalerite Dissolution in Ferric Sulphate-Sulphuric acid Media*, Yazawa International Symposium.
- [2] Aydogan, S., Aras, A., Canbazoglu, M., (2005) *Chemical Engineering Journal*, 114, 67-72.
- [3] Vogel, A.I., (1972) *A Text Book of Quantitative Inorganic Analysis Including Elementary Instrumental Analysis*, 3<sup>th</sup> ed., Longman Group Limited, London.



## **Copper recovery from ammoniacal media using hollow fibre contactors**

M. Lurdes F. Gameiro, M. Rosinda C. Ismael, M. Teresa A. Reis, Jorge M. R. Carvalho

*CPQUTL – Centre of Chemical Processes of UTL, Department of Chemical and Biological Engineering, Instituto Superior Técnico, Av. Rovisco Pais, 1049-001 Lisboa, Portugal*

### **1. Summary**

This work aims to study the recovery of copper from ammoniacal aqueous solutions using hydrophobic propylene membrane contactors. The hydroxyoxime LIX 84-I and the  $\beta$ -diketone LIX 54 (both from Cognis) were used as extractants. The results obtained showed that practically all the copper content was removed from the ammoniacal feed solutions. The recovery of copper reached nearly 100% in several extraction-stripping experiments using LIX 54 as carrier. The results were compared with the ones obtained by applying the Emulsion Liquid Membranes (ELM) technique.

Keywords: copper extraction, LIX 54, LIX 84-I, hollow fibre, waste treatment

### **2. Extended Abstract**

#### *2.1. Introduction*

The hollow fibre contactors present several advantages: a very large contact area without direct mixing of the aqueous and organic phases, the capability of treating a large amount of dilute solutions, and the reduction in equipment volume and space (Juang and Huang, 2000). Such microporous membrane-based dispersion-free extraction has been developed to avoid many of the problems associated with conventional liquid-liquid extraction including solvent losses, emulsion formation, phase separation, and the shortcomings due to flooding in conventional column contactors and mixer-settlers.

The ammoniacal leaching is an attractive approach to process concentrates, wastes, and by-products containing copper since this metal ion is easily solubilised through the formation of ammine complexes. The recovery of copper from such leach solutions can be carried out by solvent extraction processes due to their versatility to remove/separate efficiently metal ions from aqueous solutions when a suitable extractant is used.

#### *2.2. Experimental*

Non-dispersive solvent extraction (NDSX) was carried out using Liqui-Cel<sup>®</sup> Extra-Flow 2.5"×8" phase contactors (Celgard, USA) the fibres being X-50 type. The experimental procedure was according to Cichy *et al.*, 2001. The ELM runs were carried out as described elsewhere (Gameiro *et al.*, 2007). Analyses of copper were performed with an atomic absorption spectrophotometer (Perkin Elmer, AAnalyst 200).

### 2.3. Discussion

The influence of the aqueous and organic throughputs on the extraction rate was studied in order to select the optimum hydrodynamic conditions. From the results obtained (data not shown), it was decided to keep the phases flow rates at 300 mL/min in the subsequent experiments. Simultaneous extraction and stripping experiments using different volume phase ratios were carried out. Typical concentration profiles in the aqueous feed and stripping phases for both extractants are shown in Figure 1. Table 1 summarises the results obtained from the NDSX and ELM experiments. As Figure 1 illustrates, the stripping kinetics is much faster using the carrier LIX 54. The flux entering in the stripping phase should control the overall process of copper extraction. The copper recovery obtained with ELM is lower than the one obtained by NDSX, due to non-ideal phenomena occurrence, like water transport and break-up. However, the time necessary for achieving the same absolute amount of transferred copper was found to be 1-2 times higher for the hollow fibres, which might be due to the significant contribution of stripping membrane resistance to the overall mass transfer.

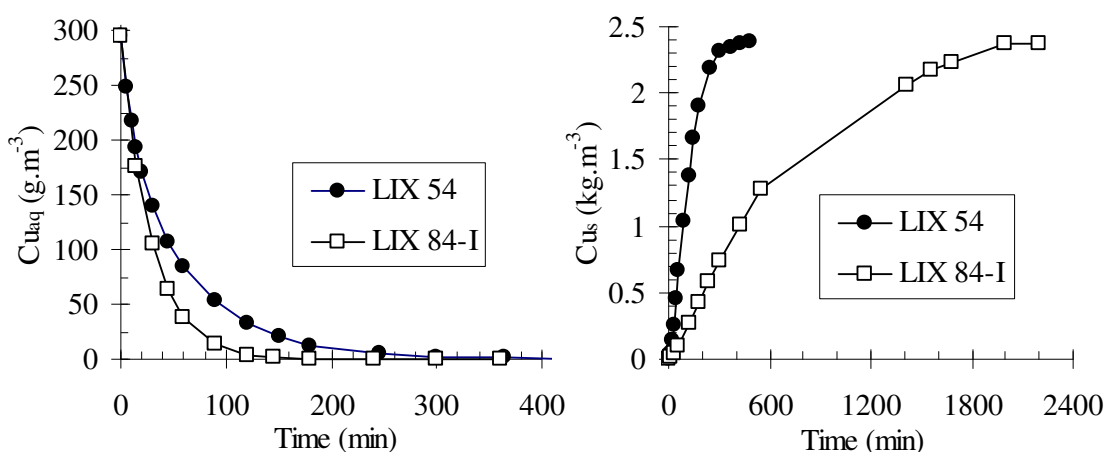


Figure 1: Copper concentration profiles in the aqueous phases (feed: aq and stripping: s) during extraction-stripping experiments. Initial aqueous phase:  $0.3 \text{ kg m}^{-3} \text{ Cu}$ ; pH 9.53.  $V_{aq}/V_s=8$ .

Table 1: NDSX versus ELM – Copper recovery and concentrations reached in the raffinate and stripping phases

Technique	$V_{aq}/V_s$	Extractant	$Cu_{aq} \text{ (g m}^{-3}\text{)}$	$Cu_s \text{ (kg m}^{-3}\text{)}$	Cu recovery (%)
NDSX	8	LIX 54	0.18	2.4	$\approx 100$
		LIX 84-I	0.01	2.4	98
	20	LIX 54	0.36	5.8	99
		LIX 84-I	0.01	5.5	91
ELM (4 min)	8	LIX 54	0.60	2.3	96
		LIX 84-I	0.33	2.7	92
	20	LIX 54	2.10	5.6	92
		LIX 84-I	0.27	6.1	92

Initial feed phase:  $Cu_{aq} = 0.3 \text{ kg m}^{-3}$ ,  $(NH_4)_2SO_4/NH_3$ , pH 9.53; Organic phase: extractant ( $0.06 \text{ kmol m}^{-3}$ ), surfactant ECA 4360J (2 wt.%) and Shellsol T;  $V_{org}/V_s=2$ ; Stripping phase:  $150 \text{ kg m}^{-3} \text{ H}_2\text{SO}_4$ .

### References

- Cichy, W., Schlosser, S. and Szymanowski, J., (2001) *Solv. Extraction and Ion Exchange*, 19, 905-923.
- Gameiro, M.L.F., Bento, P., Ismael, M.R.C., Reis, M.T.A. and Carvalho, J.M.R., (2007) *Journal of Membrane Science*, 293, 151-160.
- Juang, R.-S. and Huang, I-P., (2000) *Ind. Eng. Chem. Res.*, 39, 1409-1415.

## Thermodynamic topological analysis at infinite and finite conditions for reactive mixtures of acetates

C.A.Cardona<sup>a</sup>, F.A.Perdomo<sup>a</sup>, F.E Lopez<sup>b</sup>

<sup>a</sup>Department of Chemical Engineering, National University of Colombia at Manizales, Cra 27 N° 64 – 60 OF. 505, Manizales Colombia

<sup>b</sup>Departament of Inorganic Chemical, University of Alicante. Carretera San Vicente del Raspeig s/n - 03690 San Vicente del Raspeig – Alicante, Spain

### 1. Summary

When designing conventional and non-conventional distillation processes shortcut methods for predicting feasible separations are widely used. The thermodynamic topological analysis based on phase equilibrium and distillation maps study is a good approach allowing the knowledge of basic tower configuration at extreme conditions (infinite efficiency: total reflux and infinite number of stages). At these conditions usually the prediction is qualitatively approximate to that at total reflux. However some times the prediction strong differs from that, found during rigorous simulation. Additionally because of the infinite efficiency these regimes are not the optimal from the point of view of energy consumption. Making the thermodynamic topological analysis at finite reflux gives a closed region into the concentration simplex where feasible separations take place with a limit of minimal reflux number (minimal energy consumption).

Three component nonideal mixtures from acetates with different arranges of distillation maps are studied and the distillation configuration as well as parameters for rigorous simulation are presented. The mathematical method for solving the differential equations systems involved in phase equilibrium models is innovative and characterized by accuracy and low time calculations. All this information is used and explained as a way for the analysis of reactive distillation processes at finite reflux.

Keywords: conceptual design and simulation, thermodynamic topological analysis, reactive distillation

### 2. Extended Abstract

The reactive mass-exchange process is a process where, the chemical reaction and separation of the reaction mixture occur *simultaneously and combined* (in one apparatus) *with predominant removing of target reaction products*. As was shown by Pisarenko and coworkers today the design of reactive distillation processes consists of several stages. These stages could be resumed in three basic blocks: shortcut methods, rigorous methods and experiments. However this design strategy as many more showed in the literature

does not consider the technological optimization looking for improvements in the final synthesized process. Shortcut methods based on thermodynamic-topological analysis are very helpful to minimize simulation and laboratory experiments and also allow understanding further possibilities in higher conversion and selectivity achievement. In this work this kind of modification to these shortcut strategies are explained and complemented with new developments in analysis of finite and infinite efficiency RD columns. For the reactive distillation relatively few systematic methods or approaches exists (Pisarenko, et al, 2001), however no all methods maximizes the synergy effect between reaction and the separation. The short-cut methods, based on the study of the topology of the system (topological thermodynamic), are very used to obtain a first approach, allowing the reduction of simulation and experimentation time. In addition, the prediction of the limiting steady states (Static analysis at infinite reflux), characterized by the maximum conversion and selectivity is included in this stage. This work developed a methodology for better understanding of interactions between phase and chemical equilibrium at finite conditions of operation, determining the real separation possibilities for the reactive distillation process. Then one could have a range of ideas in the conceptual design of the process, minimum demanded energy and catalyst requirements. From this information the rigorous simulation can be made on the basis of theoretical validated parameters. This kind of modifications to the short methods represents a powerful tool for better conceptual design of reactive distillation columns as it is demonstrated in the Figure 1, where Isopropyl acetate process is analyzed. Here the area limited by the maximal demand (residue curve) and minimal demand of energy (pinch point line) give the unique thermodynamic possibilities of the process.

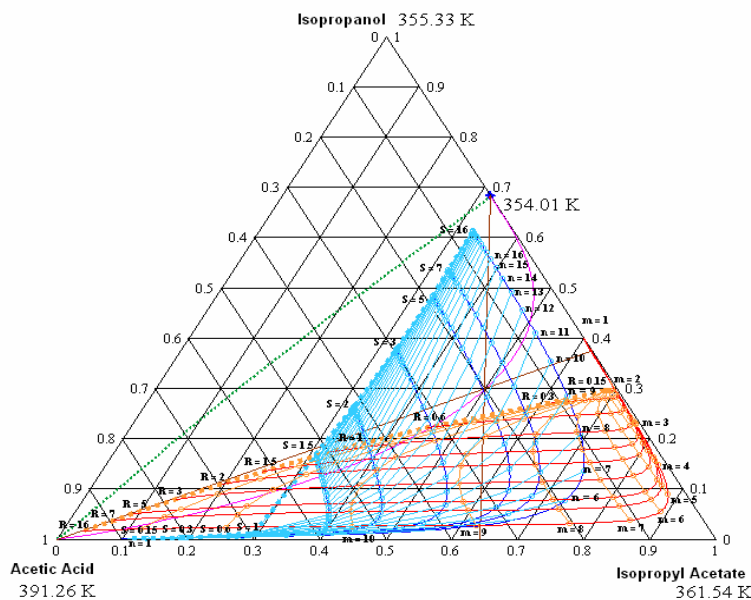


Figure 1. Analysis of separation possibilities to finite operation conditions for IP acetate

## References

- Pisarenko, Y.A., Serafimov, L.A., Cardona, C.A., Efremov, D.L., Shuwalov, A.S. (2001). *Reviews in Chemical Engineering - Freund Publishing House Israel-England*. Vol. 17, No. 4, 76 pp.

## **Regimes of extractive distillation in ethanol production**

N. Vyazmina<sup>a</sup>, D. Baranov<sup>b</sup>, A. Vyazmin<sup>b</sup>

<sup>a</sup>*Joint-Stock Company "Topaz" Distillery, ul. Oktyabr'skaya 46, Pushkino, Moscow region, 141200, Russia*

<sup>b</sup>*Department of Chemical Engineering, Moscow State University of Environmental Engineering, ul. Staraya Basmannaya 21/4, 105066, Moscow, Russia*

### **1. Summary**

The influence of operating conditions to the effectiveness of extractive distillation process was investigated. The experiment took place on an industrial vacuum plant of purification ethanol. It is obtained that the concentration of different impurities depends on the temperature and the volumetric flow rate of extractive solvent. Proposed method allows us to choose the extractive distillation regime that guarantees the necessary quality of ethanol. The values of operating conditions of extractive distillation for the best total purification from the attendant impurities are estimated.

Keywords: distillation process, industrial vacuum plant, extractive solvent, impurities

### **2. Extended Summary**

One method of production of alimentary ethyl alcohol is based on the distillation solution obtained in the fermentation. In this process, purification from various impurities occurs which were formed during fermentation and which are harmful (e.g., methyl, propyl, and other higher alcohols, various ethers, acids, aldehydes, etc.). According to the volatility with respect to ethanol, these impurities are subdivided into volatile, low-volatile, and intermediate ones. It is especially difficult to separate the latter class of impurities because they form azeotropic solutions with ethanol.

To separate intermediate impurities, a special distillation column of preliminary purification is used. In order to make it more efficient, one uses extractive distillation consisting in the extractive solvent (water) feed on the plates in the concentration part of the column. This enables to lower the concentration of ethanol and to shift the equilibrium for impurities to the transition from liquid to the vapor. Among the process parameters which define the efficiency of extractive distillation are the volumetric flow rate and the temperature of input water. The effect of the parameters on the purification degree of ethanol was studied on a commercial distillation column by measuring amounts of impurities in the products of distillation using highly effective gas chromatograph.

In order to select the volumetric flow rate  $Q_h$  and the temperature  $t_h$  of input water (water is used as the extractive solvent), at which the highest degree of purification from impurities is achieved, it is convenient to use the method of mathematical modelling and to represent the experimental data in the form of empirical formulas. The parameters  $Q_h$  and  $t_h$  for each impurity should be chosen so that the relative concentrations of impurities in product to concentrations in feed  $\alpha_{wi}/\alpha_{fi}$  is minimum.

As a parameter characterizing efficiency of purification it is natural to consider the ratio of total impurity content in the product to the total content in the initial mixture

$$I = \frac{\sum_{i=1}^m k_i (\alpha_{wi}/\alpha_{fi})}{\left( m \sum_{i=1}^m k_i \right)},$$

where  $m$  is the number of impurities. The coefficient  $k_i$  shows relative concentrations of impurities in initial mixture. The results of calculation of the  $I$  dependence on  $Q_h$  and  $t_h$  according to the experimental data are presented in Figure 1.

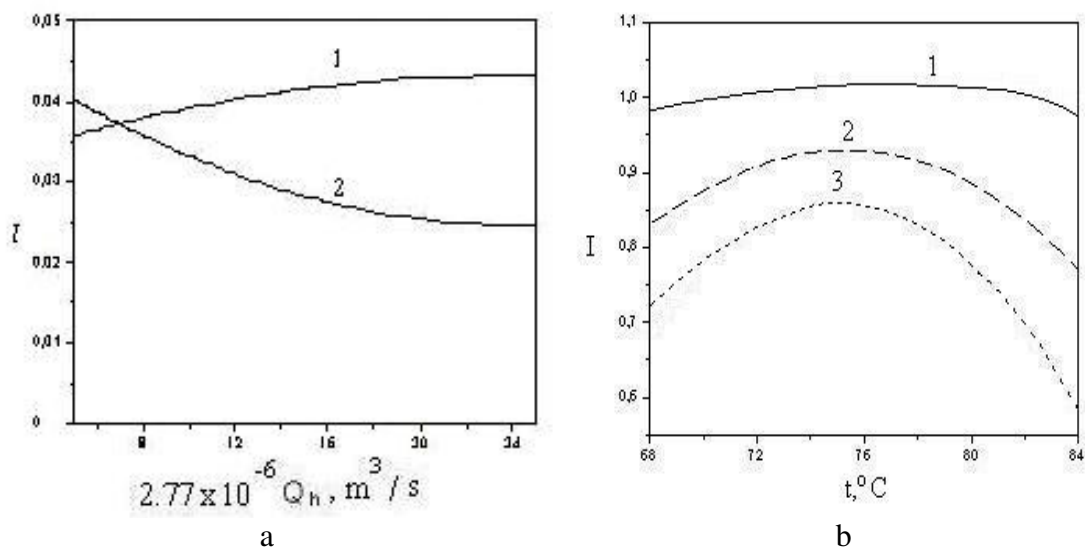


Figure 1: Dependence of  $I$  on  $Q_h$  (a) and  $t_h$  (b)

The results of calculation shown that in a separately taken column of preliminary purification (curve 1 in Fig. 1a) a slight decrease of the total (with respect to all impurities) degree of purification is observed if the volumetric flow rate of extractive solvent increases. From the results of calculation with the account taken on the correction for the selectivity of purification from different impurities (curve 2 in Fig. 1a), one may achieve a significant enhancement of the total degree of purification with respect to all impurities by simply increasing the volumetric flow rate of extractive solvent supplied for extractive distillation.

Fig. 1b depicts the calculation results for ratios of the total concentration of impurities in the product leaving the preliminary distillation column to their concentration in the initial mixture versus the extractive solvent temperature. Curve 1 corresponds to the highest degree of purification of ethanol from all main impurities. Curve 2 corresponds to the highest degree of purification from all impurities except those to be removed in the further columns, and curve 3 corresponds to the highest degree of purification from volatile and intermediate impurities only.

## **Design and Construction of a Novel Oldershaw-type Distillation Column for Measurement and Scale-up of Tray Efficiencies**

Montazer-Rahmati\*, M. M., Shafaghieh, H., Amouei, M.

*Department of Chemical Engineering, Faculty of Engineering, University of Tehran, \* E-mail: mrahmati@ut.ac.ir*

### **1. Abstract**

A new bench-scale, glass distillation column was designed and constructed in this work. This column is quite flexible with adjustable tray spacing and could be used to study various types of systems both foaming and non-foaming, each requiring different tray spacing. Tray efficiencies were measured in this three-inch diameter glass distillation column for two binary systems at total reflux. The results were compared with those obtained for a one-inch diameter Oldershaw-type column and the efficiencies obtained from an industrial column. The results of this work for the cyclohexane/n-heptane system show better efficiency than both the Oldershaw and the industrial column. With regards to methanol/n-propanol system, our data seem to follow the correct trend and are actually closer to the industrial data at lower percentages of flooding.

Keywords: Distillation column, trays, efficiency, scale-up, predictive models

### **2. Extended Abstract**

#### *2.1. Introduction*

In order to design distillation columns using the equilibrium approach, one needs to estimate the column efficiency. HTU and HETP concepts are used to design packed columns whereas overall and Murphury efficiencies are used to design tray columns [1]. Efficiency for tray columns depends on three main factors: the system involved, the flow conditions, and the tray geometry. The following methods are usually used for predicting tray efficiencies:

1. Using data from an existing similar industrial column.
2. Using empirical correlations.
3. Using theoretical or semi-empirical mass transfer models.

We are using a fourth, seldom-used method here, which uses the efficiency data obtained in a lab-scale column to predict the efficiency for industrial-scale columns. If this could prove to be a valid method, its simplicity would make it very useful for the study of complicated and non-ideal systems.

The distillation column designed in this work has the following characteristics. The shell is made of glass and all the internal parts including the perforated plates, the down-comers, and the central shaft on which the plates are located are made of stainless steel. The perforation pattern on all trays was triangular. Unlike typical Oldershaw columns, which have a circular pipe in the center as the down-comer, we used half-cylindrical down-comers on the sides. These were rectangular plates extending from tray to tray, the top part of which formed the weir on each tray.

The various components comprising the column are shown schematically in Figure 1.

### 2.2. Results and discussion

The results of this work for the cyclohexane/n-pentane system and for the methanol/n-propanol system have been compared to the data for an Oldershaw column [2] and an industrial column [3, 4] in Figure 2.

As can be seen in Figure 2, the results of this work are in good agreement with both the Oldershaw and the industrial column. The data available from the industrial column were limited. Therefore, it may not be wise to draw a firm conclusion from the comparison indicated in Figure 2b. Our data seem to follow the correct trend and are actually closer to the industrial data at lower percentages of flooding.

1. Tray hole locations      2. Down-comer      3. Silicone gasket      4. Central shaft hole

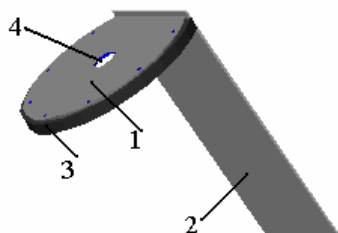
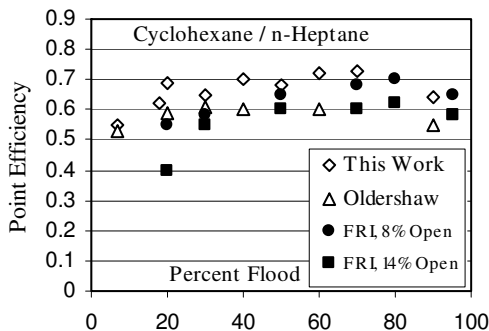
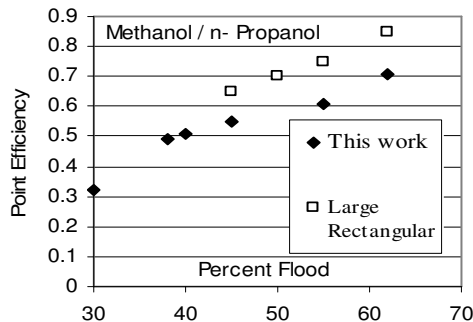


Figure 1: Details of the adjustable tray and weir



(a)



(b)

Figure 2: a) Comparison of point efficiencies for the cyclohexane /n-heptane system with the data for an Oldershaw column [2], and an industrial column [3]. b) Comparison of the point efficiencies for the methanol/n-propanol system with the data for an industrial column with rectangular trays [4].

### References

1. Montazer-Rahmati, M. M., Rekabi-Zadeh, D., and Amouei, M., "Suitability of using Brass Ferrules as packing in a glass distillation column and presenting a new relationship between HETP and pressure drop," Accepted in Iranian Journal of Chemistry and Chemical Engineering IJCCCE, (2007)
2. Fair, J. R., Null, H. R., and Bolles, W. L., Ind. Eng. Chem., Proc. Des., Vol. 22, 1983.
3. Yanagi, T. and Sakata, M., Ind. Eng. Chem., Proc. Des. & Dev., Vol. 21, 1982.
4. Biddulph, M. W., and Dribika, M. M., AIChE J., 1986.



## **Supercritical fluid extraction of bioactive compounds from sunflower leaves: comparison of analytical and pilot-scale extraction**

L. Casas,<sup>a</sup> C. Mantell,<sup>a</sup> M. Rodríguez,<sup>a</sup> A. Torres,<sup>b</sup> F. A. Macías,<sup>b</sup> E. J. Martínez de la Ossa,<sup>a</sup>

<sup>a</sup>Department of Chemical Engineering, Food Technology and Environmental Technologies, Faculty of Science, University of Cadiz, Box 40, 11510 Puerto Real, Cadiz, Spain.

<sup>b</sup>Department of Organic Chemistry, Faculty of Science, University of Cadiz, Box 40, 11510 Puerto Real, Cadiz, Spain

### **1. Summary**

Supercritical fluid extraction (SFE) from natural products has been widely studied as an alternative to the use of traditional techniques in the production of bioactive compounds. The work described here involved the extraction of bioactive compounds from the sunflower (*Helianthus annuus* L) with CO<sub>2</sub> and CO<sub>2</sub>+H<sub>2</sub>O. The extractions were carried out in an analytical Isco extractor and in a pilot plant from Thar Technology. The experimental data obtained of both were compared and the implications of this analysis on the development of scale-up procedures were also discussed. The SFE method was scaled-up for preparative applications using a pilot plant. Large-scale SFE was technically feasible with pure CO<sub>2</sub> as the extracting fluid. However, the use of CO<sub>2</sub> modified with water was not effective at the pilot plant scale.

Keywords: supercritical fluid extraction, *Helianthus annuus* L., analytical scale, pilot plant scale

### **2. Extended Abstract**

Interference of weeds with agricultural crops causes huge economic losses to farmers in two ways [1]. In this regard, greater attention has recently been paid to the use of allelopathic plants and their products to manage weeds in a sustainable manner [2]. Chemical studies of *Helianthus annuus* L (sunflower) have shown that this species is a rich source of compounds with a wide spectrum of biological activities, including potential allelopathy.

SFE from natural products has been widely studied as an alternative to the use of traditional techniques in the production of bioactive compounds. In most of these studies carbon dioxide was used as the solvent. However, quantitative extraction of polar analytes requires the addition of a modifier.

The work described here involved the extraction of bioactive compounds from the sunflower with CO<sub>2</sub> and CO<sub>2</sub>+5% H<sub>2</sub>O. The extractions were carried out in an analytical Isco extractor with one extractor with a maximum capacity of 10 ml and in a pilot plant from Thar Technology provided with an extraction vessel with a capacity of 2 L. The experimental data obtained of both were compared and the implications of this analysis on the development of scale-up procedures were also discussed.

The extracts obtained from CO<sub>2</sub>, show better results in terms of bioactivity than the extracted obtained from CO<sub>2</sub> and 5% water, nevertheless the best extraction yields were achieved using 5% water as a modifier and drying the sample under different conditions of pressure and temperature.

The SFE method was scaled-up for preparative applications using a pilot plant. Large-scale SFE was technically feasible with pure CO<sub>2</sub> as the extracting fluid. Dimensionless analysis (Reynolds) is the most relevant parameter for scale-up when CO<sub>2</sub> is using as solvent. The dimensions (H/d) are similarly in order to maintain geometric similarity. The ration 5 too is similar in analytical and plant pilot scale. Another important parameter is the residence time of the solvent in the extractor. Nevertheless, in this case this parameter is very difference between the analytical and pilot scale at 10 g/min, reason why it is not adapted to have presents on the process of sacle-up. Therefore, the scaling criterion of maintaining a constant residence time is not sufficient to ensure equivalent process during scale-up.

However, the use of CO<sub>2</sub> modified with water was not effective at the pilot plant scale. Although the form factor continues being he himself, in this case is not similarity between the reason considered (Q<sub>m</sub>d/M and Re). It is important to note that the effect that causes of cosolvent is different in analytical and pilot plant scale. It has been reported [3] that water is only 0.3% soluble in supercritical CO<sub>2</sub> but, despite this limited solubility, could play an important role in the extraction process. At analytical scale the passage of the solvents is descendent and the water is forced to leave the extractor increased solubility of the substances and therefore the yield. On the other hand, al pilot plant scale the passage of solvents are ascending and great part of this one does not solubility in CO<sub>2</sub> and remain in the extractor.

## References

1. Pimentel, D., McNair, S., Janecka, J., Wightman, J., Simmonds, C., O'Connell, C., Wong, E., Russel, L., Zern, J., Aquino, T. and Tsomondo, T. (2001) *Agriculture, Ecosystems & Environment*. 84, 1-20.
2. Singh, H., Batish, D., and Kohli R.(2003) *Critical Reviews in Plant Sciences*. 22, 239-311.
3. Lang, Q and Wai, C. (2001) *Talanta*. 53, 771-782.

## **Sorption Dynamics of Rare Metals into a Matrix-Type Microcapsule Containing an Organophosphorus Extractant**

Kazuo Kondo<sup>a</sup>, Michiaki Matsumoto<sup>a</sup>, Eiji Kamio<sup>b</sup>

<sup>a</sup>*Department of Chemical Engineering and Materials Science, Doshisha University, Kyotanabe-shi, Kyoto 610-0321, Japan*

<sup>b</sup>*Department of Environmental Chemistry and Materials, Okayama University, Okayama-shi, Okayama 700-8530, Japan*

### **1. Summary**

In this study, sorption dynamics model for microcapsule system is derived. The investigated system is sorption of gallium and indium into a matrix type microcapsule containing 2-ethylhexylphosphonic acid mono-2-ethylhexyl ester (EHPNA). The proposed model takes into account of both the complexation reaction of metal ion and EHPNA at the interface between aqueous bulk and EHPNA phase, which exists on the microcapsule surface, and the intraparticle diffusion of the formed metal-EHPNA complex. The proposed model describes the pH and the metal concentration dependencies on sorption behavior not using any fitting parameters. As a result, the sorption mechanism of metals into a microcapsule is estimated as follows: (1) diffusion of metal ion through the aqueous film surrounding a microcapsule, (2) complexation reaction of metal ion and extractant adsorbed on the interface, and (3) diffusion of the extracted complex into a microcapsule through the pore.

Keywords: microcapsule, rare metal, sorption, organophosphorus extractant

### **2. Extended Abstract**

Considering that the microcapsules containing EHPNA exhibit strong hydrophobicity at  $\text{pH} < 4$  and do not behave as ideal mixing, we measured the kinetic data by the shallow bed method. A 0.05g of the microcapsules was packed into the bed. The feed solution containing gallium or indium ion was introduced for appropriate periods. It was found in the preliminary experiments that  $70 \text{ cm}^3/\text{min}$  of the flow rate is enough to ignore liquid film diffusion resistance surrounding a microcapsule. As soon as the desired time passed, a scrubbing solution of  $\text{pH}=3.0$  was introduced into the bed to remove the feed solution remaining in the bed. Then the microcapsules were collected and contacted with the stripping solution for 1 day. The stripping solutions used are 1 and  $5 \text{ mol/dm}^3 \text{ H}_2\text{SO}_4$

solution for gallium and indium, respectively. The metal concentration in the stripping solution was measured with inductively coupled plasma spectrometer. The experiments were carried out at 313K.

The fractional attainment of sorption equilibrium,  $F(t)$ , decreased with decrease in pH from 2.5 to 2.0 and increased with decrease in pH from 2.0 to 1.3. In addition,  $F(t)$  increased with increase in metal concentration in the aqueous bulk and the corresponding calculated results illustrate well these tendency. The calculated uptake curves for gallium sorption, which are based on the proposed model, well correspond to the experimental data, that is to say, it is suggested that the proposed kinetics model is adequate for metal sorption system with the microcapsules. In the case of indium sorption, the calculated results fit to the experimental data only at the initial stage of sorption. The uptake curves of indium sorption depend on pH as well as the case of gallium sorption. The calculated uptake curves also describe its pH dependency well. Effect of indium concentration on the uptake also shows the same dependency in the experimental data and calculated results. Especially in the case of low loading condition, the calculated results show good agreement with the experimental data. However, the calculated results under the high pH and metal concentrations stray off from the experimental data with passing time. This disagreement occurs due to pore closing by formation of the indium-EHPNA condensate on the surface of the microcapsule. Namely, in the case of indium sorption, where the complexation rate is fast, it is suggested that the complexes formed on the surface of the microcapsule aggregate with each other and are hard to diffuse into the center of a microcapsule.

## References

- Kondo, K. and Matsumoto, M., (1998) *Separation and Purification Technology*, 13, 109-115.  
Kamio, E. and Kondo, K., (2005) *Industrial & Engineering Chemistry Research*, 44, 2266-2272.

## Characterizing a Brazilian Petroleum Residue by Molecular Distillation Process

Winter, A.<sup>a</sup>, Batistella, C.B.<sup>a</sup>, Wolf Maciel, M.R.<sup>a</sup>, Maciel Filho, R.<sup>a</sup>, , Medina, L.C.<sup>b</sup>

<sup>a</sup> Separation Process Development Laboratory, Faculty of Chemical Engineering, State University of Campinas (UNICAMP), Zip.code: 13080-570, Campinas, Brazil [winter@feq.unicamp.br](mailto:winter@feq.unicamp.br), [doutorbatistella@uol.com.br](mailto:doutorbatistella@uol.com.br), [wolf@feq.unicamp.br](mailto:wolf@feq.unicamp.br), [maciel@feq.unicamp.br](mailto:maciel@feq.unicamp.br)

<sup>b</sup> CENPES/PETROBRAS, Rio de Janeiro, Brazil [lmolina@petrobras.com.br](mailto:lmolina@petrobras.com.br)

### 1. Summary

The increasing evolution of the quality of petroleum derivatives and the increase of heavy petroleum leads to the need of a better characterization and utilization of this oil. The properties of natural petroleum and petroleum products make use of the True Boiling Point (TBP) distillation analyses and this is very useful for petroleum characterization, for design and operation of refinery units, for the classification of petroleum, for the development of petroleum property correlations and it has been used worldwide. Two conventional methods specified by the American Society for Testing and Material (ASTM) are necessary for determination of the boiling point of crude oil distribution. The first method, ASTM D2892, is satisfactory for the distillation below 400°C. The second method, ASTM D5236, is used at reduced pressures (50-0,1 mmHg). The maximum atmospheric equivalent temperature reached with ASTM D5236 method, can be 565°C. In this work, the TBP curve was extended above 700°C. The molecular distillation process is a potential technique for fractionating products of high molecular weight and it was used in this work for extending the TBP curve.

Keywords: petroleum, True Boiling Point curve, molecular distillation

### 2. Extended Abstract

Oils are evaluated in function of the distillation curve TBP (True Boiling Point). Two conventional methods specified by the American Society for Testing and Material (ASTM) can reach temperatures up to 565°C. For higher temperatures, a well established method does not exist. In this work, it was developed a methodology for generating, from molecular distillation process, the liquid volume percentage in relation to temperature, to build up the distillation curve, using one of the streams (distilled) of the process. In

Batistella (1999), Burrows (1960) and Boduszynski and Altgelt (1994), it can be verified the robustness of this method since it enables operation at low temperatures, short residence times, being ideal for working with high molecular weight and thermally sensitive compounds. In Batistella et al. (2005), data of temperature and percentage of distilled from molecular distiller, obtained experimentally, were used in the TBP curve extension, and a new correlation (FRAMOL correlation) was presented. This correlation allows conversion of the operating temperature of molecular distiller to equivalent atmospheric temperatures, which are, indeed, used in the conventional TBP curves.

In Figure 1 the TBP curve was extended using FRAMOL correlation. The extension of the curve reached approximately 700°C+ and present continuity and good agreement with the ASTM curve. The accumulated percentage of distilled for residue Beta 540°C+ arrived values next to 76%. The increase in distilled percentage is approximately 19%. Molecular Distillation process made possible the extension of TBP curve with very good precision using the FRAMOL correlation and this is very important to define better strategies and operating conditions for heavy petroleum processing, leading to upgrade these fractions. The developments achieved in this work are very important since no standard methodology is available for calculating the TBP extended curve, considering the large amount of heavy petroleum today encountered.

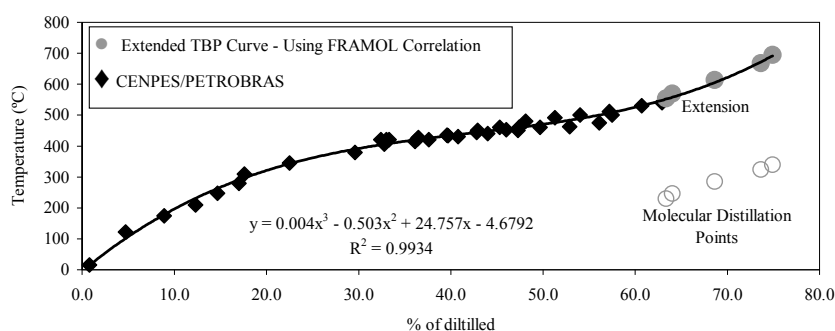


Figure 1: Extension of the true boiling point curve for Beta 540°C+ petroleum through molecular distillation considering FRAMOL correlation.

## 1. References

- Batistella, C. B., *PHD Thesis (in Portuguese)*, (1999), UNICAMP, SP, Brazil.
- Batistella, C. B., Sbaite, P., Wolf Maciel, M.R., Maciel Filho, R., Winter, A., Gomes, A., Medina, L., Kunert, R. Heavy Petroleum Fractions Characterization: A New Approach Through Molecular Distillation, *2<sup>nd</sup> Mercosul Congress on Chemical Engineering & 4<sup>th</sup> Mercosul Congress on Process Systems Engineering*, (2005), Costa Verde – RJ, Brazil.
- Boduszynski, M.M E Altgelt, K.H., *Composition end Analysis of Heavy Petroleum Fractions*. (1994) Marcel Dekker, Inc.,NY.
- Burrows, G. *Molecular Distillation*. (19960), Oxf. Univ. Press (Oxford).

## Carbon dioxide absorption from flue gases using Sodium Hydroxide as liquid solvent

F. Yazdanbakhsh, A. Soltani, H. Hashemipour

*Department of Chemical Engineering Shahid Bahonar University – Kerman – Iran  
Kerman- Jomhoori Blvd- School of engineering- Chemical engineering Department*

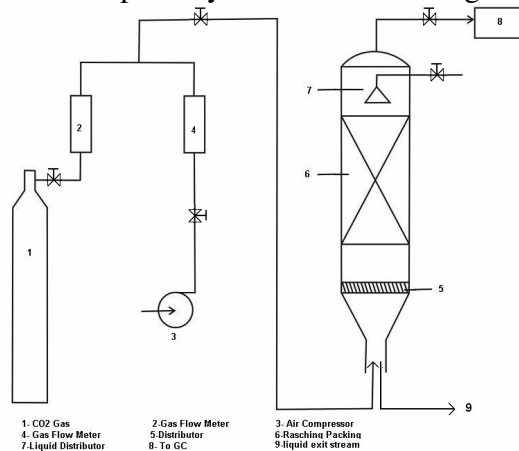
### 1. Summary

In this research absorption of carbon dioxide into sodium hydroxide solution has been investigated. By making mass and energy balance around a differential height of the absorber, governing equations were obtained and solving these equations using boundary conditions predicted the axit parameters. comparing these simulation data with experimental data shows the accuracy of the model.

### 2. Extended Abstract

In recent years, the removal of CO<sub>2</sub> from industrial gas streams has become important. This has resulted from the environmental concern for reduction of greenhouse gas emissions from industrial sources. Here, CO<sub>2</sub> is considered to be the largest contributor to the global warming problem, and is thus the major target for reduction. The removal of CO<sub>2</sub> from gas streams can be achieved by absorption into a liquid solvent. This separation process usually takes place in the columns packed with packing materials to promote direct contact between irrigating liquid and the continuous gas phase. in this study simulation of carbon dioxide absorption by Sodium Hydroxide solution in a packed bed has been investigated.

A schematic diagram of the absorption system is shown in figure (1):



Figure(1)- absorption system

first, mass and energy balances were applied around a differential height of the bed. So, the governing equations were obtained. These equations are related to both phases: gas phase and liquid phase. Gas phase consists of carbon dioxide and air which we just consider carbon dioxide in the equations. On the other hand liquid phase consists of sodium hydroxide, water and sodium carbonate. So we have a general differential equation for each phase and one equation for each substance in both phases. ie. Carbon dioxide concentration in gas phase was calculated using this equation:

$$\frac{dy_{CO_2}}{dz} = \frac{[-N_{CO_2}(1-y_{CO_2})]}{G} \cdot a$$

Surface renewal theory by Danckwerts was used to represent the mass transfer operation:

$$N_{CO_2} = \left( \frac{k_{gCO_2} k_L EH}{k_{gCO_2} + k_L EH} \right) (P_{CO_2} - P_{CO_2e}) = K_{gCO_2} (P_{CO_2} - P_{CO_2e})$$

In which E is enhancement factor and is presented by:

$$E = \sqrt{1 + \frac{D_{CO_2} \cdot k}{k_L^2}}$$

The differential equations we obtained should be solved to represent the exit concentration of carbon dioxide in gas phase. Since half of the boundary conditions were not known we used shooting method to estimate these boundary conditions and fourth order runge-kutta method was used to solve the differential equations by MATLAB software. A verification of model was carried out by comparison with the experimental data taken from the packed bed. Gas samples were analyzed by gas chromatography. The predicted results and actual data represent an appreciable agreement. Obtained data are listed in table (1):

Gas load(L/min)	Gas entrance conc.	Gas exit conc.	Predicted gas exit conc.	%error
50	4.0863	2.6728	2.89	7.51
70	3.8957	3.0283	3.17	4.47
90	4.1756	3.4215	3.34	2.44
50	6.0724	4.5728	4.36	4.88
70	5.8745	4.6254	4.78	3.23
90	5.9246	5.2327	5.03	4.03
50	8.0748	5.6114	5.84	3.91
70	8.1249	6.7592	6.4	5.61
90	7.8953	6.9631	6.73	3.62
50	10.2741	7.1418	7.33	2.57
70	10.3426	8.3504	8.02	4.12
90	9.8597	8.5273	8.43	1.15

Table(1) - comparison of experimental data from the absorption column with model in liquid concentration of .2 M and liquid load of 4 (L/min)

## References

- AL. Kohl, FC Riesenfeld . "Gas purification", (5<sup>th</sup> ed).. Huston, Texas:Gulf publication Co, 1985  
 G. Sartori , DW Savage . Sterically hindered amines for CO<sub>2</sub> removal from gases.Ind Eng Chem Fundam 1983;22:239-49  
 A.Z. Kashkooli, M.Sc. Thesis , Shiraz University, Shiraz, Iran 2002  
 P. Tontiwachwutikul, A Meisen Co2 absorption by NaOH , monoethanolamine and 2-amino-2-methyl-1-propanol solutions in packed column. Chem Eng Sci 47 (1992) 381-390  
 P.V Dankwerts, Gas-Liquid Reactions, McGraw-hill, 1970.



## Numerical simulation to determine the mass transfer Coefficient in gas - liquid phase in an absorbed column

Basher Sohbi

Libyan Petroleum Institute/ Department of Separation technology, Gergarsh road, P.O. Box: 6431 Tripoli  
-Libya, Email: bsohbi04@yahoo.com

### 1. Summary

In this paper, a numerical simulation is used to predict the mass transfer coefficient  $k_{L,a}$ , for both liquid and gas phases, the value of the mass transfer coefficient would change until the experimental data were in agreement with the calculated data using MS Excel program. The mass transfer coefficient  $k_{L,a}$  in gas/liquid system was measured by the unsteady state dynamic method, the water was as liquid phase and the oxygen was as gas phase. In special cases for both liquid and gas phases the mass transfer coefficient  $k_{L,a}$  could be determined with analytic method. The agreement between the results of a numerical simulation and analytical method is found to be perfect.

Keywords: gas-liquid, mass transfer coefficient; absorption; numerical and analytic method

### 2. Extended Abstract

Absorption and stripping are widely used in many applications such as: chemical, petrochemical, bio-reactions, and waste water treatment. Most studies on gas-liquid phase were devoted to the experimental determination of the design parameters for gas-liquid phase, such as flow regime, individual mass transfer, gas-liquid specific interfacial area and more specifically, of the mass transfer coefficient  $k_{L,a}$  [Sohbi *et al*, 2006 and, Nikakhtari *et al*, 2005]. The value of the mass transfer coefficient  $k_{L,a}$  in the equation (1) for the Gas phase and the equation (2) for the Liquid phase would be simulated using the numerical technique, until the experimental data were equal to the calculated data. As shown in the figure (1) for the Liquid phase, the agreement between the results of a numerical simulation and analytical method is shown in the figure (2) in the Gas phase

$$\frac{\partial C_G}{\partial h} = \frac{A_s(1-\phi_G)}{V_G} \cdot (k \cdot C_G - C_L) \cdot k_{L,a} \quad (1)$$

$$\frac{\partial C_L}{\partial t} = -\frac{V_G}{A_s(1-\phi_G)} \cdot \frac{\partial C_G}{\partial h} \quad (2)$$

The mass transfer coefficient  $k_{La}$  in gas/liquid system was measured in four different Positions by the unsteady state dynamic method.

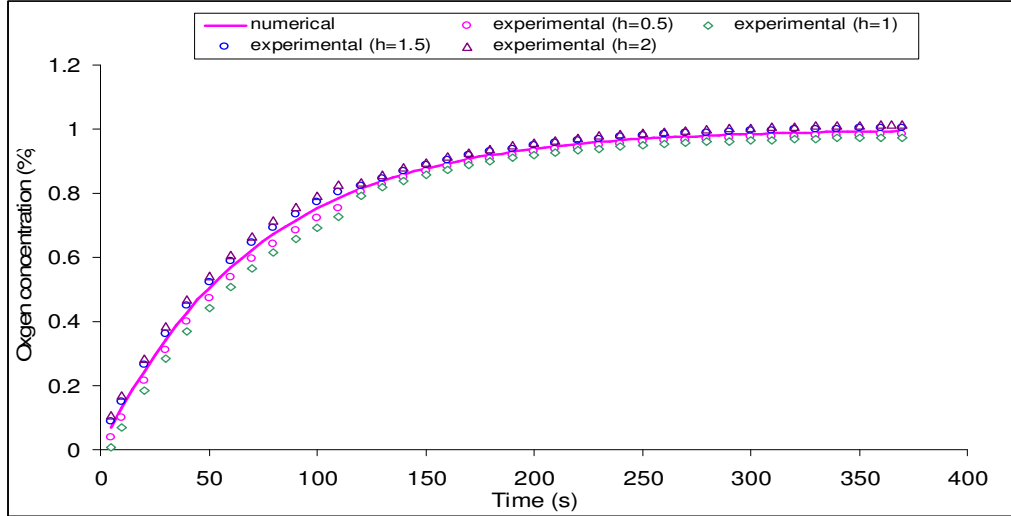


Figure1. Experimental data compared to calculated data in Liquid phase at Gas velocity = 0.01 m/s

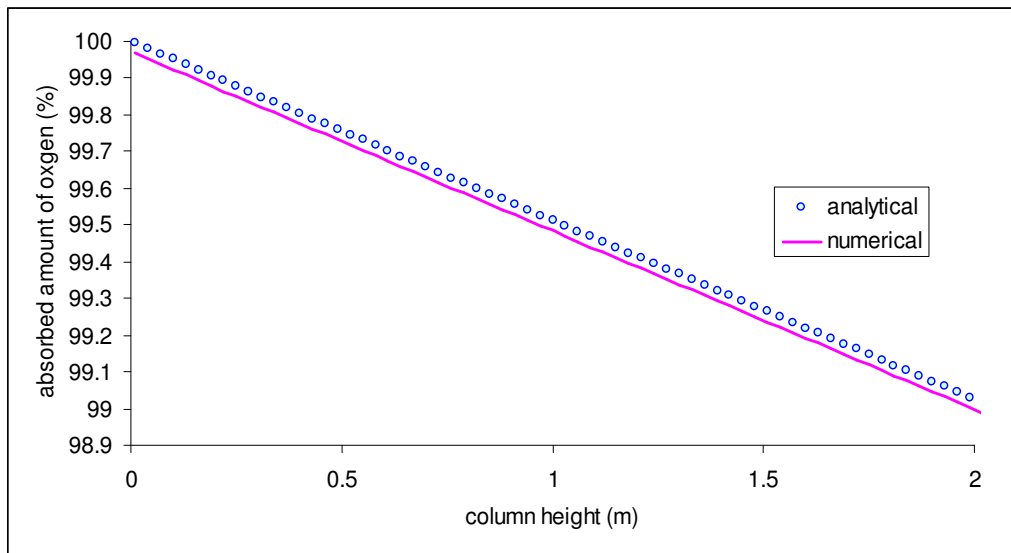


Figure 2. Comparison between numerical simulation and analytical method in the Gas phase

## References

- Sohbi, B., Edreder, E., (2006) 17<sup>th</sup> *International Congress of Chemical and Process Engineering* 27 - 31 August 2006, Prague - Czech Republic, Conference proceeding.  
 Nikakhtari, H., Hill, G.A., (2005) *Ind.Eng. Chem. Res.* 44: 1067-1072.

## Session T2-11a: Filtration – I

<b>Abstract Number</b>	<b>Paper Title &amp; Authors</b>	<b>Included</b>
401	Investigating the influence of bed structure on pulp washing using a novel measurement technique J Lindau, H Theliander	Yes
2137	Applying core-shell colloids as a tool for understanding solid/ liquid separation of slurries mainly containing organic materials M Hinge, K Keiding	Yes
2326	Pressure effects in dead-end filtration of skimmed milk: Analysis of cake properties A Bouchoux, F Garnier, A Harouna, G G Guiziou	Yes
3358	Filtration of Ultrafine Aerosols: Small Particles, Many Questions G Mouret, D Thomas , S Callé-Chazelet , D Bémer	Yes

Session T2-11a

## **Investigating the influence of bed structure on pulp washing using a novel measurement technique**

J. Lindau,<sup>a</sup> and H. Theliander,<sup>a</sup>

<sup>a</sup>*Department of Chemical and Biological Engineering, Chalmers University of Technology, 412 96 Gothenburg, Sweden*

### **1. Summary**

The influence of bed structure on pulp washing was investigated in this work using an in-situ measurement technique. The experimental equipment was a test piston filter press equipped with a  $\gamma$ -radiation source and a scintillation detector that was used to measure concentrations and porosity within the pulp bed during the washing process. Two types of pulp were investigated: groundwood and kraft pulp. Both the influence of flocculation and a porosity gradient on washing efficiency were examined. It was shown that washing efficiency was lower for a flocculated bed than for a corresponding non-flocculated bed. It was also shown that the porosity gradients obtained in this study do not virtually affect the washing efficiency. Local dispersion coefficients were also obtained and it was shown that they were independent of the measurement height.

Keywords: washing, dispersion, experimental, paper pulp, bed structure

### **2. Extended Abstract**

In the sulphate paper pulping process, the pulp is washed after the delignification stage in order to recover spent cooking chemicals and remove dissolved organic compounds. There are two ways to wash pulp, either by dilution/separation or by displacement. In an ideal displacement washer all of the chemicals and dissolved organic compounds are recovered by one void volume of wash water. This is, however, not the case in a real washer. There are several different phenomena responsible for this deviation from the ideal case, e.g. adsorption, as well as various phenomena related to the structure of the cake and the flow conditions; these, together with diffusion, are collectively called dispersion. Much work has been performed on determining what factors influence the washing efficiency. The results have however been somewhat contradictory and a full explanation on how factors such as different pulp types, temperature and pulp consistency influence pulp washing is yet to be presented. One explanation for this might be the experimental technique used in practically all of the earlier experiments. This technique involves measuring the concentration of some interesting specie, usually  $\text{Na}^+$  or lignin in the collected filtrate. The drawback of this experimental method is that it gives very little information about what happens inside the cake itself. A new method of measuring concentrations

within the pulp bed during the washing process was therefore developed and presented in (Lindau et al., 2007a). In (Lindau et al., 2007b) the new measurement technique was used to study the influence of pulp types on displacement washing.

In this work the novel experimental technique has been used in order to investigate the influence of bed structure on pulp washing. The experiments have been divided into five different groups. The way in which the groups differed from each other is explained in Table I. The previously developed method has also been extended in this work to incorporate the measuring of porosity within the bed.

Table I. Experimental groups.

Group	A	B	C	D	E
Type of pulp	kraft	groundwood	kraft	groundwood	kraft
Bed height [cm]	3	3	7	3	3
Inlet consistency [%]	0.36	0.36	0.36	5.2	4.8

The porosity measurements showed that a porosity gradient could only be found in the kraft pulp cakes in Group C. The porosity measurement technique can also be used to determine the presence of even a small amount of air within the cake: air was indeed detected in the Group E pulp cakes. It was however shown that the small amount of air present had no effect on the washing efficiency.

The filtrate measurements showed that, for both groundwood and kraft pulps the non-flocculated beds had lower dispersion coefficients and higher Peclet number than the beds. This is an expected result, and can be explained by the fact that diffusion from the flocs occurs in flocculated beds thus increasing the dispersion.

The effect of a porosity profile was investigated by comparing Group C, where a porosity profile was present, with Group A, where no such profile was found. The results were difficult to analyze since several parameters differ between the groups besides the presence of a porosity profile. The conclusion was that a major cause of the difference in dispersion coefficient was the difference in velocity and nothing conclusively could be said about the influence of the porosity profile.

The local measurements were used to obtain local breakthrough curves. These breakthrough curves were used to calculate local dispersion coefficients, and it was indicated that the local dispersion coefficients virtually did not depend on the measurement height.

## References

- Lindau, J., Sedin, P. and Theliander, H., (2007a) *Chem. Eng. Res. Des.* 85(A3), 357-364.  
 Lindau, J., Sedin, P. and Theliander, H., (2007b) *Nord. Pulp Paper Res. J.* 22(1), 80-86.

## **Applying core-shell colloids as a tool for understanding solid/ liquid separation of slurries mainly containing organic materials**

M. Hinge and K. Keiding

*Department of Biotechnology, Chemistry and Environmental Engineering,, Aalborg University,DK-9000 Aalborg, Denmark*

### **1. Summary**

It is not always possible to predict or scale up the separation process of organic materials (e.g. activated sludge) with the existing mathematical models. A new approach of designing, synthesising and dewater core-shell model colloids have been applied in order to investigate the filtration behaviour of organic materials. The results showed that it is possible to investigate the effect of one specific physical or chemical material property on the dewatering process.

Keywords: Dewatering, Model colloids, Water swollen materials

### **2. Extended Abstract**

Sometimes it is not possible to apply the traditional mathematical models when predicting or scaling up the separation process for dewatering of organic material (e.g. activated sludge). A plausible reason for this is that the traditional mathematical models have been developed and verified on data generated from filtration experiments performed on inorganic model materials (e.g. titanium dioxide). Therefore there is a need for further understanding of the mechanisms taking place during dewatering of organic materials. Designing organic model materials and performing filtration experiments on such might reveal some of the mechanisms taking place in the organic material during filtration. This will open the possibility for further development of the mathematical filtration models to include organic materials.

A new strategy has been applied in order to investigate the filtration behaviour of organic materials. The method comprises the synthesis of monodisperse core-shell colloids with a variation in one specific physical or chemical material property and performance of filtration experiments on these colloids. Three series of core-shell colloids have been synthesized and applied in filtration experiments. The first series have a solid core and varying amount of a water swollen anionic shell, the second series is colloids with a varying diameter of the solid core with a water swollen anionic shell. The final set has a solid core and varying amount of a non-ionic water swollen shell. The filtration experiments were performed on the water swollen core-shell colloids at different filtration pressures. Based on the results from the synthesis, characterization and filtration experiments a conceptual model for the interaction of the water swollen core-shell colloids during filtration has been proposed.

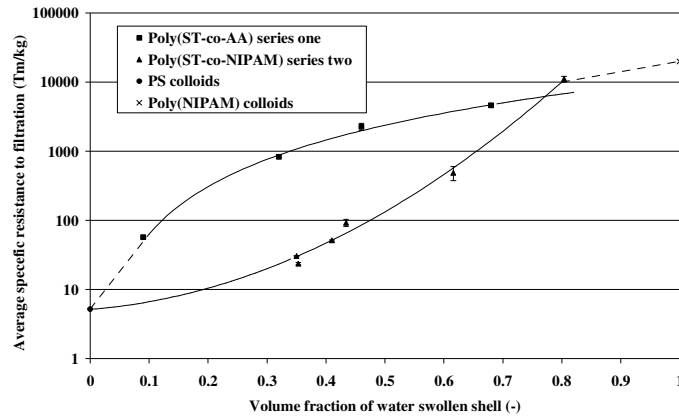


Figure: Example of a specific filtration result obtained. The specific resistance to filtration increases with volume fraction of water swollen shell. Dashed line: extrapolation and solid line: interpolation.

These findings indicate that the method of designing polymeric colloids that targets the effect from one specific physical or chemical material property on filtration is promising with respect to further development of the filtration theory and should be pursued further.



## Pressure effects in dead-end filtration of skimmed milk: Analysis of cake properties

A. Bouchoux<sup>a</sup>, F. Garnier<sup>a</sup>, A. Haroun<sup>a</sup>, G. Gésan-Guiziou<sup>a</sup>

<sup>a</sup>INRA, Agrocampus Rennes, UMR1253, Science et Technologie du Lait et de l'Oeuf, F-35000 Rennes, France

### 1. Summary

Ultra- and microfiltration are now widely used in the dairy industry as tools for the separation and the fractionation of specific solutes and proteins in milk [1]. The performances of these operations, in terms of permeability and selectivity, are ruled by the formation of concentrated layers at the membrane surface during the course of filtration. Understanding the properties of these layers and the mechanisms involved in their formation is of major importance for developing strategies to improve membrane-based processes in the dairy industry [2-3].

This work focuses on the analysis of controlled dead-end filtrations of skimmed milk at various transmembrane pressures. We show that: (i) the concentrated layers formed during the filtrations exhibit high specific resistances which indicate a possible deformation and/or destructuration of the casein micelle, the major constituent of the fouling layers; (ii) these layers are sensitive to transmembrane pressure and are clearly compressible.

Keywords: milk, membrane, filtration, cake, compressibility

### 2. Extended Abstract

Filtrations were performed in dead-end mode (Fig.1a) with ultrafiltration membranes (PES Membrane of  $100 \text{ kg}\cdot\text{mol}^{-1}$  MWCO, Novasep, France) at  $50^\circ\text{C}$ , i.e. the temperature commonly used in the dairy industry.

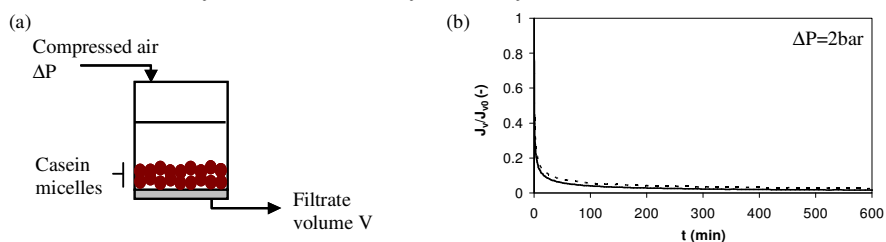


Figure 1: (a) Dead-End filtration principle. (b) Normalized instantaneous flux as a function of time for  $\Delta P=2\text{bar}$ . Skimmed milk. The dashed and solid lines are flux profiles for duplicate experiments.

For all the pressures investigated from 1 to 4 bar (Fig.1b shows typical results for  $\Delta P=2\text{bar}$ ), flux decline was severe and very fast, indicating a relatively high fouling resistance. After about 1 h of filtration, permeation flux was very low and still slowly decreased.

As it is commonly done in colloids filtration, the average specific resistance to filtration ( $\alpha_{\text{ave}}$ ) was classically determined from the slope of  $dt/dV$  vs  $V$  (Fig.2a, Eq.1). Here,  $\alpha_{\text{ave}}$  is the specific resistance of the entire concentrated region formed at the membrane surface, i.e. region divided into a concentration polarization layer and a more concentrated cake or gel layer [2]. Additionally, the specific resistance  $\alpha_{\text{gel}}$  of the gel layer itself was also determined from the absolute remaining resistance after rinsing of the cell.

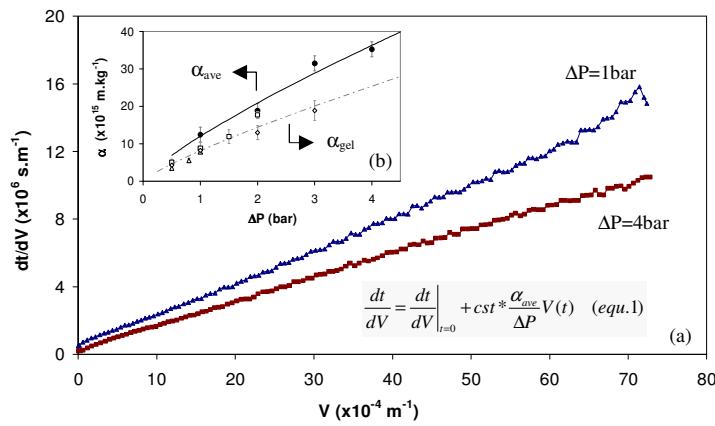


Figure 2: (a) The classical plot  $dt/dv$  vs  $v$  for dead-end filtration of skimmed milk for  $\Delta P= 1$  and  $4$  bar. (b) Effect of filtration pressure on the specific resistances  $\alpha_{\text{ave}}$  (as determined from  $dt/dV$  vs  $V$ ) and  $\alpha_{\text{gel}}$  (as determined from the absolute remaining gel resistance).

In all cases,  $\alpha_{\text{ave}}$  and  $\alpha_{\text{gel}}$  are remarkably comparable (Fig.2b). However, the values obtained are typically two orders of magnitude higher than resistances calculated from the Carman-Kozeny approximation for a deposit formed by closely packed casein micelles of roughly  $150\text{nm}$  in diameter ( $\approx 3.10^{14}\text{m.kg}^{-1}$ ). This discrepancy is probably due to the deformation and/or the shrinkage of the micelles upon filtration. This assumption was further confirmed by comparing the casein micelle hydration in non-concentrated milk with the dry matter content of the remaining gels after filtration.

Finally, our results clearly show that the specific resistances  $\alpha_{\text{ave}}$  and  $\alpha_{\text{gel}}$  are highly sensitive to transmembrane pressure (Fig.2b). The relevance of such a compressibility to the possible structure of concentrated dispersions of casein micelles will also be discussed.

## References

- [1] Brans, G., Schroen, C. G. P. H., van der Sman and R. G. M., Boom, R. M., (2004) *Journal of Membrane Science*, 243, 263-272.
- [2] Gésan-Guiziou, G., Jimenez; A., and Arcelin, C., (2006) *Desalination*, 199, 20-22
- [3] Kromkamp, J., Rijnsent, S., Huttenhuis, R., Schroën, K. and Boom, R., (2007) *Journal of Food Engineering*, 80, 257-266

## Filtration of Ultrafine Aerosols: Small Particles, Many Questions

G. Mouret <sup>a</sup>, D. Thomas <sup>a</sup>, S. Callé-Chazelet <sup>a</sup>, D. Bémer <sup>b</sup>

<sup>a</sup> Nancy-Université/LSGC/CNRS – 1, rue Grandville - BP 20451 - 54001 NANCY Cedex, France

<sup>b</sup> INRS - Avenue de Bourgogne - 54501 Vandoeuvre les Nancy Cedex, France

### 1. Summary

In 1991, Wang and Kasper challenged filtration theories with the thermal rebound effect: according to them, filtration efficiency of filters could decrease below 10 nanometers. The experimental study of Cu-nanoparticles penetration through grounded wire screens at 5 cm/s shows no evidence of efficiency loss down to 4 nm.

Keywords: nanoparticles, filtration, efficiency, thermal rebound

### 2. Extended Abstract

Filtration efficiency is determined by several mechanisms: inertial deposition, interception and diffusion as the most important. Despite these different mechanisms, a maximum of penetration is reached for particles in the 0.1-0.5  $\mu\text{m}$  size range: bigger particles are stopped by inertia and tinier ones are expected to be collected by Brownian diffusion. But in the early nineties, a theory was developed establishing that filtration efficiency could decrease again in the nanometric domain because velocity of particles would be too high to enable their caption: it is the thermal rebound effect.

Experimental study of filtration efficiency of nanoparticles has been carried out in metallic grids of different characteristics (table 1 and figure 1).

Table 1 – Physical parameters of tested wire screens

		SS25	SS40	SS75	SS150	SS355
fiber diameter	$\mu\text{m}$	25	36	50	100	200
solid volume fraction	/	0.3927	0.372	0.3142	0.3142	0.283

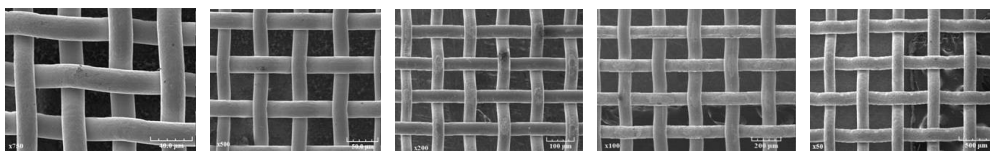


Figure 1 – SEM images of wire screens. From left to right: SS25, SS40, SS75, SS150 and SS355

An aerosol generator Palas<sup>®</sup> GFG-1000 and a condensation particle counter 3022A of TSI<sup>®</sup> are the main components of the setup. Spark-generated Cu-nanoparticles are size-selected between 4 and 30 nm thanks to a TSI<sup>®</sup> nano-DMA 3080. To avoid mistaken results, awareness of some metrological biases is needed:

- shift in diameter selection due to argon presence in generated aerosol
- different CNC counting modes depending on particle concentration

Figure 2 shows the penetration through the wire screens at a face velocity of 5 cm/s.

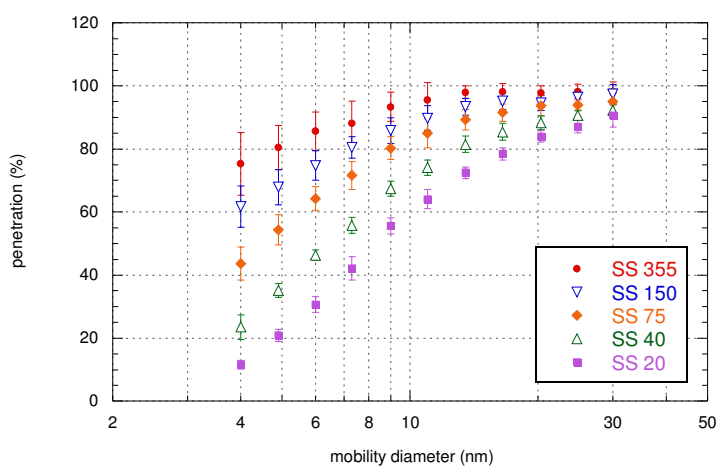


Figure 2 – Cu-nanoparticles penetration at 5 cm/s

Particle penetration continuously decreases down to 4 nm. This observation agrees with latest results obtained by Heim *et al.* and Kim *et al.*: they report no evidence of thermal rebound down to 2.5 and 3 nm respectively. The smaller the particle diameter is, the higher the screen efficiency. Likewise, the more compact the wire screen, the less the penetration.

## References

- Wang, H.-C. and Kasper, G., (1991) *Journal of Aerosol Science*, 22, 1, 31-41.
- Heim, M., Mullins, B.J., Wild, M., Meyer J. and Kasper, G., (2005), *Aerosol Science and Technology*, 39, 782-789
- Kim, S.C., Harrington, M.S. and Pui, D.Y.H., (2007) *Journal of Nanoparticle Research*, 9, 117-125

## Session T2-11b: Filtration – II

<b>Abstract Number</b>	<b>Paper Title &amp; Authors</b>	<b>Included</b>
285	Electrically enhanced ultrafiltration of enzyme solutions A D Enevoldsen, E Hansen, G Jonsson	Yes
589	Computation of optimal production intervals for an ultrafiltration plant processing surface water E Zondervan, B Blankert and B Roffel	Yes
1067	Evaluation of tubular ceramic ultrafiltration membranes for the recovery of vanillin from Kraft black liquor M Zabkova, E A B Silva, A E Rodrigues	Yes
2391	The fouling and cleaning of ultrafiltration membranes for black tea liquor clarification. P J Evans, M R Bird	Yes
2604	The effects of cross diffusion on the mass transport in the ultrafiltration of water/ lysozyme/ NaCl solutions V Magueijo, V Semiao, M N Pinho	Yes

Session T2-11b

## Electrically enhanced ultrafiltration of enzyme solutions

A.D. Enevoldsen,<sup>a,b</sup> E. Hansen,<sup>a</sup> G. Jonsson<sup>b</sup>

<sup>a</sup> Recovery Development, Novozymes A/S, Smørumsevej 9, 3AM, DK-2880 Bagsværd, Denmark.

<sup>b</sup> Department of Chemical Engineering, The Technical University of Denmark, DK-2800 Lyngby, Denmark

### 1. Summary

Electro-ultrafiltration (EUF) is an efficient method to reduce fouling and concentration polarization during filtration of enzyme solutions. Flux improvements in the range 3-7 times have been achieved during filtration of amylase solutions. The greatest improvement is gained at high concentrations. This makes EUF a useful method for filtering solutions with a high concentration, and applicable as a final concentration step during production. The conductivity of the solution must however be low to minimize the energy consumption of the electric field, since the energy requirements increases proportional to the conductivity.

Keywords: Crossflow filtration; Enzyme; Electrophoresis; Electrofiltration; Membrane fouling

### 2. Extended Abstract

Fouling and concentration polarization are well know problems in crossflow ultrafiltration of proteins. Usually a high crossflow velocity is needed to enhance the shear at the membrane surface and thereby reduce concentration polarization. Application of an external dc (direct current) electric force field across the membrane is a promising method to reduce fouling and concentration polarization. The electric field imposes an electrophoretic force on the charged proteins dragging them away from the membrane surface. The concentration polarization layer is thereby reduced and the flux increases. The solvent flow through the membrane might also be enhanced by the electroosmotic effect; but this effect is considered secondary.

In this work, crossflow electro-ultrafiltration (EUF) is carried out on industrial enzyme solutions from Novozymes A/S, Denmark. The aim is to investigate the use of EUF in industrial production.

The EUF cell is based on a commercial available electro dialysis module. It consists of a UF membrane (10 kDa ETNA membrane from Alpha Laval) placed between two cation-exchange membranes. The cation-exchange membranes are necessary in order to prevent direct contact between the electrodes and the enzyme solutions; and make a multi compartment module possible.

Figure 1 shows the effect of a constant dc electric field when filtering two different amylase solutions. The flux increases 2-3 times at an electric field strength around 1500 V/m. The greatest improvement is achieved for the amylase-F solution, which also has the highest electrophoretic mobility of the two enzymes.

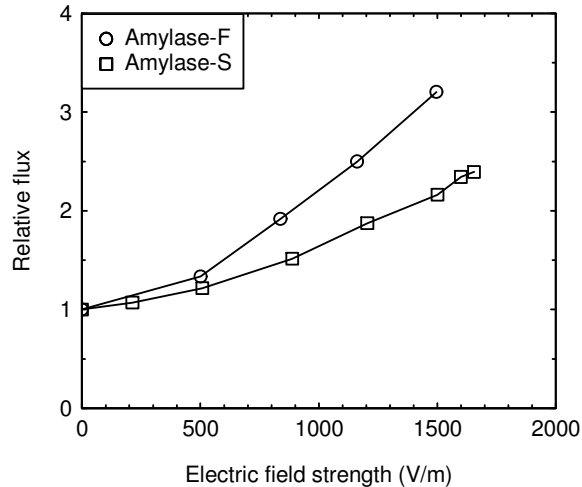


Figure 1: Relative flux improvement during filtration of two 12 g/L amylase solution at increasing electric field strength. Crossflow = 0.07 m/s and trans membrane pressure 1.5 bar.

The relative flux improvement increases at increasing enzyme concentration. The flux increases around 6-7 times at a concentration around 100 g/L. EUF will therefore be best as a final concentration step during production.

The effect of a pulsed electric field has also been tested, but showed no improvement compared to a constant electric field due to the build-up of the concentration polarization layer.

The effect of salt concentration, TMP and crossflow velocity has also been studied. An increased TMP and crossflow did not improve the flux appreciably -since the process is controlled by the strength of the electric field. Increasing the conductivity of the enzyme solution by adding  $\text{CaCl}_2$  did not change the flux, but the energy consumption increased.

The salt concentration in the enzyme solution is a key factor for the feasibility of the EUF process; since the energy requirements increases proportional to the conductivity of the enzyme solution. Calculations have shown that EUF is profitable when filtering solutions of high concentration, while conventional UF is profitable when filtering solutions of low concentration. However, if the conductivity becomes too high, the advantage of using EUF disappears.

## References

- H. Yukawa, K. Shimura, A. Suda and A. Maniwa, *Cross flow electroultrafiltration for colloidal solution of protein*, Journal of Chemical Engineering of Japan, **16** (1983) 305.
- T. Weigert, J. Altmann, S. Ripperger, *Crossflow electrofiltration in pilot scale*, Journal of Membrane Science, **159** (1999) 253.
- H.M. Huotari, G. Trägårdh and I.H. Huisman, *Crossflow membrane filtration enhanced by an external dc electric field: A review*, Trans IChemE, **77** (A) (1999) 461.



## **Computation of optimal production intervals for an ultra filtration plant processing surface water**

E. Zondervan, B. Blankert and B. Roffel

*Department of Chemical Engineering, University of Groningen, 9747AG Groningen, the Netherlands*

### **1. Summary**

In this paper a chemical cleaning sequence model is proposed that can be used to predict the fouling status of a membrane during multiple chemical cleaning cycles. The proposed model is used to minimize the overall operating costs - based on chemicals consumption, energy consumption and investment costs - over a fixed time horizon, guaranteeing production of a specified volume of permeate, where the numbers of cycles, the net production flux, the duration of a production phase and the duration of a subsequent cleaning phase are computed. The membrane fouling status should not exceed certain operating limits. Numerical results are presented, where optimal net production fluxes, operating- and cleaning intervals are calculated. It was found that at chemical cleaning cycle level, optimization of the cleaning variables do not strongly influence operational costs, however, optimization of the chemical cleaning cycle is useful as means of effective fouling control.

Keywords: Ultra filtration, modeling, cyclic behavior, multi-level-optimization.

### **2. Extended Abstract**

Ultra filtration (UF) is increasingly used as a surface water purification technique. UF membranes have a high selectivity, are easy to scale up and have become economically attractive during the last fifteen years. However, during filtration, UF membranes are subject to fouling, and frequent cleaning is required. In the short term, membrane fouling is removed from the membrane by means of backwashes, and in the long-term the membrane is treated with cleaning chemicals. Currently operating settings for UF membranes are based on rules of thumb and pilot plant studies. The settings are generally conservative and it is expected that operating costs can be significantly reduced by means of process optimization. The main objective of this paper is to investigate the influence of chemical cleaning on the total operational costs.

An UF process shows a cyclic behavior (switching between filtration, backwashing and chemical cleaning). The process takes place over different time horizons and optimization should subsequently be performed at different levels.

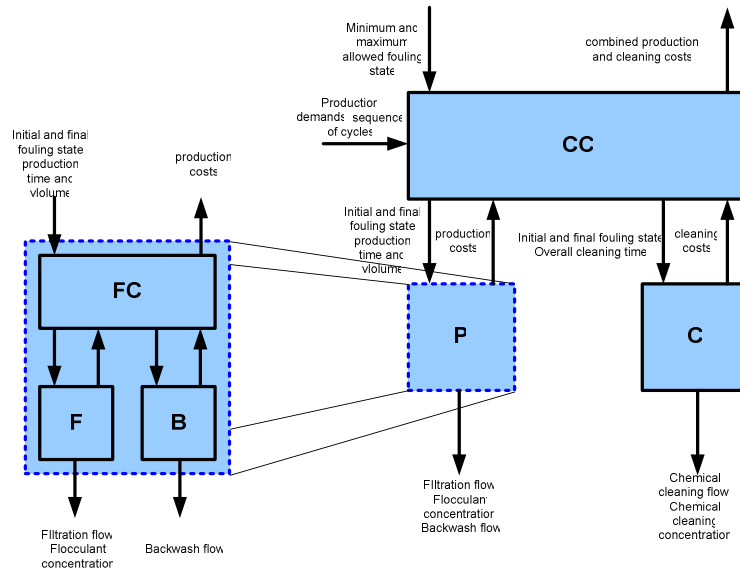


Fig. 1. Hierarchical representation of the ultra filtration process F: filtration phase, B: Backwash phase, FC: Filtration cycle (one filtration phase followed by one backwash phase), P: Production phase (a sequence of filtration cycles), C: a Chemical cleaning phase and CC: a chemical cleaning cycle (a sequence of filtrations followed by a chemical cleaning phase).

Multi-level (or hierarchical) optimization may be very useful if a process can be divided into several decision layers. In figure 1 the cyclic nature of an UF process as studied in this paper, is visualized.

After formulation of the process models, the objective function and the constraints a bi-level optimization problem is formulated, containing four continuous variables and two discrete variables. Optimal values for the optimization variables are subsequently calculated using a direct search method.

The results of the optimization show that chemical cleaning settings (cleaning time, cleaning agent volume and the number of chemical cleanings) do not significantly influence the operational costs, however, optimization of the chemical cleaning cycle is useful as means of effective fouling control.

## **Evaluation of tubular ceramic ultrafiltration membranes for the recovery of vanillin from Kraft black liquor**

M. Zabkova, E.A. Borges da Silva, A.E. Rodrigues

*Laboratory of Separation and Reaction Engineering – LSRE, Department of Chemical Engineering, Faculty of Engineering, University of Porto, Dr. Roberto Frias s/n, 4200-465, Porto, Portugal*

### **1. Summary**

The *Kraft* pulp liquor coming from paper industry is a waste which must be treated before disposal. On the other hand, organic compounds present in liquors, especially lignin, are very useful raw material from which many substances or materials can be produced (vanillin, vanillic acid, dispersing agents etc). The main purpose of lignin removal from the liquor is to separate the cooking chemicals, NaOH and Na<sub>2</sub>S to avoid losses of these chemicals from the mill. Fractionation of the cooking liquor from *Kraft* and sulphite pulps by ultrafiltration has been studied for thirty years. In most of the applications the objective of ultrafiltration process was to purify the lignin fraction in order to use it as a fuel or valuable product. In the process of *Kraft* lignin oxidation to produce vanillin the reaction media contains degraded molecules of lignin and sodium salt of vanillin (vanillate) and other species. The isolation of vanillate from the oxidized solution is an important stage in the vanillin production. During the ultrafiltration process vanillin goes to the permeate stream and the lignin as a macromolecule stays in the retentate. Therefore, the ultrafiltration technique can be used as a first step in the process of recovery of vanillin from *Kraft* lignin oxidation. The goal of this work is to evaluate the membrane ultrafiltration process focused on the recovery of vanillin from Kraft lignin oxidation media. For this purpose, ultrafiltration using tubular ceramic membranes with different molecular weight cut-off is investigated.

Keywords: vanillin; tubular ceramic membrane; ultrafiltration; *Kraft* black liquor.

### **2. Extended Abstract**

The experiments are carried out in the batch concentration mode, in which retentate is recirculated to the feed tank and permeate is withdrawn to a separated reservoir. This work assumes that the formation of a boundary layer takes place on the membrane surface and thus influences the separation process because it is responsible for significant flux decline. In Table 1, the highest value of lignin rejection is obtained

with the membrane 1 kDa cut-off. Membranes with small cut-off show significant decline of permeate flux comparing with the membranes with larger cut-off.

The influence of the lignin and vanillin concentration and pH of the mixture on the ultrafiltration process is studied. Results from literature<sup>1</sup> attest our experiment results using the membrane of 15 kDa cut-off when increasing pH of the solution leads to a decrease of lignin rejection, but they are in contradiction with those observed on the membrane of 1 kDa cut-off (although, for the 1 kDa cut-off membrane, different feed flow-rates have been used in ultrafiltration of the mixture at pH=8.5 and pH=12.5). This disagreement can be related to a change of governing mechanism of the association of lignin molecules, which is strongly dependent on the molecular weight and pH of filtrated macromolecular solution.<sup>2</sup>

The association of the molecules at high pH lead to particle size increase mostly due to polyelectrolyte swelling and dissociation of ionisable functional groups while when pH decreases the association is due to the formation of hydrogen bonds.<sup>2</sup> One can believe that at pH=12.5, the larger molecules provide many sites for association and it reduce small molecules in this UF operation using 1 kDa membrane, while using 15 kDa membrane even associated molecules can pass through the membrane to the permeate. On other hand, the association of molecules at lower pH can be predominant leading to the formation of bigger aggregates which are not allowed to pass through the membrane of 15 kDa cut-off.

Table 1: Experimental conditions (in gray)\* and measured values\* in ultrafiltration of the lignin/vanillin mixture using tubular ceramic membranes ( $Q_f$ , feed flowrate;  $C_f$ , feed concentration;  $VR$ , volume reduction;  $V_o$ , initial feed volume;  $R_{obs}$ , observed rejection;  $\eta$ , viscosity of solution;  $R_m$ , membrane hydraulic resistance).

$Q_f$ (L h <sup>-1</sup> )	$C_f$ (g L <sup>-1</sup> )		pH	$V_o$ (L)	VR	$R_{obs}$ (Lignin)	$\eta \times 10^{-3}$ (kg m <sup>-1</sup> s <sup>-1</sup> )	$R_m \times 10^{13}$ (m <sup>-1</sup> )
	Lignin	Vanillin						
<b>1 kDa cut-off</b>								
130	60	6	8.5	5	0.102	0.951	1.19	2.806
120	60	6	12.5	4	0.103	0.972	1.19	
<b>5 kDa cut-off</b>								
120	60	5	12.5	4	0.275	0.968	1.19	1.222
<b>15 kDa cut-off</b>								
109	5	0.5	8.5	5	0.500	0.916	0.887	0.2806
102	20	2	8.5		0.440	0.958	0.954	
102	20	2	12.5		0.440	0.873	0.954	
101	60	6	8.5		0.313	0.943	1.190	
101	60	6	12.5		0.340	0.865	1.190	

(\*) Transmembrane pressure:  $\Delta P$ (1 and 5 kDa cut-off)= 1.55 bar;  $\Delta P$ (15 kDa cut-off)= 1.30 bar.

(†)  $R_{obs}$  (Vanillin)  $\approx 0$  for all ultrafiltration run.

## References

1. D.F. Ross, T.B. Cartwright, M.R. Doshi, and H.S. Dugal, IPC technical paper series, 199 (1986).
2. W.G.Glasser, S. Sarkanen (Eds.), *Lignin Properties and Materials*, ACS Symp. Series 397, American Chemical Society, Washington, DC, 1989.

## **The fouling and cleaning of ultrafiltration membranes for black tea liquor clarification.**

P.J. Evans and M.R. Bird

*Department of Chemical Engineering, University of Bath, UK..*

### **1. Summary**

The presentation will briefly discuss black tea and the issues involved in the production of Ready To Drink (RTD) or iced tea. The use of ultrafiltration will be suggested as a potential method for clarification and thus increased stability of final product. Experimental results demonstrate that a range of different membrane materials and pore sizes were effective at producing a stable, clarified liquor at commercially viable fluxes. A thorough analysis of membrane surface properties and the mechanisms by which the membranes are fouled will also be discussed.

### **2. Extended Abstract**

A problem associated with the production of Ready To Drink (RTD) or iced tea is a phenomenon known as 'tea creaming', which gives the product a hazy or muddy appearance which can be detrimental to both appearance and taste. Membranes offer the possibility of producing a clarified liquor without the need for chemical addition or thermal processing, thus leading to a more natural product.

This paper reports experimental findings concerning the ultrafiltration of hot tea extract reconstituted from black tea powder. The filters studied were 10, 30 and 100kDa Fluoropolymer (FP) and Regenerated Cellulose (RC) ultrafiltration membranes. Colour, haze and stability of clarified permeate were analysed, and total solids determined. Theaflavin and caffeine content were measured using HPLC and total polyphenols measured using the Folin-Ciocalteu assay. Membranes were effective at producing a stable, clarified liquor at commercially viable fluxes.

An analysis of the changes in membrane surface properties through a complete fouling / cleaning cycle has been comprehensively studied. FTIR analysis was used to investigate tea species removal from RC and FP membranes due to NaOH cleaning. The importance of roughness, hydrophobicity and surface charge are discussed for each membrane type through the fouling / cleaning cycles.

The variation in adhesive forces between model functional groups and different membrane surfaces will also be reported.

Fouling flux decline curves were fitted using a modified Hermia analysis to provide a mechanistic description of the fouling occurring under various processing conditions. Fouling mechanisms were found to be dominated by cake filtration.

Book of Abstracts  
European Congress of Chemical Engineering (ECCE-6)  
Copenhagen, 16-20 September 2007

## **The effects of cross diffusion on the mass transport in the ultrafiltration of water/ lysozyme/ NaCl solutions**

V. Magueijo,<sup>a</sup> V. Semiao,<sup>b</sup> M. N. de Pinho<sup>a</sup>

<sup>a</sup> *Department of Chemical and Biological Engineering*

<sup>b</sup> *Department of Mechanical Engineering*

*Technical University of Lisbon, Instituto Superior Técnico, Av. Rovisco Pais 1, 1049-001 Lisbon, Portugal*

### **1. Summary**

This work addresses the ultrafiltration of water/ lysozyme/ NaCl solutions. In particular, it addresses the effects of cross diffusion on the concentration polarization of the solutes and on the membrane permeation rates. Modelling the UF of ternary systems, such as the studied aqueous solution containing a protein and a salt, requires an accurate description of the multicomponent nature of the mass transport, which can be accomplished through a sophisticated tool like Computer Fluid Dynamics (CFD). In UF, due to the concentration polarization phenomenon, the species being separated do not have uniform concentrations at the membrane vicinity, and therefore, the cross diffusion of the solutes may play an important role in the overall mass transport.

Ultrafiltration experiments with ternary aqueous solutions of lysozyme (0.3 kg m<sup>-3</sup>) and NaCl (ranging from 0 to 0.5 M) were carried out in a rectangular cell. The cell top wall is impermeable while the bottom wall supports a semi-permeable membrane. Three cellulose acetate membranes – M1, M2 and M3 – used in this work, were prepared in the laboratory using the phase inversion method and were characterized through the permeation of pure water and reference solutes. Membrane M3 has the largest hydraulic permeability, whereas membrane M1 has the smallest one.

Using CFD, the fluid flow and mass transport modelling allows the prediction of the concentration polarization and permeation fluxes. The predicted fluxes were compared with experimental ones and the results show that cross diffusion plays an important role in the overall mass transport. This importance, however, depends on the permeation and selectivity characteristics of the membrane.

**Keywords:** Protein ultrafiltration; Modelling; CFD; Multicomponent diffusion

## 2. Extended Abstract

### 2.1. Results

Using CFD, the model yields the prediction of the concentration polarization and permeation fluxes as a function of the transmembrane pressure,  $\Delta P$ , and at a wide range of salt concentrations,  $C_{S0}$ . Figure 1 exemplifies the trends verified in the three studied membranes: the results predicted from simulations incorporating cross-diffusion are in excellent agreement with the experimental ones. If cross diffusion is ignored, the simulations overestimate the permeation fluxes and the deviations between estimated and experimental values increase with the increase of the membrane hydraulic permeability.

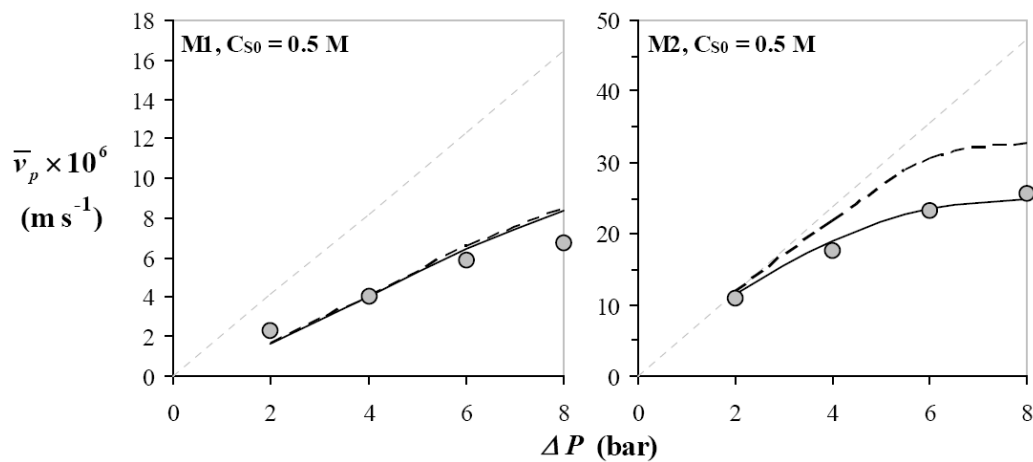


Figure 1: Permeation fluxes for the UF of lysozyme solutions with different membranes. Simulation results with cross diffusion (full black lines) and without cross diffusion (dashed black lines) are compared to the experimental values (dots). Note: the membranes used have high apparent rejection coefficients for lysozyme.

### 2.2. Conclusions

In membranes with high protein rejections, the importance of cross diffusion phenomenon to the overall mass transport increases with the membrane hydraulic permeability. For different feed salt concentrations and transmembrane pressures, the incorporation of the protein/salt cross diffusion in the model is mandatory as it leads to a much better agreement between calculated and experimental permeation fluxes.

## References

- Annunziata, O., Paduano, L., Pearlstein, A.J., Miller, D.G. and Albright, J.G., (2000) *Journal of the American Chemical Society*, 122, 5916-5928.
- Magueijo, V., Semião, V., de Pinho, M.N., (2005) *International Journal of Heat and Mass Transfer*, 48, 1716-1726.
- Magueijo, V., Semião, V. and de Pinho, M.N., (2006) *Journal of Membrane Science*, 286, 133-143.



## Session T2-11P: Filtration – Poster

Abstract Number	Paper Title & Authors	Included
593	A vibrating membrane bioreactor operated at supra- and sub-critical flux: Influence of EPS from yeast cells S P Beier, G Jonsson	Yes
735	Assessment of must concentration by nanofiltration membranes I Catarino, V Geraldés, M N Pinho	Yes
897	Modified polyethersulfone membranes for micellar enhanced ultrafiltration of chromium G Poźniak, R Poźniak	Yes
928	Effect of physicochemical conditions on crossflow microfiltration of mineral dispersions using ceramic membranes P Mikulášek, P Velikovská, J Horčíčková	Yes
1032	The role of ultrafiltration on sheep milk rennet clotting properties I Catarino, A P L Martins, E Duarte, M N Pinho	Yes
1103	Particle Fouling in Air-Sparged Cross-Flow Microfiltration K J Hwang, Y J Wu	Yes
1704	Ultrafiltration of hydrolysis products from xylan Eucalyptus wood M J G Muñoz, H Domínguez, J C Parajó	Yes
2141	Demonstration of "creep" during filtration K Keiding, M Hinge, M L Christensen	Yes
2147	Cake creep during filtration of flocculated manure M L Christensen, K Keiding	Yes

Session T2-11P

## **A vibrating membrane bioreactor operated at supra- and sub-critical flux: Influence of EPS from yeast cells**

Søren Prip Beier<sup>a</sup>, Gunnar Jonsson<sup>a</sup>

*<sup>a</sup>CAPEC/Department of Chemical Engineering, Technical University of Denmark, DK-2800 Kgs. Lyngby, Denmark*

### **1. Summary**

A vibrating microfiltration membrane bioreactor (MBR) has been tested at constant flux filtrations above (supra-critical) and below (sub-critical) an experimentally determined critical flux. The extent of fouling is reduced by vibrations and the critical flux seems to be a flux interval rather than a specific value. In filtration of yeast cell suspensions the influence of extracellular polymeric substances (EPS) is very dependent on whether the flux is above or below the critical level.

Keywords: Vibrating microfiltration, Membrane bioreactor, Critical flux, Yeast cell suspensions, Extracellular polymeric substances.

### **2. Extended Abstract**

Submerged suction pressure driven membrane units are of expanding interest. When connected to, or submerged into, a fermentation tank, waste water tank or another tank or reactor, from which water or eventually a solute has to be continually removed, such a set-up is called a membrane bioreactor (MBR). In contrast to more conventional membrane filtration systems, which are operated at constant pressure, MBR's are often operated at constant flux with a relatively low trans-membrane pressure (TMP).

The fouling problems in our microfiltration MBR are reduced by letting the membrane module vibrate. The system has already been tested in filtration of yeast cell suspensions [Beier et al., 2006] and in separation of an  $\alpha$ -amylase enzyme from yeast cells [Beier & Jonsson, 2007]. The system has the advantage of being able to operate at a very low feed flow velocity ( $< 1$  cm/s) and a very low TMP ( $< 100$  mbar) with critical fluxes from  $10 - 50$  L/(m<sup>2</sup>·h), depending on degree of vibration, for a module consisting of PES hollow fibers. The aim of this paper is to present data from constant flux experiments. The critical flux concept is discussed by comparison of constant flux filtrations above (supra-critical) and below (sub-critical) an

experimentally determined critical flux. Permeabilities, membrane resistances and fouling resistances are calculated from the constant flux experiments, which are depicted in figure 1.

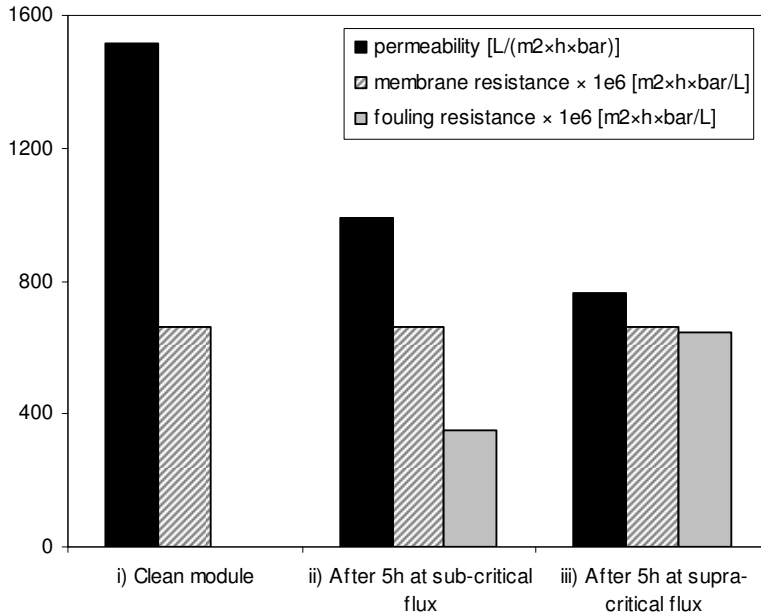


**Figure 1:** Permeability, membrane resistance and fouling resistance for i) clean module and after 5 h filtration of a 4 g/L yeast suspension with a vibration degree of 25 Hz and 0.7 mm amplitude at ii) sub-critical flux (14 L/(m<sup>2</sup>×h)) and at iii) supra-critical flux (30 L/(m<sup>2</sup>×h)).

At the conditions given in figure 1, a critical flux of 15 L/(m<sup>2</sup>×h) has been determined earlier [Beier et al., 2006]. The membrane resistance is, of course, constant, but the fouling resistance is twice as large after 5 hours at supra-critical flux compared to at sub-critical flux. Furthermore, the final permeability has decreased less after 5 hours at sub-critical flux compared to at supra-critical flux. However, since a fouling resistance and a drop in permeability is observed at sub-critical conditions, the critical flux seems to be a flux interval rather than a specific value.

The influence of EPS, which is diffusing or being washed out from the yeast cells, is also evaluated by comparing the permeability drop and fouling resistance obtained by flux increasing experiments done on a clean and a pre-fouled membrane module. EPS is being washed out from the yeast cells during filtration, but the extent of washing-out turns out to be very dependent on whether the flux is below or above the critical flux.

## References

Beier, S. P., Guerra, M., Garde, A., Jonsson, G., (2006), *Journal of Membrane Science*, 281, 281-287.

Beier, S. P., Jonsson, G., (2007) *Separation & Purification Technology*, 53, 111-118.

## Assessment of must concentration by nanofiltration membranes

I. Catarino,<sup>a</sup> V. Geraldes,<sup>a</sup> M. N. de Pinho<sup>a</sup>

*<sup>a</sup>Department of Chemical and Biological Engineering, Instituto Superior Técnico, Av. Rovisco Pais, 1 1049-001 Lisboa, Portugal*

### 1. Summary

This work addresses the investigation at lab scale of grape must concentration using nanofiltration (NF). Five NF membranes and one ultrafiltration (UF) membrane were tested which had molecular weight cut-offs (MWCO) between 100 to 1000 Da. A solution of grape must prepared through the dilution of rectified grape must (to a total sugar concentration of 120 g l<sup>-1</sup>) and a sample of grape must used in the production of “Vinho Verde” were tested. NF experiments were carried out in total recirculation mode in six flat-sheet cells of 13.2x10<sup>-4</sup> m<sup>2</sup> membrane surface area.

The NF membranes with MWCO between 100 to 300 Da displayed high rejections for sugars (range from 90% to 99%) while the rejections for organic acids varied from 68% to 99%, being the ones for malic acid smaller than the ones for tartaric acid.

Keywords: nanofiltration, grape must; organic acids

### 2. Extended Abstract

The enrichment of must prior to fermentation plays an important role in the wine production industry. The enrichment is performed by adding sugar-containing products, sucrose or grape musts (concentrated must and rectified concentrated must). Among the classical forms of producing concentrated must are evaporation and reverse osmosis (RO). Those processes enable to increase the sugar concentration, as well as all other components. Furthermore both techniques have high energy-consumption (Versari et al., 2003; Kiss et al., 2004; Ferrarini et al., 2001; Mietton-Peuchot et al., 2002).

NF technique appears to provide an alternative to the classical processes of concentrated must production.

The aim of this work was to investigate the potential of several NF membranes in must concentration and evaluated its potential for the partial removal of organic acids. NF/UF experiments were carried out in total recirculation mode in six flat-sheet cells of 13.2x10<sup>-4</sup> m<sup>2</sup> membrane surface area equipped with five commercial membranes supplied by Alfa Laval, Denmark (ETNA 0.1 PP and NFT 50) and Flimtec Corporation, USA (NF 90, NF 200 and NF 270) and one laboratory made (Kunst and Sourirajan, 1974) cellulose acetate membrane. The membrane characteristics are described in Table 1.

Membranes	CA27-87.5	NFT 50	NF 90	NF 200	NF 270	ETNA0.1PP
L <sub>p</sub> (Kg/h/m <sup>2</sup> /bar)	1,8	9,9	8,6	2,1	19,2	-
f <sub>NaCl</sub> (%)	91%	72%	97%	76%	46%	13%
f <sub>Na<sub>2</sub>SO<sub>4</sub></sub> (%)	99%	100%	100%	99%	99%	67%
f <sub>MgSO<sub>4</sub></sub> (%)	98%	100%	100%	99%	99%	51%
f <sub>fructose</sub> (%)	100%	97%	100%	96%	82%	17%
f <sub>glucose</sub> (%)	100%	96%	100%	97%	76%	16%
f <sub>tartaric acid</sub> (%)	94%	52%	100%	72%	35%	14%
f <sub>malic acid</sub> (%)	81%	42%	100%	54%	25%	10%

Table 1: Membrane characterization. L<sub>p</sub>; hydraulic permeability, f<sub>NaCl</sub>; rejection coefficient to NaCl, f<sub>Na<sub>2</sub>SO<sub>4</sub></sub>; rejection coefficient to Na<sub>2</sub>SO<sub>4</sub>, f<sub>MgSO<sub>4</sub></sub>; rejection coefficient to MgSO<sub>4</sub>, f<sub>fructose</sub>; rejection coefficient to fructose, f<sub>glucose</sub>; rejection coefficient to glucose, f<sub>tartaric acid</sub>; rejection coefficient to tartaric acid, f<sub>malic acid</sub>; rejection coefficient to malic acid.

The permeation of reference solutions, for membrane characterisation, as well as permeation of grape must solutions were performed at feed recirculation flow rate of 130 L h<sup>-1</sup> and a transmembrane pressure of 30 bar.

For the must solution prepared through the dilution of rectified grape must (no acid content), the rejection coefficients observed for the glucose and fructose presented the same values for a given membrane and are always higher than 90 % for NF membranes. The UF membrane (ETNA 0.1 PP) had low sugar rejection coefficients.

The presence of organic acids, grape must used in the production of “Vinho Verde”, induced an increase in the sugar rejection coefficients, which was specially enhanced for the UF membrane. NF membranes presented high acids rejection coefficients, being the ones for malic acid smaller than the ones for tartaric acid. Nevertheless a rejection gap between acids and sugars was observed for membrane NF 270. This rejection gap can be enhanced by varying other parameters that might lead to an effective fractionation of sugars from organic acids.

The effect of each organic acid in the sugars rejection coefficients and of the feed concentration is investigated in work under development

## References

Versari A., Ferrarini R., Parpinello G., P. and Galassi S., (2003) Concentration of grape must by nanofiltration membranes, *Trans IChemE*, 81, Part C, 275.

Kiss I., Vatai Gy. and Bekassy-Molnar E., (2004) Must concentrate using membrane technology, *Desalination*, 162, 295.

Ferrarini R., Versari A. and Galassi S., (2001) A preliminary comparison between nanofiltration and reverse osmosis membranes for grape juice treatment, *Journal of Food Engineering*, 50, 113.

Mietton-Peuchot M., Milisic V. and Noilet P., (2002) Grape must concentration by using reverse osmosis. Comparison with chaptalization, *Desalination*, 148, 125.

Kunst B. and Sourirajan S., (1974) An approach to the development of cellulose acetate ultrafiltration membranes, *Journal of Applied Polymeric Science*, 18, 3423.

## **Modified polyethersulfone membranes for micellar enhanced ultrafiltration of chromium**

G. Poźniak,<sup>a</sup> R. Poźniak,<sup>a</sup>

<sup>a</sup>*Department of Chemistry, Wrocław University of Technology, 50-370 Wrocław, Poland*

### **1. Summary**

Separation properties of ultrafiltration membranes made from polyethersulfone, sulfonated and aminated polyethersulfone have been characterized and their suitability for chromium (III) and (VI) ions removal from aqueous media by means of solubilized hexadecylpyridine chloride and sodium dodecyl sulfate has been evaluated.

Keywords: sulfonated polyethersulfone, aminated polyethersulfone, environmental protection, membrane separation

### **2. Extended Abstract**

The increasing contamination of water by toxic heavy metals, such as chromium, is a serious environmental problem. Chromium exists in nature mostly in two valence states: hexavalent and trivalent chromium. In past years the metal finishing industry has shown an increase in the use of trivalent chromium electroplating baths to replace hexavalent chromium ones due to its lesser toxicity. Although the effluents generated in these processes are less toxic than the hexavalent chromium ones, they are still highly dangerous to the environment and must be treated prior to disposal [1].

Membrane separation processes play today an important role in the field of wastewater purification and reuse. This well consolidated technology is very interesting because of low operative costs, conceptual simplicity, modularity, optimal quality of treated water, and being more ecological than conventional separation techniques [2]. The micellar enhanced ultrafiltration (MEUF) has been shown to be a promising method for removal of low levels of toxic heavy metal ions from industrial effluents. In MEUF an anionic surfactant at a concentration higher than the critical micelle concentration (cmc) is added to the aqueous stream containing the dissolved solutes. The negatively charged micelles cause the cations to bind or adsorb at the micelle interface. Micelles containing absorbed ions are then separated by UF using membrane of suitable porosity, capable of retaining micelles [3].

Thermo-resistant polymers of good mechanical strength, biological and chemical stability and film-forming properties are the most frequently used materials for membrane preparation. Among them polyethersulfone (PES) is a popular one in last time. However, it has hydrophobic character that facilitates adsorption of many substances during filtration processes. Deposition of solute on/in membrane causes the negative effect – a significant drop of the permeate flux. This harmful phenomenon is called membrane fouling. There are many ways to protect membrane from fouling. One of them is introduction of ionic groups to the membrane materials by chemical or plasma treatment. Porous ion exchange membranes prove to be very useful in ultrafiltration of charge-bearing solutes. The improvement in solute rejection and decrease in the membrane fouling ability are the main profits coming from the use of such membranes [4-6].

Transport properties of membrane made from polyethersulfone (PES), aminated (APES) and sulfonated polyethersulfone (SPES) in micellar enhanced ultrafiltration of chromium (VI) and chromium(III) in presence of hexadecylpyridine chloride (CPC) and sodium dodecyl sulfate (SDS) micelles, respectively, were characterized. It was found that separation of investigated metal ions by MEUF depends on the kind of membrane and concentration of surfactant. At concentration of surfactants equal to 5 x cmc the best results for separation of Cr(III) through SPES membrane and Cr(VI) through APES membrane were obtained. Additionally, the effect of ligand (ethylenediaminetetraacetic acid (EDTA) added to a receiving solution) on Cr(III) ions transport through SPES membrane was studied. The ligand forms a complex with the target ion of interest and becomes incorporated in the micelles. In ligand-modified micellar enhanced ultrafiltration (LM-MEUF), the best rejection of Cr(III) at concentration of CPC equal to 1 x cmc was obtained. In comparison with unmodified PES, aminated and sulfonated membranes show a significant improvement of performance in micellar enhanced ultrafiltration of chromium.

#### **Acknowledgement:**

*This work was supported by the Polish Committee for Scientific Research grant 3 T09B 047 28.*

#### **References**

1. Bagchi, D., Stohs, S. J., Downs, B. W., Bagchi, M. and Preuss, H. G., (2002) *Toxicology*, 180, 5-22.
2. Mulder, M., *Basic principles of membrane technology*, Kluwer Academy Pub., Dordrecht, Holland (1991).
3. Sadaoui, Z., Azoug, C., Charbit, G. and Charbit, F., (1998) *Journal Environmental Engineering ASCE*, 124, 695-700.
4. Poźniak, G., Bryjak, M. and Trochimczuk, W., (1995) *Angewandte Makromolekulare Chemie*, 233, 23-31.
5. Bryjak, M., Poźniak, G., Gancarz, I. and Tylus W., (2004) *Desalination*, 163, 231-238.
6. Poźniak, G., Gancarz, I. and Tylus, W., (2006) *Desalination*, 198, 215-224.



## **Effect of physicochemical conditions on crossflow microfiltration of mineral dispersions using ceramic membranes**

P. Mikulášek, P. Velikovská, J. Horčíčková

*Department of Chemical Engineering, Faculty of Chemical Technology, University of Pardubice, CZ-532 10 Pardubice, Czech Republic*

### **1. Summary**

The characteristic permeate flux-time behaviour and effects of operating variables on flux data have been presented for aqueous titanium dioxide dispersions that were crossflow microfiltered in a ceramic membrane tube. The influence of a coagulant type, the dispersion pH, and ionic strength on the process performance was analyzed. The flux-time curve, and the steady state permeate flux, are functions of all the operating variables studied, i.e. inlet crossflow velocity of bulk dispersion, bulk solids volume fraction and transmembrane pressure difference. Predicted fluxes show a notable correspondence with experimentally measured values. The model thus gives a basis for estimating the optimal parameters for the design of crossflow microfiltration systems operating on concentrated dispersions.

Keywords: microfiltration, pH, ionic strength, coagulation, membrane fouling

### **2. Extended Abstract**

Crossflow microfiltration experiments were performed on aqueous dispersions of titanium dioxide through a 0.1  $\mu\text{m}$  pore size ceramic membrane at various operating parameters. The influence of a coagulant type, the dispersion pH, and ionic strength on the process performance was analyzed. The initial transient flux decline follows dead-end filtration theory, with the membrane resistance determined from the initial flux and the cake resistance determined from the rate of flux decline due to cake build-up. For long times, the observed fluxes reach steady or nearly steady state values, presumably as a result of the cake growth being arrested by the shear exerted at its surface. The steady state fluxes increase with increasing inlet crossflow velocity and decreasing feed concentration.

The extreme sensitivity with the nature of the coagulant and dispersions pH was observed, whereby the dispersion particle size can be changed by as much as an order of magnitude with pH variation at constant volume fraction.

The steady state permeate flux values were determined from the steady state model based on the Kozeny-Carman equation for cake resistance and Darcy's law applied over the filter area to relate filtration rate to average pressure difference between the feed and permeate sides of the filter. The model includes a cake resistance of the cake layer, which was determined for the titanium dioxide dispersions by fitting the experimental flux data to the model.

The results of the experiments show that during the ceramic membrane microfiltration of  $\text{TiO}_2$  dispersion the value of steady state permeate flux was significantly affected by the presence of coagulant. The comparison of the two types of coagulant is shown in Fig. 1. From this figure is evident that aluminium sulphate is better coagulant for titanium dioxide dispersion. The results of the experiments show that the pre-treatment of the feed by aluminium sulphate led to four or five times higher permeate flux than that without any pre-treatment and more than two times higher permeate flux than with pre-treatment by the PRAESTOL 511 K.

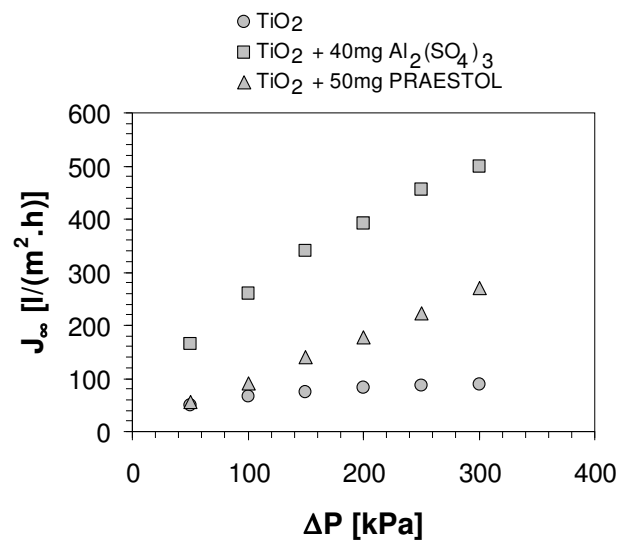


Figure 1: The comparisons of the effects of optimal doses of coagulants on permeate flux

The resulting fluxes obtained from the model using simple values for the membrane resistance, cake resistance, and physicochemical parameters for each data set are in good agreement with the measured fluxes.

#### Acknowledgements

This work was financially supported by the Ministry of Education, Youth and Sports of the Czech Republic, Project MSM0021627502.

#### References

- Mikulášek, P., Wakeman, R.J. and Marchant, J.Q., (1998) *Chemical Engineering Journal*, 69, 53-61.  
 Mikulášek, P., Doleček, P., Šmídová, D., Pospíšil, P., (2004) *Desalination*, 163, 333-343.  
 Velikovská, P., Mikulášek, P., (2006) *Desalination*, 200, 292-293.

## **The role of ultrafiltration on sheep milk rennet clotting properties**

I. Catarino<sup>a</sup>, A. P. L. Martins<sup>b</sup>, E. Duarte<sup>c</sup>, M. N. de Pinho<sup>a</sup>

<sup>a</sup>*Instituto Superior Técnico, Av. Rovisco Pais, 1 1049-001 Lisboa, Portugal*

<sup>b</sup>*Estação Agronómica Nacional, DTPA. Instituto Superior de Agronomia, Tapada da Ajuda, 1349-017 Lisboa Portugal*

<sup>c</sup>*Instituto Superior de Agronomia, Tapada da Ajuda, 1349-017 Lisboa Portugal*

### **1. Summary**

This work addresses the investigation of sheep milk ultrafiltration (UF) and its effect on the rennet clotting properties (RCP), namely rennet clotting time (RCT), rate of curd firming ( $k_{20}$ ) and curd firmness. UF experiments were carried out in concentration mode by varying the concentration factors from 1.2 to 2.0.

Significant increased on curd firmness was detected with increasing protein concentration, whereas a decreased on the curd firming rate was observed. The behavior of curd firmness and curd firming rate with the protein concentration was linear and correlations were established.

Skimmed milk concentrated by ultrafiltration leads to the improvement of RCP evaluated by the firmness parameters.

Keywords: ultrafiltration, sheep milk, renneting properties

### **2. Extended Abstract**

In the cheese-making process, ultrafiltration (UF) is use to concentrate the milk proteins. Rennet clotting properties (RCP) are extremely depended on the concentration factor and therefore is critical a systematic study of the ultrafiltration's influence.

Portuguese cheeses made from sheep milk have peculiar characteristics, since milk composition variability, like protein content, can influence the coagulation and curd formation, determinant for the cheese characteristics, is of extreme importance to determine the effect of these parameters in the cheese making process.

Although several studies have been done with cow's milk (Kosikowski, 1986; Lelievre et al, 1988; Hinrichs, 2001), the results shouldn't be extrapolated for sheep milk, given the differences in milk composition (Espinoza and Calvo, 1998), namely the calciumphosphate equilibrium and the micelle's characteristics (Remeuf and Raynal 2001).

In this work the influence of sheep milk ultrafiltration on the rennet clotting properties was investigated. UF experiments were carried out in concentration mode by varying the concentration factors from 1.2 to 2.0 that represented protein contents ranging from 4.8% to 10.6%. The UF unit (laboratory unit P28 from Celfa) with

$25.5 \times 10^{-4} \text{ cm}^2$  of membrane surface area was equipped with a laboratory made (Kunst and Sourirajan, 1974) cellulose acetate membrane. The membrane characteristics are described in Table 1.

$L_p$ (kg/(h.m <sup>2</sup> .bar))	22.4
MWCO (Da)	7000
$f_{\text{NaCl}}$ (%)	3
$f_{\text{CaCl}_2}$ (%)	3
$f_{\text{lactose}}$ (%)	10

Table 1: Membrane characterization.  $L_p$ ; hydraulic permeability, MWCO; molecular weight cut-off,  $f_{\text{NaCl}}$ ; rejection coefficient to NaCl,  $f_{\text{CaCl}_2}$ ; rejection coefficient to CaCl<sub>2</sub>,  $f_{\text{lactose}}$ ; rejection coefficient to lactose.

Half a liter of milk was heated at 32 °C and pumped through the membrane module while the transmembrane pressure was kept at 3.0 bar. The permeate volume was monitored continuously to determine the reduction in milk volume and to establish the permeate flux evolution with time. At determined volume concentration factor, VCF, samples of permeate and concentrate were collected.

The milk behavior was monitored by Optigraph ® (Ysebaert Dairy Division, Frepillon, France) after the intensity of the emitted signal was set to 7 volts. All tests were run for 60 min. Three parameters were analysed, namely: rennet clotting time (RCT), rate of curd firming ( $k_{20}$ ) and curd firmness.

Rennet clotting time increased when milk concentration by UF had occurred, besides protein concentration, salts concentration had a major effect on the rennet clotting time. The increase of milk protein content influences the curd firmness and the rate of curd firming. When considering curd firmness, a significant increase was observed with the increase of protein concentration, whereas the rate of curd firmness decreased considerably. The results show the existence of linear correlations between these two rennet clotting properties and the protein concentration.

## References

- Espinoza, N. A. and Calvo, M. M. (1998), Effect of heat treatment and ultrafiltration process of cow's, ewe's or goat's milk on its coagulation properties, *Journal of Agriculture and Food Chemistry*, 46, 1547-1551.
- Hinrichs, J. (2001), Incorporation of whey proteins in cheese, *International Dairy Journal*, 11, 495-503.
- Kosikowski, F. (1986), New Cheese-Making Procedures Utilizing Ultrafiltration, *Food Technology*, June, 71-77.
- Kunst, B., and Sourirajan, S. (1974), Approach to development of cellulose acetate polymeric membranes, *Journal of Applied Polymer Science*, 18, 3423.
- Lelievre, J., and Lawrence, R.C., (1988), Manufacture of cheese from milk concentrated by Ultrafiltration – Review Article, *Journal of Dairy Research*, 55, 565-478.
- Remeuf, F. and Raynal K. (2001), Effets de différents traitements de correction sur les aptitudes à la coagulation des laits de chèvre, de brebis et de vache chauffés, *Lait*, 81, 381-399.

## Particle Fouling in Air-Sparged Cross-Flow Microfiltration

Kuo-Jen Hwang, Ya-Ju Wu

*Department of Chemical and Materials Engineering, Tamkang University,  
Tamsui, Taipei Hsien 25137, Taiwan*

### 1. Summary

The particle fouling in air-sparged cross-flow microfiltration is studied on a microscopic viewpoint. Since the injection of air bubbles increases the shear stress acting on the membrane surface and decreases the deposition probability of solid particles, this is an efficient method to enhance the flux in cross-flow microfiltration. The filtration flux and cake properties under various operating conditions, such as cross-flow velocity, filtration pressure, particle size distribution, bubble size and sparging intensity are analyzed based on hydrodynamics. The results indicate that the filtration flux can be markedly enhanced by increasing air-sparging velocity due to the reduction of particle fouling. Furthermore, the filtration flux increases with both increasing cross-flow velocity and filtration pressure. These trends can be reasonably explained by the variations of cake properties under various conditions. A relationship among filtration flux, shear stress and overall filtration resistance is also derived based on the force balance model; the resulting equation can be verified by experimental data.

Keywords: cross-flow microfiltration, particle fouling, membrane separation, air-sparging, cake properties

### 2. Materials and Methods

Spherical particles made of polymethyl methacrylate (PMMA) were dispersed in a de-ionized water to prepare the suspension used in experiments. The mean diameter and the density of the particles were  $0.4\ \mu\text{m}$  and  $1219\ \text{kg/m}^3$ , respectively. The temperature of the suspension was kept at  $20^\circ\text{C}$  during filtration. The cellulose ester-membrane with a mean pore size of  $0.22\ \mu\text{m}$  was used as a filter medium.

A two-parallel-plate type microfilter with a clearance of  $1.0 \times 10^{-3}\ \text{m}$  was used in experiments. The cross-flow microfiltration was carried under constant pressure. The relationship between received filtrate volume and filtration time was recorded during

the filtration. When the experiment was terminated, the cake formed on the filter membrane was sent to analyze its wet and dry mass or proceeded SEM analysis.

### 3. Results and Discussion

Figure 1 shows the effects of air-sparging velocity on the cake mass and the pseudo-steady flux. The cross-flow liquid velocity and filtration pressure are kept at 0.1 m/s and 20 kPa, respectively. A sparged air can significantly reduce the particle fouling due to increasing the shear stress acting on the membrane surface, i.e., the cake mass decreases with the increase of air-sparging velocity. This indicates that sparging air is an efficient way to reduce the cake formation. It can be found that the cake mass under  $u_g=0.12$  m/s is only 1/3 of that under no air-sparging. This phenomenon can reasonably explain why the filtration flux can be enhanced by the sparging air, which is also shown in Fig.1. The filtration flux increases two-fold as air-sparging velocity increases from 0 to 0.12 m/s.

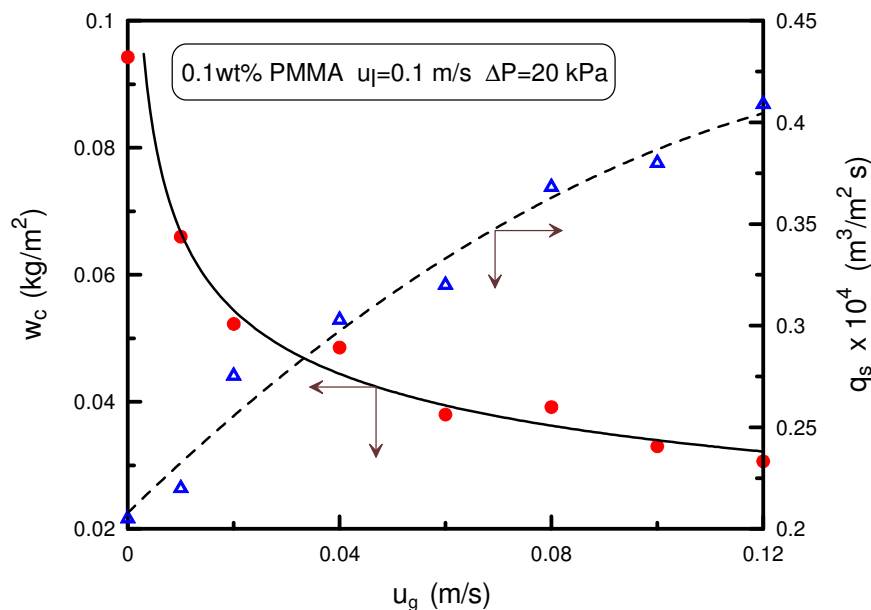


Fig.1 Effects of air-sparging velocity on the cake mass and filtration flux.

### 4. Acknowledgements

The authors wish to express their sincere gratitude to the National Science Council of the Republic of China for its financial support.

## **Ultrafiltration of hydrolysis products from xylan *Eucalyptus* wood**

M.J. González-Muñoz, H. Domínguez, J.C. Parajó

*Department of Chemical Engineering, University of Vigo (Campus Ourense). As Lagoas. 32004 Ourense. Spain.*

### **1. Summary**

The aim of this work was the purification of xylooligosaccharides (XOS) from *Eucalyptus globulus* wood autohydrolysis liquors using ultrafiltration membranes. Tubular ceramic membranes with cut-offs in the range 1 to 50 kDa were used to process autohydrolysis liquors to obtain concentrates containing XO of increased purity, owing to the preferential removal of both monosaccharides and non-saccharide compounds in permeates.

Keywords: *Eucalyptus globulus* wood, xylooligosaccharides, membranes, purification

### **2. Extended Abstract**

#### **2.1. Introduction**

Xylooligosaccharides can be used as ingredients for functional food due to its prebiotic effect. When ingested in diet, XOS behave as non-digestible oligosaccharides, reaching the gut, where they favour the proliferation of healthy microorganisms as *Bifidobacteria* and facilitate the reduction of entero-putrefactive and pathogenic intestinal bacteria by increasing the production of short chain fatty acids.

#### **2.2. Autohydrolysis processing of rice husks**

*Eucalyptus globulus* wood samples were milled to a particle size lower than 8 mm and mixed with distilled water at a water to dry solid ratio of 8 kg/kg. The mixture was heated in a stirred pressurized reactor until reaching 196 °C, the optimum temperature to produce XOS (Garrote, 2002). At the end of treatments, the solids were separated by filtration and the liquors were recovered, analyzed and processed with membranes. Table 1 shows the composition of the autohydrolysis liquors obtained with *Eucalyptus globulus* wood under the conditions employed in this study.

#### **2.3. Membrane processing of liquors**

Experiments at full recirculation mode were carried out with autohydrolysis liquors to determine the optimum conditions for concentration and purification. The assays were

performed measuring the time dependence of permeability at the considered transmembrane pressure (TMP) , and increasing the TMP once stable flow was achieved.

Additional experiments were run in concentration mode (removing the permeate) at the optimum TMP determined previously.

Table 1. Composition of *Eucalyptus wood* autohydrolysis liquors obtained at 196 °C.

a) Mass fraction of non volatile compounds (NVC) (kg NVC/kg liquor) = 0.02731; Composition of NVC:

Component	Mass fraction (kg/kg NVC)
Glucose	0.02410
Xylose	0.16982
Arabinose	0.03015
Acetic acid	0.03619
Glucooligosaccharides (GOS)	0.02733
Xylooligosaccharides (XOS)	0.48696
Acetyl groups linked to oligosaccharides	0.07338
Uronic acids	0.05810
ONVC <sup>1</sup>	0.13017

<sup>1</sup>ONVC: Other non-volatile compounds.

Figure 1 shows the retention of the different components of the autohydrolysis liquor at different TMP in experiments performed with a membrane of 5 kDa cut-off. In this case, near the 80 % of XOS contained in feed were present in the retentate, in comparison with 20 % of the initial monosaccharides.

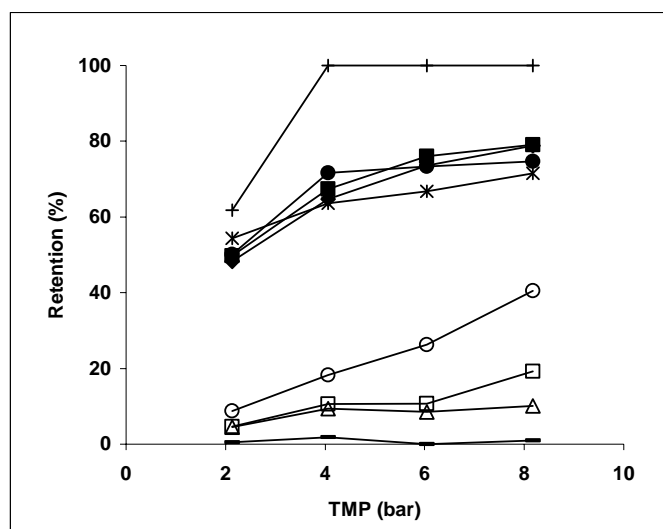


Figure 1. Retention of the different components of the autohydrolysis liquors using a 5 kDa ceramic membrane. (○) glucose; (□)xylose; (△)arabinose; (-) acetic acid; (●) GOS; (■) XOS; (◆)acetyl groups linked to oligosaccharides; (\*) uronic acids; (+) ONVC.

## References

Garrote, G., Parajó, J.C., (2002) Non-isothermal autohydrolysis of *Eucalyptus* wood, *Wood Science and Technology*, 36, 111–123.



## Demonstration of "creep" during filtration

K. Keiding, M. Hinge, M. L. Christensen,

*Department of Biotechnology, Chemistry, and Environmental Engineering, Aalborg University, DK-9000 Aalborg, Denmark*

### 1. Summary

A model for filtration of soft materials e.g. activated sludge has been developed. This model takes into account that creep may occur during the filtration stage. This effect of creep during filtration is demonstrated and discussed with respect to blinding and scaling.

Keywords: Creep, Filtration, Modelling, Sludge, Soft materials

### 2. Extended Abstract

The classical filtration theory assumes a unique relationship between the local filter cake porosity and the local effective pressure. For a number of compressible materials, it has however been observed that during the consolidation stage this may not be the case. It has been found that the production of filtrate also depends on the characteristic time for the filter cake solids to deform.

This is formulated in the Terzaghi-Voigt model in which a secondary consolidation is introduced. The secondary consolidation may be visualized by plots of the relative cake deformation ( $U$ ) v.s. the square root of time ( $t^{1/2}$ ). Even more clearly it is demonstrated by plotting the liquid pressure at the cake piston interface ( $p_L$ ) v.s.  $t^{1/2}$  (Fig. 1). The phenomenon of a secondary consolidation processes is in short called creep.

Provided that the secondary consolidation rate is of the same magnitude as the primary consolidation (defined by the hydraulic retardation), the creep phenomenon may occur during filtration. This will lead to Ruth's plot characterized by a concave curve (Fig. 2). This has been observed and modelled for dewatering experiment activated sludge (Christensen and Keiding 2007).

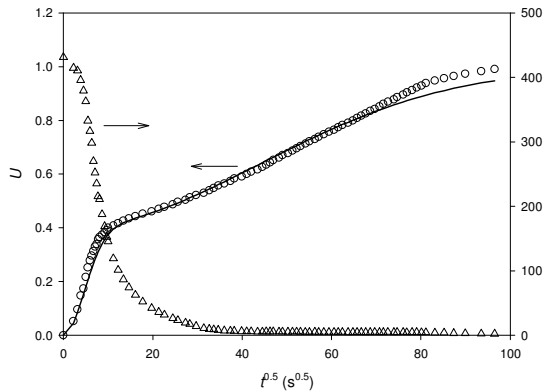


Figure 1: Consolidation of soft particle

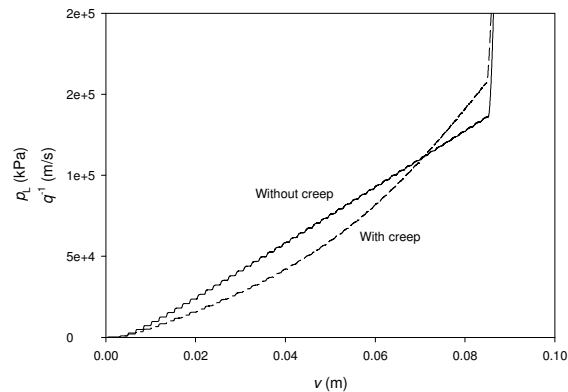


Figure 2: Simulation of filtration

The creep phenomenon has been adopted in the conventional filtration models by introducing an excess pressure ( $p_{\text{excess}}$ ).

$$\frac{dp_{\text{excess}}}{dt} = k \frac{dp_s}{dt} - \frac{p_{\text{excess}}}{\tau}$$

$p_{\text{excess}}$  has been inserted in the constitutive equations for calculating the local cake porosity ( $\epsilon$ ) and local resistance ( $\alpha$ ):

$$\left( \frac{1 - \epsilon}{1 - \epsilon_0} \right)^{1/\beta} = \left( \frac{\alpha}{\alpha_0} \right)^{1/n} = 1 + \frac{p_s - p_{\text{excess}}}{p_a}$$

Such a model can be used to study the creep phenomenon during filtration. It will be argued that although a strong resemblance between blinding and creep exists, these two effects may readily be distinguished by virtue of their dependency of the solid content. Finally a comment on the problem of the scaling of soft materials will be given, in which it will be suggested that the scaling problems may well be related to the existence of creep.

## References

Christensen ML, Keiding K (2007). Filtration Model for Suspensions that Form Filter Cakes with Creep Behaviour. *AIChE J.* 53: 598-609.

## **Cake creep during filtration of flocculated manure**

M. L. Christensen, K. Keiding

*Department of Biotechnology, Chemistry, and Environmental Engineering, Aalborg University, DK-9000 Aalborg, Denmark*

### **1. Summary**

It is shown how the filtrate volume for filtrations of flocculated manure can be simulated by adopting cake creep in one of the conventional filtration models.

Keywords: Creep, Manure, Phosphorus, Solid-Liquid separation

### **2. Extended Abstract**

Animal production is becoming increasingly concentrated on large farms. Large amounts of manure are produced of which the N:P ratio often differs from the crop requirements. A possible solution is to separate manure into a P-rich solid fraction and a liquid fraction, which would improve the distribution of N and P on the fields. Filtration is a useful method for such a separation. Furthermore, chemicals can be added to flocculate the solids and thereby increase the filterability i.e. the specific filter-cake resistance can be reduced from  $10^{15}$  m/kg to  $10^{11}$  m/kg. Both the amount of added chemicals, and the mixing procedure affect the result, and lab-scale experiments are often used to study how these pre-treatments influence the filtration process. However, the existing mathematical filtration models are based on filtration of inorganic particles and cannot simulate the filtration data obtained when manure is filtered. Hence, it is not possible to scale up the experiments, and it is therefore difficult to optimize the flocculation and estimate the needed filter media area. Similar problems have been observed when sewage sludge and synthetic core-shell colloids are filtered, and it has been suggested that the discrepancy between the filtration theory and the observed filtration behaviour is due to a time-dependent collapse of the formed cake (creep). This can also explain the observed behaviour when flocculated manure is filtered. The filtration data can be simulated if cake creep is adopted in the filtration model. The calculation shows that the specific filter-cake resistance increases by a factor of 3 during the filtration. Thus, the impact of cake creep is significant when organic materials such as manure are filtered.

Book of Abstracts  
European Congress of Chemical Engineering (ECCE-6)  
Copenhagen, 16-20 September 2007

## Session T2-12a: Polymer Science & Engineering – I

<b>Abstract Number</b>	<b>Paper Title &amp; Authors</b>	<b>Included</b>
1620	A Study of SEC Chromatograms on the Basis of Polymer Structure Properties Y Wang, O Hassager	Yes
1691	Preparation and Characterization of Organic/Inorganic Polymer Nanocomposites G Schmidt-Naake	Yes
1787	Synthesis and kinetics study of UV curable epoxy acrylate resi M Ebrahimi, P Kardar, S Bastani	Yes
2474	On the gas penetration in periodically constricted circular tubes filled with viscoelastic liquids Y Dimakopoulos, J Tsamopoulos	Yes

Session T2-12a

## A Study of SEC Chromatograms on the Basis of Polymer Structure Properties

Yanwei Wang, Ole Hassager

*Department of Chemical Engineering, Technical University of Denmark, DK-2800 City, Denmark*

### 1. Summary

In Size Exclusion Chromatography (SEC) measurements polymer molecules are fractionated by their sizes, but what size to use has been a matter of debate for many decades. In this study we define a new characteristic size, which correlates to the equilibrium partitioning of macromolecules in confining geometries, and use it to predict calibration curves for nonlinear polymers based on that determined experimentally for linear polymers. The experimental data obtained by Sun et al. [1] are used to demonstrate quality of the prediction by this approach.

Keywords: Size Exclusion Chromatography, universal calibration, calibration curve, equilibrium partition

### 2. Extended Abstract

We adopt a simple model of a polymer molecule:  $N$  point beads are connected by bonds of length  $b$  to form a desired chain architecture defined by a connection matrix  $Z$ . We assume that polymer molecules are fractionated in SEC by a single size  $R_c$ , and therefore a nonlinear polymer defined by  $(N, b, Z)$  will stay in the same retention volume as a linear polymer defined by  $(N_0, b, Z_0)$  of the same  $R_c$ . We define a branching parameter  $g$  as

$$g = \frac{R_c^2(N, b, Z)}{R_c^2(N, b, Z_0)} = \frac{R_c^2(N_0, b, Z_0)}{R_c^2(N, b, Z_0)} = \left( \frac{N_0}{N} \right)^{2\nu}$$

where  $\nu$  is the Flory exponent describing the solvent condition. The SEC calibration curve for nonlinear polymer can thus be obtained by shifting upwards the calibration curve for a linear polymer of the same repeating units by  $\log_{10} g^{-1/(2\nu)}$ .

Now the question is to find this characteristic size  $R_c$ , i.e. the separation principle of SEC. Grubisic et al. [2] found experimentally that polymer molecules are separate in

SEC column according to a hydrodynamic volume  $V_H = M[\eta]/6^{3/2}$ . Theoretical studies assume a thermodynamic separation principle for SEC, and use the radius of gyration  $R_g$  as the relevant size parameter, and recent work by Sun et al. [1], Teraoka [3], Farmer et al. [4] have shown that the hydrodynamic radius  $R_h$  correlates better with elution behaviour of branched polymers than does  $R_g$ .

In this study we define a new characteristic size  $R_C$ , which is relevant to the equilibrium partitioning of polymers into a confining slit. The experimental data by Sun et al. [1] are used to demonstrate the quality of different approaches. As shown in Figure 1, the calibration curve predicted based on  $R_C$  shows an excellent agreement with the experimental data.

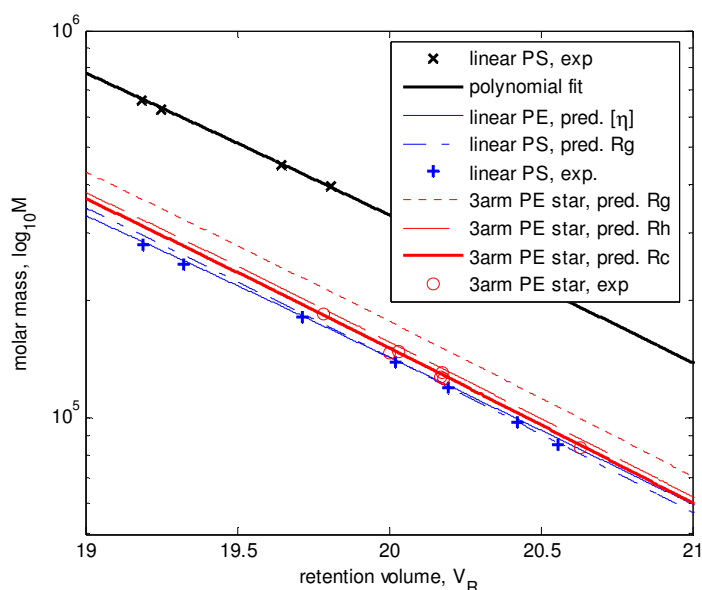


Figure 1 SEC calibration curves. Symbols (x, +, o) denote experimental data for linear PS, linear PE and 3-arm symmetric PE star respectively [1]. The calibration curve for linear PS is fitted to a polynomial, and used to predict calibration curves for linear PE by universal calibration  $[\eta]$  and by  $R_g$ . The predicted calibration curve by  $R_g$  is then used to predict calibration curves for 3-arm PE star by  $R_g$ ,  $R_h$  and  $R_c$  respectively. The prediction by  $R_c$  shows an excellent agreement with the experimental data. No fitting parameter is used in all predictions.

## References

- [1] Sun, T., Chance, R. R., Graessley W. W. and Lohse D. J., (2004) *Macromolecules*, 37, 4304-4312
- [2] Grubisic, Z., Rempp, P. and Benoit, H., (1967) *J. Polym. Sci. Part B Polym. Lett.* 5, 753-759
- [3] Teraoka, I., (2004) *Macromolecules*, 37, 6632-6639
- [4] Farmer, B. S., Terao, K. and Mays J. W., (2006) *International Journal of Polymer Anal. Charact.*, 11, 3-19



## Preparation and Characterization of Organic/Inorganic Polymer Nanocomposites

Gudrun Schmidt-Naake

Technische Universität Clausthal, Institut für Technische Chemie, Erzstraße 18, D-38678 Clausthal-Zellerfeld, Germany. Tel.: +49 5323 72 2036; fax: +49 5323 72 3655  
*e-mail address:* gudrun.schmidt@tu-clausthal.de

The combination of polymers with inorganic materials is a research field of steadily growing interest and importance. Especially, the synergism of polymeric properties such as elasticity and chemical resistance with organic ones like hardness, stability, electrical conductivity and other properties offer a vast potential concerning new materials and applications.

The preparation of polymer composites does not always lead to the desired synergetic effects. Due to the complementary properties of the components often phase separation occurs, giving rise to unsatisfactory material properties. This problem can be solved by linking organic and inorganic part covalently. Typical coupling agents for this purpose are substituted alkyl trialkoxysilanes and tetraalkoxysilanes.

Different styrene and acrylate based org./inorg. polymer composites incorporating magnesium hydroxide were successfully synthesized using 3-(methacryloxy)propyl-trimethoxysilane (MPTMS) as coupling agent and  $MgCl_2$  as inorganic precursor<sup>[1,2]</sup>. The polymer composites were prepared by free radical emulsion polymerization.

Another interesting field of research is devoted to the encapsulation of inorganic particles by polymers, the so called core-shell particles.

The main focus of our study are the preparation of functionalized hybrids<sup>[3,4]</sup>. Therefore, inorganic cores were produced, varying from silica cores to  $Al_2O_3$  - ,  $ZrO_2$  - and  $TiO_2$  -cores with polymerizable functionalities. Those cores have been copolymerized in miniemulsion using sodium dodecyl sulphate as surfactant and potassium peroxy disulphate as initiator with styrene or other monomers as matrix and glycidyl methacrylate, styrene sulfonic acid (SSA) and aminoethyl methacrylate hydrochloride and other as comonomers. This leads to functionalized emulsion products. The comonomer concentration was varied to achieve different polymer compositions and thus different rates of functional groups at the surface. The received emulsions were investigated with respect to thermal stability, rate of functionalization at the surface and particle size distribution, using a dynamic light scattering machine, equipped with a cross correlation system which enables the investigation of emulsions in reaction-state concentration.

The sol-gel-process is a powerful method for preparing polymer/silica organic-inorganic hybrids, in which a nanometer-size silica component is dispersed in a polymer matrix. This process can be carried out also in the polymer melt. The steady-shear rheological behaviour show that the polymer composites are viscoelastic solids. We discuss the role and functional mechanism of the silane coupling agent. At high inorganic content storage and loss compliance become nearly independent from frequency due to extensive cross-linking.

- [1] O. Pankow and G. Schmidt-Naake, *Macromol. Mater. Eng.* 2004, 289, 990
- [2] O. Pankow and G. Schmidt-Naake, *Macromol. Mater. Eng.* 2006, 291, 1348
- [3] M. Valencia, W. Dempwolf, F. Günzler, O. Knöpfelmacher, G. Schmidt-Naake, *Macromolecules*, 2007, 40, 40
- [4] O. Töpfer, G. Schmidt-Naake, *Macromol. Chem. Phys.* 2006, submitted

Book of Abstracts  
European Congress of Chemical Engineering (ECCE-6)  
Copenhagen, 16-20 September 2007

## **Synthesis and kinetics study of UV curable epoxy acrylate resin**

M..Ebrahimi,<sup>a</sup> P. Kardar,<sup>a,b</sup> S. Bastani<sup>b</sup>

<sup>a</sup>*Department of Polymer Engineering, Amirkabir University of Technology, 15875-4413, Tehran, Iran*

<sup>b</sup>*Institute for Colorants, Paints and Coatings, No. 59, Vafamanesh, Hossein abad, Sq., Tehran, Iran.*

### **1. Summary**

In this research, an epoxy acrylate resin was synthesized using a bisphenol-A epoxy (EEW=190) and acrylic acid. The reactions were carried out in the presence of triethylamine as catalyst and in the temperature range of 60-90 °C. The results showed that the reaction followed a first-order kinetics in the reaction conditions. The results obtained in the excess method also revealed that the reaction was first- and zero-order with respect to acrylic acid and epoxy, respectively. The activation energy of the reaction was found to be 45-48 kJ mol<sup>-1</sup> and the frequency factor was calculated to be about 1.1x10<sup>5</sup> min<sup>-1</sup>. FTIR analysis was used to identify the formation of epoxy acrylate resin. The synthesized resin was mixed with different amounts of multifunctional diluents and cured by UV. The results showed that all of the coatings had an excellent gloss with a good harness and scratch resistance.

Keywords: Epoxy acrylate resin, UV curing, Kinetics, Multifunctional monomers

### **2. Extended Abstract**

#### **2.1. Introduction**

In the recent years, the use of UV curable coatings has considerably increased [1]. This coating system considered as one of the most environment friendly coating systems. Having both good properties of epoxy and acrylic resins, epoxy acrylate resins are among the most frequently used resins in UV curing systems [1, 2]. Bajpai et al. [2] studied the synthesis of novolac and bisphenol-A based epoxy acrylate resins but they did not report any kinetics parameter. Pal et al. [3] investigated the kinetics of esterification of bisphenol-A based epoxy resin with acrylic acid in presence of triphenylphosphine. They reported a first-order kinetics for the reaction.

#### **2.2. Experimental**

A bisphenol-A based epoxy resin (EEW=190), acrylic acid, triethylamine, hydroquinone was used for the synthesis of epoxy acrylate resin. In addition, trimethylol propane triacrylate (TMPTA), tripropane glycol diacrylate (TPGDA) and 1, 6 hexanediol diacrylate (HDDA) were used as multifunctional diluents for the formulation of an UV curing coating.

### 2.3. Results and Discussion

The FTIR spectra of epoxy resin, acrylic acid and epoxy acrylate resin showed that the esterification reaction was the main reaction.

The acid value (AV) of the reactor content was used for kinetics studies. The obtained results were interpreted by differential and integral method and the overall reaction order was found to be one (Fig. 1). The results obtained in the excess method also revealed that the reaction was first- and zero-order with respect to carboxylic and epoxide groups, respectively. The specific rate constant was found to obey Arrhenius expression and activation energy and frequency factor were found to be 45-48 kJ/mol and  $1.1 \times 10^5 \text{ min}^{-1}$ , respectively.

The synthesized resin was mixed with different amounts of multifunctional diluents (Table 1), benzophenon and a co-initiator and then cured by UV radiation. Important properties of the cured resins were measured and presented in Table 1.

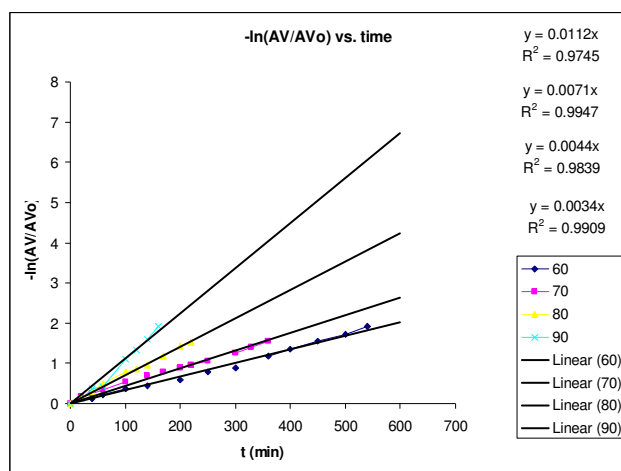


Figure 1: Ln (AVo/Av) versus time

Table 1: Formulation of epoxy acrylate resins and their physical and mechanical properties

Epoxy Acrylate	TMPTA	DPGDA	HDDA	Viscosity (cp)	Hardness (s)	Scratch (mN)	Gloss (60°)
40	27.5	5	27.5	70	100	450	Fully gloss
40	25	30	5	300	120	350	Fully gloss
44.5	20.5	17.5	17.5	190	90	400	Fully gloss
55	21	19	5	1350	100	400	Fully gloss

### 2.4. References

- [1] Koleske, J., *SRadiation Curing of Coatings*, ASTM International, USA (2002).
- [2] Bajpai, M., Shukla, V. and Kumar, A., (2002), *Progress in Organic Coatings*, 44, 271-278.
- [3] Pal, N., Srivastava, A. and Rai, J.S.P., (2004), *International Journal of Chemical Kinetics*, 36, 280-285.

## **On the gas penetration in periodically constricted circular tubes filled with viscoelastic liquids**

Yannis Dimakopoulos<sup>a</sup>, John Tsamopoulos<sup>a</sup>

*<sup>a</sup>Laboratory of Computational Fluid Dynamics, Department of Chemical Engineering, University of Patras, 26500 Patras, Greece*

### **1. Summary**

We examine the displacement of viscoelastic liquids by pressurized air from harmonically undulated tubes of finite length. This unsteady process gives rise to a long open bubble of varying radius, increasing length and surrounded by the liquid. The viscoelastic part of the liquid stresses is governed by either the exponential PTT or the Oldroyd-B constitutive law. In general, the thickness of the liquid film that remains on the tube wall is non-uniform. Under creeping flow conditions, it varies periodically, but with a phase difference from the tube radius, while at high values of the Reynolds number,  $Re_p$ , the film thickness increases with the axial distance, and the periodicity of the velocity and stress fields ahead of the bubble tip is broken. At even higher Reynolds numbers, recirculating vortices develop inside each tube expansion and when the undulation ratio,  $S$ , also decreases significantly, nearly isolated bubbles are formed in each tube segment, while the free surface exhibits small-wavelength variations.

Keywords: gas penetration, liquid displacement, undulated tube, periodic coating, viscoelastic liquids

### **2. Extended Abstract**

The displacement of viscoelastic liquid by a gaseous phase is a problem of fundamental importance in the chemical and petrochemical industry. There are many practical applications and physical operations, such as the enhanced oil recovery, the pulmonary airway reopening and the gas assisted injection moulding, which have as a common basic feature the effective displacement of a liquid by gas. In addition all these processes take place in geometries which are more complicated than a single straight tube. Numerous researchers have approximated them with a tube with sinusoidally varying cross-section. Although this cannot describe the latitudinal dispersion, it simulates the converging-diverging character of these flows. Here we extend our previous study for viscous liquids in periodic tubes (Dimakopoulos & Tsamopoulos (2006)) to the displacement of viscoelastic ones.

The flow geometry consists of three parts: an introductory segment, a harmonically varying middle part and an exit segment. The middle segment is made up of number of identical sinusoidal units of wavelength  $\lambda$ , while  $S$  is the ratio of the minimum to the maximum radii. The viscoelastic liquid which initially occupies the whole undulated tube comes into contact with the ambient air on the left side of the liquid. The displacement process begins after a step change in the pressure of air.

Governing equations are the mass and momentum balances and the constitutive equation for the viscoelastic part of the liquid stresses. The latter is either the exponential PTT or the Oldroyd-B constitutive law. In order to accurately and efficiently solve these equations, we have chosen the mixed finite element method to discretize the velocity and pressure fields together the Discontinuous Galerkin method for the viscoelastic stresses and a system of quasi elliptic partial-differential equations capable of generating a boundary-fitted discretization of the highly deforming domain occupied by the liquid (Dimakopoulos & Tsamopoulos (2003a, 2003b, 2005)).

This unsteady process gives rise to a long open bubble of varying radius, increasing length and surrounded by the liquid. In general, the thickness of the liquid film that remains on the tube wall is non-uniform. Under creeping flow conditions, it varies periodically, but with a phase difference from the tube radius, because of the periodicity of the velocity and stress fields in front of the bubble. The liquid fraction remaining in each periodic segment of the tube increases as the  $S$ , decreases, whereas it tends to an asymptotic value for straight tubes, as  $S \rightarrow 1$  or as the wavelength of the tube undulation increases, although here the flow is accelerating. The evolution of both the tip and the exit velocity are also affected by the  $S$ . Moreover, the liquid fraction depends strongly on the solvent viscosity and the exponential parameter of the PTT model,  $\varepsilon_{PTT}$ . It increases as any of the two parameters decreases and tends to the Newtonian limit as the  $\varepsilon_{PTT}$  takes large enough values. At high values of the Reynolds number,  $Re_p$ , the film thickness increases with the axial distance, and the periodicity of the velocity and stress fields ahead of the bubble tip, which exists under creeping flow conditions, is broken. In fact the bubble tries to follow a straighter way and avoid the large undulations of the tube wall. At even higher Reynolds numbers, recirculating vortices develop inside each tube expansion and when  $S$  also decreases significantly, nearly isolated bubbles are formed in each tube segment, while the free surface exhibits isolated variations of increasing amplitude and small wavelength.

## References

- Dimakopoulos, Y., and Tsamopoulos, J., (2006) *AICHE J.*, 52(8), 2707-2726.
- Dimakopoulos, Y. and Tsamopoulos, J., (2005) *J. Non-Newt. Fluid Mech.*, 117, 117-139.
- Dimakopoulos, Y. and Tsamopoulos, J., (2003a) *J. Comput. Phys.*, 192, 494-522.
- Dimakopoulos, Y. and Tsamopoulos, J., (2003b) *Phys.Fluids*, 15(7), 1973-1991.

## Session T2-12b: Polymer Science & Engineering – II

<b>Abstract Number</b>	<b>Paper Title &amp; Authors</b>	<b>Included</b>
2145	Kinetic Studies and Monte Carlo Simulations of radical Ter- and Tetrapolymerisations M Drache, G Schmidt-Naake	Yes
2347	Control of Emulsion Polymerisation Processes: A Control-Relevant Model for Particle Size Distribution M A Pinto, C D Immanuel, J R Richards, J P Congalidis	Yes
2513	Batch Processing of Poly (ethylene terephthalate)-Based Masterbatches: The Effect of Carrier Molecular Weight and Pigment Concentration S S Hosseini, A Mehrabani-Zeinabad, A Zadhoush	Yes
2955	Reinforcing of expanded polymer morphology using peroxy radical initiatorse K Aleksieva, A Sassi, K Jerabek	Yes
3823	Effect of Processing Parameters and Composition on Mechanical Properties of Glass fiber Reinforced, EPR-g-MA Toughened Polyamide 6 Using Taguchi experimental design method A Shojaei, M Fereydoon, A Ramazani	Yes

Session T2-12b



## Kinetic Studies and Monte Carlo Simulations of radical Ter- and Tetrapolymerisations

Marco Drache, Gudrun Schmidt-Naake

Technische Universität Clausthal, Institut für Technische Chemie, Erzstraße 18, D-38678 Clausthal-Zellerfeld, Germany. Tel.: +49 5323 72 2048; fax: +49 5323 72 3655  
*e-mail address:* marco.drache@tu-clausthal.de

Radical polymerisation of three and more monomers with different reactivities can lead to polymers with extremely different copolymer compositions during the polymerisation process. A Monte Carlo (MC) simulation method will be presented to describe the copolymer composition dependent on the conversion, the integral and differential copolymer mixture, the comonomer conversions and sequence distributions of the comonomers. The results were verified by experimental investigations of ter- and tetrapolymerisations of donor-, acceptor-, and neutral monomers in batch and semibatch experiments.

For the conversion dependent simulation of these ter- and tetrapolymerisations, the  $r$ -values of the corresponding binary systems and the initial molar compositions of the reaction mixture are required. The applied MC simulation processes a defined total number of monomer molecules of  $n_{\text{tot}}=1 \cdot 10^8$  that are distributed among the given monomer species according to the initial molar composition of the feed. Every single step in this MC simulation represents the incorporation of one monomer unit into the polymer based upon the effective reaction probabilities for the given reaction conditions. The results of the simulation are tracked at steps of 1% of total monomer conversion and are analyzed in respect to the integral composition of the polymer, composition of the monomer feed mixture and conversion of the given monomers. By comparison with the result of the preceding analysis step, the differential polymer composition is calculated. Moreover, analysis of the sequence of monomer units provides information about the numbers for each sequence length of all involved monomers at every analysis step.

The Monte Carlo simulation procedure is executed by the *mcCopolymer* program, programmed in C++ with a Tcl-interface, and employing the *Mersenne Twister* high-level 623-dimensionally equidistributed uniform pseudo-random number generator [1].

Comparison between the experimental results and the MC simulation for radical polymerisations of donor, acceptor and neutral monomers with highly different reactivities, demonstrates the precision of the presented Monte Carlo model for terpolymerisations and tetrapolymerisations. If the  $r$ -values of the binary sub-systems are correctly known, copolymer compositions, comonomer compositions and monomer conversions can be described in good agreement with experimental data up to high conversions. The calculated, differential copolymer compositions and sequence distributions lead to a better understanding of the correlations between polymer structure and feed composition for multicomponent polymerisations. Furthermore, these MC simulations are a powerful tool for the development of semi-batch regimes for the synthesis of chemically uniform polymers.

- [1] M. Matsumoto, T. Nishimura, *ACM Trans Model Comp. Simul.* **1998**, 8, 3

Book of Abstracts  
European Congress of Chemical Engineering (ECCE-6)  
Copenhagen, 16-20 September 2007

## **Control of Emulsion Polymerisation Processes: A Control-Relevant Model for Particle Size Distribution**

Mark A. Pinto,<sup>a</sup> Charles D. Immanuel,<sup>a</sup> John R. Richards,<sup>b</sup> John P. Congalidis<sup>b</sup>

<sup>a</sup>*Centre for Process Systems Engineering, Department of Chemical Engineering, Imperial College London, London, UK*

<sup>b</sup>*DuPont Engineering and Research, Experimental Station Laboratory, Wilmington, DE, USA*

### **1. Summary**

Emulsion polymerization is an important process for the manufacture of several polymeric materials. In this process, the particle size distribution (PSD) is an important control variable due to its strong influence on the end-product properties. However, comprehensive population balance models of the PSD are computationally expensive and are suitable primarily for off-line open-loop control studies. In this paper, a lumped model of emulsion polymerization is formulated in which the total number and volume of particles in the system are considered in lieu of the complete PSD. However, all other phenomena present in the comprehensive model are considered in detail. It is observed that the predictions of the lumped model are comparable to that of the detailed model though the prediction error increases over time. It is concluded that this lumped model, in combination with a state/parameter estimator, would be suitable for on-line feedback control.

Keywords: emulsion polymerisation, particle size distribution, inferential control, on-line feedback control, model-based control

### **2. Extended Abstract**

Emulsion polymerisation is a commercially important technology to produce polymeric materials for both conventional and novel applications. In this paper, firstly, an analysis will be presented identifying an inferential control scheme for the emulsion polymerisation process. Secondly, a control-relevant model will be described that is computationally less demanding, and thereby ideally suited for on-line applications. This model will serve as a useful complement for a more detailed population balance model that is imperative for off-line purposes such as open-loop optimisation. These two aspects are elaborated in the rest of the abstract.

In emulsion polymerisation, the polymer is produced within particles that span the sub-micron size range. The particle size distribution (PSD) plays a strong role in determining several end-use properties of the emulsion polymers. In particular, the PSD determines the rheology of the emulsion polymers by influencing the maximum packing factor of the particles in the latex. Thus, in addition to the conversion of the monomers and the polymer content of the latex, the PSD constitutes the most crucial control variable in the process. The PSD itself is determined by three particle-level

phenomena, namely, nucleation, growth and coagulation, which interact with each other through an integrated internal feedback mechanism, resulting in a highly nonlinear process. The inferential control of rheology through PSD control facilitates the complex and non-convex rheology control problem by providing a guarantee for the identification of a control move that would lead to the desired rheology. It is also clear that the identification of the target PSD that would lead to the desired rheology will be strongly influenced by the process imposed reachability restrictions as well as interactions among the process variables.

Typical industrial operation of emulsion polymerisation reactors is in the batch mode. A detailed model of PSD in emulsion polymerisation is obtained through the use of population balances, which is the ideal basis for the open-loop optimisation of (semi-) batch operation, to determine the operating conditions and feed policies. For on-line feedback control using a model-based control framework, a less-extensive model would be preferable. Such a model could be formulated based on a lumping approximation using simpler material balances, instead of the population balances. While the population balances consider the time evolution of the particle population distribution over the size range of about 5 nm to 500 nm, the lumped material balances consider the time evolution of the total number of particles over the entire size range and their average size. The lumped model proposed here, which is computationally substantially simpler than the population balance model, retains all the features of the more intensive population balance model, including phase partitioning of monomers, surfactants and other reagents; kinetics and associated balances in the aqueous and particle phases; and the major particle phenomena of nucleation, growth and coagulation. However, all size-dependent properties are calculated based on the average particle size.

The differences in the predictions of the simple lumped model and the comprehensive population balance model for two classes of PSD of interest have been studied (unimodal monodisperse PSD, and bimodal PSD). It is seen that the primary difference is in the prediction of the secondary nucleation while considering bimodal PSD classes. Until this secondary nucleation event occurs, the predictions of the two models are in good agreement. Further, the predictions of important measurable quantities such as conversion and solids content are comparable to those obtained from the distributed model throughout the duration of the process. Thus, it is clear that this simpler model can be used for on-line control purposes, when combined with a state/parameter estimator. The estimator would use on-line measurements to implement a lumped correction to the model with regard to the nucleation parameters, and thereby produce a better prediction of any secondary nucleation for control of the PSD. When unimodal distributions are considered, the results are significantly better with the lumped model deviating only gradually from the predictions of the comprehensive model. These results further strengthen the conclusion that the lumped model, in combination with a state/parameter estimator, would be appropriate for on-line control applications. This holds better promise than the use of the comprehensive distributed model for on-line control purposes. As part of future work, it is of interest to study the ability of this lumped model to predict the oscillatory dynamics exhibited by continuous emulsion polymerisation reactors.

## **Batch Processing of Poly(ethylene terephthalate)-Based Masterbatches: The Effect of Carrier Molecular Weight and Pigment Concentration**

Seyed Saeid Hosseini<sup>a,b</sup>, Arjomand Mehrabani-Zeinabad<sup>a</sup>, Ali Zadhoush<sup>c,\*</sup>

<sup>a</sup>*Department of Chemical Engineering, Isfahan University of Technology, Isfahan, 84154, Iran*

<sup>b</sup>*Department of Chemical and Biomolecular Engineering, National University of Singapore, Singapore, 119260, Singapore*

<sup>c</sup>*Department of Textile Engineering, Isfahan University of Technology, Isfahan, 84154, Iran*

### **1. Summary**

The main objective of this study is to conduct a laboratory scale experiments on mass pigmentation process to produce suitable coloring masterbatches for PET by using pigment powders and PET as polymeric carrier. In addition to providing the appropriate conditions for this process, a comprehensive investigation is carried out on the vital processing variables like the effect of carrier molecular weight and pigment concentration on the compounding process. Applying image analysis along with interpretation of index curves of compounding process provides a comprehensive insight the state of dispersion and quality of products.

Keywords: Poly(ethylene terephthalate), Masterbatch, Batch processing, Dispersion, Optical analysis.

### **2. Extended Abstract**

#### **Experimental**

Four types of PET samples each one possessing stipulated molecular weight (24200, 20200, 12250 and 9300) were used as the carrier for preparation of masterbatches. The compounding of polymer and pigments, Cromophtal red 214 BN, (Ciba Switzerland). was carried out through batch process in a laboratory scale internal mixer model TL2000 (Brabender, Germany). Granules of carrier and pigment particles were physically pre-mixed and were fed in between the two counter-rotating rotors while in motion. The speed of rotors and processing temperature were controlled at 30 rpm and 290°C, respectively. The compounding period was set to 10 minutes for all the samples.

#### **Results and Discussion**

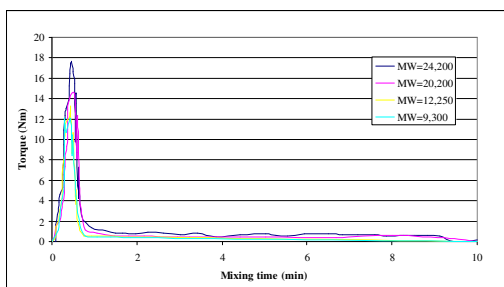


Fig.1 Effect of carrier molecular weight on Torque-Time diagrams of compounding process for production of masterbatch. (pigment loading= 4%).

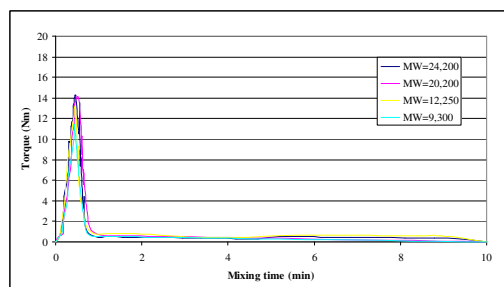


Fig.2 Effect of carrier molecular weight on Torque-Time diagrams of compounding process for production of masterbatch. (pigment loading= 8%).

Mass pigmentation technique<sup>1</sup> was adopted in order to prepare the coloring masterbatches based on poly(ethylene terephthalate) (PET) as the carrier medium. A set of appropriate processing conditions was determined to prevent the polymer degradation while achieving the desired quality. The effect of compound formulation, including the molecular weight of carrier and pigment concentrations were studied. The best dispersion quality was obtained from the compound having lower molecular weight, mainly due to the less viscosity and chain entanglements which rendered less resistance for the transport of pigments into the carrier medium. Increase of the pigment loading for a fixed carrier resulted in the decrease in dispersion energy which was ascribed to the direct effect of compound formulation and the difference in nature of the materials. The produced masterbatches were accordingly applied to the host polymer to enable the qualitative analysis of the dispersion process via optical microscopy. The better dispersion quality and less agglomeration were observed for the samples prepared from low molecular weight carrier. The results indicate high quality PET-based coloring masterbatches can be successfully produced through the optimized condition of batch compounding. Furthermore, an appropriate selection of carrier molecular weight and pigment loading are prerequisite for achieving a masterbatch compound with desired properties.

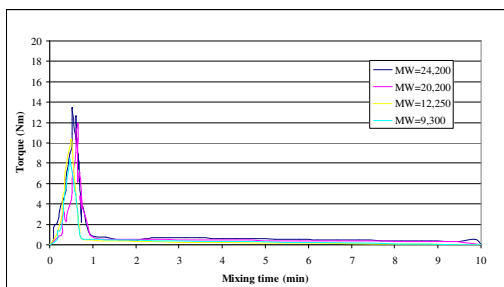


Fig.3 Effect of carrier molecular weight on Torque-Time diagrams of compounding process for production of masterbatch. (pigment loading= 12%).

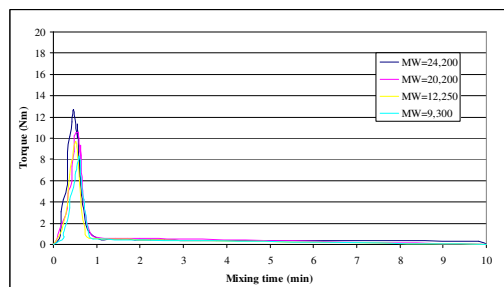


Fig.4 Effect of carrier molecular weight on Torque-Time diagrams of compounding process for production of masterbatch. (pigment loading= 16%).

## References

- 1 Marcinčin A., Modification of fiber forming polymers by additives, Prog. Polym. Sci., 27 (2002)

## **Reinforcing of expanded polymer morphology using peroxy radical initiator**

K. Aleksieva<sup>a</sup>, A. Sassi<sup>b</sup>, K. Jerabek<sup>a</sup>

<sup>a</sup>*Institute of Chemical Process Fundamentals, Academy of Sciences of the Czech Republic, 165 02 Prague 6, Czech Republic*

<sup>b</sup>*Istituto di Scienze e Tecnologie Molecolari-CNR, Università di Padova, Padova I-35131 Italy*

### **1. Summary**

For applications requiring high porosity of the functional polymer is advantageous to reinforce the polymeric skeleton against collapse during drying. The process is known as post-polymerisation crosslinking.

In this contribution we report an attempt to increase the rigidity of functional polymers by post-polymerization treatment based on utilization of the residual vinyl groups in simple free radical reaction in presence of a strong radical initiator and thermodynamically good solvent. In order to better understand the effect of radical initiator action, polymers with different degree of crosslinking were used. Additional polymerization of residual double bonds and/or polyrecombination reaction is studied in terms of their overall effect on the polymer morphology and surface area and by <sup>13</sup>C MAS NMR.

Keywords: post-crosslinking, surface area, pores, macroreticular, residual double bonds

### **2. Extended Abstract**

Accessibility of the interior of functional polymers like adsorbents or catalysts supports is the highest when the polymer is swollen by the suitable solvent. After removal of the swelling solvent e.g., by drying, the polymer morphology at least partially collapses. Extent of the collapse depends on the rigidity of the polymer skeleton. For applications requiring high porosity of the functional polymer even in absence of swelling solvents is advantageous to reinforce the polymeric skeleton against collapse by post-polymerisation crosslinking. Already know methods for this purpose uses Friedel-Crafts catalysed addition of chloromethyl groups or residual double bonds on benzene rings in styrenic polymers.

In this contribution we report an attempt to increase the rigidity of functional polymers by post-polymerization treatment based on utilization of the residual vinyl groups in simple free radical reaction in presence of a strong radical initiator and thermodynamically good solvent. New crosslinks possibly stabilizing the expanded position of polymer chains can be formed either from those residual double bonds,

which do have in close vicinity another reaction partner or by polyrecombination mechanism involving macroradicals created by splitting of a labile hydrogen atom from aliphatic chain by an energetic radical initiator.

For better understanding the post-crosslinking effect of the radical initiator, we have used a few styrenic polymers with different divinylbenzene content and different concentrations of free double bonds having diverse values of apparent specific surface area (Table 1).

Measurements of nitrogen physical adsorption and inverse steric exclusion chromatography (ISEC) provided information on polymer morphology in dry and swollen state, respectively. Changes in vinyl groups and/or in aliphatic part of the polymer structure have been followed using  $^{13}\text{C}$  MAS NMR.

Polymer sample	BET surface area, m <sup>2</sup> /g Original samples	BET surface area, m <sup>2</sup> /g after post-crosslinking
XAD-4, highly crosslinked	870.8	918.7
XAD-2, moderately crosslinked	340.2	358.8
ST-DVB10%, low crosslinked	0.69	0.60

#### References:

Davankov, V., Tsyurupa, M., (1990) *React. Polym.* 13, 27.

Ando K., Ito T., Kusano H., in *Ion Exchange in Industry*, M. Streat Ed., Ellis Horwood Ltd, Chichester, p.232, 1988

Aleksieva, K., J. Xu, Li min Wang, Sassi A., Pientka Z., Zhang, Z., Jerabek K. (2006) *Polymer* 47, 6544.

V. V. Korshak V. V., Sosin, S. L. V. M. Chistyakova, (1960) *Polymer Science U.S.S.R.*, vol. 1, Issue 3, , 341.



## **Effect of Processing Parameters and Composition on Mechanical Properties of Glass fiber Reinforced, EPR-g-MA Toughened Polyamide 6 Using Taguchi experimental design method**

*A. Shojaei\*<sup>a</sup>, M. Fereydoon<sup>a</sup> and A. Ramazani<sup>b</sup>*

Department of Chemical and Petroleum Engineering Department, Sharif University of Technology, Tehran 11365-9465, Iran [mfereydoon77@yahoo.com](mailto:mfereydoon77@yahoo.com)

### **1. Summary**

In this study the role of composition and processing conditions including feed rate, screw speed and temperature on phase morphology and mechanical properties of nylon 6 toughened with maleated ethylene propylene random copolymer (EPR-g-MA) and reinforced with glass fiber is examined. In order to reduce the number of experiments and explore the contribution of each component in the final properties of the blend, Taguchi design of experiments is used. Main factors of the systems investigated in this study include the concentration of glass fiber and EPR-g-MA in the range of 10–20 wt%, feed rate ranges 100-250 kg/hr, compounding temperature varying between 230-260 °C and screw speed from 100-450 rpm. After designing the experiments by using the Taguchi method. The results obtained from experiments and analysis with Qualitec-4 software show that processing parameters such as temperature, screw speed and feed rate do not influence considerably the mechanical properties and phase morphology of blends. The results obtained from SEM show although rubber made a separated phase through matrix but adhesion of rubber phase to polyamide is good and rubber particles distributed completely in spherical shape through the polyamide matrix. Moreover, rubber content has a dominant effect on impact strength of the blend. When the rubber content increases, rubber particle size decreases and caused the narrow distribution size of particle size. This could be attributed to reduction of surface tension between the rubber phase and the PA6 matrix caused by grafting reactions of rubber with polyamide.

### **2. Extended Abstract**

The effect of EPR-g-MA contents and processing conditions on the morphology and tensile and Izod impact performance of blends on nylon6 were examined. Based on L-9 and M-16 orthogonal array of Taguchi's method, 9 compounding conditions were designed for PA/EPR-g-MA blends and 16 compounding conditions were designed for reinforced PA/EPR-g-MA blends with glass fiber. The results obtained from

experiments and analysis with Qualitec-4 software show that processing parameters such as temperature, screw speed and feed rate do not influence considerably the mechanical properties and phase morphology of blends. However, the content of the rubber phase has a dominant role on the mechanical properties, toughness as well as rubber particle size. Consequently, increasing the rubber content and decreasing the rubber particle size leads to a significant increase of the impact strength of PA6, i.e. from 4j/m to 53.1 j/m in 20 volume percent of EPR-g-MA. This results show that the morphology of the blends more especially the rubber particle size is affected considerably by the rubber content. Degree of adhesion of the rubber and matrix phase takes place by incorporating functional groups into the elastomer that can react with polyamide. The grafting process, provide the adhesion needed and dramatically affect the ability to disperse the elastomer and resulting particle size. As expected the adhesion of nylon6 to EPR-g-MA is significantly greater at higher content of elastomer in the blends, where more chemical bonds can be formed at the interface so more toughening will be taken place. The results obtained from Qualitec-4 software results show that functionalization does improve adhesion and causes smaller rubber particle size. There seems to be a critical value of the particle size about 400 nm, below which the blend is super-tough. Clearly a tremendous reduction in particle size of the rubber is caused by the grafting reaction. Adding 20Wt% rubber to PA matrix produces small particles that are effective for toughening and improving Izod impact strength. The Izod impact strength is often used indicator of toughness. By plotting the Izod impact strength as a function of rubber content, processing temperature, feed rate and screw speed, it was shown that mechanical properties are affected only by rubber content. Rubber causes though blend and Izod impact increased. Morphology, rubber particle size, shape, and the distribution of rubber particle among the matrix of blends, have an important rule on the Izod impact. Rubber content controls the amount of Izod impact. When fiberglass content increased, Izod impact of blends decreased. When feed rate increased, average of fiber length increased, when in feed rate range by increasing the feed rate average of shear flow increased, and the more fiber has broken the average fiber length with screw speed have descending trend. There is a critical fiber length for each composite. If the fiber length is more than the critical value the system is stiff and strength and if the fiber length of system is less than critical length the properties of un reinforced blends. In fact, in this system fibers have not any rule in reinforcement of composite.

## References

- [1] Oshinski, A.J., Keskkula, H., Paul, D.R., (1992), *Polymer*, 33, 268-283.
- [2] Montgomery Douglas C., *Design and Analysis of Experiments*, John Wiley & Sons Inc, 3rd edition, (1991).
- [3] K. Ranjit, Roy, *Design if Experiments Using the Approach: 16 Steps to Product and Process Improvement*, April (2001).
- [4] Takeda Y., Keskkula H., Paul D.R., (1992) *Polymer*, 33, 3173-3181.
- [5] Oshinski, A.J., Keskkula, H., Paul, D.R., (1992), *Polymer*, 33, 284-293.
- [6] Oshinski, A.J., Keskkula, H., Paul, D.R., (1996), *Polymer*, 37, 4891-4908.
- [7] Oshinski, A.J., Keskkula, H., Paul, D.R., (1996), *Polymer*, 37, 4909-4918.
- [8] Laura, D. M., Keskkula, H., Paul, D.R., (2003), *Polymer*, 44, 3347-3361.

## Session T2-12P: Polymer Science & Engineering – Poster

<b>Abstract Number</b>	<b>Paper Title &amp; Authors</b>	<b>Included</b>
1946	Thermal behavior of whey protein films laminated with corn zein protein F Jabbari, R Oromiehie, B Ghanbarzadeh, S N Khorasani	No
2593	Study on effective parameters on phase separation in segmented polyurethanes M Amrollahi, G M M Sadeghi	Yes
2688	The Curing Reactions of the Epoxy/Intercalated Clay Resin Systems S G Hong, C W Kuo	Yes
3451	Kinetic Study of Methyl Methacrylate/Lauryl Methacrylate Inhibited Free Radical Copolymerization by Differential Scanning Calorimetry A Habibi, J D Wilde	Yes

Session T2-12P

## **Study on effective parameters on phase separation in segmented polyurethanes**

M. Amrollahi , G. Mir Mohamad Sadeghi \*

*Department of Polymer Engineering, Amirkabir University of Technology, 15875/4413 Tehran, Iran*

### **1. Summary**

Phase separation in segmented polyurethanes is an important phenomenon which affects on characteristic properties of polyurethanes. Morphology, formation and distribution of microdomains (hard segments and soft segments) are effective parameters on adhesion and interfacial interaction of polyurethane system. In this work segmented polyurethanes based on 4,4 -diphenylmethane diisocyanate (MDI) and 1,4-butanediol (BDO) were synthesized and the effect of hard segment content as well as type of polyol on phase separation of synthesized polyurethanes has been studied and also correlation between microstructural factors on final properties of polymer well defined.

Keywords: Polyurethane, Phase separation, Hard Segment, Hydrogen bonding

### **2. Introduction**

Segmented polyurethanes that consist of alternating soft and hard segments offer unique possibilities of tailor-made polymers by varying block length and composition [1]. Thermodynamic immiscibility between hard and soft segments induces phase separation and generates a two-phase morphology in these segmented block copolymers. There are some reports on evaluation of structure-properties in these segmented polyurethanes [2-4].

In the present study the effect of hard segment content and type of polyol on the thermo-mechanical properties as well as size of soft and hard domains and micro phase separation of synthesized polyurethane networks have been studied.

### **3. Experimental**

The polybutadien-ol were prepared locally [5] with low vinyl microstructures and  $M_n$  being about 2500 gr/mol. PTMG and polycaprolactone with  $M_n=2300$  and  $M_n=2600$  respectively obtained from Merck and used as received.

Polybutadiene-ol and other polyols were degassed at 50 °C for 24 hr before use. MDI (4,4-diphenylmethane diisocyanate), BDO(1,4-butane diol ) from Merck were used after drying at 50 °C and 800 mm-Hg vacuum for 8 hr.

#### 4. Synthesize method

All the polyurethanes synthesized using one-shot method. The procedure was as follows: Polyol, MDI and BD were mixed vigorously for a few minutes. The above mixture was poured in a rectangular mould. The mould was preheated and coated with silicon before use. The mould was in an 85°C oven for 3 days. All of tests were carried out on the specimens that maintained in a desiccator for 7 days. Final cross linked products (networks) were insoluble in common solvents. Polyurethanes were synthesized in various molar ratios and hard segment contents of 25 %, 40% and 55%.

#### 5. Analytical techniques

A VPO Knauer apparatus was used to determine Mn of polyols. Toluene as solvent at 90°C and benzyl was used for calibration. DMTA analysis was carried out through heating rate of 4 C/min from -100°C to 250° C. A Polymer-Lab DSC was used. The DSC runs were performed under nitrogen using a heating rate of 10°C/min with sample weight of 10 mg. AFM (Atomic Force Microscopy) was used to study of two phases in network. Surfaces for AFM analysis prepared from fractural area of samples broken in liquid Nitrogen. The static mechanical properties were carried out by MTS tensile machine with a separation speed of 500 mm/min. FTIR(Bruker) spectroscopy was used to study of hydrogen bonding and phase separation of networks.

#### Conclusion

Experiments showed that as the hard segment content of polyurethanes as well as type of polyol affect on thermo mechanical properties as well as phase separation of polyurethanes. AFM results show that one can recognized relationship between hard segment content of and domain sizes in polyurethanes.

#### References

- Speckhard,T.A;Cooper,S , (1986) *Rubb.Chem.Tec.*, 59 ,405-413  
Cuve,L;Pascault,J.P.;Boiteux,G.;Boiteux,G. (1993) *Polymer*, 33,18  
Ono,K;Shimada,H,Nishimura,T, (1977) *J.Appl.Polym.Sci.*, 21,3223, 1977  
Huang, G. *J. Appl. Polym. Sci.* (1997) ,63,1309  
Mir Mohamad Sadeghi G., Morshedian,J., Barikani M.(2003) *Polym.International*,  
,52 ,1083  
Kincal D.,Ozkar S. *J. (1997) J.Applied Polymer Science*,66,1979-1983

## The Curing Reactions of the Epoxy/Intercalated Clay Resin Systems

S. G. Hong, C. W. Kuo

*Department of Chemical Engineering & Materials Science, Yuan-Ze University, Chung-Li 320, Taiwan*

### 1. Summary

The curing reactions of different intercalated clay/epoxy resin systems are studied by using thermogravimetric analysis (TGA), differential scanning calorimetry (DSC), wide angle X-ray diffraction, and Fourier transform infrared spectroscopy (FTIR). The results of X-ray diffraction indicate that the intercalation distance of the clay increases in the order of unmodified clay < phosphorus epoxy intercalated clay < organic amine intercalated clay < siloxane intercalated clay. The results of TGA confirm that the amount of various compounds intercalated increases in the order of organic amine < phosphorus epoxy < siloxane. Due to the difference in reactive functional groups of intercalated compounds, it is shown from DSC and FTIR analyses that the curing kinetics, reaction extents, and exotherms of the epoxy resin are significantly affected by the presence of different intercalated clays. The curing reactions of the epoxy systems also change with respect to the clay content and the curing temperature used.

Keywords: epoxy, clay, intercalation, curing, kinetics

### 2. Extended Abstract

The curing behaviours of the model epoxy system filled with montmorillonite (clay) intercalated with different organic compounds are demonstrated. As shown in Table 1 from the wide angle X-ray diffraction, the d-spacing of clay is changed with respect to the intercalated organic compound used.

SAMPLE	(001) (2 $\theta$ )	d spacing (Å)
pureclay	7.59	11.64
orgclay	2.96	29.84
Org8411clay	2.34	32.56
phoclay	5.68	15.56

Table 1: The intercalated distance of various clay specimens

The long chain amino and siloxane compounds can effectively widen the d-spacing of the clay while the effect from the use of phosphorus epoxy resin is limited.

The amount of intercalated organic compounds in the clay can be obtained from the TGA thermograms shown in Figure 1. The modified clay with the larger d-spacing also has the greater amount of organic compound penetrated into the clay.

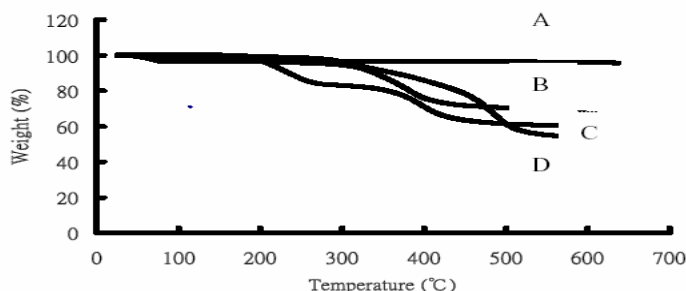


Figure 1: The TGA thermograms obtained from (A) unmodified clay and clay intercalated by (B) phosphorus epoxy resin (C) amino compound and (D) siloxane compound.

The curing characteristics of the epoxy systems are affected by the addition of different intercalated clay due to the reactive groups in the intercalated compounds and the effect from the solid clay filler. Consequently, the curing speed, the exothermic heat, and the reaction order are influenced by the type and the amount of modified clay added (see Table 2). The curing speeds of various systems follow the order of blank > pureclay > phoclay > org8411clay > orgclay. The reaction heat increases with the use of phoclay due to the increase of the epoxide content. The curing reactions of the epoxy systems are also changed by the amount of clay added and the curing temperature used. The DSC data is consistent with the results obtained from the FTIR analysis during cure.

SAMPLE	°C	k	n	m
blank	160	0.436	1.67	0.33
	170	0.732	1.69	0.31
	180	1.356	1.64	0.36
1 phr pureclay	160	0.333	1.71	0.29
	170	0.74	1.64	0.36
	180	1.26	1.66	0.34
1 phr orgclay	160	0.155	1.63	0.37
	170	0.487	1.51	0.49
	180	1.022	1.53	0.47
1 phr 8411clay	160	0.256	1.70	0.30
	170	0.521	1.73	0.27
	180	0.869	1.75	0.25
1 phr phoclay	160	0.288	1.68	0.32
	170	0.39	1.69	0.31
	180	0.71	1.74	0.26

Table 2: The curing kinetics of different specimens calculated from isothermal DSC thermograms



## **Kinetic Study of Methyl Methacrylate/Lauryl Methacrylate Inhibited Free Radical Copolymerization by Differential Scanning Calorimetry**

A. Habibi,<sup>a</sup>, J. De Wilde,<sup>a</sup>

<sup>a</sup>*Department of Materials and Process Engineering (IMAP), Université catholique de Louvain, Réaumur, Place Sainte Barbe 2, B-1348 Louvain-la-Neuve, Belgium, habibi@imap.ucl.ac.be*

### **Abstract**

The solution copolymerization kinetics of isobutyl methacrylate (*i*-BMA) with lauryl methacrylate (LMA) was studied by designing a set of inhibited in-situ polymerization experiments with Differential Scanning Calorimetry (DSC). The kinetic parameters of copolymerization were retrieved using a robust *M*-estimation method. The initiation parameter,  $\bar{k}_d$ , inhibitor transfer parameter,  $\bar{C}_z$  and the number of radicals terminated per each inhibitor molecule (stoichiometric ratio) are determined from the extracted data of induction period. The enthalpy of copolymerization and dependence of  $\bar{k}_d$  and  $\bar{k}_p / \bar{k}_t^{0.5}$  on the monomer phase composition are determined from the data of uninhibited portion of the thermograms. It is indicated that robust *M*-estimation outperforms existing methods of estimation in terms of statistical precision and computational speed, while keeping good robustness properties.

**Key Words:** Copolymerization Kinetics, Inhibition, Methacrylate, Differential Scanning Calorimetry (DSC), Robust *M*-Estimation.

### **1. Introduction**

Interpretation of polymerization kinetics demands knowledge of reliable kinetic parameters. They form the basis for more accurate design of polymerization reactors and better insight into the behavior of an existing reactor. Kinetic modelling of copolymerization systems is subjected to variability of the rate parameter values, which are both usually composition and conversion dependent. In general by using the “Pseudo-kinetic rate constant” (PKRC) method (Tobita and Hamielec, 1991), the

kinetic treatment of a multicomponent polymerization can be reduced to that of homopolymerization. This method applies to chain statistics based on terminal unit model, as well as higher order Markov chain statistics such as penultimate unit model.

DSC has found several applications in determination of reaction kinetics. It provides a continuous history of the heat evolved during the polymerization. In comparison to classical methods of experimental kinetics only small amounts of sample are needed and the rate parameters as well as the heat of reaction can be obtained from a single run. Application of DSC for kinetic studies of copolymerization systems is less clear-cut. Horie (1970) applied the DSC method in conjunction with lump kinetic model for kinetic study of copolymerization systems. The lumped kinetic model defines a heat of reaction that depends on the initial feed composition but does not vary with compositional drift during the course of polymerization. In fact in copolymerization systems, the heat of reaction changes with conversion due to compositional drift, preventing simple reduction of calorimetric data to rate data. In this work the exact dependence of polymerization heat on conversion is taken into account. The calculation procedure allows fully capturing the variability of the copolymerization heat with conversion and avoiding from the limitations of lump kinetic models.

For kinetic parameter estimation, the robust  $M$ -estimator is employed due to its robustness with respect to the outliers and low computational effort (Wakeling and MacFie, 1992). Its major advantage over other techniques is mainly apparent in datasets consisting of blocks of variables subject to problems such as multicollinearity. It is indicated that the dependence of coupled rate parameter,  $\bar{k}_p / \bar{k}_t^{0.5}$  on monomer feed composition is well represented by the Implicit Penultimate Unit Effect Model (IPUM) of Fukuda et al. (1992).

## References

- Tobita H., Hamielec A.E., (1991) *Polymer*, 32/14, 2641.  
Horie K., (1970), *J. Polym. Sci.:Part A-1*, 8, 1357.  
Wakeling I.N., MacFie H.J.H., (1992), *J. Chemometr.*, 6, 189.  
Fukuda T., Kubo K., Ma Y.D., *Prog. (1992), Polym. Sci.*, 17, 875.

## Session T2-13a: Catalysis – I

<b>Abstract Number</b>	<b>Paper Title &amp; Authors</b>	<b>Included</b>
851	Optimum water/syngas molar ratio in the feed for minimizing deactivation by coke in the single step synthesis of DME I Sierra, J Ereña, A T Aguayo, J M Arandes, M Olazar, J Bilbao	Yes
1572	Deactivation of SCR catalysts by aerosols of potassium compounds: Elucidation of mechanisms by lab and pilot scale experiments A D Jensen, J E Johnsson, Y Zheng	Yes
1657	Tailored Distribution of MoO <sub>3</sub> in the TiO <sub>2</sub> and ZrO <sub>2</sub> Supported Catalysts by Water-Assisted Spreading L Kaluža, D Gulková, Z Vít, M Zdražil	Yes
2995	Deactivation of Commercial SCR Vanadia-based Catalysts by Fuel Additives F Castellino, A D Jensen, J E Johnsson	Yes
3261	High Throughput Experimentation and Modeling as Tools for the Development of Green Alkylation Catalysts E A Dejaegere, K Mantri, G V Baron, J F M Denayer	Yes

Session T2-13a

## **Optimum water/syngas molar ratio in the feed for minimizing deactivation by coke in the single step synthesis of DME**

I. Sierra, J. Ereña, A. T. Aguayo, J. M. Arandes, M. Olazar, J. Bilbao

*Departamento de Ingeniería Química, Universidad del País Vasco, Apartado 644, 48080 Bilbao, Spain.  
Phone: +34-94-6015363, Fax: +34-94-6013500, e-mail: javier.arena@ehu.es*

### **1. Summary**

This paper deals with the one-step synthesis of dimethyl ether (DME) from H<sub>2</sub> and CO over CuO-ZnO-Al<sub>2</sub>O<sub>3</sub>/γ-Al<sub>2</sub>O<sub>3</sub> bifunctional catalysts. The strategy of co-feeding water with syngas has been studied in order to limit the formation of coke, which is severe in this process. However, water in the feed has an unfavourable effect in the initial yield of DME, due to the thermodynamic limitations of the reaction and to the water adsorption capacity of the γ-Al<sub>2</sub>O<sub>3</sub>. Taking into account this effect, a serie of experiments with different water/syngas molar ratio in the feed has been carried out. A water/syngas molar ratio of 0.20 effectively reduces deactivation by coke without a significant decrease in the initial activity of the catalyst.

Keywords: dimethyl ether, syngas, catalyst deactivation, coke

### **2. Extended Abstract**

Considerable attention is being paid in the literature to the synthesis of DME from hydrogen and CO in a single step for the following reasons: i) DME is considered to be one of the clean fuels with greater potential for use in the medium term; ii) this process allows for using alternative sources to oil (natural gas, coal and biomass) and has better perspectives for CO<sub>2</sub> incorporation as reactant; and iii) the use of a single reaction step allows for shifting the reaction equilibrium towards DME production (Semelsberger et al., 2006).

Unfortunately, deactivation by coke deposition is severe in this reaction, which gives way to a pronounced decrease in the yield of DME with time on stream. This paper approaches the viability of co-feeding water with the synthesis gas as an efficient strategy for minimizing deactivation by coke. However, this strategy of co-feeding water has the inconvenience of reducing the initial DME yield, due to the thermodynamic limitations of the reaction and to the adsorption of water in the acidic function (Aguayo et al., 2005). Thus, another aspect of this study is to find the optimum water/syngas molar ratio in the reactor feed.

The bifunctional catalyst used is CuO-ZnO-Al<sub>2</sub>O<sub>3</sub>/γ-Al<sub>2</sub>O<sub>3</sub>, prepared by mixing the dry metallic function (CuO-ZnO-Al<sub>2</sub>O<sub>3</sub>, for the methanol synthesis from H<sub>2</sub> and CO) and the acidic function (γ-Al<sub>2</sub>O<sub>3</sub>, for the dehydration of methanol to DME) in an aqueous solution at a ratio of 2/1 by mass (Ereña et al., 2005). The reaction conditions selected are the following: 275 °C (low enough to avoid CuO sintering), 30 bar, H<sub>2</sub>/CO molar ratio= 3/1, space time= 12.8 (g of catalyst) h<sup>-1</sup> (mol of reactants)<sup>-1</sup>, time on stream= 30 h. Under these conditions, the catalyst undergoes severe deactivation by coke.

As is observed in Figure 1, a water/syngas molar ratio of 0.20 (corresponding to a water flowrate of 0.005 ml/min) effectively reduces the deactivation by coke of the bifunctional catalyst (the DME yield hardly decreases with time on stream), without a significant decrease in the initial yield of DME. A higher water/syngas molar ratio (Figure 1 shows, as an example, the results for a ratio of 0.60) is not advisable, as the initial DME yield is severely affected by thermodynamic limitations and water adsorption on the Lewis sites of the γ-Al<sub>2</sub>O<sub>3</sub>. Water/syngas molar ratios lower than 0.20 (e.g. 0.08) do not lead to an acceptable limitation of deactivation by coke. These results are confirmed in Table 1, where the values of coke content on the catalyst are shown for different feeds into the reactor.

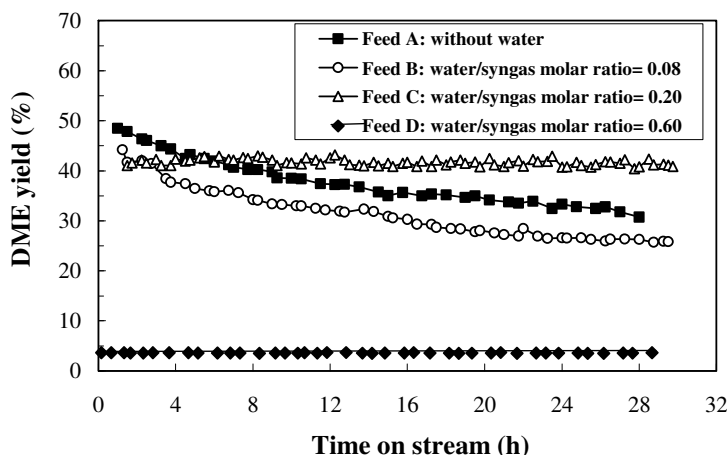


Figure 1. Evolution with time on stream of DME yield for different water/syngas molar ratios in the feed.

Table 1: Effect of the feed on the coke content on the catalyst (wt.%).

	Feed A	Feed B	Feed C	Feed D
Coke content (wt.%)	5.5	4.2	1.3	0.2

## References

- Aguayo, A. T., Ereña, J., Sierra, I., Olazar, M. and Bilbao, J., (2005) *Catal. Today*, 106, 265-270.  
 Ereña, J., Garoña, R., Arandes, J. M., Aguayo, A. T. and Bilbao, J., (2005) *Catal. Today*, 107, 467-473.  
 Semelsberger, T. A., Borup, R. L., Greene, H. L., (2006) *J. Power Sources*, 156, 497-511.

## **Deactivation of SCR catalysts by aerosols of potassium compounds: Elucidation of mechanisms by lab and pilot scale experiments**

A.D. Jensen, J.E. Johnsson, Y. Zheng

*Department of Chemical Engineering, Technical University of Denmark, Building 229, DK-2800 Kgs. Lyngby, Denmark*

### **1. Summary**

An experimental investigation of the deactivation of commercial  $V_2O_5$ - $WO_3$ - $TiO_2$  SCR catalysts under biomass combustion conditions is reported. Catalyst plates were exposed to a layer of KCl particles or fly ash from biomass combustion in a lab-scale reactor, and full-length monolith catalysts were exposed to pure KCl or  $K_2SO_4$  aerosols in a bench scale reactor. Exposed samples were characterized by activity measurements, SEM-EDX and  $NH_3$  chemisorption. The results show that aerosols of KCl and  $K_2SO_4$  are strong poisons for the catalyst because they react with the active sites making them inactive. In the bench scale reactor KCl aerosols cause a deactivation rate of about 1 %/day, while exposure to  $K_2SO_4$  results in about 0.4 %/day. Much slower deactivation was observed for catalyst plates exposed to a layer of KCl or biomass fly ash (a mixture of KCl and  $K_2SO_4$ ). This shows that deposition of potassium aerosols followed by diffusion into the catalyst material is the main cause of the fast deactivation of SCR catalysts observed in biomass fired systems.

Keywords: SCR;  $NO_x$ ; potassium; aerosol; deactivation; biomass combustion

### **2. Extended Abstract**

Selective catalytic reduction (SCR) was developed for reducing  $NO_x$  from stationary sources burning fossil fuels. However, the use of biomass for power generation has increased in recent years to reduce the net  $CO_2$  emissions, and in some countries such as Sweden and Denmark, the SCR process is now being used on plants burning pure biomass or mixtures of biomass and others fuels such as coal, gas or oil. Unfortunately, it has been found that the SCR catalysts may deactivate fast in biomass fired systems. The purpose of the present work was to increase the understanding of SCR catalyst deactivation in biomass fired systems, by performing well-controlled lab and pilot scale experiments extending up to several thousand hours.

Laboratory tests in a flow reactor showed that slight deactivation (about 10 %) was observed for catalyst plates with a composition similar to that of the commercial

monoliths, when exposed to a layer of KCl particles at 350 °C for 2397 h. No deactivation was found for catalyst plates exposed for 2970 h to fly ash (consisting mainly of KCl and K<sub>2</sub>SO<sub>4</sub>) collected from a straw fired power plant. These results were supported by SEM-EDX analysis of the exposed plates. In the case of exposure to pure KCl, potassium did penetrate 10-20 μm into the catalyst wall with had a total thickness of 1000 μm while no potassium was found within the structure of the catalyst plates exposed to biomass fly ash.

Exposure to potassium aerosols was made in the bench scale setup shown in figure 1. The aerosols were generated by injecting a solution of either KCl or K<sub>2</sub>SO<sub>4</sub> in water into a hot (1100 °C) flue gas from a natural gas burner. The salts evaporate and during cooling, condense to form aerosols. Figure 2 shows the results for exposure to KCl for 850 hours and then stopping the KCl addition. The rate of deactivation for catalysts when exposed to KCl aerosols at 350 °C was about 1% per day. Tests with chemisorption of NH<sub>3</sub> were also carried out in the bench scale reactor, and figure 2 shows that the NH<sub>3</sub> adsorption capacity decreases even faster than the activity. This shows that the active sites for NH<sub>3</sub> adsorption (-V-OH) react with potassium and become inactive. It can further be seen that the loss of activity stops when no aerosol flows through the catalyst. This indicates that aerosol particles are needed for deactivation to progress. SEM analysis revealed that the potassium salt had partly deposited on the catalyst outer wall which may to some extent decrease the diffusion rate of NO and NH<sub>3</sub> into the catalyst. However, potassium also penetrated into the catalyst wall and the average K/V ratios (0.5-0.75) in the catalyst structure are high enough for significant chemical deactivation. Similar results were observed for exposure to K<sub>2</sub>SO<sub>4</sub> aerosols although the deactivation rate was smaller, ~0.4 %/day.

The conclusion is that chemical poisoning of active sites caused by deposition of potassium aerosol species (KCl/K<sub>2</sub>SO<sub>4</sub>) is the dominating deactivation mechanism of SCR catalysts in biomass fired systems.

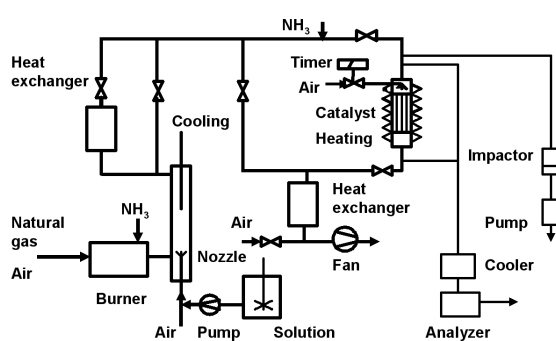


Figure 1. Schematic drawing of the bench scale reactor for catalyst monolith deactivation test.

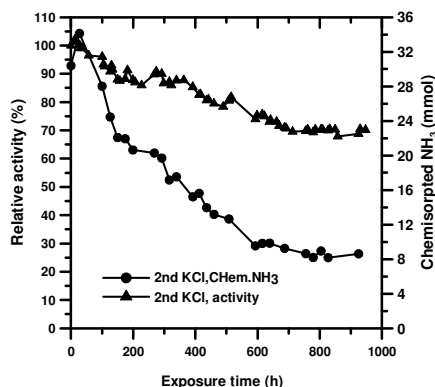


Figure 2. Activity and chemisorbed NH<sub>3</sub> on the catalyst during exposure to KCl aerosols at 350 °C as a function of exposure time.



## Tailored Distribution of MoO<sub>3</sub> in the TiO<sub>2</sub> and ZrO<sub>2</sub> Supported Catalysts by Water-Assisted Spreading

Luděk Kaluža\*, Daniela Gulková, Zdeněk Vít, Miroslav Zdražil

*Institute of Chemical Process Fundamentals, Academy of Sciences of the Czech Republic, Rozvojová 135, 165 02 Prague 6 – Suchbát, Czech Republic; \*Email: kaluza@icpf.cas.cz*

### 1. Summary

A new method for preparation of both eggshell and uniformly distributed MoO<sub>3</sub> in titania and zirconia supported catalysts was studied. Spreading of MoO<sub>3</sub> onto the supports in water was followed by electron probe microanalysis and visually after sulphidation. Eggshell type distribution with saturation adsorption loading 3.3 and 3.2 Mo atoms per nm<sup>2</sup> of TiO<sub>2</sub> and ZrO<sub>2</sub> was formed before the uniform distribution was reached. The thickness of the eggshell was found to be easily controlled either by MoO<sub>3</sub> amount used for the spreading or by reaction time. The uniformly saturated catalysts MoO<sub>3</sub>/TiO<sub>2</sub> and MoO<sub>3</sub>/ZrO<sub>2</sub> were tested in hydrodesulphurisation of thiophene and benzothiophene in their sulphidic states. They exhibited the same hydrodesulphurisation activity and relative selectivity hydrogenation/hydrogenolysis as their counterparts prepared by conventional impregnation from solution of ammonium heptamolybdate, which confirmed good dispersion of Mo species achieved by water-assisted spreading method.

Keywords: eggshell catalysts, solvent-assisted spreading, hydrodesulphurisation, MoO<sub>3</sub>/TiO<sub>2</sub>, MoO<sub>3</sub>/ZrO<sub>2</sub>

### 2. Extended Abstract

Catalysts MoO<sub>3</sub> supported on TiO<sub>2</sub> and ZrO<sub>2</sub> are studied because of their activity in various industrially important reactions, such as hydrodesulphurisation, partial oxidation of methanol, vapour-phase ammoxidation of toluene, the water-gas shift reaction, epoxidation of allyl acetate with tert.-butyl hydroperoxide, oxidation of 1-butene and butadiene, and selective catalytic reduction of NO<sub>x</sub> by NH<sub>3</sub>. A controlled distribution of MoO<sub>3</sub>, eggshell/uniform, in the TiO<sub>2</sub> and ZrO<sub>2</sub> is both of theoretical and practical interest. The eggshell catalysts find application when a rate-determining step is internal diffusion. A desirable reaction product is transported from the eggshell structure more easily than from the interior of the catalyst particles preventing it from further and unwanted consecutive reactions.

A new method proposed here for preparation of both eggshell and uniformly distributed MoO<sub>3</sub> titania and zirconia supported catalysts is based on reaction (spreading) of MoO<sub>3</sub> (Fluka, activated in a planetary mill for 27 h) with the support (TiO<sub>2</sub> of S.A. 140 m<sup>2</sup>g<sup>-1</sup>, or

ZrO<sub>2</sub> of S.A. 108 m<sup>2</sup>g<sup>-1</sup>; both 1/8" pellets, AlphaAesar, Germany) in water. Points of zero charge 5.5 and 6.0 of the TiO<sub>2</sub> and ZrO<sub>2</sub>, respectively, were found to be well above the pH 2.1 of the aqueous impregnation slurry of MoO<sub>3</sub>. An adsorption of dissolved Mo anionic species was therefore enhanced. The dissolved species that penetrated the pellets of support adsorbed there to form gradually saturated adsorption monolayer of MoO<sub>3</sub>. After filling that monolayer, the impregnation continued deeper into the carrier up to the point where uniform distribution throughout the supports was achieved. A thickness of a desired eggshell is easy to control either by amount of MoO<sub>3</sub> or by reaction time. The process of water-assisted spreading was followed by electron probe microanalysis and visually after samples sulphidation (white MoO<sub>3</sub> was transformed to black MoS<sub>2</sub>, supports remained white). The MoO<sub>3</sub> concentration in the eggshell of TiO<sub>2</sub> pellets, for example, was high, about 9-10 wt.%. The content of MoO<sub>3</sub> in the saturated pellets with the uniform MoO<sub>3</sub> distribution was additionally determined by chemical analysis AAS and was about 10 and 7.6 wt% in MoO<sub>3</sub>/TiO<sub>2</sub> and MoO<sub>3</sub>/ZrO<sub>2</sub> catalyst, respectively. These values corresponded to the density of a saturated monolayer of 3.3 and 3.2 atoms Mo per nm<sup>2</sup> of TiO<sub>2</sub> and ZrO<sub>2</sub>, respectively, which was closed to the value 3.4 atoms Mo.nm<sup>-2</sup> obtained previously with MoO<sub>3</sub>/Al<sub>2</sub>O<sub>3</sub> systems. It was also found that high temperature speed up the water-assisted spreading. For example, uniform saturation of whole TiO<sub>2</sub> pellets was achieved after 45 h at 95 °C, whereas the eggshell of about 0.6 mm thick was obtained at 25 °C after 52 h. The spreading over ZrO<sub>2</sub> pellets was considerably slower probably due to its lower S.A. in comparison with TiO<sub>2</sub>. Uniform Mo distribution was received after 20-day reaction including 75-hour heating at 95 °C.

Activity of the prepared and reference catalysts were tested in hydrodesulphurisation (HDS) of thiophene and benzothiophene after presulphiding in H<sub>2</sub>S/H<sub>2</sub> mixture. The uniformly saturated pellets were crushed to particle size 0.16-0.32 mm. Particles 0.16-0.32 mm of both carriers were also impregnated with (NH<sub>4</sub>)<sub>6</sub>Mo<sub>7</sub>O<sub>24</sub> for comparison. The thiophene test was used to evaluate the HDS activity and the benzothiophene test was chosen to evaluate both the HDS activity and the relative C=C hydrogenation/ C-S hydrogenolysis (HYD/HYG) selectivity of the deposited phase because it is believed that the HYD/HYG selectivity refers on quality of the active sites formed. It was determined that the samples obtained by solvent-assisted spreading exhibited the same activity and the HYD/HYG selectivity as the sample impregnated conventionally, which confirmed good dispersion of molybdenum species achieved by water-assisted spreading. MoO<sub>3</sub>/TiO<sub>2</sub> and MoO<sub>3</sub>/ZrO<sub>2</sub> catalysts, furthermore, exhibited relative HDS activity, normalized per gram of reference MoO<sub>3</sub>/Al<sub>2</sub>O<sub>3</sub> catalyst (15wt.% MoO<sub>3</sub>, S.A. 210 m<sup>2</sup>g<sup>-1</sup>, BASF M8-30, Germany), of about 1.5 and 1.0, respectively, and possessed similar relative selectivity as the reference catalysts. It was additionally concluded that quality of the active phase were basically the same over all the support studied and that the relatively high activity of the TiO<sub>2</sub> and ZrO<sub>2</sub> supported catalysts resulted from an increased number of the active sites deposited over those supports.

Financial support of the Grant Agency of the Czech Republic is gratefully acknowledged. L.K. acknowledges Grant No. 104/06/P034 and D.G., Z.V., and M.Z. acknowledge Grant No. 104/06/0705.

## Deactivation of Commercial SCR Vanadia-based Catalysts by Fuel Additives

F. Castellino, A.D. Jensen, J.E. Johnsson

*Department of Chemical Engineering, Technical University of Denmark, DK-2800 Kgs. Lyngby, Denmark*

### 1. Summary

Among the negative aspects of biomass firing at power stations, high rate of corrosive ash deposition on the super-heater exchanger and SCR catalysts deactivation are among the most important ones. The use of P-Ca-containing-additives to the biomass is considered by the Danish power companies as a promising way to solve the ash deposition-related problem.

In order to evaluate the effects of the addition of such species on the vanadia-based SCR catalysts, commercial full-length monoliths have been exposed in a SCR pilot-scale reactor to a flue gas containing the additives and the possible products of addition. The expositions have been carried out for up to 700 hours and the activity of the elements have been periodically measured during the whole exposure.

This presentation mainly focuses on deactivation by  $H_3PO_4$  and  $K_3PO_4$  aerosols, which are considered the main products of the addition process.

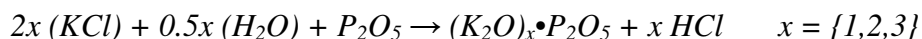
Keywords: SCR, deactivation, biomass combustion.

### 2. Extended Abstract

#### 2.1. Introduction

When biomass is fired at power stations, the resulting ashes are mainly constituted by KCl and  $K_2SO_4$ . These two compounds have a relatively low melting point temperature and so the ashes tend to stick on the super-heater surfaces reducing the heat transfer. Moreover, the chlorine present in the ashes makes the deposits very corrosive.

It has been shown that when a high molar ratio of P/(Na+K) (from 1.94 to 3.19) and a molar ratio of P/Ca from 0.78 to 0.88 is obtained during combustion, the ashes have a lower tendency to deposit, and, most importantly, almost all the chlorine is released in the gas phase according to the following reactions (Jensen et al., 2005):



In order to meet the above mentioned conditions, P and Ca may thus be added to the biomass during combustion. So far, orthophosphoric acid  $H_3PO_4$ , mono- and di-calcium phosphates have been tested as potential additives.

Both P and Ca are known to be mild poisons for the vanadia-based catalysts (Chen et al., 1990). However, very fast deactivation rates have been reported when burning P-rich fuels (Bech et al., 2005). Our investigations are aimed at i) clarifying the possible effects of the addition process on the activity of the SCR catalyst, thus supporting the Danish power companies in evaluating the global effects of the addition process on their power plants; ii) better understanding the mechanisms of deactivation due to P and K aerosols.

## 2.2. Experimental

The experiments are carried out at a pilot-scale reactor. The setup mainly consists of a 50 kW natural gas burner, a lance for injection of solutions in the flue gas, ammonia storage and addition line, and a reactor hosting an SCR catalyst monolith  $7.5 \times 7.5 \times 50 \text{ cm}^3$  in size. The catalysts employed are commercial full-length Haldor Topsøe A/S DNX 3%  $V_2O_5$ - $WO_3$ - $TiO_2$ . The activity measurements have been performed at  $350^\circ\text{C}$ , in the presence of 500 ppmv NO and 600 ppmv of  $NH_3$  in the pilot scale reactor. The catalyst activities are calculated assuming plug flow and a first order reaction. Different catalyst elements have been exposed to flue gases containing 10, 100, 1000 ppm of  $H_3PO_4$  and 10 ppm  $K_3PO_4$ . These have been introduced into the system by spraying a water solution of the different compounds directly into the hot flue gas. Both the aerosol particle sizes and concentrations at the inlet of the SCR reactor have been measured by a TSI SMPS. Both the fresh and the spent catalysts have been characterized by Hg-porosimetry, SEM analysis, chemical composition, FTIR and in-situ EPR.

## 2.3. Results

The addition of  $H_3PO_4$  resulted in the formation of a high particle concentration of sub-micron particles constituted by polyphosphoric acids. These were able to deactivate the catalyst both physically, by surface masking and pore blocking, and chemically, by reducing the redox properties of the element as shown by in-situ EPR measurements. It was shown that P may deactivate the catalyst extremely fast, in contrast to lab-scale tests, but in agreement with some full-scale tests.

The addition of  $K_3PO_4$  also resulted in a very fast deactivation. During the whole period of exposure (720 hours) the catalyst lost 1.2% of activity per day.

## References

- Beck, J., Muller, R., Brandenstein, J., Matschenko, B., Matschke, J., Unterberger, S. and Hein, K.R.G., (2005) *Fuel*, 84, 1911-1919
- Chen, J.P., Buzanowski, M.A. and Yang, R.T., (1990) *J. Air Waste Manage. Assoc.*, 40, 1403-1409
- Jensen, P.A., Sørensen, L.H., Hu, G., Holm, J.K., Frandsen, F. and Henriksen, U.B., (2005) *CHEC internal report*, Rep. No. 0504

## High Throughput Experimentation and Modeling as Tools for the Development of Green Alkylation Catalysts

E.A. Dejaegere, K. Mantri, G.V. Baron, J.F.M. Denayer

*Department of Chemical Engineering, Vrije Universiteit Brussel, Pleinlaan 2, B-1050 Brussels, Belgium*

### 1. Summary

For the development of green alkylation catalysts, research has been performed to predict the behavior of zeolite catalysts for the bromobenzene alkylation with allyl acetate. Reaction experiments were performed on a high throughput continuous flow parallel reactor setup with a frontal analysis technique. For the modeling of this data, a set of equations describing the chemical reaction, adsorption and deactivation effects was implemented in the Athena software package.

Keywords: modeling, alkylation, zeolite, high throughput

### 2. Extended Abstract

The general trend in industrial Friedel-Crafts reactions is to move towards greener chemistry and cleaner production. One of the alternatives to the traditional polluting Friedel-Crafts catalysts are zeolites. When a chemical reaction is performed on zeolites instead of in the homogeneous liquid phase, the entire process becomes more complex, as besides the chemical reaction itself, other processes also play a role. In the case of zeolites, it is well known that deactivation by products often occurs, mainly influenced by how the several components interact and adsorb in the zeolite pores. Strong adsorption of some of the reactants or products often negatively influences the efficiency of the chemical reaction (Mantri *et al.*, 2007).

In this study, a method is presented to extract critical information to understand what happens inside the zeolite packed reactor. As an example, the alkylation of bromobenzene with allyl acetate is performed on a high throughput continuous flow parallel reactor setup with a frontal analysis technique (Van der Beken *et al.*, 2005a). During the transient operation of reaction and deactivation, samples are collected and analyzed automatically. A detailed kinetic model was derived incorporating the main alkylation products (allylbromobenzene, cis- and trans-propenyl bromobenzene, each present in 3 isomeric forms and di-alkylated products), the side products (acetic acid and 1,2-propanediol diacetate) and the polymers causing deactivation. The model

obviously includes equations describing the deactivation and the adsorption equilibria inside the zeolite pores. Independent adsorption experiments are performed to complete the information fed to the model. The Athena software package was used to solve the set of equations. Model discrimination was performed between several possible reaction mechanisms, including several deactivation mechanisms (Van der Beken *et al.*, 2005b).

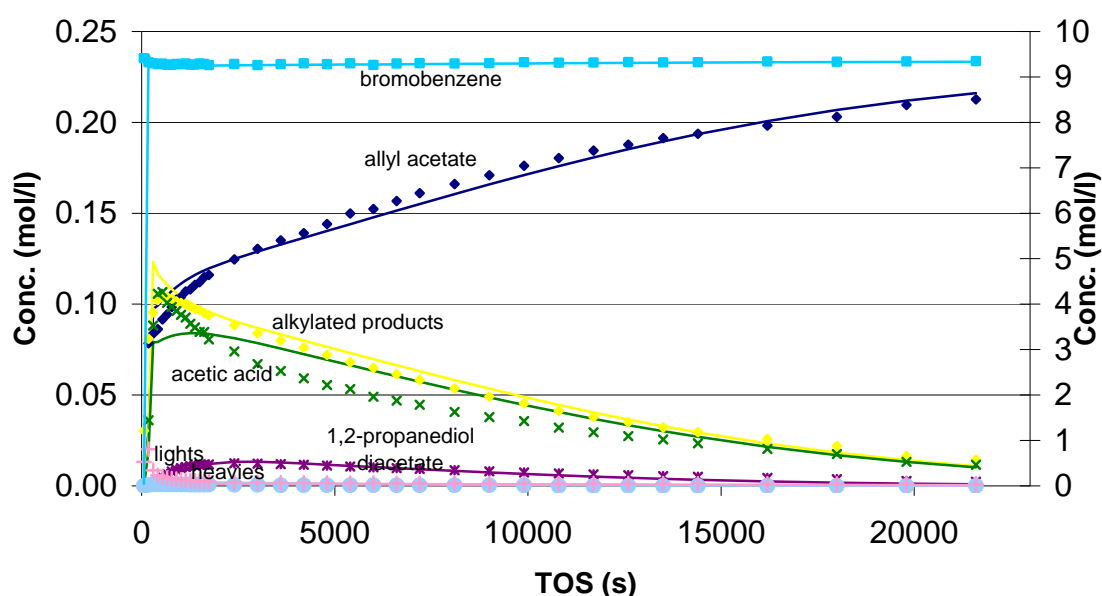


Figure 1: Reactor effluent for the alkylation of bromobenzene with allyl acetate: modeling (lines) of the experimental data (points).

In this way, the model is able to simultaneously predict the catalytic activity, the adsorption effects and clarify the process of deactivation. Such model can then be used for the selection of the best zeolite catalyst, and to derive the optimal operation conditions.

## References

- Mantri, K., Dejaegere, E., Baron, G.V., Denayer, J.F.M., (2007) *Applied Catalysis A: General*, 318, 95-107.
- Van der Beken, S., Dejaegere, E., Tehrani, K. A., Paul, J. S., Jacobs, P. A., Baron, G. V. and Denayer, J.F.M., (2005a) *Journal of Catalysis*, 235, 128–138.
- Van der Beken, S., Dejaegere, E., Verelst, H., Baron, G.V. and Denayer, J.F.M., (2005b) *International Journal of Chemical Reactor Engineering*, Volume 3, Article A23

## Session T2-13b: Catalysis - II

<b>Abstract Number</b>	<b>Paper Title &amp; Authors</b>	<b>Included</b>
1578	Thermal stability of SCR catalysts containing vanadia on silica-titania for the use in diesel applications C U I Odenbrand	Yes
875	Comparison of acid catalysts for the dehydration of methanol to dimethyl ether I Sierra, J Ereña, A T Aguayo, J M Arandes, A G Gayubo, J Bilbao	Yes
960	Photocatalytic reactivity of the titanium oxide loaded on a stainless steel screen by a spraying method F Shiraishi, T Itoh, Y Oda, H Nagayoshi, T Higuchi, K Tateishi	Yes
2966	Synthesis and characterization of copper-zirconia based catalysts for DeNOX in biomass fired units S B Rasmussen, J D Hansen, A L Kustov, A D Jensen, P Simonsen, R Fehrmann, M Yates, J Blanco	Yes





## **Thermal stability of SCR catalysts containing vanadia on silica-titania for the use in diesel applications**

C.U. Ingemar Odenbrand

*Department of Chemical Engineering, University of Lund, P.O. Box 124, SE-221 00 Lund, Sweden*

### **1. Summary**

The effect of reaction temperature, water content, and vanadia content on the sintering of vanadia on model silica-titania SCR catalysts has been investigated. A comparison is also made to a vanadia/titania catalyst submitted to conditions simulating at least 500 000 km driving on a diesel truck. The variation of the surface area, the XRD spectra including crystallite size on thermal treatment in dry and moist air was investigated. The support stabilises after 5 hours at 450 °C in wet and dry conditions. The support without vanadia sinters to a much lower degree than the complete catalyst. The vanadia crystallite size increases to fill the pores of the support. The effect of vanadia is to increase the rate of the conversion of the anatase phase of the support to rutile and to lower the transition temperature.

Keywords: Thermal stability, Vanadia based SCR catalysts, Diesel SCR catalysts

### **2. Extended Abstract**

The introduction of the SCR technique to reduce nitrogen oxides on diesel vehicles in 2005 has renewed the interest in these catalysts. There is very little information in literature about the thermal stability of these catalysts. That is why we conducted a study on this topic using model catalysts as well as a commercial one.

XRD (peak broadening) was used to determine the crystallite size. Adsorption of nitrogen at 77 K using either a one-point or a complete adsorption and desorption isotherm method was used to measure surface area and pore volume.

First we studied the sintering of the support (50/50 mol % TiO<sub>2</sub>/SiO<sub>2</sub>), the preparation and characterisation of which is given by Odenbrand et al. 1990. Before the sintering studies all materials were presintered at 450 °C for 5 hours in dry air. The XRD spectrum of the support, sintered at 450 °C, shows a typical anatase pattern and a broad peak for amorphous silica. The support surface area was stable after 5 hours at 450 °C both in dry and wet conditions.

The vanadia catalysts were prepared by an incipient wetness method for final contents of 10, 20 and 30 % V<sub>2</sub>O<sub>5</sub>. They were sintered for 5 hours at 500, 550 and 600 °C. The surface area decreased with an increased amount of vanadia at all temperatures and the

effect is largest at 600 °C. The 20 % catalyst was further sintered in 2 % water for times up to 350 hours. Both the size of the anatase and the vanadia domains increase rapidly with sintering time as shown in the Figure 1.

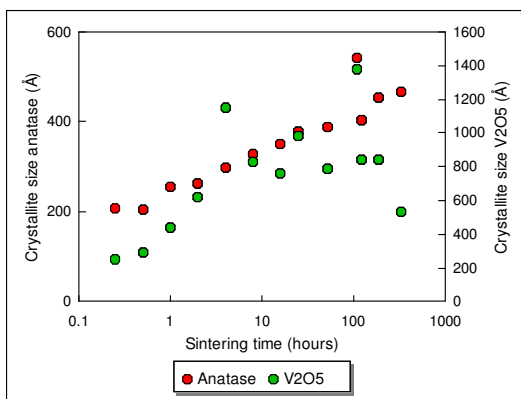


Figure 1. Sintering of 20 % V<sub>2</sub>O<sub>5</sub>/SiO<sub>2</sub>-TiO<sub>2</sub> at 450 °C in 2 % water vapour.

From fitting measured experimental surface areas to a SPLE model and determining the activation energy it was possible to simulate the surface area loss determined experimentally of a 5.6 % V<sub>2</sub>O<sub>5</sub>/TiO<sub>2</sub> monolithic catalyst deactivated on a rig at Volvo (Figure 2).

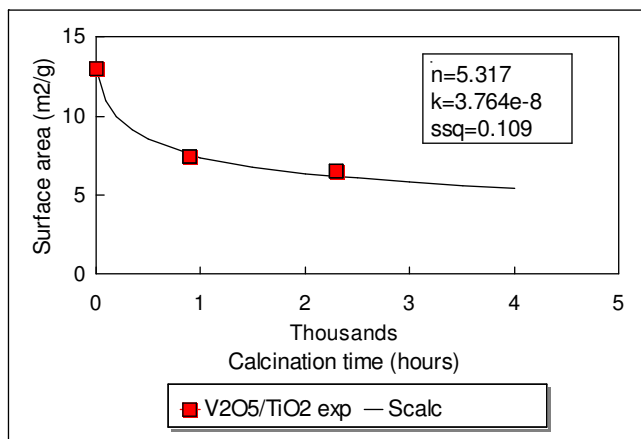


Figure 2. Sintering of 5.6 % vanadia on titania applied on a monolith at Volvo.

## References

Odenbrand, C.U.I., Andersson, S.L.T., Andersson, L.A.H., Brandin, J.G.M. and Busca G., (1990), *J. Catal.*, 125, 541-553.

## Comparison of acid catalysts for the dehydration of methanol to dimethyl ether

I. Sierra, J. Ereña, A. T. Aguayo, J. M. Arandes, A. G. Gayubo, J. Bilbao.

*Departamento de Ingeniería Química, Universidad del País Vasco, Apartado 644, 48080 Bilbao, Spain.  
Phone: +34-94-6015363, Fax: +34-94-6013500, e-mail: javier.arena@ehu.es*

### 1. Summary

The aim of this work is to compare the performance of three acid functions in the dehydration of methanol to dimethyl ether (DME):  $\gamma$ -Al<sub>2</sub>O<sub>3</sub>, NaHZSM-5 (obtained from NaZSM-5 zeolite subsequent to ion exchange) and HZSM-5 zeolite pretreated with NaOH. Ion exchange and treatment with NaOH allow for reducing the acidity of the zeolite, in order to favor methanol dehydration and to avoid the production of C<sub>1</sub>-C<sub>4</sub> paraffins, which is important at temperatures above 260 °C. In the 200-275 °C range, higher DME yields are obtained with the catalysts based on ZSM-5 zeolite than with the  $\gamma$ -Al<sub>2</sub>O<sub>3</sub>. Above 260 °C the catalyst that has been treated with NaOH performs slightly better than the one obtained by ion exchange.

Keywords: dimethyl ether, methanol dehydration, acid function

### 2. Extended Abstract

$\gamma$ -Al<sub>2</sub>O<sub>3</sub> acid function is used widely in the dehydration of methanol to dimethyl ether. Good performance is reported in the literature for this and other acid functions in the transformation of synthesis gas to DME in a single step on bifunctional catalysts such as CuO-ZnO-Al<sub>2</sub>O<sub>3</sub>/ $\gamma$ -Al<sub>2</sub>O<sub>3</sub> and CuO-ZnO-Al<sub>2</sub>O<sub>3</sub>/NaHZSM-5. These catalysts are made up of a metallic function for methanol synthesis and an acid function for the dehydration of methanol to DME (Ereña et al., 2005a,b).

The aim of this paper is to compare the performance of three acid functions in the second reaction step (dehydration of methanol to dimethyl ether). These acid functions are:  $\gamma$ -Al<sub>2</sub>O<sub>3</sub>, NaHZSM-5 (obtained from NaZSM-5 zeolite subsequent to ion exchange with 1M NH<sub>4</sub>Cl) and HZSM-5 zeolite pretreated with 0.2M NaOH dissolution. Both partial ion exchange and pretreatment with NaOH allow for obtaining moderate acid sites in the zeolite, which on the one hand are active in the dehydration of methanol and, on the other, are of low activity in the formation of hydrocarbons.

The following operating conditions have been used: temperature, in the 200-275 °C range; pressure, 15 bar; space time, 5.6 g of catalyst<sup>-1</sup> (mol of methanol)<sup>-1</sup>. DME yield ( $Y_{DME}$ ) has been measured as the percentage of carbon atoms fed in the methanol that converts to DME:

$$Y_{DME} = \frac{2n_{DME}}{(n_{MeOH})_0} 100 \quad (1)$$

where  $n_{DME}$  and  $(n_{MeOH})_0$  are the molar flowrates of DME in the product stream and of methanol in the feed.

As it is observed in Figure 1, higher DME yields are obtained with the catalysts based on ZSM-5 zeolite than with the  $\gamma$ -Al<sub>2</sub>O<sub>3</sub>. DME yield is almost the same (between 90 and 93 %) up to temperatures of 260 °C, for NaHZSM-5 and HZSM-5 pretreated with NaOH, and there is a slight difference above this temperature. The more severe treatment with NaOH allows for obtaining a zeolite with a more suitable acid strength for avoiding the formation of olefins and the decrease in DME yield.

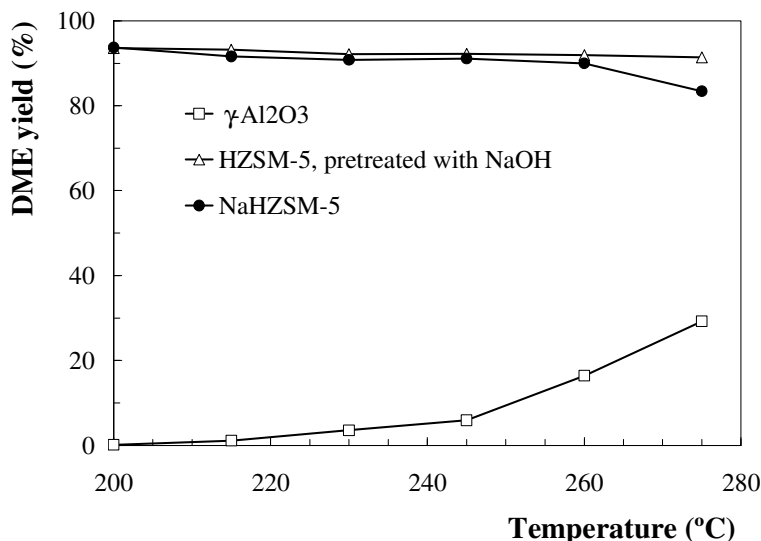


Figure 1. Evolution of DME yield with temperature for different acid catalysts.

## References

- Ereña, J., Garoña, R., Arandes, J. M., Aguayo, A. T. and Bilbao, J., (2005) *Int. J. Chem. Reactor Eng.*, 3, A44.  
 Ereña, J., Garoña, R., Arandes, J. M., Aguayo, A. T. and Bilbao, J., (2005) *Catal. Today*, 107-108, 467-473.

## Photocatalytic reactivity of the titanium oxide loaded on a stainless steel screen by a spraying method

F. Shiraishi<sup>a</sup>, T. Itoh<sup>a</sup>, Y. Oda<sup>a</sup>, H. Nagayoshi<sup>b</sup>, T. Higuchi<sup>b</sup>, K. Tateishi<sup>c</sup>

<sup>a</sup>Department of Systems Design, Bio-Architecture Center, Kyushu University, Fukuoka 812-8581, Japan

<sup>b</sup>FUJICO Co., Ltd., 4-31, Makiyamashinmachi, Kitakyushu 804-0054, Japan

<sup>c</sup>I-Quark Corporation, 1-36-14, Matsushima, Higashi-ku, Fukuoka 812-0062, Japan

### 1. Summary

To reduce a film-diffusional resistance in the very vicinity of the photocatalyst surface, titanium oxide particles are immobilized on a stainless steel screen by a spraying method and its performance is investigated by decomposing organic compounds in water. This preparation gives higher rates of decomposition under a condition of lower linear velocity. The preparation with uniformly distributed zeolite particles is further increased. A simple mathematical model is used to explain this phenomenon.

Keywords: photocatalyst, spraying method, water purification, film-diffusional resistance

### 2. Extended Abstract

The photocatalytic decomposition of organic compounds is strongly influenced by a large film-diffusional resistance. In the photocatalytic purification of air, it was relatively easy to remove this resistance by increasing the recirculation flow rate (Shiraishi *et al.*, 2003, 2005a & b). This operation was also effective in water systems (Shiraishi and Kawanishi, 2004; Shiraishi *et al.*, 2006); for instance,  $>0.8 \text{ m s}^{-1}$  with formic acid. However, such a high flow rate requires a high-performance pump and consumes a large amount of electricity. In addition, a shearing force by water causes a gradual exfoliation of the photocatalyst film.

There is a rust prevention technique called *spraying method*, in which fine metal particles are sprayed with a gun so that a stiff metallic film is formed on a solid plate. This method may be able to not only reduce the film exfoliation problem but also uniformly distribute adsorbent particles such as zeolite over the film of titanium oxide particles since these two types of particles can readily be well-mixed before spraying, which may be able to reduce the film-diffusional resistance remarkably at a lower linear velocity. In the present work, therefore, we examined the performance of the photocatalyst prepared by the spraying method by means of decomposing 2, 4-dinitrophenol (DNP) in water.

The batch-recirculation reactor system consisted of a peristaltic pump, perfectly-mixed flow vessel, and annular-flow type reactor with a 6W germicidal lamp (Shiraishi and Kawanishi, 2004). The stainless steel screen (wire diameter; 0.1 mm, gap between wires;

0.1 mm) was used as a support, on which titanium oxide particles or 3-10 % zeolite/titanium oxide particles were sprayed. This preparation (14mm×8.8mm) was rounded and then fixed in the reactor. The DNP concentration was determined by a spectrophotometer.

The initial rates of decomposition of DNP,  $\nu_0$ , were measured at various linear velocities of a reaction mixture in the range of 0-0.051 m s<sup>-1</sup>. The result is shown in Fig.1. The  $\nu_0$  value for the glass tube that loaded titanium oxide particles increased with an increase of the linear velocity and gave the highest value at above 0.037 m s<sup>-1</sup>. This variation is due to a reduction in the film-diffusional resistance with the increased linear velocity. The  $\nu_0$  value of the stainless steel screen that loaded titanium oxide particles was strongly influenced by the zeolite content. Even in the case of no zeolite content, the preparation gave a higher  $\nu_0$  value than the glass tube. In the case of 5%-zeolite content, the  $\nu_0$  value became higher at a lower linear velocity, probably because the photocatalytic decomposition was accelerated by the adsorption of DNP on titanium oxide itself and zeolite. However, the  $\nu_0$  value of the 10 %-zeolite content was lowered, probably due to a decreased amount of titanium oxide. A comparison of the experimental data at  $\nu_0=0.003$  m s<sup>-1</sup> clearly shows that the photocatalyst prepared by the spraying method has a higher activity at a lower linear velocity. The enhancement in the activity was successfully explained by a simple mathematical model.

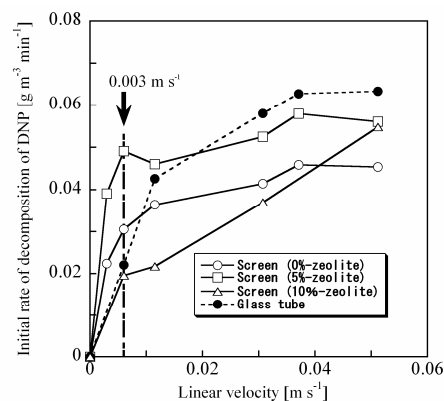


Fig.1 Relationship between initial rates of photocatalytic decomposition of DNP and linear flow velocity

## References

- Shiraishi, F., Yamaguchi, S., Ohbuchi, Y., (2003) *Chem. Eng. Sci.*, 58, 929-934.  
 Shiraishi, F., Ohkubo, D., Toyoda, K., Yamaguchi, S., (2005) *Chem. Eng. J.* 114, 153-159.  
 Shiraishi, F., Toyoda, K., Miyakawa, H., (2005) *Chem. Eng. J.*, 114, 145-151.  
 Shiraishi, F., Nagano, M., Wang, S., (2006) *J. Chem. Technol. Biotechnol.*, 81, 1039-1048.  
 Shiraishi, F., Kawanishi, C., (2004) *J. Phys. Chem.*, 108, 10491-10496.

## Synthesis and characterization of copper-zirconia based catalysts for DeNO<sub>x</sub> in biomass fired units

S.B. Rasmussen<sup>a,b,c</sup>, J. Due-Hansen<sup>b</sup>, A.L. Kustov<sup>b</sup>, A.D. Jensen<sup>c</sup>, P. Simonsen<sup>d</sup>, R. Fehrmann<sup>b</sup>, M. Yates<sup>a</sup>, J. Blanco<sup>a</sup>

<sup>a</sup>*Instituto de Catal sis y Petroleoqu mica, CSIC, C/Marie Curie no 2, Cantoblanco, 28049 Madrid, Spain*

<sup>b</sup>*Center for Sustainable and Green Chemistry, Department Chemistry, Technical University of Denmark, Denmark*

<sup>c</sup>*CHEC, Department of Chemical Engineering, Technical University of Denmark, S ltofts Plads, Building 22, DK-2800 Kgs. Lyngb, Denmark*

<sup>d</sup>*DONG Energy, Research & Development Dep., Teglholmen, A. C. Meyers V nge 9, DK-2450 Copenhagen SV, Denmark*

### 1. Summary

Selective catalytic reduction (SCR) of nitric oxide with ammonia performed in boiler units based on biomass combustion, suffer from a number of deactivation phenomena due to the exposure to alkali containing particulates. Apart from fouling and coating, the industrial V<sub>2</sub>O<sub>5</sub>/TiO<sub>2</sub> based catalyst also suffer from chemical deactivation due to a reaction between alkali salts from the particulates with the active V=O and V-OH sites on the catalyst. The effect of alkaline metals on the activity of V<sub>2</sub>O<sub>5</sub>/TiO<sub>2</sub> catalysts has been reported by several authors [1-4]. Most of them conclude that poisonous additives affect the Br nsted acid sites which are responsible for the ammonia adsorption, thus decreasing both their number and activity in NO reduction. Use of biomass as an alternative to fossil fuels is desirable, since it is considered as a CO<sub>2</sub> neutral fuel, regarding human impact on the CO<sub>2</sub> release to the atmosphere. Therefore new DeNO<sub>x</sub> catalysts more resistant to deactivation by alkali metals are needed. One of the possible ways to increase catalyst resistance to alkaline poisons is the use of supports, revealing high or super-acidic properties which would interact more strongly with potassium than vanadium species. Since potassium oxide affects Br nsted acid sites of the catalyst to a much larger extent than Lewis sites, another possible solution for NO removal in biomass-related applications is the use of other metal oxides as active components, which posses mainly Lewis acidity [2]. In this context we have synthesised and studied CuO<sub>x</sub>/ZrO<sub>2</sub>-SO<sub>4</sub> catalysts with respect to the performance of NH<sub>3</sub>-SCR in biomass fired boiler units. We find that the optimal loading of our catalysts is 3 wt % CuO, both in terms of activity and selectivity.

Keywords: NH<sub>3</sub>-SCR, Biomass, ZrO<sub>2</sub>-SO<sub>4</sub>, Copper, deactivation

## 2. Extended Abstract

The catalytic reduction of NO<sub>x</sub> with ammonia increases with the CuO loading up to 3 wt %, as seen from Figure 1. At higher loadings powder XRD measurements revealed formation of crystalline CuO commences. Furthermore, as shown in Figure 2, the selectivity, expressed as the molar consumption ratio between NO and NH<sub>3</sub>, also exhibit a maximum for the 3 wt % CuO/ZrO<sub>2</sub>-SO<sub>4</sub> catalyst. Thus, it appears that non-crystalline dimeric and polymeric CuO species are responsible for the catalytic activity. A conformed (plates) catalyst of this type is currently being tested in a biomass fired power plant, where prolonged exposure to fly ash from straw combustion will reveal whether the increased resistance towards alkali poisoning observed at laboratory scale [5], also translates into an improved catalyst at industrial scale.

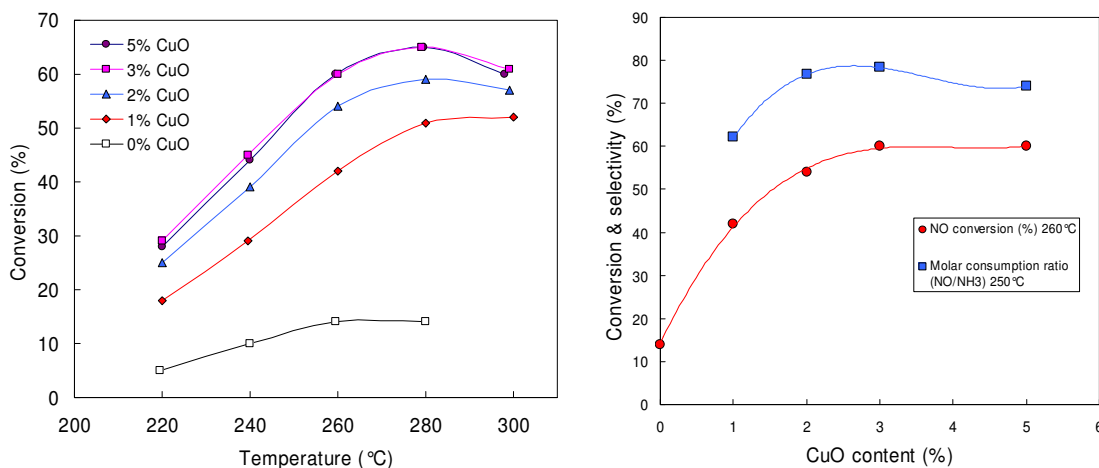


Figure 1 (left) & 2 (right): 1) Conversions of NO by NH<sub>3</sub>-SCR for different metal oxide loadings of CuO on ZrO<sub>2</sub>-SO<sub>4</sub>. The operating conditions were: [NO] = 500 ppm, [NH<sub>3</sub>] = 500 ppm, [O<sub>2</sub>] = 3 vol.%, balance in N<sub>2</sub>, GHSV(N.T.P.) = 36000 h<sup>-1</sup>. 2) Conversion and molar consumption ratio as a function of CuO content at 260°C.

### Acknowledgements

The authors gratefully acknowledge the CYTED Program (Project V 7), the CAM (project ref: GR/AMB/0751/2004), the ELFOR PSO FU520 project as well as LAB S.A. for financial support.

### References

- J. Chen, R. Yang, *J. Catal.* 125 (1990) 411.
- H. Kamata, K. Takahashi, C.U.I. Odenbrand, *J. Mol. Catal. A* 139 (1999) 189.
- I.E. Wachs, B.M. Weckhuysen, *Appl. Catal. A* 137 (1997) 67.
- D. Bulushev, F. Rainone, L. Kiwi-Minsker, *Langmuir* 17 (2001) 5276.
- A. L. Kustov, S. B. Rasmussen, R. Fehrmann, and P. Simonsen, *J. Appl. Catal. B*. Accepted.



## Session T2-13c: Catalysis – III

Abstract Number	Paper Title & Authors	Included
247	Oxidative dehydrogenation of propane under steady-state and transient regimes over alumina-supported isopolyanionic catalysts S Paul, M F Kaezar, J G Eon	Yes
417	Catalytic wet air oxidation of aqueous solution of phenol over Pt/CNF catalysts C Díaz, G Ovejero, A Rodríguez, J García	Yes
926	Effect of tetralol and tetralone in the tetralin oxidation with copper and chromium heterogeneous catalysts O Casanova, R Galiasso, A Corma	Yes
1898	Catalytic wet peroxide oxidation of phenol over Cu/ZSM-5 catalyst K M Valkaj, I Kranjčec, O Wittine, A Katović, S Zrnčević	Yes
3261	High Throughput Experimentation and Modeling as Tools for the Development of Green Alkylation Catalysts E A Dejaegere, K Mantri, G V Baron, J F M Denayer	Yes
3688	Phase Transfer Catalysis-Continuous Contact T Sankarshana, J S Murthy, A A kumar	Yes
4070	Methane catalytic decomposition over Cu-Ni-Al catalyst: reaction rate and catalyst regeneration T E Machado, M A Lansarin, O W P Lopez	Yes

Session T3-13c

## **Oxidative dehydrogenation of propane under steady-state and transient regimes over alumina-supported isopolyanionic catalysts**

S. Paul<sup>a</sup>, M. França Kaezar<sup>b</sup>, J.G. Eon<sup>b</sup>

<sup>a</sup>*Unité de Catalyse et de Chimie du Solide (UMR CNRS 8181), Ecole Centrale de Lille, Cité Scientifique BP48, 59651 Villeneuve d'Ascq Cedex, France*

<sup>b</sup>*Instituto de Química, Universidade Federal do Rio de Janeiro – Cidade Universitaria, Ilha do Fundão, 21945-970 Rio de Janeiro, Brazil*

### **1. Summary**

This communication deals with the oxidative dehydrogenation (ODH) of propane into propylene. A global approach integrating the development of an innovative catalyst coupled to the development of a new process is followed. The opportunity of using a reactor working in transient conditions is actually studied to take into account the specific properties of the ODH reaction. In this work the preparation method, characterization and performances for the steady-state and the transient regimes of catalysts based on the  $V_2W_4O_{19}^{4-}$  Linqvist isopolyanion and supported on alumina are presented. The influence of the countercations and the role of water in the feed gas are more particularly discussed. To get these results it has been necessary to specially design a polyvalent experimental set-up, which is also described in details in this communication.

Keywords: heterogeneous catalysis, propane, oxidehydrogenation, steady-state and transient reactors, Linqvist isopolyanions.

### **2. Extended Abstract**

The world economy is growing rapidly, implying a strong demand in raw materials. In this context, the so-called oil depletion and, in a further future, of natural gas and the concomitant increase of their prices incite to a more rational use of these natural resources. For instance it is proposed to use light alkanes (ethane, propane, isobutane...) as sources of important intermediates of the chemical industry (olefins, acids, aldehydes...) instead of mainly burning them to produce energy. The low costs of these materials are of course encouraging these developments at an industrial scale.

This work deals with the oxidative dehydrogenation (ODH) of propane into propylene. This reaction might be in a near future a complementary way of production of propylene today mainly produced by vapocracking. The drawback of this process is the simultaneous production of ethylene which demand is increasing at a lower rate than the propylene one.

It is generally admitted that the use of alkanes will only be possible if a global approach integrating the developments of new catalysts (active, selective and stable) and of new processes probably including new types of reactor in order to take into account the specific properties of oxidation reactions. As a matter of fact the well-known fixed-bed reactor technology does not seem to be adequate because of the important exothermicities of the reactions involved.

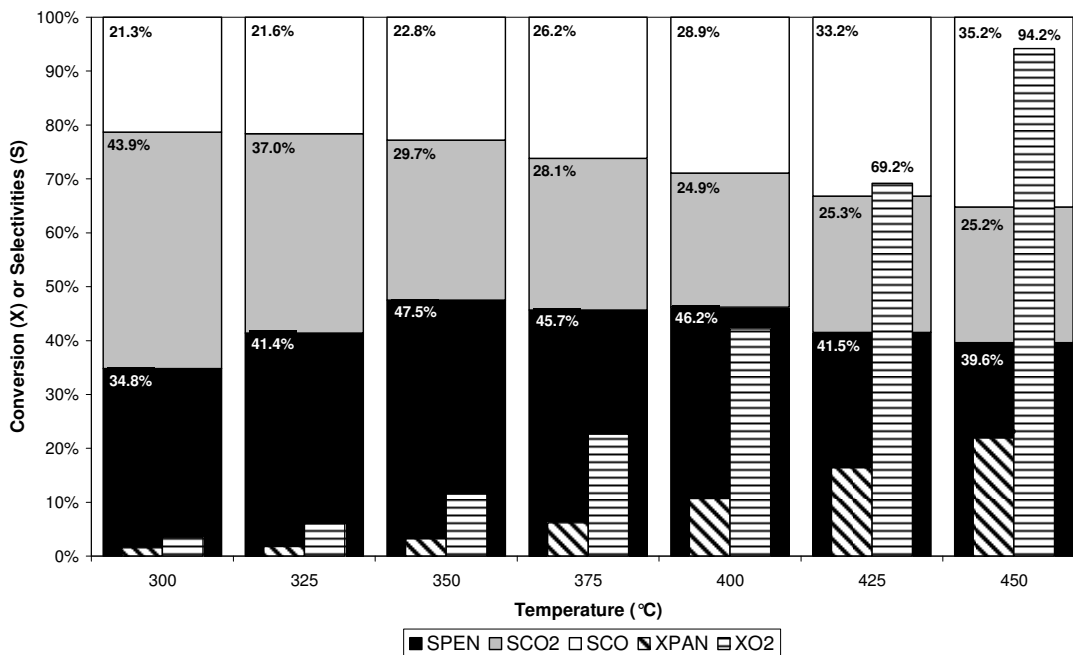
One of the proposed solutions is to separate the reduction and oxidation steps of the catalyst (redox decoupling). In this case the catalyst is used as an oxygen reservoir when placed in contact with the hydrocarbon and should be able to be reoxidized without loss of performances in a further reductive step.

In this work a global approach integrating the simultaneous developments of an innovative catalyst coupled to those of a new process is followed. To this aim a polyvalent laboratory experimental set-up has been designed. It is described in details in this communication. It allows carrying out catalytic tests in both the transient and steady-state regimes.

The preparation method, characterization and performances in the propane ODH in steady-state and transient regimes of innovative catalysts based on the  $V_2W_4O_{19}^{4-}$ -Linqvist isopolyanion and supported on alumina are also presented. As an example of the results presented in this communication the role of the temperature on the catalytic performances of  $Na_4V_2W_4O_{19}$  catalyst supported on alumina is shown on Figure 1.

The influence of the counteraction and the role of water in the feed gas are more particularly discussed in the communication.

Figure 1: Catalytic performances of  $Na_4V_2W_4O_{19}$  catalyst supported on alumina vs temperature (dry conditions).



## Catalytic wet air oxidation of aqueous solution of phenol over Pt/CNF catalysts

C. Díaz,<sup>a</sup> G. Ovejero,<sup>a</sup> A. Rodríguez,<sup>a</sup> J. García<sup>a</sup>

<sup>a</sup>*Grupo de Catálisis y Procesos de Separación (CyPS). Departamento de Ingeniería Química, Universidad Complutense de Madrid. Avda. Complutense s/n, 28040 Madrid, Spain.*

### 1. Summary

Catalytic wet air oxidation (CWAO) of phenol, as model organic compound of many industrial wastewaters, was investigated using 2 wt.% platinum supported on commercial carbon nanofibers (CNFs) as catalyst in a continuous trickled bed reactor. The effect of process parameter like temperature, pressure, catalyst load, air and liquid flow rates, has been studied. Samples were taken periodically to measure phenol conversion as well as total organic carbon (TOC) evolution. High phenol conversion and TOC removal can be reached over this catalyst at mild reaction temperature (433 K) and moderate pressure (2.0 MPa). According to the results, a Langmuir-Hinshelwood kinetic model was used to fit experimental data.

### 2. Extended Abstract

During the past two decades, carbon nanofibers (CNFs), including multiwalled carbon nanotubes (MWNTs), have attracted extensive interest and attention from both academia and industry. Due to their novel physico-chemical and mechanical properties, CNFs exhibit growing perspectives in a number of potential applications, especially in heterogeneous catalysis (G. Ovejero, 2006). One of the advantages of CNFs used as catalysts and catalyst supports is the possibility of tailoring their microstructures by proper selection of preparation method and controlling their surface chemistry via surface modification (P. Serp, 2003).

Therefore, the main objective of this work has been the study of variables that concern the CWAO of phenol in continuous operation, using platinum catalysts supported on CNFs.

The commercial carbon support does not possess a high amount of functional groups on its surface, so it was subjected to an acid treatment with nitric acid 5 M. The platinum supported on CNF catalysts was prepared by incipient wetness using an aqueous solution containing an appropriate amount of  $\text{PtCl}_4(\text{NH}_4)_2$ . The Pt load was fixed in 2 wt.%. The activation of the catalyst was performed by reduction under  $\text{N}_2/\text{H}_2$  (2:1) atmosphere at 623K.

The characterization of the catalyst was done by means of transmission electron microscopy (Figure 1b), XRD and  $\text{N}_2$  physisorption (244 and 188  $\text{m}^2/\text{g}$  BET surface for the support, CNF, and the catalyst, Pt/CNF, respectively, Figure 1a).

The catalytic activity of the prepared catalysts was verified by tests realized in a continuous trickled bed reactor, taking samples with reaction time.

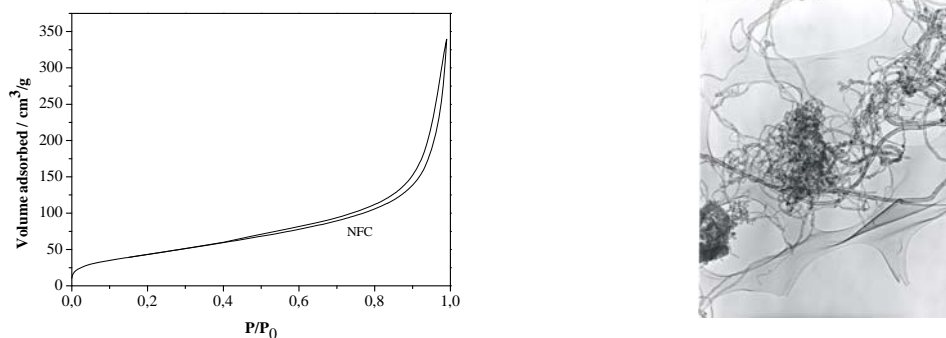


Figure 1: N<sub>2</sub> adsorption/ desorption isotherm and TEM micrograph of CNF.

Samples were analyzed in a high performance liquid chromatography (HPLC), to identify the products of the reaction, and total organic carbon (TOC) was determined. The operational variables studied were: pressure, temperature, catalyst load, air and liquid flow rates. The results are shown in Table 1.

Table 1: Catalytic wet air oxidation of phenol

Run	P (MPa)	T (K)	Q <sub>Phe</sub> (mL/min)	Catalyst load (g)	Q <sub>air</sub> (mL/min)	X <sub>phe</sub> (%)	X <sub>TOC</sub> (%)
1	2.0	433	0.5	0	300	1.30	4.8
2	2.0	433	0.5	1	300	96.9	81.6
3	1.0	433	0.5	1	300	72.9	68.3
4	3.0	433	0.5	1	300	98.6	28.4
5	2.0	433	0.5	1	300	90.6	32.2
6	2.0	453	0.5	1	300	93.7	87.0
7	2.0	433	1	1	300	78.2	65.9
8	2.0	433	2	1	300	64.7	50.6
9	2.0	433	0.5	0.5	300	69.8	60.0
10	2.0	433	0.5	2	300	99.7	93.2
11	2.0	433	0.5	1	150	76.1	72.4
12	2.0	433	0.5	1	400	95.7	65.1

The experimental dates were satisfactory fitted to a Langmuir-Hinshelwood kinetic model. The conversion of phenol increases with the temperature, pressure and catalyst load.

It was demonstrated that Pt/CNF is an efficient catalyst for the CWAO of phenol. High phenol conversion and TOC removal can be reached over this catalyst at mild reaction temperature (433 K) and moderate pressure (2.0 MPa).

## References

- [1] Ovejero G., Sotelo J. L., Romero M. D., Rodríguez A., Ocaña M. A., Rodríguez G., García J. (2006). *Industrial Engineering Chemistry and Research*, 45, 2206-2212.
- [2] Serp P., Corrias M., Kack P. (2003). *Applied Catal. A*, 253, 337-358.

## Acknowledgement

The authors gratefully acknowledge the financial support from MEC (Grant: CTQ2004/05141) and by Comunidad de Madrid through REMTAVARES Network S-505/AMB/0395.

## **Effect of tetralol and tetralone in the tetralin oxidation with copper and chromium heterogeneous catalysts**

O. Casanova, R. Galiasso, A. Corma

*Instituto de Tecnología Química (UPV-CSIC) Av. Naranjos, 46022 Valencia, Spain*

### **1. Summary**

The production of oxygenated organic derivatives is an area of high interest in the field of chemicals and petrochemicals. A comparison between the oxidation of tetralin under mild conditions with air using Cu and Cr/PVP catalysts has demonstrated that Cu/PVP is able to perform this reaction efficiently yielding tetralone preferentially. Tetralol has proved to act in that case as a catalytic inhibitor, however in Cr/PVP catalysts this was not observed. Characterization of both fresh and used catalysts with FTIR, CNMR and magnetic measurements brings to light both metal-pyridine coordination and the adsorption of products during the reaction, in order to explain the mechanism of the reaction.

Keywords: tetralin oxidation, Cu/PVP, Cr/PVP catalyst, tetralol

### **2. Extended Abstract**

The oxidation of naphteno-aromatics molecules is important in the production of oxygenated diesel to reduce emissions, as well as for the Fine Chemistry Industry to produce ketone type derivatives. In particular the development of a selective catalyst able to perform this oxidation with high stability is an important area of research. In this paper we have studied the conversion of tetralin into tetralone – probe type molecules for the oxidation reactions- using air, Cu/PVP and Cr/PVP catalysts.

The kinetics of the reaction was studied in a semi continuous stirred tank reactor in presence of different concentration of products (tetralone and tetralol) and time on stream, to study their effect on catalyst activity, selectivity and stability. The products were analyzed by GC-MS and the solid characterized by chemical analysis, FTIR, CNMR, and magnetic measurements. We have found that tetralin is oxidized via adsorption on the metal and then transformed into an on-surface peroxide. That starts the cycle of oxidation which progresses towards ketone, alcohol and polyoxygenated products by reducing the metal. The presence of oxygen regenerates the active species. The work shows that for Cu/PVP (poly(4-vinylpyridine)) catalysts, the presence of tetralol at a certain concentration inhibits the reaction (90°C, atmospheric pressure, and bubbling air for 24 hours). If tetralol was added either at the beginning or after starting

the reaction, this was inhibited; however if the selectivity to tetralone was high enough, i.e. tetralol is rapidly oxidized, the level of alcohol in the reaction media is always low, and the oxidation smoothly progresses. When  $\text{Cr}^{+3}$  is used instead of  $\text{Cu}^{+2}$ , the catalytic behavior changes and the inhibiting effect of tetralol is lower. It was also verified that the partial reoxidation of tetralol occurred faster with Cr/PVP and that tetralone did not inhibit the reaction. FTIR characterization of both fresh and used catalysts revealed that the C-N stretching band shifts towards higher wavenumber due to metal coordination. The intensity of the IR band decreases as a result of tetralol adsorption onto the metal site. The preferential adsorption of tetralol, results in gradual loss of activity since no metal leaching was detected. Catalysts were reused three times without an observable decrease in activity. However, the presence of adsorbed species retarded the start up of the reaction (induction period) when used catalysts were employed and no conversion was detected before 8 hours. Magnetic measurements of the spent catalyst provide additional information to this respect. The paper discusses the mechanism of reaction.

## **References**

- Corma, A., García, H., (2002) *Chemical Reviews*, 102, 3837-3892.  
Goe, G., Marston, C., Scriven, E. and Showers, E. “*Applications of Pyridine Containing Polymers in Organic Chemistry*”, Prentice Hall, (1990).



## Catalytic wet peroxide oxidation of phenol over Cu/ZSM-5 catalyst

K. Maduna Valkaj<sup>a</sup>, I. Kranjčec<sup>a</sup>, O. Wittine<sup>a</sup>, A. Katović<sup>b</sup>, S. Zrnčević<sup>a</sup>

<sup>a</sup>University of Zagreb, Faculty of Chemical Engineering and Technology, 10000 Zagreb, Marulićev trg 19, Croatia

<sup>b</sup>Università della Calabria, Dip. Ingegneria Chimica e dei Materiali, Rende, Italia

### 1. Summary

In this work oxidation of phenol with hydrogen peroxide on Cu/ZSM-5 catalyst prepared by direct hydrothermal synthesis was studied. Characterization of the catalyst extends to X-ray diffraction (XRD), and scanning electron microscopy (SEM), while the adsorption techniques were used for the measurement of the specific surface area.

The catalytic test was carried out in a stainless steel Parr reactor in batch operation mode at the atmospheric pressure and the temperature range from 323 to 353 K. The mass ratio of the active metal component on the zeolite was in the range of 1.62-3.24 wt. %. The initial concentration of phenol and hydrogen peroxide was 0.01 mol dm<sup>-3</sup> and 0.1 mol dm<sup>-3</sup>, respectively. The influence of catalysts preparation method on their catalytic performance was monitored in terms of phenol conversion and degree of metal leached into aqueous solution.

Keywords: wastewater treatment; pollutant degradation, catalyst preparation, phenol oxidation, kinetics modeling

### 2. Extended Abstract

Organic compounds, which are extremely toxic and refractory in nature, are common pollutants in many industrial wastewaters. To remove the pollutants there are many remediation technologies, of which only reactive destruction results in the mineralization of the waste. CWAO is an efficient technique to eliminate a variety of organic compounds from wastewater, but the reaction is performed at high operating pressure from 1 to 10 MPa and high temperature from 80 °C to 200 °C, which makes the investment rather costly. But if hydrogen peroxide is used as an oxidant, reaction can be performed under atmospheric pressure and temperature below 323 K on a great number of different catalysts, as example different metals supported on metal oxides, clays, graphite, polymers, and carbon, supported and unsupported metal oxides and so on.

Therefore, in this research heterogeneous CWPO was studied as an organic wastewater treatment technology using phenol as a model compound, because phenol and its derivatives are a common industrial pollutant found in many wastewaters. The objectives

of this study were to investigate the activity and stability of Cu/ZSM-5 catalyst prepared by direct hydrothermal synthesis.

The kinetic experiments and activity tests were carried out in stainless steel Parr reactor in batch operation mode at temperature between 50 °C and 80 °C and atmospheric pressure. The mass ratio of the active metal component on the zeolite was in the range of 1.62-3.24 wt. %, and the initial concentration of phenol and hydrogen peroxide was 0.01 mol dm<sup>-3</sup> and 0.1 mol dm<sup>-3</sup>, respectively. A detailed description of the experimental procedure is found elsewhere (Zrnčević and Gomzi, 2005). The catalyst samples (Cu/ZSM-5) were prepared by direct hydrothermal synthesis. Catalyst preparation method was described elsewhere (Maduna Valkaj et al., 2006). Characterization of the catalysts extends to X-ray diffraction (XRD) and scanning electron microscopy (SEM), while the adsorption techniques were used for the measurement of the specific surface area. The stability of the catalyst samples to leaching of the active metal ingredient was verified by atomic absorption of the filtered solution samples.

The obtained experimental data was tested to a proposed kinetic model for phenol oxidation and hydrogen peroxide decomposition.

$$-\frac{dc_{\text{Ph}}}{dt} = k_{\text{Ph}} c_{\text{Ph}}^n c_{\text{HP}} \quad (1)$$

$$-\frac{dc_{\text{HP}}}{dt} = k_{\text{HP}} c_{\text{HP}} + k_{\text{Ph}} c_{\text{Ph}}^n c_{\text{HP}} \quad (2)$$

The kinetic parameters in eqs. 1 and 2 were estimated using the Nelder-Mead method of nonlinear regression. The rate of phenol oxidation is almost second order toward the concentration of phenol and first order toward the concentration of H<sub>2</sub>O<sub>2</sub>. The rate of H<sub>2</sub>O<sub>2</sub> decomposition is the sum of rates of phenol oxidation and peroxide decomposition.

Table 1. Effect of Cu loading on the rate constant in phenol removal and hydrogen peroxide decomposition at different temperatures.

Y <sub>Cu</sub> , wt. %	k <sub>Ph</sub> · 10 <sup>3</sup> , dm <sup>3</sup> mol <sup>-1</sup> min <sup>-1</sup>						k <sub>HP</sub> · 10 <sup>3</sup> , min <sup>-1</sup>						E <sub>a</sub> , kJ mol <sup>-1</sup>	
	50 °C	55 °C	60 °C	65 °C	70 °C	80 °C	50 °C	55 °C	60 °C	65 °C	70 °C	80 °C	Ph	HP
<b>1.62</b>	2.67	3.97	8.48	16.23	20.65	45.40	0.72	0.88	0.24	3.39	5.33	11.01	92.45	90.62
SD · 10 <sup>3</sup>	4.5	4.3	5.5	11.0	9.5	7.5	4.5	4.3	5.5	11.0	9.5	7.5		
<b>2.75</b>	3.40	5.25	9.82	24.50	23.15	67.20	1.49	2.04	6.45	11.81	5.35	15.52	85.10	73.88
SD · 10 <sup>3</sup>	5.7	4.5	5.0	15.3	11.0	15.0	5.7	4.5	5.0	15.3	1.1	1.5		
<b>3.24</b>	8.98	10.53	24.87	69.30	41.88	97.10	3.46	3.11	7.16	24.21	8.72	19.41	66.20	47.81
SD · 10 <sup>3</sup>	5.7	10.6	5.0	11.1	11.0	15.0	5.7	10.6	5.0	11.1	11.0	15.0		

SD - standard deviation of measured and calculated values

It can be seen (table 1) that the increasing the temperature and loading of catalytic active material on catalyst support have a profound effect on rate constants for phenol oxidation and peroxide decomposition.

## Reference

Maduna Valkaj, K., Katović, A. and Zrnčević, S., (2007) *Journal of Hazardous Material*, 144, 663-667.

Zrnčević, S. and Gomzi, Z., (2005) *Industrial Engineering Chemical Research*, 44, 6110-6114.

## Phase Transfer Catalysis-Continuous Contact

Talapuru Sankarshana, Josyula Suryanarayana Murthy, Adla Anil kumar

*University College of Technology, Osmania University, Hyderabad – 500 007, India.*

### 1. Summary

Most of the reactions using phase transfer catalysis are carried out in batch operation. However the separation of the catalyst after the reaction is not economical. Hence the catalyst is supported on solids like polymer, silica gel etc which can be easily separated and the reactions can be carried out under continuous conditions. But in this case, it is reported that the rate of reaction decreases to a large extent. In the present study reactions were carried out under continuous conditions and the phase transfer catalyst was used without the support. Continuous contact column was used to study the reaction of n-hexanol in benzene by potassium permanganate in aqueous phase employing the phase transfer catalyst, Aliquat 336. This catalyst is insoluble in the aqueous phase but soluble in the organic phase. Oxidation of n-hexanol by potassium permanganate renders the product in aqueous phase, which is processed for the product. The organic phase containing the catalyst and n-hexanol can be recycled.

Keywords: continuous contact, phase transfer catalysis

### 2. Extended Abstract

When two immiscible liquids containing reactants are brought together the reaction will be slow or will not take place at all due to inaccessibility of the reactants. The reaction can be made faster by adding a little amount of phase transfer catalyst. These types of reactions have been investigated mostly using batch reactors. The catalyst will be present in one of the phases or either of the phases depending on their solubility. The removal of the catalyst which is present in small quantities, after the reaction will be cumbersome and the reactions cannot be carried out under continuous conditions. Hence some of the reactions were investigated by supporting the catalyst on solids like polymer, silica gel, alumina etc. In such cases removal of catalyst becomes easy and also the reactions can be carried out under continuous flow conditions. However the literature indicates, in most of the cases the rate of reaction decreases when the catalyst is supported on a solid compared to when it is not supported. But with catalysts which are soluble in one of the phases and the product formed in the other phase, the reactions can be carried under continuous contact conditions. In the present study, the aqueous phase containing potassium permanganate is used to oxidize n-hexanol in benzene phase. The phase transfer catalyst is tri caprylyl methyl ammonium chloride (Aliquat 336) and is insoluble in the aqueous phase. The product thus formed will be in the aqueous phase.

Under continuous contact conditions, the aqueous phase containing the product can be easily separated from the organic phase. The organic phase containing unconverted alcohol and the catalyst can be recycled. For this a column of 0.7 m in length and 0.01m in diameter was used. The inlets for organic and aqueous phases were at the bottom. The organic liquid was dispersed in the aqueous phase under continuous co-current conditions. At the outlet(top) the two phases were separated and analysis was made when required. The experimental runs were made for different flow rates of organic and aqueous phases and also varied the catalyst and alcohol concentration in the organic phase.

The enhancement in the conversions was observed with the catalyst. The rate of extraction of potassium permanganate was found to increase with the catalyst concentration. With increase in n-hexanol concentration the rate of extraction was found to remain same. For a particular concentration of the catalyst the extent of extraction decreased with the flow rate of potassium permanganate solution. With increase in the flow rate of organic phase, the percentage of extraction of potassium permanganate increased. A model equation has been developed.

## **Methane catalytic decomposition over cu-ni-al catalyst: reaction rate and catalyst regeneration**

T. E. Machado, M. A. Lansarin, O. W. Perez-Lopez

*Departamento de Engenharia Química – Universidade Federal do Rio Grande do Sul, Rua Eng. Luiz Englert s/n. CEP 90040-040, Porto Alegre, RS, Brasil. E-mail - marla@enq.ufrgs.br*

### **1. Summary**

The objective of this work is the kinetic study and the reaction rate determination of methane catalytic decomposition over Cu-Ni-Al catalyst for pure hydrogen production. The reaction was carried out in a thermobalance with different temperatures (500 to 600°C) and methane concentrations (0.5 to 1.2 mol m<sup>-3</sup>) to determining the reaction rate. It was observed that the reaction is of first order, with activation energy of 50655 J mol<sup>-1</sup>. The reaction also forms carbon. The carbon oxidation for catalyst regeneration was also investigated. Repeated reaction-regeneration cycles were carried out, being the regeneration composed by oxidation or by oxidation and reduction. The oxidation was carried out at different temperatures (500 to 600°C) and times (20 to 75min) The best regeneration condition was determined. It was also observed that the deposited carbon is in the nanotubes form, which has exceptional properties. The structure of carbon nanotubes formed during the reaction was analyzed by Scanning Electron Microscopy (SEM).

Key words: hydrogen (production); natural gas; methane decomposition; coprecipitated catalyst; carbon nanotubes.

### **2. Extended Abstract**

The objective of the present work is the kinetic study and determination of the methane catalytic decomposition reaction rate ( $\text{CH}_4 \rightarrow \text{C} + \text{H}_2$ ) over Cu-Ni-Al catalyst in order to produce high purity hydrogen. The regeneration on the catalyst was also studied by oxidation of the produced carbon.

The catalyst was prepared by continuous co precipitation method, starting from solution metals nitrate and sodium carbonate as precipitating. After the precipitate will be crystallized, filtrate and dried, samples were calcined at 600°C, using synthetic air. The activation was carried out with a H<sub>2</sub>/N<sub>2</sub> mixture. Than the methane decomposition was carried out with CH<sub>4</sub>/N<sub>2</sub> mixtures at different temperatures, during two hours. More details can be found else where (Machado, 2007). The catalytic tests were carried out in a thermobalance SDT Q600 of TA instruments.

The effects of diffusion in porous catalyst and of the operation conditions in the reaction rate were appraised. In the studied conditions, the diffusion effect is not limiting.

The Cu-Ni-Al co-precipitated catalyst stability was shown for temperatures above 500°C, and it began to lose activity at 700°C. So, the temperature range chosen for tests were 500 to 600°C. The catalyst was shown quite stable up to nine hours of reaction, when the test was interrupted due to pan capacity limitation.

The methane decomposition was carried out under different temperatures and methane concentrations for reaction rate determination. Methane concentrations between 0.5 and 1.25 gmol m<sup>-3</sup> were used. The reaction rate grows quickly in the initial minutes and then, after 140 min time-on-stream, reaches a constant value. The kinetic parameters were obtained and it was observed that the reaction is first order.

Since the reaction forms carbon which is deposited on the catalyst surface causing its deactivation, regeneration studies were carried out. The regeneration was done by oxidation with air and its effects on the catalyst activity were also investigated. The catalyst was submitted to reaction-regeneration cycles. After two hours of reaction (600°C), the methane was removed of the line by purge with nitrogen and air was added. Firstly, a 30 minutes long regeneration was carried out in temperatures between 500 and 600°C. After, 20, 30 and 45 min. long regenerations were carried out at 560°C. It was done at least three reaction-regeneration cycles for each case. The best regeneration condition, that is to say, that allows a larger number of cycles with low activity loss, was done at 560°C during 30 min. In this condition the catalyst could be regenerated three times, with loss of 20% of the activity.

During the regeneration, besides the carbon oxidation, metallic Ni and Cu can be partially converted to the oxide form, what requests a new catalyst activation stage after regeneration. In the reaction-regeneration cycles mentioned previously, the methane acting as gas reducer during the reaction stage beginner. The activation was evidenced by a weight loss in the first minutes of the reaction. A test using H<sub>2</sub>/N<sub>2</sub> reduction stage, after regeneration, was carried out (560°C during 30 min). This test result was better, being the catalyst after the first regeneration more active than the fresh catalyst. Four cycles reduction-reaction-regeneration was carried out and the catalyst lost 15% of its activity after the third regeneration.

## References

Machado, T. E., *Decomposição catalítica do metano sobre catalisador Cu-Ni-Al: taxa da reação e regeneração do catalisador*. Universidade Federal do Rio Grande do Sul, Brasil (2007).

## Session T2-13P: Catalysis – Poster

Abstract Number	Paper Title & Authors	Included
171	Catalyst deactivation by polyaromatics during LCO upgrading to high quality diesel R G Tailleux	Yes
422	Esterification of aromatic olefins with acetic acid in the presence of sulphuric acid as a catalyst (Abstract 422) P J Martinez, E Rus, S Rojano	Yes
547	Semiempirical molecular orbital studies of the acylation step in the lipase-catalyzed ester hydrolysis J H Zhao, H L Liua	Yes
618	Phase transfer catalyzed reaction of n-Octanol T Sankarshana, J S Murthy	Yes
664	Effect of metal oxide additives on the properties of Cu/ZnO/Al <sub>2</sub> O <sub>3</sub> catalysts in methanol synthesis from syngas F Meshkinia, M T Mazandarania, M Bahmanib	Yes
777	Catalytic decomposition of nitrous oxide on nano sized palladium catalysts: The influence of precursor and the method of preparation P S S Reddya, N Lingaiaha, P S S Prasada, I V Raob	Yes
852	Coherent – Synchronous Oxidation of CH <sub>4</sub> , C <sub>2</sub> H <sub>6</sub> , C <sub>3</sub> H <sub>8</sub> by Hydrogen Peroxide T Nagiev	No
895	Influence of textural properties and iron content on the activated carbon performance for catalytic wet air oxidation of phenol M Baricot, S A Dastgheib, J Font, A Fortuny, F Stüber, C Bengoa, A Fabregat, L Le Coq, J Font	Yes
905	Study of the interaction of ozone with phenantroline for the determination of the oxidation kinetic of iron (II) with a FIA system J N Laboulais, A Cerver, J I Torregrosa, M J Palomo	Yes
918	Influence of Preparation Method of Fe <sub>3</sub> O <sub>4</sub> -Cr <sub>2</sub> O <sub>3</sub> Catalysts for Water Gas Shift Reaction J Dufour, C Martos, A Ruiz	Yes
1037	Reactivity of several olefins in the HDS of full boiling range FCC gasoline over PtPd/USY S Magyar, J Hancsók, D Kalló	Yes
1167	Synthesis of copper catalysts by coprecipitation of Cu(II) and Chitosan onto Alumina U I Castro, I Sanchez, A Fortuny, F Stüber, A Fabregat, J Font, P Haure, C Bengoa	Yes
1393	Synthesis of isobutyl propionate using Amberlyst 15 as a	Yes

	catalyst	
	A I Citak, H L Hosgun	
1462	Effects of Nickel Impregnation Profiles on Partial Oxidation Ethanol Reaction	Yes
	C Diana, J Tatiana, C Gabriel, G J Mario, M J Carlos, G Liliana	
1686	Dehydrocondensation of 1-hexanol to di-n-hexyl ether (DNHE) on Amberlyst 70	Yes
	E. Medina, R Bringué, J Tejero, M Iborra, C Fité, J F Izquierdo, F Cunill	
1790	Hydrogenation of CO Over a Cobalt/Cerium Oxide Catalyst for Production of Lower Olefins	Yes
	M Haghshenas Fard, L Maleki, M Khoshnoodi , F Banitaba	
1826	Activity and synergetic effects of Mo sulfide catalysts promoted by Pd, Rh, Pt and Ru in HDS of benzothiophene	Yes
	D Gulková, Z Vít, L Kaluža, M Zdražil	
1986	SCR of NO by C <sub>3</sub> H <sub>6</sub> over Cu-Fe-PILC in the presence of oxygen and steam	Yes
	P B García, F Dorado, A D Lucas, A D LConsuegra, A N Márquez, J L Valverde, A Romero	
1989	Influence of the reaction temperature on the electrochemical promoted catalytic behaviour of Pt impregnated catalyst for the reduction of Nitrogen oxides under lean burn conditions	Yes
	F Dorado, A D L Consuegra, P B García, A N Márquez, J L Valverde	
1996	Catalytic Growth of Structured Nitrogen-Containing Carbon over Unsupported and Y Zeolite Supported Ni and Co Catalysts	Yes
	A N Márquez, A Romero, P B García, M A Keane, J L Valverde	
2061	The Effect of Lanthanum on the Performance of Pt-Sn/Al <sub>2</sub> O <sub>3</sub> Reforming catalysts	Yes
	I C Andrade, T V García	
2272	Esterification with cation exchange resin catalysts: The concept of an active surface layer	No
	Willie Nicol	
2390	Characteristics of the support and active phases of Monolithic Co/Al <sub>2</sub> O <sub>3</sub> -SO <sub>4</sub> catalysts for CH <sub>4</sub> -SCR	Yes
	S B Rasmussen, J C Martin, M Yates, P Avila	
2572	Catalysts on the base of layered oxides for the decomposition of water and waste compounds	Yes
	I Zvereva, A Toikka, J C Liu	
2796	Kinetic consideration of non-catalytic and catalytic oxidation of soot	Yes
	V Tomašić, I Brnardić, H Jenei, S Zrnčević	
3290	Cyclohexane dehydrogenation for the evaluation of metallic sites accessibility in naphtha reforming bimetallic catalysts.	Yes
	B Iñarra, M P G Marcos, J M Guil, M A G Ortiz	
3551	Effect of preparation method on perovskite catalyst structure for synthesis of Acetic acid from natural gas	Yes
	H R Arandiyán, M Parvari	
	A new perovskite catalytic system consisting of LaMoV for Acetic acid direct synthesis from Ethane and CO <sub>2</sub>	Yes
	H R Arandiyán, M Parvari	
4036	The investigation of Ru based Fischer Tropsch catalyst for the	Yes



production of synthetic liquid fuels derived from bio-syngas  
S Tungkamani, P Narataruksa, H Sukkathanyawat, N Kraikul,  
S Nivitchanyong, B Sakakini  
4144 <sup>1</sup>H and <sup>13</sup>C-DEPT PFG NMR Studies of Diffusion in Catalysts Yes  
D Weber, E H Stitt, L F Gladden



## **Catalyst deactivation by polyaromatics during LCO upgrading to high quality diesel**

Roberto Galiasso Tailleur

*Department of Chemical Engineering, University of Texas A&M College Station Texas 77840*

### **1. Summary**

During the hydrotreatment of LCO the WNiPd/TiO<sub>2</sub>Al<sub>2</sub>O<sub>3</sub> acid sites dedicated to ring opening deactivated faster than those acid sites used for cracking and than the metal sites, thus the cetane number is reduced as a function of time on stream.

Keywords: LCO upgrading, low aromatic diesel, catalyst deactivation

### **2. Extended Abstract**

The upgrading of LCO and SR Diesel fractions to produce a ultralow sulfur and aromatics high-cetane-number diesel is a growing area of interest. The commercial operation of a hydrotreating unit had shown an important deactivation of the catalyst when treated feeds contain LCO to produce 15 ppm diesel. The cycle length depends on the rate of losing the cetane number in the hydrotreated product. In the plant the temperature has been increased along the cycle to have constant sulfur in the product. This paper is focuses in studying the relative deactivation of the hydrogenation and ring opening reaction active sites, which improve the cetane number, respect to those of desulfurization sites along the cycle length when pure LCO was upgrade to low emission diesel

The performances of a new generation hydrotreating catalyst (WNiPd/TiO<sub>2</sub>Al<sub>2</sub>O<sub>3</sub>) [1] was evaluated in a pilot plant as a function of time on stream using 100% of LCO (1.5% of sulfur 55% of aromatics) as feed. two set of experiments were performed to produce 15 or 50 ppm sulfur in the product during three months, taking samples along the cycle length. The temperature along the cycle length was changed to keep the sulfur constant in the product. The catalysts at the end of run were tested with 100% of LCO (Feed I) and a synthetic feed composed by benzothiophene (15000 ppm of S), 30% of naphthalene and 10% of tetraline in hexadecane (Feed II). The products and spent catalyst samples were obtained at the end of the three months on stream. (Spent 1 and 2 catalyst and characterized by TPD, CO and pyridine adsorptions, XPS, CNMR and FTIR.

**Products of Feed I / II as a function of time on stream.**  
**(12.5 MPa, 0.2 h<sup>-1</sup>, 20 (mol) H<sub>2</sub>/HC, WNiPd/TiO<sub>2</sub>-Al<sub>2</sub>O<sub>3</sub>)**

Properties wt% (Feed1 / Feed 2)	Fresh cat.		Spent 1		Spent 2	
Operating Temperature °C	354		372		382	
Sulfur (ppm wt)	58	3	55	6	65	4
Nitrogen (ppm wt)	22	-	42	-	55	-
Mono-aromatics / alkyl benzenes	13	10	10	9	8	10
Di-aromatics / methyl naphthalene	9	11	12	13	13	13
Mono-naphthene / alkyl cyclohexanes	9	8	7	5	6	2
Naphthen-Aromatic/ methyl tetralin	16	11	22	13	25.5	13
Di-naphthenes / methyl decaline	22	7	20	6	19	6
Other aromatics and naphthenes	4.5	9	4.2	9.5	2.4	10
C <sub>10</sub> -C <sub>20</sub> paraffins	18	18	16	22	13	23
C <sub>4</sub> -C <sub>10</sub>	6	28	8	24	10	23
C <sub>1</sub> -C <sub>4</sub> paraffins	2.3	5.8	3.9	6.9	4.3	7.2
Cetane number (-)	44	-	38	-	<38	-

The pilot plant study demonstrated, like it was observed in commercial plant, that both spent catalyst in spite of produce 50 ppm sulfur specification had increase the aromatics and naphthenic content respect to the fresh catalyst, thus their lost cetane number. The results were verified with the synthetic feed were we can confirm the effect of deactivation in hydrogenation, the ring opening and cracking. We postulated that there is two different acid sites one that produce the isomerization and endo-cycle cracking and other that produce the exo-cycle cracking. The first acid function was responsible for the naphthenic rings opening that improve the cetane number, and the other to the dealkylation and paraffinic branches break up that reduce the cetane number. Higher is the deactivation higher is the average weight temperature need for the catalyst to maintain the sulfur constant in the product, the higher the exocycle cracking and the lower the isomerization. Pyridine and CO adsorption and XPS analysis of the spent catalyst demonstrated a larger survival of the metal sites than the acid sites and a change in the strength of acid sites due to the deactivation.

**Reference:** Galiasso Tailleur R and .Ravigli J., Applied Catalysis, A: General, 293, 192 (2005)

## **Esterification of aromatic olefins with acetic acid in the presence of sulphuric acid as a catalyst (Abstract 422)**

Pedro J. Martinez,<sup>a</sup> Eloisa Rus,<sup>a</sup> Santiago Rojano<sup>a</sup>

<sup>a</sup>*Department of Chemical Engineering, Faculty of Sciences, University of Malaga  
29071 Malaga, Spain  
E-mail: cuesta@uma.es*

### **1. Summary**

Esterification reactions of aromatic olefins (ethenyl benzene and its derivatives) were carried out with acetic acid. A strong acid, sulphuric acid, was used as a catalyst. A study was made on influence of different variables have on the olefin conversion. From the obtained results it can be deduced the following conclusions: an increase in temperature and catalyst concentration positively influences the conversion of the corresponding olefins. The substituted radical and the occupied position on the aromatic ring ("meta" or "para") exerts a very important influence on the reaction conversion. For identical substitute type, the substituted derivatives in position "para" present a bigger reactivity and olefin conversion than substituted derivatives in position "meta". A thermodynamic and kinetic study has been done with the calculation of the corresponding parameters. Finally we studied the influence of acidity on reaction rate constant by Hammet equation.

### **2. Extended Abstract**

Most of the commercially available esters are obtained by the reaction between an alcohol and an organic acid, or an organic anhydride, generally in the presence of a strong mineral acid that acts as a catalyst. However, the direct esterification of an olefin by an organic acid should be the most appropriate, and therefore more economic method, to reach the same result of the classic reaction. The addition of acetic acid to ethenyl benzene and its derivatives compounds in the presence of sulphuric acid as a catalyst registers inside the study of the homogeneous catalysis in solution. The esters of organic acids are a very important group of compounds. They are used for a wide variety of chemical reactions. In this sense, the scientific investigations of the last years are directed fundamentally toward the election of the most appropriate catalysts to carry out this type of processes, among those we can mention to the heteropolyacids. Nowadays, a group of new catalysts are used in the olefin esterification reaction with a carboxylic acid, such as cerium sulphate (Horiuchi, 2003); sulfamic acid (Wang, 2004); iridium complex (Kiyooka, 2005); SO<sub>3</sub>H-functionalized ionic liquids as dual catalyst-solvent (Gu, 2004) and protic ionic liquids based on 2-methylpyridinium (Duan, 2006).

For the different processes of acetic acid addition to ethenyl benzene and its derivatives compounds using sulphuric acid as a catalyst that were carried out, a study was made of the influence that temperature, catalyst concentration and type of substituted radical have on the conversion of all studied compounds. It is observed that an increment of the temperature influences positively the olefins conversion. When the catalyst concentration influence on the olefin conversion was studied, it was observed that catalyst concentration effects positively the conversion of olefin.

Finally, it was possible to prove the important influence of the substituted radicals in the m- or p- positions on the conversion of the studied olefins, presenting growing reactivity in the following order: 1-ethenyl-3-nitro benzene, 1-ethenyl-3-chloro benzene, 1-ethenyl-4-chloro benzene, 1-ethenyl-3-methyl benzene and 1-ethenyl-4-methyl benzene. For the same substitute type, those derivatives substituted in position p- present a bigger reactivity and a bigger conversion of the olefin than derivatives substituted in position m-.

A kinetic and thermodynamic study has been done, and the corresponding kinetic parameters have been calculated in each one of the cases with an adequate fitting.

The effect of the substitute on the ring benzene over the reaction rate constant of the esterification process can be studied by the application of the Hammett equation:

$$\log k = \log k_o + \sigma \cdot \rho$$

where  $k$  is the reaction rate constant of substituted compound and  $k_o$  is the reaction rate constant of non-substituted compound (ethenyl benzene in this case) that takes as reference value. The parameter  $\sigma$  is called the substitution constant. The parameter  $\rho$  is called the reaction constant. The Hammett equation is valid for a series of compound aromatic that has in common a reaction centre. It was possible to determinate the reaction constant.

T (°C)	$\rho$
20	4.665
25	4.654
30	4.644
35	4.634

**Table:** Esterification of p- or m- substituted derivatives.  
Determination of reaction constant.  $[\text{H}_2\text{SO}_4] = 2 \text{ mol/L}$

Finally, we studied the influence of medium acidity on the reaction rate constant. From mathematical expressions developed in previous works and with the values of the Hammett constant ( $H_o$ ) taken from the bibliography (Mollard, 1966), it has been proven that, for various concentrations of catalyst, the experimental data fits the following equation:

$$\log k = -\alpha \cdot H_o - \beta$$

We have calculate the parameters  $\alpha$  and  $\beta$ ; an adequate fitting is obtained, since the correlation coefficients is sufficiently acceptable.

### 3. References

- Duan Z., Gu Y., Zhang J., Journal of molecular catalysis A: Chemical, 250, 163-168 (2006).
- Gu Y., Feng S., Deng Y., Journal of molecular catalysis A: Chemical, 212, 71-75 (2004).
- Horiuchi C.A., Fukushima T., Journal of Chemical Research, Vol 2003, Number 5, 270-272 (2003).
- Kiyooka S., Ueno M. Tetrahedron Letters, 46 (27), 4639-4642 (2005).
- Mollard M., Torck B., Hellin M., Cousement I., Bull. Soc. Chim. France 1, 83-94 (1966).
- Wang B., Gu Y., Catalysis Letters, 96, 71-74 (2004).

## Semiempirical molecular orbital studies of the acylation step in the lipase-catalyzed ester hydrolysis

Jian-Hua Zhao<sup>a</sup> and Hsuan-Liang Liu<sup>a,b</sup>

<sup>a</sup>*Department of Chemical Engineering and Biotechnology, National Taipei University of Technology, 1 Sec. 3 ZhongXiao E. Rd., Taipei, Taiwan 10608*

<sup>b</sup>*Graduate Institute of Biotechnology, National Taipei University of Technology, 1 Sec. 3 ZhongXiao E. Rd., Taipei, Taiwan 10608*

### 1. Summary

In this study, we present the results from the semiempirical molecular orbital calculations for the acylation step in the lipase-catalyzed ester hydrolysis. The results reveal that the lowest energy path for the formation of the tetrahedral intermediate is for the serine residue of the catalytic triad to attack the substrate, followed by coupling heavy atom movement and proton transfer. The calculations of four active site models show that the cooperation of the aspartate group and the oxyanion hole is capable of lowering the activation energy by about 16 kcalmol<sup>-1</sup>. Our results further suggest that the lipase-catalyzed ester hydrolysis adopts the single proton transfer mechanism.

Keywords: semiempirical molecular orbital calculations, acylation, lipase, oxyanion hole

### 2. Extended Abstract

#### 2.1 Introduction

Lipases, a class of enzymes belonging to the serine hydrolases, have been proven to be efficient for resolving racemic alcohols and esters. Many lipases are heat-stable and can be used in organic solvents. It is of great interest to use molecular modeling for predicting the ability of these enzymes in discriminating the enantiomers of a particular substrate. So far, vast amounts of molecular modeling studies have been performed with the aim of rationalizing and/or predicting the enantioselectivity of triacylglycerol lipases toward various substrates [1-5].

It is well known that most lipases are functioned with the catalytic triad (Asp-His-Ser) located in the active site [6]. The reason for this arrangement is presumably to make the Ser oxygen sufficiently nucleophilic before it attacks the carbonyl carbon of the amide or ester substrate. The most commonly accepted mechanism of serine hydrolases is divided into two steps: the acylation and the deacylation steps [7].

## 2.2 Methods

The crystal structure of the *Burkholderia Cepacia* lipase in complex with hexylphosphonic acid (R)-2-methyl-3-phenylpropyl ester (PDB code: 1YS1) [6] was used to construct the lipase model. In our molecular orbital calculations, Ser87, His286, Asp264 and substrate were modeled by methanol, imidazole, formate anion and methyl formate, respectively. In addition, Leu17 and Gln88 were represented by two water molecules to mimic the formation of two hydrogen bonds with the carbonyl oxygen of the substrate.

Semiempirical molecular orbital calculations were carried out using the AM1 [8] and PM3 [9] molecular models, which are implemented within the MOPAC module in the InsightII program. All calculations of this study were made in gas phase. All the reactions were examined by using the reaction coordinate method [10].

The potential energy surface for the formation of the tetrahedral intermediate was calculated by restraining two reaction coordinates: 1) the distance between the hydroxyl oxygen of Ser and the carbonyl carbon of the substrate ( $R_a$ ) and 2) the difference of the distances between the donating and the accepting oxygen atoms and the transferring proton ( $R_b$ ), which describes the abstraction of a proton from the Ser oxygen to the His nitrogen.

## 2.3 Results and discussion

The aim of this study is to gain insights into the mechanistic aspect of the acylation step in the lipase-catalyzed ester hydrolysis using quantum chemical approaches. We further examined the effect of the Asp residue of the catalytic triad and the oxyanion hole on decreasing the activation energy by four active site models. Double proton transfer mechanism was also investigated in this study.

The calculations of four active site models show that the cooperation of the aspartate group and the oxyanion hole is capable of lowering the activation energy by about 16 kcalmol<sup>-1</sup>. Our results further suggest that the lipase-catalyzed ester hydrolysis adopts the single proton transfer mechanism

## References

- Holmquist, M., Häffner, F., Norin, T. and Hult, K., (1996) *Protein Sci.*, 5,83-88  
Häffner, F., Norin, T. and Hult, K., (1998) *Biophys. J.*, 74,1251-1262  
Tuomi, W.V., and Kazlauskas, R.J., (1999) *J. Org. Chem.*, 64,2638-2647  
Scheib, H., Pleiss, J., Kovac, A., Paltauf, F. and Schmid, R.D., (1999) *Protein Sci.*, 8,215-221  
Schulz, T., Pleiss, J. and Schmid, R.D., (2000) *Protein Sci.*, 9,1053-1062  
Mezzetti, A., Schrag, J.D., Cheong, C.S. and Kazlauskas, R.J., (2005) *Chem. Biol.*, 12,427-437  
Topf, M., and Richards, W.G., (2004) *J. Am. Chem. Soc.*, 126,14631-14647  
Dewar, M.J.S., Zorbisch, E.G., Healy, E.F. and Stewart, J.J.P. (1985) *J. Am. Chem. Soc.*, 107, 3902-3909  
Stewart, J.J.P. (1989) *J. Comput. Chem.* 10, 209-220  
Dewar, M.J.S. and Kirschner, S.J. (1971) *J. Am. Chem. Soc.* 93, 4290-4294



## Phase transfer catalyzed reaction of n-Octanol

Talapuru Sankarshana and Josyula Suryanarayana.Murthy

*University College of Technology, Osmania University, Hyderabad – 500 007, India.*

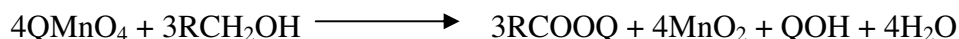
### 1. Summary

Kinetics of oxidation reaction of n-octanol by potassium permanganate was investigated using the phase transfer catalyst (PTC), tricaprylyl methyl ammonium chloride (Aliquat 336) under both homogeneous and heterogeneous conditions. The rate constants obtained are compared under these conditions. Oxidation of n-octanol by permanganate was first order with respect to each of the reactants resulting in an overall second order rate expression. The second order rate constant determined under both homogeneous and heterogeneous agreed well. Among the catalysts used Aliquat 336 was proved to be more effective and gave the enhancement factor of 7. Extractability of quaternary ammonium permanganate ion from aqueous phase into the organic phase reached its saturation value within three minutes.

Keywords: Phase transfer catalysis, Kinetics, Enhancement factor

### 2. Extended Abstract

Experiments were conducted in a batch reactor to determine the homogeneous kinetics. Purple benzene containing tricaprylyl methyl ammonium permanganate,  $QMnO_4$  was prepared by contacting aqueous potassium permanganate solution with benzene consisting of the phase transfer catalyst, tricaprylyl methyl ammonium chloride. Benzene layer (purple benzene) was separated and used for reactions by adding n-octanol at different conditions. The oxidation reaction of n-octanol by  $QMnO_4$  can be represented as follows.



In all the experiments the concentration of n-octanol was maintained at a very large value compared to the concentration of  $QMnO_4$  so that the change in n-octanol concentration was negligible and the reaction was considered to be negligible. From the obtained concentration versus time values, the rate constant was determined.

A 0.06 m diameter borosilicate agitated reactor with baffles was used to find the kinetics under heterogeneous conditions. Experiments were performed by dispersing benzene containing n-octanol and PTC in aqueous potassium permanganate solution. At different

time intervals the samples were analyzed for potassium permanganate concentration. From these values the average rate of reaction was determined and the order and the rate constant were calculated. The results indicated that the oxidation of n-octanol by permanganate was first order with respect to each of the reactants resulting in an overall second order rate expression.

The second order rate constant determined under both homogeneous and heterogeneous conditions agreed well.

Different phase transfer catalysts like, tricaprylyl methyl ammonium chloride (Aliquat 336), triethyl benzyl ammonium chloride (TEBAC), tetra butyl ammonium bromide (TBAB), tetra butyl ammonium iodide (TBAI) were compared for their effectiveness. Aliquat 336 was proved to be more effective and gave the highest enhancement factor of 7. The activities of these catalysts were found to be consistent with findings in literature.

Runs were made to find the extractability of quaternary ammonium permanganate ion at different speeds of agitation and for different volume ratios of organic and aqueous phases. The results show that the concentration of permanganate ion in organic phase reaches its saturation value within three minutes for the stirrer speeds above 450 rpm and is equal to the initial concentration of catalyst.

## Effect of metal oxide additives on the properties of Cu/ZnO/Al<sub>2</sub>O<sub>3</sub> catalysts in methanol synthesis from syngas

F. Meshkini<sup>a</sup>, M. Taghizadeh Mazandarani<sup>a</sup>, M. Bahmani<sup>b</sup>

<sup>a</sup>Chemical Engineering Department, Faculty of Engineering, Mazandaran University, P.O.Box:484, Babol, Iran, E-mail: taghizadehfr@yahoo.com, Tel: +98111-3234204, Fax: +98111-3234201

<sup>b</sup>Catalyst Research Group, Petrochemical Research and Technology Co., National Petrochemical Co., P.O.Box: 14458, Tehran, Iran

### 1. Summary

The Cu/ZnO/Al<sub>2</sub>O<sub>3</sub> catalysts, prepared by co-precipitation method, has been modified by adding small amount of Mn, Mg, Zr, Cr, Ba, W and Ce oxide using design of experiments (<sup>1</sup>/<sub>16</sub> full factorial design). The structure and morphology of catalysts were studied by X-ray diffraction (XRD) and Surface area (S<sub>BET</sub>). Performance of the prepared catalysts for CO/CO<sub>2</sub> hydrogenation to methanol was evaluated by using a stainless steel fixed-bed reactor at 5MPa and 513 K. The oxide additives were found to influence the catalytic activity, dispersion of Cu, Cu crystallite size, surface composition of catalyst and stability of catalysts during their operations. The results showed that the Mn, Zr and Ba promoted catalysts have high performance for methanol synthesis from syngas.

Keywords: Methanol synthesis, Cu/ZnO/Al<sub>2</sub>O<sub>3</sub> catalysts, metal oxide additives

### 2. Extended Abstract

The oxide precursors of Cu/ZnO/Al<sub>2</sub>O<sub>3</sub>/MO (M<sub>2</sub>O<sub>3</sub> or MO<sub>2</sub>), where M is Mn, Mg, Zr, Ce, Ba, Cr and W, with a nominal composition of 65 mol% Cu, 25 mol% ZnO and 10 mol% Al<sub>2</sub>O<sub>3</sub> and 2 mol% of each promoter were prepared by the conventional co-precipitation method. An aqueous solution of metal nitrate (only tungsten was introduced as Ammonium tungstate) and an aqueous solution of Na<sub>2</sub>CO<sub>3</sub> were added simultaneously to a vessel containing deionized water under vigorous stirring. The precipitation was carried out at 343 K and a constant pH 7. The precipitates were aged in mother liquid at 343 K for 5 hr under stirring.

CO/CO<sub>2</sub> hydrogenation tests were carried out using a stainless steel tubular, down flow, high pressure, fixed bed reactor (interior ID: 10 mm), which contained 1.1 gr (1 Cm<sup>3</sup>) catalysts placed between two layers of SiC. All catalysts were reduced in diluted H<sub>2</sub> (3% in N<sub>2</sub>) flow at 513 K and atmospheric pressure for 15 h before syngas exposure.

The catalytic activity in the methanol synthesis was determined at 5 MPa pressure and 513 K with a mixture of CO/CO<sub>2</sub>/H<sub>2</sub> = 1/1/14.5 and GHSV=12400 hr<sup>-1</sup>. The outlet gases (products and unconverted feed) were cooled up to 255K and the water and methanol in

liquids were analyzed by Varian Star GC (CP-3800). H<sub>2</sub>, CO, CO<sub>2</sub> and small amount of CH<sub>4</sub> were determined by RGA (Agilent 6890N) chromatographs.

The results of catalytic activity tests on catalysts with different promoters are given in Table 1. Figure 1 shows the variations of the methanol yield with time on stream for the catalyst without any promoter (A) and the catalyst having the high activity and stability (A-Mn-Zr).

Table 1: The activity and selectivity of the catalysts for methanol synthesis

Catalyst name	MeOH Space time yield (gr <sub>CH<sub>3</sub>OH</sub> /Kg <sub>Cat</sub> .hr)		Carbon conversion (mol%)	MeOH selectivity
	Initial activity	Activity after 64 hr		
A-Zr-Ba-Mn	684.06	642.04	28.77	99.49
A-Mn-Cr-W	608.33	505.43	24.78	99.62
A-Mg-Zr-Cr	599.38	567.29	24.85	99.49
A-Mg-Ba-W	574.69	481.89	23.18	99.08
A-Mn-Mg-Ce	488.14	507.00	21.68	98.32
A-Ce-Ba-Cr	440.63	400.24	18.41	99.17
A-Zr-Ce-W	423.06	440.63	18.77	98.54
A-Mn-Mg-Zr-Ba-Ce-W-Cr	376.68	395.44	16.69	98.97

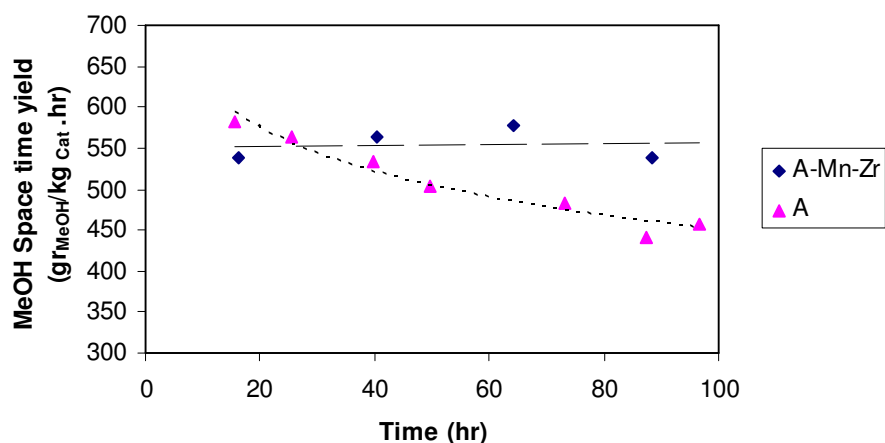


Figure 1: MeOH Space time yield for Catalyst A and Catalyst A-Mn-Zr.

## References

- Jingang Wu, Masahiro Satio, Hirotaka Mabuse, (2000) *Catalysis Letters*, 68, 55-58.  
 Toyir, J., P. R. Piscina, J. L. G. Fierro, N, Homs, (2001) *Applied Catalysis B: Environmental*, 29, 207-215.  
 Chen, H.Y., J. Lin, K.L. Tan, J. Li, (1998) *Applied Surface Science*, 126, 323-331.  
 Cabrera, I. M., M.L. Granados, J.L. Fierro, (2002) *Journal of Catalysis*, 210, 285-294.  
 J. Słocynski, R. Grabowski, P. Olszewski, A. Kozłowska, J. Stoch, M. Lachowska, J. Skrzpek, (2006) *Applied Catalysis A: Gneral*, 310, 127-137.

## Catalytic decomposition of nitrous oxide on nano sized palladium catalysts: The influence of precursor and the method of preparation

P. Siva Sankar Reddy<sup>a</sup>, N. Lingaiah<sup>a</sup>, P. S. Sai Prasad<sup>a</sup>, I.V. Rao<sup>b\*</sup>

<sup>a</sup> I & PC Division, Indian Institute of Chemical Technology, Hyderabad 500 007, India

<sup>b</sup> College of Technology, Osmania University, Hyderabad 500 007, India

### 1. Summary

Alumina-supported palladium catalysts were prepared by the deposition precipitation (DP) and impregnation (IMP) methods. The DP catalysts showed higher activity than those of their IMP analogues for decomposition of nitrous oxide. The DRIFTS analysis revealed preferential formation of partially oxidized Pd<sup>+1</sup> species on the surface of DP-Cl catalyst. The high activity of DP-Cl catalyst prepared by DP method is related to the formation of electron deficient Pd sites during the preparation and their occupancy in the octahedral vacancies of alumina.

### 2. Extended Abstract

Nitrous oxide (N<sub>2</sub>O) has been recognized as an important greenhouse gas responsible for stratospheric ozone depletion. With a lifetime of 150 years at atmospheric conditions, it also exhibits a global warming potential 310 times that of carbon dioxide. With the increase in concern for environmental protection, efforts have been made to convert N<sub>2</sub>O into N<sub>2</sub> and O<sub>2</sub> [1] and in this process catalytic direct decomposition is found to be advantageous.

Alumina-supported palladium catalysts were prepared by the deposition precipitation (DP) and impregnation (IMP) methods with 1 wt. % PdCl<sub>2</sub> or Pd (NO<sub>3</sub>)<sub>2</sub> precursors. The catalyst preparation, characterization methods and activity measurements were well reported in our previous studies [2]. The activity profiles obtained on the catalysts for the decomposition of N<sub>2</sub>O are shown in Fig. 1 (a). The conversion plots follow S-shaped curves for all the catalysts. In the case of IMP-N and DP-N catalysts the decomposition started at 300 °C and the complete conversion occurred above 525 °C. The DP N catalyst showed relatively high activity than IMP N at a given temperature. On the IMP Cl catalyst the decomposition was initiated at 300 °C and complete conversion occurred above 600 °C, whereas on the DP-Cl catalyst the initiation of decomposition occurred at 250 °C and completed at 500 °C. Thus, the DP-Cl catalyst showed complete conversion relatively at low temperature than that of other three catalysts. Generally, chloride-based catalysts are inactive for the N<sub>2</sub>O decomposition. In contrast, the present investigation showed that with change of method of preparation of the catalyst this disadvantage can be easily overcome.

In order to understand the nature of Pd surface species formed during method of preparation CO DRIFTS adsorption studies have been carried out. In our recent studies [2] on Ru catalysts, it was proved that partially reduced Ru is responsible for catalytic conversion of  $N_2O$  to  $N_2$ . In the same way to know the oxidation states of the Pd, DRIFTS experiments were conducted using CO as a probe molecule. Fig. 1 (b) shows the infrared spectra of CO adsorbed at room temperature on palladium catalysts. The stretching frequency is often an excellent indicator of the way CO binds to the substrate. Linearly adsorbed CO absorbs at frequencies between  $2000-2130\text{ cm}^{-1}$ , bridged-bonded CO between  $1880-2000\text{ cm}^{-1}$ . Therefore, the IR band at  $2070\text{ cm}^{-1}$  can be assigned to linearly bonded CO to  $Pd^0$ , and the  $1980$  and  $1930\text{ cm}^{-1}$  bands to bridge-bonded  $Pd^0$  to CO. In the IR spectrum for IMP-Cl, additional IR bands assignable to monocarbonyl  $Pd^{2+}-CO$  and  $Pd^{1+}-CO$  species were also observed at  $2160$  and  $2125\text{ cm}^{-1}$ , respectively, indicating that the surface property of palladium on IMP-Cl prepared from palladium chloride seems to be different from that on the other catalysts. The IMP-N catalyst did not show formation of any cationic species. Nitrate based precursors are reduced relatively at lower temperatures than that of chloride based precursors. In the case of DP-Cl catalyst there is a clear formation of  $Pd^{1+}-CO$  species at  $2129\text{ cm}^{-1}$ . This is due to the fact that the DP-Cl based method of preparation can create strong metal support interactions during the preparation of the catalyst.

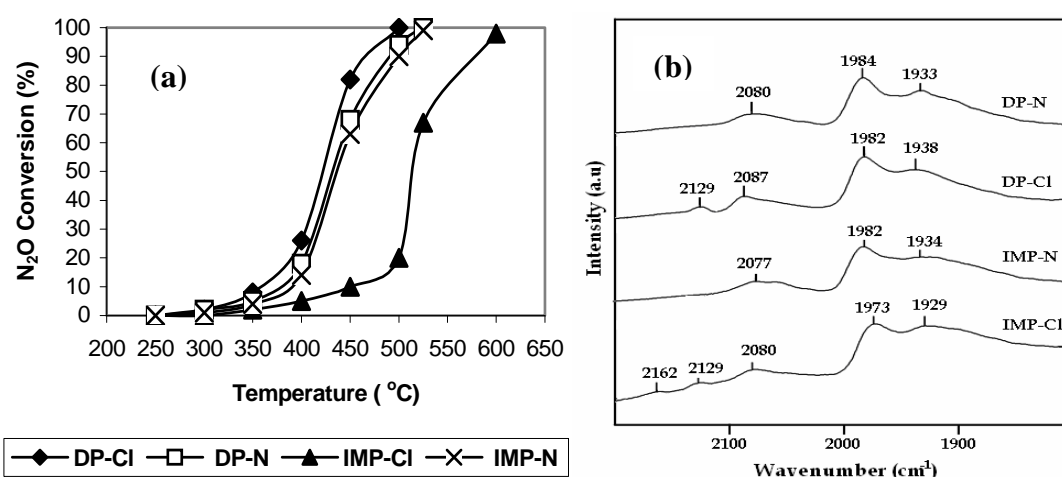


**Fig. 1.** (a)  $N_2O$  Conversion on Pd/  $Al_2O_3$  catalysts with temperature. (b) CO adsorbed DRIFTS spectra on Pd/  $Al_2O_3$  catalysts at room temperature

**Conclusions:** Palladium chloride supported  $Al_2O_3$  catalyst prepared by deposition – precipitation method was found to be highly active among the four catalysts. The Pd catalysts prepared by DP method with chloride precursor provide a convenient approach for the preparation of active catalysts for catalytic decomposition of nitrous oxide reaction. The high activity of DP - Cl catalyst seems to be manifestation of forming an active site wherein Pd exists in its cationic form.

## References

1. Kapteijn, F., Mirasol, J.R. and Moulijn, J.A., (1996) Appl. Catal. B, 9, 25-55.
2. Siva Sankar Reddy, P., Nayeem Pasha., Chalapathi Rao, M.G.V., Lingaiah, N., Suryanarayana, I. and Sai Prasad., P.S., (2007) Cat.Com, 8, 1406- 1410.

## **Influence of textural properties and iron content on the activated carbon performance for catalytic wet air oxidation of phenol**

M. Baricot<sup>a</sup>, S.A. Dastgheib<sup>a</sup>, J. Font<sup>a</sup>, A. Fortuny<sup>b</sup>, F. Stüber<sup>a</sup>, C. Bengoa<sup>a</sup>, A. Fabregat<sup>a</sup>, L. Le Coq<sup>c</sup>, J. Font<sup>a</sup>

<sup>a</sup>*Departament d'Enginyeria Química, ETSEQ, Universitat Rovira i Virgili, Av. Països Catalans, 26, Campus Sescelades, 43007 Tarragona, Catalunya, Spain*

<sup>b</sup>*Departament d'Enginyeria Química, EPSEVG,, Universitat Politècnica de Catalunya, 08800 Vilanova I la Geltrú, Catalunya, Spain*

<sup>c</sup>*Ecole des Mines de Nantes, GEPEA, UMR CNRS 6144, 44307 Nantes Cedex 3, France*

### **1. Summary**

A commercial activated carbon (AC), with proven catalytic activity in phenol catalytic wet air oxidation (CWAO) has been characterised and modified to explore the effect of the iron content and mesoporous volume in the catalytic activity.

Keywords: activated carbon, catalyst, phenol oxidation, iron content, trickle bed

### **2. Extended Abstract**

Nowadays, increasingly stringent regulations about the disposal of hazardous chemical substances force the development of new low-cost and efficient alternatives for the treatment of effluents. Many of the available wastewater treatments are based on the oxidation of the substances at high temperature and pressure using some oxidants. The use of dedicated catalysts allows to temper the operation conditions. In turn, AC has been used for years in water remediation (Dabrowski et al. 2005), typically, in adsorption. AC can be made from almost any carbonaceous source such as wood and coal.; even great results have been obtained using sewage sludge as raw material (Rio et al. 2004). Different physico-chemical characteristics of AC, such as porosity and surface chemistry, can be obtained by controlling the media and conditions during the activation step. Also, post-manufactured treatments look like alternatives to improve the performance of AC in different applications. For instance, heat treatment under inert atmosphere has shown to be effective in reducing the surface oxygen content and increasing the adsorption capacity towards phenolic compounds, which are well-known pollutants because of their high toxicity and poor biodegradability (Ania et al., 2002; Tessmer et al., 1997). AC has also shown to possess catalytic activity for certain reactions. Pereira et al. (1999), and Stüber et al. (2001) have used AC carbon as catalyst in oxidative dehydrogenation (ODH) of ethyl benzene and CWAO of phenol, respectively. However, the specific physical

and/or chemical characteristics that provided these catalytic activities are not yet well identified. Using heat treatment to partially remove surface oxygen, Pereira et al. (1999) found that surface quinones groups were responsible for the catalytic activity shown by AC in ODH. Nevertheless, the surface oxygen groups that might be partially responsible for the catalytic activity of AC in the CWAQ of phenol have not been clearly identified. In order to highlight which properties could influence the catalytic behaviour, a commercial AC with proven catalytic activity has been altered using several modification methods. It was found that a basic and stable to reoxidation AC surface, such as that obtained after a heat treatment under H<sub>2</sub>, can increase the steady state phenol conversion up to 10%. Previous results obtained after acid treatment of the AC demonstrated that an increase in the surface oxygen content gave worse final phenol conversion (Santiago et al., 2005). Moreover, Fe content also seems to have some impact on the catalytic activity shown by AC, since previous studies made with demineralised samples showed a lower phenol conversion. However, the effect of textural properties has not been sufficiently studied, as all the treatments conducted until now have not practically changed either the surface area or the porosity. Therefore, the impact of porosity and Fe/Ca content on the CWAQ of phenol was also investigated. A commercial AC was initially subjected to either Ca or Fe impregnation by ion exchange, and then heated under N<sub>2</sub> at 1000°C. An enhancement in the mesoporosity of the samples was observed due to carbon pore enlargement. Surface area and pore size distribution of carbons were characterised by N<sub>2</sub> adsorption. The oxygen content was determined by elemental analysis while surface oxygen groups were characterised by Boehm method. The performance of these modified samples was evaluated by phenol adsorption and CWAQ of phenol in a trickle bed reactor. Results have demonstrated that iron content, rather than pore distribution, is the main factor responsible of the catalytic activity.

## References

- Ania, C.O., J.B. Parra, and J.J. Pis, (2002) *Fuel Process. Technol.*, 79, 265-271.
- Dabrowski, A., P. Podkościelny, Z. Hubicki and M. Barczak, (2005) *Chemosphere*, 58, 1049-1070.
- Pereira, M.F.R., J.J.M. Orfao, and J.L. Figueiredo, (1999) *Appl. Catal., A.*, 184, 153-160.
- Rio, S., Faur-Brasquet, C., Le Coq, L., Lecomte, D., and P. Le Cloirec, (2004) *Water Sci. Technol.*, 49, 139-146.
- Santiago, M., F. Stüber, A. Fortuny, A. Fabregat and J. Font, (2005) *Carbon*, 43, 2134-2145.
- Stüber, F., I. Polaert, H. Delmas, J. Font, A. Fortuny, and A. Fabregat, (2001) *J. Chem. Technol. Biotech.*, 76, 743-751.
- Tessmer, C.H., R.D. Vidic, and L.J. Uranowski, (1997) *Env. Sci. Technol.*, 31, 1872-1878.



## **Study of the interaction of ozone with phenantroline for the determination of the oxidation kinetic of iron (II) with a FIA system**

J.Navarro-Laboulais<sup>a</sup>, A.Cerver<sup>a</sup>, J.I.Torregrosa<sup>a</sup>, and M.J.Palomo<sup>b</sup>

<sup>a</sup> *Department of Chemical and Nuclear Engineering, Escuela Politécnica Superior de Alcoy (EPSA). Universidad Politécnica de Valencia. Paseo Viaducto 1, 03801 Alcoy (Alicante) Spain*

<sup>b</sup> *Department of Chemical and Nuclear Engineering, Escuela Técnica Superior de Ingenieros Industriales (E.T.S.I.I.), Universidad Politécnica de Valencia, Camino de Vera s/n, (Valencia), Spain*

### **1. Summary**

The aim of this work has been the preliminary study of the kinetic process when ozone is used to oxidize Fe(II) to Fe(III) in a G/L reactor and the proposal of an experimental set-up for the determination of the different substances involved in the reaction. Experiments to study the effect of temperature, ozone gas concentration, and the interaction between ozone+phenantroline and ozone+complex Fe and phenantroline has been done.

Keywords: ozone, iron, FIA, phenantroline.

### **2. Extended abstract**

Electroplating wastewaters are characterized for high concentrations of iron (II) up to 20g/100 ml. The removal of this pollutant in wastewaters is desirable for reasons of protecting wastewater treatment systems. Iron can be eliminated by oxidation followed by precipitation or absorption. This preoxidation treatment can be done by bubbling ozone in a G/L reactor due to this gas is capable of oxidize iron (II) to iron (III). In order to study the kinetic of this process it is convenient an automated process for the on-line measurement of the variation in concentration of the dissolved ferrous ions in the solution. One of the most popular methods for the determination of iron is the measurement of the absorbance of Fe(II) - 1,10-phenanthroline complex. This method can be combined with FIA system, which makes possible to carry out a large number of determinations with a minimum consumption of samples and reagents.

For the experiments a G/L reactor of 0.5 L capacity has been used. Ozone has been produced with a Multiozono generator. Solutions of iron (II) have been prepared

with ultra pure water using Mohr's salt (Merck). Phenantroline has been used as chelating agent (Merck). The absorption spectra have been measured with a Diode Array Multispec-1501 (Shimadzu).

Results of ozonation of a phenantroline solution show that ozone is not consumed during the experiment so oxidation rate of ozone+phenantroline is insignificant or null. Kinetic experiments with and without iron-phenantroline complex in the G/L reactor show that the presence of phenantroline decreases significantly the oxidation rate of iron (II) to iron (III). There have not been appreciated any effects in the kinetic of the reaction in the range of temperatures studied. From the analysis of the variation of ozone gas concentration during the experiments is observed that consumption of ozone in the reactor (Figure 1) is significant while Fe(II) is present in the solution, fact that could be related with a fast kinetic process. The analysis of absorption spectra of a non complexed iron solution during the ozonation experiments shows that a peak at 303 nm appears as the oxidation occurs, reaching a maximum when the ozonation is completed. This peak has been associated to the presence of Iron (III) in the solution.

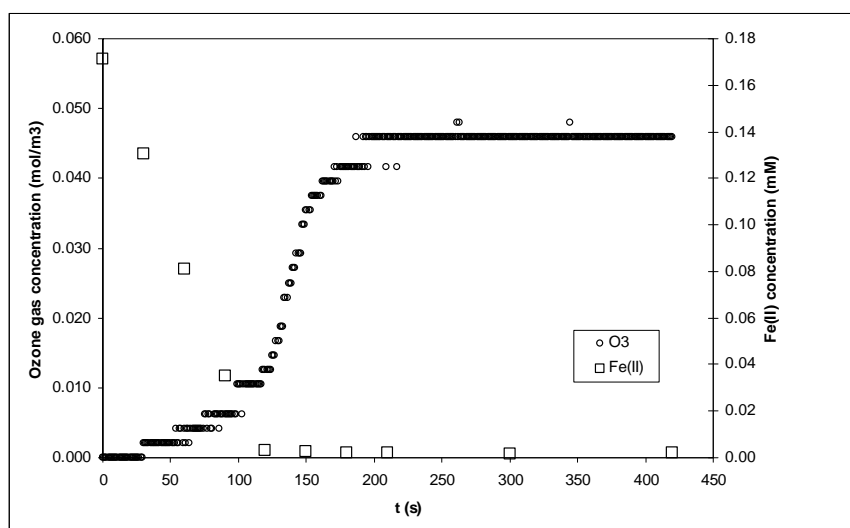


**Fig. 1.-** Variation of ozone gas concentration and Fe(II); T=20 °C, pH=3.5, Inlet ozone gas concentration 2.3 g/m<sup>3</sup>.

The authors gratefully acknowledge the Conselleria d'Empresa, Universitat i Ciència de la Generalitat Valenciana for financial support of this work under project ref. GV06/083.

## References

- Reckhow, D.A., Knocke, W.R., Kearney, M.J. and Parks, C.A., (1991) *Ozone Science and Engineering*, 13, 675-695.  
 Radionova, T.V.; Beklemishev, M.K., Dracheva, L.V. and Zolotov, Y.A., (1992) *Journal of Analytical Chemistry*, 47 (7), 888 -892.  
 Mortatti, J., Drug, F.J., Pessenda, L.C.R., Zagatto, E.A.G., (1982) *Analyst*, 107, 659-663.

## **Influence of Preparation Method of Fe<sub>3</sub>O<sub>4</sub>-Cr<sub>2</sub>O<sub>3</sub> Catalysts for Water Gas Shift Reaction**

J. Dufour, C. Martos, A. Ruiz

*Department of Chemical Engineering, Rey Juan Carlos University, E-28933 Móstoles (Madrid), Spain*

### **1. Summary**

High temperature water gas shift catalysts are prepared by oxiprecipitation and compared to materials obtained by the traditional coprecipitation method. Catalysts synthesized by oxiprecipitation are composed of magnetite crystals surrounded by smaller high chromium containing particles. On the contrary, chromium is in solid solution within the magnetite lattice in materials obtained by coprecipitation.

Keywords: water gas shift reaction, catalysts synthesis, oxiprecipitation.

### **2. Extended Abstract**

Water gas shift reaction ( $\text{CO} + \text{H}_2 \leftrightarrow \text{CO}_2 + \text{H}_2\text{O}$ ) is an important step in the industrial manufacture of high-purity hydrogen. The reaction is slightly exothermic and reversible, and is usually carried out in two stages to overcome equilibrium limitations. The first stage involves a high temperature (HTWGS) catalyst based on Fe<sub>3</sub>O<sub>4</sub>/Cr<sub>2</sub>O<sub>3</sub>, while the second one uses a low temperature catalyst based on Cu/ZnO/Al<sub>2</sub>O<sub>3</sub>. A new approach is performance the reaction in a membrane reactor, so hydrogen can be continuously removed. This allows carrying out this process in a single stage using a high temperature water gas shift (WGS) catalyst.

The active phase in HTWGS catalyst is magnetite (Fe<sub>3</sub>O<sub>4</sub>), which in absence of chromium oxide rapidly loses its activity by sintering. There is some controversy about the role of Cr<sub>2</sub>O<sub>3</sub> in the stabilisation of the catalyst structure. Some researchers have proposed that the reduced catalyst forms an inverse spinel-type structure with Cr<sup>3+</sup> ions in solid solution within the Fe<sub>3</sub>O<sub>4</sub> lattice [1]. On the other hand, several authors suggest that Cr<sub>2</sub>O<sub>3</sub> appears as fine particles that physically block Fe<sub>3</sub>O<sub>4</sub> sintering [2].

In this work, we study the oxiprecipitation method to obtain WGS catalysts directly in active phase. These materials are compared to those obtained by the usual method which consists of coprecipitation, thermal treatment and reduction.

The solids obtained by oxiprecipitation were prepared through a previously reported procedure [3]. The variables studied were pH, air flowrate and temperature. The materials

obtained by coprecipitation were prepared from  $\text{FeCl}_3$  or  $\text{FeCl}_3$  and  $\text{FeCl}_2$  solutions and  $\text{NaOH}$  as precipitating agent. The solid was filtered and washed out with demineralised water. Then it was dried at  $110^\circ\text{C}$  and calcined at  $250^\circ\text{C}$  or  $600^\circ\text{C}$  depending on the experiment. Catalysts were characterized by X-ray diffraction (XRD), Fourier transform infrared spectroscopy (FTIR), transmission electron microscopy (TEM), nitrogen adsorption/desorption at  $77\text{ K}$ , Raman spectroscopy and temperature programmed reduction (TPR). From these analyse, the best oxiprecipitation conditions were  $\text{pH} = 7$ , air flowrate =  $1,1\text{ L/min}$  and  $T = 70^\circ\text{C}$ .

The solids obtained by coprecipitation were synthesized as  $\alpha\text{-Fe}_2\text{O}_3$  or  $\gamma\text{-Fe}_2\text{O}_3$  and partially reduced to active phase ( $\text{Fe}_3\text{O}_4$ ). Fig. 1 shows FTIR results of samples with 8 wt %  $\text{Cr}_2\text{O}_3$  obtained by the above explained methods. The samples prepared by oxiprecipitation and coprecipitation-reduction showed the typical IR band of magnetite ( $565\text{ cm}^{-1}$ ). TEM and  $\text{N}_2$  adsorption results showed that oxiprecipitation materials were composed of  $\text{Fe}_3\text{O}_4$  crystals surrounded by smaller high chromium containing particles and high BET surface ( $>100\text{ m}^2/\text{g}$ ). In the case of coprecipitated samples,  $\text{Cr}_2\text{O}_3$  was in solid solution and BET surface was lower as result of thermal treatment.

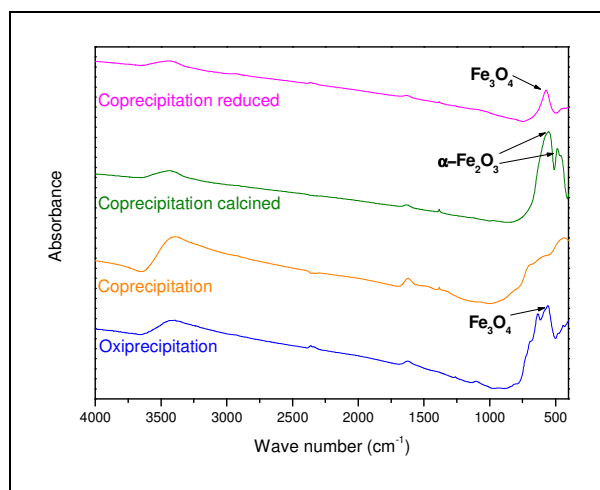


Fig.1. FTIR spectra obtained from samples prepared with different synthesis methods.

ACKNOWLEDGEMENT: The Ministry of Education and Science of Spain is acknowledged for funding through project ENE2004-07758-C02-02

## References

- H. Topsöe; M. Boudart. *Journal of Catalysis* (1973), 31(3), 346-59.  
G. C. Chinchén; R. H. Logan; M. S. Spencer. *Applied Catalysis*, 12 (1984) 69-88.  
J. Dufour; C. Martos; A. Ruiz; A. Carrasco; M. Maroño. "Synthesis of  $\text{Fe}_3\text{O}_4\text{-Cr}_2\text{O}_3$  catalysts by oxy-coprecipitation for water gas shift reaction". 10th Mediterranean Congress of Chemical Engineering (2005).

## **Reactivity of several olefins in the HDS of full boiling range FCC gasoline over PtPd/USY**

Szabolcs Magyar<sup>a</sup>, Jenő Hancsók<sup>a</sup>, Dénes Kalló<sup>b</sup>

<sup>a</sup>*Department of Hydrocarbon and Coal Processing, University of Pannonia, H-8201 Veszprém, P.O. Box 158, Hungary*

<sup>b</sup>*Chemical Research Center, Institute of Surface Chemistry and Catalysis, Hungarian Academy of Sciences, H-1525, Budapest, P.O. Box 17, Hungary*

### **1. Summary**

Reactivity of C<sub>4</sub>-C<sub>6</sub> olefins during the selective HDS of a full boiling range FCC gasoline over PtPd/USY catalyst was studied under various process conditions. Effect of the structure and carbon number of olefins on their conversion is discussed. It was found that the rate of hydrogenation decreases with the carbon number of linear olefins. Terminal olefins are converted to internal olefins by double bond shift to approach the equilibrium composition of olefin isomers.

Keywords: HDS, FCC gasoline, olefin hydrogenation, PtPd/USY

### **2. Extended Abstract**

#### *2.1. Introduction*

Desulphurization of FCC gasoline is a key process in refineries for blending gasoline of ultra low sulphur content (<10 mg/kg). Hydrodesulphurization (HDS) of highly olefinic cracked naphtha fractions on conventional CoMo/Al<sub>2</sub>O<sub>3</sub> catalysts results in significant olefin saturation and high H<sub>2</sub> consumption, making this process unsuitable for cracked naphtha upgrading. Quite a number of new catalyst have been developed, which are suitable for the desulphurization of cracked naphthas with minimized olefin saturation (Song, 2003; Brunet et al., 2005). In our previous works we showed that PtPd/USY catalyst can selectively desulphurize FCC gasoline fractions containing 50-150 mg/kg sulphur due to the selective poisoning of the hydrogenation active sites (Hancsók et al. 2002 & 2007). The dissimilar reactivity of various olefins can have a significant effect on the octane number of the products, because the difference in the RON or MON between a certain olefin and its saturated paraffin derivative can greatly depend on its structure and carbon number. Therefore, in this work the reactivity of C<sub>4</sub>-C<sub>6</sub> olefins in the HDS of a full boiling range FCC gasoline over PtPd/USY catalyst was studied.

## 2.2. Experimental

The tests were carried out in a *pilot scale HDS unit*. The effective volume of the down-flow fix-bed HDS reactor is 100 cm<sup>3</sup>. The test system contained all the equipments and devices, which are applied in full-scale commercial gasoline desulphurization units. The tests were carried out in continuous operation. Full boiling range FCC gasoline of 66 mg/kg sulphur content was used as a *feedstock* of the HDS tests. Its hydrocarbon composition expressed in w/w% was the following: *n*-paraffins: 4.0; *i*-paraffins: 31.8; olefins: 24.9; naphthenes: 7.6; aromatics: 31.7. The *catalyst* was PtPd/USY with a Pt content of 0.15% and Pd content of 0.45%. *Composition* of the feedstock and liquid products were determined by gas chromatography according to a modified version of NF M07-086 method. Sulphur contents were measured according to ISO 20846 standard (Multi EA 3100 analyzer). The following *process conditions* were applied: temperature: 220-280°C; LHSV: 1.0-3.0; H<sub>2</sub>/hydrocarbon ratio: 300 Nm<sup>3</sup>/m<sup>3</sup>.

## 2.3. Results and discussion

The results showed that the rate of olefin hydrogenation under the conditions of gasoline HDS over PtPd/USY catalyst decreases with the carbon number of the olefin. Although hydrogenation of *n*-pentenes is significantly faster than those of methyl butenes, the conversion of *n*-hexenes is barely higher than those of methyl pentenes. These findings are in accordance with Lebedev's rule.

The results also showed that double-bond migration took place during the HDS of the FCC gasoline feed, because the conversion of certain olefins (e.g. *trans*-2-pentene and 2-methyl-2-butene) was negative, indicating that more of these olefins formed from other olefin isomers than they were consumed in their saturation to paraffins.

After hydrogenation the composition of *n*-pentenes in the product does not seem to depend on the contact time; it remains almost constant (11-13 wt% 1-pentene; 27-28 wt% *trans*-2-pentene and 59-60 wt% *cis*-2-pentene) while their hydrogenation clearly increases. In fact, the composition of *n*-pentene isomers is also practically constant as function of the temperature in the investigated range of 220-280°C. This suggests that under gasoline HDS conditions the rate of double-bond shift is much higher compared to that of hydrogenation, leading to a near-equilibrium composition of olefins that are taking part in double-bond shift reactions.

Consequently, the different conversion of olefin compounds can be attributed to double-bond isomerization instead of the different hydrogenation rates of various olefin isomers.

## References

- Brunet, S., Mey, D., Pérot, G., Bouchy, C. and Diehl, F., (2005), *Appl. Catal. A*, 278, 143-172.  
Hancsók, J., Magyar, Sz., Lengyel, A. (2002) *Hung. J. Ind. Chem.*, 30, 299-303.  
Hancsók, J., Magyar, Sz., Juhász, K., Kalló, D., (2007) *Top. Cat.*, DOI: 10.1007/s11244-007-0267-y (in press)  
Song, C., (2003) *Catalysis Today*, 86, 211-263.

## Synthesis of copper catalysts by coprecipitation of Cu(II) and Chitosan onto Alumina

U.I. Castro<sup>a\*</sup>, I. Sanchez<sup>a</sup>, A. Fortuny<sup>b</sup>, F. Stüber<sup>a</sup>, A. Fabregat<sup>a</sup>, J. Font<sup>a</sup>, P. Haure<sup>c</sup>, C. Bengoa<sup>a</sup>

<sup>a</sup>*Departament d'Enginyeria Química, Escola Tècnica Superior d'Enginyeria Química, Universitat Rovira i Virgili, Av. Països Catalans 26, 43007 Tarragona, Catalonia, SPAIN.*

<sup>b</sup>*Departament d'Enginyeria Química, EPSEVG, Universitat Politècnica de Catalunya, Av. Víctor Balaguer s/n, 08800 Vilanova i la Geltrú, Barcelona, Catalonia, SPAIN.*

<sup>c</sup>*Departamento de Ingeniería Química, INTEMA, Universidad Nacional de Mar del Plata, Avda. Juan B. Justo4302, Mar del Plata, ARGENTINA.*

### 1. Summary

Four Cu/chitosan composite catalysts were prepared by coprecipitation of a Cu-Chitosan complex onto cylindrical pellets and spheres of  $\gamma$ -alumina in subsequent impregnation steps. Samples were used in the WPO of phenol solutions at 30°C and 1 atm. All catalysts were active for phenol degradation, showing up to 88% of phenol conversion. Leaching of the active species during reaction was detected.

Keywords: coprecipitation, copper, alumina, chitosan, catalytic oxidation.

### 2. Extended Abstract

The use of heterogeneous systems for CWPO has received considerable attention in the last years. Transition metal complexes supported on diverse surfaces were investigated as potentially active catalysts in a variety of reaction systems. Particularly, a growing number of studies reporting on Chitosan as a catalytic support have been published over the last two decades (Guibal, 2005). This biodegradable polysaccharide is one of the most abundant natural polymers and exhibits an remarkable capability to adsorb metal ions. It is obtained from chitin (a material found in crab or shrimp shells) by deacetylation. Chitosan-supported catalysts were used in several processes (Guibal et al., 2005 and Sulakova et al., 2007) mostly in the form of flakes, powder or hydrogel beads. Under typical reaction conditions, it has the tendency to agglomerate, to form gel or even to dissolve in the aqueous medium. To overcome this problem, SiO<sub>2</sub>-Chitosan composites have been developed (Kucherov et al, 2003). In this context, the aim of this work is to both synthesise and characterize new Cu/Chitosan composite catalysts obtained by coating Cu-chitosan complexes onto  $\gamma$ -alumina in subsequent impregnation steps. Catalysts were used in the WPO of phenol solutions at 30°C and 1 atm. Samples were prepared by coprecipitation of the Cu-Chitosan complex onto cylindrical pellets and

spheres of  $\gamma$ -alumina. The Cu-Chitosan complex, obtained by dissolving 2g of Chitosan and 4g of Cu(II) (as  $\text{CuCl}_2$ ) into 300 mL of HCl (0,1M),. was used to impregnate a known amount of  $\gamma$ -alumina. In each impregnation cycle, the particles were immersed into the complex solution for 15 minutes. Then, the liquid was drained and the excess of superficial copper complexes or copper ions were removed by washing with distilled water. The catalyst was dried at room temperature in air. The drying process was completed in a stove at 100°C during 30 min.. Following the same experimental protocol, four catalysts were prepared: **P1**, **P2** and **P3**, in which  $\gamma$ -alumina pellets were exposed to one, two or three impregnation steps, and catalyst **S1**, in which alumina spheres were exposed to one impregnation cycle. Preliminary activity experiments were performed and fresh and used samples were characterized by AA, TPR and TGA. Table 1 lists results obtained after 2h of reaction. All catalysts were active for phenol degradation. Leaching of the active phase is significant, so the occurrence of homogeneous reactions can not be neglected.

TABLE 1 Catalytic behaviour for WPO of phenol

<b>Sample</b>	<b>Cu content (mg·g<sup>-1</sup>)</b>	<b>Phenol conversion (%)</b>	<b>Cu leached (%)</b>
<b>P1</b>	<b>20.38</b>	<b>76</b>	<b>5.4</b>
<b>P2</b>	<b>31.81</b>	<b>88</b>	<b>5,3</b>
<b>P3</b>	<b>33.34</b>	<b>87</b>	<b>6,1</b>
<b>S1</b>	<b>12.76</b>	<b>46</b>	<b>2,1</b>

## References

- Guibal E., (2005) Heterogeneous catalysis on chitosan-based materials: a review, 30, 71-109.  
 Kucherov A.V., Kramareva N.V., Finashina E.D., Koklin A.E., Kustov L.M., (2003) Heterogenized redox catalysts on the basis of Chitosan matrix. 1. Copper complexes, 198, 377-389.  
 Sulakova R., Hrdina R., Soares G.M.B., (2007) Oxidation of azo textile soluble dyes with hydrogen peroxide in the presence of Cu(II)-chitosan heterogeneous catalysts, 73, 19-24.



## **Synthesis of isobutyl propionate using Amberlyst 15 as a catalyst**

Alime Izci Citak and Halit L. Hosgun

*Department of Chemical Engineering, University of Eskisehir Osmangazi, 26480 Eskisehir, Turkey.*

### **1. Summary**

In this study, the adsorption equilibrium constants of adsorbed species and the kinetic parameters of the reaction of isobutanol with propionic acid catalyzed by an acidic ion-exchange resin (Amberlyst-15) were investigated. Experiments were carried out in a stirred batch reactor using dioxan as a solvent. The chemical equilibrium composition was measured at temperature ranges of 318-348 K and kinetic information was also obtained at the same temperature intervals at various starting compositions of the reactants and products. For this reaction, the mechanism was found to follow the Eley-Rideal theory. The rate limiting step is the surface reaction. The activation energy of the esterification reaction was determined to be 44.57 kJ/mol. The heat of adsorption for isobutanol and water was also calculated as -29.07 kJ/mol and -33.26 kJ/mol, respectively.

Keywords: Esterification, Heterogeneous Catalyst, Isobutyl propionate, Kinetics.

### **2. Extended Abstract**

#### *1.1. Introduction*

Esterification is one of the most important reactions in the organic process industry. In an esterification reaction, a carboxylic acid reacts with an alcohol to produce ester and water. Esters are widely used as a solvent, flavour and fragrance compounds and precursors to a gamut of pharmaceuticals and agrochemicals (Yadav and Thathagar, 2002; Gubicza et al., 2000; Zhao, 2000; Carey, 1990). Catalyst such as mineral acid, p-toluen sulphonic acid and ion exchange resins are always used in liquid phase esterification reactions to raise the product yield. Although homogeneous catalysts have high catalytic activity, there are some problems as corrosion, side reactions and separation from the reaction mixture (Ahtiokka and Citak, 2003; Teo and Saha, 2004; Ali and Merchant, 2006). In this study, the kinetics of the reaction of isobutanol with propionic acid in the presence of Amberlyst 15 was investigated.

## 1.2. Experimental section

Isobutanol (98.5 %) and propionic acid (99 %) were used in the experiments. 1,4 Dioxan (99.8 %) was used as solvent. Amberlyst 15 was washed metanol and distilled water, then, dried at 348 K under vacuum for 48 hours approximately before use. The reaction temperature was maintained by means of a thermostatic water bath. It was used a reactor that was fitted with a reflux condenser to prevent any loss of products. Samples were taken at regular intervals and analyzed by Gas Chromatography. The water content of samples was analyzed by Karl-Fischer method.

## 1.3. Results and discussion

From the experimental data, while isobutanol molecule in the bulk is not adsorbed on the catalyst surface, propionic acid molecule is adsorbed. Accordingly, the mechanism was found to follow the Eley-Rideal theory in which an adsorbed and protonated propionic acid molecule reacted with an isobutanol molecule in the bulk. Depending on this approach, the general reaction rate expression can be given as:

$$-r_A = \frac{k_f \frac{m}{V} (C_A C_B - \frac{C_E C_W}{K_e})}{1 + K_B C_B + K_W C_W} \quad (1)$$

Where subscripts A, B, E and W refer to acid, alcohol, ester and water respectively,  $k_f$  is forward reaction rate constant,  $K_e$  is equilibrium constant of the reaction,  $K$ 's are adsorption equilibrium constants,  $m$  is quantity of dry-resin, and  $V$  is the volume of the reaction mixture. Applying the Arrhenius equation to the values obtained from experiments, the temperature dependency of the constants were found to be:

$$k_f = \exp(5.706 - 5361/T) \quad L^2 (\text{g-dry resin})^{-1} \cdot \text{mol}^{-1} \cdot \text{min}^{-1} \quad (2)$$

$$K_B = \exp(3496/T - 11.455) \quad L \cdot \text{mol}^{-1} \quad (3)$$

$$K_W = \exp(4000/T - 11.065) \quad L \cdot \text{mol}^{-1} \quad (4)$$

## References

- G.D. Yadav, M.B. Thathagar, (2002) *Reactive & Functional Polymers*, 52, 99-110.  
 L. Gubicza, A. Kabiri-Badr, E. Keoves, K. Belafi-Bako, (2000) *Journal of Biotechnology*, 84, 193-96.  
 Z. Zhao, (2000) *Journal of Molecular Catalysis A: Chemical*, 154, 131-35.  
 F.A.Carey, *Advanced Organic Chemistry*, Plenium Press, New York (1990)  
 M.R. Altiokka, A. Citak, (2003) *Applied Catalysis A : General*, 239, 141-148.  
 H. T. R. Teo, B. Saha, (2004) *Journal of Catalysis*, 228, 174-182  
 S. H. Ali, S. Q. Merchant, (2006) *International Journal of Chemical Kinetics*, 38, 593-612.

## Effects of Nickel Impregnation Profiles on Partial Oxidation Ethanol Reaction

Caro Diana<sup>a</sup>, Jerez Tatiana<sup>a</sup>, Camargo Gabriel<sup>a</sup>, Gomez Jorge Mario<sup>a</sup>, Moreno Juan Carlos<sup>b</sup>, Giraldo Liliana<sup>c</sup>

<sup>a</sup>*Department of Chemical Engineering, Universidad de los Andes Bogotá Colombia*

<sup>b</sup>*Department of Chemistry, Universidad de los Andes, Bogota, Colombia*

<sup>c</sup>*Department of Chemistry, Universidad Nacional de Colombia, Bogota Colombia.*

### 1. Summary

In this job, the effects of distribution profiles of Ni/  $\gamma$  Al<sub>2</sub>O<sub>3</sub> support, in the partial oxidation of ethanol was analyzed. The catalysts were elaborated by impregnation process. The four distribution profiles (uniform, egg shell, egg white and egg yolk) were obtained when the impregnation time, previous state of support (dry or wet), pH of impregnation solution, second impregnated substance and the impregnations sequence were the variables investigated. The support and catalyst were characterized by TGA, XDR, BET, AAS, SEM, TPD, TPR, and immersion calorimetric.

Keywords: distribution profiles, catalysts prepared by impregnation, egg yolk, egg white

### 2. Extended Abstract

This work explores the impregnation of Ni on gamma alumina, because Colombia is a producer of palm oil and the Chemical Engineering Department (Universidad de Los Andes), is interested in the extraction of the essential oils and further development of catalytic process to obtain products of higher value. The initial goal is to design of catalysts for the production of the intermediated derived from these oils.

The catalysts, with four distributions obtained (Fig. 1) were tested in a packed bed reactor for the partial oxidation ethanol reaction at several W/F<sub>A0</sub> ratios. The products and conversion were measured by gas chromatography. The results show that the conversion of ethanol depends on Nickel loading (Fig. 2), and that the catalysts with the egg white and egg yolk distributions were more selective to acetaldehyde (fig 3)



Fig. 1. Types of impregnation distribution profiles

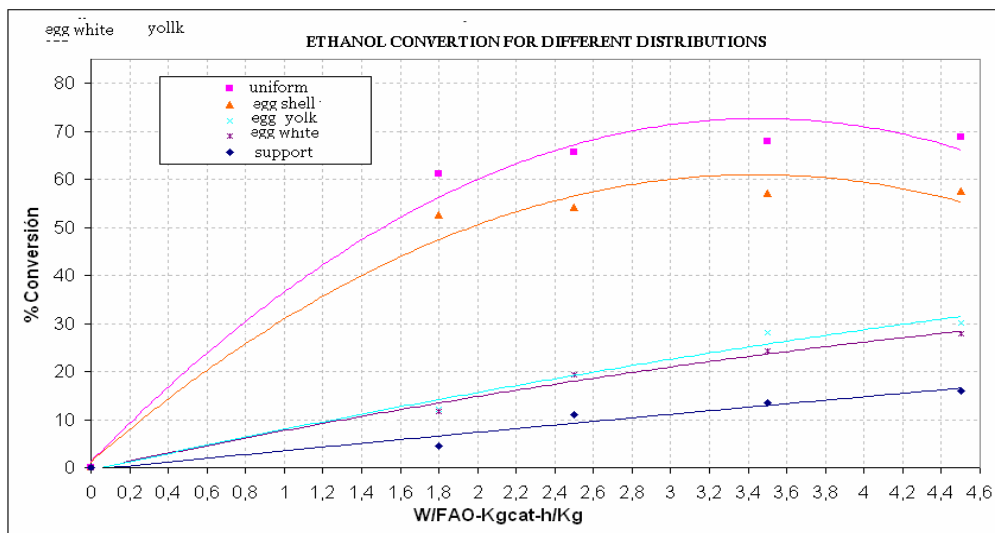


Fig. 2 Ethanol conversion as function of distribution profiles for Ni/  $\gamma$ Al<sub>2</sub>O<sub>3</sub> catalyst.

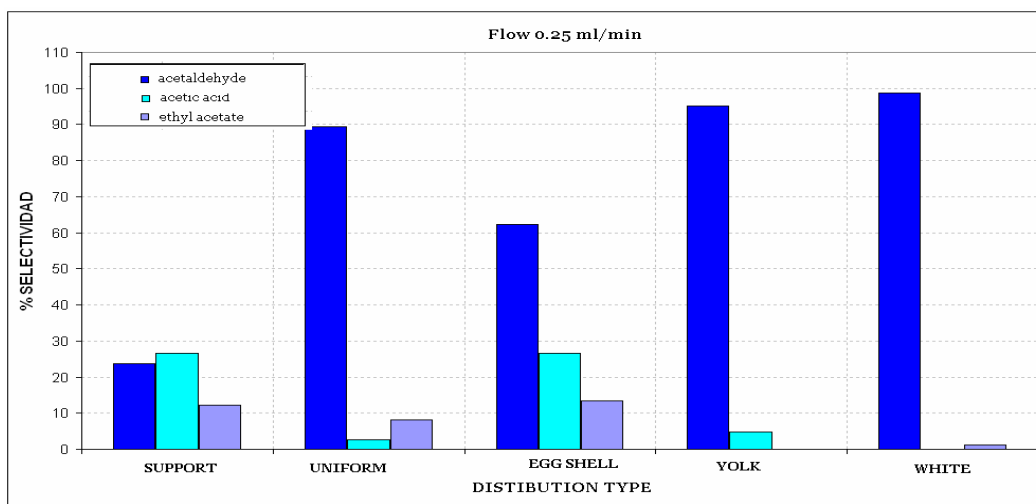


Fig. 3. Selectivity of partial oxidation of ethanol as function of distribution profiles for Ni/  $\gamma$ Al<sub>2</sub>O<sub>3</sub> catalyst.

References

ZHANG. J, Et al. Applied Catalysis A General 243 (2003) 451-459. Elsevier Science Publishers. B.V.  
 PATCAS F. et al. Catalysis Today (69) 379-383 (2001).

## Dehydrocondensation of 1-hexanol to di-n-hexyl ether (DNHE) on Amberlyst 70

E. Medina, R. Bringué, J. Tejero, M. Iborra, C. Fité, J.F. Izquierdo, F. Cunill

*Department of Chemical Engineering, University of Barcelona. C/ Martí i Franquès, 1. 08028-Barcelona. Spain*

### 1. Summary

Conversion, selectivity, yield and kinetics of 1-hexanol liquid phase dehydrocondensation to di-n-hexyl ether (DNHE) were determined at 150-190 °C on the thermally stable resin Amberlyst 70 in a batch reactor. At 190°C, 1-hexanol conversion of about 71 %, with selectivity to ether of 87 % was obtained after 6-h reaction time. A kinetic model stemming from an Eley-Rideal mechanism in which 1-hexanol from the liquid phase reacts with 1-hexanol adsorbed on a single centre to give water adsorbed on a single site represents data suitably. Activation energy was computed to be 130 kJ/mol.

Keywords: di-n-hexyl ether, 1-hexanol, Amberlyst 70, dehydrocondensation reaction.

### 2. Extended Abstract

Diesel fuelled cars park in EU is nowadays larger than that of gasoline counterparts. Due to higher demand in processing heavier oils, refiners are blending in diesel fuels streams containing high length chain compounds, usually aromatics, of boiling point range from 200 to 390°C. In addition, thermal efficiency of diesel engines has been improved by raising the compression ratio to 20:1 and the combustion temperature in the chamber. As a result, higher energy efficiency is gained, but also emissions raise, especially NO<sub>x</sub> and smog. However, standard emissions combustion limits of such pollutants are increasingly stricter.

A clean burning diesel fuel composition may be attained by using alkyl ethers with 6 to 24 carbon atoms. Linear ethers can be blended with all kind of diesel fuel streams. In all cases, diesel cetane number is improved, and emissions reduced by enhancing cold weather driveability. Di-n-hexyl ether (DNHE, blending cetane number 118) may be a reliable option for quality diesel fuels. It can be obtained from 1-hexanol, a product of the hydroformylation and hydrogenation of 1-pentene from C<sub>5</sub> cuts.

The dehydration reaction of 1-hexanol to DNHE has been studied at 150-190°C in a stainless steel 100 cc batch reactor on macroporous resin Amberlyst 70 [A70] (max. operation temperature 200°C, exchange capacity 3 eq/kg, surface area 36 m<sup>2</sup>/g). To keep

reacting mixture in the liquid phase pressure was set at 2 MPa by using N<sub>2</sub> as inert gas. Catalyst was dried at 110°C and 0.1 MPa for 15 h, and then at vacuum for 2 h. Runs lasted 6 h. and liquid samples were analyzed online in an HP-GLC apparatus.

Preliminary experiments performed at 190°C by using catalyst mass from 0.5 to 5 g, stirring rates from 50 to 800 rpm, and up to six A70 fractions of bead size ranging 0.45-0.8 mm, showed that diffusion and external mass transfer influence on reaction rate is negligible within the limits of the experimental error, operating at 200-700 rpm, with 0.45-0.8 mm beads, and less of 3 g of catalyst.

Runs performed at 150-190°C, 500 rpm and 2.0 MPa by using 1-3 g of resin shows that DNHE synthesis is fairly temperature-sensitive and proceeds readily at the higher temperatures of the range. Table shows results obtained with 1 g of resin. As it is seen, the reaction is quite selective to ether; dehydration to olefins being the main side reaction. Compared to the related reaction of 1-pentanol dehydration to di-n-pentyl ether (DNPE) performed in the same set-up (Bringué, 2006), DNHE synthesis on that resin is a bit faster but less selective. However, yields in ether are of the same order.

T(°C)	X <sub>HeOH</sub> (%)	S <sub>DNHE</sub> (%)	Y <sub>DNHE</sub> (%)	S <sub>alkenes</sub> (%)	S <sub>ethers</sub> (%)	r <sup>0</sup> (mol/h.kg)
150	16.5	97.7	16.1	1.5	0.8	10.7
160	29.7	96.2	28.6	2.4	1.4	18.7
170	47.6	94.3	44.9	3.5	2.1	32.3
180	63.7	91.1	58.0	5.9	3.0	73.3
190	70.9	86.9	61.7	9.4	3.6	151

T(°C)	X <sub>PeOH</sub> (%)	S <sub>DNPE</sub> (%)	Y <sub>DNPE</sub> (%)	S <sub>alkenes</sub> (%)	S <sub>ethers</sub> (%)	r <sup>0</sup> (mol/h.kg)
190	67.7	90.8	61.4	5.8	3.4	112

The following kinetic model stemming from an Eley-Rideal mechanism wherein a 1-hexanol molecule from the liquid phase reacts with an alcohol molecule adsorbed on the catalyst surface giving place to water adsorbed on the resin and ether directly released to the liquid (the surface reaction being the rate-limiting step), represented appropriately rate data. Activation energy was estimated to be 130 kJ/mol.

$$r = k \left( a_{\text{HeOH}}^2 - a_{\text{w}} a_{\text{DNHE}} / K_{\text{eq}} \right) / \left( a_{\text{HeOH}} + (K_{\text{w}} / K_{\text{HeOH}}) a_{\text{w}} \right)$$

Additional experiments carried out by adding DNHE or water to 1-hexanol fed at 180, 170 and 160°C, disclosed that reaction rate hardly changed when DNHE was initially added, but with water it highly decreased, what proves the relevant role of water in the kinetics of DNHE synthesis on Amberlyst 70.

## Reference

Bringué, R., Iborra, M., Tejero, J., Izquierdo, J. F., Cunill, F., Fité, C. and Cruz, V. J., (2006) *Journal of Catalysis*, 244, 33-42.

## Hydrogenation of CO Over a Cobalt/Cerium Oxide Catalyst for Production of Lower Olefins

M. Haghshenas Fard<sup>a</sup>, L. Maleki<sup>b</sup>, M. Khoshnoodi<sup>b</sup>, F. Banitaba<sup>b</sup>

<sup>a</sup>Department of Chemical Engineering, Islamic Azad University, Shahreza branch, Isfahan, Iran

<sup>b</sup>Department of Chemical Engineering, University of Sistan Baluchestan, Zahedan, Iran

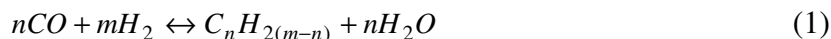
### 1. Summary

A cobalt/ceria catalyst has been found to be receptive for production of lower olefins from synthesis gas by Fischer Tropsch synthesis. Catalysts were prepared in a 0 and 165 minute ageing time. These catalysts were tested at various temperatures and pressures in a stainless steel micro reactor. It was found that a catalyst with 165 minute ageing time was highly receptive to ethylene and methane.

Keywords: Fischer Tropsch, olefins, synthesis gas, cobalt catalyst

### 2. Extended Abstract

The aim of this study was to investigate the role of ageing time in product selectivity and to evaluate the catalyst performance under the various process conditions. The main reaction for the production of hydrocarbons is



#### *Experimental*

The reaction equipment used was a fixed bed microreactor, which allows for working up to 50 bar and 600°C. One gr of catalyst was transferred into the microreactor. After controlling temperature, pressure and flow rate, feed gas passes through the microreactor.

#### *Results and Discussion*

The performance of the catalysts in the screening microreactor at various temperatures, pressure and space velocity (GHSV) is summarized in Table 1.

%Selectivity					%Conv.	H <sub>2</sub> /CO	GHSV hr <sup>-1</sup>	P atm	T°C	Ageing time min
C <sub>4</sub> H <sub>10</sub>	C <sub>3</sub> H <sub>6</sub>	C <sub>2</sub> H <sub>4</sub>	C <sub>2</sub> H <sub>6</sub>	CH <sub>4</sub>						
-	-	0.1	-	-	40	1	3600	1	350	0
-	0.1	0.6	-	0.1	31	1	3600	1	400	
-	1.6	4	-	4	21	1	3600	1	450	
0.3	1.9	4.5	-	3.5	19	1	7200	1	450	
-	0.6	0.9	0.3	4	30	1	7200	5	450	
-	-	0.5	-	1.3	50	1	3600	1	350	165
-	0.7	1.8	-	1.5	38	1	3600	1	400	
0.1	0.7	44	-	48	17	1	3600	1	450	
-	0.5	2	0.3	4	40	2	3600	1	450	

Table 1. Result of 0 and 165 min age Co/CeO<sub>2</sub> catalyst

These catalysts showed high methane and high alkenes content in ethylene fractions.

### Conclusions

In this paper, effective parameters such as ageing time, temperature, pressure of the reaction and space velocity were investigated. The Co/CeO<sub>2</sub> catalyst in the 165 minute ageing time has been found to be selective for light alkenes production from synthesis gas. In high pressure and H<sub>2</sub>/CO>1, production of olefins is very low. In general, high temperature, low pressure and low H<sub>2</sub>/CO are effective for the production of light olefins with high selectivity.

### References

- Varma, R. L. & Bakhshi, N. (1990). *Ind. Eng. Chem. Res.*, 29, 1753-1757.  
 Rabo, J. A., Risch, A. P. & Poustma, M. L. (1978). *J. Catal*, 53, 287-294.  
 Kuipers, E. W., et. al, (1996)., *J. Catal*, 158, 228-300.  
 Schulz, S., Beck, K. & Erich, E. (1988). *Fuel Proc. Tech.*, 18, 293-304.  
 Snel, R. (1987). *Catal. Rev. Sci. Eng.*, 29, 361-445.  
 Bukur, D. B., Mukesh, D. & Patel, S. A. (1990). *Ind. Eng. Chem. Res.*, 29, 194-204.  
 Steynbery, A. P., Espinoza, R. L., Jager, B. & Vosloo, A. C. (1999). *Appl. Catal. A: General* 186, 41-54.



## Activity and synergetic effects of Mo sulfide catalysts promoted by Pd, Rh, Pt and Ru in HDS of benzothiophene

D. Gulková, Z. Vít, L. Kaluža, M. Zdražil

*Institute of Chemical Process Fundamentals, Academy of Sciences of the Czech Republic, Rozvojová 135, 165 02 Prague 6, Czech Republic*

### 1. Summary

Alumina-supported Mo sulfide catalysts were promoted by small amounts of Pd, Rh, Pt and Ru (< 0.8 wt.%). Their activity in hydrodesulfurization (HDS) of benzothiophene (BT) was compared with activities of the conventional Mo/Al<sub>2</sub>O<sub>3</sub> (BASF M8-30) and CoMo/Al<sub>2</sub>O<sub>3</sub> (Shell 344) catalysts at 330-390°C and 1,6 MPa. The addition of noble metals (NM) led to the improvement of activity and to synergetic effects (SE) up to about 4. The Pd promoted sample was the most active from all NM based catalysts, but less active in comparison with the CoMo system. This can be explained by much lower Pd loading than that of Co. However, the specific synergetic effect per atom of NM was higher than that of Co.

Keywords: noble metal sulfides, hydrodesulfurization, benzothiophene

### 2. Extended Abstract

The catalysts were prepared by impregnation of the sulfided Mo catalysts by NM acetylacetonates in ethanol (1). They were characterized by ICP/AAS, N<sub>2</sub> adsorption and some of them by TEM.

The activity in HDS of BT was tested in a fixed bed flow reactor with the reaction mixture in the gas phase at a pressure of 1,6 MPa and temperature of 330-390°C. The catalysts were in situ presulfided in a flow of H<sub>2</sub>S/H<sub>2</sub> mixture (1:10) at 400°C. The products were dihydrobenzothiophene (DHBT) and ethylbenzene (EB). HDS activity of catalysts was expressed by first-order rate constants for overall BT disappearance ( $k_{BT}$ ) and EB formation ( $k_{EB}$ ). The synergetic effects in BT removal ( $SE_{BT}$ ) and EB formation ( $SE_{EB}$ ) were expressed by the  $k_{BT}$  ( $k_{EB}$ ) ratios of the promoted and the unpromoted Mo/Al<sub>2</sub>O<sub>3</sub> catalysts.

Fig. 1 shows the composition of the reaction mixture at different values of the space time W/F over the prepared PdMo(S) catalyst. The addition of Pd significantly suppressed the formation of intermediate dihydrobenzothiophene, similarly as was observed with the Co promoter.

The Pd-Mo(S)/Al<sub>2</sub>O<sub>3</sub> was the most active both in the overall BT conversion and EB formation. The activities of all NM based catalysts were lower than that of conventional CoMo system (see Fig. 2), which is obviously given by much lower content of NM than Co.

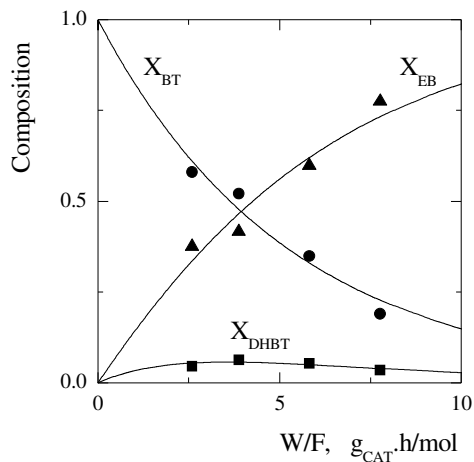


Figure 1: Composition of the reaction mixture versus space time in HDS of BT at pressure of 1.6 MPa and temperature of 360°C over PdMo(S) catalyst

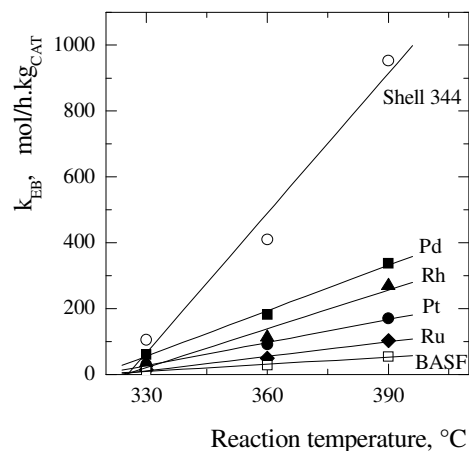


Figure 2: Activity of Mo, CoMo and noble metal promoted catalysts as a function of reaction temperature

On the other hand, the specific synergetic effect calculated per atom of noble metals (SSE) was higher than that of CoMo/Al<sub>2</sub>O<sub>3</sub> and decreased in the order Pt > Rh > Pd > Ru (Table 1).

	0.76 % Pd-Mo(S)	0.36 % Rh-Mo(S)	0.52 % Pt-Mo(S)	0.63 % Ru-Mo(S)	2.4 % Co-Mo (Shell 344)
SE <sub>EB</sub>	4.2	2.6	2.1	1.1	9.5
SSE <sub>EB</sub>	5.9	7.5	7.9	1.8	2.3

Table 1: Synergetic effects in HDS of BT evaluated at 360°C

The synergetic effects observed for Pd and Pt promoted catalysts were less temperature dependent than those for Rh, Ru and the CoMo system, suggesting a different quality of the active sites participating in hydrodesulfurization.

#### Acknowledgements

The authors thank Grant Agency of the Czech Republic for financial support (Grants No. 104/06/0870 and 104/06/P034).

#### References

Vít, Z., Cinibulk, J. and Gulková, D., (2004) *Appl. Catal. A*, 272, 99-107.

## SCR of NO by C<sub>3</sub>H<sub>6</sub> over Cu-Fe-PILC in the presence of oxygen and steam

P.B.García, F. Dorado, A. de Lucas, A. de Lucas-Consuegra, A. Nieto-Márquez, J.L. Valverde, A. Romero

*Department of Chemical Engineering, University of Castilla La Mancha, Avda. Camilo José Cela 10, 13005, Ciudad Real, Spain. Tel.: +34926295300 ext 3509. Fax.: +34926295318. Corresponding author e-mail: PradoBelen.Garcia@uclm.es*

### 1. Summary

Cu-Fe-PILCs were tested in the Selective Catalytic Reduction (SCR) of NO by propene in the presence of water in the feed. These catalysts showed deactivation under wet reaction conditions, with a catalytic activity decrease of 15 – 30 points in the range of temperature studied. NO and C<sub>3</sub>H<sub>6</sub> adsorption over Cu<sup>2+</sup> active sites showed inhibition. However, C<sub>3</sub>H<sub>6</sub> adsorption over CuO clusters was much more affected by the presence of water. The catalytic activity of the samples with CuO aggregates was similar to that obtained for the sample with only Cu<sup>2+</sup> sites, as the promoting effect of CuO for the propene oxidation was totally inhibited by the presence of water. It was observed that inhibition by water was fully reversible. Thus, after removal of water from the feed, NO conversion was completely recovered. This kind of catalysts showed hydrothermal stability after 48 h on stream, and their textural properties were not modified under wet conditions.

Keywords: copper oxides, NO reduction, water inhibition, SCR, pillared clays

### 2. Extended Abstract

The use of hydrocarbons as an alternative reductant to NH<sub>3</sub> has received great attention as the most promising deNO<sub>x</sub> technology for stationary and oxygen-rich mobile sources [1]. Most of NO<sub>x</sub> emissions sources contain water in the concentration ranges of 2 to 18 % [2]; therefore, high catalytic activity is essential for a commercial application but it also required from the view of catalyst life water tolerance. For this purpose, the present study will focus on testing the catalytic activity of Cu ion-exchanged iron pillared clays in the HC-SCR in the presence of water.

Table 1 summarizes temperatures and yields corresponding to the maximum NO conversion reached for all catalysts tested. Under wet conditions, the catalytic activity decreases, depending on the sample, between 15 and 30 points, and the maximum NO conversion shifts to higher temperatures. As copper loading increased, catalysts showed higher inhibition by water, and the C<sub>3</sub>H<sub>6</sub> yield to CO<sub>2</sub> decreased. This fact indicates that

copper species in the samples are affected by the steam. In a previous work [3] the distribution of the copper species present in this kind of catalysts was widely studied. Sample prepared without pH control (Cu3.3-5.4) showed in its structure only isolated  $\text{Cu}^{2+}$ , while samples prepared under alkali conditions showed in their structure copper as  $\text{Cu}^{2+}$  and CuO clusters. The proportion of CuO clusters increased with the pH valued. Under wet conditions, the samples with CuO in their structure presented higher deactivation due to the inhibitor effect of water. At this point, it could be concluded that both  $\text{Cu}^{2+}$  and CuO show similar affinity to  $\text{H}_2\text{O}$  molecules than NO and  $\text{C}_3\text{H}_6$  molecules, but notably, the  $\text{C}_3\text{H}_6$  adsorption over CuO is strongly inhibited by the presence of water.

From the point of view of industrial application, it is interesting to study the reversibility of the NO conversion when water is removed from the feed stream. Therefore, after testing the catalytic activity of the catalysts in absence and presence of water, regeneration of the catalysts was carried out under a helium flow of 100 mL/min for 10 h at 180 °C. All the catalysts showed the same behaviour. It was observed that the deactivation was reversible, so that when water is removed from the feed, NO conversion is completely recovered.

On the other hand, hydrothermal stability of catalysts Cu6.2-9.0 was examined under simulated wet conditions for 48 h at 260 °C (temperature corresponding to maximum NO conversion under dry conditions). Moreover, nitrogen adsorption runs were carried out on catalysts after reaction tests under wet conditions to check textural characteristics with the aim of verifying whether metal sinterization or damage in the support has occurred. Catalysts showed hydrothermal stability after 48 h on stream, and their textural properties were not modified under wet conditions.

Table 1. Temperatures and yield corresponding to maximum NO conversion.

Catalysts	$T_{\text{max}}$ (°C)	NO yield to $\text{N}_2$ (%)	$\text{C}_3\text{H}_6$ yield to $\text{CO}_2$ (%)
Cu3.3-5.4	280	36.2	81.5
Cu3.3-5.4*	320	31.6	91.2
Cu4.8-7.0	260	43.0	81.2
Cu4.8-7.0*	320	34.8	89.0
Cu6.2-9.0	260	53.9	86.7
Cu6.2-9.0*	320	38.0	87.6
Cu6.5-10.5	280	45.2	95.6
Cu6.5-10.5*	320	38.7	82.0

\* Wet reaction conditions (10 %  $\text{H}_2\text{O}$ ).

## References

- Kim, M.H., Nam, I-S., (2001) *Korean Journal Chemical Engineering*, 18 (5), 725-740.  
 Li, Y., Battavio, P., Armor, J.N., (1993) *Journal of Catalysis*, 142, 561-571.  
 Dorado, F., de Lucas, A., García, P.B., Valverde, J.L., Romero, A., (2006) *Applied Catalysis B: Environmental*, 65, 175-184.

## **Influence of the reaction temperature on the electrochemical promoted catalytic behaviour of Pt impregnated catalyst for the reduction of Nitrogen oxides under lean burn conditions**

F. Dorado, A. de Lucas-Consuegra, P.B. García, A. Nieto-Márquez, J.L. Valverde

*Department of Chemical Engineering, University of Castilla La Mancha, Avda. Camilo José Cela 10, 13005, Ciudad Real, Spain. Tel.: +34926295300 ext 3509. Fax.: +34926295318. Corresponding author e-mail: Antonio.Lconsuegra@uclm.es*

### **1. Summary**

The aim of this work was to study the influence of the reaction temperature on the efficiency of the electrochemical promotion to improve the catalytic performance of a Pt impregnated catalyst for the reduction of nitrogen oxides under lean burn conditions. Open circuit catalytic and potential measurements were carried out in order to explain the potentiostatic behaviour of the electrochemical catalyst under different reactions temperatures. At low temperature (220 °C), the application of negative polarization increased the NO reduction rate by a factor of 1.4 (electrophilic behaviour). But as the reaction temperature was higher, the efficiency of electrochemical promotion to improve the catalytic activity decreased, even leading to a poisoning effect at 300 °C (electrophobic behaviour). Nevertheless, at all explored reaction temperatures, the presence of sodium promoter gave a large increase in N<sub>2</sub> selectivity, reaching 90%. These results demonstrated that electrochemical promotion is a suitable technique to improve the catalytic performance of Pt catalyst for the practical development of HC-SCR process to removal nitrogen oxides.

Keywords: Electrochemical Promotion, NEMCA effect, Selective Catalytic Reduction, Pt catalyst.

### **2. Extended Abstract**

The catalytic performance of a metal catalyst can be enhanced by the phenomenon of electrochemical promotion [1]. This new phenomenon occurs when catalytic reactions take place on a variety of metal films in contact with a solid electrolyte, where the latter acts as a source of electrochemically controlled promoter species that directly modify the behaviour of the catalyst film (working electrode). In the present work the electrochemical catalyst consisted of a porous, continuous thin Pt film deposited on a side of a Na-βAl<sub>2</sub>O<sub>3</sub> disk [2], while gold counter and reference electrode were deposited on the other side to polarize the sample. The effect of catalyst polarization on the catalytic activity (Fig. 1) was investigated under different reaction temperatures by

characterization of the rate enhancement ratio ( $\rho$ ) defined as,  $\rho=r/r_0$ , where  $r_0$  is the catalytic reaction rate under unpromoted conditions ( $V_{WR}=1500$  mV) and  $r$  is the catalytic reaction rate under promoted conditions ( $V_{WR}<1500$  mV). The inserted abscissa in Fig. 1, provides an estimation of the sodium coverage ( $\theta_{Na}^*$ ) on Pt catalyst surface.

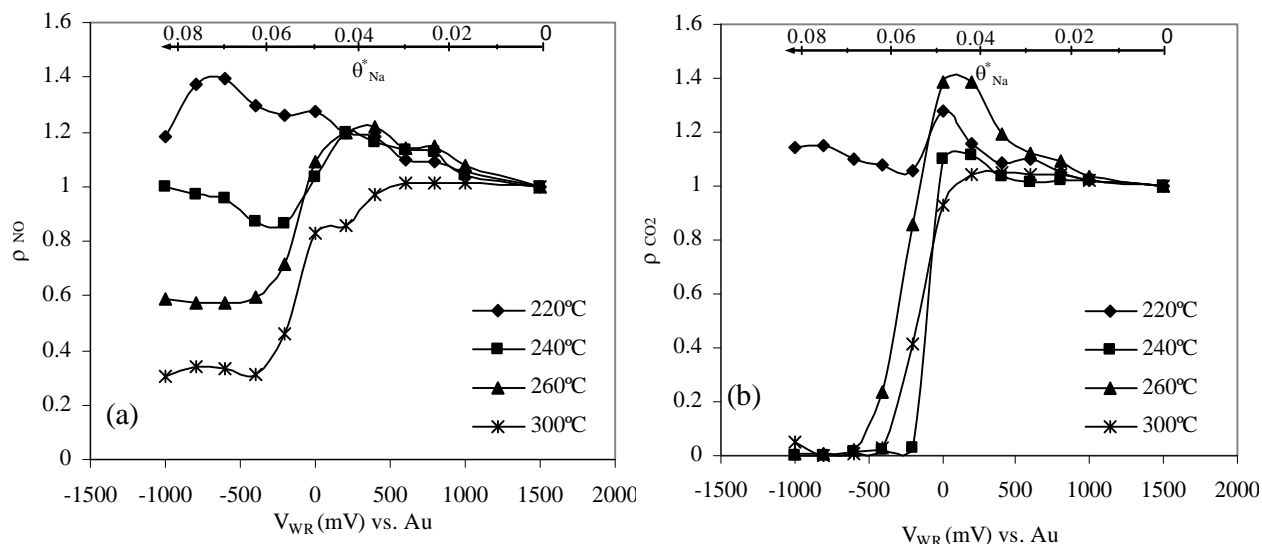


Figure 1. Effect of catalyst potential on the rate enhancement ratio ( $\rho$ ) for NO (a) and  $C_3H_6$  at different reaction temperatures. Conditions:  $C_3H_6/NO/O_2=2000$  ppm(2000 ppm/ 5 %, He balance, total flow rate 12 L/h.

It can be observed that a catalyst potential decrease led to changes for the NO and  $C_3H_6$  reaction rates. A decrease in the catalyst potential produced a decrease in the catalyst work function due to electrochemical pumping of  $Na^+$  from the electrolyte to the catalyst which modify its chemisorption properties. A decrease in the catalyst potential weakened the Pt chemical bond with electron-donor adsorbates, such as  $C_3H_6$  and strengthened those with electron-acceptors ones, such as  $O_2$  and NO [2]. At low temperature the catalyst is mainly covered by propene and therefore a decrease in the catalyst potential produced an increase in the catalytic activity. However, for high sodium coverage the catalyst exhibit poisoning, due to blocking of Pt active sites by Na compounds [3]. On the other hand, as the reaction temperature increase a progressive suppression of the promoting effect could be observed. It is due to an increasing adsorption of  $O_2$  at the expenses of the other reactants. As the reaction temperature is higher the initial  $O_2$  coverage on the catalyst increases. As a consequence, increasing the reaction temperature under promoted conditions resulted in a relative increase of the surface coverage of O adsorbed atoms at the expense of  $C_3H_6$  and NO molecules, thus causing a decrease in the level of promotion. Nevertheless, for the whole temperature range the presence of  $Na^+$  on the Pt catalyst strongly enhanced the N-O dissociation, giving values for  $N_2$  selectivity close to 90 %.

## References

- Vayenas, C.G., Bebelis, S., Ladas, S., (1990) *Nature*, 343, 625-627.  
 Dorado, F., de Lucas-Consuegra, A., Vernoux, P., Valverde, J.L., (2007) *Applied Catalysis B: environmental*, 73, 42-50.  
 Vernoux, P., Gaillard, F., Lopez, C., Siebert, E., (2004) *Solid State Ionics*, 175, 609-613.

## Catalytic Growth of Structured Nitrogen-Containing Carbon over Unsupported and Y Zeolite Supported Ni and Co Catalysts

A. Nieto-Márquez<sup>a</sup>, A. Romero<sup>a</sup>, P.B. García<sup>a</sup>, M.A. Keane<sup>b</sup>, J.L. Valverde<sup>a</sup>

<sup>a</sup>Department of Chemical Engineering, Faculty of Chemistry, University of Castilla-la Mancha Av. Camilo José Cela, 10. 13005 Ciudad Real, Spain. Tel.: +34-926-295300; Fax: +34-926-295318.

<sup>b</sup>Chemical Engineering, School of Engineering and Physical Sciences, Heriot-Watt University, Edinburgh E.H 14 4 AS, Scotland, United Kingdom. Corresponding author: antonio.nieto@uclm.es

### 1. Summary

The discovery of structured carbonaceous materials with a diversity of unique chemical and physical properties has attracted a significant research effort focused on alternative syntheses and new applications in gas adsorption, H<sub>2</sub> storage, and electronics. In addition, structured carbon has been used as catalyst support and as an electrochemical promoter in fuel cells. Doping these carbonaceous structures with heteroatoms, such as nitrogen or boron, is an effective means of modifying surface and electronic properties. Indeed, it has been established [1] that the incorporation of nitrogen in nanotubes results in enhanced conductivity, polarity and basicity while modifying surface hydrophilicity. In earlier work, we reported the growth of structured carbon *via* the decomposition of ethylene over Y zeolite supported Ni [2,3] and recorded reproducible yields of uniformly sized carbon nanofibers. This work has since been extended to consider carbon growth over bulk and Y zeolite supported Ni and Co, using acetonitrile as the carbon precursor. In this presentation, the effect of temperature, reaction time and the nature of the active metal on carbon yield is considered, the role of the support is addressed and the structural diversity (morphology, aspect ratio and graphitic nature) of the carbon product is demonstrated. The viability of incorporating nitrogen in the carbon growth is also discussed.

Keywords: acetonitrile, nickel, cobalt, metal-support interactions, carbon morphology

### 2. Extended Abstract

Unsupported and Y zeolite supported nickel and cobalt catalysts have been tested for the growth of nitrogen-doped structured carbon *via* the chemical vapour decomposition (CVD) of acetonitrile where  $550^{\circ}\text{C} \leq T \leq 1150^{\circ}\text{C}$ . A range of carbonaceous structures, including straight and coiled carbon filaments of varying diameter and lattice structure as well as carbon nanospheres were obtained. The graphitic character of the carbon product has been evaluated by means of temperature programmed oxidation (TPO) and XRD measurements. The surface area and porosity of both catalyst and carbon product has

been assessed by N<sub>2</sub> adsorption-desorption analyses and the morphological features determined by scanning and transmission electron microscopy (SEM and TEM). Carbon yield and morphology was strongly dependent on reaction temperature, the nature of the active metal and the use of a support. Carbon yield increased with increasing temperature (up to 1050°C) to give maximum values in the order Ni < Co < Ni-Y < Co-Y. The supported catalysts delivered significantly higher carbon yields (up to 30 g<sub>carbon</sub>/g<sub>metal</sub>) and initiated carbon growth at temperatures up to 300°C lower than that observed for the bulk metals. A loss of catalyst activity with time-on-stream was a feature of reaction over the supported metals. Carbon generated over Ni/Y and Co/Y at 750°C took the form of straight nanofibres with a switch to a coiled filament growth at higher temperatures and ultimately a predominant production of nanospheres at 1150°C. On the basis of TPO analysis, the graphitic nature of the carbon growth over both zeolite supported and bulk metal increased with increasing synthesis temperature. Elemental (CHN) analysis of the carbon product has revealed a nitrogen content up to 5 mol %. Critical structural and compositional characteristics of the carbon obtained from the four catalyst systems are summarised in Table 1 for three representative reaction temperatures.

<i>Catalyst/ Reaction Temperature</i>	<i>BET area (m<sup>2</sup>g<sup>-1</sup>)</i>	<i>Ext. surface area (m<sup>2</sup>g<sup>-1</sup>)</i>	<i>Total pore volume (cm<sup>3</sup>g<sup>-1</sup>)</i>	<i>d<sub>pore</sub> (nm)</i>	<i>d<sub>002</sub> (nm)</i>	<i>%mol Carbon</i>	<i>%mol Hydrogen</i>	<i>%mol Nitrogen</i>
<b>Ni/Y @750°C</b>	49	36	0.09	7.4	0.343	90.5	5.0	4.5
<b>Ni/Y@ 950°C</b>	31	26	0.09	12.1	0.339	92.6	5.9	1.5
<b>Ni/Y@1150°C</b>	8	7	0.04	21.1	0.339	95.2	2.6	2.2
<b>Co/Y@750°C</b>	100	96	0.33	13.2	0.343	95.9	2.5	1.6
<b>Co/Y@950°C</b>	19	12	0.05	12.1	0.339	95.2	3.6	1.2
<b>Co/Y@1150°C</b>	5	2	0.02	11.8	0.339	92.5	4.9	2.6
<b>Ni+Y@950°C</b>	8	5	0.04	17.5	0.339	91.1	5.7	3.2
<b>Ni+Y@1150°C</b>	5	2	0.01	9.2	0.341	91.7	4.8	3.5
<b>Co+Y@950°C</b>	5	<1	0.01	8.8	0.343	89.0	6.0	5.0
<b>Co+Y@1150°C</b>	5	<1	0.01	9.9	0.338	90.7	5.7	3.6

Table 1: BET surface area, porosity, crystalline parameters and elemental (CHN) composition of representative carbon obtained from reaction over bulk and Y-zeolite supported Co and Ni catalysts.

## References

- Maiyalagan, T., Viswanathan, B., (2005) *Mater. Chem. Phys.*, 93, 291-295.  
 De Lucas, A. Garrido, A., Sánchez, P., Romero, A., Valverde, J.L., (2005) *Ind. Eng. Chem. Res.*, 44, 8225-8236.  
 Park, C., Keane, M.A., (2001) *Langmuir* 17, 8386-8396.



## The Effect of Lanthanum on the Performance of Pt-Sn/Al<sub>2</sub>O<sub>3</sub> Reforming catalysts

I. Contreras-Andrade<sup>a,b</sup> and T. Viveros-García<sup>b</sup>

<sup>a</sup>Facultad de Ciencias Químico-Biológicas, Universidad Autónoma de Sinaloa, 01354, Culiacán, Sinaloa, México.

<sup>b</sup>Universidad Autónoma Metropolitana- Iztapalapa, Departamento de Ingeniería de Procesos e Hidráulica, México D.F., Av. San Rafael Atlixco, No. 186, Col. Vicentina, 09340. Tel. +52 (55) 58044925, Fax. +52 (55) 58044900, e-mail: [tvig@xanum.uam.mx](mailto:tvig@xanum.uam.mx).

### 1. Summary

In the present work the effect of lanthanum on the catalytic behavior of the bifunctional PtSn/Al<sub>2</sub>O<sub>3</sub> reforming catalyst has been investigated. Lanthanum was introduced during the synthesis of the Al<sub>2</sub>O<sub>3</sub> by the sol-gel method to form an Al<sub>2</sub>O<sub>3</sub>-La<sub>2</sub>O<sub>3</sub> mixed oxide. The *n*-heptane reforming at 500°C was used as a test reaction and according to our results lanthanum seems to be one of the most promising additives because it provides a total benzene inhibition and long lifetime (17% deactivation after 50 min. on stream). Changes in the catalytic behavior due to differences of the acidity and the support-metal interaction were observed. The surface area is increased with lanthanum content, reaching its maximum at 15% of La<sub>2</sub>O<sub>3</sub> content. Acid site density is diminished, while the base site density is increased with the introduction of lanthanum. Furthermore, the higher base site density (at 15 wt% of La<sub>2</sub>O<sub>3</sub>) correlates very well with the inhibition of benzene and resistance to deactivation of the PtSn/Al<sub>2</sub>O<sub>3</sub>-La<sub>2</sub>O<sub>3</sub>-15. By FTIR-pyridine thermo-desorption it was determined that alumina has mainly Lewis acid sites. The strength of the Lewis acid sites decreased according to the La content. Crystalline micro-domains of LaAl<sub>11</sub>O<sub>18</sub> detected by EDX could be responsible for the changes in the acid-base properties of the support. The introduction of La into Al<sub>2</sub>O<sub>3</sub> framework was observed by NMR. Al<sup>V</sup> site can be promoted through La addition in the sol-gel procedure.

Key words: Catalytic Reforming, PtSn/Al<sub>2</sub>O<sub>3</sub>-La<sub>2</sub>O<sub>3</sub>, catalysts deactivation, <sup>27</sup>Al NMR.

### 2. Experimental

The Al<sub>2</sub>O<sub>3</sub>-La<sub>2</sub>O<sub>3</sub> (5 and 15 wt% of La<sub>2</sub>O<sub>3</sub>) supports were prepared by the sol-gel method [1] and after calcinations were impregnated with hexachloroplatinic acid and tin (II) chloride to obtain PtSn/Al<sub>2</sub>O<sub>3</sub>-La<sub>2</sub>O<sub>3</sub> (1% Pt and 0.6% Sn). In such a way, the role of La<sub>2</sub>O<sub>3</sub> is not limited to a surface effect, since La can be incorporated into the alumina framework. The characterization of the synthesized material was done by physisorption of nitrogen, temperature programmed desorption (TPD) of ammonia and CO<sub>2</sub>, magic angle spinning (MAS) <sup>27</sup>Al NMR spectroscopy, electron transmission

microscopy and H<sub>2</sub> chemisorption. The catalytic activity of the materials was determined by *n*-heptane reforming at 500°C. Support preparation has been described in details elsewhere [1].

### 3. Results and discussion

Table 1. Textural and acidity-basicity properties of the supports.

Sample	N <sub>2</sub> Physisorption			Acidity-Basicity Properties		
	S <sub>BET</sub> , m <sup>2</sup> /g	Pore volume, cc/g	Pore diameter, Å	Temperature Programmed Desorption		
				Acid site density (mole NH <sub>3</sub> /m <sup>2</sup> ) X10 <sup>4</sup>	Base site density (mole CO <sub>2</sub> /m <sup>2</sup> ) X10 <sup>5</sup>	Ψ
Al <sub>2</sub> O <sub>3</sub>	327	1.26	156	2.72	2.70	10.07
Al <sub>2</sub> O <sub>3</sub> -La <sub>2</sub> O <sub>3</sub> -5	345	1.00	115	2.32	3.88	5.97
Al <sub>2</sub> O <sub>3</sub> -La <sub>2</sub> O <sub>3</sub> -15	355	0.82	93	1.99	4.35	4.57
La <sub>2</sub> O <sub>3</sub>	30	0.23	330	1.11	8.03	1.38

Al<sub>2</sub>O<sub>3</sub>-La<sub>2</sub>O<sub>3</sub>-5: with 5 wt% of La<sub>2</sub>O<sub>3</sub>, Al<sub>2</sub>O<sub>3</sub>-La<sub>2</sub>O<sub>3</sub>-15: with 15 wt% of La<sub>2</sub>O<sub>3</sub> and ψ: acid/base site ratio

The sol-gel method yielded mesoporous materials of high surface areas. It has been observed a small increase in the BET surface area for Al<sub>2</sub>O<sub>3</sub>-La<sub>2</sub>O<sub>3</sub> mixed oxide compared with bare Al<sub>2</sub>O<sub>3</sub> (327m<sup>2</sup>/g) due to lanthanum insertion in the framework of Al<sub>2</sub>O<sub>3</sub>. Moreover, changes in coordination spheres of Al were detected by NMR. A decrease of aluminum in octahedral environment Al<sup>VI</sup> (3.5 ppm) as well as an increase of the pentahedrally coordinated Al<sup>V</sup> (32 ppm) as a function of the lanthanum content was observed. The former gives a modification in the acid-base properties of the support (table1). On the other hand, the acid/base site ratio (ψ) diminishes with the introduction of lanthanum and base site correlates very well with the activity of the catalysts (table1). Furthermore, lanthanum clearly modifies both the yield of the catalysts inhibiting the benzene production (table 2) and the selectivity to toluene. In fact, it seems to be that the 15% of La<sub>2</sub>O<sub>3</sub> is the optimum concentration to increase both the activity and the resistance to deactivation.

Table 2. Catalytic behavior of Pt and PtSn catalysts for the *n*-heptane dehydrocyclization after 50 min. on stream.

Catalyst	%D <sup>a</sup>	Rate X 10 <sup>4</sup> (molg <sup>-1</sup> s <sup>-1</sup> )	Yield, (%)			Toluene Selectivity <sup>b</sup> , (%)
			C <sub>1</sub> -C <sub>4</sub>	Benzene	Toluene	
PtSn/Al <sub>2</sub> O <sub>3</sub>	46	1.56	4.38	1.00	12.32	69.6
PtSn/Al <sub>2</sub> O <sub>3</sub> -La <sub>2</sub> O <sub>3</sub> -5	30	1.53	1.80	0.5	15.03	86.7
PtSn/Al <sub>2</sub> O <sub>3</sub> -La <sub>2</sub> O <sub>3</sub> -15	17	3.52	0.52	-	39.40	98.7
PtSn/La <sub>2</sub> O <sub>3</sub>	95	0.16	1.8	-	0.01	0.55

<sup>a</sup> % of deactivation and <sup>b</sup> Calculated as yield of toluene/total conversion

The effect of lanthanum over the catalytic behavior of the catalysts studied is in disagreement with the reported by Del Angel et al [2]. In our study, this catalytic behavior can be attributed to the closer intimate contact between the platinum-lanthanum-acid sites. That is to say, La performs as auto-regeneration agent, hydrogenating the coke precursors. As main conclusion, the result shows a promising alternative for production of ecological benzene-free gasoline in RC process.

### 4. References

- [1] Contreras, I., Perez, G., and Viveros, T. Int. J. React. Eng., 3 (2005) A32.
- [2] Del Angel, G., Bonilla, A., Peña, Y., Navarrete, J., Fierro, J.L.G., Acosta, D.R., J. Catal., 219 (2003) 63.

## Characteristics of the support and active phases of Monolithic Co/Al<sub>2</sub>O<sub>3</sub>-SO<sub>4</sub> catalysts for CH<sub>4</sub>-SCR

S.B. Rasmussen<sup>a,b</sup>, J.C. Martin<sup>a</sup>, M. Yates<sup>a</sup>, P. Avila<sup>a</sup>

<sup>a</sup>*Instituto de Catal sis y Petroleoqu mica, CSIC, C/Marie Curie no 2, Cantoblanco, 28049 Madrid, Spain*

<sup>b</sup>*Center for Sustainable and Green Chemistry, Dep. Chemistry, Technical University of Denmark, Denmark*

### 1. Summary

Selective catalytic reduction (SCR) of nitric oxide with methane in presence of excess oxygen has been studied in this work. CoO<sub>x</sub>/γ-Al<sub>2</sub>O<sub>3</sub> showed low SCR activity, but high activity for the unwanted CH<sub>4</sub> combustion. By pre treating the γ-Al<sub>2</sub>O<sub>3</sub> with H<sub>2</sub>SO<sub>4</sub>, a promoting effect on the catalytic activity as well as the selectivity was obtained. The UV-Vis- and EPR- spectroscopic techniques were used to elucidate the structural rearrangements responsible for the improvement of the catalyst. The coordination chemistry of CoO<sub>x</sub> dispersed over γ-Al<sub>2</sub>O<sub>3</sub>-SO<sub>4</sub> and γ-Al<sub>2</sub>O<sub>3</sub> was altered by sulphatisation of the carrier material, such that cobalt was stabilised as a tetrahedral Co(II) complex bonded to sulphate ligands. The analogue unsulphated carrier did not exhibit the same stabilising properties, and cobalt oxide was instead found as the mixed valence spinel structure Co<sub>3</sub>O<sub>4</sub>. Activity measurements suggest that the tetrahedral Co<sup>2+</sup> surface complex is the active species for the CH<sub>4</sub>-SCR reaction.

Keywords: monolithic catalyst, EPR, UV-VIS, sulphated γ-alumina, cobalt

### 2. Extended Abstract

The catalytic reduction of NO<sub>x</sub> with hydrocarbons (HC) in the presence of excess oxygen (lean conditions) constitutes an interesting alternative process for elimination of emitted NO<sub>x</sub> from mobile sources, as well as for certain stationary (hydro-carbon fuelled) installations. In these types of applications use of methane is especially attractive since this compound is readily available from the fuel itself. However, CH<sub>4</sub>-SCR suffers from low catalytic activity, due to the challenge of activating the methane molecule. Cobalt based catalysts supported by zeolites [1] and sulphated zirconia [2] have been demonstrated as promising materials for this process. Earlier [3] we have shown that pre treatment of alumina with H<sub>2</sub>SO<sub>4</sub> improved the catalytic activity and selectivity compared to treatments with other mineral acids.

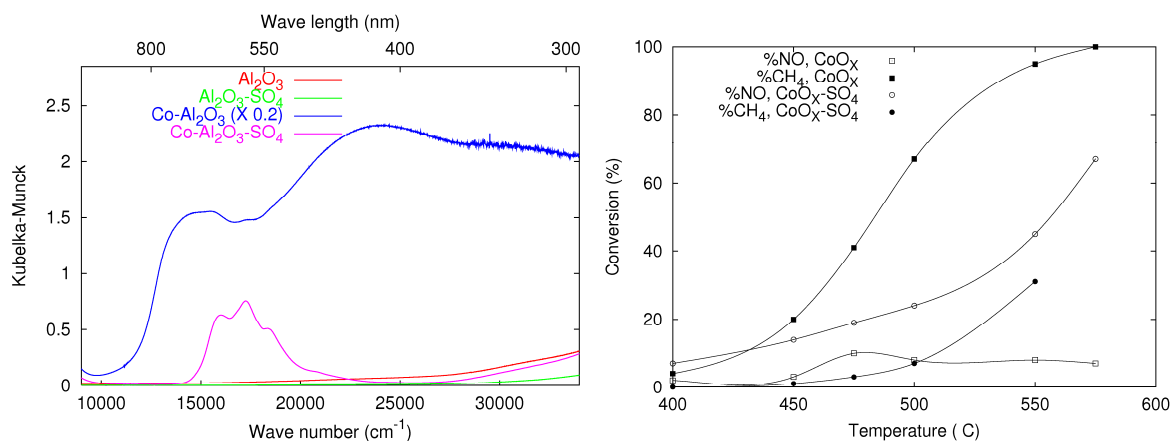


Figure 1 (left) & 2 (right): 1) UV-VIS spectras of sulphated and non-sulphated monolithic aluminas with and without Co-impregnation. 2) Conversions of NO by CH<sub>4</sub>-SCR and CH<sub>4</sub> combustion for sulphated and non-sulphated Co-catalysts. The operating conditions were: [NO] = 500 ppm, [CH<sub>4</sub>] = 1000 ppm, [O<sub>2</sub>] = 5 vol.%, balance in N<sub>2</sub>, GHSV(N.T.P.) = 5120 h<sup>-1</sup>.

As seen in Figure 1, treatment of alumina monoliths with sulphuric acid induces changes of the structure of the active CoO<sub>x</sub> phase, which can be seen clearly by the change in the UV-Vis spectra, where the Co-bands change from octahedral to tetrahedral conformation. Simultaneously, the presence of pure ionic Co-SO<sub>4</sub> bonds, instead of cobalt aluminate improves the catalytic activity of the monoliths in the CH<sub>4</sub>-SCR of NO<sub>x</sub> reaction and lowers the overall oxidation (combustion) of CH<sub>4</sub>. Furthermore additional EPR spectroscopic results show that Co<sup>2+</sup> on the sulphated catalyst has sulphate ligands, Thus, sulphate probably acts as a catalyst promoter both by increasing the surface acidity and by structurally rearranging the active Co<sup>2+</sup> site.

### Conclusion

An improved cobalt catalyst using sulphated  $\gamma$ -alumina as support in monolithic form has been obtained. The structural chemistry of the active species responsible for the catalytic properties have been studied by spectroscopic methods and are found to consist of isolated Co<sup>2+</sup> entities in tetrahedral conformation with sulphate ligands. Thus the benefits of sulphatisation with these catalysts are not limited to the well known enhanced acidity effect – since it also modifies the active cobalt species, forming a tetrahedral complex with improved catalytic properties.

### Acknowledgements

The authors gratefully acknowledge the CYTED Program (Project V 7), the CAM (project ref: GR/AMB/0751/2004) and the ELFOR PSO FU520 project for financial support.

### References

- Y. Li y J. N. Armor, *Appl. Catal. B*, 1 (1992) L31.
- N. Li, A. Wang, J. Tang, X. Wang, D. Liang, T. Zhang, *Appl. Catal. B*, 43 (2003) 195.
- J.C.Martin, P.Avila, S.Suarez, M. Yates, A.B.Martín-Rojo, C. Barthelemy, J.A.Martín, *Appl. Catal. B*. 67 (2006) 270.

## Catalysts on the base of layered oxides for the decomposition of water and waste compounds

Irina Zvereva<sup>a</sup>, Alexander Toikka<sup>a</sup>, Jhy-Chern Liu<sup>b</sup>

<sup>a</sup>*Department of Chemical Thermodynamics and Kinetics, Saint-Petersburg State University, Universitetskiy pr. 26, 198504, Saint-Petersburg, Russia*

<sup>b</sup>*Department of Chemical Engineering, National Tawan University of Science and Technology, 43 Keelung road., sec. 4, Taipei 106, Taiwan*

### 1. Summary

Photocatalysis has great potential for the conversion of photon energy into chemical energy and to decompose pollutants in solution. Photocatalytic water splitting with the use of solar energy or UV-light irradiation is an attractive route for energy conversion. The reaction of water splitting into H<sub>2</sub> and O<sub>2</sub> is of fundamental and industrial importance because it converts water directly into hydrogen. In our work we report the result of the research of photocatalytic properties of materials based on perovskite-type layered oxides. We consider the advantages of Ruddlesden-Popper, Dion-Jacobson and Aurivillius phases as photocatalysts. The preparation of these photocatalytic materials, investigation and design of the structure, the study of stability of layered oxide and their photocatalytic properties are the main goal of presentation.

Keywords: Photocatalysts, photocatalytic reactions, water splitting, hydrogen energy, layered materials

### 2. Extended Summary

Photocatalytic water splitting reaction has received much attention as a method for solar energy conversion into chemical energy because of its potential to directly obtain clean hydrogen. The construction of an efficient artificial photosynthesis system for solar energy conversion and storage is one of the fascinating goals to solve the global energy problem. Application of photocatalytic reactions is much perspective for sterilization of water for different waste products

Nowadays some technological methods are not useful in practice, because there are no proper materials and substances. There is considerable interest at present in layered oxides. A variety of mixed metal oxides such as perovskite-type and another layered structures, have been extensively studied as substances able to decompose water under irradiation. Use of layered materials is especially interesting because of the possibility of modifying the chemical composition as well as microstructure by means of ion-exchange

or intercalation, which is useful for designing photocatalysts based on semiconducting metal oxide sheets.

Report focuses on the structural design and photocatalytic properties of materials based on perovskite-type layered oxides. We consider oxides with photocatalytic activity for the process of water splitting and decomposition of waste compounds.

The preparation potential photocatalytic materials, investigate their structure, phase stability and photocatalytic properties are the main aspects of presentation. This provides understanding of the structural and electronic factors responsible for photo-initiated decomposition processes in the interlayer space of layered structures. The knowledge of these properties would open a route towards new materials for the solving environmental and ecological problems.

The possibilities of layered oxides and their derivatives with interplay between layered type of structure, cationic ordering, electric polarization are not comprehensively studied. A new way to improve photocatalytic activity for the decomposition of compounds by introduction of ordered perovskites is related to creating ordered arrangements of cations with local dipoles. The analysis covers wide range of oxides which belongs to layered perovskite-type structures (Ruddlesden-Popper, Dion-Jacobson and Aurivillius phases with various thickness of perovskite slabs), investigation of oxides with variable anisotropy of structure and chemical content (titanates, tantalates, niobates, aluminates), kinetics of photocatalytic processes, methods of synthesis and using photocatalysts at practical conditions.

#### *Acknowledgements*

Authors are grateful for the financial support of the Federal Education Agency of Russia. The present contribution was developed within the framework of the project "Innovative educational environment in the classical university" by the St. Petersburg State University.

## **Kinetic consideration of non-catalytic and catalytic oxidation of soot**

Vesna Tomašić<sup>a</sup>, Ivan Brnardić<sup>b</sup>, Hrvoje Jenei<sup>c</sup>, Stanka Zrnčević<sup>a</sup>

<sup>a</sup>*Department of Reaction Engineering and Catalysis, Faculty of Chemical Engineering and Technology, University of Zagreb, HR-10000 Zagreb, Croatia*

<sup>b</sup>*Department of Physical Chemistry, Faculty of Chemical Engineering and Technology, University of Zagreb, HR-10000 Zagreb, Croatia*

<sup>c</sup>*PLIVA Croatia, Generics IP, HR-10000 Zagreb, Croatia*

### **1. Summary**

Diesel engines are considered as the main source of emission of the particulate matter (soot particles) originating from the uncomplete fuel combustion (Neeft et al., 1996; Stanmore et al., 2001). These particles are very harmful to human health, due to their carcinogenic effect.

The aim of this work was to investigate the influence of the applied catalysts (Mn- and Pt-based catalyst) on the soot oxidation. Special emphasis was put on the kinetics of both non-catalyzed and catalyzed reaction. The Kissinger-Akahira-Sunose (Kissinger, 1957) isoconversional method was used and the obtained Arrhenius parameters (activation energy and pre-exponential factor) are analysed and discussed.

Keywords: soot oxidation, kinetics, thermo-oxidative degradation

### **2. Extended Abstract**

Active carbon supplied by Kemika, was selected as model carbon material to simulate diesel soot combustion. Commercial Pt-based catalyst (code F 105 R/W), supplied by Degussa-Huls AG was thermal pretreated at 60 °C for 24 hours. Mn-based catalyst was prepared by wet impregnation of Mn(SO<sub>4</sub>)-4H<sub>2</sub>O solution on the alumina support.

The thermo-oxidative degradation and catalytic oxidation of the active carbon were investigated by means of dynamic thermogravimetric analysis in an excess of air. An appropriate amount of the active carbon or mixture of active carbon and catalyst (in the ratio of 1:1) was loaded in the crucible and heated from 40 °C to 1000 °C. The experiments were carried out at constant heating rates (5, 10, 15, 20 and 25 °C min<sup>-1</sup>). The mass loss and the sample temperature were monitored by computerised data acquisition system. The oxidant was dry air (30 and 150 cm<sup>3</sup>min<sup>-1</sup>) flowing downwards on the cylindrical sample holder.

The preliminary experiments were performed with varying gas flow rate of dry air (30-150 cm<sup>3</sup> min<sup>-1</sup>) in order to investigate the influence of the external mass transfer

limitations on the results of thermoanalytical measurements. It was observed that under the experimental conditions employed in this study, the conversion versus temperature curves remained unchanged within the range of experimental uncertainty. Due to a small size fraction of the soot sample used, the intraphase mass transfer was also neglected.

Figure 1 shows comparison of the results obtained during non-catalytic and catalytic oxidation of the soot at constant heating rate of  $20^{\circ}\text{C min}^{-1}$ . It can be seen that the characteristic temperature of the soot oxidation was shifted to the low temperature region in the presence of the Pt-based catalyst. Maximum temperature for catalytic oxidation of the AC-Pt catalyst mixture was by approximately  $180\text{--}200^{\circ}\text{C}$  lower than for thermo-oxidative degradation in the absence of the catalyst. Conversely, the Mn-based catalyst had no influence on combustion rate of the active carbon sample. That was surprising, because some researchers had observed good activity of the Mn-based catalyst in the soot oxidation. Presumably, wet impregnation is not the appropriate method for preparation of the Mn-based catalyst active in the soot oxidation. Further work is currently undertaken to investigate the influence of other preparation methods and preparation conditions on the activity of the Mn-catalyst.

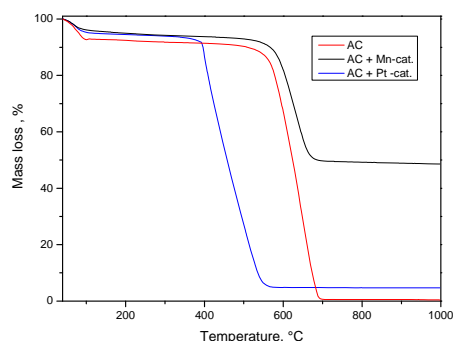


Figure 1: Experimental data obtained at constant heating rate of  $20^{\circ}\text{C min}^{-1}$  for non-catalytic and catalytic oxidation of the soot

The values of kinetic parameters, such as activation energy ( $E_a$ ) and Arrhenius pre-exponential factor ( $A$ ) were calculated using Kissinger-Akahira-Sunose (KAS) isoconversional method. The obtained values of the activation energy were in good agreement with the literature data (López-Fonseca et al., 2005). At 50 % conversion the activation energies were  $88.39\text{ kJ mol}^{-1}$  and  $173\text{ kJ mol}^{-1}$  for the catalytic and non-catalytic soot oxidation respectively. Linear relationship between activation energy and pre-exponential factor was observed and defined by the compensation effect.

## References

- Kissinger, H.E. (1957) *Anal. Chem.* 29, 1702.  
 López-Fonseca, R., Elizundia, U., Landa, I., Gutiérrez-Ortiz, M.A., González-Velasco, J.R. (2005) *Appl. Catal. B: Environ.* 61, 150.  
 Neeft, J.P.A., Makkee, M., Moulijn, J.A. (1996) *Fuel Process. Technol.* 47 (1) 1.  
 Stanmore, B.R., Brilhac, J.F., Gilot, P. (2001) *Carbon* 39, 2247.



## Cyclohexane dehydrogenation for the evaluation of metallic sites accessibility in naphtha reforming bimetallic catalysts.

B. Iñarra<sup>a,c</sup>, M.P. González-Marcos<sup>a,c,\*</sup>, J.M. Guil<sup>b,c</sup>, M.A. Gutiérrez-Ortiz<sup>a,c</sup>

<sup>a</sup>*Dpto. Ingeniería Química, Facultad de Ciencias, Universidad del País Vasco/E.H.U., P.O. Box 644, E-48080 Bilbao (Spain),*

<sup>b</sup>*Instituto de Química Física "Rocasolano", CSIC, c/Serrano, 119, E-28006 Madrid (Spain)*

<sup>c</sup>*Unidad asociada al CSIC "Grupo de Tecnologías Químicas para la Sostenibilidad Ambiental"*

### 1. Summary

Catalysts characterisation is of paramount importance in any catalytic process. Furthermore, if catalysts undergo deactivation, monitoring of catalysts properties becomes the key for the process performance. Naphtha reforming is one of the most important operations of petroleum treatments. The evolution of catalysts, from classic Pt/Al<sub>2</sub>O<sub>3</sub> to Pt-Re/Al<sub>2</sub>O<sub>3</sub> or Pt-Sn/Al<sub>2</sub>O<sub>3</sub>, and operation units, from cyclic units to CCR, necessitates a close catalyst evaluation. When evaluating metallic sites accessibility, the use of hydrogen chemisorption, or hydrogen-oxygen titration, is well established for monometallic Pt/Al<sub>2</sub>O<sub>3</sub> catalysts. However, classical methods do not provide reliable values for bimetallic catalysts and the use of pilot plants is expensive and time-consuming. Problems are mostly related with the uncertainties of the oxidation state of the second metal and its interaction with platinum and the support. In order to solve this problem, we propose in this work the use and standardisation of test reactions to characterise these catalysts. Cyclohexane dehydrogenation (CH) is a structure-insensitive reaction that can be easily used for the evaluation of metallic sites accessibility.

Keywords: naphtha reforming catalysts, Pt-Re, Pt-Sn, test reactions, catalyst characterization

### 2. Extended Abstract

A wide range of purposely prepared catalysts (Pt/Al<sub>2</sub>O<sub>3</sub>, Pt-Re/Al<sub>2</sub>O<sub>3</sub> and Pt-Sn/Al<sub>2</sub>O<sub>3</sub>) and industrial fresh and aged catalysts (Pt-Re/Al<sub>2</sub>O<sub>3</sub> and Pt-Sn/Al<sub>2</sub>O<sub>3</sub>) were studied with classical techniques and tested in CH. Catalyst preparation methods and details of classical techniques are described elsewhere [González-Marcos et al., 2004]. CH test reactions were carried out at atmospheric pressure in a fixed-bed reactor with differential operation, high linear gas space velocity, in order to avoid external and internal diffusion controls.

Results show that H<sub>2</sub> chemisorption presents a low sensitivity to Sn/Pt or Re/Pt ratio (Table 1, H/Pt column). However, catalytic tests reveal important changes in the catalyst behaviour: while Sn decreases catalyst activity, Re enhances it.

Assuming a constant TOF, equal to that obtained with Pt/Al<sub>2</sub>O<sub>3</sub> catalysts (the reaction is structure-insensitive), allows recalculation of metallic dispersion (Table 1, CH/Pt column for Sn-containing and CH/Pt+Re for Re-containing catalysts).

Sn-containing fresh and aged industrial catalysts show similar metallic dispersion evaluated by H<sub>2</sub> chemisorption, while their CH reaction rate show a clear and progressive decrease with the use in the industrial process. All aged Re-containing catalysts present similar metallic dispersion evaluated by H<sub>2</sub> chemisorption, lower than that of the fresh catalyst, although catalytic tests show a progressive diminution of CH reaction rate with ageing.

Cyclohexane dehydrogenation test reactions can be concluded to be a powerful tool to achieve cheap, quick and reliable information for the evaluation of metallic site accessibility of industrial naphtha reforming catalysts in order to improve catalyst regeneration and process operation.

### Acknowledgements

The authors wish to thank the Spanish *Ministerio de Ciencia y Tecnología* (MCYT, MAT2001-2082), the *Universidad del País Vasco/E.H.U.* (9/UPV-13517) for their financial support and the *Departamento de Educación, Universidades e Investigación del Gobierno Vasco* for the Grant of B. Iñarra (*Programa de Formación de Investigadores*, BFI02.51).

### References

González-Marcos, M. P., Iñarra, B., Guil, J. M. and Gutiérrez-Ortiz, M. A., (2004) *Applied Catalysis A: General*, 273, 259-268.

Table 1: Nomenclature, metallic content and dispersion of evaluated samples.

	Actual metallic content		Dispersion	
	Pt	Sn	H/Pt	CH/Pt
03S00	0.25	0.00	0.71	0.71
03S03	0.29	0.33	0.54	0.11
03S10	0.27	1.02	0.63	0.01
10S00	0.91	0.00	0.56	0.56
10S03	0.90	0.32	0.63	0.33
IS-F	0.23	0.24	0.52	0.11
IS-1	0.24	0.24	0.60	0.01
IS-2	0.24	0.24	0.56	0.01
	Pt	Re	H/Pt	CH/Pt+Re
03R00	0.21	0.00	0.95	0.95
03R03	0.21	0.25	0.62	0.53
03R10	0.27	0.97	0.57	0.26
10R00	0.71	0.00	0.94	0.94
10R03	0.77	0.28	0.52	0.91
10R10	0.73	0.92	0.43	0.73
IR-F	0.26	0.27	0.74	0.44
IR-1	0.26	0.27	0.20	0.29
IR-2	0.26	0.27	0.20	0.20
IR-3	0.26	0.27	0.22	0.10
IR-4	0.26	0.27	0.19	0.05

## Effect of preparation method on perovskite catalyst structure for synthesis of Acetic acid from natural gas

H. R. Arandiyani and M. Parvari\*

*Department of Chemical Engineering, Iran University of Science and Technology, Tehran, Iran*

### 1. Summary

Different synthesis of acetic acid have been studied and compared. The most important objective of the development of new acetic acid processes is, to reduce raw material consumption, energy requirements, and investment costs. Different methods have been presented for synthesis of acetic acid in literature but industrial processes for the production of acetic acid are dominated by methanol carbonylation and the oxidation of hydrocarbons such as acetaldehyde, ethylene, n-butane, and naphtha. In addition of comparison synthesis methods, application of the product is investigated and advantages of the methods have been presented. In this regard, proper process for production of acetic acid can be selected. Finally results showed that the using methanol carbonylation method is proper because of high purity, low production cost, reaction condition, yield and also no undesired byproduct as the best choice for production acetic acid.

Keywords: perovskite catalyst, acetic acid, natural gas, sol-gel

### 2. Extended Abstract

Acetic acid is an important industrial product with world-wide production over eight million tons per year, Acetic acid is produced commercially by methanol carbonylation, ethylene or acetaldehyde oxidation and butane/naphtha oxidation Smejkal, Q. et al. Halder topsoe, et al. is promoting technology for acetic acid from natural gas. Showa denko, Sano, K. et al. uses a one step process to produce acetic acid by direct oxidation of ethylene. Sabic has disclosed an improved catalyst for coproduction of ethylene and acetic acid from ethane. Chiyoda and UOP, Noriyuki, Y. et al. introduced the acetica process, based on a heterogeneous Rh catalyst in which the active Rh complex is chemically immobilized on a polyvinyl pyridine resin. Now days, Wei, H. et al. a great research is being carried out in the development of direct synthesis of acetic acid from natural gas, because can be an alternative to methanol carbonylation process because of its high selectivity and because of the cheap feedstock.

In this work, we present the mixed-oxide  $\text{LaMo}_x\text{V}_{1-x}\text{O}_n$  ternary perovskites with  $X=0$  for  $\text{LaVO}_n$  and  $X=1$  for  $\text{LaMoO}_n$  as catalyst precursor are synthesized by a sol-gel method to ensure a good homogeneity of the mixed-oxides that calcined in different conditions have been tested in direct synthesis of acetic acid in ethane dry reforming reaction. The effects

of temperature and pressure and catalyst activity have been studied in a fixed bed micro reactor with 200 mg catalyst loading. Reaction temperature has been changed in range of 450°C to 750°C and pressure has been changed in range of 1atm to 8 atm.  $\text{LaMo}_{0.3}\text{V}_{0.7}\text{O}_n$  mixed oxide calcined in 750°C show more activity respect to other samples. Ethane conversion and acetic acid selectivity in 750°C reach to 78% and 9% respectively. In this regards it has been shown that acetic acid selectivity increase with increasing the pressure and temperature.

## References

- Denko, Japanese Patent Koukai 9-67298 (1995) to Denko.  
Noriyuki, Y., Satoru, K., Makoto, Y., Peter, P., Steve. W., (2001) *Applied Catalysis A: General* 221 , 253–265.  
Sano, K., Uchida, H., *Shokubai* 41 (4) (1999) 290.  
Smejkal, Q., Linke, D., Baerns, M., (2005) *Chemical Engineering Processing* 44, 421-428.  
Topsoe, US patent 5728871 (1998) to Topsoe.  
Wei, H., Cuihong, Z., Lihua, Y., Kechang, X., (2004) *Journal of Natural Gas Chemistry* 13, 113-115.

## **A new perovskite catalytic system consisting of LaMoV for Acetic acid direct synthesis from Ethane and CO<sub>2</sub>**

H. R. Arandiyani, M. Parvari\*

*Department of Chemical Engineering, Iran University of Science and Technology, Tehran, Iran*

### **1. Summary**

LaMo<sub>x</sub>V<sub>1-x</sub>O<sub>n</sub> Perovskite systems were prepared to be used in natural gas for producing acetic acid. The perovskite systems have been obtained via a sol-gel related method using water as solvent. In order to understand the role of the precursor nature and calcinations conditions on the formation of LaMo<sub>x</sub>V<sub>1-x</sub>O<sub>n</sub> an identification using FTIR, XRD, SEM, EDS, TPR, and Carbon Analysis was made. The precursor structure is a function of raw material and calcinations conditions. It is shown that the nitrate salts of lanthanum, molybdenum and vanadium and calcinations at 750 °C for 4 hours gave pure LaMo<sub>x</sub>V<sub>1-x</sub>O<sub>n</sub> perovskite with good homogeneity. These systems are highly efficient catalysts in direct synthesis of acetic acid from natural gas. Studies on the state of these systems after test show the stabilization of perovskite structures. The best-mixed perovskite for the direct synthesis acetic acid from natural gas is LaMo<sub>0.7</sub>V<sub>0.3</sub>O<sub>n</sub>

Keywords: Perovskite, LaMoO<sub>n</sub>, LaVO<sub>n</sub>, Direct Synthesis, Acetic acid

### **2. Extended Abstract**

Acetic acid is an important industrial chemical produced at an annual rate of more than 8 million tons worldwide, Acetic Acid.Chemical Week. Acetic acid is used primarily as a raw material for vinyl acetate monomer (VAM) and acetic anhydride synthesis, and as a solvent for purified terephthalic acid (PTA) production. Using over 44% of the acetic acid produced in 2006, vinyl acetate production is the largest consumer of acetic acid, Agreda, V. et al. The conversion of light hydrocarbons to more valuable products is of high industrial interest, Wei, H. et al. The direct synthesis of ethane to acetic acid can be an alternative to methanol carbonylation process because of its high selectivity and because of the cheap feedstock, Roussel, M. et al. The main target of the novel acetic acid process studies is to find process conditions, where the process economy can compete with the state-of-the-art methanol carbonylation process at the same acetic acid quality, Smejkal, Q. et al. The ethane direct oxidation (EDO) process is not yet commercialized, although SABIC announced in July 2002 a 30 kt/year acetic acid plant based on the EDO process, which has been developed by their Research and Development Center in Riyadh, Saudi Arabia, Wilcox, E. et al.

In this work, we present the mixed-oxide  $\text{LaMo}_x\text{V}_{1-x}\text{O}_n$  ( $0 < x < 1$ ) as catalyst precursor are synthesized by a sol-gel method and characterized by physicochemical techniques such as: FTIR, XRD, SEM, EDS, BET, TPR, Carbon analysis and tested in direct synthesis of acetic acid from Ethane.

FTIR diagram of the precursor solutions of the raw materials show that no change in chemical composition has been occurred during gel formation, to assess the structural features of the perovskites, the solids were characterized as-synthesized and after catalytic tests by means of different techniques such as X-ray diffraction (XRD) patterns of the fresh and used samples were recorded with Cu Ka ( $\lambda = 1.5406 \text{ \AA}$ ) analyses. JCPDSICDD standard spectra software was used to determine the phases, surface areas measurements were carried out by using the (BET) method based on the  $\text{N}_2$  physisorption capacity at 77K and under reduction of each catalyst was monitored by means of temperature programmed reduction (TPR) in an  $\text{H}_2$  flow from ambient temperature to 700 K. The catalysts were studied by scanning electron microscopy (SEM), For the determination of the chemical composition of crystalline phases, by means of energy-dispersive spectroscopy (EDS). The amount of deposited carbon on each catalyst after the reaction was quantified by Carbon Analysis (CA). A preliminary study on the preparation method and on the raw material for the formation of the  $\text{LaMo}_x\text{V}_{1-x}\text{O}_n$  solid solution. All compounds of these  $\text{LaMo}_x\text{V}_{1-x}\text{O}_n$  series have been successfully prepared from a sol-gel related method using water as solvent. The characterizations by (SEM) and (XRD) have demonstrated the formation of the La-Mo-V solid solution and the good homogeneity of the prepared systems have been proved by constant local elemental distribution given by (EDS). The elemental composition in the series of  $\text{LaMo}_x\text{V}_{1-x}\text{O}_n$  perovskites determined by elemental analysis presents a good balance between the theoretical and experimental values, it is defined that preparation method is suitable. Furthermore, the (BET) surface area of catalysts is close to  $5 \text{ m}^2 \text{ g}^{-1}$ . Then these systems are efficient catalysts for direct synthesis from ethane to Acetic acid.

## References

- Acetic Acid. Chemical Week, (2002). 164(21), 30-33.
- Agreda, V. and Zoeller, J., Acetic Acid and its Derivatives. (1993), *New York: Marcel Dekker*
- Noriyuki, Y., Satoru, K., Makoto, Y., Peter, P., Steve. W., (2001) *Applied Catalysis A: General* 221 , 253–265.
- Roussel, M., Bouchard, M., Bordes-Richard, E., Karim, K., Al-Sayari, S., (2005) *Catalysis Today* 99 , 77–87
- Smejkal, Q., Linke, D., Baerns, M., (2005) *Chemical Engineering Processing* 44, 421-428.
- Wei, H., Cuihong, Z., Lihua, Y., Kechang, X., (2004) *Journal of Natural Gas Chemistry* 13, 113-115.
- Wilcox, E., George, Roberts, W., Spivey, J. (2003) *Catalysis Today* 88 , 83–90.

## The investigation of Ru based Fischer Tropsch catalyst for the production of synthetic liquid fuels derived from bio-syngas

Sabaithip Tungkamani<sup>a</sup>, Phavanee Narataruksa<sup>b</sup>, Hussanai Sukkathanyawat<sup>a</sup>, Natthakorn Kraikul<sup>a</sup>, Siriluck Nivitchanyong<sup>c</sup>, Bahij Sakakini<sup>d</sup>

<sup>a</sup>Department of Industrial Chemistry, King Mongkut's Institute of Technology North Bangkok, 1518 Pibulsongkarm Rd., Bangsue, Bangkok, Thailand 10800

<sup>b</sup>Department of Chemical Engineering, King Mongkut's Institute of Technology North Bangkok, Thailand 10800

<sup>c</sup>National Metal and Materials Technology Center (MTEC), 114 Thailand Science Park, Paholyothin Rd., Pathumthani, Thailand 12120

<sup>d</sup>The School of Chemistry, The University of Manchester, Sackville street, P.O. Box 88, Manchester, UK, M60 1QD

### 1. Summary

The present research is aimed at exploring the feasibility of producing synthetic liquid fuel from bio-syngas over Ru supported on mixed oxide catalyst via Fischer-Tropsch synthesis. Attention is mainly focused on the development and improvement of Fischer-Tropsch catalysts. A series of magnesium oxide modified Ru/Al<sub>2</sub>O<sub>3</sub> catalysts were prepared and characterized by XRD and BET technique. The catalytic behavior of catalysts prepared is elucidated in Fischer Tropsch reaction using transient and steady state conditions. The experiment has been carried out in a fixed bed reactor under the flow of CO/H<sub>2</sub> mixture over Ru/Al<sub>2</sub>O<sub>3</sub> and Ru/Al<sub>2</sub>O<sub>3</sub>-MgO catalyst. The transient study reveals that the hydrogenation of pre-adsorbed CO using TPSR technique was observed at 80°C and TPSR profile shows peak maximum at ~ 200°C. The steady state reaction illustrates that the production of higher hydrocarbons (C<sub>5</sub><sup>+</sup>) was obtained. The modification of magnesium oxide on alumina support catalyst has an effect on the catalytic performance of Ru catalysts.

### 2. Extended Abstract

Utilization of biomass to produce gaseous, liquid and solid fuel has become the most attractive resource in Thailand. This could sustain the energy adequacy and economy stabilization at the same time. Although an indirect liquefaction of biomass via Fischer-Tropsch synthesis to produce clean liquid transportation fuels such as gasoline (C<sub>5</sub>-C<sub>12</sub>) and diesel (C<sub>12</sub>-C<sub>20</sub>) is extremely interesting, the program is not popular in commercial view according to a high cost of technology. However, this problem could be overcome by the development of Fischer-Tropsch catalysts and the system configurations that served the long-term with large scale production. To approach this, a present research attempts to develop the Fischer Tropsch catalyst for the production of long chain hydrocarbons.

The effect of mixed metal oxide support used for catalyst preparation and reaction conditions on Fischer Tropsch reaction was intensively studied. The results obtained from the characterization of the supports show that  $\gamma$ -Al<sub>2</sub>O<sub>3</sub> prepared gives high surface areas in the range of 253-273 m<sup>2</sup>/g. A MgO-Al<sub>2</sub>O<sub>3</sub> support gives lower surface area of 173-200 m<sup>2</sup>/g. A

series of Ru/MgO-Al<sub>2</sub>O<sub>3</sub> was prepared. The catalytic activity was determined by Fischer Tropsch reaction using transient and steady state conditions. A transient experiment was studied by temperature programmed surface reaction (TPSR) of pre-adsorbed CO with H<sub>2</sub>. The catalytic results obtained from TPSR reveal that hydrogenation of pre-adsorbed CO produces mainly methane. The profile starts at 80°C and temperature peak (T<sub>max</sub>) were observed around 200°C for all catalysts investigated. The Fischer Tropsch reaction at different operating conditions was investigated under steady state experiment. A portion of Ru based catalyst was pretreated under a flow of hydrogen and then subjected to the Fischer Tropsch Reaction at different operation condition. The catalytic behavior illustrates that operating conditions at low pressure and high temperature, all catalysts investigated produce much methane, whereas at high pressure and low temperature, the production is selective towards higher hydrocarbons (C<sub>5</sub><sup>+</sup>), especially in the range of gasoline (see Figure 1.). The selectivity of Ru based catalyst for the production of diesel hydrocarbons was also observed at low pressure and low temperature (see Figure 2.). The modification of magnesium oxide on alumina support catalyst has an effect on the catalytic performance of Ru catalysts.

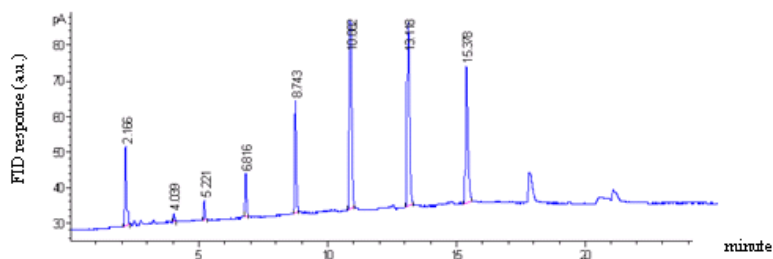


**Figure 1.** The reaction at high pressure and low temperature gives selectivity for higher hydrocarbons (C<sub>5</sub><sup>+</sup>), especially in the range of gasoline.

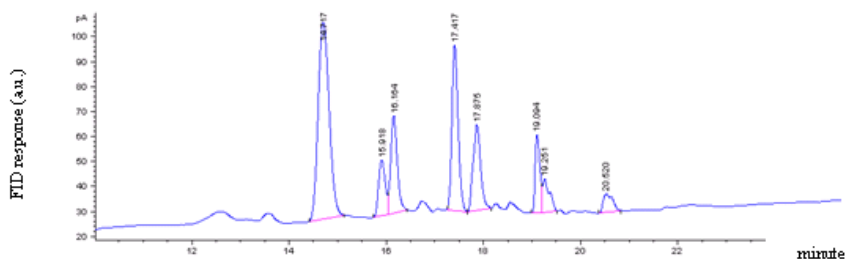


**Figure 2.** The selectivity for diesel hydrocarbons was observed on catalyst investigated at low pressure and low temperature.

### Acknowledgement

This recent project has been financially supported by the National Metal and Materials Technology Center (MTEC), National Science and Technology Development Agency, Thailand. The authors are gratefully appreciated.

### References

- Dry M.E., *Catalysis Today*, 71, 227, 2002.
- Sharifnia S., Mortazavi Y. and Khodadadi A., *Fuel Processing Technology*, 86, 1253-1264, 2005.
- Sie S.T. and Krishna R., *Applied Catalysis A: General*, **186**, 55-70, 1999.
- Spadaro L., Arena F., Granados M.L., Ojeda M., Fierro J.L.G. and Frusteri F., *J. Catal.*, **234**, 451-462, 2005.
- Tijjimensen M.J.A., Faaij A.P.C., Hamelinck C.N., van Hardeveld M.R.M., *Biomass and Bioenergy*, **23**, 129-152, 2002.



## $^1\text{H}$ and $^{13}\text{C}$ -DEPT PFG NMR Studies of Diffusion in Catalysts

D. Weber<sup>a</sup>, E.H. Stitt<sup>b</sup>, L.F. Gladden<sup>a</sup>

<sup>a</sup>Department of Chemical Engineering, University of Cambridge, CB23RA Cambridge, United Kingdom

<sup>b</sup>Johnson Matthey Catalysts, P.O. Box 1, Billingham, TS23 1LB Cleveland, United Kingdom

### 1. Summary

Quantifying molecular diffusion within porous catalysts is central to advancing our ability to design heterogeneous catalysts and catalytic processes. In particular, measurement of diffusion processes is relevant to furthering our understanding of the performance of catalysts used in trickle-bed reactor processes. In these systems, there is a need to characterise liquid transport phenomena and hence identify potential mass transport limitations, which lead to loss of catalyst effectiveness. Nuclear Magnetic Resonance (NMR) techniques have proved to be an invaluable tool characterising transport in porous media; measurements of molecular diffusion, dispersion and flow are possible. The study of diffusion phenomena with Pulsed Field Gradient (PFG) NMR techniques evolved in the 1960s and is nowadays part of the standard NMR toolbox. This project addresses two new implementations of PFG NMR, which will open up significant, new opportunities in studying catalytic systems *in situ*. First, the study of molecular diffusion within porous catalysts over a range of observation times is employed to discriminate between diffusion on the internal surface of the catalyst and in the bulk of the pore space. Second, measurement of diffusion coefficients using natural abundance  $^{13}\text{C}$  PFG NMR is discussed. This development opens up opportunities for measuring chemically-specific diffusion coefficients within catalysts.

Keywords: diffusion, porous media, DEPT, PFG, NMR

### 2. Extended Abstract

PFG NMR techniques offer us the ability to quantify diffusion both in the presence and absence of a concentration gradient. The motivation for this project is to develop and implement novel PFG NMR methods to characterise diffusion on the internal surface of the catalyst (i.e., a surface diffusion coefficient) and in the bulk pore space (i.e., a pore diffusion coefficient) of heterogeneous catalysts. Further, we wish to explore the extent to which it is possible to make these measurements chemically-specific.

Figure 1 shows the results of recent experiments which enable us to estimate surface and pore diffusion coefficients. In this set of experiments we have applied the Alternating Pulsed Field Gradient Stimulated Echo (APGSTE) PFG NMR pulse sequence (Cotts *et al.*, 1989), employing  $^1\text{H}$  observation, to study the diffusion of 1-octene in the pores of a porous alumina support and the catalyst pellets derived from this support. The principle of the measurement is that as the 'observation time' of the experiment is increased, the root-mean-square displacement of the molecules within the pore space increases. Thus, at

D. Weber *et al.*

longer observation times, more molecules interact to a greater extent with the pore wall; i.e., the surface of the catalyst. By recording data for a range of observation times, estimates of pore and surface diffusion coefficients are obtained. In Figure 1, signal attenuation ( $I/I_0$ ) as a function of a set of data acquisition parameters (b-factor) is plotted; the gradient of this plot yields the diffusion coefficient. Data are shown for 1-octene diffusion within a 1 wt% Pd/Al<sub>2</sub>O<sub>3</sub> catalyst. We see that for all observation times and at small values of b-factor, the gradient of all the lines converge; this limiting gradient gives an estimate of the pore diffusion coefficient. In this case the pore diffusion coefficient takes the value of  $1.3 \pm 0.2 \times 10^{-9} \text{ m}^2 \text{ s}^{-1}$ , suggesting a value of tortuosity of  $\sim 1.8$ . At large b-factor values and long observation times, a diffusion coefficient, assigned here to surface diffusion, of  $5 \pm 3 \times 10^{-11} \text{ m}^2 \text{ s}^{-1}$  is observed. In these studies negligible difference was observed for diffusion coefficients within a pure support and the related catalyst. More detailed analysis (Karger *et al.*, 1988) provides an estimate of the exchange time for molecules moving between these two populations.

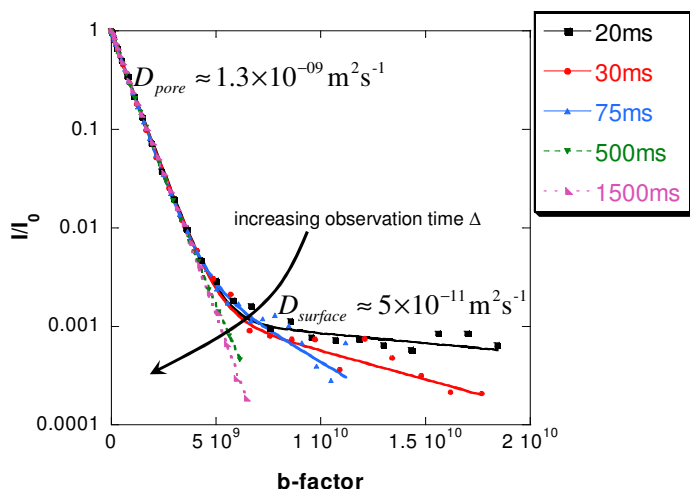


Figure 1: Stejskal-Tanner plots for varying observation times  $\Delta$ . Data are shown for 1-octene diffusing in 1 wt% Pd/Al<sub>2</sub>O<sub>3</sub> catalyst pellets.

The second aspect of the work addresses the use of <sup>13</sup>C PFG NMR instead of <sup>1</sup>H observation to measure molecular diffusion coefficients. The advantage of using <sup>13</sup>C as opposed to <sup>1</sup>H observation is that the <sup>13</sup>C nucleus has a much wider spectral range than <sup>1</sup>H (0-200 ppm for <sup>13</sup>C vs. 0-14 ppm for <sup>1</sup>H), thereby allowing direct identification of NMR signals associated with different chemical species within a mixture. However, the signal available from <sup>13</sup>C measurements is  $\sim 3$  orders of magnitude less than that from <sup>1</sup>H. We are employing polarisation transfer techniques to enhance the <sup>13</sup>C signal so that <sup>13</sup>C measurements can be made without need to employ costly <sup>13</sup>C isotopic enrichment techniques. We have now implemented a <sup>13</sup>C Distortionless Enhancement by Polarisation Transfer (DEPT) PFG NMR technique, which we have fully validated against <sup>1</sup>H measurements for a range of systems. Future work will employ these new measurements to study molecular diffusion during catalytic reactions *in situ*.

## References

- Cotts, R. M., Hoch, M. J. R., Sun, T. and Markert, J. T., (1989) *Journal of Magnetic Resonance*, 82.  
 Karger, J., Pfeifer, H, Heink, W., (1988) *Advances in Magnetic Resonance*, 12.

## Session T-14a: Electrochemical Engineering – I

<b>Abstract Number</b>	<b>Paper Title &amp; Authors</b>	<b>Included</b>
75	Removal of fluoride from photovoltaic wastewater by electrocoagulation and sludge characteristics N Drouiche, M Hecini	Yes
365	Use of ion-exchange composites based on natural zeolites for cleaning of water solutions with purpose to create environmentally safe technologies V P Nesterenko	No
767	Electrochemical oxidation of activated carbon fibre – an efficient way of enhancing toxic metal ion sorptive capacity I D Harry, B Saha, I W Cumming	Yes
1967	Selective separation of Chromium (III) from electroplating effluents by ion-exchange processes L Ferreira, S A Cavaco, M J Quina	No

Session T2-14a

## Removal of fluoride from photovoltaic wastewater by electrocoagulation and sludge characteristics

N. Drouiche<sup>a\*</sup>, M.Hecini<sup>a</sup>

<sup>a</sup>Silicon Technology Development Unit (UDTS). 2, Boulevard Frantz Fanon, Alger  
BP 140 Alger-7 merveilles, Alger 16200Tel/Fax: 213 21433511, Email: [nadjibdrouiche@yahoo.fr](mailto:nadjibdrouiche@yahoo.fr)

### Introduction

Efficient treatment of fluoride-containing wastewater efficiently has been important for environmental engineers in Algeria, following the fast development of the photovoltaic industry. An appropriate concentration of fluoride in drinking water is required to prevent dental cavities, but longterm ingestion of water that contains more than a suitable level of fluoride causes bone disease and mottling of the teeth [1,2]. The discharge standard of fluoride in industrial wastewater is  $15\text{mg L}^{-1}$  in Algeria. The wastewater from a U.D.T.S. photovoltaic plant was characterized by high suspended solids, high turbidity (NTU), chemical oxygen demand (COD) concentration up to  $7\ 00\ \text{mg l}^{-1}$  and fluor concentration up to  $1000\ \text{mg l}^{-1}$ . When the fluoride concentration is high, lime precipitation is commonly used to form  $\text{CaF}_2$  precipitate. Depending on the discharge standards of industrial wastewaters, a polishing step may be necessary. Currently, the cheapest way to remove fluoride from semiconductor wastewater is to produce calcium fluoride ( $\text{CaF}_2$ ) by adding lime or another calcium salt, such as  $\text{CaCl}_2$ . The aim of this paper is to propose an efficient and low cost treatment of chemical mechanical polishing wastewater process based on electrocoagulation with iron bipolar electrodes. The performance of a pilot scale electrochemical reactor equipped with iron bipolar electrodes and an anode active area surface of about  $220\ \text{cm}^2$  was studied, In addition, sludge settling after electrocoagulation were characterized.

### Materials and Methods

Experiments were conducted in a small bipolar batch reactor with two iron electrodes connected in parallel (fig.1), The volume of the reactor cell is about 1 l. A steady temperature of 293K was maintained for all test runs and a constant applied potential was maintained using a P.Fontaine MC 3030C generator. The dimensions of the bipolar electrodes are  $100\text{mm}\times 85\text{mm}$ . The fluorinated water is injected into the electrochemical reactor cell, centrifugal Fontaine M7 feed pump, which allows flow rates of up to 460 l/h are used to maintain well mixing of the CMP wastewater during electrocoagulation process. The purity of the iron electrodes used was about 99.5%.



Fig.1 Electrochemical reactor

### Results and discussions

Fig. 2 reveals respectively 34 and 40% fluoride removal was achieved in 40 min of electrocoagulation for 20 and 30 V and there is under the Algerian standards discharge. The electrocoagulation process will take significant longer to achieve comparable fluoride removal for an applied potential of 10 V. This is due primarily to insufficient amount of electric power supply at 10 V for complete destabilization of the suspended oxide particles in the aqueous solution. Hence both 20 and 30 V will be good operating potential for the present electrocoagulation with the latter requiring shorter treatment time less than 40 min. Therefore, 30 V offers the best overall performance for the present work because the discharge standard are obtained in less time with relatively lower energy consumption. Fig.3 shows that discharge standards of fluoride are obtained in more time than using synthetic solution. This difference can be explained by the fact that co-existing anions are present in the fluoride containing wastewater. Among these co-existing anions,  $\text{SO}_4^{2-}$ ,  $\text{HCO}_3^-$  and  $\text{H}_2\text{PO}_4^-$  and the competition of fluoride and this anions reduce treatment efficiency of fluoride.

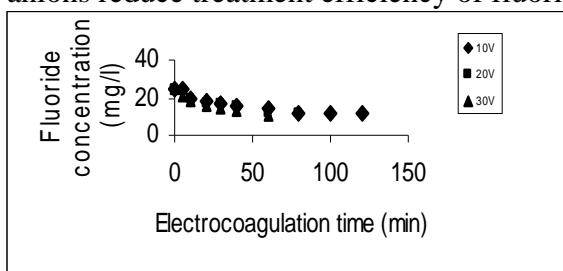


Figure n°2:Defluorination in continuous mode with laboratory cell.  $T=20^{\circ}\text{C}$ ,  $I=1$  A, and  $V= 11$

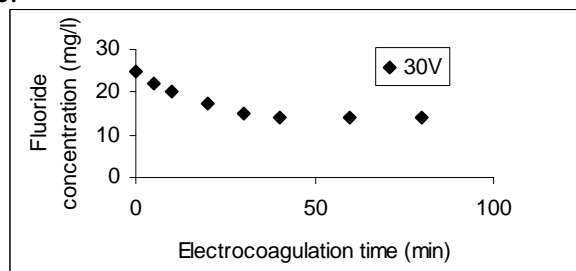


Figure n°3:Defluorination in continuous mode with laboratory cell of wastewater.  $T=20^{\circ}\text{C}$ ,  $I=1$  A, and  $V=11$

Fig.4.shows the morphology of the sludge generated by the electrocoagulation the aggregates observed showed a different two geometrical appearance, spherical (a) and prismatic (b). spherical solids are approximately 100 nm in diameter and prismatic solids are approximately 600nm. This result can mean that the final crystallographic features of the sludge are prismatic morphology.

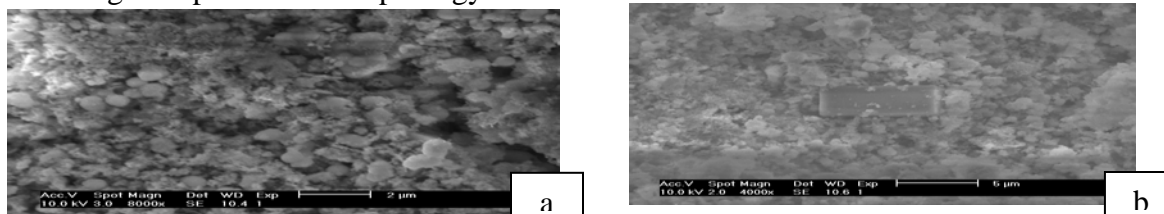


Fig.4.(a,b) MEB images of sludge in the wastewater

## Conclusion

Electrochemical treatment of chemical mechanical polishing wastewater containing fluoride in small bipolar batch reactor was investigated. This work has uncovered some aspects of electrocoagulation that provide promise for improved wastewater treatment. Treatment of real wastewater indicate that some cations and anions interfere with fluoride removal. Cost calculations show that, in the case of iron electrode.

## References

- [1] Brown, W.E., Gregry, J.M., Chow, L.C., 1977. Effects of fluoride on emanal solubility and cariostasis. *Caries Res.* 11, 118–141.
- [2] Lynch, C.F., 1987. Relationship of fluorine in drinking waters to other drinking waters parameters. *Arch. Environ. Health* 42, 5–13.

## **Electrochemical oxidation of activated carbon fibre – an efficient way of enhancing toxic metal ion sorptive capacity**

I. D. Harry, B. Saha, I. W. Cumming

*Advanced Separation Technologies Group,  
Department of Chemical Engineering, Loughborough University, LE11 3TU, Loughborough,  
Leicestershire, United Kingdom*

### **1. Summary**

A viscose rayon based activated carbon cloth (ACC) was electrochemically oxidised under a wide variety of current conditions to modify the surface properties. The ACCs were characterised in detail. A loss of 49% BET surface area and a significant loss in microporosity were observed on the electrochemically oxidised ACC (EO) and attributed to blockage of pores through formation of carboxylic acidic groups. Increase in surface acidity shifted the point of zero charge (PZC) from pH of 6.8 to 2.8 and the isoelectric point from pH of 3 to 1.15. The optimum constant current for electrochemical oxidation was found to be 1.1 A. Batch sorption experiments confirmed that EO is more effective for the removal of lead and copper ions compared to unoxidised ACC (UO) for both competitive and non-competitive sorption. The non-competitive copper and lead sorption capacities of EO sample are approximately 17 times and 4 times greater than the non-competitive sorption capacities of UO sample, respectively.

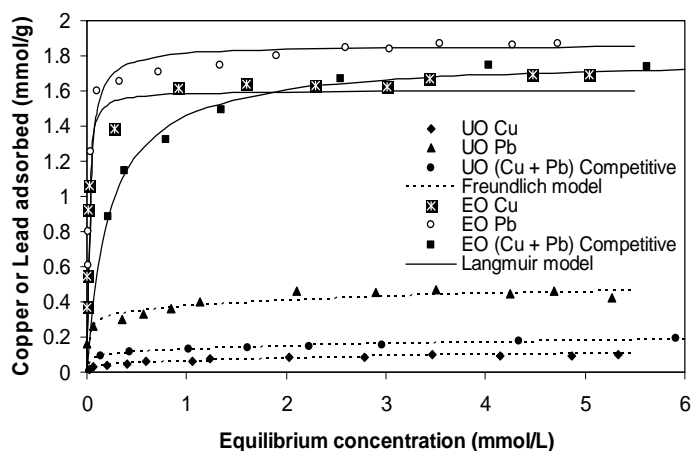
Keywords: Viscose rayon based activated carbon cloth; Lead; Copper; Electrochemical oxidation; Competitive and non-competitive sorption.

### **2. Extended Abstract**

#### **Effect of electrochemical oxidation on lead and copper sorption equilibrium**

The sorption capacities of EO and UO samples were evaluated for copper and lead ions. Figure 1 shows the copper and lead sorption of EO and UO samples evaluated at pH 5 and 298 K. The maximum non-competitive copper and lead sorption capacities of EO sample are 1.69 mmol/g and 1.87 mmol/g, respectively while the maximum non-competitive copper and lead sorption capacities of UO sample are 0.098 mmol/g and 0.47 mmol/g, respectively (Harry *et al.*, 2006; Harry *et al.*, 2007). The non-competitive copper and lead sorption capacities of EO sample are approximately 17 times and 4 times greater than the non-competitive sorption capacities of UO sample, respectively. The maximum competitive copper and lead sorption capacities of EO sample are 0.75 mmol/g and 1.01 mmol/g, respectively and the maximum competitive

copper and lead sorption capacities of UO sample are 0.085 mmol/g and 0.12 mmol/g, respectively.



The competitive copper and lead sorption capacities of EO sample are approximately 8.8 times and 8.6 times greater than the competitive sorption capacities of UO sample, respectively. Therefore, electrochemical oxidation of ACC markedly increased its sorption capacity for both competitive and non-competitive sorption of

lead and copper ions.

Figure 1. Non-competitive and competitive (Cu + Pb) sorption isotherms of copper and lead onto UO and EO at pH 5.

### Mechanism of lead and copper sorption onto EO and UO ACC

The PZC for EO and UO samples are at pH 2.8 and 6.8, respectively. The highest pH at which the batch sorption experiments were performed was pH 5. This is below the PZC of UO, so the ACC surface was positively charged. However, the greater electron distribution over the more electronegative oxygen atoms makes it possible for lead and/or copper ions to be attached to them, therefore, complex formation between the metal ions and the UO surface is the likely mechanism for sorption of lead and copper onto UO. A pH of 5 is above the PZC of EO. So, the surface of the EO sample was negatively charged. The EO therefore, behaved as a cation exchanger indicating that the sorption process was ion exchange. This explains why the solution pH decreased during the lead and copper sorption indicating that  $H^+$  ions were released from the surface of the EO sample. Mass balance to obtain the maximum  $H^+$  ions released were performed using the volumes of 0.1 M sodium hydroxide added to adjust the solution pH. The experimentally determined maximum non-competitive copper and lead sorption capacities of EO are 1.69 mmol/g and 1.87 mmol/g, respectively and the maximum  $H^+$  ions released are 3.352 mmol/g and 3.68 mmol/g, respectively. It is obvious that one  $Pb^{2+}$  or  $Cu^{2+}$  ion was sorbed for approximately every two  $H^+$  ions released from the EO surface. This confirms that the sorption of lead and copper onto EO is mainly governed by ion exchange mechanism.

### References

Harry, I. D., Saha, B. and Cumming, I. W. (2006) *Journal of Colloid and Interface Science*, 304, 9-20.

Harry, I. D., Saha, B. and Cumming, I. W. (2007) *Carbon*, 45, 766-774.



## Session T2-14b: Electrochemical Engineering – II

<b>Abstract Number</b>	<b>Paper Title &amp; Authors</b>	<b>Included</b>
1771	Mechanism of capture of ionic impurities from electrolytes, based on a bipolar cell of oscillating porous electrodes, spaced by the equilibrium distances O C Bustos, G M Cifuentes, R M Perez, J C Santana, J T Torres	No
3250	Treatment of textile wastewater by electrocoagulation using Al and Fe electrodes F Lopicque, I Zongo, J-P Leclerc, J Wethe	No
3449	P-Graph Methodology for Cost-Effective Reduction of Carbon Emissions Involving Fuel Cell Combined Cycles F Friedler, P Varbanova, J Klemeš	Yes
3585	Pilot plant study of the electrooxidation of landfill leachates using BDD anodes A Urriaga, A Cabeza, A Anglada, G Perez, I Ortiz	Yes

Session T2-14b

## **P-Graph Methodology for Cost-Effective Reduction of Carbon Emissions Involving Fuel Cell Combined Cycles**

Ferenc Friedler<sup>a</sup>, Petar Varbanov<sup>a</sup>, Jiří Klemesš<sup>b</sup>

<sup>a</sup>*Department of Computer Science, Faculty of Systems and Information Technology, University of Pannonia, Egyetem u. 10, H-8200, Veszprem, Hungary, friedler@dcs.vein.hu, varbanov@dcs.vein.hu*

<sup>b</sup>*Centre for Process Integration, CEAS, The University of Manchester, PO Box 88, M60 1QD Manchester, UK, j.klemes@manchester.ac.uk*

### **1. Summary**

Fuel cells are currently under extensive investigation for building combined energy cycles due to the higher efficiencies they offer. Two kinds of High-Temperature Fuel Cells (HTFC) are considered as best candidates for Fuel Cell Combined Cycles (FCCC) – Molten Carbonate Fuel Cells (MCFC) and Solid Oxide Fuel Cells (SOFC). The current paper presents a procedure for evaluating energy conversion systems including FCCC and utilising biomass and/or fossil fuels. This involves significant combinatorial complexity, efficiently handled by the P-graph methodology (Friedler et al., 1995). Promising system components are evaluated using the P-Graph framework and a methodology for the synthesis of cost-optimal FCCC configurations is developed, accounting for the carbon footprint of the various technology and fuel options. The results show that such systems employing renewable fuels can be economically viable for wide range of economic conditions.

Keywords: CO<sub>2</sub> minimisation; Combined Energy Cycles, Energy Efficiency, High-Temperature Fuel Cells

### **2. Extended Abstract**

Reducing significantly the CO<sub>2</sub> emissions at reasonable costs is a priority, dictated by the need for cleaner energy. Recent results on integrating HTFC with ST and GT indicate possibility to achieve both high efficiencies (Massardo and Bosio, 2002) and economic viability (Varbanov et al., 2006). Systems for FCCC-based CHP feature a large number of alternative topologies, leading to combinatorial complexity. The initial approach to solving such problems employed Mathematical Programming (MP). For realistic systems the optimisation problems become too large. The huge number of the available options makes it rather difficult to build the necessary

problem superstructures heuristically and it is easy to miss low-cost options and optimal solutions.

For handling such problems of a practical complexity the Process Network Synthesis methodology based on the P-Graph (Process Graph) has been applied in this investigation. Its associated axioms ensuring representation unambiguity (Friedler et al., 1992), algorithms generating the maximal network structure (Friedler et al., 1993) and for generation of all possible solution structures (Friedler et al., 1995), make the approach superior to MP in solving process synthesis problems because the approach is algorithmic – performing the task of superstructure construction automatically, following the rules and options specified by the operators thus minimising subjectivity. It also eliminates infeasible combinations of process units prior to examination. As a result, P-graph PNS drastically reduces the combinatorial search space and is orders of magnitude more efficient than pure MP (Friedler et al., 1996).

Another important issue is the correct evaluation of the CO<sub>2</sub> minimisation potential. Although biomass is nominally carbon-neutral, its harvesting and transportation contribute to certain small carbon footprint (Bulatov et al., 2007), which is taken into account.

The presented evaluation procedure identifies FCCC systems and conditions favourable for CO<sub>2</sub> reduction. The objective function is Total Annualised Cost.

#### ACKNOWLEDGEMENTS

The financial support from the European Community EMINENT2 project TREN/05/FP6EN/S07.56209/019886 is gratefully acknowledged.

#### References

- Friedler, F., K. Tarjan, Y.W. Huang, and L.T. Fan. 1992, Graph-Theoretic Approach to Process Synthesis: Axioms and Theorems, *Chem. Eng. Sci.*, 47(8):1972-1988.
- Friedler, F., K. Tarjan, Y.W. Huang and L.T. Fan, 1993, Graph-Theoretic Approach to Process Synthesis: Polynomial Algorithm for Maximal Structure Generation, *Comput. Chem. Eng.*, 17(9):929-942.
- Friedler, F., J.B. Varga, and L.T. Fan. (1995), Decision-Mapping: a Tool for Consistent and Complete Decisions in Process Synthesis, *Chem. Eng. Sci.*, 50(11):1755-1768.
- Friedler, F., J.B. Varga, E. Fehér, and L.T. Fan, 1996, Combinatorially Accelerated Branch-and-Bound Method for Solving the MIP Model of Process Network Synthesis, In: *State of the Art in Global Optimization*, ed. Floudas, C.A. and P.M. Pardalos, Kluwer Academic Publishers.
- Massardo, A.L. and B. Bosio, 2002, Assessment of Molten Carbonate Fuel Cell Models and Integration with Gas and Steam Cycles, *J of Eng for Gas Turb & Power*, 124:103-9.
- Nagy, A.B., R. Adonyi, L. Halasz, F. Friedler and L.T. Fan, 2001, Integrated Synthesis of Process and Heat Exchanger Networks: Algorithmic Approach, *Applied Thermal Engineering*, 21:1407-1427.
- Varbanov, P., J. Klemeš and F. Friedler, 2007, Critical Analysis of Fuel Cell Combined Cycles for Development of Low-Carbon Energy Technologies, *Chemical Engineering Transactions*, Ed. J.Klemeš, 12:739, AIDIC, PRES'07, June 24-27, Naples, Italy.

## Pilot plant study of the electrooxidation of landfill leachates using BDD anodes

A. Urriaga, A. Cabeza, A. Anglada, G. Perez, I. Ortiz

*Department of Chemical Engineering, University of Cantabria. Av. de los Castros s/n, 39005 Santander, Spain.*

### 1. Summary

The design, building and start-up of an electrooxidation pilot plant for the treatment of landfill leachates are presented. The previous analysis performed at the laboratory scale using a 70 cm<sup>2</sup> boron doped diamond (BDD) anode conducted to the kinetic equations of the removal of COD and ammonium (1). Based on this modeling, the pilot plant unit with a total anode surface of 1.05 m<sup>2</sup> was designed and built. In the start-up methodology, experiments are conducted both at the laboratory and pilot plant scales under equivalent conditions. Comparison of results will permit to identify the main factors that affect the output of the electrooxidation process at larger scales.

Keywords: electrooxidation, BDD anode, landfill leachate, green engineering

### 2. Extended Abstract

Leachates from municipal landfills are highly polluted effluents, characterized by the high loading of ammonium and COD and the poor biodegradability (table 1). In the framework of the present project, different treatment technologies have been considered. The biological treatment showed a limited efficiency. Fenton's oxidation, a cost effective system characterized by its simplicity of application, obtained a significant COD reduction, although ammonium reduction was not sufficient.

	pH	COD	BOD <sub>5</sub> /COD	N-NH <sub>4</sub> <sup>+</sup>	Cl <sup>-</sup>
Raw leachate	8.35	4430	0.14	1930	3230
Leachate after biological treatment	7.61	900-2100	0.10	1100-1400	1740
Leachate after Fenton's oxidation	8.5	360-470		560-630	1350

Table 1: Landfill leachate composition: raw leachate and after biological and Fenton's treatments.

The treated leachate obtained at the outlet of Fenton's oxidation has been used as the feed in the electro-oxidation tests performed at the pilot plant. The unit has 150 electrochemical compartments set up in three parallel ways; each compartment has a BDD anode and a stainless steel cathode, both electrodes with a surface of 70 cm<sup>2</sup>.

The total anode area is 1.05 m<sup>2</sup>. The electrical current is provided by 3 power suppliers 750 A, 16 V DC. The leachate is stored in a 725 L tank and is pumped through the cell in closed circuit. Figure 1 shows a diagram of the pilot plant after installation in the leachate treatment facilities located at the landfill site.

In figure 2, the evolution of COD and ammonium is plotted vs. Q (specific charge), the parameter that permits direct comparison of experiments performed with different feed volumes. After 6 hours of experimental runs, COD is totally removed, both at the laboratory and the pilot plant. Despite the experimental variability, that is more significant in COD data, it seems that the pilot plant efficiency is reduced if compared with the laboratory output. Factors affecting this behavior are now under study.

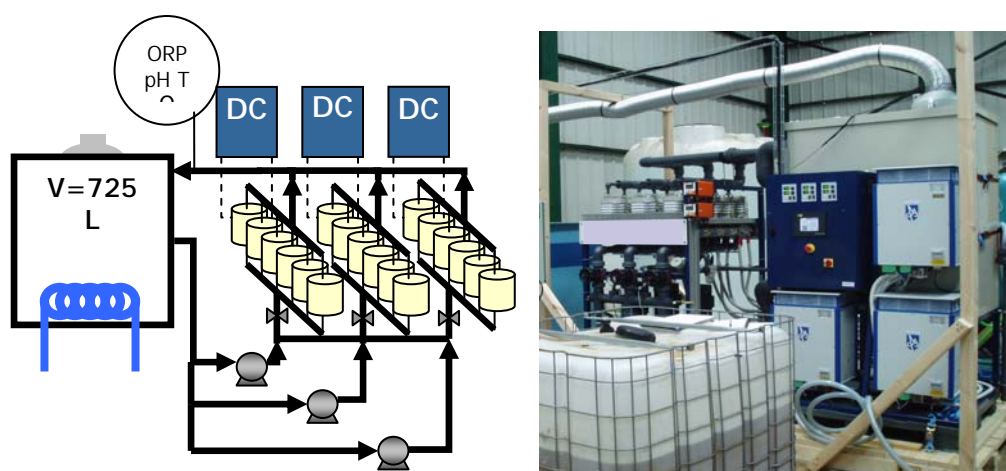


Figure 1. Diagram and photograph of the Electrooxidation pilot plant

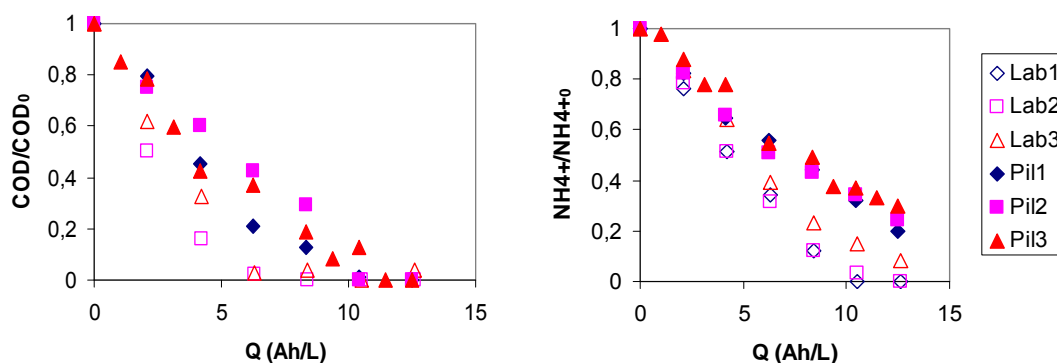


Figure 2. COD and ammonia evolution in pilot plant and laboratory experiments. Dimensionless data referred to the initial concentration

Financial support of projects MMA 2.5-216/2005/3-B, PET2005\_0169 and MARE is gratefully acknowledged.

## References

- (1) Cabeza, A., Urriaga, A.M. and Ortiz, I. (2007) *Ind. Eng. Chem. Res.*, 46, 1439-1446.

## Session T2-14P: Electrochemical Engineering – Poster

Abstract Number	Paper Title & Authors	Included
464	Dynamic Response of Oxygen Electrodes. Signal Deconvolution by Regularization Methods F López, A Abad, J N Laboulais	Yes
1190	Porous electrodes based on Ti, Zr and Co oxides for electrochemical oxygen sensors G Y Kolbasov, V S Vorobetz, N D Ivanova, O A Stadnik	Yes
1201	Elimination of organic compounds in wastewater by advanced oxidation technologies S Rojano, Á Fernández	No
2110	Kinetic and thermodynamic study of the adsorption of natural organic matter on granular activated carbon N C Alanís, B P Ayo, U I Velasco, J I Á Uriarte, J R G Velasco	Yes
2396	Electrochemical generation of Fenton's reagent to treat spent caustic wastewater in oil production H K Hansen, P Nuñez, N Rodriguez, J Guzman	Yes
3489	Recovery of zinc by electrochemical remediation of zinc oxide-containing waste F Lopicque, P Guillaume, N Leclerc, C Boulanger	No
3593	Cd(II) removal from aqueous solutions by adsorption onto activated carbon F Natale, A Erto, A Lancia	Yes
3693	Water condensation in gas distribution plates of PEMFCs: flow and removal from the grooved patterns of the plates C Bonnet, J Ramousse, N Doss, F Lopicque, M Boillot	Yes

Session T2-14P



## **Dynamic Response of Oxygen Electrodes. Signal Deconvolution by Regularization Methods**

F. López, A. Abad, J. Navarro Laboulais

*Dpt. Chemical and Nuclear Engineering. Universidad Politécnica de Valencia (UPV-EPVA). Plaza Ferrándiz y Carbonell s/n. 03801 Alcoy (Alicante) Spain*

### **1. Summary**

Three functions are used for characterized oxygen electrodes with oxygen steps at different temperatures. The transfer functions of the electrodes are used for data deconvolution in dynamic oxygen-transfer experiments and for the determination of the  $k_{La}$ . The deconvolution data is based on Tikhonov's regularization method. This method allows to do hypothesis about the function to be obtained in order to reduce the error in its determination. The results show that when the dynamic response of the electrode is similar to the dynamics of the process to be measured, the signal deconvolution is necessary to reduce the error on the parameter estimation, e.g. the mass transfer coefficient,  $k_{La}$ .

Keywords: Oxygen Electrodes, Deconvolution, Gas-Liquid Mass Transfer, Bubble-Column Reactor

### **2. Extended Abstract**

Oxygen electrodes are commonly used in monitoring biological reactors or for the determination of the volumetric oxygen mass-transfer coefficient in a bubble-column reactor. The measuring principle is based on the electrochemical reduction of the oxygen of a gold electrode covered by a gas-permeable polymeric membrane. The measured reduction current is proportional to the oxygen gradient near the electrode. Then, when these electrodes are used in dynamic experiments this gradient changes with time leading to systematic errors in the interpretation of the data.

The deduction of a transfer function of this kind of electrodes must contain information about the gas transport across the membrane and the distortion of the diffusion field near the edges of the gold cathode. An analytical function is proposed derived from the solution of the one-dimensional diffusion equation [1]. This theoretical transfer function is compared with the experimental two-zone transfer

function proposed by Linek et al [2], and with another function obtained from the analysis of results the previous functions

$$f(t) = 1 + 2A \sum_{n=1}^{\infty} (-1)^n \text{Exp}[-n^2 \pi^2 kt] \quad (1)$$

Where A and k are experimental constants to be determined from oxygen-steps experiments. The best fits were obtained with the equation (1) (see Fig. 1).

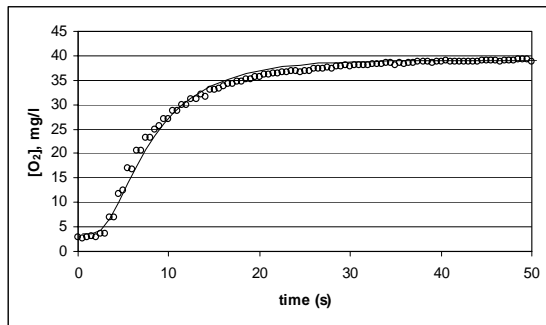


Figure 1: Oxygen- step data (—) for a T=25°C and fitted data (□) with equation (1)

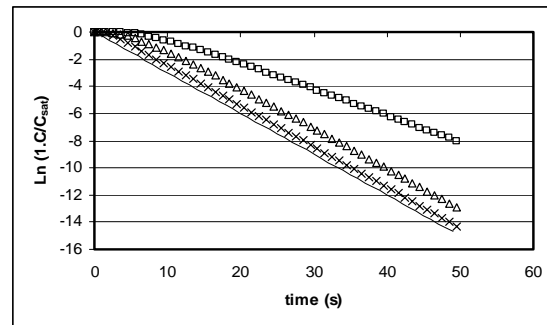


Figure 2: Theoretical data (—) and simulate data for k=0,02 s<sup>-1</sup> (□), k=0,04 s<sup>-1</sup> (Δ), and k=0,1 s<sup>-1</sup> (×)

The electrode transfer function is used for data deconvolution of dynamic oxygen mass-transfer experiments. The method attempts to obtain a numerical approximation to the solution of the convolution equation

$$R(t) = \int_0^t H(t-\theta)S(\theta)d\theta \quad (2)$$

To solve the integral equation we use the Tikhonov's regularization method which avoids the numerical instability of the numerical inversion and allows to include hypothesis about  $R(t)$  to improve the calculation. The method is shown in detail elsewhere [3].

Fig. 2 shows the classical representation for  $k_L a$  calculation. If raw data are used instead the deconvolved ones, the slopes of the lines provides a systematic error on the  $k_L a$  determination. The theoretical value of  $k_L a$  in Fig 2 is  $0.3 \text{ s}^{-1}$  but the slopes of the lines are  $0.191$ ,  $0.276$  and  $0.297 \text{ s}^{-1}$  respectively. The experimental value of  $k$  for the oxygen electrodes is close to  $0.03$  leading to errors on  $k_L a$  determination without the deconvolution of the data.

The authors wish to acknowledge the Conselleria d'Empresa, Universitat i Ciència de la Generalitat Valenciana for the financial support to this work under the project Ref GV05/190.

## References

- 1.- J. Crank, *The Mathematics of Diffusion. 2nd Ed.*; Oxford University Press: Oxford, 1999.
- 2.- V.Linek, V.Vacek, J.Sinkule, P.Benes, *Measurement of Oxygen by Membrane Covered Probes*; Ellis Horwood Lim, Chichester, (1988)
- 3.- A.Abad, SC.Cardona, J.I.Torregrosa, F.López, J.Navarro-Laboulais, (2005) *J. Math. Chem.* 38, 271-92

## **Porous electrodes based on Ti, Zr and Co oxides for electrochemical oxygen sensors**

G.Ya. Kolbasov, V.S. Vorobetz, N.D. Ivanova, O.A. Stadnik

*Institute of General & Inorganic Chemistry,  
32-34 prospect Palladina, 03142 Kiev, Ukraine*

### **1. Summary**

The porous electrodes for electrochemical oxygen sensors based on Ti, Zr and Co oxides nanoparticles were produced. Catalytic properties of electrodes were investigated in the processes of oxygen electroreduction in physiological solution of NaCl (0,9%) and in blood plasma. It has been found for the TiO<sub>2</sub> - ZrO<sub>2</sub> oxides that the potential of oxygen reduction shifts more negative values with increasing ZrO<sub>2</sub> content. The relative change in conduction band potential and valence band potential of TiO<sub>2</sub>-ZrO<sub>2</sub> electrodes depending on ZrO<sub>2</sub> content has been determined.

Keywords: oxygen electroreduction, electrochemical oxygen sensors, Ti, Zr, Co oxides nanoparticles

### **2. Extended Abstract**

The TiO<sub>2</sub> nanoparticles were produced by sol-gel method on a Ti substrate from solutions containing titanium chloride. The nanoparticles of mixed TiO<sub>2</sub> - ZrO<sub>2</sub> oxides were produced by sol-gel method on a Ti substrate from solutions containing titanium and zirconium tetraisopropoxides. The electrodes were annealed in air at 500-550<sup>0</sup>C. The cobalt oxide compounds of nonstoichiometric composition were obtained on a Ni anode by the electrooxidation of Co<sup>2+</sup> ions from an electrolyte containing CoSO<sub>4</sub> and NH<sub>4</sub>F. The cobalt oxide compounds had the composition Co<sub>x</sub>O<sub>y</sub>(OH)<sub>z</sub>, where x=0.65–0.71, y=1.34–1.79, z=1.3–1.52. The average size of nanoparticles on the Ti surface depended on the deposition conditions, and was no more than 10 nm, the average thickness of the deposited layers was 300 – 1500 nm. The cobalt oxide particles size was 80-120 nm; the coating thickness was 2-3 μm.

The polarization curves for process of oxygen electroreduction in physiological solution of NaCl (0,9%) and in blood plasma for all electrodes exhibited one current wave, which corresponded to oxygen reduction limiting current. We have found that the overall O<sub>2</sub> reduction process involves two electrons, and that the reaction proceeds without hydrogen peroxide formation. It has been found for the TiO<sub>2</sub> - ZrO<sub>2</sub> oxides that the potential of oxygen reduction shifts more negative values with increasing ZrO<sub>2</sub> content. The layers which contained 5-10% ZrO<sub>2</sub> were most stable in

time. For the Co oxides, increasing the  $\text{NH}_4\text{F}$  content of the starting solution from 20 to 40 g/l enhanced the electrocatalytic properties of the electrodes, reducing by  $\approx 200$  mV the oxygen reduction overpotential as against that at the Ni substrate.

The relative change in conduction band potential and valence band potential of  $\text{TiO}_2\text{-ZrO}_2$  electrodes has been determined from photoelectrochemical measurements [1] depending on the film composition. It has been found that the conduction band potential of electrodes did not vary, but the valence band potential increased in anodic region with increasing  $\text{ZrO}_2$  content, which accounts for the improvement of their oxidative properties. The shift of the oxygen reduction potential to cathodic region for the electrodes with high  $\text{ZrO}_2$  content we associate with a change in their catalytic activity.

The electrodes investigated were distinguished by a high sensitivity to dissolved oxygen ( $(4-5) \cdot 10^{-6}$  g/l) and high reproducibility of characteristics in long-time cycling. These electrodes promise much as reusable electrode materials in electrochemical sensors for the determination of oxygen concentration.

## **References**

- [1] Smirnova, N., Gnatyuk, Y., Eremenko, A., Kolbasov, G., (2005) 8<sup>th</sup> International Conference on Solar Energy and Applied Photochemistry, 20 – 25 February 2005, Luxor, Egypt. Book of Abstracts, p. 100-101.

## **Kinetic and thermodynamic study of the adsorption of natural organic matter on granular activated carbon**

N. Chimeno-Alanís, B. Pereda-Ayo, U. Iriarte-Velasco, J. I. Álvarez-Uriarte, J. R. González-Velasco.

*Department of Chemical Engineering. Faculty of Science and Technology. University of the Basque Country, P.O. Box 644, E-48080, Bilbao, Spain. Tel: +034 946015415, e-mail: juanra.gonzalezvelasco@ehu.es*

### **1. Summary**

Adsorption equilibrium and kinetics of natural organic matter (NOM) onto two different granular activated carbons (GAC) were studied. Firstly physical and chemical properties of both carbons were evaluated and significant differences were observed. The influence of the initial concentration of NOM and adsorbent particle size were investigated. The kinetic data were fitted using the pseudo-first-order equation, the pseudo-second-order equation, the intraparticle diffusion model and the modified pseudo-first-order equation. The corresponding kinetic parameters for these models are presented. The results show that the pseudo-second-order model generated the best agreement with the experimental data for the NOM/GAC A and NOM/GAC F system. Finally, the adsorption equilibrium data were correlated with Freundlich and Langmuir isotherms.

**Keywords:** Drinking water treatment; Natural organic matter; Granular activated carbon; Adsorption kinetics; Isotherms.

### **2. Extended Abstract**

During the disinfection of drinking water the reaction between disinfectant and natural organic matter generates disinfection by-products (DBPs). When chlorine is used as disinfectant, these harmful products include trihalomethanes (THMs) and haloacetic acids (HAAs). Nowadays, numerous rules make provisions for minimizing the formation of undesirable DBPs.

Adsorption by activated carbon is regarded as one of the best available technologies for removing dissolved contaminants such as natural organic matter (NOM) from drinking water. At the moment, NOM adsorption equilibrium data are available in the literature, but residence times at water treatment plants are not long enough and the process seldom reaches equilibrium. Therefore, not only equilibrium but also kinetic

data were evaluated in this study, looking for the activated carbons with both high removal capacity and increased kinetics.

Two different GACs were used for DBPs precursors elimination, one coal based (GAC F) and one coconut based (GAC A) carbon. Firstly, physical and chemical properties were evaluated. Significant differences were observed between both carbons. It was evidenced that surface specific area, pore size distribution, point of zero charge ( $\text{pH}_{\text{pzc}}$ ), superficial basicity and inorganic content controlled the NOM adsorption process. NOM removal was evaluated by measurements of UV absorbance spectra for wavelengths between 200 and 500 nm. Preliminary bench scale experiments demonstrated that the NOM initial concentration and adsorbent particle size were the most significant factors on adsorption rate. This behaviour was attributed to mass transfer phenomena.

Adsorption equilibrium data were correlated with two well-known equilibrium isotherm models, Freundlich and Langmuir equations. A comparison of the characteristic parameters obtained from each fitting indicated that NOM adsorption process is favoured for GAC F.

Finally, obtained kinetic data, Figure 1, were fitted to several adsorption models. The pseudo-first-order equation (PPO), the pseudo-second-order equation (PSO), the intraparticle diffusion model (ID) and the modified pseudo-first-order equation (MPPO) were used. The results showed that the adsorption mechanism in the NOM/GAC F and NOM/GAC A systems followed the PSO equation throughout all adsorption curve. Moreover, PSO generates the best agreement with the experimental equilibrium data. This behaviour was maintained regardless of the initial NOM concentration.

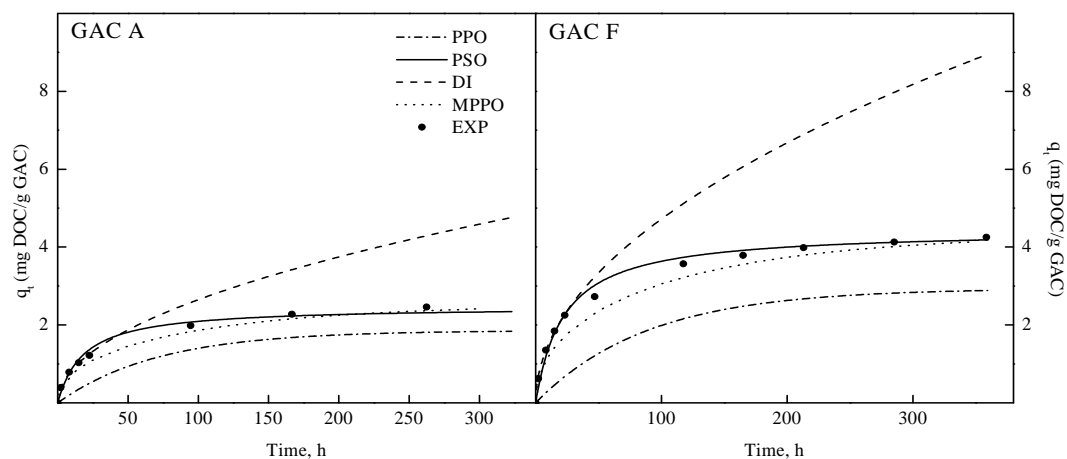


Figure 1: Kinetics of MON adsorption on GAC A and GAC F. ( $\text{pH} 7.0$ ,  $C_0 = 5 \text{ mg/l DOC}$ ,  $30 \text{ }^\circ\text{C}$ ,  $200 \text{ rpm}$ ,  $d_p = 0.25\text{-}0.3 \text{ mm}$ ).

## References

- Oztürk N., Bektas T.E., (2004). *Nitrate removal from aqueous solution by adsorption onto various materials*. Journal of Hazardous materials, B112, 155-162.
- Yang X., Al- Duri B., (2005). *Kinetic modelling of liquid-phase adsorption of reactive dyes on activated carbon*. Journal of Colloid and Interface Science, 287, 25-34.

## **Electrochemical generation of Fenton's reagent to treat spent caustic wastewater in oil production**

H. K. Hansen, P. Nuñez, N. Rodriguez, J. Guzman

*Departamento de Procesos Químicos, Biotecnológicos y Ambientales, Universidad Técnica Federico Santa María, Avenida España 1680, Valparaiso, Chile, e-mail: henrik.hansen@usm.cl*

### **1. Summary**

In an experimental cell, the electrochemical production of Fenton's reagent and the use in the oxidation of spent caustic solutions was tested. The efficiency was measured as reduction of chemical oxygen demand (COD). Results showed a 10000 ppm COD solution could be reduced to under 500 ppm using the reactor to produce Fenton's reagent electrochemically.

### **2. Extended abstract**

An important wastewater stream from oil refineries is the spent caustic. Caustic solutions are used as scrubbing agent during the desulphurisation process to eliminate sulphur and mercaptans from oil and gasses. Spent caustic is classified as D003 (reactive sulphide) hazardous waste under the US Resource Conservation and Recovery Act (RCRA). Spent caustic is a highly specific effluent. Typically, relative small volumes (0.1 to 8 m<sup>3</sup>/h) are discharged, and these vary depending on the refinery's size and layout. The harmful effects are considerable due to the concentration in S<sup>2-</sup> (around 10000 ppm) and phenols (2500 ppm). The wastewater has typically a COD of around 10000 ppm.

An efficient treatment is the oxidation with Fenton's reagent. Fenton's reagent is a solution of hydrogen peroxide and an iron catalyst that is used to oxidize contaminants or waste waters. Mixing iron and hydrogen peroxide in the right manner, it results in the generation of highly reactive hydroxyl radicals ( $\cdot\text{OH}$ ) or peroxide radicals ( $\cdot\text{OOH}$ ). Ferrous iron(II) is oxidized to ferric iron(III) by hydrogen peroxide to a hydroxyl radical and a hydroxyl anion. In order to have an efficient process, the procedure requires: a) adjusting the wastewater to pH 3-5, b) adding the iron catalyst (for example as a solution of FeSO<sub>4</sub>), and c) adding slowly the H<sub>2</sub>O<sub>2</sub>. If the pH is too high, the iron precipitates as Fe(OH)<sub>3</sub> and catalytically decomposes the H<sub>2</sub>O<sub>2</sub> to oxygen.

Fenton's reagent can be produced by electrochemical oxidation of iron(0) and adding H<sub>2</sub>O<sub>2</sub> simultaneously. If iron plates are used in an electrolytic cell, continuous anodic oxidation of iron will occur at the plate surface and liberate the catalyst for Fenton's reagent. The advantages with the electrochemical in-situ production of Fe<sup>2+</sup> are:

- No generation of residual products.
- The process does not need to be heated.
- Better Fe<sup>2+</sup> dosage by controlling the electric current.
- Less operational costs (no use of chemicals).

In an experimental cell, the electrochemical production of Fenton's reagent and the use in the spent caustic treatment was tested. Both batch and continuous operation was investigated. During the process different parameters were analysed such as pH, temperature, electric current density and H<sub>2</sub>O<sub>2</sub> addition rate. Figure 1 shows the experimental set-up in principle.

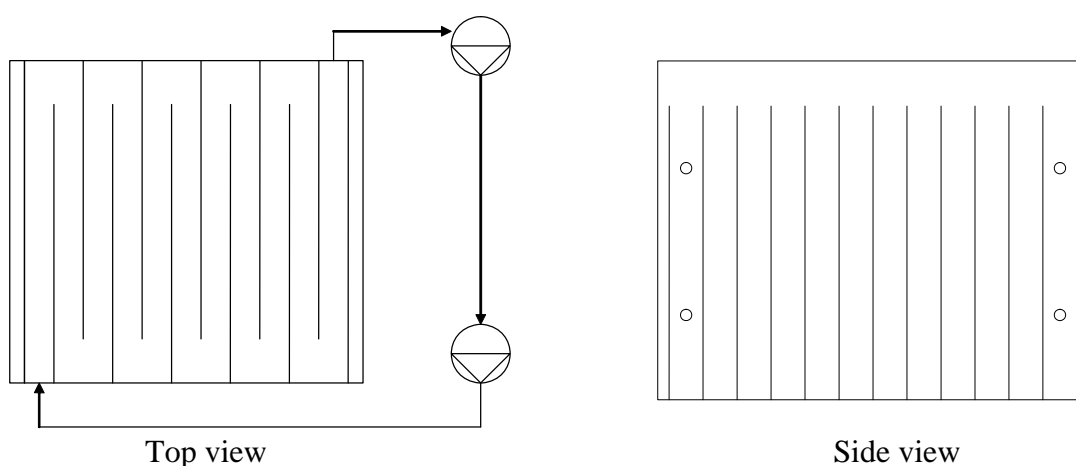


Figure 1. Experimental set-up

Applying electric DC current for one hour generated the Fe<sup>2+</sup> catalyst. Thereafter H<sub>2</sub>O<sub>2</sub> was added, and the COD reduction was measured with time. Table 1 shows a summary of important experimental results. The results showed that the electro assisted process to treat spent caustic was a promising alternative to wet air oxidation that operates at 25-90 bar and 200-300 C. 96 % of phenols and sulphides (in form of COD) could be oxidized in the spent caustic solutions applying 1.0 A for one hour at 40 °C and pH 2. Initial COD was 10000 ppm.

Experiment	pH	Electric current (A)	Temperature (°C)	COD reduction (%)
1	2	0.5	30	94
2	2	1.0	40	96
3	4	0.5	30	89
4	4	1.0	30	95

Table 1. Experimental details and results.



## **Cd(II) removal from aqueous solutions by adsorption onto activated carbon**

F. Di Natale<sup>a</sup>, A. Erto<sup>a</sup>, A. Lancia<sup>a</sup>,

*Department of Chemical Engineering, University of Naples Federico II,  
P.le Tecchio, 80 – 80125 Naples – Italy*

### **1. Summary**

This paper documents the results of an experimental study on cadmium removal from model aqueous solutions by adsorption onto a granular activated carbon (Aquacarb 207EA<sup>TM</sup>). Adsorption isotherms have been carried out at different pH, salinity and temperature levels. Cadmium adsorption is the highest at neutral pH levels while it strongly decreases by decreasing pH. Due to Cd(OH)<sub>2</sub> precipitation, the adsorption becomes irrelevant in alkaline systems. On the contrary, temperature and salinity have more limited effects on cadmium capture by the GAC.

### **2. Introduction**

Cadmium is a highly toxic inorganic micro-pollutant whose emissions are widely diffused giving rise to a large-scale environmental pollution. Adsorption on a granular activated carbon can be a reliable technique to reduce cadmium concentration in wastewater. Process design and optimization requires the knowledge of adsorption thermodynamics and kinetics. This paper presents experimental results on cadmium removal from model aqueous solution by adsorption onto a commercially available granular activated carbon (Aquacarb 207EA).

### **2. Experimental analysis**

The Aquacarb 207EA<sup>TM</sup> is a non impregnated granular activated carbon. Its morphological and chemical properties are reported in Di Natale et al. (2006).

Adsorption isotherms are obtained from batch tests at constant temperature (10 ÷ 40°C). Experiments are carried out by using HNO<sub>3</sub> and NaOH to adjust pH and NaNO<sub>3</sub> to alter salinity. Adsorption isotherms show the typical shape of a Langmuir-like isotherm. Experimental results reveal that the adsorption capacity,  $\omega$ , is the highest at neutral pH and lower salinity levels (Figure 1). Due to the occurrence of Cd(OH)<sub>2</sub> precipitation, the adsorption becomes irrelevant in alkaline systems. Furthermore, it slowly decreases by increasing temperature.

Breakthrough curves are obtained at neutral pH for different feed concentrations and flow rates (Figure 2). They show the classical sigmoidal shape with lower breakpoint times for higher flow rates and cadmium concentrations.

Desorption tests are conducted with 0.1 M nitric acid solution. The complete regeneration of a column saturated with 4 mg of cadmium is obtained with less than 100 ml of acid solution, giving a concentration factor of about 8. This result suggests a possible recovery of cadmium from wastewaters by means of adsorption-desorption cycles.

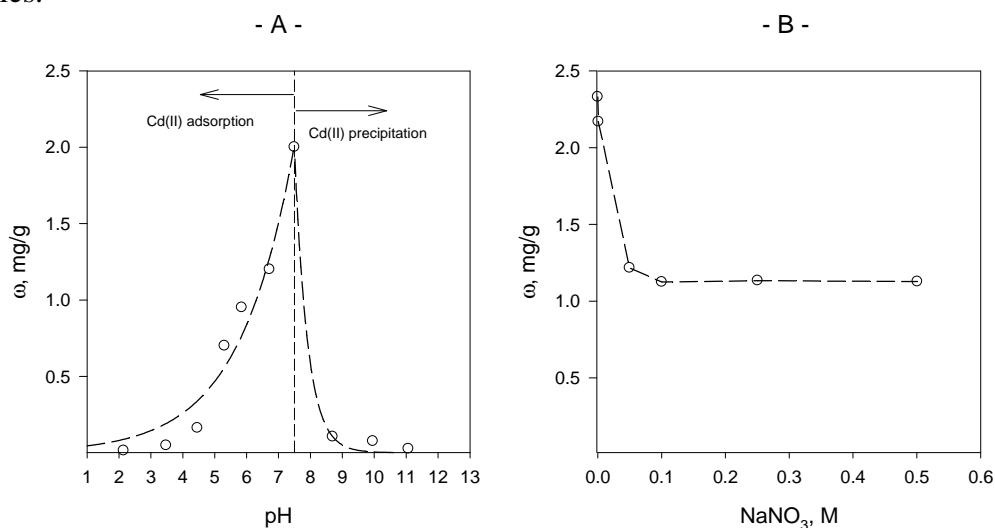


Figure 1 –A– Effect of solution pH on cadmium adsorption;  $m/V = 7.5$  g/l, –B– Effect of solution salinity on cadmium adsorption;  $m/V = 5$  g/l ( $T = 20^\circ\text{C}$ ,  $c^\circ = 25$  mg/l)

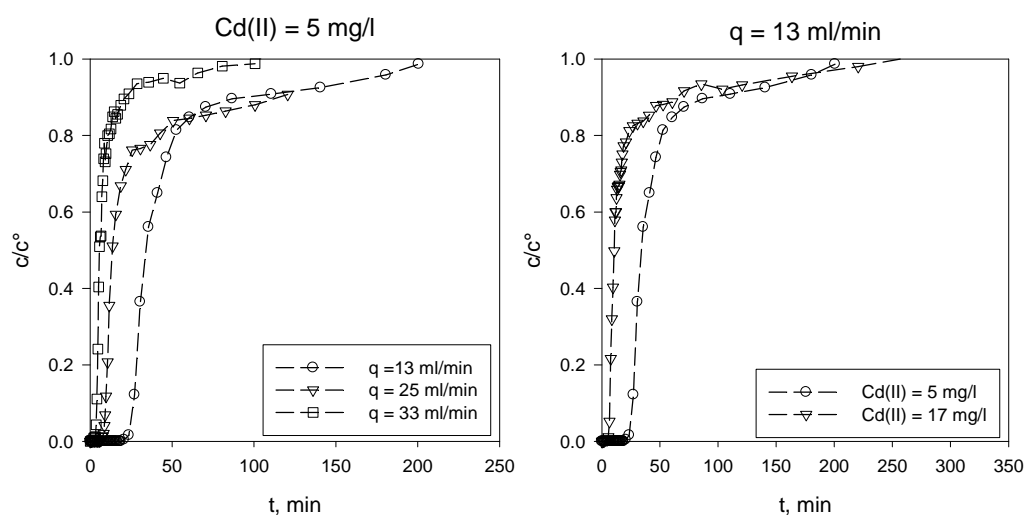


Figure 2 – Cadmium breakthrough curves in function of feed concentration and feed flow rate. Mass of carbon: 20 g; Bed height: 40 cm; Inert material: glass beads 800  $\mu\text{m}$ ;  $T = 20^\circ\text{C}$

## References

Di Natale F., Lancia A., Molino A., Karatza D., Musmarra D., Adsorption of chromium by activated carbon and char, *Journal of Hazardous materials*, available online from 19-11-2006; DOI:10.1016/j.jhazmat.2006.11.028. Reference HAZMAT 6252, ISSN:0304-3894

## **Water condensation in gas distribution plates of PEMFCs: flow and removal from the grooved patterns of the plates**

C. Bonnet,<sup>a</sup> J. Ramousse,<sup>b</sup> N. Doss,<sup>a</sup> F. Lopicque,<sup>a</sup> M. Boillot,<sup>a</sup>

<sup>a</sup>*Laboratoire des Sciences du Génie Chimique, CNRS-ENSIC, 1 rue Grandville, BP 20451, F- 54001 Nancy, France*

<sup>b</sup>*Institut de Recherche sur l'Hydrogène, Université du Québec à Trois-Rivières, 3351, boul. des Forges, C.P. 500, Trois-Rivières (QC) G9A 5H7, Canada*

### **1. Summary**

The effect of the gas dynamics on the mobility of the water droplets in two different designs of bipolar plate channels was studied. With the serpentine design, water-clogging in the channels and storage in the collecting segments at the edge were observed. This has been confirmed by the modelling of the gas velocity. With the column-flow pattern, liquid droplets are removed under the gas pressure and gravity.

Keywords: PEMFC, water condensation, bipolar plate channels

### **2. Extended Abstract**

While necessary in the membrane for proton conduction, water produced in PEMFC for the production of heat and electricity can be partly in the form of liquid for high hydration of the inlet gases and high current densities. Presence of liquid water in too a significant amount can result in water-clogging in the channels of the bipolar plates, in the structure of the diffusion media, as well as in the catalyst layers. Hence the activity of some parts of the fuel cell will reduce, and instability of the voltage will appear. It is well known that temperature, flow rates and hydration have to be carefully chosen for efficient operation at the nominal current. However, the bipolar plate design also is to exert a significant effect on the water management as shown by Sholta and al. (2006). Ramousse et al. (2007) shown that the condensation of the water occurs preferentially at the ribs of the bipolar plate channels.

Little is known on the effect of the gas dynamics on the mobility of the water droplets in the fuel cell channels. The present investigation was aimed at observing the flow of liquid water in the grooved structures of the bipolar plate in emulation experiments. Graphite Electrochem plates with an area of 25 cm<sup>2</sup> were used, considering two different designs: i) The so-called serpentine design actually consisted in the series of seven sets of five parallel channels 47.7 mm long, with collecting and redistribution segments at the edge which are deeper than the parallel channels. (ii) In the column-flow pattern, the gas was distributed through thirteen squared orifices, then circulated

around 2.0 mm squares tiles placed regularly on the plate surface, before being collected by the outlet tube.

The bipolar plate considered was simply covered by a Perspex polymeric plate, allowing visual observations, and humidified air was driven into the half inert cell. The rear face of the bipolar plate was cooled by tap water at 18 °C allowing partial condensation of water. In order to keep things clear, this abstract only presents a part of our results. Gas flow rates and hydration of the gas were adjusted as representative operating conditions of actual FC tests: 150 NmL min<sup>-1</sup> of dry air which corresponds to a current density equals to 0.12 A cm<sup>-2</sup> with a stoichiometric factor of 3. The dry air was humidified by bubbling it through water at a controlled temperature of 75 °C. High-speed camera allowed continuous observation of the two-phase flow (Figure 1).

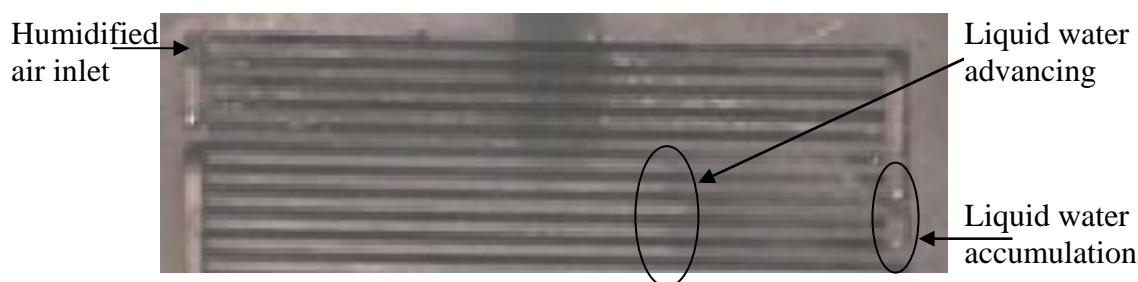


Figure 1: Zoom in the upper part of the serpentine design

The serpentine pattern was shown to favour slug flow in the channels. After complete wetting of the graphite surface, droplets of water can be attached in the segments at the edge, before being suddenly removed by a slight overpressure of the gas.

For 150 NmL min<sup>-1</sup>, the gas modelling in 2-D by solving the Navier-Stokes equations velocity is given in Figure 2 (the lighter colour corresponds to the higher velocity).

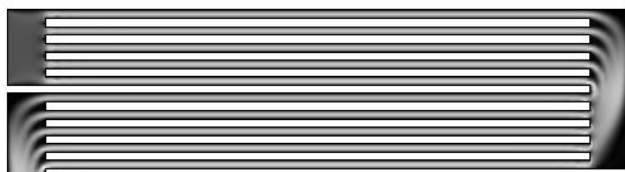


Figure 2: Modelling of the gas velocity in the serpentine design

The velocity seems rather homogeneous in the five parallel channels which could explain progression of the liquid water in Figure 1. However a negligible velocity is calculated in the edge of the lateral part, what could favour the accumulation of liquid water as observed.

In the column-flow pattern plate, liquid droplets formed are more regularly removed under the pressure of the gas and gravity: droplets falling entrain liquid water in their fall, in sort of avalanche phenomena, and stagnant liquid water can only be observed in the gas collection channel at the outlet of the cell.

## References

- Scholta, J., Escher, G., Zhang, W., Küpper, L., Jörissen, L., Lehnert, W., (2006) *Journal of Power Sources*, 155, 66-71.
- Ramousse, J., Didierjean, S., Lottin, O., Maillet, D., (2007) *Hydrogen and fuel cell 2007*, Vancouver, Canada